MARTIN MARIETTA ENERGY SYSTEMS LIBRARIES
4456 0285561 2

ORNL-NSIC-

OAK RIDGE NATIONAL LABORATORY

operated by

UNION CARBIDE CORPORATION

for the

U.S. ATOMIC ENERGY COMMISSION

U. S. REACTOR CONTAINMENT TECHNOLOGY

A COMPILATION OF CURRENT PRACTICE IN ANALYSIS, DESIGN, CONSTRUCTION, TEST, AND OPERATION

VOL. I

OAK RIDGE NATIONAL LABORATORY
CENTRAL RESEARCH LIBRARY
CIRCULATION SECTION
4500N ROOM 175
LIBRARY LOAN COPY
DO NOT TRANSFER TO ANOTHER PERSON
If you wish someone else to see this report, send in name with report and the library will arrange a loan.

Wm. B. Cottrell and A. W. Savolainen
Editors

NUCLEAR SAFETY INFORMATION CENTER

NSIC

ORNL-NSIC-5

UC-80 - Reactor Technology
TID-4500 (42nd ed.)

Contract No. W-7405-eng-26

U.S. REACTOR CONTAINMENT TECHNOLOGY

A Compilation of Current Practice in Analysis, Design, Construction, Test, and Operation

Volume I

Wm. B. Cottrell and A. W. Savolainen
Editors

Prepared by Oak Ridge National Laboratory
and Bechtel Corporation

AUGUST 1965

OAK RIDGE NATIONAL LABORATORY
Oak Ridge, Tennessee
operated by
UNION CARBIDE CORPORATION
for the
U.S. ATOMIC ENERGY COMMISSION

MARTIN MARIETTA ENERGY SYSTEMS LIBRARIES

3 4456 0285561 2

Printed in USA. Price $14.00 for Vols. I and II. Available from the Clearinghouse for Federal Scientific and Technical Information, National Bureau of Standards, U.S. Department of Commerce, Springfield, Virginia.

LEGAL NOTICE

This report was prepared as an account of Government sponsored work. Neither the United States, nor the Commission, nor any person acting on behalf of the Commission:

A. Makes any warranty or representation, expressed or implied, with respect to the accuracy, completeness, or usefulness of the information contained in this report, or that the use of any information, apparatus, method, or process disclosed in this report may not infringe privately owned rights; or

B. Assumes any liabilities with respect to the use of, or for damages resulting from the use of any information, apparatus, method, or process disclosed in this report.

As used in the above, "person acting on behalf of the Commission" includes any employee or contractor of the Commission, or employee of such contractor, to the extent that such employee or contractor of the Commission, or employee of such contractor prepares, disseminates, or provides access to, any information pursuant to his employment or contract with the Commission, or his employment with such contractor.

FOREWORD

As a consequence of preparation of the quarterly technical progress review Nuclear Safety, it became apparent both to the Oak Ridge National Laboratory editorial staff and to cognizant persons in the AEC Division of Reactor Development that there existed a wealth of uncorrelated information on the subject of reactor containment. Accordingly, in the fall of 1962, the Laboratory was authorized to undertake the present compilation, which was essentially completed in its present form in the spring of 1964.

In an effort to make the compilation as comprehensive and as authoritative as practical, the Laboratory subcontracted the responsibility for preparation of four of the 12 chapters (i.e., Chapters 8, 9, 10, and 11) to Bechtel Corporation, a major architect-engineer and fabricator of reactor containment structures. The authorship of the remaining chapters was then assigned to senior Laboratory personnel, supplemented in many instances by experts from other installations. Thus in addition to the literally hundreds of persons who reviewed the various drafts, numerous persons have made substantial original contributions to this work. Although these persons and the extent of their contribution are indicated at the beginning of each chapter, they are all listed alphabetically below in order that we may collectively acknowledge their contributions.

Contributor	Organization	Chapter
A. M. Appleford	Bechtel Corporation	8
L. Baker, Jr.	Argonne National Laboratory	5
C. J. Barton	Oak Ridge National Laboratory	4
S. A. Bernsen	Bechtel Corporation	9
J. R. Buchanan	Oak Ridge National Laboratory	1,7,12
W. B. Cottrell	Oak Ridge National Laboratory	1
G. H. Dyer	Bechtel Corporation	8,9,10
W. K. Ergen	Oak Ridge National Laboratory	5
M. H. Fontana	Purdue University	4
G. R. Fowles	Stanford Research Institute	6
B. L. Greenstreet	Oak Ridge National Laboratory	6
R. F. Griffin	Bechtel Corporation	8,9,10,11
J. R. Hawthorne	U. S. Naval Research Laboratory	8
H. W. Hoffman	Oak Ridge National Laboratory	6
G. W. Keilholtz	Oak Ridge National Laboratory	4
J. O. Kolb	Oak Ridge National Laboratory	5
R. R. Maccary	AEC Division of Reactor Licensing	10
J. E. Mott	University of Minnesota	6
W. E. Nyer	Phillips Petroleum Company	5
P. F. Pasqua	University of Tennessee	6
S. Peterson	Oak Ridge National Laboratory	5
T. W. Pickel	Oak Ridge National Laboratory	6
H. B. Piper	Oak Ridge National Laboratory	3,7,8
G. C. Robinson	Oak Ridge National Laboratory	10
M. A. Salmon	Illinois Institute of Technology Research Institute (formerly Armour Research Foundation)	6

R. W. Schneider	Oak Ridge National Laboratory	2
L. E. Steele	U.S. Naval Research Laboratory	8
H. W. Wahl	Bechtel Corporation	9
C. S. Walker	Oak Ridge National Laboratory	9
N. A. Weil	Illinois Institute of Technology Reactor Institute (formerly Armour Research Foundation)	6
C. A. Whitmarsh	Lewis Research Center	2,5

Of the many persons listed above, both within and without the Laboratory, we would like to express particular thanks to M. I. Lundin, who coordinated the Bechtel Corporation subcontract, and to H. B. Piper who, in addition to his contributions as an author, coordinated the review of all the chapters and prepared the index.

In order to make the greatest possible use of this compilation, readers should familiarize themselves with Chapter 1, which, in addition to providing essential background material, contains a section specifically designated "Guide to the Use of this Report." In addition, an extensive index is available.

It will be appreciated that a compilation of this type – particularly the first of its kind – on a relatively new subject and one upon which there is considerable research and development will be subject to frequent evaluation and change, at least until a much higher plateau of knowledge and experience is attained. Thus the editors are aware of the limited timeliness of the material herein and anticipate, circumstances permitting, that the material will be revised every two or three years. Toward that end, this document is being distributed in a loose-leaf binder, and recipients wishing to receive revisions of this material are asked to advise the editor of any changes in address.

The editors also wish to acknowledge the support, encouragement, and constructive criticism of the sponsors within the AEC Division of Reactor Development, particularly J. A. Lieberman, Assistant Director for Nuclear Safety; S. A. Szawlewicz, Chief, Research and Development Branch; and R. N. Newton, Research and Development Branch, without whom this work would not have been possible. However, the reader is cautioned not to regard the inclusion of any information here as giving that information any official sanction as far as the AEC Division of Compliance or Division of Reactor Licensing is concerned. This report does no more than reflect the current state of the art to the satisfaction of the Oak Ridge National Laboratory and the Bechtel Corporation. Furthermore, it cannot anticipate what changes in containment technology may evolve from research and development or the official attitudes regarding the adequacy of containment provisions for a particular application that may evolve from the continuing deliberation of either the Advisory Committee on Reactor Safeguards or the Division of Reactor Licensing.

Editors
Wm. B. Cottrell
A. W. Savolainen

PREFACE

Although this report was not prepared by or under the auspices of the Nuclear Safety Information Center, it is being distributed as an NSIC report for the following reasons: (1) containment is one of the most important interests of the NSIC and (2) the NSIC can provide the continuity, as well as the source material, for future revisions. The Nuclear Safety Information Center was established in March 1963 at the Oak Ridge National Laboratory under the sponsorship of the U.S. Atomic Energy Commission. The Center serves as a focal point for the collection, storage, evaluation, and dissemination of information in the following areas:

Containment of nuclear facilities
Fission-product release, transport, and removal
Nuclear instrumentation, control, and safety systems
Radioactive effluent control monitoring, movement, and dosage
Reactor transients, kinetics, and stability
Meteorological considerations
Operational safety and experience

In addition to state-of-the-art reports in the above subject areas, the Center prepares the quarterly technical progress review Nuclear Safety and has a reference file stored on magnetic tape for the computer search of safety information and the preparation of a quarterly indexed bibliography of the nuclear safety literature.

Inquiries concerning the services, capabilities, and operation of the Center should be addressed to:

Wm. B. Cottrell, Director
Nuclear Safety Information Center
Oak Ridge National Laboratory
P. O. Box Y
Oak Ridge, Tennessee 37831

GUIDE TO THE USE OF THIS REPORT

Purpose

In order to make use of the information that may be found in this report, not only should the specific purposes be known but also the subjects that are excluded. For the purposes to stand out clearly, it is pertinent to note that this report does not propose to

1. evaluate the safety of specific systems for specific applications,
2. present information on the design, integrity, or performance of the primary system,
3. discuss extensively the behavior of fission products after leaving the reactor-containment system (see Sec. 4.5.1),
4. establish criteria by which containment systems must be designed, fabricated, tested, and operated.

On the other hand, it is the purpose of this report to

1. describe the containment features of existing reactor installations,
2. describe some of the calculational techniques that have been employed to determine fluid dynamics and radiological loads on containment systems,
3. present experimental data pertinent to items 1 and 2,
4. describe pertinent details of the design, construction, and test of containment systems,
5. present existing data on the cost of containment systems,
6. review the current research and development pertinent to the above items.

Pertinent matters of significant interest to the containment designer and fabricator or to the plant operator concerning the containment system have been considered in this report. Thus it is concerned not only with the design of the many existing containment systems but also with how and why these designs were developed and why particular containment systems appear more suitable in certain reactor systems for certain applications. The capabilities and limitations of the various containment systems and also the accidents for which the containment is provided are discussed. The existing regulatory requirements that must be met at a particular place and time are cited. Unfortunately, none of these requirements are fixed and it is not possible to speak in absolute terms except with regard to what has been done. The information presented provides a point of departure for more advanced designs, improved engineered safeguards, and possibly even changes in the siting requirements.

Chapters 2 through 6 set forth the salient basic information regarding containment requirements for particular reactors and sites. Chapter 2 gives the pertinent regulations and existing criteria. Chapter 3 discusses the nature and scope of the accidents that are examined for every reactor in order to identify the accident that is considered the maximum credible for that reactor and which in turn determines the containment requirements. Chapter 4 gives the amounts and nature of the fission products that must be contained. Chapter 5 discusses the energy that the containment system must be designed to cope with. Chapter 6 gives a summary of the special

analytical techniques frequently involved in containment analyses. Chapter 7 describes existing containment systems; Chapter 8 gives design considerations; Chapter 9 describes auxiliary components; and Chapter 10 lists the performance tests required. In Chapter 11 the identifiable costs associated with various containment systems and parts thereof are tabulated. Chapter 12 presents a resume of current research pertinent to all aspects of containment.

Limitations and Use

At the present stage in the development of both reactor and containment technology, it is not possible to develop a definitive relationship between reactor type, power level, and containment system that can be employed to identify the most economical containment system for use with a given reactor installation. Examination of the trends discussed here, as well as considerations of the obvious points of compatibility and incompatibility between various reactor and containment types, will, however, point to combinations of interest. The cost information in Chapter 11 is of limited value because of the uncertainty in the cost accounts that were available, the apparent wide range in costs for similar systems, and the many subtle differences in superficially similar reactor installations. Trends do become evident with data presented here, although these trends may have been apparent anyway. The most pertinent advice that can be offered regarding costs of different containment systems for a given application is that, assuming no obvious mismatch (see Table 1.12) and that the safety provided by each is acceptable to the regulatory authorities, the best containment system (i.e., the least expensive) must be determined from a cost analysis of a fairly detailed design of two and sometimes more arrangements.

It should also be appreciated that most of the containment information reported here has been derived from a reactor technology that has been and still is oriented toward a water-cooled and -moderated reactor. It is not surprising that starting with this background, the containment systems provided for other types of reactor are adaptations of, and subject to, much of the same rationale as those that developed out of the technology of water-cooled power reactors. It is quite conceivable that starting from another frame of reference, for example, the gas-cooled graphite-moderated reactors, which form the basis of the United Kingdom nuclear power program, the accepted containment systems might have been considerably different. It is also possible that they might have afforded comparable protection.

The containment analyst is also cautioned against regarding the criteria and designs described here as being fixed. The past several years have witnessed many innovations in containment design, increasing expenditures in containment research and development, and the establishment of the first reactor siting criteria. The present rapid pace in the development of containment technology cannot help but have significant ramifications in containment design and criteria.

The reader is also cautioned not to regard the inclusion of any information here as giving that information any official sanction as far as the AEC Divisions of Compliance or Reactor Licensing are concerned. Even in

instances where members of these AEC regulatory divisions may have received or supplied material for use herein, that does not per se establish that material or any other portion of this report as an official regulation, standard, or criterion that must be followed in the analyses, design, construction, testing, or operation of a containment system. This report does, however, attempt to include all relevant information and in so doing includes many criteria that are frequently associated with containment systems, some of which have been approved for specific sites and specific reactors.

CONTENTS

Volume I

	Page
Foreword	iii
Preface	v
Guide to the Use of This Report	vii
1. INTRODUCTION	1.1
1.1 Philosophy	1.1
1.1.1 Definitions	1.1
1.1.1.1 Reactor Containment	1.1
1.1.1.2 Engineered Safeguards	1.1
1.1.1.3 Maximum Credible Accident	1.2
1.1.2 Need for Containment	1.2
1.1.3 Evolution of Containment	1.2
1.1.4 Safety Factors	1.4
1.1.4.1 Exposure Calculations	1.4
1.1.4.2 Energy Release Calculations	1.4
1.1.4.3 Mechanical Design	1.5
1.2 Ramifications of Reactor Containment	1.6
1.2.1 Reactor Site Criteria	1.6
1.2.1.1 Stipulations of Current Criteria	1.8
1.2.1.2 Calculational Procedures	1.8
1.2.1.3 Conclusions	1.15
1.2.2 Nuclear Merchant Ship Site Criteria	1.16
1.2.2.1 Essential Features of Ship Site Criteria	1.17
1.2.2.2 Other Aspects of the Criteria	1.18
1.2.2.3 Discussion	1.19
1.2.3 Reliability of Reactor Systems	1.21
1.2.3.1 Control and Safety Systems Reliability	1.21
1.2.3.2 Reliability of Containment Systems	1.21
1.2.3.3 Reliability in Operating Versus Shutdown Condition	1.22
1.2.4 Nuclear Safety Economics	1.23
1.2.4.1 Emergency Supply Systems	1.24
1.2.4.2 Containment Structures	1.24
1.2.4.3 Site Costs	1.25
1.2.4.4 Conclusions	1.28
1.2.5 Liability and Indemnity	1.28
1.3 General Description of Reactor Types	1.32
1.3.1 Water-Cooled Reactors	1.32
1.3.1.1 Pressurized-Water Reactors	1.32
1.3.1.2 Boiling-Water Reactors	1.34
1.3.1.3 Homogeneous Reactors	1.36
1.3.1.4 Heavy-Water Reactors	1.36
1.3.2 Liquid-Metal-Cooled Reactors	1.37
1.3.2.1 Thermal Reactors	1.37
1.3.2.2 Fast Reactors	1.38

1.3.3 Gas-Cooled Reactors 1.38
1.3.4 Organic-Cooled Reactors 1.39
1.3.5 Fused-Salt Reactors 1.40
1.3.6 University Reactors 1.41
1.4 General Description of Containment Systems..... 1.42
1.4.1 Pressure Containment..... 1.42
1.4.2 Pressure-Suppression Containment..... 1.44
1.4.3 Pressure-Release Containment..... 1.46
1.4.3.1 Pressure-Venting Containment..... 1.46
1.4.3.2 Pressure-Relief Containment..... 1.48
1.4.4 Multiple Containment..... 1.49
1.4.4.1 High-Pressure Double Containment..... 1.50
1.4.4.2 Pressure-Suppression Double Containment..... 1.51
1.4.5 State of the Art..... 1.52
References..... 1.55

2. CODES, CRITERIA, AND REGULATIONS..... 2.1
2.1 Introduction..... 2.1
2.2 Regulatory Organizations..... 2.2
2.2.1 Atomic Energy Commission..... 2.2
2.2.1.1 Division of Reactor Licensing..... 2.5
2.2.1.2 Division of Compliance..... 2.5
2.2.1.3 Office of the General Counsel..... 2.5
2.2.1.4 Atomic Safety and Licensing Board..... 2.5
2.2.2 Advisory Committee on Reactor Safeguards..... 2.6
2.2.3 Joint Committee on Atomic Energy..... 2.7
2.2.4 State Activities in Atomic Energy..... 2.7
2.3 Federal Licensing and Authorization Procedures..... 2.12
2.3.1 General..... 2.12
2.3.2 Code of Federal Regulations..... 2.13
2.3.3 Construction Permit..... 2.13
2.3.4 Operating License..... 2.15
2.3.5 Containment Description in Final Safety Analysis Report..... 2.16
2.4 Codes and Regulations for Steel Containment Structures.. 2.17
2.4.1 General..... 2.17
2.4.2 ASME Codes..... 2.17
2.4.3 ASME Code Cases..... 2.18
2.4.3.1 Case 1270N-5..... 2.19
2.4.3.2 Case 1271N..... 2.19
2.4.3.3 Case 1272N-5..... 2.19
2.4.3.4 Case 1273N-7..... 2.19
2.4.3.5 Case 1274N-10..... 2.20
2.4.3.6 Case 1275N..... 2.20
2.4.3.7 Case 1276N-2..... 2.20
2.4.3.8 Cases Applicable to Section III..... 2.20
2.4.4 ASME Provisions for Steel Containment Vessels at Pressures Under 5 psi..... 2.20
2.4.5 Manufacturers of ASME Code Boilers and Pressure Vessels..... 2.21
2.4.6 The National Board..... 2.21

2.4.7 Tabulation of States, Cities, and Counties Having Boiler or Pressure Vessel Laws..... 2.22
2.4.8 Uniform Boiler and Pressure Vessel Laws Society Inc..... 2.26
2.4.9 ASA Containment Vessel Standard..... 2.26
2.4.10 Other Containment Vessel Codes..... 2.26
2.4.10.1 Navy Code..... 2.26
2.4.10.2 API-ASME Code..... 2.27
2.5 Codes and Standards for Pressure Piping..... 2.27
2.6 Codes and Regulations for Confinement Structures..... 2.29
2.7 High-Efficiency Filters as a Part of Containment..... 2.30
2.7.1 General..... 2.30
2.7.2 Testing Individual New High-Efficiency Filters..... 2.31
2.7.3 Determining Efficiency of Filter Systems..... 2.31
2.8 Status of Activities in the Development of Nuclear Standards..... 2.32
References..... 2.43

3. CREDIBLE ACCIDENTS..... 3.1
3.1 Typical Accidents..... 3.2
3.1.1 Startup Accident..... 3.2
3.1.2 Control Rod Withdrawal Accident..... 3.3
3.1.3 Poison Removal Accident..... 3.3
3.1.4 Cold Coolant Accident..... 3.5
3.1.5 Control Rod Drop Accident..... 3.6
3.1.6 Loss of Coolant Flow Accident..... 3.6
3.1.6.1 Circulating Pump Stoppage..... 3.6
3.1.6.2 Blocked Flow Channel..... 3.8
3.1.7 Loss of Load Accident..... 3.8
3.1.8 Step Increase in Load Accident..... 3.8
3.1.9 Accidental Release of Primary Fluid and Interchange of Primary and Secondary Fluids..... 3.8
3.1.9.1 Indirect Cycle..... 3.11
3.1.9.2 Direct Cycle..... 3.11
3.1.10 Loss of Coolant Accident..... 3.11
3.1.11 Fuel-Handling Accidents..... 3.13
3.1.11.1 Mechanical Failure..... 3.13
3.1.11.2 Insufficient Cooling..... 3.13
3.1.11.3 Misoperation..... 3.13
3.1.12 Fuel Element Failures..... 3.13
3.1.13 Chemical Reactions..... 3.14
3.1.14 General..... 3.14
3.2 Maximum Credible Accident..... 3.14
3.2.1 Reference Description..... 3.15
3.2.1.1 Fuel Material Conditions..... 3.15
3.2.1.2 Primary Coolant Conditions..... 3.16
3.2.1.3 Release and Dispersion Conditions..... 3.16
3.2.2 Analysis..... 3.18
3.2.3 Examples of Assumed MCA's..... 3.19
3.2.3.1 Conventional Types..... 3.19
3.2.3.2 Mechanistic Type..... 3.28

3.3 Component Failures 3.31
3.3.1 Pressure Vessels 3.32
3.3.2 Piping 3.33
3.4 Probabilities 3.34
3.5 Reactor Accident Experience 3.37
References 3.41

4. FISSION-PRODUCT RELEASE AND TRANSPORT 4.1
4.1 Introduction 4.1
4.2 Radioactivity Generation 4.3
4.2.1 Fission-Product Distribution 4.3
4.2.2 Radioactivity of Fission Products 4.8
4.2.3 Calculation of Fission-Product Inventories 4.36
4.2.3.1 Calculation of Fission-Product Accumulation in Circulating Fuels 4.83
4.2.3.2 Summary and Comments on Evaluating Fission-Product Buildup and Decay 4.87
4.3 Fission-Product Release from Fuel Elements 4.89
4.3.1 Introduction 4.89
4.3.2 Predicting Cladding Failure 4.90
4.3.2.1 Release of Fission Gases from UO_2 During Irradiation 4.90
4.3.2.2 Pressure Buildup and Cladding Stress in a Fuel Rod 4.102
4.3.3 Release from Fuel After Cladding Failure 4.103
4.3.3.1 Release from Oxidized UO_2 ..... 4.105
4.3.3.2 Release from Molten UO_2 ..... 4.106
4.3.4 Release from Non-UO_2 Fuel 4.115
4.3.4.1 Release from Metallic Uranium 4.115
4.3.4.2 Release from Graphite-Matrix Fuel Elements 4.117
4.3.5 Particulate Generation During Fuel Meltdown 4.118
4.4 Fission-Product Transport 4.119
4.4.1 Transport Within the Primary System 4.119
4.4.2 Chemical and Physical Behavior of Released Fission Products 4.123
4.4.2.1 Release Experiments 4.123
4.4.2.2 Fission-Product Behavior 4.123
4.4.2.3 Chemical States 4.129
4.4.3 Transport Effects of Small Particles 4.132
4.4.4 Fission-Product Behavior Within the Outer Containment Building 4.133
4.4.4.1 Behavior of Fission Products in Water Droplets 4.133
4.4.4.2 Behavior of Iodine in Reactor Containment Buildings 4.134
4.4.4.3 Removal of Iodine from Containment Vessel Atmosphere by Sprays 4.143
4.4.4.4 Behavior of Particulates in Containment Vessels 4.162
4.4.4.5 Release of Activity from Three-Barrier Containment Systems 4.172

4.5 Effects External to Containment Barriers..... 4.178
4.5.1 Atmospheric Dispersion..... 4.178
4.5.2 Biological Hazards and Dose Calculations..... 4.186
4.5.2.1 Deposition of Activity from the Cloud... 4.192
4.5.2.2 Hazards Due to Iodine..... 4.193
4.5.2.3 Contamination of Exposed Food with Iodine..... 4.198
4.5.2.4 Hazards Due to ^{137}Cs..... 4.199
4.5.2.5 Inhalation and Ingestion Hazards of ^{90}Sr and ^{89}Sr..... 4.199
4.5.2.6 Ranges of Hazards — Summary 4.199
References..... 4.209

5. ENERGY SOURCES..... 5.1
5.1 Introduction..... 5.1
5.2 Chemical Reactions..... 5.2
5.2.1 Metal-Water Reactions..... 5.3
5.2.1.1 General..... 5.3
5.2.1.2 Analytical Considerations..... 5.3
5.2.1.3 Full-Scale Excursions..... 5.9
5.2.1.4 Small-Scale Meltdown Tests in TREAT..... 5.11
5.2.1.5 Out-of-Pile Studies..... 5.12
5.2.1.6 Specific Reactions..... 5.12
5.2.1.7 Analysis of Cladding-Water Reaction During Reactor Accidents..... 5.50
5.2.2 Oxidation Reactions..... 5.56
5.2.2.1 Graphite Oxidation..... 5.56
5.2.2.2 Sodium Oxidation..... 5.71
5.2.2.3 Organic Coolants..... 5.78
5.2.2.4 Hydrogen-Oxygen Reaction..... 5.78
5.2.3 Graphite-Steam Reactions..... 5.84
5.2.3.1 Reactions in a Graphite-Steam Environment..... 5.84
5.2.3.2 Reaction Rate Kinetics..... 5.85
5.2.3.3 Hazards Calculations..... 5.86
5.3 Nuclear Energy..... 5.89
5.3.1 Fission Energy..... 5.89
5.3.2 Power Excursions..... 5.90
5.3.2.1 Introduction..... 5.90
5.3.2.2 Nuclear Excursion Models..... 5.92
5.3.2.3 Thermal Burst Shape Properties..... 5.94
5.3.2.4 Some Comparisons of Thermal Models and Thermal Excursion Reactor Data..... 5.99
5.3.2.5 Energy in Fast Reactor Excursions..... 5.110
5.3.2.6 Excursion Energy for Use in Accident Calculations..... 5.112
5.3.3 Delayed Neutrons..... 5.116
5.3.4 Decay Heat Generation..... 5.117

5.4 Other Heat Sources..... 5.128
5.4.1 Heat Content of Materials..... 5.128
5.4.2 Stored Energy in Graphite (Wigner Energy)..... 5.128
5.4.2.1 Effect of Irradiation..... 5.130
5.4.2.2 Energy Release..... 5.131
References..... 5.133

6. ANALYTICAL TECHNIQUES AND PERTINENT EXPERIMENTAL DATA..... 6.1
6.1 Introduction..... 6.1
6.2 Heat Transfer Problems..... 6.2
6.2.1 Conduction..... 6.3
6.2.2 Convection..... 6.5
6.2.2.1 Forced Convection..... 6.5
6.2.2.2 Free Convection..... 6.10
6.2.3 Radiation..... 6.12
6.2.4 Condensation..... 6.19
6.2.4.1 Condensation Without Inert Gas Present.. 6.20
6.2.4.2 Condensation With Inert Gas Present..... 6.21
6.2.4.3 Direct Contact of Liquid and Gas..... 6.21
6.2.5 Boiling..... 6.22
6.3 Pressure, Volume, and Temperature Relations..... 6.26
6.4 Hydraulic Problems..... 6.35
6.4.1 Jet Impingement Forces..... 6.36
6.4.2 Two-Phase Flow..... 6.44
6.4.2.1 Quality and Void Fractions in a Non-slip Flow System..... 6.46
6.4.2.2 Slip Flow System..... 6.47
6.4.2.3 Friction Drop in a Boiling Channel..... 6.53
6.4.2.4 Acceleration Pressure Drop..... 6.55
6.4.2.5 Expansion and Contraction Losses in Two-Phase Flow..... 6.56
6.4.2.6 Critical Flow..... 6.60
6.4.2.7 Equilibrium Two-Phase Annular Critical Flow 6.62
6.4.2.8 Nonequilibrium or Metastable Two-Phase Critical Flow..... 6.68
6.4.2.9 Transitional Critical Flow..... 6.71
6.4.2.10 Metastable Flow..... 6.71
6.4.2.11 Pressure-Flow-Time History..... 6.72
6.4.3 Shock Generation and Transmission..... 6.76
6.4.3.1 Rankine-Hugoniot Conservation Laws..... 6.77
6.4.3.2 Wave Forms..... 6.81
6.4.3.3 Shock Transfer Across an Interface..... 6.84
6.4.3.4 Initial Pressure Generation..... 6.86
6.4.3.5 Spray Pressure..... 6.87
6.4.3.6 Energy Dissipation..... 6.89
6.4.4 Jet Condensation..... 6.91
6.5 Structural Problems..... 6.92
6.5.1 Introduction..... 6.92
6.5.1.1 Limitations of Analysis..... 6.92
6.5.1.2 Nomenclature..... 6.94

6.5.2 Mechanical Properties of Materials..... 6.94
6.5.2.1 Fundamentals of the Plastic Behavior of Metals Under Biaxial States of Stress... 6.94
6.5.2.2 Uniaxial Stress-Strain Relations..... 6.95
6.5.2.3 Yield Criteria for Biaxial States of Stress..... 6.100
6.5.2.4 Flow Rule..... 6.103
6.5.2.5 Behavior of Materials Subjected to Dynamic Loading..... 6.106
6.5.3 Static Plastic Strength of Thin Cylindrical Shells with Various End Closures Under Internal Pressure..... 6.122
6.5.3.1 Comparison of Exact Solutions with Test Results..... 6.122
6.5.3.2 Approximate Theories..... 6.133
6.5.3.3 Accuracy of the Approximate Theory..... 6.137
6.5.3.4 Conclusions..... 6.147
6.5.3.5 ENDCON..... 6.148
6.6 Shock and Missile Protection..... 6.150
6.6.1 Missile Generation..... 6.150
6.6.1.1 Shock-Generated Missiles..... 6.151
6.6.1.2 Self-Propelled Missiles..... 6.152
6.6.1.3 Jet-Propelled Missiles..... 6.153
6.6.1.4 Spalling..... 6.155
6.6.2 Penetrability of Shells..... 6.156
6.6.2.1 Penetration Experiments..... 6.157
6.6.2.2 Conclusions..... 6.163
6.6.3 Blast Shielding..... 6.164
6.6.3.1 Blast Shield Theory..... 6.165
6.6.3.2 Absorption Mechanism..... 6.167
6.6.3.3 Criteria for Ideal Absorbers..... 6.168
6.6.3.4 Reduction Factor Formula..... 6.169
6.6.3.5 Materials..... 6.171
6.6.3.6 Maximum Absorber Thickness..... 6.176
6.6.3.7 Composite Design..... 6.179
6.7 Computer Programs..... 6.179
References..... 6.185

Volume II

7. DESCRIPTIONS OF SPECIFIC CONTAINMENT SYSTEMS..... 7.1
7.1 Introduction..... 7.1
7.1.1 General Design Considerations..... 7.5
7.1.1.1 High- and Low-Pressure Containers..... 7.5
7.1.1.2 Pressure Suppression..... 7.9
7.1.1.3 Pressure Venting..... 7.9
7.1.1.4 Pressure Relief..... 7.10
7.1.2 Example of Containment System Planning..... 7.10
7.2 High-Pressure Containment..... 7.11
7.2.1 Spherical Containers..... 7.15
7.2.1.1 Yankee..... 7.15
7.2.1.2 Indian Point..... 7.15
7.2.1.3 Dresden..... 7.15

7.2.2 Cylindrical Containers..... 7.20
7.2.2.1 Hemispherical Top and Hemiellipsoidal Bottom..... 7.20
7.2.2.2 Hemispherical Top and Bottom..... 7.27
7.2.2.3 Hemispherical Top and Flat Bottom..... 7.30
7.2.3 Other Shapes..... 7.33
7.2.3.1 PWR..... 7.33
7.2.3.2 HRT..... 7.36
7.2.3.3 NS Savannah..... 7.36
7.2.4 Proof Tests..... 7.39
7.2.4.1 NS Savannah..... 7.39
7.2.4.2 Indian Point..... 7.41
7.2.4.3 CVTR..... 7.41
7.2.4.4 Future Testing..... 7.41
7.2.4.5 Leakage-Rate Specifications..... 7.43
7.2.5 Materials and Specifications..... 7.44
7.2.6 Penetrations..... 7.44
7.2.7 Containment Protection..... 7.55
7.2.7.1 External Protection..... 7.55
7.2.7.2 Shock Protection..... 7.57
7.2.7.3 Missile Protection..... 7.58
7.2.8 Coolant Properties..... 7.58
7.2.9 Energy Sources..... 7.58
7.2.9.1 Boiling-Water Reactors..... 7.62
7.2.9.2 Pressurized-Water Reactors..... 7.63
7.2.9.3 Pressure-Tube Reactors..... 7.65
7.2.9.4 Sodium-Cooled Reactors..... 7.65
7.2.9.5 Gas-Cooled Reactors..... 7.65
7.2.10 Fission-Product Release and Dispersion..... 7.66
7.2.10.1 Power History..... 7.66
7.2.10.2 Fission-Product Release..... 7.70
7.2.10.3 Direct Radiation..... 7.71
7.2.10.4 Leakage from the Building..... 7.71
7.2.10.5 Leakage and Transport..... 7.72
7.3 Low-Pressure Containment..... 7.75
7.3.1 Design Parameters..... 7.78
7.3.2 Proof Tests..... 7.78
7.3.3 Material Specifications..... 7.81
7.3.4 Penetrations..... 7.81
7.3.5 Building Protection..... 7.84
7.3.5.1 External Protection..... 7.84
7.3.5.2 Missile Protection..... 7.84
7.3.6 Moderator and Coolant..... 7.85
7.3.7 Design Accident..... 7.86
7.3.8 Fission-Product Release and Transport..... 7.88
7.4 Pressure-Suppression Containment..... 7.91
7.4.1 Description and Design..... 7.95
7.4.2 Tests..... 7.97
7.4.3 Codes..... 7.98
7.4.4 Penetrations..... 7.98
7.4.5 Containment Protection..... 7.100

7.4.6 Coolant Properties..... 7.100
7.4.7 Accidents..... 7.102
7.4.8 Activity Release..... 7.103
7.5 Pressure-Venting Containment..... 7.109
7.5.1 Building Concept..... 7.109
7.5.2 Pressure and Leakage Requirements..... 7.109
7.5.3 Building Construction..... 7.115
7.5.4 Penetrations..... 7.115
7.5.5 Building Protection..... 7.116
7.5.6 Building Design Basis..... 7.117
7.5.7 The Maximum Accident..... 7.119
7.6 Pressure-Relief Containment..... 7.123
7.6.1 Building..... 7.124
7.6.2 Tests..... 7.124
7.6.3 Penetrations..... 7.127
7.6.4 Accident Analysis..... 7.127
7.7 Underground Containment..... 7.127
7.7.1 Building Concept..... 7.128
7.7.2 Tests..... 7.128
7.7.3 Penetrations..... 7.130
7.7.4 Protection..... 7.130
7.7.5 Basis for Design..... 7.130
7.7.6 Doses..... 7.131
7.8 Multiple Containment..... 7.132
7.8.1 Indian Point..... 7.132
7.8.2 NS Savannah..... 7.134
7.8.3 Ravenswood..... 7.134
7.8.4 Design Parameters..... 7.134
7.8.4.1 Building Design..... 7.134
7.8.4.2 Vacuum System..... 7.136
7.8.5 Proof Tests..... 7.136
7.8.6 Material Specifications..... 7.136
7.8.7 Penetrations..... 7.136
7.8.8 Building Protection..... 7.139
7.8.9 Moderator and Coolant..... 7.141
7.8.10 Design Accident..... 7.141
7.8.11 Fission-Product Release..... 7.143
7.8.11.1 Indian Point..... 7.143
7.8.11.2 NS Savannah..... 7.143
7.9 Engineered Safeguards..... 7.145
7.9.1 Core Cooling Systems..... 7.146
7.9.1.1 Water Reactor Systems..... 7.148
7.9.1.2 Gas-Cooled Systems..... 7.148
7.9.2 Building Spray Systems..... 7.151
7.9.2.1 Spray and Dousing Systems..... 7.153
7.9.2.2 External Spray Systems..... 7.153
7.9.3 Filter Systems..... 7.154
7.9.4 Multiple Containment..... 7.157
7.9.5 Combination of Engineered Safeguards..... 7.157
7.10 Bibliography..... 7.158
References..... 7.160

8. STRUCTURAL DESIGN CONSIDERATIONS..... 8.1
8.1 General Design Considerations..... 8.1
8.1.1 Site Conditions..... 8.2
8.1.1.1 Topography and Soil Conditions..... 8.2
8.1.1.2 Meteorology and Hydrology..... 8.7
8.1.1.3 Seismology..... 8.10
8.1.2 Containment Envelope Boundaries..... 8.14
8.1.3 Plant Layout and Structural Considerations..... 8.15
8.1.3.1 Size..... 8.16
8.1.3.2 Shape..... 8.17
8.1.3.3 Materials..... 8.19
8.1.4 Additional Requirements..... 8.19
8.1.4.1 Containment Shielding..... 8.19
8.1.4.2 Site Layout..... 8.20
8.1.4.3 Refueling..... 8.20
8.1.5 Examples of Design Considerations Leading to Various Containment Shapes..... 8.20
8.1.5.1 Spherical..... 8.21
8.1.5.2 Cylindrical..... 8.22
8.1.5.3 Flat-Walled Rectangular Prisms..... 8.22
8.2 Choice of Materials..... 8.23
8.2.1 Steel..... 8.23
8.2.2 Concrete..... 8.27
8.2.2.1 Reinforced Concrete..... 8.30
8.2.2.2 Prestressed Concrete..... 8.33
8.2.3 Combination Steel and Concrete..... 8.37
8.2.4 Low-Leakage-Rate Conventional Buildings..... 8.37
8.3 Special Design Features..... 8.39
8.3.1 Containment Foundation and Support..... 8.39
8.3.2 Penetrations in Containment Vessels..... 8.41
8.3.3 Thermal and Other Motions of Containment Vessels..... 8.42
8.3.4 Shock and Missile Protection..... 8.44
8.3.5 Attachments and Accessories..... 8.45
8.4 Construction..... 8.46
8.4.1 Single-Stage Construction..... 8.46
8.4.2 Multistage Construction..... 8.50
8.4.3 Lined Concrete..... 8.53
8.4.3.1 Metal Linings..... 8.54
8.4.3.2 Nonmetallic Coatings..... 8.56
8.4.4 Fabrication and Erection Techniques..... 8.57
8.5 Brittle Fracture of Steel..... 8.58
8.5.1 Transition Temperature Tests..... 8.59
8.5.1.1 Impact Tests..... 8.59
8.5.1.2 Drop Weight Test..... 8.60
8.5.1.3 Explosion Bulge Test..... 8.61
8.5.1.4 Crack-Arrest Test..... 8.61
8.5.2 Low-Temperature Brittleness..... 8.62
8.5.2.1 Three Conditions for Fracture..... 8.62
8.5.2.2 Significance and Practical Use of the Fracture Analysis Diagram..... 8.64
8.5.2.3 Comments Pertinent to Pressure Vessel Fabrication..... 8.68

8.5.3 Neutron Embrittlement of Steel..... 8.68
8.5.3.1 Effects of Irradiation on Notch Ductility of Steels..... 8.69
8.5.3.2 Postirradiation Heat Treatment and Cyclic Irradiation and Annealing..... 8.76
8.5.3.3 Effects of Irradiation on Tensile Properties..... 8.77
8.5.3.4 Reactor Surveillance Programs..... 8.79
8.5.4 Summary..... 8.79
8.6 Containment Protection..... 8.80
8.6.1 Insulation..... 8.80
8.6.2 Paint..... 8.81
8.6.3 Cathodic Protection..... 8.82
8.7 Inspection and Control..... 8.82
8.7.1 Concrete..... 8.83
8.7.2 Steel..... 8.83
8.7.3 Welding and Other Field Fabrication Operations... 8.84
8.7.4 Nonmetallic Coatings..... 8.85
References..... 8.86

9. CONTAINMENT ACCESSORIES..... 9.1
9.1 Introduction..... 9.1
9.2 Access Penetrations..... 9.2
9.2.1 General..... 9.2
9.2.2 Air Locks..... 9.7
9.2.3 Air-Lock Accessories and Details..... 9.8
9.2.3.1 Locking Devices..... 9.8
9.2.3.2 Seals and Gaskets..... 9.10
9.2.3.3 Power Systems for Air-Lock Operation.... 9.12
9.2.3.4 Interlocks and Interlock Bypasses..... 9.12
9.2.3.5 Equalizing Valves..... 9.12
9.2.3.6 Removal Floor Systems..... 9.13
9.2.4 Doors in Low-Leakage Buildings..... 9.13
9.2.4.1 Quick-Acting Watertight Ship's Door..... 9.13
9.2.4.2 Bulkhead Door with Inflatable Seals..... 9.13
9.2.4.3 Shielding Door..... 9.13
9.2.5 Testing of Access Penetrations..... 9.14
9.2.5.1 Shop Testing..... 9.14
9.2.5.2 Field Testing..... 9.14
9.2.5.3 Retesting..... 9.14
9.3 Piping Penetrations..... 9.16
9.3.1 General..... 9.16
9.3.2 Piping Penetration Designs..... 9.16
9.3.3 Isolation Valves..... 9.21
9.3.3.1 Criteria..... 9.21
9.3.3.2 Types of Valves..... 9.24
9.3.4 Penetrations and Isolation Valving in Conventional Structures..... 9.25
9.3.5 Testing..... 9.27
9.4 Fuel Transfer Penetrations..... 9.28
9.4.1 General..... 9.28
9.4.2 Fuel Transfer Mechanism Designs..... 9.29

9.5 Electrical Penetrations 9.29
9.5.1 General 9.29
9.5.2 Electrical Cables 9.33
9.5.3 Electrical Penetration Assemblies 9.34
9.5.3.1 Packed 9.36
9.5.3.2 Potted 9.37
9.5.3.3 Gasketed 9.40
9.5.3.4 Nonseparable Hermetic Connectors 9.40
9.5.3.5 Separable Connectors 9.41
9.5.4 Penetrations in Conventional Walls 9.41
9.5.5 Testing 9.41
9.6 Ventilation and Pressure Control Systems 9.45
9.6.1 General 9.45
9.6.2 Ventilation Systems 9.45
9.6.3 Ventilation Stacks 9.47
9.6.4 Vacuum-Relief Devices 9.48
9.6.5 Inert Atmosphere Systems 9.49
9.6.6 Negative-Pressure Systems 9.50
9.6.7 Pressure-Relief Systems 9.50
9.6.8 Pressure-Suppression Systems 9.51
9.6.8.1 Pool Pressure Suppression 9.52
9.6.8.2 Water Spray Systems 9.52
9.7 Fission-Product Removal and Trapping Systems 9.53
9.7.1 General 9.53
9.7.2 Particulate Filters 9.55
9.7.2.1 Prefilters 9.55
9.7.2.2 High-Efficiency Filters 9.55
9.7.2.3 Moisture Separators 9.57
9.7.3 Iodine-Removal Devices 9.60
9.7.3.1 Caustic Scrubbers 9.60
9.7.3.2 Heated Silver Nitrate Beds 9.60
9.7.3.3 Silver-Plated Wire Beds 9.60
9.7.3.4 Activated Charcoal 9.61
9.7.4 Containment Atmosphere Cleanup Systems 9.62
9.7.4.1 Recirculating Filter Systems 9.62
9.7.4.2 Spray Systems 9.63
9.7.4.3 Fog Systems 9.63
9.7.4.4 Foams 9.63
9.7.5 Testing 9.64
9.7.5.1 Particulate Filters 9.64
9.7.5.2 Iodine-Removal Systems 9.65
9.7.5.3 Requirement for Filter Testing 9.66
9.8 Operation of Containment Systems 9.66
9.8.1 System Reliability 9.67
9.8.1.1 Protective Channels 9.69
9.8.1.2 Testing and Monitoring 9.70
9.8.1.3 Independence of Channels 9.71
9.8.2 Operational Requirements of System Components 9.73
9.8.2.1 Valves 9.73
9.8.2.2 Air Locks 9.77
9.8.2.3 Spray Systems 9.78
9.8.2.4 Other Systems and Related Components 9.78

9.9 Electric Power Systems..... 9.78
9.9.1 Primary Power System..... 9.79
9.9.2 Auxiliary Power System..... 9.82
9.9.3 Emergency Power Sources..... 9.82
9.9.4 Power for Instrumentation..... 9.83
References..... 9.84

10. PERFORMANCE TESTS..... 10.1
10.1 Introduction..... 10.1
10.2 Strength Testing..... 10.2
10.2.1 General..... 10.2
10.2.2 Steel Containment Vessels..... 10.3
10.2.2.1 Code Requirements..... 10.3
10.2.2.2 Test Procedure..... 10.4
10.2.2.3 Equipment..... 10.6
10.2.2.4 Precautions..... 10.6
10.2.2.5 Scheduling..... 10.7
10.2.3 Other Containment Structures..... 10.7
10.2.3.1 Conventional Buildings..... 10.8
10.2.3.2 Concrete Containment Structures..... 10.8
10.2.3.3 Pressure-Suppression Containment.... 10.9
10.2.3.4 Multiple-Barrier Containment..... 10.9
10.3 Local Leak Testing Techniques..... 10.9
10.3.1 General..... 10.9
10.3.2 Bubble Observation Tests..... 10.12
10.3.2.1 Soap Bubble Test..... 10.12
10.3.2.2 Water Submersion Test..... 10.14
10.3.3 Vacuum Test..... 10.14
10.3.4 Sonic Tests..... 10.14
10.3.5 Adulterant Gas Tests..... 10.15
10.3.5.1 Air-Ammonia Test..... 10.15
10.3.5.2 Halogen Sniffer Test..... 10.16
10.3.5.3 Helium Mass Spectrometer Test..... 10.16
10.3.5.4 Additional Adulterant Gas Methods... 10.17
10.4 Leakage-Rate Testing..... 10.17
10.4.1 General..... 10.17
10.4.2 Leakage-Rate Criteria..... 10.19
10.4.3 Terminology..... 10.22
10.4.4 Standards..... 10.23
10.4.4.1 ANS Proposed Standard..... 10.23
10.4.4.2 ASA Proposed Standard..... 10.25
10.4.5 Nature of Leakage..... 10.26
10.4.5.1 Theoretical..... 10.26
10.4.5.2 Predominant Leakage Characteristics..... 10.40
10.4.5.3 Leak Locations..... 10.42
10.4.6 Variation of Leakage Rate with Pressure..... 10.43
10.4.6.1 Leakage-Rate Definition..... 10.44
10.4.6.2 Extrapolation of Leakage Rates..... 10.45
10.4.6.3 Leakage-Rate Test Data Interpretation..... 10.57
10.4.6.4 Significance of Tests for Leakage Prediction..... 10.64

10.4.7 Theory and General Procedure for Pressure-Decay Leakage-Rate Testing..... 10.65
10.4.7.1 Theory..... 10.65
10.4.7.2 General Procedure..... 10.66
10.4.7.3 Equipment Required..... 10.66
10.4.7.4 Precautions..... 10.67
10.4.8 Absolute Method..... 10.67
10.4.8.1 Method..... 10.67
10.4.8.2 Experience..... 10.69
10.4.9 Reference Vessel Method..... 10.71
10.4.9.1 Method..... 10.71
10.4.9.2 Experience..... 10.75
10.4.10 Other Methods..... 10.76
10.4.10.1 Measurement of Makeup Air..... 10.76
10.4.10.2 Adulterant Gas Method..... 10.78
10.4.10.3 Checking Individual Penetrations..... 10.78
10.4.10.4 Resistance Thermometry..... 10.79
10.4.11 Comparison of Leakage-Rate Testing Methods.. 10.79
10.4.12 Refinements in Leakage-Rate Determinations.. 10.84
10.4.12.1 Correction for Changes in Water Vapor..... 10.85
10.4.12.2 Change of Volume..... 10.90
10.4.12.3 Variation of R..... 10.91
10.4.12.4 Other Corrections..... 10.91
10.4.12.5 Error Considerations..... 10.92
10.4.12.6 Experimental Checks on Leakage-Rate Determinations..... 10.96
10.4.13 Special Considerations for Various Types of Containment Structures..... 10.97
10.4.13.1 Conventional Buildings..... 10.97
10.4.13.2 Low-Pressure Containment..... 10.99
10.4.13.3 Pressure-Relief Containment..... 10.99
10.4.13.4 Pressure-Suppression Containment. 10.100
10.4.13.5 Underground Containment..... 10.100
10.4.13.6 Multiple-Barrier Containment..... 10.101
10.5 A Typical Initial Integrity Testing Procedure..... 10.101
10.6 Retesting..... 10.107
10.6.1 Requirements for Retesting..... 10.107
10.6.2 Limitations..... 10.108
10.6.3 Methods..... 10.109
10.6.4 Experience..... 10.110
10.7 Maintenance of Containment..... 10.111
10.7.1 Design Features..... 10.111
10.7.2 Operating Procedures..... 10.112
References..... 10.112

11. ECONOMICS 11.1
- 11.1 Introduction 11.1
- 11.2 Economic Impact of Containment 11.2
  - 11.2.1 General 11.2
  - 11.2.2 Effect of Containment on Total Plant and Power Costs 11.2
    - 11.2.2.1 Capital Cost 11.3
    - 11.2.2.2 Power Cost 11.3
    - 11.2.2.3 Containment Cost Penalty 11.6
  - 11.2.3 Effect of Containment on Plant Location 11.6
    - 11.2.3.1 Engineered Safeguards vs Distance Requirements 11.6
    - 11.2.3.2 Transmission Costs 11.8
    - 11.2.3.3 Site Costs 11.10
    - 11.2.3.4 Evaluation 11.10
  - 11.2.4 Effect of Containment on Plant Design and Construction 11.11
    - 11.2.4.1 Design Changes 11.11
    - 11.2.4.2 Construction Requirements 11.12
- 11.3 Unit Costs of Containment Components 11.12
  - 11.3.1 General 11.12
  - 11.3.2 Steel Containment Vessels 11.13
  - 11.3.3 Concrete Containment Vessels 11.16
  - 11.3.4 Other Concrete Structures 11.18
  - 11.3.5 Excavation 11.18
  - 11.3.6 Air Locks and Doors 11.19
  - 11.3.7 Heating, Ventilating, and Air Conditioning 11.19
  - 11.3.8 Filters 11.21
  - 11.3.9 Stacks 11.21
  - 11.3.10 Penetrations 11.23
  - 11.3.11 Isolation Valves 11.24
  - 11.3.12 Protective Coatings 11.25
- 11.4 Cost Experience on Constructed Facilities 11.25
- 11.5 Typical Cost Evaluations 11.30
  - 11.5.1 General 11.30
  - 11.5.2 Reactor Containment Design Study 11.31
  - 11.5.3 Selection of the Containment Structure for the Dresden Nuclear Power Station 11.34
  - 11.5.4 Cost Normalization Study 11.36
  - 11.5.5 Economic Aspects of Reactor Safety 11.38
  - 11.5.6 Steel Containment Vessel Costs 11.39
  - 11.5.7 Conventional Building Costs 11.44
  - 11.5.8 Underground Containment Cost Study 11.44
  - 11.5.9 Filter System Costs 11.44
- 11.6 Cost Estimating 11.47
  - 11.6.1 General 11.47
  - 11.6.2 General Cost Estimating Procedure 11.47
  - 11.6.3 Detailed Cost Estimate of the HWCTR Containment Structure 11.51
- 11.7 Summary 11.51
  - References 11.55

12. RESEARCH..... 12.1
12.1 Introduction..... 12.1
12.2 Studies of the Response of Vessels, Piping, and Outer Containment Structures to Accidents..... 12.2
12.2.1 Aberdeen Proving Ground..... 12.2
References..... 12.2
12.2.2 Illinois Institute of Technology Research Institute..... 12.5
References..... 12.5
12.2.3 Atomics International..... 12.6
References..... 12.6
12.2.4 Battelle Memorial Institute..... 12.7
References..... 12.7
12.2.5 General Electric Company..... 12.7
References..... 12.7
12.2.6 Naval Ordnance Laboratory..... 12.8
References..... 12.8
12.2.7 Southwest Research Institute..... 12.8
References..... 12.9
12.2.8 Stanford Research Institute..... 12.9
References..... 12.9
12.3 Loss-of-Coolant Accident Studies..... 12.10
12.3.1 Illinois Institute of Technology Research Institute..... 12.10
References..... 12.10
12.3.2 Babcock & Wilcox..... 12.10
References..... 12.12
12.3.3 Hanford Laboratories..... 12.12
References..... 12.12
12.3.4 Phillips Petroleum Company..... 12.12
References..... 12.13
12.3.5 University of Minnesota..... 12.13
References..... 12.14
12.4 Metal-Water Reactions and Metal Ignitions..... 12.14
12.4.1 Argonne National Laboratory..... 12.14
References..... 12.16
12.4.2 Atomics International..... 12.17
References..... 12.17
12.5 Studies of Fission-Product Release, Aerosol and Particulate Generation, and Transport of Radioactivity.. 12.17
12.5.1 Atomics International..... 12.19
References..... 12.19
12.5.2 Brookhaven National Laboratory..... 12.19
References..... 12.19
12.5.3 Hanford Laboratories..... 12.20
References..... 12.20
12.5.4 Harvard Air Cleaning Laboratory..... 12.20
References..... 12.20
12.5.5 Oak Ridge National Laboratory..... 12.21
References..... 12.22

12.6 Aims of Future Containment Research Programs 12.23
12.6.1 Transient Tests 12.24
12.6.2 Metal-Water Reactions 12.24
12.6.3 Power Burst Facility 12.24
12.6.4 Fission-Product Release and Large-Scale Tests 12.25
12.6.5 Conclusion 12.27

Appendix A. Code of Federal Regulations, Title 10, Part 100 — Reactor Site Criteria

Appendix B. Description of Containment System in Final Safety Analysis Report

Appendix C. Criteria of Section III of the ASME Boiler and Pressure Vessel Code for Nuclear Vessels

Appendix D. Article I of Section III of the ASME Boiler and Pressure Vessel Code for Nuclear Vessels

Appendix E. Safety Standard for Design, Fabrication and Maintenance of Steel Containment Structures for Stationary Nuclear Power Reactors

Appendix F. Standard Accounts

Appendix G. Behavior of Iodine in Reactor Containment Systems

Index

1. INTRODUCTION

Wm. B. Cottrell

1.1 PHILOSOPHY

1.1.1 Definitions

1.1.1.1 Reactor Containment

Reactor containment is a general term which, for the purpose of this report, is defined to include all structures, systems, mechanisms, and devices that can be provided to attain with a high degree of reliability some specified attenuation in the radioactivity presumed to be released from the primary system in a reactor accident and might otherwise be released to the surrounding environment. Most containment enclosures generally incorporate some radiation shielding in order to restrict the direct radiation exposure therefrom in the event of a major fission-product release. Containment is usually not required for routine operations and need not be absolute, and, in fact, generally is not. Containment systems are normally referred to as "leak-tight" structures, which, in reality, leak a finite amount. Thus as a consequence, containment systems may consist of integrated complexes of structures, processes, and subsystems, which combine to control the activity release in a prescribed manner with a high degree of reliability. To the extent that activity may also be released from refueling buildings and chemical processing plants, similar containment and other engineered safeguard features are commonly provided with these facilities also.

1.1.1.2 Engineered Safeguards

Reactor safeguards literature is full of discussions of engineered safeguard features, a designation that includes emergency cooling systems, filters, sprays, etc., as well as containment enclosures themselves. Engineered safeguards are discussed in the site criteria guide[1] in the following connotations: "unique or unusual features having a significant bearing on the probability or consequences of accidental release of radioactive material" and "such safety features that are to be engineered into the facility. ... Where unfavorable physical characteristics of the site exist, the proposed site may nevertheless be found to be acceptable if the design of the facility includes appropriate and adequate compensating engineering safeguards." The definition encompasses features whose function is to prevent the occurrence of an accident, as well as those designed to mitigate the consequences thereof; only the latter are discussed extensively in this report. However, licensing procedures and safety analyses have always included both preventive and consequence-limiting safeguards in their considerations as a part of the "safety in depth" engineered in a reactor facility. It is possible that certain reactors at a particular site might not be approved if certain engineered safeguards, in addition to containment, were not provided, although credit may not have been explicitly given for their operation in the event of a severe accident.

1.1.1.3 Maximum Credible Accident

In considering the safety of any reactor system a large number of potential accidents are examined in terms of their probable consequences. The maximum credible accident (mca) (also sometimes referred to as the maximum design accident) is that accident whose consequences, as measured by the radiation exposure of the surrounding public, would not be exceeded by any other accident whose occurrence during the lifetime of the facility would appear to be credible. It is immediately obvious that this definition is singularly dependent upon what is considered "credible," and upon further reflection it will be seen that this credibility must be ascertained at least twice for any reactor accident, once for the credibility of the initiating event and again for the credibility of the performance of the various consequence-limiting safeguards.[2] In the former evaluation a double-ended primary pipe rupture, but not a gross pressure vessel failure, is frequently considered to be the initiating event; and in the latter the continuous integrity of the containment envelope is assumed credible, but the operation of the core cooling system, although likely, may not be deemed to be sufficiently certain for credit to be confidently assigned in the event of an accident.

The maximum credible accident is generally the accident that releases the greatest amount of fission products to the containment. However, this is not necessarily so, inasmuch as the particular safeguard features in use at a given installation may be more effective for some accidents than for others.

1.1.2 Need for Containment

The need for a containment system in the large power reactor installation is well established by convention and precedent in the United States, and the specific design requirements are determined by the reactor safety analysis. Philosophically, containment is provided so that the risk that cannot be dissociated from the operation of a particular reactor can be reduced to acceptable proportions with respect to the corresponding gain that is expected to result from its operation. However, such a balance of gain versus risk is impossible to attain on a quantitative basis, and only the risk enters into the evaluation that is made in connection with every reactor safety analysis. The specific function of the containment system is to reduce the consequences of the maximum credible accident so that a particular facility may fulfill siting requirements as defined in the Code of Federal Regulations.[1] On this basis, containment systems may be called upon to effect a reduction in activity released in an accident by a factor of 10^2 to 10^5.

1.1.3 Evolution of Containment[3]

As defined, containment is the provision for controlling the public exposure following an mca to acceptable levels. This "control"

was first attained in this country by the use of large exclusion areas surrounding the first reactor installations. Thus, in 1943 the Clinton pile was located in a portion of a 60,000-acre restricted area in Tennessee, designated Oak Ridge, the graphite production reactors were located in an even larger restricted area, designated Hanford, in the Washington desert near the Columbia River, and the National Reactor Testing Station was established in the desert of Idaho. In each of these instances the distance from the reactors to the site boundary was intended to permit adequate control (i.e., reduction) of any activity that might be accidentally released. The required size of controlled (exclusion) areas generally dictated locations in remote areas.

Several things have occurred to change this picture. Most prominent of these is the fact that location in remote areas is not compatible with today's need to provide electric power for our industrial complexes, since this need implies location near heavily populated areas. The use of reactors in marine propulsion systems may also bring power reactors nearer to population centers. In addition, there is an increasing desire and need to use reactors for experiments and research. In fact, the first so-called "containment vessel," which was located at the West Milton facility of the Knolls Atomic Power Laboratory, was conceived because of a desire to conduct large-scale experiments on power reactors near the Laboratory rather than at the National Reactor Testing Station in Idaho.

For reactors not located in remote areas the philosophy of public protection required, first, a thorough examination of the circumstances and conditions under which initial loss of control of the radioactive material inventory might arise. Since it was generally found impossible to guarantee absolutely the absence of either an accident or the release of the radioactive materials from the multiple series of containers normally present, e.g., fuel elements, cladding, reactor pressure vessel, and piping, an additional container usually was provided around the reactor complex. This additional container was first envisioned as a static pressure envelope with few penetrations and with appropriate pressure and leakage specification to contain any accident without exceeding a given leakage requirement related to the activity to be contained and the site in question.

From these rudimentary concepts of containment, as exemplified by the West Milton sphere, containment practice has gone on to the use of dynamic containment structures in which a multiplicity of penetrations must be closed at the time of the accident in order to effect the "leak-tight" enclosure and to more complicated versions that attempt to reduce accident pressures or to directly return leakage to the containment by additional outer barriers and pumping circuits. Also of significance in the evolution of containment systems and philosophy are the recent efforts to establish a reasonable upper boundary on some of the inherent release and transport phenomena, which also act to limit the public exposures that might result from a reactor accident.

1.1.4 Safety Factors

Inasmuch as containment is provided principally in order to limit the public exposure as the result of significant activity release, it is of interest to consider the various safety factors involved in the evaluation of exposure. These safety factors fall into two classes: first, those associated with conservative assumptions employed in the analytical representations of fission-product transport and, second, those associated with the designed integrity and performance of engineered safeguards, including the containment enclosure itself.

The term "safety factor" does not necessarily imply the uniform application of a particular integer (e.g., 3 or 5) to adjust design data in a direction of overdesign. It does describe a philosophy — the use of values in design that are realistic but conservative. Although both concepts attempt to establish a margin of safety in order to compensate for unknown or uncertain effects, the two differ primarily in their degree of uncertainty. The term "safety factor" implies that the basic value of a given parameter has been established through considerable experience, whereas "degree of conservatism" implies the use of values much more pessimistic than otherwise indicated in order to cover the lack of experience.

1.1.4.1 Exposure Calculations

Calculations of exposure to radioactivity resulting from a postulated maximum accident are not completely confirmable in terms of amounts and behavior of the fission products released. Thus conservative methods that reflect the designer's judgment as to the safety of the results are utilized. The accepted approach is to exercise extreme conservatism in uncertain situations owing to the severity of possible consequences.

As data become available, values can be estimated for these uncertainties that can be designated degrees of conservatism. An example of this is given in an AEC document[4] relating to siting calculations, and the estimates are listed in Table 1.1. Great uncertainty in these calculations and assumptions is illustrated by the wide range of estimated values.

1.1.4.2 Energy Release Calculations

The safety factors involved in energy release calculations, while much smaller, have not been as thoroughly documented. Thus, it is frequently assumed that all the energy in the primary system is released into the containment structure with no heat losses. Practically speaking, that would, of course, be impossible. Similarly, the energy contributions due to chemical reactions and nuclear energy are each conservatively applied to cover lack of knowledge of the subject.

Table 1.1. Estimated Degrees of Conservatism in Exposure Calculations[a]

Calculation or Assumption	Degree of Conservatism
Removal of iodine from containment vessel atmosphere by various physical phenomena such as adsorption, adherence, and settling	3–10
Removal of iodine by protective safeguards such as cooling spray and filtration of internal-air-recirculating systems	10–1000
Vessel leakage rate calculated at constant peak pressure	5–10
Wind direction shift during extended period of time	2–50
Wind meandering from centerline direction	~3
Atmospheric dispersion under other than inversion conditions	5–1000
Particulate fallout from radioactive cloud	2–5
Direct gamma dose neglecting shielding from structures and topography	2–1000

[a]From DiNunno et al., ref. 4.

1.1.4.3 Mechanical Design

The term safety factor in its strictest sense means the ratio of the magnitude of a parameter at failure to the magnitude of the same parameter used for design purposes. The parameter may be stress, force, pressure, repetitive cycles of loading, etc. Unfortunately, the situation is not clear-cut, since a definition of failure is also involved. Yielding, excessive deformation, brittle fracture, leakage, and the formation of fatigue cracks all may constitute modes of failure in certain circumstances.

The permissible design stresses in the ASME Codes[5] are based on a fraction of the smallest of several values: the minimum specified or expected ultimate tensile strength, yield strength, creep rate, and stress-rupture. For most ferritic materials of construction operating at temperatures below their creep range, the specified fraction of the ultimate tensile strength governs the permissible design stress. This fraction is 1/4 in Section VIII of the ASME Boiler and Pressure Vessel Code and 1/3 in Section III. Generally, the membrane stresses are thus limited to 1/4 or 1/3 of the ultimate tensile strength of the material; however, stresses due to structural discontinuities, thermal gradients, etc., are allowed to exceed these values. In neither case is the term safety factor used in

the strict sense nor is this safety factor per se a reliable indicator of the relative safety of vessels built to the two Codes. The various ASME Codes rather carefully avoid the use of the term safety factor.

The economical utilization of materials, without sacrificing safety, is the aim of Section III of the ASME Code. It accomplishes this by (1) placing clearly defined limits on the various types of stresses, (2) requiring detailed stress analyses based on rigorous methods of experimental methods, (3) requiring thorough materials inspections, (4) requiring thorough vessel inspection during fabrication and, finally (5) clearly defining the responsibilities of the purchaser, fabricator, and authorized inspector.

While Section VIII appears to use lower allowable design stresses, certain stresses may be significantly higher than in a comparable vessel designed to Section III. This is due to the fact that the rules of Section VIII are less restrictive (by omission) regarding discontinuity stresses, thermal stresses, materials inspection, testing, and so forth.

One important feature that is dependent on mechanical design, but is not covered in any detail by the ASME Boiler Code, is leakage. Generally, the smallest leakage rate that can be reasonably obtained from the standpoints of economics, fabricability, and measurability is specified, provided the maximum permissible exposure is not exceeded at the exclusion area perimeter in the event of an accident. At present this figure for large steel or steel-lined containment vessels can be reduced to less than 0.1% of the contained volume per day at design or acceptance test pressure.

1.2 RAMIFICATIONS OF REACTOR CONTAINMENT

As this report shows, the reactor containment technology has many and varied ramifications, not all of which are well understood. While some of these may seem quite remote from the structure itself, all are involved in its specification, design, fabrication, test, or operation in some way.

1.2.1 Reactor Site Criteria

The Atomic Energy Commission (AEC) has established guides for use in the evaluation of proposed sites for stationary power and test reactors licensed by the AEC. These guides apply only to reactors in which the probability of any accident occurring is small. The approved site criteria guides were released in the Federal Register on April 12, 1962, and were subsequently incorporated in Title 10, Code of Federal Regulations, as Part 100. The approval of these guides was preceded by more than three years of intensive study during which time proposed guides appeared twice in the Federal Register[6,7] for comments, which were profuse on both occasions,[8,9] and following which the proposed guides were extensively

revised. The last revision incorporated many of the comments, and the published document has been designated a guide for an interim period until enough experience can be accumulated with reactors to permit the writing of more definite standards.

The approved site guides differ from their immediate predecessors in several significant points. A predominant point of objection was the inclusion of a sample calculation of environmental and distance characteristics as an appendix to the proposed guides on the grounds that (1) the definite numerical values used in the sample calculation gave an aspect of undue rigidity to the guides and (2) the example tended to overemphasize the concept of environmental isolation. This objection was resolved not only by deleting the sample calculation from the guide and placing it in a separate document[4] but also by identifying the criteria as interim measures and by stating that the "applicants are free and indeed encouraged to demonstrate to the Commission the applicability and significance of considerations other than those set forth in the guides."

Other changes in the criteria were incorporated in an attempt to clarify the intent of the Commission on specific subjects and to cover additional points that were raised by the comments. Thus some further clarification is now included on the following issues: (1) multiple reactors at one site, (2) dependence upon isolation versus engineered safety features, (3) applicability to mobile reactors, (4) effect of population growth, and (5) population-center-distance concept, as follows:

1. The siting criteria for multiple reactors at one site may be determined on the basis of the evaluation of individual reactors if the reactors are independent to the extent that an accident in one does not result in a simultaneous accident or otherwise adversely affect the safety of operation of adjacent reactors.

2. The revised guides still reflect the Commission's emphasis on isolation, although the phraseology has been modified to indicate a potential willingness to accept demonstrably reliable engineered safety features on proven plants in lieu of isolation.

3. Although the general safety concepts that are embodied in these criteria may be expected to be applicable to all power reactors, these guides were not meant to be directly applicable to other than stationary plants.

4. Potential future population growth in the vicinity of a reactor is considered in its hazards evaluation and it is anticipated that each nuclear installation will acquire sufficient experience with engineered safeguards to make it possible to rely on such factors, rather than isolation, as the surrounding population increases.

5. The population-center-distance concept, although not entirely satisfactory, provides an insight into current siting practice and philosophy. It was said to be retained in lieu of any better technique of both (a) limiting the total population exposure and (b) providing protection against excessive exposure doses to people in large centers where protective measures may not be feasible. The man-roentgen equivalent man (rem) concept suggested both in Nuclear Safety[10] and by the Advisory Committee on Reactor Safeguards[11] is a direct means of specifying population exposure and has been given consideration for inclusion in the siting guide.

1.2.1.1 Stipulations of Current Criteria

The published site-criteria document does not differ substantially in principle from the previous draft. The criteria in effect define three distances from the reactor that must meet certain conditions. These distances are (1) the exclusion area, (2) the low-population zone, and (3) the population-center distance. The population-center distance is defined as the distance from the reactor to the nearest boundary of a densely populated area containing more than about 25,000 residents and is somewhat arbitrarily taken as 1 1/3 of the low-population zone. On the other hand both the low-population zone and the exclusion area are related to exposures, which are calculated at the outer perimeter of those areas following the maximum credible accident. The exclusion area is the area immediately surrounding the reactor that is under the control of the reactor operator and which is of such size that an adult located at the boundary for 2 hr immediately following the maximum credible accident would not receive a total radiation dose in excess of 25 rem to the whole body or 300 rem to the thyroid. The low-population zone may contain residents, but the total number and density must be such that there is a reasonable probability that appropriate measures could be taken in their behalf in the event of a serious accident. This zone is of such size that an adult located at any point on its outer boundary during the entire time of passage of the activity released from the maximum credible accident would not receive a total radiation dose in excess of 25 rem to the whole body or 300 rem to the thyroid.

The site criteria also list the following factors that are to be taken into consideration when evaluating sites (and hence also when calculating exposures at the specified distances):

1. characteristics of the reactor, which include the utilization of the reactor, design of the facility, features affecting activity release, and engineering safety features;
2. population density and use characteristics of the site environs, which include the exclusion area, low-population zone, and the population-center distance;
3. physical characteristics of the site, which include seismology, meteorology, geology, and hydrology.

1.2.1.2 Calculational Procedures

The sample calculational procedure that was included in the second draft as an appendix, as mentioned above, was deleted from the criteria, expanded, and incorporated into a separate report.[4] The report recognizes that there will be significant differences between different reactors and different containment systems. The analytical example presented refers specifically to the maximum credible accident, which is defined for pressurized- and boiling-water reactors with high-pressure containment. It is noted that for other types of reactor it will be necessary "to postulate...corresponding maximum credible accidents...by similar analyses." However, the calculational procedures were never intended to be rigid rules, and the applicant is free to propose his own analytical

techniques for approval. The fundamental assumptions on which the calculations were based are quoted, along with some estimation of the degree of conservatism represented.

The report[4] states that:

"1. Experts agree and experience to date, though limited, confirms that there is only an exceedingly small probability of a serious accident in reactors approved or likely to be approved for construction.[12] The probability is still lower for an accident in which significant amounts of fission products are released into the confined primary coolant system and a great deal lower for accidents which would release significant quantities of radioactivity from the primary system into the reactor building.

"2. It is assumed that the reactor is a pressurized water type for which the maximum credible accident will release into the reactor building 100 percent of the noble gases, 50 percent of the halogens and 1 percent of the solids in the fission product inventory. Such a release represents approximately 15 percent of the gross fission product activity.

"3. Fifty percent of the iodines in the containment vessel is assumed to remain available for release to the atmosphere. The remaining fifty percent of the iodines is assumed to absorb onto internal surfaces of the reactor building or adhere to internal components. Rather than the assumed reduction factor of two, it is estimated that removal of airborne iodines by various physical phenomena such as adsorption, adherence and settling could give an effect of 3-10 reduction in the final result. Credit has not been taken for the effects of washdown or filtering from protective safeguards such as cooling sprays and internal air recirculating systems. Washdown features and filtering networks could provide additional reduction factors of 10-1000.

"4. The release of available (airborne) radioactivity from the reactor building to the environment is assumed to occur at a constant leakage rate of 0.1 percent per day. The leakage and pressure conditions are assumed to persist throughout the effective course of the accident, which for practical purposes, would be until the iodine activity becomes insignificant. The maximum pressure within the reactor building and the leakage rate would actually decrease with time as the steam condenses from contact with cooling surfaces. By assuming no change in leak rate as a function of pressure drop, it is estimated that the final off-site doses calculated may be too high by factors of 5-10.

"5. Atmospheric dispersion of material from the reactor building is assumed to occur according to the well-known relationship developed by O. G. Sutton[13] involving meteorological factors of wind velocity, atmospheric stability, and diffusion parameters. Application of this treatment to reactor hazards analysis was discussed in WASH-740 (ref. 12) and AECU-3066

(ref. 14). Recently a simplified method of dispersion calculation has been proposed, by Pasquill[15] and Meade,[16] which reflects recent dispersion field trials, as well as current dispersion theories. This method gives the same numerical results as the Sutton method in the present application to a distance of about seven miles. Beyond this distance, the new method predicts somewhat greater concentrations.

"6. The assumption is made that a shift in wind direction does not occur for the duration of the leakage of the fission products from the containment barrier. If leakage from the containment barrier is assumed to occur over a significant time period (in the order of days), a reduction factor of 2-50 could result from shifts in wind directions. Wind meandering from any one centerline direction might also result in a reduction factor of approximately 3.

"7. Atmospheric dispersion is assumed to occur under inversion type weather conditions. For weather conditions which exist for 75 percent or so of the time at most sites, the atmospheric dispersion conditions could be more favorable, by factors of 5-1000.[17]

"8. Cloud depletion as ground deposition (particulate fallout) is not assumed during cloud travel. Such deposition during cloud travel could reduce the low population zone distance by factors of 2-5.

"9. In calculating the direct gamma dose, credit is not taken for shielding by the containment structure and applicable reactor shielding or topography. In some cases it is recognized that such shielding could reduce the direct gamma dose by a factor of 2-1000.

"10. Decay of fission products is assumed while they are confined to the containment building but is not assumed during their transit to the receptor point. The decay enroute is not significant for the conditions of release considered here but would lower the calculated doses slightly if included.

"11. In determining the whole body direct gamma dose, only the external gamma dose due to the fission products contained in the reactor building was considered significant for the assumed conditions. The whole body direct gamma dose due to the cloud passage for the assumed conditions would contribute on the order of 1-10 percent of the total whole body direct gamma dose at the exclusion and low population zone distances.[14]"

The report[4] explains that:

"...even if the postulated maximum credible accident should occur and if the external containment shell remained intact, the resulting exposure doses would probably be many times lower than those calculated by the indicated method.

"On the other hand, there are potential, conceivable conditions which would result in larger fission product releases than those assumed to be released in the maximum

credible accident, and the consequences could be more hazardous. Other potentially more hazardous factors than those represented by the example calculation include the following conditions.

"1. Total radioactivity releases to the containment vessel could theoretically be up to six times as large as those assumed. Release of long-lived fission products to the containment vessel could theoretically be up to 99 times as large as that assumed. These greater releases would affect doses to the lung, bone, and total body.

"2. For some sites, the atmospheric diffusion conditions for a small proportion of time could be worse than those assumed in these calculations. Such diffusion conditions could result in an increase in the inhalation doses.

"3. If the external containment structure should be rendered completely ineffective at the outset of the accident, the consequences of the 'maximum credible' accident would be increased many orders of magnitude. In such a case, the dose from the cloud and ground contamination could become significant in determining the external dose."

With the above frame of reference, the report then outlines, in detail, the analytical techniques and procedures common to many reactor hazards reports for calculating external and internal exposures from a fission-product cloud. Data are presented for meteorological conditions, as given below, that are indicative of the slow dispersion conditions expected to apply between 15 and 25% of the time in most areas of the United States:

Wind speed, u	1 m/sec
Horizontal virtual diffusion coefficient, C_y	0.40 $m^{n/2}$
Vertical virtual diffusion coefficient, C_z	0.07 $m^{n/2}$
Stability parameter, n	0.5 (dimensionless)

The results of calculations employing a containment-structure leakage rate of 0.1%/day were used (as an example only) to determine values of distances for water-cooled and -moderated reactors of various power levels. The values thus obtained are listed in Table 1.2.

Further from ref. 4:

"The estimated radii for power reactors are graphically represented in [Figs. 1.1 and 1.2]. For the exclusion distance, doses from both direct gamma radiation from the reactor building and from iodine in the cloud escaping from the reactor building were calculated, and the distance established on the basis of the effect requiring the greater isolation. [Figure 1.1] shows the controlling dose for various power levels.

"Under the conditions assumed, the doses resulting from the inhalation of the isotopes of iodine are controlling for the low population zone distance and population center

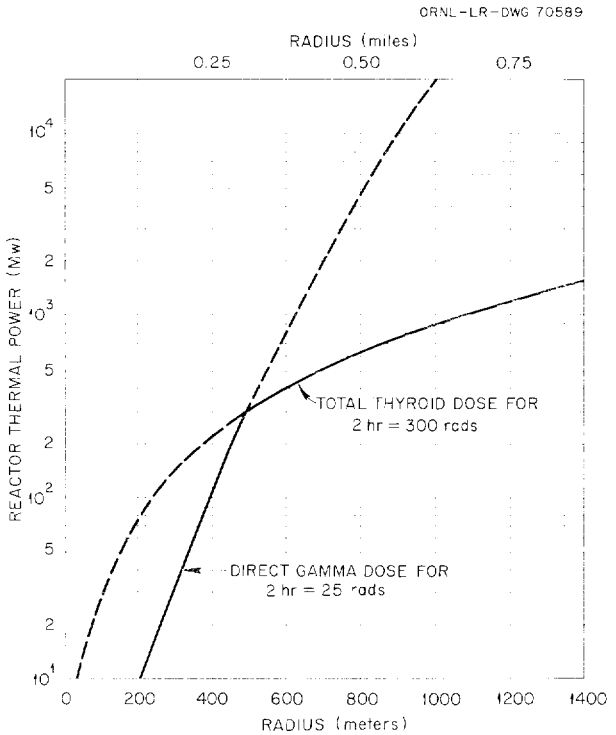

Fig. 1.1. Exclusion-Area Radius Determination Using Sample Calculation of Ref. 4.

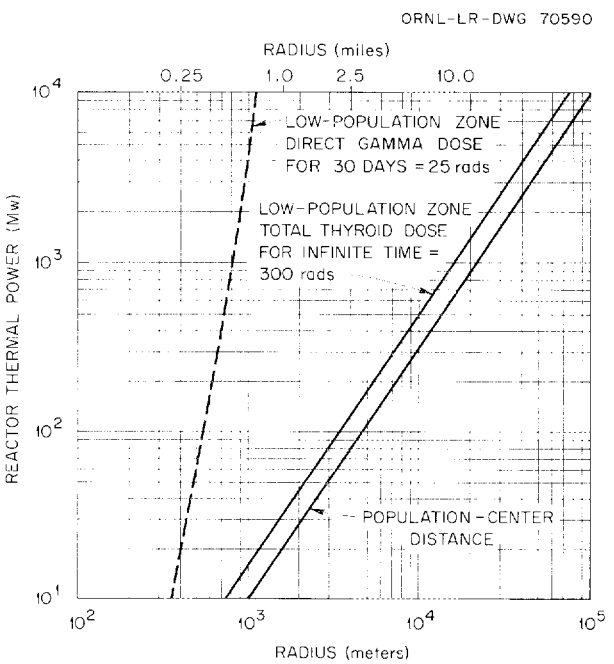

Fig. 1.2. Population Radius Determination.

Table 1.2. Calculated Site-Criteria Radii for Reactors of Various Power Levels[a]

Thermal Power Level (Mw)	Exclusion-Area Radius (miles)	Low-Population-Zone Distance (miles)	Population-Center Distance (miles)
1500	0.88	13.3	17.7
1200	0.77	11.5	15.3
1000	0.67	10.3	13.7
900	0.63	9.4	12.5
800	0.58	8.6	11.5
700	0.53	8.2	10.9
600	0.48	7.2	9.6
500	0.43	6.5	8.7
400	0.37	5.4	7.2
300	0.31	4.5	6.0
200	0.29	3.4	4.5
100	0.25	2.2	2.9
50	0.21	1.4	1.9
10	0.13	0.5	0.7

[a]Based on data of ref. 4.

distance.* However, it is possible that such may not always be the case and this should be checked for each case under consideration. The low population zone distance results from integrating the effects of iodine 131 through 135. The population center distance equals the low population zone distance increased by a factor of one-third. [Figure 1.2] shows the relationship between the inhalation and direct dose for various power levels."

The document[4] concludes with a comparison of the site distances obtained by the analytical method described above with those authorized for operating reactors or reactors approved for construction. The values of these example calculations are given in Table 1.3.

---

*Editor's note: Most hazards evaluations refer to the controlling dose for ingestion, inhalation, or whole-body exposure. In cases where no single dose reaches emergency limits but more than one approaches them, the cumulative effect must be considered.

Table 1.3. Calculated[4] and Actual Site Distances for Selected Reactors

Reactor	Thermal Power Level[a] (Mw)	Exclusion-Area Radius (miles)		Calculated Low-Population-Zone Distance (miles)	Population-Center Distance (miles)	
		Calculated	Actual		Calculated	Actual
Dresden	630	0.50	0.50	7.4	9.9	14.0
Consolidated Edison	585	0.48	0.30	7.0	9.4	17.0
Yankee	485	0.42	0.50	6.3	8.4	21.0
PRDC	300	0.31	0.75	4.5	6.1	7.5
PWR	270	0.31	0.40	4.1	5.6	7.5
Consumers	240	0.30	0.50	3.9	5.2	135.0
Hallam	240	0.30	0.25	3.9	5.2	17.0
Pathfinder	203	0.29	0.50	3.4	4.6	3.5
PG&E	202	0.29	0.25	3.4	4.6	3.0
Philadelphia Electric	115	0.26	0.57	2.4	3.2	21.0
NASA	60	0.22	0.50	1.6	2.1	3.0
CVTR	60	0.22	0.50	1.6	2.1	25.0
Elk River	58	0.22	0.23	1.5	2.1	20.0
VBWR	50	0.21	0.40	1.4	1.9	15.0
Piqua	48	0.21	0.14	1.4	1.8	27.0

[a]The thermal power levels shown were those employed by the AEC for the calculations in ref. 4. The power level of several of the reactors has since changed; see Chapter 7 for more recent values.

1.2.1.3 Conclusions

In advocating the acceptance of the draft of the Reactor Site Criteria,[1] the Director of Licensing and Regulation commented:

> "One may justly conclude, as the Commission had done, that although it is generally recognized that insufficient experience with reactors has been accumulated to permit the writing of definitive standards that would provide a quantitative correlation of all factors significant to the question of acceptability of reactor sites, it is possible to provide more guidance than currently exists as to the factors considered by the commission in evaluating reactor sites. The proposed guide...is intended as an interim measure until the state of the art allows more definitive standards to be developed. The guide is a starting point that gives the nuclear community an understanding of the basis on which the Commission will review proposed sites while providing flexibility and freedom for any applicant to demonstrate the applicability and significance of considerations other than those set forth in the guides. The proposed guides do not represent a different approach to reactor siting than has been used to date but rather they represent an attempt to articulate those practices. Application of these criteria will result in reactor sites in general agreement with those approved to date but sufficient flexibility has been provided to allow for considerations that might lead to locations that vary from current practice."

It is of interest to note that both the conservative and nonconservative factors involved in the determination of exposures at the specified distances are tabulated in ref. 4. Excluding the assumed atmospheric dispersion (which appears on both lists), the conservatism in the calculation of inhalation exposure may range from 10^3 to 10^6. However, three "potential conceivable conditions" could result in higher exposures. These conditions are (1) greater activity release, (2) poorer atmospheric diffusion, and (3) simultaneous failure of the containment structure. Whether or not these three factors are conceivable is a question of semantics. If they are taken as conceivable, it is theoretically possible for the total activity release to be up to six times as large as that assumed (since the release assumed was approximately 15% of the total). However, many responsible technical people would conclude that 100% release is not conceivable in view of (1) the fuel-meltdown experiments that have been performed, (2) the limit on the attainable temperature, even in a core meltdown, and (3) the known chemical reaction behavior of the fission-product elements. For the second nonconservative factor – poorer atmospheric diffusion – the assumptions include a moderate inversion, low wind speed, and a narrow dispersion angle persisting for a long period of time compared with the half-life of the released activity. Although there is a 25% probability that such poorer conditions may exist at any time, there is much less likelihood that such a weather condition will persist for a long time. In any event, the condition is to be weighed against the other conservative factors that are involved in the calculation.

The point of greatest concern, however, involves "conceivable," i.e., incredible but imaginable, accidents that could render ineffective the containment vessel or, for that matter, any other engineered safety features. Present technology is adequate to provide containment or safety features or both for nuclear facilities that would permit their location in population centers and still meet the existing requirements for exclusion area and low-population zone. This possibility is precluded, however, in the present site criteria by the specified population-center distance. As experience is acquired and safety analyses become more sophisticated, it may be anticipated that the present site criteria, which are based on distance, will give way to criteria that will be based on total population exposure. Such site criteria might, for example, still employ the exclusion-area concept as a means for limiting the maximum exposure to any one off-site individual, and the low-population zone and population-center distances might evolve into a total-population-exposure requirement. The AEC encourages applicants "to demonstrate to the Commission the applicability and significance of considerations other than those set forth in the guides" in order to take into consideration additional containment and engineering safeguards that may reduce the exclusion area, low-population zone, and population center distances.

It may be many years, however, before sufficient experience has been developed to permit a major reorientation of siting policy. In the meantime the existing site criteria provide a workable and generally consistent basis for siting reactors.

1.2.2 Nuclear Merchant Ship Site Criteria

The safeguards review of the N.S. Savannah by the Advisory Committee on Reactor Safeguards (ACRS) and the Division of Licensing and Regulation was concluded during the summer of 1962 with authorization, on August 3, for interim operation extending over a six-month period and covering approximately six port areas. As a consequence of the study that led to this authorization, the Maritime Administration-AEC Joint Group developed a guide for the "Port Operation of Shipboard Reactors."[18] The principal part of this guide modified the AEC Reactor Site Criteria[1] in such a manner as to make some allowance for the mobility of the ship reactor and to arrive at criteria that would be compatible with both the inherent aspects of nuclear merchant vessels and the safety philosophy expressed in the existing site criteria.

1.2.2.1 Essential Features of Ship Site Criteria

One of the most important developments was the adaptation of a criterion for total population exposure in lieu of the city distance stipulation in the existing guide.[1] As an interim measure, a criterion of a permissible exposure dose of 2,000,000 man-rem was established, as had previously been proposed.[19] This exposure is in addition to the individual exposure limit of 25-rem whole body (and 300-rem thyroid) that is employed for calculating various defined zones around the ship berth site in a manner similar to the zones around a stationary reactor site.

Other unique features of the ship site criteria involve the removal of the vessel after an accident (as a means of limiting the total population exposure), the manipulation of the ship's reactor power history to match the capability of the berth to provide adequate exclusion distances for a given fission-product inventory, and provisions for the exposure potential during the time the ship is entering and leaving a port. Since ship mobility is accepted as a safety factor upon which port safety evaluations are based, if the potential mobility were lost for some reason (e.g., adverse weather), consideration would have to be given to shutting down the reactor and possibly, also, depressurization of an appropriate type.

The guide[18] developed for mobile reactors, such as the N.S. Savannah, established three zones that vary in distance from the reactor, as follows:

> "1. Controlled Zone - that area in which all persons are under the direct control of ship's personnel so that in the event of an accident evacuation could be effected within two hours without any person receiving more than 25 rem whole body or 300 rem thyroid, and any individual general public member standing at its outer boundary for two hours would not receive an exposure exceeding 25 rem whole body or 300 rem thyroid.
>
> "2. Low Population Zone - that area in which it is reasonable to expect that, in the event of an accident, total evacuation or protective measures could be carried out in a graded fashion within 24 hours so that no person would receive more than 25 rem whole body or 300 rem thyroid; and any member of the general public standing at its outer boundary for 24 hours would not receive an exposure exceeding 25 rem whole body or 300 rem thyroid.
>
> "3. Dense Population Zone - that area which is immediately adjacent to the outer boundary of the low population zone and cannot be evacuated, controlled, or protected.
>
> "It can be seen that the establishment of these zones is not only a function of the fixed port environment, but also a function of the potential reactor accident. If the port environment remains fixed, the reactor's potential maximum accident can be adjusted. Therefore, the basic requirement for suitability for any berth is that the reactor accident potential be adjusted by controlled reactor power history so that the zone boundaries for exposure limitation are equal to or less than those boundaries established on population control or ship mobility.

"To ensure appropriate limitations to long-term effects on the population as a whole, the criteria set forth a 2,000,000 man-rem whole body limitation on the exposure to the total population in all three zones surrounding the reactor for the duration of the accident. Because of the inherent mobility of a shipboard reactor, the duration of the accident is taken to be 24 hours maximum.

"It is this very mobility, however, that makes it necessary to consider the varying position of the reactor with respect to the port environment. Thus, irrespective of an acceptable zone boundary based on individual exposures, the total population dose level should also be met at all times."

1.2.2.2 Other Aspects of the Criteria

In view of the many unique differences between siting a stationary power reactor and berthing a nuclear merchant vessel, the ship site criteria set forth in some detail the conditions for port entry and the arrangements that must be made. Such conditions and arrangements implement the general objectives of the criteria and ensure their attainment.

The specified conditions for port entry[18] include the following:

1. invitation from port authorities,
2. evaluation of environmental conditions,
3. evaluation of port emergency capabilities,
4. notification of all organizations involved,
5. screening of suitable berths,
6. evaluation of access and egress routes,
7. preparation of detailed accident analysis,
8. availability of tugboats,
9. testing of emergency equipment,
10. approval of emergency plans,
11. limitations on shipboard visitors,
12. reporting and approval of above factors.

In addition to the above conditions for port entry, the ship site criteria[18] give 24 "additional measures applied to initial operations." These additional measures are specific provisions with respect to the calculation of the specified zones or operating procedures and accident assumptions that would, in effect, introduce extreme safety in the operation of the vessel and extreme conservatism in the calculation of the exposure that might result from the maximum credible accident. The additional measures to be applied for initial operations are as follows:

1. use actual reactor power history,
2. take no credit for emergency cooling,
3. assume 50% iodine plateout in the containment vessel only,
4. assume containment-vessel leakage rate to be 2.5% per day,
5. assume iodine filter efficiency to be 99%,
6. take no credit for variable wind direction over the 24-hr period,
7. take no credit for other than inversion conditions over the 24-hr period,

8. base dispersion calculations on 1 m/sec wind speed, $C_y = 0.4$, $C_y = 0.07$, $n = 0.5$, $h = 0$,
9. establish specific emergency plan,
10. test auxiliary boilers in port,
11. maintain vacuum on main condenser,
12. limit ship visitors to one-half the acceptable number,
13. limit site visitors to one-half the acceptable number,
14. conduct evacuation drills regularly on ship and on site,
15. test reactor compartment integrity and emergency system operability periodically,
16. test containment-vessel leakage rate, filter efficiency, and duct tightness periodically,
17. have senior nuclear staff member aboard ship in port,
18. have health-physics staff member aboard at all times reactor is operating,
19. get approval of port analysis report by regulatory authorities,
20. establish conservative zone boundaries for 25 rem in specified time (1 hr, 480 ft; 2 hr, 650 ft; 24 hr, 1600 ft),
21. assume instantaneous release of fission products to containment vessel,
22. assume maximum number of persons in controlled zone in calculating total population exposures,
23. do not consider individual exposures of less than 0.05 rem,
24. take no credit for holdup in the reactor compartment.

1.2.2.3 Discussion

Since the Reactor Site Criteria[1] were specifically intended to reflect stationary-reactor siting practice in the U.S., the criteria not only did not cover many of the new problems introduced by a mobile reactor but also would have specifically excluded nuclear ships from most harbors. As has been previously noted,[20,21] the provision that made it impossible to apply the stationary-reactor criteria to mobile reactors was the stipulated city distance, that is, "at least 1-1/3 times the distance from the reactor to the outer boundary of the low-population zone." Since the specified low-population-zone boundary increases from 1.6 miles for a 60-Mw(t) reactor, it is readily apparent that city distances 1 1/3 times the above would deny a nuclear merchant ship access to most ports in the world. This being the case, it is important to know what the function of the city-distance criterion was. As stated in the Reactor Site Criteria:[1]

> "One basic objective of the criteria is to assure that the cumulative exposure dose to large numbers of people as a consequence of any nuclear accident should be low in comparison with what might be considered reasonable for total population dose. Further, since accidents of greater potential hazard than those commonly postulated as representing an upper limit are conceivable, although highly improbable, it was considered desirable to provide for protection against excessive exposure doses to people in large centers, where effective protective measures might not be feasible."

Although both these objectives are not readily achievable by a single criterion, the mobile-reactor site criteria effect the former by use of a total-population-exposure limit and the latter by safety features in the design, emergency procedures, and the special arrangements for port operation.

Once having established reasonable criteria, it is most important to demonstrate that the criteria can actually be attained in all circumstances. Of particular concern is the capability of removing the ship from its berth in less than 24 hr. Many studies have been made of the exposures as a function of time and position following the maximum credible accident. These are formally summarized, so far as the N.S. Savannah project is concerned, in the Port Analysis Reports (for example, the reports for Savannah, Ga.,[22] Norfolk, Va.,[23] Panama Canal[24]) and in an ORNL report,[25] which presents in more detail the probable exposures, independent of any port or berth conditions. From these studies it is concluded that the exposures of the tugboat personnel involved in moving the ship would be less than 1-r/hr submersion dose and less than 80-r thyroid inhalation dose for the several hours that might be required for the emergency removal of the ship, even if all personnel remained downwind of the release during that time.

The ship criteria also provide for the relatively large number of persons who might be on site (i.e., within the controlled zone), as well as for those who might be aboard ship. In both instances these persons must be evacuable before they have received 25-rem whole-body or equivalent exposure. Their evacuation must be possible in the specified time, that is, less than 2 hr, or their presence is not permitted. In this connection it is noted that, even assuming the pessimistic leakage and release rates indicated in the interim criteria, the close-in exposures would be substantially less than in most stationary power plants because of the double containment; thus the planned evacuation of personnel is considered feasible.

It appears that the mobile-reactor criteria have provided a reasonable extension of the Commission's Reactor Site Criteria to meet the needs of ship reactors. In so doing, certain concepts have been introduced or, at least, extended that may assume greater significance in siting considerations as nuclear technology develops. In addition to the total-population-exposure limit, the following concepts are implicit or explicit in the ship criteria:

1. controlled release of activity from the accident,
2. dependence on operating procedures to minimize the consequences of the maximum credible accident,
3. dependence on administrative control to assure the integrity of certain features (i.e., the reactor compartment).

The fact that each of the concepts is involved in conditions that were authorized for the N.S. Savannah does not imply approval of the concepts themselves but rather that, given justifiable reasons, modifications to existing practice will be considered. This is really no more or less than the approved Reactor Site Criteria[1] (for stationary reactors) pointed out in the statement that a "unique or universal feature having a significant bearing on the probability or consequences of accidental release of radioactive materials...would be taken into consideration."

1.2.3 Reliability of Reactor Systems

The reliability of a reactor system depends on instruments and control systems to a degree that is largely determined by the skill of the reactor designer in meeting the sometimes conflicting objectives of high performance and safety of the plant. The degree of reliability attainable in instrument systems and the degree of reliability needed in various reactor applications have been widely discussed.[26,27] It should also be recognized that accident prevention and consequence-limiting systems, including the containment system, should have a degree of reliability comparable with that of the reactor safety system.

Siddall[26] defines reliability as the sum of safety and serviceability and defines "The propensities to be free from unsafe failures and safe failures...respectively...as 'safety' and 'serviceability'... ." For the purposes of this report, reactor control systems are considered to be those systems having serviceability as the main objective, and safety (or protection, including containment) systems as those having safety as the principal objective. Limited attempts are sometimes made to improve the serviceability of safety systems, but excessive efforts in this direction may degrade reliability.

1.2.3.1 Control and Safety Systems Reliability

It is useful to consider reliability to be of two classes: (1) control-system reliability and (2) safety-system reliability. In a reliable control system, the interlocks, annunciators, relays, controllers, etc., are for the purpose of causing the reactor to operate in the manner intended by the designer and for minimizing damage to equipment from operator mistakes. The consequence of failure of these devices is a shutdown of the reactor, either directly because of the failure or indirectly through an increase of reactor power and subsequent action by the reactor safety system. The reliability of the system will therefore be based on economic considerations, with continuous operation of the plant a major objective. Even when adopted for a reactor, the system usually has no more than ordinary control-system reliability.

The reliability of the safety system, however, must be of an order sufficiently high not only to protect the core from failure of the control system but also to protect the operating personnel. Such reliability is obtainable through the use of redundant independent channels completely tested and monitored. This high degree of reliability is mandatory because the consequence of failure to operate correctly when required could be damage or destruction of the core and exposure of individuals.

1.2.3.2 Reliability of Containment Systems

The pressure vessel and its related piping constitute the primary barrier to the release of radioactivity for many reactors (after the fuel element itself). Because of the structural requirements for pressurized operation, the integrity is considered to be high, and thus this primary system constitutes an important barrier to the dispersion of

fission products. The failure of the primary system could, in many power-reactor plants, result in core meltdown and dispersal of fission products into the containment system. It is suggested therefore that the consequence of failure of the primary system is potentially greater than that of the failure of the reactor safety system, and its reliability and the reliability of instrumentation upon which its integrity may be dependent should be comparable to that of the safety system.

The containment system is the last barrier between the reactor and the general public and is provided to protect the public when all other barriers have failed. Since failure of this system to operate correctly when correct operation is required will be catastrophic, its reliability must be at least as great as that of any other reactor system safety device. The necessity in some systems for ventilating the containment vessel imposes a reliability problem in that valves must close the ventilating ducts, and reliable closure depends on the correct operation of instruments and control systems. The problem is aggravated by the requirement that all the valves must be tightly closed to effect containment. This is in contrast to the reactor safety system that is usually required to insert only a fraction of the total number of rods to effect shutdown. Hanauer[28] reviewed the closure systems of eight power-reactor containment systems and found the reliability in several cases to be below that of a reactor safety system.

1.2.3.3 Reliability in Operating Versus Shutdown Condition

There is a growing conviction that a reactor is safer in operation than in the shutdown condition. In discussing the NRX and NRU reactors, Breckon and Collins[29] state that

> "The (NRX) accident pointed out quite clearly that a reactor capable of operation but in a shut down state is potentially more hazardous than when it is operating at full power, a fact which has been borne out by other reactor accidents throughout the world."

This conclusion would, of course, not be true for a fluid-fueled reactor in which the fuel is drained from the reactor system when the reactor is shut down. In any event, it is probably true that while a shut down reactor may have a far greater chance of an accident, the magnitude of the accident potential under this condition is likely to be much smaller than in the operating condition. Nevertheless, Canadian practice is to do as much maintenance testing and fuel handling as possible with the reactor in operation so that the first error will result in a noticeable perturbation, and thus errors will be less likely to accumulate than would be the case if testing and fuel handling were done with the reactor shut down.

Most reactors must be loaded and unloaded by manual manipulation of the fuel. During such fuel-handling operations, the reactor may be without the protection of the safety system and the pressure-vessel cover is usually removed. In this condition the power reactor resembles the critical experiments in which a number of prompt-critical excursions have resulted from errors in manual manipulation. The hazard is increased by

the presence of fission products in spent fuel and by the infrequence of the operation and consequent unfamiliarity of plant personnel with procedures.

The only protection against the loading accident becomes administrative procedure and an adequate shutdown margin. Bates,[30] in reviewing the shutdown systems for 18 power reactors, states the criteria for shutdown margin as applied to ORNL reactors and concludes that for economic reasons the shutdown margin in power reactors is minimal, with the result that in several installations (e.g., Yankee and Saxton) a soluble poison, as well as rod insertion, is required. It is evident why the fuel-loading procedures usually contain the provision that the containment system be tightly closed until sufficient fuel has been removed to provide an adequate shutdown margin. Finally, the vulnerability to the loading accident has been forcibly brought into prominence by the SL-1 accident.[31]

1.2.4 Nuclear Safety Economics

Experience has shown that it is good, sound economics to emphasize safety in all conventional plants and operations; however, in the case of nuclear plants, the tie-in between safety and economics is considerably more important. This greater emphasis occurs not only because of the conditions under which nuclear energy was introduced into society but also because the fission reaction gives rise to harmful radiation and radioactive byproducts. Thus a nuclear reaction not only requires faster response of the control system than a combustion reaction, but the consequences of a control failure or malfunction can be more serious if adequate engineered safeguards are not provided. The magnitude of the problem of nuclear safety becomes obvious when it is realized that one 500-Mw(e) reactor contains about 12 billion curies of radioactive fission products during operation. If even a small fraction of this amount of radioactivity were released to the surroundings, it could conceivably contaminate a large area surrounding the plant. Thus a paramount factor in the design of a nuclear plant is the incorporation of adequate means for controlling the release of radioactive materials under all circumstances.

Some studies of nuclear safety economics[32,33] have attempted to identify the nuclear plant cost factors attributable to the presence of radioactivity. It has been shown[34] that safety considerations necessitated by radioactivity contribute directly and indirectly from 20% to as much as 65% of the total plant costs.

The objective of studying nuclear safety economics, however, is not merely to single out costs attributable to the presence of radioactivity but, rather, to establish the minimum cost of protecting plant personnel and the public against the accidental release of radioactivity. This problem can be approached by identifying costs of individual protective devices and measures and finding which of these are redundant. In this way it would be hoped that the most economical solution to the problem of radiological safety could be found. The discussion of nuclear safety economics is therefore limited to a summary of costs associated only with the possible accidential release of radioactive material from the facility. The primary contributors to nuclear plant costs that belong to this category

are (1) the emergency supply systems, (2) the containment systems and other engineered safeguards systems, and (3) the site, including land and the extra transmission lines needed because of the remote plant location. It should be remembered that in addition to protecting public safety, safeguards are commonly also included in the design of a facility to protect the capital investment by minimizing damage. Detailed data on the costs associated with the containment system are presented in Chapter 11.

1.2.4.1 Emergency Supply Systems

Certain auxiliary systems, such as the emergency cooling system, emergency filter system, and emergency power supply, are provided in most plants for use in the event of possible unusual circumstances. Only systems that are not used during normal routine operation of the plant can be assigned to nuclear safety costs, although normally operating systems generally provide for the safe operation or shutdown of the plant under abnormal circumstances. However, extra auxiliary and emergency power supplies, over and above those which might be found in a conventional plant, may be desirable to ensure that power will not be lost to the emergency coolant-circulating pumps. Items of this nature can be properly considered to contribute to nuclear safety costs, whereas items such as the control system, water-treatment system, and radiation-monitoring systems cannot. Kallman and Hanson[32] estimated the costs of extra emergency supply systems for a 500-Mw(t) pressurized-water reactor at $1,400,000 or $10/kw(e). The absolute costs of emergency supply systems might be expected to be relatively insensitive to the size of the nuclear plant; therefore, in a large nuclear plant, unit costs would be considerably less than in a small plant. If the 0.6-power rule is used as a basis for extrapolating to plants in the 500- to 1000-Mw(e) range, the unit costs of emergency supply systems would drop to $4 to $6/kw(e).

1.2.4.2 Containment Structures

In many reactor systems the coolant is in a high energy state — high temperature and high pressure — and any sudden break in the primary system will vaporize part of the fluid (if a pressurized liquid) and, in any event, release it to the containment enclosure. The resulting increase in pressure in the container must either be sustained or relieved in some way. Various methods of doing this have been proposed, each of which leads to a number of different types of containment, such as (1) pressure containment for high or low pressures, (2) pressure-suppression containment, and (3) pressure-release containment by relief or venting. All these types of containment are described in subsequent sections of this report and will not be further described at this point. Some cost data developed from actual construction, as well as cost estimates, are summarized here, but the subject of containment costs is covered in full in Chapter 11.

Containment costs for several small reactors are listed in Table 1.4. As may be seen, these costs range from $20/kw(e) to $169/kw(e) and constitute from 5 to 12% of the total plant cost. Unit containment costs for

Table 1.4. Containment Costs for Existing Nuclear Plants[a]

Nuclear Plant	Electrical Power Level (Mw)	Total Costs Chargeable to Containment (millions of dollars)	Cost per Unit Electrical Output ($/kw)	Containment Cost Relative to Total Cost (%)
EBR-2	16.5	2.78	169	11.1
Elk River	20	1.42	71	11.6
Hallam	75	5.24	70	12.2
Pathfinder	59	1.15	19.5	5.2
Piqua	11.4	0.95	83	8.0
HWCTR	15[b]	1.18[c]	79	
Yankee	185[d]	3.27	18[d]	7.5
EGCR	21.9	2.02	91	5.0
BONUS	16.3	1.24	76	9.7

[a]This tabulation is based on the accounts of ref. 34. The figures presented are the best estimates available from AEC. However, because final costs are not yet available in many cases and because the TID-7025 (ref. 35) accounts have not been used consistently, these figures should be considered preliminary and not necessarily comparable.

[b]Calculated from thermal power of 61 Mw.

[c]Includes indirect costs.

[d]Recent information from the reactor operator.

various sizes and types of reactor are plotted in Fig. 1.3. The results indicate that standard containment costs of large-scale plants [~500 Mw(e)] fall in the range of $7 to $27/kw(e), whereas pressure-relief containment costs may be as low as $2 to $3/kw(e).

1.2.4.3 Site Costs

1. Exclusion Area Costs. With the nuclear plant siting criteria given in the AEC cost evaluation guide[34] as a basis, it is found that the cost of the site ranges from $5/kw(e) for 40-Mw(e) plants down to $1/kw(e) for 400-Mw(e) plants. Thus site costs constitute about 0.5 to 1% of the total plant costs and are a relatively unimportant addition to total power costs. However, potential increases in site costs where large exclusion distances would possibly be required for large plants could make this item become a significant factor in nuclear safety costs.

2. Costs of Remote Location. Most conventionally fueled power plants are located as close as practical to the center of load density. If nuclear plants are located remote from load centers for safety reasons,

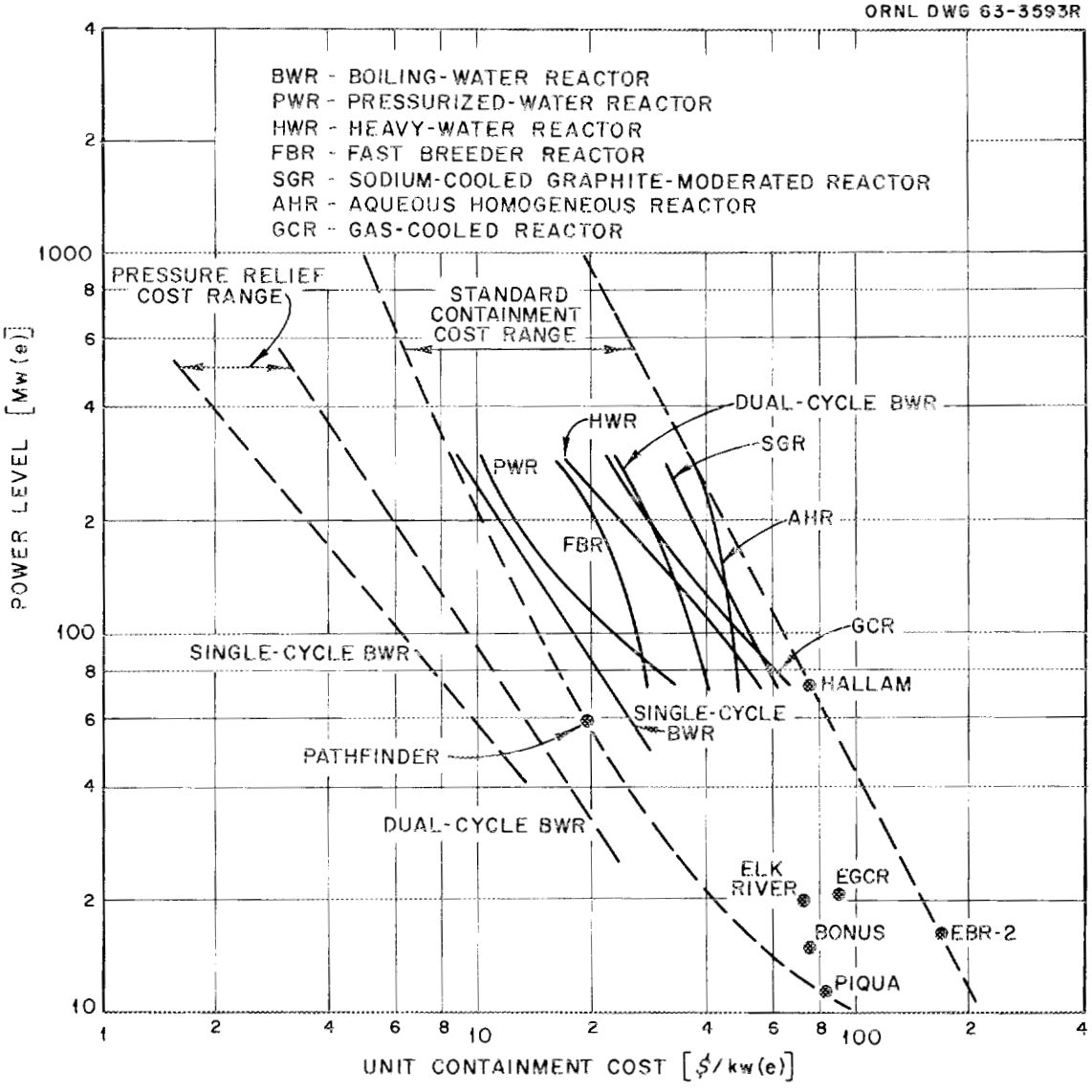

Fig. 1.3. Unit Containment Costs Versus Plant Size and Type of Reactor.

additional transmission costs are incurred. For relatively short distances, that is, less than 100 miles, the investment in transmission lines will be of the order of $60,000 per mile. For longer lines, higher voltages are necessary and the cost increases to about $150,000 per mile, as shown in Table 1.5. Corresponding power costs for 100- to 350-mile lines for 500-Mw(e) plants range from 0.3 to 2.2 mills/kwhr. Actual costs for construction and operation can vary widely depending upon the voltage to be transmitted and the type of lines used.

Table 1.5. Transmission Costs for Remote Siting of 500-Mw(e) Plants

Transmission distance, miles	100	150	300
Transmission voltage, kv	230	345	500
Line cost per mile, $	61,000	91,000	150,000
Total line cost, $	6,100,000	13,600,000	54,600,000
Transmission costs,[a] mills/kwhr	0.3	0.6	2.2

[a]At an interest charge of 14.0% and a 0.8 load factor.

It is apparent that some sort of balance can be achieved between the type and cost of containment and the additional transmission costs incurred because of remote siting. This is illustrated by Table 1.6, which gives containment and incremental transmission costs for a 500-Mw(e) direct-cycle boiling-water reactor. This sort of analysis should, of course, be done for each type of reactor, since there is no general relation that represents unit containment costs as a function of method of containment for all types of reactors.

Table 1.6. Containment Plus Incremental Transmission Costs for a 500-Mw(e) Direct-Cycle Boiling-Water Reactor

Containment Method	Unit Containment Cost ($/kw)	Incremental Transmission Distance for Equal Power Costs (miles)
Standard	7.50	0
Pressure suppression	4.00	30
Pressure relief	2.00	45

1.2.4.4 Conclusions

Nuclear safety costs are summarized in Table 1.7 along with comments as to the possible cost reductions. It is evident from this table that, in large-scale nuclear plants, most costs attributable to nuclear safety are either quite low or not amenable to much of a cost reduction. The one exception appears to be the costs of standard containment. Alternate types of containment, such as pressure suppression or pressure relief, may result in savings in the containment portion of the plant.

The main conclusion that can be drawn from this review of nuclear safety economics is that in large-scale plants the cost of components properly belonging to the category of "nuclear safety" is not large. Thus it appears that the widespread idea that the cost of nuclear safety represents an insurmountable barrier to the achievement of economic nuclear power is not valid.

1.2.5 Liability and Indemnity

Containment per se is not directly involved in the consideration of insurance on nuclear installations, inasmuch as experience (either with or without containment) is so limited and varied that the conventional insurance practice of determining rates is not applicable. Thus a nominal standard rate schedule exists, and the coverage is available to those facilities which the government has licensed.

The possibility of excessively large financial liability and property damage resulting from a nuclear accident necessitated the provision of insurance for companies operating nuclear installations in order to "spread the risk." This demand by industry for third-party liability policies with exceptionally high limits and for physical-property-damage coverage of high-value plants led to the formation of private insurance company pools and to government indemnification via the Price-Anderson Act.[35] The evolution of nuclear insurance and indemnity practice by the AEC is the subject of a book[36] that should be consulted for more detailed information than presented here.

Insurance coverage of nuclear facilities by the government was provided in 1957 by the Price-Anderson Indemnity Act, which added Section 170 to the Atomic Energy Act. Under that amendment, licensed facilities were required to have and maintain financial liability protection in amounts required by the AEC up to a maximum of $60,000,000. This private insurance protection is supplemented by governmental indemnity of $500,000,000. The Act provides indemnity to a licensee and anyone else who may be liable for a nuclear incident. One novel concept is the extension of the government indemnity to include damage to the property of a person or organization legally liable for a nuclear incident, with the exception of property located at the site of and used in connection with the activity where the nuclear incident occurred. Apparently, it was felt that such coverage was desirable since property insurance is not generally available against such

Table 1.7. Summary of Nuclear Safety Costs in Large Plants

Cost Component	Unit Cost[a] ($/kw)	Comments on Possible Reductions in Cost
Emergency supply systems	4–10	Reductions in cost will occur primarily as the result of larger plant sizes and of experience with the operation of existing plants, which may indicate that various emergency systems can be eliminated
Containment	0–60	
Standard pressure vessel	7–30	Reductions in cost may be achieved by reducing the volume of the primary coolant system, but this means higher pumping costs or a larger temperature difference across the reactor
Pressure suppression	3–10	Appears to be an excellent means for reducing containment costs for certain types and sizes of reactors
Pressure relief	2–6	A more remote site might be required because of momentary venting of fission gases to atmosphere; an overall saving could probably be achieved, however
Low pressure	20–40	Not a good approach to economic containment
Underground	~60	Construction of plants underground appears to be too costly to warrant this type of containment
Conventional structure	0	This containment means is analogous to the pressure-relief method of containment and would be subject to the same criteria
Exclusion area	1–2	Cost is sufficiently low and close to costs for conventional plants that cost reductions are relatively unimportant
Transmission	3–6[b]	Added transmission investment costs amount to $60,000 per mile; corresponds to only 0.02 to 0.04 mill/kwhr for a 300- to 500-Mw(e) plant located an extra 30 miles from population center

[a]The ranges indicated are not additive, since the lower containment costs tend to be associated with the higher costs of other factors.

[b]Cost per 30 miles.

a hazard. Government indemnification does not provide coverage for damage to a reactor and other on-site property involved in a nuclear incident. The basis[37] for determining the amount of liability insurance or other financial protection to be maintained on nuclear reactors is given in Table 1.8.

Table 1.8. Liability Requirements

Power Level	Required Coverage
10 kw(t) or less	$ 1,000,000
10 kw(t) to 1 Mw(t)	1,500,000
1 Mw(t) to 10 Mw(t)	2,500,000[a]
10 Mw(t) to 100 Mw(e)	$150 × [Power in Mw(t)] × [Population factor][b]
100 Mw(e) or more	$60,000,000

[a]Except testing reactors and demonstration reactors.

[b]Establishment of a satisfactory formula has been difficult, and the current formula suggests that a base amount of $150 per thermal kilowatt of capacity be multiplied by a population factor of between 1.0 and 2.0, depending on local population density.

Federal agencies and nonprofit educational institutions that operate reactors are exempt from financial protection requirements. However, government indemnity is still available to them. Table 1.9 summarizes, as of December 1963, the indemnity agreements entered into by the AEC, the reactor power level, and the amount of financial protection required of the licensee in order to qualify for the indemnification.

The private insurance coverage is provided by groups of companies in order to achieve the required underwriting capacity. The two principal syndicates are the Nuclear Energy Liability Insurance Association (NELIA)[38] and the Mutual Atomic Energy Liability Underwriters (MAELU).[39] A Nuclear Insurance Rating Bureau, which determines the final rates for the insured nuclear risks, has been established. Coverage is provided for public liability and for on-site property damage.

The nuclear energy liability policy issued by either of the above organizations does not afford separate limits of liability for bodily injury and property damage but contains a single aggregate limit of liability for all losses and loss expenses. The policy provides protection not only to the operator of a nuclear facility but also to any other person or organization who may be liable for injury or damage caused by the nuclear energy hazard. Another feature of the policy is continuous coverage. The nature of the radiation hazard (damage might result from repeated

Table 1.9. Indemnity Agreements[a]

Organization	Thermal Power Level	Private Financial Protection Required
Yankee Atomic Electric Co.	600,000 kw	$60,000,000
Commonwealth Edison Co.	700,000 kw	60,000,000
Consolidated Edison Co.	585,000 kw	60,000,000
Pacific Gas & Electric Co.	165,000 kw	29,700,000
Consumers Power Co.	157,000 kw	23,600,000
General Electric Co.	50,000 kw 30,000 kw	12,000,000
Carolinas Virginia Nuclear Power Associates, Inc.	44,300 kw	6,645,000
Saxton Nuclear Experimental Corp.	23,500 kw	4,300,000
Industrial Reactor Laboratories, Inc.	5,000 kw	2,500,000
Union Carbide Corp.	5,000 kw	2,500,000
Battelle Memorial Institute	2,000 kw	2,500,000
General Dynamics Corp.	1,500 kw	2,500,000
The Babcock & Wilcox Co.	1,000 kw	1,500,000
Lockheed Aircraft Corp.	1,000 kw	1,500,000
Power Reactor Development Co.	1,000 kw	1,500,000
Northern States Power Co.[b]		1,000,000
Northrop Corp.	100 kw	1,500,000
Armour Research Foundation of Illinois Institute of Technology	75 kw	
Westinghouse Electric Corp.	2 kw	1,000,000
North American Aviation, Inc.	200 w	1,000,000
Alco Products, Inc., and Allis-Chalmers Manufacturing Co.	100 w	1,000,000
Allis-Chalmers Manufacturing Co.	100 w	1,000,000
United Nuclear Corp.	100 w	1,000,000
Martin-Marietta Corp.	50 w	1,000,000
Aerojet-General Nucleonics	20 w	1,000,000
American Radiator & Standard Sanitary Corp.	15 w	1,000,000
49 educational institutions and federal agencies		None

[a]Information taken from AEC annual report for 1963.

[b]Personal communication, A. E. Swanson, Northern States Power Company, April 2, 1963.

exposures over a long period of time or damage from a single exposure might not become apparent for many years) makes a continuous policy necessary.

The physical-property-damage policy provides coverage for financial losses incurred due to damage to the reactor itself and other on-site installations. It is in the form of an all-risk package policy, since the exact cause of an accident may be difficult to determine. However, the policy covers only nuclear perils; other hazards must be covered by conventional forms of insurance.

1.3 GENERAL DESCRIPTION OF REACTOR TYPES

Short descriptions of the various types of nuclear reactors that exist or are in an advanced stage of design are given below in order to identify the principle features of each system that relate to its containment requirements. Reactors may be classified according to the kind of coolant utilized. Those cooled by (1) water, (2) liquid metal, (3) gas, (4) organic material, and (5) fused salts are considered. Some information on the extremes of several reactor parameters is given in Table 1.10 for each of the major reactor types. All these reactors require some form of containment. The type that is best suited for a particular reactor is the one that can economically and adequately limit the consequences of the "design accident" while being otherwise compatible with the system. In addition, all systems incorporate some engineered safeguards for which credit may or may not be given but which are considered in licensing (see also Sec. 7.9).

1.3.1 Water-Cooled Reactors

1.3.1.1 Pressurized-Water Reactors

In the pressurized-water reactor, shown schematically in Fig. 1.4, water at temperatures up to about 600°F and pressures up to about 2150 psia is pumped through the primary system. Boiling in the reactor vessel is prevented by utilizing electrical heaters in the loop pressurizer to keep the system pressure above the liquid saturation pressure. The circulating water serves to cool and, usually, to moderate a critical fuel assembly of fissionable material in the core. Heat removed from the fuel assembly is transported by the water to a heat exchanger where it serves to generate steam. The steam portion of the generator is part of the secondary system, which also includes a turbine where the heat energy is converted to electrical energy.

Counting naval reactors, over 100 pressurized-water reactors have been or are presently being built in the world. Since the concept required the least developmental work, these reactors received early emphasis. The Shippingport plant was the first U.S. nuclear plant built as part of a public utility. As a result of the early start, pressurized-water technology is relatively well developed. In addition, water is well known as a heat transfer medium, and the cooling system is simple.

Table 1.10. U.S. Reactor Types[a]

Reactors Categorized by Type of Coolant	Primary Coolant					Core Power Density (kw/liter)	Steam System	
	Pressure (psia)	Core Outlet Temperature (°F)	Weight of Coolant (lb)	Heat of Vaporization (Btu/lb)	Heat Capacity (Btu/lb·°F)		Pressure (psia)	Temperature (°F)
Water								
Pressurized	2150[b]	~600	163,000	1060 (15°C)	1.54 (600°F)	75	650	~500
Boiling	~1000	~545	376,000	1060 (15°C)	1.54 (600°F)	50	~1000	~550
Circulating fuel	1800	~570	7,000	1060 (15°C)	1.54 (600°F)	17	520	470
Heavy water	2150	~570	~15,000	1030 (15°C)	1.68 (600°F)	3	650	~500
Low pressure (research)	<100	~270		1060 (15°C)	1.02 (270°F)	494	(c)	(c)
Liquid metal								
Thermal	<100	~960		1809	0.30	117	815	825
Fast	<100	~900		1809	0.30	890	1250	850
Gas	500	2400	~1,000	(c)	1.25	10	1450	1000
Organic material	~200	>600	65,600	125 (495°F)	0.68 (675°F)	30	440	550
Fused salt	<50	1225	10,500	(c)	0.46 (1200°F)	17	None[d]	

[a]These data are for the extreme cases for U.S. reactors under each general type. Information chosen for the table is that which bears upon containment design.

[b]The Russian Reactor Lenin reports a primary coolant pressure of 2850 psi.

[c]Not applicable

[d]The experimental system being built will dump its heat to the atmosphere.

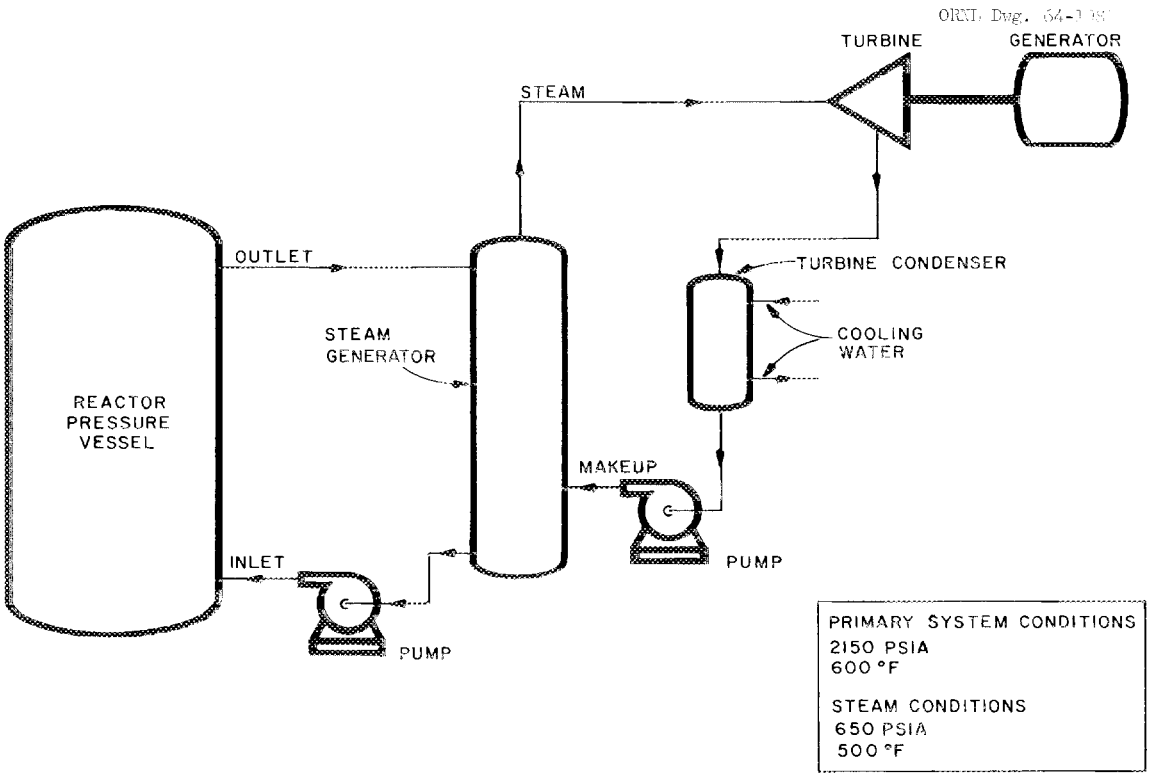

Fig. 1.4. Pressurized-Water Reactor.

Since the primary coolant passes through the core vessel, it absorbs neutrons that cause some induced radioactivity. Small amounts of fission products may also be present if there are any fuel element cladding ruptures. Cleanup facilities are provided that limit the fission-product buildup in the primary coolant. The secondary coolant, which is separated from the core by an additional barrier (the steam generator), does not contain radioactivity except in the event of a heat exchanger leak. The primary system components and the steam generator are enclosed in some type of containment vessel to prevent large quantities of fission products from being released to the atmosphere in case of a reactor accident. Most often the turbine and other secondary system equipment are located outside the container. Isolation or block valves in those portions of the secondary loop that penetrate the container are essential parts of the containment system.

High-pressure containment has been used quite generally for pressurized-water plants because of the large amount of stored energy inherent with these reactors. Pressure-suppression or pressure-relief also may be adapted to contain this type of reactor.

1.3.1.2 Boiling-Water Reactors

The boiling-water direct-cycle reactor is shown schematically in Fig. 1.5. In this cycle, water is converted directly to steam in the core, eliminating the need for a heat exchanger for steam generation.

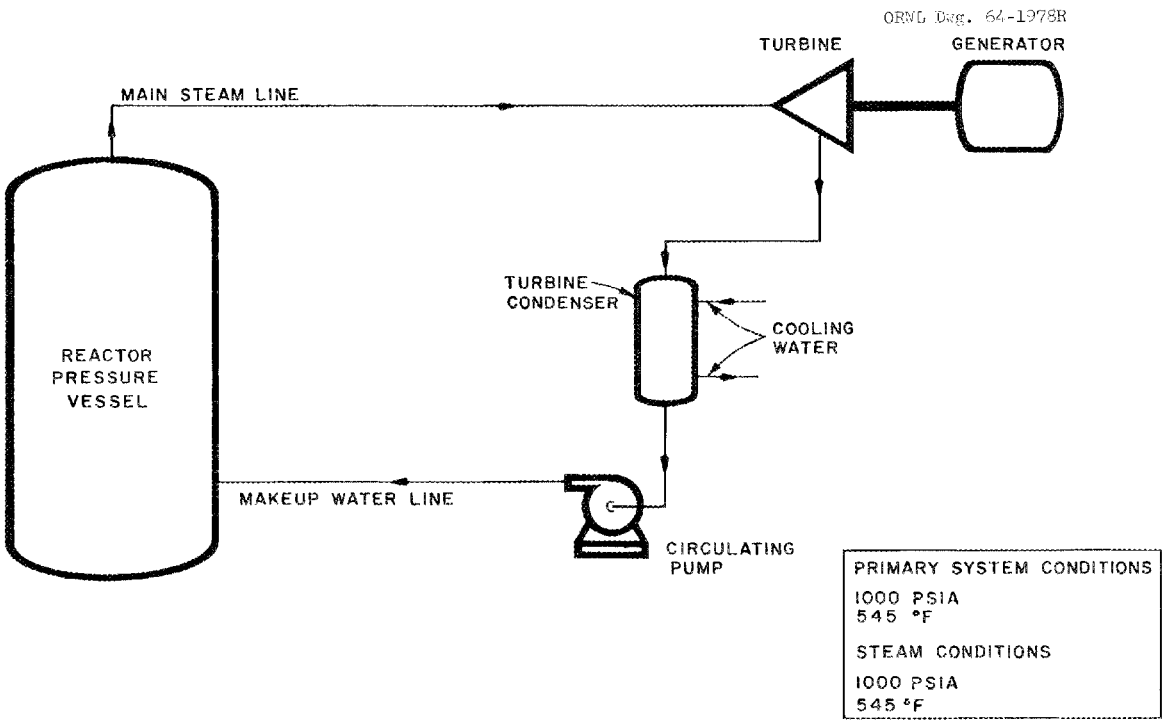

Fig. 1.5. Boiling-Water Reactor.

These systems operate at somewhat lower pressures than the pressurized-water systems. Coolant or steam pressures are usually in the range of 600 to 1000 psi, although some higher pressures are reported. So far, over 25 boiling-water reactors have been built or are now being constructed.

Except for the fact that large steam-generating heat exchangers are not used for a boiling-water reactor, the other items of equipment are quite similar to those of the pressurized-water systems. There may be, however, steam entrainment separators, which are usually located inside the reactor vessel. The steam is dried so that its quality is satisfactory for turbine operation. Some boiling-water reactors have means for superheating the steam, employing either nonnuclear heat or steam-cooled fuel elements around the periphery or in the center of a boiling core. While a postulated accident for a plant with nuclear superheat is more complex than that for a conventional boiling-water system, adequate design can ensure that there is no compromise in the safety of the system.

Present-day boiling-water reactor plants usually locate the steam turbine outside the containment system, even though the location of any portion of the primary system outside the containment system requires special considerations in plant containment design. Both the pressure-suppression and high-pressure containment systems have been employed with such an arrangement, although other systems, such as a low-pressure system or a pressure-relief system, could conceivably be adopted.

1.3.1.3 Homogeneous Reactors

The homogeneous reactor is one in which the fuel is intimately mixed with the water coolant, which also acts as moderator. There are no fuel elements and generally no control rods. The fuel, since it circulates, is cooled externally in the steam generator. The coolant and fuel circulate through the reactor vessel, coolant circulating pump, and steam generator and make these components internally radioactive. These components must be operated at high pressures comparable to those of the pressurized-water systems in order to prevent boiling. Fission products also circulate through the low-pressure system, which employs evaporators to adjust the concentrations of the fuel solution of the high-pressure loop.

No aqueous homogeneous reactors are operating in this country at present, although there were four reactor experiments that operated at one time or another in the past 10 years. The sulfate system (HRT) operated at a maximum temperature of 570°F and a pressure of 1800 psia. The steam pressure was about 520 psia. The aqueous homogeneous solutions became highly radioactive during reactor operation, and the hazard of a solution leak was a potent problem. Precautions were taken to prevent accumulation of a critical mass in parts of the system other than the reactor core. Both the loop and the low-pressure components were contained, since the fission-product-containing fuel circulated through them. The turbine could be located outside the container with steam block valves completing the containment scheme. High-pressure containment was used effectively.

1.3.1.4 Heavy-Water Reactors

Deuterium oxide, or heavy water, is attractive as a coolant and moderator for thermal nuclear reactors because it has an appreciably smaller cross section for the capture of thermal neutrons than ordinary water and is feasible to use with natural uranium. So far it has not found frequent use for power reactors. This has been due in large degree to the high cost of heavy water (now $15 per lb, down from $28 per lb).

Except for the core, most of the reactor components are similar to those of a conventional pressurized-water reactor. The core must be of different design because of the large size needed to attain criticality with natural uranium fuel. One approach is to contain the core in a large pressure vessel, while the alternative is to use an individual pressure tube around each fuel element. Both the Carolinas-Virginia Tube Reactor (CVTR) and the Plutonium Recycle Test Reactor (PRTR) have taken the latter approach.

There is considerable design and operating experience available on heavy-water reactors from the Savannah River production reactors. Also, a few reactors that fall in other categories, such as the circulating-fuel HRT, used D_2O. In principle, containment considerations for these reactors are essentially the same as for conventional pressurized-water reactors. In actual practice reactors of this type have employed the pressure-tube core design, which makes the maximum credible accident somewhat less severe.

High-pressure containment has been used; however, pressure suppression and pressure relief are also adaptable to such plants.

1.3.2 Liquid-Metal-Cooled Reactors

1.3.2.1 Thermal Reactors

Liquid metals, such as liquid sodium, are attractive as reactor coolants because their thermal properties permit the attainment of high operating temperatures without the need for high pressures. In such reactor systems the coolant system pressure is only that of the dynamic head, and temperatures of up to 1300°F are readily obtained. The high temperatures allow attainment of steam conditions (approaching a steam temperature of 1000°F) that give net plant efficiencies greater than in water reactors. Graphite usually serves as moderator for these plants. Use of the moderator, of course, makes this a thermal-neutron plant and distinguishes it from the fast breeder reactor discussed below. Any reactor employing liquid sodium as the primary coolant must cope with the ^{24}Na activity which is formed from the neutron activation of the coolant.

Plants using alkali-metal coolants require two heat transfer systems, as shown schematically in Fig. 1.6, to eliminate the hazard of the possible generation of radioactive fumes by the chemical reaction of water and the coolant metal. Such plants may also be expected to be designed with special reactor cells and double-walled piping, etc., in order to eliminate the possibility of uncovering the core in any accident. The secondary coolant system necessitates another heat exchanger and coolant pump. So far, fewer than ten liquid-metal-cooled thermal reactors have been built.

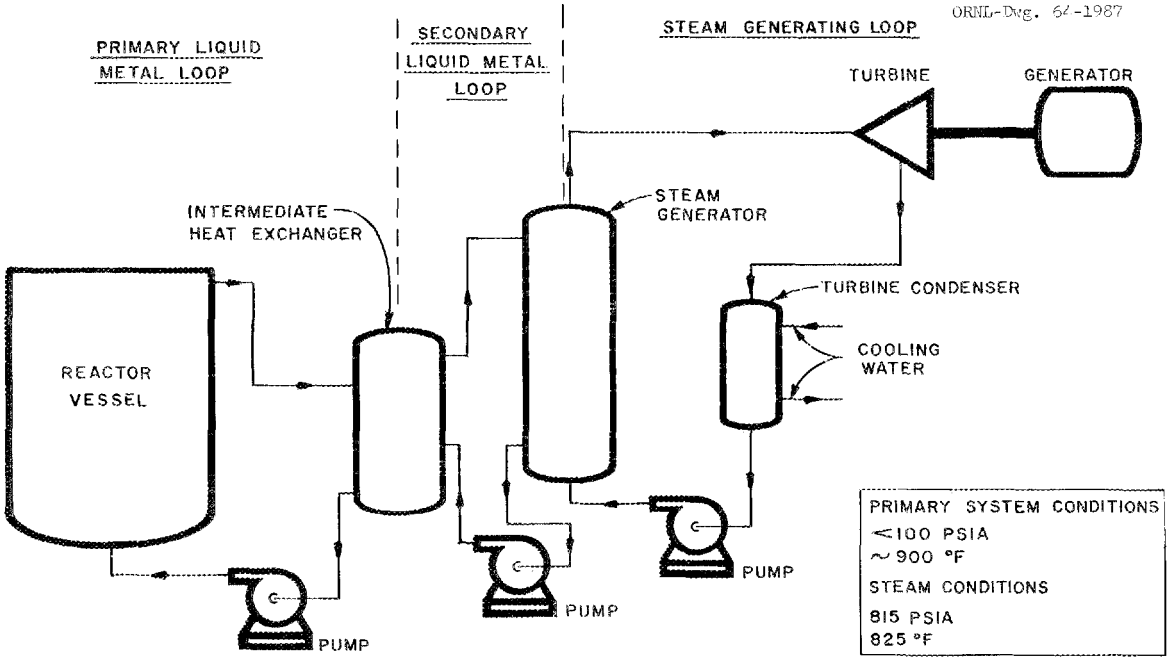

Fig. 1.6. Liquid-Metal-Cooled Reactor.

Containment pressure requirements are not great if air is excluded from the alkali-metal systems. This is accomplished at the Hallam Reactor by locating the reactor vessel and radioactive sodium heat transfer system in shielded compartments below the reactor room floor. A nitrogen atmosphere is maintained in these cells. The reactor building at Hallam utilizes the negative-pressure containment concept. The capability of using this concept indicates that the containment problem for this type of reactor is less severe than for some other types.

1.3.2.2 Fast Reactors

Fast reactors must use liquid metals or other nonmoderating coolants because of the moderating effect of either light or heavy water. Sodium or sodium-potassium mixtures have been used exclusively, although gas coolants are being considered. The excellent heat transfer properties of the liquid metals are exceedingly valuable, since the core of a fast reactor is usually small and as a consequence has limited heat transfer area.

The equipment is much the same as that required for a liquid-metal-cooled thermal plant. Again it is necessary to use two heat transfer systems so that the highly radioactive primary coolant will be separated by an additional barrier from the steam system. There are fewer than ten fast reactor systems operating throughout the world.

It may be possible to design fast reactor systems so that the negative pressure containment concept can be applied. However, high-pressure containment is being used for the current fast reactors. The design basis has been that of a severe nuclear excursion resulting from fuel element meltdown. This excursion might assume some of the characteristics of a TNT explosion,[40] producing high pressures and shock waves.

1.3.3 Gas-Cooled Reactors

Gases such as helium and carbon dioxide are used as reactor coolants. In the gas-cooled concept shown in Fig. 1.7, the reactor heat is removed from the fuel by the gas and is transmitted to a heat exchanger where steam is generated to drive the turbine. The use of a gaseous coolant allows attainment of high temperatures without the high pressures associated with water-cooled systems. The gas-cooled reactor has been popular in several countries other than the U.S. because it can be designed to use natural uranium as fuel. In fact, 33 gas-cooled power reactors, over 75% of the gas-cooled reactors in the world, are located in the United Kingdom and France.

Graphite-moderated gas-cooled reactors, because of the nature of the coolant, have, in general, less stored energy than pressurized-water reactors. It is possible to design gas-cooled reactors so that the after-heat can be removed by natural convection. There are potential hazards, however, because of the storage of Wigner energy in the graphite at lower temperatures and graphite reactions with air and water at higher temperatures. The former problem is usually avoided by designs that maintain a graphite temperature at which Wigner energy releases do not present a

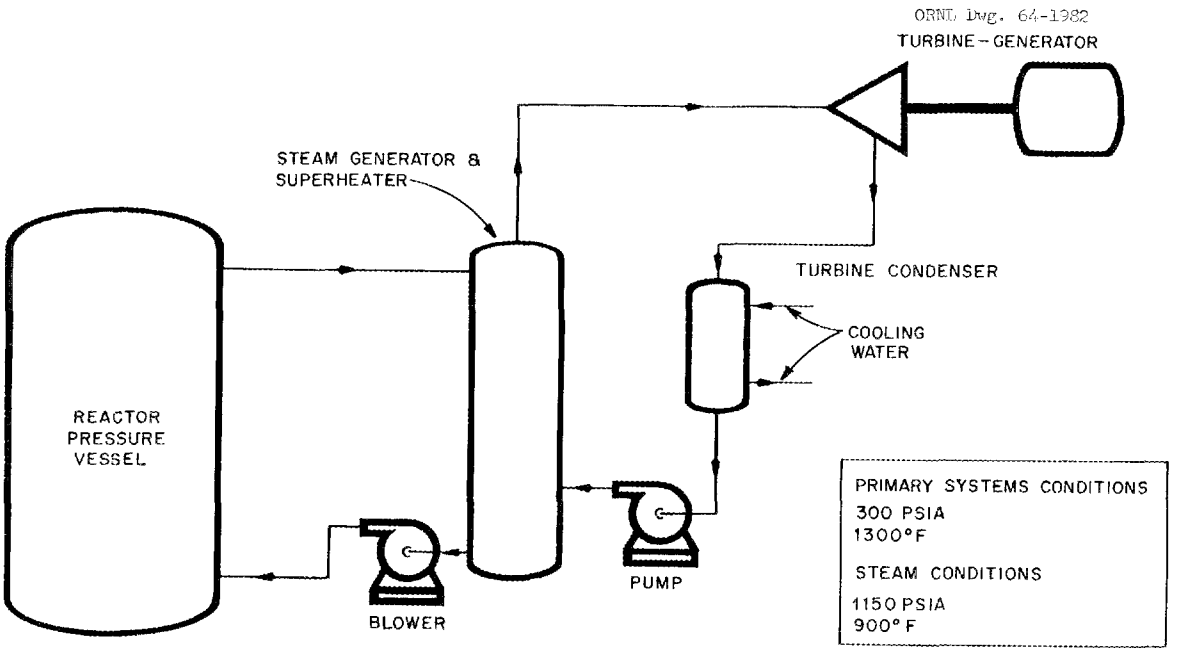

Fig. 1.7. Gas-Cooled Reactor.

problem. In general, containment pressure requirements for a gas-cooled plant are not as strenuous as those for a comparable pressurized-water plant. The design pressure for a high-pressure container could be expected to be less for a gas-cooled reactor, and it should be possible to design suitable low-pressure or pressure-relief containers. Pressure-suppression containment, however, would not be suitable.

1.3.4 Organic-Cooled Reactors

Several organic liquids are attractive as coolant-moderators because of their high boiling points and ease of handling. In many of the concepts, reactor heat that is removed from the fuel by the coolant is transferred to the steam system via the steam generator, as shown schematically in Fig. 1.8. Steam drives the turbine. High coolant pressures are not required, and temperatures of up to 700°F can be attained at pressures of 200 psia or less. Steam pressures range up to about 600 psia. Most organic coolants are quite combustible, so it is desirable to limit the oxygen content of the containment in order to prevent fire in the event of a coolant leak. In 1962 there were only five organic-moderated reactors in the world.

Containment pressure requirements of an organic reactor are not as demanding as those for a water-cooled reactor. Total containment with a low container design pressure is illustrated by the Piqua reactor. The design pressure in this case is 5 psig. The vessel is cylindrical with hemispherical heads.

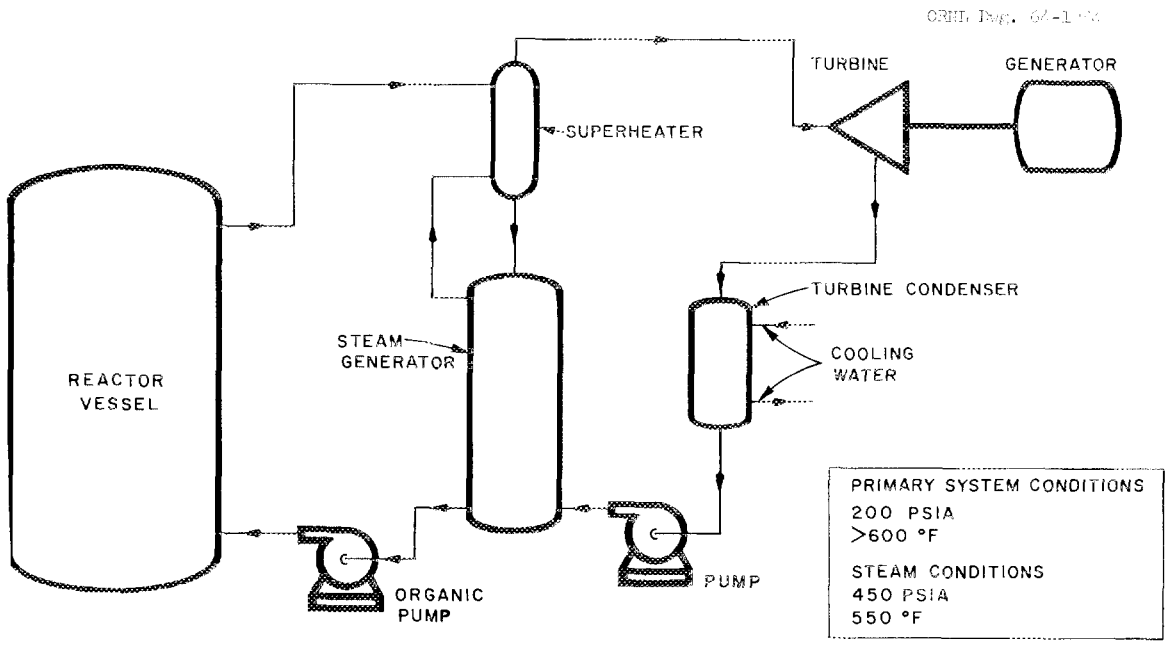

Fig. 1.8. Organic-Cooled Reactor.

1.3.5 Fused-Salt Reactors

Fused inorganic materials, such as the fluoride salts of uranium, lithium, beryllium, zirconium, and thorium, show promise of providing a circulating-fuel power reactor system of low pressure and high temperature. The Molten Salt Reactor Experiment (MSRE) will use a coolant-fuel of this type and will employ a graphite moderator. It is being built to operate at a temperature of greater than 1200°F and a pressure of less than 50 psig. Much of the technology for this concept was developed for the now discontinued aircraft reactor project.

The MSRE will use a pressure-containment shell and possess the capability for pressure suppression. This enabled the reactor to be placed in an existing containment vessel originally intended for use in the aircraft reactor project. Otherwise the reactor design accident pressure for total containment would have exceeded the permissible pressure of the existing vessel. Reactors of this concept could be contained adequately by total containment structures of the high- or low-pressure type if they were designed specifically for the particular reactor. Pressure-relief containment would probably not be satisfactory, since the fuel is an integral part of the coolant.

1.3.6 University Reactors

University, or teaching reactors, which usually operate at power levels of 10 kw or less and handle little excess reactivity, generally require no or only modest containment. Information on the main classes of these reactors is given in Table 1.11. Because of the safety features designed into these reactors and their low power levels, the safety of university reactors seems to be well established. Inherent characteristics such as the negative temperature and void coefficients are incorporated to contribute to the safe control of these systems.[41] The low power levels

Table 1.11. University Reactors

Reactor Class	Type	Excessive Reactivity (% k_{eff})	Negative Temperature Coefficient ($\Delta k/k$ per °C)	Negative Void Coefficient [$(\Delta k/k)$/% void]	Power Level (w)
Argonaut[a]	Water-moderated graphite-reflected core with plate-type fuel elements	0.75	10^{-4}	0.25	10^4
UTR-10[b]	Water-moderated graphite-reflected core with plate-type fuel elements	0.5	6.83×10^{-3}	0.17	10^4
Triga Mark II[c]	Solid, homogeneous, 20%-enriched uranium-zirconium hydride fuel elements (plate type) operating in a pool of light water	1.6	9.6×10^{-5}[d]	2.1×10^{-3}[d]	10^5
Triga Mark F[c]	Solid, homogeneous, 20%-enriched uranium-zirconium hydride fuel elements (cylindrical type) light-water cooled and reflected	4.9[d]	1.26×10^{-4}[d]	Uncertain[d]	10^6[d]
GE University Reactor[e]	Fully enriched, MTR-type fuel elements operating in a pool of light water	0.5	0.5×10^{-4}	2×10^{-3}	10 to 3×10^6 g
AGN-201[f]	Graphite-reflected core with fuel elements consisting of 20%-enriched UO_2 powder homogeneously dispersed in disks of polyethylene moderator		3.6×10^{-4}		10^{-1}
AGN-211[f]	Core similar to that of AGN-201 but operated in a pool	0.2	3.6×10^{-4}		1

[a]Original designed by Argonne National Laboratory, has served as a model for several commercial units.

[b]University Test Reactor built by the Advanced Technology Laboratories. Units of the same type are also built by General Nuclear Engineering Corporation, Nucledyne Company, and AMF Atomics, Inc.

[c]A commercial unit built by General Atomic, Division of General Dynamics Corp.

[d]Personal communication from Thomas R. Moffette, May 17, 1964.

[e]In addition to the General Electric Company, these units are built by Bendix Aviation Corporation and Lockheed Aircraft Corporation.

[f]Units built by Aerojet-General Nucleonics.

[g]Personal communication from J. M. Smith of the General Electric Company, San Jose, California.

at which most of the units operate limit the fission-product inventory to such an extent that large quantities of contaminants cannot be released even if an accident occurs.

1.4 GENERAL DESCRIPTION OF CONTAINMENT SYSTEMS

Reactor containment is usually the final safety device in the complex system provided for the protection of the life and property of the public from all possible effects of a reactor accident. The containment structure encloses the reactor and (usually) the entire primary reactor system in such a fashion as to control, in conjunction with other engineering safeguards of demonstrable reliability, the dispersal of activity to acceptable levels in the event of a maximum credible reactor accident. The containment structure thus defined may take many different sizes and shapes, have a wide range of design requirements, have various materials of construction, and be based upon many different operating requirements. Nevertheless, whether it looks like a pressure vessel or just another industrial building, whether designed for 200 psig or 2 psig, if it is capable of limiting the consequences of the reactor maximum credible accident (mca), it constitutes a containment system or a part thereof.

There are three basically different types of containment system and many variations of each of these three types. A specific containment system may contain features of more than one basic type so that it becomes hard to characterize it. The three general types are distinguishable by how they treat the primary and secondary fluids released in the accident and are known as (1) pressure (or vapor) containment, (2) pressure-suppression containment, and (3) pressure-release containment. In addition to containment systems that are a cross of some of the above the use of more than one containment barrier or system in series on a single nuclear installation has recently given rise to the designation "multiple containment." The general characteristics of each of these systems is discussed below. Detailed data on specific examples of each of these are presented in Chapter 7.

1.4.1 Pressure Containment

In the simple pressure-containment system, all the energy released in the reactor maximum credible accident (mca) is contained in a pressure-containment structure that encloses the reactor. The structure usually also encloses all of the primary system and frequently much of the secondary. Although these structures generally have many lines that penetrate the containing membrane, all such lines that might constitute a significant leak at the time of the mca are equipped with one or more valves that close to complete the isolation of the contained volume.

Pressure-containment structures are frequently steel but are not necessarily limited to this material. Steel-lined concrete containment vessels have been used and some forms of underground concrete-lined containers may be designed as a pressure-containment system. It is of interest to note that the containment pressure may range from a few pounds to over a

hundred pounds, depending upon the energy released in the accident and the volume enclosed. If the entire plant, including the turbine-generators, is contained, as shown schematically in Fig. 1.9, the large resulting containment volume will give rise to a low containment pressure. Although not typical for boiling-water reactors, such a containment system was employed on the BONUS facility in Puerto Rico. On the other hand, the contained volume may be minimized by the enclosure of only the reactor and the primary system, as shown schematically in Fig. 1.10, and the resulting pressure will be relatively high. The new ASME Code, designated Section III, Rules for Construction of Nuclear Vessels, covers containment vessels having a design pressure greater than 5 psig. This pressure is now generally considered the dividing line between high-pressure containment and low-pressure containment. The division is merely one of definition, and the design considerations previously noted will establish design pressure of a containment structure either at or below 5 psig or substantially greater.

ORNL Dwg. 64-1989R

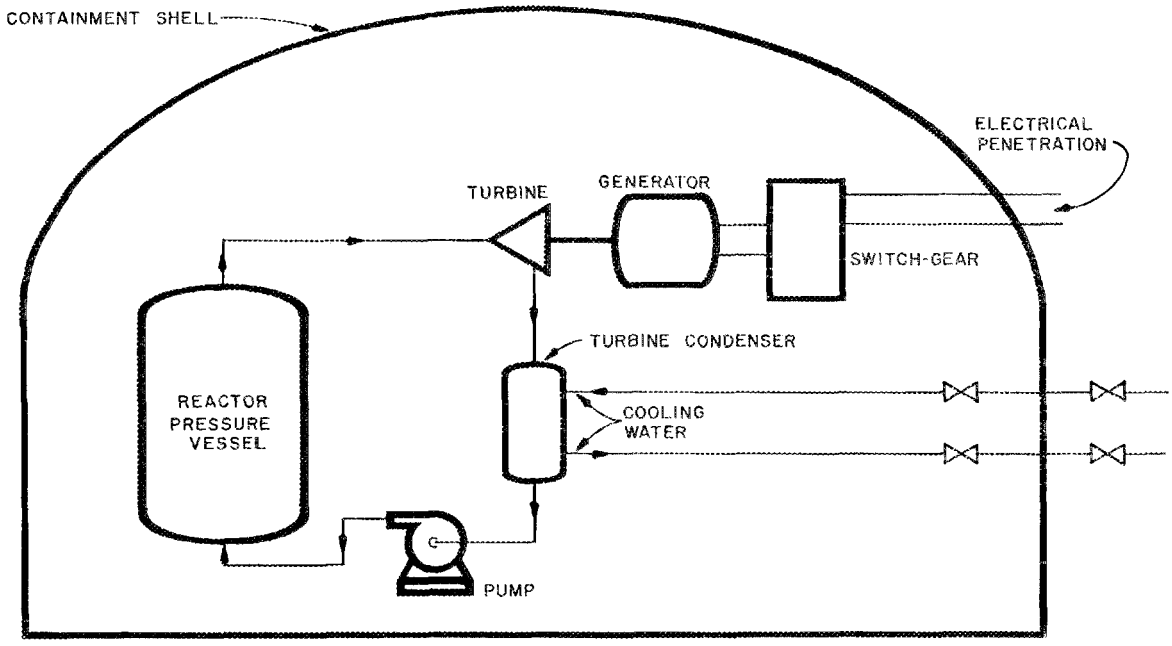

Fig. 1.9. Low-Pressure Containment Shown with Boiling-Water Reactor.

ORNL Dwg. 64-1179

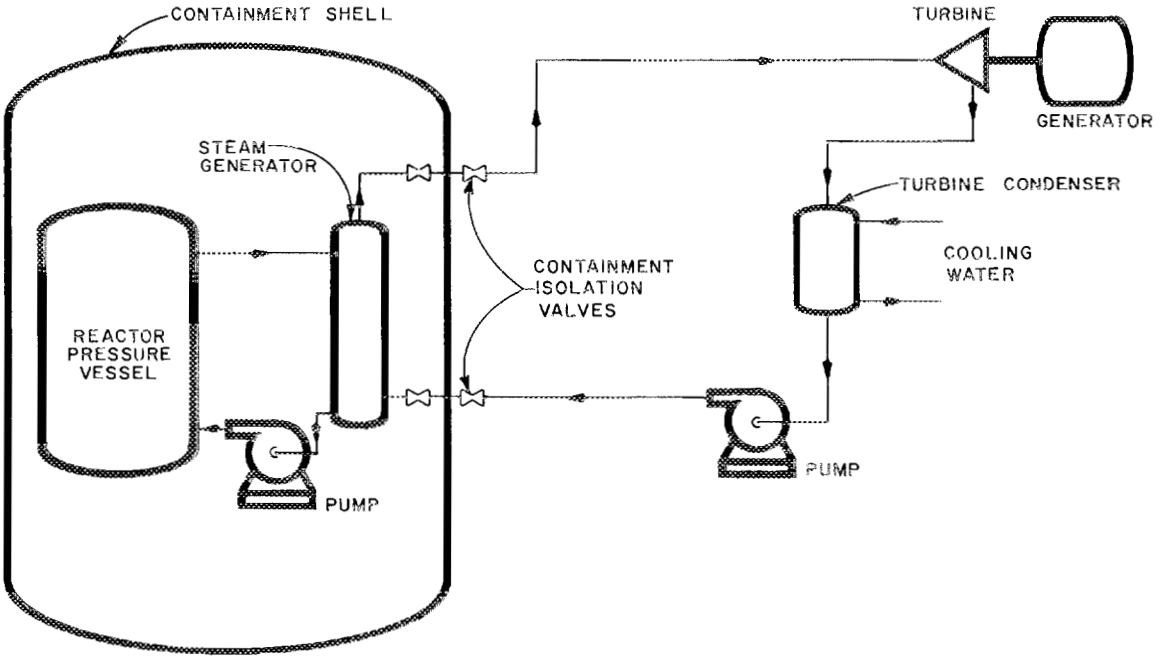

Fig. 1.10. High-Pressure Containment Shown with Pressurized-Water, Gas-Cooled, or Organic-Cooled Reactors.

In any event the leakage rate from a pressure-containment system is usually held to a small fraction of the contained volume; the maximum permissible leakage rate is a function of the reactor site and the activity released from the reactor system. Pressure containment is commonly employed for the pressurized-water and boiling-water reactors where large volumes of the pressurized coolant may be released by the accident concurrent with or soon followed by large amounts of activity. This form of containment was the earliest developed and therefore has also been used on several other reactor systems.

1.4.2 Pressure-Suppression Containment

Pressure-suppression (or, as it is sometimes called, vapor-condensation) containment is based on deposition of the energy resulting from a reactor by condensing the vapor in a pool of water as it is released. Obviously this technique is only applicable to reactor accidents that release a condensable vapor, such as steam. The pressure-suppression containment system shown schematically in Fig. 1.11 is composed of two main

ORNL Dwg. 64-1988R

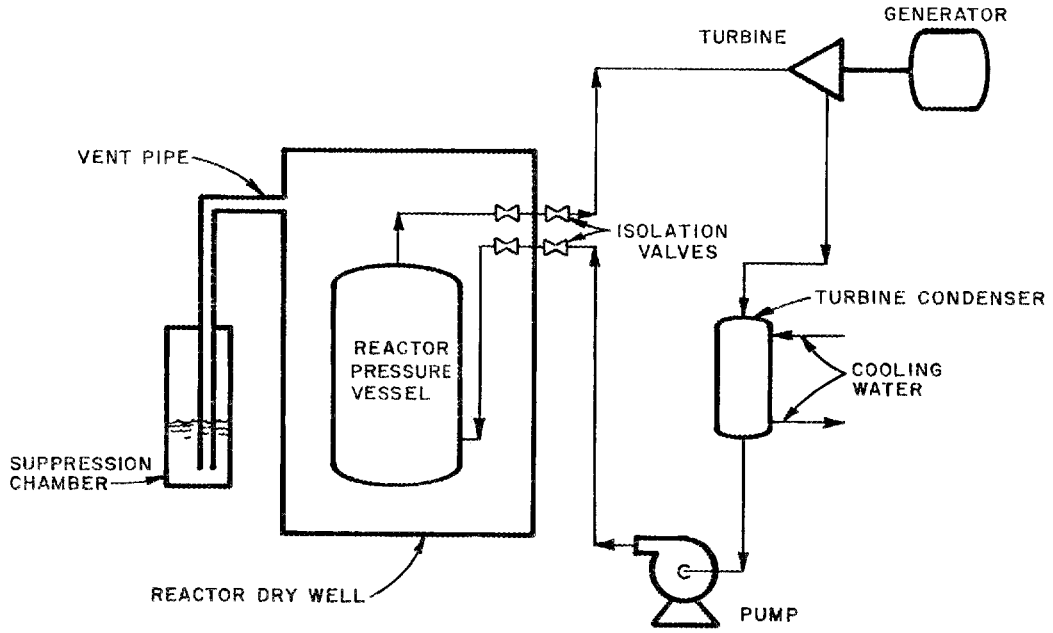

Fig. 1.11. Pressure-Suppression Containment Shown with Boiling-Water Reactor.

components: (1) a pressure vessel or "dry-well" enclosing at least the reactor and (2) a pressure-suppression chamber or "wet-well" partly full of water. The dry well vents through a number of pipes whose discharge ends are submerged in the water within the suppression chamber. Although intended primarily to condense steam, the water pool may perhaps also remove some of the condensable fission products and some particulate and gaseous fission products.

The dry well is designed to withstand the static and dynamic pressures and such other loadings as would result from the maximum credible accident. The suppression chamber experiences relatively low accident pressure, which is a function of the efficiency of the suppression system, volume of the noncondensables, transport from the dry well, and the size of the air chamber.

Pressure-suppression containment systems are attractive in some applications because the size of the dry-well vessel is less than that of a complete containment shell. This advantage, however, is compromised by the fact that, in general, only the reactor and a portion, but not all, of the primary system are contained within the inner vessel. Thus in order to preclude the occurrence of a major loss-of-coolant accident occurring outside the containment, the primary system lines penetrating the containment must be provided with isolation valves. These valves must be provided in duplicate as insurance against the failure of a single valve or to account for breaks inside and outside the containment.

A type of containment employing a form of pressure suppression is effected in systems that employ a water spray within the containment structure as a means of limiting the pressures attained therein. Such an arrangement would be most effective where the condensable vapor was released over a period of time, since sudden releases would not allow time for suppression of the pressure.

Pressure-suppression containment systems consisting of separate dry-well and wet-well volumes are commonly employed with boiling-water reactor systems. All plants have some portions of the dry-well and suppression chamber in a vented building containment system, and, as shown in Fig. 1.16 (sec. 1.4.4), the entire plant may be contained in a vented building. This system represents a logical extension of the concept that is known as "multiple containment." Pressure suppression appears to be most suited to boiling-water reactor systems because the boiling-water system, exclusive of the turbine, can be enclosed in the relatively small dry-well.

1.4.3 Pressure-Release Containment

In the pressure-release method of containment the pressure in the containment structure is relieved by venting to the atmosphere. This venting is limited, in some systems, to the period of the primary (or secondary) system blowdown and, in others, may extend over the course of the accident. The former case is commonly called "pressure-relief" containment and the latter is variously described as "confinement," "vapor-venting," "pressure-venting," "building-type," or in some applications, "negative-pressure" containment. For the purposes of the subsequent discussion, the two types will be called pressure relief (where the pressure is relieved only during the initial release from the accident) and pressure venting (where the contained volume is more or less continuously vented, often through filters, during the course of the accident in order to maintain a given pressure within the contained volume).

In either case, the suitability of this containment technique is critically dependent on the amount of fission products that are released to the atmosphere during the release period. Air-cleaning systems so far proposed for such applications do not provide for the efficient removal of radioactive noble gases and some forms of other fission products such as methyl iodide, and this would be an important consideration in the use of such systems.

1.4.3.1 Pressure-Venting Containment

Although the containment atmosphere is more or less continuously discharged to the outside, it is generally discharged through a stack and then only after the fission-product contamination in the discharge effluent has been reduced to acceptable levels by filters, scrubbers, or both techniques. The success of this type of containment, shown schematically in Fig. 1.12, is often dependent upon the effectiveness of the cleanup system in maintaining a safe level of activity in the effluent and the ability to maintain the exhaust rate high enough to

ORNL Dwg. 64-1986

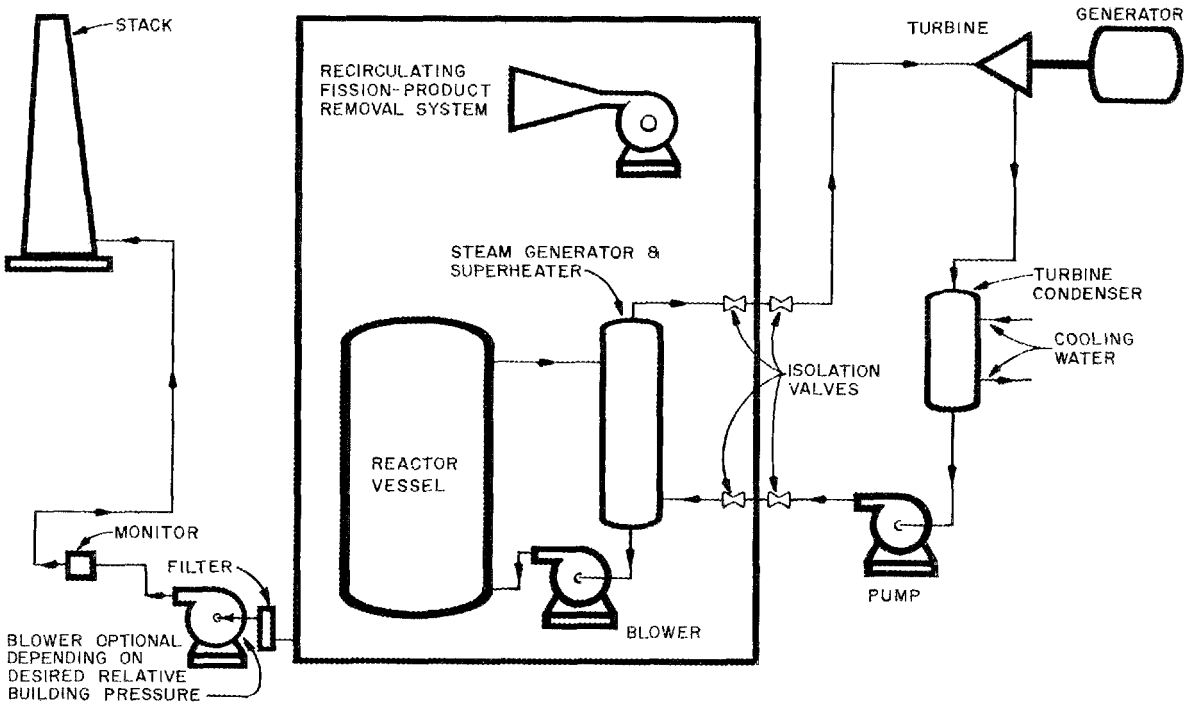

Fig. 1.12. Pressure-Venting Containment Shown with a Gas-Cooled Reactor.

avoid developing an excessive pressure in the containment structure (building). An additional recirculating fission-product-removal system would not necessarily be required for all applications but would be a function of the specific need of a specific reactor and site for containment-atmosphere cleanup.

The applicability of confinement or vapor-venting containment is quite dependent on the reactor type and, in turn, can be characterized by the maximum credible accident. In general, confinement containment has been used for reactor systems associated with relatively low-energy mca's. Those systems in which the energy release is sufficiently small that continuous exhausting of the building atmosphere keeps the building pressure below that of the atmosphere are known as negative-pressure systems. Obviously the structures required for such a containment system are not subjected to high-pressure loads and may be of steel frame construction with metal-panel siding. Usually exterior windows are omitted, all joints are caulked and sealed, and doors are gasketed. Such a building may be operated at a slightly negative pressure to produce inleakage and to channel all discharge through the filtered stack exhaust system. This type of containment is used for swimming pool reactors, the Oak Ridge Research Reactor, and graphite reactors.

1.4.3.2 Pressure-Relief Containment

In the pressure-relief method of containment, shown schematically in Fig. 1.13, the air and steam are purposely released immediately through an exhaust duct and then sprays or deluge systems are activated to prevent excessive pressures from subsequently developing in the containment structure due to decay heat, etc.

In this technique the containment atmosphere is discharged only during the initial primary system blowdown. It is applicable only where the initial blowdown precedes the release of fission products from the core by a sufficient margin that the once-"relieved" system may be effectively sealed before significant amounts of fission products are released. Inasmuch as the principal virtue of this system is the low structure design pressure, the structure is frequently provided with sprays to prevent excessive pressures from developing after the initial relief. Some activity

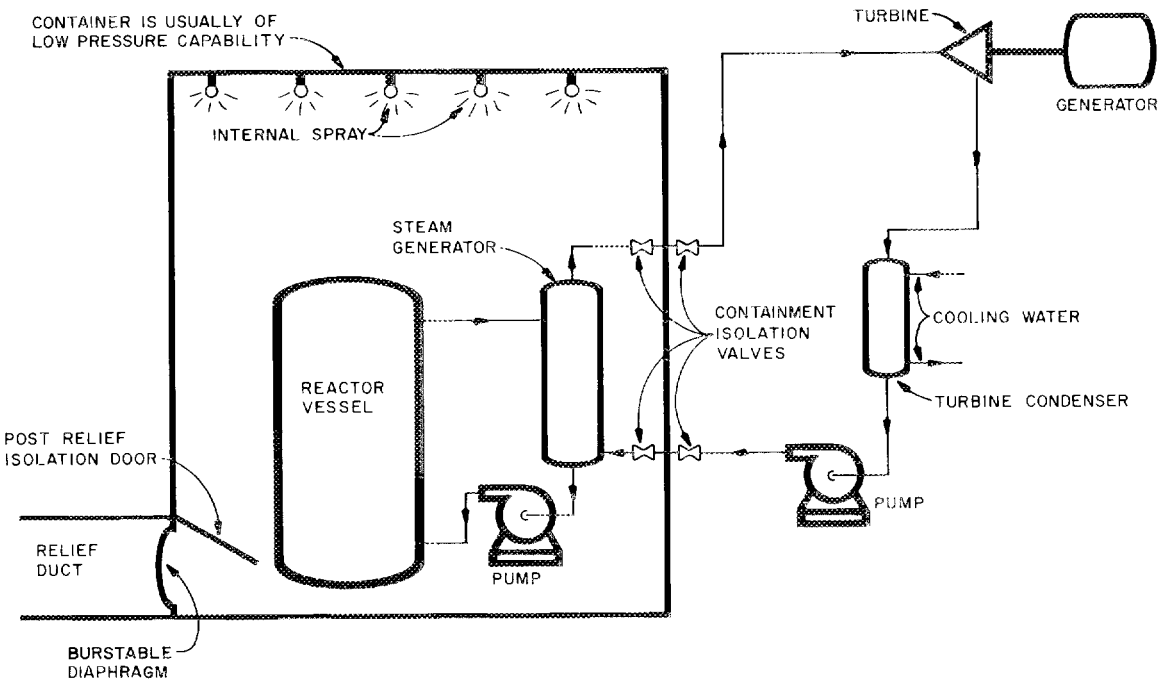

Fig. 1.13. Pressure-Relief Containment Shown with Pressurized-Water Reactor.

will inevitably be released during the initial venting and this system is only applicable where this initial release is tolerable. Activity subsequently released to the atmosphere is minimized by closing the exhaust-duct vent before core overheating occurs. The containment vessel or confinement structure must be designed to withstand the pressure that may be generated after the exhaust duct is closed following the initial release of air and steam. This type of containment has been considered for several reactor plants. As employed at the New Production Reactor at Hanford, this type of containment is coupled with pressure-venting containment, since a small amount of vapor may be vented through filters and released to the stack even after the initial blowdown.

1.4.4 Multiple Containment

Since "multiple containment" is receiving considerable attention for containing power reactors to be located in heavily populated areas, it is discussed separately here. Multiple containment denotes any one of a number of methods of providing two or more complete containment barriers around the primary reactor system.

The two most common forms of multiple containment are (1) that in which a high-pressure containment structure is surrounded by another envelope from which the atmosphere may either be cleaned up and released or pumped back into the containment vessel, and (2) that in which a pressure-suppression system is surrounded by a vented envelope. A major concern with multiple containment systems is that the two containment barriers are never completely independent, so there remains the possibility, however remote, that a single event, e.g., sabotage, could violate both systems.

The various multiple containment systems described here, some involving the use of an intermediate negative pressure zone in connection with a monitoring device to detect leakage, permit much lower leakage rates than is practical to attain with simple pressure containment. This is an important fact when siting close to populations is concerned.

1.4.4.1 High-Pressure Double Containment

Perhaps the first power reactor to require and provide multiple containment was the N.S. Savannah. In this nuclear ship, the pressurized-water-reactor plant is first contained in a conventional pressure containment system, and this system, in turn, is located in a sealed ship compartment that is continuously vented through filters. The effluent from the filters is released at the top of the ship's mast. This type of system is shown in Fig. 1.14.

A similar form of multiple containment exists at the Consolidated Edison Indian Point Plant, although its capability was not exploited or required in order for that plant to meet its initial siting requirements. However, the existing annular space between the pressure containment shell and the outer shell, initially provided for concrete forming, is vented to the facility stack and thus effects pressure-venting containment.

Another version of high-pressure double containment, shown in Fig. 1.15, has been proposed for both the Malibu Nuclear Plant of the city of Los Angeles and the now tabled Ravenswood plant. In this system, an annular space 30 in. wide is formed by two 0.25-in.-thick carbon steel shells. The annulus is filled with pervious concrete, and an additional 5 1/2 ft

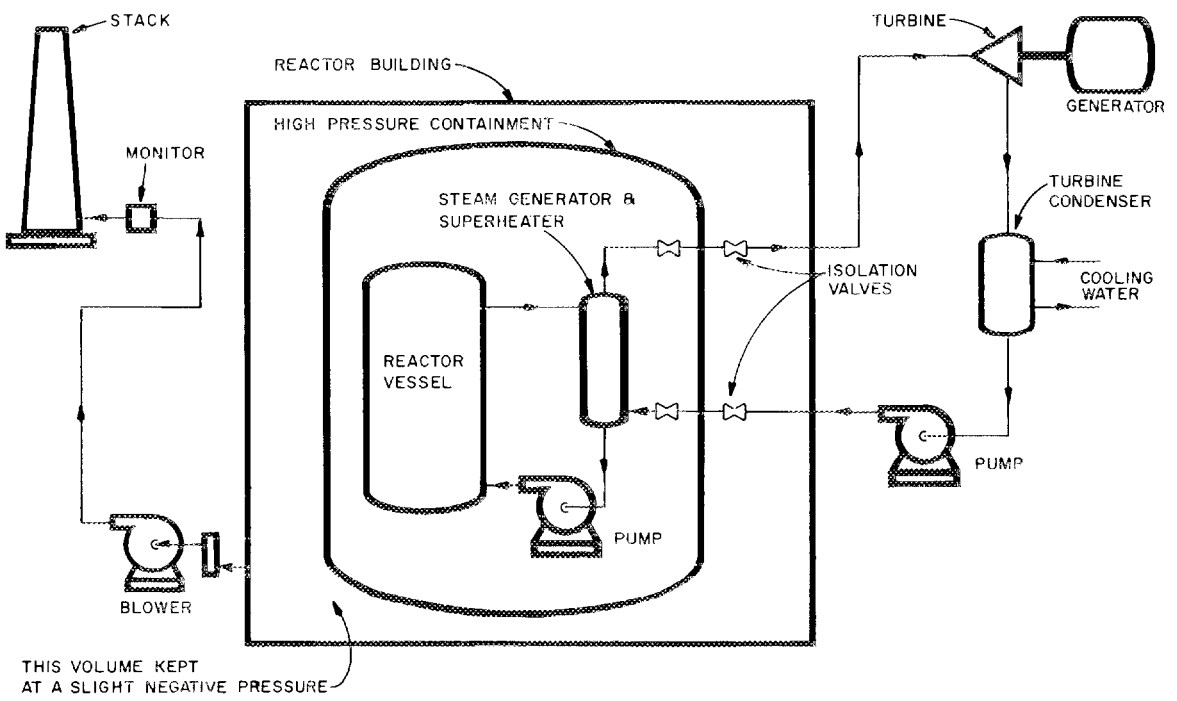

Fig. 1.14. Multiple Containment (Basic Application) Shown with Pressurized-Water Reactor.

ORNL Dwg. 64-19813

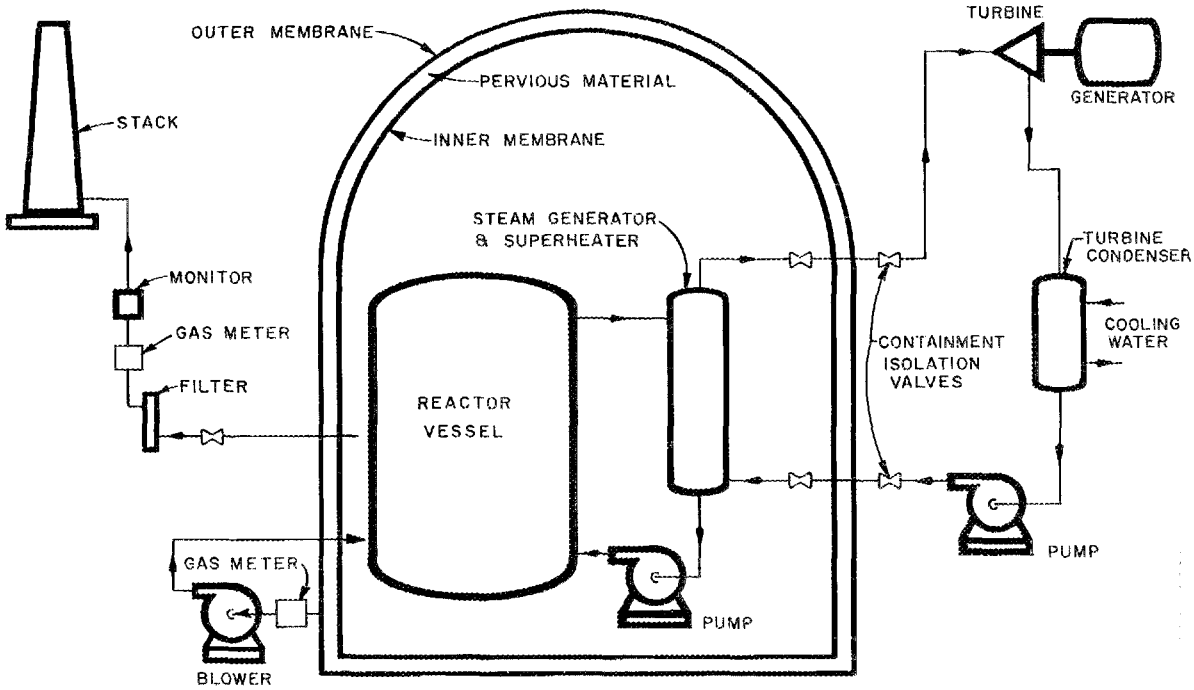

Fig. 1.15. Multiple Containment (Advanced Concept) Shown with Pressurized-Water Reactor.

of normal-density reinforced concrete encompasses the outer membrane. However, the resulting poor heat transfer through the concrete to the environment required that a decay heat removal system be added. The normal ventilation air exhaust from the containment vessel is filtered before being released to the atmosphere through a stack. In the event of pressure buildup within the vessel, the pervious concrete plus the two steel membranes would transmit the forces to the outer reinforced concrete vessel (layer), which is designed to carry the pressure produced by an mca. The annulus is maintained at a negative pressure to assure inward leakage flow at all leakage points. The negative pressure zone (annulus) is continuously monitored for leakage, which is returned to the containment vessel by a pump-back compressor.

1.4.4.2 Pressure-Suppression Double Containment

In the pressure-suppression version of multiple containment, the simple pressure-suppression system (see Fig. 1.11) is located within a building that may be vented through filters to a stack, only when isolation is called for, as shown in Fig. 1.16. In order to meet siting requirements, all proposals involving boiling-water reactors with pressure-suppression containment more closely resemble the double containment of Fig. 1.16 than simple pressure suppression only.

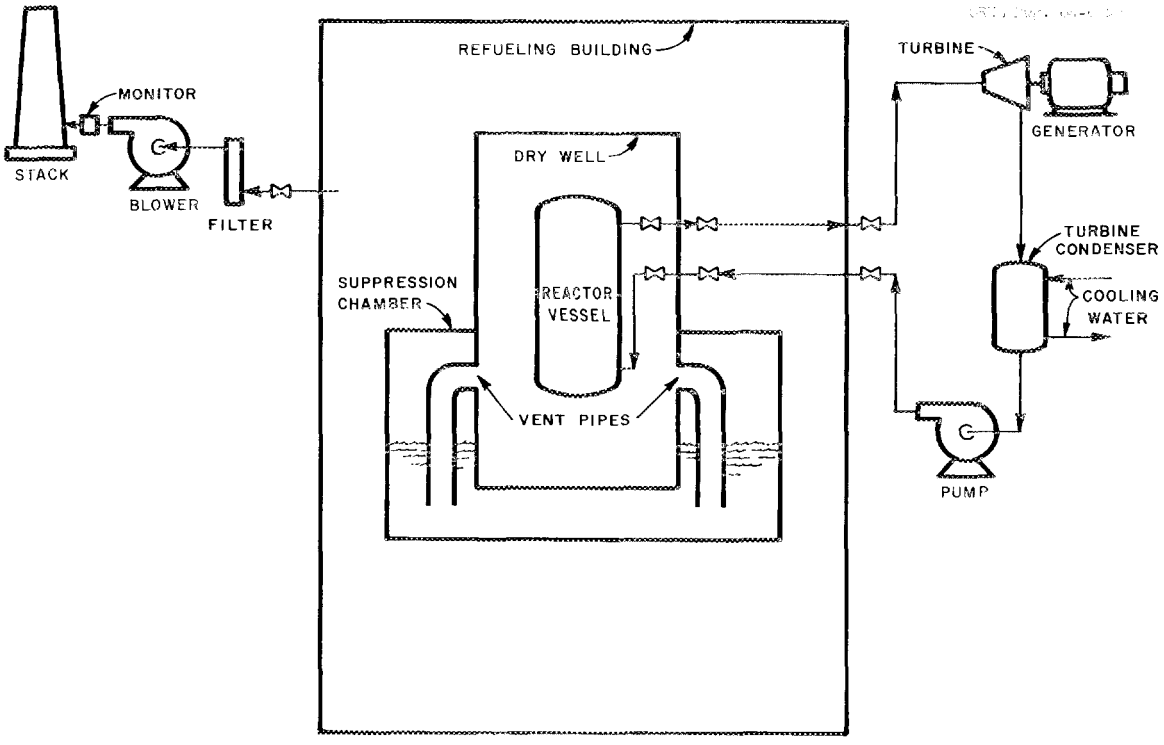

Fig. 1.16. Multiple Containment Shown with Boiling-Water Reactor.

1.4.5 State of the Art

As nuclear power comes increasingly into contention as one of the economic means of generating electricity, costs such as those associated with containment will come under increasing scrutiny. Indeed, the scrutiny is even now well under way, as evidenced by the substantial research and development programs. The further exploitation of engineered safeguard techniques could have as decisive an effect on nuclear technology in the next decade as the concept of dependence upon the containment enclosure had in the past. Included in the extensive research and development programs are the many projects reviewed in Chapter 12.

For the immediate future, nuclear plants will continue to incorporate containment enclosures. Which containment system to use with a particular reactor is still an open question, although the experience of the past decade can narrow the choice somewhat. Table 1.12 presents a qualitative attempt to relate reactor and containment system, first on the basis of "apparent" compatibility and second on the basis of experience. The

Table 1.12. Compatibility of Various Reactor and Containment Systems

Apparent Compatibility	Current Usage
A — Well matched	1 — Wide use (three or more)
B — Compatible	2 — Some use (less than three)
C — Not well matched	3 — Regarded as possible
D — Incompatible	4 — Regarded as unlikely

Reactor Type[a]	Containment System[b]				
	High Pressure	Low Pressure	Pressure Suppression	Pressure Relief	Pressure Venting
Pressurized water	A-1	B-3	B-3	B-3	C-4
Boiling water	A-1	B-2	A-1	B-3	C-4
Aqueous homogeneous	A-2	C-3	C-3	D-4	D-4
Heavy-water moderated	A-2	B-3	B-3	B-2	C-3
Liquid-metal cooled, thermal	B-3	A-3	D-4	B-3	A-2
Liquid-metal cooled, fast	A-2	B-3	D-4	D-4	C-3
Gas cooled	A-2	B-3	D-4	B-3	A-1
Organic moderated	B-3	A-2	C-4	B-3	B-3
Fused-salt fueled	B-2	A-3	C-3	C-3	B-3
Test	A-1	B-3	C-4	B-3	A-1
University research	B-3	B-2	C-4	C-3	A-1

[a]See Section 1.3 for a general description of reactor types.

[b]See Section 1.4 for a general description of containment systems.

table does not consider multiple containment systems nor should all combinations listed be regarded as comparably safe, since many have not been evaluated by licensing and regulatory authorities.

In using the information of Table 1.12, the following limitations should be kept in mind:

1. Some combinations may involve safety features or philosophy whose acceptability has not been evaluated by U.S. regulatory authorities.

2. The reactor and containment system combinations considered do not include military or production reactors.

3. The evaluations are based on U.S. experience where available; where not, the most comparable foreign experience was considered.

The table is intended to apply only to the systems described in Sections 1.3 and 1.4 above. Many variations, modifications, adaptations, or combinations of the general containment systems listed, either with each other or with other engineered safeguards, could have been reflected in the apparent compatibility rating given in Table 1.12, but, obviously, it is not feasible to consider all such combinations in a tabulation of this type.

Some further definition of the basis for the apparent compatibility classification is also necessary. This classification was generally arrived at for a particular type of reactor by considering the suitability or appropriateness of each of the five containment systems and then designating the "most-effective" containment system "A" and the others, as appropriate, in descending order. This yardstick, however, is misleading in situations in which the reactor mca might not produce high pressures (e.g., organic-moderated and fused-salt-fueled reactors) and thus the reactor would be well matched with low-pressure containment, or in which pressure containment would be inherently capable of greater protection than the reactor accident could conceivably require (e.g., university reactors).

References

1. Code of Federal Regulations, Title 10, Part 100, Reactor Site Criteria; see also Federal Register, April 12, 1962.

2. C. K. Beck, Engineering Out the Distance Factor, AEC press release, September 25, 1963.

3. R. O. Brittan, Reactor Containment, Including a Technical Progress Review, USAEC Report ANL-5948, Argonne National Laboratory, May 1959.

4. J. J. DiNunno et al., Calculations of Distance Factors for Power and Test Reactor Sites, USAEC Report TID-14844, March 23, 1962.

5. ASME Boiler and Pressure Vessel Code, Sections I, III, and VIII, American Society of Mechanical Engineers, United Engineering Center, 345 East 47th Street, New York, N.Y.

6. Power and Test Reactors, Notice of Proposed Rule Making, Federal Register, 24(10): 4184–4185 (May 23, 1959).

7. Code of Federal Regulations, Title 10, Part 100, Proposed Reactor Site Criteria; see also Federal Register, Notice of Proposed Guides, 26(28): 1224 (Feb. 11, 1961).

8. W. B. Cottrell, Site Selection Criteria, Nuclear Safety, 1(1): 4–5 (September 1959).

9. J. R. Buchanan, Comments on Proposed Reactor Site Criteria, Nuclear Safety, 3(2): 73–76 (December 1961).

10. W. B. Cottrell, Site Selection Criteria, Nucl. Safety, 1(2): 2–5 (December 1959).

11. Letter from ACRS Chairman L. Silverman to Hon. John A. McCone, September 26, 1960, Subject: Criteria for the Evaluation of Reactor Sites.

12. U.S. Atomic Energy Commission, Theoretical Possibilities and Consequences of Major Accidents in Large Nuclear Power Plants, USAEC Report WASH-740, March 1957.

13. O. G. Sutton, A Theory of Eddy Diffusion in the Atmosphere, Proc. Roy. Soc. (London), 135A: 143 (1932).

14. U.S. Weather Bureau, Meteorology and Atomic Energy, USAEC Report AECU-3066, July 1955.

15. For discussion of proposal by Pasquill, see F. A. Gifford, Jr., Use of Routine Meteorological Observations for Estimating Atmospheric Dispersion, Nucl. Safety, 2(4): 47–51 (June 1961).

16. P. J. Meade, Meteorological Aspects of the Safety and Location of Reactor Plants, World Meteorological Organization, Technical Note No. 33, pp. 13–22, 1960.

17. C. R. Hosler, Low-Level Inversion Frequency in Contiguous United States, Monthly Weather Review, 89: 319–339 (September 1961).

18. Port Operation of Shipboard Reactors, prepared by AEC-Maritime Administration Joint Group, No. 970/5053, August 1, 1962, submitted for the public hearing on the interim sea and port operation of the N.S. Savannah.

19. Wm. B. Cottrell, L. A. Mann, F. L. Parker, and G. D. Schmidt, Environmental Analysis of N.S. Savannah Operation at Camden, Appendix C, USAEC Report ORNL-2867 (Rev.), Oak Ridge National Laboratory, January 24, 1961.

20. Wm. B. Cottrell, Reactor Site Criteria, Nucl. Safety, 4(1): 11–16 (September 1962).

21. J. R. Buchanan, Comments on Proposed Reactor Site Criteria, Nucl. Safety, 3(2): 73–76 (December 1961).

22. Port Analyses Report: Savannah, Ga., prepared by the AEC and Maritime Administration, August 7, 1962, and submitted for the public hearing on the interim sea and port operation of the N.S. Savannah.

23. Port Analyses Report: Norfolk, Va., prepared by the AEC and Maritime Administration, August 15, 1962, No. 970/4592, and submitted for the public hearing on the interim sea and port operation of the N.S. Savannah.

24. Port Analyses Report: Panama Canal, prepared by the AEC and Maritime Administration, August 22, 1962, No. 970/4603, and submitted for the public hearing on the interim sea and port operation of the N.S. Savannah.

25. Wm. B. Cottrell et al., Activity Releases from the N.S. Savannah in the Maximum Credible Accident, USAEC Report ORNL-3361, Oak Ridge National Laboratory, October 2, 1963.

26. E. Siddall, Reliability of Reactor Control Systems, Nucl. Safety, 4(4): 1–7 (June 1963).

27. E. P. Epler, Reliability of Reactor Systems, Nucl. Safety, 4(4): 72–76 (June 1963).

28. S. H. Hanauer, Instrumentation for Containment, Nucl. Safety, 3(1): 41–46 (September 1961).

29. D. G. Breckon and J. H. Collins, Control and Safety in the Operation of the NRX and NRU Reactors, Canadian Report AECL-1486, April 1962.

30. A. E. G. Bates, Control Rods and Control-Rod Drives in Power Reactors, Nucl. Safety, 2(4): 17–37 (June 1961).

31. J. R. Buchanan, SL-1 Final Report, Nucl. Safety, 4(3): 83–86, (March 1963).

32. D. Kallman and O. G. Hanson, Some Economic Aspects of Reactor Safety, Reactor Safety Conference, New York City, October 31, 1957, USAEC Report TID-7549, Pt. 2, pp. 1–6.

33. S. J. Harris, Nuclear Power Safety Economics, Pilot Books, New York 1961.

34. U.S. Atomic Energy Commission, Guide to Nuclear Power Cost Evaluation, USAEC Report TID-7025, Mar. 15, 1962, and Supplement No. 1, Sept. 30, 1962.

35. Public Law 85-256, 71 Stat. 576 (amends sections 2, 11, and 53, and adds section 170 to the Atomic Energy Act of 1954).

36. J. F. Hennessey, Indemnification of the USAEC's Contractors Against Liability for Nuclear Incidents, Law and Administrative Series X, Progress in Nuclear Energy, Pergamon Press, 1962.

37. Code of Federal Regulations, Title 10, Part 140, Financial Protection Requirements and Indemnity Agreements; see also Federal Register.

38. Nuclear Energy Liability Insurance Association (NELIA), 85 John St., New York 38, N.Y.

39. Mutual Atomic Energy Liability Underwriters (MAELU), 919 North Michigan Avenue, Chicago, Illinois.

40. W. McGuire and G. P. Fisher, Containment Studies of the Enrico Fermi Atomic Power Plant, pp. 19–36, Cornell University, Ithaca, New York, 1959.

41. T. H. Row, Safety of University Reactors, Nucl. Safety, 3(4): 17–21 (June 1962).

2. CODES, CRITERIA, AND REGULATIONS

R. W. Schneider*

2.1 INTRODUCTION

Containment structures are used to enclose nuclear facilities and are designed to control the dispersal of activity in the event of an accident. The structure must contain all credible accidents, including the maximum credible accident. Although a steel pressure vessel is the most common type of containment structure for power reactors in the United States, containment structures may assume many forms, such as confinement buildings with filtered and scrubbed exhaust, concrete, prestressed concrete, or underground buildings. In general any containment system may be employed with any reactor, but in practice some containment systems are more compatible with certain reactor systems.

At the present time the reviewer's judgement plays a large role in evaluating reactor systems for the granting of construction permits and operating licenses. Attempts have been made and are being made to codify requirements, for example, Code of Federal Regulations, Title 10, Part 100, "Reactor Site Criteria"[1] (see Chapter 1), but it is not yet possible to eliminate judgement from the hazards evaluation process. However, at the present state of experience the most fundamental principles that could be included in codes vary over an extremely broad range and, for the most part, comprehensive data are not available. Many people believe that criteria written at this time might impede progress to such an extent that new designs and concepts might not be investigated. As a result, there are few nationally recognized and accepted codes available on criteria and design of containment structures.

The boiler and pressure vessel codes, which existed before the nuclear age, have been revised and supplemented to provide rules for the design of pressure containment structures, and new rules are forthcoming A comprehensive discussion of codes and criteria for steel (metal) pressure containment vessels is presented in Section 2.4. Since most power reactors in the United States use steel containment vessels, there is considerable experience available on this type of containment scheme, and therefore the discussion here of steel containment vessels is more comprehensive than for the other types of reactor containment or confinement.

---

*The work on this chapter was initiated in 1962 by C. L. Whitmarsh, Jr., now of the Lewis Research Center, and was completed by R. W. Schneider of ORNL in 1964. The author is indebted to F. W. Catudal of Travelers Indemnity Co., E. A. Fenton of American Welding Society, Inc., Henry G. Lamb of Nuclear Standards Board, E. C. Miller of ORNL, J. D. Wilding of ASME, R. R. Maccary of Division of Reactor Licensing, AEC, L. P. Zick of Chicago Bridge and Iron and others for aid in this work.

Before any containment and confinement schemes can be regarded as acceptable to the Division of Reactor Licensing of the Atomic Energy Commission, their performance must be demonstrated to the satisfaction of the Commission. Since nationally recognized codes for nuclear confinement structures and containment vessels (other than steel) are essentially nonexistent, the consideration of applicable codes for these structures, as in Section 2.6, must be of a general nature.

It must be appreciated that code rules, in general, provide minimum safety requirements. The ASME Boiler and Pressure Vessel Codes do not cover the deterioration that might occur in service as a result of radiation effects, corrosion, erosion, etc. Nevertheless, these effects and many others must be considered in order to be reasonably assured of achieving the specified life of the vessel. In general, design parameters must be established before the codes can serve a useful purpose.

Approval to construct and operate a nuclear facility is granted by the Division of Reactor Licensing of the U. S. Atomic Energy Commission and is directly related to compliance with pertinent regulations and, thus, indirectly to the application of appropriate codes and criteria. Guidance is provided here by a discussion of pertinent federal, state, and local regulations and the federal-state relationship.

2.2 REGULATORY ORGANIZATIONS

2.2.1 Atomic Energy Commission

The U. S. Atomic Energy Commission (AEC) was established by the Atomic Energy Act of 1946 and later modified by the Atomic Energy Act of 1954.[2] Its prime functions are (1) to regulate the atomic energy industry in a manner to protect the health and safety interests of the public, (2) to control and regulate the use and possession of special nuclear materials, (3) to foster international cooperation in the use and development of nuclear energy, and (4) to encourage industry participation in research and development. In addition, it is a federal law that no one may build or operate an atomic power plant without first obtaining a construction permit and then an operating license from the U. S. Atomic Energy Commission.

An organization chart for the entire AEC is shown in Fig. 2.1 and that of the Divisions under the Director of Regulation are shown in Fig. 2.2. The functions of the divisions associated with the approval and licensing of reactor systems, including the containment structure, are described below.

The present organizational structure was established in April and May of 1961 (ref. 3) as a result of a Commission decision to separate its regulatory functions from those of operations and development. Prior to that time the activities of the various divisions now reporting to the Director of Regulations, a position that was created in May 1961, reported to the AEC General Manager, who was also responsible for all Commmission operations and development.

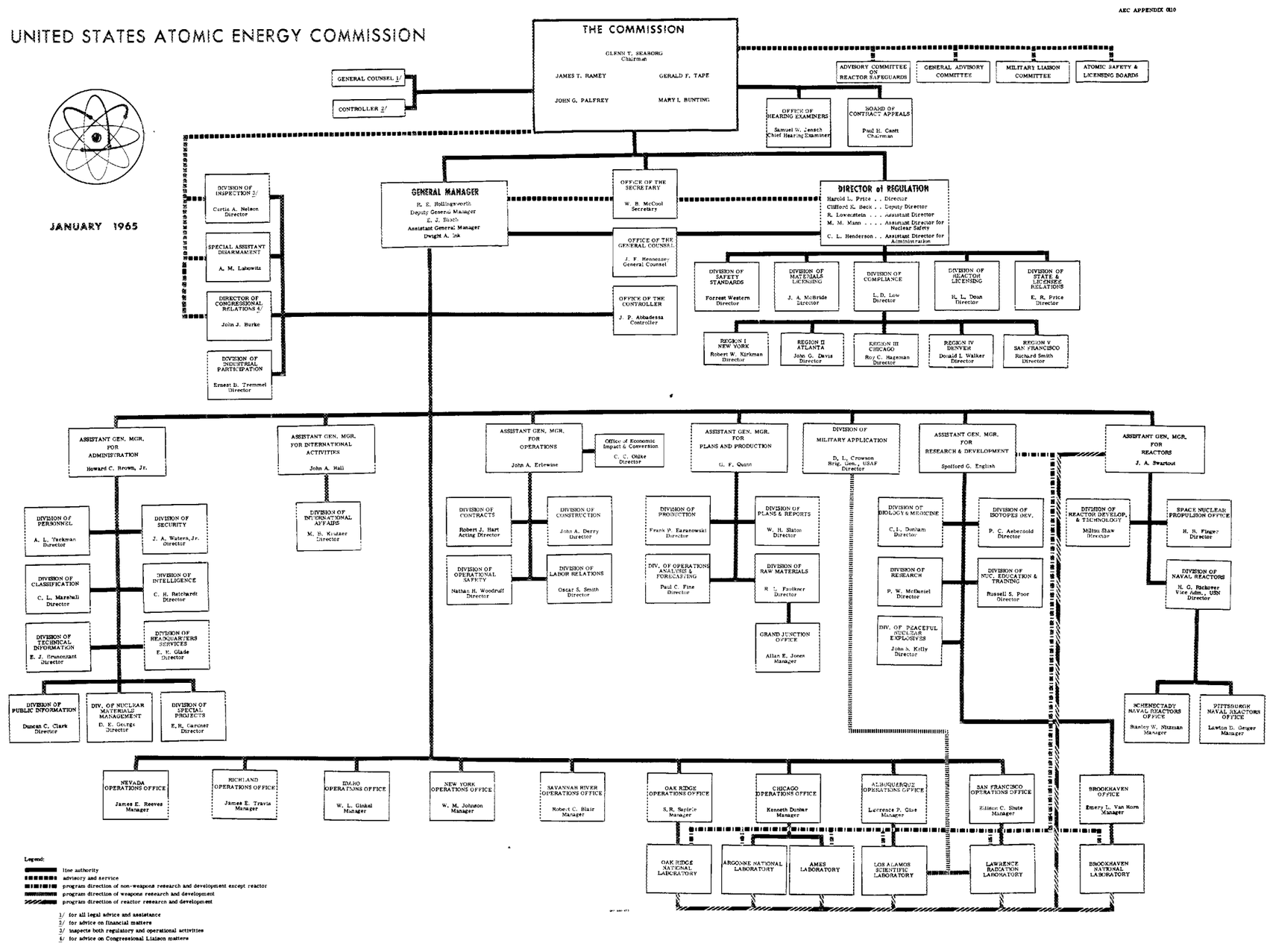

Fig. 2.1. Organization Chart for the U.S. Atomic Energy Commission.

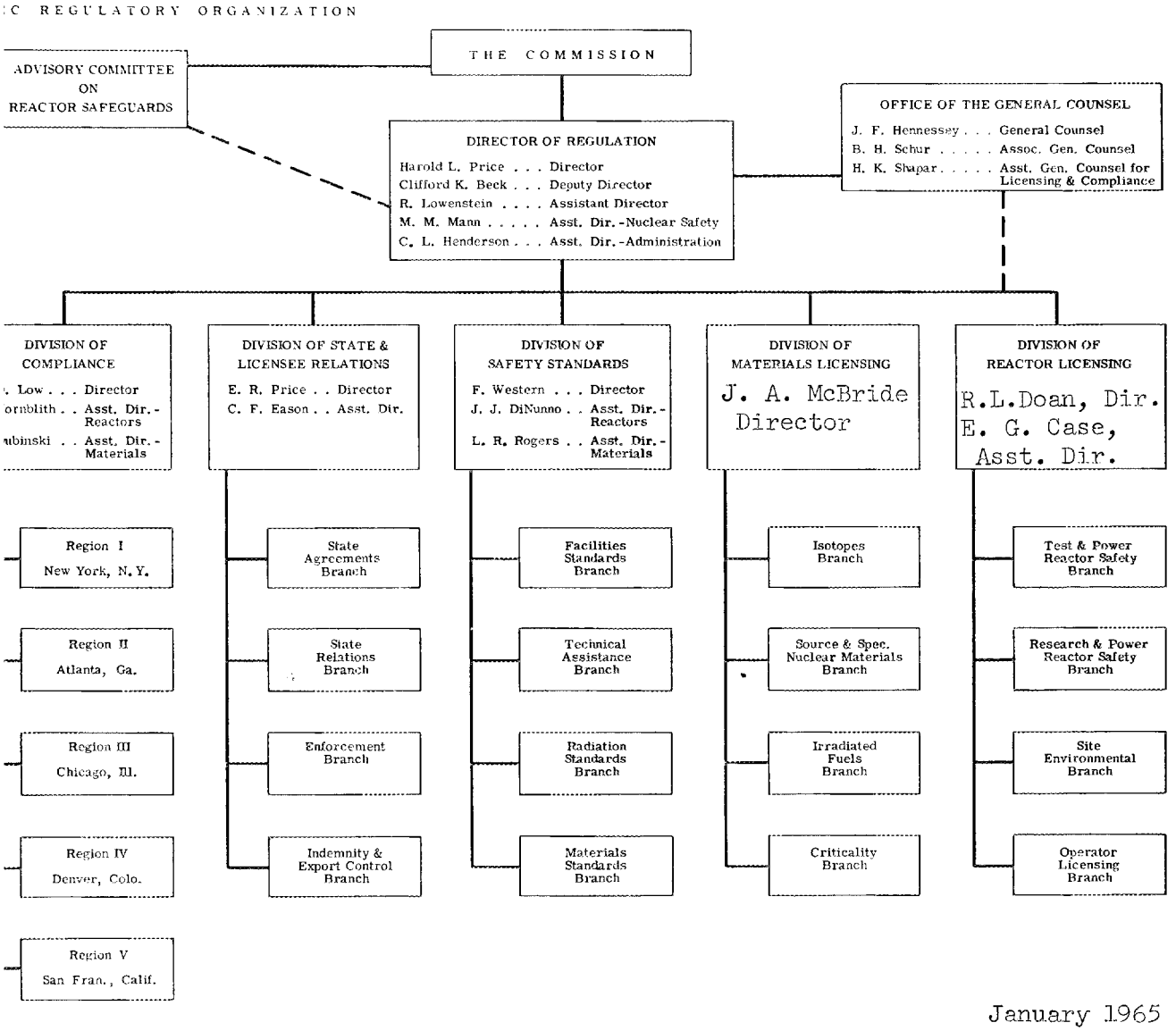

Fig. 2.2. Organization Chart of Divisions Under Director of Regulation.

As may be seen from Fig. 2.2 the significant AEC divisions concerned in the licensing of nuclear facilities are the Division of Reactor Licensing and the Division of Compliance. In addition the AEC General Counsel's Office and the Atomic Safety and Licensing Boards play important roles in the process. The functions of each of these four groups are briefly summarized below.

2.2.1.1 Division of Reactor Licensing

The Division of Reactor Licensing is directly concerned with all aspects of administering the Commission's program of reactor licensing. The Division has the responsibility of developing licensing and regulatory policies in close cooperation with the several advisory groups that are available to it. This includes development of regulations for particular uses, development of criteria for issuance of specific and general licenses, evaluation of health and safety features of proposed activities, determination of technical and financial qualifications of applicants, allocation of special nuclear material, and development and application of the indemnity program. The Division has the further responsibility of licensing all private activities in the U. S. involving the use of source and special materials.

2.2.1.2 Division of Compliance

The purpose of the Division of Compliance is to direct the program for the inspection and investigation of materials and facilities to determine compliance. The Division provides guidance and assistance to the licensee's inspection staff. Although not responsible for development of regulations, the Division through its experience, is able to recommend regulation and regulatory changes.

2.2.1.3 Office of the General Counsel

The Office of the General Counsel is closely involved in the legal aspects of all phases of AEC licensing, regulatory, compliance, and inspection activities. The most substantial participation of the Office of the General Counsel in the regulatory program is through counsel to the Division of Reactor Licensing and the Division of Compliance. In licensing cases the Office closely follows, from the legal standpoint, all documents and testimony submitted by the licensee and other interested parties.

2.2.1.4 Atomic Safety and Licensing Board

The Atomic Safety and Licensing Board has the responsibility of conducting hearings and issuing orders and decisions in licensing cases. The Board performs no direct role in the development of general Commission regulatory policies, except to the extent that such policies may be developed in a decision or order which becomes the action of the Commission or becomes a final order in the absence of review by the Commission.

The Board is separated from the staff and the Commission and does not communicate with counsel, members of the staff, or parties to a proceeding, except upon the record or as otherwise permitted by law.

2.2.2 Advisory Committee on Reactor Safeguards

The Advisory Committee on Reactor Safeguards (ACRS) was established to review the design (including containment provisions) of all proposed power reactors. An advisory service was initially intended, but the Atomic Energy Act of 1954 was amended[4] in Section 29 on September 2, 1957 to give ACRS statutory status and to make hearings mandatory on specified facility licenses. The ACRS has an authorized membership of 15, and each member is a recognized expert in some phase of nuclear reactor technology. These men are appointed to four-year terms by the AEC.

The 1957 amendment to the Atomic Energy Act authorized the Commission to request advice from the ACRS on any reactor safety problem and directed the Commission to obtain such counsel on all power and test reactors considered for licensing by the Commission. Subsequently, by issuance of Part 115, Title 10, Code of Federal Regulations,[5] the Commission was also required to obtain these services for other nuclear reactors, e.g., Commission-owned reactors which would otherwise be exempted from licensing requirements. The procedures for the review of such facilities are known as "parallel procedures," since the procedures "parallel" those for licensed facilities, even though such a license is not required for Commission-owned facilities.

ACRS concern regarding some aspects of containment and related safety features was indicated by recommendations made to Chairman Seaborg of the AEC on September 11, 1961. Some of these recommendations were that[6]

> "(1) Except in special units, all nuclear vessels and piping be designed, built, and inspected in accordance with one of the recognized codes and that no deviation be permitted except as provided by the code used;
>
> "(2) In selection of vendors for supplying equipment for use in nuclear installations, recognition be given to the need for care beyond code requirements in selection of materials, control of fabrication, and testing;
>
> "(3) In the Hazards Summary Report, (a) the code used be specified, and (b) assurance be given that adequate concomitant material selection, manufacturing procedure, and testing will be used; ...."

As noted earlier the containment system is but one of several engineered safeguards that have been used or considered for use with nuclear facilities. The ACRS also expressed itself in a letter of April 18, 1963, to AEC Chairman Seaborg regarding the testing requirements for engineered safeguards:

> "The increasing pressure to locate nuclear power plants near population centers requires that designers of these plants incorporate in their designs engineered safeguards to reduce the magnitude of postulated radioactivity releases.

"The Advisory Committee on Reactor Safeguards is of the opinion that, as a principle, where such engineered safeguards are incorporated in plants, they should be so designed and built that their reliability can be tested continuously or at least frequently under design conditions, or under conditions such that conservative extrapolation to design conditions can be made. This would insure that no deterioration occurs that could lead to increases in the postulated effects of accidents."

2.2.3 Joint Committee on Atomic Energy

Legislation pertaining to atomic energy would normally originate in the Joint Committee on Atomic Energy (JCAE). The Committee is composed of nine members of the Senate and nine members of the House of Representatives. The functions of this committee include a continuing survey of the activities of the AEC and of problems relating to the development, use, and control of atomic energy. In the past several years the Committee has held hearings on the following subjects related to containment:

1. Radiation safety and regulation,[7] June 12-15, 1961,
2. Radiation standards, including fallout,[8] June 4-7, 1962,
3. Development, growth, and state of atomic energy industry,[9] February 20-21, 1963,
4. Fallout, radiation standards, and countermeasures,[10] June 3-6, 1963.

2.2.4 State Activities in Atomic Energy

The activities of the various states in the regulation of radiation hazards are described in the following quotation from the AEC publication Safety Standards:[11]

"Development of atomic energy for peaceful purposes in the last two decades brought with it the need to protect from radiation hazards the persons who work with it or are otherwise likely to be exposed to ionizing radiation. It was evident that special health and safety hazards were involved and special protective regulation necessary.

"Early regulations were issued in some States under general safety authority already existing. For instance, in 1945, the Arkansas State Board of Health issued a code that prescribed 'minimum sanitary requirements for the protection of health of all employees,' referring specifically to 'radiation' and 'radioactive materials.' Effective in 1947, an Ohio Public Health Council code included radiation exposure limits for X-ray, radium, and radon. In 1952, a New Jersey State Department of Health code required that all radiation sources be 'shielded, transported, handled, used and kept in such manner as to prevent

all users thereof and all persons within effective range thereof from being exposed to excessive dosage of radiation.'

"In 1954, the Federal Government took an important step when Congress enacted an amendment to the Atomic Energy Act of 1946. One purpose of the new act (designated as the Atomic Energy Act of 1954) was to provide a program to 'encourage widespread participation in the development and utilization of atomic energy for peaceful purposes to the maximum extent consistent with the common defense and security and with the health and safety of the public.' The act specified that the licenses issued by the Atomic Energy Commission could cover any type of utilization or production facility which was sufficiently developed to be of practical value for industrial or commercial purposes, and it directed that the licenses be subject to safety standards to protect health and minimize danger to life or property.

"About the same time, 'model codes' containing suggested language for State radiation-control legislation were issued by several groups, among them the Council of State Governments, the National Committee for Radiation Protection, the New England Committee on Atomic Energy, and the University of Michigan Law School.

"Then too, the States began to realize that studies of the problems involved and coordination of atomic energy activities were essential. In 1955, six States (Connecticut, Illinois, Maine, Michigan, New Hampshire, and Rhode Island) adopted laws authorizing studies to be made in the field of atomic energy developments, including consideration of the need for legislative changes because of such developments. Other States adopted similar laws in the next several years: for example, Massachusetts, New Jersey, and South Carolina in 1956; Tennessee in 1957; Kentucky in 1958; and Alaska, Kansas, Missouri, and Texas in 1959. Laws in Arkansas, Florida, Ohio, and Washington, in 1957, provided for studies to be made and for coordination of atomic energy activities. Other States providing for coordination included Connecticut and New York in 1955, and California, North Carolina, and Oklahoma in 1959.

"Congress, in a 1959 amendment to the Atomic Energy Act of 1954, authorized the Atomic Energy Commission under certain conditions to make agreements with individual States, permitting the latter to exercise control over certain specified sources of radiation. This gave added impetus to the States to pass more comprehensive legislation for the actual control of activities involving radiation and, since 1959, 29 States have passed new laws or amended existing ones. Many provisions in these laws are based on the studies made by the States in the previous few years.

"At present 42 States have laws or regulations specifically designed to control radiation hazards. [See following tabulation]

States With Radiation Hazards Control*

Alabama	Maine	North Dakota
Alaska	Maryland	Ohio
Arkansas	Massachusetts	Oklahoma
California	Michigan	Oregon
Colorado	Minnesota	Pennsylvania
Connecticut	Mississippi	South Carolina
Delaware	Missouri	South Dakota
Florida	Nebraska	Tennessee
Idaho	Nevada	Texas
Illinois	New Hampshire	Virginia
Indiana	New Jersey	Washington
Kansas	New Mexico	West Virginia
Kentucky	New York	Wisconsin
Louisiana	North Carolina	Wyoming

*See last paragraph of this article.

"These have certain major features in common, although not all of the provisions are found in each of the laws. These features include rule-making authority, licensing or registration requirements, or both, recordkeeping requirements, and naming a specific regulatory agency. The laws of some States authorize the Governor to enter into agreement with the Federal Government for transfer to the State of certain AEC responsibilities in connection with the control of sources of ionizing radiation; and authorize the regulatory agency to enter into agreements with the Federal Government, other States, or interstate agencies for cooperative inspections or performance of other radiation control functions.

"Rulemaking Authority

"Authority to make rules for radiation protection is specific in 35 States. Under such authority, at least 24 of the States have issued safety codes. Four additional States have issued radiation codes under their general safety rulemaking authority.

"There is considerable variance among the provisions of the radiation codes of the States. Requirements that are commonly found include: that the employer furnish instruction and training in the use of all necessary safeguards and procedures to employees who handle radioactive material or operate machines that produce radiation, and that he furnish safety devices, protective clothing, and appropriate personnel monitoring equipment for all persons for whom there is a reasonable possibility of their receiving amounts of radiation in excess of some percentage of the maximum permissible amounts specified.

"Registration and Licensing

"Of the 42 States, all but 2 provide for either registration or licensing, or both, by the State regulatory agency of the 'source of ionizing radiation,' 'operators of a radiation installation,' or 'all who possess or use radiation producing machines or devices or equipment utilizing by-product, source, special nuclear materials,' or similarly described persons or processes concerned with radioactive materials.

"Thirty-six States provide for registration and 24, for licensing, either by statutory requirement, statutory authorization, or regulation. As mentioned above, some of these States require both registration and licensing.

"Recordkeeping

"Two principal types of recordkeeping are required in the laws: (1) records of the sources of radiation and (2) records of personal exposure to radiation, termed 'personnel monitoring.'

"The laws of 16 States require records of the sources of radiation and the disposal or transfer thereof. In most of these, the provisions are worded similarly, requiring persons who acquire, possess, or use sources of ionizing radiation to maintain records relating to their receipt, storage, transfer, or disposal, and such other records as the regulatory agency may deem necessary.

"The personnel monitoring provision requires each person who possesses or uses a source of ionizing radiation to maintain appropriate records showing the radiation exposure of individuals for whom personnel monitoring is required by rules and regulations of the regulatory agency.

"Administrative Agency

"Of the 42 States, the labor department is the administrative agency in one, Wisconsin. The labor department and the industrial accident board have joint responsibility in Idaho. In Massachusetts and New York, the health department is responsible for the public health aspects and the labor department for the protection of employees in industrial establishments; however, the activities of the two departments are coordinated through a separate agency. In South Carolina, the Governor, when he determines that the public health and safety so require, is authorized to designate the health department as the regulatory agency. In the other 37 States, the health department is designated as the regulatory agency.

"Federal-State Agreements

"As already mentioned, the 1959 amendment (Public Law 86-373) to the Atomic Energy Act authorizes AEC, upon request by the State, to enter into an agreement with the Governor providing for release to the State of certain aspects of AEC's licensing and regulatory authority over radiation sources.

Such agreements are contingent upon a finding by AEC that the State's regulation and control program is adequate and compatible with that of AEC.

"The criteria for compatibility of the State's program with AEC's include the concept of comprehensiveness. This is interpreted to mean that the State should regulate all sources of ionizing radiation and not limit its program to the segment which the AEC may legally transfer to the State under Public Law 86-373.

"Twenty-seven States have authorized such Federal-State agreements, and the Atomic Energy Commission reports that six of these have concluded agreements, thus transferring certain responsibilities for radiation control to Arkansas, California, Kentucky, Mississippi, New York, and Texas.

"Southern Interstate Nuclear Compact

"In 1958, at the 24th annual meeting of the Southern Governors' Conference, a project was approved to create the Nation's first regional interstate compact on atomic energy. The Regional Advisory Council on Nuclear Energy, created by the Governors' Conference in 1956, had recommended the Compact.

"The Southern Interstate Nuclear Compact declares that the proper employment of nuclear energy can assist substantially in the industrialization of the South, and that optimum benefit from an acquisition of nuclear resources and facilities requires systematic encouragement, guidance, and assistance from the party States on a cooperative basis.

"The Compact creates the Southern Interstate Nuclear Board, composed of one representative from each member State. Among its duties, the Board is empowered to encourage the development and use of nuclear energy facilities, and to study and recommend changes in industrial health, safety, and other laws and regulations of the party States.

"The Compact lists 16 Southern States which are eligible to join; it was to become effective when enacted by 7 of the States, and approved by the U. S. Congress. It went into effect following approval of Public Law 87-563, July 31, 1962. The following 13 States have become members: Alabama, Arkansas, Florida, Georgia, Kentucky, Louisiana, Maryland, Mississippi, South Carolina, Tennessee, Texas, Virginia, and West Virginia.

"In 1963, bills proposing membership were introduced into the legislatures of the remaining three eligible States; those in North Carolina and Oklahoma were not passed. The Delaware bill is still pending, as the 1963 legislative session in that State was carried over into 1964.

"1964 Legislative Developments

"Since the foregoing analysis was made, and as this issue goes to press, further evidence of continuing interest and activity comes from 3 additional States. Laws were enacted by the legislatures of Arizona and Georgia (States which

formerly had no radiation control legislation) and in Virginia (which had a registration requirement for certain radiation sources but no other provisions) to provide for comprehensive radiation control by the States. These laws designate a regulatory agency, giving it rulemaking authority, and require licensing and registration and recordkeeping. They also give the Governor authority to enter into an agreement with the Federal Government for the State's assumption of control of radiation hazards."*

States having entered into agreements with the AEC for transfer of responsibilities are listed below, along with the date of the agreement and designation of the responsible state agency:

State	Date of Agreement with AEC	Responsible State Agency
Arkansas	July 1, 1963	State Board of Health
California	July 1, 1962	State Department of Public Health
Kentucky	March 26, 1962	Kentucky Atomic Energy Authority
Mississippi	July 1, 1962	State Board of Health
New York	October 15, 1962	Office of Atomic Development
Texas	March 1, 1963	State Department of Health

2.3 FEDERAL LICENSING AND AUTHORIZATION PROCEDURES

2.3.1 General

Licensing and authorization of a reactor installation are usually accomplished in two major steps: the issuance of a construction permit early in the history of the project and the issuance of an operating license upon the successful completion of fabrication. A provisional license is frequently issued for a specified period of time, and upon the successful completion of trial runs, an operating license is issued.

Before a license is granted by the Commission's Division of Reactor Licensing (DRL), the Division must be satisfied that the facility as designed and fabricated and as proposed to be operated will not result in undue hazard to the health and safety of the public. The reactor safety analysis reports** submitted by the applicant are the principal documents upon which the Commission (and the ACRS, as applicable) base their reviews.

---

*"Note: This summary was prepared from sources currently available in the Bureau of Labor Standards. Further details on this subject are given in Fact Sheet No. 9-B, 'Brief Summary of State Laws and Regulations for the Control of Radiation Hazards,' Division of State Services, Bureau of Labor Standards."

**The previous terminology was "hazards summary report."

Throughout the course of the review of a nuclear facility as part of the procedure leading to a construction permit or an operating license, copies of all pertinent documents submitted by the applicant or prepared by the AEC are filed in the Public Document Room, 1717 H Street, Washington 25, D. C., where they may be examined.

A guide to the purpose, organization, and contents of safety analysis reports has been prepared by DRL.[12] The material that follows is intended to be a guide to codes, criteria, and regulations as applied to containment and should not be construed as an interpretation of Commission regulations or the specific process of evaluating the safety of a given reactor application.

2.3.2 Code of Federal Regulations

All federal regulations pertaining to atomic energy are published in Atomic Energy Rules and Regulations, Title 10, Code of Federal Regulations.[13] The Code is a loose-leaf document because continual revisions are necessary to keep pace with an inherently dynamic situation. The following parts are pertinent to the subject of codes, criteria, and regulations:

1. Part 20 Standards for Protection Against Radiation
2. Part 50 Licensing of Production and Utilization Facilities
3. Part 100 Reactor Site Criteria
4. Part 115 Procedures for Review of Certain Nuclear Reactors Exempted from Licensing Requirements

The Commission regulations are, in effect, summarized in the subsequent sections of this chapter. Proposed regulations are published in the Federal Register for comments, and the comments are reviewed. When deemed advisable, they are incorporated into the final version of the regulation, which is then placed in effect by decree.

2.3.3 Construction Permit

As discussed in Part 50 of the Code, "Licensing of Production and Utilization Facilities," a permit must be issued by the AEC before construction of a "utilization facility" may commence. "Utilization facility" is defined in the Code, Sect. 50.2(b), as any nuclear reactor other than one designed or used primarily for the production of plutonium, in which event the reactor would be a production facility under Sect. 11t of the Act and Sect. 50.2(a) of the Code. Reactors are licensed under Sect. 103, 104, and 185 of the Act. The permit or license is explicit in setting out the conditions under which the facility may be constructed and operated. The permit or license also usually contains the authority to receive and use special nuclear material in certain amounts, source material as required by the type of facility, and certain by-product material that may be produced incidentally by operation of the facility. The term "construction" does not include site exploration, site excavation, preparation of the site for construction of the facility, or construction of roadways, railroad

spurs, and transmission lines. In addition, the term "construction" does not include construction of nonnuclear facilities (such as turbine-generators and turbine buildings) and temporary buildings, such as construction equipment storage sheds.

There are several steps involved in the issuance of a construction permit; in the typical case they would include the following:

1. application for a construction permit, submittal of a preliminary safety analysis report (also called a site evaluation report because of the function which it is intended to serve),
2. review of case by Commission staff (DRL),
3. review of case by Advisory Committee on Reactor Safeguards,
4. public hearing before an Atomic Safety and Licensing Board appointed by the Commission,
5. granting or denial of the construction permit.

The above list is not intended to imply that the review procedures follow in the sequence indicated without any intermediate steps. Following steps 2 or 3 or both the applicant is frequently asked to supply additional information to supplement that in the preliminary safety analysis report. The application is then evaluated in light of this additional information, which usually becomes a part of the license application.

The request for a construction permit is made to the Commission early in the history of the project. As the name implies, it is a request for authorization to begin fabrication and erection of the reactor complex. A preliminary safety analysis report is submitted with the request. Its purpose is to provide sufficient information to permit an evaluation of the potential hazards that might be encountered during normal operation, as well as the consequences of these accidents, including the maximum credible accident (mca). It should contain as much meaningful information concerning the installation and safety status as is practical to develop, considering the conceptual state of the design. Some areas of major importance that should be covered in the report include descriptions of the following:

1. reactor site,
2. containment system,
3. reactor,
4. primary coolant system,
5. power conversion system,
6. instrumentation and control systems,
7. accidents, potential hazards, maximum credible accident, and detailed consideration of proposed safeguards.

At the construction permit stage all design details and reactor behavior may not be firmly established. The applicant is thus expected to indicate some upper boundary for the hazards so that subsequent systematic analyses will (in all probability) show credible accidents to be below the prescribed upper boundary.

The application for a construction permit, accompanied by a preliminary safety analysis report, is submitted to the local AEC Operations Office as the first formal step in the licensing process. The application and report, with AEC Operations Office review comments and recommendations,

are transmitted to the Division of Reactor Licensing. The state in which the facility is to be located is also notified at this time.

Concurrent with the review of the preliminary safety analysis report by the Commission staff, a review is initiated by the Advisory Committee on Reactor Safeguards. The applicant is usually requested to discuss the report with the Committee. If the Commission staff and the ACRS arrive at a favorable decision, the Commission is required to hold a public hearing, as provided for by a 1957 amendment to the Atomic Energy Act.

The public is notified of the intent to hold a hearing through the publication of a notice in the Federal Register. Notice is also given to the chief executive of the state or county in which the project is to be located. The hearing is held no sooner than 30 days after publication of the notices. It provides the opportunity for the departments of the state in which the reactor complex is to be situated, as well as interested persons, to express their position for the public record of the hearing.

Following the presentation of the applicant at the hearing, an analysis of the proposed project, which includes the findings of the ACRS, is presented by the Commission's regulatory staff. Upon completion of the presentations, the Hearing Examiner takes the matter under consideration and subsequently delivers an Intermediate Decision. The decision becomes final after a prescribed period of time unless the Commission decides to review the matter further. If the decision is favorable, the Division of Reactor Licensing is authorized to grant the construction permit for the designated site. When an applicant has not initially supplied all of the technical information required to complete the application and support the issuance of a construction permit that approves all proposed design features, the Commission may issue a provisional construction permit (for additional information, see Part 50 of the Code).

The issuance of a construction permit does not automatically assure the applicant of the right to an operating license. It is granted on the basis of a reasonable assurance that the proposed facility can be designed, built, and operated in a manner that will not result in undue hazard to the health and safety of the public.

2.3.4 Operating License

Application for an operating license is made when the construction of a reactor facility has progressed to the point where the time for initial operation can be reliably predicted. A final safety analysis report is usually submitted with the application for an operating license. The final safety analysis report should emphasize those aspects of the facility as constructed and the plans and procedures for operation actually prepared for the as built facility insofar as they directly or indirectly affect safety. The final safety analysis report must also, in particular, assess with a greater certainty the likelihood and consequences of potential accidents and show that adequate public safety is maintained.

The processing of the application for an operating license follows substantially the same path as that previously described for the construction permit, specifically:

1. application for an operating license, submittal of a final safety analysis report,
2. review of case by Commission staff,
3. review of case by Advisory Committee on Reactor Safeguards,
4. inspection of facility by Commission personnel,
5. public hearing before an Examiner appointed by the Commission,
6. granting or denial of an operating license.

In contrast to the construction permit, which is based on the applicant meeting certain qualifications and demonstrating that there is reasonable assurance that the facility can be built and operated without undue hazard to the health and safety of the general public, the operating permit is based on the applicant demonstrating that the facility was built and will be operated without undue hazard to the health and safety of the public.

2.3.5 Containment Description in Final Safety Analysis Report

The preceding discussion pertains to the entire reactor system and was presented because the adequacy of a proposed containment structure depends upon the system contained. Further, the relationship of the entire system to the containment structure is important when considering codes and criteria.

The final safety analysis report is the major source of information upon which the Commission and the Advisory Committee on Reactor Safeguards base their judgement as to whether or not a license or authorization for construction or operation is warranted. In this respect, it should be of paramount interest to an applicant to submit a report adequate for the purpose it will serve. An outline of the material concerning the containment system that would be expected to be included in the report for a typical nuclear power facility is presented in Appendix B, which was taken from an August 28, 1962 draft copy of an AEC Licensing Guide[12] entitled, "Purpose, Organization, and Contents of Hazards Summary Reports for Power Reactors." Appendix A is not intended to serve as an interpretation of Commission regulations but, rather, as a convenient list of important items that require consideration on the subject of containment.

Obviously not all reactor systems are similar, and they will not have the same containment system. Consequently, the outline in Appendix A is not necessarily complete. The material presented in the safety analysis report on containment should provide information appropriate for a determination of the effectiveness of the containment system in limiting the release of radioactive materials.

2.4 CODES AND REGULATIONS FOR STEEL CONTAINMENT STRUCTURES

2.4.1 General

Reference is made to design codes in the AEC Licensing Guide,[12] which have generally been interpreted to mean nationally recognized standards. In the case of steel pressure containment shells, the design codes would be the applicable Boiler and Pressure Vessel Codes published by the American Society of Mechanical Engineers. The design of a pressure containment shell based on an ASME code is one of the means of demonstrating partial compliance with Title 10 of the Code of Federal Regulations, but designing and fabricating to an ASME code does not intrinsically constitute full compliance with the containment requirements of Title 10 of the federal code. Design codes should be taken as representing only minimum requirements, and each containment system should be examined for conformance to governing legal criteria and for adequacy of provisions for preservation of public safety. There are no codes uniquely applicable to multibarrier containment systems, but existing codes generally cover these needs. The codes and regulations discussed in this section (2.4) are applicable to containment vessels or dry wells of reactor systems utilizing pressure-suppression or vapor-condensation containment, as well as to pressure containment shells.

2.4.2 ASME Codes

In the early 1800's there was a mounting toll of disastrous boiler explosions in the United States. Very little legislative action was taken until 1907, at which time Massachusetts enacted the first code of rules for the construction of steam boilers. Shortly thereafter several other States did likewise, but the laws were different in the various States. Thus the boilers could not be freely shipped between the jurisdictional areas and confusion resulted.

The need for uniform rules for construction became apparent. In 1911, the American Society of Mechanical Engineers appointed a committee to prepare a set of rules for the construction of steam boilers and unfired pressure vessels. (The committee is known today as the Boiler and Pressure Vessel Code Committee.) The first ASME Code was approved and published in 1915.

The ASME recognized that compliance with the new code could be accomplished only by laws that might be adopted by the states and municipalities. A Conference Committee was therefore established to cooperate with the states and to obtain their assistance. It consisted of chief inspectors of all states and cities that assumed legal jurisdiction over boilers and pressure vessels.

Shortly after the publication of the first ASME Code in 1915, the Committee was burdened with inquiries regarding the intent of certain rules. To handle the problems the Committee issued Code Interpretations that made the replies a matter of public record. Periodically, addenda to the ASME Codes are prepared that incorporate many of the existing code interpretations, and the interpretations are then annulled. On the

average of once every three years the codes are republished to incorporate the existing addenda and code interpretations.

The ASME Codes do not have a legal status. However, many states and cities of the United States and Provinces of Canada have adopted one or more sections and, thus, by reference, the Codes assume a legal status.

Many containment vessels have been built in accordance with Section VIII of the ASME Unfired Pressure Vessel Code[14] and Code Cases 1270N, 1271N, and 1272N. Since a new ASME Code for the construction of nuclear vessels (Section III) has been released, the cases have been annulled and Section VIII will apply only to the extent it is cross referenced by Section III. The new code was released in March 1964, but the publication is dated 1963 because it was adopted at that time.

The new ASME Boiler and Pressure Vessel Code, Section III, Rules for Construction of Nuclear Vessels,[15] gives rules for three classes of vessels; namely, Class A (reactor and primary vessels), Class B (containment vessels), and Class C (vessels other than Class A and Class B, i.e., secondary vessels). The rules for Class B vessels apply when the design pressure is greater than 5 psi. Section III covers, in considerable detail, (1) design, (2) examination of materials in the product form, (3) inspection of vessel during fabrication, (4) welding and weld inspection, and (5) the use of material with adequate low-temperature notch toughness. In addition, it clearly defines the responsibilities of the purchaser, fabricator, and the authorized (Code) inspector.

The design philosophy of the new ASME Code is presented in a document entitled "Criteria of Section III of the ASME Boiler and Pressure Vessel Code for Nuclear Vessels." It is included here as Appendix C. Although this document discusses fatigue, it is to be noted that the Code does not require a fatigue analysis for the conventional containment vessel. Because of its pertinence, Article I of Section III is also included as Appendix D.

2.4.3 ASME Code Cases

At the present time two ASME Codes are available for the design of containment vessels; namely, Sections III and VIII of the Boiler and Pressure Vessel Code plus Cases 1270N-5, 1271N, and 1272N-5. Altogether, there are seven Code Cases that apply to the design of nuclear vessels and which are intended to be used in conjunction with one or more of the following ASME Boiler and Pressure Vessel Codes:

Section I	Power Boilers
Section VIII	Unfired Pressure Vessels
Section IX	Welding Qualifications

The cases contain the suffix N, which indicates "for nuclear application." The latest nuclear case interpretations, which apply to Sections I, VIII, and IX, but not to Section III, are:

Case 1270N-5	General Requirements for Nuclear Vessels
Case 1271N	Safety Devices
Case 1272N-5	Containment and Intermediate Containment Vessels

Case 1273N-7	Nuclear Reactor Vessels and Primary Vessels
Case 1274N-10	Special Material Requirements
Case 1275N	Inspection Requirements
Case 1276N-2	Special Equipment Requirements

These nuclear case interpretations were annulled on January 12, 1965. The delay between the adoption of Section III and this annullment was to allow adoption of Section III by states, cities, and counties of the United States having boiler or pressure vessel laws (see Sect. 2.4.7). Since Section III was written specifically for the design, construction, and fabrication of nuclear vessels, its use is recommended whenever possible. The annulled cases are discussed below.

2.4.3.1 Case 1270N-5

Case 1270N-5 is an introductory case that defines the various vessels in a reactor system; for example, primary, calandria, containment, intermediate containment, and secondary. This case emphasizes that where differences exist between the requirements of the cases and the requirements of Section I or Section VIII, the cases take precedence over the Code rules for the particular subject covered.

2.4.3.2 Case 1271N

The literal application of Sections I and VIII of the Code to safety and relief valves and to pressure-indicating devices would be hazardous. Case 1271N covers those modifications of the various safety requirements that are designed to avoid these hazards. Pressurized-water and boiling-water reactors and their containment vessels are considered.

2.4.3.3 Case 1272N-5

Case 1272N-5 provides design requirements for containment and intermediate containment vessels. Special consideration is given to the use of materials with adequate low-temperature notch toughness when the containment vessel is exposed to the atmosphere. Radiographic and stress relief requirements are also given. This case gives the procedure for waiving inspection during the pneumatic test of welded joints in the lower part of the vessel that were covered by concrete during construction.

2.4.3.4 Case 1273N-7

Case 1273N-7 describes special requirements for primary reactor vessels; for example, membrane and thermal stresses, bolt design criteria, penetrations, radiation effects, mechanical shock, vibratory loading, and welding.

2.4.3.5 Case 1274N-10

A compilation of special material requirements for use in construction of nuclear vessels is presented in Case 1274N-10. The materials covered include AISI type 403 modified forgings, castings, bolting, types 304L and 316L stainless steel, and Inconel.

2.4.3.6 Case 1275N

Case 1275N is intended to cover all special inspection requirements, although to date this inquiry and the reply pertain only to ultrasonic inspection of welded joints.

2.4.3.7 Case 1276N-2

Case 1276N-2 covers the use of expansion joints on primary and secondary vessels.

2.4.3.8 Cases Applicable to Section III

Since Section III is not complete, new cases will be added from time to time. Specifically, cases are to be added for materials not yet covered by ASTM Standards and to cover the high-temperature range of all materials. The following cases have been issued and apply to nuclear construction under Section III:

Case 1330 Special Equipment Requirements (Expansion Bellows)
Case 1331 Nuclear Vessels in High Temperature Service
Case 1332 Requirements for Steel Forgings
Case 1333 Requirements for Steel Castings
Case 1334 Requirements for Corrosion-Resisting Steel Bars
Case 1335 Requirements for Bolting Materials
Case 1337 Requirements for Special Type 403 Modified Forgings and Bars

The new code cases no longer carry the suffix "N" to indicate "for nuclear applications."

Copies of the ASME Code and the various case rulings may be obtained from the American Society of Mechanical Engineers, 345 East 47th Street, New York 17, New York. The ASME Codes and Case Interpretations are subject to revision, and it is important that the latest revision be consulted in any design (see Sect. 2.4.7). The ASME maintains a Case Interpretation service that supplies subscribers with copies of these revisions as they are published.

2.4.4 ASME Provisions for Steel Containment Vessels at Pressures Under 5 psi

Section VIII of the ASME Boiler and Pressure Vessel Code states that vessels with an internal pressure of less than 15 psi are not considered

to be within the jurisdiction of the Code. However, the Code permits ASME Code stamping of such vessels provided they conform in all respects with the applicable rules. The same philosophy appears to apply to containment vessels built under the rules of Case Interpretation 1272N-5. Section III, Rules for Construction of Nuclear Vessels, applies to containment vessels with a design pressure greater than 5 psi.

Steel containment vessels with a design pressure of less than 5 psi may be designed to meet the intent of Case 1272N-5 or Section III whether or not Code stamping is possible. The materials, design, fabrication, and inspection requirements are valid and essentially independent of the design pressure of the vessel. Special consideration must be given to low-pressure containment vessels, both above and below 15 psi, since an unstable structure may result if only pressure stresses and stresses due to imposed loads are considered. Frequently, the ability of the structure to support its own weight (plus wind and snow loads) will establish the design of a low-pressure, pressure-containment vessel.

2.4.5 Manufacturers of ASME Code Boilers and Pressure Vessels

Only those manufacturers who possess an ASME "Certificate of Authorization" are permitted to possess and apply the appropriate Code symbol to boilers and pressure vessels. Any manufacturer of boilers and pressure vessels may apply to the Boiler and Pressure Vessel Committee of the American Society of Mechanical Engineers for permission to build ASME Code equipment. Permission to use the stamp may be granted or withheld by the Society (ASME) at its absolute discretion. If the stamp is granted, the applicant must agree to use it according to the rules and regulations of the Code and must not permit its use by any other manufacturer. Paragraphs UG-116 (m) of Section VIII, P-332 of Section I, and N-831 of Section III of the ASME Boiler and Pressure Vessel Codes describe the "Certificates of Authorization." Lists of manufacturers holding "Certificates of Authorization" are available from ASME and the National Bureau of Casualty Underwriters. The National Board of Boiler and Pressure Vessel Inspectors also publishes a list of manufacturers who have ASME "Certificates of Authorization" and who are registered with the National Board as ASME National Board boiler and pressure vessel fabricators.

2.4.6 The National Board

The ASME Codes state in part: "Only a state inspector, a municipal inspector, or an inspector regularly employed by an insurance company, may be accepted as a qualified inspector. The inspector shall not be in the employ of the manufacturer. The qualifications of an inspector shall have been determined by examinations as prescribed under the rules of any state or municipality which has adopted this Code... ."

Most authorized inspectors hold commissions issued by the National Board of Boiler and Pressure Vessel Inspectors. The National Board of Boiler and Pressure Vessel Inspectors is composed of chief inspectors of

states and municipalities in the United States and of provinces in the Dominion of Canada that have adopted one or more sections of the Boiler and Pressure Vessel Code.

Two of the prime objects of the organization are:

1. to promote uniform enforcement of boiler and pressure vessel laws and rules, and
2. to promote one uniform code of rules for, and one standard stamp to be placed on, all boilers and pressure vessels constructed in accordance with the requirements of that code, and one standard of qualifications and examinations for inspectors who are to enforce the requirements of that code.

In general, ASME Code vessels stamped "National Board" are acceptable in most jurisdictions and may be shipped freely between states and municipalities. A few jurisdictions require, however, that the inspector hold a commission of the particular state. Purchasers and fabricators of ASME Code vessels should consult the law of the state that has jurisdiction over a particular vessel for pertinent rules regarding construction and stamping. The National Bureau of Casualty Underwriters, 125 Maiden Lane, New York 38, New York, has prepared a helpful publication entitled "Synopsis of Boiler and Pressure Vessel Laws, Rules and Regulations by States, Cities, Counties, and Provinces — United States and Canada."

2.4.7 Tabulation of States, Cities, and Counties Having Boiler or Pressure Vessel Laws

The issuance of a construction permit and, subsequently, an operating license by the U. S. Atomic Energy Commission is predicated upon the requirement that the containment vessel (and the other reactor components) comply with Title 10 of the Code of Federal Regulations. The applicant for a permit for a privately-owned reactor facility is also obliged to comply with all pertinent laws relating to boilers and pressure vessels of the jurisdiction in which the reactor system is to be located. States, cities, counties, and provinces that have laws relating to boilers and pressure vessels have either adopted the ASME Codes by reference or have written their own codes using the ASME Codes as the basis of their law.

None of the states have accepted Section III of the ASME Boiler and Pressure Vessel Code at this time. Therefore it may not be legally possible to follow this section of the code until such time as it is adopted. Since Section III is more comprehensive than the Nuclear Case Interpretations, it should be possible to design, fabricate, and test (in the interim) in accordance with it and have the vessel code stamped according to the applicable "N" Case. However, laws are subject to change and some jurisdictions do not automatically accept ASME Case Interpretations, so the user should refer to the state laws and boards for particular details. A summary of all states, cities, and counties of the United States that have boiler or pressure vessel laws is presented in Table 2.1.

Table 2.1. Rules for Construction and Stamping or for Field Inspection of Boilers and Pressure Vessels

Jurisdiction	Boilers	Pressure Vessels	Cognizant Department
Alabama	No	No	
Alaska	Yes	Yes	Department of Labor
Arizona	No	No	
Arkansas	Yes	Yes	Department of Labor
California	Yes	Yes	Department of Industrial Relations
Colorado	Yes	No	Industrial Commission
Connecticut	Yes	No	Labor Department
Delaware	Yes	No	Board of Boiler Rules
District of Columbia	Yes	Yes	Department of Licenses and Inspections
Florida	No	No	
Georgia	No	No	
Hawaii	Yes	No	Department of Labor and Industrial Relations
Idaho	Yes	Yes	Industrial Accident Board
Illinois	Yes	No	Department of Public Safety
Indiana	Yes	Yes	Indiana Boiler and Pressure Vessel Board
Iowa	Yes	Yes	Bureau of Labor
Kansas	Yes	Yes	Department of Labor
Kentucky	Yes	No	Department of Public Safety
Louisiana	Yes	No	Department of Labor
Maine	Yes	No	Department of Labor and Industry
Maryland	Yes	No	Department of Labor and Industry
Massachusetts	Yes	Yes	Department of Public Safety
Michigan	Yes	No	Department of Labor
Minnesota	Yes	Yes	Industrial Commission
Mississippi	No	No	Bureau of Industrial Hygiene and Factory Inspection
Missouri	No	No	
Montana	No	No	Industrial Accident Board
Nebraska	Yes	Yes	Department of Labor
Nevada	Yes	Yes	Industrial Commission
New Hampshire	Yes	No	Department of Labor
New Jersey	Yes	Yes	Department of Labor and Industry
New Mexico	No	No	
New York	Yes	No	Department of Labor
North Carolina	Yes	Yes	Department of Labor

Table 2.1. (continued)

Jurisdiction	Boilers	Pressure Vessels	Cognizant Department
North Dakota	Yes	Yes	Workmen's Compensation Bureau
Ohio	Yes	Yes	Department of Industrial Relations
Oklahoma	Yes	No	Department of Labor
Oregon	Yes	Yes	Bureau of Labor
Pennsylvania	Yes	Yes	Department of Labor and Industry
Rhode Island	Yes	No	Department of Labor
South Carolina	No	No	
Tennessee	Yes	Yes	Department of Labor
Texas	Yes	No	Bureau of Labor Statistics
Utah	Yes	Yes	Industrial Commission
Vermont	Yes	Yes	Department of Industrial Relations
Virginia	Yes	Yes	
Washington	Yes	Yes	Department of Labor and Industries
West Virginia	Yes	No	Department of Labor
Wisconsin	Yes	Yes	Industrial Commission
Wyoming	No	No	
Albuquerque, New Mexico	Yes	No	Department of Public Works
Buffalo, New York	Yes	Yes	Department of Public Works
Chicago, Illinois	Yes	Yes	Department of Inspection of Steam Boilers
Dearborn, Michigan	Yes	Yes	Department of Public Works
Denver, Colorado	Yes	Yes	
Des Moines, Iowa	Yes	No	Department of Heating and Ventilating Inspection
Detroit, Michigan	Yes	Yes	Department of Buildings and Safety Engineering
East St. Louis, Illinois	Yes	Yes	
Greensboro, North Carolina	Yes	Yes	Department of Public Works
Kansas City, Missouri	Yes	Yes	Public Works Department
Los Angeles, California	Yes	Yes	Building and Safety Department
Memphis, Tennessee	Yes	Yes	Department of Public Service
Miami, Florida	Yes	Yes	Building Department
Miami Beach, Florida	Yes	Yes	City Building Department

Table 2.1. (continued)

Jurisdiction	Boilers	Pressure Vessels	Cognizant Department
Milwaukee, Wisconsin	Yes	Yes	Department of Building Inspection and Safety Engineering
Mount Vernon, New York	Yes	Yes	Department of Boiler Inspection
New Orleans, Louisiana	Yes	Yes	Department of Safety and Permits
New York City, New York	Yes	No	Department of Buildings, Boiler Division
Niagara Falls, New York	Yes	No	City Executive Department
North Miami Beach, Florida	Yes	Yes	Department of Boiler Inspection
Oklahoma City, Oklahoma	Yes	Yes	Building Department
Omaha, Nebraska	Yes	Yes	Building Department
Phoenix, Arizona	Yes	Yes	City Mechanical Section
Richmond, Virginia	Yes	Yes	Department of Public Safety
St. Joseph, Missouri	Yes	Yes	City Boiler Inspection Department
St. Louis, Missouri	Yes	Yes	Department of Public Safety
San Francisco, California	Yes	Yes	Department of Public Works
Seattle, Washington	Yes	Yes	Department of Buildings
Spokane, Washington	Yes	Yes	Department of Public Works
Tacoma, Washington	Yes	Yes	Department of Public Works
Tampa, Florida	Yes	Yes	Bureau of Plumbing, Gas, and Boiler Inspection
Tulsa, Oklahoma	Yes	Yes	Board of Commissioners
Tucson, Arizona	Yes	Yes	Inspection Division
University City, Missouri	Yes	No	City Manager
Yonkers, New York	Yes	No	Bureau of Steam Boiler Inspection
Panama Canal Zone	Yes	Yes	Panama Canal Company
Puerto Rico	Yes	Yes	Department of Labor
Arlington County, Virginia	Yes	No	Department of Inspection
Dade County, Florida	Yes	Yes	Planning, Zoning, and Building Department
Jefferson Parish, Louisiana	Yes	Yes	Department of Regulatory Inspections
St. Louis County, Missouri	Yes	Yes	Department of Public Works

2.4.8 Uniform Boiler and Pressure Vessel Laws Society, Inc.

The Uniform Boiler and Pressure Vessel Laws Society, Inc. is a nonpolitical, noncommercial, and nonprofit organization supported by its membership. Its objective is to secure uniformity in the laws, rules, or regulations and administration which affect the boiler and pressure vessel industry, inspection agencies, and users. The Society believes that such laws and rules should follow nationally accepted codes and standards. It recommends the ASME Boiler and Pressure Vessel Codes as the standards for construction and the Inspection Code of the National Board of Boiler and Pressure Vessel Inspectors for administration and inspection.

2.4.9 ASA Containment Vessel Standard

Subcommittee N6.2 of the American Standards Association Sectional Committee N6, Reactor Safety, has prepared a standard for the design of steel containment structures. It is titled, "Safety Standard for Design, Fabrication, and Maintenance of Steel Containment Structures for Stationary Nuclear Power Reactors." It is intended to cover containment structures for pressures both above and below 5 psi; some information not covered by ASME Case Interpretation 1272N-5 or by Section III of the ASME Boiler and Pressure Vessel Code is included. Because of its pertinence, it is included as Appendix E. It should be noted that requirements for periodic testing, means for extrapolation to other pressures, and testing under accident temperatures and wet atmospheres are not covered in the proposed standard.

2.4.10 Other Containment Vessel Codes

A number of standards, specifications, and codes are used in addition to the ASME Boiler and Pressure Vessel Code in special problem areas. The most prominent among these are:

1. PB 151987, "Tentative Structural Design Basis for Reactor Pressure Vessels and Directly Associated Components," available from the Office of Technical Services, U. S. Department of Commerce, Washington, D. C.
2. American Petroleum Institute (API) Tentative Standard 620, "Recommended Rules for the Design and Construction of Large, Welded Low-pressure Storage Tanks," available from the American Petroleum Institute, New York, N. Y.

2.4.10.1 Navy Code

Document PB 151987 is frequently referred to as the "Navy Code." It was prepared for application in the Naval Reactor Program, and it establishes general loading assumptions, performance and design criteria, and

essential minimum limitations for assuring acceptable structural reliability and safety of reactor pressure vessels and directly associated components. The code covers in considerable detail the calculation of pressure and thermal stresses and examples are provided.

Although PB 151987 was originally prepared for the Naval Reactor Program, it has been widely used for industrial reactor design because of the detailed provisions included therein. In ASME Case 1273N-7, for example, certain requirements are stated in general terms such as "due regard shall be given to the creep and stress-rupture properties...," "each design detail shall be carefully considered to provide against operational failure such as might occur from thermal stress...," and "... particular consideration shall also be given to materials, construction, and inspection... ." The ASME case places limits on thermal stresses and primary and secondary stresses produced by the design pressure, but detailed methods for calculating the stresses and combining them are not included. Conformance with the intent of such parts of Case 1273N-7 has often been based on the detailed requirements of the "Navy Code." Since Section III of the ASME Boiler and Pressure Vessel Code has been officially released, it is not expected that the Navy Code will have much further application.

2.4.10.2 API-ASME Code

In 1931 the American Petroleum Institute and the American Society of Mechanical Engineers cooperated in the formulation of the "API-ASME Code for Unfired Pressure Vessels for Petroleum Liquids and Gases." The first API-ASME Code was published in 1934 and was revised in 1936, 1938, 1943, and 1951. Although the code was primarily intended for vessels that would contain petroleum liquids and gases, it was also intended to cover other vessels integral with the petroleum industry's plants. In most respects the code was similar to the ASME Unfired Pressure Vessel Code except that it did not cover high alloy steels and nonferrous materials and it contained basic differences in inspection requirements.

By a joint declaration of ASME and API, the API-ASME Code was discontinued as of December 31, 1956. The ASME Code was then considered to adequately cover the petroleum industry's pressure vessel needs.

2.5 CODES AND STANDARDS FOR PRESSURE PIPING

Pressure piping in a nuclear facility frequently constitutes an integral part of the containment system because of the many piping penetrations in the vessel wall and the existence of entire subsystems external or internal to the containment vessel that should remain intact in the event of a reactor accident. The boundary between vessel and piping is usually defined by the code that is being consulted. In the case of the ASME Code, Section III states that

> "The jurisdiction of this Section of the Code is intended to include only the vessel and its appurtenances and

to terminate at the following points where connections are provided for attachment to piping which is external to the vessel:

(a) The first circumferential joint exclusive of the connecting weld in welded connections.

(b) The face of the first flange in bolted flange connections.

(c) The first threaded joint in screwed connections."

Nuclear piping design presently follows the rules of Section I of American Standard B 31.1-1955, Code for Pressure Piping, with addenda ($5.00, American Standards Association). Work is under way to revise Section I to include nuclear application, and this may eventually be published as a separate code. The ASA Sectional Committee B31, Code for Pressure Piping, sponsored by ASME, is presently working on a code for nuclear piping that will be similar in scope to the Boiler and Pressure Vessel Code, Section III. This committee is also responsible for revisions of the Piping Code and has issued a number of Piping Code Case Interpretations intended to make the Piping Code applicable to nuclear service. The Nuclear Case Interpretations are described below:

1. Case N-1 establishes the section of the Code to be used in nuclear power plant piping design and construction as well as what piping is to be considered as nuclear.

2. Case N-2 defines the requirements for valves used in nuclear piping systems.

3. Case N-3 covers the use of screwed connections as the only seal in a nuclear piping system.

4. Case N-4 establishes whether nuclear piping systems need to adhere to the temperature limit of the hydrostatic media at 100°F maximum set in section 1, paragraph 121C, of the Code.

5. Case N-7 gives a list of several types of stainless steel to be used and requirements for their use for aqueous-type power piping in nuclear energy installations under the rules of Section 1 of the Code.

6. Case N-8 handles the same questions raised in Case N-7, except that liquid sodium and sodium-potassium mixtures are considered.

7. Case N-9 defines conditions for the use of centrifugally cast austenitic stainless steel pipe in nuclear piping systems within the scope of Section 1.

8. Case N-10 considers the same basic question as Case N-9, except that it is for cast austenitic steel butt-welded fittings.

9. Case N-11 gives recommendations for means of providing for thermal expansion in a nuclear piping system.

10. Case N-12 gives the procedure for qualifying new material for use in nuclear piping systems.

All Nuclear Case Interpretations are published in the Mechanical Engineering journal, under the section Codes and Standards Workshop, as the interpretations of the Sectional Committee are released. The Piping Code has been adopted as mandatory by some regulatory agencies. Work is presently under way by the General Electric Company at San Jose[16-19] that deals with frequency and probability of piping failures and also modes of failure.

2.6 CODES AND REGULATIONS FOR CONFINEMENT STRUCTURES

A steel pressure vessel (for pressure containment) is the most common type of containment structure for power reactors in the United States. Since only limited experience is available with the use of confinement-type containment structures, no nationally recognized codes exist that deal specifically with confinement buildings.

Before a construction permit or an operating license is granted by the Commission, the Commission must be satisfied that the facility as designed and fabricated and as proposed to be operated will not result in undue hazard to the health and safety of the public. Therefore the burden of proof of the adequacy of a proposed containment scheme rests with the applicant and its performance must be demonstrated to the satisfaction of the Commission. The AEC has sponsored an experimental program at North American Aviation, Inc., on the containment performance of low-pressure buildings and their components.[20] However, these studies have not progressed to the point where a code can be formulated.

In lieu of specific codes the following are a few of the more important items that should be considered in the design of a confinement structure with a filtered or filtered and scrubbed exhaust:

1. The building must withstand the loads imposed by normal operation under the specified negative pressure or positive pressure conditions.
2. In-leakage for negative pressure designs and out-leakage for buildings with positive pressure designs must be controlled.
3. The exhauster capacity must be adequate to prevent a positive pressure from developing during the postulated maximum credible accident in structures designed to operate under a negative pressure. For buildings designed to withstand a positive pressure the building design pressure shall not be exceeded.
4. The high-efficiency particulate air filters, scrubbers, and adsorbers must effectively maintain their specified decontamination factors under performance conditions within the limits defined in the safety analysis reports upon which licensing by the Commission was based.

Construction of conventional buildings that house reactors and also serve as containment structures is usually based on the Uniform Building Code[21] or the Southern Standard Building Code.[22] The choice of codes is determined primarily by local ordinances. The Southern Code is utilized in the region east of the Mississippi River and south of the Ohio River and the State of Pennsylvania, whereas the Uniform Building Code is used in the rest of the United States.

The following standards may be referred to for additional information:

1. "Specification for the Design, Fabrication and Erection of Structural Steel for Buildings," $0.50, American Institute of Steel Construction, 101 Park Avenue, New York 17, N.Y., American Standard A57.1-1952.
2. "Building Code Requirements for Reinforced Concrete," $1.00, American Concrete Institute, P.O. Box 4754, Redford Station, Detroit 19, Michigan, American Standard A89.1-1957.
3. "Building Code Requirements for Masonry," $0.20, National Bureau of Standards, Superintendent of Documents, U.S. Government Printing Office, Washington 25, D.C., NBS Miscellaneous Publication 211, American Standard A41.1-1953.

4. "Light Gauge Steel Design Manual," $1.00, American Iron and Steel Institute, 150 East 42nd Street, New York 17, N.Y.

5. "Standard Specifications for Open Web Steel Joist Construction Shortspan Series," $1.30, Steel Joist Institute, 1346 Connecticut Avenue, N.W., Washington 6, D.C., ASA American Standard A87.1-1957.

6. "Standard Code for Arc and Gas Welding in Building Construction," $1.00, American Welding Society, 345 East 47th Street, New York 17, N.Y.

7. "National Design Specifications for Stress Grade Lumber and Its Fastenings," National Lumber Manufacturers Association, 1319 18th Street, N.W., Washington 6, D.C.

8. "National Electrical Code," $1.00, National Board of Fire Underwriters, 85 John Street, New York 38, N.Y.

9. "Heating, Ventilating and Air Conditioning Guide," $12.00, American Society of Heating and Air-Conditioning Engineers, 62 North Street, New York 13, N.Y.

10. "National Plumbing Code," $4.50, issued jointly by the U.S. Department of Commerce and the Housing and House Finance Agency, Office of Administration, Washington 25, D.C., American Standard A40.8-1955.

2.7 HIGH-EFFICIENCY FILTERS AS A PART OF CONTAINMENT

2.7.1 General

Reactor containment and confinement structures are used to contain the activity released by an accident to the extent that any leakage from the structure will be within tolerable limits. In some reactor confinement systems the pressure in the building is maintained at a low level by an exhaust system. Before the effluent is discharged to the atmosphere following an accident, it is treated to reduce activity to a tolerable level. Usually the particulate material is removed by high-efficiency particulate air filter units and iodine by a charcoal adsorber installed in the exhaust system. In such systems, the filters are as important as the confinement structure itself in limiting the release of activity and would therefore be subject to the same reliability requirements as imposed upon the containment vessel (see Sects. 1.2.3 and 8.9).

Some pressure containment systems use high-efficiency filters to filter the normal building air before it is exhausted to the stack. The filters must function efficiently and reliably, especially in the period between the detection of an accident and the time when all containment penetrations are closed. In this period the filters form an integral part of the containment scheme. There are, however, no codes to cover the performance of filter units in such instances. The information below summarizes briefly the present status of filter requirements.

2.7.2 Testing Individual New High-Efficiency Filters

A high-efficiency particulate filter consists of a continuous pleated filter medium installed and sealed within a suitable frame. One or more such units installed within a filter housing comprise the filter system. Such filters are capable of removing 0.3-μ particles with an efficiency of 99.97% or better under controlled conditions.

The efficiency of individual filters is checked by the manufacturer in accordance with MIL-STD-282.[23] In addition, participants in the atomic energy program are urged to have new filters checked by one of the two AEC Quality Assurance Stations.[24]

The efficiency test consists of confronting a filter with an aerosol of dioctyl phthalate with an average particle size of 0.3 μ. Efficiency is calculated from the concentration of the aerosol measured before it enters and after it leaves the filter. While such a test will give some assurance as to the initial integrity of the filter, it may not be significant as to the filter performance under accident conditions.

2.7.3 Determining Efficiency of Filter Systems

No standards or codes exist covering in-place testing of systems containing high-efficiency filters including either or both particulate filters and iodine absorbers. A few companies are testing particulate-filter systems in place by using a technique that is basically the same as that employed by the AEC Quality Assurance Stations for testing individual new filters, and an in-place iodine filter test was developed for testing the iodine adsorber efficiency in the N.S. SAVANNAH containment system.[25] The in-place particulate filter tests differ in the method of generating the aerosol of dioctyl phthalate. The thermal aerosol generators used by the AEC stations produce an aerosol with an average particle size of 0.3 μ. Since thermal generators are not suitable for field work, air-operated generators are usually used for testing installations in place.[26] While the air-operated units produce an aerosol with a slightly larger average particle size, the difference has been shown to be unimportant when evaluating filter systems.[27] Tacit approval has been given to the method which employs air-operated aerosol generators, since the results of numerous tests have been used and accepted as the basis of review by the Commission for licensing purposes.

The use of sound filters alone does not ensure having a filter installation with an adequate filtration efficiency or ensure its performance under accident conditions. The sound filters must be properly handled and properly installed in a structurally adequate housing[27,28] with due concern for corrosion problems and sealing to the filter container. The results of hundreds of in-place efficiency tests have disclosed the critical need for determing the filtration efficiency of filter systems with operating filters in place and for rechecking them at an established frequency. An even more important concern is the performance of the filter under accident conditions as opposed to normal conditions. The effects of shock, overpressure, temperature, fission-product heating, flow velocity, moisture,

and overloading must all be considered in establishing filter performance under accident conditions.

2.8 STATUS OF ACTIVITIES IN THE DEVELOPMENT OF NUCLEAR STANDARDS[29,30]

By the Atomic Energy Acts of 1946 and 1954, many areas of the nuclear industry were placed under regulatory control of the government because of military aspects and the possibility of catastrophic accidents. As technology advances, however, the extent of regulatory coverage is diminishing, and the regulations are being modified into voluntary standards. The development of nuclear standards in the United States is primarily the responsibility of the various technical societies, scientific organizations, trade associations, manufacturers, and other groups directly affected by these standards. To be useful, that is, to have wide acceptance, a standard must be approved by all affected organizations, With this in mind, the American Standards Association (ASA), a federation of technical societies, trade associations, government agencies, and numerous companies, provides a mechanism for nation-wide agreement on standards.

Within the ASA, all nuclear standards work is coordinated by the Nuclear Standards Board under which the sectional committees N1 through N7 and their subcommittees are organized. When the need for a standard is determined, the sectional committees try to interest member groups in developing the required information, with the ASA acting in a coordinating or an editorial function. If this fails, the ASA sectional committee proceeds to develop the standard. Approval of a standard by ASA is indicated by the official designation American Standard. To attain this, the standard, during the course of development, must receive acceptance by a consensus of all concerned.

There are, in addition, many company standards and technical society standards that have never been submitted to ASA for approval. Such standards are nonetheless valid when accepted by those concerned, and some are nationally recognized. One of the best examples of this is the Boiler and Pressure Vessel Code, a standard of the American Society of Mechanical Engineers (ASME), the application of which to containment vessels was discussed above.

An informal cooperative relation is maintained between ASA and AEC, since compatibility between industry standards and government regulations must exist. Also, ASA represents the United States in the International Organization for Standardization (ISO). Technical Committee 85 of the ISO is concerned with international standardization in the broad field of nuclear energy.

Although many groups are involved with the production of standards through ASA, many technical and professional societies with nuclear interest prepare and publish documents that are regarded as standards as far as that society is concerned. The following tables list, for the ASA and each organization that conducts its own standards studies, both the various committees which have been established by the organization

and the standards which have been published. The table numbers and the organizations described are listed below:

Table 2.2	American Standards Association - Nuclear Standards Board
Table 2.3	American Standards Association - Miscellaneous
Table 2.4	American Nuclear Society
Table 2.5	American Society of Civil Engineers
Table 2.6	American Society of Mechanical Engineers
Table 2.7	American Society for Testing and Materials
Table 2.8	American Institute of Electrical and Electronic Engineers
Table 2.9	National Electrical Manufacturers Association
Table 2.10	National Bureau of Standards
Table 2.11	Society of Naval Architects and Marine Engineers

Although many other organizations are involved in the production of standards relating to nuclear interests, the above list includes those that have produced significant results relative to reactor containment. For presentation here, only published documents generated by standards organizations are listed, although many other documents exist in draft form and others are being generated.

Table 2.2. American Standards Association - Nuclear Standards Board

---

The American Standards Association (ASA) was founded in 1918 by five engineering societies which were soon joined by three departments of the Federal Government. Today it is a federation of 68 technical societies, trade associations, and consumer groups with 67 similar groups as associate members. The ASA offices are at 10 East 40th Street, New York, N.Y.

ASA was formed primarily as a national clearinghouse for standards of all types, and it functions as the machinery through which standards or ideas for standards may be coordinated. The ASA program basically calls for the development by industry of standards which are believed to be advantageous. The standards of interest here are those that make uniform provisions for health and safety.

ASA performs its judicial functions through the Standards Council, which has vested its authority for approving standards in a Board of Review, elected from its own members. A Committee on Procedures advises the Standards Council on all constitutional and procedural questions.

The ASA Standards Council is assisted by 15 Standards Boards, each of which is responsible for a special field. The Nuclear Standards Board was established in June 1956 and is responsible for standards projects for industrial and commercial applications in the field of nuclear energy. The Nuclear Standards Board does not formulate standards, and it is not concerned with their technical content except to ensure coordination with other American Standards.

The members of the Nuclear Standards Board represent 34 technical societies, trade associations, and government agencies. The Board supervises the work of seven Sectional Committees and numerous Subcommittees. The sectional committee designations, names, and sponsors are listed below:

Table 2.2 (continued)

ASA N1. Sectional Committee N1 was disbanded following publication of ASA N1.1-1957, A Glossary of Terms in Nuclear Science and Technology. This standard was developed by a conference under the leadership of the National Academy of Sciences, National Research Council, and was approved by ASA under the Existing Standards Method. Sectional Committee N2 will handle all revisions and additions to the glossary.

ASA N2. General and Administrative Standards for Nuclear Energy. Sponsor: Atomic Industrial Forum, Inc., 850 Third Ave., New York 22, N.Y. This committee has 23 organization members. It studies standards, specifications, and methods of administration associated with the peaceful uses of nuclear energy, including color codes, symbols, nomenclature, qualifications of professionals, records and reporting systems and procedures, and accountability of materials. The following subcommittees have been established:

N2-1 Ionizing Radiation Symbol, Color Code, Signs, Labels, and Other Indentifying or Warning Devices
N2-2 Occupational Radiation Exposure Records Systems
N2-3 Qualifications of Nuclear Professionals
N2-4 Nuclear Terminology
N2-5 Model Codes and Regulations
N2-6 Administrative Practices in Radiation Monitoring

ASA N3. Nuclear Instrumentation. Sponsor: Institute of Electrical and Electronic Engineers, 345 East 47th Street, New York 17, N.Y. This committee has 26 organization members. It studies standards, specifications, and testing methods for instrumentation in the nuclear field, including instruments for personnel protection, reactor control, industrial processes, analysis and laboratory work, radiation calibration equipment, and components therefor. Its subcommittees are the following:

N3-1 Index of Nuclear Standardization Work
N3-2 Topical Structure

ASA N4. Electric Apparatus and Systems for the Nuclear Field. Sponsors: Institute of Electrical and Electronics Engineers, 345 East 47th Street, New York 17, N.Y.; Electric Light and Power Group, consisting of Edison Electric Institute, 750 Third Avenue, New York 17, N.Y., and Association of Edison Illuminating Companies, 51 East 42nd Street, New York 17, N.Y.; and National Electric Manufacturers Association, 155 East 54th Street, New York 17, N.Y. This committee has 14 organization members. Standards for electric power apparatus, systems, and controls used in the nuclear field are considered by this committee.

N4-1 Electrical Power Apparatus
N4-2 Auxiliary Electrical Power Systems
N4-3 Electrical Control Systems and Apparatus
N4-4 Environmental Classifications

Table 2.2 (continued)

ASA N5. Nuclear Fuel Cycle Engineering. Sponsor: American Institute of Chemical Engineers, 345 East 47th Street, New York 17, N.Y. This committee has 23 organization members. It considers standards, specifications, tolerances, and methods of testing for the chemical engineering aspects of the nuclear field, including the refining, processing, separation, purification, treatment, packaging, handling, and disposal of fuels, radioisotopes, industrial chemicals, pharmaceuticals with isotope tracers, and radioactive wastes (gases, liquids, and solids); the use of radioactive sources for tracers and for processing foods and other materials; the application and use of chemically resistant coatings; and the cleaning of contaminated equipment and facilities. Its subcommittees are the following:

N5-1 Fuel Manufacture and Fabrication
N5-2 Radioactive Waste Disposal
N5-3 Recovery of Irradiated Fuel
N5-4 Use and Handling of Radioisotopes and High-Energy Radiation
N5-5 Packaging and Transportation of Radioactive Material

ASA Sectional Committee N6. Reactor Safety Standards. Sponsors: American Nuclear Society, 244 East Ogden Avenue, Hinsdale, Ill., and American Society of Mechanical Engineers, United Engineering Center, 345 East 47th Street, New York 17, N.Y. This committee has 36 organization members. It considers codes and standards concerned with the hazards involved in the design, location, construction, and operation of nuclear reactors and of potentially critical assemblies. Its subcommittees are the following:

N6-1 Site Evaluation (dissolved, refer to ANS-2)
N6-2 Containment
N6-3 Fluid Systems of the Reactor and Fuel Within the Reactor
N6-4 Reactor Dynamics and Control Requirements (dissolved, refer to ANS-4)
N6-5 Instrumentation and Execution of Control Requirements
N6-6 Operation, Operator Qualifications, Inspection and Maintenance
N6-7 Failure Probabilities and Maximum Credible Accidents (dissolved, refer to ANS-5)
N6-8 Fissionable Material Outside Reactors (normally subcritical systems) (dissolved, refer to ANS-8)
N6-9 Index of American and Foreign Nuclear Safety Standards

ASA N7. Radiation Protection. Sponsors: Atomic Industrial Forum, Inc., 850 Third Ave., New York 22, N.Y., and National Safety Council, 425 North Michigan Avenue, Chicago 11, Ill. This committee has 25 organization members. It studies safety standards for the protection of persons employed in facilities associated with the production and utilization of fissionable materials against the normal, routine hazards present in such facilities (mines, mills, refineries, separation plants, fuel-element-fabrication plants, critical assembly facilities,

Table 2.2 (continued)

processing and reprocessing plants, working areas around reactors, and transportation and purification of radioactive materials). Its subcommittees are the following:

N7-1 Radiation Protection Standards in Uranium Mines and Mills
N7-2 Radiation Protection Standards in Uranium and Thorium Refineries
N7-3 Radiation Protection Standards in Isotopic Separation Plants
N7-4 Radiation Protection Standards for Fuel-Element Fabrication Plants
N7-5 Radiation Protection Standards for Nuclear Reactors
N7-6 Radiation Protection Standards for Transportation of Radioactive Materials

Standards Issued

1. American Standard, A Glossary of Terms in Nuclear Science and Technology, ASA N1.1-1957.
2. American Standard Radiation Symbol, ASA N2.1-1960.
3. American Standard Guide to Practice in Transportation of Source and Special Nuclear Materials Before Irradiation, ASA N5.1-1962.
4. American Standard Radiation Protection in Uranium Mines and Mills (Concentrators), ASA N7.1-1960.
5. American Standard Radiation Protection in Nuclear Fuel Fabrication Plants, ASA N7.2-1963.
6. American Standard Design Guide for a Radioisotope Laboratory Type B, N5.2-1963.

Table 2.3. American Standards Association - Miscellaneous

American Standards Association Committees on standards closely allied with nuclear safety but not under the jurisdiction of the ASA Nuclear Standards Board are listed below:

ASA Sectional Committee Z54. Industrial Use of X-Rays and Radiation. Sponsor: National Bureau of Standards. The following subcommittees have been established:

Z54-1 General Provisions: Methods and Materials of Protection
Z54-2 Health Provisions and Monitoring
Z54-3 X-Ray Protection for Installations Up to 2 Million Volts
Z54-4 Protection for Installations Above 2000 Kv
Z54-5 Gamma-Ray Sources for Industrial Radiography
Z54-6 Electrical Protection
Z54-7 X-Ray Diffraction, Fluorescence Analysis, and Microradiography
Z54-8 Sealed Beta-Ray Sources
Z54-9 Contamination Levels for Industrial Materials

Table 2.3 (continued)

ASA Sectional Committee B31. Code for Pressure Piping. Sponsor: American Society of Mechanical Engineers. This committee considers piping from the reactor to the power unit. Materials covered to date are primarily stainless steels. Future plans include the development of standards for carbon and alloy steels and nonferrous metals, as well as a revised version for nuclear piping.

Standards Issued

1. Safety Standard for Non-Medical X-Ray and Sealed Gamma-Ray Sources, Part I - General, Z54.1-1963
2. Safe Design and Use of Industrial Beta-Ray Sources, Z54.2-1958.

Table 2.4. American Nuclear Society Standards Committee

The American Nuclear Society (ANS) is an organization of scientists and engineers. Its offices are located at 244 East Ogden Ave., Hinsdale, Illinois. It was founded in 1954 in Washington, D.C., by a group of men active in nuclear science and technology. The main objectives of the Society are the advancement of nuclear science and engineering, together with allied sciences and arts, and the integration of the several disciplines constituting nuclear science and technology. Other objectives include the encouragement of research, the establishment of scholarships, the dissemination of technical information, the holding of meetings devoted to scientific and technical papers, and the cooperation with governmental agencies, educational institutions, and other organizations having similar purposes.

To qualify for membership in ANS, a person must have a record of attainment of leadership in some area related to nuclear science and technology. To conduct its program, the Society has seven divisions, each of which concerns itself with a particular area of the technology. These are:

1. Shielding
2. Isotopes and Radiation
3. Hot Laboratories
4. Reactor Mathematics and Computations
5. Reactor Operations
6. Aerospace
7. Materials Technology

The Society is managed by a Board of Directors that may delegate any or all of its powers to an Executive Committee of seven members. Among its standing committees is a Standards Committee which considers and investigates all matters relating to units, terminology, standards, and practices that pertain to nuclear science and engineering. This Committee also coordinates the work of the technical committees with respect to the

Table 2.4 (continued)

making or revising of Society Standards. The ANS standards committees work closely with the ASA Nuclear Standards Board and its Sectional Committees. ANS cosponsors ASA Sectional Committee N6, Reactor Safety, together with ASME.

The subcommittees of the ANS Standards Committee are described below:

ANS 1. Critical Experiments. The aim of this committee is to establish standards of performance of critical experiments.

ANS 2. Site Evaluation. (See also ASA N6-1 and N6-2.) The aim of this committee is to develop standards relative to site selection other than plant design and operation.

ANS 3. Reactor Operator Qualifications. (See also ASA N2-3 and ASA N6-6.) This committee was dissolved because of the work being done by ASA N6-6.

ANS 4. Reactor Dynamics and Control. (See also ASA N6-4.) The aim of this committee is to establish standards for the general design of those systems and components related to the overall aspects of reactor dynamics and control.

ANS 5. Energy and Fission-Product Release. (See also N6-7.) The aim of this committee is to establish standard methods for estimating the release of energy and fission products under nonstandard or accident conditions and the subsequent distribution and disposition of radioactive materials throughout the reactor facility.

ANS-6. Reactor Operation. (See also ASA N6-6.) This committee was dissolved because of work being done by ASA N6-6.

ANS-7. Reactor Components. (See also N3, N5, N6, and N7.) The aim of this committee is to establish standards for design, production, and testing of components of reactor systems.

ANS-8. Fissionable Materials Outside Reactors. (See also N6-8.) The aim of this committee is to establish standards providing guidance in the prevention of nuclear chain reactions in all procedures for handling, storing, transporting, processing, and treating fissionable nuclides.

ANS-9. Nuclear Terminology and Reactor Systems Classification. (See also N2-4.) In cooperation with N2-4, this committee is responsible for preparing suggested definitions for inclusion in the International Standards Organization trilingual glossary and is assisting in the revision of the American Standard N1.1-1957, A Glossary of Terms in Nuclear Science and Technology. It is a further aim of this committee to prepare standards for classifying nuclear reactors and related systems.

ANS-10. Standard Units for Nuclear Industry. The aim of this committee is to develop standard units, parameters, and definitions, including

Table 2.4 (continued)

abbreviations, for the nuclear industry. A further aim is to promote the use of a suitable metric system of units, in cooperation with educational institutions, professional societies, and publishers of technical literature.

Table 2.5. American Society of Civil Engineers

The American Society of Civil Engineers (ASCE) was organized for the purpose of advancing the science and profession of engineering. Specialization within civil engineering has brought about the creation of 14 separate Technical Divisions in the Society, and a number of these are active in radiation protection. The Administrative Committee on Nuclear Structures and Materials, Address: 345 East 47th Street, New York 17, N.Y., has the following task committees:

Task Committee on Hot Laboratories
Task Committee on Live Loads Due to Heat and Incidence
Task Committee on Structural Aspects of Nuclear Incidents
Task Committee on Structural Materials in Reactor Design

Table 2.6. American Society of Mechanical Engineers

The American Society of Mechanical Engineers (ASME) was organized to promote the art and science of mechanical engineering and to further mechanical construction for scientific purposes. Address: 345 East 47th Street, New York 17, N.Y. Its governing body is the Council, under which there are a number of boards and committees. ASME has representatives on the ASA Nuclear Standards Board and its Sectional Committees N2, N3, N4, N5, N6, and N7. It sponsors ASA Sectional Committee B31, Code for Pressure Piping, and cosponsors ASA Sectional Committee N6, Reactor Safety. ASME prepares and distributes many ASME standards of direct and indirect bearing on nuclear safety, in addition to other standards (e.g., ASME Boiler and Pressure Vessel Code). The ASME committees working in the nuclear field are listed below:

Subcommittee on Nuclear Power. In 1955 this committee was established by the Boiler and Pressure Vessel Committee to extend the use of the construction rules of the Code to vessels used in nuclear installations, to modify them where necessary, and to develop such additional rules as required for the special construction and uses involved. Adopted rules are presently grouped under seven general headings and

Table 2.6 (continued)

bear case numbers 1270N to 1276N, 1330 to 1335, and 1337. A new section of the Code has been released to cover vessels for nuclear service; namely, ASME Boiler and Pressure Vessel Code, Section III, Rules for Construction of Nuclear Vessels.

Special Committee to Review Code Stress Basis. This committee was set up to assemble the related requirements to permit the use of higher basic allowable stresses in all sections of the Code without sacrificing the integrity or safety of the vessels. This group worked closely with the Subcommittee on Nuclear Power in drafting Section III because of this need. Their work will now be directed toward Section VIII of the Code and the standing subcommittees will assist the Subcommittee on Nuclear Power in answering inquiries on Section III.

Research Committee on Effects of Radiation on Materials. The objective of this committee is to convert research data to a form useful to engineers and designers, as well as to develop new data where needed.

Table 2.7. American Society for Testing and Materials

The American Society for Testing and Materials has a Special Administrative Committee on Nuclear Problems. Address: 1916 Race Street, Philadelphia, Pa. The following subcommittees are working on standards in the nuclear energy field:

ASTM A-1	Steel
ASTM A-5	Corrosion of Iron and Steel
ASTM A-10	Iron-Chromium, Iron-Chromium-Nickel, and Related Alloys (six groups)
ASTM B-2	Nonferrous Metals and Alloys
ASTM B-7	Light Metals and Alloys Cast and Wrought
ASTM C-9	Concrete and Concrete Aggregates (with special subcommittee on shielding)
ASTM C-21	Ceramic Whiteware and Related Products
ASTM D-2	Petroleum Products and Lubricants
ASTM D-9 and D-20	Joint Subcommittee on Effects of Nuclear and High-Energy Radiation (insulating materials and plastics)
ASTM D-18	Soils for Engineering Purposes
ASTM D-19	Industrial Water
ASTM E-1	Methods of Testing
ASTM E-2	Emission Spectroscopy
ASTM E-3	Chemical Analysis of Metals
ASTM E-7	Nondestructive Methods of Testing
ASTM E-10	Radioisotopes and Radiation Effects
ASTM E-14	Mass Spectroscopy

Table 2.8. Institute of Electrical and Electronic Engineers

The Institute of Electrical and Electronic Engineers (IEEE) is located at 345 East 47th Street, New York, N.Y. IEEE has representatives on the ASA Nuclear Standards Board and Sectional Committees N3 and N6, and it sponsors ASA Sectional Committee N3. It also has the following committees working on standards in the nuclear field:

Committee 13 on Nuclear Techniques. The scope of the standards work affecting nuclear safety includes (1) the selection of terms and the preparation and maintenance of standard definitions in the fields of nuclear radiation and nuclear instrumentation, (2) the preparation and maintenance of standards covering methods of measurement in these fields, (3) the compilation of information relating standards in these fields, and (4) coordination with activities of other IEEE committees and other professional societies and liaison with technical organizations engaged in allied work.

Nucleonics Committee. IEEE cosponsors ASA Sectional Committee N4 and has worked closely with ASA Committees N2 and N6 in developing standard qualifications for personnel.

Standards and Safety Committee. This committee is developing a code for qualifications of Nuclear Reactor and Accelerator Operators that relates to nuclear safety.

Table 2.9. National Electrical Manufacturers Association

National Electrical Manufacturers Association (NEMA) is located at 155 East 44th Street, New York, N.Y. NEMA has representatives on the ASA Nuclear Standards Board and Sectional Committees N3, N4, and N6. NEMA has developed standards for canned-motor pumps for nuclear applications.

Table 2.10. National Bureau of Standards

The U.S. Department of Commerce, National Bureau of Standards, publications are available from the Superintendent of Documents, U.S. Government Printing Office, Washington 25, D.C. NBS prepares handbooks summarizing the recommendations of the National Committee on Radiation Protection and Measurements (NCRP), which works closely with the International Commission on Radiological Protection (ICRP). The NCRP was organized by and continues to operate under sponsorship of the National Bureau of Standards. Forty-one main committee members and 18 subcommittees are listed, with their respective chairmen, in NBS Handbook 69, Maximum Permissible Body Burdens and Maximum Permissible Concentrations of Radionuclides in Air and in Water for Occupational Exposure, issued June 5, 1959.

The following NBS handbooks that relate directly to safety in utilization of nuclear energy have been issued:

1. Safe Handling of Radioactive Isotopes, NBS-42, 1949
2. Control and Removal of Radioactive Contamination in Laboratories, NBS-48, 1951
3. Recommendations for Waste Disposal of Phosphorous-32 and Iodine-131 for Medical Users, NBS-49, 1951
4. X-Ray Protection Design, NBS-50, 1952
5. Radiological Monitoring Methods and Instruments, NBS-51, 1952
6. Maximum Permissible Amounts of Radioisotopes in the Human Body and Maximum Permissible Concentrations in Air and Water, NBS-52, 1953
7. Recommendations for the Disposal of Carbon-14 Wastes, NBS-53
8. Protection Against Radiations from Radium, Cobalt-60 and Cesium-137, NBS-54, 1954
9. Protection Against Betatron-Synchrotron Radiations up to 100 Million Electron Volts, NBS-55
10. Photographic Dosimetry of X and Gamma Rays, NBS-57
11. Radioactive Waste Disposal in the Ocean, NBS-58, 1954
12. Permissible Dose From External Sources of Ionizing Radiation, NBS-59, 1954
13. Regulation of Radiation Exposure by Legislative Means, NBS-61, 1955
14. Protection Against Neutron Radiation Up to 30 Million Electron Volts, NBS-63, 1957
15. Design of Free-Air Ionization Chambers, NBS-64, 1957
16. Safe Handling of Bodies Containing Radioactive Isotopes, NBS-65, 1958
17. Safe Design and Use of Industrial Beta-Ray Sources, NBS-66, 1958
18. Maximum Permissible Body Burdens and Maximum Permissible Concentrations of Radionuclides in Air and in Water for Occupational Exposure, NBS-69, 1959
19. Measurement of Neutron Flux and Spectra for Physical and Biological Applications, NBS-72, 1960
20. Protection Against Radiations from Sealed Gamma Sources, NBS-73, 1960

Table 2.10 (continued)

21.	Measurement of Absorbed Dose of Neutrons and of Mixtures of Neutrons and Gamma Rays, NBS-75, 1961
22.	Medical X-Ray Protection Up to Three Million Volts, NBS-76
23.	Stopping Powers for Use with Cavity Chambers, NBS-79, 1961
24.	A Manual of Radioactivity Procedures, NBS-80, 1961
25.	Radiation Quantities and Units, NBS-84, 1962
26.	Physical Aspects of Irradiation, NBS-85, 1962
27.	Radioactivity, NBS-86, 1962
28.	Radiobiological Dosimetry, Recommendations of the International Commission on Radiological Units and Measurements, NBS-88, 1962
29.	Methods of Evaluating Radiological Equipment and Materials, NBS-89

Table 2.11. Society of Naval Architects and Marine Engineers

The Society of Naval Architects and Marine Engineers, Ships Machinery Committee, M-13 Panel (Address: 74 Trinity Place, New York 6, N.Y.) prepared Technical Research Bulletin 3-6, "Safety Considerations Affecting the Design and Installation of Water-Cooled and Water-Moderated Reactors on Merchant Ships," at the request of the U.S. Coast Guard.

References

1. Code of Federal Regulations, Title 10, Part 100, Reactor Site Criteria; see also Federal Register, April 2, 1962.

2. Atomic Energy Act of 1954, Public Law 83-703.

3. R. Lowenstein, Announcement No. 72, Organizational Changes, Division of Licensing and Regulation, May 10, 1961.

4. Atomic Energy Act of 1954 as amended in Section 29 by Public Law 85-744 Sept. 2, 1957.

5. Code of Federal Regulations, Title 10, Part 115, Procedures for Review of Certain Nuclear Reactors Exempted from Licensing Requirements; see also Federal Register, May 18, 1961.

6. Letter from T. J. Thompson, ACRS Chairman, to Hon. Glenn T. Seaborg, Sept. 11, 1961, Subject: Nuclear Reactor System Mechanical Design; available at AEC Public Document Room.

7. Hearings Before the Joint Committee on Atomic Energy, Congress of the United States, Radiation Safety and Regulation, June 12-15, 1961, U.S. Government Printing Office, Washington, D.C.

8. Hearings Before the Joint Committee on Atomic Energy, Congress of the United States, Radiation Standards, Including Fallout, June 4-7, 1962, U.S. Government Printing Office, Washington, D.C.

9. Hearings Before the Joint Committee on Atomic Energy, Congress of the United States, Development, Growth, and State of the Atomic Energy Industry, Feb. 20-21, 1963, U.S. Government Printing Office, Washington, D.C.

10. Hearings Before the Joint Committee on Atomic Energy, Congress of the United States, Fallout, Radiation Standards, and Countermeasures, June 3, 4, and 6, 1963, U.S. Government Printing Office, Washington, D.C.

11. Florence C. Johnson, "Progress in State Regulation of Radiation Hazards," Safety Standards, XIII(3): 7-9 (May-June 1964).

12. AEC Licensing Guide, Purpose, Organization, and Contents of Hazards Summary Reports for Power Reactors, USAEC Division of Licensing and Regulation, Draft, Aug. 28, 1962.

13. Atomic Energy Commission, Rules and Regulations, Title 10 of Code of Federal Regulations, June 1, 1962, Office of the General Council, U.S. Atomic Energy Commission, Washington, D.C.

14. ASME Boiler and Pressure Vessel Code, Section VIII, Unfired Pressure Vessels, Available from ASME United Engineering Center, 345 East 47th Street, New York 17, New York.

15. ASME Boiler and Pressure Vessel Code, Section III, Rules for Construction of Nuclear Vessels, Available from ASME United Engineering Center, 345 East 47th Street, New York, 17, New York.

16. General Electric Company, A Survey of Reactor Design and Operation for Use in a Study of Water Cooled Reactor Primary System Reliability, USAEC Report GEAP-4445.

17. General Electric Company, A Survey of Piping Failures, USAEC Report GEAP-4474.

18. General Electric Company, A Review of Fracture Modes as Related to Reactor Primary Coolant Pipe Rupture, USAEC Report GEAP-4446.

19. General Electric Company, Mechanical Design Considerations in Primary Nuclear Piping, USAEC Report GEAP-4578.

20. R. L. Koontz et al., Low Pressure Containment Buildings, Component Tests and Design Data, USAEC Report NAA-SR-7234, Atomics International, March 15, 1963.

21. Uniform Building Code, International Conference of Building Officials, 50 South Los Robles, Pasadena, California.

22. Southern Standard Building Code, Southern Building Code Congress, Brown-Marx Building, Birmingham, Alabama.

23. Filter Units, Protective Clothing, Gas-Mask Components and Related Products: Performance - Test Methods, Method 102.9.1, pp. 33-38, MIL-STD-282, May 28, 1956.

24. Health and Safety Information, USAEC Issue 151, December 14, 1962.

25. R. E. Adams and W. E. Browning, Jr., Iodine Adsorption Studies, pp. 10-18, Maritime Reactor Program Annual Progress Report for Period Ending Nov. 30, 1962, USAEC Report ORNL-3416, Oak Ridge National Laboratory.

26. W. H. Echols and J. A. Young, Studies of Portable Air-Operated Aerosol Generators, Naval Research Laboratory Report 5929, July 26, 1963.

27. E. C. Parrish and R. W. Schneider, Tests of High-Efficiency Filters and Filter Installations at ORNL, USAEC Report 3442, Oak Ridge National Laboratory, May 1963.

28. H. Gilbert and J. H. Palmer, Inspection, Storage, Handling, and Installation of High-Efficiency Particulate Air Filter Units, USAEC Report TID-7023, August 1, 1961.

29. C. L. Whitmarsh, Status of Activities in Nuclear Standards, Nucl. Safety, 3(4): 1-12 (June 1962).

30. Selected Bibliography of Radiation Protection Organizations, Committee of Ionizing Radiation, American Conference of Governmental Industrial Hygienists, 1963.

3. CREDIBLE ACCIDENTS

H. B. Piper*

The credible accidents that may occur in a nuclear plant cover a broad range from the inconsequential to the maximum credible accident. When discussing such accidents, however, it is important to bear in mind that there has been little experience on which to base any evaulation as to their probability or severity. In the safety analysis of a reactor facility, all types of accidents that could occur must be studied.

The word "credible" is used here in describing accidents that, in the judgment of safety analysts, must be provided for in the design of the facility. In many cases, very severe accidents may be thought of, but they may be incredible or could not occur. For example, to the person unfamiliar with nuclear mechanics, it may appear that a reactor could explode like a bomb, since the "atomic bomb" and the nuclear reactor contain the same fuel. There is, however, no imaginable set of circumstances under which this could happen. Since the nuclear explosion of a reactor is incredible, it is not further pursued when evaluating the safety of a reactor.

There are, however, many credible accidents that must be considered by the designer. These include the possibilities of component failures, design deficiencies, and operating errors. Further, it is possible for instruments to fail, so frequently more than one instrument is employed for a given task, and their signals are connected so that simultaneous failures of more than one item are required for a given accident to occur.

Since reactor vessels and associated piping are generally of conventional metals, these components may fail although carefully fabricated to pressure standards and routinely inspected where possible. However, portions of primary nuclear systems are not usually amenable to periodic inspection after operation, so extreme care must be exercised in the construction and initial inspection of these systems. Components are heat treated and stress relieved and welds are x-rayed and further checked with dye penetrant. This sort of care during construction leads to increased confidence in the "as-constructed" reactor system.

Many types of accidents could occur and must be considered when a safety analysis is performed. In general no single credible accident could render substantial damage to the surrounding environment, but some combination or sequence of credible accidents may be postulated that would result in the accident that is called the Maximum Credible Accident (mca). The mca is the credible accident that can cause the most serious consequences as far as radiation exposure to the surrounding off-site populace is concerned. There are limits beyond which these consequences cannot be allowed to extend, and if for a given facility the consequences are beyond those limits, more effective containment measures must be assured if the facility is to be built and operated.

---

*Oak Ridge National Laboratory.

3.1 TYPICAL ACCIDENTS

In the safety reports of existing reactors, many typical accidents are cited. Usually the accidents are categorized and described, and their effects are analyzed. Some of the accidents considered are listed below:

1. Startup accident,
2. Control rod withdrawal accident,
3. Poison removal accident,
4. Cold coolant accident,
5. Control rod drop accident,
6. Loss of coolant flow accident,
7. Loss of load accident,
8. Step increase in load accident (i.e., break in steam line to turbine),
9. Accidental interchange of primary and secondary fluids,
10. Loss of coolant accident,
11. Fuel-handling accident,
12. Fuel element failure,
13. Chemical reactions.

These accidents, which are discussed below are general in nature; that is, they are not inherently limited to one type of reactor, although some accidents may be more pertinent to some reactor types than to others. In fact, it may be expected that it will be necessary to consider all these accidents in the safety analyses of all types of reactor. Nuclear transients are a significant feature of the first five accidents, but in contrast to fast reactors (which are discussed in sec. 5.3), nuclear transients do not constitute the maximum credible accident in thermal reactors.

3.1.1 Startup Accident

The startup accident is one that is caused by insertion of reactivity at the maximum possible rate with the reactor initially in the shutdown condition and the neutron flux at the source level. Generally the temperature is assumed to be that which will result in the most severe nuclear transient. Even so, this type of accident is minimized in low-enrichment reactors by the fact that the Doppler coefficient is quite effective under these conditions.

In general, this accident can be severe enough to cause core damage only in the case of misoperation and failure of conventional reactor safety channels. Rapid withdrawal of a control rod, by the operator, from the shutdown condition should constitute misoperation. A fast period on low-, intermediate-, and high-flux channels should cause the rod withdrawal to stop or, if the period were fast enough, a scram and high-power indication should cause a scram. With these safety interlocks the startup accident should cause little or no damage to the system. If by some manner this accident should continue unchecked, it would result in a severe core temperature transient, which, by one of several mechanisms, would be self limiting but might destroy the reactor core. Even so, if the primary system remained intact, no significant fraction of the fission products would be released to the reactor containment system.

The temperature transient that would be experienced as a result of a startup incident at the Piqua (organic-cooled) reactor[1] is shown in

Fig. 3.1. The temperature and power would continue to rise until film boiling occurred, at which time the voids produced by boiling would introduce negative reactivity. Continued power production would eventually result in melting and rearrangement of the central elements. This incident is assumed to take place with full coolant flow established; the effects would be adversely magnified by any reduction in flow.

3.1.2 Control Rod Withdrawal Accident

An accident could be initiated by the continuous withdrawal of one or more control rods at the maximum rate when the reactor was operating. Except for the fact that the reactor would be operating, this accident would be the same as the startup accident. The potential consequences could be worse, however, because in this case the reactor would be at some power and the core would have accumulated fission-product activity proportional to the power and the time at power. However, if the primary system did not fail, none of the fission products would be released to the containment structure. As in the startup accident, if the several safety channels did not cause the reactor to scram, severe overheating of the core could occur, which would ultimately result in the termination of the excursion either by expulsion of the moderating coolant or by loss of fuel from the core.

The control rod withdrawal accident was analyzed for the Big Rock Point plant as follows:[2]

> "The continuous withdrawal of control rods at power will cause a flux peaking in the area from which the rods are withdrawn. There will be no excursion however, due to the strong negative void coefficient of reactivity. The rate of increase of power in this case is a function of the rate of rod removal, the particular rods removed, and the control rod and void configuration at the time of the incident. In any event, the local power flux, and the over-all steam formation will increase smoothly. The bypass valve will continuously increase its opening to receive the larger steam flow. Before the flow capacity of the bypass valve is reached, the reactor will safely shut down from the over-flux signal that will arise from the flux monitoring instrumentation."

3.1.3 Poison Removal Accident

The accidental removal of poison (other than control rod poison) could occur in those reactors that use soluble poisons in the coolant for reactivity contol or burnable poisons to extend core life. In the case of the soluble poison, if administrative control were not properly exercised, the poison concentration might decrease at a time when some maximum nuclear transient could occur as a result. The Indian Point plant uses soluble boron in the primary coolant as a burnable poison[3] to aid in control. In reactors where insoluble burnable poison is used, a strip of

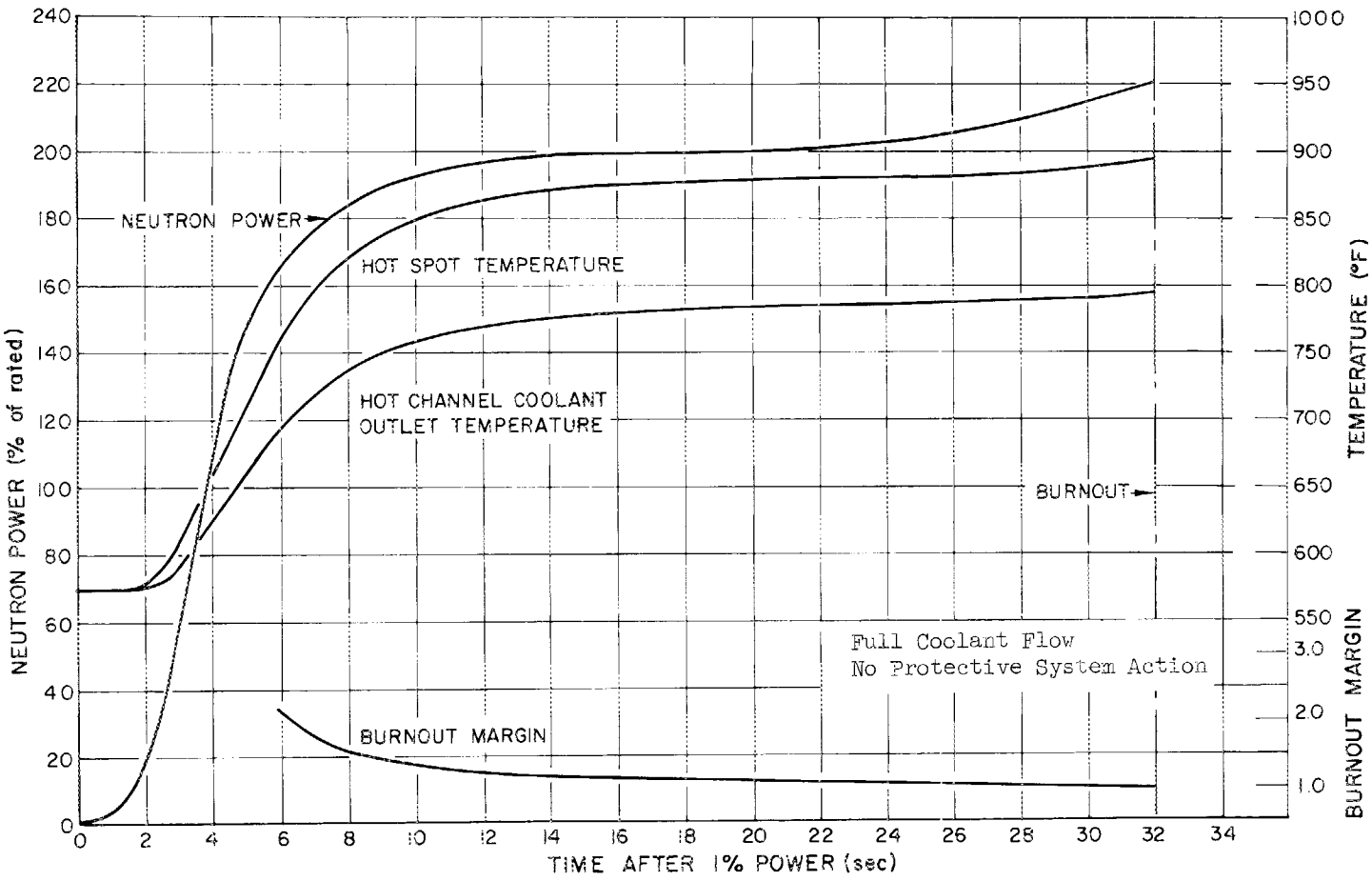

Fig. 3.1. Transients Resulting from Startup Accident in the Piqua Reactor. (From ref. 1)

the poison may be attached to the fuel element. The depletion of the poison compensates for the fuel that is burned and thereby provides a core with a longer lifetime. Such strips of poison could become separated from the fuel element and drop from the active core region, thus adding reactivity to the system. By the very nature of this accident it would be inconceivable for all the poison to fall from the core at the same time, and so the severity would be minimized by virture of the fact that the accident would occur over a period of time. Reactivity increases were noted in the SL-1 that were found to be caused by this phenomenon.[4]

3.1.4 Cold Coolant Accident

The cold coolant accident would occur if some or all of the coolant circulated through the core had been cooled below the normal inlet temperature. In general, reactors have a negative temperature coefficient of reactivity, and therefore, with a reduction of temperature, there is an increase in reactivity. This increase in reactivity can logically be called a transient in the core, and the severity of the transient is determined by the value of the temperature coefficient and by the degree to which the inlet coolant is subcooled and the coolant flows through the core. In some cases this incident could result in severe core damage. In plants where this could be a serious problem, safeguards must be established to prevent this accident.

One probable cause of this accident would be the starting of a coolant loop that had been idle for a period of time sufficient to allow the coolant in the loop to become subcooled. This could be prevented by interlocks on the valves that isolate the loop or by administrative control through the proper use of loop startup procedures, which should include heating of the loop prior to starting the pump.

Considerable attention has been given to this accident at the Yankee reactor, which has a large negative temperature coefficient. The analysis of the problem is as follows:[5]

> "Since the Yankee reactor has a relatively large negative temperature coefficient of reactivity, a lowering of temperature represents an addition of reactivity. Such a downward temperature change might come about through opening valves which previously had isolated a coolant loop containing water at a temperature below that of the water in the reactor core. Protection against such an occurrence is afforded by the following:
>
> "1. Temperature interlock which prevents valve opening unless the cold leg loop temperature is within 30°F of the highest cold leg temperature in the other loops.
>
> "2. Slow opening valve permits mixing of isolated loop water with water in the active loops. Loop transit time is short compared to valve opening time which increases mixing, as does the configuration of reactor piping and internals.
>
> "3. Cold leg low temperature alarm.

"4. Startup rate protection and 25% power level scram, if at low power levels, and 120% power level scram, if at power.
"5. Administrative control dictates that the isolated loop will be borated when it is more than 30°F cooler than the highest core inlet water temperature.
"6. Administrative control dictates that temperature and boron concentration will be matched before a loop is cut in."

3.1.5 Control Rod Drop Accident

The accidental dropping of one or more control rods into the active core of a reactor would cause a flux depression and a power loss. From the safety standpoint, this accident, which causes the reactor conditions to change in the direction of shutdown, does not present a problem. It is an unusual circumstance, however, that could precipitate another accident which might have serious consequences. This incident is usually analyzed for the sake of completeness of the safety investigation.

The control rod might also drop out of the core. If this were the case, the accident would be similar to the startup and control rod withdrawal accidents (secs. 3.1.1 and 3.1.2).

3.1.6 Loss of Coolant Flow Accident

Loss of coolant flow accidents can be of various magnitudes, depending on the mechanism that causes the impairment in coolant flow.

3.1.6.1 Circulating Pump Stoppage

The loss of one or all of the circulating pumps could be responsible for the loss of flow accident. The portion of flow lost would determine the severity of the incident. A complete loss of flow could result in severe core damage because localized overheating of the fuel elements would occur. In many cases, however, thermally induced convection would provide sufficient flow to prevent extensive overheating, even in the event of complete flow loss, and, when possible, this is a design requirement. It is tacitly assumed that upon stoppage of flow, the appropriate sensors will initiate a scram and shut down the reactor. If this is not the case, overheating of the core may occur. However, the loss of flow and concurrent failure of the control system constitute a compound accident involving the failure of two independent components, which could possibly occur from a single initiating event.

The accident analyzed for the N.S. Savannah was based on the assumption that a scram would occur 0.50 sec after the loss of flow was initiated. As indicated in the following discussion, no cladding failures would be anticipated as a result of this accident.[6]

"The variation of clad temperatures after the loss of flow is very sensitive to the assumption of the value of the heat transfer coefficient at the clad surface. Fig. 20 [see Fig. 3.2, this report] gives the fuel pin surface and pellet-center temperatures for the case in which the heat transfer coefficient accounted for local and net boiling at the surface of the clad. The thermal conductivity of the mixed helium and fission products in the gap was assumed to be 0.03 Btu/hr-ft-°F. Because of substantial resistance to heat transfer in the gap between the pellet and the clad, the clad temperature seeks the temperature of the coolant for any reasonable value of surface heat transfer coefficient. In this case, the maximum clad surface temperature was 625°F. Fig. 20 represents the conditions actually anticipated in the event of a complete loss of coolant flow."

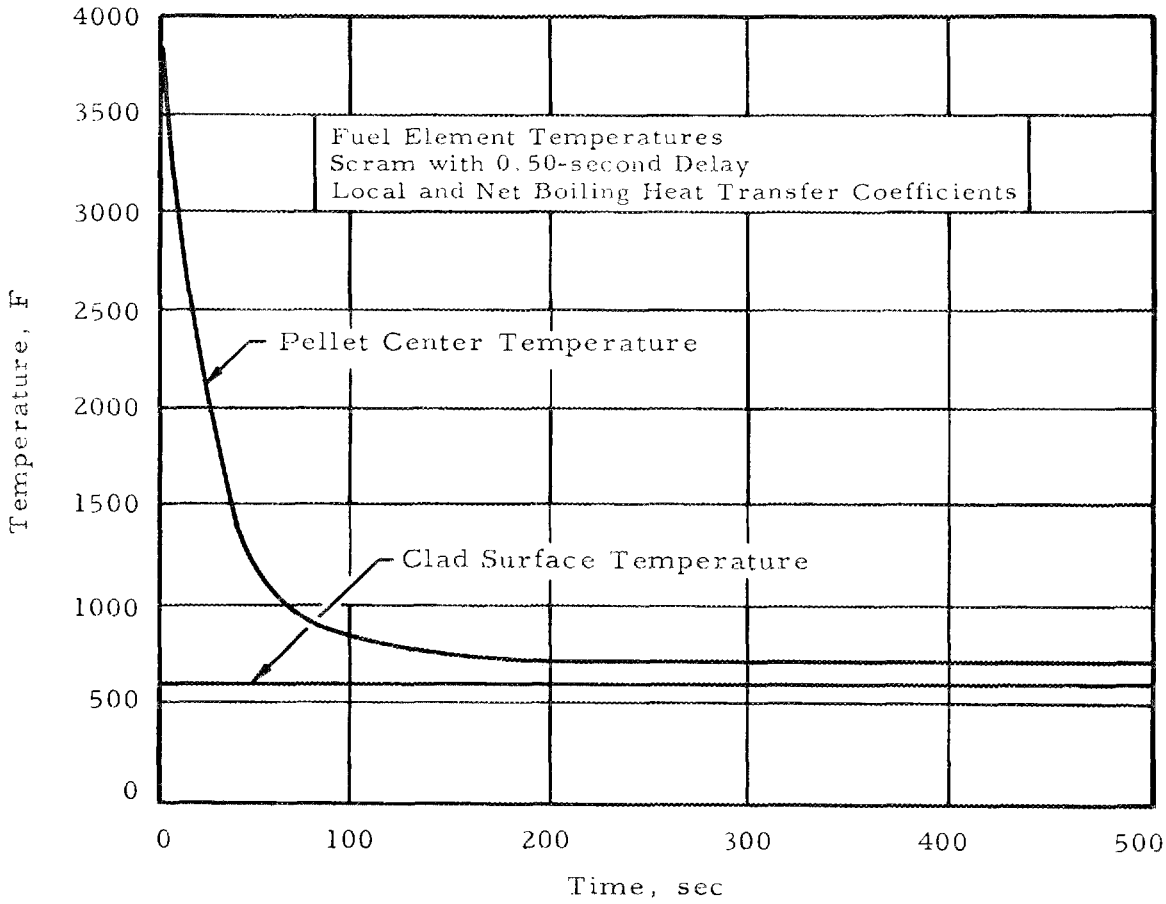

Fig. 3.2. Fuel and Cladding Temperatures Resulting from Complete Loss of Coolant Flow in the N.S. Savannah Reactor. (From ref. 6)

3.1.6.2 Blocked Flow Channel

An accident with much less severe consequences but with a greater probability of occurrence is the blocked flow channel accident. This is a variation of the loss of flow accident in which the flow to a single (or a few) channel(s) is either stopped or limited to the extent that departure from nucleate boiling can take place. In this event the fuel element would overheat, and melting of the cladding might occur with resulting release of fission products to the coolant stream. The coolant activity monitor would indicate this trouble, and steps would be taken to rectify the potentially unsafe situation. (See also sec. 3.5.)

3.1.7 Loss of Load Accident

Upon loss of load, the reactor would start on a transient that could become severe unless a scram were initiated. With loss of load the average coolant temperature would go up, cooling of the core would be reduced, and some fuel melting could occur. However, a scram signal would generally be initiated by a loss of load, and a further scram signal might be given by the coolant volume change that would occur as a result of the increased average temperature; the volume change would be sensed as a high level in the pressurizer.

The loss of load accident at full power was analyzed for the Yankee reactor, assuming both scram and nonscram conditions. Figures 3.3 and 3.4 show the behavior of the important parameters upon occurrence of the accident.

3.1.8 Step Increase in Load Accident

In general, reactors behave quite well under the influence of load changes, but if the reactor is operating at full power and a substantial load increase is imposed, the resulting effects may be quite severe. For example, if the steam line to the turbine suddenly ruptured, the heat removal from the primary system would increase and cause an immediate temperature change in the primary fluid. The control system would insert reactivity to compensate for this change, and the change itself, in lowering the average temperature, might also insert reactivity if the system had a negative temperature coefficient. The high power set point would be exceeded and a scram would be initiated that would end the transient. If the control system failed to shut the reactor down, severe core damage could be caused by the core temperature transient that would follow.

3.1.9 Accidental Release of Primary Fluid and Interchange of Primary and Secondary Fluids

Some fuel elements may be expected to rupture or slowly leak fission products into the primary coolant stream. The existence of one or more failed fuel elements does not constitute an accident condition, since power reactors are designed to operate under such a condition. Various accidents could, however, cause the failure of many more fuel elements.

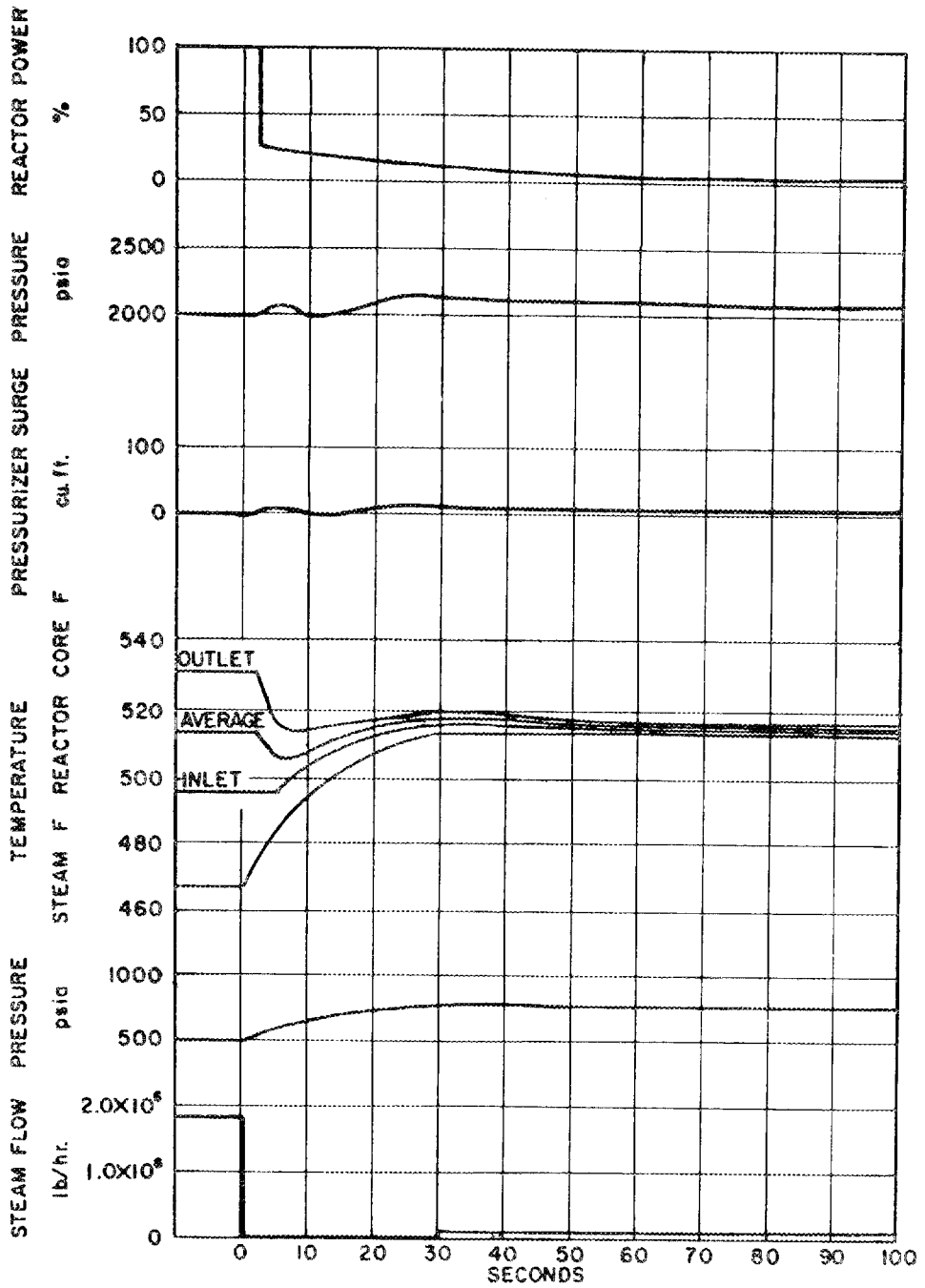

Fig. 3.3. Effect of Automatic Reactor Scram on Parameters of Yankee Reactor Upon Loss of Load When Operating at 485 Mw(t). (From ref. 5)

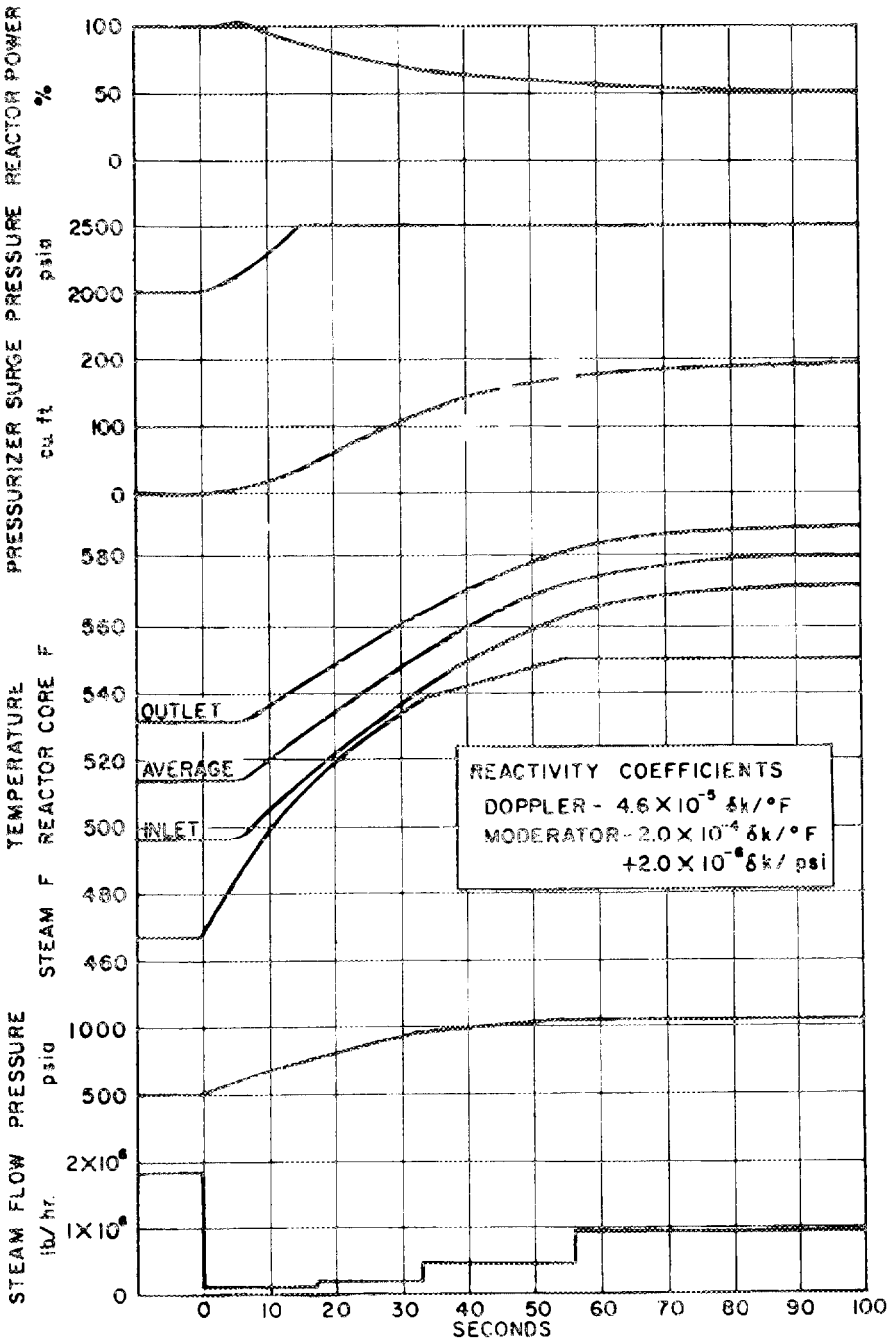

Fig. 3.4. Effect of Loss of Load Without a Reactor Scram on Parameters of Yankee Reactor When Operating at 485 Mw(t). (From ref. 5).

In a pressurized system the fission products would normally be confined by the primary system, but they could enter the secondary system through some break between the two systems. In a boiling system, the small amounts of gaseous fission products flowing with the steam can be safely released to the atmosphere after a decay period.

3.1.9.1 Indirect Cycle

With the indirect-cycle systems in which the primary coolant gives heat to a secondary (or tertiary) coolant which, in turn, drives the turbine, the possibility of a leak occurring in the heat exchanger must be investigated. Some concentration of fission products may accumulate in the primary system without causing undue alarm because the activity is contained. If an interconnection (by tube failure, etc.) between primary and secondary systems occurs, dispersal of the radioactive primary coolant may be minimized by designs in which the secondary system is maintained at a higher operating pressure. If an interchange is established between the two coolant systems, however, the fission products may reach a dangerous concentration in the secondary working fluid. Close observation of fission-product activity in all coolant streams and administrative control that would initiate shutdown and repair in case the activities became excessive would preclude any serious discharge of contaminants.

3.1.9.2 Direct Cycle

In the direct-cycle system, the primary coolant is also the working fluid; that is, it drives the turbine. In this case any steam leak would be the primary fluid and if fission products were present, they could thus escape from the primary containment system. It is obvious that this could impose a more severe limitation on the activity in the primary coolant in order that the contamination at the turbine remain of negligible radiological significance.

3.1.10 Loss of Coolant Accident

Loss of coolant could range from that escaping through a small leak, which could be accommodated by the feed pumps, to the loss of coolant within seconds. The accident might be initiated by a small leak or by failure of some component such as a flange, valve, pipe, or even a large pressure vessel. In this accident, coolant would drain from the primary loop. If the drainage were slow enough to allow the feed pumps or emergency injection systems to provide cooling for the core, minor ill effects would be suffered; but, if the release of coolant were sufficiently sudden to uncover the core, the fuel elements would suffer a severe temperature increase that might result in meltdown of the core and subsequent release of fission products to the reactor containment vessel through the failure that allowed the loss of coolant. The loss of coolant accident based on instantaneous depressurization of the primary system was analyzed for the Bodega Bay plant. The assumptions relevant to the fuel transients were as follows:[7]

"(1) A fully effective core spray would preclude significant core damage and result in little or no off-site radiological effect. However, this analysis assumes a highly improbable independent failure, partial ineffectiveness of the core spray, which would permit half the core to overheat from decay heat.

"(2) The core heat-up curves are shown in Fig. VII-2 [see Fig. 3.5, this report]. These curves were estimated assuming that coolant loss occurs in about 8 sec., as shown by test results, and that no decay heat would be lost from the uncooled fuel.

The fuel melting curves are conservative because thermal radiation and other heat loss possibilities which have been neglected would be expected to limit temperatures and the extent of meltdown in the overheated fuel."

Other, less severe accidents of this nature might be costly and troublesome, but they would be of less consequence as far as hazards to the environment were concerned. In most reactors, the complete loss of coolant accident is the maximum credible accident, and it is this accident for which the containment structure is designed in most cases.

The foregoing discussion is based on water-cooled reactors; similar accidents could occur, however, in systems cooled with gas or molten metal or salt. The immediate severity and the long-term effects might be different from those expected with water-cooled reactors, but this type of accident must be considered regardless of the reactor type.

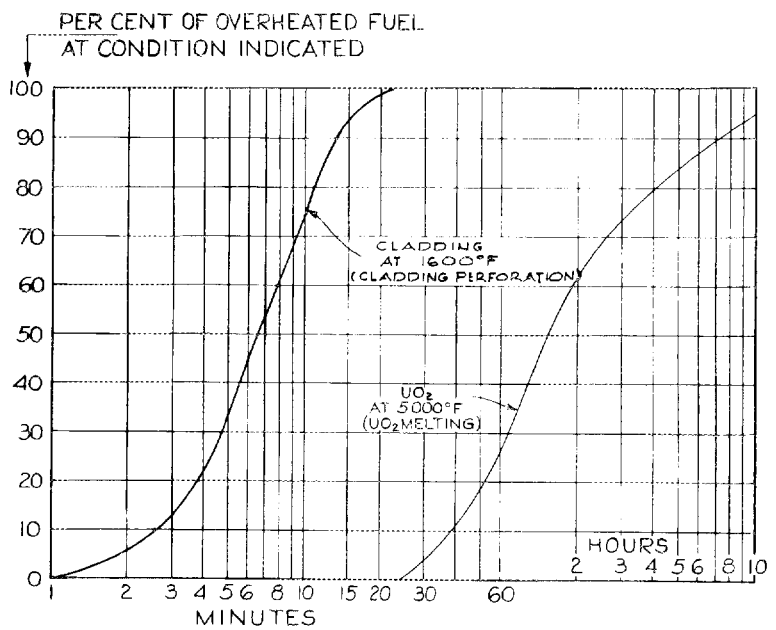

Fig. 3.5. Fuel Temperature Transient After Loss of Coolant Accident in the Bodega Bay Plant. (From ref. 7)

3.1.11 Fuel-Handling Accidents

Fuel elements that are removed from a reactor soon after operation offer opportunities for serious accidents. Such elements contain fission products and, furthermore, they may be damaged, broken, or weakened by their use in the reactor or by handling during removal. Since these elements have been irradiated, they represent an appreciable heat source, and if the decay heat is not removed, the temperature within the element may reach the cladding melting temperature in a short time. The fuel-handling accidents generally considered are of two types: mechanical failure, which leads to fission-product release, and insufficient cooling of the removed element, which could lead to melting. Although generally regarded as not a severe accident, in some facilities such an accident could constitute the maximum credible accident.

3.1.11.1 Mechanical Failure

Broken, damaged, or warped elements may present difficulty in the removal operation since the fuel transfer cask is normally designed to accommodate the "new" fuel element with ample clearance for minor changes. The possible accidents are typified by the fuel element that becomes jammed in the fuel transfer cask. In this case the element may be broken or pulled apart or possibly, because of its improper position in the cask, have insufficient cooling. All these occurrences may lead to fission-product release to the refueling room (see sec. 3.5).

3.1.11.2 Insufficient Cooling

Loss of cooling or of coolant could result in overheating, along with cladding failures that would allow fission-product release. Efforts should be made in design and operation to minimize the probability of loss of cooling of the transfer cask.

3.1.11.3 Misoperation

During handling of fuel the human element must also be considered. Improper procedures in the use of any of the fuel-handling equipment could result in either or both of the difficulties mentioned above.

3.1.12 Fuel Element Failures

By far the most prevalent incidents in reactor operation have been fuel element failures. The effects are usually minor, contributing only a minor source of activity to the circulating coolant. Fuel element failures may be caused by a number of mechanisms, as follows: (1) overheating due to hot spots or coolant flow restrictions, (2) stress or fatigue cracking, (3) swelling of elements caused by oxidizing metallic fuel or fission-product-gas accumulation, and (4) possibly incompatibilities between cladding and either fuel or coolant at various temperatures or flux densities.

3.1.13 Chemical Reactions

Some reactors use a coolant or a moderator that may, when thermally hot, react with air, water, or steam. Sodium-cooled reactors could be subject to a severe accident involving chemical reaction of the coolant with air or water upon rupture of the primary system. A graphite-moderated system could be subject to graphite-air or graphite-steam reactions that could add greatly to the hazards of operation. In these and other cases, steps are taken to control the atmosphere surrounding the reactor to exclude the presence of materials that could react with coolant or moderator. For example, the emergency cooling loop in the EGCR is designed to add nitrogen to the reactor system to prevent excessive oxidation of the graphite moderator. In some accident situations, cladding-fuel and cladding-coolant reactions may be of concern. Chemical reactions involving reactor materials are discussed in detail in Chapter 5.

3.1.14 General

There is virtually no limit to the failures that may cause accidents of various proportions. Each system must be analyzed for its own peculiar characteristics that may be the initiating mechanisms for an accident.

Some accidents may occur as a function of location. For example, during a hurricane a palm tree may be hurled through the vapor container of the BONUS Reactor (Puerto Rico). The Enrico Fermi Plant (Detroit, Michigan) designers considered the possibility of an airplane engine falling onto that plant. An earthquake was considered by those analyzing the safety of the Humboldt Bay Reactor (California). The SM-1 and SM-1A (Army Reactors) operators considered the possibility of acts of war or sabotage. These and "act of God" types of accidents are countless, but the more possible ones should be included in any safety analysis.

3.2 MAXIMUM CREDIBLE ACCIDENT

The accident that could occur and would have associated with it the most severe set of consequences as far as the radiation exposure of off-site personnel is termed the "maximum credible accident" (mca). Although this accident is a characteristic of a given plant, there are only two types of accidents that comprise the mca. The first is the loss of coolant accident, with subsequent core melting or possible nuclear excursion and release of fission products. The second is the fuel-handling accident in which a fuel element, or assembly, is dropped or allowed to fail in such a way that its fission products are released. After these initiating events occur, the released fission products disperse through the system and leak to the environment at some rate determined by the containment vessel in question.

Those who define the mca must analyze the set of circumstances that will determine the seriousness of the accident. This is a difficult problem because of the lack of the firm guide lines needed to make a "cut-and-dried" decision. Judgment is necessary when postulating the accident

and inevitably involves a subjective evalution of the product of probability of occurrence and hazardous consequences.

It was initially the policy to assume a very severe accident (really a series of accidents) for the mca; that is, one that would have extremely damaging effects and likewise little chance of occurring. Historically the occurrence of an accident that would now be regarded as incredible was postulated for the early power and power-demonstration reactors, but since the first reactor installations were in remote locations, the effect of this "incredible" accident on the general public was negligible. As the desire for development of nuclear power increased, it became obvious that remote sites for reactors would not often be available, so more realism had to be injected into the evolution of the maximum hazard. Of course, realism could not exceed knowledge on a given subject, so a compromise between the completely realistic approach and the pessimistic assumption of the worst conceivable accident had to be drawn. As was mentioned before, the product of probability times the hazard itself is involved in determining the accidents to be analyzed. Knowledge of the subjects pertinent to reactor safety is still not as abundant as desired, but progress has been and is being made. There is now a great amount of operating experience to draw from, as well as some reasonable approaches to accident analysis from the mechanistic point of view. Although the mechanistic approach has been used in the analysis of only a few plants to date, it is reasonable to assume that, as ability to assign a probability of failure to a given device or system increases, this is the next step in the evolution of a logical accident analysis.

3.2.1 Reference Description

The accident most often postulated, for water-cooled reactors at least, is (1) complete severance of a main coolant pipe so that coolant may be discharged unimpeded from both ends of the broken pipe, (2) rapid expansion of this fluid to vapor that contributes to the pressure loading of the reactor enclosure, and (3) meltdown (partial or complete) of the fuel with partial release of the contained fission products to the reactor containment system. This accident, or some modification of it, can also be postulated for other types of reactor, such as liquid-metal-cooled, gas-cooled, etc. In general, this accident is assumed to occur at a time when system conditions result in the most severe set of consequences.

3.2.1.1 Fuel Material Conditions

In all cases it is assumed that the reactor has operated at maximum power for a period of time sufficient to accumulate a large fission-product inventory. This means, for the purpose of accident analysis, that the amount of fission-product activity is defined. It is usually defined as the greatest amount of activity that is thought possible to obtain in the given reactor during operation for a long period of time at maximum power (see also Chapter 7). In special cases, such as the N.S. Savannah, the

accident at a particular location may be predicated on the power history of the reactor immediately prior to its arrival at that location.

An assumption must be made as to the fraction of contained activity that would be released upon occurrence of the accident. Of course, it could be assumed that all the contained activity would be released, but this would be unrealistic. It has been shown under simulated meltdown conditions that not all fission products are released from the melted fuel.[8] In many cases, when fuel is melted, relatively small amounts of activity are released. As may be seen in Table 3.1, the fraction of a given fission product that is released may be dependent upon the fuel material. It can be seen that the noble gases, iodine, tellurium, and cesium are the constituents that are released most readily; the others, in most cases, are negligible by comparison, although the transport behavior and relative maximum permissible concentrations must be considered in evaluating the relative importance of the various released activities. (Fission-product releases from fuels are discussed more fully in Chapter 4.) The sample calculation used by the AEC[9] is based on 100% release of the noble gases, 50% release of the halogens, and 1% release of the remaining fission products from the reactor system to the container (building) following fuel meltdown. It is further assumed that 50% of the released iodines are absorbed on surfaces within the reactor containment system.

3.2.1.2 Primary Coolant Conditions

In most cases the normal operating conditions are not assumed for the coolant at the time of the postulated accident, but rather the conditions specified are those that would yield the greatest amount of stored energy in the coolant. In some cases the reactor is assumed to be in the hot standby condition; this means that the average temperature of the coolant is at its highest, and consequently the stored energy is greatest. This condition is, however, not necessarily compatible with the condition producing the maximum possible amount of fission products; even so, these two assumptions are occasionally made, that is, maximum possible amount of fission products and maximum stored energy.

With the coolant conditions specified to yield the greatest amount of stored energy, the largest pipe in the system is assumed to break and allow coolant to issue unimpeded from both ends of the ruptured pipe. This assumption results in an additional degree of conservatism, since such a rupture is considered extremely improbable.[9]

Examples of mca's that have been postulated for various reactors are given in Section 3.2.3. For the calculational techniques involved in applying these accidents to the problem of containment, see the discussion in Chapter 6.

3.2.1.3 Release and Dispersion Conditions

As was mentioned above (sec. 3.2.1.1), not all the fission products that escape from the fuel after meltdown are considered to be available for release from the reactor building; for example, for the sample calculation used by the AEC[9] and based on information then available, it was assumed that 50% of the iodine released within the reactor building would be removed by deposition.

The contents of the building are assumed to leak at a rate that is equivalent to the specified leak rate of the containment system. In the

Table 3.1. Fission-Product Release from Various Fuels[a]

Material	Release Temperature (°C)	Release Upon Fuel Meltdown (%)								Source of Data
		Noble Gases	Iodine	Tellurium	Cesium	Ruthenium	Strontium	Barium	Rare Earths	
Metallic uranium	1200–1300	60	25	15	15	4				Windscale accidental melting and burning
Uranium-aluminum alloy	750–800	100	50		10					ORNL experiments
UO_2	~3000	100	100	100	90–98	50–90	0.2–2	0.5–5	0.5–5	ORNL experiments

[a]This table was prepared with the help of G. W. Parker of the Oak Ridge National Laboratory.

example given in ref. 9, the leak rate is assumed to be 0.1% of the containment volume per day, and this is assumed to remain constant for the duration of the accident.

After leakage from the building, the fission products are dispersed by diffusion and fallout from the atmosphere. Meteorological effects are not treated in this report, except to note that weather conditions typified by a severe inversion generally result in the greatest possible calculated doses at or beyond the site boundary. For more complete discussions of atmospheric diffusion it is suggested that refs. 9 and 10 be consulted.

3.2.2 Analysis

An approach to the mca analysis through studies of various mechanisms that might operate simultaneously or sequentially and yield, finally, some set of serious consequences is known as mechanistic analysis. This method consists of analyzing all possible accident sequences and their consequences to determine the most severe accident. A great number of possible combinations of events exist in any given analysis, and therefore the greatest difficulty is in determining, by individual analysis of each set of events, which accident will be the mca.

The typical failure sequence that is generally assumed consists of

1. Primary coolant loop failure with subsequent loss of coolant,
2. Secondary coolant loop failure with at least partial loss of that coolant,
3. Instantaneous fuel element failure caused by the rapid depressurization of the core,
4. Continued failure of elements because of decay heat.

These failures appear to be the same as those taken for the nonmechanistic analysis, but the manner in which each failure is determining in the overall accident is different.

The first two steps may be discussed together. A rupture of the primary coolant loop is assumed, but instead of assuming instantaneous loss of coolant, the piping loop is analyzed for the position where a break would be the most serious and would have a real probability of occurring. A break of finite size is assumed to occur at that point. Knowing the size of rupture, the upstream pressure, and the coolant inventory, the time for blowdown of the loop is calculated. The same sort of analysis is then made of the secondary coolant system. With these two rates of energy addition to the containment system specified, pressure and temperature versus time curves can be drawn. Then, based on conservative heat transfer rates to the building, to the atmosphere, or to the structures inside the container, the pressure and temperature versus time curves may be revised downward to fit this more realistic case. The revised curves specify the containment design pressure.

Failures of the fuel elements specify the fission-product inventory available for leakage over the accident period. It is assumed that a number of elements will fail initially as a result of the rather sudden depressurization of the primary loop. This number is calculable when the physical condition of the fuel element cladding can be evaluated or estimated. Then as decay heat begins to build in at a predictable rate,

other elements will fail and release fission products to the container. Again these are predictable failures, since the temperature of an element can be calculated (conservatively) and the temperature at which the cladding will fail is known (by experiment). Once the fuel elements have failed, assumptions concerning release and plate out must be made based either on special experiments or on general experiments such as those that provided the basis for the numbers in ref. 9, that is, 100% release of the noble gases, 50% release of the halogens, and 1% release of the solids, with 50% of the iodines retained in the container and the rest available for release from the containment system.

This type of study requires extensive research and analysis with regard to the initial failure and equally extensive experimentation in the area of fuel element failure. However, it yields a result that is more realistic than the conventional mca analysis. All safety analyses contain the mechanistic approach to some degree and include the effectiveness of various countermeasures, even though credit may not always be allowed. The EGCR analysis is an example of a thoroughly mechanistic one[11] (see sec. 3.2.3.2).

3.2.3 Examples of Assumed MCA'S

3.2.3.1 Conventional Types

1. Pressurized-Water Reactor. The Yankee Atomic Electric Company postulated for their reactor that in the event of the loss of coolant accident, core meltdown would be prevented by the emergency injection system. However, it was further shown that, even in the case of fuel meltdown, no danger would be presented to the public. Therefore a more severe accident was analyzed as the basis for the mca. The most extensive danger afforded by the nuclear plant was the possibility of release of fission products. Because of this unique danger to the public, all reasonable measures were taken to guard against even the very unlikely accident that could cause radiation hazards outside the plant area. The accident considered is outlined below.[5]

It was assumed that a 20-in. pipe in the primary system would be severed, resulting in depressurization and virtually complete loss of water from the primary system. Blowdown of the primary system would result in an initial pressure rise in the vapor container to 33.85 psig, which would decrease to approximately 15 psig after 2 hr (see also chap. 7). It was further assumed that, for unexplained reasons, the safety injection system would not function and that partial core meltdown would occur. No criticality of the fuel pellets released by melting of the cladding would occur, but 20% of the gaseous and volatile fission products present in the core after 10,000 hr of reactor operation at 485 Mw would be released to the vapor container and dispersed homogeneously therein. It was also assumed that the gaseous and volatile fission products would be released instantaneously from the fuel into the vapor container, although the release actually would occur after a finite time interval that would begin several minutes after the start of the accident. The vapor container has a leak rate of 70 ft^3 (STP)/hr with the vapor container at an internal pressure at 15 psi above atmosphere, and this leak rate and driving head were assumed to continue indefinitely.

For many pressurized-water reactors, failure of the secondary loop piping, either partial or total, is also assumed. This assumption would add to the loading of the containment shell.

The temperature transient in the core resulting from the loss of coolant and failure of the safety injection system would bring on core melting. Core melting as a function of time is shown in Fig. 3.6.

2. Boiling-Water Reactors. The mca for the BONUS Reactor, a boiling-water reactor, is also the rapid loss of coolant, with subsequent core meltdown. The postulated accident is outlined below:[12]

> "The worst credible reactor-rupture accident is considered to be a rupture of the reactor primary water system which is equivalent to a cross-sectional area of a 16-in. line at the bottom of the pressure vessel, since this has the highest probability of releasing the maximum amount of fission products.

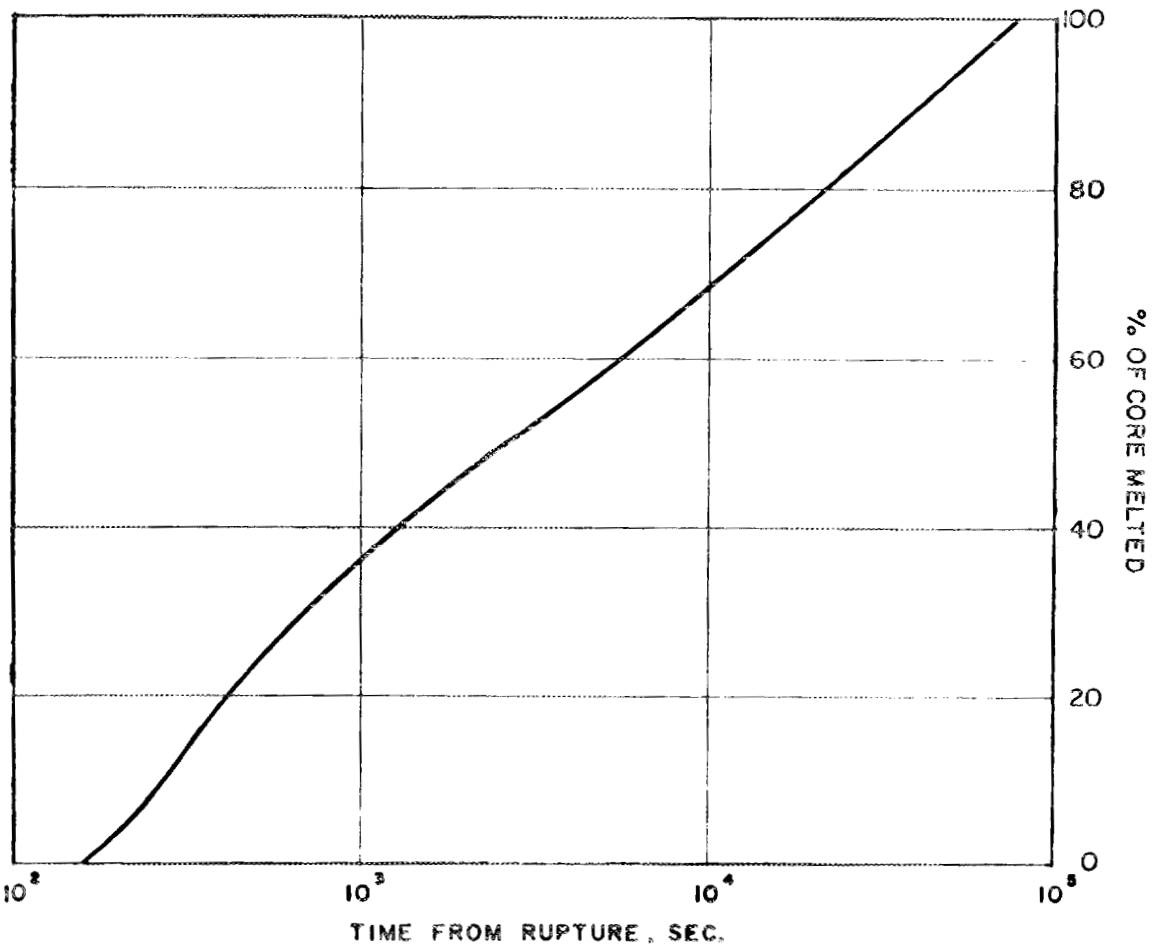

Fig. 3.6. Core Meltdown Following Rupture of a 20-in. Primary Coolant Pipe, with No Safety Injection, in the Yankee Pressurized-Water Reactor. (From ref. 5)

The various assumptions used as a basis for calculating the effects of a maximum credible accident are listed below. The assumptions regarding quantities of various fission products released from the molten fuel are the same as typical values listed in a reactor siting calculation example given in the Code of Federal Regulations (10 CFR 100). Experimental fuel meltdown data justify the use of these values. The siting criteria assumptions used for the dosage calculation are:

1) the core has been operating at full power for an extended period of time when a pipe rupture occurs;
2) the reactor will become subcritical by 10% Δk a few seconds after the break;
3) the emergency core spray system fails to operate;
4) all the water in the pressure vessel is discharged in approximately 4 seconds [see Fig. 3.7];

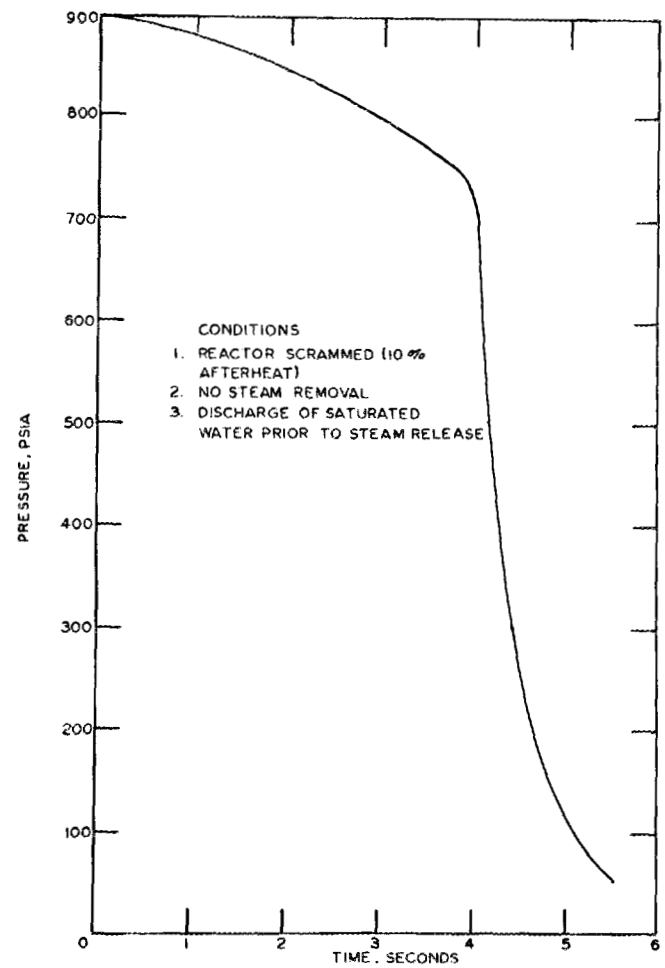

Fig. 3.7. Reactor Vessel Pressure as a Function of Time After Rupture of 16-in. Recirculating Water Line in the BONUS Reactor. (From ref. 12)

5) all the fuel melts, releasing 100% of the noble gases (Xe, Kr) to the containment building;
6) fifty per cent of the halogen gases (I, Br) escape from the reactor vessel and are dispersed into the containment building (half of this material plates out on the walls and internal structures of the containment building);
7) one per cent of the "non-volatile" fission products (products other than noble gases or halogens) escape from the reactor vessel into the containment building and are plated out on building structures;
8) no credit is taken for the natural shielding provided by the hills surrounding the BONUS site;
9) no credit is taken for scrubbing of fission products or reduction of containment pressure by the water moat in the pump room;
10) no credit is taken for any heat energy transferred to the containment building walls and other structures;
11) all fission products released to the containment building are assumed to remain above the main floor;
12) the containment building is pessimistically assumed to pressurize to 4.3 psig and to have a constant leakage rate of 0.4% of the contained air per day throughout the course of the accident, which is assumed to last for a period of 90 days; the 0.4% value is the containment building allowable leakage rate at the design pressure of 5 psig;
13) the building spray comes on 30 seconds after the building becomes pressurized and removes 95% of the halogens still suspended in the building atmosphere but does not remove any of the material deposited on internal surfaces.*

"If it is pessimistically assumed that no heat is lost from the fuel once coolant flow ceases, the hottest spot in the superheater will reach the clad melting temperature (2500 to 2600°F) approximately 60 seconds after the break occurs. Most of the superheater is, of course, operating at power levels well below those assumed to exist at the hottest spot. As a result, the clad temperature of an average element will take more than 11 minutes to reach the melting temperature. Although melting of the clad will start in about one minute, the UO_2 will remain relatively unaffected until it reaches the melting point of approximately 5000°F. Even for the hottest element, it will take more than 7 minutes for this to occur; for the average superheater element it will take 48 minutes for the UO_2 to reach the melting point.

"For the boiler fuel the results of loss of water are similar to those described for the superheater except that

---

*This assumption is made, but even when credit is not taken for it, the off-site dose is not in excess of the minimums set forth in the Code of Federal Regulations, Title 10, Part 100.

the cooling following the scram is more effective for the boiling during the 4 second period required for the vessel to lose all its water. The cladding at the hottest spot will reach the melting temperature (3270°F) in approximately 80 seconds if the core spray fails to come on and no cooling is provided. However, 16 minutes will have elapsed before the clad on the average boiling element reaches the melting temperature. The UO_2 at the hot spot in the boiler will reach its melting point in approximately 4 minutes, but the UO_2 from an average boiling element will require 33 minutes to reach this temperature.

"It should be noted that the meltdown described in the above paragraph, will occur only if the emergency core spray system fails. If the gravity actuated spray is turned on at any time before melting has occurred, the fuel will again be cooled and fuel temperature conditions similar to those which occurred with stoppage of steam flow will be produced."

3. Liquid-Metal-Cooled Reactor. Since liquid-metal-cooled reactors operate with near ambient pressures in the primary coolant loop, there is little reason to designate as credible the loss of coolant accident. Furthermore it is possible to design the system so that the reactor cavity and vessel are at the lowest point in the system, and thus no break in the primary system can allow the core to be drained. Since the heat transfer of the convecting sodium is sufficient to remove the afterheat from the fuel, core melting is not considered credible for such a system. Since the mca is defined as that accident which offers the most danger to the public, a careful analysis of all other possible accidents and their consequences must be made in order to identify the mca.

The maximum credible accident for the Hallam Nuclear Power Facility is the dropping of one fuel slug (or its equivalent in small pieces) from the fuel-handling machine. The likelihood of this accident occurring is minimized by various safety interlocks and well-trained operating personnel.

The accident was determined to be the mca from several possibilities, as listed in Table 3.2. As may be seen in Table 3.2, several accidents were analyzed for both credibility and hazard to the public, and from the tabulation the worst credible accident was clearly evident.

The arguments that pertain to the mca, the fuel-handling accident, are contained in the following discussion:[13]

"The design features of the fuel handling machine make it highly unlikely that any fuel slugs could be dropped from the cask during a normal fuel transfer operation. However, a non-routine situation is postulated where one or more slugs might fall from the handling cask. Possible consequences of such situations have been made based on pessimistic values of heat generation, temperature, fuel oxidation rate, and radioactivity released. Specific cases considered are:

1) The hottest slug of the element drops intact.
2) The hottest slug drops in several pieces.
3) All slugs of one rod drop intact.
4) All slugs of one element drop intact.

Table 3.2. Summary of Hallam Reactor Postulated Incidents[a]

Postulated Incident	Possible Causes	Safeguards Against Incident	Remarks	Building Dose or Dose Rate	Site Boundary Dose or Dose Rate	Credible
1. Meltdown of one fuel element	Foreign matter in primary system or maloperation of variable orifice	Primary system kept clean; channel outlet temperature monitored	Cover gas activity increased to 10,000 $\mu c/cm^3$	Negligible	Negligible	Yes
2. Core meltdown	Complete failure of control and protective systems and no action by operator	Failsafe circuitry	Leads to ultimate shutdown	Negligible	Negligible	No
3. Fuel element rupture in wash cell	Excessive sodium holdup in element	If elements known to have ruptured, cladding will not be washed	4×10^3 curies in wash cell condensate; 1.3×10^2 curies in cover gas	Negligible	Negligible	Yes
4. Fuel-handling incident						
Element meltdown in fuel-handling machine	Loss of helium cooling in fuel-handling machine	About 30 min to remove element following blower failure	2.1×10^4 $\mu c/cm^3$ in handling machine atmosphere	17 mr/hr	Negligible	Yes
Fuel slug dropped from fuel-handling machine	Transfer of damaged element with gate valve at bottom of machine open (requires interlock bypass)	Key to interlocks with shift supervisor	Elements known to be damaged will be allowed extra decay time	530 r/hr direct at 10 ft	Direct: 7 mr (1 hr) Iodine: 8×10^{-5} rad (1 hr) Noble gas: 4×10^{-5} mr (1 hr)	Yes
Complete and instantaneous oxidation of entire dropped fuel element	None known			80,000 r/hr direct at 10 ft	Direct: 1 r (1 hr) Iodine: 190 rads (1 hr) Noble gas: 100 mr (1 hr)	No
5. Pressurization of inert atmosphere in						
Reactor cavity	Sodium leak into reactor cavity	Reactor vessel and outer vessel prevent leak; cavity vent system and rupture disks prevent pressure	Primary fill tank keeps core covered with Na; rupture disks go at 10 psig	None	None	No
Intermediate heat exchanger cell	Large sodium spill in intermediate heat exchanger cell	See item 6 below	Nitrogen cooling system limits temperature to 242°F and pressure to 2.8 psig	None	None	No
	Nitrogen cooling system fails	100% cooling capacity continuously available	Pressure rises 1.8 psig in 15 min	None	None	No
6. Sodium spill						
Small (~100 lb)	Equipment or piping leak	Careful design, construction, and testing	No fire or radioactivity release	None	None	Yes
Large (160,000 lb)	Primary pipe rupture (no known reason)	Careful design and construction	Cell gas temperature and pressure rise to 242°F; no fire or radioactivity release	Negligible	Negligible	No
Large spill following core meltdown	Primary pipe rupture (no known reason)	Careful design, construction, and testing	Leakage of Xe and Kr decay products from halides in Na	0.033 $\mu c/cm^3$ (dose rate not calculated)	820 mr	No

[a]From ref. 13.

Table 3.2 (continued)

Postulated Incident	Possible Causes	Safeguards Against Incident	Remarks	Building Dose or Dose Rate	Site Boundary Dose or Dose Rate	Credible
7. Radioactive sodium fire						
Small	Small spill in area open to atmosphere	Careful handling of hot sodium		Negligible except close to spill	Negligible	Yes
Large	Gross disregard of procedures during a maintenance operation	Lock and tag procedure during maintenance	Dry scrubber and filters remove all but 81 lb of radioactive sodium from building exhaust	Extremely large (not calculated)	Direct: 0.4 r in 2 hr; 16 r in infinite time Cloud: 8.0 mr in 2 hr; 65 mr in infinite time Ground deposition at 1.75 miles: 2.4 mr in 2 hr; 2.2 r in infinite time	No
8. Steam generator leak (complete rupture of duplex tube)	Unknown	Monitor system detects leaks before two walls fail	Large, nonradioactive fire results	None	None	No
9. Control rod thimble leak	Thimble leak above sodium level plus failure of helium supply	Observation of helium supply system; leaking thimbles removed	Cover gas collects in actuator housing	520 mr/hr at 1 ft from actuator housing	Negligible	Yes
10. Gas leakage through loading face shield						
1% failed fuel rods	Seals omitted from one shield plug	Operating procedures	Estimated leakage, 120 ft^3/day	5 mr	0.014 mr	No
Core meltdown	Same as above; see item 2	Same as above; see item 2	Same as above	<25 r (50 min)	260 mr	No
11. Gas leakage from primary pump	Broken sight glass	Location, sturdy construction	Incident can be stopped by closing valve	1.1 r	0.76 mr	Yes
12. Loss of reactor heat sink	Complete loss of primary or secondary coolant systems	Three independent cooling systems	58 hr before sodium boiling	None	None	No

"Case 2 represents the most likely of the situations considered. Construction of the lower rod hanger beneath the fuel is such that it acts as a screen to keep the fuel within the process tube; thus, an intact fuel slug will not fall through it. For purposes of analysis, pieces of the broken slug are assumed to have the same surface-to-volume ratio as a cylindrical section 1/10 as long as a whole slug, and it is assumed that the slug breaks into ten pieces.

"Heat generation rates are based on a maximum decay power of .071 kw for a 6-in. slug, 10 hours after reactor shutdown. The axial power distribution is assumed to have a cosine shape with peak-to-average ratio of 1.5, as shown in Fig. B-2 [see Fig. 3.8, this report]. Temperatures of dropped slugs are calculated by taking into account radiation and convection cooling. The slug temperature as a function position in the fuel rod is plotted in Fig. B-2 [Fig. 3.8]. Surface oxidation rates (Fig. B-3) [Fig. 3.9] are based on experimental data(1) [ref. 14, this report] which gives a maximum rate of 5 mg/cm^2-hr. for 800°F UC in moist air for 1 hr. To extrapolate oxidation rates for lower temperatures, the variation of oxidation rate of metallic uranium in air with temperature was used.(2) [ref. 15, this report] The UC oxidation rate as a function of the slug position in a rod is shown in Fig. B-2 [Fig. 3.8].

"Results of these slug oxidation calculations are presented in Table B-1 [see Table 3.3, this report]."

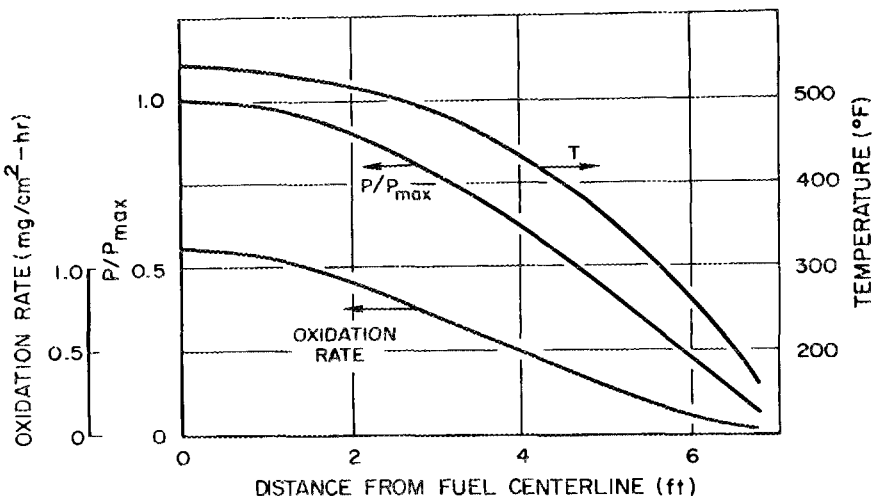

Fig. 3.8. Fuel Slug Relative Power, Temperature, and Oxidation Rate for Uranium Carbide Element Dropped on the Floor of the Hallam Reactor. (From ref. 13)

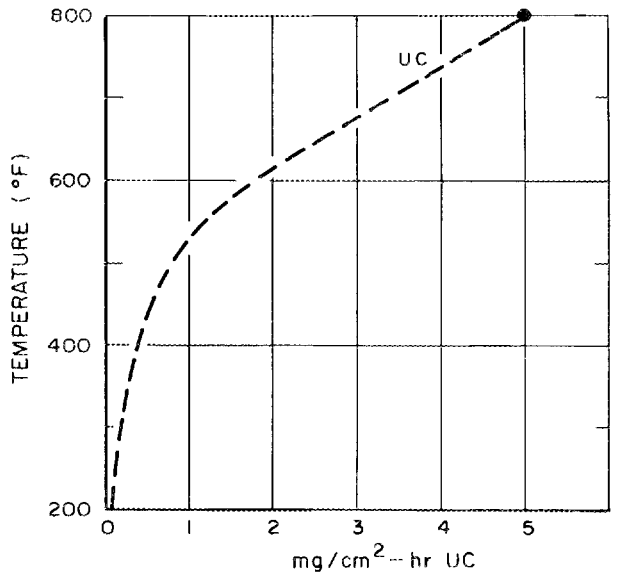

Fig. 3.9. Oxidation Rate of Uranium Carbide as a Function of Temperature in the Hallam Reactor. (From ref. 13)

Table 3.3. Temperature, Oxidation Rates, and Radiation from UC Fuel Slugs on the Reactor Floor of the Hallam Reactor[a]

	Hottest Slug	Broken Slug	One Rod	Entire Element
Fuel temperature,[b] °F	540	430	540–160	540–160
Oxidation rate, mg(UC)/cm²·hr	1.1	0.5	0.62 av	0.62 av
Noble gases				
Activity released in 1 hr, curies	0.56	0.39	7.1	57
Building activity, c/cm³	5.1×10^{-6}	3.5×10^{-6}	6.5×10^{-5}	5.2×10^{-4}
Dose at site boundary				
Neutral,[c] stack release, mr	3.4×10^{-4}	2.3×10^{-4}	4.3×10^{-3}	3.5×10^{-2}
Strong lapse, stack release, mr	2.2×10^{-4}	1.5×10^{-4}	2.8×10^{-3}	2.2×10^{-2}
Iodine				
Activity released in 1 hr, curies	0.63	0.44	8.0	64
Dose at site boundary during strong lapse,[c] stack release, rads	6.5×10^{-4}	4.5×10^{-4}	8.3×10^{-3}	6.6×10^{-2}
Direct radiation to site boundary in 1 hr, mr	9.5	9.5	171	1370

[a]From ref. 13.

[b]Based on one year of operation at 1.8 Mw(t) and 10 hr of decay after shutdown.

[c]Most unfavorable weather conditions.

4. Organic-Cooled Reactors. The maximum credible incident for the Piqua Nuclear Power Facility was designated as the group of incidents in which the control rods would be withdrawn from the core in a continuous and uncontrolled manner during the startup of the reactor following shutdown from extended operation at full power. This incident would be terminated by void formation and the meltdown of 50% of the six central fuel elements, which could release 7.5% of the core fission products. The total amount of energy released during the transient would be 2750 Mw-sec, which would cause a temperature increase in the coolant of less than 100°F. The pressure increase in the reactor system due to this temperature rise would be small.

In the uncontrolled startup incident, simultaneous malfunction of the control rod drive system and failure of at least two complete channels of the protective system (i.e., the period circuitry and the power flow comparator circuitry) were assumed. The resulting transient is shown in Fig. 3.1, in which the neutron power, hot-spot temperature, hot-channel outlet coolant temperature, and burnout margin are plotted against the time after sensible heat generation (assumed 1% of rated). The burnout margin is defined as the ratio of critical heat flux to maximum operating heat flux, where the critical heat flux is that heat flux necessary for the inception of film boiling.

By reference to Fig. 3.1, it can be seen that burnout would occur 32 sec after sensible heat generation, and, since the conservatively assumed minimum shutdown margin is 3% Δk in this case, it would take at least 332 sec (over 5 min) from the start of rod withdrawal to reach burnout. The peak power at burnout is 221% of rated power, the highest power level attained in any of the incidents. Once the critical heat flux was reached, film boiling would occur. If it is assumed that no heat would be transferred through the film, fuel plate melting would occur approximately 2 sec after burnout. Referring again to Fig. 3.1, it can be seen that the power level at burnout would increase slowly because the reactivity would be only slightly above that required for criticality. Melting of less than 50% of the six central elements would make the core subcritical in the complete absence of control rods. The energy released during the transient (from the start of the accident to the time at which shutdown occurred due to fuel melting) would be approximately 2750 Mw-sec, as mentioned above. This would present no radiological hazard because the melted fuel would be contained within the reactor coolant system.[1]

Since this accident was unlike any previously considered by the AEC, a more conventional analysis was made by Biles of the Reactor Safety Branch (see sec. 7.3.8 of chap. 7). He concluded that the "...hypothetical worst possible situation probably would not result in injurious dose rates, particularly in view of the opportunity for evacuation from the nearby areas. Any credible accidents would cause substantially lower exposure possibilities."

3.2.3.2 Mechanistic Type

The Experimental Gas-Cooled Reactor (EGCR) is an example of a power reactor facility for which the mechanistic approach to the evaluation of its hazards was used. The mechanistic approach is tedious in that it

requires the evaluation of many sequences of events to finally arrive at the mca. The following is a description and discussion of the accident:[11]

"The most severe class of accidents that can occur in the EGCR is the loss of coolant (depressurization) accidents. These accidents, in general, result in the most severe fuel element temperature transients. In addition to these temperature transients, the external pressure on the fuel element cladding is reduced thereby changing the force acting on the cladding from an external or collapsing force to an internal or bursting force. This internal pressure combined with the severe temperature transients results in the largest number of predicted fuel element failures.

"The maximum credible accident, however, cannot be determined solely on the basis of fuel element failures since these govern only the release of activity to the containment shell. It is quite possible that the accident which results in the largest activity release from the reactor may not be the accident which results in the greatest release of activity beyond the containment shell. For this reason, the maximum credible accident in the EGCR is a composite accident, and includes the most severe features of several depressurization accidents.

"The MCA for the EGCR is identified as a rupture of the primary coolant piping which depressurizes the primary system, suppresses core coolant flow for 30 sec and causes internal failure of the steam generator in the ruptured coolant circuit. From the end of the depressurization to the end of the accident the most severe reactor condition from the standpoint of reactor cooling is assumed. From one hour to several days after the accident, the emergency cooling loop and the nitrogen pure gas system to control graphite oxidation are assumed to be in operation.

"Approximately 330 fuel elements fail during the first 30 sec of the accident. No subsequent fuel element failures occur. [Fuel clad temperatures as a function of time for the several core positions are shown in Fig. 3.10.] Concurrent with controlled graphite oxidation, the UO_2 within the failed fuel elements is assumed to oxidize at the rate given as follows:

$$\frac{df}{dt} = be^{-bt}$$

where:

f = the fraction of exposed UO_2 oxidized
b = the oxidation rate coefficient (sec^{-1})
t = time (sec).

"For the purpose of calculating release from the containment shell, a constant internal pressure of 9 psig is assumed for the first 24 hr after the accident. It is next assumed

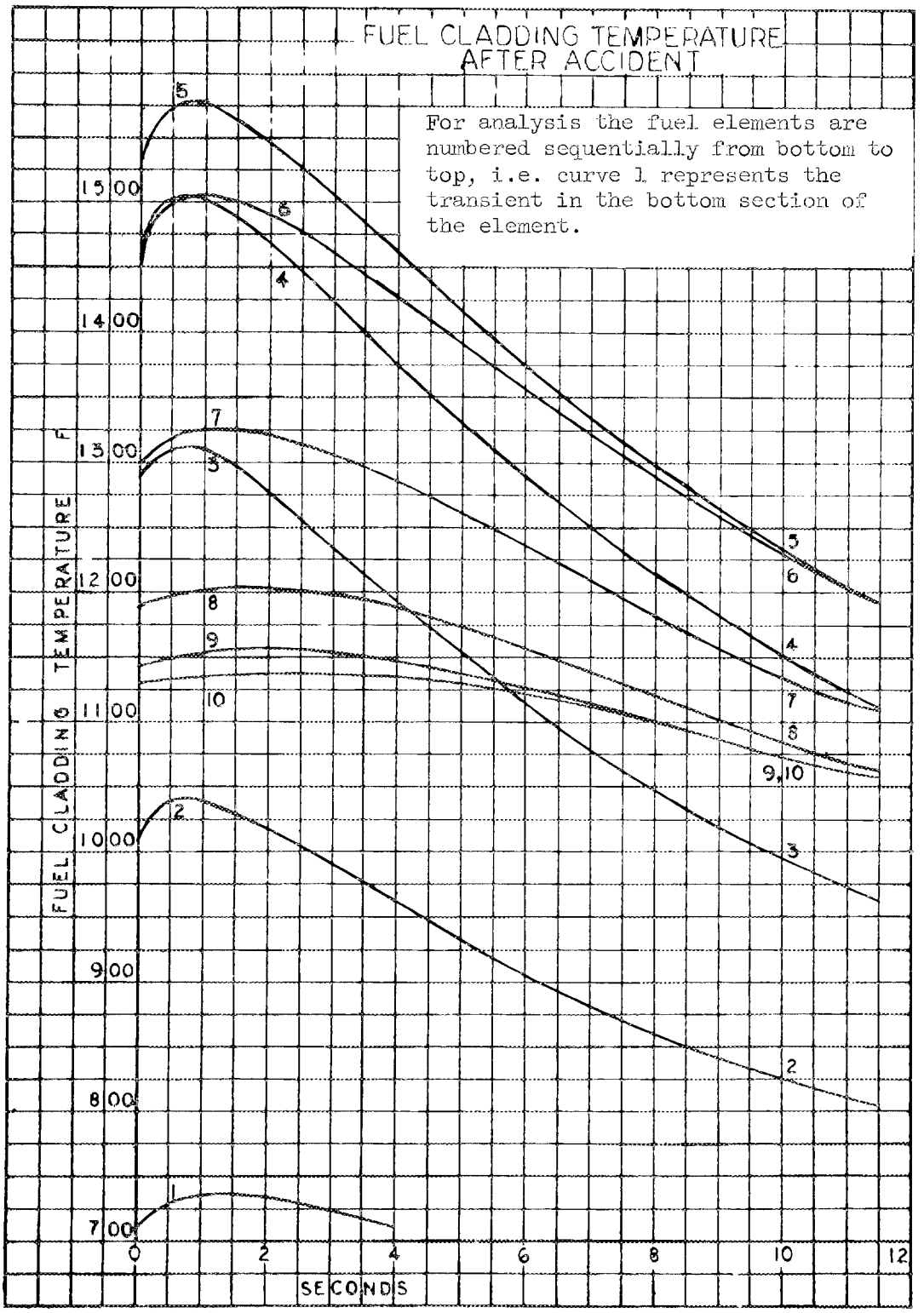

Fig. 3.10. Post Accident Fuel Cladding Temperatures for the EGCR. (From ref. 11)

that at 24 hr after the accident the containment shell internal pressure is reduced to 4.2 psig and remains constant from 24 to 61 hr after the accident. At 60 hr after the accident the pressure in the containment shell is assumed to be reduced to zero psig. Containment shell leakage is based on 0.3% of the contained mixture per day at 9 psig.

"The assumed containment shell internal pressures are conservative, based upon the calculated pressure transient following the accident, and the capacity of the containment shell fission product removal system. It is assumed that the reactor operator places the fission product removal system into operation 24 hr after the accident.

"For the first 24 hr after the accident, the dose to the public is due only to the leakage (assumed to be at ground level) from the containment shell. From 24 to 61 hr, the dose is due both to containment shell leakage and the effluent from the fission product removal system (at stack level). During this period the stack discharge rate is conservatively assumed to be constant at the initial rate. From 61 hr to 3 days the dose is due to the fission product removal system effluent only. During this period the stack discharge is assumed constant.

"After 3 days, the nitrogen purge is stopped; consequently, the effluent from the stack and the activity release from the containment shell stops. A continued release of activity to the containment shell due to oxidation of the UO_2 is conservatively assumed to occur until 64 days after the start of the accident.

"The requirement for afterheat removal from the reactor core terminates at approximately 3 months after the start of the accident."

3.3 COMPONENT FAILURES

The pressure vessels and the high-pressure piping used in nuclear reactor systems are not unlike those used in the steam-generation systems that employ a conventional heat source. Mechanisms that tend to produce failure in a conventional system are present in all systems designed to contain thermally hot fluids under pressure. Wear, creep, corrosion, fatigue, stress, graphitization, sigma-phase precipitation, etc., are present in all systems fabricated from conventional steels; and similar mechanisms are usually present in the more exotic alloys now being used in the manufacture of some nuclear plants. These mechanisms are usually fairly well understood, qualitatively at least, and by proper consideration in design the associated failures can largely be eliminated. This is evidenced by the low frequency of failures that have been sustained in conventional steam power plants.

If a break occurs in a conventional plant, steam or hot water may be released, and operating personnel may sustain injury; but, in general,

this is an inconvenience or hazard only to the operators of the plant. If, however, a similar release occurs in a nuclear plant, it may have associated with it the additional hazard of radioactivity release. For this reason, more rigorous adherence to design criteria is necessary. Furthermore, there is one additional mechanism that may contribute to the failure probability in a nuclear plant – radiation embrittlement of steel. Fast neutrons have a tendency to harden steels and make them more susceptible to brittle fracture at a given temperature. Quite fortunately this effect is seen only in the vessel containing the active core; and furthermore, it is generally confined to that part of the vessel which is nearest the core. Provision for all these factors in the design of a plant increases the confidence in that plant from the safety standpoint.

3.3.1 Pressure Vessels

The possibility of catastrophic failure of the reactor pressure vessel has not been considered credible in power reactors. Since there is little experience with pressure vessels as applied to the nuclear field, it is necessary to draw from experience with high-pressure steam boilers. In the Humboldt Bay safety analysis,[16] a statement of fact and statistical evidence is made to lend support to the assumption that catastrophic failure of the reactor pressure vessel is incredible. It reads as follows:

> "Statistics on reactor vessels are not available because of the relative newness of this application. However, good statistics are available on power boilers, and these statistics seem generally applicable to reactor vessels. It is conservatively estimated that there are 400-500 boilers in the United States designed to operate at a pressure over 600 psia, and that they represent not less than 4000 boiler-years of operating experience. The first such boiler was designed over 30 years ago. An examination of the Hartford Steam Boiler Inspection and Insurance Company power boiler statistics shows no failures of steam drums in power boilers designed to operate over 600 psia. In no case have the materials used in these drums been superior to those used in fabrication of reactor vessels... . The allowable design stress for the ASME Code vessel is less than one-fourth the ultimate strength of the material. A ductile shear type of failure resulting from loadings which exceed the ultimate strength of the material over a significant section of the reactor vessel could occur only from extreme overpressure or extreme overloading of a large section."

Reactor vessels are not easily examined on a periodic basis as are vessels for nonnuclear use, and for this reason design and construction of nuclear vessels is more conservative. With the greater degree of conservatism in manufacture, the confidence in the "as built" vessel is greater. With nuclear vessels, special attention is given to stress concentrations. It would not be reasonable to expect that a vessel could be built without areas of high stress; nozzles, openings, and supports

must be provided, and these features give rise to geometric discontinuities,[17] and hence local stresses, but these stresses may be minimized. There are two experimental programs under way to investigate pressure vessel failure: a British study directed at fast fractures of pressure vessels[18] and a study of responses to cyclic stresses that is being done by the Southwest Research Institute in this country. (See also the discussion on embrittlement of steels, sec. 8.5.)

3.3.2 Piping

Except for the catastrophic rupture of the pressure vessel, the event that would generally result in the most severe accident in a nuclear facility would be rupture of the largest pipe in the system. It is frequently considered that the mca is initiated by the rupture of the primary piping and that the break releases fluid in such a way that maximum flow is possible from both ends of the broken pipe, that is, a "double-ended" rupture.

It was pointed out by Helmut Thielsch[19] that "pipe is pipe" and whether used in a steam plant, refinery, or nuclear plant, the same design considerations are imposed. When piping is properly designed, sized, and supported, the possibility of failure is virtually eliminated. A survey[20] made of piping failures (nonnuclear) over the last 30 years showed that there have been many small leaks, cracks, and ruptures in pipes, tubing, and fittings, but only four ruptures in large piping have been reported, and these failures were attributed to inferior materials or manufacture.

Recently a review of fracture modes as related to primary coolant system rupture was published. The work, which cites nearly 100 references in the study of fracture mechanics, is summarized by the following conclusions:[21]

1. With the proper application of present knowledge, fractures by fibrous ductile fracture due to gross overstress or by brittle cleavage can be virtually ruled out as credible events (unless cyclic strain aging is found to raise the brittle-ductile transition temperature above the service temperature for carbon steels).

2. With the proper application of present knowledge, fracture by creep-rupture at 500 to 650°F can be virtually ruled out, although combined creep and fatigue should be further studied with respect to superheat plant piping.

3. Relationships exist that could be used to eliminate any possibility of impact erosion failures if the critical velocity parameters were determined for the specific piping steels.

4. The remaining possible fracture modes, fatigue, low-energy ductile fracture, and localized corrosion cracking, are now well enough understood that the probability of their occurrence is acceptably low.

Important questions that cannot be answered on the basis of present knowledge are:

1. Can long, shallow, crack-like defects develop undetected due to fatigue or localized corrosion, and can such defects, if developed, propagate to large-area fractures by unstable ductile rupture?

2. Is the time for serious fatigue or corrosion crack (or leak) propagation, in the specific materials of interest, fast or slow compared with the inherent response time for flaw and leak detection procedures?

3. Can service experience thus far, and short-term experimental results showing freedom from localized corrosion fracture, be taken to imply complete immunity from attack over a 10- to 40-year service exposure?

A method of calculating the maximum size of a ductile rupture was suggested by H. B. Ketchum.[22] The method is subject to some criticism but has been used in many cases in an effort to define some minimum values as guide lines to system design. It must be noted, however, that this paper[22] deals with ductile ruptures, which are generally less severe than the brittle rupture. Increased knowledge and experience in this field may lend credence to the mechanistic approach to the analysis of the mca. As was stated before, almost all failures in piping and tubing have been of the ductile type, and they were minor in importance as far as catastrophic events are concerned. Ketchum,[22] in his effort to compare his computed results with actual experience, accumulated data on the pipe and tubing failures that have occurred. Table 3.4 contains much of this information. A second group of data was also assembled that included information on ruptures under test conditions which resulted in stresses in excess of those found under normal conditions in an operating system. Under these conditions, the relationship developed by Ketchum predicted failure sizes considerably smaller than actual. The statement is made[22] that when the ratio of the stress to the yield-point stress (σ/σ_{yp}) is greater than about 70%, Ketchum's method becomes useless in predicting failure sizes. Table 3.5 gives the information taken under these inapplicable conditions.

3.4 PROBABILITIES

In order to establish probabilities, a large amount of experience must be accumulated with a sizeable number of events taking place. The probability might be thought of as a fraction, with the number of opportunities for the occurrence of an event being the denominator and the number of actual events occurring being the numerator. As the absolute values of these two numbers increase, the confidence in the resulting fraction, or probability, increases. With this simplified picture in mind, it becomes obvious that a given function must be repeated many times to establish, with good confidence, the likelihood of some occurrence in that function. For example, many cars must travel many miles to establish the rate (on a per mile basis, for example) at which flat tires will occur. Using the same line of reasoning, many nuclear plants must operate many hours to establish the frequency of accidents, both serious and minor. Such experience will not be accumulated in a sufficient amount for a number of years. It is necessary and sensible to apply the experience accumulated in other industries faced with similar problems, and this is done when nuclear plants are discussed.

The chemical industry has been faced with the production and transportation of invidious reagents for many years. The containment of a

Table 3.4. Data on Pipe and Tubing Failures[a]

Description	Material	Fluid	Temperature (°F)	Pressure (psig)	Inside Diameter (in.)	Outside Diameter (in.)	Wall Thickness (in.)	Calculated Failure Length (in.)		Stress Ratio, σ/σ_{yp} (%)	Failure Length (in.)	Failure
								Maximum	Minimum			
8-in. main steam line	Type 347 stainless steel	Steam	1050	1800	8	10.2	1.1	6.06	3.66	21.9	2.4 (est.)	Crack 9.6 in. long (outside), estimated 9.6 × 2/8 = 2.4 in. (inside)
1/2-in. aircraft hydraulic line	Aluminum	Hydraulic oil	Room	3000	0.3	0.5	0.1	8.81	6.07	11.9	8 (est.)	Flap length parallel to tubing axis
1-in. test loop line	Type 304 stainless steel	Water	450	2000	0.957	1.315	0.179	8.73	2.86	25.1	3	Split longitudinally parallel to pipe axis
6-in. turbine steam lead	Type 304 stainless steel	Steam	900	850	5.761	6.625	0.432	8.47	2.62	27.4	4	Split longitudinally parallel to pipe axis
6-in. steam lead	Type 347 stainless steel	Steam	1050	1500	6.000	7.436	0.718	6.35	3.79	19.36	2	Crack 8 in. long outside; 2 in. long inside
Atkomatic valve	Type 316 stainless steel	Water	210	3000	0.814	1.000	0.093	4.25	1.56	43.1	2.5	Split parallel to axis
Turbine lead slip joint	Type 347 stainless steel	Steam	1050	2000	6	8	1	6.29	3.76	19.4	2	Crack at weld
Turbine steam lead	Type 347 stainless steel	Steam	1050	2000	4.745	6.625	0.94	7.25	4.34	16.9	2	Crack adjacent to weld in parent metal
1-in. feed line	Type 347 stainless steel	Water	550	1750	0.957	1.315	0.179	9.35	4.36	16.8	6	Split parallel to pipe axis
Test pipe creep rupture	SA-210 steel	Water	950	3150	1.668	2.0	0.166	2.555	1.035	58.4	1	Crack
Test pipe creep rupture	SA-210 steel	Water	950	2750	1.660	2.0	0.170	3.04	1.293	49.8	0.75	Crack
Test pipe creep rupture	SA-210 steel	Water	950	1700	1.678	2.0	0.161	4.71	2.155	32.6	0.50	Crack
Turbine steam lead	A-302 carbon-molybdenum steel	Steam	950	1375	6.813	8.625	0.906	11.1	6.40	11.5	4	Crack in radial plane adjacent to bend (in 1954) graphitization
Nonreturn 12-in. 1500-psi valve	A-302 carbon-molybdenum steel	Steam	950	1300	14	19.5	2.75	15.92	9.2	8.0	6	Crack graphitization; three other smaller cracks in similar valves
Turbine steam lead	Type 347 stainless steel	Steam	1050	2000	6	7.88	0.940	5.98	3.56	20.4	2.5	Crack adjacent to weld in parent metal
Turbine steam lead	A-302 carbon-molybdenum steel	Steam	950	1375	6.813	8.625	0.906	11.1	6.40	11.5	5	Two cracks, each 5 in. long, in radial plane adjacent to bend with 1 in. of sound metal between (in 1955); graphitization
1-in. test loop line	Type 304 stainless steel	Water	1100	4500	0.957	1.315	0.179	2.885	0.746	0.82		Split parallel to pipe axis

[a]From ref. 21.

Table 3.5. Inapplicable Data on Pipe and Tubing Failures[a]

Description	Material	Fluid	Temperature (°F)	Pressure (psig)	Inside Diameter (in.)	Outside Diameter (in.)	Wall Thickness (in.)	Calculated Failure Length (in.)		Stress Ratio, σ/σ_{yp} (%)	Failure Length (in.)	Failure
								Maximum	Minimum			
Test pipe creep rupture	SA-210 steel	Water	950	8000	1.682	2.0	0.159	0.668		155.5	9.2	Split
Test pipe creep rupture	SA-210 steel	Water	950	3700	1.678	2.0	0.161	2.065	1.29	71	6.5	Split
Test tubing	Copper	Oil	Room	3590	1.449	1.585	0.068	0.684		125	2.79	Split
Test tubing	Copper	Oil	Room	3660	1.546	1.680	0.067	0.76		119	2.10	Split
Test tubing	Copper	Oil	Room	3750	1.570	1.720	0.075	0.986		103	2.15	Split
Test pipe	Medium carbon steel	Oil	Room	9200	1.250	1.450	0.100	0.48		144.5	2.4	Split
Model pressure vessel	SA-201 steel	Water	70	6250	10.5	12	0.75	0.645		119	43	Split

[a]From ref. 22.

highly toxic substance under a significant pressure is a common problem in chemical and petroleum plants. Accidents have occurred in these areas that resulted in substantial property damage and, in many cases, loss of life. These events have contributed to experience and have provided for reasonable extensions of design considerations. Also there is a wealth of knowledge available from the experience of the power industry. For many years, high-pressure and high-temperature boilers and piping have been used in steam-generating plants. Studies[16,19] have been made to accumulate information concerning large ruptures of pipes and vessels. The results show that no boiler designed for high-pressure service has failed in 30 years (4000 boiler years) of experience and that only four large pipe ruptures have been reported in a similar length of time. Small leaks that required repair did occur during this time, but no failures of a major or catastrophic nature, except those mentioned above, have occurred.

This sort of information from industries closely akin to the nuclear industry should permit the application of these statistics to the accident analysis of a reactor plant. Several years ago, an estimate of the probability[23] of a major nuclear accident occurring that would have an effect on the general public was made. This estimate was based on accident statistics from the entire industrial community, which were applied in a conservative manner. The probability was one chance in 10^5 to 10^9 for an accident for each reactor per year.

As can be seen from the foregoing discussion, the state of the art with regard to accident probabilities in the nuclear industry is such that existing experience in nonnuclear fields must be applied. To be consistent with the general philosophy of the nuclear industry relevant to safety, pessimistic application of existing failure experience is made. This problem has been recognized and efforts are being made to gain experience through several extensive failure probability studies.[24-26]

3.5 REACTOR ACCIDENT EXPERIENCE

No reactor accident approaching the maximum credible accident has yet occurred, so it is not possible to ascertain from actual experience how conservatively these accidents have been analyzed. This situation, however, makes the problems of the safety analyst difficult, since he depends upon the use of probabilities for evaluation, and probabilities must be based on the occurrence of events. Since no accident of "maximum" proportions has taken place, the lesser accidents must be used as a basis for the safety evaluation of a reactor.

Tables 3.6, 3.7, and 3.8 list some of the accidents that have occurred in operating reactor systems in recent years. The tables deal with accidents resulting from (1) reduction in cooling, (2) nuclear excursions, and (3) assorted miscellaneous failures. More detailed information on these accidents is available in the references cited. In general, component or instrument failure, design deficiencies, or operator errors initiate accidents, and a column is included in each table that indicates which of these is the probable cause.

It should be noted that the reactors listed in the tables are, for the most part, experimental or research reactors. The production reactors at Hanford, the Windscale reactor (No. 1), and the two Army reactors

Table 3.6. Reactor Accidents Involving Reduction in Cooling

Date	Reference	Location	Reactor	Cause[a]	Nature of Incident	Remarks
June 1954	27	Arco, Idaho	MTR	DD	Fuel plates failed because bulging of plates limited coolant flow to affected areas and caused hot spots; the fuel elements were modified to correct this	No injury; no release of activity
Jan. 4, 1955	28	Hanford, Washington	"KW"	OE	Cooling water flow to one process tube was blocked; some elements in the tube melted and caused damage to that channel	No significant release of activity; no radiation exposures; considerable damage to the reactor
April 13, 1958	27	Saclay, France	EL-3	DD	An aluminum channel holding a fuel element fell as a result of vibration and lack of support; this stopped coolant flow to that element and resulted in fuel element failure	No injury; no activity release
July 24, 1959	29	Santa Susana, California	SRE	CF	Fuel element failure (melting) occurred as a result of reduced cooling; the reduction was caused by fouling of coolant channels by the decomposition products of tetraline (auxiliary coolant), which had leaked into the primary coolant	No release of activity
April 3, 1960	30, 31	Pittsburg, Pennsylvania	WTR	CF	Because of reduced coolant flow and possibly inadequate metallurgical bonding between meat and cladding, overheating and subsequent fuel element failure occurred	Contamination of primary coolant, and some activity released to atmosphere
Dec. 12, 1961	32	Idaho Falls, Idaho	ETR	OE	Six fuel elements overheated and failed as a result of foreign matter (part of a plastic sight box) lodging in flow channels and reducing cooling	No significant release of activity
Nov. 13, 1962	33	Idaho Falls, Idaho	MTR	OE	A small portion of one plate in a fuel element melted because of reduced coolant flow; this was caused by a blockage of the coolant channel by debris identified as gasket material	Building was evacuated but no significant exposures or damage occurred
July 1963	34	Oak Ridge, Tennessee	ORR	OE	Partial meltdown of one plate in an element soon after startup; the meltdown was caused by insufficient coolant flow as a result of restriction by a large gasket lodged in the coolant channel	Building was evacuated but no injuries occurred and only minor damage was done to the reactor

[a]Probable initiating cause: DD — Design Deficiency; OE — Operation Error; CF — Component Failure.

Table 3.7. Reactor Accidents Involving Nuclear Excursion

Date	Reference	Location	Reactor	Cause[a]	Nature of Incident	Remarks
Dec. 12, 1952	35, 36	Chalk River, Ontario, Canada	NRX	OE	While making reactivity measurements, the reactor suddenly became divergent, the shutoff rods would not drop (mechanical defect), and the cooling water (a poison, in this case) began to boil; all these things contributed to the core melting that ensued	Melted fuel, contaminated cooling water, and other contaminants were released to the room below the reactor
Oct. 3, 1954	28	Hanford, Washington	Production reactor	OE	Startup proceeded too rapidly and localized heating occurred; this caused thermal stress rupture of fuel elements; the effected elements were located and removed	No significant release of activity; no radiation exposures
Nov. 29, 1955	37	Idaho Falls, Idaho	EBR	OE	An experiment was being performed with automatic control bypassed; when shutdown was requested, operator error resulted in a slow shutdown that allowed overheating and fuel element melting	Building was evacuated; no injuries; no overexposures; no release of activity
Jan. 6, 1956	28	Hanford, Washington	Production reactor	OE	The reactor was started and the power rise was allowed to be so rapid that severe damage was feared; the excursion was stopped and the reactor shut down before any serious consequences occurred	No release of activity
Oct. 15, 1958	38	Boris Kidrich Institute of Nuclear Science, Vinca, Yugoslavia	Critical assembly	OE	Primary reactor control is by varying D_2O level in the reactor tank; while working on an experiment near the unshielded assembly, D_2O was inadvertently added to the reactor tank making the system critical; the smell of ozone was the first indication of trouble	Several individuals received significant exposures; five victims received bone marrow transplants; one of the five died
Nov. 18, 1958	39	NRTS, Idaho Falls	HTRE-3	OE	During tests to determine control values, instrumentation settings had to be changed from normal; as a result, when the desired power was reached the servo called for more rod removal; the incident was ended by core rearrangement due to melting	No injury; limited contamination at the site
March 15, 1960	40	Saclay, France	Alize I	OE	Experiments requiring specific periods at low power were being run; rod position for this period was determined (by experiment), then the rods were reinserted; but the position was inadvertently established with only one rod out, and when the run was made, both rods were withdrawn, thus initiating an excursion; this, followed by the failure of instrumentation to scram the reactor, allowed the power to go to 10 Mw	Negligible exposure; no activity release
Jan. 3, 1961	4, 41–44	Idaho Falls, Idaho	SL-1	OE	With the reactor shut down and the head opened to do maintenance, there was a gross reactivity insertion (withdrawal of the central control rod) which initiated a nuclear excursion; rapid steam generation caused a "water hammer," which resulted in considerable damage	Three operators were killed; in the recovery operation, 14 persons received doses ranging from 5 to 27 r; severe core damage occurred and contamination was extensive; no contamination or exposure to the public occurred

[a]Probable initiating cause: OE – Operation Error.

Table 3.8. Accidents Involving Miscellaneous Failures

Date	Reference	Location	Reactor	Cause[a]	Nature of Incident	Remarks
Oct. 10, 1957	27	Windscale, U.K.	Windscale, No. 1	DD	During annealing operation to reduce the Wigner energy of the graphite pile, there was overheating of the graphite that caused fuel cladding failures which led to oxidation of the exposed uranium fuel and subsequently to fire in the graphite and uranium	Fourteen workers exposed greater than 3 rem; maximum exposure 4.66 rem, maximum thyroid dose 9.5 rad; iodine, tellurium, cesium, and strontium were released and caused contamination in the vicinity
May 23, 1958	45	Chalk River, Ontario, Canada	NRU	CF	Part of a broken fuel rod fell from the fuel transfer cask; the rod ignited and burned for 15 min; it was covered with wet sand to extinguish the fire	Serious contamination resulted in 1000 r/hr fields near the elements; a total of ~650 men were used in cleanup; one man received 19 r; 2, ~10 r; the rest, less than 5 r
Nov. 7, 1959	31, 46	Idaho Falls, Idaho		CF	Rupture of an in-pile tube containing an experiment released contaminated liquid	Considerable contamination, but no injury or overexposures
Oct. 7, 1962	47	McMurdo Sound, Antarctica	PM-3A	CF	Hydrogen, leaking from the primary system (probably from a valve bonnet), collected in the top of one of the three containment tanks and was ignited by an electrical short in an instrument line	No injury; no activity release

[a]Probable initiating cause: DD — Design Deficiency; CF — Component Failure.

are the only ones that could be considered as being other than experimental, and in these cases the installation is, for practical purposes, experimental. The point is that no reactor built for power production has experienced an accident that released enough activity to cause significant irradiation of human beings.

References

1. North American Aviation, Final Hazards Summary Report for the Piqua Nuclear Power Facility, USAEC Report NAA-SR-5608.

2. Consumers Power Company, Revised Hazards Summary Report for Big Rock Point Plant, Oct. 14, 1960.

3. Consolidated Edison Co. of New York, Inc., Indian Point Intermediate Hazards Summary Report.

4. W. B. Cottrell, The S1-1 Accident, Nucl. Safety, 3(3): 67-74 (March 1962).

5. Yankee Atomic Electric Co., Final Hazards Summary Report, Yankee Nuclear Power Station, Sept. 15, 1959.

6. Babcock and Wilcox Co., N.S. Savannah Safety Assessment.

7. Pacific Gas and Electric Co., Preliminary Hazards Summary Report for the Bodega Bay Plant.

8. G. E. Creek et al., Experiments on the Release of Fission Products from Molten Reactor Fuels, USAEC Report ORNL-2616, Oak Ridge National Laboratory, July 1959.

9. J. J. DiNunno et al., Calculation of Distance Factors for Reactor Sites, USAEC Report TID-14844, March 1962.

10. Meteorology and Atomic Energy, USAEC Report AECU-3066, July 1955.

11. Oak Ridge Operations Office, Experimental Gas-Cooled Reactor Final Hazards Summary Report, USAEC Report ORO-586, Oct. 10, 1962.

12. Puerto Rico Water Resources Association and General Nuclear Engineering Co., Boiling Nuclear Superheater (BONUS) Power Station, Final Hazards Summary Report, USAEC Report PRWRA-GNEC-5, Feb. 1, 1962.

13. North American Aviation, Hallam, Nuclear Power Facility, Final Summary Safeguards Report, USAEC Report NAA-SR-5700.

14. R. S. Neymark, Oxidation of UC in Air, Technical Data Record No. 5924, Atomics International, Nov. 30, 1960.

15. Reactor Handbook, Vol. 3, p. 405, USAEC Report AECD-3647.

16. Pacific Gas and Electric Company, Final Hazards Summary Report for the Humboldt Bay Plant.

17. John F. Harvey, Pressure Vessel Design: Nuclear and Chemical Applications, Van Nostrand, Princeton, 1963.

18. E. Bevitt and A. L. Stott, Fast Fracture of Pressure Vessels, UKAEA TRG Report 477(C), April 1963.

19. Helmut Thielsch, Failures in High-Temperature, High-Pressure Piping, Nucl. Safety, 4(3): 1-24 (March 1963).

20. I. R. Finrock, Jr., D. E. Hetrick, and D. R. Rees, Preliminary Hazards Summary Report, USAEC Report NP-7757, Saxton Nuclear Experimental Corp., 1959.

21. A. J. Brothers et al., A Review of Fracture Modes as Related to Reactor Primary Coolant Pipe Rupture, Report GEAP-4446, General Electric Company, May 1964.

22. H. B. Ketchum, A Simple Method for Calculating the Maximum Size of Ductile Ruptures in Pressurized Systems, USAEC Report WAPD-TM-56, Westinghouse Atomic Power Division, July 1957.

23. Theoretical Possibilities and Consequences of Major Accidents in Large Nuclear Power Plants, USAEC Report WASH-740, March 1957.

24. D. N. Sunderman et al., Critical Analyses of the Blowdown Accident, paper presented at the International Symposium on Fission Product Release and Transport Under Accident Conditions, Oak Ridge, April 5-7, 1965, Conf. 650407 (to be published).

25. B. J. Garrick et al., A Study of Test Reactor Operating and Safety Experience, Report HN-172, Holmes and Narver, May 10, 1963.

26. B. J. Garrick et al., A Study of Research Reactor Operating and Safety Experience, Report HN-180, Holmes and Narver, June 12, 1964.

27. H. B. Smets, A Review of Nuclear Reactor Incidents, Proceedings of the Symposium on Reactor Safety and Hazards Evaluation Techniques, Sponsored by the International Atomic Energy Agency and Held in Vienna, 14-18, May 1962.

28. J. R. Buchanan, Hanford Reactor Incidents, Nucl. Safety, 4(1): 103-107 (September 1962).

29. W. B. McDonald and J. H. DeVan, Sodium Reactor Experiment Incident, Nucl. Safety, 1(3): 73-75 (March 1960).

30. R. B. Korsmeyer, Westinghouse Testing Reactor Incident, Nucl. Safety, 2(2): 70-73 (December 1960).

31. W. B. Cottrell, Accidents in Nuclear Energy Operations, Nucl. Safety, 2(4): 55-63 (June 1961).

32. J. R. Buchanan, Accidents in Nuclear Energy Operations, Nucl. Safety, 3(4): 90-96 (June 1962).

33. R. A. Costner, Jr., MTR Fission-Break Incident, Nucl. Safety, 4(4): 144-147 (June 1963).

34. A. L. Colomb and T. M. Sims, ORR Fuel Failure Incident, Nucl. Safety, 5(2): 203-207 (Winter 1963-1964).

35. W. B. Lewis, The Accident to the NRX Reactor on December 12, 1952, Canadian Report AECL-232, Atomic Energy of Canada, Limited.

36. D. A. Hurst, The Accident of the NRX Reactor, Part II, Canadian Report AECL-233, Atomic Energy of Canada Limited.

37. D. F. Hayes, A Summary of Accidents and Incidents Involving Radiation in Atomic Energy Activities, June 1954-December 1955, USAEC Report TID-5360.

38. A. D. Callihan, Kidrich Institute Accident, Nucl. Safety, 1(1): 38-40 (September 1959).

39. E. P. Epler, HTRE-3 Excursion, Nucl. Safety, 1(2): 57-59 (December 1959).

40. E. P. Epler, Failure of Alize I Reactor Safety System, Nucl. Safety, 5(2): 172-173 (Winter 1963-1964).

41. J. R. Buchanan, SL-1 Final Report, Nucl. Safety, 4(3): 83-86 (March 1963).

42. J. R. Buchanan and L. J. King, Accidents in Nuclear Energy Operations, Nucl. Safety, 4(4): 147-155 (June 1963).

43. Nuclear Incident at the Sl-1 Reactor, USAEC Report IDO-19302, May 1961.

44. SL-1 Recovery Operations, January 3 to May 20, 1961, USAEC Report IDO-19301, June 1961.

45. J. W. Greenwood, Contamination of the NRU Reactor in May 1958, Canadian Report AECL-850, Atomic Energy of Canada Limited.

46. A Summary of Industrial Accidents in USAEC Facilities, Suppl. 3, p. 16, USAEC Report TID-5360, December 1961.

47. J. R. Buchanan, PM-3A Nuclear Power Plant Fission, Nucl. Safety, 4(3): 86-89 (March 1963).

4. FISSION-PRODUCT RELEASE AND TRANSPORT*

M. H. Fontana**

4.1 INTRODUCTION

Energy, which is the main useful product in a nuclear reactor, results from the fission of a heavy nuclide into two nuclides of generally unequal weight and charge. These fission products are initially in a highly excited state and decay to more stable states, usually by beta decay, with the release of excess energy in the form of gamma rays. The fundamental problem of nuclear safety is the protection of operating personnel and the general public from the harmful effects of these fission products.

In order to assess the degree of hazard, it is necessary to evaluate the amount of hazardous fission products present and, given a mode of accidental failure of the reactor system, to determine the degree of release to the surroundings and the effects on the nearby population. The importance of a fission-product element from a safety standpoint depends on its radiological half-life and the energy of its rays, its volatility and ability to be transported through long distances, and its biological uptake and half-life. Tables 4.1 and 4.2 present some characteristics of the hazardous fission products (see ref. 1). It is the function of this chapter to present means of computing the fission-product inventory and to report the results of recent experiments on and analyses of fission-product release from molten fuels, the transport behavior of fission products within the containment vessel, and the consequences of their release into the atmosphere.

The reader will notice a greater amount of usable material in some areas than in others. This reflects the relative state of knowledge of the various topics covered by this chapter. For instance, the fission-product inventories can be calculated quite well, if the neutron flux, irradiation time, and decay time are known. On the other hand, the determination of fractions of various fission products released from molten fuels under various conditions, and their transport behavior, can only be crudely estimated. The nomenclature common to the particular field of interest has been retained; this results in different usages within this chapter. This situation is unfortunate but is preferable to presentation of material in strange nomenclature.

---

*See Appendix G for relevant information published since this chapter was prepared.

**Mr. Fontana, now with Purdue University, left the Oak Ridge National Laboratory after completing the initial draft of this chapter. The review and final revisions were the responsibility of G. W. Keilholtz and C. J. Barton of ORNL, who are indebted to R. K. Hilliard of General Electric Company (Hanford) and D. A. Collins, F. G. May, and H. M. Nicholson of the United Kingdom Atomic Energy Authority, as well as others, for significant contributions to this work.

Table 4.1. Characteristics of Important Short Half-Life Fission-Product Isotopes[a]

Isotope	Half-Life	Activity in Kilocuries per Mw of Thermal Power		Boiling Point (°C)	Volatility	Health Physics Properties
		At Shutdown	1 Day After Shutdown			
Br-83	2.3 h	3	0	59	Highly volatile	External whole body radiation, moderate health hazard
-84	32 m	6	0	"	" "	
-85	3 m	8	0	"	" "	
-87	56 s	15	0	"	" "	
Kr-83m	114 m	3	0	-153	Gaseous	External radiation, slight health hazard
-85m	4.4 h	8	0.2	"	"	
-87	78 m	15	0	"	"	
-88	2.8 h	23	0.1	"	"	
-89	3 m	31	0	"	"	
-90	33 s	38	0	"	"	
I-131	8 d	25	23	185	Highly volatile	External radiation, internal irradiation of thyroid, high radiotoxicity
-132[b]	2.3 h	38	0	"	" "	
-133	21 h	54	25	"	" "	
-134	52 m	63	0	"	" "	
-135	6.7 h	55	4.4	"	" "	
-136	86 s	53	0	"	" "	
Xe-131m	12 d	0.3	0.3	-108	Gaseous	External radiation, slight health hazard
-133m	2.3 d	1	0.7	"	"	
-133	5.3 d	54	47	"	"	
-135m	15.6 m	16	0	"	"	
-135	9.2 h	25	4	"	"	
-137	3.9 m	48	0	"	"	
-138	17 m	53	0	"	"	
-139	41 s	61	0	"	"	
Te-127m	105 d	0.5	0.5	Released from oxidizing uranium		External radiation, moderate health hazard
-127	9.4 h	2.9	0.5	" "	" "	
-129m	34 d	2.3	2.3	" "	" "	
-129	72 m	9.5	0	" "	" "	
-131m	30 h	3.9	2.2	" "	" "	
-131	25 m	26	0	" "	" "	
-132	77 h	38	31	" "	" "	Health hazard from I-132 daughter[b]
-133m	63 m	54	0	" "	" "	External radiation, moderate health hazard
-133	2 m	54	0	" "	" "	
-134	44 m	63	0	" "	" "	
-135	2 m	55	0	" "	" "	

[a]From Beattie, ref. 1, pp. 10–11.

[b]38 kc of ^{132}I per Mw of thermal power is generated in the reactor by decay of ^{132}Te. Analyses that follow will also consider the ^{132}I formed outside the reactor by decay of ^{132}Te released from a reactor accident.

At the time of this writing, an active research program is under way at the Oak Ridge National Laboratory (ORNL) and other facilities throughout the country that should develop an increasing amount of knowledge on fission-product behavior and thereby make the data reported in parts of this chapter subject to change and improvement. It is important, therefore, that anyone interested in applying these results consult the latest progress reports, such as the ORNL Semiannual Nuclear Safety Program Progress Reports. The material covered in this chapter is also treated

Table 4.2. Characteristics of Important Long Half-Life Fission-Product Isotopes[a]

Isotope	Half-Life	Activity in Kilocuries per Mw of Thermal Power[b]		Boiling Point (°C)	Volatility	Health Physics Properties
		After 1 Year of Irradiation	After 5 Years of Irradiation			
Kr-85	10.4 y	0.12	0.62	-153	Gaseous	Slight health hazard
Sr-89	54 d	39	39	1366	Moderately volatile	Internal hazard to bone and lung
-90	28 y	1.2	6.0	1366	Moderately volatile	
Ru-106	1.0 y	5	10	4080 *	Highly* volatile oxides, RuO_3 and RuO_4	Internal hazard to kidney and GI tract
Cs-137	33 y	1.1	5.3	670	Highly volatile	Internal hazard to whole body
Ce-144	282 d	30	50	3470*	Slightly* volatile	Internal hazard to bone, liver, and lung
Ba-140	12.8 d	53	53	1640*	Moderately volatile	Internal hazard to bone and lung

[a]From Beattie, ref. 1, pp. 10-11, with a few corrections indicated by asterisks.

[b]38 kc of ^{132}I per Mw of thermal power is generated in the reactor by decay of ^{132}Te. Analyses that follow will also consider the ^{132}I formed outside the reactor by decay of ^{132}Te released from a reactor accident.

in some detail in the AEC-sponsored book Safety Information for the Technology of Reactors to be published in two volumes by the MIT Press during the latter part of 1964.

4.2 RADIOACTIVITY GENERATION

In designing a nuclear facility, it is necessary to determine the amounts and kinds of hazardous materials generated, released from the fuel, and available for release from the surrounding structure. This knowledge, in turn, dictates the means to be taken to control the hazardous material. Since this report is primarily intended for the nuclear engineer, nuclear physics will be kept to a minimum; the emphasis is being placed on the calculation of fission-product inventory as a function of irradiation time and decay time.

4.2.1 Fission-Product Distribution

The fissionable nuclei are ^{232}Th, ^{238}U, ^{239}Pu, ^{233}U, and ^{235}U. Of these, only ^{239}Pu, ^{233}U, and ^{235}U are fissionable by thermal neutrons; the others require higher energy neutrons to cause fission. Of the latter

three, ^{235}U is by far the most commonly used isotope at this time, and most of the discussion here will be directed to evaluation of its fission products; however, the others will be considered because of the current attention being given to them. At any rate, from the hazards point of view, the fission-product distribution is not radically different among the heavy nuclides.

Each fission process results in two elements that are generally of unequal weight; the mass numbers peak at approximately 90 to 100 and 134 to 144 for ^{235}U. With increasing mass of the fissioning nucleus, the position of the heavy group of products remains fixed, while the light group shifts to higher mass.[2]

The mass yields for slow neutron-induced fission are shown in Figs. 4.1, 4.2, and 4.3 for ^{235}U, ^{233}U, and ^{239}Pu, respectively. The yield is the probability that a fragment of a given mass number will be formed in fission. The effects of different neutron energies are shown in Fig. 4.4 for the fission of ^{235}U and ^{238}U by thermal neutrons and by 8- and 14-Mev neutrons. The effect of higher neutron energies is to increase the trough yield, that is, to yield more symmetric products.

The fission process can be written as follows:

$$
\begin{gathered}
{}_{Z}M^{A} = {}_{Z_1}M^{A_1} + {}_{Z_2}M^{A_2} + \nu n + E_n + E_M + E_\gamma \ , \\
Z_1 + Z_2 = Z \ , \\
A_1 + A_2 + \nu = A \ ,
\end{gathered}
\tag{4.1}
$$

where

$_{Z}M^{A}$ = mass of the original nucleus,
$_{Z_1}M^{A_1}$, $_{Z_2}M^{A_2}$ = masses of the products,
ν = number of neutrons of rest mass n emitted,
E_n = kinetic energy of the neutrons,
E_M = kinetic energy of the fragments,
E_γ = energy of prompt gamma rays emitted during fission,
Z_1, Z_2 = atomic number of products,
A_1, A_2 = mass of products,
Z = atomic number of fissioning nucleus,
A = atomic mass of fissioning nucleus.

It can be seen from Eq. (4.1) that a large variety of A_1 and A_2 and of Z_1 and Z_2 is possible. The distribution of charge (Z_1 and Z_2) for a given mass appears to be normally distributed about a most probable charge (Z_p). In thermal fission of uranium, the width of this distribution appears to be similar for all masses and can be plotted as shown in Fig. 4.5. The yield on the curve is the independent yield. The term $Z-Z_p$ is the difference between the charge of the particular isobar in question and the most probable charge for its mass. In order to use Fig. 4.5, it becomes necessary to evaluate the most probable charge (Z_p). Glendenin's rule is that light and heavy fragments would be equally far from stability.

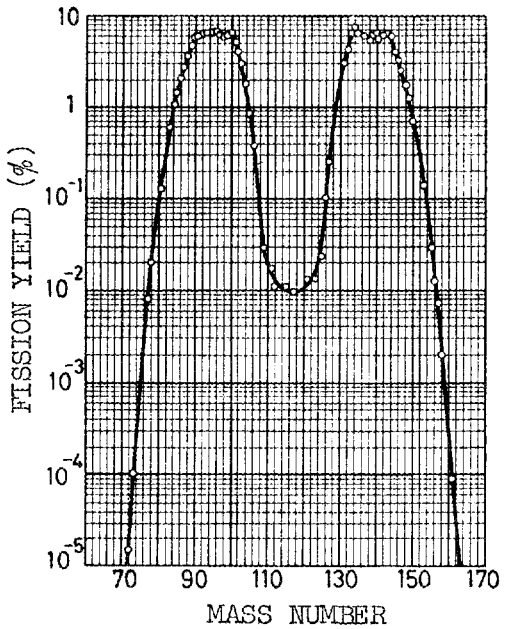

Fig. 4.1. Yield-Mass Curve for Slow-Neutron-Induced Fission of ^{235}U. (From Steinberg and Glendenin, ref. 2, p. 11.)

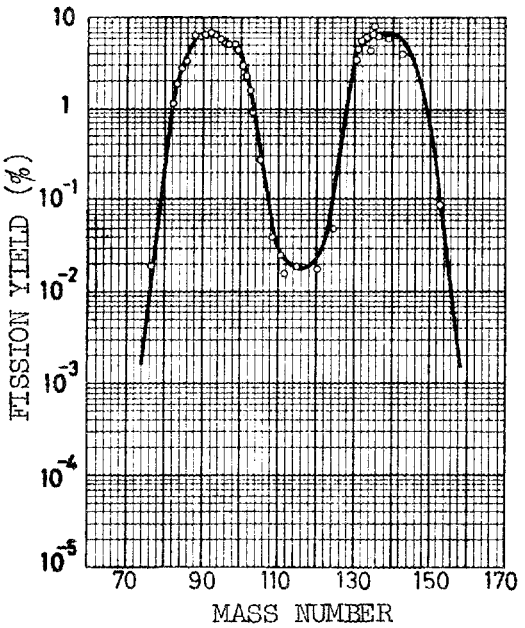

Fig. 4.2. Yield-Mass Curve for Slow-Neutron-Induced Fission of ^{233}U. (From Steinberg and Glendenin, ref. 2, p. 11.)

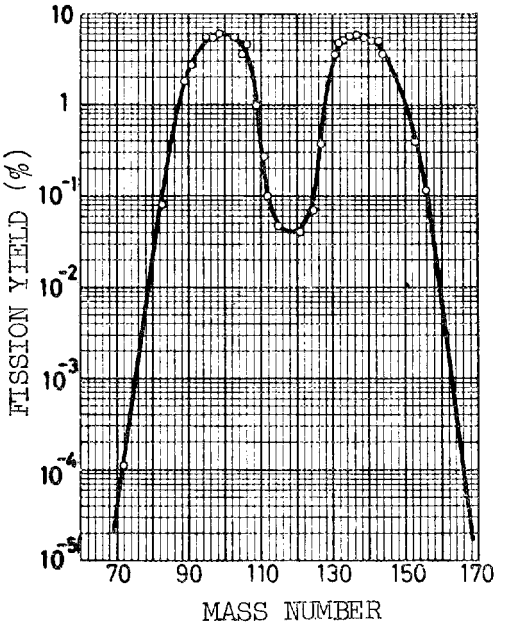

Fig. 4.3. Yield-Mass Curve for Slow-Neutron-Induced Fission of ^{239}Pu. (From Steinberg and Glendenin, ref. 2, p. 14).

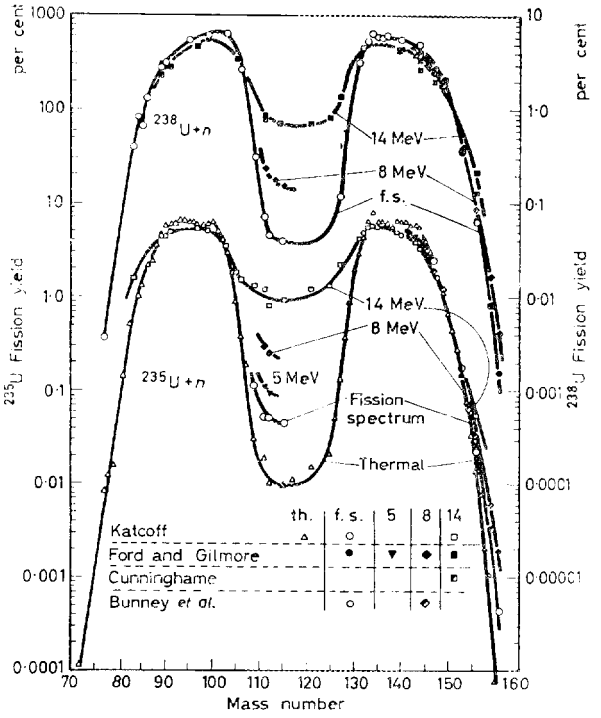

Fig. 4.4. The Measured Mass Yields from Fission of ^{235}U and ^{238}U Induced by Neutrons of Various Energies (th. = Thermal Neutrons; f.s. = Fission Spectrum Neutrons). (From Leachman, ref. 3.)

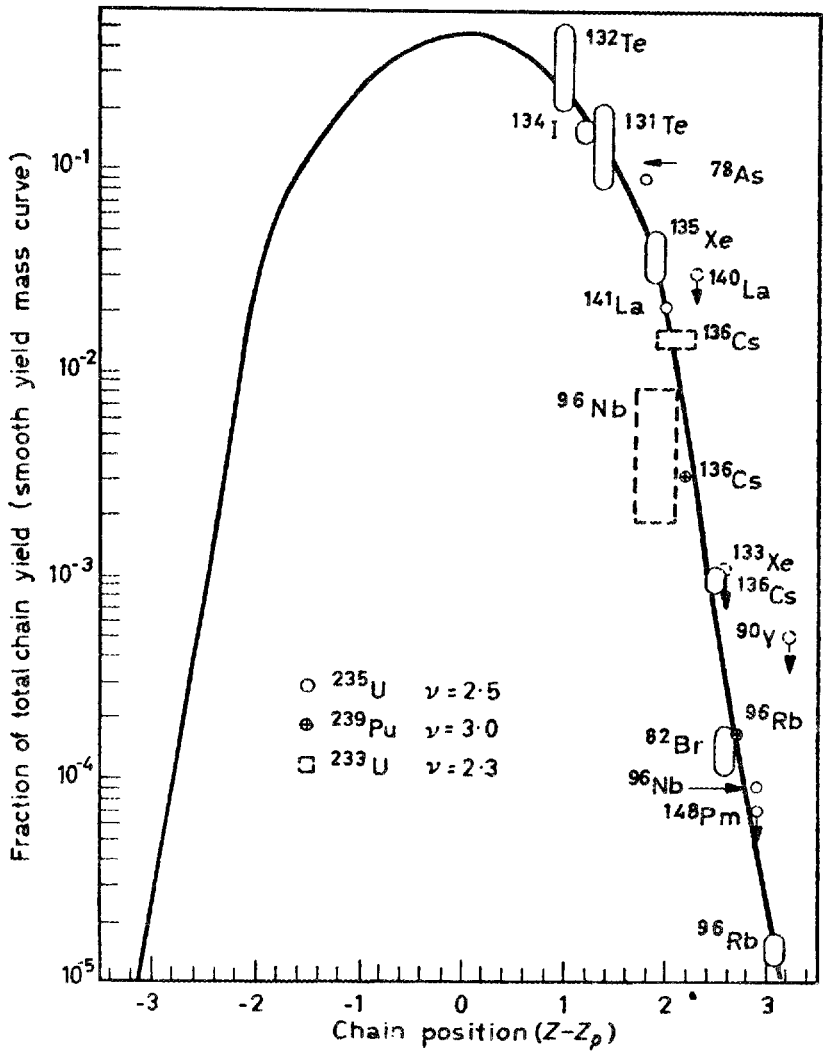

Fig. 4.5. Variation of Yield with Nuclear Charge. (From Pappas, ref. 4.)

This allows independent yields to be plotted, as in Fig. 4.5. The formula for Z_p is

$$Z_p = 46 - \frac{Z_{A_2} - Z_{A_1}}{2} , \qquad (4.2)$$

$$A_1 + A_2 = A - \nu ,$$

When Z_{A_1} is the most stable charge for the mass in question (see Table 4.3).

Table 4.3. Most Stable Charge for Fission Chains[a]

Mass	Z_A	*Mass*	Z_A	*Mass*	Z_A
70	31·2	100	44·0	130	53·9
1	31·5	1	44·4	1	54·3
2	31·9	2	44·8	2	54·6
3	32·2	3	45·2	3	55·0
4	32·6	4	45·6	4	55·4
5	33·0	5	46·0	5	55·8
6	33·4	6	46·4	6	56·2
7	33·8	7	46·7	7	56·6
8	34·2	8	47·1	8	57·0
9	34·6	9	47·4	9	57·5
80	35·0	110	47·7	140	58·0
1	35·4	1	48·1	1	58·5
2	35·8	2	48·4	2	59·0
3	36·3	3	48·7	3	59·5
4	36·7	4	49·0	4	60·0
5	37·1	5	49·3	5	60·5
6	37·6	6	49·6	6	60·9
7	38·0	7	49·9	7	61·4
8	38·5	8	50·2	8	61·8
9	38·9	9	50·5	9	62·2
90	39·4	120	50·8	150	62·5
1	39·9	1	51·1	1	62·9
2	40·3	2	51·4	2	63·2
3	40·8	3	51·7	3	63·5
4	41·3	4	52·0	4	63·8
5	41·7	5	52·4	5	64·1
6	42·2	6	52·7	6	64·4
7	42·6	7	53·0	7	64·6
8	43·1	8	53·3	8	64·9
9	43·6	9	53·6	9	65·2

[a]From Glendenin *et al.*, Ref. 5.

The values of ^{Z}A and $^{Z}A_2$ are uncertain for any particular mass, especially in the region of closed nuclear shells (Z = 2, 8, 20, 28, 50; N = 2, 8, 20, 28, 50, 82, 126), by as much as one unit.[6]

4.2.2 Radioactivity of Fission Products

The fission products formed in low-energy fission tend to be formed with a neutron excess and are generally in an excited state. In reaching stability, the only processes apparent to any great extent in the fission products are gamma emission (as a nucleus passes to lower energy levels) and beta emission (as the excess neutrons are changed to protons). Direct neutron emission also occurs in a few instances from nuclides that have short half-lives. These are the so-called "delayed" neutrons, which are so important to reactor control. However, these are of no significance

in safety considerations not involving reactor kinetics. In high-energy fission the charge distribution of the initial product can be sufficiently broad to include neutron-deficient isobars, atoms or elements having the same atomic weight but different atomic numbers, and in these cases other kinds of radioactive decay can occur.

The fission products can exist as different isomers, i.e., different excited states of the same nuclear configuration. The transformation between levels is effected by the emission of gamma photons or by internal conversion. In internal conversion, one of the electrons in the atomic shell is emitted with an energy equivalent to the difference between the transition energy and the binding energy of the electron in the atom. Most frequently, this atom comes from the K shell that is closest to the nucleus (actually the probability of an electron being near the nucleus in the K shell is greater than it is in the L shell, and so on). The hole in the K shell is filled by an electron from the L shell and holes appear in each shell that can be filled by electrons from the next distant shell and lead to a cascade. This is accompanied by x radiation as the electron cascades from higher to lower shells and can release further electrons with a kinetic energy equal to the x-ray energy characteristic of the difference in shell levels minus the binding energy of the emitted electron. These are known as Auger electrons.

Beta decay is accompanied by the emission of a neutrino, which is of no significance so far as exposure hazards are concerned. A theory of beta and gamma decay is available that can be used to predict half-lives and energy transitions dependent on nuclear spin, parity, atomic and charge numbers, and beta maximum kinetic energy, but it will not be used in this discussion.

Table 4.4 gives the fission-product chains in the order of increasing atomic number, and Table 4.5 gives the mass numbers, half-lives, decay constants, neutron absorption cross sections (in barns), yields, maximum and average beta energies (and the percent of the transition yielding them), gamma energies (and percent of transition yielding them), total gamma energies, shielding groups, and total energy of radiation. Yield values not in parentheses are recommended by Glendenin and Steinberg[3] while those in parentheses are calculated values. Branching ratios are subject to some uncertainty.[6]

Table 4.5 gives the nuclear properties of ^{235}U fission products.[7] In addition to the cumulative and chain yields, independent yields are given where known. The average beta energies were computed as one-third the maximum beta energies. Those yields calculated by the method of equal-charge displacement are shown in parentheses. Experimental values of decay energies were used when available; when none were available, the energies were estimated either by use of Q values or on the basis of mass difference. For shielding purposes the gamma transitions were classified into four energy groups: group I, 0 to 0.25 Mev; group II, 0.26 to 1.00 Mev; group III, 1.01 to 1.70 Mev; group IV, 1.71 Mev and higher. The gamma energy transition values are given and can be grouped as required.

In Tables 4.4 and 4.5, the superscript a denotes an independent fission yield; b shows that it is an energy value computed from the mass change by means of the table of atomic masses;[8] c denotes a nuclide which decays, in part, by K-electron capture or positron emission; and d denotes an energy computed from the total disintegration energy (or Q value).

Table 4.4. ^{235}U Fission-Product Decay Chains[a]

Mass No.	Atomic No. 30	31	32	33	34	35	36
72	49.0h Zn 1.5×10^{-5}	→ 14.3h Ga 1.5×10^{-5}	→ Stable Ge				
73	<2m Zn (9.8×10^{-5})	→ 5.0h Ga 1×10^{-4}	→ Stable Ge				
74			Stable Ge 3×10^{-4}[a]				
75			82m Ge 8×10^{-4}	→ Stable As			
76			Stable Ge 2×10^{-3}[a]	26.6h As	→ Stable Se		
77			52s Ge 5.4×10^{-3} ↓ 12h Ge 3.7×10^{-3}	38.8h As 9.1×10^{-3}	<2% → 17.5s Se $<2 \times 10^{-4}$ ↓ >98% → Stable Se		
78			86m Ge 0.018	→ 91m As 0.02	→ Stable Se		
79				9m As 0.04	→ 3.5m Se 0.04 ↓ → 6.5×10^{4}y Se 0.04	→ Stable Br	
80					Stable Se 0.08[a]		

Table 4.4 (continued)

Mass No.	Atomic No. 33	34	35	36	37	38
81	<10m As (0.125) →	56.5m Se 0.008 ↓ 17m Se 0.133 →	Stable Br			
82		Stable Se 0.25^a	35.87h Br 3.8×10^{-5a} →	Stable Kr		
83		67s Se 0.30 ↘ >90% ; ↓ <10% ; 25m Se 0.21 →	2.4h Br 0.48 → ; ⇢	114m Kr 0.48 ↓ ; Stable Kr		
84		~2m Se 1.1 →	30m Br 1.1 →	Stable Kr		
85			3.00m Br 1.5 → ; ⇢	4.36h Kr 1.5 ↘ 80% ; ↓ 20% ; 10.27y Kr 0.3 →	Stable Rb	
86				Stable Kr 2.1^a	19.5d Rb 2.8×10^{-5a} →	Stable Sr

Table 4.4 (continued)

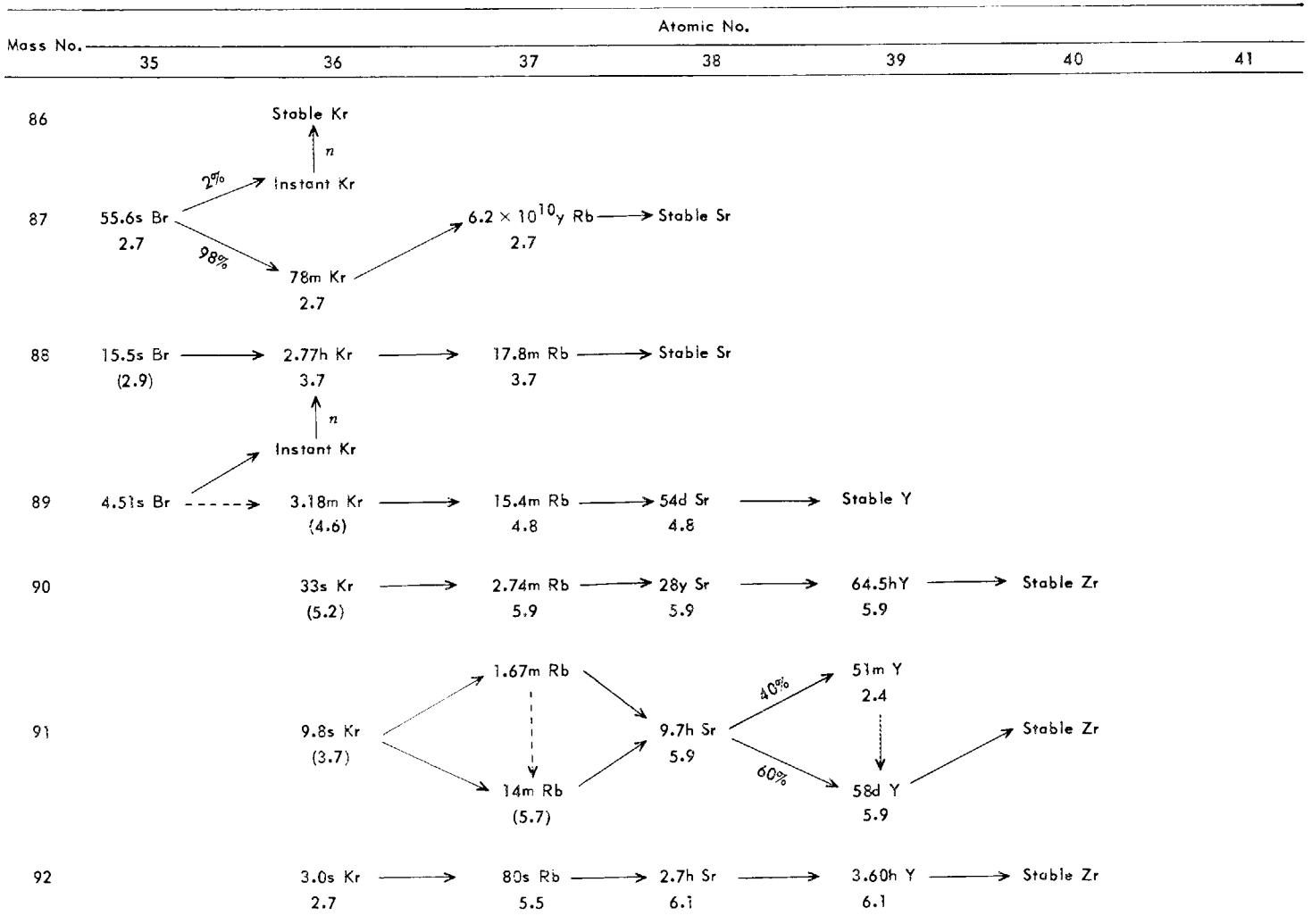

Table 4.4 (continued)

Mass No.	Atomic No. 36	37	38	39	40	41	42
93	2.0s Kr (1.3) →	Short Rb (4.4) →	7m Sr (6.4) →	10.0h Y 6.5 →	1.1×10^6y Zr 6.5	33% → 4.2Y Nb 2.1 → Stable Nb; 67% → Stable Nb	
94	1.4s Kr (0.6) →	Short Rb (2.9) →	2.0m Sr (5.8) →	16.5m Y 6.5 →	Stable Zr		
95	Short Kr (0.2) →	Short Rb (1.6) →	Short Sr (4.7) →	10.5m Y 6.4 →	63d Zr 6.4	1% → 90h Nb 0.06 → 35d Nb 6.4; 99% → 35d Nb 6.4	→ Stable Mo
96					Stable Zr 6.4[a]	23.4h Nb 5.7×10^{-4}[a]	→ Stable Mo
97	~1s Kr (~0) →	Short Rb (0.1) →	Short Sr (1.7) →	Short Y (4.8) →	17.0h Zr 6.2	→ 60s Nb 6.2 → 72.1m Nb 6.2	→ Stable Mo

Table 4.4 (continued)

Mass No.	Atomic No. 42	43	44	45	46
98	Stable Mo 5.9[a]				
99	67h Mo 6.1	~10% → 6.04h Tc ~0.6 ↓ ~90% → 2.12×10^5y Tc 6.1	→ Stable Ru		
100	Stable Mo 6.5[a]	15.8s Tc →	Stable Ru		
101	14.6m Mo →	14.0m Tc →	Stable Ru		
102	12m Mo →	<25s Tc →	Stable Ru		
103			41d Ru 2.9 >95% → 54m Rh 2.9 ↓ <5% → Stable Rh		
104			Stable Ru 1.8[a]	4.4m Rh ↓ 42s Rh →	Stable Pd

Table 4.4 (continued)

Mass No.	Atomic No. 42	43	44	45	46	47	48
105	~5m Mo (0.6) →	Short Tc (0.9) →	4.5h Ru 0.9 →	45s Rh 0.9 ↓ 36.5h Rh 0.9 →	Stable Pd		
106			1.0y Ru 0.38 →	30s Rh 0.38 →	Stable Pd		
107		<1.5m Tc (0.16) →	4m Ru 0.2 →	26m Rh 0.2 →	7.5×10^6y Pd 0.2 → 44.3s Ag ↓ Stable Ag		
108					Stable Pd 0.08^a		
109				<1h Rh (0.028) →	13.6h Pd 0.028 → 39.2s Ag 0.028 ↓ Stable Ag		
110					Stable Pd 0.02^a	270d Ag 2×10^{-7a} ~97% → Stable Cd; ↓ ~3% → 24.2s Ag $\sim 6 \times 10^{-9}$ → Stable Cd	

Table 4.4 (continued)

Mass No.	Atomic No. 46	47	48	49	50
111	22m Pd 0.018	7.6d Ag 0.018	Stable Cd		
112	21h Pd 0.011	3.2h Ag 0.011	Stable Cd		
113		5.3h Ag 0.01	5.1y Cd Stable Cd	Stable In	
114		2m Ag 0.01	Stable Cd		
115		20m Ag (~0.01)	43d Cd 7.1×10^{-4} 53h Cd 9.8×10^{-3}	4.50h In 9.8×10^{-3} 6×10^{14}y In 9.9×10^{-3}	Stable Sn
116			Stable Cd 0.01^{a}	54.2m In 13s In	Stable Sn

Table 4.4 (continued)

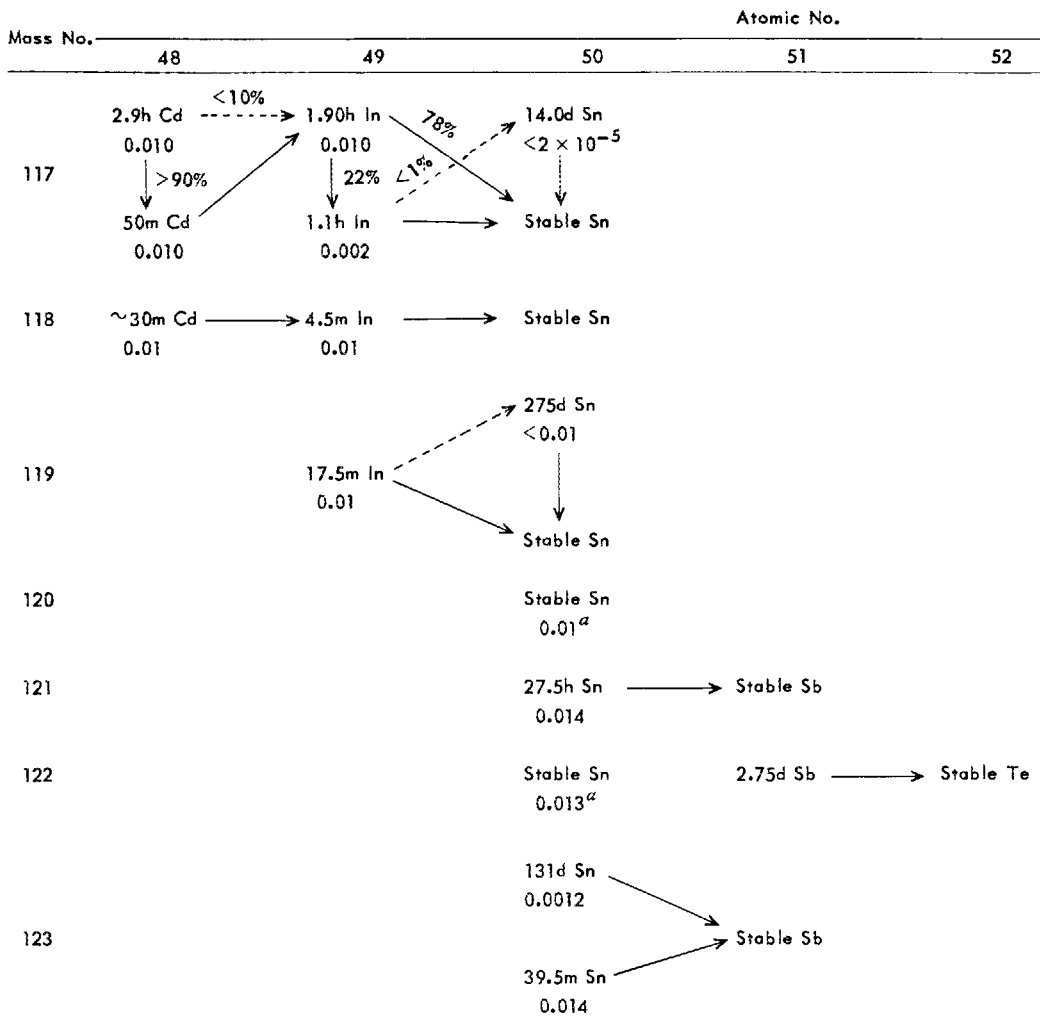

Table 4.4 (continued)

Mass No.	Atomic No. 50	51	52	53	54
124	Stable Sn 0.02[a]				
125	9.4d Sn 0.012 9.5m Sn 0.011	~2.7y Sb 0.023	14% → 58d Te 3×10^{-3} 86% → Stable Te		
126	50m Sn 0.1 →	9h Sb 0.1 →	Stable Te		
127	1.5h Sn (0.24) →	93h Sb 0.25	~16% → 90d Te 0.056 ~84% → 9.3h Te 0.25	→ Stable I	
128		1.1h Sb 0.5 →	Stable Te	24.98m I →	Stable Xe
129		4.6h Sb 1.0	~24% → 33d Te 0.34 ~76% → 72m Te 1.0	→ 1.72×10^{7}y I 1.0 →	Stable Xe 4×10^{-4}[a]
130		12m Sb 2.0 →	$>10^{15}$y Te	12.6h I →	Stable Xe

Table 4.4 (continued)

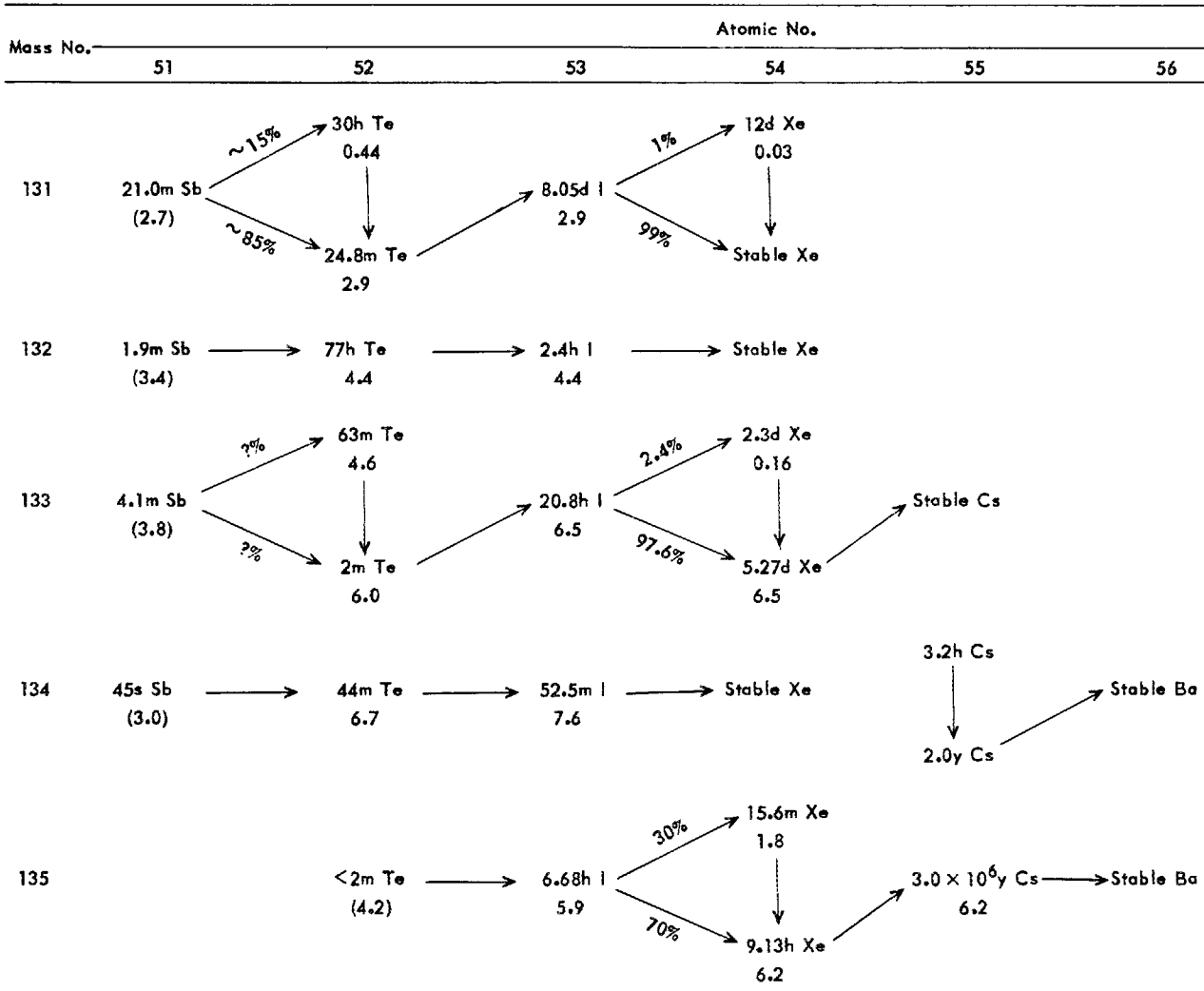

Table 4.4 (continued)

Mass No.	Atomic No. 53	54	55	56	57	58	59	60
136	86s I 3.1 →	Stable Xe 3.2^a	13d Cs 0.0060^a →	Stable Ba				
		↑ n Instant Xe						
137	22.0s I (4.9) ~6% →			2.60m Ba 5.4				
	~94% →	3.9m Xe (5.9) →	26.6y Cs 5.9	92% → ↓ 8% →	Stable Ba			
138	5.9s I (3.4) →	17m Xe (5.5) →	32m Cs 5.8 →	Stable Ba				
139	2.7s I (1.8) →	41s Xe (4.7) →	9.5m Cs (5.9) →	85m Ba 6.0 →	Stable La			
140		16s Xe (3.7) →	66s Cs (6.0) →	12.80d Ba 6.3 →	40.2h La 6.3 →	Stable Ce		
141		1.7s Xe (1.8) →	Short Cs (4.7) →	18m Ba 5.9 →	3.7h La 6.0 →	32d Ce 6.0 →	Stable Pr	
142			~1m Cs (3.4) →	6m Ba (5.6) →	74m La 5.9 →	Stable Ce	19.3h Pr →	Stable Nd
143		1s Xe (0.2) →	Short Cs (1.9) →	<0.5m Ba (4.9) →	19m La 6.2 →	32h Ce 6.2 →	13.7d Pr 6.2 →	Stable Nd
144		~1s Xe (~0) →	Short Cs (1.0) →	Short Ba (3.5) →	Short La (5.8) →	290d Ce 6.1 →	17.5m Pr 6.1 →	1.5×10^{15}y Nd

Table 4.4 (continued)

Mass No.	Atomic No. 58	59	60	61	62	63	64
145	3.0m Ce →	6.0h Pr →	Stable Nd				
	4.2	4.2					
146	13.9m Ce →	24.4m Pr →	Stable Nd				
	(3.2)	3.3					
147			11.3d Nd →	2.6y Pm →	1.4×10^{11}y Sm		
			2.6	2.6			
148			Stable Nd	5.3d Pm →	Stable Sm		
			1.8^a				
149			2.0h Nd →	54h Pm →	Stable Sm		
			1.3	1.3			
150			$>2 \times 10^{15}$y Nd		Stable Sm		
			0.74^a				
151			15m Nd →	27.5h Pm →	93y Sm →	Stable Eu	
			(0.48)	0.5	0.5		
152					Stable Sm	9.2h Eu → Stable Gd 13y Eu → Stable Gd	
					0.3^a		
153					47h Sm →	Stable Eu	
					0.15		
154					Stable Sm	16y Eu →	Stable Gd
					0.09^a		

Table 4.4 (continued)

Mass No.	Atomic No. 62	63	64	65	66
155	23.5m Sm → 0.031	1.7y Eu → 0.031	Stable Gd		
156	~10h Sm → 0.013	15.4d Eu → 0.013	Stable Gd		
157		15.4h Eu → 7.4×10^{-3}	Stable Gd		
158		60m Eu → 2×10^{-3}	Stable Gd		
159			18.0h Gd → 1.1×10^{-3}	Stable Tb	
160			Stable Gd 3×10^{-4} [a]	73.5d Tb →	Stable Dy
161			3.6m Gd → 8.0×10^{-5}	7.0d Tb → 8.0×10^{-5}	Stable Dy

[a] From Blomeke and Todd, Ref. 7, Table 1.

Table 4.5. Nuclear Properties of ^{235}U Fission Products*
Arranged According to Increasing Order of Atomic Number and Mass

Nuclide	Mass Number, A	Half-life, $t_{1/2}$	Decay Constant, λ (sec^{-1})	Absorption Cross Section σ_a (barns)	Yield, Y (%)	Energy of Radiation: Beta Particles: E_b (Mev)	Beta Particles: (%)	Beta Particles: Av. E_b (Mev)	Gamma Transitions: E_g (Mev)	Gamma Transitions: (%)	Shielding: Group	Shielding: (%)	Total E_g (Mev)	Total E (Mev)
$_{30}Zn$	72	49h	3.93×10^{-6}	---	1.5×10^{-5}	0.3	~95	~0.122	---	---	II	~100	0.91[b]	1.03
						1.6	~5							
	73	<2m	5.75×10^{-3}	---	(9.8×10^{-5})	4.9[b]	100	1.6[b]	---	~0	---	---	~0	1.6[b]
$_{31}Ga$	72	14.3h	1.351×10^{-5}	---	1.5×10^{-5}	0.6	40	0.390	2.51	26	II	~126	2.70	3.09
						0.9	32		2.21	33	III	~12		
						1.5	11		1.87	8	IV	~67		
						2.52	8		1.59	5				
						3.15	9		1.20	<2				
									1.05	5				
									0.84	100				
									0.68	<2				
									0.63	24				
	73	5.0h	3.85×10^{-5}	---	1×10^{-4}	1.4	100	0.47	0.054	100	I	200	0.068	0.538
					(2×10^{-6})[a]				0.0135	100				
$_{32}Ge$	72	Stable	0	0.94	1.5×10^{-5}	0	0	0	0	0	---	---	0	0
	73	Stable	0	13.7	1×10^{-4}	0	0	0	0	0	---	---	0	0
	74	Stable	0	0.60	3×10^{-4}[a]	0	0	0	0	0	---	---	0	0
	75	82m	1.41×10^{-4}	---	8×10^{-4}	0.614	15	0.353	0.572	---	II	15	0.08[d]	0.43
						1.137	85		0.418	---				
									0.265	---				
	76	Stable	0	0.015 + 0.30	2×10^{-3}[a]	0	0	0	0	0	---	---	0	0
	77m	52s	1.340×10^{-2}	---	5.4×10^{-3}	2.7	100	0.90	0.215	100	I	200	0.384	1.27
									0.159	---				
	77	12h	1.60×10^{-5}	---	3.7×10^{-3}	0.71	23	0.523	0.26	---	I	~100	0.89[d]	1.41
						1.379	35		0.21	---	II	~100		
						2.196	42							
	78	86m	1.34×10^{-4}	---	1.8×10^{-2}	0.9	100	0.3	0	0	---	---	0	0.3
$_{33}As$	75	Stable	0	4.1	8×10^{-4}	0	0	0	0	0	---	---	0	0
	77	38.8h	4.96×10^{-6}	---	9.1×10^{-3}	0.700	~100	~0.233	0	0	---	---	0	0.233
	78	91m	1.27×10^{-4}	---	2×10^{-2}	1.4	30	1.10	0.27	---	II	~300	0.8[d]	1.90
					2×10^{-3}[a]	4.1	70							
	79	9m	1.28×10^{-3}	---	4×10^{-2}	2.1	100	0.7	0	0	---	---	0	0.7
	81	<10m	1.16×10^{-3}	---	(0.125)	5.1[b]	100	1.7[b]	---	~0	---	---	~0	1.7[b]
$_{34}Se$	77m	17.5s	3.96×10^{-2}	---	$<2 \times 10^{-4}$	0	0	0	0.162	100	I	100	0.162	0.162
	77	Stable	0	40	9.1×10^{-3}	0	0	0	0	0	---	---	0	0
	78	Stable	0	0.4	2×10^{-2}	0	0	0	0	0	---	---	0	0
	79m	3.9m	1.28×10^{-3}	---	4×10^{-2}	0	0	0	0.096	100	I	100	0.096	0.096
	79	6.5×10^{4}y	3.38×10^{-13}	---	4×10^{-2}	0.160	100	0.053	0	0	---	---	0	0.053
	80	Stable	0	0.03 + 0.5	8×10^{-2}	0	0	0	0	0	---	---	0	0
	81m	56.5m	2.04×10^{-4}	---	8×10^{-3}	0	0	0	0.103	100	I	100	0.103	0.103

Table 4.5 (continued)

Nuclide	Mass Number, A	Half-life, $t_{1/2}$	Decay Constant, λ (sec^{-1})	Absorption Cross Section σ_a (barns)	Yield, Y (%)	Energy of Radiation: Beta Particles E_b (Mev)	Beta Particles (%)	Beta Particles Av. E_b (Mev)	Gamma Transitions E_g (Mev)	Gamma Transitions (%)	Shielding Group	Shielding (%)	Total E_g (Mev)	Total E (Mev)
$_{34}Se$	81	17m	6.80×10^{-4}	---	0.133	1.38	100	0.46	0	0	---	---	0	0.46
	82	Stable	0	2	0.25[a]	0	0	0	0	0	---	---	0	0
	83m	67s	1.03×10^{-2}	---	0.30	3.4	100	1.13	0	---	---	---	---	~1.13
	83	25m	4.62×10^{-4}	---	0.21	1.5	100	0.5	0.950	---	I	~200	~3.1[b]	~3.6
									0.176	---	II	~200		
									0.061					
									0.04					
	84	~2m	5.78×10^{-3}	---	1.1	2.94[b]	100	0.98[b]	---	~0	---	---	~0	0.98[b]
$_{35}Br$	79	Stable	0	2.6 + 7.6	3.7×10^{-2}	0	0	0	0	0	---	---	0	0
	81	Stable	0	2.6	0.133	0	0	0	0	0	---	---	0	0
	82	35.87h	5.37×10^{-6}	---	3.8×10^{-5}[a]	0.465	100	0.155	1.312	---	II	~100	3.6[b]	~3.8
									1.031	---	III	~200		
									0.823	---				
									0.766	---				
									0.692	---				
									0.608	---				
									0.547	---				
	83	2.4h	8.02×10^{-5}	---	0.48	0.940	100	0.313	0.051	100	I	100	0.051	0.364
	84	30m	3.85×10^{-4}	---	1.1	1.72	35	1.065	1.89	---	II	~150	2.4[b]	3.5
						2.53	16		0.89	---	IV	~50		
						3.56	9							
						4.68	40							
	85	3.0m	3.85×10^{-3}	---	1.5	2.5	100	0.83	0	0	---	---	0	0.83
	87	55.6s	1.25×10^{-2}	---	2.7	2.6	70	1.41	5.4	56	IV	70	~3.78[d]	~5.19
						8.0	30		~3	14				
	88	15.5s	4.47×10^{-2}	---	(2.9)	8.70[b]	100	2.90[b]	---	~0	---	---	~0	2.90[b]
	89	4.51s	1.54×10^{-2}	---	?	7.10[b]	100	2.37[b]	---	~0	---	---	~0	2.37[b]
$_{36}Kr$	82	Stable	0	45	3.5×10^{-5}	0	0	0	0	0	---	---	0	0
	83m	114m	1.01×10^{-4}	---	0.48	0	0	0	0.0322	100	I	200	0.0415	0.0415
									0.0093	100				
	83	Stable	0	205	0.48	0	0	0	0	0	---	---	0	0
	84	Stable	0	1.0 + 0.06	1.1	0	0	0	0	0	---	---	0	0
	85m	4.36h	4.41×10^{-5}	0.096	1.5	0.835	80	0.233	0.305	20	I	80	0.181	0.414
									0.1495	80	II	20		
	85	10.27y	2.14×10^{-9}	<15	0.3	0.695	99+	~0.232	0	~0	---	---	~0	0.232
	86	Stable	0	0.06	2.1[a]	0	0	0	0	0	---	---	0	0
	87	78m	1.48×10^{-4}	<470	2.7	1.27	25	1.01	2.3	<25	II	~20	0.56[d]	1.57
						3.63	75		1.89	<25	IV	~25		
									0.41	<25				
	88	2.77h	6.95×10^{-5}	---	3.7	0.52	70	0.331	2.40	35	I	49	2.07	2.40
					(0.8)[a]	0.9	10		2.19	18	II	28		
						2.7	20		1.85	15	III	18		
									1.55	14	IV	68		
									1.20	4				
									0.85	23				
									0.365	5				
									0.191	35				
									0.163	7				
									0.028	7				

Table 4.5 (continued)

Nuclide	Mass Number, A	Half-life, $t_{1/2}$	Decay Constant, λ (sec^{-1})	Absorption Cross Section σ_a (barns)	Yield, Y (%)	Energy of Radiation: Beta Particles E_b (Mev)	(%)	Av. E_b (Mev)	Gamma Transitions E_g (Mev)	(%)	Shielding Group	Shielding (%)	Total E_g (Mev)	Total E (Mev)
$_{36}$Kr	89	3.18m	3.63×10^{-3}	---	(4.6)	4.0	100	1.3	0	0	---	---	0	1.3
	90	~33s	2.10×10^{-2}	---	(5.2)	3.2	100	1.07	0	0	---	---	0	1.07
	91	9.8s	7.08×10^{-2}	---	(3.7)	3.6	100	1.20	0	0	---	---	0	1.20
	92	3.0s	0.231	---	(3.7)	5.0[b]	100	1.67[b]	---	~0	---	---	~0	1.67[b]
	93	2.0s	0.347	---	(1.3)	8.0[b]	100	2.66[b]	---	~0	---	---	~0	2.66[b]
	94	1.4s	0.495	---	(0.6)	6.4[b]	100	2.14[b]	---	~0	---	---	~0	2.14[b]
	95	Short	---	---	(0.2)	9.3[b]	100	3.1[b]	---	~0	---	---	~0	3.1[b]
	97	~1s	0.693	---	(~0)	10.6[b]	100	3.5[b]	---	~0	---	---	~0	3.5[b]
$_{37}$Rb	83	Stable	0	0.05 + 0.85	1.5	0	0	0	0	0	---	---	0	0
	86	19.5d	4.11×10^{-7}	---	2.8×10^{-5}[a]	0.68	12	0.543	1.076	12	III	12	0.130	0.673
						1.76	88							
	87	6.2×10^{10}y	3.54×10^{-19}	0.14	2.7	0.275	100	0.092	0	0	---	---	0	0.092
	88	17.8m	6.49×10^{-4}	<200	3.7	2.5	9	1.61	2.8	---	II	5	0.47[d]	2.08
						3.6	13		1.86	---	IV	22		
						5.3	78		0.9	---				
	89	15.4m	7.50×10^{-4}	---	4.8	4.5	100	1.5	0	0	---	---	0	1.5
					(0.2)[a]									
	90	2.74m	4.22×10^{-3}	---	5.9	5.7	100	1.9	0	0	---	---	0	1.9
					(0.7)[a]									
	91m	1.67m	6.93×10^{-3}	---	?	4.6	100	1.5	?	?	---	---	?	~1.5
	91	14m	8.25×10^{-4}	---	(5.7)	3.0	100	1.0	?	?	---	---	?	~1.0
					(2.0)[a]									
	92	80s	8.66×10^{-3}	---	(5.5)	7.59[b]	100	2.5[b]	---	~0	---	---	~0	2.5[b]
					(2.8)[a]									
	93	Short	---	---	(4.4)	6.04[b]	100	2.0[b]	---	~0	---	---	~0	2.0[b]
					(3.1)[a]									
	94	Short	---	---	(2.9)	8.97[b]	100	3.0[b]	---	~0	---	---	~0	3.0[b]
					(2.3)[a]									
	95	Short	---	---	(1.6)	7.43[b]	100	2.5[b]	---	~0	---	---	~0	2.5[b]
					(1.4)[a]									
	97	Short	---	---	(0.1)	8.75[b]	100	2.9[b]	---	~0	---	---	~0	2.9[b]
$_{38}$Sr	86	Stable	0	1.3 + ?	2.8×10^{-5}	0	0	0	0	0	---	---	0	0
	87	Stable	0	---	2.7	0	0	0	0	0	---	---	0	0
	88	Stable	0	0.005	3.7	0	0	0	0	0	---	---	0	0
	89	54d	1.48×10^{-7}	<130	4.8	1.463	100	0.487	0	0	---	---	0	0.487
	90	28y	7.85×10^{-10}	~1	5.9	0.61	100	0.20	0	0	---	---	0	0.20
	91	9.7h	1.99×10^{-5}	---	5.9	0.62	7	0.533	1.413	7	II	62	0.845	1.38
					(0.2)[a]	1.09	33		1.025	33	III	40		
						1.36	29		0.747	7				
						2.03	4		0.66	22				
						2.665	27		0.64	33				

Table 4.5 (continued)

Nuclide	Mass Number, A	Half-life, $t_{1/2}$	Decay Constant, λ (sec^{-1})	Absorption Cross Section σ_a (barns)	Yield, Y (%)	Energy of Radiation: Beta Particles: E_b (Mev)	(%)	Av. E_b (Mev)	Gamma Transitions: E_g (Mev)	(%)	Shielding: Group	(%)	Total E_g (Mev)	Total E (Mev)
$_{38}Sr$	92	2.7h	7.13×10^{-5}	---	6.1	1.14[b]	100	0.4[b]	---	~0	---	---	~0	0.4[b]
					(0.6)[a]									
	93	7m	1.65×10^{-3}	---	(6.4)	4.13[b]	100	1.4[b]	---	~0	---	---	~0	1.4[b]
					(2.0)[a]									
	94	2.0m	5.78×10^{-3}	---	(5.8)	2.63[b]	100	0.9[b]	---	~0	---	---	~0	0.9[b]
					(2.9)[a]									
	95	Short	---	---	(4.7)	5.55[b]	100	1.8[b]	---	~0	---	---	~0	1.8[b]
					(3.1)[a]									
	97	Short	---	---	(1.7)	6.90[b]	100	2.3[b]	---	~0	---	---	~0	2.3[b]
					(1.6)[a]									
$_{39}Y$	89	Stable	0	1.4	4.8	0	0	0	0	0	---	---	0	0
	90	64.5h	2.98×10^{-6}	<6.5	5.9	2.18[d]	100	0.73	1.4	0.4	III	0.4	~0	~0.73
	91m	51m	2.26×10^{-4}	---	2.4	0	0	0	0.551	100	II	100	0.551	0.551
	91	58d	1.38×10^{-7}	---	5.9	1.537	~100	0.512	1.22	0.3	III	0.3	~0	~0.512
	92	3.60h	5.35×10^{-5}	---	6.1	1.3	---	~1.2[b]	0.6	---	II	---	~0	~1.2[b]
						2.7	---							
						3.6	---							
	93	10.0h	1.93×10^{-5}	---	6.5	3.1	100	1.03	0.7	100	II	100	0.7	1.73
					(0.1)[a]									
	94	16.5m	7.00×10^{-4}	---	6.5	5.4	100	1.8	1.4	100	III	100	1.4	3.2
					(0.7)[a]									
	95	10.5m	1.10×10^{-3}	---	(6.4)	3.66[b]	100	1.2	0	0	---	---	0	1.2
					(1.7)[a]									
	97	Short	---	---	(4.8)	5.06[b]	100	1.7[b]	---	~0	---	---	~0	1.7[b]
					(3.1)[a]									
$_{40}Zr$	90	Stable	0	0.1	5.9	0	0	0	0	0	---	---	0	0
	91	Stable	0	1.5	5.9	0	0	0	0	0	---	---	0	0
	92	Stable	0	0.2	6.1	0	0	0	0	0	---	---	0	0
	93	1.1×10^6y	2.31×10^{-14}	<4	6.5	0.063	100	0.021	0	0	---	---	0	0.021
	94	Stable	0	0.07	6.5	0	0	0	0	0	---	---	0	0
	95	63d	1.27×10^{-7}	---	6.4	0.364	57	0.127	0.717	98	II	99	0.733	0.860
						0.396	42							
						0.883	1							
	96	Stable	0	0.05	6.4[a]	0	0	0	0	0	---	---	0	0
	97	17.0h	1.13×10^{-5}	---	6.2	1.91	100	0.64	---	---	II	100	0.75[d]	1.39[d]
					(1.4)[a]									
$_{41}Nb$	93m	4.2y	5.24×10^{-9}	---	2.1	0	0	0	0.0292	100	I	100	0.0292	0.0292
	93	Stable	0	1.1	6.5	0	0	0	0	0	---	---	0	0
	95m	90h	2.14×10^{-6}	---	0.06	0	0	0	0.235	100	I	100	0.235	0.235
	95	35d	2.29×10^{-7}	---	6.4	0.160	100	0.053	0.745	100	II	100	0.745	0.798

Table 4.5 (continued)

Nuclide	Mass Number, A	Half-life, $t_{1/2}$	Decay Constant, λ (sec^{-1})	Absorption Cross Section σ_a (barns)	Yield, Y (%)	Energy of Radiation: Beta Particles E_b (Mev)	Beta Particles (%)	Beta Particles Av. E_b (Mev)	Gamma Transitions E_g (Mev)	Gamma Transitions (%)	Shielding Group	Shielding (%)	Total E_g (Mev)	Total E (Mev)
$_{41}$Nb	96	23.4h	8.23×10^{-6}	---	5.7×10^{-4}[a]	0.37	8	0.240	1.187	32	I	17	2.40	2.64
						0.750	92		1.078	52	II	210		
									0.840	16	III	84		
									0.804	6				
									0.770	100				
									0.560	61				
									0.451	27				
									0.238	10				
									0.216	7				
	97m	60s	1.16×10^{-2}	---	6.2	0	0	0	0.747	100	II	100	0.747	0.747
	97	72.1m	1.60×10^{-4}	---	6.2	1.267	100	0.422	0.665	100	II	100	0.665	1.087
$_{42}$Mo	95	Stable	0	13.4	6.4	0	0	0	0	0	---	---	0	0
	96	Stable	0	1	5.7×10^{-4}	0	0	0	0	0	---	---	0	0
	97	Stable	0	2	6.2	0	0	0	0	0	---	---	0	0
	98	Stable	0	0.13	5.9[a]	0	0	0	0	0	---	---	0	0
	99	67h	2.88×10^{-6}	---	6.1	0.45	~13	0.376	0.780	---	I	90	0.24[d]	0.616[d]
						1.23	~87		0.740	---	II	10		
									0.181	---				
									0.140	---				
									0.041	---				
	100	Stable	0	0.2	6.5[a]	0	0	0	0	0	---	---	0	0
	101	14.6m	7.91×10^{-4}	---	5.0	1.2	70	0.5	0.960	70	I	100	0.864	1.36
						2.2	30		0.191	100	II	70	---	
	102	12m	9.63×10^{-4}	---	4.2	0.92[b]	100	0.31[b]	---	~0	---	---	~0	0.31[b]
	105	~5m	2.31×10^{-3}	---	(0.6)	4.94[b]	100	1.65[b]	---	~0	---	---	~0	1.65[b]
$_{43}$Tc	99m	6.04h	3.19×10^{-5}	---	~0.6	0	0	0	0.141	100	I	100	0.141	0.141
	99	2.12×10^{5}y	1.04×10^{-13}	19	6.1	0.290	100	0.097	0	0	---	---	0	0.097
	101	14.0m	8.25×10^{-4}	---	5.0	1.20	100	0.40	0.30	100	II	100	0.30	0.70
	102	<25s	2.77×10^{-2}	---	4.2	3.31[b]	100	1.10[b]	---	~0	---	---	~0	1.1[b]
	105	Short	---	---	(0.9)	3.24[b]	100	1.08[b]	---	~0	---	---	~0	1.1[b]
				---	(0.3)[a]									
	107	<1.5m	7.7×10^{-3}	---	(0.16)	4.5[b]	100	1.5[b]	---	~0	---	---	~0	1.5[b]
$_{44}$Ru	99	Stable	0	---	6.1	0	0	0	0	0	---	---	0	0
	101	Stable	0	2.46	5.0	0	0	0	0	0	---	---	0	0
	102	Stable	0	1.2	4.2	0	0	0	0	0	---	---	0	0
	103	41d	1.96×10^{-7}	---	2.9	0.217	95	0.080	0.498	95	II	95	0.473	0.567
						0.698	5							
	104	Stable	0	0.7	1.8[a]	0	0	0	0	0	---	---	0	0
	105	4.5h	4.28×10^{-5}	---	0.9	1.150	100	0.383	0.726	100	II	100	0.726	1.109
	106	1.0y	2.20×10^{-8}	---	0.38	0.0392	100	0.0131	0	0	---	---	0	0.0131
	107	4m	2.89×10^{-3}	---	0.2	2.81[b]	100	0.94[b]	---	~0	---	---	~0	0.94[b]
					(0.04)[a]									

Table 4.5 (continued)

Nuclide	Mass Number, A	Half-life, $t_{1/2}$	Decay Constant, λ (sec^{-1})	Absorption Cross Section σ_a (barns)	Yield, Y (%)	Energy of Radiation: Beta Particles E_b (Mev)	Beta Particles (%)	Beta Particles Av. E_b (Mev)	Gamma Transitions E_g (Mev)	Gamma Transitions (%)	Shielding Group	Shielding (%)	Total E_g (Mev)	Total E (Mev)
$_{45}$Rh	103m	54m	2.14×10^{-4}	---	2.9	0	0	0	0.040	100	I	100	0.04	0.04
	103	Stable	0	12 + 138	2.9	0	0	0	0	0	---	---	0	0
	105m	45s	1.54×10^{-2}	---	0.9	0	0	0	0.130	100	I	100	0.130	0.130
	105	36.5h	5.27×10^{-6}	---	0.9	0.25	10	0.183	0.322	10	II	10	0.032	0.215
						0.570	90							
	106	30s	2.31×10^{-2}	---	0.38	~1.0	6	1.05	2.41	0.25	II	38	0.245	1.30
						2.0	3		1.55	0.5	III	2.5		
						2.44	12		1.045	2	IV	1		
						3.1	11		0.87	1				
						3.53	68		0.624	12				
									0.513	25				
	107	26m	4.44×10^{-4}	---	0.2	1.2	100	0.4	0	0	---	---	0	0.4
	109	<1h	1.93×10^{-4}	---	(0.028)	2.39[b]	100	0.8[b]	---	~0	---	---	~0	0.8[b]
$_{46}$Pd	105	Stable	0	---	0.9	0	0	0	0	0	---	---	0	0
	106	Stable	0	---	0.38	0	0	0	0	0	---	---	0	0
	107	7.5×10^6y	2.92×10^{-15}	---	0.2	0.04	100	0.01	0	0	---	---	0	0.01
	108	Stable	0	0.07 + 11	0.08[a]	0	0	0	0	0	---	---	0	0
	109	13.6h	1.42×10^{-5}	---	0.028	0.961	100	0.32	0	0	---	---	0	0.32
	110	Stable	0	? + 0.4	0.02[a]	0	0	0	0	0	---	---	0	0
	111	22m	5.25×10^{-4}	---	0.018	2.13	100	0.71	0.73	---	II	~0	~0[b]	0.71
									0.65	---				
									0.56	---				
									0.38	---				
	112	21h	9.17×10^{-6}	---	0.011	0.2	100	0.07	0.018	100	I	100	0.018	0.088
$_{47}$Ag	107m	44.3s	1.57×10^{-2}	---	<0.2	0	0	0	0.094	100	I	100	0.094	0.094
	107	Stable	0	30	0.2	0	0	0	0	0	---	---	0	0
	109m	39.2s	1.77×10^{-2}	---	0.028	0	0	0	0.088	100	I	100	0.088	0.088
	109	Stable	0	2 + 82	0.028	0	0	0	0	0	---	---	0	0
	110m	270d	2.98×10^{-8}	---	2×10^{-7}[a]	0.087	58	0.128	1.516	---	I	~3	~2.6[d]	2.7[d]
						0.530	35		1.389	---	II	~295		
						2.12	3		0.935	---	III	~50		
						2.86	3		0.885	---				
									0.814	---				
									0.759	---				
									0.706	---				
									0.676	---				
									0.656	---				
									0.116	---				
	110	24.2s	2.86×10^{-2}	---	6×10^{-9}	2.16	60	0.811	0.66	100	II	100	0.66	1.48
						2.84	40							
	111	7.6d	1.06×10^{-6}	---	0.018	0.70	8	0.337	0.243	1	I	1	0.030	0.367
						0.80	1		0.340	8	II	8		
						1.04	91							

Table 4.5 (continued)

Nuclide	Mass Number, A	Half-life, $t_{1/2}$	Decay Constant, λ (sec^{-1})	Absorption Cross Section σ_a (barns)	Yield, Y (%)	Energy of Radiation: Beta Particles E_b (Mev)	Beta Particles (%)	Beta Particles Av. E_b (Mev)	Gamma Transitions E_g (Mev)	Gamma Transitions (%)	Shielding Group	Shielding (%)	Total E_g (Mev)	Total E (Mev)
$_{47}Ag$	112	3.2h	6.02×10^{-5}	---	0.011	1.0	15	1.04	1.40	---	II	~0	~0[b]	1.04
						2.7	20		0.62	---	III	~0		
						3.5	40							
						4.1	25							
	113	5.3h	3.63×10^{-5}	---	0.01	2.0	100	0.67	0	0	---	---	0	0.67
	114	2m	5.78×10^{-3}	---	0.01	4.11[b]	100	1.37[b]	---	~0	---	---	~0	1.37[b]
	115	20m	5.78×10^{-4}	---	(~0.01)	3.0	100	1.0	0	0	---	---	0	1.0
$_{48}Cd$	110	Stable	0	0.2 + ?	2×10^{-7}	0	0	0	0	0	---	---	0	0
	111	Stable	0	---	0.018	0	0	0	0	0	---	---	0	0
	112	Stable	0	0.02 + ?	0.011	0	0	0	0	0	---	---	0	0
	113m	5.1y	4.30×10^{-9}	---	?	0.59	100	0.20	0	0	---	---	0	0.20
	113	Stable	0	25,000	0.01	0	0	0	0	0	---	---	0	0
	114	Stable	0	0.14 + 1.1	0.01	0	0	0	0	0	---	---	0	0
	115	43d	1.86×10^{-7}	---	0.00071	0.7	2	0.53	1.28	---	II	~0	0.05[d]	0.58[d]
						1.61	98		0.96	---	III	~0		
									0.50	---				
									0.46	---				
	115	53h	3.63×10^{-6}	---	0.0098	0.58	42	0.296	0.525	---	II	42	0.56[d]	0.86[d]
						1.11	58		0.50	---				
									0.360	---				
	116	Stable	0	1.4 + ?	0.01[a]	0	0	0	0	0	---	---	0	0
	117m	2.9h	6.66×10^{-5}	---	0.01	---	<10	---	2.00	---	II	>90	<0.79[b]	<0.79[b]
									1.55	---	III	~0		
									1.27	---	IV	~0		
									0.84	---				
									0.43	---				
									0.33	---				
									0.28	---				
									0.27	---				
	117	50m	2.31×10^{-4}	---	0.010	~1.6	---	<0.79[b]	---	~0	---	---	~0	<0.8[b]
						~3.0	---							
	118	~30m	3.85×10^{-4}	---	0.01	1.09[b]	100	0.36[b]	---	~0	---	---	~0	0.36[b]
$_{49}In$	113	Stable	0	60 + 2	?	0	0	0	0	0	---	---	0	0
	115m	4.50h	4.28×10^{-5}	---	0.0098	0.83	6	0.017	0.335	94	II	94	0.317	0.334
	115	6×10^{14}y	3.66×10^{-23}	145 + 52	0.0099	0.63	100	0.21	0	~0	---	---	~0	0.21
	117m	1.90h	1.01×10^{-4}	---	0.010	1.62	23	0.449	0.311	22	II	22	0.194	0.643
						1.77	55		0.161	78	I	78		
	117	1.1h	1.75×10^{-4}	---	2×10^{-3}	0.740	100	0.247	0.565	---	I	~10	0.09[b]	0.34[b]
									0.161	---	II	~15		
	118	4.5m	2.57×10^{-3}	---	0.01	1.5	100	0.5	?	---	---	---	?	~0.5
	119	17.5m	6.60×10^{-4}	---	0.01	2.7	100	0.9	0	0	---	---	0	0.9

Table 4.5 (continued)

Nuclide	Mass Number, A	Half-life, $t_{1/2}$	Decay Constant, λ (sec^{-1})	Absorption Cross Section σ_a (barns)	Yield, Y (%)	Energy of Radiation: Beta Particles E_b (Mev)	Beta Particles (%)	Beta Particles Av. E_b (Mev)	Gamma Transitions E_g (Mev)	Gamma Transitions (%)	Shielding Group	Shielding (%)	Total E_g (Mev)	Total E (Mev)
$_{50}Sn$	115	Stable	0	---	0.01	0	0	0	0	0	---	---	0	0
	117m	14.0d	5.73×10^{-7}	---	$<2 \times 10^{-5}$	0	0	0	0.162	100	I	200	0.321	0.321
									0.159	100				
	117	Stable	0	---	0.010	0	0	0	0	0	---	---	0	0
	118	Stable	0	0.01 + ?	0.01	0	0	0	0	0	---	---	0	0
	119m	275d	2.91×10^{-8}	---	<0.01	0	0	0	0.0653	100	I	200	0.0895	0.09
									0.0242	100				
	119	Stable	0	---	0.01	0	0	0	0	0	---	---	0	0
	120	Stable	0	~0.001 + 0.03	0.01[a]	0	0	0	0	0	---	---	0	0
	121	27.5h	7.00×10^{-6}	1.2×10^{-2}	0.014	0.383	100	0.128	0	0	---	---	0	0.128
	122	Stable	0	0.001 + 0.1	0.013[a]	0	0	0	0	0	---	---	0	0
	123	131d	6.12×10^{-8}	---	0.0012	1.42	100	0.47	0	0	---	---	0	0.47
	123	39.5m	2.92×10^{-4}	---	0.014	1.26	100	0.42	0.153	100	I	100	0.153	0.57
	124	Stable	0	0.75	0.02[a]	0	0	0	0	0	---	---	0	0
	125	9.4d	8.53×10^{-7}	---	0.012	0.40	5	0.76	1.90	5	IV	5	0.095	0.86
						2.37	95							
	129	9.5m	1.22×10^{-3}	---	0.011	0.51	---	~0.7	0.326	100	II	100	0.326	~1.03
						1.17	---							
						2.04	~100							
	126	50m	2.31×10^{-4}	---	0.1	2.55[b]	100	0.85[b]	---	~0	---	---	~0	0.85[b]
	127	1.5h	1.28×10^{-4}	---	(0.24)	4.84[b]	100	1.61[b]	---	~0	---	---	~0	1.61[b]
$_{51}Sb$	121	Stable	0	5.7	0.014	0	0	0	0	0	---	---	0	0
	123	Stable	0	0.03 + 0.03 + 2.5	0.015	0	0	0	0	0	---	---	0	0
	125	2.7y	8.14×10^{-9}	---	0.023	0.125	29	0.102	0.637	---	I	28	0.46[d]	0.56[d]
						0.300	45		0.601	---	II	72		
						0.414	12		0.465	---				
						0.612	14		0.425	---				
									0.175	---				
									0.110	---				
									0.035	---				
	126	9h	2.14×10^{-5}	---	0.10	1.0	100	0.33	0.90	100	II	200	1.3	1.63
									0.4	100				
	127	93h	2.07×10^{-6}	---	0.25	1.2	100	0.4	0.72	100	II	100	0.72	1.12
					(0.01)[a]									
	128	1.1h	1.75×10^{-4}	---	0.5	5.68[b]	100	1.9[b]	---	~0	---	---	~0	1.9[b]
	129	4.6h	4.32×10^{-5}	---	1.0	4.42[b]	100	1.5[b]	---	~0	---	---	~0	1.5[b]
	130	12m	9.63×10^{-4}	---	2.0	6.68[b]	100	2.2[b]	---	~0	---	---	~0	2.2[b]
	131	21.0m	5.50×10^{-4}	---	(2.7)	5.44[b]	100	1.8[b]	---	~0	---	---	~0	1.8[b]
	132	1.9m	6.08×10^{-3}	---	(3.4)	7.64[b]	100	2.6[b]	---	~0	---	---	~0	2.6[b]
	133	4.1m	2.82×10^{-3}	---	(3.8)	6.41[b]	100	2.1[b]	---	~0	---	---	~0	2.1[b]
	134	45s	1.54×10^{-2}	---	(3.0)	8.57[b]	100	2.9[b]	---	~0	---	---	~0	2.9[b]

Table 4.5 (continued)

Nuclide	Mass Number, A	Half-life, $t_{1/2}$	Decay Constant, λ (sec^{-1})	Absorption Cross Section σ_a (barns)	Yield, Y (%)	Energy of Radiation: Beta Particles E_b (Mev)	(%)	Av. E_b (Mev)	Gamma Transitions E_g (Mev)	(%)	Shielding Group	Shielding (%)	Total E_g (Mev)	Total E (Mev)
$_{52}$Te	125m	58d	1.38×10^{-7}	---	3×10^{-3}	0	0	0	0.110	100	I	100	0.110	0.110
	125	Stable	0	1.5	0.023	0	0	0	0	0	---	---	0	0
	126	Stable	0	0.07 + 0.7	0.10	0	0	0	0	0	---	---	0	0
	127m	90d	8.82×10^{-8}	---	0.056	0	0	0	0.0885	100	I	100	0.09	0.09
	127	9.3h	2.07×10^{-5}	---	0.25	0.7	100	0.23	0	0	---	---	0	0.23
	128	Stable	0	0.016 + 0.14	0.5	0	0	0	0	0	---	---	0	0
	129m	33d	2.43×10^{-7}	---	0.34	0	0	0	0.106	100	I	100	0.106	0.106
	129	72m	1.60×10^{-4}	---	1.0	1.8	100	0.6	0.8	100	II	200	1.1	1.7
									0.3	100				
	130	$>10^{15}$y	~0	<0.01 + 0.3	2.0	0	0	0	0	0	---	---	0	0
	131m	30h	6.42×10^{-5}	---	0.44	0	0	0	0.177	100	I	100	0.177	0.177
	131	24.8m	4.66×10^{-4}	---	2.9	1.4	45	0.577	0.7	45	I	100	0.475	1.052
					(0.2)[a]	2.0	55		0.16	100	II	45		
	132	77h	2.50×10^{-6}	---	4.4	0.22	100	0.073	0.231	100	I	100	0.231	0.961
					(1.0)[a]									
	133m	63m	1.83×10^{-4}	---	4.6	0	0	0	0.4	100	II	100	0.4	0.4
	133	2m	5.78×10^{-3}	---	6.0	1.3	70	0.54	1.0	70	II	170	1.3	1.84
					(2.2)[a]	2.4	30		0.6	100				
	134	44m	2.63×10^{-4}	---	6.7	3.80[b]	100	1.27[b]	---	~0	---	---	~0	1.27[b]
					(3.7)[a]									
	135	<2m	5.78×10^{-3}	---	(4.2)	5.98[b]	100	2.0[b]	---	~0	---	---	~0	2.0[b]
$_{53}$I	127	Stable	0	6.1	0.25	0	0	0	0	0	---	---	0	0
	129	1.72×10^{7}y	1.28×10^{-15}	11	1.0	0.15	100	0.05	0.039	100	I	100	0.04	0.09
	131	8.05d	9.96×10^{-7}	600	2.9	0.250	2.8	0.191	0.722	3	II	97.3	0.39	0.58
						0.335	9.3		0.637	9				
						0.608	87.2		0.364	80				
						0.815	0.7		0.284	5.3				
	132	2.4h	8.02×10^{-5}	---	4.4	0.7	15	0.434	2.2	2	II	226	1.992	2.43
						0.9	20		1.96	5	III	19		
						1.16	23		1.40	11	IV	7		
						1.53	24		1.16	8				
						2.12	18		0.96	20				
									0.777	75				
									0.673	100				
									0.624	6				
									0.528	25				
	133	20.8h	9.25×10^{-6}	---	6.5	0.5	6	0.45	1.4	1	II	99	0.555	1.01
					0.3[a]	1.4	94		0.85	5	III	1		
									0.53	94				
	134	52.5m	2.20×10^{-4}	---	7.6	1.5	70	0.60	1.78	~35	II	3	~1.27	~1.92
					0.9[a]	2.5	30		1.10	~35	III	35		
									0.86	~30	IV	35		
									0.20	~0				
									0.12	~0				

Table 4.5 (continued)

Nuclide	Mass Number, A	Half-life, $t_{1/2}$	Decay Constant, λ (sec^{-1})	Absorption Cross Section σ_a (barns)	Yield, Y (%)	Energy of Radiation: Beta Particles E_b (Mev)	Beta Particles (%)	Beta Particles Av. E_b (Mev)	Gamma Transitions E_g (Mev)	Gamma Transitions (%)	Shielding Group	Shielding (%)	Total E_g (Mev)	Total E (Mev)
$_{53}I$	135	6.68h	2.89×10^{-5}	---	5.9	0.5	35	0.308	1.8	~50	III	~50	1.54	1.85
					(1.7)[a]	1.0	40		1.27	~50	IV	~50		
						1.4	25							
	136	86s	8.06×10^{-3}	---	3.1	3.6	---	~2.1	2.9	---	III	~0	~0	~2.1
						5.0	---		1.38	---	IV	~0		
						6.4	~100		1.38	---				
	137	22.0s	3.15×10^{-2}	---	(4.9)	0.56	100	0.19	0	0	---	---	0	0.19
	138	5.9s	1.17×10^{-1}	---	(3.4)	7.69[b]	100	2.56[b]	---	~0	---	---	~0	2.56[b]
	139	2.7s	2.57×10^{-1}	---	(1.8)	6.48[b]	100	2.16[b]	---	~0	---	---	~0	2.16[b]
$_{54}Xe$	129	Stable	0	45	1.0	0	0	0	0	0	---	---	0	0
					4×10^{-4}[a]									
	$131m_2$	12.0d	6.68×10^{-7}	---	0.03	0	0	0	0.163	100	I	100	0.163	0.163
	131	Stable	0	120	2.9	0	0	0	0	0	---	---	0	0
	132	Stable	0	? + 0.2	4.4	0	0	0	0	0	---	---	0	0
	133m	2.3d	3.49×10^{-6}	---	0.16	0	0	0	0.233	100	I	100	0.233	0.233
	133	5.270d	1.52×10^{-6}	---	6.5	0.345	100	0.115	0.081	100	I	100	0.081	0.196
	134	Stable	0	? + 0.2	7.6	0	0	0	0	0	---	---	0	0
	135m	15.6m	7.40×10^{-4}	---	1.8	0	0	0	0.52	100	II	100	0.52	0.52
	135	9.13h	2.11×10^{-5}	2.8×10^{6}	6.2	0.548	5 .	0.302	0.60	4	I	96	0.268	0.570
					0.3[a]	0.910	95		0.37	1	II	5		
									0.250	96				
	136	Stable	0	0.15	6.3	0	0	0	0	0	---	---	0	0
					3.2[a]									
	137	3.9m	2.96×10^{-3}	---	(5.9)	4.0	100	1.33	0	0	---	---	0	1.33
					(1.3)[a]									
	138	17m	6.79×10^{-4}	---	(5.5)	3.02[b]	100	1.0[b]	---	~0	---	---	~0	1.0[b]
					(2.1)[a]									
	139	41s	1.69×10^{-2}	---	(4.7)	5.15[b]	100	1.7[b]	---	~0	---	---	~0	1.7[b]
					(2.9)[a]									
	140	16s	4.33×10^{-2}	---	(3.7)	3.97[b]	100	1.3[b]	---	~0	---	---	~0	1.3[b]
	141	1.7s	4.08×10^{-1}	---	(1.8)	6.07[b]	100	2.0[b]	---	~0	---	---	~0	2.0[b]
	143	1s	6.93×10^{-1}	---	(0.2)	6.95[b]	100	2.3[b]	---	~0	---	---	~0	2.3[b]
	144	1s	6.93×10^{-1}	---	(~0)	5.78[b]	100	1.9[b]	---	~0	---	---	~0	1.9[b]
$_{55}Cs$	133	Stable	0	0.16 + 26	6.5	0	0	0	0	0	---	---	0	0
	135	3.0×10^{6}y	7.33×10^{-15}	15	6.2	0.21	100	0.07	0	0	---	---	0	0.07
	136	13d	6.17×10^{-7}	---	6×10^{-3}[a]	0.35	100	0.12	0.9	100	II	100	0.9	1.02
	137	26.6y	8.27×10^{-10}	<2	5.9	0.523	92	0.192	0	0	---	---	0	0.19
						1.17	8							
	138	32m	3.62×10^{-4}	8.7	5.8	2.0	33	1.08	1.44	100	II	100	2.01	3.09
						2.9	10		0.98	43	III	100		
						3.4	67		0.463	33				
	139	9.5m	1.22×10^{-3}	---	(5.9)	3.82[b]	100	1.3[b]	---	~0	---	---	~0	1.3[b]
					(1.2)[a]									

Table 4.5 (continued)

Nuclide	Mass Number, A	Half-life, $t_{1/2}$	Decay Constant, λ (sec^{-1})	Absorption Cross Section σ_a (barns)	Yield, Y (%)	Energy of Radiation: Beta Particles E_b (Mev)	(%)	Av. E_b (Mev)	Gamma Transitions E_g (Mev)	(%)	Shielding Group	Shielding (%)	Total E_g (Mev)	Total E (Mev)
$_{55}$Cs	140	66s	1.05×10^{-2}	0.63	(6.0)	5.93[b]	100	2.0[b]	---	~0	---	---	~0	2.0[b]
					(2.3)[a]									
	141	Short	---	---	(4.7)	4.75[b]	100	1.6[b]	---	~0	---	---	~0	1.6[b]
					(2.9)[a]									
	142	~1m	1.16×10^{-2}	1.76	(3.4)	6.83[b]	100	2.3[b]	---	~0	---	---	~0	2.3[b]
	143	Short	---	---	(1.9)	5.66[b]	100	1.9[b]	0.29	~0	I	~0	~0	1.9[b]
					(1.7)[a]				0.12	~0	II	~0		
	144	Short	---	---	(1.0)[a]	7.72	100	2.6[b]	---	~0	---	---	~0	2.6[b]
$_{56}$Ba	135	Stable	0	5.6	6.2	0	0	0	0	0	---	---	0	0
	136	Stable	0	0.4	6×10^{-3}	0	0	0	0	0	---	---	0	0
	137m	2.60m	4.44×10^{-3}	---	5.4	0	0	0	0.661	100	II	100	0.661	0.661
	137	Stable	0	4.9	5.9	0	0	0	0	0	---	---	0	0
	138	Stable	0	0.68	5.8	0	0	0	0	0	---	---	0	0
	139	85m	1.36×10^{-4}	4	6.0	0.82	19	0.220	1.43	19	I	66	0.380	0.600
					(0.1)[a]	2.23	66		0.163	66	III	19		
						2.38	15							
	140	12.80d	6.27×10^{-7}		6.3	0.480	40	0.268	0.54	30	I	110	0.237	0.505
					(0.3)[a]				0.30	10	II	40		
						1.022	60		0.16	10				
									0.03	100				
	141	18m	6.42×10^{-4}	---	5.9	2.8	100	0.93	0	0	---	---	0	0.93
					(1.2)[a]									
	142	6m	1.93×10^{-3}	---	(5.6)	2.26[b]	100	0.75[b]	---	~0	---	---	~0	0.75[b]
					(2.2)[a]									
	143	30s	2.31×10^{-2}	---	(4.9)	4.34[b]	100	1.5[b]	---	~0	---	---	~0	1.5[b]
					(3.0)[a]									
	144	Short	---	---	(3.5)	3.18[b]	100	1.1[b]	---	~0	---	---	~0	1.1[b]
					(2.5)[a]									
$_{57}$La	139	Stable	0	8.9	6.0	0	0	0	0	0	---	---	0	0
	140	40.2h	4.79×10^{-6}	3	6.3	1.32	70	0.495	3.0	1	I	1.8	2.11	2.61
						1.67	20		2.5	5.4	II	73.4		
						2.26	10		1.596	94	III	94		
									0.8151	29	IV	6.4		
									0.4867	39				
									0.3286	5.4				
									0.093	1.8				
	141	3.7h	5.20×10^{-5}	---	6.0	0.9	5	0.785	1.5	5	III	5	0.075	0.86
					0.1[a]	2.43	95							
	142	74m	1.56×10^{-4}	---	5.9	2.5	100	0.83	0.87	10	II	150	0.66	1.49
					(0.3)[a]				0.63	90				
	143	19m	6.08×10^{-4}	---	6.2	3.05[b]	100	1.0[b]	---	~0	---	---	~0	1.0[b]
					(1.3)[a]									
	144	Short	---	---	(5.8)	5.12[b]	100	1.7[b]	---	~0	---	---	~0	1.7[b]
					(2.3)[a]									

Table 4.5 (continued)

Nuclide	Mass Number, A	Half-life, $t_{1/2}$	Decay Constant, λ (sec^{-1})	Absorption Cross Section σ_a (barns)	Yield, Y (%)	Energy of Radiation: Beta Particles E_b (Mev)	Beta Particles (%)	Beta Particles Av. E_b (Mev)	Gamma Transitions E_g (Mev)	Gamma Transitions (%)	Shielding Group	Shielding (%)	Total E_g (Mev)	Total E (Mev)
$_{58}Ce$	140	Stable	0	0.6	6.3	0	0	0	0	0	---	---	0	0
	141	32d	2.51×10^{-7}	---	6.0	0.442	67	0.163	0.145	67	I	67	0.097	0.260
						0.581	33							
	142	Stable	0	1.8	5.9	0	0	0	0	0	---	---	0	0
	143	32h	6.01×10^{-6}	---	6.2	0.71	30	0.355	0.660	15.2	I	12.1	0.334	0.689
						[illegible]	40		0.356	12.1	II	87.9		
						1.39	30		0.289	60.6				
									0.126	12.1				
	144	290d	2.76×10^{-8}	---	6.1	0.170	30	0.087	0.134	~10	I	~50	0.043[d]	0.130[d]
					(0.3)[a]	0.300	70		0.100	~10				
									0.0807	~10				
									0.054	~10				
									0.0337	~10				
	145	3.0m	3.85×10^{-3}	---	4.2	2.67[b]	100	0.89[b]	---	~0	---	---	~0	0.9[b]
	146	13.9m	8.31×10^{-4}	---	(3.2)	0.7	100	0.23	0.32	12	I	72	0.327	0.56
									0.27	24	II	64		
									0.22	36				
									0.142	7				
									0.110	~57				
$_{59}Pr$	141	Stable	0	11	6.0	0	0	0	0	0	---	---	0	0
	143	13.7d	5.85×10^{-7}	---	6.2	0.932	100	0.311	0	0	---	---	0	0.31
	144	17.5m	6.60×10^{-4}	---	6.1	0.8	3	0.97	2.185	1	II	4	0.08	1.05
						2.3	2		1.480	2	III	2		
						2.98	95		0.695	4	IV	1		
	145	6.0h	3.21×10^{-5}	---	4.2	~1.7	100	~0.6	---	~0	---	---	~0	~0.6
	146	24.4m	4.73×10^{-4}	---	3.3	2.2	44	1.01	1.49	33	II	122	1.12	2.13
					(0.1)[a]	3.7	56		0.75	22	III	33		
									0.46	100				
$_{60}Nd$	143	Stable	0	290	6.2	0	0	0	0	0	---	---	0	0
	144	1.5×10^{15}y	~0	4.8	6.1	0	0	0	0	0	---	---	0	0
	145	Stable	0	52	4.2	0	0	0	0	0	---	---	0	0
	146	Stable	0	9.8	3.3	0	0	0	0	0	---	---	0	0
	147	11.3d	7.10×10^{-7}	---	2.6	0.38	25	0.228	0.532	25	I	60	0.236	0.464
						0.60	15		0.318	15	II	40		
						0.83	60		0.092	60				
	148	Stable	0	3.3	1.8[a]	0	0	0	0	0	---	---	0	0
	149	2.0h	9.63×10^{-5}	---	1.3	0.95	---	~0.5	0.650	---	I	~0	~0	~0.5
						1.1	---		0.538	---	II	~0		
						1.5	~100		0.424	---				
									0.266	---				
									0.240	---				

Table 4.5 (continued)

Nuclide	Mass Number, A	Half-life, $t_{1/2}$	Decay Constant, λ (sec^{-1})	Absorption Cross Section σ_a (barns)	Yield, Y (%)	Energy of Radiation: Beta Particles E_b (Mev)	Beta Particles (%)	Beta Particles Av. E_b (Mev)	Gamma Transitions E_g (Mev)	Gamma Transitions (%)	Shielding Group	Shielding (%)	Total E_g (Mev)	Total E (Mev)
$_{60}$Nd (continued)									0.226	---				
									0.211	---				
									0.198	---				
									0.188	---				
									0.124	---				
									0.114	---				
									0.112	---				
									0.097	---				
									0.030	---				
	150	$>2 \times 10^{15}$y	~0	2.9	0.74[a]	0	0	0	0	0	---	---	0	0
	151	15m	7.7×10^{-4}	---	(0.48)	1.93	100	0.64	1.14	---	I	~150	0.91[b]	1.55[b]
									0.73	---	II	~100		
									0.421	---	III	~50		
									0.117	---				
									0.110	---				
									0.085	---				
$_{61}$Pm	147	2.6y	8.46×10^{-9}	60 + ?	2.6	0.223	100	0.074	0	0	---	---	0	0.074
	149	54h	3.56×10^{-6}	---	1.3	1.05	100	0.35	0.285	100	II	100	0.285	0.635
	151	27.5h	7.00×10^{-6}	---	0.5	1.1	100	0.37	0.715	---	I	~100	0.5[b]	0.87[b]
					(0.02)[a]				0.340	---	II	~100		
									<0.25	---				
									0.177	---				
$_{62}$Sm	147	1.4×10^{11}y	~0	---	2.6	0	0	0	0	0	---	---	0	0
	149	Stable	0	50,000	1.3	0	0	0	0	0	---	---	0	0
	151	93y	2.37×10^{-10}	12,000	0.5	0.076	100	0.025	0.019	100	I	100	0.019	0.044
	152	Stable	0	150	0.3[a]	0	0	0	0	0	---	---	0	0
	153	47h	4.10×10^{-6}	---	0.15	0.26	10	0.219	0.538	10	I	~102	0.149	0.368
						0.64	29		0.1717	~0	II	10		
						0.70	44		0.1026	73				
						0.81	17		0.0691	29				
	154	Stable	0	5.5	0.09[a]	0	0	0	0	0	---	---	0	0
	155	23.5m	4.91×10^{-4}	---	0.031	1.8	100	0.6	0.246	100	I	200	0.35	0.95
									0.105	100				
	156	~10h	1.93×10^{-5}	---	0.013	0.9	100	0.3	?	?	---	---	?	0.3 ?
$_{63}$Eu	151	Stable	0	1400 + 7000	0.5	0	0	0	0	0	---	---	0	0
	153	Stable	0	400	0.15	0	0	0	0	0	---	---	0	0
	155	1.7y	1.29×10^{-8}	14,000	0.031	0.152	84	0.056	0.1368	---	I	~500	0.7[b]	0.76[b]
						0.252	16		0.1309	---				
									0.1045	---				
									0.0858	---				
									0.0593	---				
									0.0187	---				

Table 4.5 (continued)

Nuclide	Mass Number, A	Half-life, $t_{1/2}$	Decay Constant, λ (sec^{-1})	Absorption Cross Section σ_a (barns)	Yield, Y (%)	Energy of Radiation: Beta Particles E_b (Mev)	Beta Particles (%)	Beta Particles Av. E_b (Mev)	Gamma Transitions E_g (Mev)	Gamma Transitions (%)	Shielding Group	Shielding (%)	Total E_g (Mev)	Total E (Mev)
$_{63}Eu$	156	15.4d	5.21×10^{-7}	---	0.013	0.5	60	0.43	2.0	~60	IV	~60	1.2	1.63
						2.4	40							
	157	15.4h	1.25×10^{-5}	---	0.0074	1.0	75	0.392	0.60	100	I	100	0.8	1.19
						1.7	25		0.2	100	II	100		
	158	60m	1.93×10^{-4}	---	0.002	2.6	100	0.87	---	---	---	---	1.1[b]	2.0[b]
$_{64}Gd$	155	Stable	0	70,000	0.031	0	0	0	0	0	---	---	0	0
	156	Stable	0	---	0.013	0	0	0	0	0	---	---	0	0
	157	Stable	0	160,000	0.0074	0	0	0	0	0	---	---	0	0
	158	Stable	0	4	0.002	0	0	0	0	0	---	---	0	0
	159	18.0h	1.07×10^{-5}	---	1.1×10^{-3}	0.9	100	0.3	0.38	100	I	100	0.46	0.76
									0.055	100	II	100		
	160	Stable	0	1.5	3×10^{-4}[a]	0	0	0	0	0	---	---	0	0
	161	3.6m	3.21×10^{-3}	---	8.0×10^{-5}	1.6	100	0.5	0.36	---	I	100	0.7[b]	1.2[b]
									0.316	---	II	200		
									0.102	---				
$_{65}Tb$	159	Stable	0	44	1.1×10^{-3}	0	0	0	0	0	---	---	0	0
	161	7.0d	1.15×10^{-6}	---	8×10^{-5}	0.5	100	0.17	0.05	100	I	100	0.05	0.22
$_{66}Dy$	161	Stable	0	---	8×10^{-5}	0	0	0	0	0	---	---	0	0

*From Blomeke and Todd, Ref. 7.

[a]Independent fission yield.

[b]Energy value computed from the mass change.

[c]Nuclide which decays in part by K electron capture and positron emission.

[d]Energy computed from total disintegration energy or Q value.

4.2.3 Calculation of Fission-Product Inventories

In calculating the inventory of fission products, the following factors must be considered: irradiation time, neutron flux, independent yield, decay constant of the nuclide in question, decay constant of previous (parent) isobar in the same chain, neutron cross section of the nuclide in question, neutron cross section of the nuclide with the same atomic number in the chain of one lower mass number, branching ratios, and decay time after irradiation. The generalized decay scheme proposed by Stoughton and Halperin[9] was used by Blomeke and Todd[7] to calculate their results.

The solutions of the decay equations are, for the time after shutdown t_i,

$$N_1 = N_1^0 e^{-\lambda_1 t} , \tag{4.3}$$

$$N_2 = N_2^0 e^{-\lambda_2 t} + \lambda_1 N_1^0 \left(\frac{e^{-\lambda_1 t}}{\lambda_2 - \lambda_1} + \frac{e^{-\lambda_2 t}}{\lambda_1 - \lambda_2} \right) , \tag{4.4}$$

$$N_3 = N_3^0 e^{-\lambda_3 t} + \lambda_2 N_2^0 \left(\frac{e^{-\lambda_2 t}}{\lambda_3 - \lambda_2} + \frac{e^{-\lambda_3 t}}{\lambda_2 - \lambda_3} \right)$$

$$+ \lambda_1 \lambda_2 N_1^0 \left[\frac{e^{-\lambda_1 t}}{(\lambda_2 - \lambda_1)(\lambda_3 - \lambda_1)} + \frac{e^{-\lambda_2 t}}{(\lambda_1 - \lambda_2)(\lambda_3 - \lambda_2)} \right.$$

$$\left. + \frac{e^{-\lambda_3 t}}{(\lambda_1 - \lambda_3)(\lambda_2 - \lambda_3)} \right], \quad (4.5)$$

$$N_i = N_i^0 e^{-\lambda_i t} + \sum_{r=1}^{r=i-1} \left[N_r^0 \left(\prod_{q=r}^{q=i-1} \lambda_q \right) S\lambda_r \lambda_{r+1} \cdots \lambda_i \right], \quad (4.6)$$

where $S_{ABC} \cdots$ represents

$$\frac{e^{-At}}{(B - A)(C - A)} \cdots + \frac{e^{-Bt}}{(A - B)(C - B)} \cdots + \frac{e^{-Ct}}{(A - C)(B - C)} .$$

In calculating the decay, if branching occurs, the two resulting chains can be treated as separate systems. Blomeke and Todd calculated the solutions of decay equations for all the fission products listed in Tables 4.4 and 4.5 using a digital computer. Numerical values of N were computed for the following values of parameters:

Thermal-Neutron Flux, ϕ (neutrons/cm^2·sec)	Irradiation Time, τ (sec)	Cooling Time, t (sec)
10^{12}	10^5	10^3
10^{13}	3×10^5	10^4
3×10^{13}	10^6	10^5
10^{14}	3×10^6	10^6
3×10^{14}	10^7	10^7
10^{15}	3×10^7	10^8
	10^8	10^9

The results were presented in the form of charts, giving the ratios N_S/N_{235}^0, the saturation values of the isotope in question expressed as a fraction of the initial number of atoms of ^{235}U originally present; N_τ/N_S, the fraction of the saturation value at a time τ of irradiation at a constant flux; and N_t/N_τ, the fraction of the shutdown value at cooling time t. Thus, by referring to three charts, the fission-product inventory can be determined. The fission products of specific interest from a hazards viewpoint are indexed in Table 4.6. The information on these fission products may be found in Figs. 4.6 through 4.49 and in Table 4.7.

Table 4.6. Index of Data for Calculation of Biologically Important Fission Products

Critical Organ	Nuclide	N_s/N^0_{235}	N_τ/N_s	N_t/N_τ
Bone	54d ^{89}Sr	Fig. 4.7	Fig. 4.9	Table 4.7
	28y ^{90}Sr	Fig. 4.6	Fig. 4.10	Table 4.7
	64.5h ^{90}Y	Fig. 4.7	Fig. 4.11	Fig. 4.20
	9.7h ^{91}Sr	Fig. 4.7	Fig. 4.12	Table 4.7
	51m ^{91m}Y	Fig. 4.8	Fig. 4.12	Fig. 4.21
	58d ^{91}Y	Fig. 4.7	Fig. 4.13	Figs. 4.22, 4.23
	63d ^{95}Zr	Fig. 4.7	Fig. 4.14	Table 4.7
	90h ^{95m}Nb	Fig. 4.7	Fig. 4.14	Fig. 4.24
	35d ^{95}Nb	Fig. 4.7	Fig. 4.14	Fig. 4.25
	17h ^{97}Zr	Fig. 4.7	Fig. 4.12	Table 4.7
	60s ^{97m}Nb	Fig. 4.8	Fig. 4.12	Table 4.7
	72.1m ^{97}Nb	Fig. 4.7	Fig. 4.12	Fig. 4.26
	67h ^{99}Mo	Fig. 4.7	Fig. 4.15	Table 4.7
	6.04h ^{99m}Tc	Fig. 4.7	Fig. 4.15	Fig. 4.27
	93h ^{127}Sb	Fig. 4.7	Fig. 4.15	Fig. 4.28
	12.8d ^{140}Ba	Fig. 4.7	Fig. 4.14	Table 4.7
	40.2h ^{140}La	Fig. 4.7	Fig. 4.14	Fig. 4.29
	32d ^{141}Ce	Fig. 4.7	Fig. 4.14	Figs. 4.30, 4.31
	33h ^{143}Ce	Fig. 4.7	Fig. 4.12	Table 4.7
	13.7d ^{143}Pr	Fig. 4.7	Fig. 4.13	Fig. 4.32
	290d ^{144}Ce	Fig. 4.6	Fig. 4.13	Table 4.7
	17.5m ^{144}Pr	Fig. 4.8	Fig. 4.13	Table 4.7
	11.3d ^{147}Nd	Fig. 4.7	Fig. 4.15	Table 4.7
	2.6y ^{147}Pm	Fig. 4.6	Fig. 4.16	Figs. 4.33, 4.34
	54h ^{149}Pm	Fig. 4.7	Fig. 4.15	Fig. 4.35
Thyroid	8.05d ^{131}I	Fig. 4.7	Fig. 4.17	Table 4.7
	2.4h ^{132}I	Fig. 4.7	Fig. 4.15	Figs. 4.36 to 4.38
	20.8h ^{133}I	Fig. 4.7	Fig. 4.12	Fig. 4.26
	52.5m ^{134}I	Fig. 4.7	Unity	Fig. 4.39
	6.68h ^{135}I	Fig. 4.7	Fig. 4.12	Table 4.7
Kidney	41d ^{103}Ru	Fig. 4.7	Fig. 4.18	Table 4.7
	57m ^{103m}Rh	Fig. 4.8	Fig. 4.18	Table 4.7
	36.5h ^{105}Rh	Fig. 4.7	Fig. 4.12	Fig. 4.40
	1.0y ^{106}Ru	Fig. 4.7	Fig. 4.13	Table 4.7
	30s ^{106}Rh	Fig. 4.8	Fig. 4.13	Table 4.7
	90d ^{127m}Te	Fig. 4.7	Fig. 4.13	Fig. 4.41
	9.3h ^{127}Te	Fig. 4.8	Fig. 4.13	Figs. 4.42 to 4.44
	33d ^{129m}Te	Fig. 4.7	Fig. 4.18	Figs. 4.45, 4.46
	72m ^{129}Te	Fig. 4.8	Fig. 4.13	Figs. 4.47, 4.48
	30h ^{131m}Te	Fig. 4.8	Unity	Fig. 4.39
	24.8m ^{131}Te	Fig. 4.8	Unity	Fig. 4.49
Muscle	26.6y ^{137}Cs	Fig. 4.6	Fig. 4.19	Table 4.7
	2.60m ^{137m}Ba	Fig. 4.8	Fig. 4.19	Table 4.7

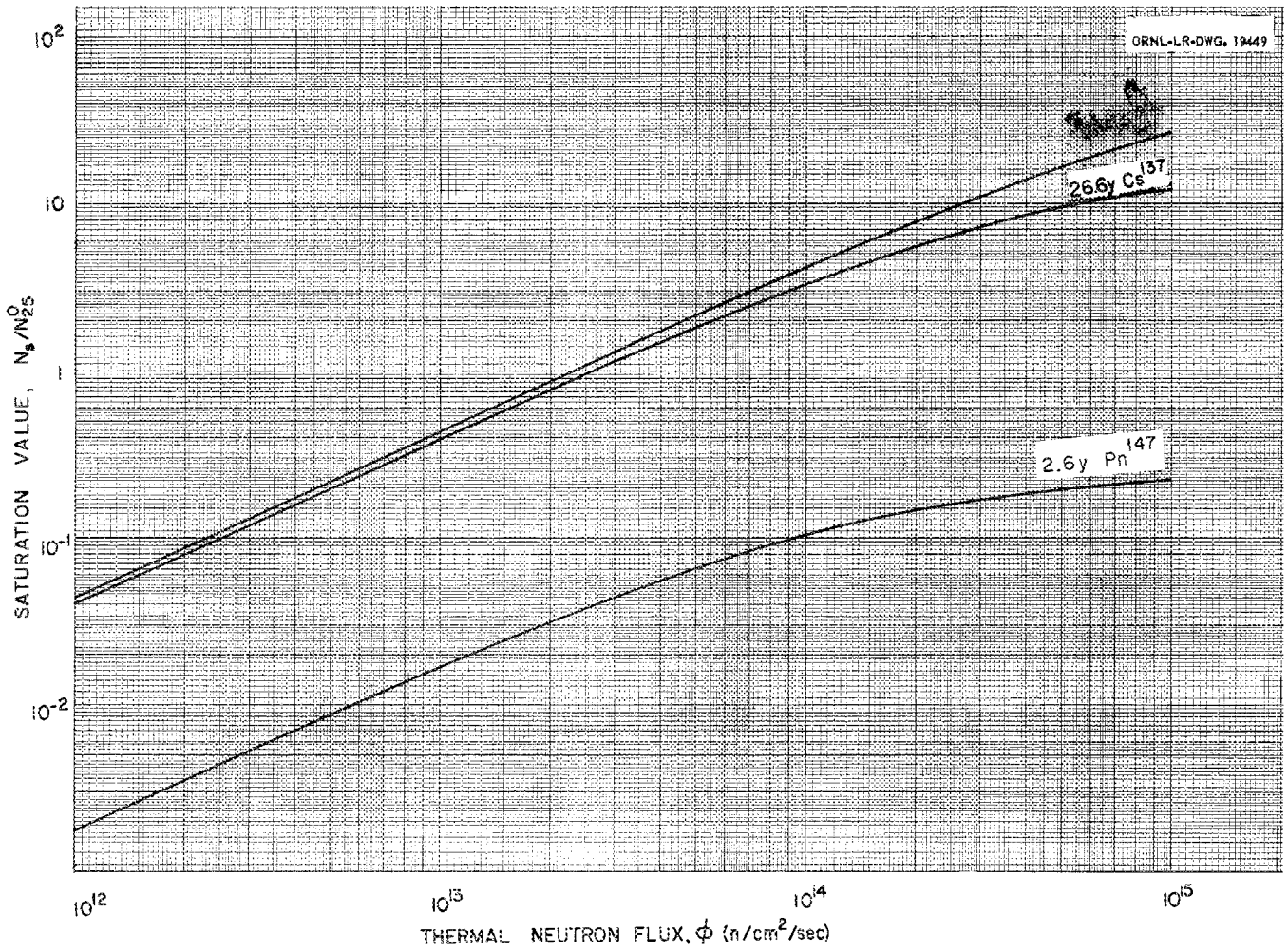

Fig. 4.6. Saturation Value of Radioactive Fission Products as a Function of Thermal-Neutron Flux. (From Blomeke and Todd, ref. 7, p. 58)

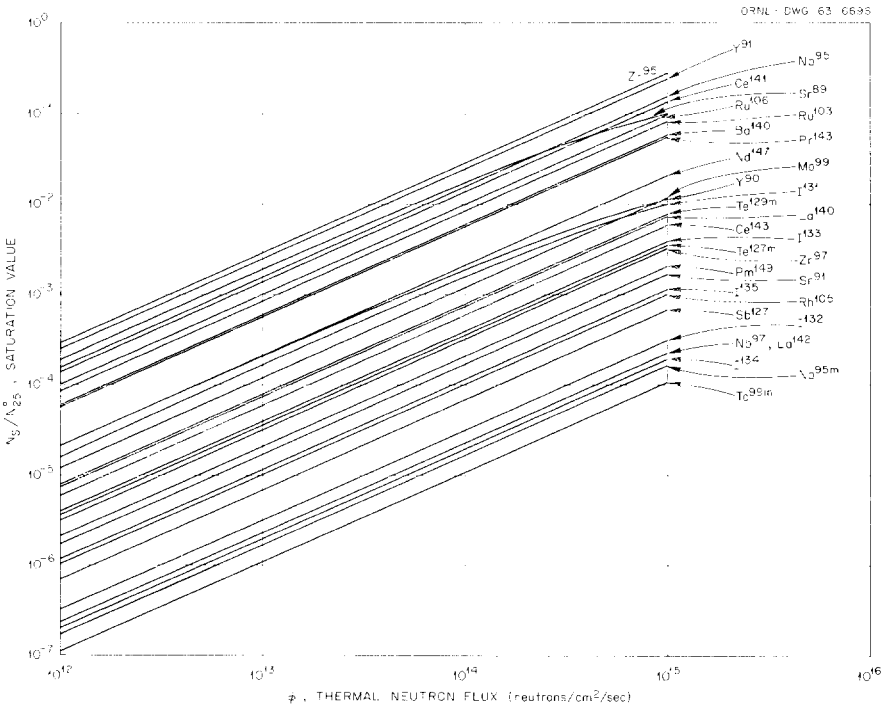

Fig. 4.7. Saturation Values of Radioactive Fission Products. (From Blomeke and Todd, ref. 7.)

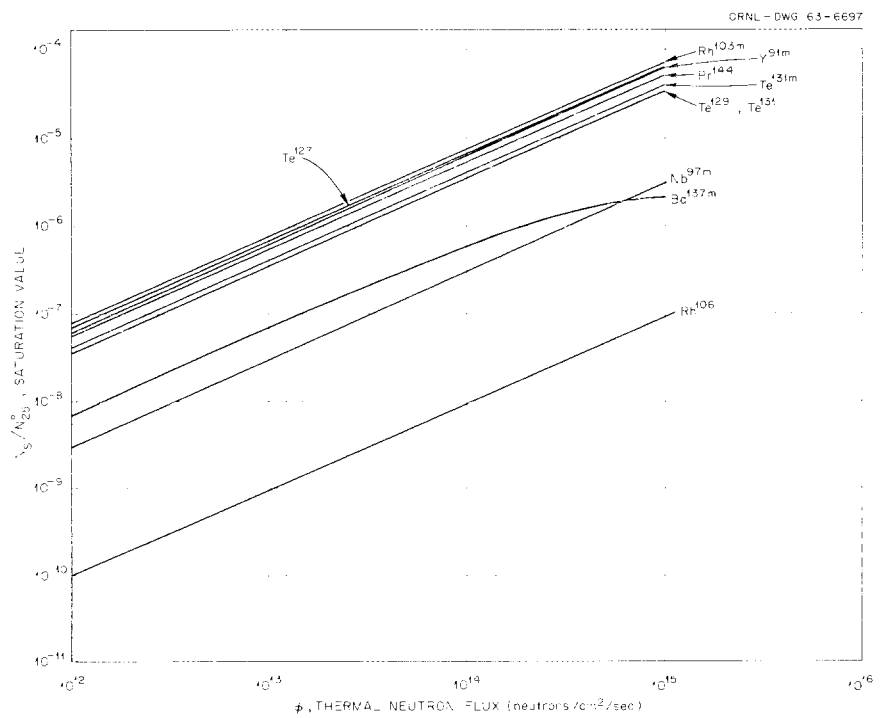

Fig. 4.8. Saturation Values of Radioactive Fission Products. (From Blomeke and Todd, ref. 7.)

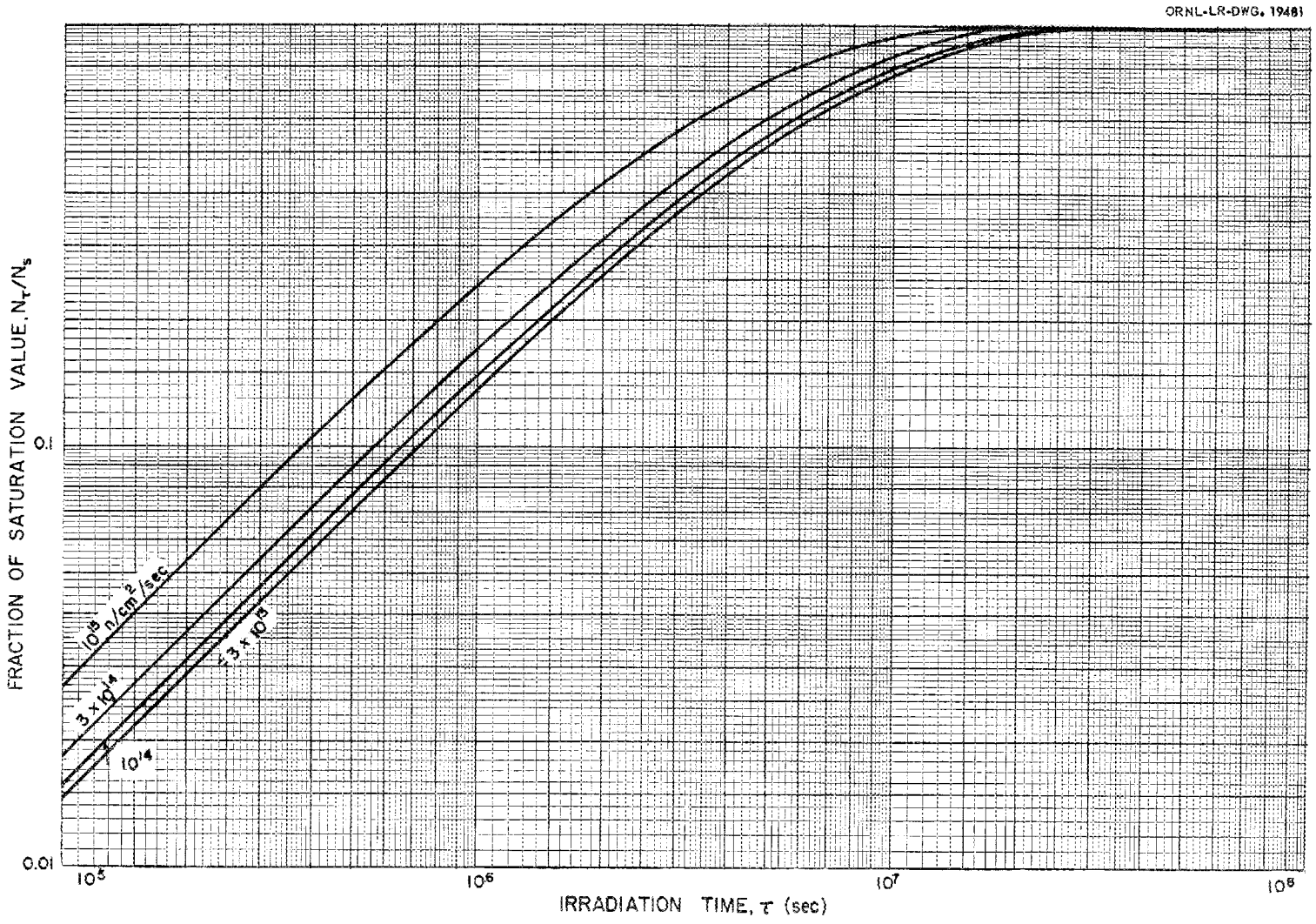

Fig. 4.9. Fraction of Saturation Value of 54d ^{89}Sr as a Function of Irradiation Time and Flux. (From Blomeke and Todd, ref. 7, p. 90.)

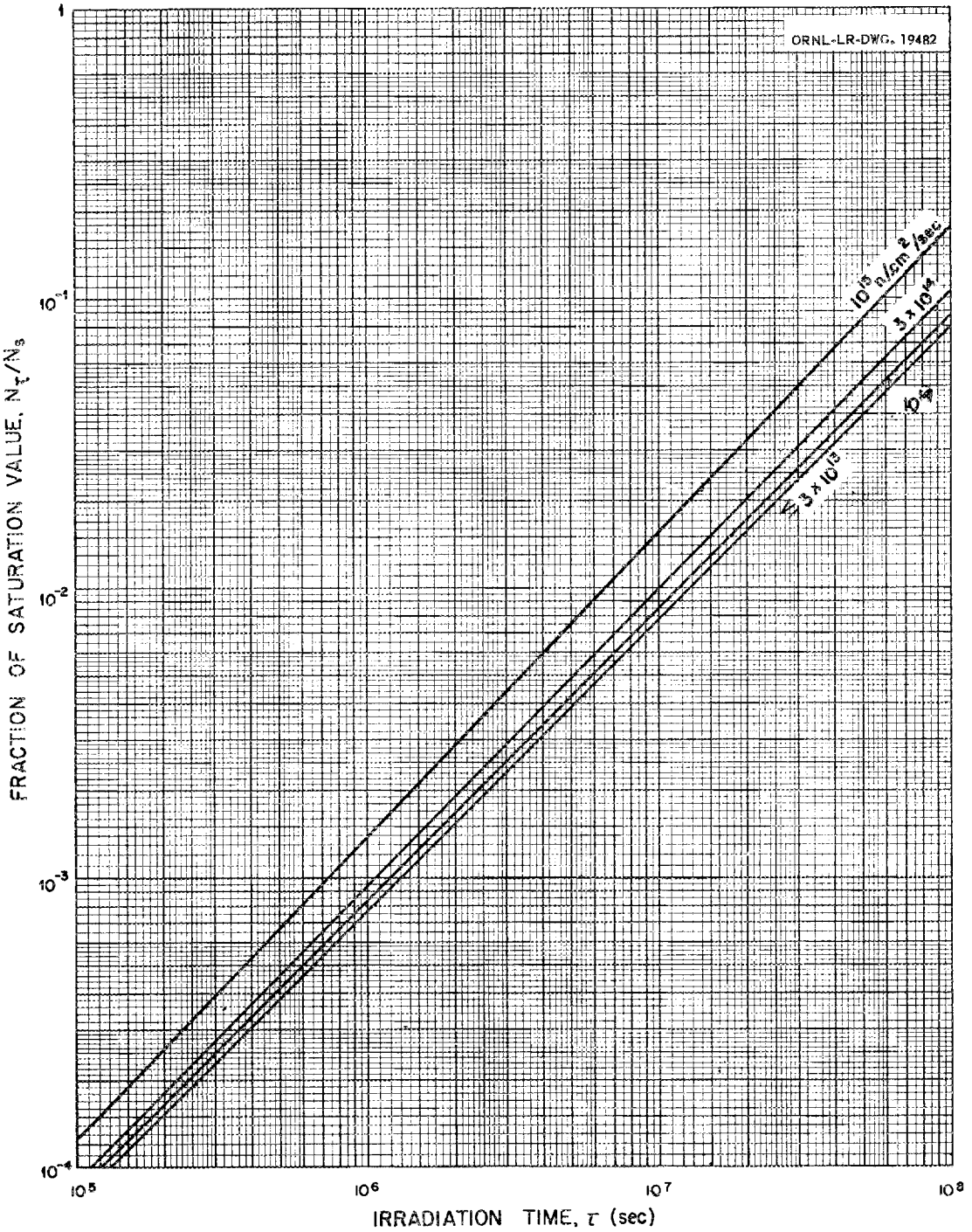

Fig. 4.10. Fraction of Saturation Value of 28y ^{90}Sr as a Function of Irradiation Time and Flux. (From Blomeke and Todd, ref. 7, p. 91.)

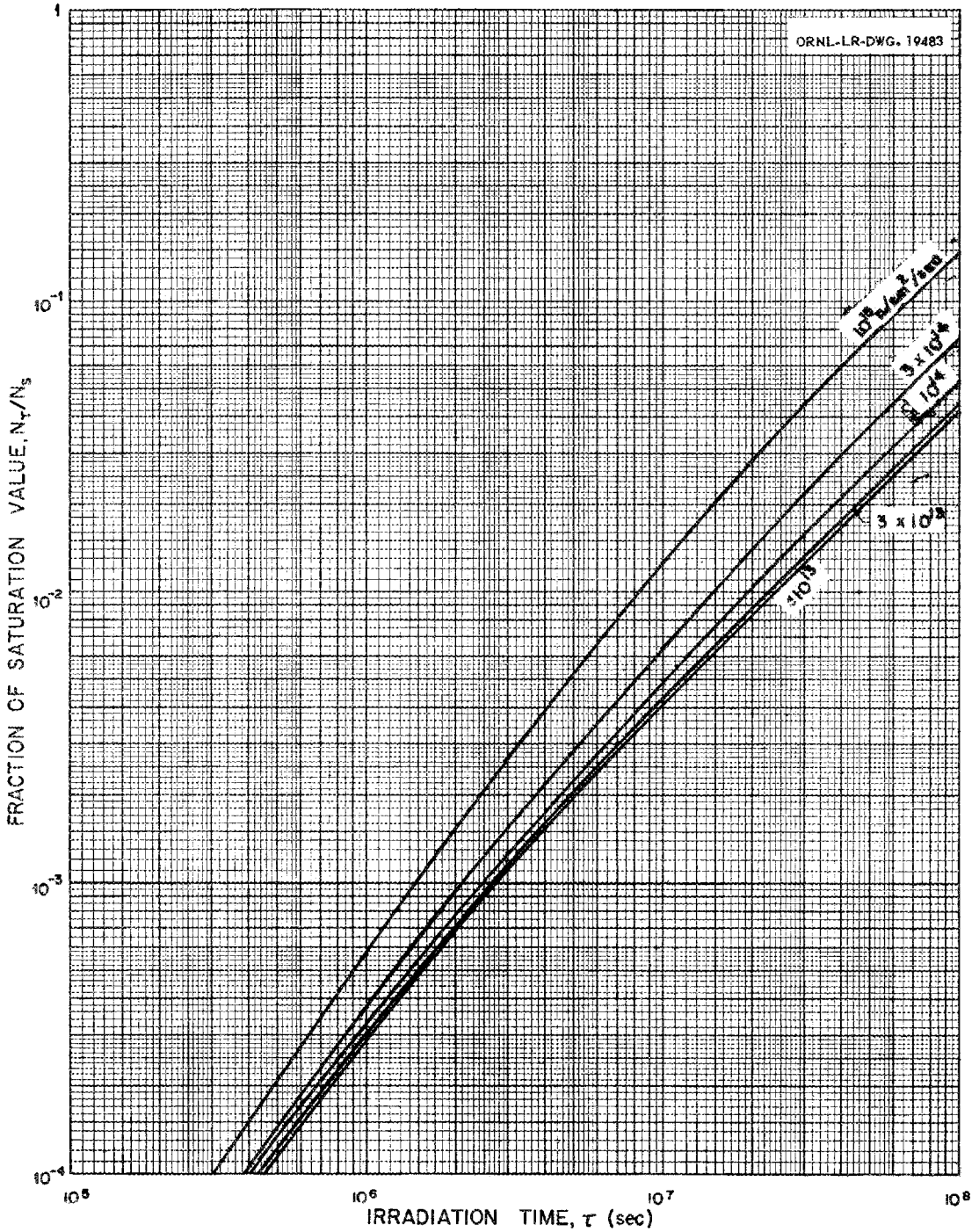

Fig. 4.11. Fraction of Saturation Value of 64.5h ^{90}Y as a Function of Irradiation Time and Flux. (From Blomeke and Todd, ref. 7, p. 92.)

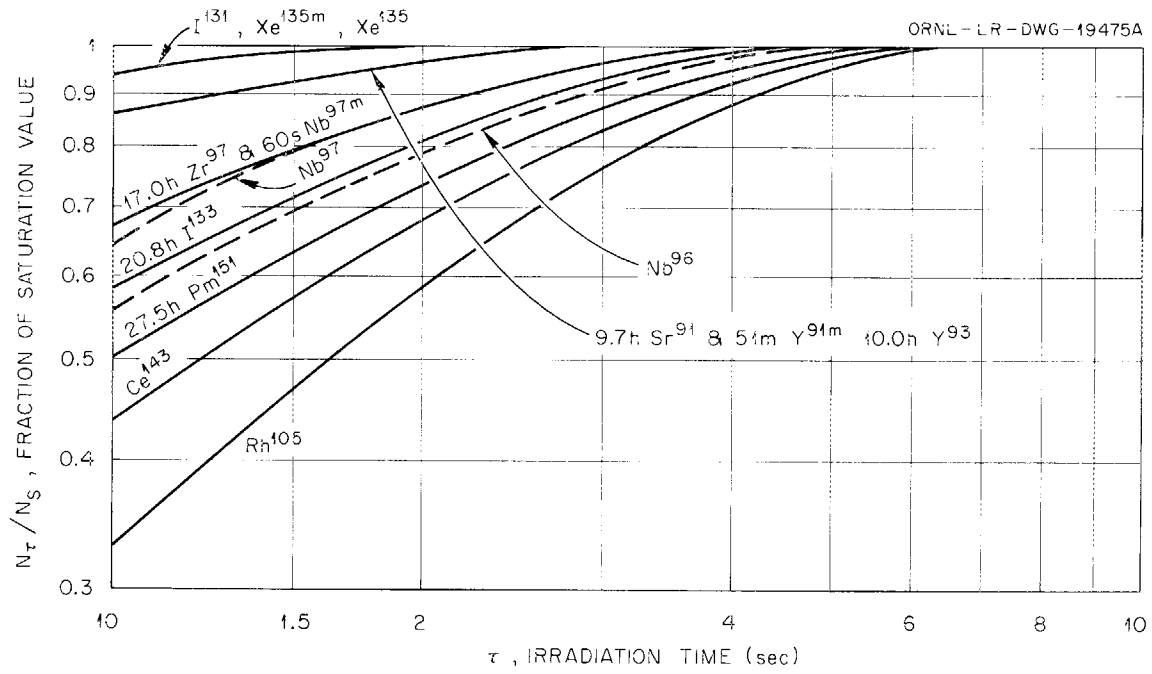

Fig. 4.12. Fraction of Saturation Value of Various Radioactive Fission Products as a Function of Irradiation Time. (From Blomeke and Todd, ref. 7.)

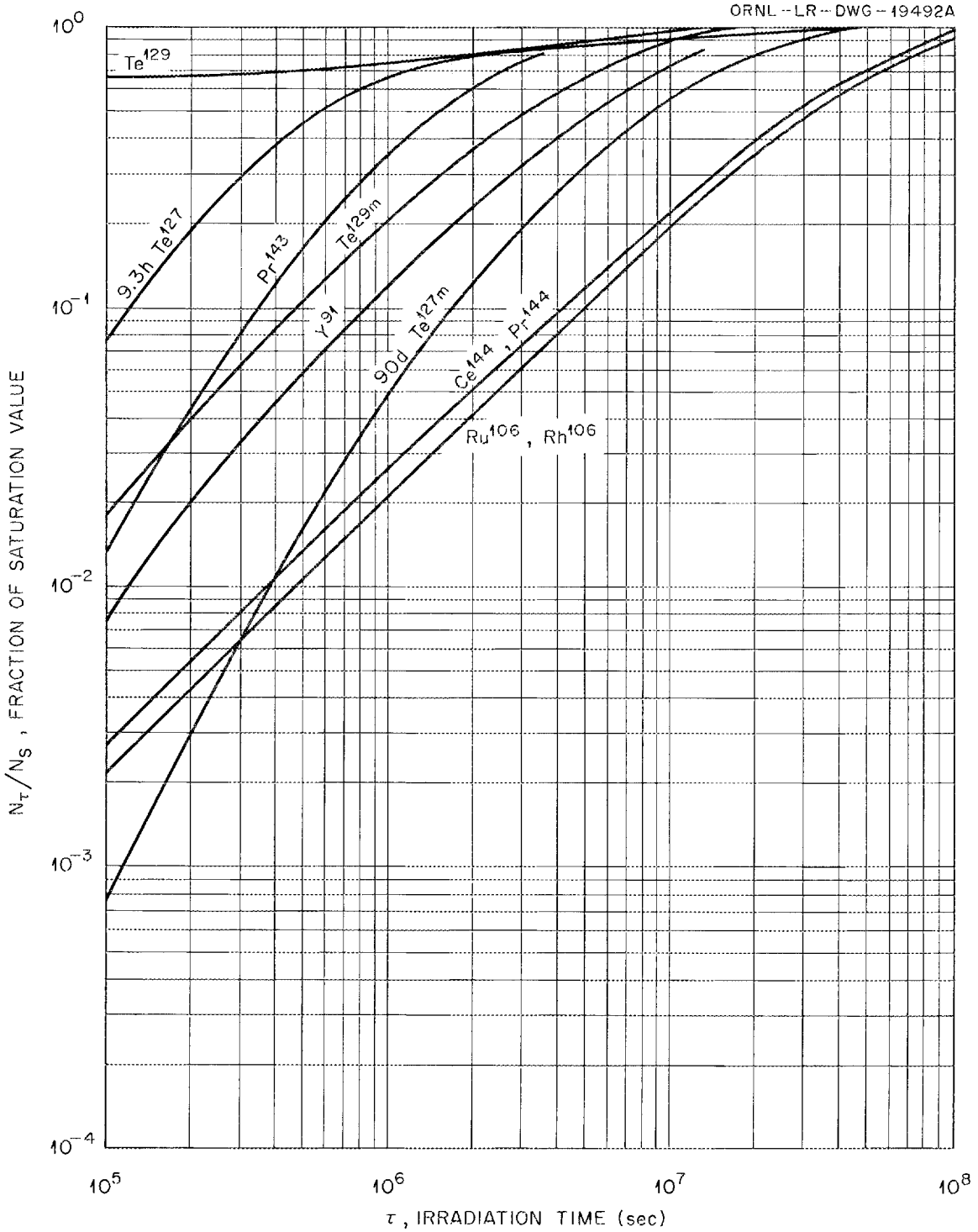

Fig. 4.13. Fraction of Saturation Value of Various Radioactive Fission Products as a Function of Irradiation Time. (From Blomeke and Todd, ref. 7, p. 101.)

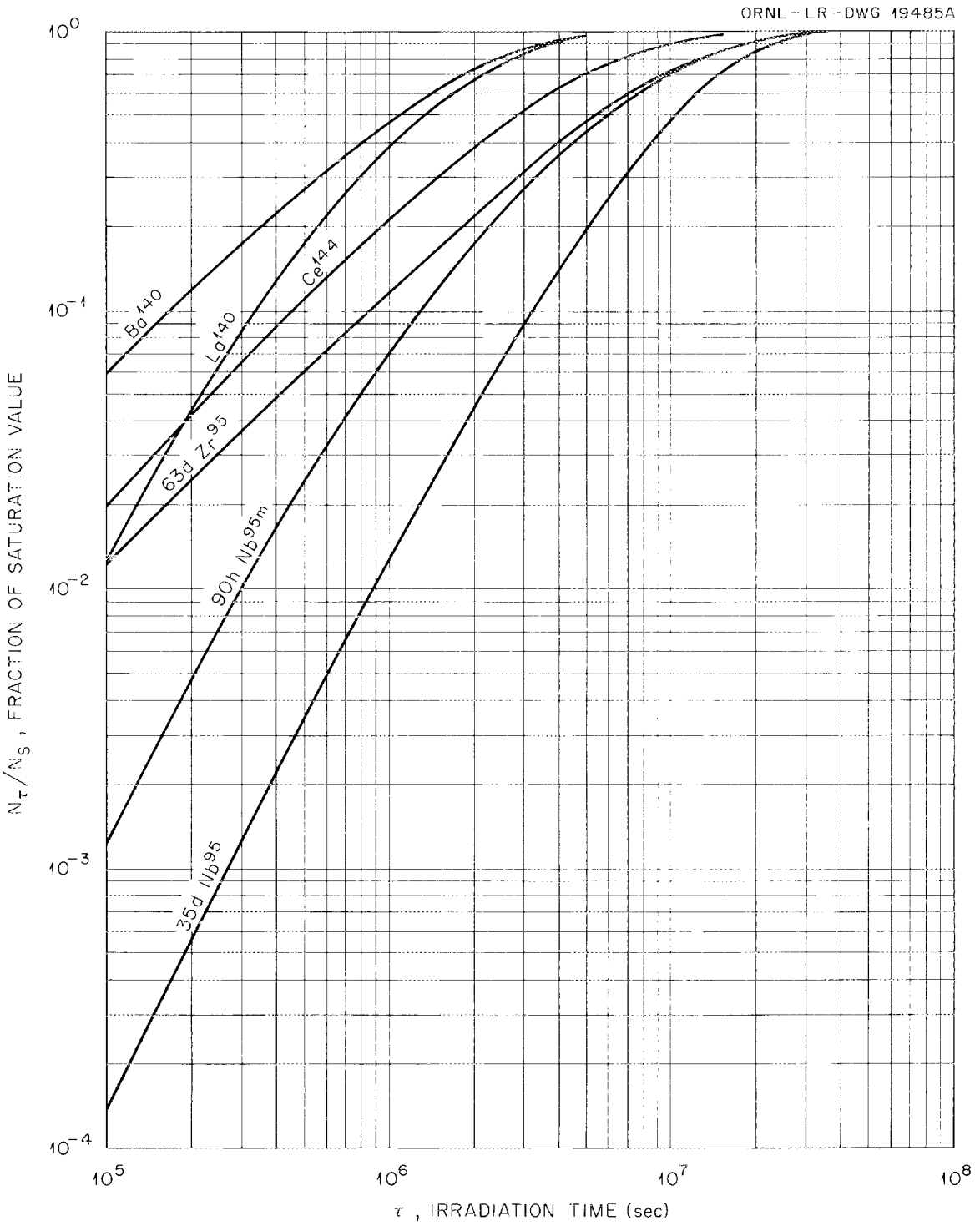

Fig. 4.14. Fraction of Saturation Value of Various Radioactive Fission Products as a Function of Irradiation Time. (From Blomeke and Todd, ref. 7, p. 94.)

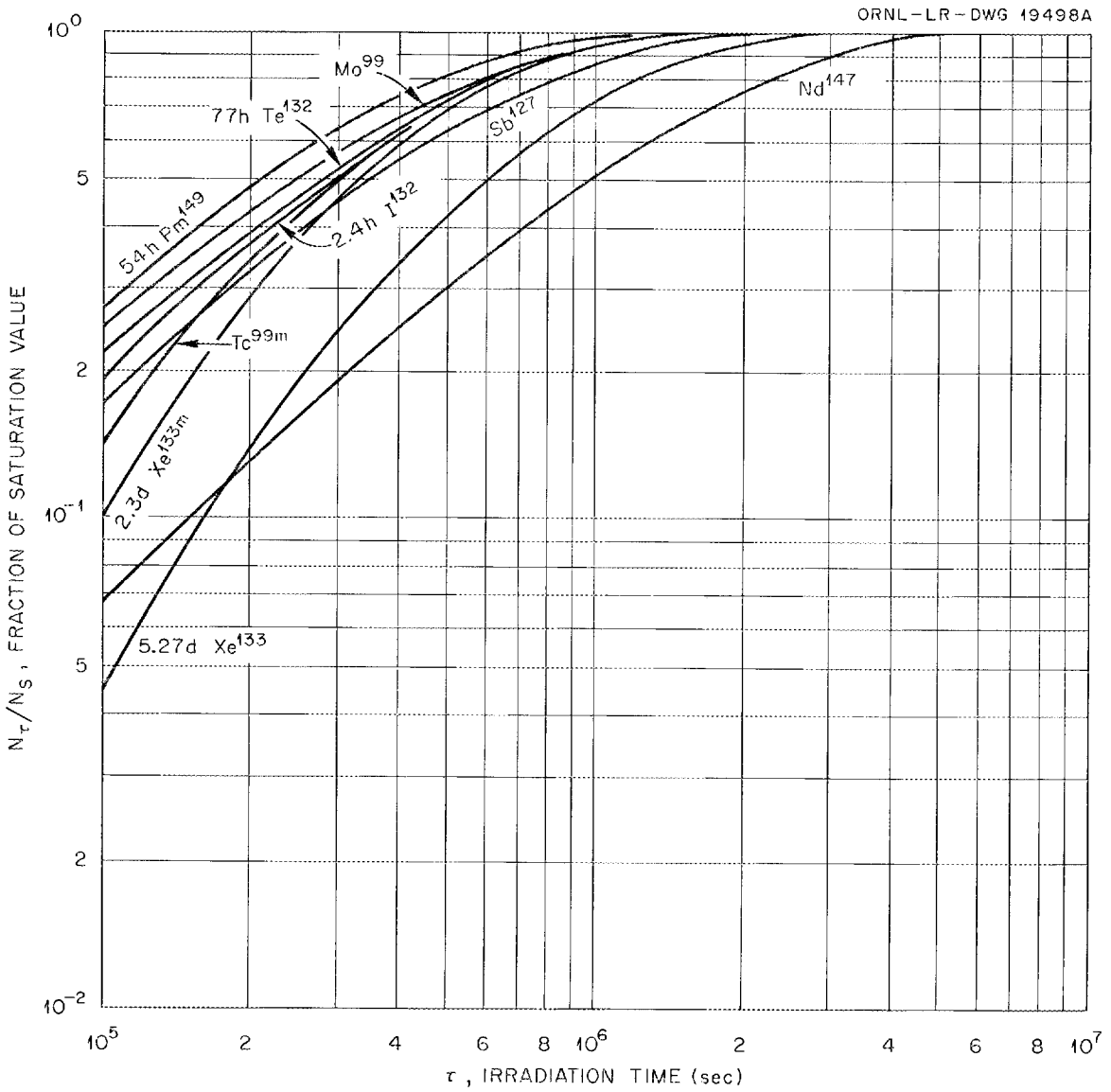

Fig. 4.15. Fraction of Saturation Value of Various Radioactive Fission Products as a Function of Irradiation Time. (From Blomeke and Todd, ref. 7, p. 107.)

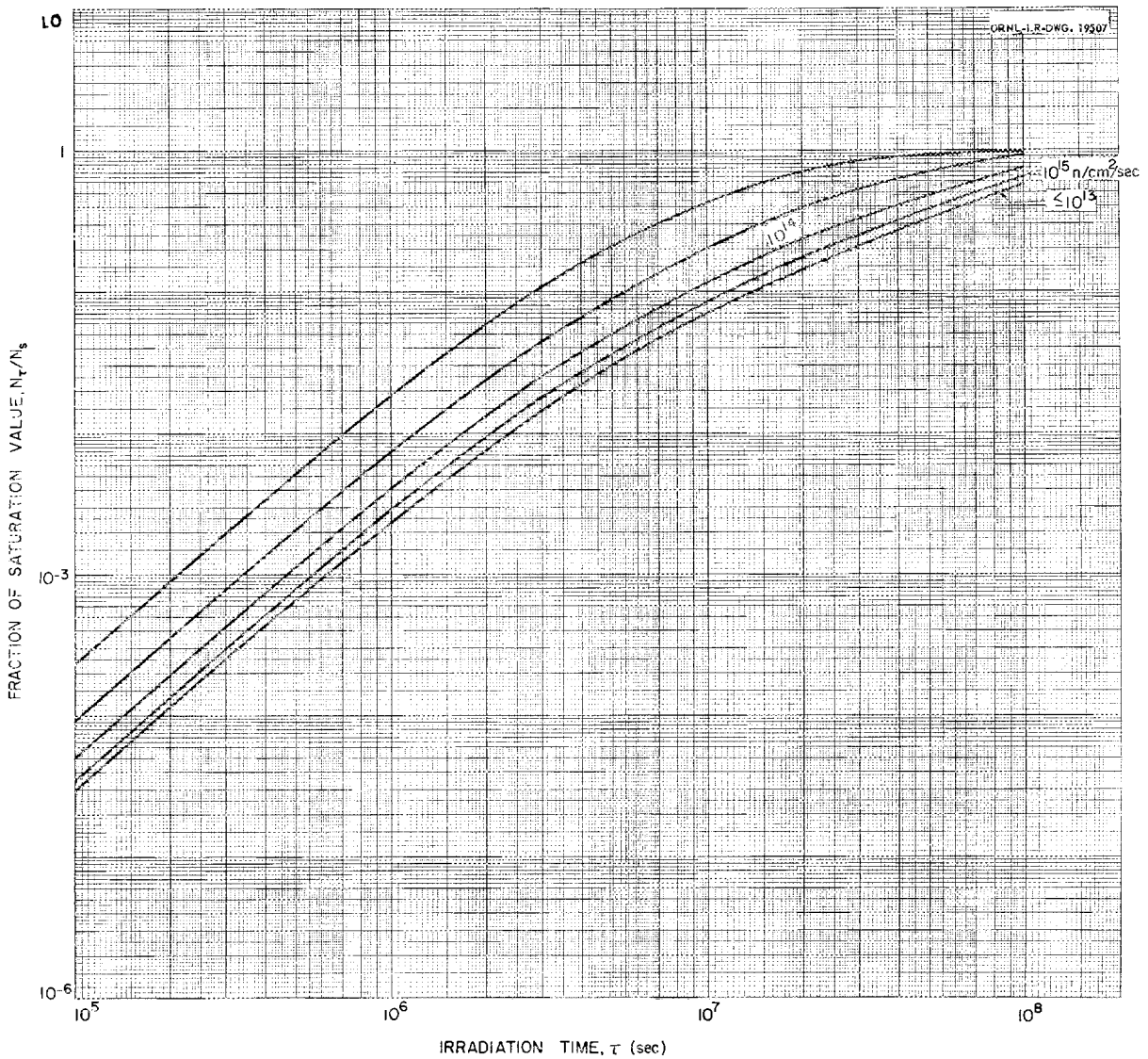

Fig. 4.16. Fraction of Saturation Value of 2.6y ^{147}Pm as a Function of Irradiation Time and Flux. (From Blomeke and Todd, ref. 7, p. 116.)

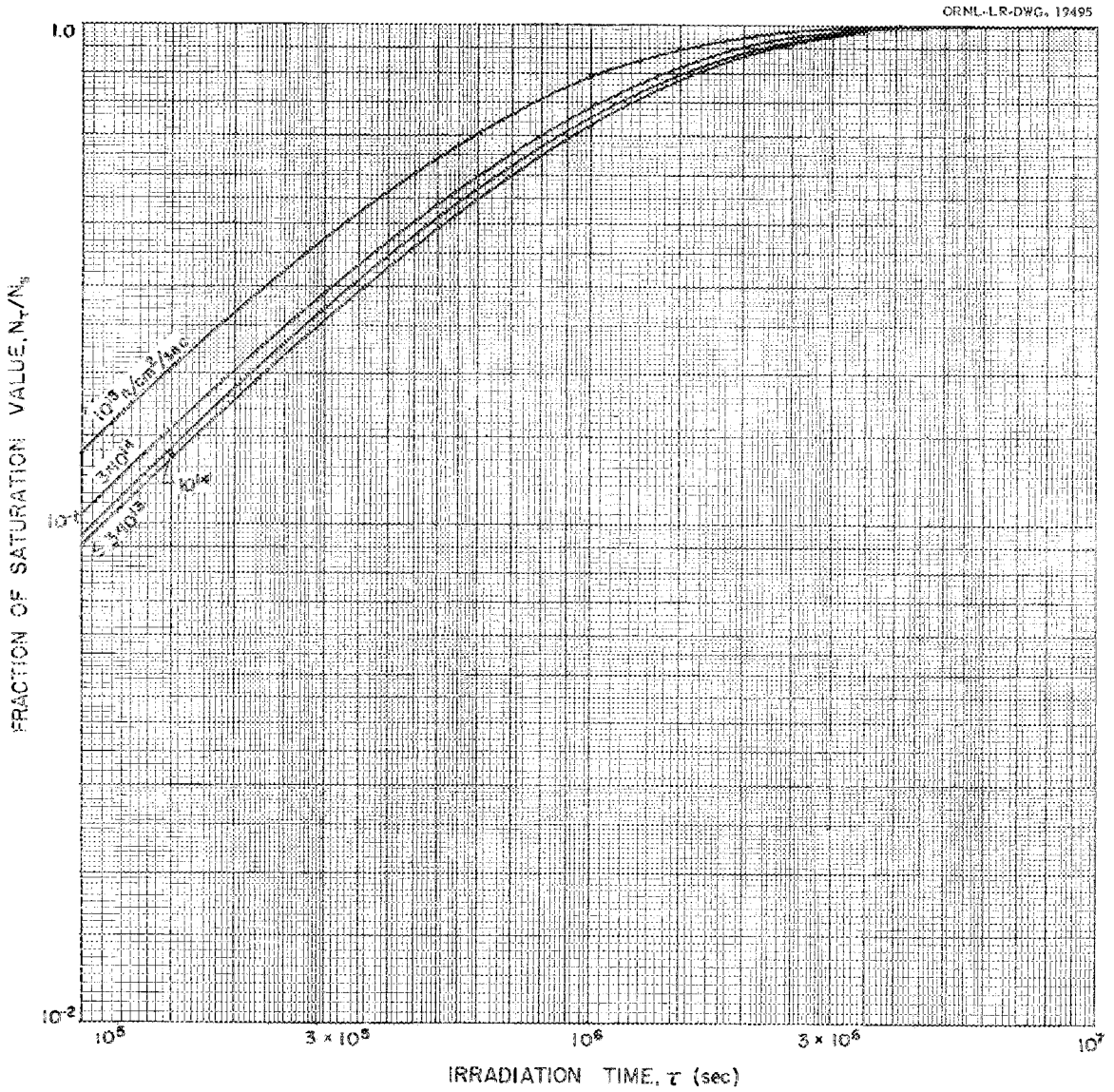

Fig. 4.17. Fraction of Saturation Value of 8.05d ^{131}I as a Function of Irradiation Time and Flux. (From Blomeke and Todd, ref. 7, p. 104.)

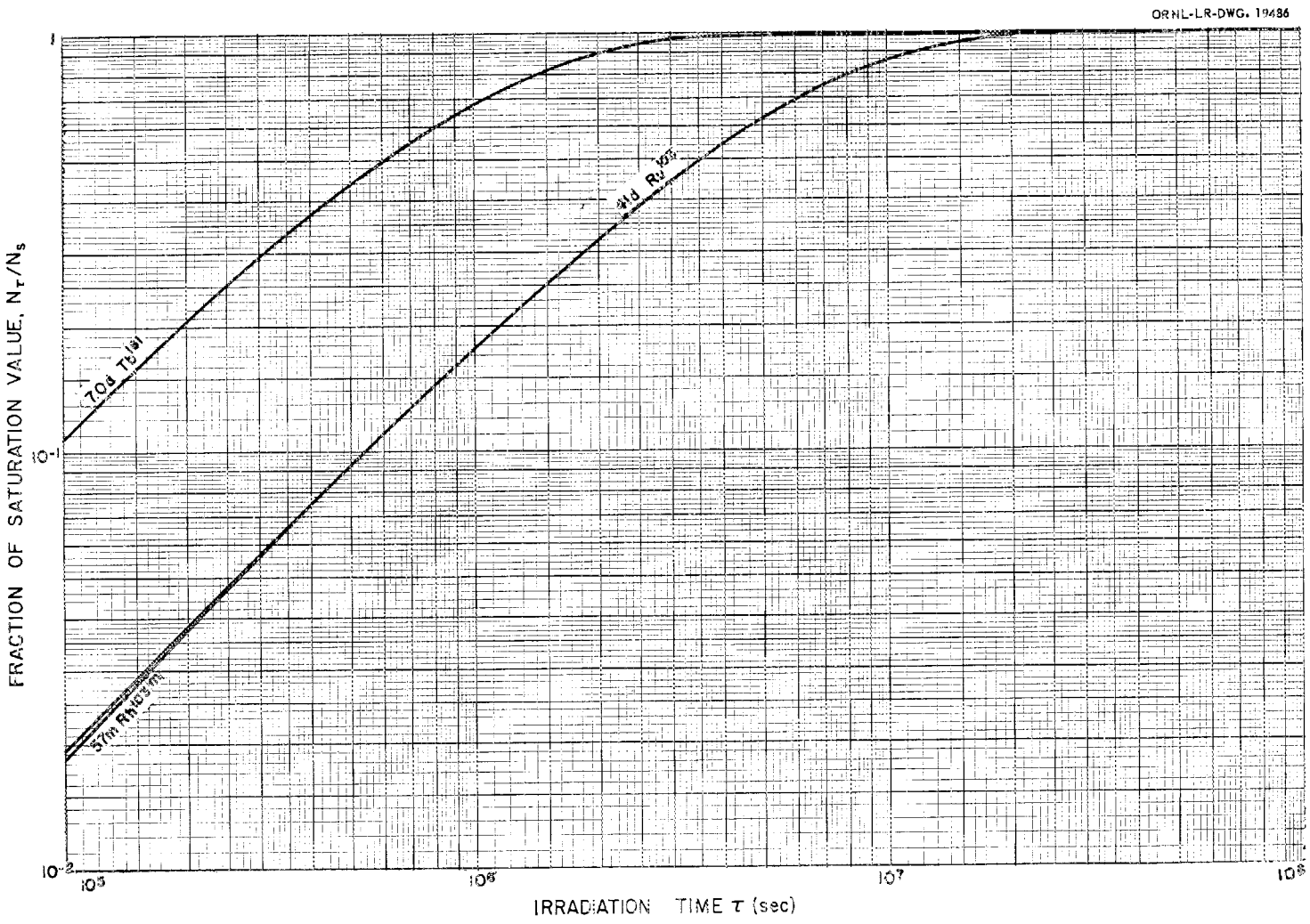

Fig. 4.18. Fraction of Saturation Value of Various Radioactive Fission Products as a Function of Irradiation Time. (From Blomeke and Todd, ref. 7, p. 95.)

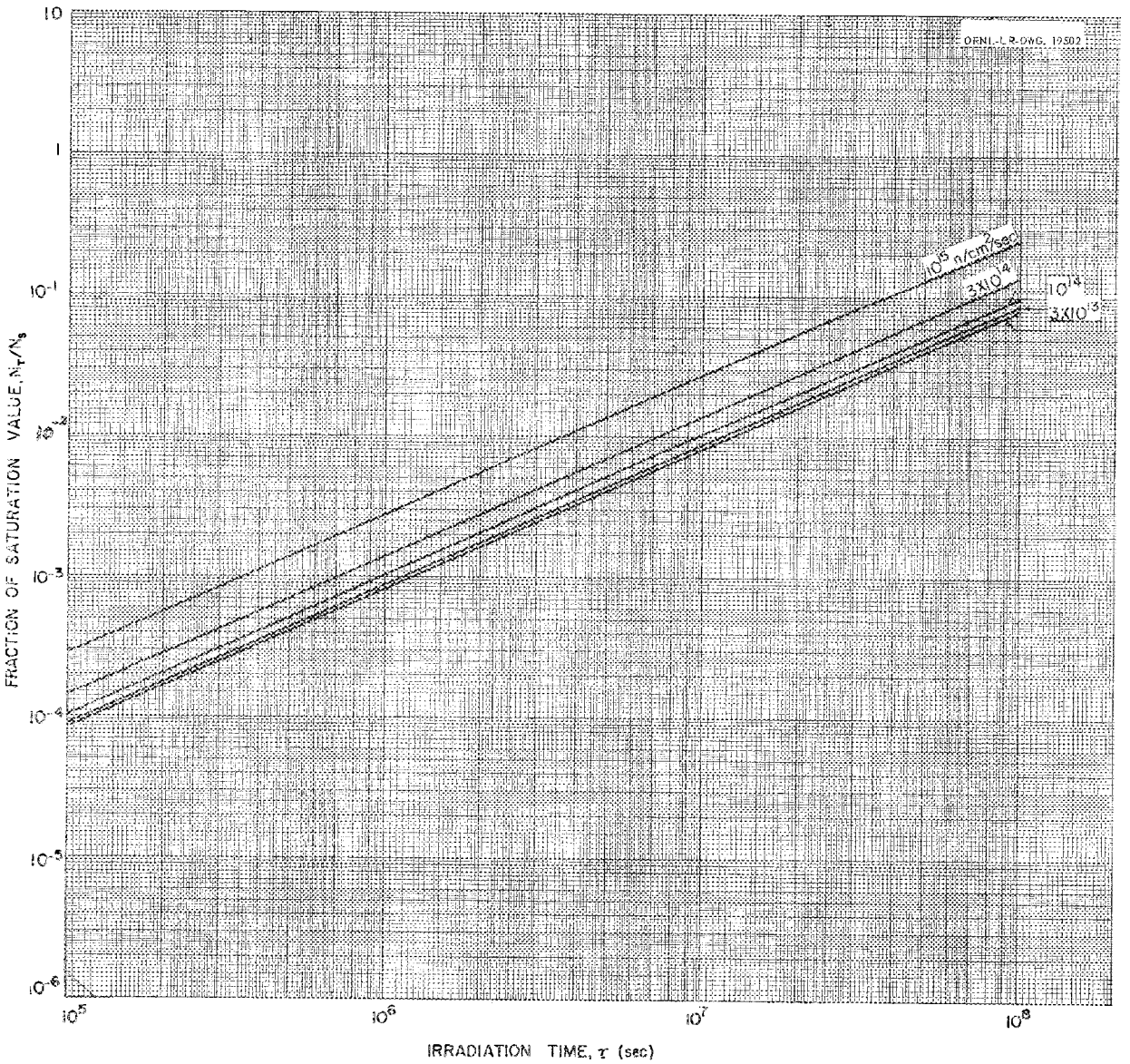

Fig. 4.19. Fraction of Saturation Value of 26.6y ^{137}Cs and 2.60m ^{137m}Ba as a Function of Irradiation Time and Flux. (From Blomeke and Todd, ref. 7, p. 111).

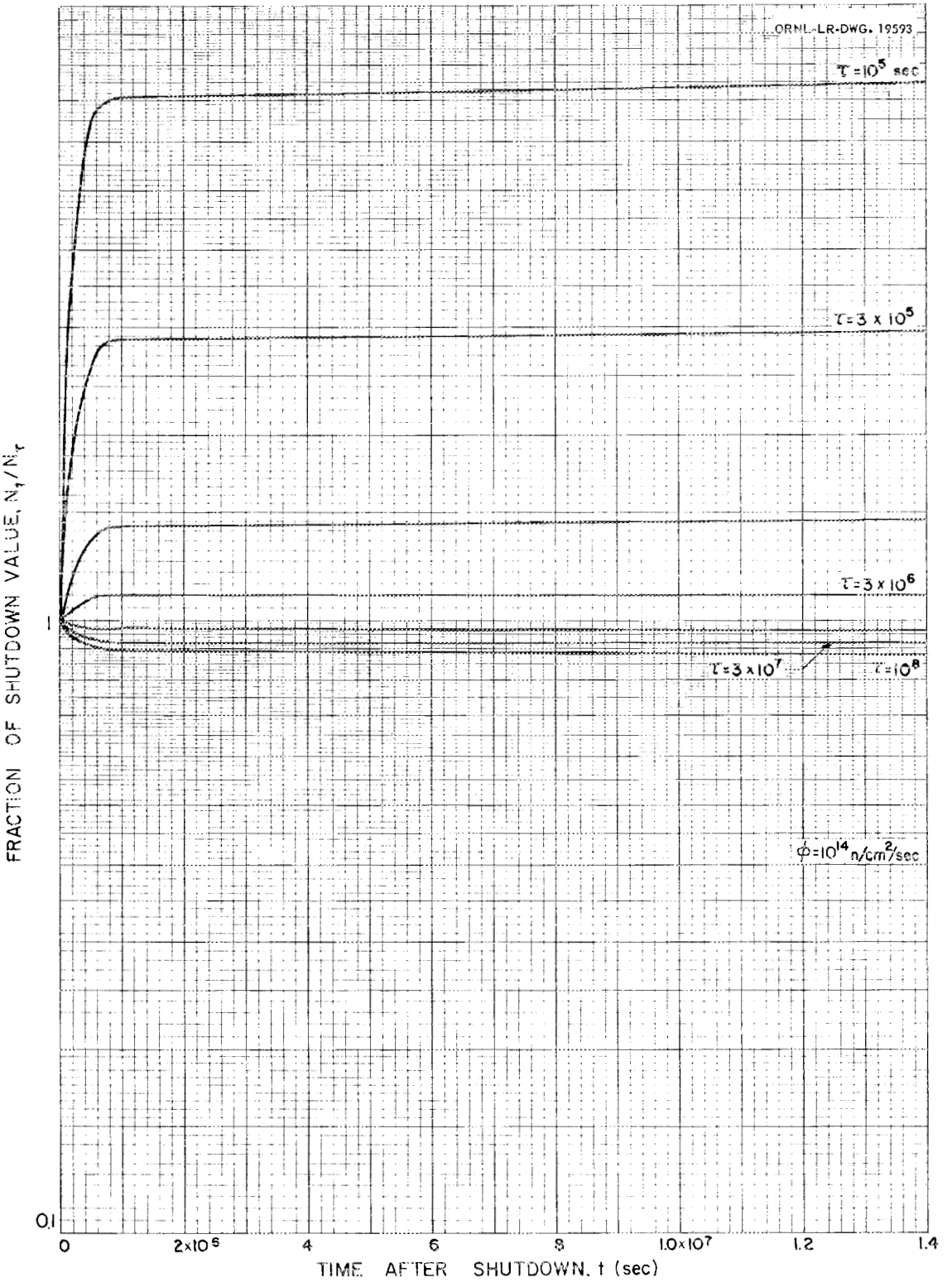

Fig. 4.20. Fraction of Shutdown Value of 64.5h ^{90}Y Remaining at Various Times After Shutdown. (From Blomeke and Todd, ref. 7, p. 202.)

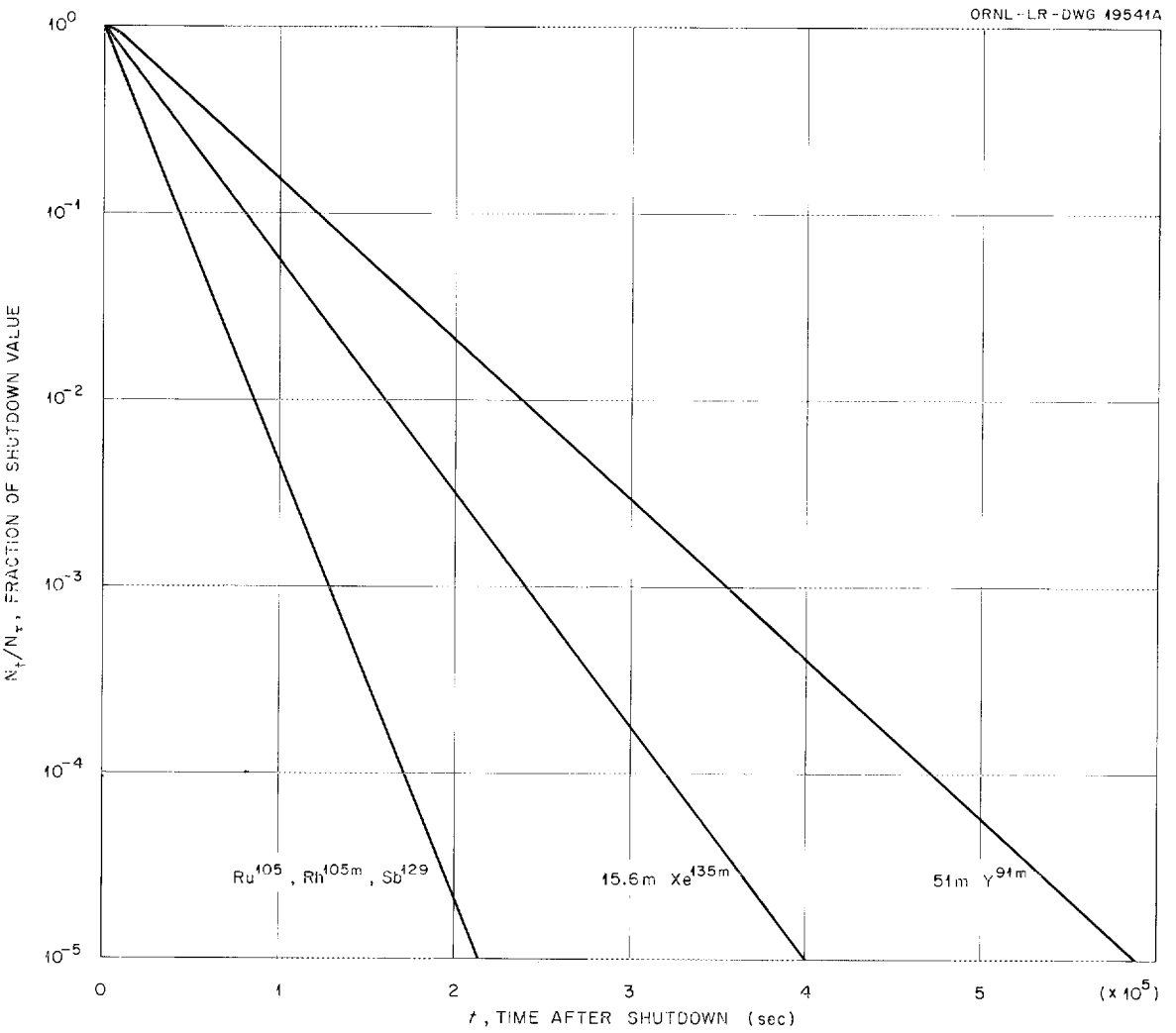

Fig. 4.21. Fraction of Shutdown Value of Radioactive Fission Products Remaining at Various Times After Shutdown. (From Blomeke and Todd, ref. 7, p. 150.)

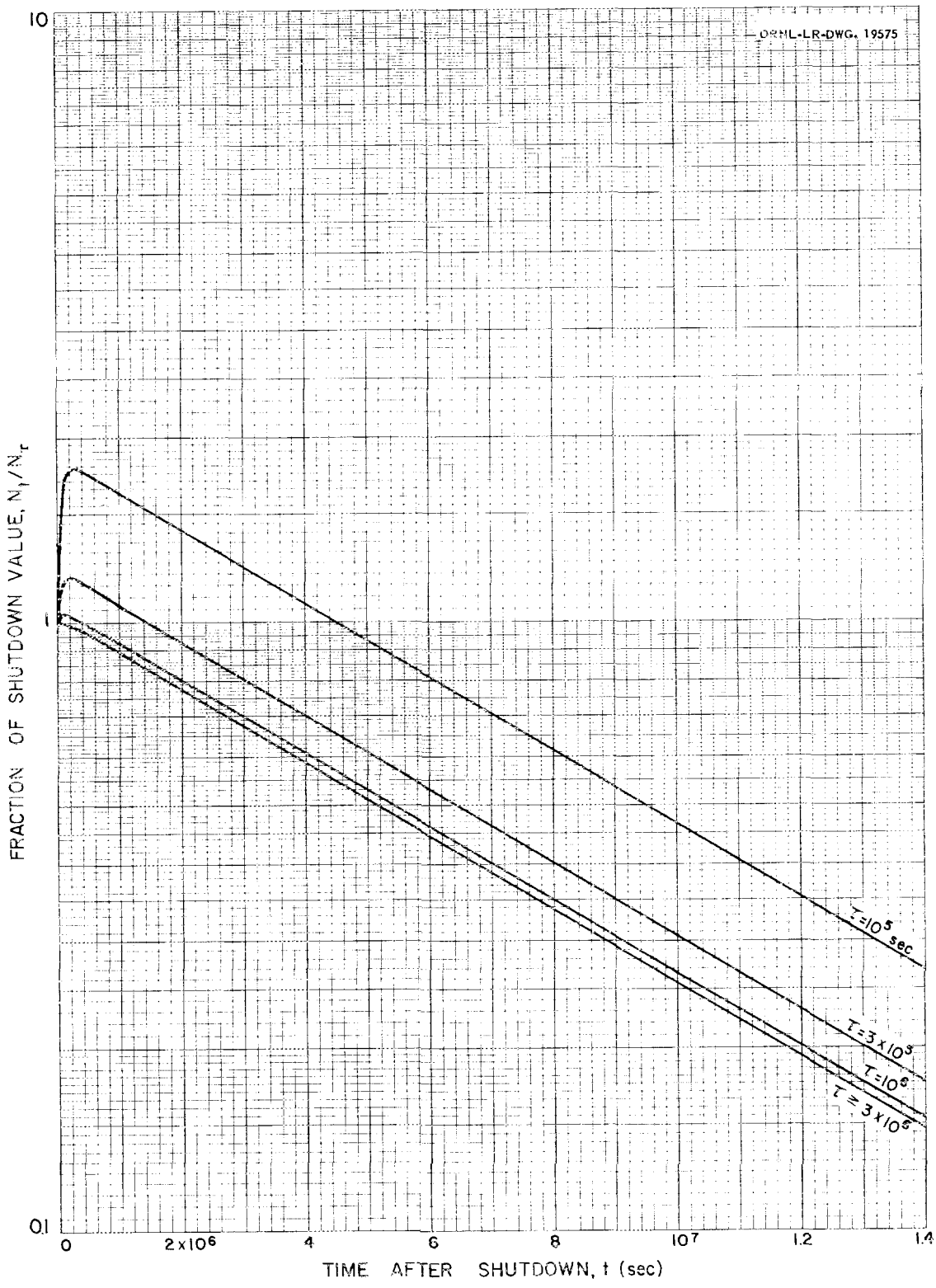

Fig. 4.22. Fraction of Shutdown Value of 58d ^{91}Y Remaining at Various Times After Shutdown. (From Blomeke and Todd, ref. 7, p. 184.)

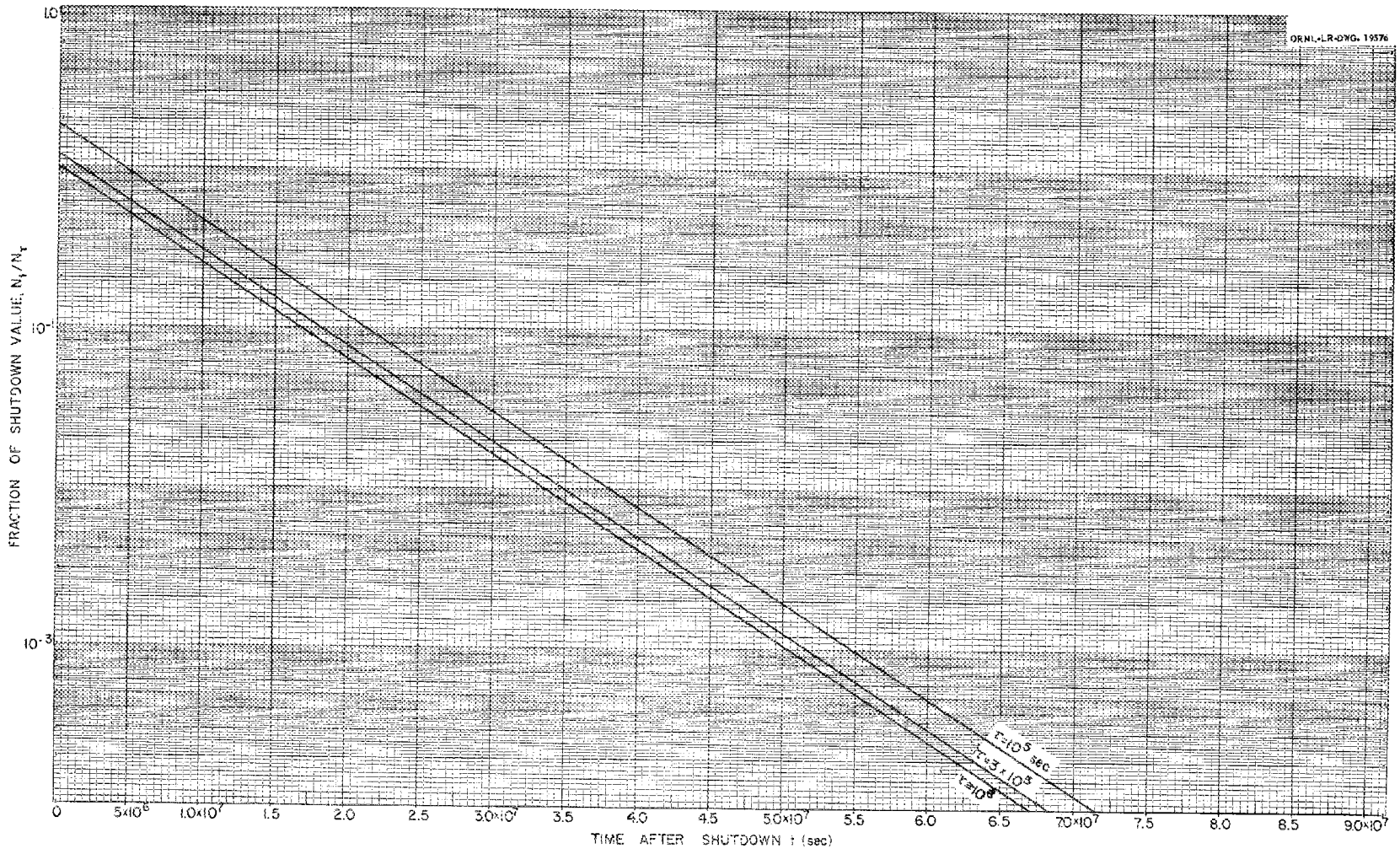

Fig. 4.23. Fraction of Shutdown Value of 58d ^{91}Y Remaining at Various Times After Shutdown. (From Blomeke and Todd, ref. 7, p. 185.)

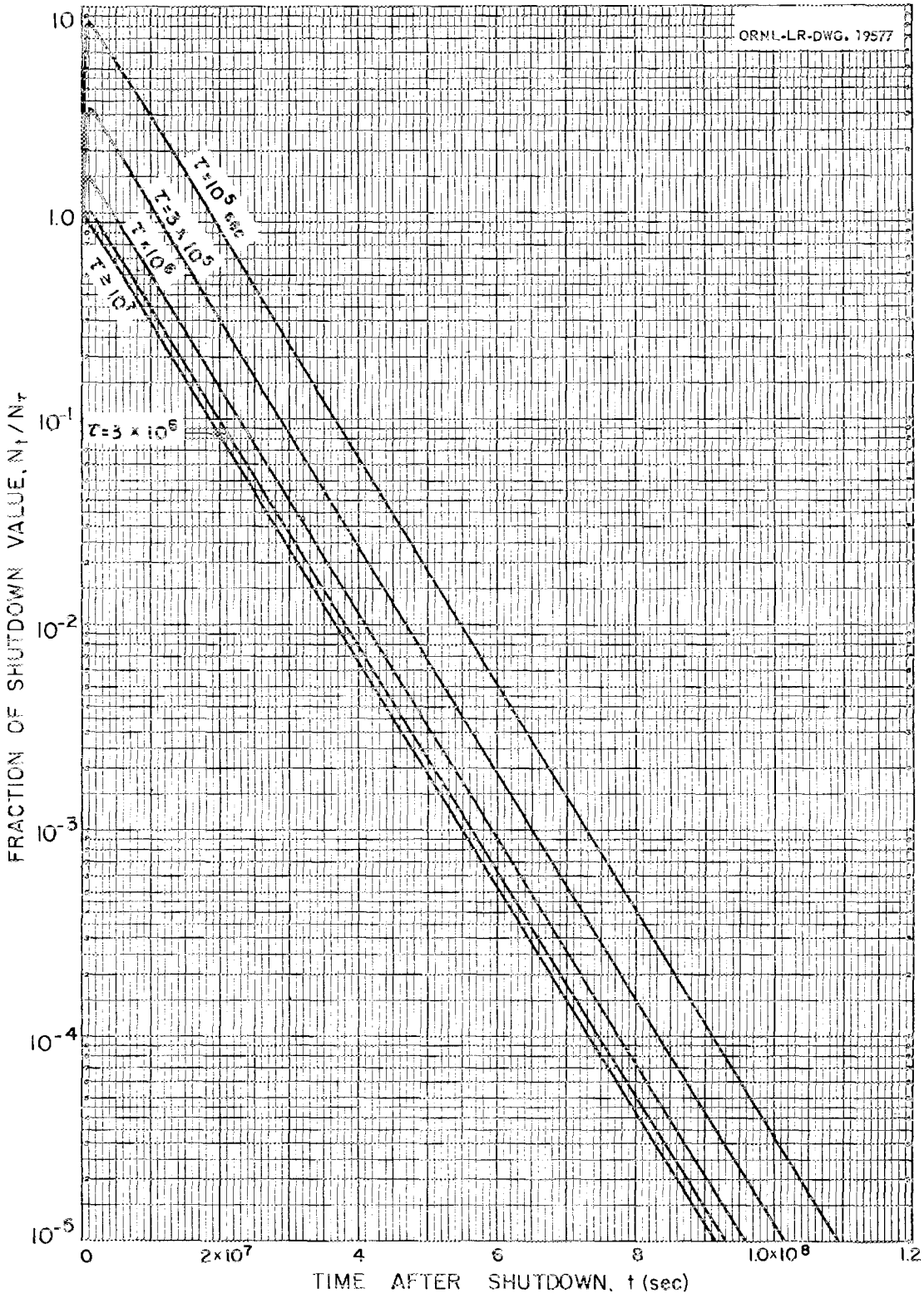

Fig. 4.24. Fraction of Shutdown Value of 90h ^{95m}Nb Remaining at Various Times After Shutdown. (From Blomeke and Todd, ref. 7, p. 186.)

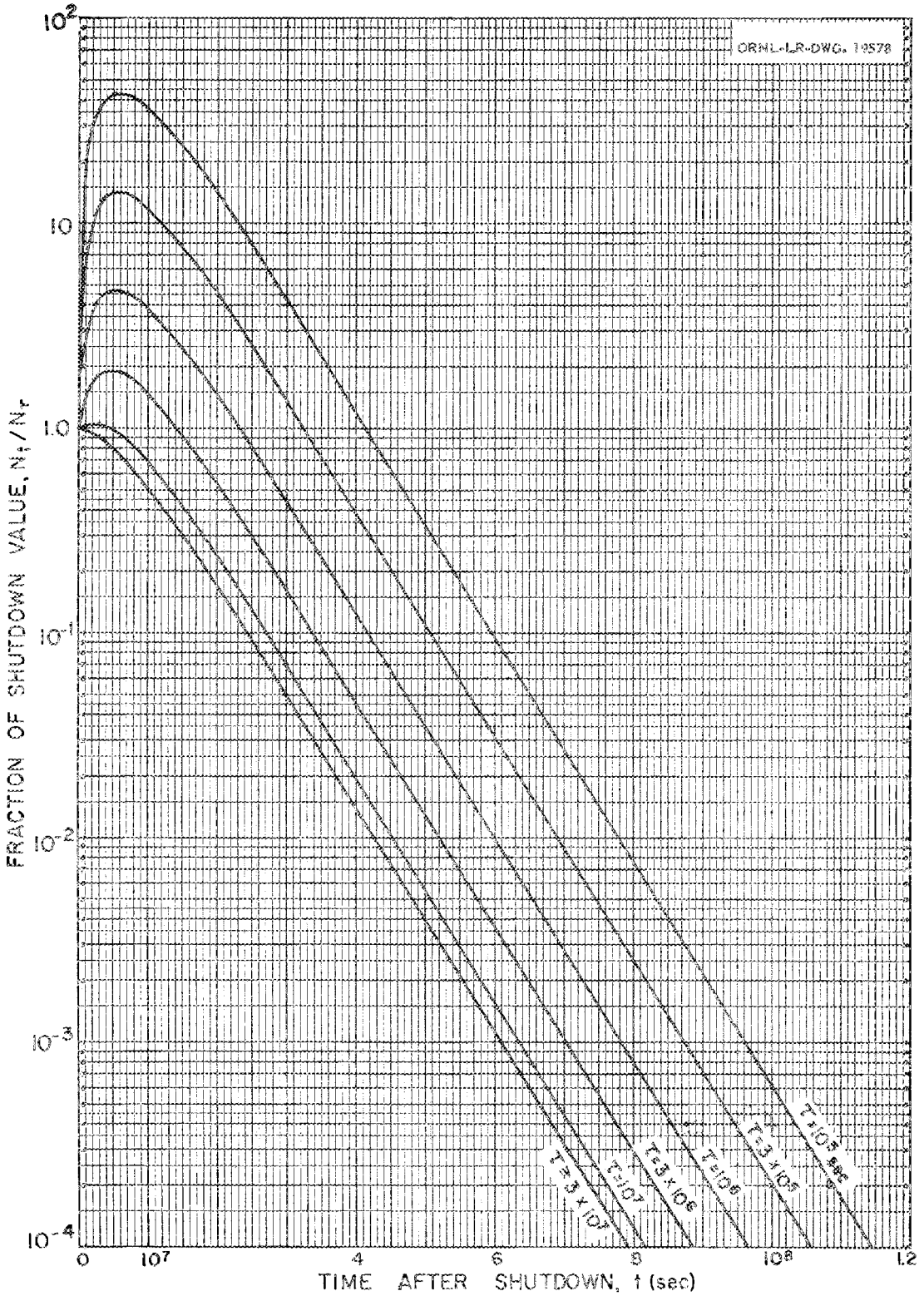

Fig. 4.25. Fraction of Shutdown Value of 35d ^{95}Nb Remaining at Various Times After Shutdown. (From Blomeke and Todd, ref. 7, p. 187.)

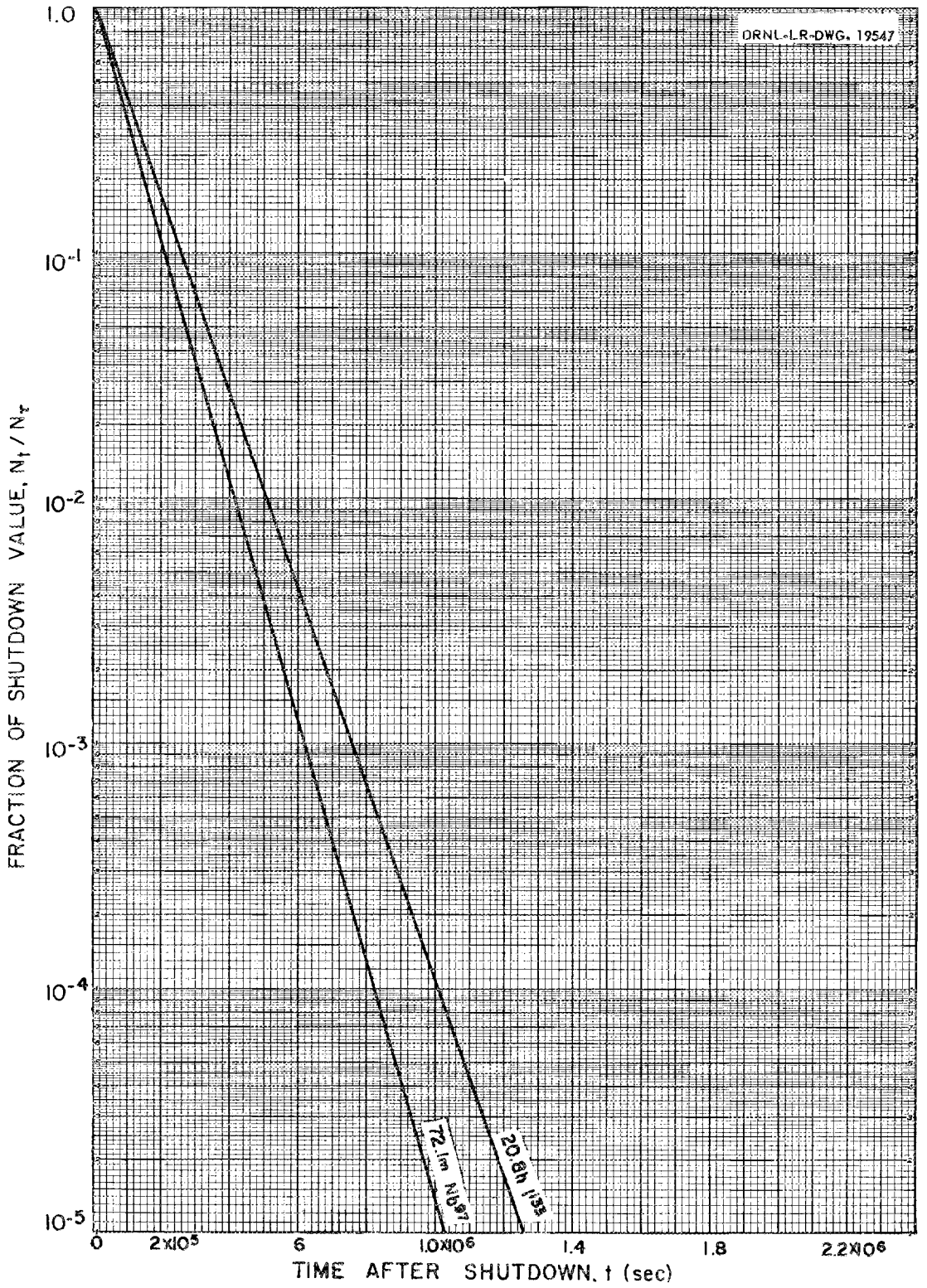

Fig. 4.26. Fraction of Shutdown Value of Radioactive Fission Products Remaining at Various Times After Shutdown. (From Blomeke and Todd, ref. 7, p. 156.)

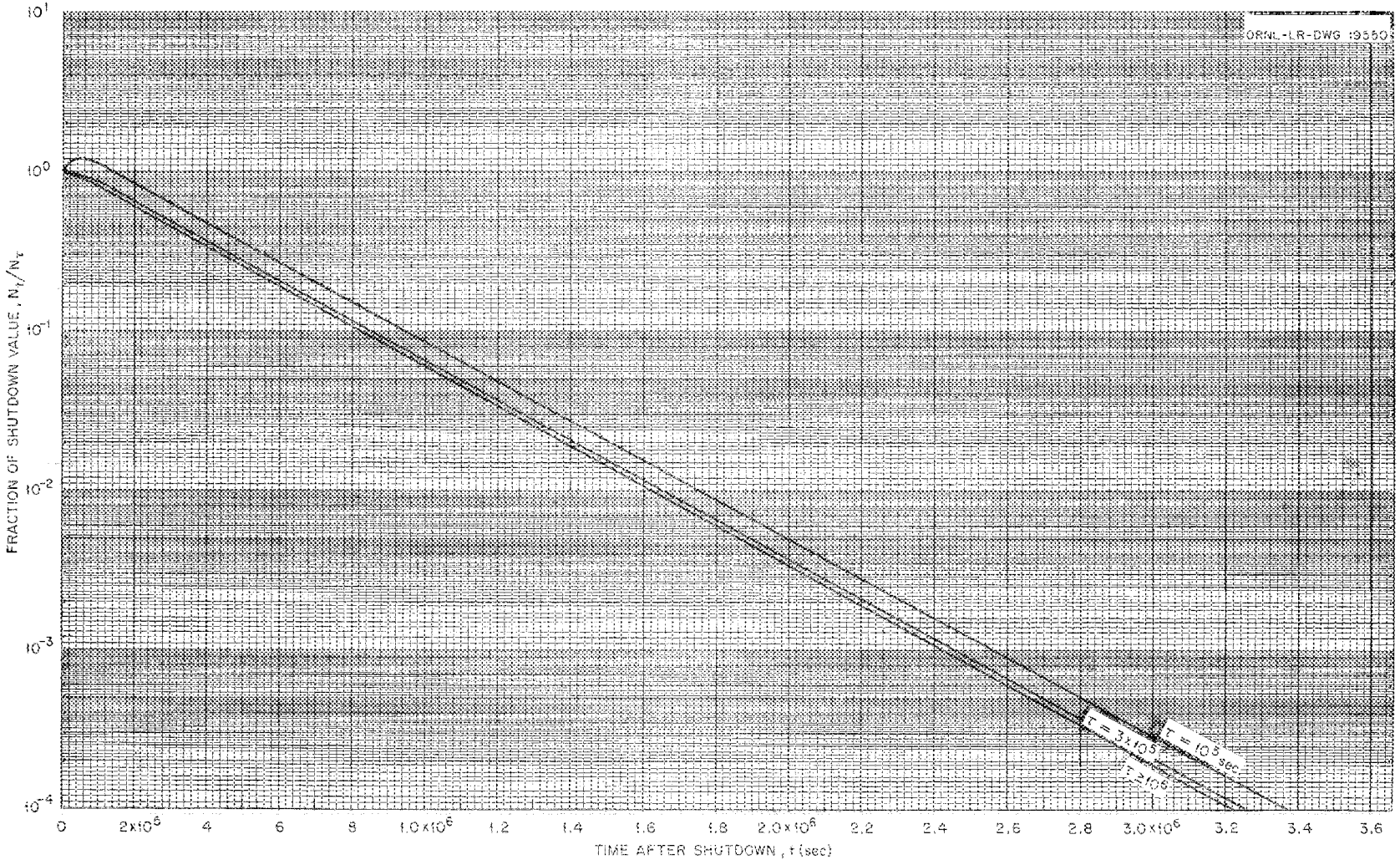

Fig. 4.27. Fraction of Shutdown Value of 6.04h ^{99m}Tc Remaining at Various Times After Shutdown. (From Blomeke and Todd, ref. 7, p. 159.)

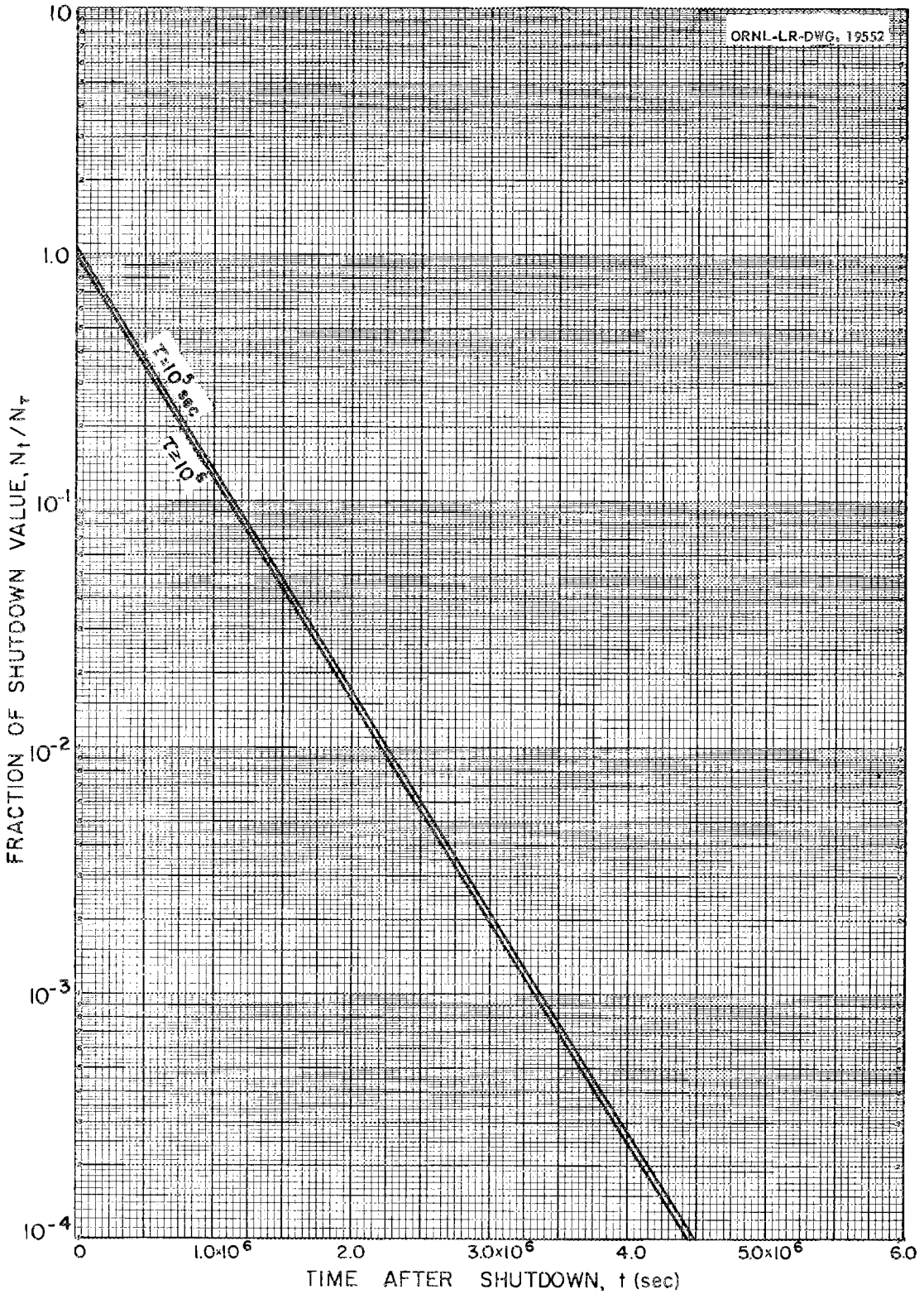

Fig. 4.28. Fraction of Shutdown Value of 93h ^{127}Sb Remaining at Various Times After Shutdown. (From Blomeke and Todd, ref. 7, p. 161.)

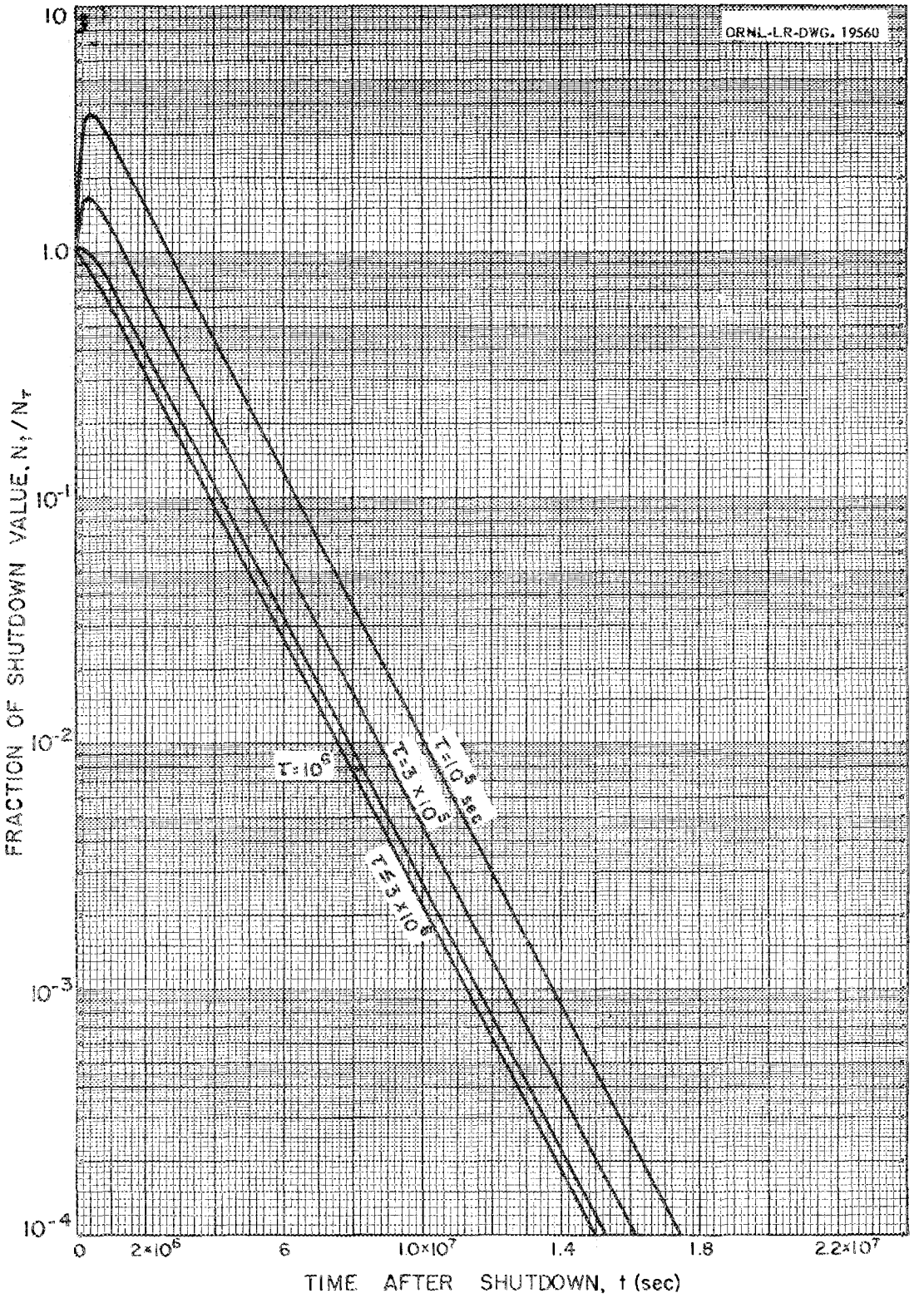

Fig. 4.29. Fraction of Shutdown Value of 40.2h ^{140}La Remaining at Various Times After Shutdown. (From Blomeke and Todd, ref. 7, p. 169.)

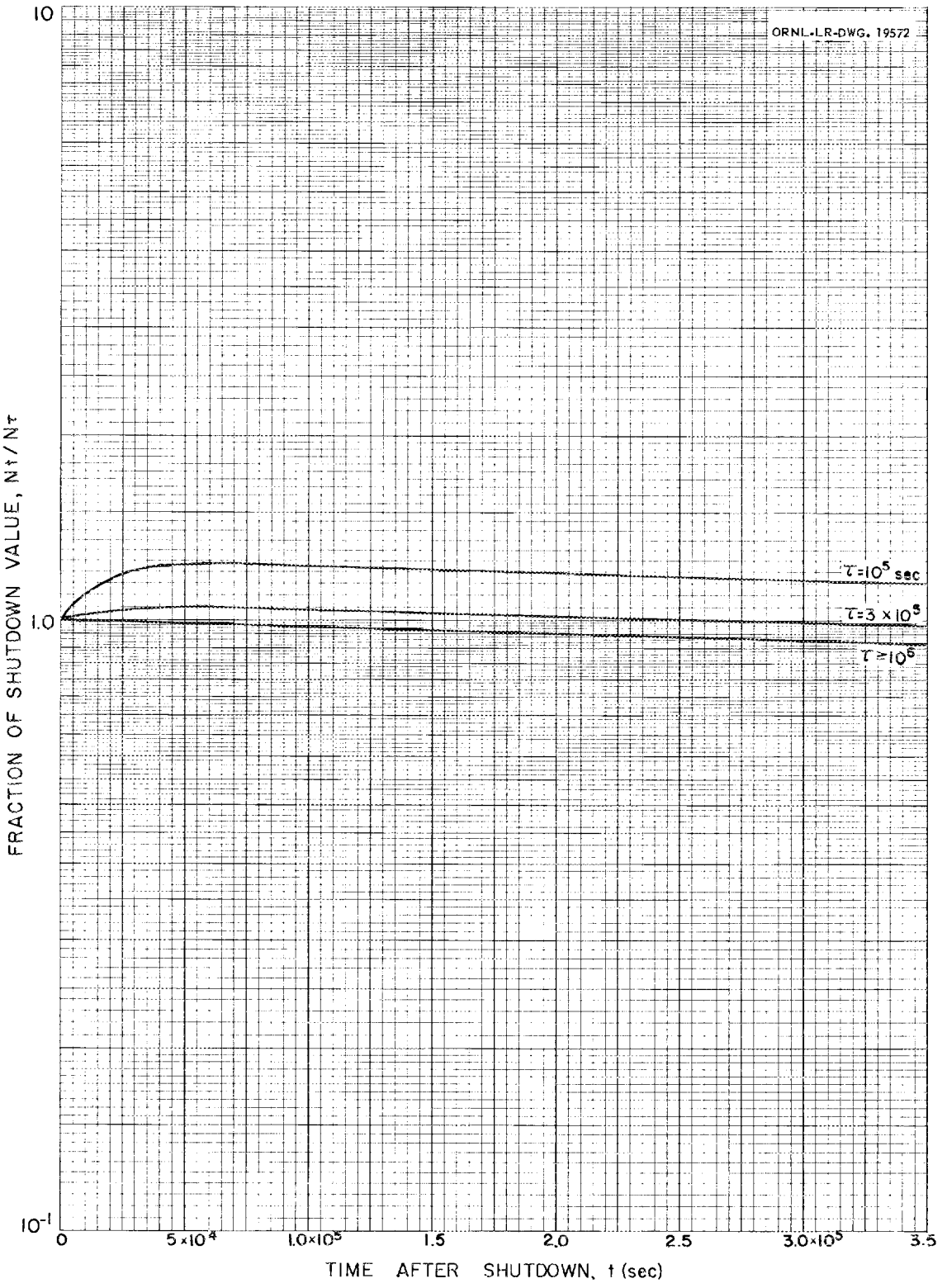

Fig. 4.30. Fraction of Shutdown Value of 32d ^{141}Ce Remaining at Various Times After Shutdown. (From Blomeke and Todd, ref. 7, p. 181.)

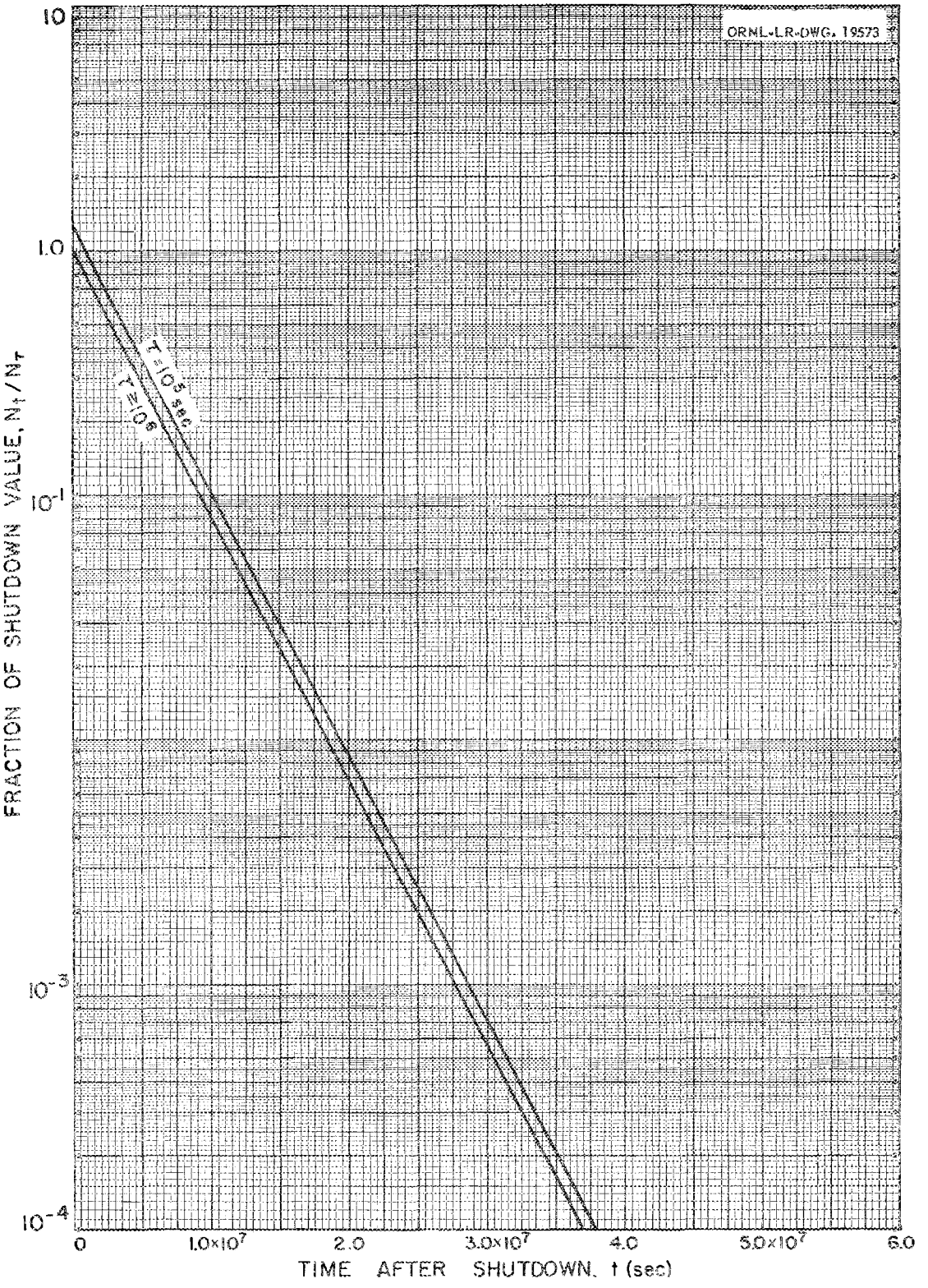

Fig. 4.31. Fraction of Shutdown Value of 32d ^{141}Ce Remaining at Various Times After Shutdown. (From Blomeke and Todd, ref. 7, p. 182.)

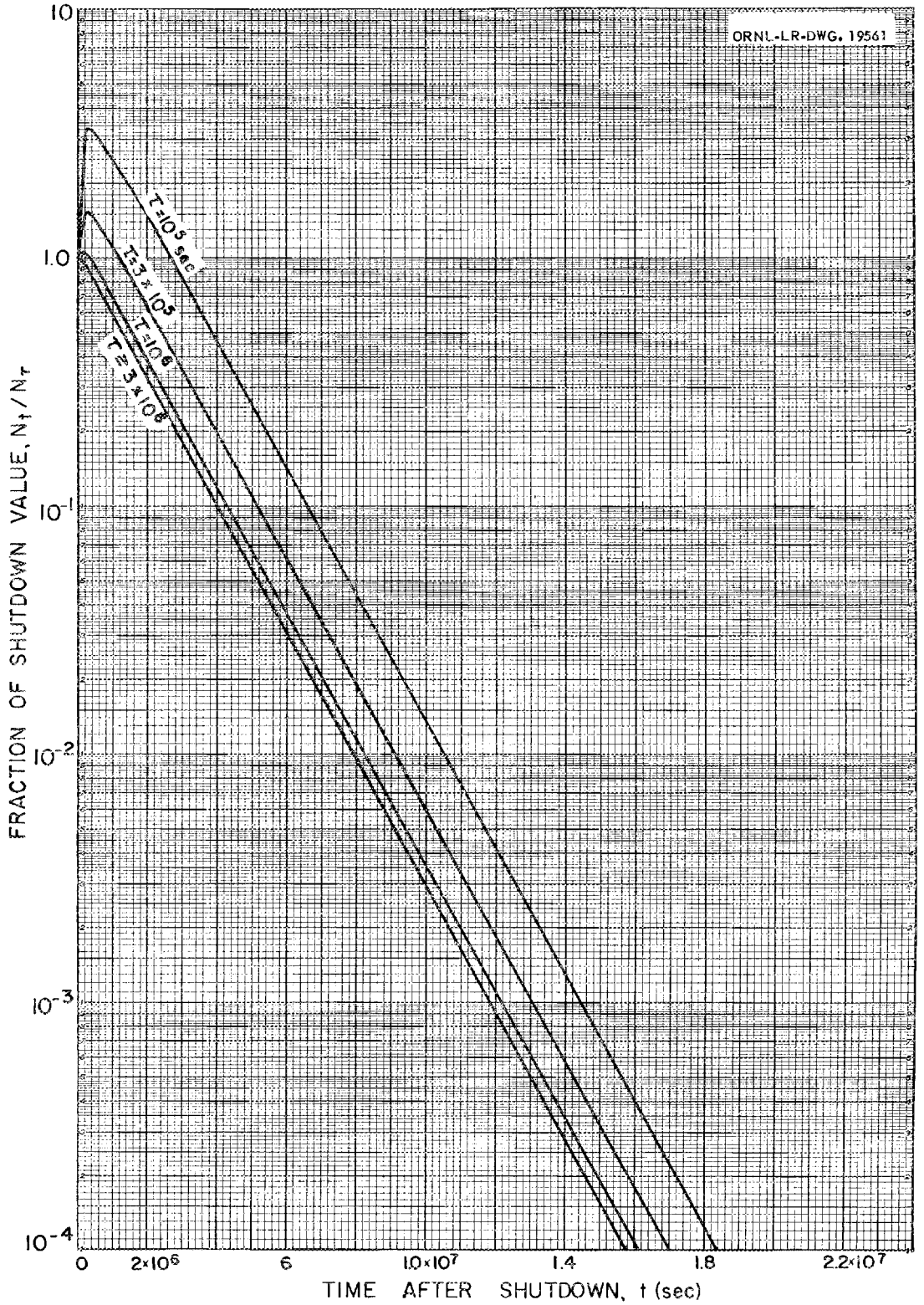

Fig. 4.32. Fraction of Shutdown Value of 13.7d ^{143}Pr Remaining at Various Times After Shutdown. (From Blomeke and Todd, ref. 7, p. 170.)

Fig. 4.33. Fraction of Shutdown Value of 2.6y ^{147}Pm at Various Times After Shutdown. (From Blomeke and Todd, ref. 7, p. 196.)

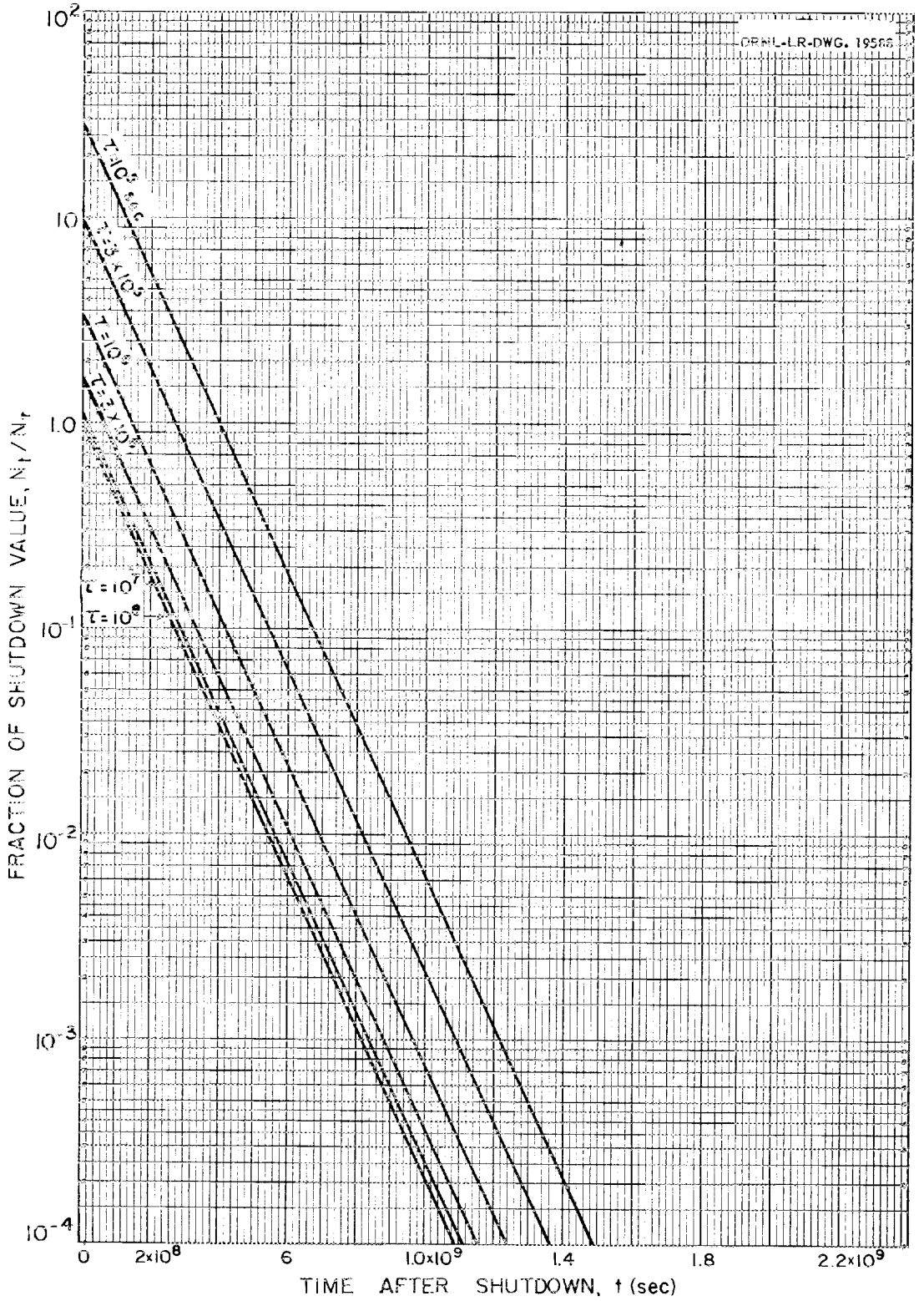

Fig. 4.34. Fraction of Shutdown Value of 2.6y ^{147}Pm Remaining at Various Times After Shutdown. (From Blomeke and Todd, ref. 7, p. 197.)

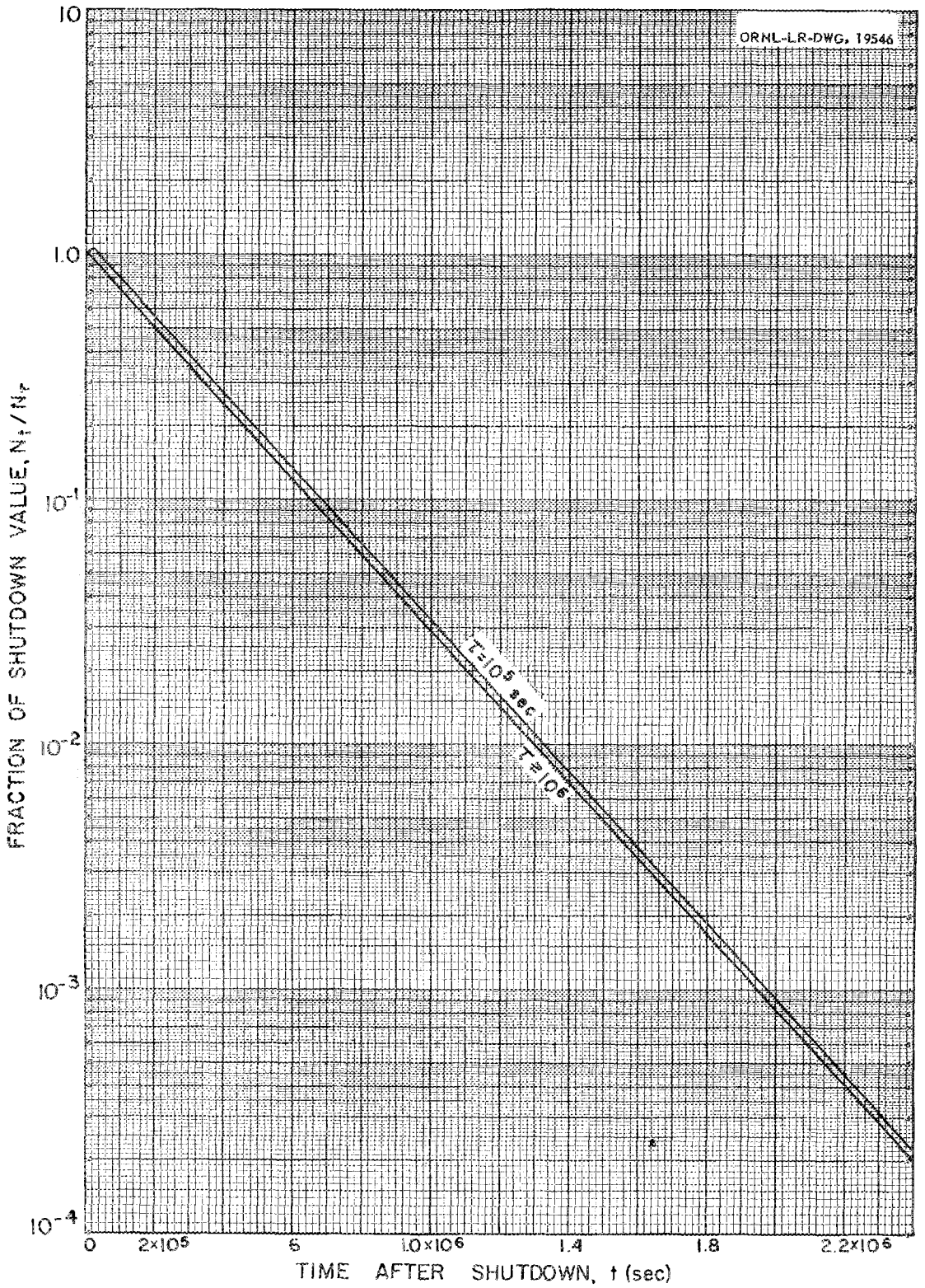

Fig. 4.35. Fraction of Shutdown Value of 54h ^{149}Pm Remaining at Various Times After Shutdown. (From Blomeke and Todd, ref. 7, p. 155.)

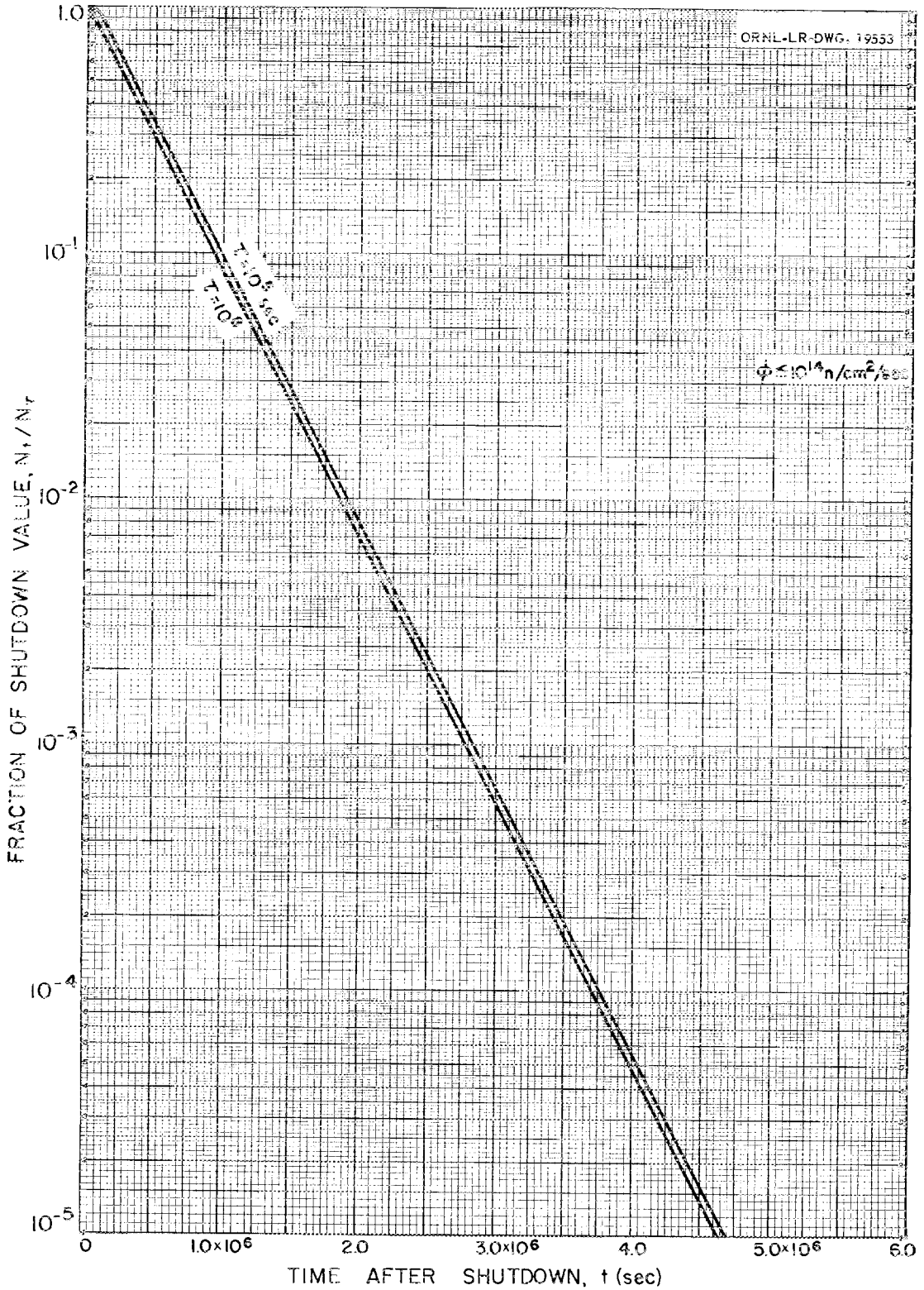

Fig. 4.36. Fraction of Shutdown Value of 2.4h ^{132}I Remaining at Various Times After Shutdown. (From Blomeke and Todd, ref. 7, p. 162.)

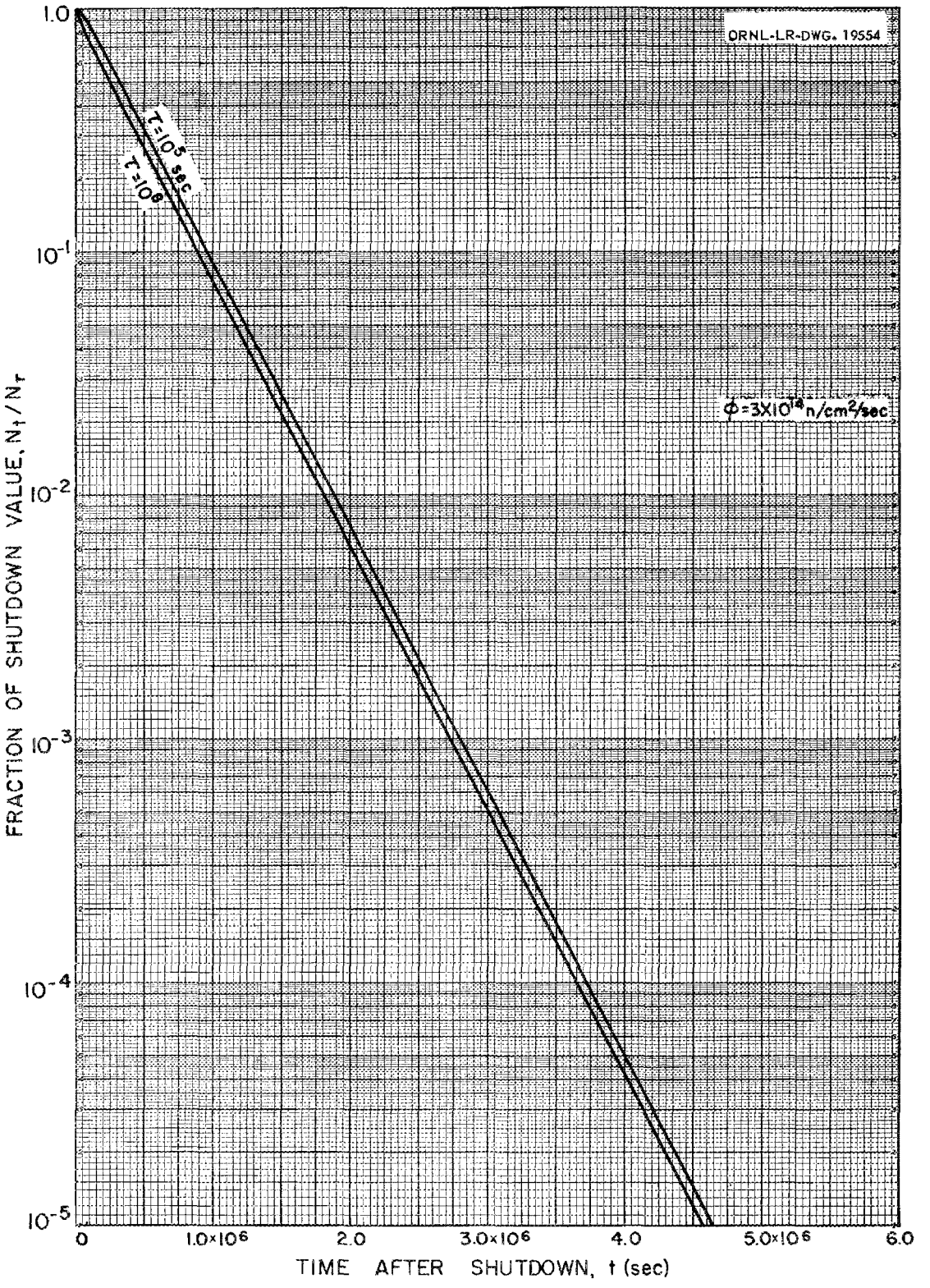

Fig. 4.37. Fraction of Shutdown Value of 2.4h ^{132}I Remaining at Various Times After Shutdown. (From Blomeke and Todd, ref. 7, p. 163.)

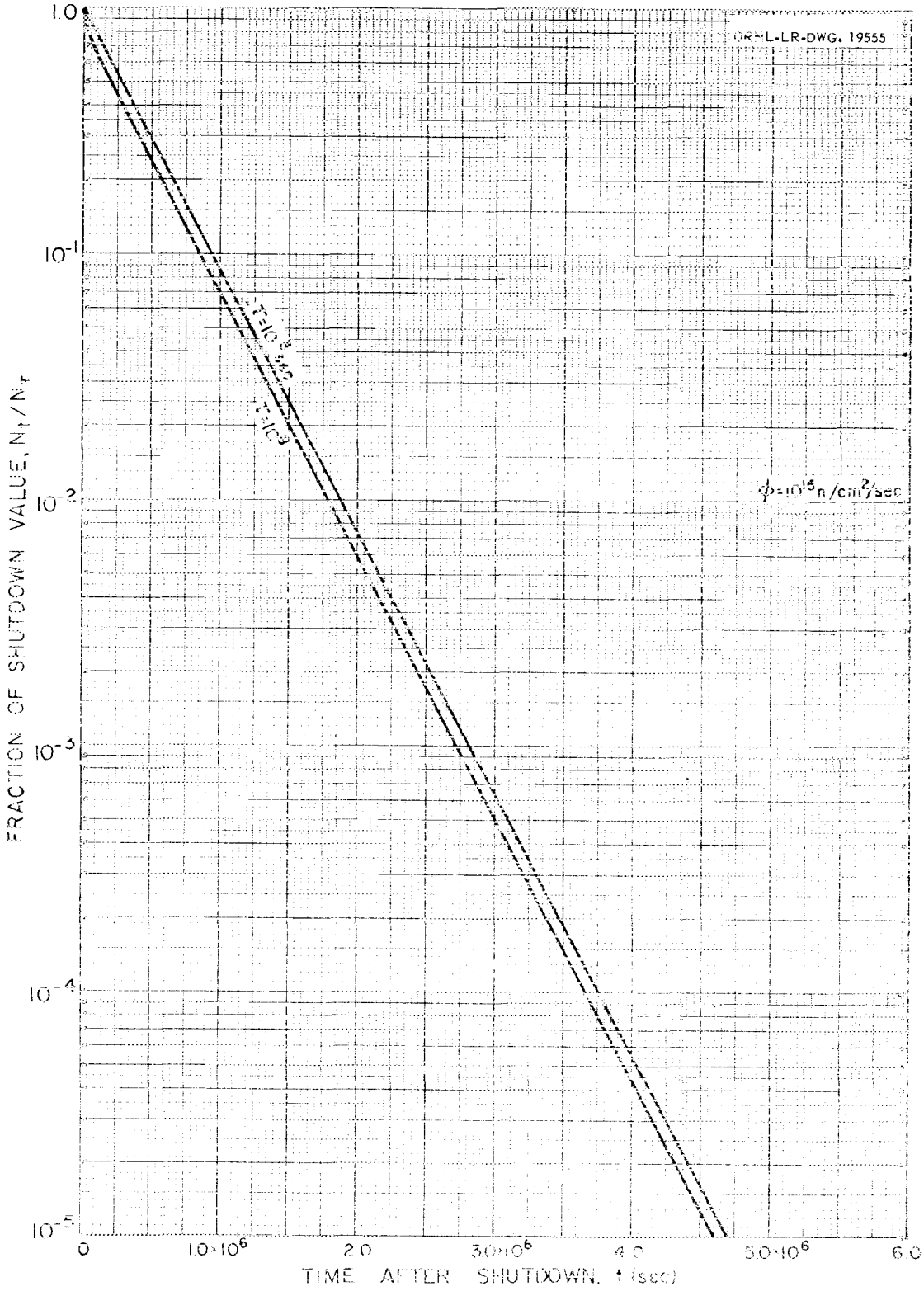

Fig. 4.38. Fraction of Shutdown Value of 2.4×10^{13} I Remaining at Various Times After Shutdown. (From Blomeke and Todd, ref. 7, p. 164.)

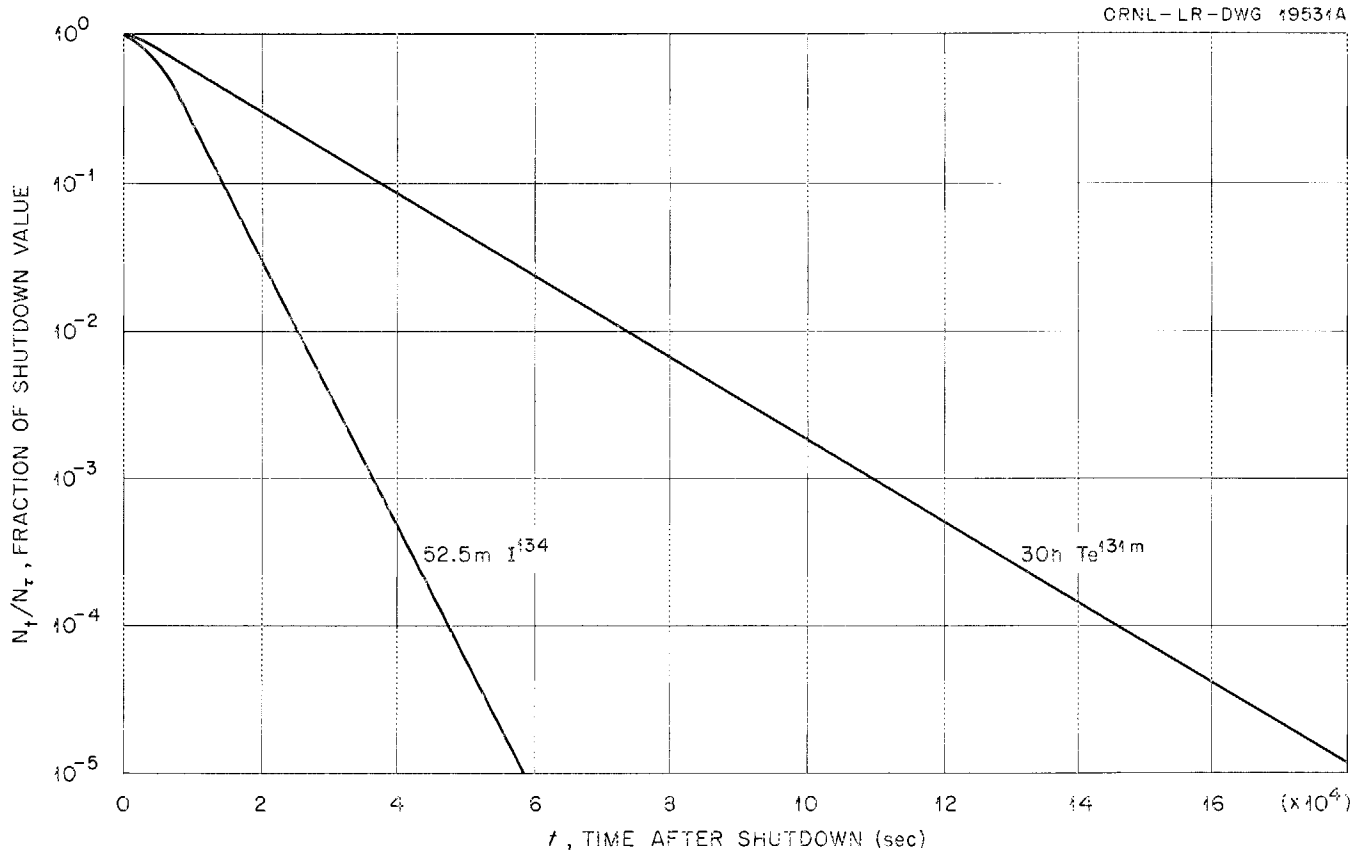

Fig. 4.39. Fraction of Shutdown Value of Radioactive Fission Products Remaining at Various Times After Shutdown. (From Blomeke and Todd, ref. 7, p. 140.)

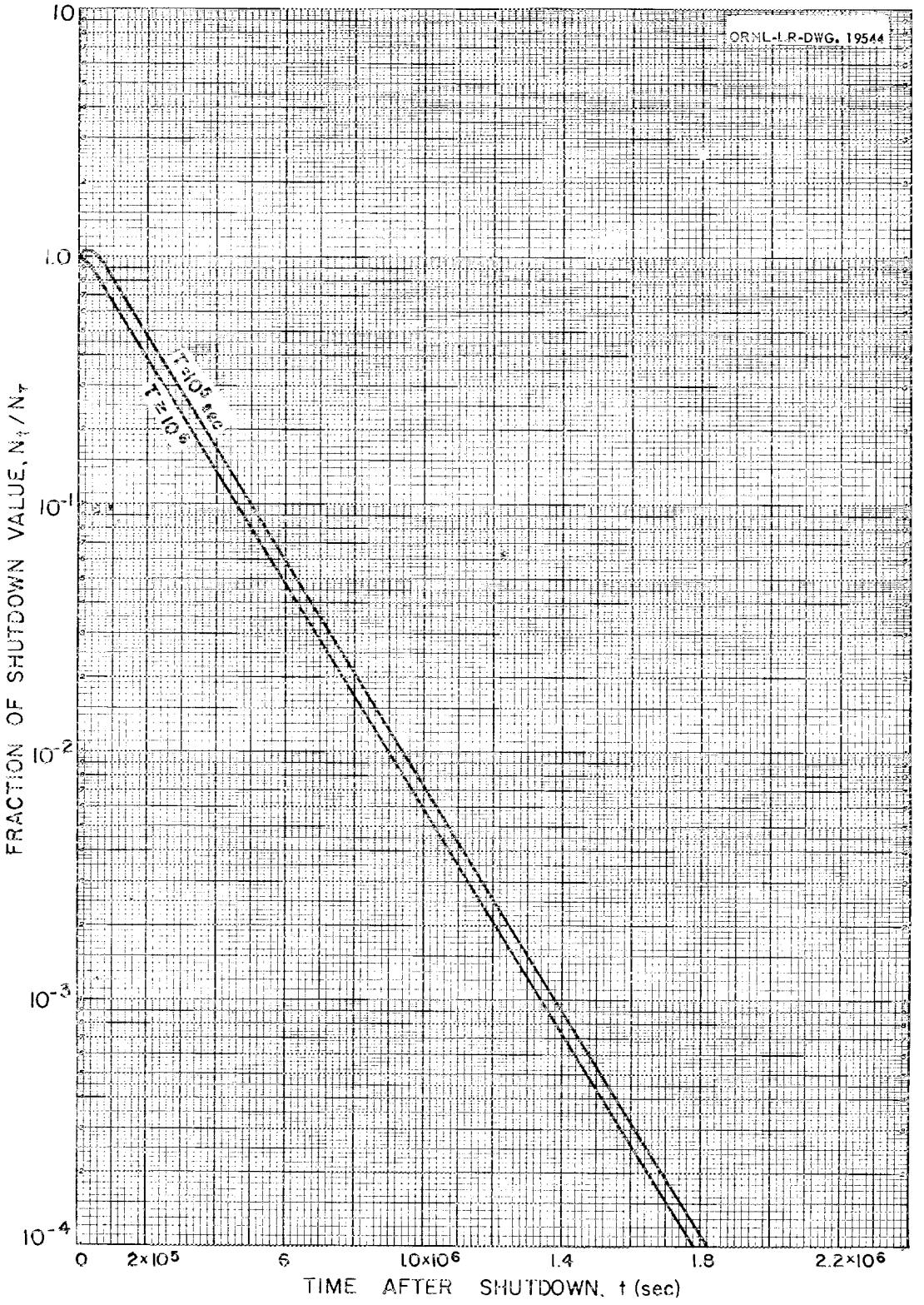

Fig. 4.40. Fraction of Shutdown Value of 36.5h ^{105}Rh Remaining at Various Times After Shutdown. (From Blomeke and Todd, ref. 7, p. 153.)

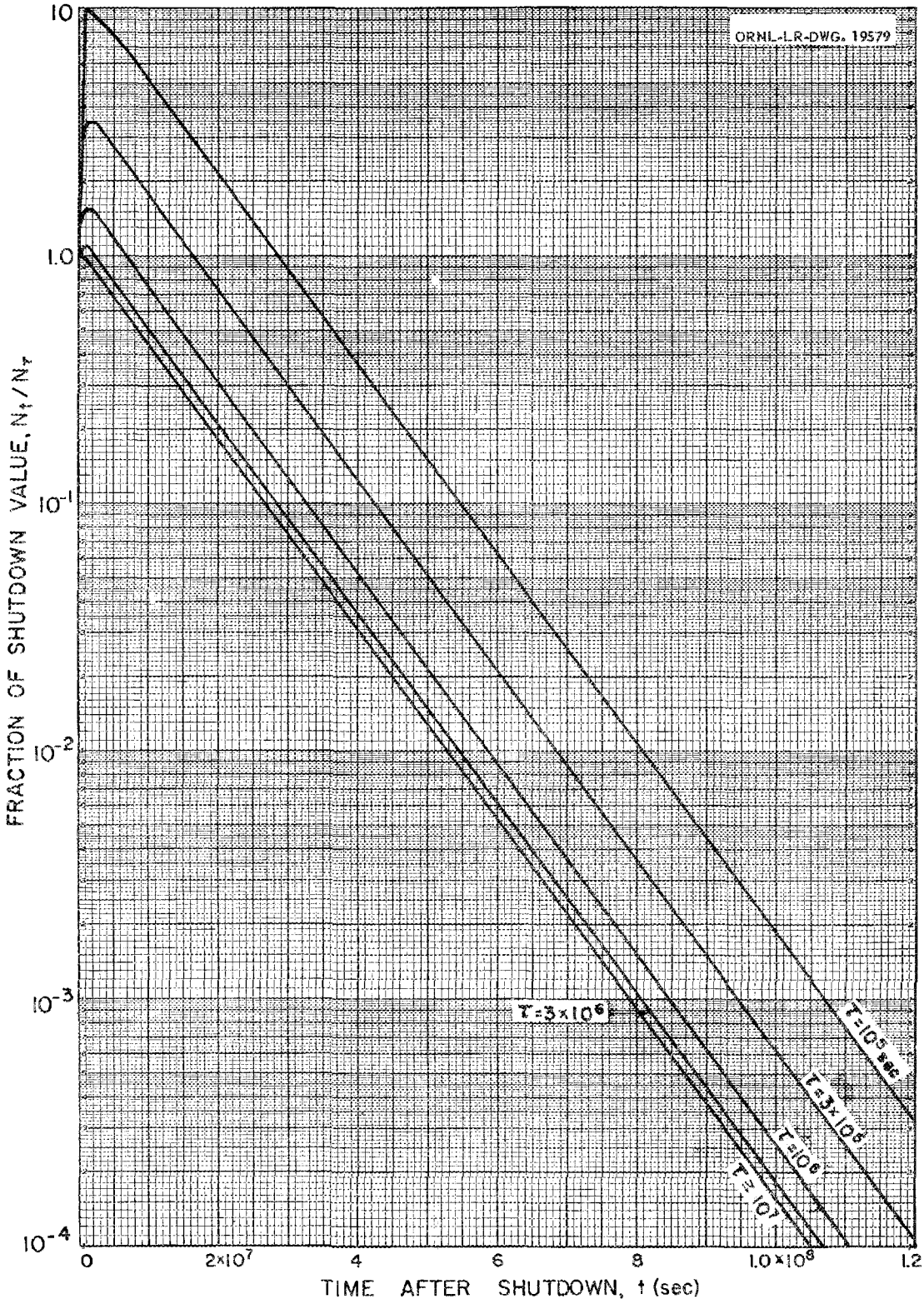

Fig. 4.41. Fraction of Shutdown Value of 90d ^{127m}Te Remaining at Various Times After Shutdown. (From Blomeke and Todd, ref. 7, p. 188.)

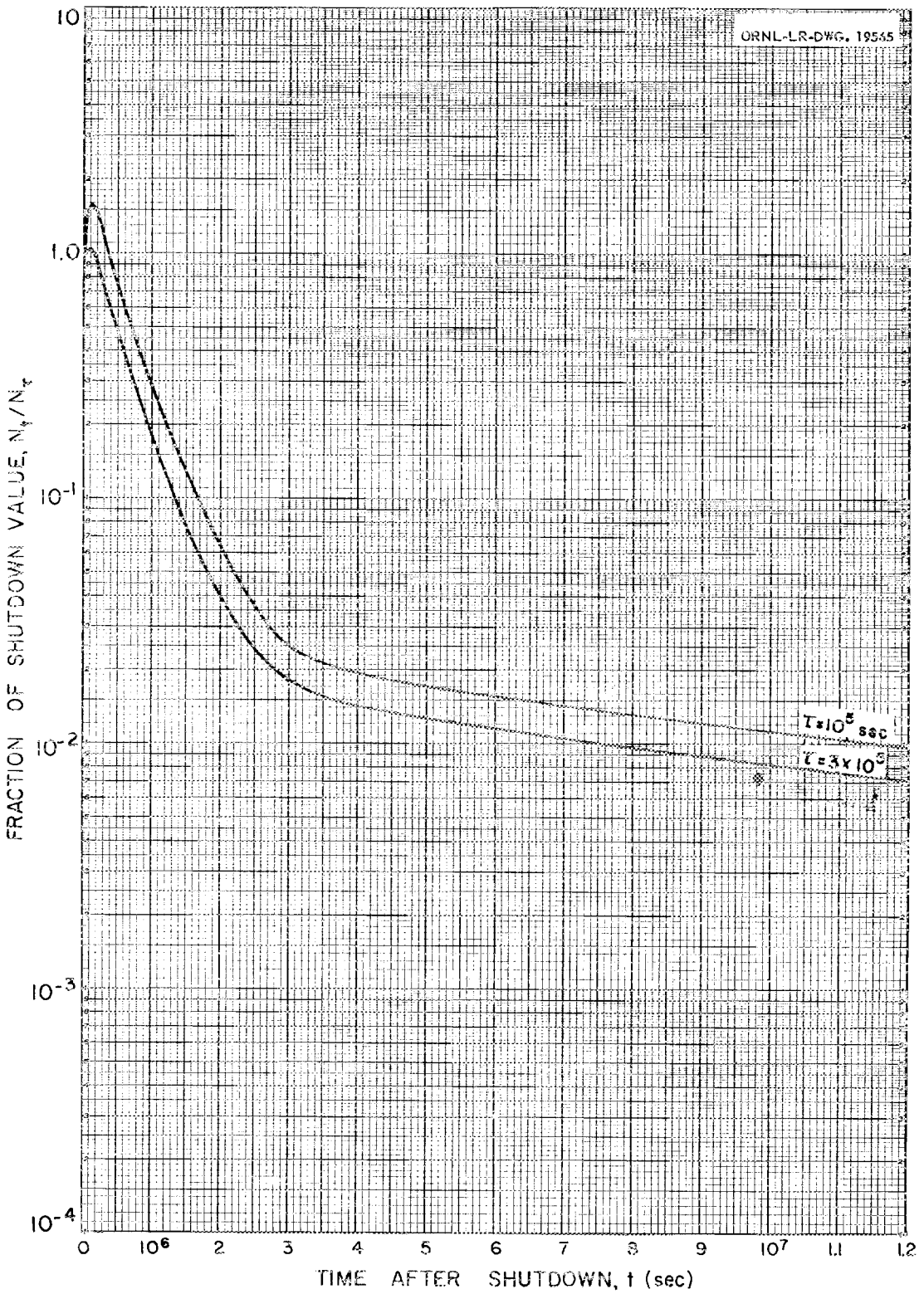

Fig. 4.42. Fraction of Shutdown Value of 9.3h ^{127}Te Remaining at Various Times After Shutdown. (From Blomeke and Todd, ref. 7, p. 174.)

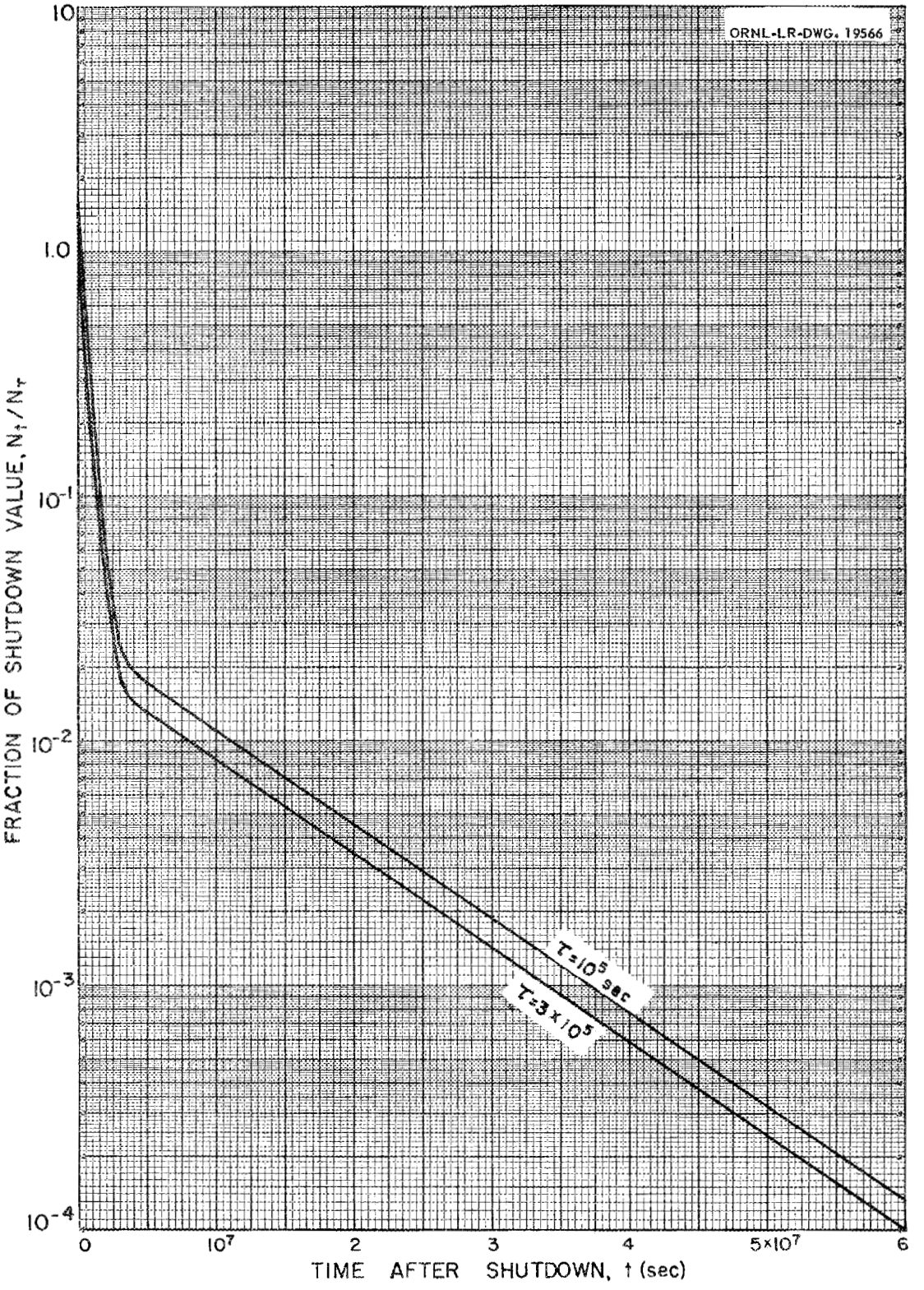

Fig. 4.43. Fraction of Shutdown Value of 9.3h ^{127}Te Remaining at Various Times After Shutdown. (From Blomeke and Todd, ref. 7, p. 175.)

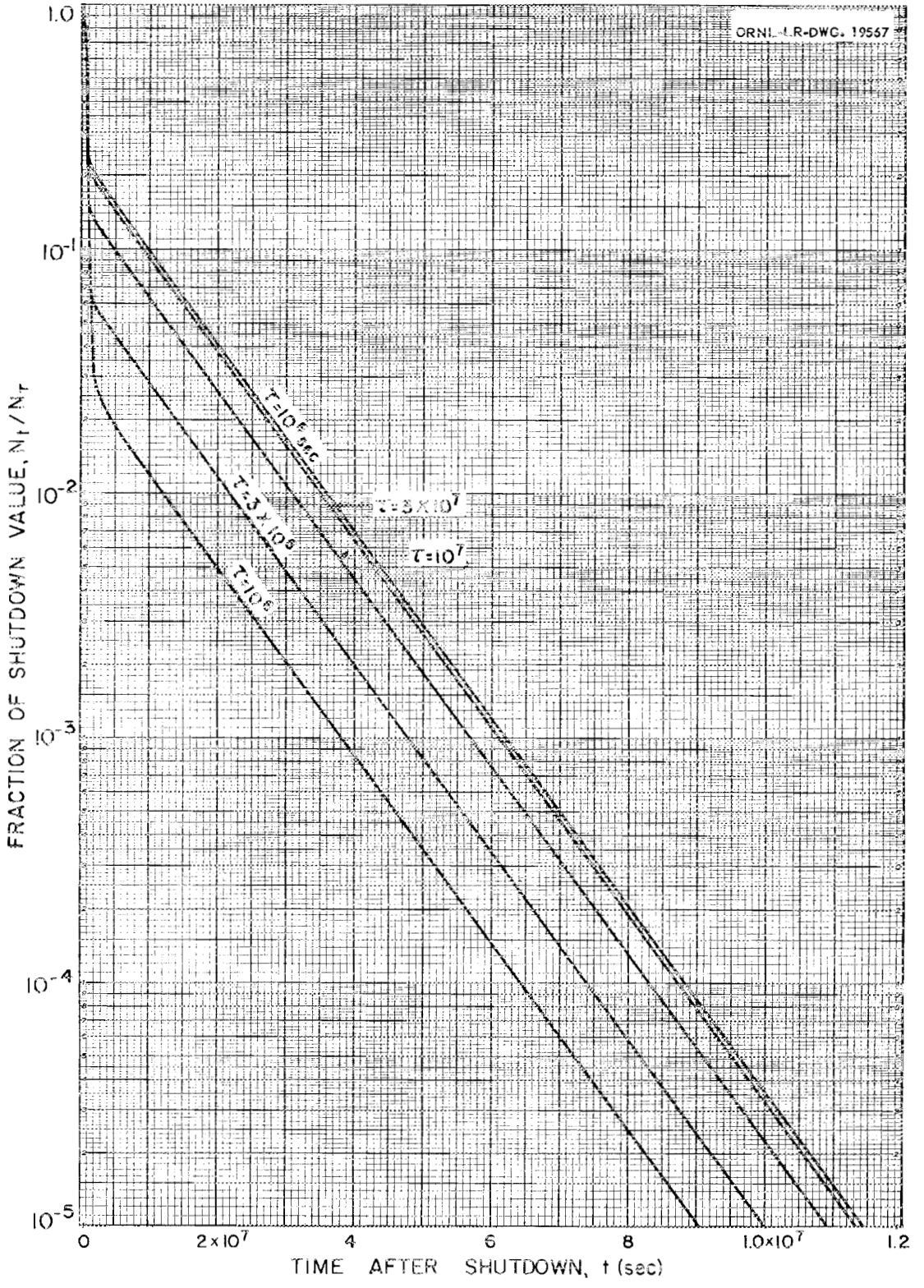

Fig. 4.44. Fraction of Shutdown Value of 9.3h ^{127}Te Remaining at Various Times After Shutdown. (From Blomeke and Todd, ref. 7, p. 176.)

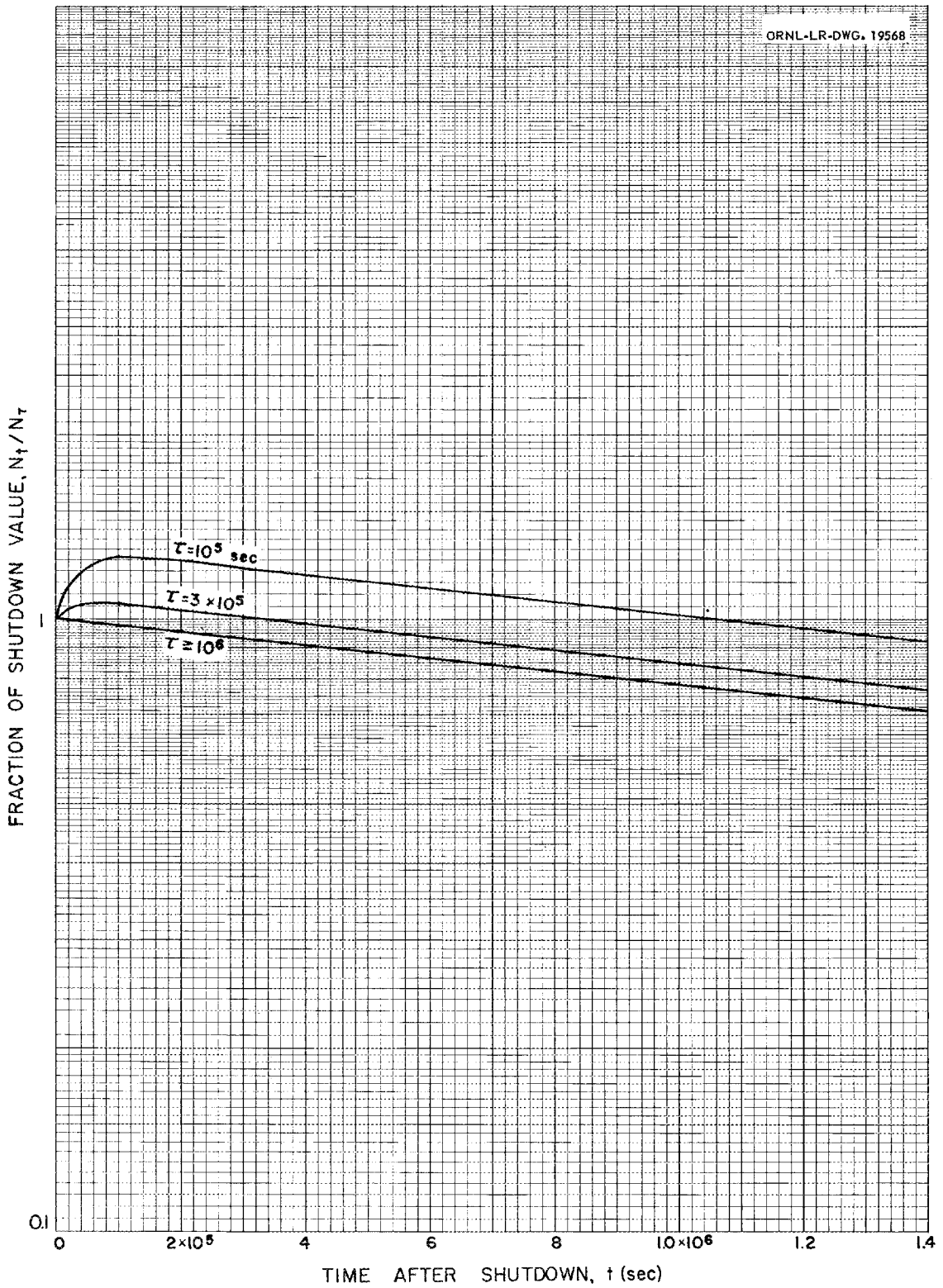

Fig. 4.45. Fraction of Shutdown Value of 33d ^{129m}Te Remaining at Various Times After Shutdown. (From Blomeke and Todd, ref. 7, p. 177.)

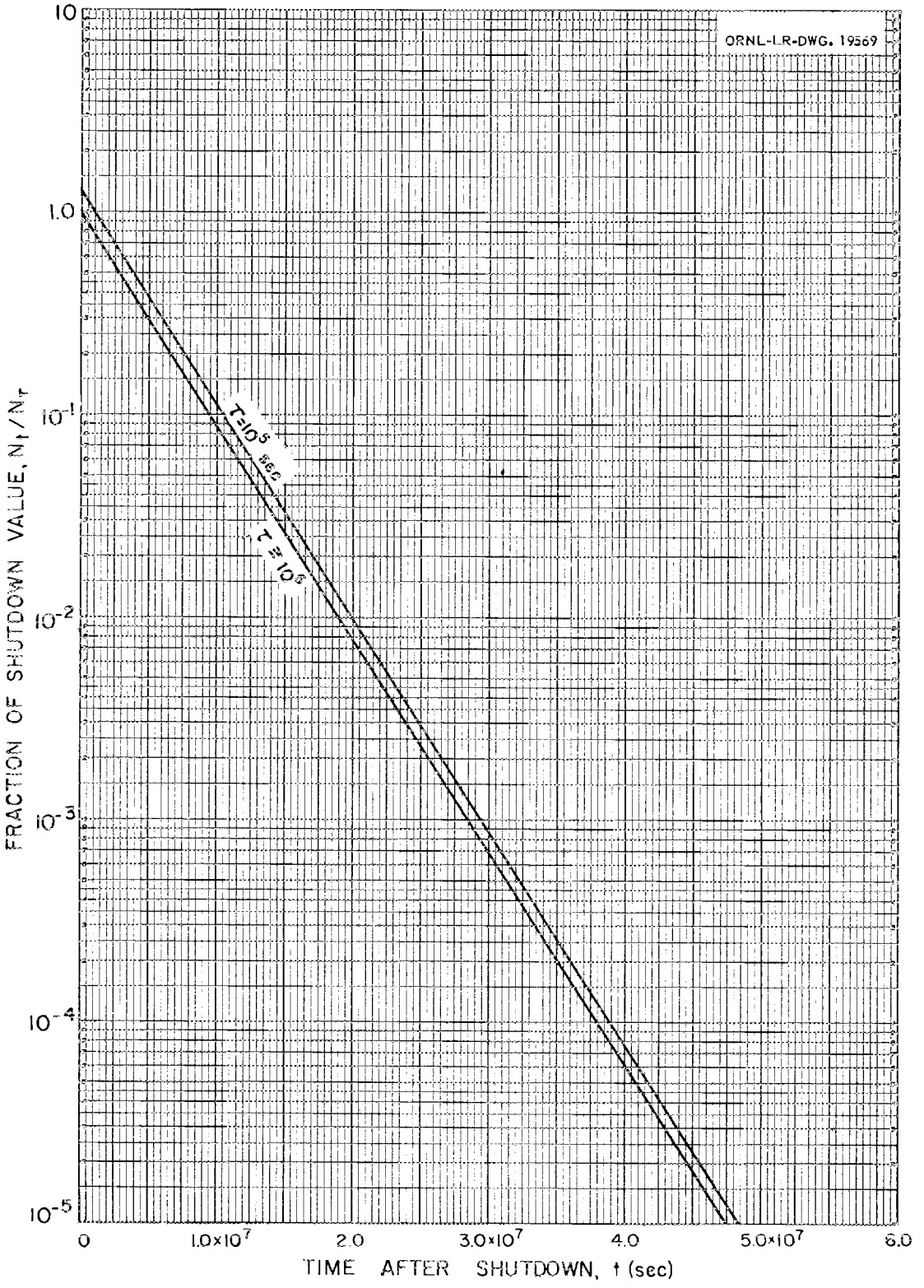

Fig. 4.46. Fraction of Shutdown Value of 33d ^{129m}Te Remaining at Various Times After Shutdown. (From Blomeke and Todd, ref. 7, p. 178.)

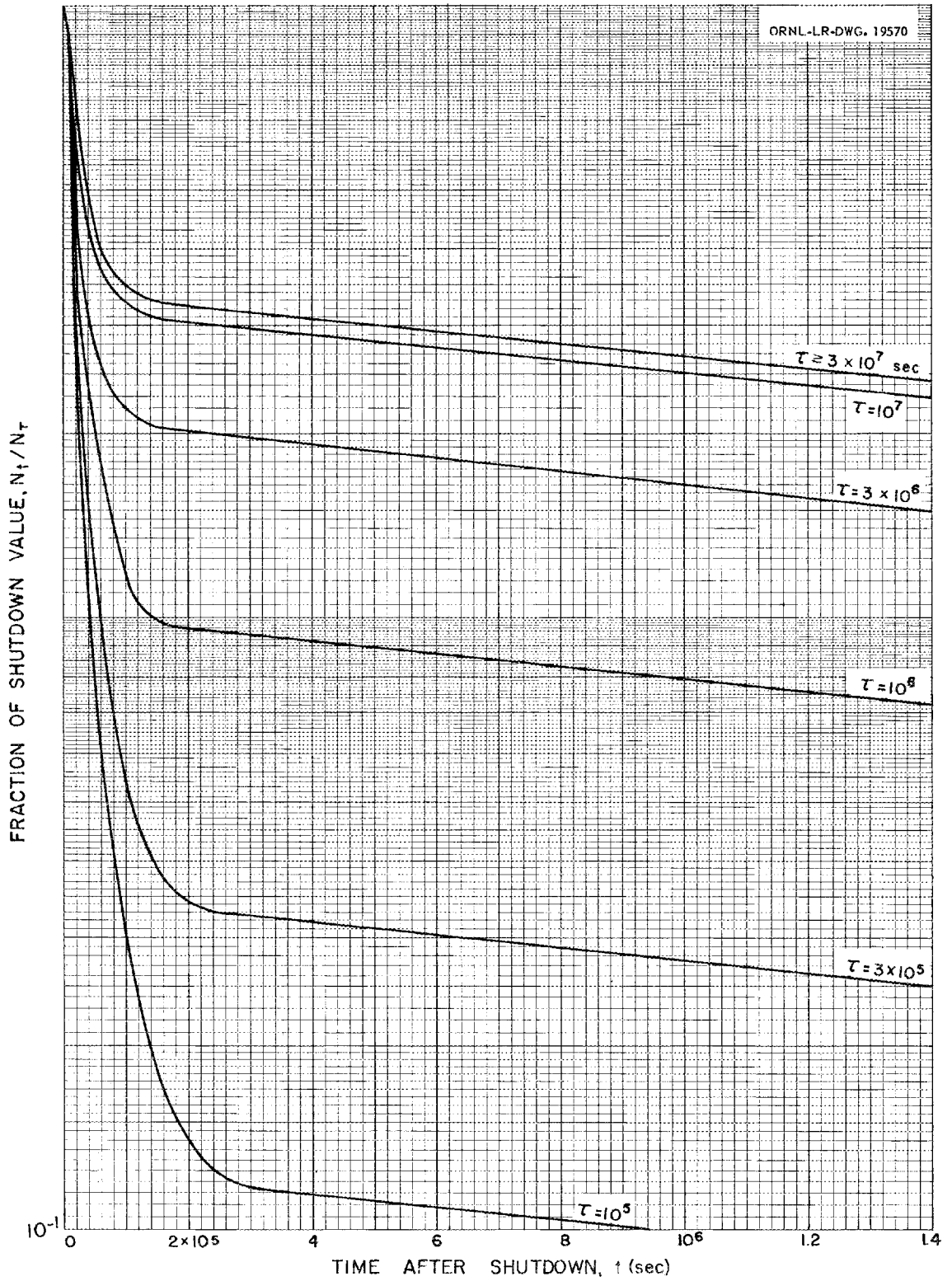

Fig. 4.47. Fraction of Shutdown Value of 72m ^{129}Te Remaining at Various Times After Shutdown. (From Blomeke and Todd, ref. 7, p. 179.)

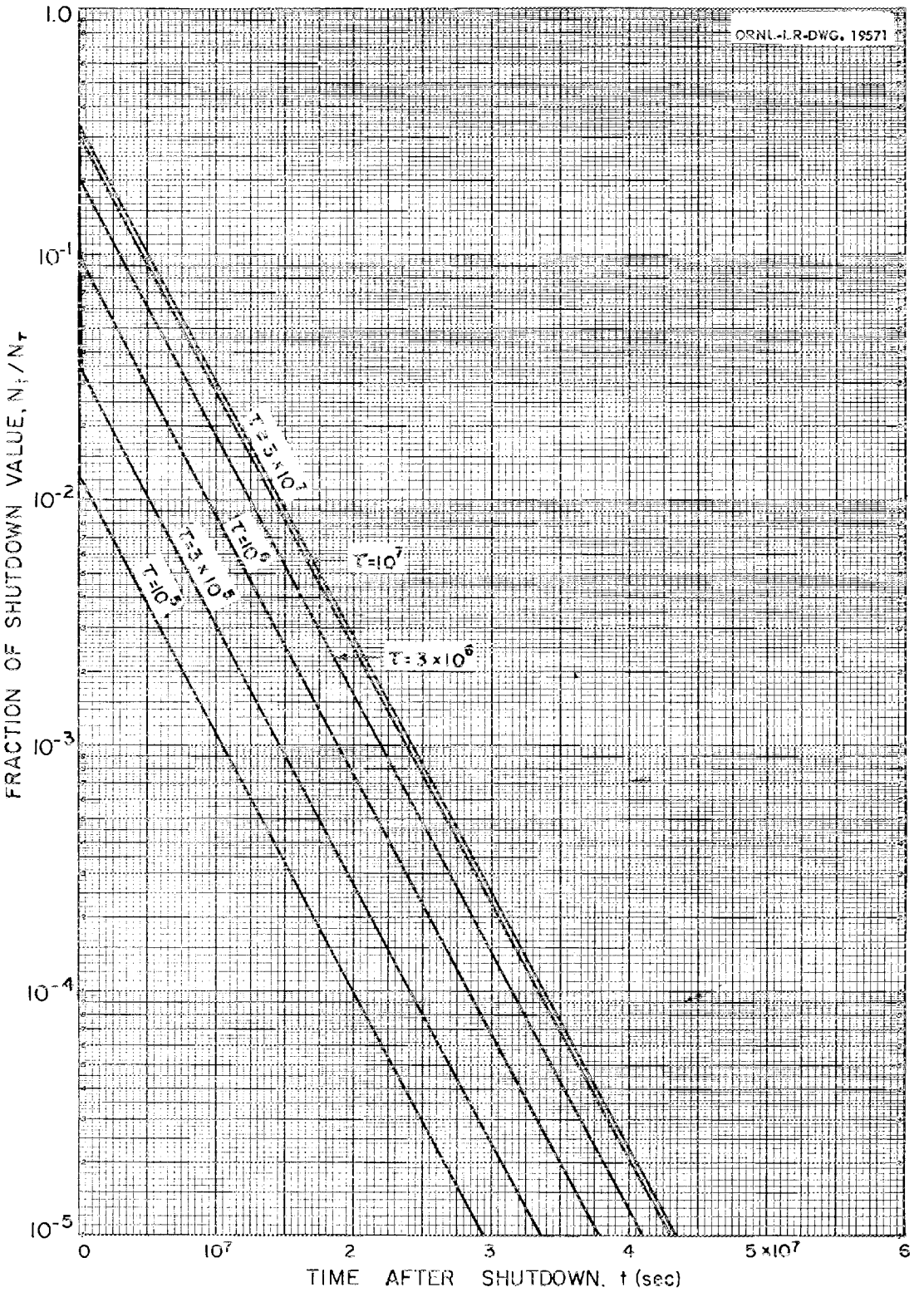

Fig. 4.48. Fraction of Shutdown Value of 72m ^{129}Te Remaining at Various Times After Shutdown. (From Blomeke and Todd, ref. 7, p. 180.)

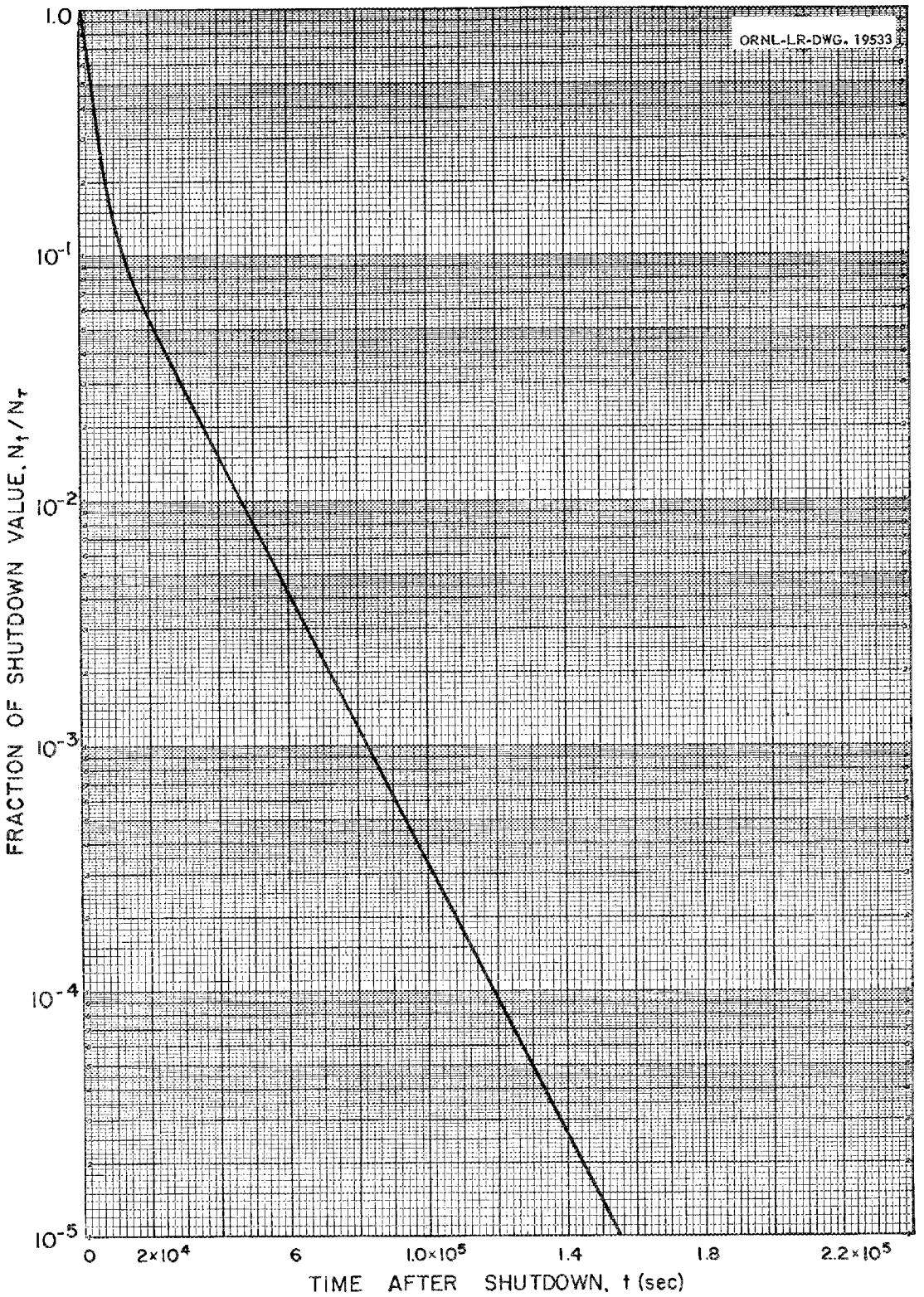

Fig. 4.49. Fraction of Shutdown Value of 24.8m ^{131}Te Remaining at Various Times After Shutdown. (From Blomeke and Todd, ref. 7, p. 142.)

Table 4.7. Fraction of Shutdown Value of Fission Products Remaining at Various Times (t, sec) After Shutdown, N_t/N_τ [Range $1 \geqslant (N_t/N_\tau) \geqslant 10^{-5}$], Accuracy ~10%

Nuclide	$\mathrm{Log}_{10}\ N_t/N_\tau$
54d ^{89}Sr	$-6.38 \times 10^{-8}\ t$
28y ^{90}Sr	$-3.41 \times 10^{-10}\ t$
9.7h ^{91}Sr	$-8.54 \times 10^{-6}\ t$
63d ^{95}Zr	$-5.55 \times 10^{-8}\ t$
17h ^{97}Zr, 90h ^{97m}Nb	$-4.9 \times 10^{-6}\ t$
67h ^{99}Mo	$-1.262 \times 10^{-6}\ t$
12.8d ^{140}Ba	$-2.73 \times 10^{-7}\ t$
33h ^{143}Ce	$-2.525 \times 10^{-6}\ t$
290d ^{144}Ce, 17.5m ^{144}Pr	$-1.203 \times 10^{-8}\ t$
11.3d ^{147}Nd	$-3.09 \times 10^{-7}\ t$
8.05d ^{131}I	$-4.31 \times 10^{-7}\ t$
6.68h ^{135}I	$-1.255 \times 10^{-5}\ t$
41d ^{103}Ru, 57m ^{103m}Rh	$-8.46 \times 10^{-6}\ t$
1.0y ^{106}Ru, 30s ^{106}Rh	$-9.62 \times 10^{-9}\ t$
26.6y ^{137}Cs, 2.60m ^{137m}Ba	$-3.635 \times 10^{-10}\ t$

In calculating the activity of fission products outside the ranges of values given by Blomeke and Todd,[7] it is often sufficient to select (by inspection) the products that will be important in the times of irradiation and cooling in question. In cases where the effects of irradiation of the fission products are negligible, the differential equations of growth can be simplified to

$$\frac{dN_1}{d\tau} = Y_1F - \lambda_1N_1 \ , \tag{4.7}$$

$$\frac{dN_2}{d\tau} = Y_2F + \lambda_1N_1 - \lambda_2N_2 \ , \tag{4.8}$$

$$\frac{dN_3}{d\tau} = Y_3F + \lambda_2N_2 - \lambda_3N_3 \ , \tag{4.9}$$

Solving this case for $N_1 = N_2 = N_3 = 0$ at $\tau = 0$ yields

$$N_1 = \frac{Y_1}{\lambda_1} F(1 - e^{-\lambda_1\tau}) \ , \tag{4.10}$$

$$N_2 = \left(\frac{Y_1 + Y_2}{\lambda_2}\right) F(1 - e^{-\lambda_2\tau}) - Y_1F\left(\frac{e^{-\lambda\tau}}{\lambda_2 - \lambda_1} + \frac{e^{-\lambda_2\tau}}{\lambda_1 - \lambda_2}\right), \tag{4.11}$$

$$N_3 = \left(\frac{Y_1 + Y_2 + Y_3}{\lambda_3}\right) F(1 - e^{-\lambda_3 \tau})$$

$$- (Y_1 + Y_2)F\left(\frac{e^{-\lambda_2 \tau}}{\lambda_3 - \lambda_2} + \frac{e^{-\lambda_3 \tau}}{\lambda_2 - \lambda_3}\right) - Y_1 F \lambda_2$$

$$\times\left[\frac{e^{-\lambda_1 \tau}}{(\lambda_2 - \lambda_1)(\lambda_3 - \lambda_1)} + \frac{e^{-\lambda_2 \tau}}{(\lambda_1 - \lambda_2)(\lambda_3 - \lambda_2)} + \frac{e^{-\lambda_3 \tau}}{(\lambda_1 - \lambda_3)(\lambda_2 - \lambda_3)}\right] . \quad (4.12)$$

In the general case for any number of nuclides i in a chain, the amount of the ith at any given time is[6]

$$N_i = F\left\{\sum_{r=1}^{r=i} Y_r \left(\frac{1 - e^{-\lambda_i \tau}}{\lambda_i}\right)\right.$$

$$\left. - \sum_{r=1}^{r=i-1}\left[\left(\sum_{p=1}^{p=r} Y_p\right)\left(\prod_{q=r}^{q=i-1} \frac{\lambda_q}{\lambda_r}\right) S\lambda_r \lambda_{r+1} \cdots \lambda_i\right]\right\}, \quad (4.13)$$

where, as before, $S_{ABC} \cdots$ represents

$$\frac{e^{-A\tau}}{(B - A)(C - A)} \cdots + \frac{e^{-B\tau}}{(A - B)(C - B)} \cdots + \frac{e^{-C\tau}}{(A - C)(B - C)} .$$

4.2.3.1 Calculation of Fission-Product Accumulation in Circulating Fuels

The problem of the accumulation of fission products in a recirculating fuel reactor has been worked out[6,10] primarily for the case of a fluid fuel reactor in which the fuel is pumped through a core and around to a heat exchanger and purification circuit in the order of a few seconds or minutes. The same problem arises, however, on a much extended time scale in any reactor where the operation is periodically intermittent or where the fuel is removed, processed, and returned for reirradiation.

The symbols for the calculation are

N_u = amount of fuel in the system (i.e., core plus circuit or reactor plus storage and processing plant),
n_u = amount of fuel in the reactor core,
N_i = total amount of fission product in whole system,
n_i = amount of fission product in core,
t_1 = time spent in the core during irradiation,
t_2 = time spent outside the core,
t_3 = time spent after leaving a processing plant and reaching the core,
T = total circuit or recycling time ($t_1 + t_2$),
t = total time of irradiation,

n = number of cycles ($t = nT$),
Y_i = independent yield of fission product i,
Y = cumulative yield.

Various cases may be considered, such as:

CASE 1 — Accumulation in a cycle in which there is no removal by processing or neutron capture.

Consider a small fragment of uranium (dN_u) either as metal or in solution. Starting from zero time, when the material first enters the reactor, the amount of a fission product (dN_i) which accumulates in the first irradiation is

$$dN_i = Y\sigma_f \phi dN_u \left(\frac{1 - e^{-\lambda_i t_1}}{\lambda_i}\right) .$$

After the first cycle (time T),

$$dN_i = Y\sigma_f \phi dN_u \left(\frac{1 - e^{-\lambda_i t_1}}{\lambda_i}\right) e^{-\lambda_i t_2} .$$

After the next irradiations,

$$dN_i = Y\sigma_f \phi dN_u \left[\left(\frac{1 - e^{-\lambda_i t_1}}{\lambda_i}\right) e^{-\lambda_i (t_1+t_2)} + \left(\frac{1 - e^{-\lambda_i t_1}}{\lambda_i}\right)\right] .$$

After two cycles,

$$dN_i = Y\sigma_f \phi dN_u \left[\left(\frac{1 - e^{-\lambda_i t_1}}{\lambda_i}\right) e^{-\lambda_i t_2}(1 - e^{-\lambda_i T})\right] .$$

After n cycles ($nT = t$),

$$dN_i = Y\sigma_f \phi dN_u \left\{\left(\frac{1 - e^{-\lambda_i t_1}}{\lambda_i}\right) e^{-\lambda_i t_2}\left[1 + e^{-\lambda_i T} + e^{-2\lambda_i T} + \ldots + e^{-(n-1)\lambda_i T}\right]\right\} .$$

Summing the geometric series ($1 + e^{-\lambda_i T} + e^{-2\lambda_i T} + \ldots$),

$$dN_i = Y\sigma_f \phi dN_u \left(\frac{1 - e^{-\lambda_i t_1}}{\lambda_i}\right) e^{-\lambda_i t_2}\left(\frac{1 - e^{-\lambda_i t}}{1 - e^{-\lambda_i T}}\right) . \qquad (4.14)$$

If the total circuit time T is short compared with the half-life $(0.693/\lambda_i)$, then

$$dN_i = Y\sigma_f \phi dN_u \left(\frac{1 - e^{-\lambda_i t}}{\lambda_i}\right) \frac{t_1}{T} . \qquad (4.15)$$

Equation (4.15) is the same as Eq. (4.10) for continuous irradiation over the whole period, except that the flux (ϕ) is replaced by a time-averaged flux

$$\overline{\phi} = \phi \frac{t_1}{T} . \qquad (4.16)$$

CASE 2 — Accumulation in a cycle in which no processing occurs, but in which the fission product is removed by neutron capture during irradiation.

For case 2, proceed in the same manner as that leading to Eq. (4.14); the following is derived:

$$dN_i = Y\sigma_f \phi dN_u \left[\frac{1 - e^{-(\lambda_i + \sigma_i \phi)t_1}}{\lambda_i + \sigma_i \phi}\right] e^{-\lambda_i t_2} \left[\frac{1 - e^{-(\lambda_i + \sigma_i \overline{\phi})t}}{1 - e^{-(\lambda_i + \sigma_i \overline{\phi})T}}\right] , \qquad (4.17)$$

where, as previously, $T = t_1 + t_2$; $t = nT$; and $\overline{\phi} = \phi(t_1/T)$.

CASE 3 — Accumulation in a cycle in which complete removal occurs at each cycle (1) of a fission product formed from an equilibrium precursor and (2) of a fission product formed directly in fission.

In case 3, (1) applies particularly to gaseous products in an aqueous homogeneous reactor, which are removed during fuel cycling, although the precursors stay in fuel solution, and (2) is more applicable to a solid fuel cycle in which both the product and its precursor are removed in each cycle. Consider the cycle in three stages, as shown in Fig. 4.50. Let

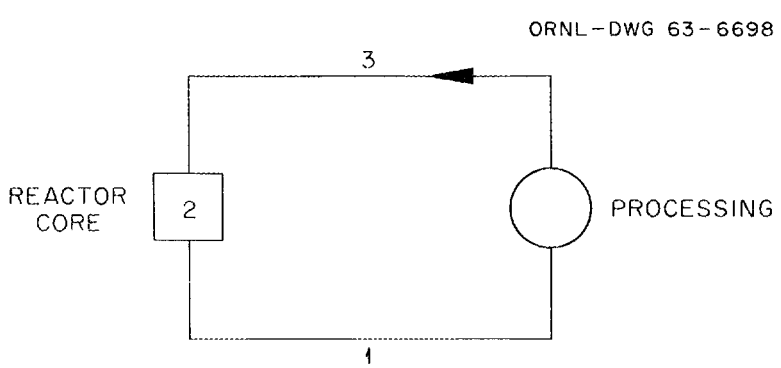

Fig. 4.50. Reactor Fuel Cycle.

the time of leaving the processing plant be t = 0, then the amount at any time t after leaving the processing plant is, in stage 3,

$$dN_i = \alpha\sigma_f\bar{\phi}dN_u\left(\frac{1 - e^{-\lambda_i t}}{\lambda_i}\right) . \tag{4.18}$$

In stage 2,

$$dN_i = \alpha\sigma_f\bar{\phi}dN_u\left\{\left(\frac{1 - e^{-\lambda_i t_3}}{\lambda_i}\right)e^{-(\lambda_i+\sigma_i\phi)(t-t_3)} + \left[\frac{1 - e^{-(\lambda_i+\sigma_i\phi)(t-t_3)}}{\lambda_i + \sigma_i\phi}\right]\right\} . \tag{4.19}$$

In stage 1,

$$dN_i = \alpha\sigma_f\phi dN_u\left\{\left(\frac{1 - e^{-\lambda_i t_3}}{\lambda_i}\right)e^{-(\lambda_i+\sigma_i\phi)t_2}\, e^{-\lambda_i[t-(t_2+t_3)]} + \left[\frac{1 - e^{-(\lambda_i+\sigma_i\phi)t_2}}{\lambda_i + \sigma_i\phi}\right]e^{-\lambda_i[t-(t_2+t_3)]} + \frac{1 - e^{-\lambda_i[t-(t_2+t_3)]}}{\lambda_i}\right\} . \tag{4.20}$$

For cycle (2), $\alpha_i\sigma_f\phi dN_u$ = rate of formation in the core; $(\lambda_i + \sigma_i\phi)dN_i$ = rate of decay in the core; and $\lambda_i dN_i$ = rate of decay outside the core. In stage 3,

$$dN_i = 0 . \tag{4.21}$$

In stage 2,

$$dN_i = \alpha_i\sigma_f\phi dN_u\left[\frac{1 - e^{-(\lambda_i+\sigma_i\phi)(t-t_3)}}{\lambda_i + \sigma_i\phi}\right] . \tag{4.22}$$

In stage 1,

$$dN_i = \alpha_i\sigma_f\phi dN_u\,\frac{\{1 - e^{-[(\lambda_i+\sigma_i\phi)t_2]}\}}{\lambda_i + \sigma_i\phi}\, e^{-\lambda_i[t-(t_3+t_2)]} . \tag{4.23}$$

The accumulation of fission products in any stage is then obtained by integrating over the time during which the uranium remains in that stage. Thus, for the core,

$$N_i = \int_{t_3}^{t_3+t} dN_i dt ,$$

where dN_i is given by Eq. (4.19) or (4.22).

4.2.3.2 Summary and Comments on Evaluating Fission-Product Buildup and Decay

In many cases, the operating time of the reactor has been sufficiently long to build up equilibrium concentrations of fission products. In this case the equilibrium value of a direct fission yield nuclide can be determined by the relation

$$\frac{dN_i}{dt} = \Sigma_f \phi Y_i - \lambda_i N ,$$

where $(dN_i/dt) = 0$. Therefore

$$N_i^{eq} = \frac{\Sigma_f \phi Y_i}{\lambda_i} . \tag{4.24}$$

This can be expressed in terms of core power, using the fact that 3.1×10^{10} fissions/sec yields 1 watt of thermal power; therefore

$$\Sigma_f \phi = (p)(3.1 \times 10^{10}) ,$$

$$N_i^{eq} = \frac{p(3.1 \times 10^{10})Y_i}{\lambda_i} , \tag{4.25}$$

where N_i is given in atoms per unit volume and p is the power in the region of the core of interest in watts per unit volume. Equation (4.25) can be expressed in terms of curies by substituting the fact that 3.7×10^{10} dis/sec = 1 curie. The activity of a nuclide is given by

$$\frac{Q_i}{V} = \frac{\lambda_i N_i}{3.7 \times 10^{10}} ,$$

$$\frac{Q_i}{V} = 0.838 p Y_i , \tag{4.26}$$

where Q_i/V is the activity of nuclide i in curies per unit volume.

The total core inventory is

$$Q_i = 0.838 Y_i \iiint_V p dV . \tag{4.27}$$

Therefore,

$$Q_i = 0.838 Y_i P \ , \tag{4.28}$$

where P is total core power. In the case of a one-precursor model,

$$\frac{dN_i}{dt} = \Sigma_f \phi Y_i + \lambda_{i-1} N_{i-1} - \lambda_i N_i \ . \tag{4.29}$$

For saturation conditions,

$$\lambda_i N_i = \Sigma_f \phi Y_i + \lambda_{i-1} N_{i-1} \ ,$$

$$N_i = \frac{\Sigma_f \phi}{\lambda_i} Y_i + \frac{\lambda_{i-1}}{\lambda_i} N_{i-1} \ . \tag{4.30}$$

When N_{i-1} is at equilibrium,

$$N_{i-1} = \Sigma_f \phi \frac{Y_{i-1}}{\lambda_{i-1}} \ . \tag{4.31}$$

Substituting

$$N_i = \Sigma_f \phi \left(\frac{Y_i + Y_{i-1}}{\lambda_i} \right) . \tag{4.32}$$

Since $Y_i + Y_{i-1}$ is the cumulative yield, Y_i^{cum},

$$N_i = \Sigma_f \phi \frac{Y_i^{cum}}{\lambda_i} \ . \tag{4.33}$$

Often it is sufficient to use a two-precursor model. Considering the case of removal by neutron capture, but no increase by neutron capture in the A-1 chain, the general equation that can be used for both buildup and decay (for a constant power level) is

$$N_i = N_i^0 e^{-\lambda_{eff}^i t} + \Sigma_f \phi \left(\frac{Y_i^{ind}}{\lambda_{eff}^i} + \frac{k Y_{i-1}^{cum} \lambda_{i-1}}{\lambda_{eff}^{i-1} \lambda_{eff}^i} \right) \left(1 - e^{-\lambda_{eff}^i t} \right)$$

$$+ \frac{\lambda_{i-1}}{\lambda_{eff}^i - \lambda_{eff}^{i-1}} \left(k N_{i-1}^0 - \frac{\Sigma_f \phi k Y_{i-1}^{cum}}{\lambda_{eff}^{i-1}} \right) \left(e^{-\lambda_{eff}^{i-1} t} - e^{-\lambda_{eff}^i t} \right) , \tag{4.34}$$

where

N_i^0 = initial value of nuclide i, atoms per unit volume,

$\lambda_{eff}^i = (\lambda^i + \sigma_i \phi)$ = effective removal decay constant, 1/sec,

Y_i^{ind} = independent yield of nuclide i,

k = branching ratio from nuclide i-1 to nuclide i, fraction of decay of N_{i-1} going to N_i.

Equation (4.34) can be used for determining the activity inventory for variations in power level by dividing the power history into periods of constant power. The value of N_i can be calculated at the end of one time period and can be used as N_i^0, the initial value for the following time period.

Considerable savings in labor can be obtained by using a digital computer to solve Eq. (4.34). The buildup and decay equations are also well suited for analysis by analog computers.

4.3 FISSION-PRODUCT RELEASE FROM FUEL ELEMENTS*

4.3.1 Introduction

The determination of the amount of fission products released from the fuel element as a consequence of an accident is obviously a difficult procedure, even when the conditions during and after the accident are well specified and of a simple enough nature to be treated analytically. Therefore the procedure is to choose a maximum credible accident (mca), the consequence of which, in terms of exposure to the public, would be worse than other credible occurrences.

Commonly, the mca is taken as a rupture of a main coolant pipe that could result in a loss of coolant, possible derangement of core compoents, blower or pump failures, and other malfunctions, depending on the particular reactor in question. The effects of this violent surge should be analyzed and the reactor built so that, at least, the control rods will insert. Under this sequence of events the fuel temperature will rise (due to afterheat generation) if adequate cooling is not available and cause eventual failure of the cladding and possibly meltdown of the fuel.

Since clad UO_2 is the predominant material used for fuel in large power reactors, the discussion here concentrates on the behavior of UO_2. With this type of fuel and an accident of the type described above, the cladding would melt (or oxidize) before the fuel and immediately release the fission products that had been released from the UO_2 fuel during its operating lifetime. The structural rigidity of the fuel would be lost with the cladding gone, and the pellets would drop to some position on the fuel support structures or to the bottom of the reactor vessel. If a pool of water remained on the bottom of the vessel, adequate cooling could be maintained to greatly reduce further fission-product release. However, if cooling were not available, the fuel would continue to rise in temperature, and

*See Appendix G for relevant information published since this chapter was prepared.

the UO_2 crystals would undergo grain growth, in which case much of the fission-product material trapped in the crystal matrix would be released. If the process were continued to the melting point of UO_2, a great deal of activity would be released. The overheating could take place in either an oxidizing or reducing atmosphere. In the former case the release would be enhanced by the oxidation of UO_2 to U_3O_8.

Some data exist for the release of fission products from molten fuels that were obtained in experiments utilizing out-of-pile, nonnuclear heating and in a small number of experiments investigating in-pile meltdown. The extrapolation of this data to a full-scale reactor is a major problem because of the differences between the experiments and the reactor and among various designs of reactors. Information already obtained in large vessels (See Sec. 4.4.4) and data that will be produced in programs just getting under way (NSPP, CSE, and LOFT) should aid in solving the extrapolation problem. The material presented in this chapter deals with the various physical processes that are likely to be involved. Experimental programs are in progress to define the release of activity more clearly, and a body of knowledge should grow quickly beyond what is given here.

4.3.2 Predicting Cladding Failure

After an accident under the conditions outlined above, the temperature of the cladding will rise. The fission gases that are volatile at these temperatures will contribute to the internal pressure on the cladding, and the pressure will increase with temperature. Also, as the temperature increases, the cladding strength will decrease, and eventually the cladding will fail. The determination of internal pressure on the cladding is basically a design problem and will not be treated here in great detail.

4.3.2.1 Release of Fission Gases from UO_2 During Irradiation

There are two major mechanisms controlling the release of fission products from UO_2 during irradiation: (1) diffusion from the crystal matrix and (2) release from the crystals undergoing grain growth. Other effects (such as recoils and knock-ons) are secondary to the major effects under most conditions and will not be treated here in detail.

1. Determination of Grain Growth. In the absence of experimental data, it may be necessary to assume that all volatile fission products will be released upon grain growth. It is therefore important to determine the extent of grain growth during operating conditions. As shown in Fig. 4.51, the grain growth is time dependent, but it will occur over a period of a few days at a temperature of 1700°C.

The determination of temperature in UO_2 is a difficult problem because of the discontinuous nature of the material after irradiation. Reactor conditions may be compared with experiment conditions by means of the conductivity integral:

$$\int K(t)dT \ , \qquad (4.35)$$

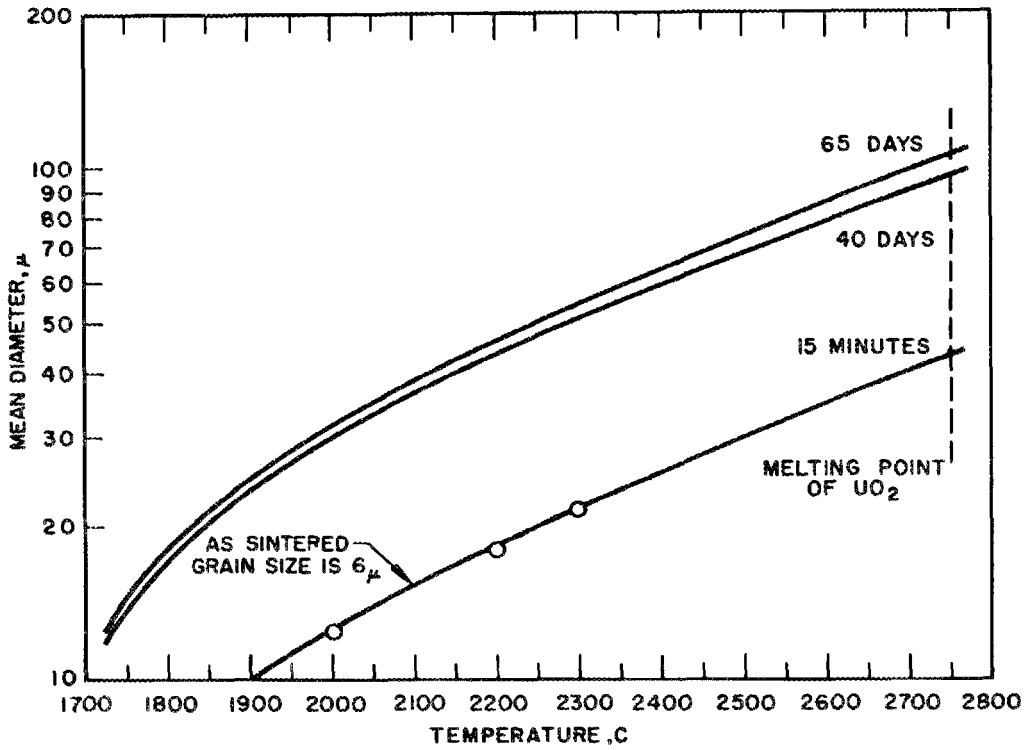

Fig. 4.51. Grain Size and Temperature Relationship for UO_2 Experimentally Derived for 15 min of Holding Time and Extrapolated to Longer Times by Use of the Equation, $D = Kt^{1.0}$. (From Eichenberg et al., ref. 11.)

where K is the thermal conductivity of the UO_2 in w/cm·°C and T is the temperature in °C. This parameter bears the following relation to the linear heat rate[12] for uniform heat generation in a solid cylindrical pellet:

$$\int_{T_s}^{T_c} K(T)dT = \frac{W}{4\pi} , \qquad (4.36)$$

where T_c is the central temperature in °C, T_s is surface temperature in °C, and W is the linear heat rate of the fuel elements in w/cm. Equation (4.36) does not require detailed knowledge of the thermal conductivity and therefore can be used to compare experimental results with the reactor data under analysis. The existence of grain growth can be checked by the inequality

$$\int_{T_{sr}}^{T_{cr}} K(T)dT < \int_{T_{se}}^{T_{gg}} K(T)dT + \int_{T_{sr}}^{T_{se}} K(T)dT , \qquad (4.37)$$

where

T_{sr} = pellet surface temperature of the reactor under study,
T_{cr} = pellet central temperature in the reactor,
T_{se} = pellet surface temperature in the experiment,
T_{gg} = grain growth temperature.

$\int_{T_{sr}}^{T_{cr}} K(T)dT$ can be determined from the reactor power from Eq. (4.36), $\int_{T_{se}}^{T_{gg}} K(T)dT$ can be obtained from experimental data, and the correction term $\int_{T_{sr}}^{T_{se}} K(T)dT$ must be calculated using the best available data for thermal conductivity. Table 9.19 in ref. 12 gives some values of $\int_{T_{se}}^{T_{gg}} K(T)dT$ for 33 experiments for various claddings, fill gases, pellet sizes, etc. The lowest useful value of $\int_{T_{se}}^{T_{gg}} K(T)dT$ reported is 23.8 w/cm for a helium fill gas; all values obtained in an argon fill gas were higher. Values for H_2O fill gas were lower, but, since it is not likely that any reactor would operate with water within the cladding during the operating lifetime under design conditions, these values are usually not considered.

The determination of the oxide surface temperature in the reactor is complicated by the uncertainty in the thermal conductance at the interface between the cladding and the UO_2. It is not sufficient to simply calculate an effective thermal conductance using the thermal conductivity of the fill gas and the diametrical clearance because the pellet would not remain centered if it were intact and, under most conditions, the pellet would fragment after irradiation. Consequently analytical prediction of the oxide-to-cladding gap conduction is impossible. The results of experiments are correlated in Fig. 4.52, in which the sheath-to-fuel thermal conductance is related to the ratio of the assembled diametrical clearance to the pellet diameter.

When the surface temperature of the cladding is known from the design conditions of the reactor, it is possible to calculate the surface temperature of the fuel for use in Eq. (4.37). The correction term $\int_{T_{sr}}^{T_{se}} K(T)dT$ can be obtained from Fig. 4.53, in which $\int_{100°C}^{T} K(T)dT$ is plotted versus the temperature T using the thermal conductivity data of Kingery[13,14] and of Hedge and Fieldhouse.[15] The Hedge and Fieldhouse data were obtained on cracked UO_2 and are generally conceded to yield a low value of conductivity. The Kingery data are believed to be accurate.

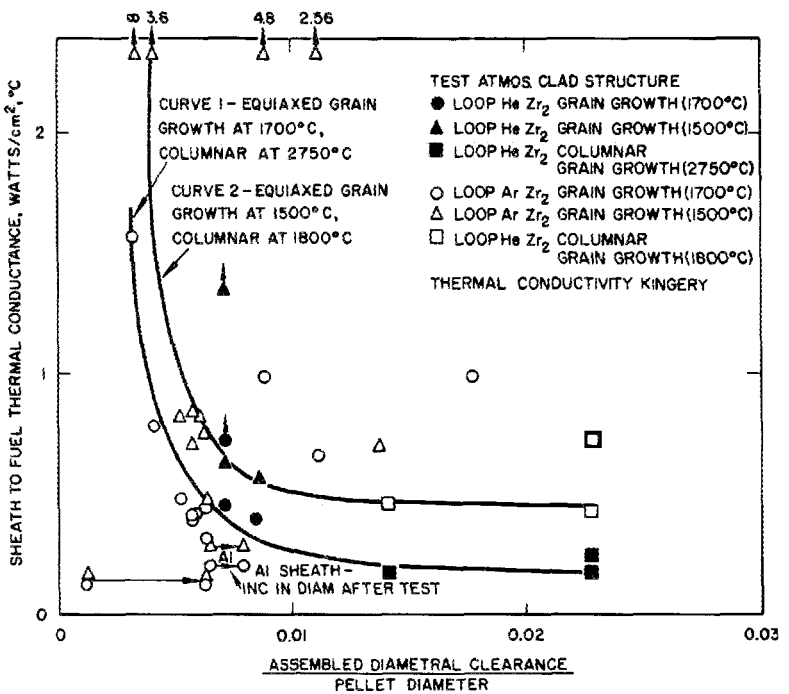

Fig. 4.52. Effect of Clearance on Gap Conductance. (From Belle, ref. 12, p. 608.)

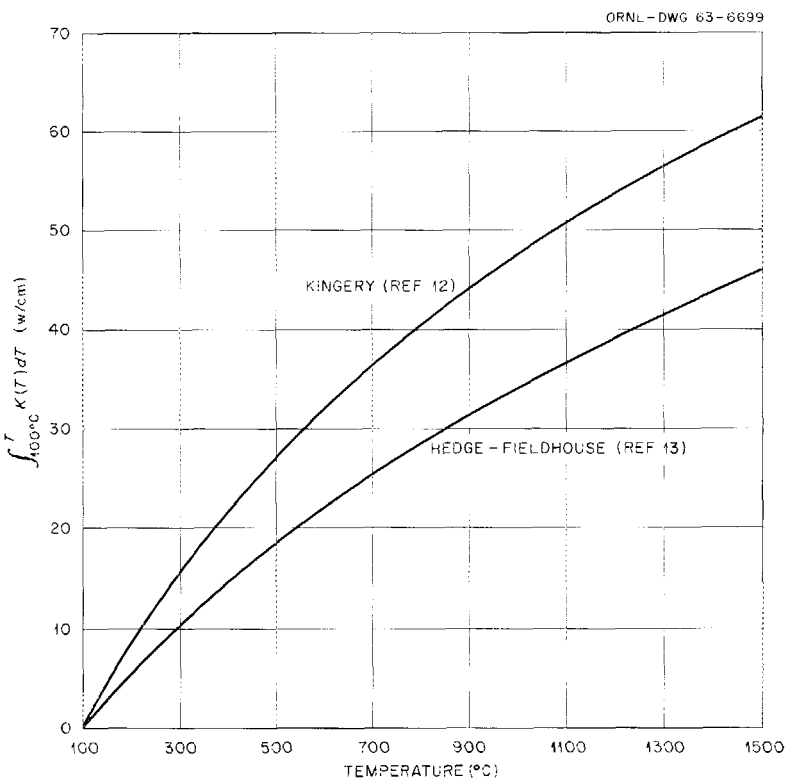

Fig. 4.53. Plot of $\int_{100°C}^{T} K(T)dT$ Versus Temperature for UO_2. (From ref. 16.)

The term $\int_{T_{sr}}^{T_{se}} K(T)dT$ can be obtained by the relation

$$\int_{T_{sr}}^{T_{se}} K(T)dT = \int_{100}^{T_{se}} K(T)dT - \int_{100}^{T_{sr}} K(T)dT \ . \qquad (4.38)$$

If the inequality of Eq. (4.37) does not hold, grain growth will occur. The extent of grain growth at a given position in the reactor can be estimated by the relation

$$\frac{V_{gg}}{V_{tot}} = 1 - \frac{\int_{T_{sr}}^{T_{gg}} K(T)dT}{\int_{T_{sr}}^{T_{cr}} K(T)dT} \ , \qquad (4.39)$$

where V_{gg}/V_{tot} is the fractional volume of UO_2 undergoing grain growth. Equation (4.39) is strictly true in cylindrical geometry for the assumption that an average thermal conductivity of the form

$$K_{av} = \frac{\int_{T_{sr}}^{T_{gg}} K(T)dT}{T_{gg} - T_{sr}}$$

holds throughout the fuel pellet, including the grain-growth region, and that constant heat generation exists in the pellet.

For hazards analyses, it is sometimes sufficient to assume that all the fission products that are volatile at grain-growth temperatures will be released from the fraction of the fuel undergoing grain growth. Table 4.8 lists the melting and boiling points for some important elemental fission products. Data[17] on diffusion rates in the temperature range spanning the grain-growth region are given in Table 4.9. Other data from the same source giving the effect of burnup or diffusion rates are listed in Table 4.10. The latter data indicate that diffusion of fission products increases with increasing burnup, except possibly for the low-volatility elements.

It is unlikely that clad UO_2, as referred to here, would be made in other than cylindrical form, but plate fuel elements have been made with UO_2 dispersed in a metal matrix to which this discussion would not be applicable. Therefore for the sake of completeness, the use of the conductivity integral to predict grain growth in slab and spherical geometry is described below.

Table 4.8. Melting and Boiling Points of Some Fission-Product Elements

Element	Melting Point (°C)	Boiling Point (°C)
Xenon	-112	-107.1
Krypton	-156.6	-152.9
Iodine	113.7	184
Tellurium	452	1390
Cesium	28.6	685
Ruthenium	2450	4080
Strontium	774	1150
Barium	725	1640

Table 4.9. Diffusion of Fission Products from UO_2 Heated 5.5 hr in Purified Helium[a,b]

Temperature (°C)	Percentage of Fission Products Released									
	Rare Gases	Gross Gamma	I	Te	Cs	Ru	Sr	Ba	Zr	U
1515	1.3	0.9	5.8	2.9	1.4	0.9	0.1			
1610	2.7	2.1	6.5	12	1.7	1.5	0.1			
1710	2.6	6.3	9.6	20	2.7	3.8	0.4	1.3		
1800	3.7	5.2	12	21	3.2	6.9	1.0			
1900	9.7	12	16	48	8.6	8.5	2.3			
1980	12	12	42	76	15	13	4.2	8.7	1.8	
2105	25	23	40	81	24	22	13	21	0.5	0.5
2150	59	18	74	95	53	49	28	40	12	0.4
2200	65	33	75	96	70	50	36	59	18	
2260	87	38	84	96	65	90	55	75	35	1.3

[a]Trace-level-irradiated PWR-type UO_2 samples heated in tantalum crucibles by RF induction.

[b]Helium purified by contact with hot zirconium sponge; flow rate, 50 cm^3/min.

Table 4.10. Effect of Burnup Level and Temperature on Diffusion of Fission Products from UO_2 Heated 5.5 hr in Pure Helium

Temperature (°C)	Irradiation Level (Mwd/ton)	Percentage of Individual Fission Products Released[a]						
		Xe-Kr	I	Te	Cs	Ru	Sr	Ba
1400	~1[b]	0.8	4.0	3.9	0.02	0.02	0.001	
	1005[c]	0.8	0.9	0.8	2.6	0.001	0.1	
	1000[b]	0.5	1.6	1.2	0.5	0.001	0.06	1.8
	4000[b]	6.1	23	16	21	0.006	0.08	0.5
1610	~1[b]	2.7	6.5	12	1.7	1.5	0.1	
	1005[c]	2.6	3.7	12	12	0.1	2.0	17
	1000[b]	6.0	5.5	27	20	0.3	0.2	12
	4000[b]	14	25	48	43	0.2	0.5	15
1780	~1[b]	3.7	12	21	3.2	6.9	1.0	
	1005[c]	12	24	67	27	0.4	9.0	39
	1000[b]	14	26	35	22	0.4	3.7	21
	4000[b]	42	59	60	40	5.7	5.8	18
1980	~1[b]	12	41	75	15	13	4.2	8.7
	1005[c]	29	53	74	84	6.0	15	57
	1000[b]	49	63	90	70	4.8	~10	51
	4000[b]	71	81	81	98	15	33	60

[a]Includes that portion adsorbed on crucible and reflector parts.

[b]PWR-type UO_2 (93 to 94% of theoretical density); only the 1 Mwd/ton pellets were full size (7g); high-burnup samples were 0.1- to 0.2-g fragments with a total weight of 1 to 2 g.

[c]EGCR-type UO_2 (97% of theoretical density); samples were similar to PWR samples in total weight and fragment size.

In an infinite slab geometry, under the same assumptions as those used in deriving the relations for the cylindrical geometry, the fraction of fuel undergoing grain growth is

$$\frac{V_{gg}}{V_{tot}} = \left[1 - \frac{\int_{T_{rs}}^{T_{gg}} K(T)dT}{\int_{T_{rs}}^{T_{rc}} K(T)dT}\right]^{1/2} . \qquad (4.40)$$

The relation between the conductivity integral and the volume heat generation is

$$\int_{T_{rs}}^{T_{rc}} K(T)dT = \frac{Q}{2} (L^2) , \tag{4.41}$$

where Q is the volume heat generation rate in w/cm^3 and L is the slab half-thickness in cm. In a spherical geometry,

$$\frac{V_{gg}}{V_{tot}} = \left[1 - \frac{\int_{T_{rs}}^{T_{gg}} K(T)dT}{\int_{T_{rs}}^{T_{rc}} K(T)dt} \right]^{3/2} \tag{4.42}$$

and

$$\int_{T_{rs}}^{T_{rc}} K(T)dT = \frac{QR^2}{6} , \tag{4.43}$$

where R is the radius of the sphere in cm.

2. Release from Regions Without Grain Growth. Once the existence of grain growth has been established, the release from the region of the UO_2 not undergoing grain growth must be determined. For low-density sintered UO_2 (91–93% of theoretical density) the Booth model[18] has been found to yield useful results. In this model the UO_2 compact is assumed to consist of an assembly of spheres communicating with the atmosphere through channels of open porosity. The radius of the spheres is taken as

$$a = \frac{3d}{S} , \tag{4.44}$$

where a is the radius of the equivalent microsphere in cm, d is fraction of theoretical density, and S is the total surface area per unit volume in cm^2/cm^3. Thus mathematical solutions of Fick's second law for spheres,[19] with appropriate boundary conditions, should represent the rate of diffusion of fission product from UO_2, assuming no resistance in the open porosity.

The diffusion equation in spherical geometry for a fission product produced at a constant rate at a constant temperature without radioactive decay is

$$\frac{\partial c}{\partial t} = D \left(\frac{\partial^2 c}{\partial r^2} + \frac{2}{r} \frac{\partial c}{\partial r} \right) + B , \tag{4.45}$$

where

c = concentration of fission products as a function of radius and time, atoms/cm^3,
r = radial position in sphere, cm,
t = time, sec,
D = diffusion coefficient, cm^2/sec,
B = rate of production, atoms/sec·cm^3.

The solution for f, the fraction of a given fission product released in time t, is[20]

$$f = 1 - \frac{6a^2}{90Dt} + \frac{6}{\pi^4 Dt} \sum_{n=1}^{\infty} \frac{1}{n^4} \exp\left(-n^2\pi^2 Dt/a^2\right) . \qquad (4.46)$$

For $f < 0.57$, corresponding to values of

$$\frac{\pi^2 Dt}{a^2} \leq 1 ,$$

the value of f is given by the approximation

$$f = 4\left(\frac{Dt}{\pi a^2}\right)^{1/2} - \frac{3Dt}{2a^2} . \qquad (4.47)$$

Again, the second term is negligible for values of

$$\frac{\pi^2 Dt}{a^2} < 0.01 .$$

For nonisothermal conditions the pellet must be subdivided into radial zones of constant temperature and the above equation applied for each zone. This is necessary because of the strong temperature dependence of the diffusion coefficient D as expressed by

$$D = D_{ref(T)} \exp\left(-Q/RT\right) , \qquad (4.48)$$

where

$D_{ref(T)}$ = the diffusion coefficient at a reference temperature, cm^2/sec,
Q = activation energy, cal/g-mole,
R = gas constant, cal/g-mole·°K,
T = absolute temperature, °K.

The above tedious procedure was followed by Robertson et al.[21] to obtain the results presented in Fig. 4.54. The calculation was done for a pellet surface temperature of 400°C and gave the fractional release of xenon as a function of D'_{1400} t and $\int_{400}^{T_c} K(T)dT$, where D'_{1400} is the value of D/a^2 at 1400°C and t is the time of irradiation. The data of Fig. 4.54 were calculated using an activation energy of 46,000 cal/g-mole, compared with the more commonly accepted 71,000 cal/g-mole.[12] The diffusion constant D for fission gases in UO_2 as a function of 1/T is shown in Fig. 4.55; note the values of a given on the figure. The values of D'_{1400} versus

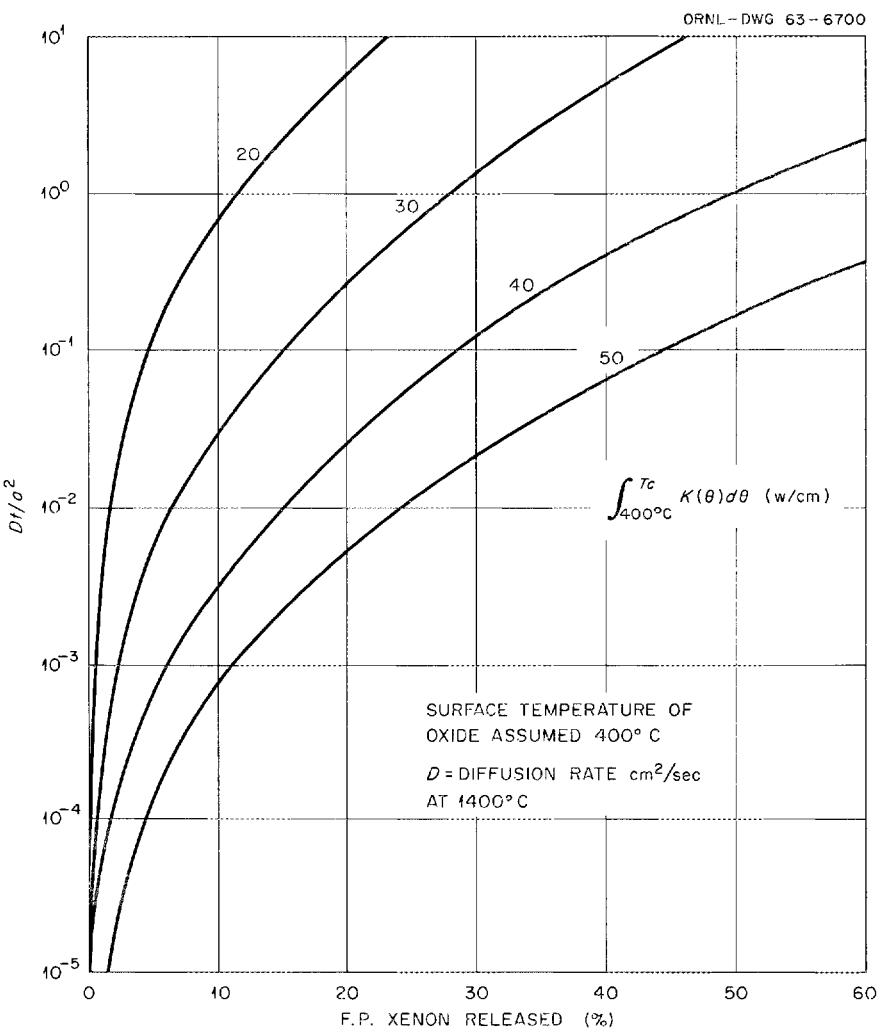

Fig. 4.54. Fractional Release of Xenon in a Cylindrical UO_2 Fuel Element as a Function of Thermal Rating, Time, and Diffusion Rate. (From Robertson et al., ref. 21.)

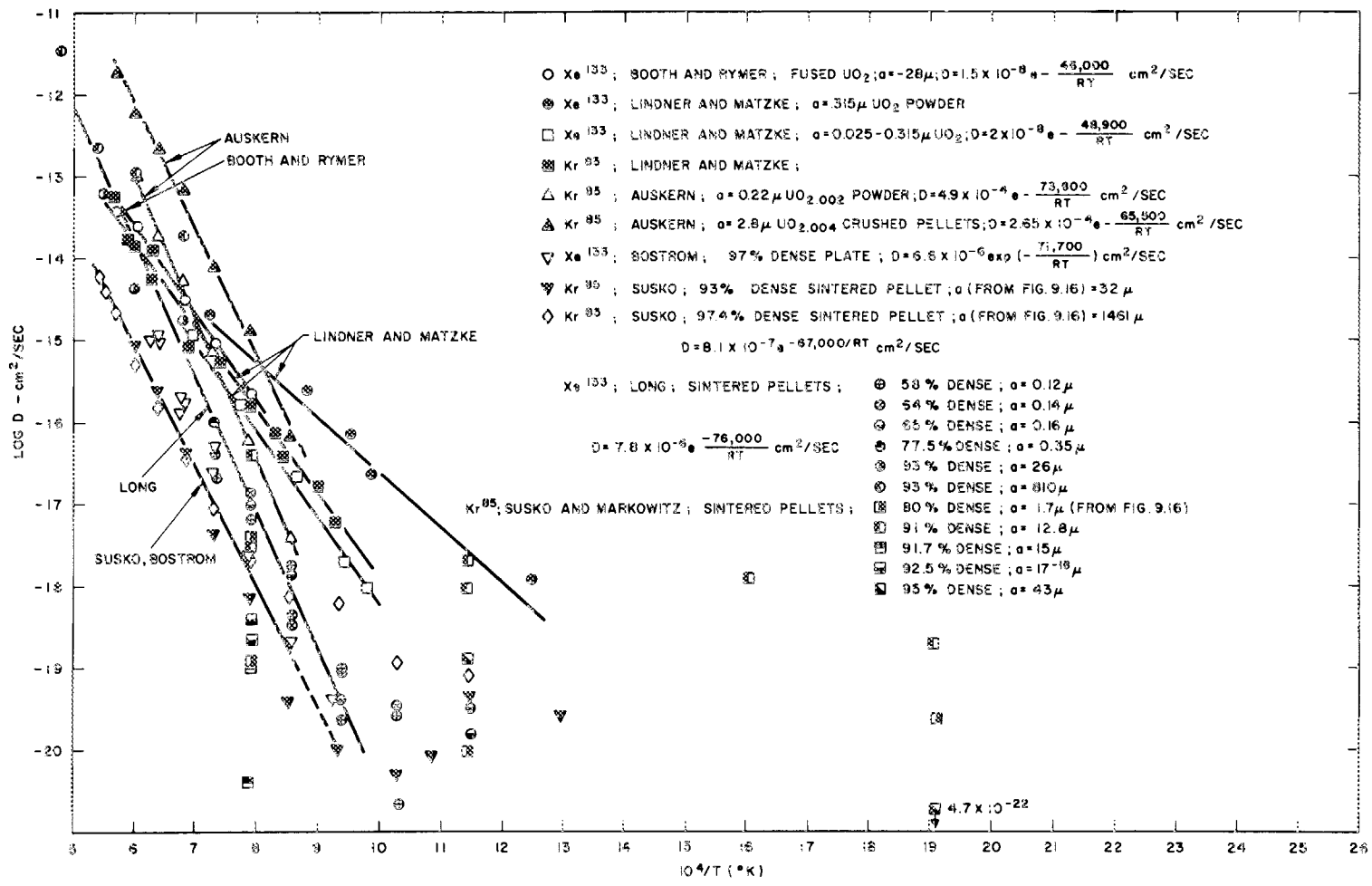

Fig. 4.55. Diffusion Constant D for Fission Gases in UO_2. (From Belle, ref. 12, p. 496.)

the density of the pellet are given in Fig. 4.56. This treatment neglects an important factor that has been shown to affect rates of escape of fission gases from UO_2 at elevated temperatures. This is the so-called burst effect, which has been noted by nearly all investigators in this field and which is still not clearly understood, although it has been subjected to rather vigorous attack. Davies and Long,[22] stated that whenever the temperature of the UO_2 sample is raised rapidly, either in-pile or out-of-pile, both the initial rate of evolution of fission gas and the total amount evolved are higher than anticipated by diffusion laws, and this phenomenon persists even after several anneals at successive temperatures.

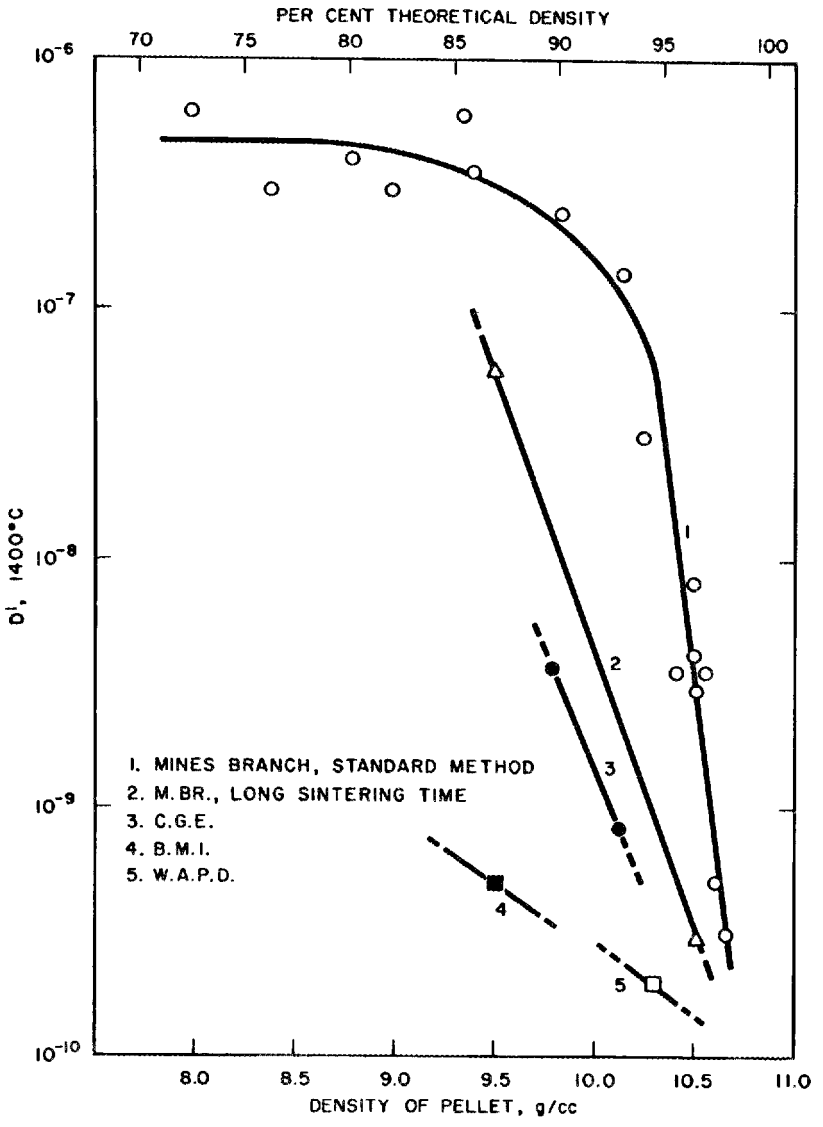

Fig. 4.56. Diffusion Constant of ^{133}Xe, $D'(D/a^2)$ at 1400°C, as a Function of Density of Sintered UO_2. (From Booth and Rymer, ref. 25.)

An investigation conducted by Stevens and his co-workers[23] indicated that an oxidized surface layer is a major cause of the burst effect with lightly irradiated UO_2. This effect was also observed to occur with highly irradiated UO_2 by Parker and his co-workers,[17] but the mechanism of release was not established.

Emission from pores and other defects in the UO_2 lattice was shown by recent studies[22] to have a significant effect on release rates of fission gases. Such defects will certainly be produced by irradiation. It seems probable, however, that the defects will have a minor effect on fission-gas release from reactor-grade UO_2, compared with the surface layer effect discussed above.

There can be little doubt that the temperature of UO_2 fuel materials will rise rapidly in loss-of-coolant accidents. Therefore the existence of the burst effect, which is not amenable to theoretical predictions, makes the value of calculations based on diffusion data alone questionable.

Higher density UO_2, i.e., UO_2 of approximately 97% theoretical density and greater, exhibits less fission-gas release than that predicted by the Booth model. For further information see refs. 12 and 24.

4.3.2.2 Pressure Buildup and Cladding Stress in a Fuel Rod

The fission gases that are released to open pores and thence to the free volume within the fuel sheath contribute to the internal pressure. In calculating the steady-state pressure, it is necessary to include the effects of the higher temperatures within the open pores in the pellets by a relation of the form

$$P_i = \frac{N_i R}{\int_V \frac{dV}{T}} , \qquad (4.49)$$

where

P_i = partial pressure due to nuclide i,
N_i = total number of moles of nuclide i released to the open pores,
V = volume of void space inside cladding available for gas storage,
T = absolute temperature, and
R = gas constant.

In practice it is possible to divide the void volume into elements of approximately uniform temperature. For this case, Eq. (4.49) can be approximated by

$$P_i = \frac{N_i R}{\left(\sum_{k'=1}^{k} \frac{\Delta V_{k'}}{T_{k'}} \right)} , \qquad (4.50)$$

where k is the number of volume elements. In the case where the temperature within the fuel is known analytically and the void space outside the fuel is at uniform temperature, Eq. 4.49 becomes

$$P_i = \frac{N_i R}{\frac{V_0}{T_0} + \int_{V_f} \frac{dV}{T}}, \qquad (4.51)$$

where

V_0 = void volume outside the fuel but inside the cladding,
T_0 = temperature of void space outside the fuel, and
V_f = volume of void space inside the fuel.

Equations (4.49) and (4.50) refer to those nuclides behaving as perfect gases at the temperature in question. If a portion of the volume walls (e.g., the cladding) is maintained at a temperature below the boiling point of a given nuclide, the contribution to the total pressure from that nuclide is the vapor pressure at the average temperature seen by the nuclide in the volume in question. Vapor pressures of some fission-product elements and compounds are given in Fig. 4.57.

In the case of an accident, as the fuel temperature increases, it can be seen that the internal pressure will rise according to Eqs. (4.50) and (4.51) for those nuclides behaving as a perfect gas at these temperatures and will further increase in steps as the cladding (the coolest part of the fuel element) in its temperature transient reaches the boiling points of abundant nuclides, such as cesium and rubidium.

If the temperature rise is relatively slow, cladding failure will occur by rapid creep. Some stress-rupture properties of type 304 stainless steel at high temperatures are given in Fig. 4.58, which shows the time required to rupture cladding that is bearing various tangential stresses at various temperatures.

In many cases of rapid temperature rise, it is sufficient to postulate that the cladding will fail at its melting point unless the cladding stress is quite high. Of course, this depends on the particular reactor design in question.

4.3.3 Release from Fuel After Cladding Failure

On failure of the cladding, the fission products released from the fuel matrix (but contained within the cladding) will be released immediately unless they react with the cladding to form alloys or stable, nonvolatile compounds. Determination of further release from the fuel is complicated by not knowing the exact condition that will exist at this time and by the scarcity of experimental and theoretical information that could be used to predict the amounts of fission products that will be released. It should be remembered that the experimental data presented

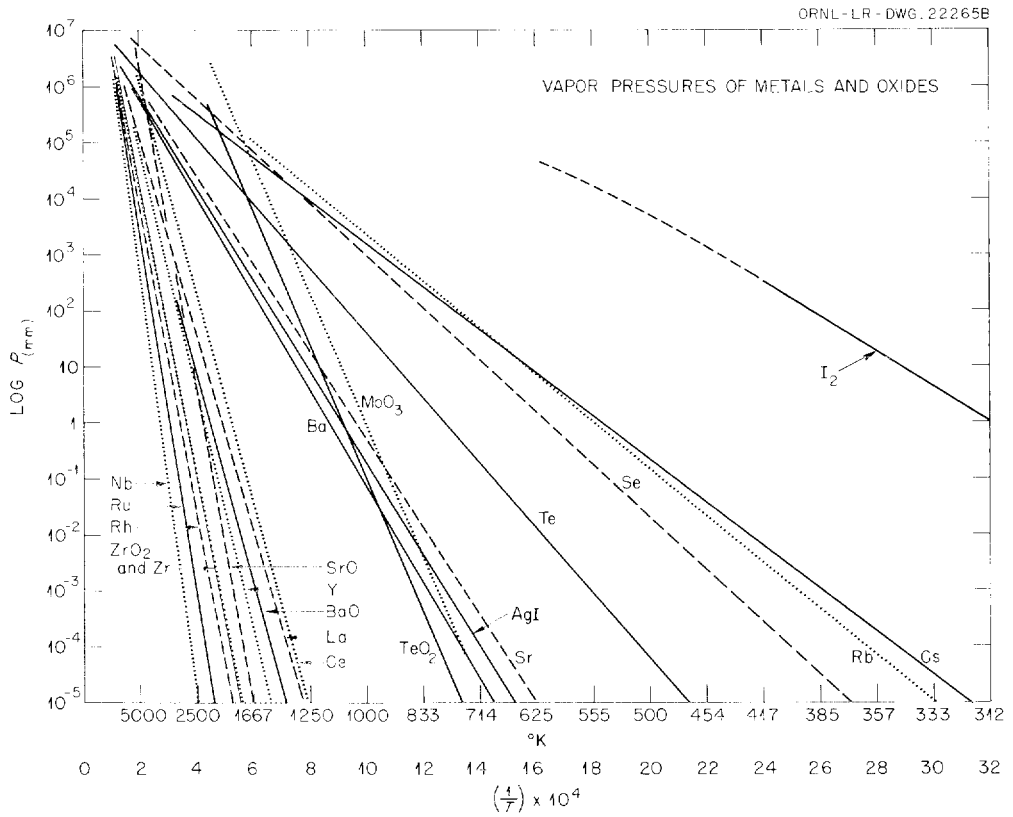

Fig. 4.57. Vapor Pressures of Metals and Oxides. (From Creek et al., ref. 26, p. 6.)

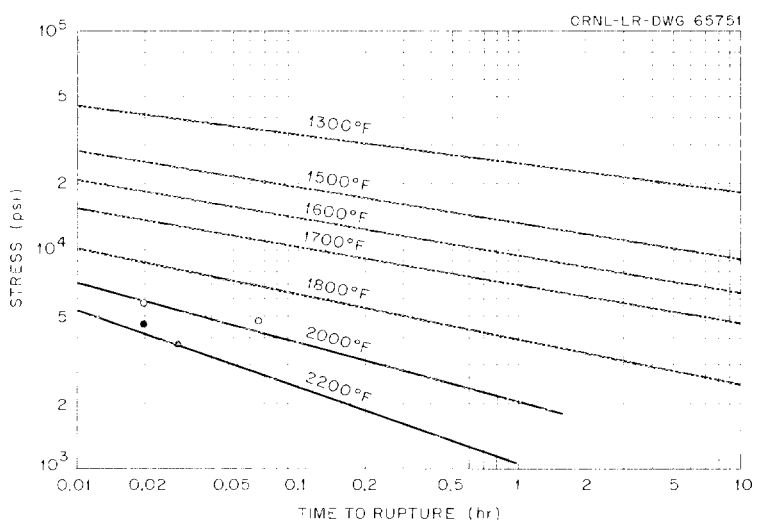

Fig. 4.58. Stress-Rupture Properties of Type 304 Stainless Steel Tube. (From Venard, ref. 27, p. 8.)

here were obtained with small fuel specimens under controlled conditions, and therefore extrapolation to full-size reactor systems in general cannot be justified at the present time. Further experiments are under way that should clarify the basic fundamental and scaleup effects of release on meltdown or overheating of fuel. Consequently, these results are subject to considerable updating in the near future.

4.3.3.1 Release from Oxidized UO_2

Release of fission products from molten UO_2 has been studied extensively in out-of-pile tests on a small scale by Parker and his associates.[28] Most of the following data are taken from ref. 28.

Results of oxidation experiments on trace-level irradiated PWR-type sintered UO_2 of 93% theoretical density are shown in Fig. 4.59. A distinct discontinuity in fission-product release can be seen in the temperature range 800 to 900°C, which is also the temperature range at which the minimum oxidation rate in air occurs after an oxidation time in excess

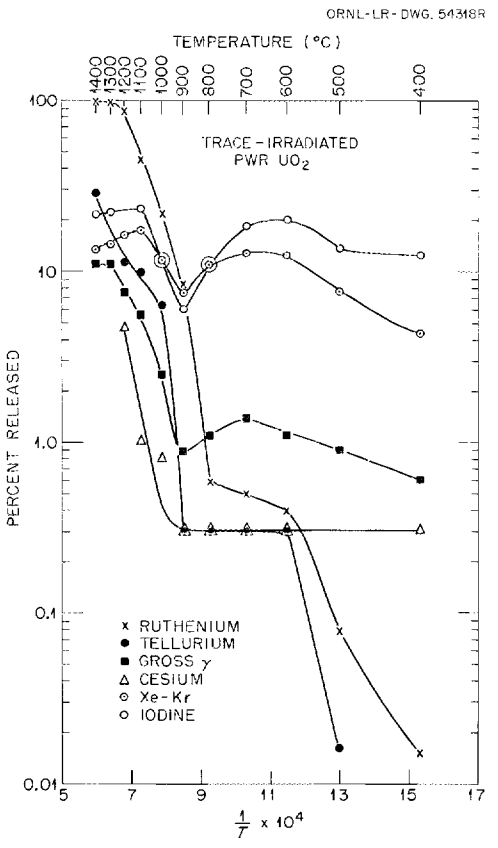

Fig. 4.59. Fission-Product Release by the Oxidation of PWR-Type UO_2 to U_3O_8 in Air (Trace-Level Irradiation). (From Parker et al., ref. 28, p. 12.)

of 1 hr. The minimum oxidation rate[29] effect can be confirmed by Fig. 4.60. Parker believes this effect to be "associated with the occurrence of the maximum degree of plastic deformation of the U_3O_8 oxidation product at this temperature, thereby affording a maximum degree of surface-layer protection against further oxidation."

Figure 4.61 shows release data for UO_2 oxidized in air after irradiation to an exposure of 1000 and 4000 Mwd/ton. The same data are shown more completely in Tables 4.11 and 4.12. Table 4.13 shows oxidation data for irradiation to an exposure of 7000 Mwd/ton.

Comparison of the data from trace-level irradiated and higher burnup samples shows that release is higher at higher burnups. Parker states that the higher oxidation rate may be due to fission-product impurity defects in the UO_2 and the greater surface area of the irradiated samples which cracked into smaller, irregular pieces during irradiation.

4.3.3.2 Release from Molten UO_2

1. Out-of-Pile Test. Table 4.14 gives results of experiments on release of fission products from very small samples of UO_2 melted in the arc-image furnace in helium, in air, and in CO_2 atmospheres after irradiation to various levels of exposure. In a reactor accident it is unlikely that UO_2 would remain molten for a long period of time because it would flow to a cooler zone in the reactor. Therefore, the experiments described in Table 4.14 were designed to maintain the UO_2 in a molten state for a short period of time. The most important condition is a simulated meltdown in a steam atmosphere. In general, the release results obtained in steam do not differ greatly from those obtained in impure helium or CO_2.

2. Effect of Scaleup. Table 4.15 shows the results of a series of meltdown experiments performed on a much larger scale (29 g of UO_2) by means of radiant heating from a tungsten crucible used as a susceptor for induction heating. Comparison of Table 4.15 with Table 4.14 for helium shows lower releases from the larger samples for all the fission products except iodine and barium. Table 4.16 shows the results of experiments using central heating of the UO_2 pellets by a tungsten resistor rod. These results appear to yield lower fractions released than those obtained using external heating from the crucible, except for ruthenium, strontium, and barium. The rare-gas release values shown in Table 4.16 indicate, however, that not all the UO_2 was molten. The fraction of xenon-krypton release can be taken as a rough measure of the fraction of fuel that was molten.

3. Effect of Cladding. Melting UO_2 in contact with stainless steel resulted in a heterogeneous, segregated residue, whereas Zircaloy apparently wet the molten UO_2 and formed a solid solution.[30] Zircaloy-clad specimens gave a reduction of about 100 in tellurium release, an increase from 1 to 10% in the release of strontium, and an increase from 3 to 7% in the release of barium. Parker states that these effects may be due to oxygen depletion of the system by hot zirconium and, also, partly due to the longer duration of heating.

4. Summary of Out-of-Pile Tests. The data presented above can be used to qualitatively evaluate the three separate methods of out-of-pile

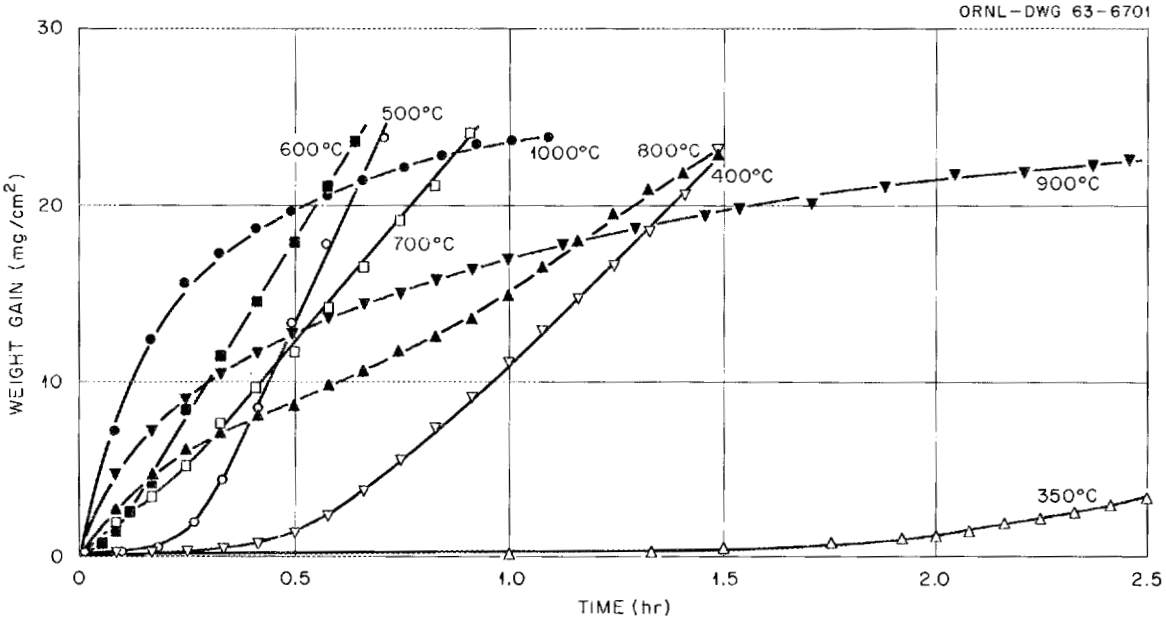

Fig. 4.60. Oxidation of UO_2 in Air at 350 to 1000°C. (From Peakall et al., ref. 29.)

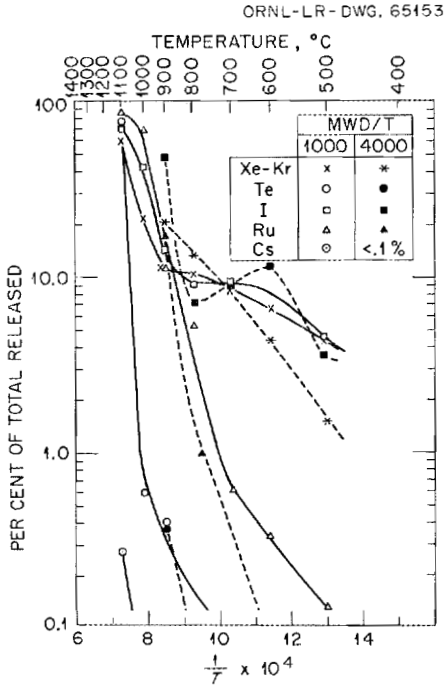

Fig. 4.61. Fission-Product Release by Oxidation of Highly Irradiated UO_2 (1000 and 4000 Mwd/ton). (From Parker et al., ref. 28, p. 12.)

Table 4.11. Fission-Product Release from UO_2 Oxidized in Air[a]

Sample: Intermediate-density PWR-type UO_2 (93–94% of theoretical)
Irradiation: 1000 Mwd/ton
Air flow: 100 cm^3/min

Temperature (°C)	Time at Temperature (min)		Percentage of Individual Fission Products Released							
	He	Air	Rare Gases	I	Te	Cs	Ru	Sr	Ba	U
500		9	4.4	4.6	<0.014	0.02	0.013	<0.001	<0.0009	
	15	13	4.0	2.5	<0.003	<0.0008	<0.014	<0.004	<0.001	
	15	90	4.0	4.7	0.008	<0.002	0.36	<0.004	<0.0008	
600		11	6.6	3.4	0.003	0.004	0.33	0.003		
	15	13	6.0	5.6	<0.003	<0.0007	<0.23	<0.001	0.0009	
	12	90	5.5	6.0	0.005	0.003	0.9	<0.0009	<0.0009	
700		12	8.5	9.4	0.01	0.001	0.63	0.001		
	15	12	7.2	10.1	<0.003	<0.003	1.25	<0.0009	<0.001	
	13	90	8.3	10.0	<0.003	0.02	3.8	<0.0008	<0.0007	
800		15	10.5	9.1	0.05	0.016	5.2	0.0006		
	13	14	8.56	11.2	0.033	0.038	6.6	0.008	0.0006	
	13.5	90	15.1	14.1	0.08	<0.007	35.3	<0.001	<0.002	
900		15	11.2	15.2	<0.4	0.005	18.9	<0.001		
	10	14	11.9	14.4	<0.85	0.03	11.5	<0.002	<0.01	
	12.5	90	13.7	26.9	0.41	<0.002	30.3	<0.001	<0.0015	
1000		26	30.3	55.2	<7.7	0.07	81.5	<0.001	<0.007	
	10	18	22.2	42.2	<0.6	~0.03	69.8	<0.001	0.002	0.007
	12	90	30.5	73.3	31.3	0.02	97.9	0.002	0.005	<0.0012
1100	8	10	60.0	70.4	75.3	2.8	85.7	<0.001	<0.002	0.002
	12.5	11	49.9	64.1	28.0	<0.01	95.5	0.001	<0.016	
	12.5	90	52.7	71.2	58.0	<0.4	99.9	<0.2	<0.2	0.19
1200	17	15	79.6	86.6	59.4	<0.1	97.8	<0.03	0.1	
	14.5	90	77.0	83.4	75.9	4.5	99.7	0.14	0.14	0.142

[a]From Parker et al., ref. 28, p. 13.

Table 4.12. Fission-Product Release from UO_2 Oxidized in Air[a]

Sample: Intermediate-density PWR-type UO_2 (93–94% of theoretical)

Irradiation: 4000 Mwd/ton
Air flow: 100 cm^3/min

Temperature (°C)	Time at Temperature (min)		Percentage of Individual Fission Products Released							
	He	Air	Rare Gases	I	Te	Cs	Ru	Sr	Ba	U
500	16	23	1.5	3.6	<0.007	<0.0004	<0.005	<0.0004		
	18	90	2.9	3.2	<0.01	<0.0007	<0.01	<0.0004	<0.0008	
600	14	18	4.4	10.3	<0.006	0.002	0.075	<0.001		
	15	90	4.5	8.0	8.4	<0.001	1.8	<0.001	<0.004	
700	14	12	9.25	9.6	0.01	0.001	1.7	<0.0002	<0.0004	
	13.5	15	7.0	10.4	0.004	<0.001	0.44	<0.0003	<0.0006	
	14	90	6.8	6.5	<0.05	<0.0005	2.3	<0.0004	<0.002	
800	13	15	13.8	7.1	0.007	0.015	1.0	<0.0004	<0.0007	
	14	90	13.8	15.6	<0.06	<0.0096	11.9	<0.0004	<0.001	
900	14	19	20.5	48.9	0.4	0.009	17.3	<0.0001	0.01	
	15	90	21.5	47.1	6.0	0.015	53.1	<0.0008	<0.004	
1000	16	15	39.5	84.	11.5	0.09	72.1	<0.0003	<0.0016	
	13.5	90	43.8	75.	31.7	0.37	91.8	0.14	0.082	0.06
1100	14	14	66.0	79.4	15.9	<0.17	90.8	<0.05	<0.0032	
	14	90	73.4	83.6	38.6	0.19	99.3	0.006	0.014	<0.003
1200	14	16.5	71.3	81.7	37.1	0.76	89.9	<0.01	<0.001	
	13	90	79.7	94.5	66.4	6.4	99.6	0.0065	0.7	<0.0025

[a]From Parker et al., ref. 28, p. 14.

Table 4.13. Fission-Product Release from UO_2 Oxidized in Air[a]

Sample: High-density PWR-type UO_2 (96% of theoretical)
Irradiation: 7000 Mwd/ton
Air flow: 100 cm^3/min

Temperature (°C)	Time at Temperature (min)		Percentage of Individual Fission Products Released						
	He	Air	Rare Gases	I	Te	Cs	Ru	Sr	Ba
500	16	90	3.1	4.1	<0.5	0.0006	0.1	<0.0007	<0.0004
600	13.5	90	4.2	3.1	<0.01	<0.002	0.7	<0.0004	<0.009
700	15.5	90	6.1	15	<0.08	<0.005	0.1	<0.0005	<0.007
800	14	90	9.4	9.0	<0.3	0.002	9.8	<0.0005	0.03
850	13.5	90	15	34	<1.4	0.02	35	<0.0005	<0.08
900	16.5	90	34	29	80	<0.01	78	<0.03	<0.8
1000	16.5	90	86	78	37	<0.03	93	<0.04	<0.2

[a]From Parker et al., ref. 28, p. 15.

Table 4.14. Effect of Burnup Level and Atmosphere on the Release of Fission Products During the Melting of UO_2[a,b]

Atmosphere	Irradiation Level (Mwd/ton)	Sample Weight (g)	Number of Results	UO_2 Vaporized (%)	Percent of Individual Fission Products Released							
					Xe-Kr	I	Te	Cs	Ru	Sr	Ba	Rare Earths
Helium (impure)	Tracer	0.22	2		99.5	89.7	92.0	91.3	61.0	2.1	4.6	2.2
	2,800	0.03	3	21.2	99.9	92.2	98.2	98.5	90.4	2.1	6.6	5.1
	11,000	0.03	2	18.0	100.0	99.7	99.6	98.7	88.1	1.7	6.5	4.1
Air	Tracer	0.2	2		98.4	94.9	79.1	37.7	67.7	0.2	0.5	0.5
	2,800	0.04	3		100.0	99.7	93.6	92.5	95.0	0.4	1.8	3.0
	11,000	0.04	3	24.7	100	99.8	99.3	97.4	92.5	0.4	1.8	3.9
CO_2	Tracer	0.2	3	14.1	80.6	76.8	71.2	60.9	44.9	0.3	1.1	0.85
	2,800	0.02	3		99.9	98.7	98.6	90.2	74.3	0.5	2.5	2.8
	11,000	0.05	3		99.9	99.9	99.0	96.6	79.1	0.6	2.9	2.3

[a]EGCR UO_2 with an oxygen-to-uranium ratio of 2.04 and an average density of 95% of theoretical.

[b]From Parker et al., ref. 28, p. 17.

Table 4.15. Fission-Product Release from UO_2 Melted in Helium by the Tungsten-Crucible Method[a]

Sample: 29 g of PWR-type UO_2, trace-irradiated
Atmosphere: purified helium, 700 cm^3/min

Time (min)		UO_2 Vaporized (%)	Percentage of Fission Products Released								
Preheat	Molten		Gross Gamma	Rare Gases	I	Te	Cs	Ru	Sr	Ba	Ce
4.75	1.0	0.097	22.6	92.9	98.1	81.0	62.5	0.45	0.33	4.8	0.05
5.0	1.5	0.157	15.1[b]	98.0	98.3	82.8	66.0	0.05	0.47	2.57	0.07
4.75	2.0	0.156	25.6	99.3	98.8	99.1	59.6	0.32	0.41	2.95	0.17
4.5	2.5	0.246	12.6[b]	99.0	95.0	98.9	72.0	0.33	0.53	2.4	0.13
4.5	1.5		13.7[b]	98.7	88.4	91.8	80.2	0.20	0.26	2.6	0.40
4.5	2.5		12.6[b]	99.3	92.9	96.2	89.4	0.70	0.50	3.6	0.10

[a]From Parker et al., ref. 30, p. 9.

[b]Decayed one week longer than previous sample.

Table 4.16. Fission-Product Release from Single-Element UO_2 Melted in a Tungsten Resistor Furnace[a]

Sample: 39 g of PWR-type UO_2, trace-irradiated
Atmosphere: pure helium flowing at a rate of 400 cm^3/min

Element	Heat Duration (min)	UO_2 Vaporized[b] (%)	Percentage of Fission Products Released								
			Gross Gamma	Xe-Kr	I	Te	Cs	Ru	Sr	Ba	Ce
UO_2	5.0	0.8	7.1	63	47	56	<44	1.6	1.6	5.3	<0.6
UO_2	4.0	0.15	5.7	50	30	42	41	0.4	0.8	2.9	<0.5
UO_2	4.4	0.3	6.9	34	25	33	>40	<0.05	1.2	4.3	0.5
UO_2[c]	4.7	0.2	5.0	56	52	31	46	0.5	1.0	4.2	<0.3
UO_2[d]	7.0	0.1	2.6	52	24	1.1	28	0.1	11	11	0.5
UO_2[d]	6.7	0.04	5.2	41	50	0.6	32	0.2	9.9	7.5	0.5
UO_2 + BeO[e]	1.5	20	30	100	90	92	91	61	2.1	4.6	2.2

[a]From Parker et al., ref. 30, p. 18 (revised).

[b]Includes material removed by spattering.

[c]Stainless steel clad.

[d]Zircaloy clad.

[e]Previous results of melting microsize sample of highly irradiated UO_2 in impure helium by use of the carbon-arc image method.

heating by expressing (as in Table 4.17) the fission-product releases as a fraction of the UO_2 that was molten, assuming that the fraction of rare-gas release is an index of the fraction that was molten. The arc-image method yielded disproportionately high values of ruthernium release. This may have been due to the use of impure helium as the atmosphere and the use of small samples, with resultant oxidation of Ru to RuO_3 or RuO_4.

5. In-Pile Tests. Tables 4.18 and 4.19 show early results obtained by Browning et al.[32,33] in a small-scale in-pile meltdown experimental program instituted to discover differences between small-scale out-of-pile meltdowns and in-pile meltdown. In these experiments, small samples of stainless-steel-clad UO_2 were allowed to build up a fission-product inventory, and then meltdown was effected by rapid insertion of the samples

Table 4.17. Summary of Fission-Product Release from Molten Unclad UO_2 by Various Methods of Meltdown in a Helium Atmosphere

$$\frac{(\%\text{ released from specimen})}{(\%\text{ rare-gas release})} \times 100 \approx \%\text{ released from molten portion}$$

Time (min)		Percentage of Fission Products Released from Molten Portion[a]								
Preheat	Molten	Rare Gas (uncorrected)	Gross Gamma	I	Te	Cs	Ru	Sr	Ba	Ce
Induction Heating Coupled on Tungsten Crucible Holding UO_2 Specimen[a]										
4.75	1.0	92.9	24.3	105	87.2	67.3	0.48	0.36	5.2	0.054
5.0	1.5	98.0	15.4	100	84.5	67.3	0.051	0.48	2.6	0.071
4.75	2.0	99.3	25.8	99.5	99.8	60.0	0.322	0.41	2.97	0.13
4.5	2.5	99.0	12.7	95.9	99.9	72.7	0.33	0.54	2.4	0.13
4.5	1.5	98.7	13.9	89.6	93.0	81.3	0.20	0.26	2.63	0.41
4.5	2.5	99.3	12.7	93.5	96.9	90.0	0.70	0.50	3.6	0.10
	High	99.3	25.8	105	99.9	90.0	0.70	0.54	5.2	0.41
	Median (low)	98.7	13.9	95.9	93	67.3	0.32	0.41	2.6	0.10
	Low	92.9	12.7	89.6	84.5	60	0.051	0.26	2.4	0.05
Center Tungsten Resistor Heating[b]										
	5	63	11	75	89	<70	2.5	2.5	8.4	<1.0
	4	50	11	60	84	82	0.8	1.6	5.8	<1.0
	4.4	34	20	74	97	>118	<0.15	3.5	13	1.5
	High	63	20	75	97	>118	2.5	3.5	13	1.5
	Median	50	11	74	89	82	0.8	2.5	8.4	<1.0
	Low	34	11	60	84	<70	<0.15	1.6	5.8	<1.0
Arc-Image Furnace Specimen Melted Simultaneously with BeO Crucible[c]										
	2	64	14.6	110	93	91.4	43.4	0.281		
	2	90.5	14.5	77.7	79.2	27.1	66.1	0.077	0.86	0.25
	2	92.7	6.47	90.3	92.4	36.1	34.5	0.173	0.971	1.2
	3	56.7	13.6	118	112	42.3	132	0.186	2.3	1.24
	3	62.8	21.8	73.7	85.3	19.4	57	0.175	4.1	0.79
	2	69.1	14.9	73.8	61.8	10.3	29.2	0.38	0.65	0.39
	2	99.4	29.8	84.7	86.3	90.2	72.1	0.20	2.0	0.7
	1 1/2	99.6	30.7	95.6	96.6	93.1	76.6	0.91	7.3	3.8
	High	99.6	30.7	118	96.6	93.1	132	0.91	7.3	3.8
	Median (low)	69.1	14.9	90.3	86.3	36.1	66.1	0.186	2.0	0.79
	Low	56.7	13.6	73.7	61.8	10.3	34.5	0.077	0.65	0.25

[a]Ratio of release of percentage release from specimen to percentage release of rare gases.

[b]From Parker, ref. 30.

[c]From Parker et al., ref. 31.

Table 4.18. Material Released from the Fuel in UO_2 Melting Experiments[a]

Experiment	Release (%)								UO_2 Vaporized (%)[b]
	^{131}I	^{132}Te	^{137}Cs	^{106}Ru	^{89}Sr	^{140}Ba	^{95}Zr	^{144}Ce	
2				83	99.8	99.8	87	93	50
3				48	93	96	87	85	43
4	99.6			81	77	94	56	59	44
5	99.4	99.2	98	91	57	55	43	44	34
6	99.0	95	99.3	59	55	52	60	49	47
7	96		96	11	5.2	14	0.91	2.5	0.72
8	99.0	98	98	57	44	70	58	43	36
9	99.7	99.1	99.0	93	71	71	72	70	70
10	97	96	96		69	72	58	59	56
11	98	99.4	96	48	18	26	12	7.6	5.1

[a]Sample length, 1 in.; diameter, 0.210 in.; sample molten 5 min except experiment 2, 10 min; helium velocity evaluated at fuel melting point, 60 fpm, except experiments 10 and 11, 125 and 350 fpm.

[b]Includes material removed by spattering.

Table 4.19. Material Released from High-Temperature Zone[a] of the Furnace in UO_2 Melting Experiments

Experiment	Release (%)								UO_2 Vaporized (%)[b]
	^{131}I	^{132}Te	^{137}Cs	^{106}Ru	^{89}Sr	^{140}Ba	^{95}Zr	^{144}Ce	
2				3.3-5.1	21	17-27	0.12	0.60	4.1
3				0.64	1.2	0.73	0.10	1.8	0.052
4	91			5.9	2.3	0.94	0.036-0.044	0.30-0.40	0.077
5	88	80	82	5.2	1.4	2.3	0.019	0.32	0.23
6	94	52	82	0.70-1.3	0.91	0.55	0.090	0.068	0.29
7	50	12	74	1.8-2.2	0.87	0.58	0.037	0.32	0.015
8	95	82	88	1.7	1.3	0.82	0.051	0.24	0.020
9	80	90	59	3.8	0.97	1.1	0.12	0.30	0.013
10	89	72	81		2.1	2.8	2.8	1.0	0.29
11	89	69-92	88	0.13-0.17	2.9	8.0	0.57	1.2	1.6

[a]High-temperature zone includes fuel material and thermal insulation; minimum temperature, 1000°C; sample length, 1 in.; diameter, 0.210 in.; sample molten 5 min except experiment 2, 10 min; helium velocity evaluated at fuel melting point, 60 fpm, except experiments 10 and 11, 125 and 350 fpm.

[b]Includes material removed by spattering.

into a higher flux region of the reactor. The conditions of the experiment are described in the tables. A diagram of the reactor furnace used for the experiments is shown in Fig. 4.62. It is to be noted that the material in closest proximity to the fuel pellet is thoria, since this material is not representative of full-scale reactors. There is qualitative agreement between the values of Tables 4.19 and 4.15, when the hot-zone data of Browning are compared with the meltdown-zone data of Parker's experiments. This further illustrates that the effect of stainless steel cladding is not too significant.

At the time of this writing, much significant work is under way, the results of which are unfortunately not presently available. Information

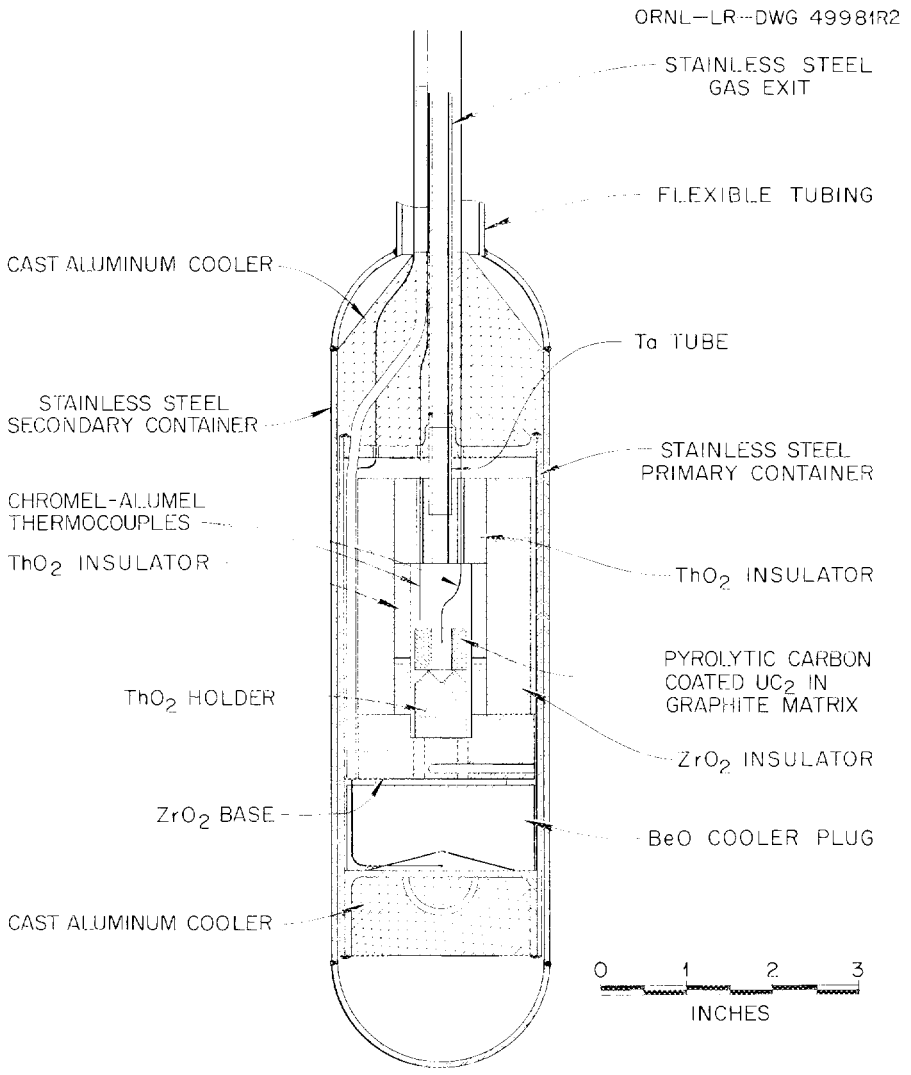

Fig. 4.62. Reactor Furnace for Meltdown Experiments. (From Browning, ref. 34, p. 30.)

in nuclear safety program semiannual progress reports published since this writing may provide a more definitive indication of the extent of fission-product release from UO_2.

The chemical nature of released fission products in many cases has not yet been experimentally determined. The best that can be done at present is to work on theoretical grounds from the known free energies of the elements involved. This is beyond the scope of this report, but the information should soon be available elsewhere.[35]

4.3.4 Release from Non-UO_2 Fuel

4.3.4.1 Release from Metallic Uranium

Metallic uranium fuel, although of decreasing importance in power reactors, is used extensively in low-temperature plutonium-production reactors. Some work has been carried out at Hanford on the release of fission products from metallic uranium and has been summarized by Hilliard and Reid.[36] The data given here are taken from that report. (Oxidation rates of uranium and fission-product release from pure uranium and uranium alloys are discussed in more detail in a forthcoming report.[35])

A series of tests on trace-irradiated natural uranium (2.5×10^{14} neutrons/cm^2) heated in air, steam, and helium showed that xenon, iodine, and tellurium were volatile, cesium and ruthenium were semivolatile, and all other fission-product elements were released in amounts less than 0.5% under the conditions used (temperatures up to 1440°C; times up to 3 hr). The volatile elements were released roughly in proportion to the percentage of uranium oxidized to U_3O_8, with release being highest in air, next highest in steam, lowest in helium. Ruthenium behaved as a nonvolatile element until all the uranium had been oxidized, after which it appeared to be volatile. This phenomenon is explainable on the basis of the free energy of formation of RuO_4 and U_3O_8.

Further tests were performed on uranium irradiated to burnups as high as 4×10^{20} neutrons/cm^2 (1340 Mwd/T). Higher irradiation levels gave greater fractional releases of xenon, iodine, and cesium but not of tellurium, strontium, barium, ruthenium, molybdenum, cerium, zirconium, neptunium, plutonium, or uranium. Table 4.20 shows the effect of irradiation level on the fractional release from 1/4-in.-diam, 3/4-in.-long specimens heated for 24 min at 1200°C.

Not only was the fractional release of xenon, iodine, and cesium greater for higher burnups, but the release occurred more rapidly; i.e., as a burst at the time the uranium melted. Figure 4.63 shows this effect for xenon. In the test on uranium irradiated to 4×10^{20} neutrons/cm^2 all the xenon had been released within 2 min, whereas for specimens with lower irradiation the release continued throughout the heating period.

Other conclusions of the study were that

1. Burnup *per se* did not influence the uranium oxidiation rate. However, as the fission-gas bubbles expanded and broke through the semiprotective oxide layer, the molten uranium flowed out and exposed greater area for oxidation, giving a net result of a larger percentage oxidized.

Table 4.20. Effect of Irradiation Level on Release of Fission Products from Metallic Uranium

Element	Fraction Released from Specimen[a] After Indicated Irradiation		
	10^{14} neutrons/cm^2	10^{18} neutrons/cm^2	4×10^{20} neutrons/cm^2
Xenon	0.70	0.95	1.00
Iodine	0.60	0.85	0.98
Cesium	0.30	0.60	0.80
Tellurium	0.65	0.65	0.65
Strontium	0.005	0.005	0.005
Barium	0.005	0.005	0.005
Ruthenium	0.001	0.001	0.04
Molybdenum	(b)	0.001	0.04
Zirconium	0.0003	0.0003	0.0003
Cerium	0.0001	0.0001	0.0001
Neptunium	(b)	0.0005	(b)
Plutonium	(b)	(b)	0.0004
Uranium	(b)	(b)	0.0003
Uranium oxidized[c]	0.70	0.70	0.92

[a] 11.7-g cylinders heated in air 24 min at 1200°C.

[b] Not analyzed.

[c] Fraction of specimen.

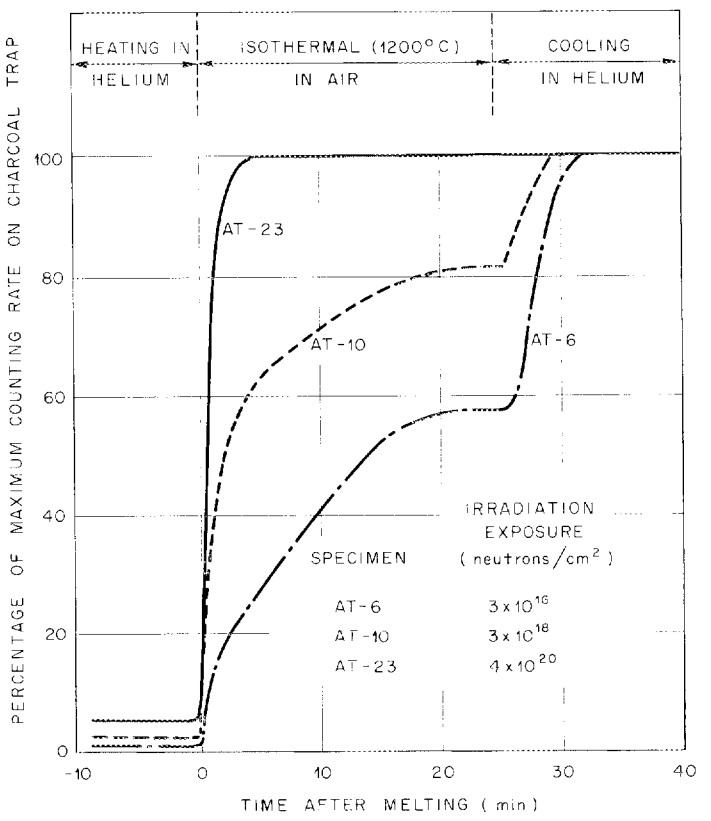

Fig. 4.63. Effect of Burnup on Rate of Release of Xenon from Metallic Uranium.

2. Ruthenium and molybdenum were released to a greater extent at the highest burnup investigated, but this was an indirect effect. As noted in the trace-level work, ruthenium was nonvolatile in the elemental form, but was very volatile when oxidized to RuO_4. In the high-level tests more surface area for oxidation provided more opportunity to form the volatile RuO_4 and MoO_3.

Full-scale meltdown tests with unirradiated fuel elements yielded the surprising conclusion that both aluminum and Zircaloy-2 cladding inhibited the flow of uranium even at 300°C above the melting point of uranium.

4.3.4.2 Release from Graphite-Matrix Fuel Elements

In-pile experiments were conducted by Browning et al.[33,37] on the release of fission products during burning of pyrolytic-carbon-coated uranium dicarbide particles in a graphite matrix. Fission and gamma heat produced sufficiently high temperatures for the fuel to burn in air at temperatures up to ~1400°C. The sample was burned for 15 min, during which about half of each specimen was consumed; however, less than half of the uranium was in the burned portion because of nonuniform distribution of fuel particles in the graphite matrix and preferential oxidation of the unfueled graphite.

The results of two of these experiments are given in Table 4.21. The relatively low release from the fuel may be due, in part, to trapping

Table 4.21. Results of In-Pile Fuel Burning Experiments with Graphite-Matrix Uranium Dicarbide Fuel Elements[a]

	Material Found (Percentage of Total in Assembly)								
	^{89}Sr	^{95}Zr	^{106}Ru	^{131}I	^{132}Te	^{137}Cs	^{140}Ba	^{144}Ce	U
Unburned fuel[b]									
Experiment 1	50.6	58.2	27.0	59.7	47.6	38.1	51.7	54.8	61.9
Experiment 3[c]	75.4	83.9	87.0	82.4	76.1	39.1	84.9	85.3	93.9
Outside of fuel residue[d]									
Experiment 1	13.8	3.7	48.2	28.9	42.7	51.3	14.5	9.05	2.12
Experiment 3	13.1	5.04	8.81	16.5	23.2	54.5	6.96	6.98	0.877
Retained in furnace									
Experiment 1	98.8	99.5	59.3	73.2	64.9	63.0	99.5	93.8	99.6
Experiment 3	98.7	98.7	94.3	85.6	85.7	58.4	99.3	97.1	99.8

[a]Sample length, 0.5 in.; diameter, 0.6 in. with 0.25-in.-diam axial hole; sample burning time, 15 min; air flow, 400 cm^3/min.

[b]58.6% of the sample was burned in experiment 1 and 41% in experiment 3.

[c]The specimen of experiment 2 was not analyzed because of its low uranium content.

[d]Fuel materials on all exposed surfaces except the unburned portion of the specimen, fuel particles and powder, and the floor of the conbustion furnace.

of fission products within the pyrolytic-carbon-coated microspheres (~150 μ), some of which fell out of the graphite matrix and did not burn completely with the matrix. The high ruthenium release was probably due to the formation of ruthenium oxide.

4.3.5 Particulate Generation During Fuel Meltdown

The generation of particulate matter during a reactor accident is of major concern because of the different transport behavior of the fission products adsorbed on particulate matter as compared with elemental forms. The sizes of particles that emanated from UO_2 melted in an arc-image furnace in helium, in air, and in CO_2 are shown in Fig. 4.64. In helium, almost all the particles, by count, were <0.06 μ in diameter.

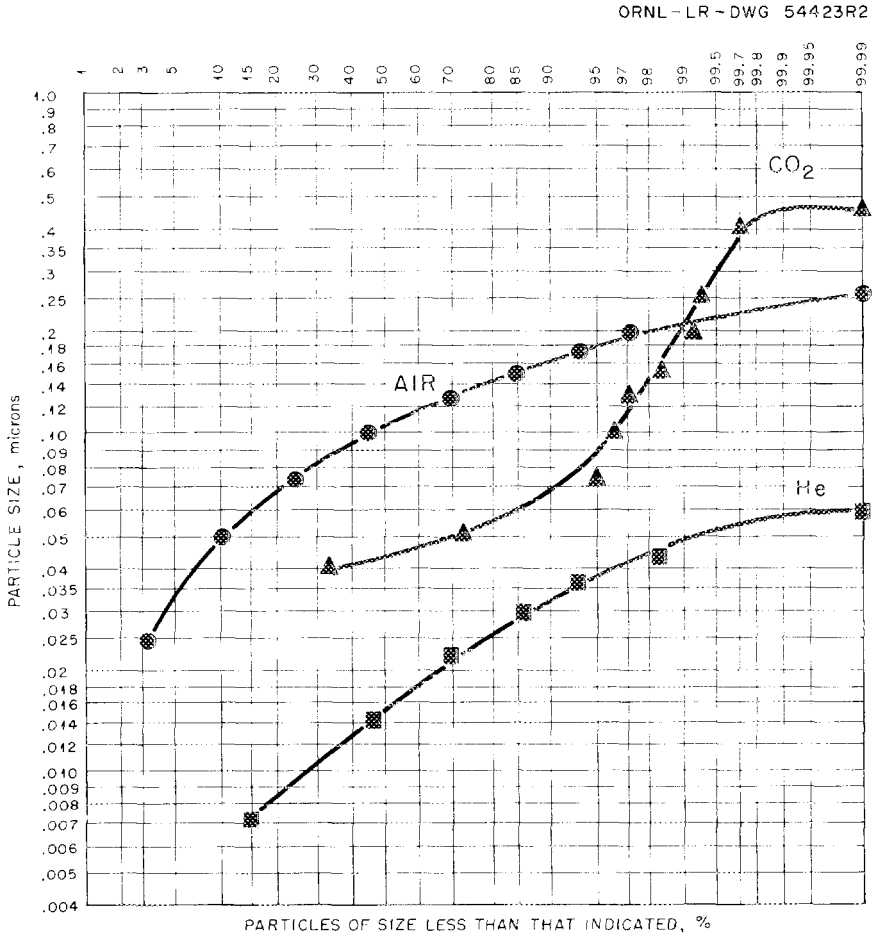

Fig. 4.64. Sizes of Particles that Emanated from UO_2 Melted in Helium, in CO_2, and in Air in an Arc-Image Furnace. (From Parker et al., ref. 28, p. 18.)

The maximum sizes in CO_2 were 0.45 μ and 0.2 μ in air; however, in CO_2 there was a larger fraction of smaller sizes than in air.

The effects of stainless steel cladding on UO_2 melted in helium are shown in Fig. 4.65. The presence of stainless steel reduced the maximum particle size, but the distribution of particles of sizes of less than 0.20 μ was similar to that for unclad UO_2. The experiments yielding the results of Fig. 4.65 were done with central heating by means of a tungsten resistor, and larger particle sizes were found than in the arc-image furnace experiments (Fig. 4.64) or a tungsten-crucible heating experiment (Fig. 4.66). The reasons for this effect are not known but may be due to faster agglomerations in the resistor-heated elements because of a larger initial concentration of particulate matter and perhaps greater agitation.

4.4 FISSION-PRODUCT TRANSPORT

4.4.1 Transport Within the Primary System*

After release from the fuel, the fission products will spread from the primary system to the interior of the containment vessel. Prediction of the fraction of the activity that will escape from the primary system is complicated and depends on the particular conditions existing in a given reactor following the accident.

In theory, the chemical composition of the effluents from molten or oxidizing fuel could be characterized, and the adsorption and chemisorption of the effluents on structural materials could be calculated for simple geometries. In practice, however, this picture is confused by the presence of particulate matter, which would have chemical properties different from those of gaseous materials. The distribution of given fission products between the free and particulate forms and the fractionation of fission products among different size particles would also need to be considered. All the above would be contingent on the knowledge of the mechanical structure of the core after the accident. The behavior of unclad pellets piled at a low point in the reactor vessel would be quite different with respect to thermal effects (natural-convection cooling, etc.) than the behavior of pellets in the coolant channels.

Research is just beginning on fundamental problems such as the characterization of fission products, fission-product fractionations, and transport under controlled conditions. Some data will be reported here, with the advice that better and more complete data should be available in the future. Results of continuing studies of fission-product deposition in a circulating helium stream have been reported[38] but will not be considered here because the conditions employed were far removed from those of probable loss-of-coolant accident conditions.

Table 4.22 gives the results of experiments on the effect of furnace air velocity in the deposition of fission products released by melting UO_2. The amounts of fission products retained in the fuel can be obtained by subtracting the total percent released from 100. It can be seen that cerium, strontium, barium, and zirconium are released in smaller

*See Appendix G for relevant information published since this chapter was prepared.

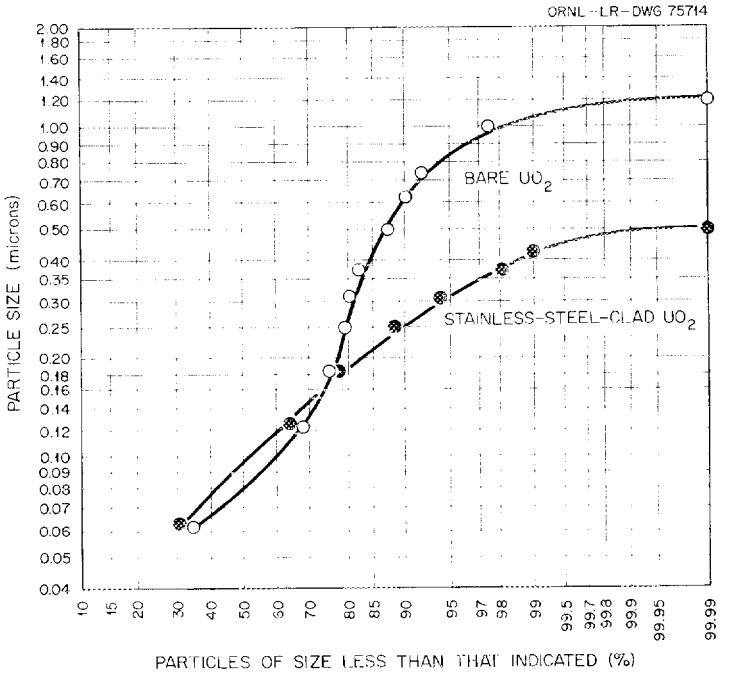

Fig. 4.65. Sizes of Particles of UO_2 Vaporized from Stainless-Steel-Clad and Bare UO_2 Fuel Pins. (From Parker et al., ref. 30, p. 24.)

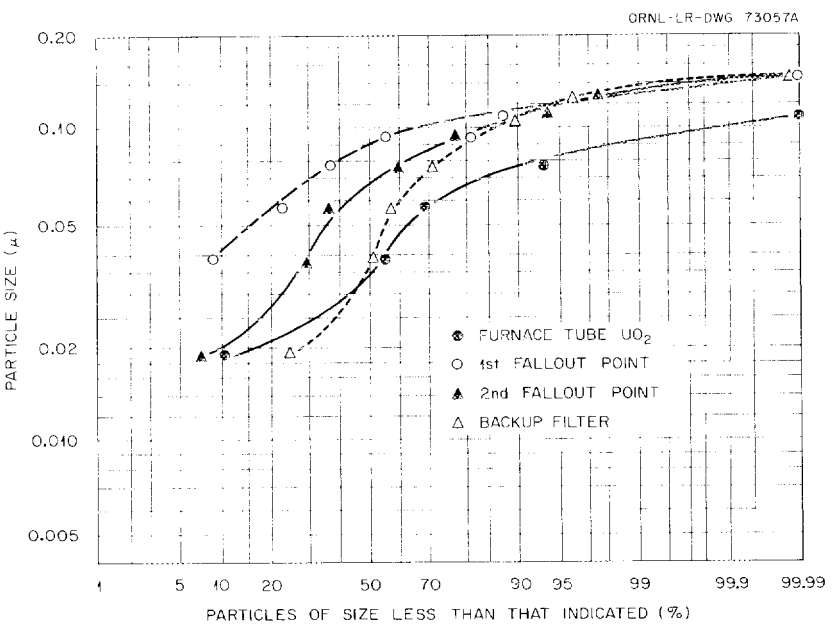

Fig. 4.66. Sizes of Particles from UO_2 Samples Melted in Helium by the Tungsten-Crucible Method. (From Parker et al., ref. 30, p. 16.)

Table 4.22. Effect of Furnace Air Velocity on Deposition of Fission Products Released by Melting Modified UO_2 Specimens at 2650°C*

	Percent of Total Activity and Its Location, with Velocity of Furnace Air as Indicated (lin ft/min)[a]							
	Furnace Tubes		Filters		Charcoal Trap		Total	
	0.3	5.0	0.3	5.0	0.3	5.0	0.3	5.0
Gross gamma	10.1	8.8	1.2	6.2	0.4	3.4	11.7	18.4
Rare gases					77.1	69.5	77.1	69.5
Iodine, γ	62.3	12.1	5.4	9.8	11.3	56.9	79.0	78.8
Tellurium, β^-	66.8	28.6	8.3	43.2			75.1	71.8
Cesium, γ	34.5	18.3	15.6	30.9			50.1	49.2
Ruthenium, γ	63.6	33.0	0.8	24.6			64.4	57.6
Cerium, β^-	0.24	0.17	0.11	0.37			0.35	0.54
Strontium, β^-	0.1	0.05	0.01				0.11	0.05
Barium, β^-	0.55	0.08	0.01	0.07			0.56	0.15
Zirconium, γ	0.02	0.02	0.01	0.01			0.03	0.03
Uranium[b]	6.4		1.4				7.8	

[a]Air flow = 200 cm^3/min or 0.3 lin ft/min or 3000 cm^3/min or 5 lin ft/min across sample; heating time = 90 sec.

[b]Vaporized as UO_3.

*From Parker et al., ref. 28, p. 18

fractions than the uranium. The more-volatile iodine, however, may be carried a considerable distance by a rapid flow of gas.

The transport effects of a helium atmosphere are indicated in Table 4.23. In this case, the furnace consisted of a tungsten crucible heated by induction heating and surrounded by a thorium oxide crucible acting as a reflector. The gas stream was passed through a miniature fallout chamber approximately 18 in. long and 3 in. in diameter, which was backed up by millipore filters placed ~9 in. downstream from the exit of the fallout chamber. Heated charcoal traps were placed 12 in. beyond that. Major differences between the two runs can be seen in Table 4.23 for iodine in the fallout chamber and in the charcoal. Differences of this magnitude were not explained.

Table 4.24 gives the distribution of released fission products from UO_2 melted in helium by the central-resistor method (unclad, stainless steel clad, and zirconium clad). The effect of zirconium cladding is a striking reduction in tellurium release at all points but shows a marked increase in strontium escape from the fuel. It can be seen, however, that strontium did not travel far in any case.

Tables 4.18 and and 4.19 (above) gave the results of some preliminary in-pile meltdown experiments with stainless steel-clad UO_2. Comparison with data in these tables shows that, although large fractions of available fission products are released from the fuel, comparatively little strontium, zirconium, ruthenium, barium, and cerium are released from

Table 4.23. Distribution of Fission Products Released from UO_2 Melted in Helium by the Tungsten-Crucible Method*

Location	Release (%)									
	Total Gamma		Iodine		Tellurium		Cesium		Strontium	
	10/24	10/31[a]	10/24	10/31	10/24	10/31	10/24	10/31	10/24	10/31
Furnace	17.8	11.6	45.3	64.1	62.9	68.5	51.6	43.6	0.2	0.4
Fallout chamber	0.8	1.1	2.8	13.5	4.7	3.0	4.5	15.8	0.1	0.04
Filter	2.8	2.3	8.0	18.1	13.4	11.3	6.4	6.8	0.02	0.04
Charcoal	1.2	0.1	42	2.8						
Total	22.6	15.1	98.1	98.5	81.0	82.8	62.5	66.2	0.32	0.48

[a]Decayed one week longer.

*From Parker et al., ref. 30, p. 10.

Table 4.24. Distribution of Fission Products Released from UO_2 Melted[a] in Helium by the Central-Resistor Method[b]

Material Released	UO_2 Specimen	Release (%)			
		Furnace Hot Zone	Base and Gas Tube	Filters	Charcoal
UO_2	Bare	0.4	0.002	0.0003	
	Stainless steel clad	0.14	0.004	0.00006	
	Zirconium clad	0.08	0.0015	0.000005	
Iodine	Bare	0.25	22	11	0.8
	Stainless steel clad	0.9	28	23	0.2
	Zirconium clad	0.2	27	9	0.4
Tellurium	Bare	2.4	33	9	
	Stainless steel clad	6	22	2	
	Zirconium clad	0.08	0.7	0.1	
Cesium	Bare	25	8	12	
	Stainless steel clad	7	25	14	
	Zirconium clad	9	15	5	
Strontium	Bare	1.2	0.02	0.001	
	Stainless steel clad	0.9	0.01	0.005	
	Zirconium clad	10	0.1	0.01	
Barium	Bare	4	0.01	0.002	
	Stainless steel clad	4	<0.02	<0.002	
	Zirconium clad	9	0.06	0.01	

[a]Bare specimens averaged 50% melting; stainless steel-clad specimen was 56% melted; zirconium-clad specimens averaged 47% melting.

[b]From Parker et al., ref. 30, p. 25 (revised).

the high-temperature zone, defined as the region having a minimum temperature of 1000°C. However, iodine, tellurium, and cesium did escape the hot zone in large quantities.

4.4.2 Chemical and Physical Behavior of Released Fission Products*

Castleman[39] at Brookhaven has done experiments on the behavior of fission-product iodine, cerium, barium, lanthanum, molybdenum, and tellurium released from metallic uranium in purified helium and in air. The following material is taken from his report.

4.4.2.1 Release Experiments

The condensation temperature of specific fission products released from an irradiated fuel sample into a helium or an air stream was measured in the apparatus shown in Fig. 4.67. The gas stream, together with the released fission products, passed through a descending temperature gradient inside of the quartz meltdown tube. Fission products that did not deposit along the tube wall were collected in a charcoal cold trap located at the meltdown-tube exit.

Prior to heating the irradiated sample, the desired temperature gradient was established along the meltdown tube. A typical temperature profile (1200°C to ambient at 80°C/in.) is shown in curve A of Fig. 4.68. Curve B of Fig. 4.68 refers to the furnace-temperature profile applicable to the third series of experiments, described below. The sample was maintained at 1205 ± 10°C throughout each run. The fuel samples were 10-g cubes of U–3.5% Mo alloy irradiated at 3 to 9 × 10^{14} neutrons/cm^2. Purified helium was used to maintain the oxygen content at a concentration low enough to prevent oxidation of the molten uranium-molybdenum sample during the run. The effect of flow rate on the fission-product deposition zone was studied. In all cases, however, a low linear velocity was used to provide sufficient contact time between the flowing stream and the tube wall to ensure fission-product deposition in a narrow band. When the temperatures reached equilibrium, the irradiated specimen was inserted into the center of the heated collar and melted at the specified experimental conditions.

4.4.2.2 Fission-Product Behavior

The typical deposition behavior of fission products released into purified helium and into air is shown in Figs. 4.69 and 4.70, respectively. The most significant result was found in the iodine deposition from a helium stream. Invariably, iodine deposited at temperatures greater than 200°C, where the vapor pressure of elemental iodine would be much in excess of 1 atm. Due to the importance of iodine in determining reactor site criteria, most of the experimental effort was placed on a better understanding of the chemical behavior of the released iodine.

---

*See Appendix G for relevant information published since this chapter was prepared.

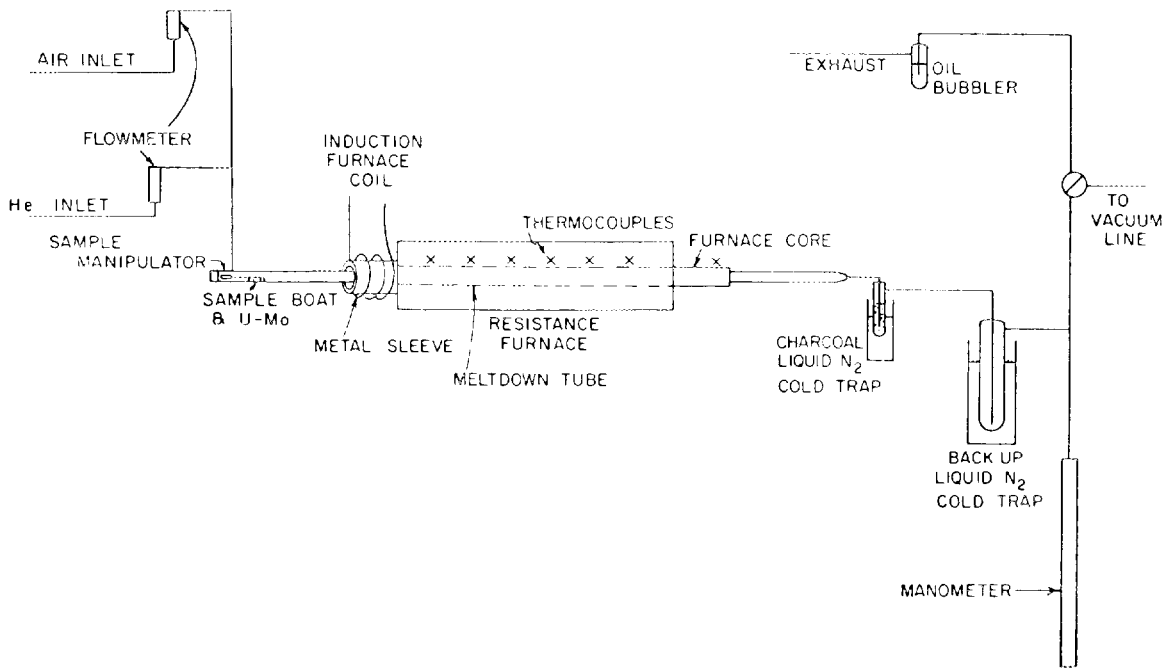

Fig. 4.67. Fission-Product Release Apparatus. (From Castleman, ref. 39.)

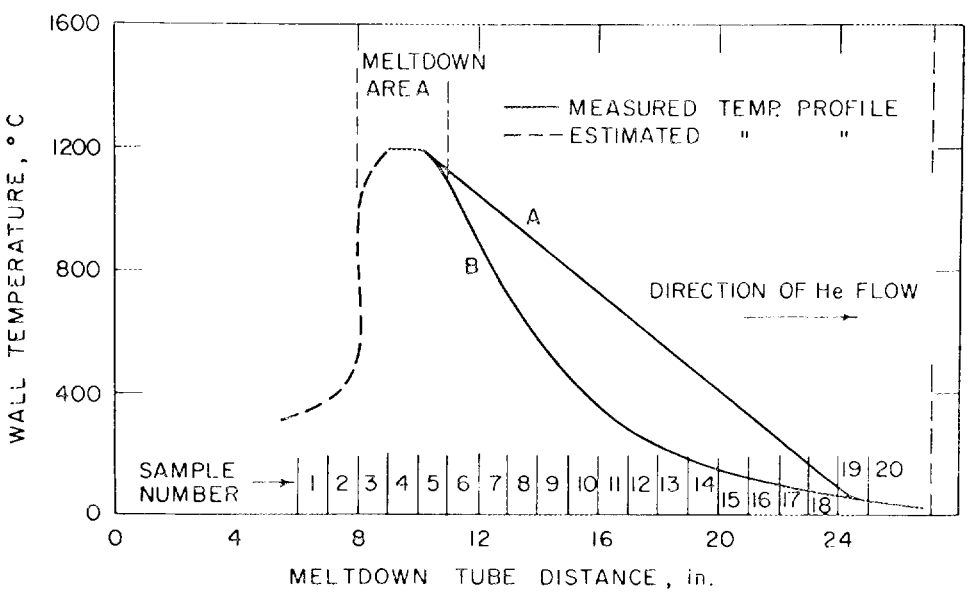

Fig. 4.68. Meltdown-Tube Temperature Profile. (From Castleman, ref. 39, Fig. 2.)

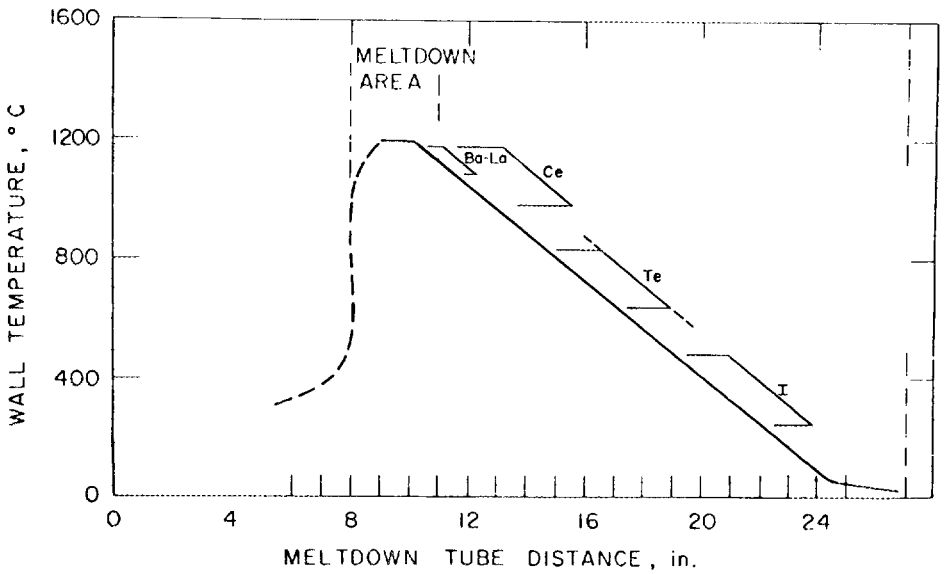

Fig. 4.69. Fission-Product Deposition from U–3.5% Mo Alloy Melted in Helium. (From Castleman, ref. 39, Fig. 3.)

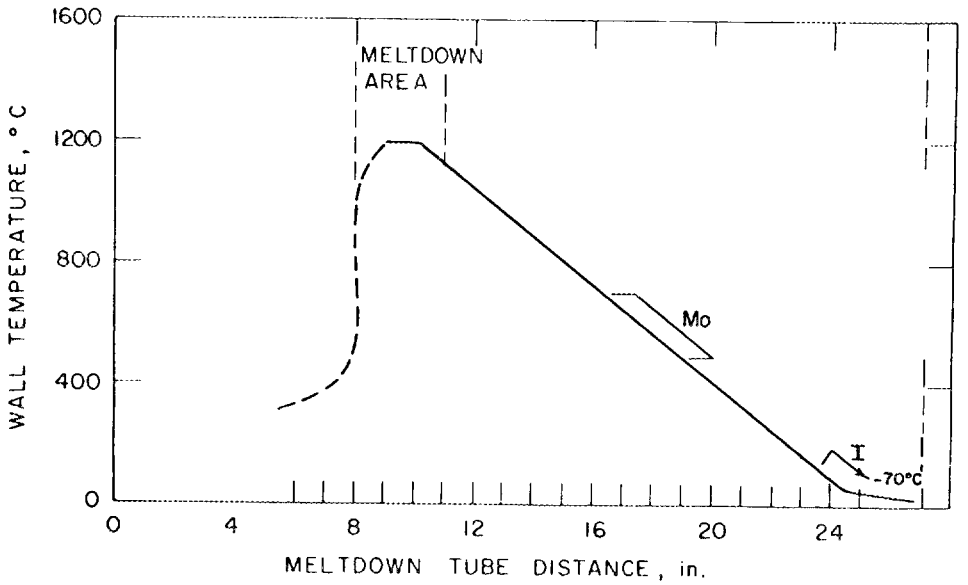

Fig. 4.70. Fission-Product Deposition from U–3.5% Mo Alloy Melted in Air. (From Castleman, ref. 39, Fig. 4.)

1. Iodine. To ensure the usefulness of the experiments for studying iodine release, it was first necessary to know what experimental variables affected the fission-product deposition distribution. The results of this investigation are given in Table 4.25. In the series 1 experiments, helium was passed across the molten uranium-molybdenum alloy specimen for 41 min at 9 cm^3/min. The temperature gradient along the meltdown tube was similar to that shown in curve A of Fig. 4.68. Less than 10% of the iodine released deposited in the region below 200°C, and the majority was in the region at 250 to 350°C. In the series 2 experiments, the helium flow rate was doubled; however, the only effect noted was that the iodine deposit was slightly more spread out. The furance temperature profile was changed to that shown in curve B of Fig. 4.68 for the third series of experiments; all other experimental conditions were identical to those used in the series 1 experiments. As seen from the results of the series 3 experiments, the iodine deposited in the identical temperature region, which in this case was four tube diameters (8 cm) closer to the meltdown zone. A comparison of these results confirmed the conclusion that there was a definite iodine condensation zone and that the iodine release was not particulate under the conditions of this experiment. The run duration for the series 4 experiments was twice that used for series 1 to 3, but no effect on the iodine deposit was noted. Therefore, the iodine deposit was relatively immobile, and a slight variation in the length of a run had no effect on the results.

Another series of experiments (series 5) was run to determine whether the crucible material had any effect on the chemical form of the released iodine and therefore on its final distribution. As seen from the results, the distribution did not depend on the boat material. Based on these experiments, the iodine was undoubtedly deposited in a combined form, dependent on the uranium matrix from which it was released. No other fission products were observed to condense in this temperature region, and, as expected, compounds of fission products would not be important based on the small concentration of the reacting species in this fuel.

The significant aspect of these studies is seen by comparison of the results obtained in helium with the results obtained in air (series 6 and 7). In these experiments, 90% of the released iodine deposited in the region below 50°C, and the major portion was collected in the cold trap. Some charcoal particles, which are known to be a good trap for elemental iodine up to several hundred degrees centigrade, were distributed at the lower end of the tube in series 7. The experimental conditions were similar to those of series 6, except that the air flow rate was increased by a factor of 5. Approximately one-half the iodine collected on these charcoal particles, and the remainder collected in the cold trap. It is therefore clear that this iodine was not merely carried along on particles in the air stream but, instead, was present in the elemental state.

2. Barium-Lanthanum. The deposition distribution of barium and lanthanum was studied under experimental conditions identical with those for the iodine study. A summary of the results is given in Table 4.26. Variations in flow rate, run duration, and boat material had no effect on the fission-product distribution, and, in all cases, the barium-lanthanum deposited in regions at 1100 to 1200°C. Both barium and

Table 4.25. Iodine Released from Uranium at 1200°C[a]

Experiment Series	Atmosphere	Flow Rate (cm^3/min)	Run Duration (min)	Boat Material	Meltdown Tube Temperature Profile[b]	Iodine Deposition Zone Temperature	Results
1	He	9	41	Ta	Curve A	Majority deposited at 250 to 350°C; less than 10% in region below 200°C	Typical behavior in helium; no other fission products in iodine deposition zone
2	He	29	35	Ta	Curve A	Same as above	Iodine deposition zone same at increased helium flow rate
3	He	9	40	Ta	Curve B	Same as above	Iodine deposition zone independent of distance from meltdown zone
4	He	9	80	Ta	Curve A	Same as above	Increased run duration had no effect on deposition region
5	He	9	40	Al_2O_3	Curve A	Same as above	Iodine release did not depend on boat material
6	Air	10	41	Al_2O_3	Curve A	Majority deposited in cold trap; less than 3% in region above 100°C	Iodine release depended on the chemical environment
7	Air	52	53	Al_2O_3	Curve A	97% deposited below 100°C; approximately one half on charcoal particles in tube and one half in cold trap	Iodine release was not particulate

[a]From Castleman, ref. 39, Table 1.

[b]Curve given in Fig. 4.70.

Table 4.26. Fission-Product Deposition[a]

Fission Product	Source	Atmosphere	Results
Ba-La	U–3.5% Mo alloy	He	100% deposited in region at 1100 to 1200°C
Ce	U–3.5% Mo alloy	He	98% deposited in region at 1000 to 1200°C
Te	U–3.5% Mo alloy	He	Widely distributed throughout tube; peak deposition in zone at 600 to 850°C
	Elemental Te	He	Wide band in region at 225 to 525°C
Mo	U–3.5% Mo alloy	He	Essentially no release
	U–3.5% Mo alloy	Air	Deposited in distinct band in region at 530 to 730°C

[a]From Castleman, ref. 39, Table 2.

lanthanum were released independently; the lanthanum was not merely the decay product of the released barium. A negligible quantity of barium-lanthanum was released from the uranium-molybdenum fuel sample into air.

3. Cerium. The cerium released from the fuel sample into helium deposited in the region at 1000 to 1200°C. The release into air was extremely small, and a negligible quantity of cerium was found outside of the sample boat.

4. Tellurium. Tellurium released in helium did not deposit in a well-defined temperature zone as did the other fission products. Although the tellurium was distributed throughout the entire tube, a major peak was observed in the region at 600 to 800°C, as shown in Table 4.26. Elemental tellurium passed through the same temperature gradient deposited at temperatures below 600°C (primarily concentrated in a wide band between 225 and 525°C).

5. Molybdenum. A U–3.5% Mo alloy fuel was used in all the experiments reported by Castleman.[39] Since the molybdenum was alloyed with the uranium matrix, the fission-product molybdenum and that molybdenum present as the alloy homogeneously mixed when the fuel melted and behaved in an identical manner chemically. The concentration of active ^{99}Mo was quite large, since it was formed both by neutron capture of natural molybdenum and as a uranium fission product. However, a negligible quantity of molybdenum was released from the molten fuel into a helium stream, as evidenced by the lack of ^{99}Mo activity in the meltdown tube.

In the release experiments run in air, however, large quantities of molybdenum were released and deposited in a well-defined zone at 530 to

730°C. The release of molybdenum in air was observed to be extremely rapid, in the order of seconds. A variation in flow rate had no effect on the region where the molybdenum deposited. In one series of experiments the flow rate was five times faster than the rate used in another, but essentially no deposition distribution difference was noted.

4.4.2.3 Chemical States

On the basis of the foregoing experiments, conclusions can be drawn regarding the probable chemical state of several released fission products. In applying these results, it must be emphasized that no attempt was made to measure the absolute condensation temperature of the individual fission products. It was sufficient (for these studies) to be able to reproduce the temperature gradient for a comparison of the fission-product deposition behavior under a variety of experimental conditions.

1. Iodine. These experiments showed that iodine is released from this molten fuel into pure helium in some combination with the matrix from which it was released. Since none of the molybdenum iodides are stable under these conditions, the iodine was undoubtedly released as one of the uranium iodides. Since the meltdown is a completely transient process, it is impossible to calculate which of the uranium iodides would be most likely to form, based solely on equilibrium considerations; however, thermodynamic estimates indicate that UI_2 gas is an important species at these temperatures. The thermodynamic calculations were made on the basis of data presented by Brewer et al. and given here in Table 4.27. The UI_2 was taken to be 1 kcal more unstable than UI_3. The UI would undoubtedly be an important species in the calculation if its free energy were estimated in a similar manner. Since its vapor pressure would be low, however, it might not be important in the release process. The results of the calculations are presented in Table 4.28, where the probable chemical states above the molten uranium are listed as UI_2 and I, although there is no reason to rule out the possibility of a mixture of UI, UI_2, and I. These would rearrange to the more stable UI_3 or UI_4 at lower temperatures.

The effect of increased fuel burnup (higher iodine concentration) has not been experimentally studied; however, it can be qualitatively estimated, based on the reactions shown in Table 4.27 and with the experimental evidence, that the iodine will be released as a uranium-iodine compound. Caution must be exercised in applying the reactions given in Table 4.27 to a fuel meltdown. The partial pressures are not fixed; rather, they change during the course of the reaction much the same way as do the reactants in a batch process. An estimation of the quantity of the various species present requires the solution of four simultaneous equations rather than a simple substitution for the estimated initial iodine partial pressure. Since the value of K_4 (the equilibrium constant for the association of atomic iodine) is small, no I_2 is present at low iodine partial pressures. Thus in reactions 1, 2, and 3 (Table 4.27), P_{I_2} should be replaced with 0.672 P_I^2. The P_{UI_4} in reaction 3 is therefore proportional to P_I to the fourth power. Even after considerable fuel burnup, the chemical activity of the iodine is still several orders of magnitude less than 1, and UI_2 will still be the most probable species

Table 4.27. Uranium-Iodine Thermodynamic Constants at 1500°K[a]

Chemical Reaction	Equilibrium Constant
1. $U + I_2 \rightarrow UI_2$	$K_1 = \frac{a_{UI_2}}{a_U a_{I_2}} \approx \frac{P_{UI_2}}{P_{I_2}} = 1.8 \times 10^8$
2. $U + \frac{3}{2} I_2 \rightarrow UI_3$	$K_2 = \frac{a_{UI_3}}{a_U a_{I_2}^{3/2}} \approx \frac{P_{UI_3}}{P_{I_2}^{3/2}} = 2.6 \times 10^8$
3. $U + 2I_2 \rightarrow UI_4$	$K_3 = \frac{a_{UI_4}}{a_U a_{I_2}^2} \approx \frac{P_{UI_4}}{P_{I_2}^2} = 3.2 \times 10^{11}$
4. $2I \rightarrow I_2$	$K_4 = \frac{a_{I_2}}{a_I^2} \approx \frac{P_{I_2}}{P_I^2} = 6.72 \times 10^{-1}$,
	since $a_U = 1$

[a]From Castleman, ref. 39, Table 3.

to be released. Therefore, the results of meltdowns using a fuel of higher burnup would probably be similar to these which have been discussed.

The uranium iodides oxidize, even at room temperature in dry air, to UO_2I_2 and I_2. The UO_2I_2 readily decomposes to UO_2 and I_2. Uranium iodides deposited along tube walls were exposed to air for long periods of time without any appreciable loss of iodine. Even though the uranium iodides liberate iodine in an oxidizing atmosphere, to a large extent the iodine remains adsorbed on the surface.

In air, the iodine was released from the uranium-molybdenum fuel as elemental iodine. This is consistent with the high-temperature reaction between the uranium iodides and oxygen:[40]

$$3UI_z + 4O_2 \rightarrow U_3O_8 + 3zI \ .$$

Based on these studies, it is probable that iodine would be released as a uranium iodide from a metallic uranium fuel element melting in a chemically inert atmosphere. It might be conjectured that if this uranium iodide deposits prior to the failure of the primary reactor containment

Table 4.28. Chemical State of Fission Products Released from Uranium[a]

Fission Product	Atmosphere	Probable Chemical Reaction	Probable Chemical State	Basis
Iodine	He	$U + 2I \rightarrow UI_2$	$UI_2 + I$ (vapor above molten U)	Thermodynamic and kinetic estimates
	He	$xUI_2 + yI \rightarrow UI_z$	UI_z, where Z = 3 or 4 (deposited)	Experimental results
	Air contact at ambient temperature after deposition	UI_z (deposited) $+ O_2 \rightarrow UO_2I_2 + I_2$ (b) $UO_2I_2 \rightarrow UO_2 + I_2$	$UO_2 + I_2$ (absorbed I_2)	Experimental results
	Air contact during release	$UI_z + O_2 \rightarrow U_3O_8 + ZI$	Elemental I	Experimental results
Molybdenum	Air	$2\ Mo + 3O_2 \rightarrow 2\ MoO_3$	MoO_3 (definite)	Identified with x-ray diffraction

[a]From Castleman, ref. 39, Table 4.

[b]From J. J. Katz and E. Rabinowitch, The Chemistry of Uranium, 1st. ed., p. 538, McGraw-Hill, 1951.

vessel and subsequent exposure to air, a large quantity of the iodine may remain on the surface. A meltdown in which the fuel material contacts air at high temperature will undoubtedly release elemental iodine.

2. Barium-Lanthanum, Cerium, and Tellurium. Barium-lanthanum and cerium deposited in the regions at 1100 to 1200°C and 1000 to 1200°C, respectively, when released in helium. However, very little, if any, of these fission products were released in air, probably because the non-volatile oxides were formed.

The behavior of the tellurium is anomalous, however, on the basis of other studies by Castleman;[39] uranium and elemental tellurium were found to react at 1200°C. It is possible that this release is a mixture of elemental tellurium and some present in a combined state with the uranium.

3. Molybdenum. Molybdenum was not released to any appreciable extent in helium. In an air environment a large fraction was rapidly released as MoO_3 (see Table 4.28). These crystals were identified by x-ray diffraction. Molybdenum trioxide is much more volatile than molybdenum and would be expected to be released to a much greater extent (b.p.: Mo, 4800°C; MoO_3, 1151°C).

4.4.3 Transport Effects of Small Particles

Browning et al.,[33] in experiments on the in-pile melting of UO_2, showed that the observed distribution of fission products could be explained, in part, on the basis of transport on very fine particles. There was apparently two particle-size groups in the millimicron range (Table 4.29). One group had an apparent size of 22 A. An average of 39% of the

Table 4.29. Average Percentage of Each Isotope and UO_2 Carried by Very Fine Particles in Exit Gas[a]

Effective Particle Diameter (A)	Material Carried	Percentage of Material Released
22	^{131}I	39
	^{89}Sr	5
	^{132}Te	3
	^{137}Cs	15
	^{140}Ba	13
30	^{95}Zr	3
	^{106}Ru	10
	^{144}Ce	13
	UO_2	9

[a]From Browning et al., ref. 33, p. 35.

iodine carried out of the reactor furnace by the exit gas was carried by these particles; values in the individual experiments ranged from 8 to 75%. In contrast to Castleman's conclusions concerning metallic uranium meltdown, no iodine having a diffusion coefficient corresponding to the vapor form was found. Some of the cesium, strontium, tellurium, and barium was also found to be associated with this group of particles. The other group of particles had a somewhat larger diameter, 30 A. Zirconium and uranium were associated with this group of particles; ruthenium and cerium also appeared to be present in one experiment. However, ruthenium and cerium were usually carried on larger particles. Work is currently under way to formulate a model that will explain the observed distribution.

It was concluded[33] that the results of both melting and burning in in-pile experiments showed that although large fractions of the fission products were released from the fuel, they were almost entirely retained inside the high-temperature zone of the furnace (with the exception of iodine, cesium, and tellurium). When oxygen was present, ruthenium was also released. The noble gases appeared to be released completely. Of the fission products released from the high-temperature zone, significant fractions were carried as particles as small as 20 to 30 A in diameter.

4.4.4 Fission-Product Behavior Within the Outer Containment Building*

In the event that fission products leave the reactor core vessel, they will enter the containment building and act as a source for leakage through the building into the atmosphere. Currently, in evaluating hazards outside the plant, no credit is taken for reduction of the source by natural effects and by the artificial effects that may be employed. Actually, the activity entering the containment vessel would be reduced by plate-out on available surfaces, settling of dust particles, condensation of steam, etc. Also artificial reduction techniques could be employed, such as recycle filtration, steam dousing, and water spray, with and without hygroscopic additives.

4.4.4.1 Behavior of Fission Products in Water Droplets

Mausteller and Campana reported[41] the results of tests in which high-temperature, high-pressure water (550°F, 2000 psi) containing simulated fission products was allowed to leak at a controlled rate into a 4000-ft^3 vessel. The fission products used were ^{24}Na, added as Na_2CO_3 to simulate soluble fission products; ^{99}Mo, which was added as MoO_3 to represent insoluble fission products; and ^{131}I in the form of I_2, representing gaseous products. Fallout coefficients of 0.1 to 0.8 hr^{-1} (half-lives of 0.9 to 7 hr) were observed with the bulk of the coefficients in the range 0.2 to 0.35 hr^{-1}. More than 80% of the activity was associated with particles in the 0.4- to 0.7-μ range according to the results of cascade-inspector tests. Only 6 to 15% of the activity was found in water droplets. It was stated that calculations showed that the life of a 10-μ-diam droplet in air at 50% relative humidity is only about 0.1 sec

*See Appendix G for relevant information published since this chapter was prepared.

while that of a 100-μ droplet is about 10 sec. Average droplet diameters in fogs and mists were said to range from 5 to 100 μ. Mention was made[41] of results of tests in which 144-liter quantities of water at 550°F and 2000 psi were allowed to expand rapidly into a 1340-ft^3 vessel. A maximum of 2% of the ^{131}I and ^{24}Na each was reported to have escaped from the container and 5% of the ^{90}Y. No details of the experiments were given.

4.4.4.2 Behavior of Iodine in Reactor Containment Buildings

Megaw and May[42] studied the behavior of elemental ^{127}I and ^{132}I released into the full-scale DIDO and PLUTO reactor containment shells in the range 0.01 to 15 $\mu g/m^3$. The importance of iodine as a biological hazard justified its individual investigation. Their study is reported in detail here.

They found that most of the iodine disappeared rapidly by deposition on surfaces in the reactor shell. Part of the remainder was airborne for periods of several hours and became attached to submicron particles in the atmosphere; part appeared to form two iodine compounds. The release of stable ^{127}I was found to cause return into the gas phase of radioactive iodine previously deposited on surfaces within the reactor containment vessel.

Details of the conditions of the experiments are given in Table 4.30. Figure 4.71 shows the PLUTO shell, including circulating fans, reactor,

Table 4.30. Details of Iodine Release Experiments in DIDO and PLUTO[a]

Reactor	Containment volume, m^3	Serial	Quantities of iodine released		Calculated added concentration		Maximum measured concentration at position 2, dis/(min)(m^3)	Remarks
			I^{127}, mg	I^{132}, mc	$\mu g/m^3$	dis/(min)(m^3)		
DIDO	7000	1	7	26	1.0	8.2×10^6	4.7×10^6	Scrubbers operated
		2	1	31	0.14	9.8×10^6	2.8×10^6	
		3	7	31	1.0	9.8×10^6	2.9×10^6	
PLUTO	7000	A	0.09	28.2	0.013	8.9×10^6	1.45×10^6	
		B	0.95	22.9	0.14	7.2×10^6	1.75×10^6	
		C	99	30.6	14.1	9.7×10^6	5.4×10^6	
		D	99	20.1	14.1	6.4×10^6	3.0×10^6	
		E	7	2.7	1.0	8.5×10^5	9.3×10^5	Scrubbers operated
		F	9.9	48.9	1.4	1.5×10^7	1.0×10^7	
		G	10	39	1.4	1.2×10^7	5.5×10^6	

[a]From Megaw and May, ref. 42, p. 428.

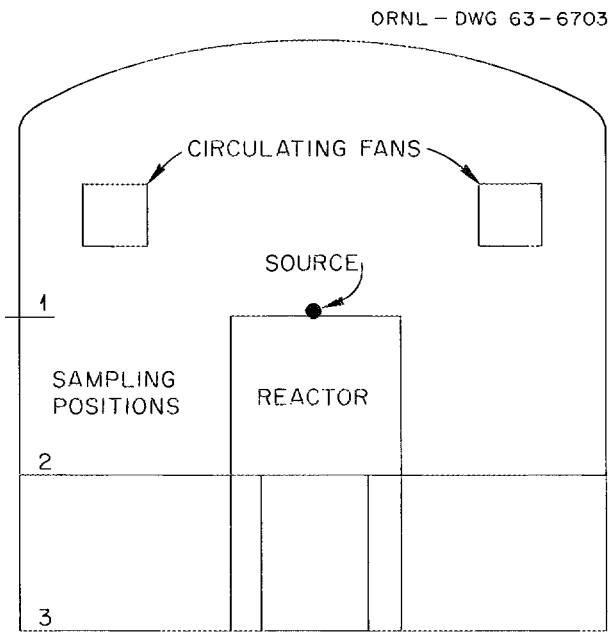

Fig. 4.71. PLUTO Reactor Shell. (From Megaw and May, ref. 42, p. 427.)

source, and sampling positions. The fans were estimated to cause complete mixing of the air in 40 min after release. The approximate internal surface area of one of the shells is 3000 m^2, of which one-third is polyvinylchloride sheet, one-third is concrete, and the remainder is metal.

Air samplers were used that could discriminate between elemental iodine and that deposited on particulates. Particular attention was paid to the behavior of iodine attached to Aitken nuclei, which are particles of a few hundredths of a micron in diameter that are always present to some extent in air. They may be of great importance in a reactor accident because they have a low diffusion coefficient (10^{-5} cm^2/sec) and yet are small enough to have a very slow settling rate under gravity (3×10^{-4} cm/sec). These nuclei are difficult to remove from air on a large scale, when in low concentrations, and could result in iodine penetration of filters designed to eliminate elemental iodine.

Figure 4.72 shows the variation of total iodine concentration with time. Except for run A, the iodine concentration falls off rapidly in the first hour and somewhat more slowly later. In run A, the mass of iodine release was smaller by a factor of 10 than the next smallest release, and it is possible that the lower concentration gradients resulted in slower diffusion to the shell wall.

1. Concentration of Iodine in Air. Figures 4.73 to 4.75 show the results of runs A, B, and D. One hundred milligrams of ^{127}I was released at the time shown by the arrow and caused an increase of the countable ^{132}I in the air. This suggests an exchange mechanism between the added stable ^{127}I and the ^{132}I that had deposited on available surfaces earlier. The curves in Figs. 4.73 to 4.75 show how the distribution of ^{132}I within

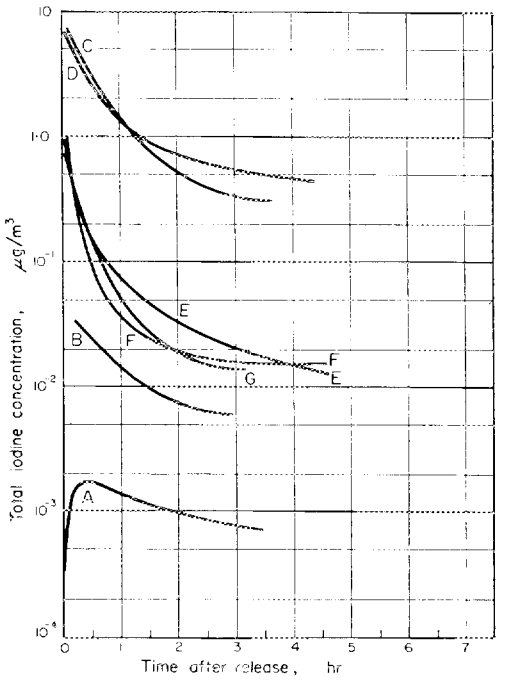

Fig. 4.72. Variation of Total Iodine Concentration with Time in PLUTO Experiment. (From Megaw and May, ref. 42, p. 431.)

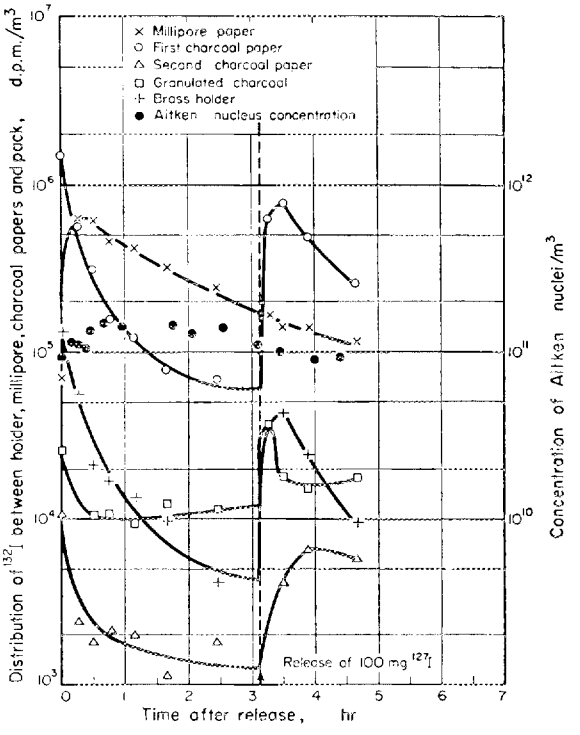

Fig. 4.73. Run B. Variation of ^{132}I Concentration with Time in PLUTO Experiment. (From Megaw and May, ref. 42, p. 431.)

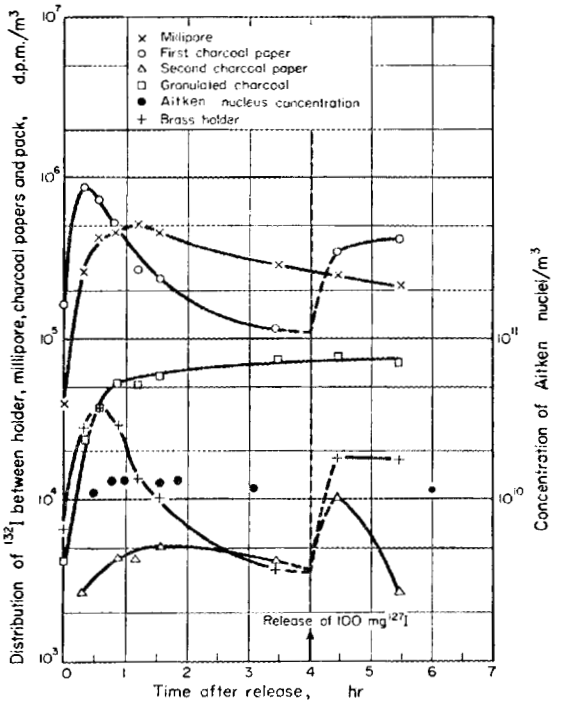

Fig. 4.74. Run A. Variation of ^{132}I Concentration with Time in PLUTO Experiment. (From Megaw and May, ref. 42, p. 431.)

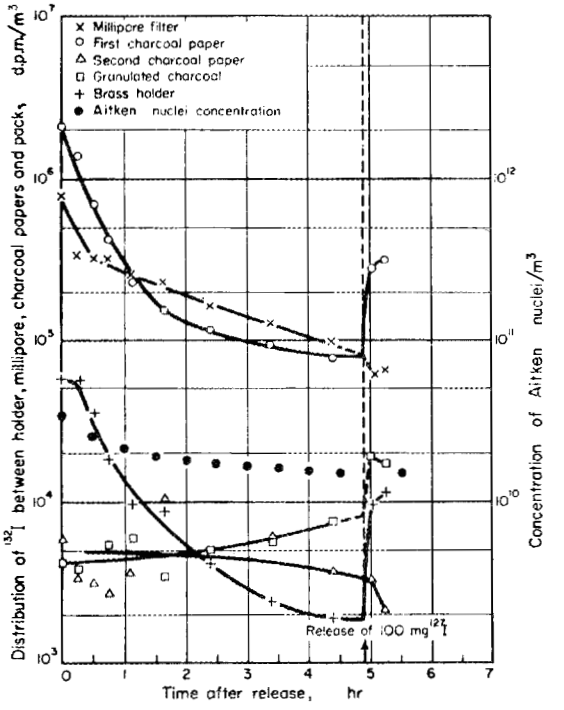

Fig. 4.75. Run D. Variation of ^{132}I Concentration with Time in PLUTO Experiment. (From Megaw and May, ref. 42, p. 431.)

the samplers varied with time. Each sampler consisted of an AA Millipore particulate filter, two charcoal-impregnated papers, and a granular charcoal bed, which were retained in that order within the brass holder.

The Millipore curve displays the amount of ^{132}I deposited on particulate matter. This effect is shown more clearly in terms of percentages in Fig. 4.76. The effects of the operation of a scrubber incorporating a high-efficiency particulate filter are shown in curves F and G. In runs A, B, and D (Figs. 4.74 to 4.76) the scrubber was not used.

2. Deposition Results. The values determined for the velocity of deposition of iodine on various surfaces exposed in the reactor atmosphere for 1 hr are shown in Fig. 4.77. Some of these deposition samples were subsequently exposed to atmospheres containing controlled concentrations of stable ^{127}I, and the ^{132}I remaining on the surface after exposure was measured. These results are shown in Fig. 4.78. Megaw and May state that the initial values of the velocity of deposition on metal surfaces and charcoal (0.1 to 0.3 cm/sec) are to be expected if the limiting factor is diffusion of iodine vapor to the surface. Figure 4.77 shows, however, that the deposition velocity decreases with time, suggesting some change in the airborne iodine. When ^{127}I was introduced, the ^{132}I deposition velocity increased.

3. Analysis of Results and Conclusions

Iodine Vapor. Comparison of Fig. 4.72 with Figs. 4.73 through 4.75 shows that the rapid decrease of iodine concentration with time occurs in the fraction of iodine that is caught on the first filter paper, which is known to be highly efficient for removing iodine vapor. It is probable that the deposition of iodine on the shell surfaces would be more important than deposition on particulate matter in the containment vessel atmosphere.

Megaw and May used the deposition velocity measurements of Fig. 4.78 to predict the air concentration in the containment vessel. If it is assumed that a uniform concentration was immediately attained throughout the vessel, the following equation holds:

$$-\frac{dq}{dt} = Av_g c = \frac{Av_g q}{V}, \qquad (4.52)$$

where

v_g = velocity of deposition, defined as (rate of deposition/cm^3·sec) divided by (volumetric concentration/cm^3), cm/sec,
A = surface available for deposition, cm^2,
q = total quantity of airborne iodine inside the shell,
V = volume of shell, cm^3,
c = uniform concentration in shell, q/V;

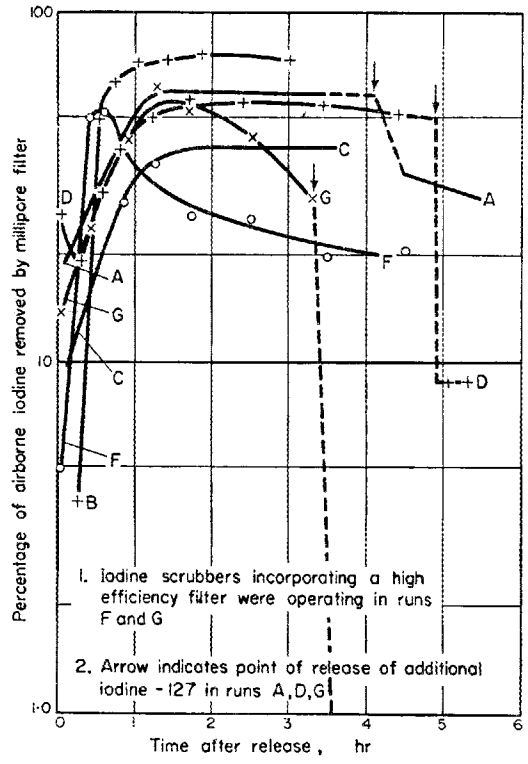

Fig. 4.76. Iodine Collected on Millipore Filter as Percentage of Total Iodine Sampled. (From Megaw and May, ref. 42, p. 432.)

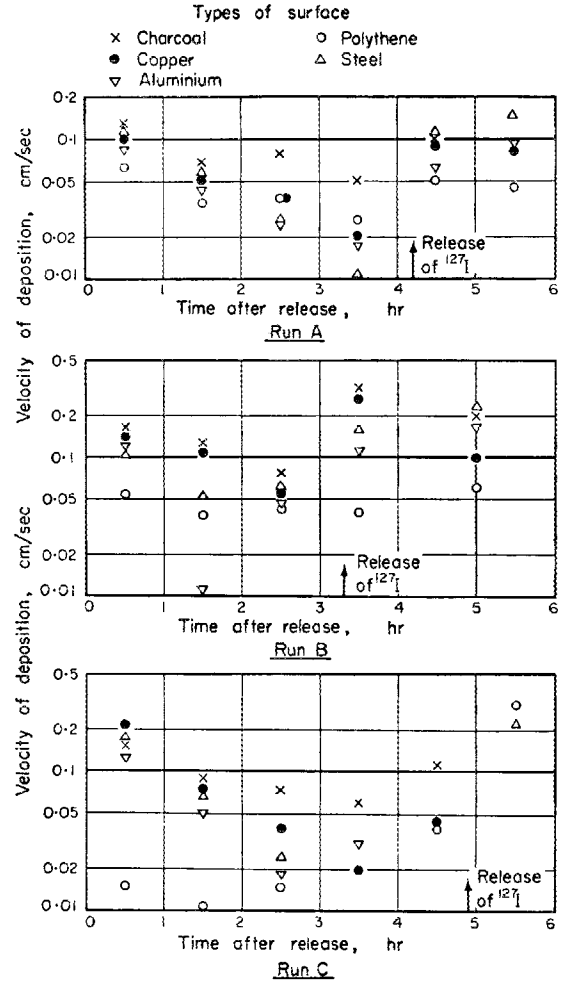

Fig. 4.77. Variation of Velocity of Deposition with Time After Release. (From Megaw and May, ref. 42, p. 432.)

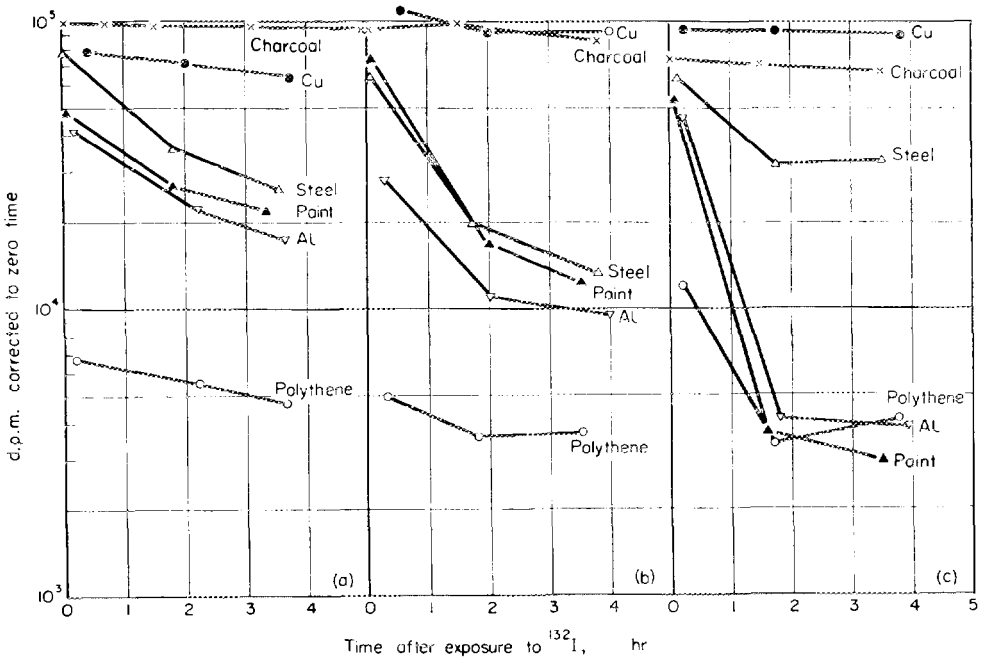

Fig. 4.78. Desorption and Exchange of Iodine from Various Surfaces. (a) Samples exposed in air; (b) samples exposed to 1 mg/m^3 of stable iodine; and (c) samples exposed to 3 g/m^3 of stable iodine. (From Megaw and May, ref. 42, p. 433.)

hence

$$-\frac{dc}{c} = -\frac{dq}{q} = \frac{Av_g}{V}\,dt$$

and

$$C = C_0 e^{-\lambda_1 t}, \qquad (4.53)$$

where $\lambda_1 = Av_g/V$.

The value of λ_1 was calculated using the concentration of iodine vapor only (remembering that other forms of iodine are present at longer aging periods), instead of the total iodine concentration. This is compared in Table 4.31 with the experimental λ (converted to half-life) in runs A, B, and D. The available area was taken as equal to the internal surface of the shell plus two extra floors. Two-thirds of the cylindrical surface and the roof were covered in polyvinylchloride sheet and were assumed to have the deposition characteristic of polyethylene sheet. The remainder of the surface area was assumed to have the deposition properties of steel.

Table 4.31. Comparison of Theoretical and Experimental Values of Half-Life of Iodine in Vapor State[a]

Run	λ_1 (sec^{-1})	Half-Life in Vapor State (min)	
		Theoretical	Experimental
A	6.2×10^{-4}	19	31
B	5.9×10^{-4}	19.5	18
D	4.8×10^{-4}	24	20

[a]From Megaw and May, ref. 42, p. 433.

Table 4.31 shows good agreement between theoretical and measured half-lives, except for run A, where the iodine concentration was very low and the assumption of immediate uniform diffusion throughout the shell was not fulfilled. Since molecular iodine was used to study the distribution of this element in reactor containment shells rather than fission-product iodine from irradiated fuel, the velocity-of-deposition data developed by Megaw and May should be employed with caution in reactor hazards analyses.

Iodine Attached to Particulates. The adsorption of gases and vapors on Aitken nuclei has been considered by Chamberlain et al.,[43] who derived the rate of adsorption as

$$\frac{1}{c}\frac{dc}{dt} = -4\pi r^2 nN\alpha \ , \qquad (4.54)$$

where

- c = concentration of gas being adsorbed,
- n = number of Aitken nuclei per cm^3,
- r = radius of Aitken nuclei, cm,
- α = the accommodation coefficient, or sticking probability, of a molecule of the adsorbed gas striking the particle surface,
- $N = (RT/2\pi M)^{1/2}$,
- R = gas constant, $cm^2\text{-}g/sec^2 \cdot g\text{-}mole \cdot {}^\circ K$,
- T = absolute temperature, °K
- M = molecular weight of adsorbed gas, g/g-mole.

The time rate of change of quantities of iodine attached on nuclei can be written as

$$\frac{dn}{dt} = \lambda_2 c - \lambda_3 n \ , \qquad (4.55)$$

where λ_2 is the rate constant for adsorption of iodine vapor on nuclei and λ_3 is the rate constant for loss of nuclei by sedimentation and diffusion to surfaces.

The value of λ_3 was determined by the slope of the Millipore curve in Figs. 4.74 to 4.77 in the last few hours of the run when the fall of the Millipore curve was exponential, indicating that attachment of vapor to particulates had nearly ceased.

The value of λ_2 was then determined using the values of n and c when $dn/dt = 0$. Then, since

$$\lambda_2 = -\frac{1}{c}\frac{dc}{dt} = 4\pi r^2 nN\alpha \ , \qquad (4.56)$$

the value of α was estimated by using a value of $r = 4 \times 10^{-6}$ cm, which was estimated from the measured diffusion coefficient. The values of α were found to be 4.7×10^{-3} for run A and 1.2×10^{-3} for run B. Such low values of the accommodation coefficient (unity is usually assumed) were taken to mean that iodine deposited only on a particular kind of nucleus rather than on the whole population, the latter being the basis of Eqs. (4.54) and (4.56). Megaw and May were unable to decide whether the particulate fraction of the iodine was a result of attachment to a relatively small proportion of chemically suitable nuclei or to an even smaller number of larger particles. They feel that the former conclusion is the more probable.

Iodine Compounds. The presence of ^{132}I on the second charcoal paper and granular charcoal stages of the sampler was almost certainly due to the formation of iodine compounds. The Millipore paper ahead of the charcoal papers did not allow significant particulate penetration. If the iodine reached the second charcoal paper as elemental vapor because the collection efficiency of the first charcoal paper was less than 100%, the activity ratio of the first to the second charcoal papers as a function of time (Fig. 4.79) would be constant. However, this ratio decreased rapidly from 150 to 250 initially when the iodine was mostly elemental vapor to a fairly constant value between 20 and 60 after 2.5 hr. It seems probable therefore that the iodine collected by the charcoal papers in the latter part of the experiments was some compound of iodine, provisionally designated[42] compound X, formed by reaction with trace contaminants in the atmosphere. The collection efficiency of the charcoal paper for compound X was in the range 95 to 98%.

The fraction of ^{132}I trapped by the granular charcoal stage of the sampler (Figs. 4.73 to 4.75) varied from run to run, being almost inversely proportional to the mass of ^{127}I released and independent of the amount of iodine on the preceding charcoal paper. This would appear therefore to be due to a second iodine compound (compound Y) for which the collection efficiency of the charcoal paper was very low.

Further work by Atkins and Eggleton[44] has confirmed these conclusions and shown that compound X is inorganic, while compound Y is a mixture of several organic iodides, predominantly methyl iodide.

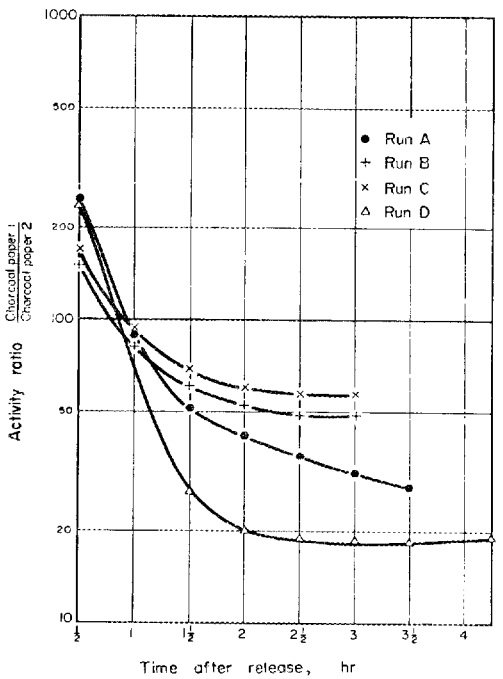

Fig. 4.79. Variation of Activity Ratio of First to Second Charcoal Papers with Time. (From Megaw and May, ref. 42, p. 435.)

Conclusions. Megaw and May concluded that the physical and chemical nature of iodine released in a reactor containment vessel change with aging. The resulting iodine is more difficult to remove from air, and it deposits less rapidly on surfaces. The release of ^{127}I to the atmosphere can cause a return to the gas phase of iodine previously deposited on surfaces. This, in conjunction with an iodine vapor scrubber, may be a promising way to decontaminate surfaces after a release of iodine.

4.4.4.3 Removal of Iodine from Containment Vessel Atmosphere by Sprays

The use of sprays has been frequently proposed as a means of reducing fission-product contamination of the containment vessel atmosphere after an accident. The subject has been covered thoroughly by Griffiths,[45] and most of his work is reproduced here. Data on the partition of iodine and water have also been reported by Watson, Bancroft, and Hoelke.[46]

1. Partition of Iodine Between Air and Water. Table 4.32 shows the solubility of iodine in water at atmospheric pressure as a function of temperature.

At higher temperatures and at pressures above 1 atm, the system exists as two liquid layers: liquid iodine and an aqueous solution of iodine. The relation between the concentrations in the gas and liquid phases and temperature is given by Henry's Law, which states that at a

Table 4.32. Solubility of Iodine in Water[a]

Temperature (°C)	Grams of Iodine Per Liter of Saturated Solution
20	0.285
60	1.00
100	4.45
112.3[b]	7.20

[a]From Griffiths, ref. 45.

[b]Invariant point, two layers formed.

given temperature

$$\frac{\text{Concentration of gas in liquid phase}}{\text{Concentration of gas in gas phase}} = R',$$

where R' is a constant that is independent of total pressure. This is strictly true only for ideal gases, and deviations are to be expected at low temperatures and high pressures. Differences in molecular form in the two phases also cause departure from ideal behavior. Thus, aqueous solutions of caustic soda, sodium, thiosulfate, and other solutions which react with iodine will not obey this law. Pure water does obey this law, and the difference between experimental and theoretical values of R' indicate the amount of iodine reacted with the water in the following possible reactions:

$$H_2O + I_2 \rightleftharpoons HOI + H^+ + I^- ,$$

$$3HOI \rightleftharpoons 2I^- + 3H^+ + IO_3^- ,$$

$$I_2 + I^- \rightleftharpoons I_3^- .$$

Figure 4.80 compares values of R' calculated using Henry's Law with experimental values found by Taylor.[47] The difference between the two curves represents the degree of compounding of iodine in the liquid phases; 20% in this case. The weight distribution of the iodine between water and air was calculated for various volume ratios based on the experimental values and the assumption that the amount of hydrolysis is a constant

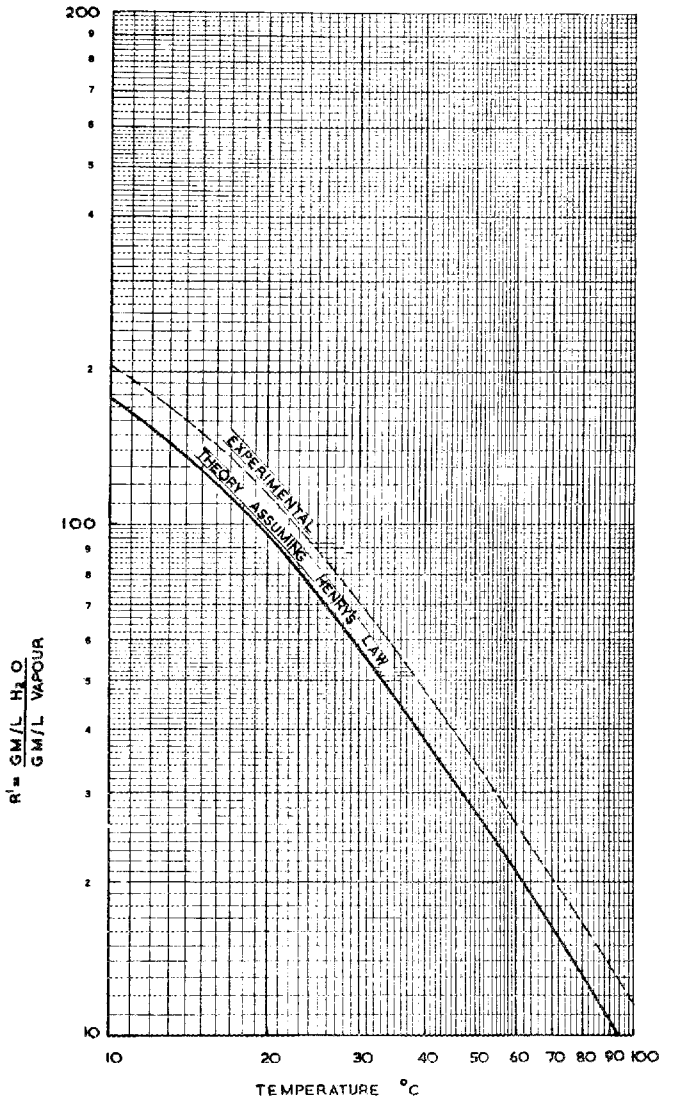

Fig. 4.80. Partition Coefficient of Iodine Between Air and Water at Normal Atmospheric Pressure. (From Griffiths, ref. 45, Fig. 1.)

fraction of the amount of iodine in the liquid phase. The results of these calculations are given in Table 4.33, which shows clearly that at 20°C, to achieve 99 wt % of the iodine in water, the volumes of air and water must be about equal. At 100°C, the volume of water must be eleven times that of the air. The use of sprays, however, is likely to lower temperatures well below 100°C.

Two ways of improving the partition are (1) continuous removal of the water from the floor of the containment vessel by recycling through an iodine-removal plant and reusing the water in a spray, and (2) the use of a liquid that combines chemically with the iodine so that the

Table 4.33. Distribution of Iodine Between Air and Water[a]

Ratio of Air Volume to Water Volume	Iodine Distribution at 20°C (%)		Iodine Distribution at 100°C (%)	
	Water	Air	Water	Air
1	99	1	91	9
10	92	8	52.5	47.5
100	54	46	9.9	90.1
1000	10.5	89.5	1.1	98.9

[a]From Griffiths, ref. 45.

partition problem does not arise (suitable solutions would be caustic soda, sodium sulfate, sodium thiosulfate, and sodium iodide).

2. Rate of Transfer of Molecular Iodine to Water Drops. The mass transfer coefficient between the gas phase and the liquid phase depends on the gas-film mass transfer coefficient, the solubility coefficient, and the liquid mass transfer coefficient from the surface of the drop to the interior.

The liquid mass transfer coefficient, k_L, is defined as (mass transferred)/(unit time)(unit area)(concentration difference), or

$$k_L = \frac{dm/dt}{\pi d^2 (c_i - c)} , \tag{4.57}$$

where

m = mass of the drop at time t,
d = diameter of the drop,
c_i = concentration at the drop surface,
c = average concentration of iodine in the liquid at time t.

The mass transfer coefficient can be expressed as[48]

$$k_L = \frac{2\pi^2}{3} \frac{D_L}{d} . \tag{4.58}$$

This is obtained by assuming that the transfer within the drop is due to diffusion only. The true value would be several times this due to the oscillation and circulation of the liquid within the drop.

The diffusivity (D_L) of iodine in water may be calculated from[48]

$$D_L = 7.4 \times 10^{-8} \frac{(Xm)^{\frac{1}{2}}T}{\mu V^{0.6}} , \qquad (4.59)$$

where

D_L = diffusivity, cm^2/sec,
T = absolute temperature, °K,
V = molecular volume (71.5 cm^3/g-mole for I_2),
m = molecular weight of solvent,
X = degree of association of solvent (2.6 for water),
μ = viscosity of solution, centipoise.

At 20°C, $D_L = 1.14 \times 10^{-5}$ cm^2/sec; and at 100°C, $D_L = 5.15 \times 10^{-5}$ cm^2/sec. Table 4.34 shows the effect of temperature and drop diameter on the transfer coefficient, k_L.

Table 4.34. Mass Transfer Coefficient of Iodine in Water Drops

Mean Drop Diameter (μ)	k_L (cm/sec)	
	At 20°C	At 100°C
50	1.5×10^{-2}	6.8×10^{-2}
100	7.5×10^{-3}	3.4×10^{-2}
200	3.75×10^{-3}	1.7×10^{-2}
500	1.5×10^{-4}	6.8×10^{-3}
1000	7.5×10^{-4}	3.4×10^{-3}
2000	3.75×10^{-4}	1.7×10^{-3}

The mass transfer coefficient can be expressed in terms of partial pressure or concentration:

$$K_G = \frac{\text{mass of constituent transferred/(sec)(unit area)}}{\text{partial pressure difference across transfer zone}} ,$$

where the units are $g/cm^2 \cdot sec \cdot atm$, and

$$K_C = \frac{\text{mass of constituent transferred/(sec)(unit area)}}{\text{concentration difference across transfer zone}} ,$$

where the units are cm/sec. Since K_C is equivalent to V_g, the velocity of deposition, the relation between the two is

$$K_C \text{ or } V_g = \frac{RT}{M} K_G .$$

For iodine at 20°C, V_g is $94.7K_G$ (cm/sec); and at 100°C, V_g is $121K_G$ (cm/sec).

The overall mass transfer coefficient is related to the gas and liquid phase coefficients by

$$\frac{1}{K_G} = \frac{1}{k_G} + \frac{1}{H_s k_L} ,$$

where

K_G = overall coefficient, $g/cm^2 \cdot sec \cdot atm$,
k_G = gas film coefficient, $g/cm^2 \cdot sec \cdot atm$,
k_L = liquid film coefficient, cm/sec,
H_s = solubility coefficient, $g/cm^3 \cdot atm$.

At 20°C, H_s is 1.25 $g/cm^3 \cdot atm$; and at 100°C, H_s is 7.4×10^{-2} $g/cm^3 \cdot atm$. Also

$$\frac{1}{V_g} = \frac{1}{v_g} + \frac{1}{R' k_L} , \qquad (4.60)$$

where

V_g = overall coefficient, cm/sec,
v_g = gas film coefficient, cm/sec,
k_L = liquid film coefficient, cm/sec,
R' = ratio of concentration in liquid phase to concentration in gas phase.

Table 4.35 gives the mass transfer coefficients for transfer of iodine to water drops. The effect of drop diameter and temperature on the overall coefficient is shown in Fig. 4.81.

These transfer coefficients may now be used to determine whether the equilibrium partition state is reached. During the time required to attain equilibrium, the drops are falling by the relation (see App. 1 of ref. 45)

$$E_M = 1 - e^{6Kt/d} ,$$

Table 4.35. Mass Transfer Coefficients for Iodine to Water Drops[a]

Mean Drop Diameter (μ)	At 20°C				At 100°C			
	k_L (cm/sec)	k_G (g/sec·cm^2·atm)	K_G (g/sec·cm^2·atm)	V_g (cm/sec)	k_L (cm/sec)	k_G (g/sec·cm^2·atm)	K_G (g/sec·cm^2·atm)	V_g (cm/sec)
50	1.5×10^{-2}	4.25×10^{-1}	1.8×10^{-2}	1.7	6.8×10^{-2}	4.22×10^{-1}	4.98×10^{-3}	6.04×10^{-1}
100	7.5×10^{-3}	2.64×10^{-1}	9.05×10^{-3}	8.56×10^{-1}	3.4×10^{-2}	2.56×10^{-1}	2.5×10^{-3}	3.03×10^{-1}
200	3.75×10^{-3}	1.93×10^{-1}	4.56×10^{-3}	4.31×10^{-1}	1.7×10^{-2}	1.82×10^{-1}	1.25×10^{-3}	1.51×10^{-1}
500	1.5×10^{-3}	1.43×10^{-1}	1.84×10^{-3}	1.74×10^{-1}	6.8×10^{-3}	1.29×10^{-1}	5.0×10^{-4}	6.05×10^{-2}
1000	7.5×10^{-4}	1.23×10^{-1}	8.7×10^{-4}	8.25×10^{-2}	3.4×10^{-3}	1.11×10^{-1}	2.5×10^{-4}	3.03×10^{-2}
2000	3.75×10^{-4}	1.04×10^{-1}	4.4×10^{-4}	4.31×10^{-2}	1.7×10^{-3}	9.1×10^{-2}	1.25×10^{-4}	1.51×10^{-2}

[a]From Griffiths, ref. 45, p. 8.

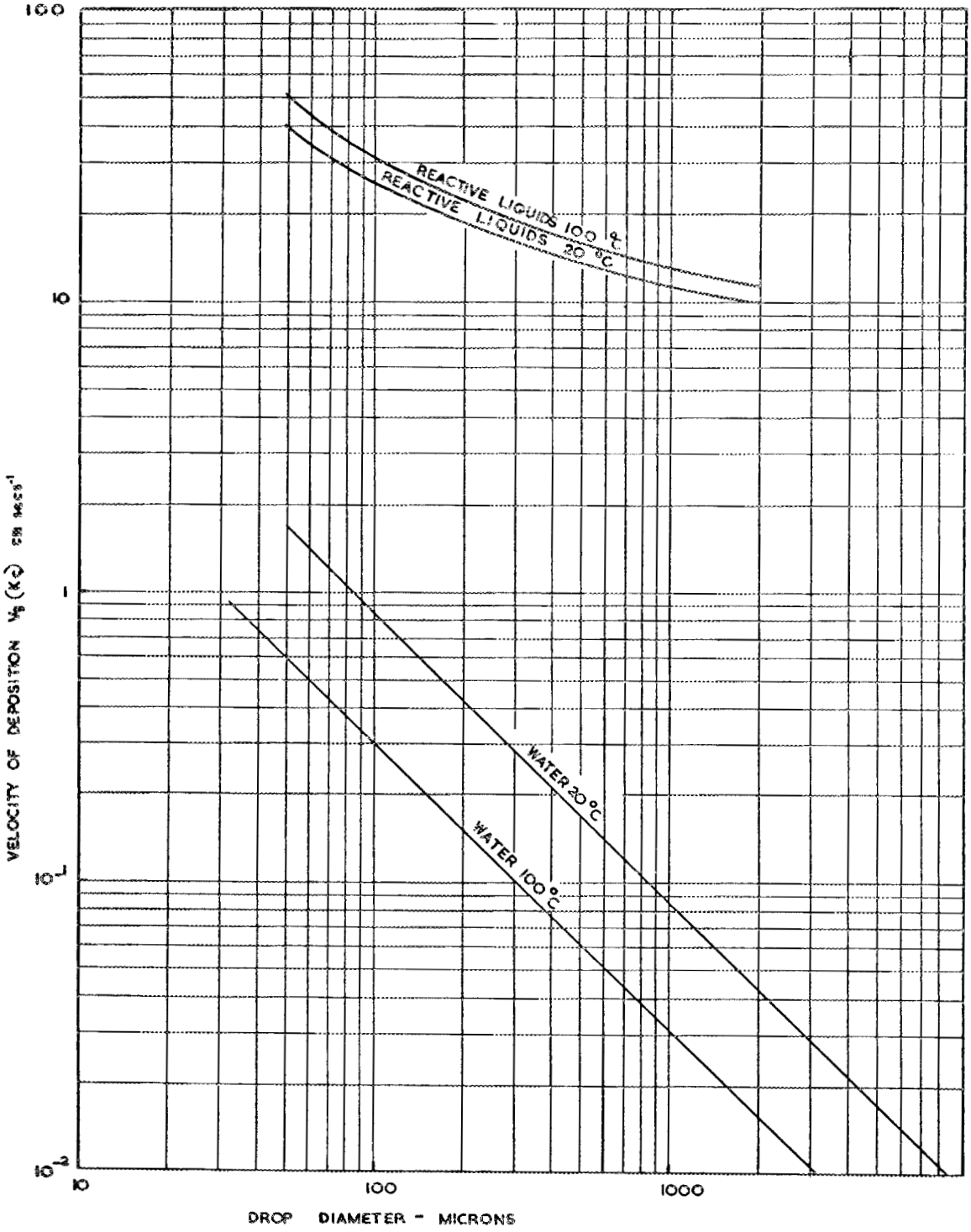

Fig. 4.81. Overall Transfer Coefficients for Transfer of Iodine to Liquid Drops. (From Griffiths, ref. 45, Fig. 2.)

where

E_M = fraction of equilibrium concentration reached in time t,
K = overall mass transfer coefficient, cm/sec,
d = diameter of drop, cm,
t = time, sec.

The height which drops must fall to reach equilibrium is shown in Fig. 4.82. It can be seen that the slowest transfer occurs with large drops at higher temperatures and that the height to reach 99% of the equilibrium values for 2000-μ drops is 65 m, which is greater than the height of most containment shells. For 1000-μ drops, the equivalent height is 10 m. Thus for all practical purposes, the removal of iodine by water drops smaller than 1000 μ would be controlled by the ratio of air to water passed through the containment.

Griffiths points out that since it is unlikely that the volume of water injected will exceed 10% of the containment volume, only 92% of the iodine would be removed at 20°C and 52% at 100°C. This is clearly a severe limitation on the use of water in removing iodine from reactor compartments.

3. Solubility of Iodine in Solutions That React with It Chemically. The increased solubility of iodine in solution is mainly due to chemical reactions according to the equations

$$OH' + I_2 \rightleftharpoons I' + HOI \ ,$$

$$3OHI \rightleftharpoons 2I' + 3H^+ + IO_3' \ .$$

As soon as I_2 has undergone reaction, it can no longer exert a partial pressure, so the major effects of liquids which react with iodine are a change in the partition that is very much in favor of the liquid phase and an increase in the mass transfer rate.

The effect on the overall mass transfer rate is shown in Fig. 4.81. The rates of transfer to solutions of caustic soda, sodium sulfite, sodium thiosulfate, and sodium iodide are similar. Alkaline solutions tend to remove grease and dirt from pipes, and filters would be required to prevent blocking of the spray nozzles. Storage of NaOH solution over long periods may present problems because of its reaction with carbon dioxide in the air to form sodium carbonate (which is fairly insoluble) and will cause blocking of the spray nozzle unless filtered. The other solutions mentioned may be more attractive from this point of view. Also, they would be less hazardous to personnel if the sprays were accidentally started.

4. Transfer of Molecular Iodine to Drops of Solutions Which React with Iodine. When the transfer rate is controlled by diffusion in the gas film, as would be the case in transfer from iodine in the air to a reactive substance in the drop, the rate of transfer can be expressed as[49]

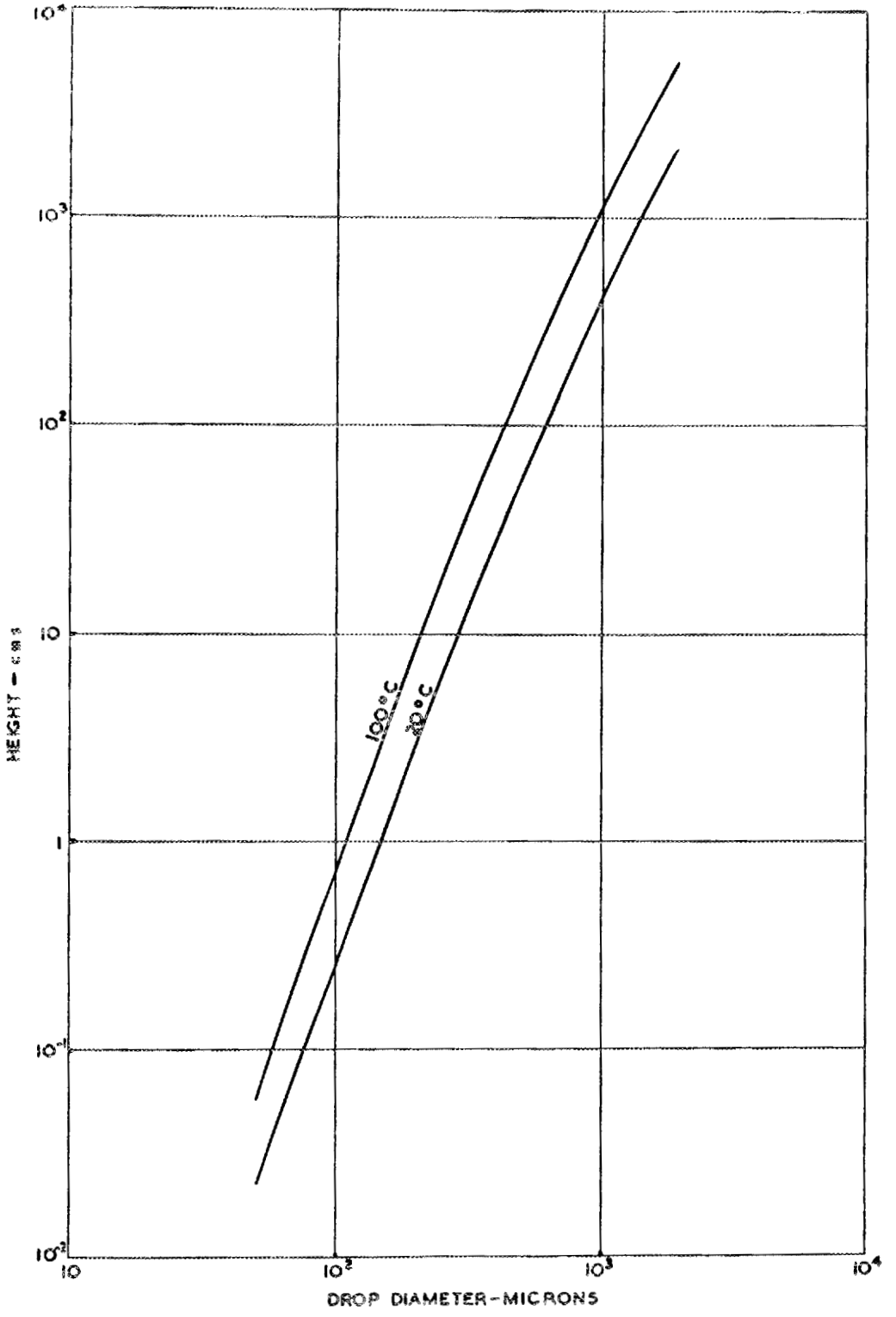

Fig. 4.82. Height in Which a Falling Drop Reaches 99% Saturation with Iodine. (From Griffiths, ref. 45, Fig. 3.)

$$k_G = \frac{D_v \rho}{M_m d P_f} \, Sh \ , \tag{4.61}$$

where

D_v = diffusion coefficient of iodine in air, cm^2/sec,
k_G = gas film mass transfer coefficient, g-moles/sec·cm·atm,
ρ = density of air, g/cm^3,
M_m = ratio of mean molecular weight of air to that of I_2 mixture in boundary layer,
d = drop diameter, cm,
P_f = partial pressure of air in the gas film, atm,
Re = Reynolds number, $\rho v d/\mu$, where ρ is density of air stream, v is velocity of air stream, and μ is viscosity of air stream,
Sc = Schmidt number, $\mu/\rho D_v$,
Sh = Sherwood number $= 2 + 0.6 Re^{1/2} Sc^{1/3}$.

At low concentrations of iodine, M_m can be taken as that of air, and P_f as the air pressure. From the gas law,

$$P_f = \frac{\rho}{M_m} RT \ ,$$

$$k_G = \frac{D_v}{d} \frac{1}{RT} (2 + 0.6 Re^{1/2} Sc^{1/3}) \ . \tag{4.62}$$

The velocity of the gas stream is taken as the terminal velocity of the drop. The mass transfer coefficients calculated from Eq. (4.62) are given in Table 4.36. Experimental results[50] show that k_G lies between 0.02 and 0.135 $g/sec \cdot cm^2 \cdot atm$. In calculating the values of k_G in Table 4.36, it was assumed that there was an excess of reactive salt at all times.

The time required for a mass flow of M' in $g/sec \cdot m^2$ to reduce the initial iodine concentration in air from X_0 to X_t at time t is given by

$$\frac{X_t}{X_0} = e^{-V_g A t} \ , \tag{4.63}$$

where V_g is the velocity of deposition given by $(RT/M)k_g$ (where M is molecular weight), and A is the area of the drops per cm^3 of atmosphere.

Figure 4.83 shows that a decontamination factor of 10^3 is reached with 1000-μ drops in 1 hr at 10-$g/sec \cdot m^2$ liquid flow. Other data show that only 6 min is required to reach the same decontamination factor at 100 $g/sec \cdot m^2$. A 200-μ drop at 10 $g/sec \cdot m^2$ gives a decontamination factor of 10^3 in about 1.5 min.

Table 4.36. Mass Transfer Coefficients (k_G) for Transfer of Iodine Into Drops of Liquid That Combine Chemically with Iodine[a]

Temperature (°C)	Drop Diameter (cm)	v (cm/sec)	μ/ρ (cm^2/sec)	D_v (cm^2/sec)	Re	Sc	$Re^{1/4}Sc^{1/3}$	Sh	k_G (g/sec·cm^2·atm)	V_g (cm/sec)
20	5×10^{-3}	7.75	0.15	0.085	0.26	1.76	0.61	2.37	0.425	40.2
	10^{-2}	25	"	"	1.67	"	1.56	2.94	0.264	25.0
	2×10^{-2}	76	"	"	10.1	"	3.84	4.3	0.193	18.2
	5×10^{-2}	200	"	"	67	"	9.9	7.94	0.143	13.5
	10^{-1}	397	"	"	264	"	19.6	13.75	0.123	11.6
	2×10^{-1}	649	"	"	866	"	35.3	23.2	0.104	9.9
100	5×10^{-3}	7.75	0.23	0.11	0.17	2.09	0.53	2.32	0.422	51.1
	10^{-2}	25	"	"	1.1	"	1.35	2.81	0.256	31.0
	2×10^{-2}	76	"	"	6.6	"	3.31	3.99	0.182	22.1
	5×10^{-2}	200	"	"	43	"	8.45	7.07	0.129	15.6
	10^{-1}	397	"	"	172	"	16.9	12.15	0.111	13.5
	2×10^{-1}	649	"	"	564	"	29.9	19.9	0.091	11.0

[a]From Griffiths, ref. 45, p. 11.

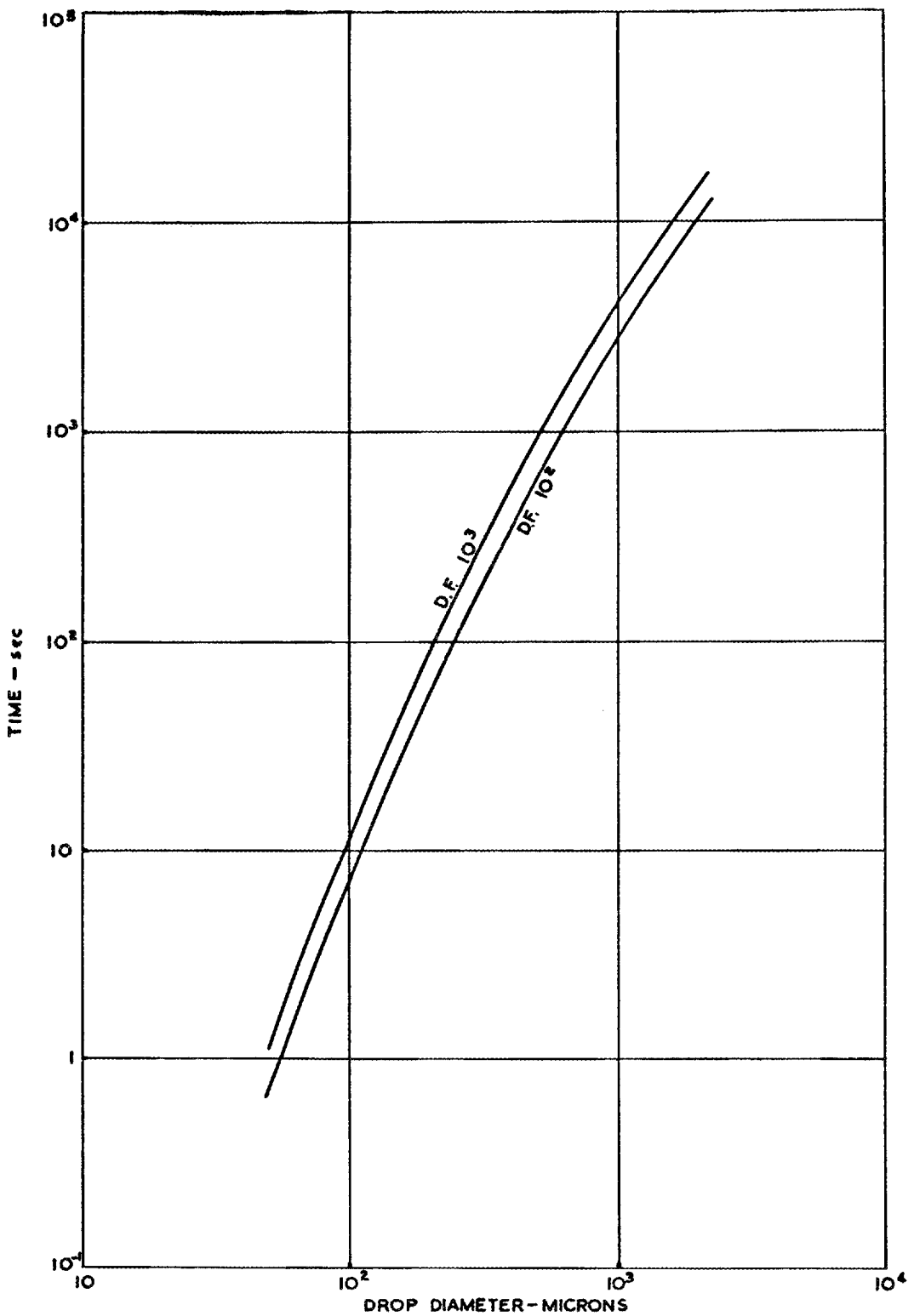

Fig. 4.83. Washout of Molecular Iodine by Reactive Sprays at a Flow Rate of 10 g/sec·m^2. (From Griffiths, ref. 45, Fig. 4.)

Griffiths states that molar solutions that would appear suitable are 4% NaOH or 24.8% $Na_2S_2O_3 \cdot 5H_2O$ or 12.6% Na_2SO_3. At concentrations of 10^{-7} g/cm^3 of iodine in the atmosphere, excess reagent would be present for drops larger than 100 μ and a distance greater than 10 m.

5. Removal of Particles by Sprays. Iodine and other fission products adsorbed on particulate matter are removed from an atmosphere by the following three main processes, all of which depend on the size and density of the particulates: (1) diffusion to solid or liquid surfaces; (2) fallout under gravity (this may be preceded by coagulation of the smaller particles); and (3) impaction on solid or liquid surfaces. This discussion will concentrate on process 3.

The fraction of the dust lying in the path of a falling drop that collides with it and is removed from the cloud is called the efficiency of impaction, E. Table 4.37 gives efficiencies of impaction of aerosol particles by water drops. Griffiths states that it is probable that submicron particles of unit density are not removed by sprays.

Table 4.37. Efficiency of Impaction of Aerosol Particles By Water Drops[a]

Particle Diameter (μ)	E, Efficiency of Impaction			
	Water Drop Diameter and Terminal Velocity			
	100 μ 25 cm/sec	200 μ 76 cm/sec	500 μ 200 cm/sec	1000 μ 400 cm/sec
1	0.0003	0.007	0.03	0.04
2	0.009	0.06	0.24	0.37
5	0.02	0.12	0.46	0.70

[a]From Griffiths, ref. 45.

The proportion of aerosol removed per second by water drops is[51]

$$\lambda = \frac{\pi d_W^2}{4} N V_W E \ , \qquad (4.64)$$

where

d_W = mean diameter of water drops,
N = number of water drops per cm^3 of air,
V_W = terminal velocity of water drops,
E = efficiency of impaction.

In the case of a spray, N is a function of the mass flow of liquid, M′ in g/sec per m^2 of floor area, and the terminal velocity of the water drops, which depends on the drop diameter,

$$N = 6 \times 10^{-4} \frac{M'}{V_W \pi d_W^{\,3}}, \tag{4.65}$$

and λ, from Eqs. (4.64) and (4.65), is given by

$$\lambda = 1.5 \times 10^{-4} \frac{EM'}{d_W} . \tag{4.66}$$

Values of λ for 1-, 2-, and 5-μ particles and a flow rate of 10 g/sec per m^2 of floor area are given in Table 4.38 and are shown in Fig. 4.84. At a mass flow rate of 100 g/sec per m^2 of floor area, the values of λ will increase by a factor of 10. Table 4.38 shows that the removal rate is fairly constant for a given particle size over a water drop range of 200 to 1000 μ. Griffiths states that the optimum would be about 500 μ.

Table 4.38. Removal Rates of Particles by Water Drops at a Flow Rate of 10 g/sec per m^2 of Floor Area[a]

Water Drop Diameter (μ)	λ (sec^{-1})		
	1-μ Particles	2-μ Particles	5-μ Particles
100	4.5×10^{-5}	1.35×10^{-3}	3×10^{-3}
200	5.2×10^{-4}	4.5×10^{-3}	9×10^{-3}
500	9×10^{-4}	7.2×10^{-3}	1.4×10^{-2}
1000	6×10^{-4}	5.5×10^{-3}	10^{-2}

[a]From Griffiths, ref. 45.

Sprays may be useful in removing UO_2 particles with densities of 10 g/cm^3 and diameters of <10 μ. They will not effectively remove submicron particles, and particles greater than 10 μ would settle out quickly under gravity, although in turbulent air this condition cannot be relied upon.

6. Spray Systems. Atomizing devices commonly used in generating aerosols may be classified as three main types:

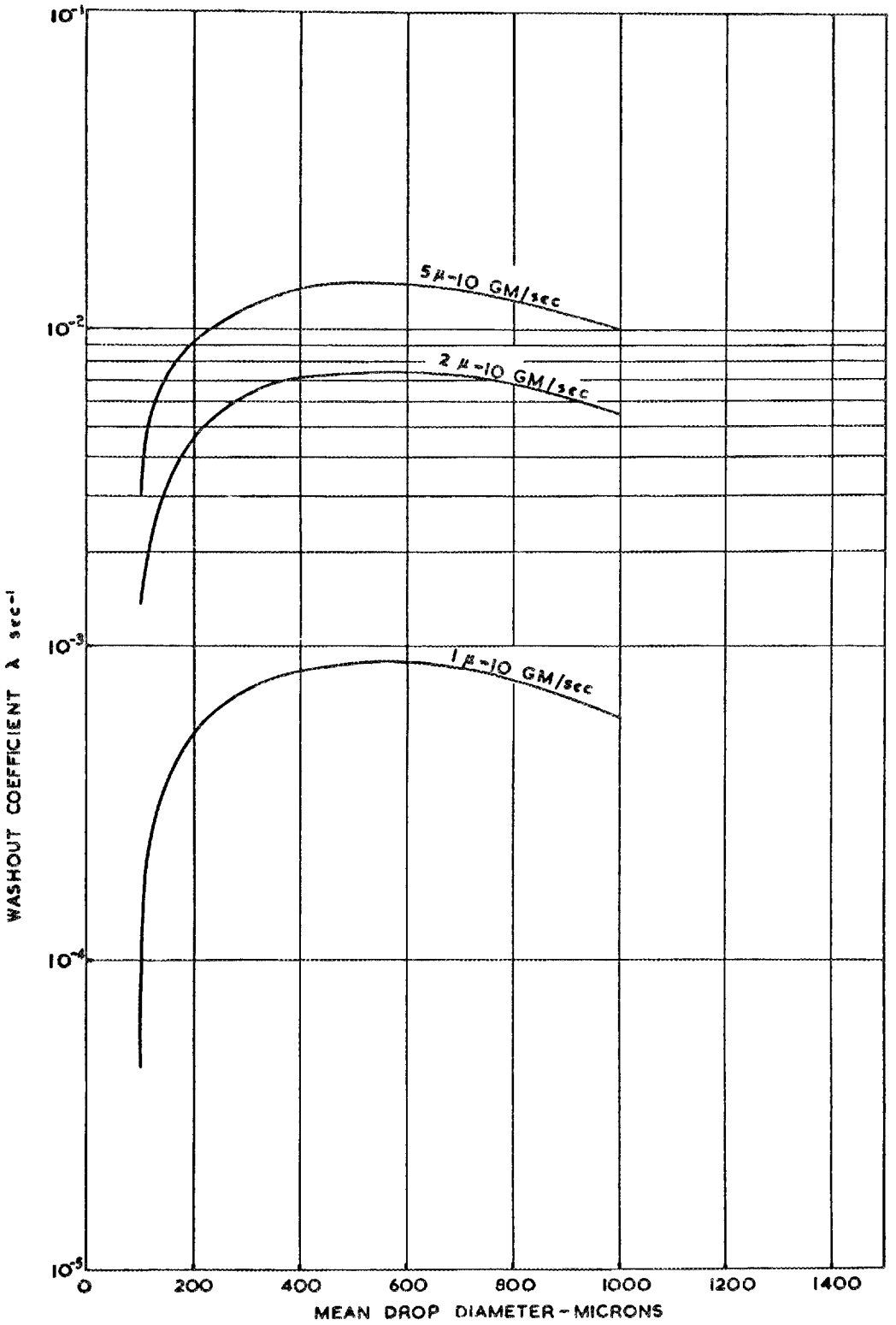

Fig. 4.84. Rates of Removal of Particles by Water Drops. (From Griffiths, ref. 45, Fig. 5.)

1. air blast or aerodynamic atomizers in which compressed air or steam is used at high velocity to break up the liquid emerging from the nozzle; a very wide range of droplet size is obtained;
2. centrifugal atomizers in which the liquid is fed onto a rotating disk and thrown off the edge; a uniform, easily controllable droplet size is obtained; and
3. The hydrodynamic type in which liquid is forced through a nozzle and breaks up into droplets.

In the swirl-chamber type of nozzle the atomizing action is caused by a spinning motion imparted to the liquid prior to spraying through a central orifice. The ways in which this may be achieved are described by Marshall.[52] A wide range of droplets (e.g., largest drops 50 to 100 times the size of the smallest drops) may be obtained; however, data by Tate and Marshall suggest that a factor of 10 between smallest and largest drops for 99% of the spray may be more realistic.

7. Choice of System. The type of atomization employed in a spray system that would be used to clean up a containment atmosphere after a fission-product release may depend on (1) the desired mean diameter of droplet, (2) the simplicity of design, and (3) energy considerations. The diameter of the droplet determines the residence time of the drop in the atmosphere, and it may be desirable in certain cases for this to be only a few minutes. For example, a 100-μ water drop falls 10 m in about 40 sec, while a 10-μ drop takes an hour to fall this distance and is therefore available for leakage from the containment atmosphere. The main advantage in producing drops smaller that 100 μ in diameter is that their ratio of surface area to volume of containment is increased. The removal of molecular iodine by water depends more on the volume of liquid introduced than the actual drop size, although above 1000 μ, equilibrium with water would not be reached in most containment heights. Removal of particulate matter would be best achieved with drops in the range 200 to 1000 μ.

With respect to simplicity of design, the liquid pressure system merely requires a pump and storage capacity. The air pressure system requires air pressure storage in addition to these. Centrifugual atomizers are ruled out on complexity of design and on cost and, indeed, have no advantage in this context.

The theoretical amount of energy required to break up a liquid into drops is very much less than that required in practice. This ratio, known as the atomization efficiency, is <1% for pressure nozzles. Marshall[52] gives the net horsepower requirement for pressure nozzles as

$$hp = 5.82MP \times 10^{-4} , \qquad (4.67)$$

where M is flow rate in gpm and P is total pressure drop in psi. The results of studies on the relation between drop diameter, flow rate, and pressure drop are confusing, but undoubtedly the type of nozzle is important. However, as a rough guide to the energy requirements for different drop sizes, the correlation suggested by Griffin and Muraszew[53] can be used. They suggested, for pressure nozzles, that

$$d_0 = K_p^{-0.42} , \qquad (4.68)$$

where d_0 is the Sauter mean diameter, K is a constant that depends on the conditions under which the spray is produced, and p is pressure drop. Griffin and Massey,[54] using a 0.0429-in. swirl-plate nozzle, found that a pressure of 70 psi and a flow of about 100 lb/hr gave a drop size distribution having a Sauter mean diameter of 100 μ. To produce a spray having d_0 = 50 μ, the pressure drop would be about 360 psi; to produce a spray of d_0 = 1000 μ, 0.3 psi.

The approximate energy requirements for the range of sprays considered in this report are given in Table 4.39, as determined from the Marshall relation [Eq. (4.67)]. It can be seen that the power requirement (e.g., 100 sprays covering a 100-m^2 area) is generally less than 1 hp. The exception would be the production of 50-μ drops at a 100 g/sec flow rate, which would require about 30 hp. The energy requirements for air-pressure atomization are invariably much greater than those for liquid pressure systems, and the limited data of Marshall suggest that under the conditions outlined above about 5 to 10 times the energy used in a liquid pressure system would be required.

Table 4.39. Energy Requirements of a Pressure Nozzle[a]

Sauter Mean Diameter (μ)	Pressure Drop (psi)	Energy Required Per Nozzle (hp)	
		At Flow Rate of 10 g/sec	At Flow Rate of 100 g/sec
50	360	3×10^{-4}	0.3
100	70	5×10^{-3}	5×10^{-2}
200	13.5	10^{-3}	10^{-2}
500	1.5	10^{-4}	10^{-3}
1000	0.3	2×10^{-5}	2×10^{-4}
2000	0.06	5×10^{-6}	5×10^{-5}

[a]From Griffiths, ref. 45.

The increase in pressure in the containment vessel may also prove embarrassing. It would seem that for most emergency systems, atomization by hydrodynamic pressure would be most suitable. For a once-through system the storage capacity required to supply 100 sprays for 1 hr would be 800 gal (3.7 m^3) at 10 g/sec and 8000 gal (37 m^3) at 100 g/sec.

8. Conclusions. Griffiths' concluded that well-distributed liquid sprays could effectively remove molecular iodine from a containment atmosphere following an accident. The fate of the particles would be rather uncertain, but the calculations suggest that particles of 10 g/cm^3 density and greater than 1 μ in diameter should be rapidly removed by sprays. The

biologically important submicron particles appear to have extremely low or zero impaction efficiencies with water drops, and it seems likely that they would not be removed. The removal of iodine compounds by liquid sprays probably depends on the partition of the compound between the gas and the liquid phases.

The removal of iodine from a containment vessel by water sprays depends on the amount of water injected and the temperature. In the case of water reactors there may be a large amount of water already available in the containment vessel for iodine dissolution. Thus two cases arise.

1. For containment systems in which no water is present intially, it is thought unlikely that the volume of water injected could exceed about 10% of the containment volume. Under these conditions about 92% of the iodine would be removed at 20°C and about 52% at 100°C.

2. For containment systems in which a large volume of water is present initially, if this volume is, say, equal to the air volume, then 99% of the iodine will be in the water at 20°C and 91% at 100°C, assuming that reasonable contact between the fission gases and water has occurred during the accident. The addition of more water by spray injection would have a marginal effect; however, it would cool the containment vessel and give better partition.

The efficiency of removal by water drops would depend on the height through which the drops fell. To achieve theoretical partition with minimum volumes of water, the whole volume of a drop must be effectively saturated. This would be so for all drops less than 1000 μ in diameter falling at least 10 m.

The problem of partition may be overcome by continuous removal of the water from the floor of the containment vessel, cleanup of the water outside the containment vessel, and then return of the water to the sprays, or by use of a liquid that combines chemically with iodine. Caustic soda, sodium sulfite, and sodium thiosulfate are all suitable, but sodium thiosulfate is probably the easiest solution to handle. The success of a chemically reactive spray depends on putting a sufficient mass of the salt into the containment to ensure an excess of reagent at all times. It is suggested that molar solutions would achieve this for initial iodine in air concentrations greater than 10^{-7} g/cm^3, i.e., 4% NaOH, 24.8% $Na_2S_2O_3 \cdot 5H_2O$, and 12.6% Na_2SO_3. It is also necessary to put the solution into the containment vessel in such a way as to enable all the liquid drops to be used. Well-dispersed small droplets at high flow rates give most rapid decontamination (Fig. 4.83).

At a flow rate of 10 g/sec, a spray would remove particles of 10 g/cm^3 density and greater than 5 μ in diameter in a few minutes. A decontamination factor of 10^3 in 15 min would be obtainable with drops in the range 200 to 1000 μ. An increase in flow rate of 100 g/sec might result in the removal of particles as small as 1 μ (density, 10 g/cm^3). The fate of smaller and less-dense particles is unknown, but the efficiency of removal is extremely low and in some cases zero. Liquid pressure sprays appear to be most attractive, and the energy requirements for 100 sprays would generally be <1 hp.

For a 1000-m^3 containment volume the storage requirements of 100 sprays working at 10 g/sec for 1 hr would be 3.7 m^3. One hundred sprays should cover an area of at least 100 m^2.

4.4.4.4 Behavior of Particulates in Containment Vessels

The fission products released from the reactor into the containment vessel could be associated with particles, as shown in Sections 4.3 and 4.4.1. The removal of particulates from the containment vessel atmosphere could take place by (1) diffusion to the walls and other available surfaces; (2) settling under gravity, often after agglomeration of smaller particles; (3) removal by spray droplets; and (4) filtration.

The removal by spray droplets was discussed in Section 4.4.4.3. Installation of filter units is discussed in Chapter 9. Diffusion to the walls would be negligible in still air in a volume as large as that of a containment vessel. However, air currents would almost certainly exist that would stir the air and change the problem from one of diffusion through large distances in still air to that of diffusion across a boundary layer next to the surface. Also, stirring of the air would greatly affect the settling of particulates under gravity forces. It is difficult to predict convection currents in a containment vessel, and perhaps the best way to evaluate these effects is to test a given vessel, as was done by Megaw and May (see Sec. 4.4.4.1).

Some information on the behavior of particulate matter will be reported here, but it is impossible to treat such a broad subject adequately. For complete treatment of this subject, see, for instance, Green and Lane[55] and Dallavalle.[56]

1. Settling of Particles. If the particle is of a large size compared with the mean free path of the gas molecules but not so large that any effects arise from the inertia of the displaced gas, then Stokes Law applies:

$$v = \frac{\rho g d^2}{18\eta} , \qquad (4.69)$$

where

v = terminal velocity of the particle, cm/sec,
g = gravitational acceleration, cm/sec^2,
d = diameter of particle, cm,
η = viscosity of air, g/sec·cm,

provided the density of the air is negligible compared with that of the particle. At Reynolds numbers of less than 0.05, deviation from Stokes Law does not exceed more than 1%. A Reynolds number of 0.05 corresponds to a 77-μ-diam sphere of unit density falling through air. For $0.05 < Re < 4$ (ref. 57),

$$Re = \frac{C_D Re^2}{24} - 2.3363 \times 10^{-4} \, (C_D Re^2)^2 + 2.0154 \times 10^{-6} \, (C_D Re^2)^3 - 6.9105 \times 10^{-9} \, (C_D Re^2)^4 . \qquad (4.70)$$

This equation is accurate for spheres of unit density that are large compared with the mean free path up to a diameter of 142 μ. The drag coefficient at terminal velocity is

$$C_D = \left(\frac{\pi}{6}\right)\left(\frac{d^3\rho g}{\frac{1}{2}\rho' v^2}\right)\left(\frac{\pi d^2}{4}\right), \tag{4.71}$$

and

$$Re = \frac{\rho' vd}{\eta}, \tag{4.72}$$

where ρ' is density of the air. Substituting Eqs. (4.71) and (4.72) into Eq. (4.70) yields a relation for v as a function of the other variables.

For particles of size comparable with the mean free path of the gas molecules, the particles can slip between the gas molecules and fall faster than predicted by hydrodynamic theory. Introducing the Cunningham correction factor into Stokes Law yields

$$v = \rho g d^2 \frac{(1 + 2A\lambda/d)}{18\eta}, \tag{4.73}$$

where λ is the mean free path of the molecule, and A is the numerical factor near unity. The mean free path is given by

$$\lambda = \frac{\eta}{0.248\rho'\bar{c}}, \tag{4.74}$$

where

$\bar{c}$ = mean molecular velocity,

$= \sqrt{8kT/\pi m}$,

$= 4.63 \times 10^2$ cm/sec at 20°C for air,

$= 4.63 \times 10^2 \sqrt{T/293}$,

and T is absolute temperature in °K. The only significant variation due to pressure is the effect on λ, since for air

$$p\lambda = 7.16 \times 10^{-4}, \tag{4.75}$$

where p is pressure in centimeters of mercury.

The slip correction factor can be expressed as[58]

$$(1 + 2A\lambda/d) = 1 + \frac{2 \times 10^{-4}}{pd} [6.32 + 2.01 \exp(-1095pd)] . \quad (4.76)$$

The terminal velocities and diffusion coefficients of rigid spheres of unit density falling in air, calculated by the appropriate equation, are listed in Table 4.40. It is to be noted that, by Eq. (4.73), the settling velocity is directly proportional to the density. The diffusion coefficient in Table 4.40 was found by

$$D = \frac{RT(1 + 2A\lambda/d)}{3N\pi\eta d} , \quad (4.77)$$

where

D = diffusion coefficient, cm^2/sec,
R = gas constant (8.3144×10^7), cm^2-g/$sec^2 \cdot$g-mole$\cdot$°K,
N = Avogadro's constant (6.02×10^{23}), at./g-mole.

Table 4.40. Terminal Velocities and Diffusion Coefficients of Rigid Spheres of Unit Density in Air at a Pressure of 760 mm Hg and a Temperature of 20°C[a]

Publication rights withheld. See original reference.

[a]From Green and Lane, ref. 55.

2. Combined Sedimentation and Diffusion of Small Particles. Davies[59] has calculated the concentration of particles that settle and diffuse while in suspension in a fluid that is uniformly dispersed in a wide vessel (i.e., the edge effects are neglected); this is a one-dimensional

problem. Although of limited use in considering a reactor containment vessel because of wall effects and air circulation, some of Davies' results are reproduced here since they may be useful for calculations of settling in compartments or other areas of still air.

The rate of increase at a point X in the suspension is given by

$$\frac{\partial C}{\partial T} = D \frac{\partial^2 C}{\partial X^2} - v \frac{\partial C}{\partial X} , \tag{4.78}$$

where

C = concentration at a point,
T = time,
D = diffusion coefficient,
v = settling velocity.

Substituting the relations $X = xl$, $T = tl/v$, $C = cC_0'$, where l is the height of the vessel, and C_0 is the initial concentration (x, t, and c are pure numbers), yields Eq. (4.78) in dimensionless form:

$$\frac{\partial c}{\partial t} = \alpha \frac{\partial^2 c}{\partial x^2} - \frac{\partial c}{\partial x} , \tag{4.79}$$

where α is D/vl. By use of the boundary conditions,

$$c(x,0) = 1 ,$$

$$c(x,\infty) = 0 \qquad (0 < x < 1) ,$$

Davies obtained solutions in eigenfunction expansions.

For the mathematical solutions, the original paper can be consulted. Figure 4.85 shows the solutions for seven values of α. These results can be used by the relations

$$\alpha = \frac{D}{v\ell} = \frac{(1.371 \times 10^{-16})(293)}{1/6\pi d^3(\rho - \rho')(981\ell)} \tag{4.80}$$

and

$$\frac{T}{t} = \frac{l}{v} = \frac{18\eta l}{d^2(\rho - \rho')gF} , \tag{4.81}$$

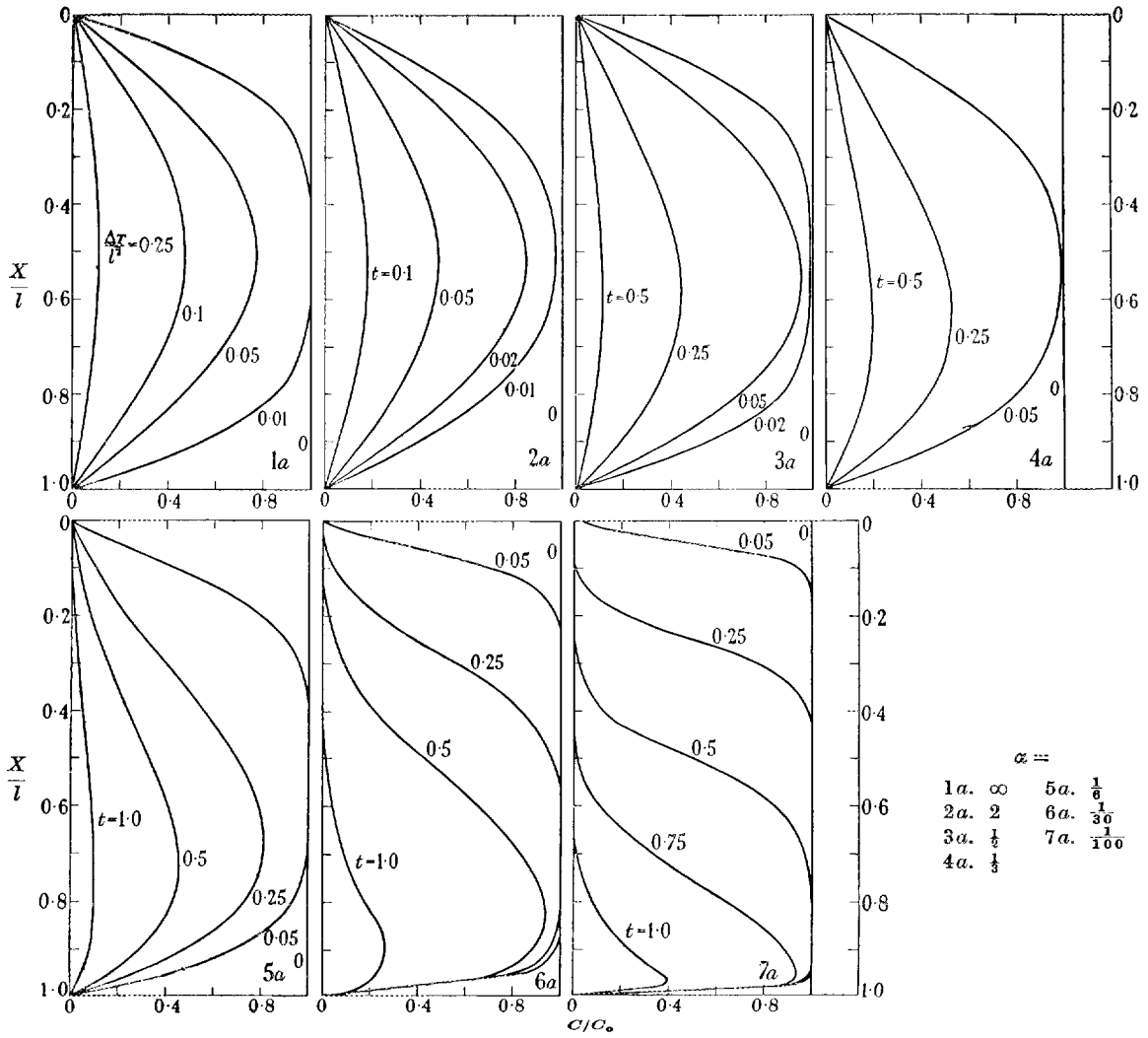

Fig. 4.85. Fluid Between Horizontal Adsorbing Planes. (From Davies, ref. 59, p. 112.)

where ρ' is the density of air and F is the slip factor. Table 4.41 is based on Eqs. (4.80) and (4.81). Given a particle size, α can be calculated from the first column and t can be multiplied by the value in column 6 to yield a relation in the real time T.

Settling (in the absence of diffusion effects for particles of equal diameter) can be expressed by[55]

$$C = C_0 e^{-vT/l} \quad . \tag{4.82}$$

(For a discussion on settling of polydisperse particles, see Green and Lane,[55] p. 169).

Table 4.41. Sedimentation Under Gravity at 20°C[a]

Particle Diameter (μ)	$\alpha(\rho - \rho')l$ (g/cm^2)	Particles in Air at 760 mm Hg				Particles in Water		
		$\frac{v}{\rho - \rho'}$	D (cm^2/sec)	F	$\frac{T}{t}\frac{\rho - \rho'}{l}$	$\frac{v}{\rho - \rho'}$	D (cm^2/sec)	$\frac{T}{t}\frac{\rho - \rho'}{l}$
		$\times 10^{-6}$	$\times 10^{-6}$			$\times 10^{-6}$	$\times 10^{-6}$	
0.05	0.625	37.7	23.5	5.02	26,500	0.135	0.0848	7,410,000
0.1	0.0781	86.4	6.77	2.89	11,600	0.54	0.0424	1,850,000
0.15	0.0232	149	3.45	2.21	6,710	1.215	0.0283	823,000
0.2	0.00977	225	2.20	1.88	4,440	2.16	0.0212	463,000
0.3	0.00298	422	1.22	1.57	2,370	4.86	0.0141	206,000
0.4	0.00122	679	0.832	1.42	1,470	8.64	0.0106	116,000
0.5	0.000625	993	0.623	1.33	1,010	13.5	0.0085	74,100
			η = 0.000182				η = 0.0101	

[a]From Davies, Proc. Roy Soc., ref. 59.

3. Particle Agglomeration. Aerosol particles, regardless of their composition, coalesce, or stick together, if they come into contact with each other. The process goes on continuously, so the aerosol becomes progressively more coarse and finally settles.[55]

Experimental data show that coagulation of particles follows the simple law

$$\frac{1}{n} - \frac{1}{n_0} = Kt \ , \tag{4.83}$$

where

n = number of particles per cm^3,
n_0 = initial number of particles per cm^3,
t = time, sec,
K = coagulation coefficient, cm^3/sec.

From Eq. (4.83) it can be seen that the rate of disappearance of particles is

$$-\frac{dn}{dt} = Kn^2 \ . \tag{4.84}$$

Thus, in any given smoke the coagulation is very rapid in the early stages, when n is large. Table 4.42 gives coagulation constants for various aerosols. It can be seen that the coagulation constant is only weakly affected by the material composition of the particles.

Table 4.42. Coagulation Constants for Various Aerosols[a]

Publication rights withheld. See original reference.

[a]From Green and Lane, ref. 55.

The theoretical expression for K when coagulation is assumed to be effected by Brownian motion is[55]

$$K = \frac{4RT}{3\eta N}\left(1 + \frac{Al}{r}\right) t \ . \qquad (4.85)$$

For example, using the values for air at 20°C ($R = 8.3 \times 10^7$, $T = 293$, $\eta = 1.82 \times 10^{-4}$, $N = 6.1 \times 10^{23}$, $Al = 9 \times 10^{-6}$, and $r = 0.125\ \mu$), $K = 0.51 \times 10^{-9}\ cm^3/sec$. Theoretical and experimental values have been shown to agree well in this case.

The above discussion is for monodisperse aerosols, that is, the particles are assumed to be of equal size. Experiments[55] have shown that smokes with particles of various sizes coagulate more rapidly than those with nondisperse particles. The existence of foreign vapors does not, in general, greatly affect the coagulation rate. Stirring increases the coagulation rate.

The effect of electric charges on aerosols cannot be predicted. Many experiments have shown an increase in coagulation rate, others have shown little effect. (For a complete discussion, see Green and Lane.[55])

The coagulation properties of aerosols are the subject of an interesting study by Fontana and Browning on the effect of particulate fission products in double containment systems with filtration equipment.[60] It was assumed that after an accident the fission products released from the core would fill the containment vessel and begin to leak out into the outer containment shell, which was swept with air that was filtered prior to exhaust into the atmosphere. It was further assumed that particles of sizes less than 0.3 μ would penetrate this secondary containment filter (the filtration efficiency for particles less than 0.3 μ is not well

known, whereas the efficiency for 0.3-μ particles is greater than 99.97%). By use of Eq. (4.83) and the relation

$$\frac{m}{V_1} = \rho \frac{\pi}{6} d^3 n \ , \tag{4.86}$$

where m is total mass of material making particles (in grams, and V_1 is total free volume of the containment vessel (in cm^3), the time required to reach a given diameter was found to be

$$t = \frac{d^3 \pi \rho}{6(m/V_1)K} - \frac{1}{n_0 K} \ . \tag{4.87}$$

Since in most cases n_0 can be expected to be very large compared with 1/K, the second term is neglected.

The integrated release from the secondary containment system up to time t compared with the rate of release from the primary containment vessel is[60]

$$\frac{A}{IR} = t - \frac{V_2}{Q} \left[1 - e^{-(Q/V_2)t}\right] \ , \tag{4.88}$$

where

A = total integrated activity released to time t, curies,
I = total activity inventory in the primary system, curies,
R = primary containment release rate, %/sec,
Q = secondary containment sweep-gas volumetric flow rate, cm^3/sec.

Figure 4.86 shows particle size versus time in the primary containment vessel, obtained from Eq. (4.87), as a function of the mass concentration of agglomerating matter in air. Figure 4.87 shows the total activity released from the secondary containment system as a function of time t, during which the filters are ineffective; the volume change time of the secondary containment is a parameter. One curve from Fig. 4.86, with $m/V_1 = 5.77 \times 10^{-7}$ g/cm^3, is superimposed on Fig. 4.87 as an example of the use of the two curves. It can be seen that if the critical particle size is 0.3 μ and a volume change time of 900 sec is used, a value of A/IR = 26 is obtained. Thus, if the leak rate R is 3%/day, this would be 3.47×10^{-7}/sec and $A/I = 26\ (3.47 \times 10^{-7}) = 9.02 \times 10^{-6}$. That is, 9.02×10^{-4}% of the inventory available within the primary containment atmosphere is released to the external atmosphere, provided the particulate matter was assumed to be made entirely of the active material.

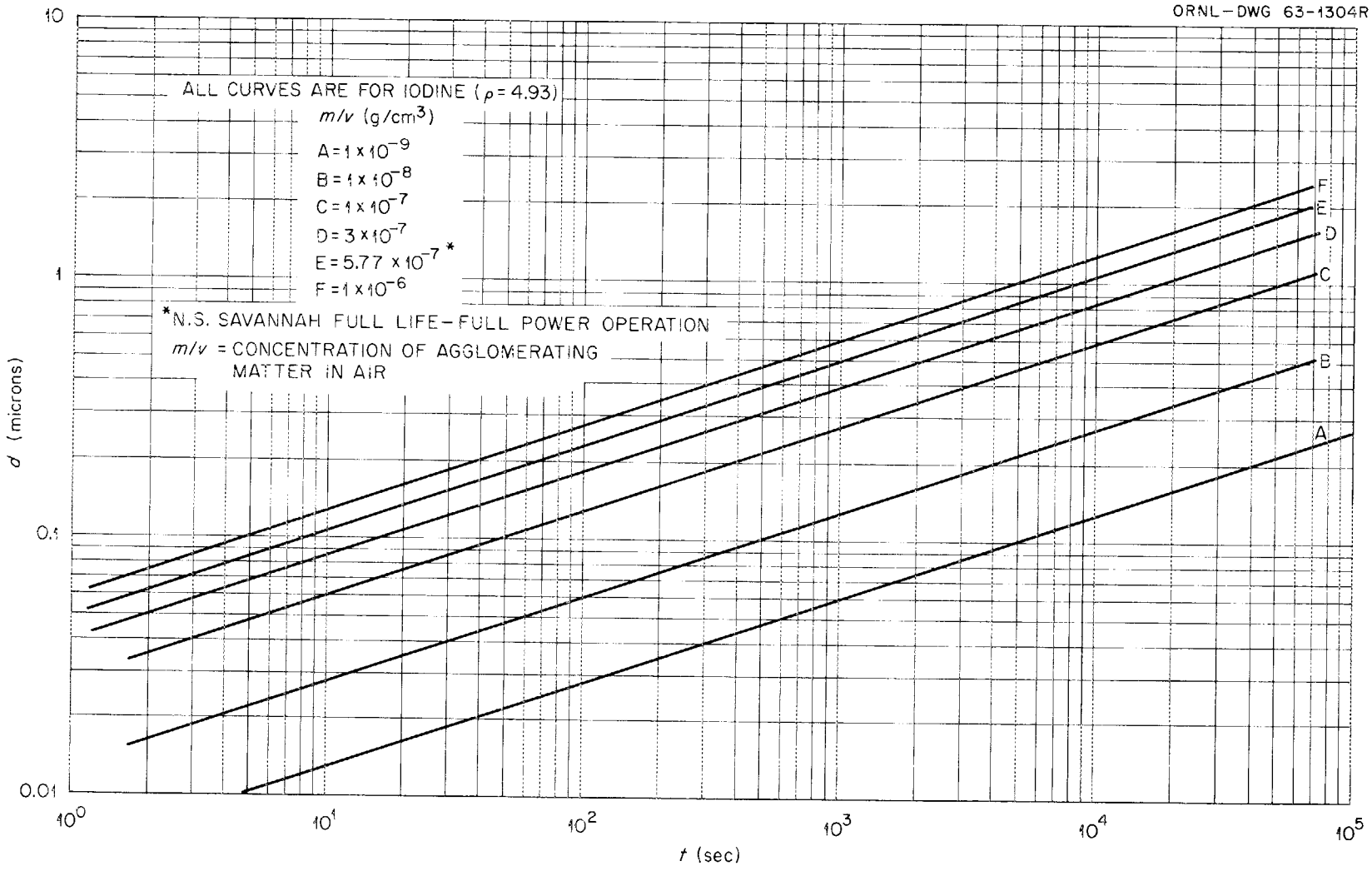

Fig. 4.86. Particle Size Versus Time as Controlled by Agglomeration. (From Fontana and Browning, ref. 60.)

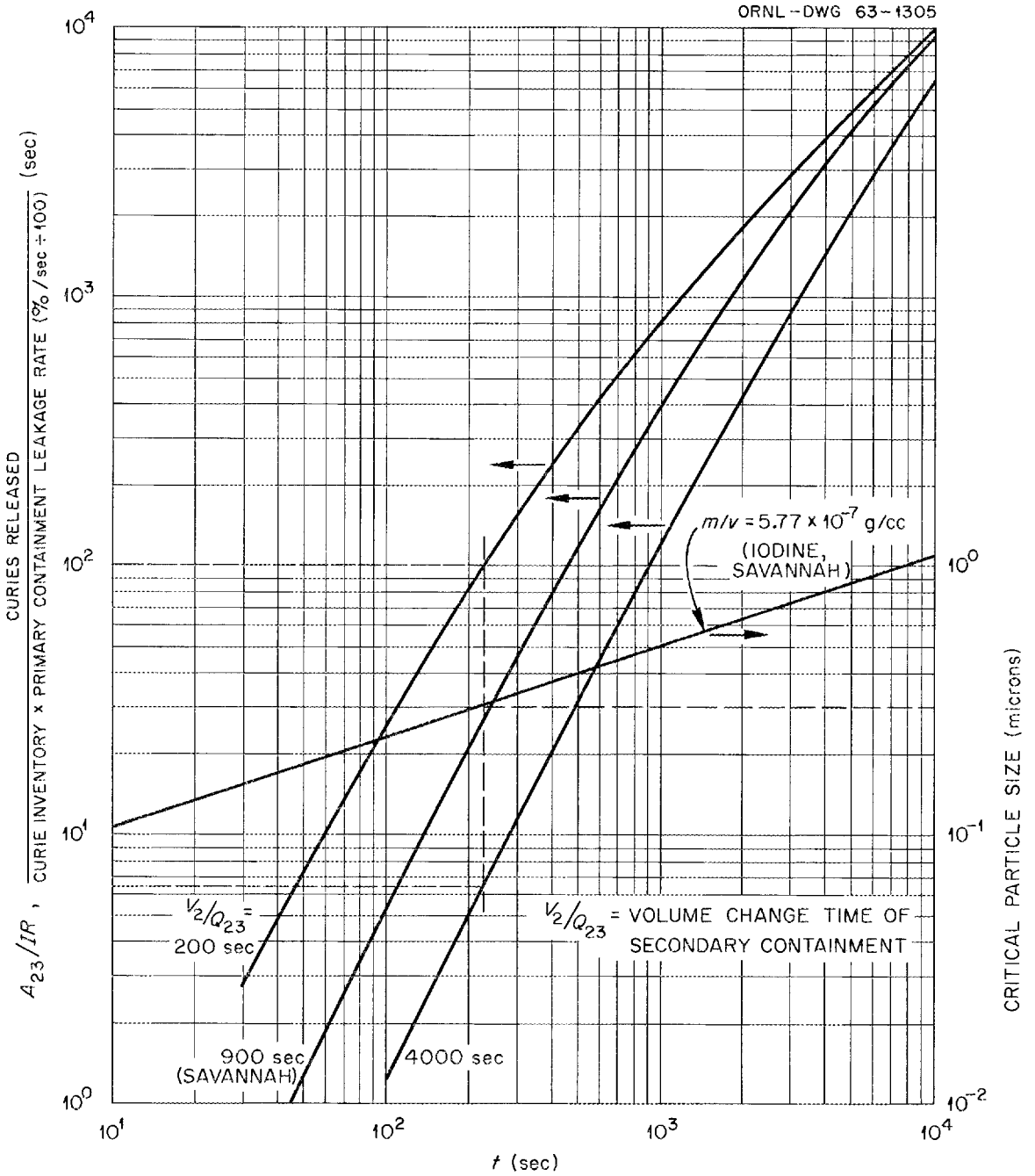

Fig. 4.87. Total Activity Released During Period of Zero Filter Efficiency Per Release Rate Versus Time. (From Fontana and Browning, ref. 60.)

Since it can be shown that

$$t = \frac{d^3\pi}{6K(V_p/V_1)} , \qquad (4.89)$$

where V_p is the volume occupied by particles, the time to reach a critical particle size would be inversely proportional to the volume occupied by the particles. Thus, addition of less-active material would increase V_p and reduce the time during which filtration is assumed to be ineffective. It also can be shown that

$$A = \frac{IR\pi d^3}{6(m_1/V_1)K} . \qquad (4.89a)$$

Thus, since I is the activity inventory associated with m_1, the material available to make particles, reducing the specific activity I/m_1 reduces the total amount of activity released.

4.4.4.5 Release of Activity from Three-Barrier Containment Systems

Anderson[61] has analyzed, in a general way, the three-barrier containment problem, i.e., a system utilizing a secondary containment vessel surrounded by a swept volume, such as is used in the NS Savannah. The model analyzed is shown in Fig. 4.88, with the following nomenclature:

$F(t)$ = fraction of the total quantity of the isotope that has escaped from the core as a gas,
$N(t)$ = total quantity of isotope existing at time t,
$R(t)$ = rate of escape of a given isotope from the reactor core into the first containment vessel,
λ_p = decay constant of precursor isotope,
$Q_p(t)$ = quantity of the precursor isotope held up in first containment vessel,
$Q(t)$ = quantity of the isotope held up in the first containment vessel,
λ = decay constant of isotope being considered,
l = leak rate constant for first containment vessel, %/day,
$U_p(t)$ = quantity of precursor isotope held up in second containment vessel,
$U(t)$ = quantity of isotope held up in second containment vessel,
m = leak rate constant for second containment vessel.

ORNL-LR-DWG 72986A

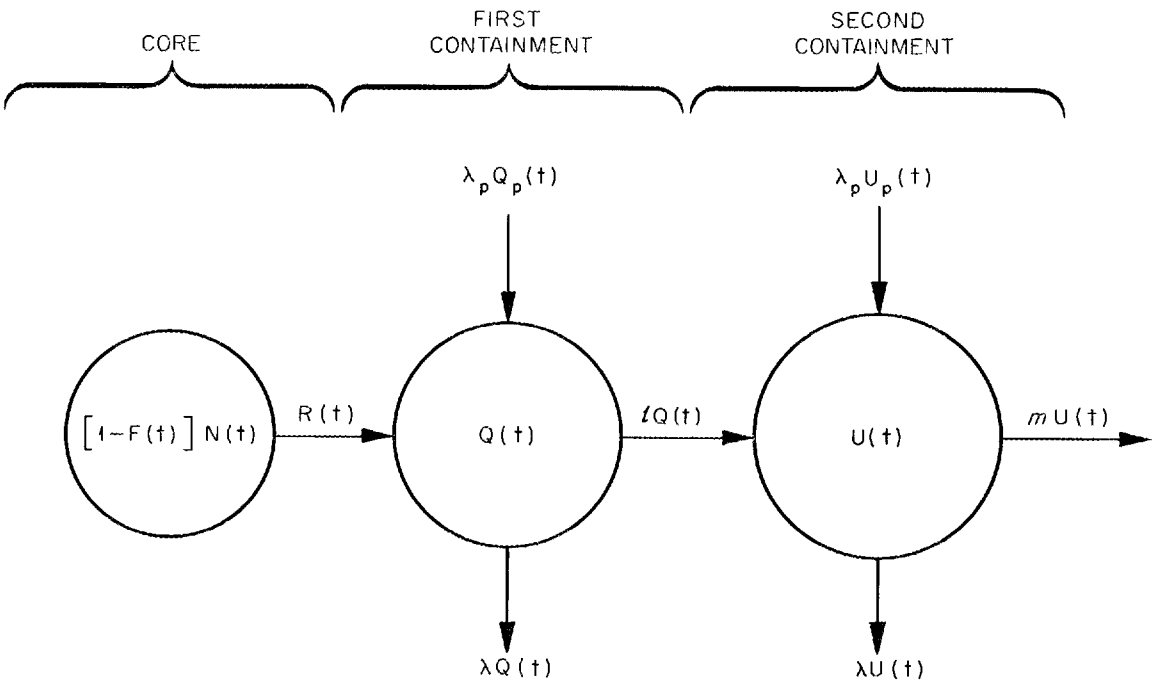

Fig. 4.88. Schematic Diagram of Containment Rate Processes. (From Anderson, ref. 61, p. 5.)

The equations for the system are

$$\frac{dq(t)}{dt} + \lambda_p \left[1 - \frac{q_p(t)}{q(t)}\right]\left[\frac{N_p(t)}{N(t)}\right] q(t) + \ell q(t)$$

$$= \frac{dF(t)}{dt} + \lambda_p[F(t) - F_p(t)] \frac{N_p(t)}{N(t)} \qquad (4.90)$$

and

$$\frac{du(t)}{dt} + \lambda_p \left[1 - \frac{u_p(t)}{u(t)}\right]\left[\frac{N_p(t)}{N(t)}\right] u(t) + mu(t) = \ell q(t) , \qquad (4.91)$$

where

$$\begin{aligned} q(t) &= Q(t)/N(t), \\ q_p(t) &= Q_p(t)/N_p(t), \\ u(t) &= U(t)/N(t), \\ u_p(t) &= U_p(t)/N_p(t). \end{aligned}$$

If it is assumed that all the precursor isotopes move through the system in the same manner as the isotope of interest, Eqs. (4.90) and (4.91) can be solved. In this case

$$F_p(t) = F(t) ,$$

$$q_p(t) = q(t) ,$$

$$u_p(t) = u(t) ,$$

and Eqs. (4.90) and (4.91) become

$$\frac{dq(t)}{dt} + \ell q(t) = \frac{dF(t)}{dt} \tag{4.92}$$

and

$$\frac{du(t)}{dt} + mu(t) = \ell q(t) . \tag{4.93}$$

With the initial conditions that $q(0) = U(0) = F(0) = 0$, the solution for $u(t)$ is

$$u(t) = \frac{\ell}{m - \ell} \left[me^{-mt} \int_0^t e^{mt} F(t)\, dt - \ell e^{-\ell t} \int_0^t e^{\ell t} F(t)\, dt \right] . \tag{4.94}$$

The leak rate to the atmosphere is given by

$$mU(t) = \frac{m\ell N(t)}{m - \ell} \left[me^{-mt} \int_0^t e^{mt} F(t)\, dt - \ell e^{-\ell t} \int_0^t e^{\ell t} F(t)\, dt \right] . \tag{4.95}$$

In the case of a single containment vessel, it is often assumed that a fraction f of the total quantity of a given fission product is released instantaneously from the core and that leakage from the containment vessel is small enough so that little depletion occurs because of the leakage. For this simple case the leakage to the atmosphere is given by $\ell fN(t)$. The leak rate given by Eq. (4.94) expressed as a fraction of the simple single-containment case is

$$\frac{mU(t)}{\ell fN(t)} = \frac{m}{f(m - \ell)} \left[me^{-mt} \int_0^t e^{mt} F(t)\, dt - \ell e^{-\ell t} \int_0^t e^{\ell t} F(t)\, dt \right] . \tag{4.96}$$

1. Case of Exponential Release from Core. In some cases it is possible to approximate the fission-product release characteristics of the reactor core by the empirical expression

$$F(t) = 0 \qquad t \leq t_0 ,$$

$$F(t) = [1 - e^{-\mu(t-t_0)}]f \qquad t > t_0 ,$$

where

t_0 = time elapsed from the start of the accident to initial fuel-element failure,
μ = rate parameter which must be determined by a detailed analysis of the core failure,
f = fractional release rate ($0 \leq f \leq 1$).

Using the above empirical expression for $F(t)$, the relative leak rate given by Eq. (4.96) is

$$L(\theta) = \frac{\kappa}{\kappa - 1}\left[\frac{\epsilon}{\kappa - \epsilon} e^{-\kappa\theta} - \frac{\epsilon}{1 - \epsilon} e^{-\theta} + \left(\frac{1}{1 - \epsilon} - \frac{\kappa}{\kappa - \epsilon}\right) e^{-\theta}\right] , \qquad (4.97)$$

where

$L(\theta) = mU(t)/lf\,N(t)$,
$\theta = l(t - t_0)$,
$\kappa = m/l$,
$\epsilon = \mu/l$.

2. Case of Step Release from Core. A conservative model for describing fission-product release from a reactor core following an accident is

$$F(t) = 0 \qquad t \leq t_0 ,$$

$$F(t) = f \qquad t > t_0 .$$

With this core model, Eq. (4.96) becomes

$$L(\theta) = \frac{\kappa}{\kappa - 1}\left(e^{-\theta} - e^{-\kappa\theta}\right) . \qquad (4.98)$$

Anderson[61] has calculated the relative leak rate $L(\theta)$ for the case of step release from the core, as given by Eq. (4.98), for a range of θ and several values of κ. The results are given in Fig. 4.89.

3. Use of Leak Rate Curve. The use of the leak rate curves given in Fig. 4.89 can best be illustrated by a few examples given by Anderson.

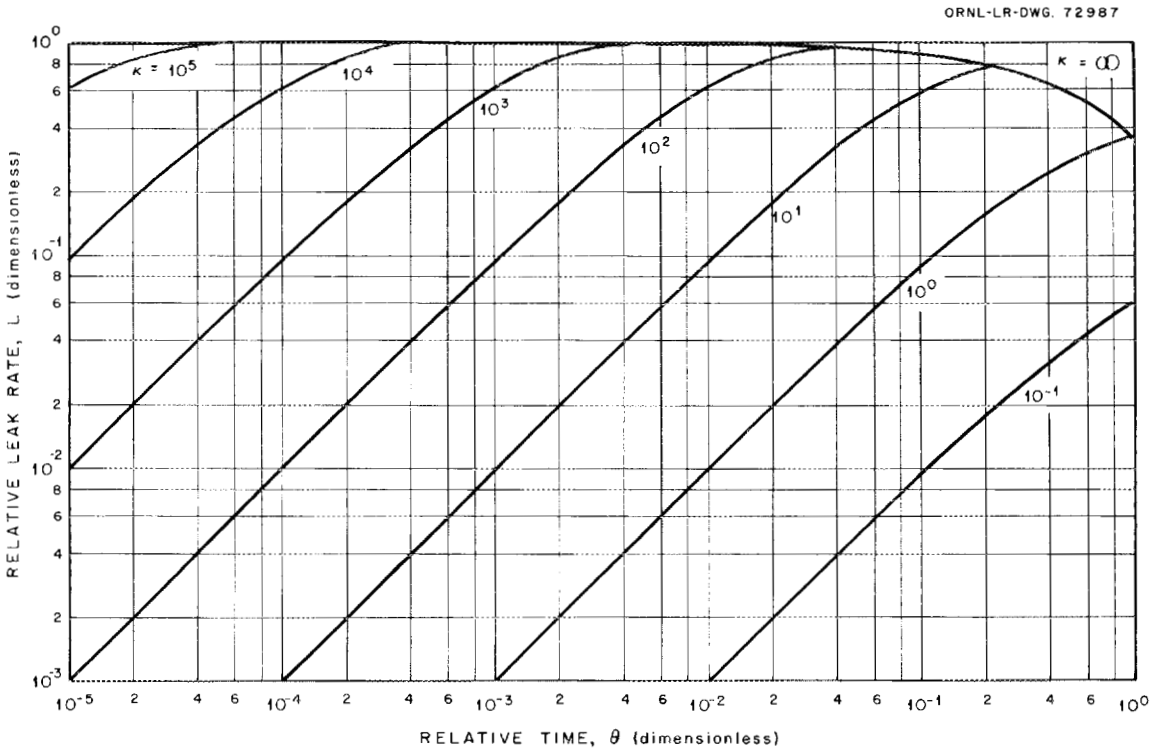

Fig. 4.89. Leak Rate to Atmosphere with Step Release from Core. (From Anderson, ref. 61, p. 11.)

Example 1

Problem: A reactor has two containment structures The first (or inner) structure leaks 1.0% of the contained gases per day; the second structure leaks at a rate of 1000% per day. It is assumed that an accident occurs when the core inventory of ^{135}I is 10^6 curies. It is also assumed that the reactor is shut down on initiation of the accident and that initial fuel-element failures occur 15 min later. If 25% of the iodine escapes from the core as a gas, what is the ^{135}I release rate to the atmosphere 1 hr after the accident?

Solution: The release rate at any time is given by

$$mU(t) = L(\theta)\lambda fN(t) \ .$$

The following values are obtainable from the statement of the problem:

$$\lambda = \frac{1.0\%/\text{day}}{100} = 0.01/\text{day} \ ,$$

$$m = \frac{1000\%/\text{day}}{100} = 10/\text{day} ,$$

$$\kappa = \frac{m}{l} = 10^3 ,$$

$$N(0) = 10^6 \text{ curies} ,$$

$$t_0 = 15 \text{ min} = \frac{1}{96} \text{ day} ,$$

$$f = 0.25 .$$

The value of θ for 1 hr is

$$\theta = l(t - t_0) = 0.01 \left(\frac{1}{24} - \frac{1}{96}\right) = 3.13 \times 10^{-4} .$$

From Fig. 4.89, $L(\theta)$ at 1 hr is $L = 0.26$. The total number of curies of ^{135}I existing at any time is given by $N(t) = N(0)e^{-\lambda t}$. The decay constant λ for ^{135}I is $\lambda = 0.1034/\text{hr}$. Therefore $N = 10^6\ e^{-0.1034} = 9.02 \times 10^5$ curies. Using the above quantities, the release rate at 1 hr is

$$(0.26)(0.01)(0.25)(9.02 \times 10^5) = 586 \text{ curies/day} .$$

Example 2

Problem: Find the amount of ^{135}I held up in the second containment structure for the reactor of example 1.

Solution: The quantity of material held up in the second containment structure is

$$U(t) = \frac{\text{release rate}}{m}$$

After 1 hr the amount of ^{135}I in the second containment vessel is

$$U = \frac{586}{10} = 58.6 \text{ curies} .$$

Example 3

Problem: If the reactor of example 1 did not have a second containment structure, what would be the release rate of ^{135}I after 1 hr?

Solution: A single containment vessel system is the same as a double containment vessel system with the outer vessel leaking at an infinite rate, i.e., $\kappa = \infty$. As can be seen from Fig. 4.89, $L(\theta)$ is approximately

unity for $\theta \lesssim 10^{-2}$ and $\kappa = \infty$. Therefore, the leak rate of ^{135}I at 1 hr is given by

$$(1)(0.01)(0.25)(9.02 \times 10^5) = 2260 \text{ curies/day} .$$

Example 4

Problem: An iodine filter having an efficiency E of 0.99 (99%) is fitted to the exhaust of the second containment vessel of the system in example 1. After 1.0 hr, what is the release rate of ^{135}I to the atmosphere with the filter installed?

Solution: Although the effect of a filter is not explicitly accounted for in the curves of Fig. 4.89, the calculation is quite straightforward. As before, the release rate from the second containment structure is mU(t). With filters, however, the quantity, mU(t), is the flow rate into the filter rather than to the atmosphere. Assuming negligible transit time through the filter, the exhaust rate from the filter and to the atmosphere is: Release rate with filter = mU(t)(1 − E). Using the result for mU(t) given in example 1, the exhaust rate of ^{135}I to the atmosphere (after 1.0 hr) with the filter is

$$(586)(1 - 0.99) = 5.86 \text{ curies/day} .$$

4.5 EFFECTS EXTERNAL TO CONTAINMENT BARRIERS

If an accident occurred that released fission products within the final containment structure, leakage from the structure would be borne downwind and diluted in the air. The exclusion distance prescribed for nuclear plants is established with cognizance of the dilution effect and is based on the maximum allowable dose to inhabitants in the vicinity of the plant. Therefore it is necessary to determine the external dose from the radioactive cloud, the internal dose received by inhalation, and the internal dose received by consumption of agricultural products.

4.5.1 Atmospheric Dispersion

The subject of atmospheric dispersion is too large to treat thoroughly here; refs. 62 through 67 should be consulted for further information on the subject. The basic equation for dispersion from continuous point sources suggested by Gifford[65] is the so-called "generalized Gaussian plume formula":

$$\chi = \frac{Q}{\pi\sigma_y\sigma_z\bar{u}} \exp\left[-\frac{1}{2}\left(\frac{y^2}{\sigma_y^2} + \frac{h^2}{\sigma_z^2}\right)\right], \qquad (4.99)$$

where

χ = ground-level air concentration, curies/m^3,
Q = source strength, curies/sec,
$\bar{u}$ = average wind speed, m/sec,
h = height of the source above the ground, m,
y = lateral (crosswind) distance from the plume axis, m.

In this equation, the x axis coincides with $\bar{u}$. The dispersion coefficients in the y and z directions are expressed as standard deviation of the plume distributions, σ_y and σ_z. Values of σ_y and σ_z are given in Figs. 4.90 and 4.91 for distances from the source of 100 to 100,000 meters for six meteorological categories,[68] as defined in Table 4.43.

Table 4.43. Meteorological Categories[a]

A: Extremely unstable conditions
B: Moderately unstable conditions
C: Slightly unstable conditions
D: Neutral conditions[b]
E: Slightly stable conditions
F: Moderately stable conditions

Surface Wind Speed (m/sec)	Daytime Insolation			Thin Overcast or ≥4/8 Cloudiness	≤3/8 Cloudiness
	Strong	Moderate	Slight		
<2	A	A-B	B		
2	A-B	B	C	E	F
4	B	B-C	C	D	E
6	C	C-D	D	D	D
>6	C	D	D	D	D

[a]From Hilsmeier and Gifford, ref. 68, p. 4.

[b]Applicable to heavy overcast, day or night.

[c]The degree of cloudiness is defined as that fraction of the sky above the local apparent horizon which is covered by clouds. [Manual of Surface Observations (WBAN), Circular N(7th ed.), paragraph 1210, U.S. Government Printing Office, Washington, July 1960.]

Hilsmeier and Gifford[68] used Eq. (4.99) and Figs. 4.90 and 4.91 to obtain charts yielding $\bar{u}(\chi/Q)$ versus distance from the source for various conditions. The term χ/Q, in units of sec/m^3, is often called the "stack factor." The charts are reproduced in Figs. 4.92 through 4.96. Figure 4.92 shows values of $\bar{u}(\chi/Q)$ at the surface for various types of weather with the source at ground level. Figures 4.93 through 4.95 show $\bar{u}(\chi/Q)$ at the surface for elevated releases of 10, 30, and 100 m, respectively.

Figure 4.96 shows the values of the area (in m^2) enclosed by ground-level concentration isopleths having the value χ_E as a function of the quantity $\chi_E(\bar{u}/Q)$ (an isopleth is a line of uniform ground concentration).

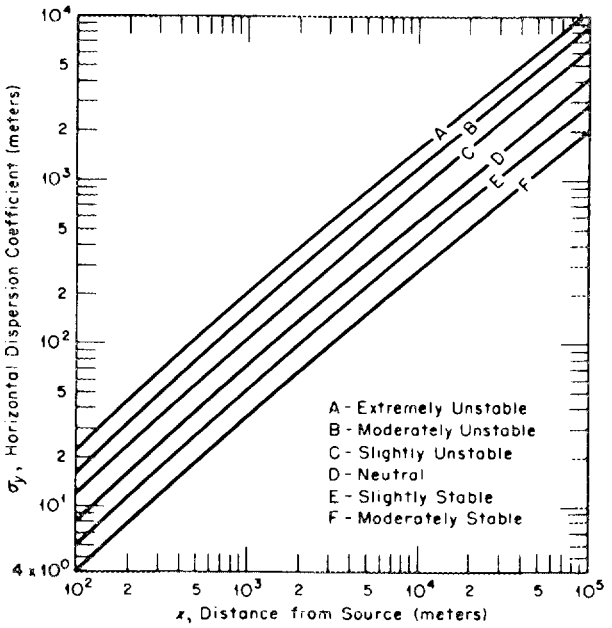

Fig. 4.90. Horizontal Dispersion Parameter, σ_y, as a Function of Downwind Distance, x, for Various Type of Weather. (From Gifford, ref. 65.)

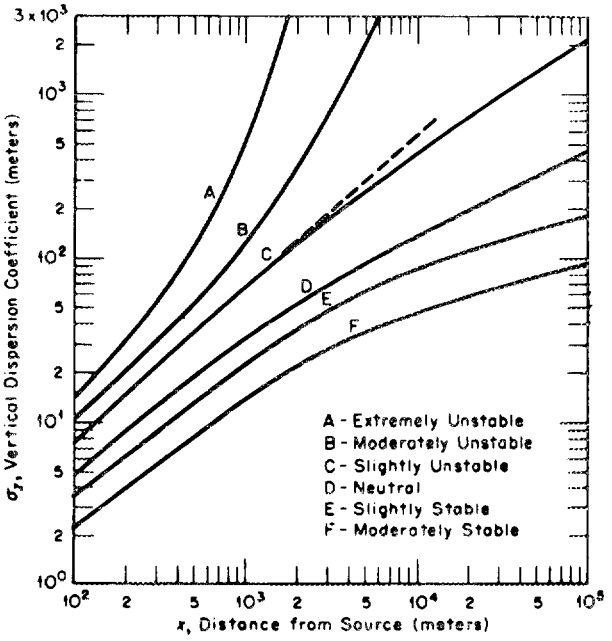

Fig. 4.91. Vertical Dispersion Parameter, σ_z, as a Function of Downwind Distance, x, for Various Types of Weather. (From Gifford, ref. 65.)

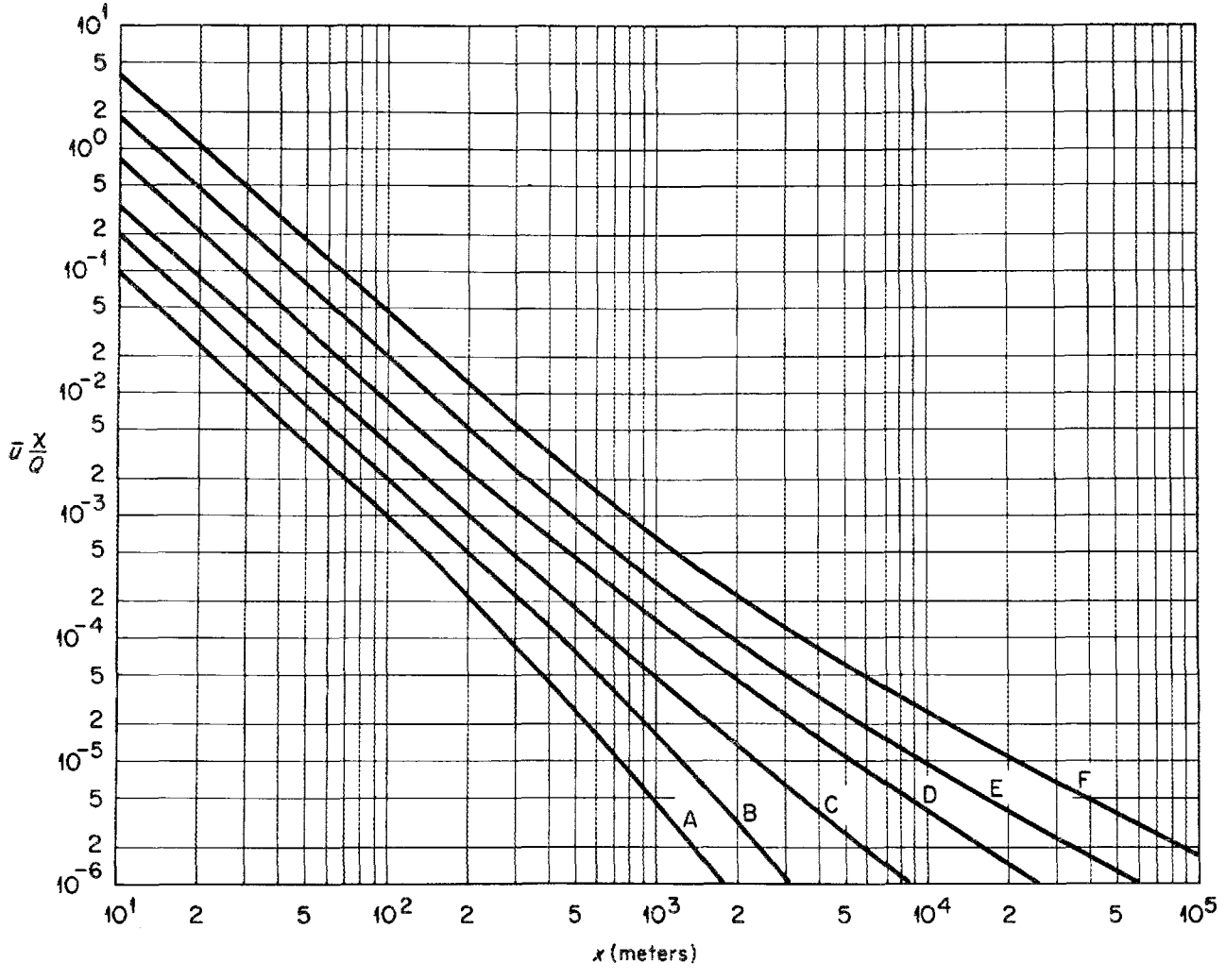

Fig. 4.92. Values of $\overline{u}X/Q$ as a Function of Downwind Distance, x, for Various Types of Weather; Source at Surface. (From Hilsmeier and Gifford, ref. 68, p. 6.)

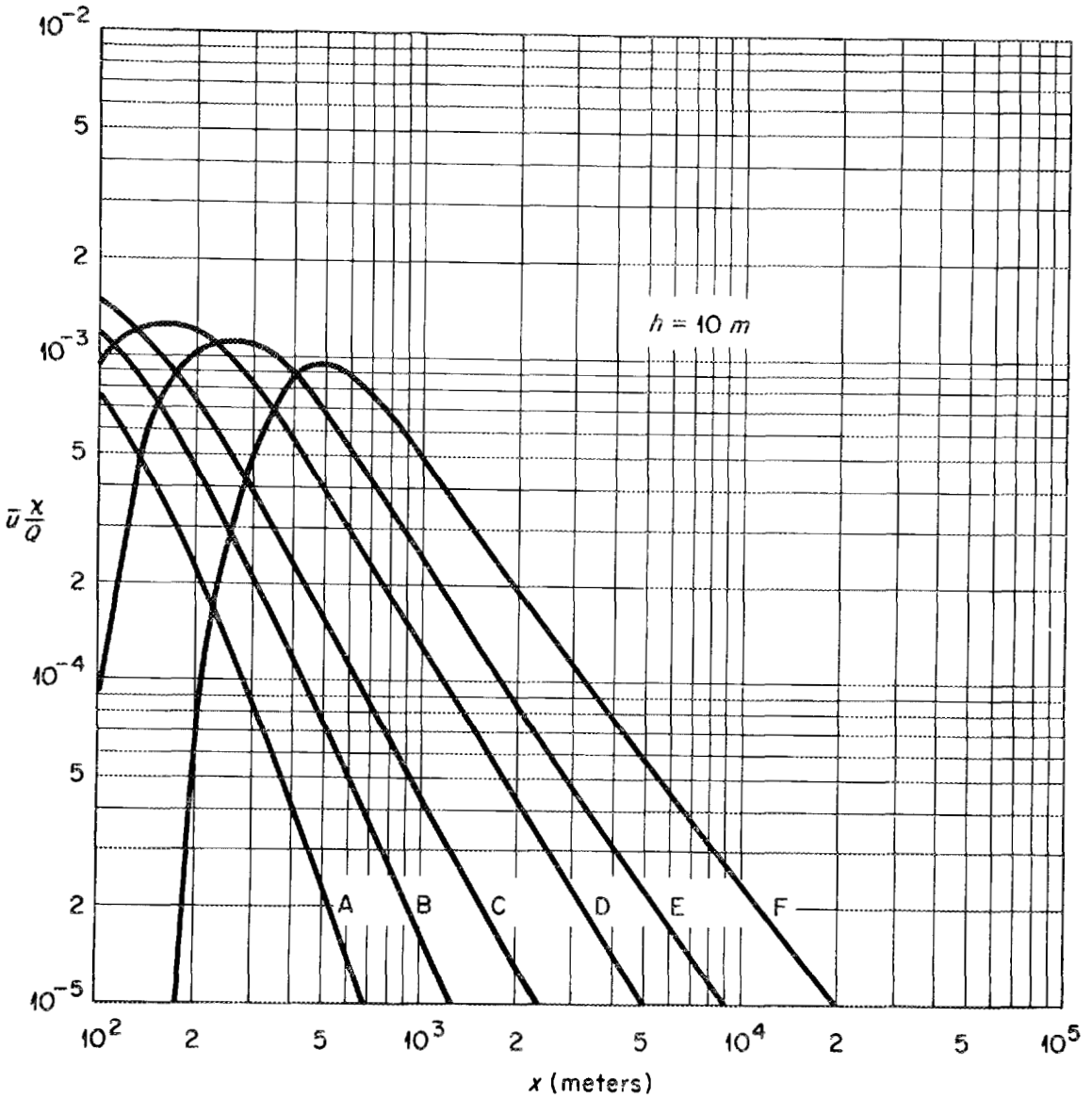

Fig. 4.93. Values of $\bar{u}\chi/Q$ as a Function of Downwind Distance, x, for Various Types of Weather; Source at Surface; h = 10 m. (From Hilsmeier and Gifford, ref. 68, p. 7.)

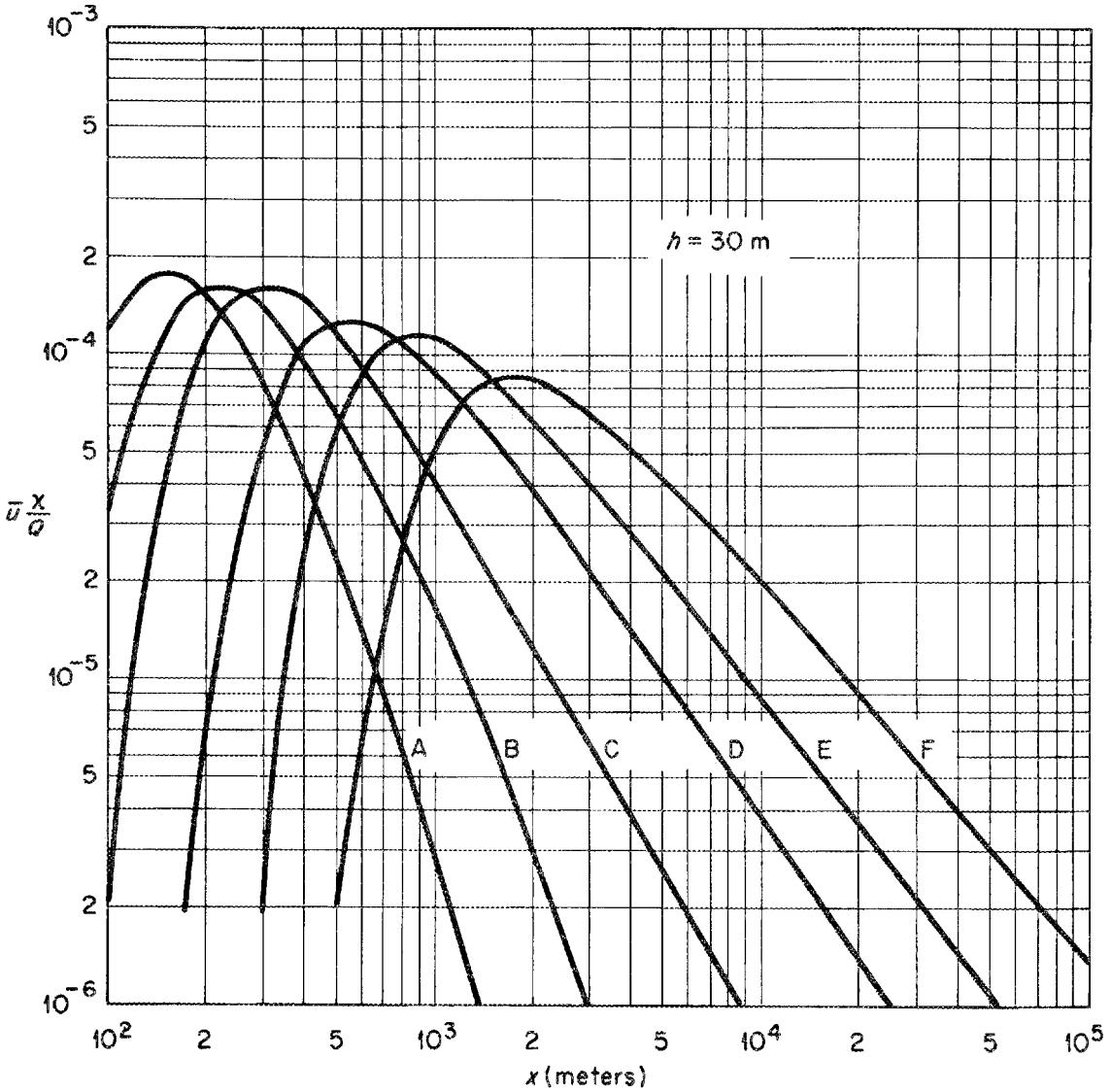

Fig. 4.94. Values of $\bar{u}X/Q$ as a Function of Downwind Distance, x, for Various Types of Weather; Source at Surface; h = 30 m. (From Hilsmeier and Gifford, ref. 68, p. 8.)

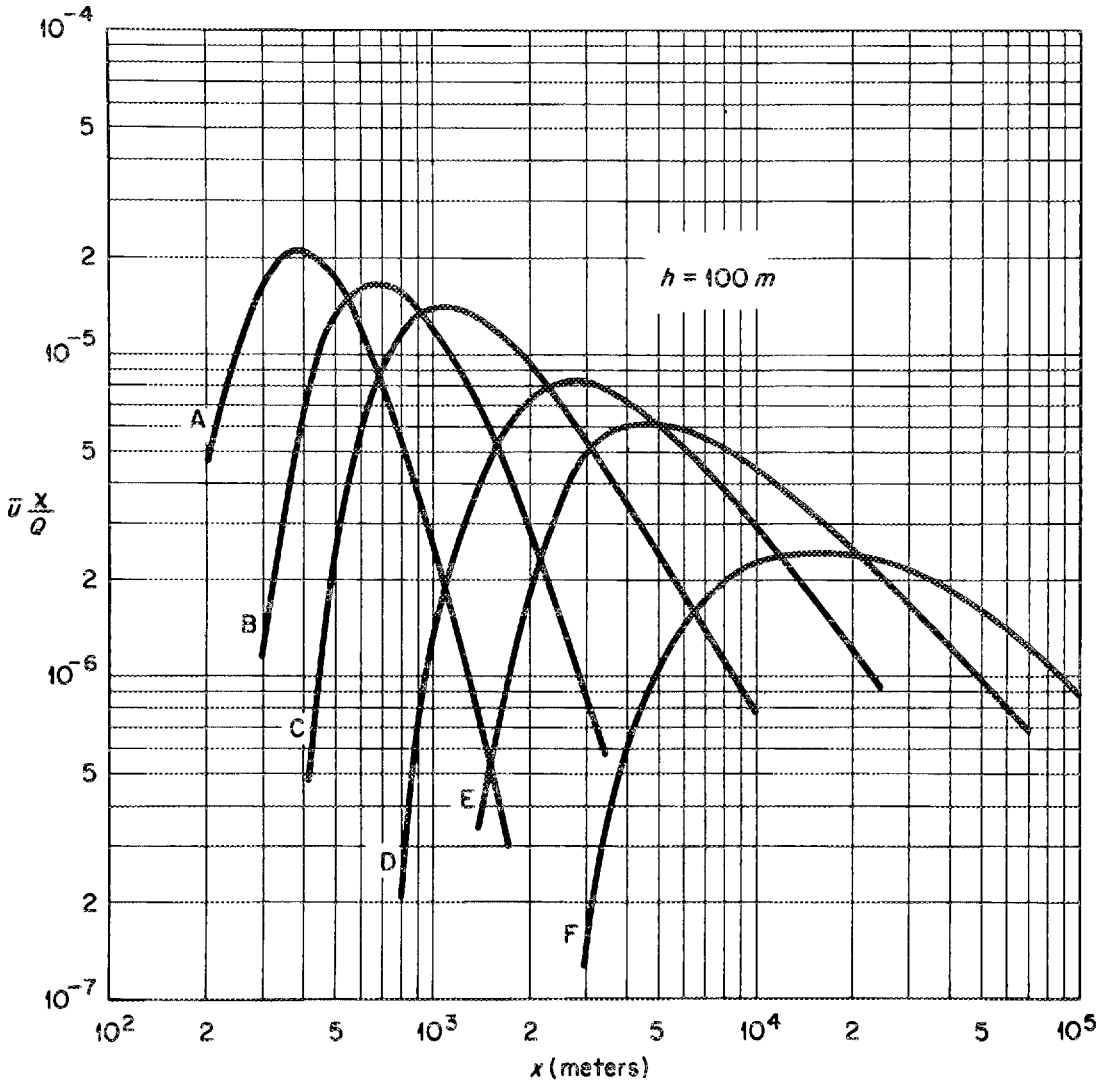

Fig. 4.95. Values of $\bar{u}X/Q$ as a Function of Downwind Distance, x, for Various Types of Weather; Source at Surface; h = 100 m. (From Hilsmeier and Gifford, ref. 68, p. 9.)

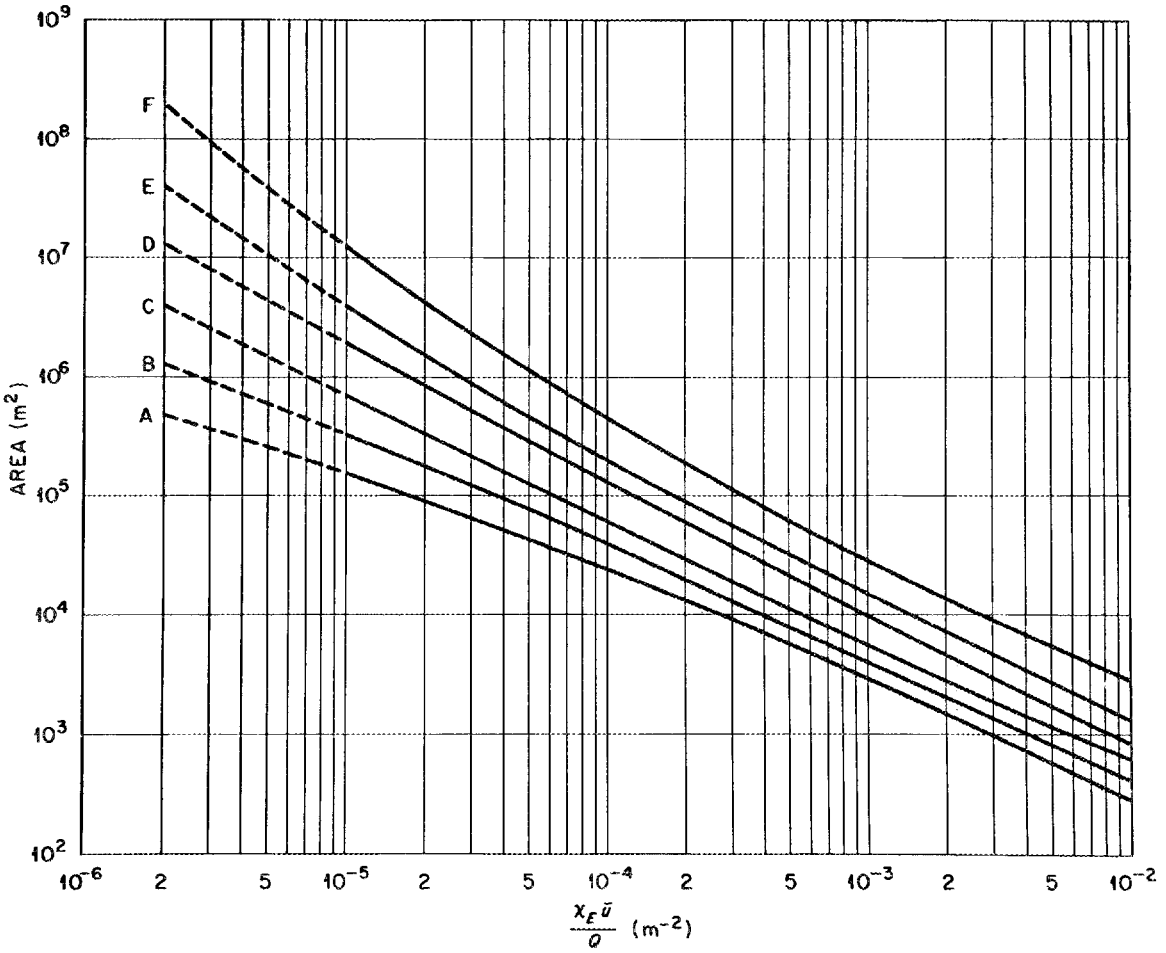

Fig. 4.96. Values of the Area Enclosed by a Ground Level Concentration Isopleth Having the Value χ_E as a Function of the Quantity $\chi_E\bar{u}/Q$. (From Hilsmeier and Gifford, ref. 68, p. 10.)

Figures 4.92 through 4.95 are useful for determining the concentration directly downwind of a release by the equation

$$C = \frac{\bar{u}\chi}{Q}\,\frac{Q}{\bar{u}}\ , \qquad (4.100)$$

where C is concentration, curies/m^3.

If the concentration in the transverse direction must be found, Eq. (4.99) can be used directly with Figs. 4.90 and 4.91 to obtain $\bar{u}(\chi/Q)$ at that point. This can be done repeatedly and can be applied to Eq. (4.100) to obtain ground-concentration isopleths.

4.5.2 Biological Hazards and Dose Calculations

The immediate hazard to people downwind from a release is that from direct radiation from the cloud and inhalation of some important isotope, notably iodine or strontium. In general, the controlling factor is the inhalation of radioiodine. Methods for calculating the effects of iodine and the other hazardous isotopes are given below.

The external exposure from submersion within a large cloud of radioactive material can be estimated[69] to be, at the maximum,

$$Z = \frac{\overline{Q}(3.7 \times 10^4)(t)(E_s)(1.6 \times 10^{-6})(1.13)(2\pi)}{(1293)(100)(4\pi)}$$

$$= 2.6 \times 10^{-7}\ E_s \overline{Q} t\ , \qquad (4.101)$$

where

Z = cumulative dose, rem,
t = exposure time, sec,
$\overline{Q}$ = average concentration, $\mu c/m^3$,
E_s = effective energy of fission-product mixture, Mev/dis.*

The inhalation intake in microcuries is

$$I = B\overline{Q}t\ , \qquad (4.102)$$

where B is breathing rate, m^3/sec. Taking B = 30 liters/min as the breathing rate, the amount inhaled (in microcuries) would be, for moderate activity,

$$I = 5 \times 10^{-4}\ \overline{Q}t\ . \qquad (4.103)$$

The total internal exposure (rem) to a body organ is

$$D = 73.8 f_a I\ \frac{NT}{m}\ \Sigma E_i (RBE)\ , \qquad (4.104)$$

---

*The effective energy is taken as the gamma energy plus one-third the beta energy. Also in Eq. (4.101) the numerical factors are 3.7×10^4 dis/sec·μc, 1.6×10^{-6} ergs/Mev, 1293 g/m^3 for air, 100 ergs/g·rad, and 1.13 is the mass stopping power of tissue relative to air.

where

m = mass of body organ, g,
f_a = fraction of inhaled material residing in organ,
I = amount of inhaled material, μc,
E_i = energy absorbed in the organ, Mev,
N = factor accounting for localized deposition,
T = effective half-life, days.

The effective half-life in days is

$$T = \frac{T_f T_r}{T_f + T_r} , \qquad (4.105)$$

where T_f is the biological half-life, and T_r is the radioactive half-life.

Burnett[69] gives the fission products of controlling importance; his table is reproduced as Table 4.44. The isotopes of Table 4.44 are grouped according to the critical organs they affect, and the energy values are those applicable to the particular organ. The D values are the total exposures calculated to result from a single inhalation of 1 μc of the respective isotope.

Burnett considered two cases of mixed fission-product inhalation in detail, that is, those resulting from 40 and 400 days of reactor operation. Table 4.45 shows the amounts of selected fission products in curies per megawatt of power. Table 4.46 gives percentages of the total of each long-lived isotope present at 40 and 400 days operation. These percentages are then applied to the exposures per inhaled microcurie of the components and totaled to give exposure per inhaled microcurie of mixture. As may be seen, the total exposure to the bones and thyroid greatly exceeds that to the kidneys or muscle.

Figure 4.97 shows exposures to the thyroid, lungs, and bones in terms of millirems per inhaled microcurie of isotope mixture as a function of reactor operating time. It should be emphasized that this assumes that the inhaled mixture is of the same composition as the fission-product inventory in the core. In a real case the isotopes would be released in different proportions, as discussed in Secs. 4.3 and 4.4.

Figure 4.98 shows comparative exposures at different operating times based on limiting the bone exposure to 25 rem. Also shown is the maximum permissible exposure (MPE) of 50 rem to the thyroid. The submersion exposure can be seen to be negligible when inhalation takes place.

In a reactor accident the more volatile fission products would be released to a greater extent than other equally hazardous, but more stable, elements such as strontium. Table 4.47 gives an example of this effect. These values of release from the Windscale incident were estimated by Beattie.[1] In this case the uranium fuel was actually burning and exhausting to the atmosphere without the presence of a containment vessel. The last column in the table lists the percentage releases which are recommended for use in future reactor safety assessments.

Table 4.44. Fission Products of Significance in Internal Exposure[a]

Isotope	Radioactive half-life, T_r	Yield, %	f_a	E_i(RBE)N,[b] Mev/dis	Eff. half-life (T), days	D, mrem/μc
Bone						
Sr^{89}[c]	50.5 d	4.8	0.28	2.8	50.	413
Sr^{90}–Y^{90}[c]	27.7 y	5.9	0.12	5.5	6400	44,200.
Sr^{91}–Y^{91m}	9.7 h	5.9	0.22	3.59	0.4	3.3
Y^{91}	57.5 d	5.9	0.19	2.9	58.	337.
Zr^{95}	65. d	6.4	0.058	0.84	48.	24.5
Nb^{95m}	90. h	0.06	0.12	1.11	3.5	4.9
Nb^{95}	35. d	6.4	0.12	0.45	21.	12.
Zr^{97}–Nb^{97m}						
Nb^{97}	17. h	6.2	0.058	6.33	0.7	3.2
Mo^{99}–Te^{99}	67. h	6.1	2×10^{-4}	2.13	2.7	0.01
Sb^{127}	93. h	0.25	0.003	3.20	2.2	0.2
Ba^{140}–La^{140}	12.8 d	6.3	0.19	4.2	10.7	91.6
Ce^{141}	33.1 d	6.0	0.1	0.93	31.	30.4
Ce^{143}	33. h	6.2	0.1	1.92	1.4	2.8
Pr^{143}	13.7 d	6.2	0.063	1.57	11.	11.4
Ce^{144}–Pr^{144}[c]	282. d	6.1	0.075	6.3	243.	1,210.
Nd^{147}	11.3 d	2.6	0.1	1.25	8.5	11.2
Pm^{147}	2.6 y	2.6	0.09	0.34	90.	28.8
Pm^{149}	54. h	1.3	0.09	1.86	2.2	3.9
Thyroid[c]						
I^{131}	8.1 d	2.9	0.23	0.23	7.6	1,484.
I^{132}	2.4 h	4.4	0.23	0.65	0.097	54.
I^{133}	20.5 h	6.5	0.23	0.54	0.87	399.
I^{134}	52.5 m	7.6	0.23	0.82	0.036	25.
I^{135}	6.68 h	5.9	0.23	0.52	0.28	124.
Kidney						
Ru^{103}–Rh^{103m}	39.8 d	2.9	0.01	0.21	13.3	6.9
Rh^{105}	36.5 h	0.9	0.02	0.19	1.5	1.4
Ru^{106}–Rh^{106}	1.0 y	0.38	0.01	1.38	19.	65.
Te^{127m}–Te^{127}	115. d	0.25	0.02	0.28	13.3	18.3
Te^{129m}–Te^{129}	33.5 d	1.0	0.02	0.89	10.4	46.
Te^{131m}–Te^{131}	30. h	2.0	0.02	1.30	1.2	7.7
Te^{132}	77.7 h	4.4	0.02	0.11	2.7	1.5
Muscle						
Cs^{137}–Ba^{137m}	33. y	5.9	0.36	0.57	17.	8.6

[a]From Burnett, ref. 69, p. 384.

[b]In the effective energy values, the nonuniform distribution factor N is taken as 5 for bones.

[c]Revised by H. N. Culver, Apr. 26, 1961.

Table 4.45. Fission Products Present at Three Periods of Reactor Operation[a]

Isotope	Radioactive Half-Life, T_r	Yield (%)	Fraction of Equilibrium		Fission Products Present (curies per kw steady power)		
			At t = 40 Days	At t = 400 Days	At t = 40 Days	At t = 400 Days	At t = ∞
Bone							
Sr^{89}	50.5 d	4.8	0.422	0.996	18.4	43.4	43.6
Sr^{90}-Y^{90}	27.7 y	5.9	0.00273	0.0270	0.146	1.45	53.6
Sr^{91}-Y^{91m}	9.7 h	5.9	1.0	1.0	53.6	53.6	53.6
Y^{91}	57.5 d	5.9	0.383	0.992	20.5	53.2	53.6
Zr^{95}	65 d	6.4	0.347	0.986	20.2	57.3	58.1
Nb^{95m}	90 h	0.06	0.307	0.985	0.2	0.6	0.6
Nb^{95}	35 d	6.4	0.114	0.970	6.6	56.4	58.1
Zr^{97}-Nb^{97m}							
Nb^{97}	17 h	6.2	1.0	1.0	56.3	56.3	56.3
Mo^{99}-Tc^{99}	67 h	6.1	0.999	1.0	55.4	55.4	55.4
Sb^{127}	93 h	0.25	0.999	1.0	2.3	2.3	2.3
Ba^{140}-La^{140}	12.8 d	6.3	0.885	1.0	50.7	57.2	57.2
Ce^{141}	33.1 d	6.0	0.567	0.999	30.9	54.5	54.5
Ce^{143}	33 h	6.2	1.0	1.0	56.3	56.3	56.3
Pr^{143}	13.7 d	6.2	0.868	1.0	48.9	56.3	56.3
Ce^{144}-Pr^{144}	282 d	6.1	0.094	0.626	5.2	34.7	55.4
Nd^{147}	11.3 d	2.6	0.914	1.0	21.6	23.6	23.6
Pm^{147}	2.6 y	2.6	0.029	0.253	0.7	6.0	23.6
Pm^{149}	54 h	1.3	1.0	1.0	11.8	11.8	11.8
(Subtotal of bone seekers)					(460)	(680)	
Thyroid							
I^{131}	8.1 d	2.9	0.967	1.0	25.5	26.3	26.3
I^{132}	2.4 h	4.4	1.0	1.0	40.0	40.0	40.0
I^{133}	20.5 h	6.5	1.0	1.0	59.0	59.0	59.0
I^{134}	52.5 m	7.6	1.0	1.0	69.0	69.0	69.0
I^{135}	6.68 h	5.9	1.0	1.0	53.6	53.6	53.6
Kidney							
Ru^{103}-Rh^{103m}	39.8 d	2.9	0.502	0.999	13.2	26.3	26.3
Rh^{105}	36.5 h	0.9	1.0	1.0	8.2	8.2	8.2
Ru^{106}-Rh^{106}	1.0 y	0.38	0.073	0.532	0.3	1.8	3.5
Te^{127m}-Te^{127}	115 d	0.25	0.214	0.910	0.5	2.1	2.3
Te^{129m}-Te^{129}	33.5 d	1.0	0.563	1.0	5.1	9.1	9.1
Te^{131m}-Te^{131}	30 h	2.9	1.0	1.0	26.3	26.3	26.3
Te^{132}	77.7 h	4.4	0.999	1.0	40.0	40.0	40.0
Muscle							
Cs^{137}-Ba^{137m}	33 y	5.9	0.00230	0.0228	1.0	1.2	53.6
Total					800	1043	1191

[a]From Burnett, ref. 54, p. 386.

Table 4.46. Exposures from Fission-Product Mixtures[a]

Isotope	Percent of Total Exposure		D, Exposure per Inhaled Microcurie (mrem)		
	At t = 40 Days	At t = 400 Days	Of Isotope	Of 40-Day Mixture	Of 400-Day Mixture
Bone					
Sr^{89}	2.30	4.16	312	7.18	12.99
Sr^{90}–Y^{90}	0.018	0.139	34,800	6.37	48.32
Sr^{91}–Y^{91m}	6.70	5.14	3.3	0.22	0.17
Y^{91}	2.56	5.10	217	5.56	11.06
Zr^{95}	2.52	5.49	24.5	0.62	1.35
Nb^{95m}	0.02	0.06	4.9	0	0
Nb^{95}	0.83	5.40	12	0.10	0.65
Zr^{97}–Nb^{97m}–Nb^{97}	7.04	5.40	3.2	0.23	0.17
Mo^{99}–Tc^{99}	6.92	5.31	0.01	0	0
Sb^{127}	0.28	0.22	0.2	0	0
Ba^{140}–La^{140}	6.33	5.49	109	6.90	5.98
Ce^{141}	3.86	5.22	30.4	1.17	1.59
Ce^{143}	7.04	5.40	2.8	0.20	0.15
Pr^{143}	6.11	5.40	11.4	0.70	0.62
Ce^{144}–Pr^{144}	0.65	3.33	1,160	7.50	38.50
Nd^{147}	2.70	2.26	11.2	0.30	0.25
Pm^{147}	0.09	0.57	28.8	0.02	0.17
Pm^{149}	1.48	1.13	3.9	0.06	0.04
(Subtotal)	(57.4)	(65.2)		(37.1)	(122.0)
Thyroid					
I^{131}	3.18	2.25	963	50.65	24.32
I^{132}	4.99	3.83	36.6	1.83	1.40
I^{133}	7.38	5.66	227	16.74	12.85
I^{134}	8.62	6.62	17.7	1.53	1.17
I^{135}	6.70	5.14	63	4.22	3.24
(Subtotal)				(55.0)	(43.0)
Kidney					
Ru^{103}–Rh^{103m}	1.65	2.52	6.9	0.11	0.17
Rh^{105}	1.02	0.78	1.4	0.01	0.01
Ru^{106}–Rh^{106}	0.03	0.18	65	0.02	0.11
Te^{127m}–Te^{127}	0.06	0.20	18.3	0.01	0.04
Te^{129m}–Te^{129}	0.64	0.87	46	0.29	0.40
Te^{131m}–Te^{131}	3.29	2.53	7.7	0.25	0.19
Te^{132}	4.99	3.83	1.5	0.08	0.06
(Subtotal)				(0.8)	(1.0)
Muscle					
Cs^{137}–Ba^{137m}	0.02	0.12	8.6	0	0.01
Lung					
All above isotopes				38.0	79.6

[a]From Burnett, ref. 69, p. 387.

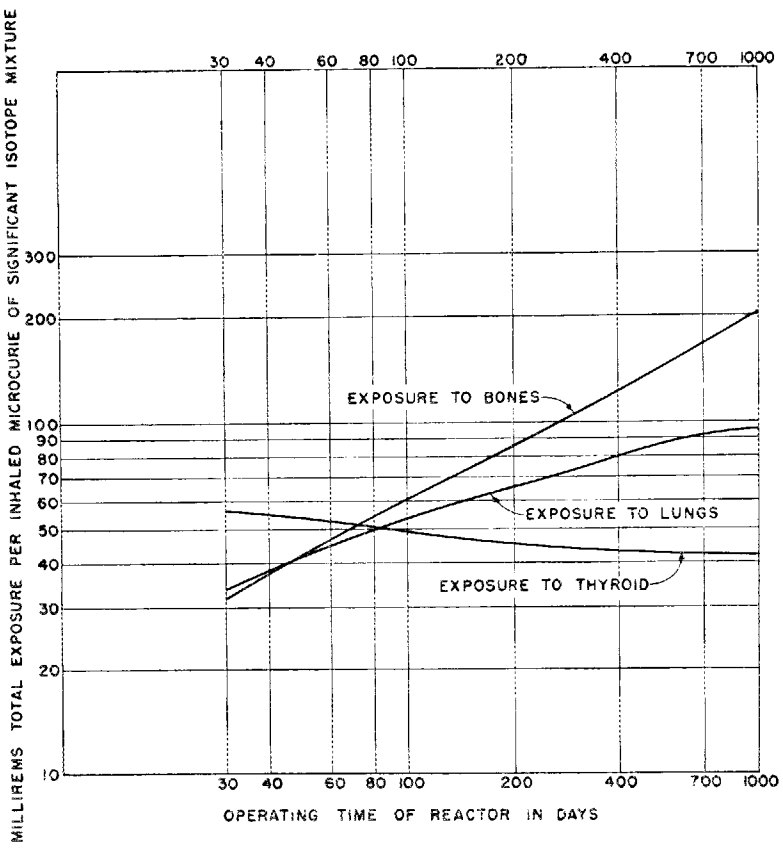

Fig. 4.97. Exposure Per Microcurie Inhaled Versus Operating Time. (From Burnett, ref. 69.)

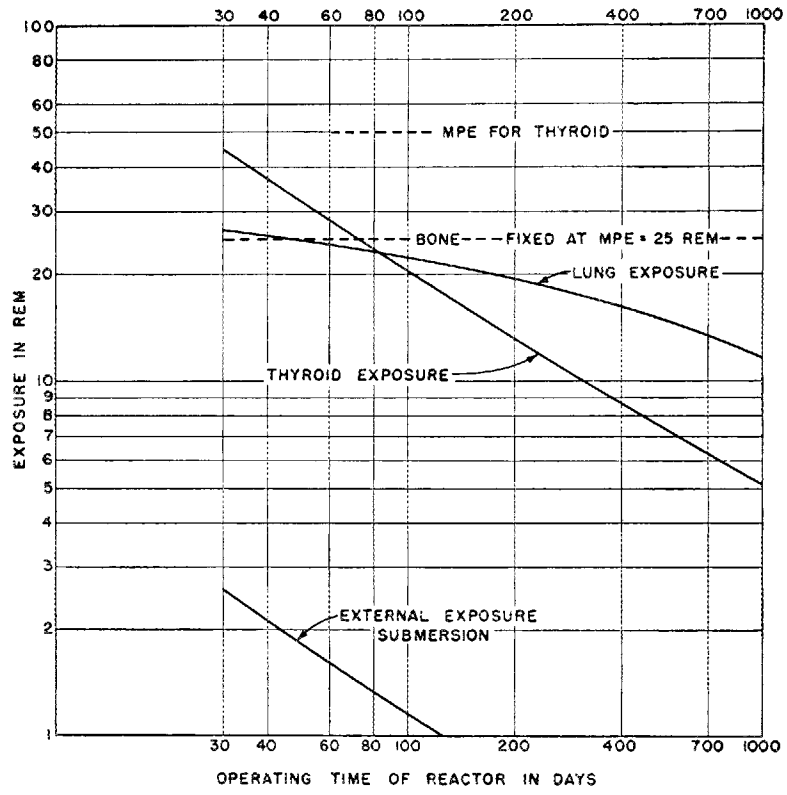

Fig. 4.98. Comparative Exposures at Different Operating Times Based on Limiting Bone Exposure to 25 rem (Power Constant). (From Burnett, ref. 69.)

Table 4.47. Windscale Accident Release as Estimated by Beattie[a]

Element or Isotope	Activity in Damaged Fuel (curies)	Activity Released from Chimney (curies)	Percentage Release from Chimney	Percentage Release Recommended For Future Assessments
Br				
Kr				60
Xe				
^{132}Te	160,000	12,000[b]	7.5	15
^{131}I	168,000	20,000	12	25
^{89}Sr	380,000	80	0.02	0.1
^{90}Sr	9,200	2	0.02	0.1
^{106}Ru	12,000	80	0.7	4
^{137}Cs	8,000	600	7.5	15
^{144}Ce	290,000	80	0.03	0.15
^{140}Ba				0.2

[a]From Beattie, ref. 1, Table 3.

[b]The ratio $^{131}I/^{132}Te$ is 1/0.6, as estimated by Chamberlain.[70]

4.5.2.1 Deposition of Activity from the Cloud

With the exception of xenon and krypton, and iodine in organic compounds and possibly also in true molecular form, the fission products released in a reactor accident would be of particulate form. As discussed previously in this chapter in conjunction with fission-product behavior within containment vessels, particles with diameters of <1 μ deposit very slowly by sedimentation. The dominant mode of removal of fine particles is diffusion and impaction. Deposition experiments can be summarized by the concept of "velocity of deposition," defined by

$$V_g = \frac{\text{total deposited activity per unit area}}{\text{cloud concentration} \times \text{time}} .$$

The values of the deposition velocity vary with the condition of the surface and wind speed. Experiments[1] done with iodine have given values of V_g from 0.01 to 5 cm/sec. Beattie feels that values between 0.1 and 1.0 cm/sec are most likely.

The effects of washout of airborne activity have been considered by Chamberlain.[70] Theoretically, the worst possible deposition by rain is eight times the worst possible deposition in dry weather, but there are so many variables that a realistic assessment is impossible. However, rain hardly ever occurs at the same time as an inversion, so the worst conditions in deposition (rain) are unlikely to coincide with the worst conditions of diffusion (inversion).[1]

Beattie calculated depletion of cloud dosage by deposition of activity of the cloud as it travels downwind. The modified cloud dosages resulting from various values of deposition velocity V_g between 0 and 1.0 cm/sec are reproduced in Figs. 4.99 and 4.100. It can be seen from these figures that the effect of ground deposition is far more pronounced during inversion conditions than it is during average conditions. (See Table 4.43 for definition of categories given on Figs. 4.99 through 4.102.)

Beattie also calculated ground deposition from a prolonged release in average wind inversion weather conditions; the results are shown in Figs. 4.101 and 4.102. When hazards due to ground deposition were calculated, Beattie used the highest values of deposition velocity (V_g = 0.1 to 10 cm/sec) that would give the highest deposition at the distance of interest in order to avoid underestimating the hazard.

4.5.2.2 Hazards Due to Iodine

In an accident, it is likely that, as a health hazard, iodine would be the controlling isotope. Beattie has calculated the amounts of the iodine isotopes that would give the maximum allowable dosage of 25 rads to the thyroid of a 6-month-old child. These results are given in Table 4.48.

Table 4.48. Maximum Permissible Cloud Dosage of Individual Iodine Isotopes[a]

	^{131}I	^{132}I	^{133}I	^{134}I	^{135}I
Effective energy, Mev[b]	0.23	0.65	0.54	0.82	0.52
Half-life, hr	192	2.3	21	0.87	6.7
Fraction, f, of isotope dose actually delivered to thyroid	1.0	0.35	0.80	0.15	0.50
Maximum permissible cloud dosage, curie-sec/m^3	0.013	1.1	0.063	5.4	0.33

[a]From Beattie, ref. 1.

[b]See ref. 71.

At equilibrium, after one or two weeks of reactor operation, the activities of the iodine isotopes are in the following ratios:

^{131}I	1.0
^{132}I	1.52
^{133}I	2.16
^{134}I	2.52
^{135}I	2.20

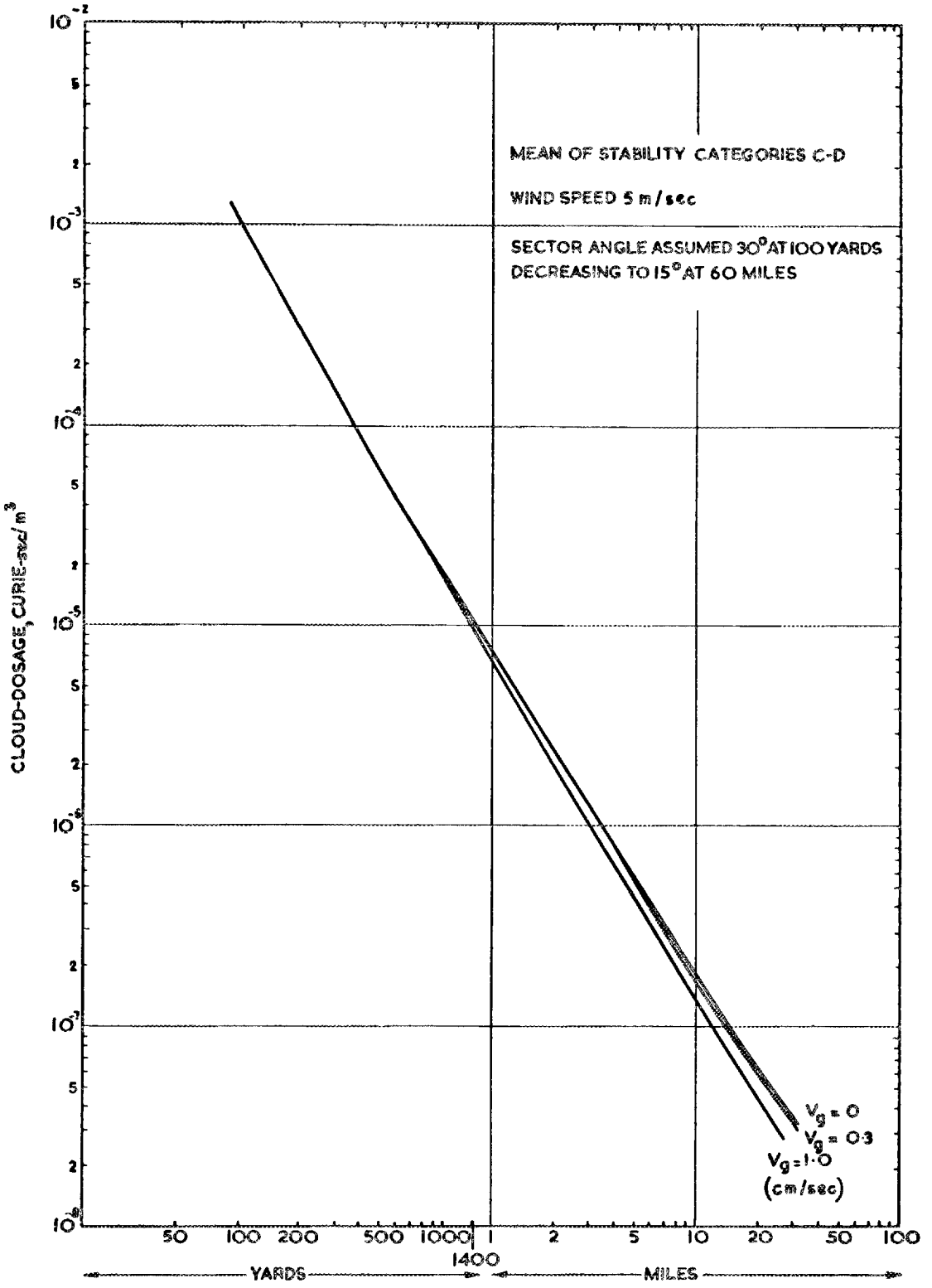

Fig. 4.99. Cloud Dosage from a Release of 1.0 Curie Over a Prolonged Period in Average Weather Conditions. (From Beattie, ref. 1, Fig. 1.)

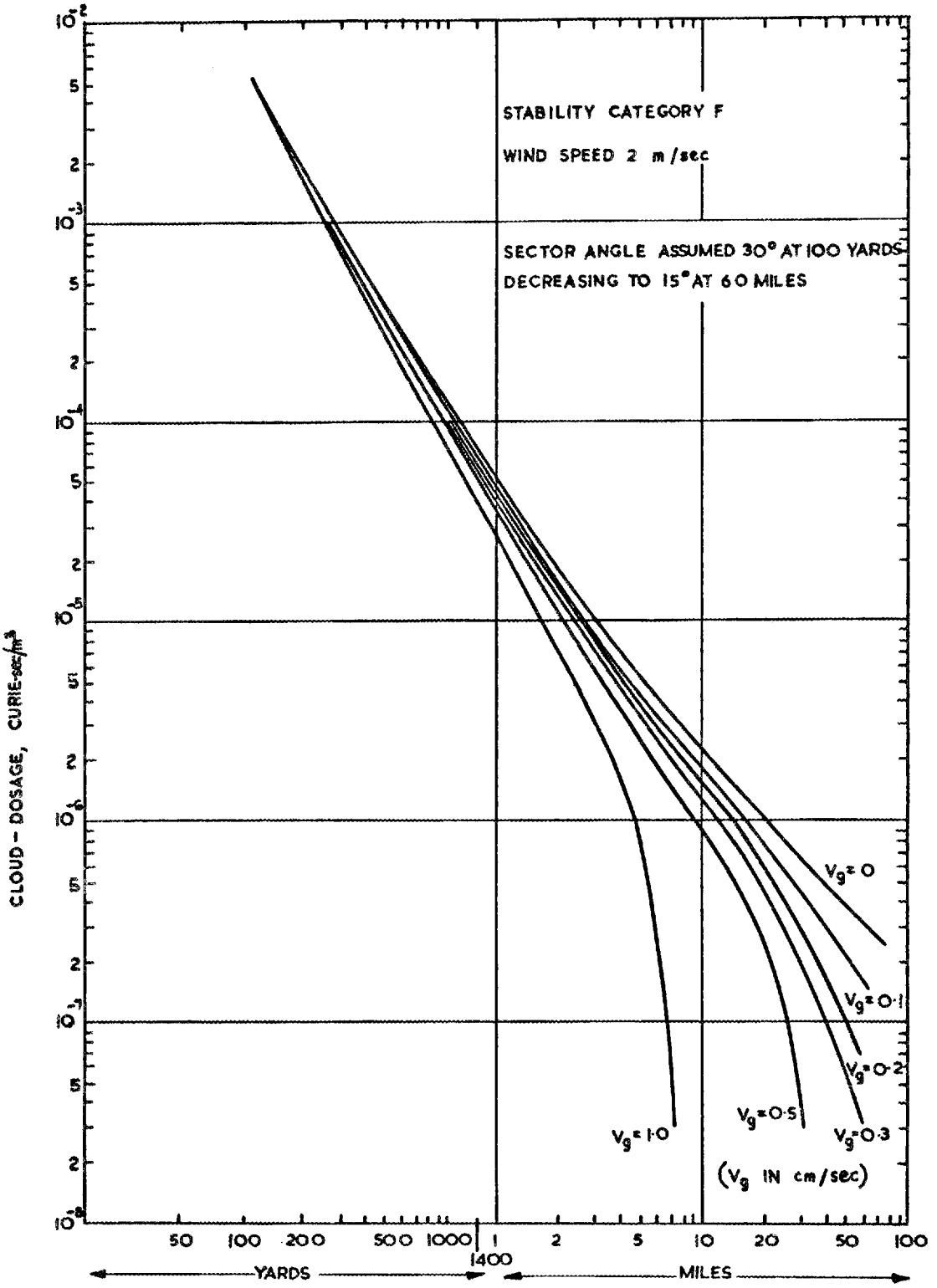

Fig. 4.100. Cloud Dosage from a Release of 1.0 Curie Over a Prolonged Period in Inversion Conditions. (From Beattie, ref. 1, Fig. 2.)

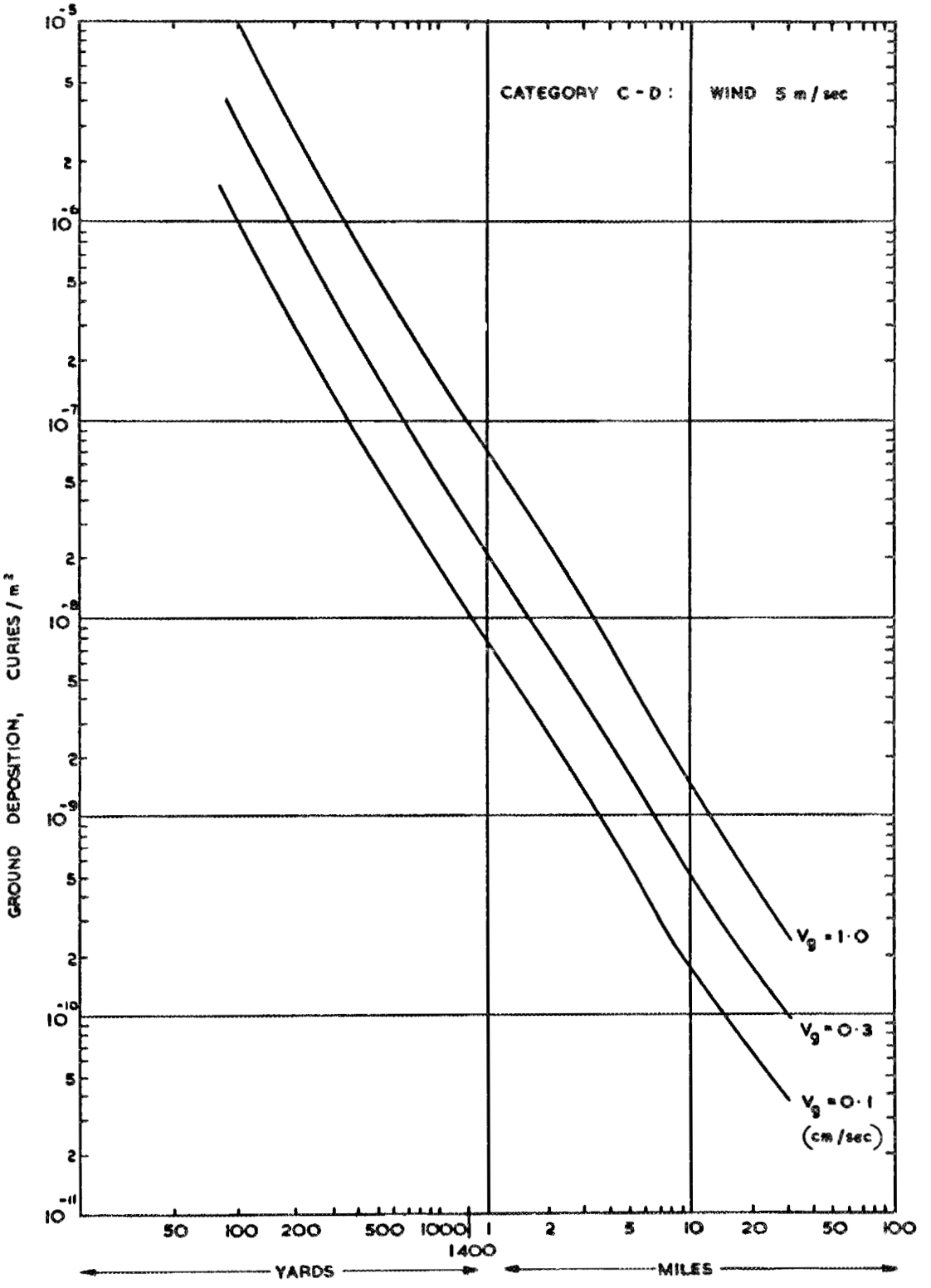

Fig. 4.101. Ground Deposition from a Release of 1.0 Curie Over a Prolonged Period in Average Weather Conditions. (From Beattie, ref. 1, Fig. 3.)

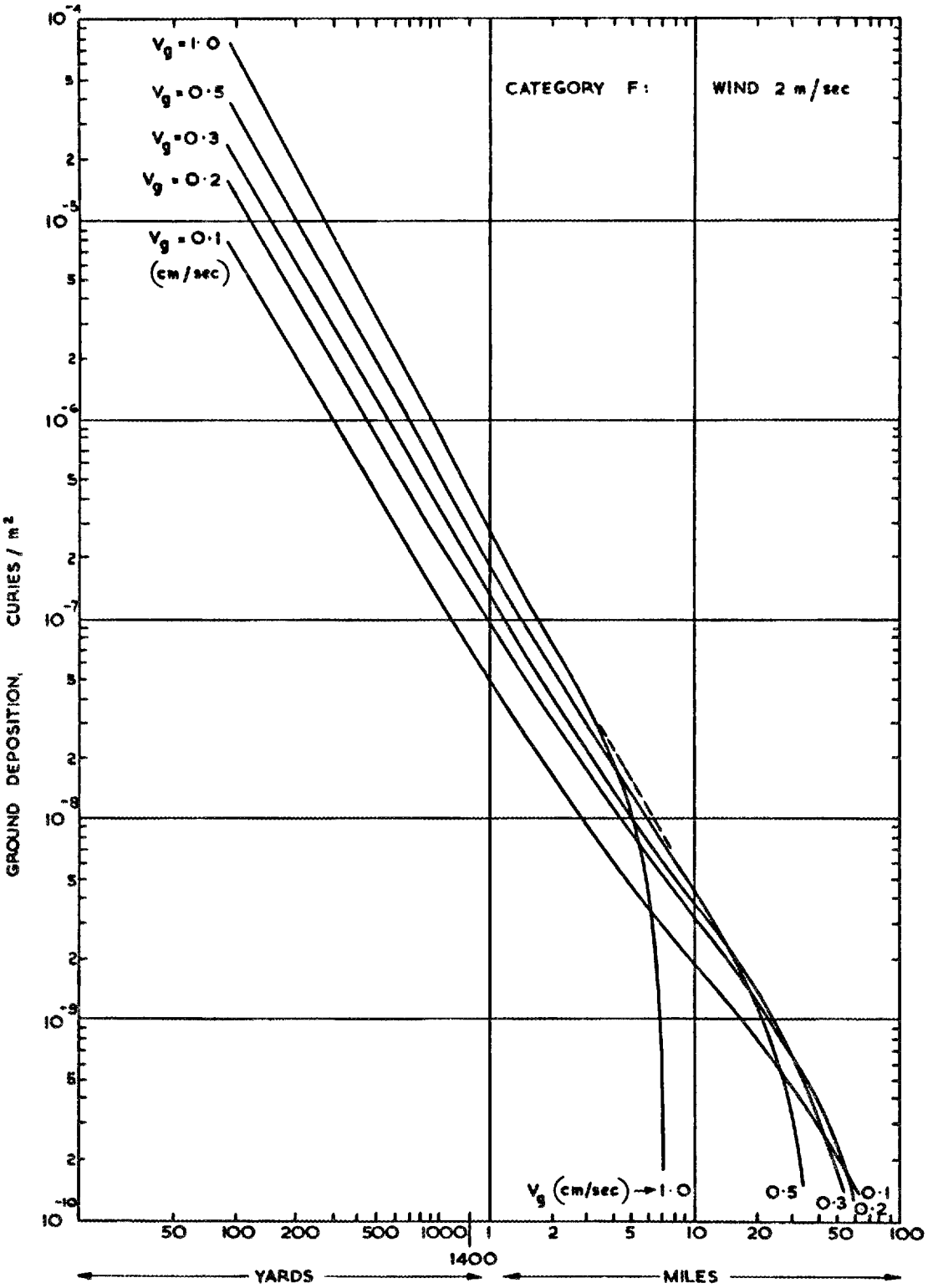

Fig. 4.102. Ground Deposition from a Release of 1.0 Curie Over a Prolonged Period in Inversion Conditions. (From Beattie, ref. 1, Fig. 4.)

The amount of iodine mixture of this composition that would yield a total thyroid dose of 25 rads is that accompanying a dosage of 0.00834 curie-sec of ^{131}I per m^3. Measured at one day after shutdown, the maximum permissible cloud dosage may be stated as 0.0077 curie-sec of ^{131}I per m^3.

When the contribution of ^{132}I arising from the decay of ^{132}Te is accounted for, the maximum permissible cloud dosage of iodine is 0.007 curie-sec of ^{131}I per m^3 measured at one day.

The above figures are based on the limit of 25 rads to the thyroid of a 6-month-old child. Table 4.49 shows the maximum permissible cloud dosages as a function of age of the subject.

Table 4.49. Maximum Permissible Cloud Dosage of Fission-Product Iodine[a,b] To Persons of Various Ages

Age	Maximum Permissible Cloud Dosage (curie-sec of ^{131}I per m^3)
6 months	0.007
3 years	0.007
10 years	0.011
20 years	0.031

[a]Expressed in terms of cloud dosage of ^{131}I which contributes the greater part of the dose to the thyroid, following inhalation, and assuming that the other iodine isotopes are present in equilibrium proportions. Allowance is also made for a contribution to thyroid dose from ^{132}I formed in this body from inhaled ^{132}Te. Curies of ^{131}I are stated as at 1 day's decay after release.

[b]From Beattie, ref. 1.

4.5.2.3 Contamination of Exposed Food with Iodine

Beattie[1] states that, where the ground concentration exceeds 5×10^{-5} curies of ^{131}I per m^2, a public warning should be issued against the consumption of green vegetables and fruit and of other food that has been exposed in the open air.

Regarding milk consumption, the British Medical Research Council[72] has recommended restrictions if the level of ^{131}I in milk exceeds 0.065 μc/liter. This level is designed to safeguard a 6-month-old child, who is at the greatest hazard from ^{131}I in milk. This level can be related to a contamination[1] on grass of $\sim 7 \times 10^{-7}$ curies of ^{131}I per m^2. The

total permissible concentration on grass and ground was taken by Beattie as 4×10^{-7} curies of ^{131}I per m^2.

Beattie states that the use of eggs of free-range hens must be restricted when the ground concentration exceeds 10^{-5} curies of ^{131}I per m^2. The hazardous effects of iodine mixtures are summarized in Figs. 4.103 and 4.104.

4.5.2.4 Hazards Due to ^{137}Cs

Cesium-137 is a beta- and gamma-emitting isotope with a 33-year half-life, which, if ingested, is absorbed mainly by muscle tissue. The maximum permissible cloud dosage of ^{137}Cs in air is 0.28 curie-sec of ^{137}Cs per m^3, based on a maximum exposure due to inhalation to a 6-month-old child. Damaging or lethal effects would follow exposure to ~5 to 10 curies-sec of ^{137}Cs per m^3.

Table 4.50 gives permissible and damaging levels of ^{137}Cs. The hazards due to ^{137}Cs are summarized in Figs. 4.105 and 4.106. In a release the effect due to ^{131}I would override the effects due to ^{137}Cs.

4.5.2.5 Inhalation and Ingestion Hazards of ^{90}Sr and ^{89}Sr

Both strontium isotopes are bone-seeking beta emitters. The British Medical Research Council has recommended that, in the period following a reactor accident, the intake of ^{90}Sr by ingestion be limited to 0.002 μc/day, corresponding to a dose rate of 1.5 rem/year. In the case of ^{89}Sr the maximum permissible daily intake is 0.2 μc, corresponding to a total dose of 15 rem, if ingestion continues until the activity has decayed to negligible proportions. Table 4.51 shows the permissible levels of ^{90}Sr as inferred by Beattie. The ranges of hazards of the ^{90}Sr component of a release in average and inversion weather conditions have been calculated and are shown in Figs. 4.107 and 4.108, respectively.

4.5.2.6 Ranges of Hazards — Summary

The work of Beattie is succinctly summarized in Tables 4.52, 4.53, and 4.54, which show the ranges of hazards from a "volatile" release in average and inversion weather conditions, respectively. These tables show the origin of the hazard due to the important fission products, the limiting dose level, possible remedial action, and the range of hazards of various types for eleven magnitudes of release measured in curies of the ^{131}I component of the release.

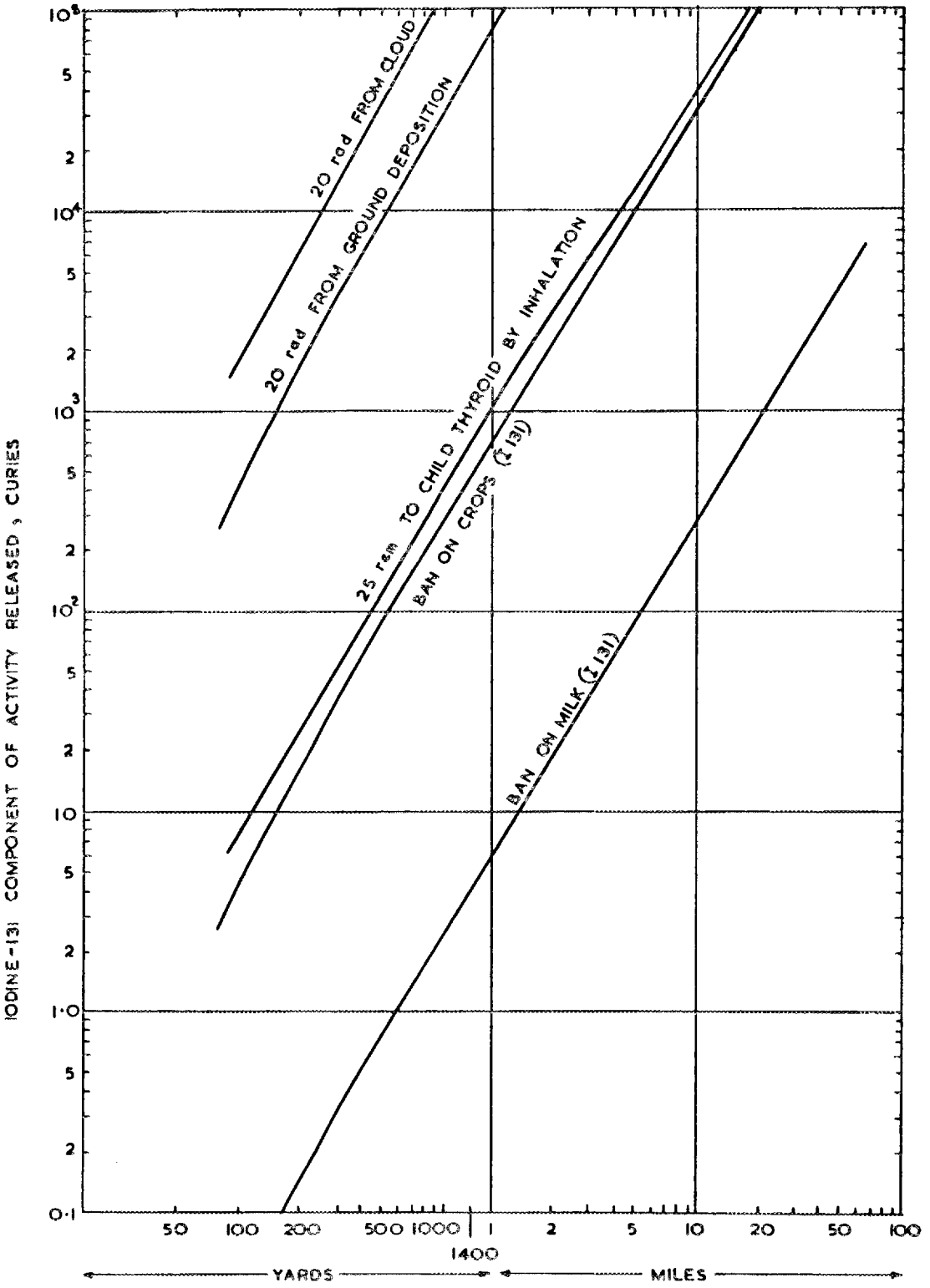

Fig. 4.103. Important Ranges of Hazard from a "Volatile" Release in Average Weather Conditions. (From Beattie, ref. 1, Fig. 10.)

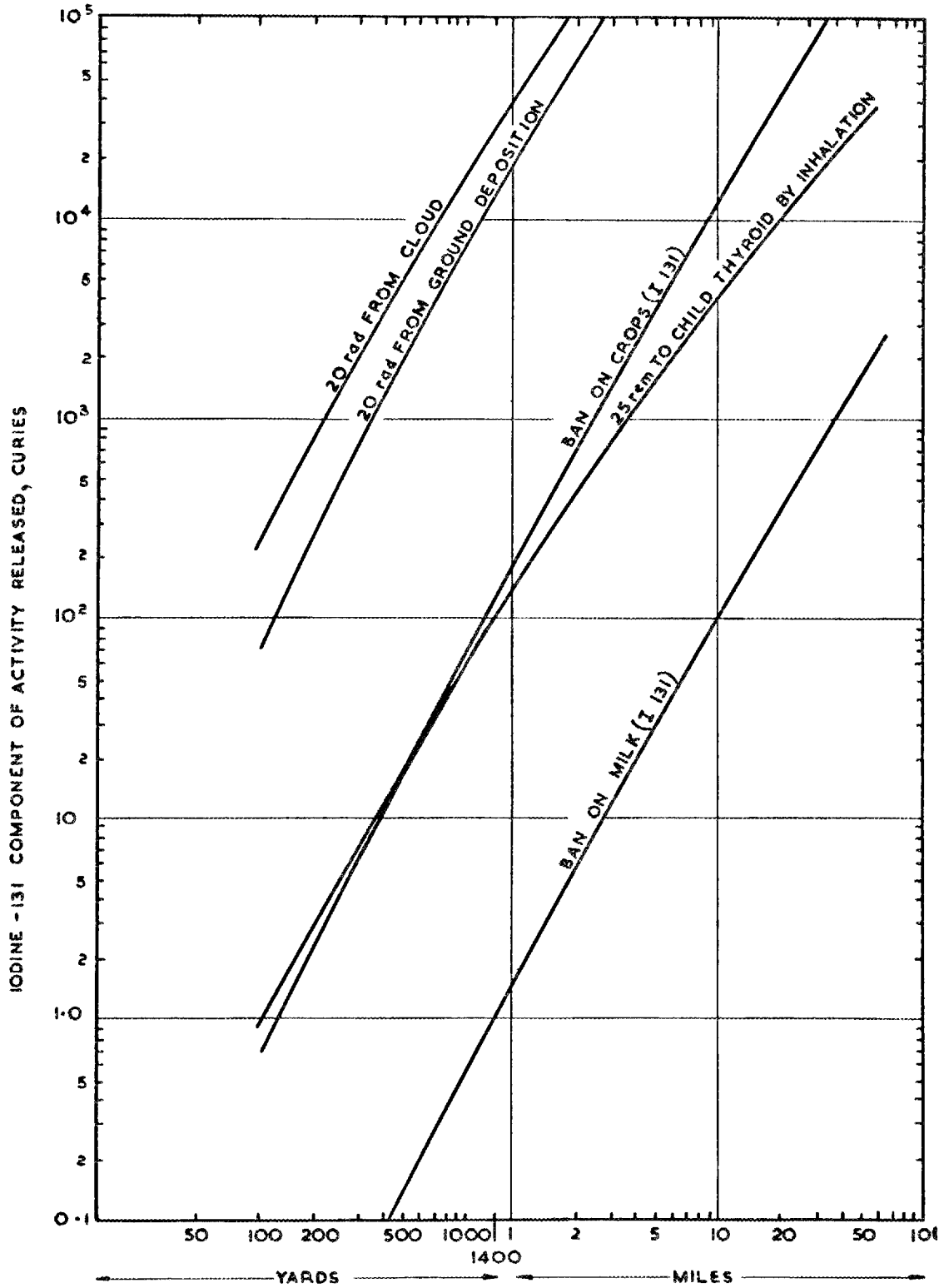

Fig. 4.104. Important Ranges of Hazard from a "Volatile" Release in Inversion Conditions. (From Beattie, ref. 1, Fig. 11.)

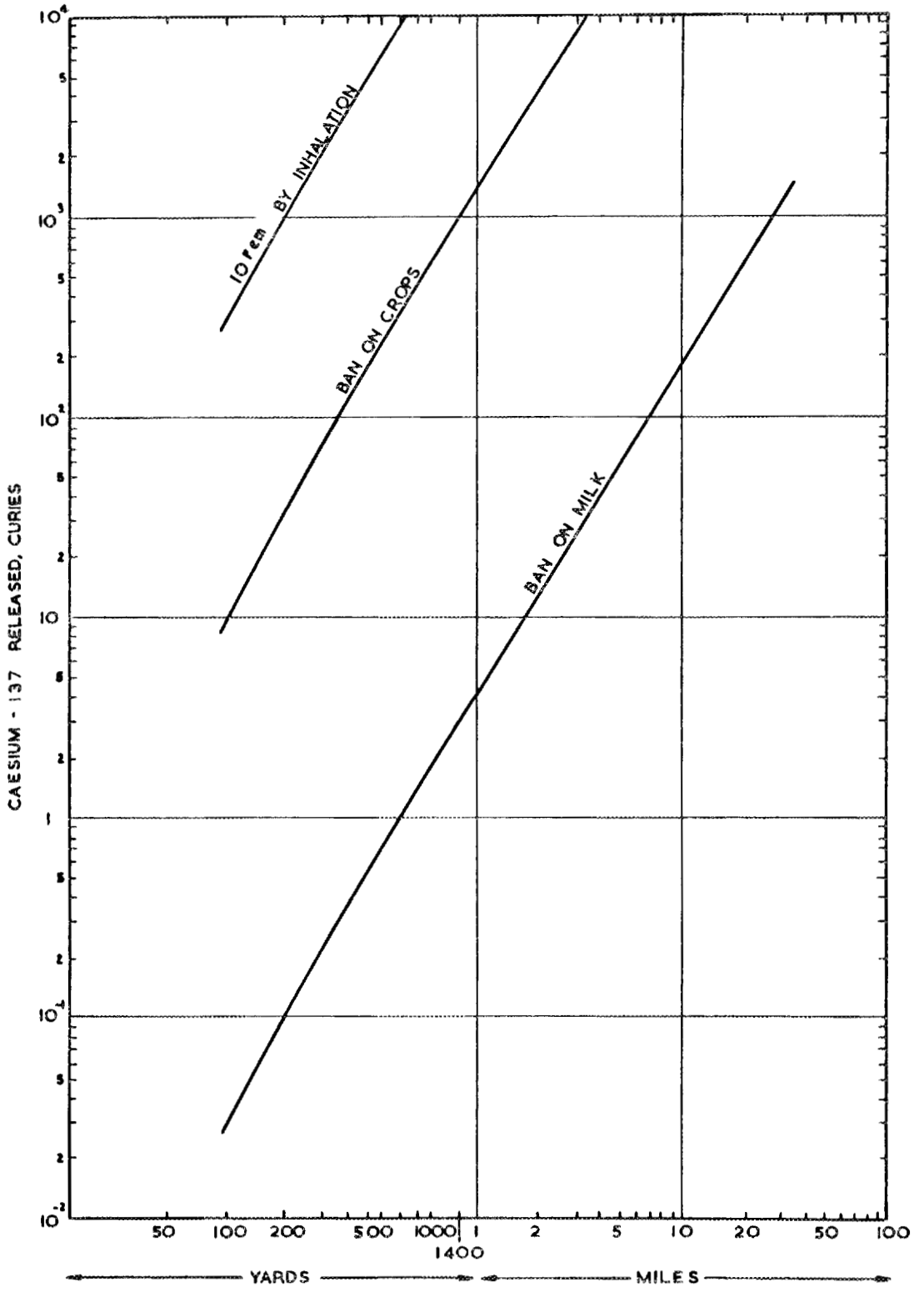

Fig. 4.105. Ranges of Hazard from the ^{137}Cs Component of a Release in Average Weather Conditions. (From Beattie, ref. 1, Fig. 12.)

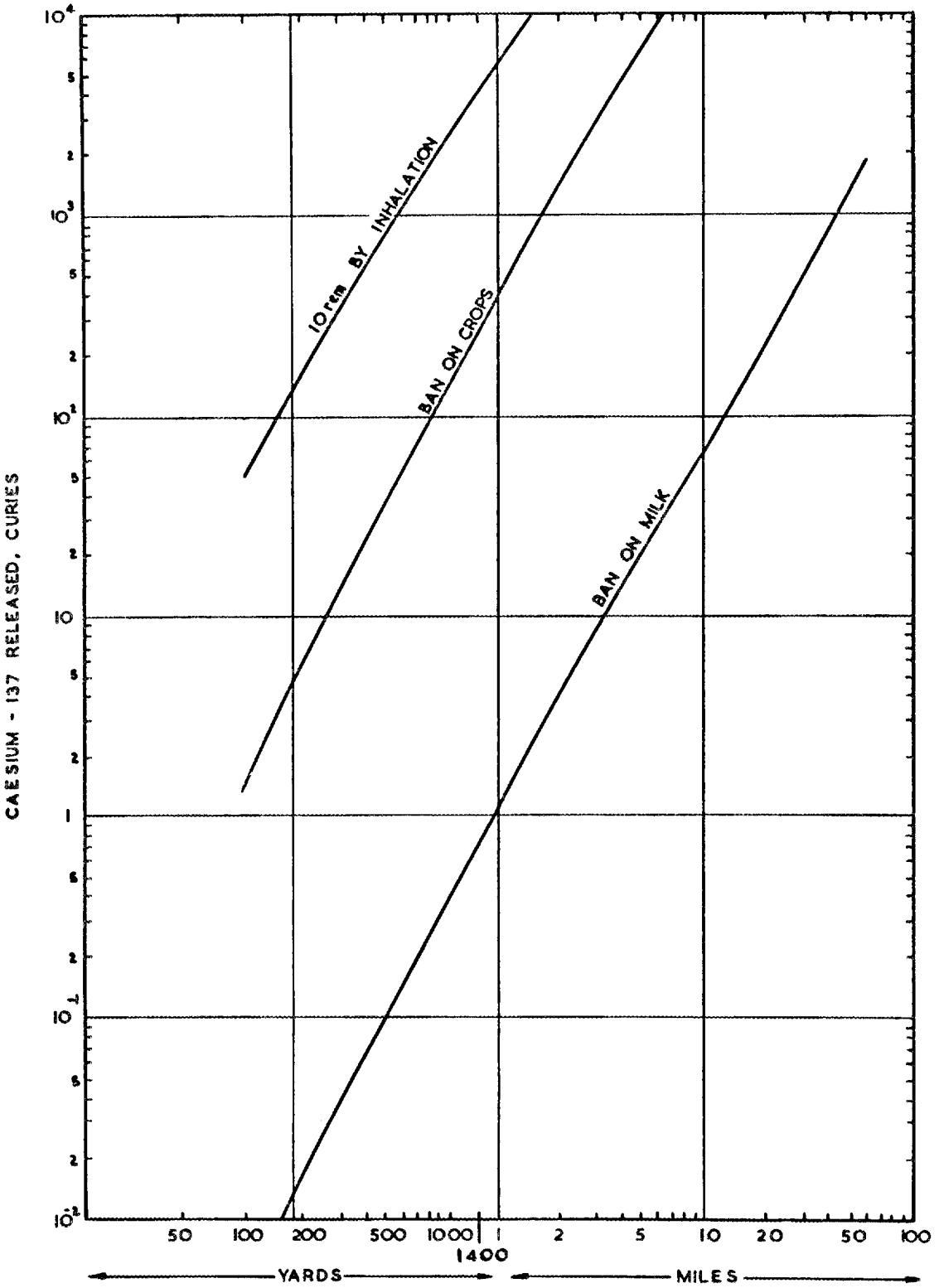

Fig. 4.106. Ranges of Hazard from the ^{137}Cs Component of a Release in Inversion Conditions. (From Beattie, ref. 1, Fig. 13.)

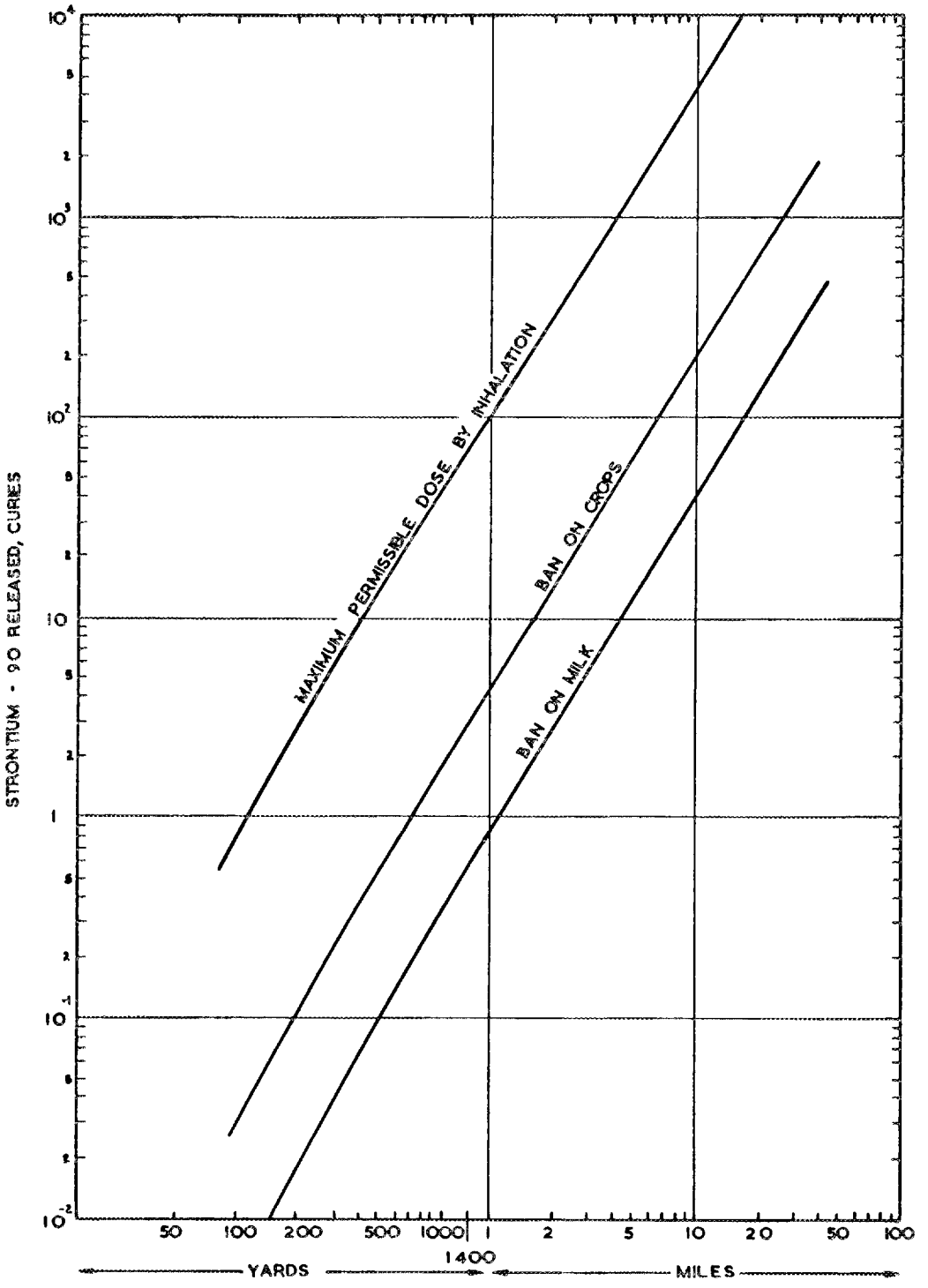

Fig. 4.107. Ranges of Hazard from the ^{90}Sr Component of a Release in Average Weather Conditions. (From Beattie, ref. 1, Fig. 14.)

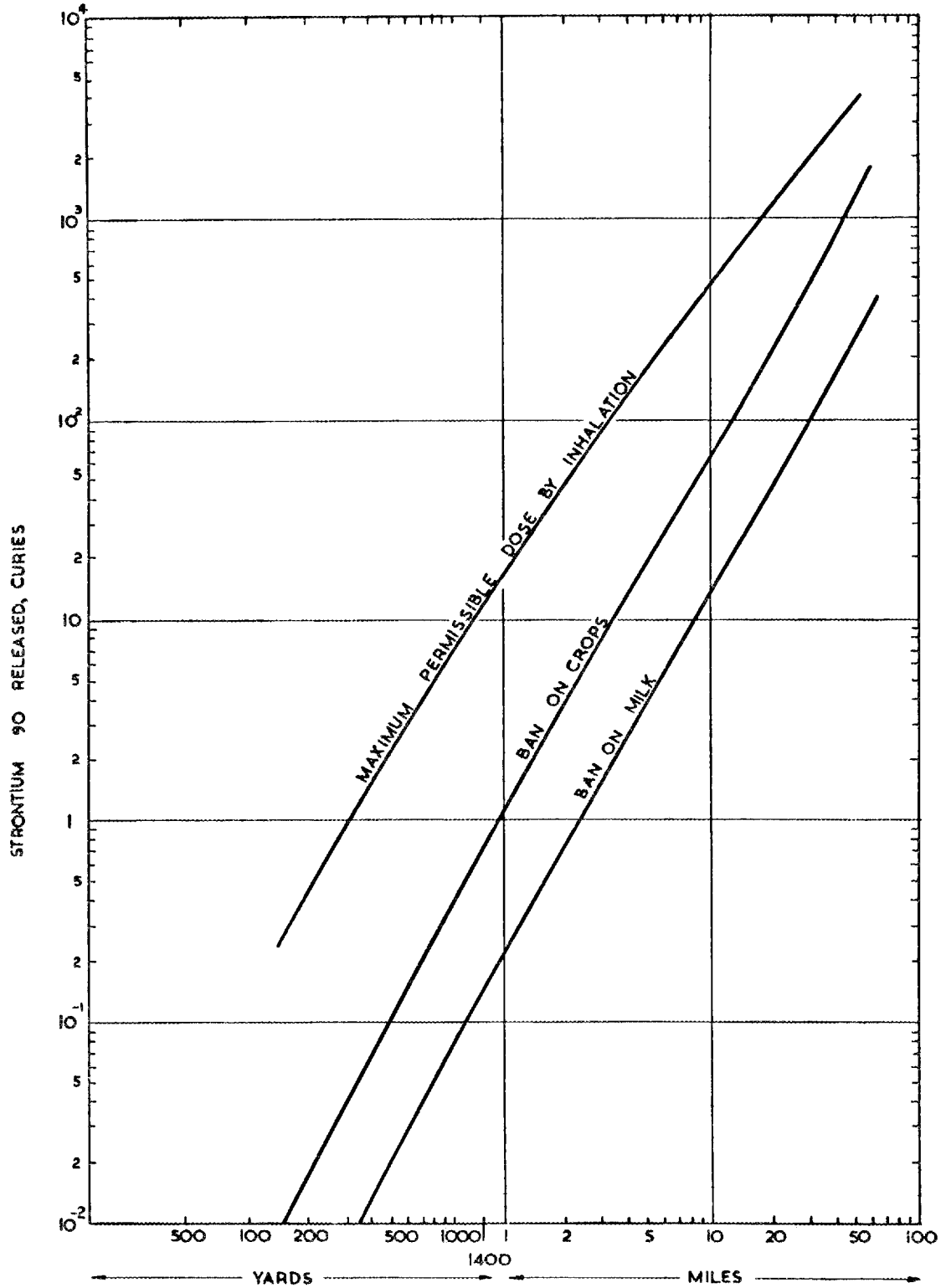

Fig. 4.108. Ranges of Hazard from the ^{90}Sr Component of a Release in Inversion Conditions. (From Beattie, ref. 1, Fig. 15.)

Table 4.50. Permissible and Damaging Levels of ^{137}Cs[a]

Level	Effect
5–10 curie-sec/m^3	Damaging or lethal effect on 6-month-old child from inhalation
0.28 curie-sec/m^3	Permissible level for inhalation; 10 rem to 6-month-old children
1×10^{-4} c/m^2	Restriction on consumption of exposed food, crops, and vegetables
0.15 μc/liter	Restriction on milk supplies
3×10^{-7} c/m^2	Probable total ground deposition of ^{137}Cs where milk supplies are restricted

[a]From Beattie, ref. 1, Table 18.

Table 4.51. Permissible Levels of ^{90}Sr[a]

Level	Remarks
8×10^{-4} curie-sec/m^3	Maximum permissible dose to mineral bone following inhalation
3×10^{-7} c/m^2	Restriction on growing green vegetables and other foods exposed in the open air
0.002 μc/liter	Restriction on milk
6×10^{-8} c/m^2	Probable total deposition of ^{90}Sr in areas where milk supplies are restricted

[a]From Beattie, ref. 1, p. 57.

Table 4.52. Ranges of Hazard from a "Volatile" Release in Average Weather Conditions[a]

(Magnitude of release specified in terms of activity of iodine-131 component of the release; activities of other isotopes in proportion given in Table 4.54. Average weather conditions, i.e., Pasquill's categories C-D, wind speed 5 metres/second. Deposition velocity assumed, 0.1 to 1.0 cm/sec; see Sec. 4.5.1.)

Origin of hazard	Element or isotope	Limiting dose or level	Remedial action	Activity in curies of iodine-131 component of release										
				1	5	10	50	100	500	10^3	5×10^3	10^4	5×10^4	10^5
				Range of hazard, yards (yd) or miles (ml)										
External beta-gamma radiation from the cloud	Iodine, xenon and other isotopes in proportion (1)	20 rad maximum permissible dose (m.p.d.)	Evacuation during period of release	-	-	-	-	-	-	-	180 yd	260 yd	700 yd	1050 yd
	(2)	400 rad lethal or damaging dose	Immediate evacuation during release	-	-	-	-	-	-	-	-	-	120 yd	180 yd
External beta-gamma radiation from ground deposition	Isotopes of iodine and tellurium (3)	20 rad (m.p.d.) to persons who remain indefinitely in area	Evacuation within 6-12 hours	-	-	-	-	-	110 yd	160 yd	360 yd	530 yd	1400 yd	$1\frac{1}{4}$ ml
	(4)	400 rad to persons who remain 12-24 h in area	Evacuation imperative within one hour	-	-	-	-	-	-	-	-	-	110 yd	160 yd
	Caesium-137 (5)	1 millirad/h persisting in the area	-	-	-	-	-	-	130 yd	180 yd	450 yd	650 yd	1 mile	$1\frac{3}{4}$ ml
				-	-	-	-	125 yd	290 yd	430 yd	1100 yd	1 mile	$2\frac{1}{2}$ ml	4 ml
Inhalation of activity from the cloud	Isotopes of iodine and tellurium (6)	25 rem to thyroids of children 0-5 years (m.p.d.)	Evacuation during period of release	-	-	125 yd	290 yd	450 yd	1200 yd	1 mile	3 ml	$4\frac{1}{4}$ ml	12 ml	19 ml
	(7)	25 rem to thyroid of 10-year-old child (m.p.d.)	" "	-	-	-	230 yd	340 yd	850 yd	1400 yd	$2\frac{1}{4}$ ml	$3\frac{1}{4}$ ml	9 ml	14 ml
	(8)	25 rem to thyroid of adult	" "	-	-	-	130 yd	190 yd	470 yd	720 yd	$1\frac{1}{4}$ ml	$1\frac{3}{4}$	$4\frac{3}{4}$	7 ml
	(9)	200 rem to thyroid of 5-year-old child	" "	-	-	-	-	140 yd	330 yd	500 yd	1400 yd	$1\frac{1}{4}$	$3\frac{1}{4}$	5 ml
	(10)	Thyroid doses 2000 rem (adult), 10,000 rem (child)	" "	-	-	-	-	-	-	-	150 yd	210 yd	530 yd	800 yd
	Caesium-137 (11)	10 rem whole-body dose to child (m.p.d.)	" "	-	-	-	-	-	-	-	-	100 yd	240 yd	360 yd
				-	-	-	-	-	-	-	170 yd	220 yd	600 yd	950 yd
	(12)	Damaging or lethal whole-body dose to child	" "	-	-	-	-	-	-	-	-	-	-	-
				-	-	-	-	-	-	-	-	-	120 yd	180 yd
	Strontium-90 (13)	Maximum permissible dose (m.p.d.) to child (bone)	" "	-	-	-	-	-	-	-	120 yd	170 yd	420 yd	640 yd
				-	-	-	-	-	-	110 yd	270 yd	400 yd	1100 yd	1 mile
	Cerium-144 (14)	Maximum permissible dose (m.p.d.) to child (bone)	" "	-	-	-	-	-	-	-	130 yd	180 yd	460 yd	700 yd
				-	-	-	-	-	-	-	170 yd	240 yd	650 yd	950 yd
	Sr89 + Ru106 + Ce144 (15)	Possibly up to 25 rad dose to lung from insoluble material	" "	-	-	-	-	-	110 yd	170 yd	400 yd	600 yd	1 mile	$1\frac{1}{4}$ ml
				-	-	-	-	-	160 yd	220 yd	580 yd	900 yd	$1\frac{1}{2}$ ml	$2\frac{1}{4}$ ml
Contamination of growing green vegetables, crops, etc.	Iodine-131 (16)	5×10^{-3} c/m² I131 ground deposition	Public warning against consumption of vegetables, crops	-	110 yd	160 yd	360 yd	530 yd	1400 yd	$1\frac{1}{4}$ ml	$3\frac{1}{4}$ ml	5 ml	13 ml	20 ml
	Caesium-137 (17)	1×10^{4} c/m² Cs137 ground deposition	" " "	-	-	-	-	-	130 yd	180 yd	440 yd	660 yd	1 mile	$1\frac{1}{2}$ ml
				-	-	-	-	110 yd	290 yd	440 yd	1100 yd	1 mile	$2\frac{1}{2}$ ml	4 ml
	Strontium-90 (18)	3×10^{-7} c/m² Sr90 ground deposition	" " "	-	-	-	-	-	200 yd	290 yd	750 yd	1100 yd	$1\frac{3}{4}$ ml	$2\frac{3}{4}$ ml
				-	-	-	140 yd	200 yd	400 yd	750 yd	1 mile	$1\frac{1}{2}$	$4\frac{1}{2}$ ml	$6\frac{1}{2}$ ml
Contamination of milk and eggs	Iodine-131 (19)	0·065 μc/litre in milk maximum permissible level	Restriction of milk supplies	600 yd	1600 yd	$1\frac{1}{2}$ ml	$3\frac{3}{4}$ ml	$5\frac{1}{2}$ ml	14 ml	23 ml	65 ml	100 ml	100 ml	100 ml
	(20)	0·05 μc/egg (free range hens)	Restriction on eggs from free-range hens	110 yd	240 yd	400 yd	900 yd	1400 yd	$2\frac{1}{4}$ ml	$3\frac{1}{4}$ ml	$8\frac{1}{4}$ ml	13 ml	35 ml	55 ml
	Caesium-137 (21)	0·15 μc/litre in milk maximum permissible level	Restriction of milk supplies	100 yd	240 yd	350 yd	900 yd	1300 yd	$2\frac{1}{4}$ ml	$3\frac{1}{2}$ ml	8 ml	12 ml	35 ml	50 ml
				230 yd	600 yd	900 yd	$1\frac{1}{2}$ ml	$2\frac{1}{4}$ ml	$5\frac{1}{4}$ ml	8 ml	22 ml	35 ml	95 ml	100 ml
	Strontium-90 (22)	0·002 μc/litre in milk maximum permissible level	" " "	-	-	-	140 yd	200 yd	490 yd	750 yd	1 mile	$1\frac{3}{4}$ ml	$4\frac{1}{2}$ ml	$6\frac{3}{4}$ ml
				-	-	140 yd	340 yd	490 yd	1200 yd	1 mile	3 ml	$4\frac{1}{2}$ ml	11 ml	17 ml
	Barium-140 (23)	0·6 μc/litre in milk probable m.p.l.	" " "	-	-	-	-	-	100 yd	150 yd	340 yd	500 yd	1300 yd	$1\frac{1}{4}$ ml

Note: Where two ranges are quoted together, these correspond to fuel with 1 year and 5 years irradiation.

[a]From Beattie, Ref. 1, Table 21.

Table 4.53. Ranges of Hazard from a "Volatile" Release in Inversion Conditions[a]

(Magnitude of release specified in terms of activity of iodine-131 component of the release; activities of other isotopes in proportions given in Table 4.54. Inversion condition assumed is Pasquill's category F, wind speed 2 metres/second. Deposition velocity assumed, 0.1 to 1.0 cm/sec; see Sec. 4.5.1.)

Origin of hazard	Element or isotope	Limiting dose or level	Remedial action	Activity in curies of iodine-131 component of release										
				1	5	10	50	100	500	10^3	5×10^3	10^4	5×10^4	10^5
				Range of hazards, yards (yd) or miles (mi)										
External beta-gamma radiation from the cloud	Iodine, xenon and other isotopes in proportion	20 rad, maximum permissible dose (m.p.d.)	Evacuation during period of release	-	-	-	-	-	150 yd	200 yd	550 yd	830 yd	1¼ mi	2 mi
		400 rad, lethal or damaging dose	Immediate evacuation during release	-	-	-	-	-	-	-	100 yd	150 yd	400 yd	550 yd
External beta-gamma radiation from ground deposition	Isotopes of iodine and tellurium	20 rad (m.p.d.) to persons who remain indefinitely in area	Evacuation within 6-12 hours	-	-	-	-	110 yd	260 yd	390 yd	880 yd	1300 yd	1¾ mi	2½
		400 rad to persons who remain 12-24 h in area	Evacuation imperative within one hour	-	-	-	-	-	-	-	-	110 yd	260 yd	390 yd
	Caesium-137	1 millirad/h persisting in the area	-	- -	- -	- 100 yd	100 yd 220 yd	140 yd 320 yd	320 yd 750 yd	460 yd 1100 yd	1100 yd 1¼ mi	1600 yd 2 mi	2 mi 5 mi	3 mi 8 mi
Inhalation of activity from the cloud	Isotopes of iodine and tellurium	25 rem to thyroids of children 0-5 years (m.p.d.)	Evacuation during period of release	100 yd	230 yd	350 yd	950 yd	1400 yd	2¼ mi	3¾ mi	12 mi	23 mi	67 mi	100 mi
		25 rem to thyroid of 10-year-old child (m.p.d.)	" " "	-	180 yd	260 yd	700 yd	1050 yd	1¾ mi	2½ mi	9 mi	16 mi	50 mi	80 mi
		25 rem to thyroid of adult	" " "	-	100 yd	150 yd	400 yd	570 yd	1550 yd	1¼ mi	4 mi	7 mi	24 mi	40 mi
		200 rem to thyroid of 5-year-old child	" " "	-	-	100 yd	250 yd	400 yd	1050 yd	1600 yd	2½ mi	4¼ mi	16 mi	26 mi
		Thyroid doses 2000 rem (adult), 10,000 rem (child)	" " "	-	-	-	-	-	120 yd	170 yd	440 yd	650 yd	1 mile	1½ mi
	Caesium-137	10 rem whole-body dose to child (m.p.d.)	" " "	- -	- -	- -	- -	- -	- 130 yd	- 180 yd	190 yd 490 yd	280 yd 700 yd	750 yd 1 mile	1150 yd 1¾ mi
		Damaging or lethal whole-body dose to child	" " "	- -	- -	- -	- -	- -	- -	- -	- 100 yd	- 140 yd	140 yd 350 yd	200 yd 520 yd
	Strontium-90	Maximum permissible dose (m.p.d.) to child (bone)	" " "	- -	- -	- -	- -	- 100 yd	100 yd 210 yd	140 yd 330 yd	340 yd 840 yd	500 yd 1300 yd	1350 yd 2 mi	1¼ mi 3½ mi
	Cerium-144	Maximum permissible dose (m.p.d.) to child (bone)	" " "	- -	- -	- -	- -	- -	100 yd 130 yd	150 yd 190 yd	410 yd 500 yd	550 yd 700 yd	1450 yd 1¼ mi	1½ mi 1¾ mi
	Sr89 + Ru106 + Ce144	Possibly up to 25 rad dose to lung from insoluble material	" " "	- -	- -	- -	- 120 yd	130 yd 170 yd	320 yd 480 yd	500 yd 700 yd	1250 yd 1 mile	1 mile 1½ mi	3¼ mi 6¾ mi	5½ mi 9 mi
Contamination of growing green vegetables, crops, etc.	Iodine-131	5×10^{-5} c/m² I131 ground deposition	Public warning against consumption of vegetables, crops	120 yd	250 yd	390 yd	900 yd	1300 yd	1¾ mi	2½ mi	6¼ mi	9½ mi	24 mi	35 mi
	Caesium-137	1×10^{-4} c/m² Cs137 ground deposition	Public warning against consumption of vegetables, crops	- -	- -	- 100 yd	100 yd 210 yd	140 yd 310 yd	320 yd 720 yd	460 yd 1050 yd	1050 yd 1¾ mi	1550 yd 2 mi	2 mi 5 mi	3 mi 7½ mi
	Strontium-90	3×10^{-7} c/m² Sr90 ground deposition	" " "	- -	- 100 yd	- 150 yd	150 yd 350 yd	210 yd 500 yd	510 yd 1200 yd	720 yd 1 mile	1 mile 2¼ mi	1¼ mi 3½ mi	3½ mi 8½ mi	5 mi 13 mi
Contamination of milk and eggs	Iodine-131	0·065 μc/litre in milk m.p.d.	Restriction of milk supplies	1400 yd	2 mi	2¾ mi	7 mi	11 mi	27 mi	39 mi	~ 90 mi	~ 100 mi	> 100 mi	> 100 mi
		0·05 μc/egg (free-range hens)	Restriction on eggs from free-range hens	250 yd	600 yd	900 yd	1¼ mi	1¾ mi	4¼ mi	6¼ mi	16 mi	24 mi	~ 55 mi	~ 75 mi
	Caesium-137	0·15 μc/litre in milk maximum permissible level (m.p.l.)	Restriction of milk supplies	250 yd 600 yd	600 yd 1400 yd	900 yd 1 mile	1½ mi 2¾ mi	1¾ mi 4 mi	4¼ mi 10 mi	6¼ mi 13 mi	16 mi 37 mi	24 mi ~ 55 mi	~ 55 mi ~ 100 mi	~ 75 mi > 100 mi
	Strontium-90	0·002 μc/litre in milk maximum permissible level (m.p.l.)	" " "	- 100 yd	100 yd 230 yd	160 yd 360 yd	360 yd 800 yd	510 yd 1200 yd	1200 yd 1½ mi	1 mile 2¼ mi	2¾ mi 5¾ mi	3½ mi 8½ mi	8½ mi 22 mi	13 mi 31 mi
	Barium-140	0·6 μc/litre in milk probable m.p.l.	" " "	-	-	-	-	100 yd	240 yd	360 yd	850 yd	1250 yd	1½ mi	2¼ mi

Note: Where two ranges are quoted together, these correspond to fuel with 1 year and 5 years irradiation.

[a] From Beattie, Ref. 1, Table 22.

Table 4.54. Activities of Fission Products Released with One Curie of ^{131}I[a]

Element or Isotope	Activity After 1 Year of Irradiation (curies)	Activity After 5 Years of Irradiation (curies)
Iodine-131	1.0	1.0
Tellurium-132	0.8	0.8
Total rare gases and volatiles, including tellurium isotopes	8.8	8.9
Cesium-137	0.029	0.138
Strontium-90	0.00021	0.0010
Strontium-89	0.0068	0.0068
Cerium-144	0.0078	0.013
Ruthenium-106	0.035	0.070
Barium-140	0.018	0.018

[a]All activities quoted as measured after one day of decay.

References

1. J. R. Beattie, An Assessment of Environmental Hazards from Fission Product Releases, British Report AHSB (S) R.64, 1963.

2. E. P. Steinberg and L. E. Glendenin, Survey of Radiochemical Studies of the Fission Process, Proceedings of Second United Nations International Conference on the Peaceful Uses of Atomic Energy, Geneva, 1958, Vol. 7, p. 3, United Nations, New York, 1958.

3. R. B. Leachman, Proceedings of Second United Nations International Conference on the Peaceful Uses of Atomic Energy, Geneva, 1958, Vol. 15, p. 229, United Nations, New York, 1958.

4. A. Pappas, Proceedings of Second United Nations International Conference on the Peaceful Uses of Atomic Energy, Geneva, 1958, Vol. 7, p. 19, United Nations, New York, 1958.

5. L. E. Glendenin, C. D. Coryell, and R. R. Edwards, Radiochemical Studies: The Fission Products, National Nuclear Energy Series, Coryell and Sugarman (Eds.), p. 489, McGraw-Hill, New York, 1951.

6. G. N. Walton, Fission and Fission Products, Chap. 1.1, in Atomic Energy Waste, Its Nature, Use, and Disposal, E. Gleukauf (Ed.), Interscience, New York, 1961.

7. J. O. Blomeke and Mary F. Todd, Uranium-235 Fission Product Production as a Function of Thermal Neutron Flux, Irradiation Time, and Decay Time. 1. Atomic Concentrations and Gross Totals, USAEC Report ORNL-2127 (TID-4500 Rev.), Oak Ridge National Laboratory, November 1958.

8. N. Metrapolis and G. G. Reteviesner, Table of Atomic Masses, USAEC Report NP-1980, Technical Information Service Extension, March 1950.

9. R. W. Stoughton and J. Halperin, Oak Ridge National Laboratory, unpublished, 1954.

10. C. J. L. Lock, Mathematics of Fission-Product Formation in Reactors with Circulating Fuel, British Report AERE c/m 278, May 1956.

11. J. D. Eichenberg et al., Effect of Irradiation on Bulk Uranium Dioxide, pp. 616–717 in Fuel Elements Conference, Paris, November 18–23, 1957, USAEC Report TID-7546 (Bk. 2), March 1958.

12. J. Belle (Ed.), Uranium Dioxide: Properties and Nuclear Applications, U.S. Government Printing Office, Washington, 1961.

13. W. D. Kingery et al., Thermal Conductivity: X. Data for Several Pure Oxide Materials Corrected to Zero Porosity, J. Am. Ceram. Soc., 37: 107 (February 1954).

14. W. D. Kingery, Thermal Conductivity: XIV. Conductivity of Multicomponent Systems, J. Am. Ceram. Soc., 42: 617 (December 1959).

15. J. C. Hedge and I. B. Fieldhouse, Measurement of Thermal Conductivity of Uranium Oxide, USAEC Report AECU-3381, Technical Information Service Extension, Sept. 20, 1956.

16. T. D. Anderson to M. H. Fontana, Oak Ridge National Laboratory, personal communication, May 1962.

17. G. W. Parker, G. E. Creek, and W. J. Martin, Fission-Product Release from Reactor-Grade UO_2 by Oxidation, Diffusion and Melting, USAEC Report TID-7622, pp. 149–159, July 1962.

18. A. H. Booth, A Method for Calculating Fission Gas Diffusion from UO_2 Fuel and Its Application to the X-2-f Loop Test, Canadian Report CRDC-721, National Research Council of Canada, September 1957.

19. J. Crank, The Mathematics of Diffusion, Clarendon Press, Oxford, 1956.

20. A. H. Booth and G. T. Rymer, Determination of the Diffusion Constant of Fission Xenon in UO_2 Crystals in Sintered Compacts, Canadian Report CRDC-720, National Research Council of Canada, August 1958.

21. J. A. L. Robertson et al., Irradiation of UO_2 Fuel Elements, Nucl. Metallurgy (Special Report Series No. 9), 6: 45–70 (1959).

22. D. Davies and G. Long, Abnormal Kinetics in the Release of Inert Gases from Uranium Dioxide, British Report AERE-M969, May 1963.

23. W. H. Stevens, J. R. MacEwan, and A. M. Ross, The Diffusion Behavior of Fission Xenon in Uranium Dioxide, USAEC Report TID-7610, June 1961.

24. D. G. Hurst, Diffusion of Fission Gas; Calculated Diffusion from a Sphere Taking into Account Trapping and Return from the Traps, Canadian Report CRRD-1124 (AECL-1550), National Research Council of Canada, November 1962.

25. A. H. Booth and G. T. Rymer, Determination of the Diffusion Constant of Fission Xenon in UO_2 Crystals and Sintered Components, USAEC Report AECL-692, Atomic Energy of Canada, Ltd., August 1958.

26. G. E. Creek, W. J. Martin, and G. W. Parker, Experiments on the Release of Fission Products from Molten Reactor Fuels, USAEC Report ORNL-2616, Oak Ridge National Laboratory, July 1959.

27. J. T. Venard, Stress-Rupture Properties of Type 304 Stainless Steel Tubing, USAEC Report ORNL TM-535, Oak Ridge National Laboratory, June 1963.

28. G. W. Parker et al., Release of Fission Products on Out-of-Pile Melting of Reactor Fuels, p. 11 in Nuclear Safety Program Semiannual Progress Report for Period Ending June 30, 1962, USAEC Report ORNL-3319, Oak Ridge National Laboratory, 1962.

29. K. A. Peakall and J. E. Antill, Oxidation of UO_2 in Air Between 350–1000°C, J. Nucl. Materials, 2(2): 194–195 (1960).

30. G. W. Parker et al., Release of Fission Products on Out-of-Pile Melting of Reactor Fuels, p. 5 in Nuclear Safety Program Semiannual Progress Report for Period Ending December 31, 1962, USAEC Report ORNL-3401, Oak Ridge National Laboratory, 1963.

31. G. W. Parker, G. E. Creek, and W. J. Martin, Fission Product Release from UO_2 by High Temperature Diffusion and Melting in Helium and Air, USAEC Report ORNL CF-60-12-14, Oak Ridge National Laboratory, February 1961.

32. W. E. Browning, Jr., et al., Behavior of Fission Products Released During In-Pile Destruction of Reactor Fuels, pp. 42–44 in Nuclear Safety Program Semiannual Progress Report for Period Ending December 31, 1963, USAEC Report ORNL-3547, Oak Ridge National Laboratory.

33. W. E. Browning, Jr., et al., Release of Fission Products on the In-Pile Melting or Burning of Reactor Fuels, p. 27 in Nuclear Safety Program Semiannual Progress Report for Period Ending December 31, 1962, USAEC Report ORNL-3401, Oak Ridge National Laboratory.

34. W. E. Browning, Jr., et al., Release of Fission Products on In-Pile Melting of Reactor Fuels, p. 29 in Nuclear Safety Program Semiannual Progress Report for Period Ending June 30, 1962, USAEC Report ORNL-3319, Oak Ridge National Laboratory.

35. T. J. Thompson and J. G. Beckerly (Eds.), Safety Information for the Technology of Reactors, an AEC-sponsored book to be published by MIT Press in two volumes in the latter half of 1964.

36. R. K. Hilliard and D. L. Reid, Fission Product Release from U — Effect of Irradiation Level, USAEC Report HW-72321, Hanford Atomic Products Operation, June 1962.

37. W. E. Browning, Jr., et al., In-Pile Burning of UC_2 Graphite Fuel, pp. 24–26 in Nuclear Safety Program Semiannual Progress Report for Period Ending June 30, 1963, USAEC Report ORNL-3483, Oak Ridge National Laboratory.

38. F. H. Neill et al., Fission-Product Transport and Deposition in Coolant Circuits, pp. 164–173 in Gas-Cooled Reactor Program Semiannual Progress Report for Period Ending March 31, 1963, USAEC Report ORNL-3445, Oak Ridge National Laboratory.

39. A. W. Castleman, Jr., The Chemical and Physical Behavior of Released Fission Products, USAEC Report BNL-6415, Brookhaven National Laboratory, 1962.

40. J. J. Katz and E. Rabinowitch, The Chemistry of Uranium, pp. 5–8, McGraw-Hill, New York, 1950.

41. J. W. Mausteller and R. J. Campana, Activity Distribution from Simulated Pressurized Water Leaks, Proceedings of Second United Nations International Conference on the Peaceful Uses of Atomic Energy, Geneva, 1958, Vol. 11, pp. 153–156, United Nations, New York, 1958.

42. W. J. Megaw and F. G. May, The Behavior of Iodine Released in Reactor Containers, J. Nucl. Energy: P. A & B, 16: 427–436 (1962).

43. A. C. Chamberlain et al., Behavior of Iodine Vapor in Air, Discussions Faraday Soc., 30: 162 (1960).

44. D. H. F. Atkins and A. E. J. Eggleton, Iodine Compounds Formed on Release of Carrier-Free Iodine-131, British Report AERE-M 1211, May 1963.

45. V. Griffiths, The Removal of Iodine from the Atmosphere by Sprays, British Report AHSB (S) R 45, January 9, 1963.

46. L. C. Watson, A. R. Bancroft, and C. W. Hoelke, Iodine Containment by Dousing in NPD-II, Canadian Report CRCE-979, October 1960.

47. R. F. Taylor, Adsorption of Iodine Vapor by Aqueous Solutions, Chem. Eng. Sci., 10(1/2): 68–80 (April 1959). (Referred to in ref. 42.)

48. C. R. Wilke and Pin Chang, Am. Inst. Chem. Eng. J., 1: 264 (1955). (Referred to in ref. 45.)

49. W. E. Ranz and W. R. Marshall, Chem. Eng. Progr., 48(141): 173 (1952). (Referred to in ref. 45.)

50. R. C. Liimatainen et al., Removal of Halogens, Carbon Dioxide and Aerosols from Air in a Spray Tower, USAEC Report ANL-5429, Argonne National Laboratory, February 1955. (Referred to in ref. 45.)

51. A. C. Chamberlain, Aspects of Travel and Deposition of Aerosol and Vapor Clouds, British Report AERE HP/R1261, United Kingdom Atomic Energy Authority, 1955. (Referred to in ref. 45.)

52. W. R. Marshall, Atomization and Spray Drying, Chem. Eng. Progr., Monograph Ser., 50(2): (1954). (Referred to in ref. 45.)

53. E. Griffin and A. Muraszew, The Atomization of Liquid Fuels, Chapman and Hall, London, 1953. (Referred to in ref. 45.)

54. E. Griffin and B. S. Massey, Some Observations on Flow in Spray Nozzles, The Motor Industries Res. Assoc. Report No. 1950/5. (Referred to in ref. 45.)

55. H. L. Green and W. R. Lane, Particulate Clouds: Dusts, Smokes and Mists, E. & F. N. Spon, Ltd., London, 1957.

56. J. M. Dallavalle, Micrometritics, The Technology of Fine Particles, 2d ed., Pitman Publishing Corp., New York, 1948.

57. C. N. Davies, Proc. Phys. Soc., 57: 259 (1945). (Referred to in ref. 55.)

58. C. N. Davies, Trans. Instr. Chem. Eng. (Suppl.), 25: (1947). (Referred to in ref. 55.)

59. C. N. Davies, The Sedimentation and Diffusion of Small Particles, Proc. Roy. Soc., A200: 100 (1950).

60. M. H. Fontana and W. E. Browning, Jr., Effect of Particle Agglomeration on the Penetration of Filters Utilized with Double Containment Systems, USAEC Report ORNL-NSIC-1, Oak Ridge National Laboratory, September 25, 1963.

61. T. D. Anderson, Time-Dependent Release of Gaseous Material from a Three-Barrier Reactor Containment System, USAEC Report ORNL-TM-397, Oak Ridge National Laboratory, November 16, 1962.

62. United States Department of Commerce, Weather Bureau, Meteorology and Atomic Energy, USAEC Report AECU-3066, Technical Information Service Extension, July 1955.

63. C. H. B. Priestly, R. A. McCormick, and F. Pasquill, Turbulent Diffusion in the Atmosphere, Technical Note No. 24, World Meteorological Organization, WMO-No. 77 TP 31, Geneva, Switzerland, 1958.

64. O. G. Sutton, Micrometeorology, McGraw-Hill, New York, 1953.

65. F. A. Gifford, Atmospheric Dispersion Calculations Using the Generalized Gaussian Plume Model, Nucl. Safety, 1(3): 48 (1960).

66. F. A. Gifford, Use of Routine Meteorological Observations for Estimating Atmospheric Dispersion, Nucl. Safety, 2(4): 47–51 (1961).

67. F. Pasquill, The Estimation of the Dispersion of Windborne Material, The Meteorological Magazine, 90: 33–49 (1961).

68. W. F. Hilsmeier and F. A. Gifford, Jr., Graphs for Estimating Atmospheric Dispersion, USAEC Report ORO-545, Oak Ridge Operations Office, July 1962.

69. T. H. Burnett, Reactors, Hazard vs. Power Level, Nucl. Sci. Eng., 2: 382–93 (1957).

70. A. C. Chamberlain, Aspects of Travel and Deposition of Aerosols and Vapour Clouds, British Report AERE HP/R-1261, United Kingdom Atomic Energy Authority, 1953. (Referred to in ref. 1.)

71. Recommendations of the International Commission on Radiological Protection, Report of Committee II on Permissible Doses for Internal Radiation, Pergamon Press, New York, 1959. (Referred to in ref. 1.)

72. Medical Reserach Council, Maximum Permissible Dietary Contamination After the Accidental Release of Radioactive Material from a Nuclear Reactor, Brit. Med. J., I(1): 967 (April 11, 1959). (Referred to in ref. 1.)

5. ENERGY SOURCES*

5.1 INTRODUCTION

The major sources of energy available for contributing to reactor accidents are nuclear core excursions and fission-product decay, chemical reaction between core, moderator, coolant, and other components, and stored heat contained in the coolant, structural materials, and components. These sources of energy are inherent to reactor systems, and the importance of their contribution to a particular accident (assuming that this availability is credible) depends on magnitude, rate, and time of release. For example, an excursion release would occur in a few milliseconds, whereas the release of a similar quantity of energy from decay heat might require a full day. The availability of the energy in an accident, however, is seldom equivalent to the energy of the source and differs for different reactors. In pressurized-water systems, chemical reactions involving as much as 60 to 70% of the available metal and catastrophic nuclear excursions are generally considered to be improbable but not impossible, and the slow rate at which decay heat is released reduces its effect. However, stored energy in the primary water system is the most important energy contribution to accidents in pressurized-water systems. Again, it should be emphasized that other systems would differ both in the inherent energy sources in the reactor and in the particular designs to cope with the release of these energies.

The relative importance of the energy sources differs with specific reactor systems. Approximate values for major energy sources in the Yankee Reactor, a pressurized-water system, are listed in Table 5.1.

---

*Contributors to this Chapter were L. Baker, Jr., Argonne National Laboratory; W. K. Ergen, Oak Ridge National Laboratory; J. O. Kolb, Oak Ridge National Laboratory; W. E. Nyer, Phillips Petroleum Company; S. Peterson, Oak Ridge National Laboratory; and C. L. Whitmarsh, Oak Ridge National Laboratory (now with NASA Lewis Research Center).

Table 5.1. Theoretical Energy Sources in the Yankee Reactor

Source of Energy	Approximate Magnitude (Btu)	Comments
Nuclear excursion	2×10^7	Vaporization of 20% of core
Chemical reaction	10^7	Metal-water reaction of all Zircaloy-2 and stainless steel in core
Decay heat	3×10^7	Integrated release over a one-day shutdown period after infinite operation
Stored energy in coolant (water)	10^8	Includes all primary system water

5.2 CHEMICAL REACTIONS

Reactions between the various materials in a nuclear reactor system under accident conditions could make major contributions to the energy release. Thermodynamic data indicate the possibility of several exothermic chemical reactions. The energy release might occur in some cases with explosive violence, e.g., hydrogen-oxygen reactions, whereas in others it could be sufficiently slow as to be of negligible importance. From the standpoint of maximum containment pressures, only those reactions need be considered that are sufficiently fast to contribute to the pressure or temperature changes which characterize that accident, although for some reactor containment combinations the consequences of the chemical reactions occurring a long time after the initiation of the accident must be accommodated. In addition to the energy from exothermic reactions, endothermic reactions must be considered if they produce materials that are potentially dangerous, for example, hydrogen from a graphite-steam reaction.

In many cases, such as metal-water reactions in pressurized-water systems, for example, the conditions necessary to initiate the chemical reactions must be generated by an accident. Therefore rate data for the appropriate conditions are needed because of the importance of knowing the time dependence of the energy release. The energy release from the chemical reaction might not occur at the same time as the maximum energy release from other sources.

In general, chemical reaction kinetics are quite sensitive to environmental conditions, such as surface area, temperature, and mixing. This sensitivity leads to considerable difficulty in predicting energy releases because the prediction of the exact conditions existing during an accident is difficult. For containment design, it would be desirable, if not essential, to know both the rate and the extent of reaction.

The major problem involved is the prediction of accident conditions, primarily the surface area available for reaction. Information relative to the prediction of accident conditions can be obtained from three sources: (1) full-scale nuclear incidents (accidental or planned), (2) small-scale meltdown tests, particularly those conducted in TREAT, and (3) out-of-pile laboratory experiments. The complex conditions affecting heat transfer in a reactor core are very difficult to simulate and measure accurately in laboratory experiments and consequently the extrapolation of these data to reactor systems must be done conservatively to ensure an adequate safety analysis.

5.2.1 Metal-Water Reactions

5.2.1.1 General

Metal-water reactions have been studied extensively because of the potential release of large amounts of heat at rapid rates under conditions postulated for reactor accidents. The exothermic reaction,

$$Me + nH_2O \rightarrow MeO_n + nH_2 + heat \ ,$$

is thermodynamically possible for certain metals. The necessary conditions for rapid evolution of a significant quantity of heat are an initial temperature sufficient to melt or vaporize the metal, some mechanism by which a reactive molten metal-steam interface is maintained, a large interfacial area, and low heat loss to the surroundings. The two reactor accidents most often considered that could lead to these conditions are nuclear excursions and loss of coolant. In principle, however, the conditions could be created by any accident which led to overheating and subsequent melting of core components.

Of particular interest are pressurized- and boiling-water reactors containing significant quantities of zirconium, aluminum, stainless steel (iron), and uranium. In some reactors liquid sodium and sodium-potassium alloy must also be considered. The evolution of hydrogen in the reaction written above is considered an indirect hazard leading to the possibility and consequences of a hydrogen explosion.

An extensive metal-water reaction might be considered a secondary hazard, since it must be preceded by some kind of accident that results in overheating and melting in the reactor. However, even if melting has occurred in the presence of water, it is not certain that a violent heat release will occur; this appears to require a special set of circumstances. Although some reaction occurs whenever reactive metals are overheated in the presence of water, a violent reaction depends upon the rapid dispersal of the reactive metal throughout the water. Experimental data and theoretical studies have not as yet adequately defined the complex nature of practical situations. Because of inadequate knowledge in this field, reactor designers have been forced to exercise caution to prevent the occurrence of overheating incidents involving reactive metals and water and to employ overly conservative calculations. These calculations are usually based on the most pessimistic accident conditions.

5.2.1.2 Analytical Considerations

1. Surface Area for Reaction. In heterogeneous reactions of the metal-water type, the chemical reaction can take place only at the interface between the reacting phases. This area dependence dictates that the metal phase be finely subdivided for the reaction to proceed to a significant extent and with sufficient rapidity to represent a significant energy contribution to the maximum containment vessel pressure. The only reasonable way this could conceivably occur in a reactor is for the metal to

become molten and thereby form small droplets. Although in principle finely subdivided solid particles, such as vaporized metal, could produce the same effect, the probability of metal being vaporized during an accident is remote. A summary of these considerations is presented in Table 5.2.

Table 5.2. Conditions Under Which Rapid Metal-Water Reactions Can Occur[a]

Form	Can Sustained Rapid Reaction Occur?	Comments
Massive solid metal	No	Process would be slowed down or halted by buildup of solid reaction products on metal surfaces
Powdered or finely divided solid metal	Yes	Experimental verification available; would require preliminary powdering of metal before injection into water (conceivable but unlikely in a nuclear accident)
Liquid metal	Yes	Experimental verification available; liquid can readily be broken into droplets with high interfacial area in contact with water (this is the case of major importance in nuclear accident considerations)
Metal vapor	Yes	Of minor importance because of low vapor pressures of metals

[a]From Epstein, ref. 1, p. 30.

2. Rate Limiting Step in Reaction. The process controlling the rate of chemical reaction depends not only on the metal under consideration but may also depend on temperature, pressure, particle size, and flow rate. The metals of interest in reactor safety, that is, zirconium, aluminum, stainless steel, and uranium, form protective oxide coatings over wide temperature ranges. The formation of a protective oxide leads to a reaction rate that decreases as the oxide film thickens. This can often be described by the parabolic rate law:

$$\frac{dw}{dt} = \frac{k_0}{2w} \exp\left(-\Delta E/RT\right) , \qquad (5.1)$$

where

w = quantity of reaction,
k_0 = reaction rate constant,
t = time,
ΔE = activation energy,
R = gas constant,
T = temperature.

The parabolic rate law is frequently expressed in integrated form:

$$w^2 = k_0 t \exp(-\Delta E/RT) . \tag{5.2}$$

Some metal-gas reactions are best described, however, by using an exponent of 3 (cubic rate law) or a fractional exponent. The parabolic law can be derived by considering the limiting process to be diffusion of an ionic species through the barrier film.

Reaction rates calculated from equations of the form of (5.1) or (5.2) become very high at a high temperature because of the exponential term, but in reality the reaction rate cannot exceed the rate at which the reactants can be brought together. For the case of metal-water reactions, the limiting process is the gas-phase diffusion of the steam toward the metal surface through the gaseous hydrogen which must diffuse away from the surface. The rate of gas-phase diffusion can be formulated as follows:

$$\frac{dw}{dt} = h_D \frac{\Delta P}{RT} , \tag{5.3}$$

where h_D is the mass transfer coefficient and ΔP is the difference in water-vapor partial pressure that drives the diffusion. A value for h_D may be obtained for small spheres by using the fact that the Nusselt number for spheres has a minimum value of 2. The Nusselt number Nu is

$$Nu = \frac{h_D L}{D} , \tag{5.4}$$

where L is the characteristic length or diameter and D is the diffusion coefficient. Diffusion coefficients for steam-hydrogen mixtures are given in Table 5.3 (ref. 2).

3. Heat Transfer. The rate of energy release from the reacting metal to the water or steam is of major importance in hazards evaluation. The temperature of individual particles of reacting metal tends to increase as a result of the heat of reaction and decay or fission heating. Self-heating is opposed by heat losses resulting from conduction, convection, and thermal radiation. The heat balance over a single spherical

Table 5.3. Diffusion Coefficients of Steam-Hydrogen Mixtures[a]

Temperature (°C)	Product of Diffusion Coefficient and Total Pressure ($cm^2 \cdot atm/sec$)
200	2.04
300	2.84
400	3.74
500	4.73
600	5.80
700	6.97
800	8.22
900	9.53
1000	10.9
1100	12.4
1200	13.9
1300	15.4
1400	17.6
1500	18.8
1600	20.5
1700	22.4
1800	24.3
1900	26.3
2000	28.4

[a]From Furman, ref. 2, p. 59.

particle has been approximated as follows:[3]

$$c_p \rho V_0 \frac{dT_m}{dt} = \underbrace{Q\rho 4\pi x^2 \left(\frac{-dx}{dt}\right)}_{\text{Chemical Heating}} + \underbrace{B(t)\ \rho V_0}_{\text{Nuclear Heating}}$$

$$- \underbrace{h(4\pi x_0^2)(T_s - T_a)}_{\text{Conduction/Convection}} - \underbrace{\sigma\epsilon(4\pi x_0^2)(T_s^4 - T_a^4)}_{\text{Thermal Radiation}} , \quad (5.5)$$

where

c_p = specific heat of metal,
ρ = density of metal,

V_0 = volume of spherical particle,
T_m = metal temperature,
t = time,
Q = heat of reaction,
x = radius of unreacted metal,
x_0 = original radius of particle,
$B(t)$ = time dependent flux or decay heating term,
h = heat transfer coefficient,
T_s = temperature of outer oxide surface,
T_a = ambient temperature,
σ = Stephan-Boltzmann constant,
ϵ = emissivity of oxide surface.

The metal temperature differs from the oxide surface temperature because of the temperature drop across the oxide. This effect has been described approximately as

$$\frac{4\pi k_{ox}}{r} \frac{x_0 x}{x_0 - x} (T_m - T_s) = h(4\pi x_0^2)(T_s - T_a) + \sigma\epsilon 4\pi x_0^2 (T_s^4 - T_a^4) , \qquad (5.6)$$

where k_{ox} is the thermal conductivity of the oxide film and r is the ratio of molar volume of oxide to that of metal. The heat loss terms not only represent the cooling rate of the particles but also the rate at which energy is deposited in the water or steam. The heat transfer coefficient, h, can be evaluated for the limiting case of small spheres by using the fact that the minimum Nusselt number for spheres is Nu = 2:

$$Nu = \frac{hL}{k_f} , \qquad (5.7)$$

where L is the characteristic length or diameter ($2x_0$) and k_f is the thermal conductivity of the steam-hydrogen film. The effect on the Nusselt number, and hence on the heat transfer rate and the gas-phase diffusion reaction rate, of violent pressure surges or irregular particle motion is an important problem area that needs additional study.

4. Solution of Equations for Small Spheres. The equations presented in the previous paragraphs were solved on an analog computer as part of a study of the zirconium-water reaction.[3] The reaction rate was initially controlled by the counterdiffusion of steam and hydrogen. At a later stage of the reaction, the rate became controlled by solid-state processes, as described by the parabolic rate law. Typical temperature vs time and percent reaction vs time curves for fully melted zirconium spheres suddenly exposed to water are given in Figs. 5.1 and 5.2. Greater reaction occurs in heated (saturated) water than in room-temperature (subcooled) water because the driving force for gas-phase diffusion is greater. The minimum convection heat loss rate (Nu = 2) and the maximum thermal radiation heat loss rate (ϵ = 1) were used for the calculations. The pause in the temperature vs time curves corresponds to the absorption of the

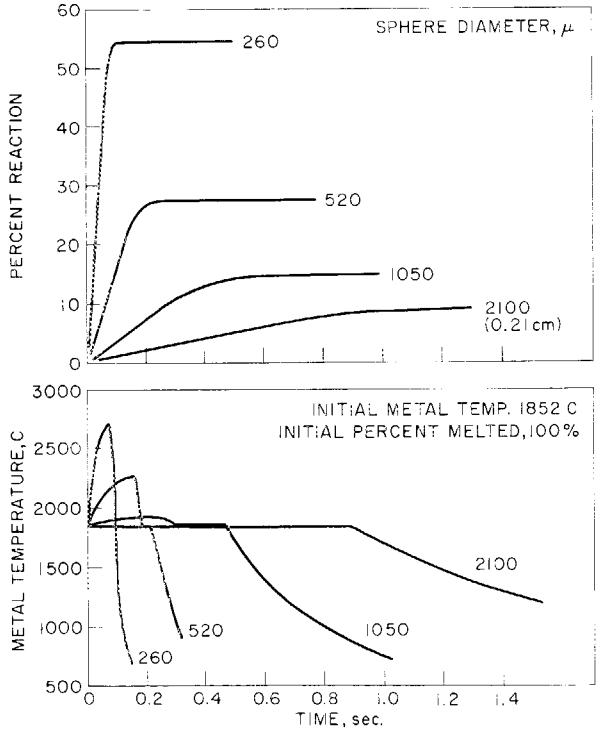

Fig. 5.1. Computed Reaction and Temperature for Molten Zirconium Spheres in Room Temperature Water.

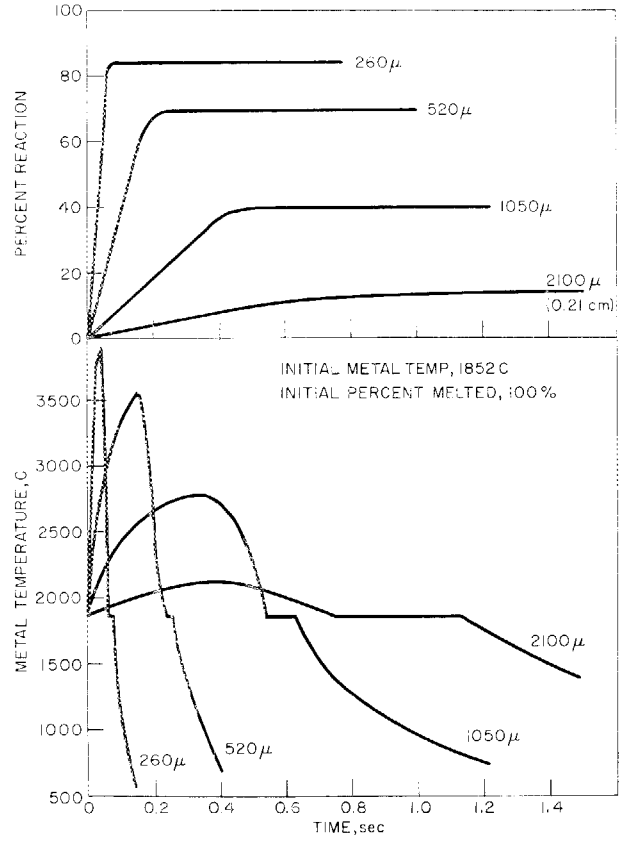

Fig. 5.2. Computed Reaction and Temperature for Molten Zirconium Spheres in Heated, 100 to 315°C, Water.

heat of fusion as the metal freezes. No fission or decay heat was included in these calculations.

The computed results for the zirconium-water reaction show that smaller particles have a greater tendency to self-heat. Reaction with smaller particles is faster and more extensive than it is with larger particles.

5. Critical Temperatures. Experimental studies of metal-water reactions have revealed the existence of "critical temperatures" where the reaction rate changes abruptly from a slower to a more rapid rate. It has been postulated[4] that metal-water reaction rates increase abruptly at the temperature at which the metal vapor pressure is 0.15 mm. More recent data have indicated, however, that observed critical temperatures may result from several different causes, some of which are unrelated to metal vapor pressure. For example, the extent of zirconium-water reaction under certain conditions increases markedly when the metal temperature reached 2400 to 2600°C.[3,5] This increase is apparently caused by the increased ability of particles to subdivide into smaller particles when the oxide (ZrO_2; mp, 2700°C) is formed as a liquid instead of as a firm solid.

Aluminum shows increased reactivity in the range above 1200 to 1400°C.[6,7] This might be caused by decreased viscosity of the molten metal, which would allow greater particle subdivision. The aluminum-water reaction shows a marked change when the metal temperature reaches 1750°C.[6] This has been shown to be the temperature at which vapor-phase burning is initiated (Al; vp, 7 mm at 1750°C). Stainless steel has been found to undergo rapid attack commencing at about 1500°C. The cause of this is presently unknown, but it is probably related to the evolution of a volatile constituent.

5.2.1.3 Full-Scale Excursions

There have been several reactor excursions in which melting of the core of a water- (or D_2O-) cooled reactor has taken place. Four separate facilities with aluminum-uranium cores have sustained nuclear excursions that resulted in extensive damage. Two of these, the NRX[8,9] and the Sl-1 (refs. 10–12), were accidents and two, Borax-1 (ref. 13) and SPERT-1 (refs. 14–16), were full-scale excursion experiments. Summary descriptions of these excursions are given in Table 5.4. Three of these transients occurred at NRTS (National Reactor Testing Station), Idaho, USA. These were the Borax-1 and SPERT-1 experiments and the SL-1 accident. All three reactors had similar cores; the fuel elements consisted of aluminum-clad, aluminum-uranium alloy plates; and the three incidents were similar. Each was initiated by the rapid removal of a control rod. In each case a large portion of the center of the core melted and fragmented. Violent movement of a large portion of the coolant water up and out of the reactor core was recorded in each incident. Both Borax-1 and SPERT-1 were open to the atmosphere (open-tank configuration), and motion pictures recorded the rise of the water spout carrying with it core material and instrumentation. Pressure records were made in both experiments; however, they were difficult to interpret because of apparently violent shock waves which destroyed transducers and overloaded recording devices.

Table 5.4. A Summary of Some Destructive Transients in Water- (or D_2O-) Cooled Reactors with Aluminum-Uranium Cores

	NRX	BORAX-1	SL-1	SPERT-1
Date of event	Dec. 12, 1952	July 22, 1954	Jan. 3, 1961	Dec. 5, 1962
Place	Chalk River, Canada	NRTS, USA	NRTS, USA	NRTS, USA
Category	Accident	Experiment	Accident	Experiment
Reactor period, sec	Few	0.0026	~0.004	0.0032
Nuclear energy, Mw-sec	~2000	135	130	31
Peak power, Mw	80	16,000 (est.)	19,000 (est.)	2300
Chemical energy, Mw-sec	Undetermined	Undetermined	24	3.5

The SL-1 reactor was a closed system. At the time of the incident, however, several flanged access holes for control rod drives (top mounted) were open. The rise of water was indicated by the apparent water hammer which lifted the entire reactor vessel and displaced several control rod drive assemblies (loose and attached). Some of the control rod mechanisms were ejected from their original positions and imbedded in loft portions of the reactor building.

In all three incidents the core debris had a similar appearance. Portions of core that had been completely melted were spongy, and considerable quantities of metallic oxides were present. No attempt was made to determine the extent of reaction of the core with water in the Borax experiment. In the postexcursion analysis of both the SL-1 accident and SPERT-1 experiment, portions of the debris were analyzed for alpha alumina. Alpha alumina is the reaction product formed at temperatures above 600°C.

The SL-1 analysis indicated appreciable quantities of alumina in several samples.[10,11] The results of these analyses and an overall material balance resulted in an estimated chemical energy release of 24 ± 10 Mw-sec, compared with the nuclear input of 130 Mw-sec. A similar analysis of debris from the SPERT-1 destructive test[15] resulted in an estimated chemical energy input of 3.5 Mw-sec, compared with the 31 Mw-sec nuclear energy release.

In all three cases, the conclusion was reached that the results of the excursion could be explained in terms of a steam explosion that resulted from the dispersion of molten metal into the water. It is presently believed that hydrogen produced by prompt metal-water reaction contributed little toward the steam explosion.

The accident to the NRX Reactor at Chalk River, Canada, was somewhat different. The reactor was D_2O moderated and primarily H_2O cooled. The excursion was initiated by the inadvertent removal of a bank of control rods. These rods failed to completely reinsert on a manual scram. After the initial power rise to 20 Mw, a sudden increase of reactivity occurred that increased the power to 80 Mw and was probably due to expulsion of light water by steam. Eventually, the dumping of the D_2O moderator ended the excursion. The total nuclear energy release was much greater than in

the three aforementioned excursions. Because of the long period of the excursion, the peak power was only 80 Mw, as compared with 16,000 and 19,000 Mw for the SL-1 and Borax excursions, respectively.

Severe damage was caused by insufficient cooling of several fuel rods in which experiments were being conducted. Melting of several rods in the core resulted. The appearance of the core material indicated that some reaction had obviously occurred. Subsequently a hydrogen explosion was postulated as an explanation for the lifting of a 4-ton dome on the gas holder above the reactor. The investigators stated,[9] "The appearance of the residual metal (uranium) in some of the worst cases can only be accounted for by considerable chemical reaction and not just melting of materials. Whether or not the highly exothermic aluminum-water reaction also had a significant role cannot be decided."

In summary, it appears that in each of these incidents the metal-water reactions played some role; however, the principal damage resulted from the nuclear energy release. One other point that should be made is that none of these reactors was operating at power at the time of the incident. The water temperatures were of the order of 25°C and the pressure in all cases was near atmospheric. The possibility of more severe chemical effects at higher initial water temperatures and steam pressures should be considered. It should also be noted that more energetic transients would increase the percentage of the reactor core metal reaching high temperatures. This would increase the chemical energy release relative to the fission energy release because of the exponential dependence of chemical reaction rates on temperature.

5.2.1.4 Small-Scale Meltdown Tests in TREAT

Extensive experimental data are available on the extent of metal-water reaction and the nature of damage produced by transient nuclear heating of small representative fuel specimens. The technique used has been to simulate a nuclear excursion accident by using fission heating from a neutron pulse to heat a few grams of fuel in a stainless steel autoclave containing water. Following the transient irradiation, the fraction of metal that reacts with water is computed from the measured quantity of hydrogen produced. The hydrogen is normally determined by a mass spectrometric analysis of the gas phase within the autoclave. Photomicrographs, macrophotographs, and particle size studies are used to characterize the physical damage sustained by the fuel specimens. Thermocouples and pressure transducers are used to determine the temperature and pressure history of the process. Thermocouples have not, however, indicated temperatures beyond the melting or fragmentation point of the specimens because of loss of contact. Pressure records have been generally unsatisfactory because of interaction between the neutron flux and the transducer circuitry. Meltdown studies with specimens containing zirconium, uranium, aluminum, and stainless steel have been carried out. The results are discussed according to the metal in Section 5.2.1.6.

5.2.1.5 Out-of-Pile Studies

Metal-water reactions have been studied in the laboratory by a wide variety of methods. These can be divided into isothermal and nonisothermal experiments. In the isothermal studies, metal samples, either solid or molten, are exposed to water or steam for a considerable period of time while the metal temperature is maintained constant. These experiments are designed to determine the reaction mechanism, rate law, and products. Nonisothermal experiments have been performed by (1) pouring or spraying molten metal into water, (2) allowing molten metal drops to fall into water, (3) dispersing molten metal by an explosive charge, and (4) heating and dispersing metal wires by discharging condensers. These methods are a somewhat better simulation of a reactor accident than the isothermal experiment; however, their principal value is to study effects resulting from a high degree of dispersion and rapidly changing temperatures.

5.2.1.6 Specific Reactions

The available information on specific metal-water reactions is discussed in this section. The stoichiometry and thermodynamics of the reactions are summarized in Table 5.5. Heat of reaction data are, in general, given for the molten metal at the melting temperature, but these can be calculated for any temperature desired.[1] The following presentation of experimental results is subdivided according to the nature of the experiment.

1. Zirconium (or Zircaloy)

Isothermal Experiments. Data[17] on the isothermal oxidation of solid Zircaloy-2 were correlated[18] by a parabolic rate law having an activation energy of 65.4 kcal/mole and also[19] by am empirical rate law with an exponent varying from 2.63 at 1200°C to 1.06 at 2200°C. These results were later replotted[3] on the assumption that the apparent failure of the parabolic law at high temperatures resulted either from a rate limitation due to the gaseous interdiffusion of steam and hydrogen or to the time required to heat the specimen in the presence of steam. The parabolic rate constants computed on this basis[3] are plotted in Fig. 5.3. They show the correlation

$$k = 33.3 \times 10^6 \exp(-45{,}500/RT) , \qquad (5.8)$$

where k is in units of $(\text{mg Zr/cm}^2)^2/\text{sec}$.

In another study the reaction of zirconium with flowing steam at temperatures between 1000 and 1690°C was correlated in terms of the parabolic rate law with an activation energy of 34 kcal/mole.[18] Recalculated parabolic rate constants are included in Fig. 5.3. An additional data point obtained by a mathematical analysis of zirconium-water reaction data obtained by a condenser discharge heating method[3] is also included in Fig. 5.3. This point was used as the basis for constructing a linear Arrhenius

Table 5.5. Thermodynamic Properties of Some Potentially Violent Chemical Reactions[a]

Reactant	State	Temperature of Reactant (°F)	Oxides Formed	ΔH_r, Heat of Reaction with Oxygen[b] (cal/g)	ΔH_r, Heat of Reaction with Water[b] (cal/g)	Hydrogen Produced in Reaction with Water[b] [liters (STP)/g]
Zr	Liquid	1852[c]	ZrO_2	-2,883	-1560	0.491
U	Liquid	1133[c]	UO_2	-1,098	-596	0.188
Al	Liquid	660[c]	Al_2O_3	-7,487	-4200	1.246
SS[d]	Liquid	1370[c]	FeO, Cr_2O_3, NiO	-1330 to 1430[e]	-144 to 253[e]	0.441
Mg	Liquid	651[c]	MgO	-6,000	-3570	0.922
Pu	Liquid	640[c]	PuO_2	-1,025	-531	0.187
Na	Solid	25	Na_2O	-2,162		
	Solid	25	NaOH		-1466	0.487
K	Solid	25	KO_2	-1,729		
	Solid	25	KOH		-857	0.287
Li	Solid	25	Li_2O	-10,260		
	Solid	25	LiOH		-7017	1.615
C	Solid	1000	CO (g)	-2,267	+2700	1.868
	Solid	1000	CO_2 (g)	-7,867	+2067	3.736
H_2	Solid	1000	H_2O (g)	-29,560		

[a]Data taken from J. P. Coughlin, Bulletin 542, U.S. Bureau of Mines, 1954, and from Reactor Handbook, Vol. I, Interscience Publishers, N.Y., 1960.

[b]Values are based on 1 g of reactant.

[c]Melting point of metal.

[d]Stainless steel.

[e]Value depends upon whether FeO (mp, 1377°C) is formed as a solid or as a molten oxide; higher value is preferred because it is likely that the oxides are a complex mixture of solids.

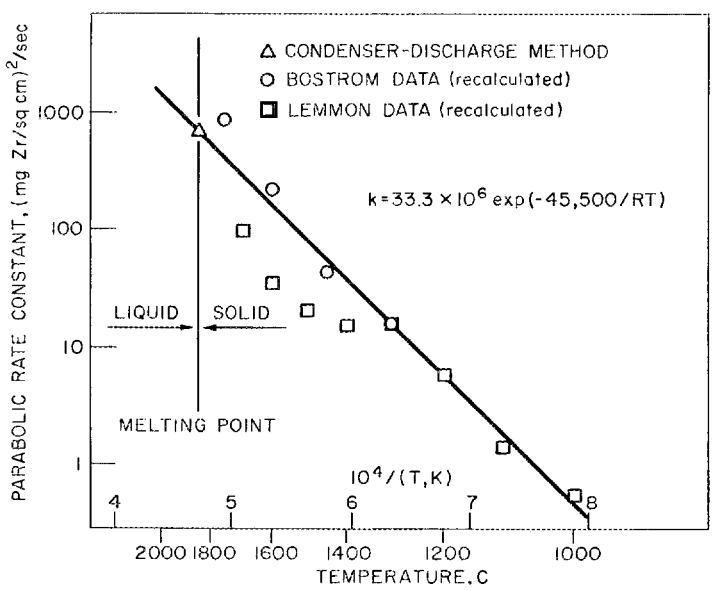

Fig. 5.3. Effect of Temperature on the Zirconium-Water Reaction.

correlation. Isothermal data[7] between 800 and 1200°C are in reasonable agreement with the correlation of Eq. 5.8. In addition, studies indicated that there was no important effect of steam pressure between 200 and 1000 psig.

Studies of the reaction of zirconium and Zircaloy-2 were carried out by using induction heating of specimens in the presence of up to 30,000 ppm of water vapor in an atmosphere of flowing helium.[2] The results of the experiments were explained on the premise that the reaction rate was controlled by the transport of the water vapor through the helium. Good agreement was obtained between experimental results and calculations employing mass transfer considerations. In these studies, the reactive metal surface was continuously exposed because of the rapid diffusion of oxygen into the metal.

Nonisothermal Experiments. Results of melting zirconium rod and dropping 2- to 10-g batches into water are summarized briefly in Table 5.6. The data indicate that the reaction is suppressed by the presence of inert gas and increased by the presence of pressurized steam.[20]

In another study, 25-mm-diam streams of molten zirconium were poured into water. Only a thin oxide coating was formed on the resulting metal globules.[21]

When molten globules of Zircaloy were dropped into water, the thickness of the oxide layer, measured as a function of water temperature, varied between 24 and 68 μ (corresponding to 2.7 and 5.8% reaction).[18]

Table 5.6. Results of Zirconium-Water Reaction Studies[a,b]

Water Vapor Pressure (psia)	Argon Pressure (psia)	Quantity of Reaction (ml of H_2/g of Zr)	Percent Reaction[c]
0.5[d]	200-1000	6.7-7.8	1.3-1.6
0.5[d]	15	8.2-12.6	1.7-2.6
1.5[d]	0	28-29	5.7-5.9
40-280	0	110-130	22-26
750	0	280	57

[a]From Milich and King, ref. 20, pp. 9, 11.

[b]From 2 to 10 g of molten zirconium at 1852°C was dropped into 130 ml of water in a 1400-ml chamber.

[c]Complete reaction corresponds to 491.2 ml of H_2 per gram of Zr.

[d]Room-temperature water at a vapor pressure of 25 mm Hg.

The cooling time for the zirconium globules increased markedly with increasing water temperature over the range 33 to 93°C.

Experiments with Dispersed Metal. One of the first demonstrations that finely divided zirconium would react extensively with water was provided by using condenser discharge heating to melt 2-mil foil strips of zirconium under water.[22] The extent of reaction was determined by collecting the hydrogen liberated by the reaction in the absence of air; it ranged between 20 and 100% in five tests with zirconium.

In experiments in which blasting caps were used to disperse molten zirconium streams under water,[21,23] the metal was largely converted into spherical particles that reacted violently. Zirconium, Zircaloy-2, and Zircaloy-B were tested. It was determined that the percent reaction was a sensitive function of particle size. The reaction could be approximated by assuming that all particles were coated with oxide to a thickness of 1 mil.

In another study, 10 to 20 g of molten zirconium was sprayed under pressure into water in an explosion dynamometer.[7] Spherical particles were formed as in the tests described above, and the extent of reaction was determined as a function of particle size by measurement of the oxide layer thickness. Mean particle diameters ranged between 10 and 18 mils, and the extent of reaction varied from 27 to 33%. Transient pressures generated within the water column were used to calculate the work, the total impulse, and the mechanical efficiency of the explosion. The explosions appeared to be uniformly violent over the range of metal temperatures from 1900 to 2575°C. The violence of the zirconium-water reaction is compared with the violence of other metal-water reactions and with a black powder explosion in Fig. 5.4 (ref. 7).

The zirconium-water reaction was recently studied extensively by the condenser discharge method.[3,5] In this study, specimen wires were heated

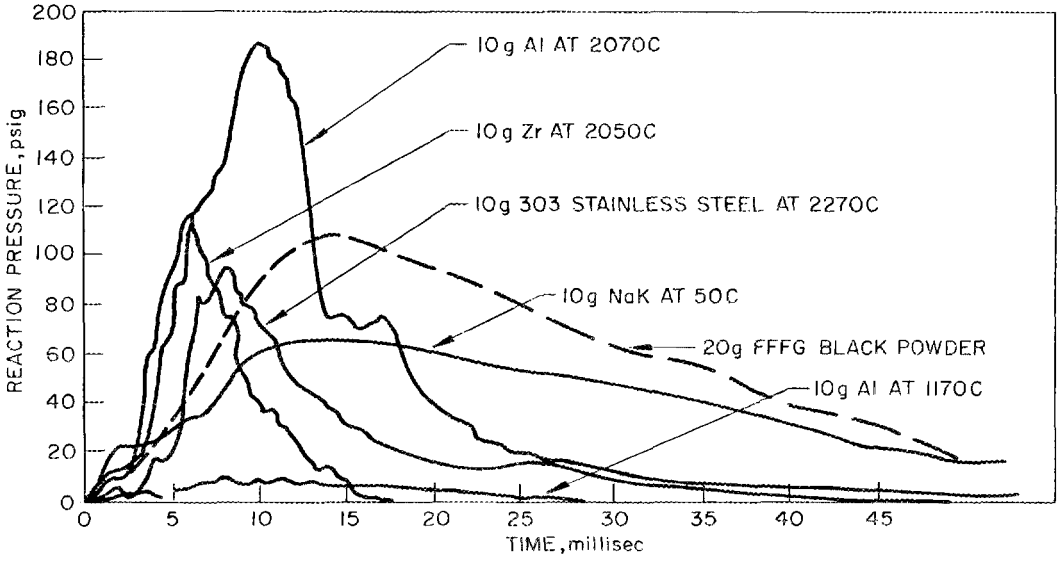

Fig. 5.4. Results of Metal-Water Reaction Tests in an Explosion Dynamometer.

almost instantaneously to temperatures between 1100 and 4000°C in water. Spherical particles were produced at temperatures above the melting point. Because the average particle size decreased continuously as the metal temperature was increased, it was impossible to separate experimentally the effects of metal temperature and particle diameter. The extent of metal-water reaction, determined by measurements of the quantity of hydrogen produced, was measured in water at temperatures from room temperature (water vapor pressure of 0.5 psi) to 315°C (water vapor pressure of 1500 psi).

The experimental results,[3] summarized in Fig. 5.5, show that more extensive reaction occurred in heated water than in water at room temperature. The extent of reaction did not increase continuously with water temperature (or vapor pressure), inasmuch as results obtained in water at 100°C (15 psi) were nominally identical with those obtained in water at 315°C (1500 psi). The extent of reaction is plotted as a function of particle size in Figs. 5.6 and 5.7 without regard to initial metal temperature.[3] Although the scatter is greater, the results indicate that the reaction may be largely independent of temperature as long as the metal is fully melted. Rates of reaction, judged from transient pressure traces, were explosive (substantial reaction in a few milliseconds) in the more energetic runs indicated in the figure and much slower (tenths of a second) in less energetic runs. Explosive reactions were found to occur with particles smaller than about 1 mm in heated water (see Fig. 5.7) and 0.5 mm in water at room temperature (see Fig. 5.6). Explosive reactions appeared to be associated with rapid particle motion.

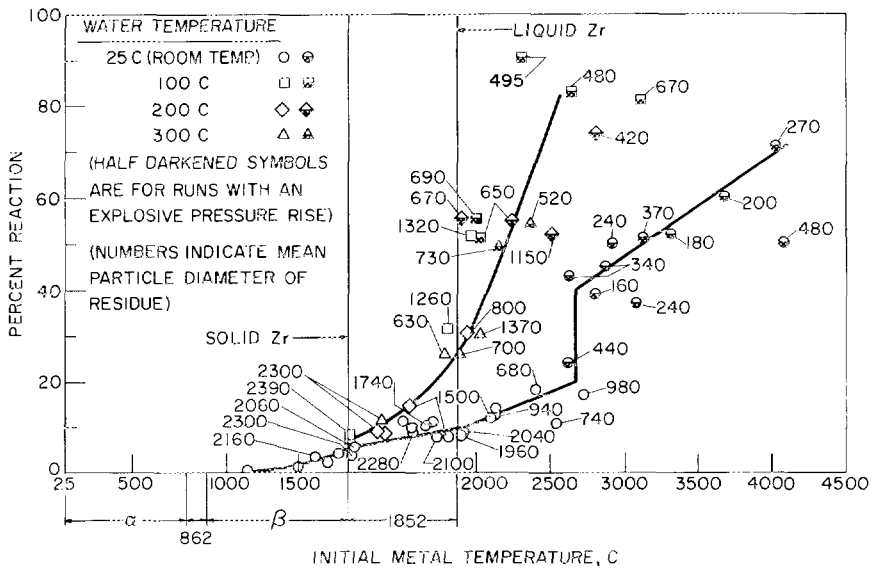

Fig. 5.5. Results of Zirconium-Water Reactions in Condenser Discharge Tests of 60-Mil Wires. The particle diameters of the residue are given in microns.

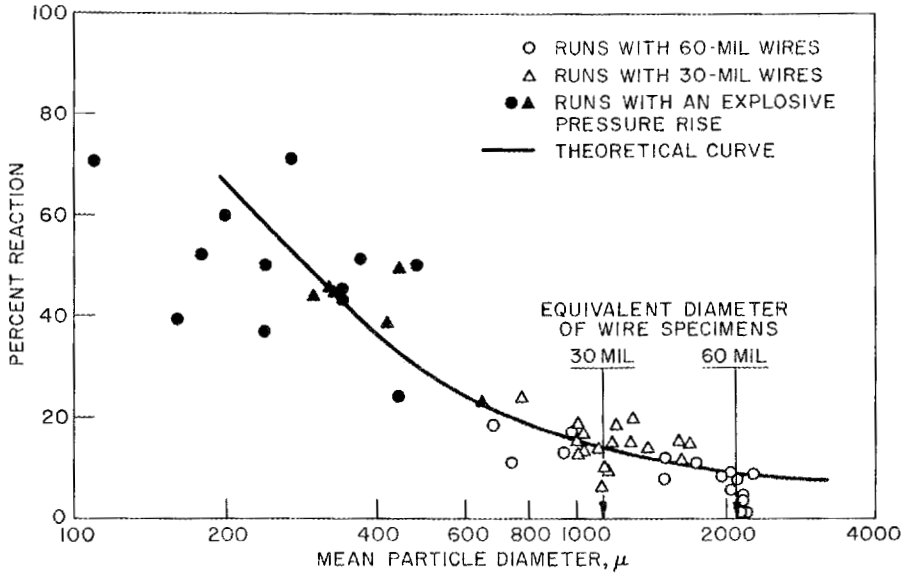

Fig. 5.6. Zirconium-Water Reactions as a Function of Particle Diameter of Residue. Tests run in room-temperature water.

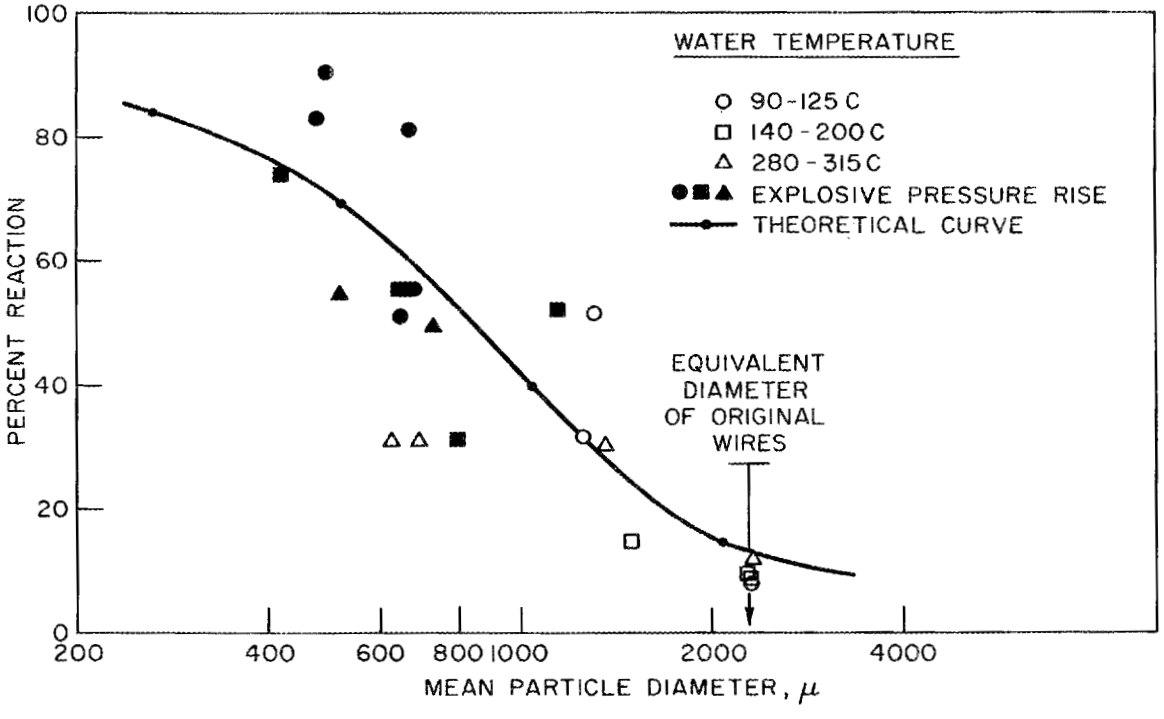

Fig. 5.7. Zirconium-Water Reactions as a Function of Water Temperature and Particle Diameter of Residue. Original wires 60 mils in diameter.

In-Pile Meltdown Tests. Studies were performed in TREAT with zirconium-uranium alloy fuel plates[24] and with Zircaloy-2-clad mixed-oxide-core fuel pins.[25] The results are summarized in Table 5.7. Calculated adiabatic core temperatures are given for the clad oxide-core specimens. It is believed that the oxide core temperatures approach the adiabatic values at temperatures below the oxide melting point because of the poor thermal conductivity of the oxide. Adiabatic temperatures are not given for metallic-core fuel specimens. The rapid rate of heat loss from metallic specimens to water prevents metallic cores from approaching adiabatic temperatures on the transient periods available in TREAT.

The zirconium-uranium alloy plates simply melted down into the alumina retaining crucible in four of the five experiments. From 6.0 to 11.5% of the metal reacted with water in these experiments. In the most vigorous experiment of the series, the metal was extensively spattered throughout the autoclave. Hydrogen analysis indicated that 67.2% of the metal reacted, and it is likely that the metal temperature reached well above 3000°C in this experiment. The results[24] are plotted in Fig. 5.8.

Table 5.7. Results of Studies of Zirconium in Submerged Fuel Specimen Meltdown Tests in TREAT

Initial water temperature: 25°C
Initial helium overpressure: 20 psia

Fission Energy Input (cal/g)	Adiabatic Core Temperature (°C)	CEN Run Number	TREAT Characteristics		Appearance of Specimen After Transient	Mean Particle Diameter (mils)	Percent of Metal Reacted
			Period (msec)	Integrated Power (Mw-sec)			
			Unclad Zirconium-Uranium Alloy Fuel Plates[a,b]				
285		100	80	208	Melted, one globule	460[c]	6.0
344		87	83	251	Melted, one globule	460[c]	5.2
510		88	79	372	Melted, one globule	460[c]	9.5
628		89	79	458	Melted, one globule	460[c]	11.5
785		101	52	573	Spattered		67.2
			Zircaloy-2-Clad Mixed-Oxide-Core Fuel Pins[d,e]				
254	1600	56	105	270	Cladding intact; core cracked	375[c]	0.3
301	1900	28	60	320	Cladding partly fragmented; core cracked and fragmented	110	4.2
362	2300	29	63	385	Cladding partly fragmented; core cracked and fragmented	107	8.0
516	2800	30	62	550	Cladding partly fragmented; core fragmented	51	14.0
609	3700	49	50	648	Cladding partly fragmented; core fragmented	49	24.0

[a] From Ivins, Testa, and Krause, ref. 24.

[b] Plates consisted of 89.4 wt % Zr and 10.6 wt % U (93% enriched); dimensions were 1.0 × 0.5 × 0.1 in.

[c] Estimated values.

[d] Liimatainen et al., ref. 25.

[e] Cladding 20 mils thick; ends capped; core 81.5 wt % ZrO_2, 9.06 wt % CaO, 0.74 wt % Al_2O_3, 8.69 wt % U_3O_8 (93% enriched); specimens were 0.33 in. in diameter and 0.53 in. long.

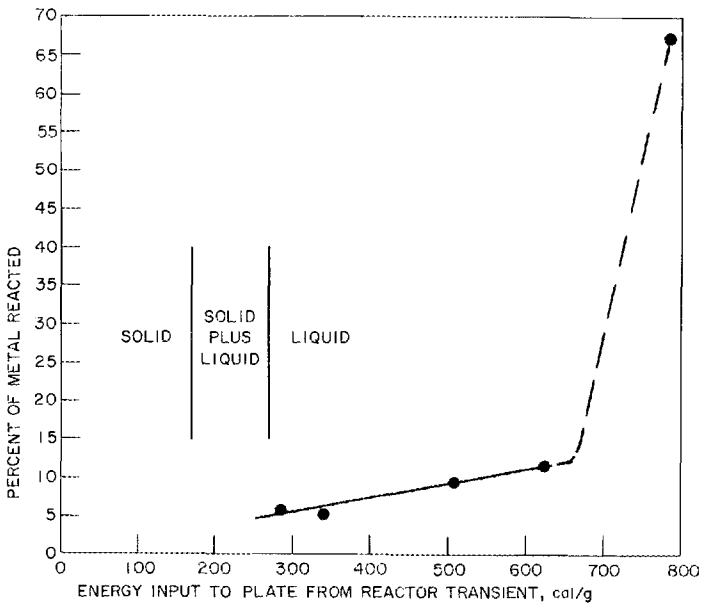

Fig. 5.8. Results of In-Pile Meltdown Tests of Zirconium-Uranium Alloy Fuel Plates. Plates consisted of 89.35 wt % Zr and 10.65 wt % U (93% enriched); their dimensions were 1.0 × 0.5 × 0.1 in.

Experiments conducted with Zircaloy-2-clad mixed-oxide-core fuel pins indicated that there was a linear relationship between the extent of metal-water reaction and the nuclear energy input over the range 250 to 600 cal/g of oxide core. The threshold for destruction was about 275 cal/g, which corresponded to an adiabatic core temperature of 1800°C. The extent of metal-water reaction as indicated by these in-pile tests, is plotted as a function of adiabatic core temperature in Fig. 5.9, where the apparent threshold for significant metal-water reaction is 1600°C.

Discussion. The experimental results overwhelmingly indicate that the quantity and rate of reaction is primarily determined by the size of the reacting particles. Only thin oxide films were formed on larger specimens, while explosions, self-sustained burning, or very extensive reaction occurred when finely divided metal was used.

Theoretical studies[3] of the reaction of heated zirconium particles with water were discussed in Section 5.2.1.2, and computed temperature vs time and extent of reaction vs time curves were given in Figs. 5.1 and 5.2. Computed results for the extent of reaction were in good agreement with experimental results obtained by the condenser discharge method, as shown in Figs. 5.10 and 5.11. The computed rates of reaction indicated in Figs. 5.1 and 5.2 agreed with measured rates only for larger particles. Particles smaller than about 1 mm in heated water and 0.5 mm in room-temperature water appeared to react in a few milliseconds. This was attributed to rapid propulsion of the particles through the water and the resulting increased rates of gas-phase diffusion.

The nature of the computed results shown in Figs. 5.10 and 5.11 indicates that the extent of reaction is nearly independent of the initial

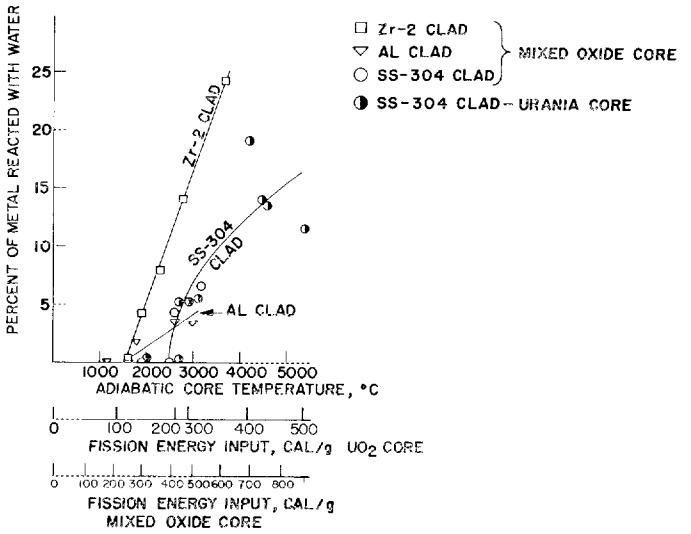

Fig. 5.9. Results of TREAT Meltdown Tests of Clad Ceramic Core Fuel Pins.

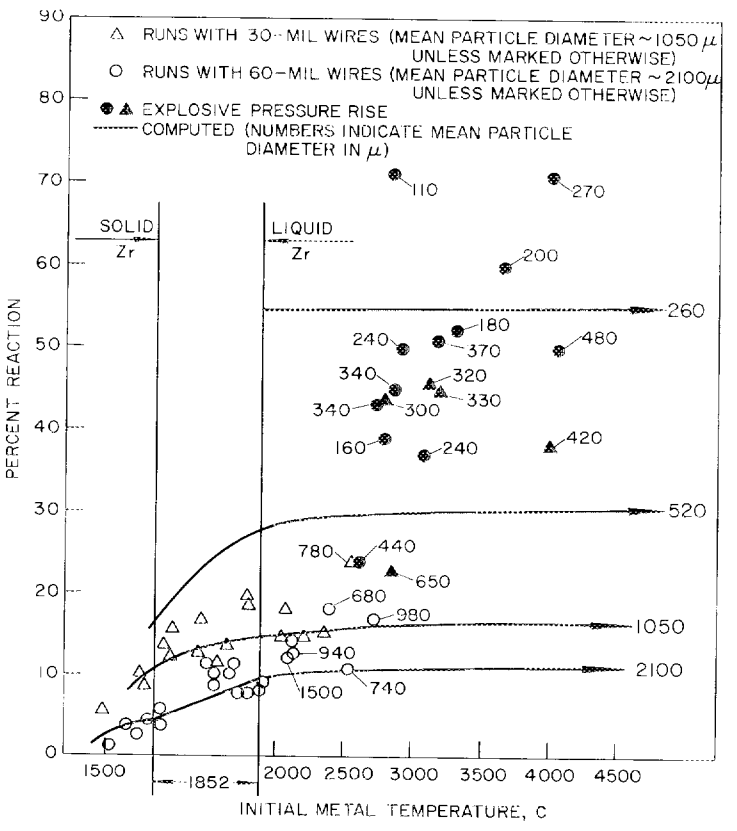

Fig. 5.10. Comparison of Computed and Experimental Results of Zirconium Reactions in Room-Temperature Water.

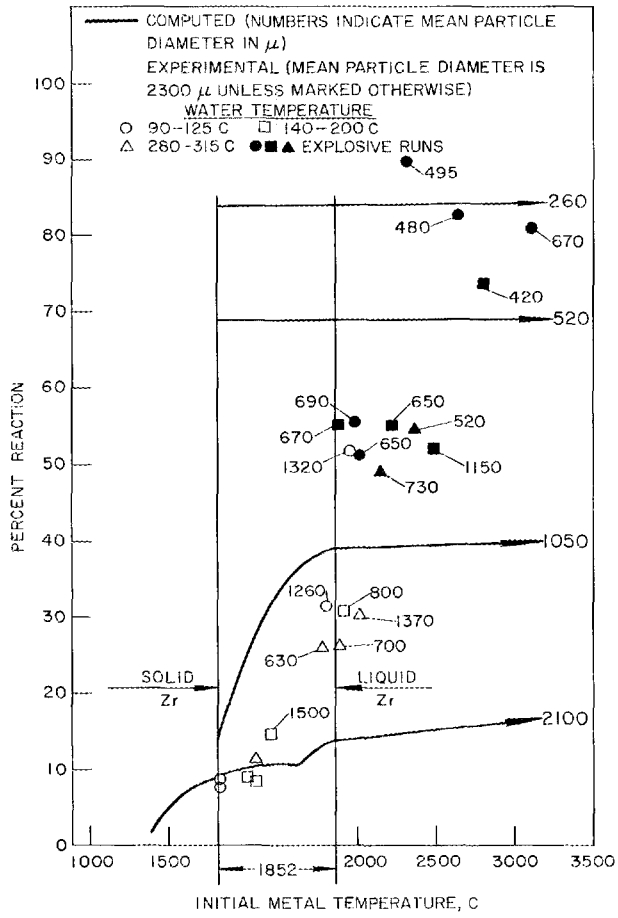

Fig. 5.11. Comparison of Computed and Experimental Results of Zirconium Reactions in Heated Water.

metal temperature as long as the particles are fully melted. The extent of reaction of molten zirconium droplets suddenly exposed to water can therefore be expressed as a function of droplet diameter, as shown in Fig. 5.12. The results for room-temperature (subcooled) water are nearly equivalent to the reaction of a uniform layer of zirconium 25 μ in depth, while the results for heated water can be represented roughly by the reaction of a layer 60 μ in depth. The computed results are therefore consistent with the Aerojet explosion dynamometer results and those obtained in the Battelle falling-drop studies.

The sharp jump in the extent of reaction occurred in condenser discharge experiments in room-temperature water (see Fig. 5.5) at an initial metal temperature of 2600°C. A similar jump occurred in the in-pile tests of zirconium-uranium alloy plates (see Fig. 5.8). These increases were caused in both cases by a sudden increase in the tendency of larger particles to fragment. This probably occurred because of the formation of molten oxide (ZrO_2; mp, 2700°C).

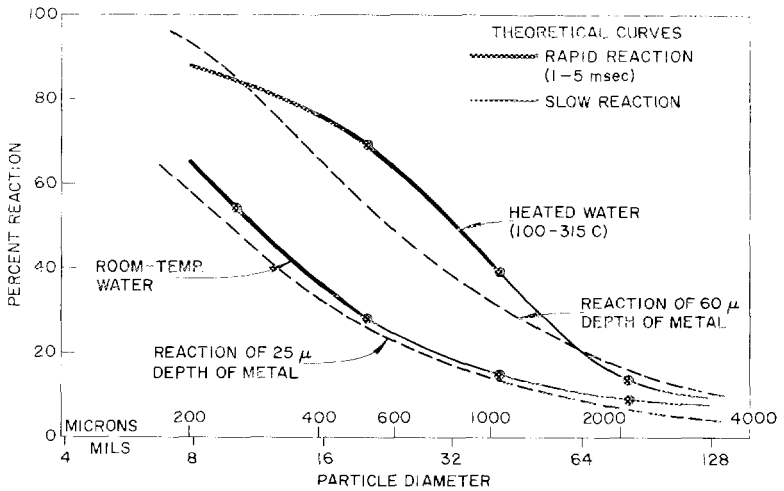

Fig. 5.12. Extent of Reaction as a Function of Particle Diameter for Molten Zirconium Spheres Formed in Water.

The in-pile results for the Zircaloy-clad oxide-core specimens could be explained in terms of the particle sizes generated by the transient heating and the extent of reaction expected for each particle size. The data are summarized in Tables 5.8, 5.9, and 5.10 and show that reasonable agreement between the calculated and experimental extent of reaction was achieved.

Table 5.8. Reactor Characteristics During In-Pile Metal-Water Reaction Experiments in TREAT[a]

	CEN Transient Experiment Number			
	28	29	30	49
Burst, Mw-sec	320	385	550	648
Period, msec	60	63	62	50
Energy, cal/g of oxide core	301	362	517	610

[a]From Baker and Just, ref. 3, p. 60, Table 10.

2. Uranium Alloys

Isothermal Experiments. It was concluded from an early study of the uranium-steam reaction at 1000°C that the reaction with massive pieces is relatively slow, requiring hours rather than seconds.[26] The oxide film formed at the rate of 11 mils/hr in a 15-min test.

Table 5.9. Particle Size and Reaction Data from In-Pile Metal-Water Reaction Experiments in Room-Temperature Water in TREAT[a]

Core material: 81.5 wt % ZrO_2, 9.1 wt % CaO, 8.7 wt % U_3O_8, 0.7 wt % Al_2O_3
Cladding material: Zircaloy-2, 20 mils thick
Overall fuel pin diameter: 0.38 in.
Overall fuel pin length: 1.05 in.

Particle Size Group (mils)	Theoretical Percent Reaction for Each Size Group[b]	Particle-Size Distribution[c] (wt %)			
		CEN Transient Experiment Number			
		28	29	30	49
1-4	70	0.0005	0.0002	0.1	0.03
4-8	60	0.01	0.024	1.3	0.2
8-16	46	0.2	0.10	6.5	2.8
16-32	28	2.1	3.0	2.0	15.2
32-64	14	11.2	9.7	12.8	25.2
64-128	9	22.3	27.8	77.3	57.6
128-256	6	64.3	59.4	0	0
256-512		0	0	0	0

[a]From Baker and Just, ref. 3, p. 60, Table 10.

[b]Data taken from Fig. 5.12.

[c]Particle-size distribution for total sample (metal and oxide).

Table 5.10. Calculated and Experimental Percentages of Metal-Water Reaction in TREAT Experiments in Room-Temperature Water[a]

	Metal Reacted with Water (%)			
	CEN Transient Experiment Number			
	28	29	30	49
Calculated	8.1	8.3	13.1	14.4
Experimental	4.1	8.0	14.0	24.0

[a]From Baker and Just, ref. 3, p. 60, Table 10.

With plate and rod specimens heated to between 160 and 1400°C in flowing steam at 1.0 atm, the reaction rate, followed gravimetrically, was found to be linear in time up to 880°C, with maximum rates at approximately 300 and 750°C.[27] Above 880°C, a parabolic rate law applied for the first 60 to 120 min, after which the reaction became linear. X-ray diffraction studies indicated that UO_2 was formed over the entire temperature range. The maximum of the reaction rate at 300°C was explained by considering the variation of the rate of uranium hydride formation with temperature.

In another study of uranium oxidation,[28] uranium cubes, supported on a thermocouple, were heated inductively in flowing steam. The reaction was followed by condensing the effluent steam and determining volumetrically the quantity of hydrogen generated. The results are summarized in Figs. 5.13 and 5.14. A rapid linear reaction occurred at 400°C, with a rate nearly identical to that reported in the gravimetric study. The reaction was nearly parabolic between 500 and 1200°C and followed a consistent rate law between 600 and 1200°C, as indicated in Fig. 5.14. The rate law was as follows:

$$w^2 = 9.16 \times 10^4 t \exp(-18{,}600/RT) , \qquad (5.9)$$

where w is milligrams of uranium reacted per square centimeter and t is

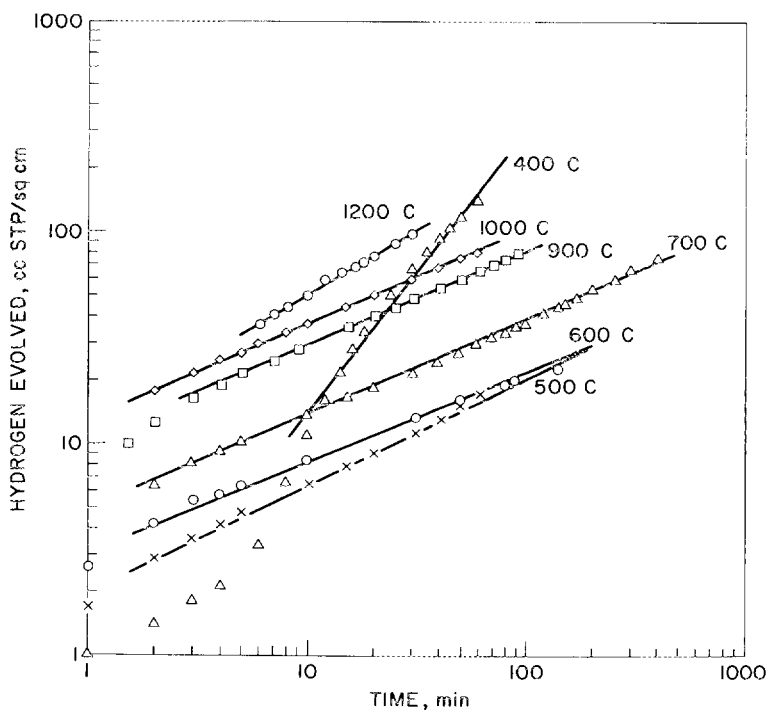

Fig. 5.13. Hydrogen Evolution in the Reaction of Steam at 1 atm with Uranium.

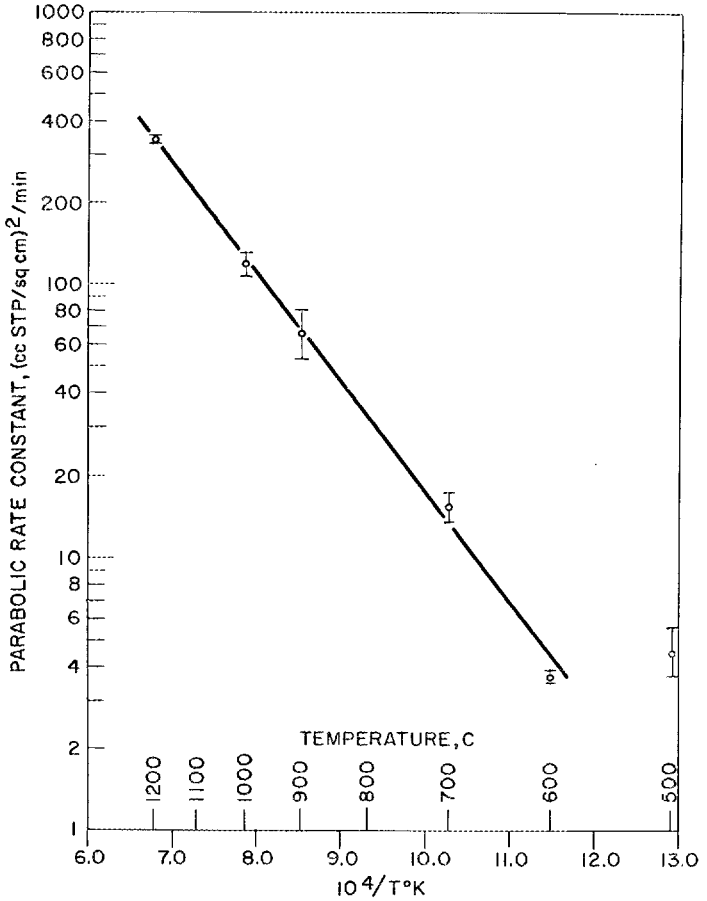

Fig. 5.14. Effect of Temperature on the Rate of Hydrogen Evolution for the Reaction of Steam with Uranium.

time in seconds. The results of the two studies[27,28] do not agree above 500°C. The wide divergence in the data was probably due to differences in impurity content or metallurgical treatment of the specimens. Ignition and oxidation studies in oxygen show clearly how alloying additions can markedly alter the uranium-oxygen reaction, especially in the temperature range above 500°C.

Nonisothermal Experiments. Natural uranium at 1540°C was poured into cold water in a series of tests.[23] Popping was heard as the evolving hydrogen ignited and burned in air; however, no explosion resulted. Thin plates of metal were found which had about 0.5 mil of oxide coating. It was estimated that from 10 to 30% reaction occurred. Similar tests with a 12% molybdenum alloy gave identical results.

Experiments with Dispersed Metal. Uranium at 1540°C poured into water and dispersed by a blasting cap[23] was partly atomized, but the bulk of the metal remained as comparatively large, irregular platelets, which were covered with surface oxidation. The percentage of reaction varied from 30 to 50. There were indications of slight explosions in four out

of five tests. Results obtained with a 12% molybdenum alloy were essentially the same, as were the results with a 5.5% zirconium-1.75% niobium ternary alloy. A single run in an explosion dynamometer indicated that uranium was not usually explosive.

Condenser discharge results obtained with uranium wires are given in Fig. 5.15. As with zirconium, considerably more reaction occurs in heated water than in room-temperature water. Runs were made only in water at 25 and 100°C because the extensive slow corrosion that occurs in water at 200°C or higher would have destroyed the specimen before the run could be completed. Transient pressure traces were similar to those obtained with zirconium. The smaller particles reacted explosively and larger particles reacted slowly. The results were consistent with the finding for zirconium that particles smaller than about 20 mils in room-temperature water and 40 mils in heated water were in violent motion and therefore reacted very rapidly because of an increased rate of gas-phase diffusion. Several factors complicated the experiments so that it was not possible to ascertain conditions for the explosive behavior of uranium with the certainty that was possible for zirconium. Larger particles (greater than about 1 mm) were not spherical, as they were with zirconium, and the oxide was not as adherent. This behavior was also reported in the Aerojet explosion studies.[7]

In-Pile Meltdown Tests. Meltdown tests in TREAT were performed[25] with pure uranium wires and rods and with the relatively corrosion-resistant uranium, 5 wt % zirconium, 1.5 wt % niobium ternary alloy. (This alloy was used in the first core loading of the EBWR.) Studies with the alloy were performed with bare pins and with Zircaloy-2 clad pins. The results, given in Table 5.11, indicate that three factors are important in governing the extent of metal-water reaction. These are the total fission energy input (see Fig. 5.16), the reactor period (see Fig. 5.17),

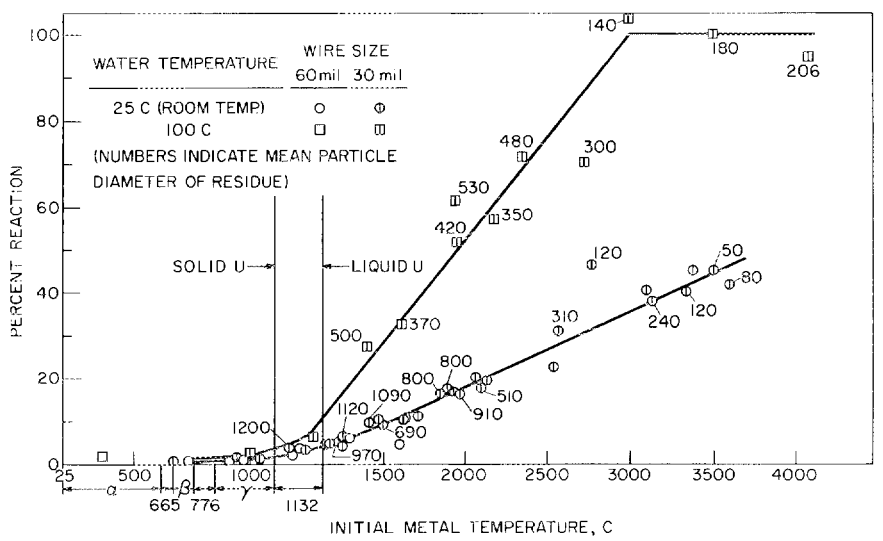

Fig. 5.15. Uranium-Water Reaction by the Condenser Discharge Method. The particle diameters of the residue are given in microns.

Table 5.11. Results of Studies of Uranium in Submerged Fuel Specimen Meltdown Tests in TREAT

Initial water temperature: 25°C
Initial helium overpressure: 20 psia

Fission Energy Input (cal/g)	CEN Run Number	TREAT Characteristics		Appearance of Specimen After Transient	Mean Particle Diameter (mils)	Percent of Metal Reacted
		Period (msec)	Integrated Power (Mw-sec)			
				Zircaloy-2-Clad Uranium-Zirconium-Niobium Alloy Fuel Pins[a,b]		
59	14	102	56	Cladding ruptured; core slightly melted	200[c]	0.9
63	15	102	60	Cladding ruptured; core partly melted	200[c]	1.7
65	13	104	62	Cladding ruptured and bulged; core partly melted	200[c]	2.0
85	10	112	81	Cladding partly melted; core melted and fragmented	200[c]	2.0
95	16	96	90	Cladding melted and fragmented; core melted and fragmented	148	9.1
136	18	104	130	Cladding melted and fragmented; core melted and fragmented	54	7.4
136	17	103	130	Cladding melted and fragmented; core melted and fragmented		7.3
179	11	100	170	Cladding melted and fragmented; core melted and fragmented	91	10.0
189	12	77	180	Cladding melted and fragmented; core melted and fragmented	140	8.6
				Unclad Uranium-Zirconium-Niobium Fuel Pins[a,d]		
37	68	100	35	Intact	844[c]	0.1
79	2	197	75	One-half melted; one globule	844[c]	1.8
84	6	100	80	Melted; one globule	844[c]	2.5
121	8	106	115	Melted; one globule	844[c]	3.2
				Unclad Pure Uranium Fuel Pins[a,e]		
50	5	125	48	Two-thirds melted; one globule	844[c]	0.2
54	3	197	52	Three-fourths melted; one globule	844[c]	1.1
				Uranium Wire[a,f]		
108	43	515	32	Intact	96[c]	0.4
146	44	304	43	Melted and fragmented	78	8.1
146	42	267	43	Melted and fragmented	32	7.5
149	45	205	44	Melted and fragmented	33	9.3
183	41	96	54	Melted and fragmented	17	17.2
305	57	152	90	Melted and fragmented	21	50.2
339	58	440	100	Melted and fragmented	23	33.2
				Zirconium Wire[a,g]		
379	35	96	47	Melted and fragmented	66	28.3
403	46	96	50	Melted and fragmented	28	12.9
410	70	1010	51	Intact	96[c]	0

[a]From Liimatainen et al., ref. 25.

[b]Pin clad with 20-mil-thick Zircaloy-2; ends capped; core 93.5 wt % U, 5 wt % Zr, 1.5 wt % Nb; U 20% enriched; dimensions were 0.2 in. in diameter and 0.5 in. long.

[c]Estimated values.

[d]Pin 93.5 wt % U, 5 wt % Zr, 1.5 wt % Nb; U 20% enriched; dimensions were 0.2 in. in diameter and 0.5 in. long.

[e]U 20% enriched; dimensions were 0.2 in. in diameter and 0.5 in. long.

[f]U 93% enriched; dimensions were 64 mils in diameter and 1.0 in. long.

[g]Dimensions were 34 mils in diameter and 1.0 in. long.

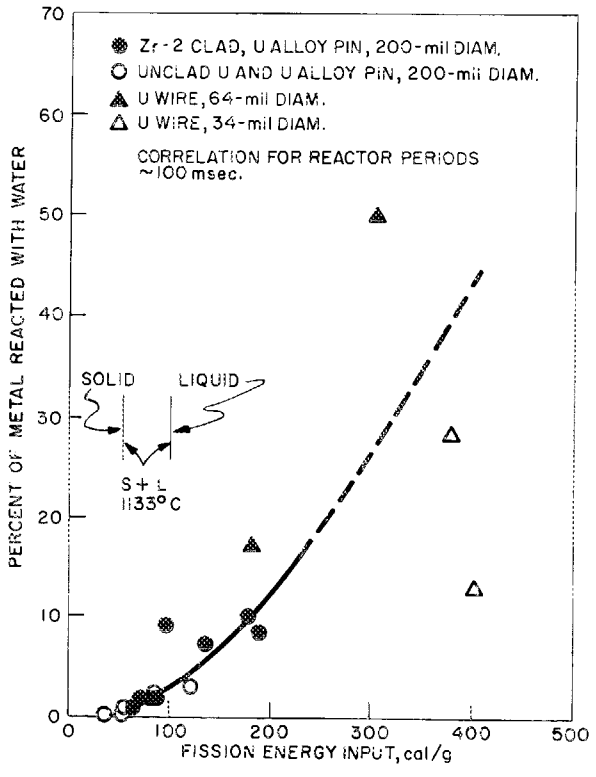

Fig. 5.16. Results of TREAT Meltdown Tests with Uranium Specimens.

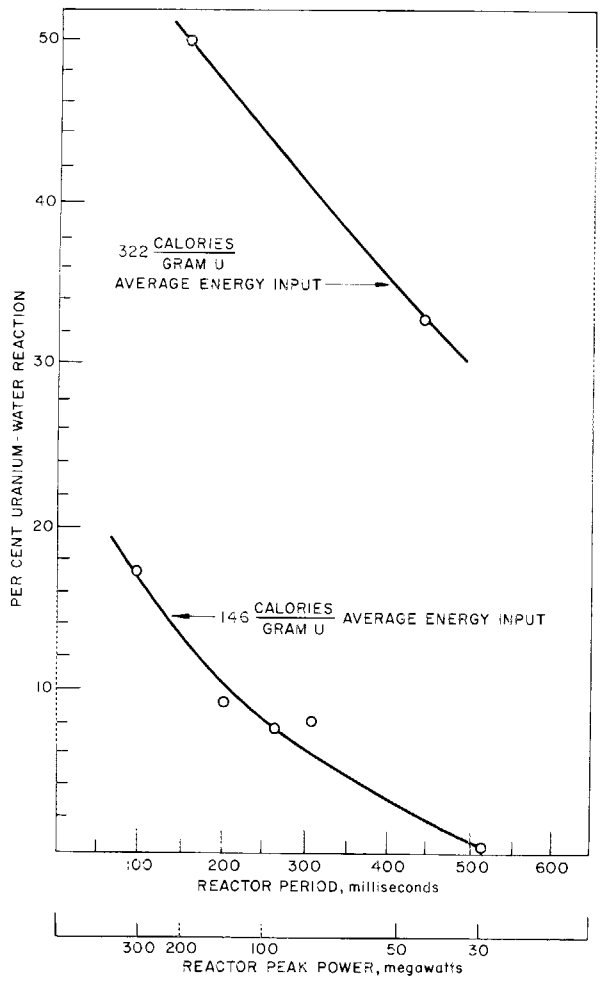

Fig. 5.17. In-Pile Metal-Water Reactions of 64-mil-diam Uranium (93% Enriched) Wires.

and the surface area of the uranium created by fragmentation (see Fig. 5.18).[25]

For a given energy input, more chemical reaction occurs as the period becomes shorter because there is less time for heat losses to occur. This increases the peak temperature reached by the metal. The behavior of uranaium, as a function of fission energy input, shown in Fig. 5.16, indicates that there are three thermal zones. At energies less than 50 cal/g the uranium remains in its original solid form with negligible chemical reaction. Above 50 cal/g, meltdown begins, and at 100 cal/g the metal has fully melted with about 3% uranium-water reaction. It is important to realize that these meltdown boundaries apply strictly to periods in the vicinity of 100 msec because of heat loss considerations. Increasing the energy progressively to 400 cal/g results in a continual increase in the amount of oxidation until about one-half the uranium has reacted with the water at a fission heat input of 400 cal/g. At this point the chemical nuclear energy ratio is about 0.75, which is appreciable. Records[25] of a typical uranium-water reaction experiment are shown in Fig. 5.19. The plot in Fig. 5.16, which expresses the extent of metal-water reaction

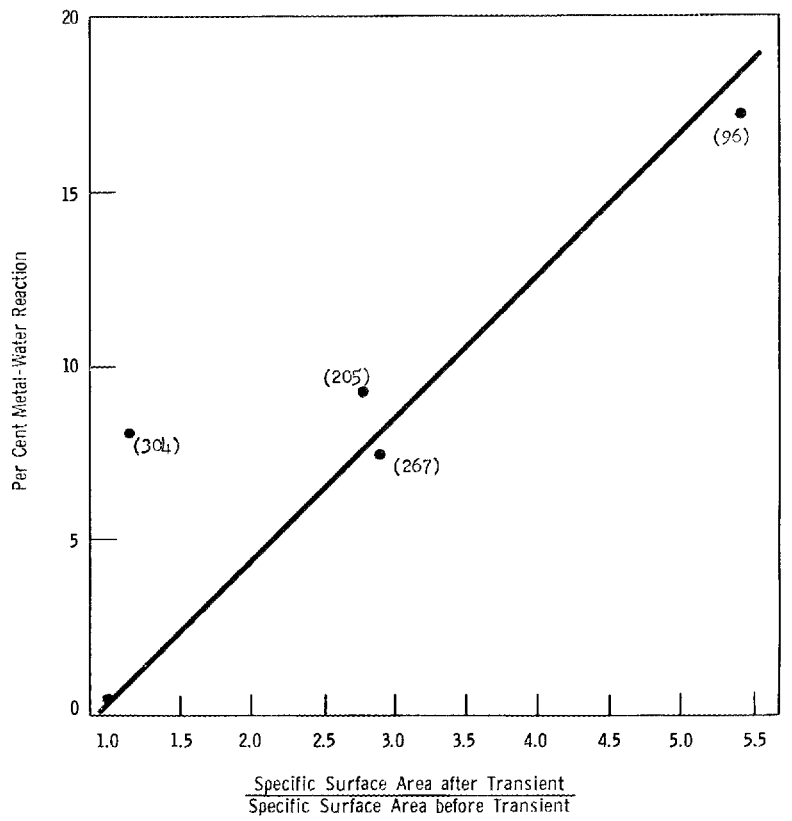

Fig. 5.18. Dependence of Extent of In-Pile Uranium-Water Reaction on Surface Area for 64-mil-diam Uranium Wires (93% Enriched). Correlation for 146 cal/g average energy input. Reactor period given in parentheses in milliseconds.

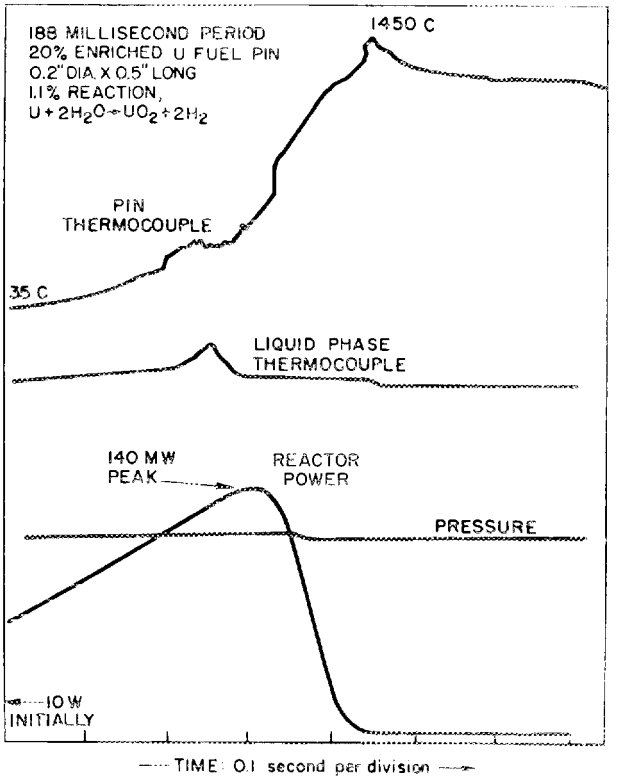

Fig. 5.19. Typical Oscillograph Record of In-Pile Meltdown Experiment with Uranium in Water.

as a function of fission energy input, shows results very similar to those obtained in condenser discharge studies of metal-water reactions in room-temperature water (see lower curve in Fig. 5.15), although the exact temperatures reached in the TREAT runs are not presently known.

Discussion. The uranium-water reaction has been studied much less thoroughly than the zirconium-water reaction. Isothermal studies above 1200°C are in progress. Preliminary studies indicate that it may not be possible to extrapolate the parabolic rate law, Eq. (5.9), to temperatures much above 1200°C, as would be required for an analysis of the type described in connection with zirconium.

It is reasonable, on theoretical grounds, to expect that the uranium-water reaction at high temperatures is somewhat less extensive than the zirconium-water reaction. The activation energy found for the zirconium reaction (45.5 kcal/mole) is considerably higher than that found for the uranium reaction, which is 18.6 kcal/mole for temperatures below 1200°C; above 1200°C a value of about 35 kcal/mole is tentatively indicated. It is therefore to be expected that greater reaction occurs with zirconium at very high temperatures. The activation energy difference also implies that uranium reacts more extensively at low temperatures, which is a well-known fact. The rate Eqs. (5.8) and (5.9) indicate that the two metals

will follow the same rate law at approximately 1460°C on the basis of hydrogen evolution. The heats of reaction are nearly identical on a molar or a volume basis but, of course, differ on a weight basis.

3. Aluminum Alloys

Isothermal Experiments. In a thermogravimetric study of the isothermal oxidation of molten aluminum in steam over the temperature range 816 to 1260°C, the reaction followed a linear rate law for pure aluminum and for a 23.4 wt % uranium-aluminum alloy. The rates reached a maximum at about 1000°C and decreased at higher temperatures.[29]

In a "pressure-pulse" study[30] of the isothermal oxidation of aluminum over the range 800 to 1200°C, the reaction followed a cubic rate law, as shown by the broken lines in Fig. 5.20. The results of the pressure-pulse and thermogravimetric studies do not agree in regard to the form of the rate law and especially in regard to the temperature dependence of the reaction rate. Both studies show, however, that at 1200°C and below the reaction is extremely slow and does not constitute a hazard.

A more recent study[6] of the aluminum-steam reaction was made using the levitation-melting method between 1200 and 1750°C. Pellets of aluminum (1/4 in.) were supported and heated by a radio-frequency field in the presence of flowing steam. Temperatures were measured and controlled by a two-color optical pyrometer. The quantity of aluminum reacting in each run was determined by a gravimetric method in which unreacted aluminum was selectively dissolved in an iodine-methanol solution, leaving the

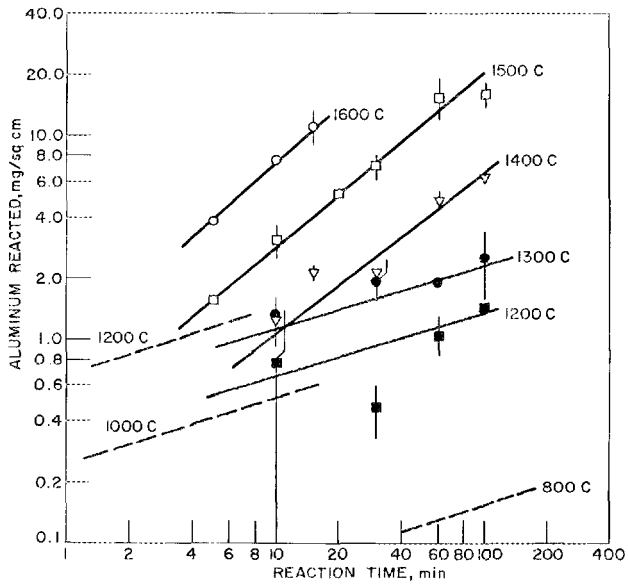

Fig. 5.20. The Reaction of Aluminum with Steam. Data points and solid lines obtained by the levitation melting method. Dashed lines obtained by the pressure-pulse method.

oxide intact. The reaction could be described by a cubic rate law at 1200 and 1300°C, as shown in Fig. 5.20. The results therefore agreed with those of the pressure-pulse study, although the measured rates differed by a factor of 2.

Studies by the levitation method between 1400 and 1600°C showed that a linear reaction occurred (see Fig. 5.20), which could be represented by the following rate law:

$$w = 3.0 \times 10^8 t \exp(-73{,}500/RT) , \qquad (5.10)$$

where w is in milligrams of aluminum reacted per square centimeter and t is time in seconds. Delayed ignitions occurred at 1600°C (18 min), at 1650°C (9 min), and at 1700°C (5 min), while immediate ignition occurred at 1750°C. Ignition began with the formation of a small hot spot, which rapidly spread across the surface of the sphere. The temperature at the hot spot reached well above 2100°C. Burning in steam appeared to be similar to the vapor-phase burning that occurred in air at 1750°C, although the voluminous white smoke was less apparent.[31]

Nonisothermal Experiments. A number of investigators have poured molten aluminum into water in an effort to evaluate the conditions needed for explosion. Injections of several pounds of molten aluminum in the form of jets at 750 to 1000°C into water gave little or no reaction; there was no appreciable steam pressure buildup noted.[32,33] Tests in which large crucibles containing molten aluminum at 900°C were smashed under water showed that pure aluminum did not react, but aluminum containing 1.0 to 7.4% lithium reacted slightly to violently. Aluminum containing 5% uranium reacted violently at 900°C in three tests and slightly in 11 tests.[21] Higher temperatures did not increase the activity. Other tests in which molten aluminum and aluminum-lithium alloys were poured into water in 1-in.-diam streams gave no violent reactions, although a thin oxide coating formed on the resulting globules in both cases.[21]

The most extensive tests of the effects of contacting large quantities of molten aluminum with water were carried out by taking 50 lb of commercially pure molten aluminum and suddenly discharging the metal into water in steel tanks. Violent explosions occurred in many cases,[34] even though the metal temperature was never higher than 900°C. Explosions occurred when the metal was discharged through holes larger than 2.75 in. but only when a certain minimum quantity of metal was used. Explosions occurred when the metal was dropped 18 in. but not when the metal was dropped 10 ft, which suggests that no explosion would occur if the stream were broken up. Breaking the stream with an iron grid prevented explosions, even with an 18-in. drop. Depth of water pool and metal temperature were interdependent. Explosions took place in a 3- or 6-in. water depth with aluminum at 670°C but required metal at 750°C with a 10-in. water depth. No explosions could be produced when the water level was 20 in. Molten metal spattering without a violent explosion took place when the water level was 2 in. or less. Wetting agents decreased the tendency toward explosion, while salt increased it. Coating the bottom of the water container with lime, gypsum, or rust promoted explosiveness, while grease, oil, or paint largely eliminated the explosions. Similar,

but less violent, explosions were produced using a molten salt mixture instead of aluminum. This finding made it almost certain that the explosions resulted primarily from steam formation and not from metal-water reaction.

Experiments with Dispersed Metal. Experiments in which blasting caps were used to disperse molten aluminum streams under water[21] showed formation of fine, metallic granules but no violent explosions. Tests in the explosion dynamometer,[7] however, showed that very violent reactions (see Fig. 5.4) could be generated when the initial metal temperature was 1400°C or higher.

Explosive reactions were initiated in moistened aluminum powder compacts by means of auxiliary explosive charges in one study.[35] Efforts to duplicate the results failed, however, to produce a violent explosion.[21]

In-Pile Meltdown Tests. Meltdown tests were performed in TREAT with aluminum-uranium alloy plates, both clad[36] and unclad,[37] unclad aluminum-U_3O_8 cermet pins,[38] and aluminum-clad mixed-oxide-core fuel pins.[25] The results are given in Table 5.12. The extent of metal-water reaction for the alloy plates and the cermet pins is plotted as a function of fission energy input in Figs. 5.21 and 5.22. The extent of reaction was slightly higher for the unclad plates (SL-1 meat) and the cermet pins than for the clad plates (SPERT-1D). The difference was probably due to the effect of cladding and geometry on the temperatures reached by the plates. The results indicate that significant metal-water reaction begins when the fission energy input reaches about 350 cal/g and increases gradually up to an energy input of 530 cal/g, where there is an apparent jump. A larger jump in metal-water reaction occurs in the vicinity of 750 cal/g.

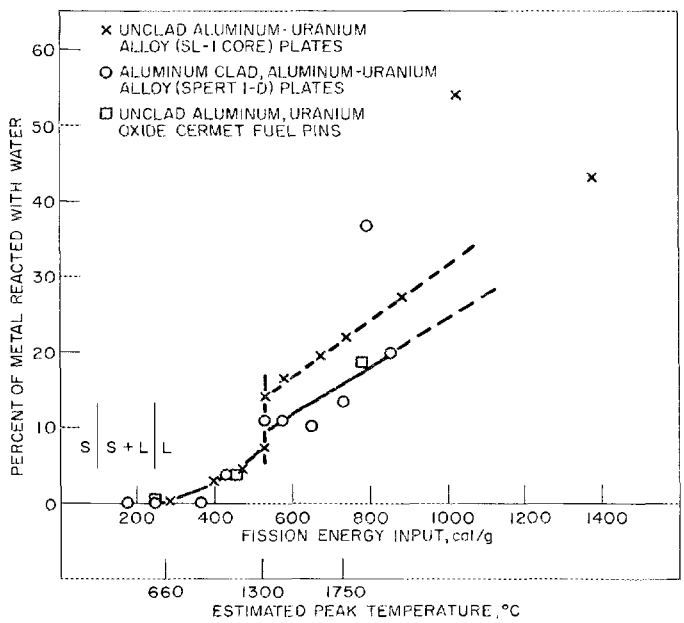

Fig. 5.21. Results of TREAT Meltdown Tests with Aluminum Alloy and Cermet Specimens.

Table 5.12. Results of Studies of Aluminum in Submerged Fuel Specimen Meltdown Tests in TREAT

Initial water temperature: 25°C
Initial helium overpressure: 20 psia

Fission Energy Input (cal/g)	Adiabatic Core Temperature (°C)	CEN Run Number	TREAT Characteristics: Period (msec)	TREAT Characteristics: Integrated Power (Mw-sec)	Appearance of Specimen After Transient	Mean Particle Diameter (mils)	Percent of Metal Reacted
			Unclad Aluminum-Uranium Alloy Plates (SL-1 Core)[a,b]				
288		114	112	174	Melted and bulged	460[c]	0.1
398		97	79	240	Melted; one globule	460[c]	2.8
473		121	79	285	Melted; one globule	460[c]	4.5
530		122	79	320	Melted; one globule	460[c]	7.2
530		123	79	320	Melted; one globule	460[c]	14.2
580		115	77	350	Melted and fragmented	110	16.4
672		116	62	405	Melted and fragmented	42	19.7
739		98	51	445	Melted and fragmented		22.2
880		137	54	530	Melted and fragmented	61	27.4
1023		99	50	616	Melted and fragmented		54.2
1378		138	41	830	Melted and fragmented	12	43.2
			Aluminum-Clad Aluminum-Uranium Alloy Plates (SPERT-1D)[d,e]				
174		109	104	169	Intact; slight melting	320[c]	0.1
245		110	96	238	Melted and bulged	320[c]	0.1
361		111	80	350	Melted; one globule	320[c]	0.3
430		112	50	417	Melted and fragmented	250[c]	3.9
527		117	52	512	Melted and fragmented	45	11.0
577		118	52	560	Melted and fragmented	24	11.0
652		113	53	633	Melted and fragmented		10.4
731		119	42	710	Melted and fragmented	22	13.6
794		120	42	770	Melted and fragmented	19	36.9
855		136	41	830	Melted and fragmented	83	20.0
			Unclad Aluminum-Uranium Oxide Cermet Fuel Pins[f,g]				
244		38	84	235	Melted; one globule	375[c]	0.7
458		37	65	440	Melted; one globule	375[c]	3.8
780		77	39	750	Melted; large fragments		19.0
			Aluminum-Clad Mixed-Oxide-Core Fuel Pins[h,i]				
159	1100	19	101	169	Cladding intact; core cracked	375[c]	0
244	1600	20	105	260	Cladding intact; core cracked	375[c]	0
272	1800	47	73	290	Cladding ruptured; core fragmented		1.7
454	2700	22	65	483	Cladding partly fragmented; core fragmented	68	3.5
508	3000	23	60	540	Cladding partly fragmented; core fragmented	26	3.6

[a] From Ivins, Testa, and Krause, ref. 37.

[b] Plate 81 wt % Al, 17 wt % U, 2 wt % Ni; dimensions were 0.2 × 0.5 × 0.5 in.

[c] Estimated values.

[d] From Ivins, Testa, and Krause, ref. 36.

[e] Plate clad with 6061 Al, 20 mils thick; core 24 wt % U (93% enriched); overall dimensions were 0.06 × 1.4 × 0.5 in.

[f] From Liimatainen, Ivins, and Testa, ref. 38.

[g] Pins 90 wt % Al, 10 wt % U_3O_8 (93% enriched); dimensions were 0.375 in. in diameter and 0.50 in. long.

[h] From Liimatainen et al., ref. 25

[i] Pins clad with 1100 Al, 20 mils thick; ends capped; core 81.5 wt % ZrO_2, 9.1 wt % CaO, 0.7 wt % Al_2O_3, 8.7 wt % U_3O_8 (93% enriched); dimensions were 0.33 in. in diameter and 0.51 in. long.

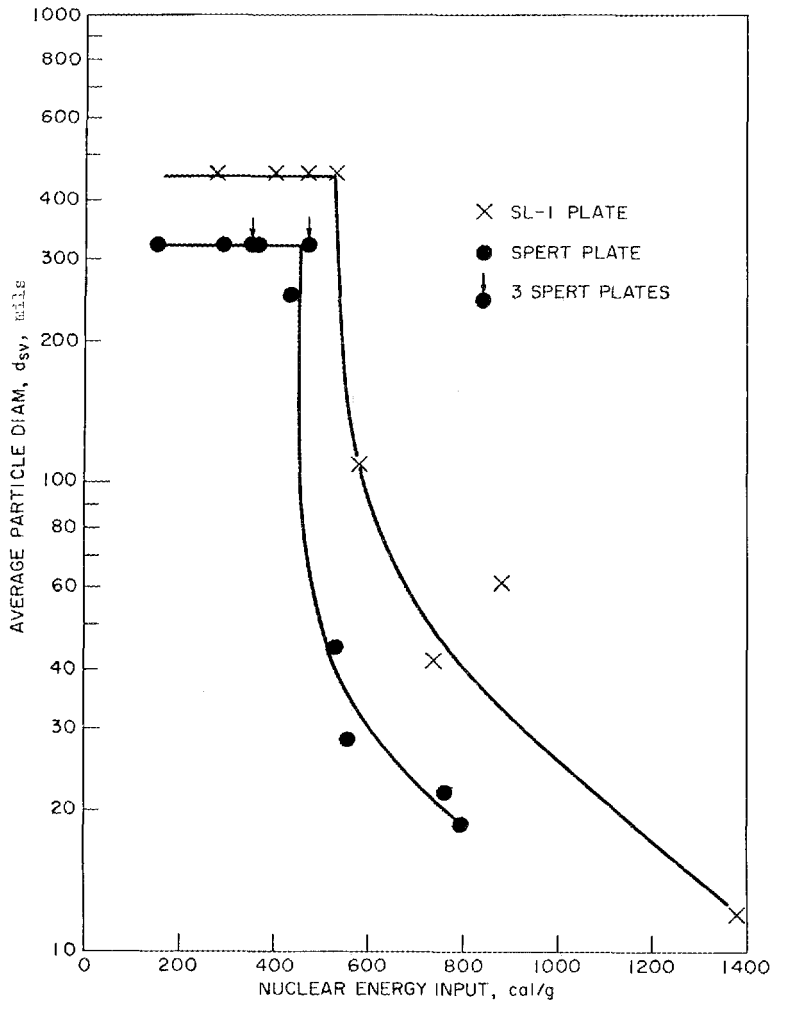

Fig. 5.22. Average Particle Size of Aluminum-Uranium Alloy Plates After Irradiation in TREAT Versus Nuclear Energy Input.

At these high energies it is likely that vapor-phase burning of aluminum is initiated. Laboratory experiments have indicated that aluminum ignition occurs at 1750°C. Photographs of the residue from experiments with clad fuel specimens (SPERT-1D),[36] shown in Figs. 5.23, 5.24, and 5.25, indicate increasing damage with increasing fission energy input. Macrographs of fragments from the clad alloy plates, shown in Figs. 5.24 and 5.25, show that increasing porosity is generated at increasing energies. Micrographs, also shown in these figures, indicate a characteristic slab-like structure at the intermediate energies and a fine-grained eutectic structure at energies in the high range (above 750 cal/g). A photomicrograph of unirradiated SPERT-1D fuel is shown in Fig. 5.26 for comparison; neither the slab-like nor the eutectic structure is evident.[36]

Results of experiments with aluminum-clad mixed-oxide-core specimens are included in Fig. 5.9; these experiments confirmed the conclusion reached

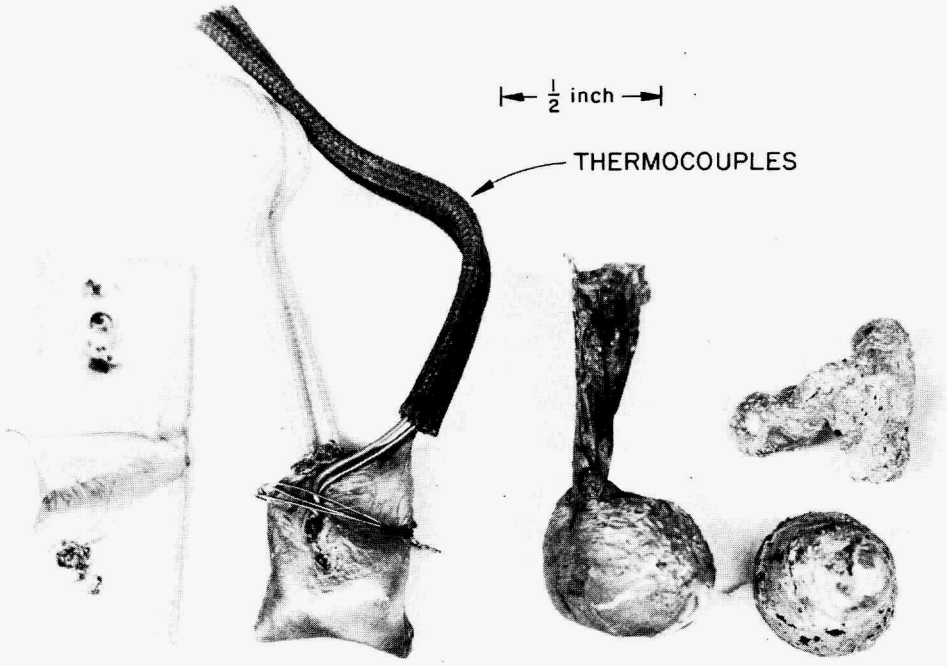

	CEN-109	CEN-110	CEN-111	CEN-112
energy:	174 cal/g	245 cal/g	361 cal/g	430 cal/g
period:	104 msec	96 msec	80 msec	50 msec
amount of metal reacted:	0.1 %	0.1 %	0.3 %	3.9 %

Fig. 5.23. Results of Meltdown Experiments in TREAT on SPERT Fuel Samples Submerged in Water.

in studies with the Zircaloy-clad mixed-oxide-core specimens that the threshold for destruction was about 275 cal/g. Considerably less metal-water reaction occurred in tests with aluminum-clad specimens than in the tests with the Zircaloy-clad specimens. It seems evident that the aluminum cladding did not reach a temperature (1750°C) where ignition and burning could occur, even though the oxide core received energies sufficient for melting the ceramic (mp, 2600°C).

Discussion. The results of experimental studies suggest strongly that the temperature reached by the aluminum metal primarily determines the nature of the reaction. Isothermal studies have shown that the oxide film is very protective up to 1300°C. This is fully consistent with the repeated failure of many investigators to obtain a vigorous metal-water reaction by pouring molten aluminum into water. Only in the explosion dynamometer tests was the metal temperature high enough to produce a significant reaction.

The explosions produced in the pouring tests were physical in nature and probably did not involve extensive metal-water reaction. The mechanism of these explosions is not fully established. The importance of physical explosions has been emphasized, with the suggestion that physical

Energy:	527 cal/g
Period:	52 msec
Amount of Metal Reacted:	11%

FRAGMENTED PLATE AFTER TRANSIENT

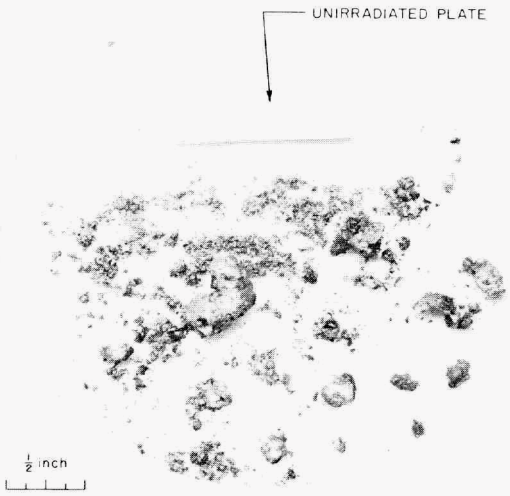

MACROGRAPH OF FRAGMENT

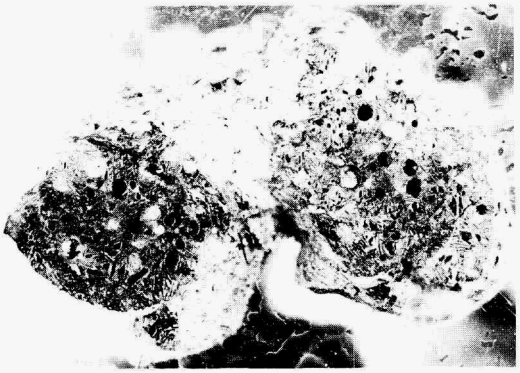

5X

PARTICLE SIZE DISTRIBUTION
d_{sv} = 44.6 mils

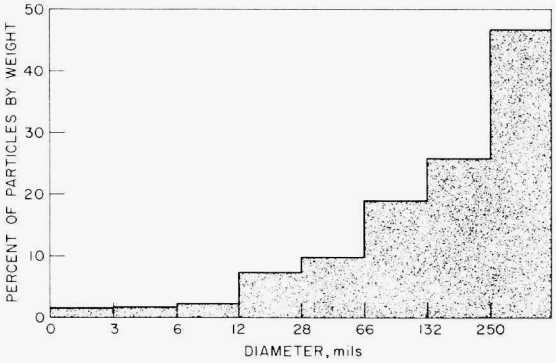

MICROGRAPH OF FRAGMENT

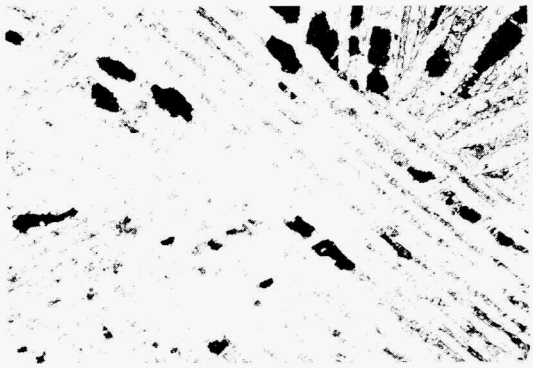

125X

Fig. 5.24. Results of Meltdown Experiments in TREAT on SPERT Fuel Samples Submerged in Water. Test CEN-117.

Energy: 794 cal/g
Period: 42 msec
Amount of
Metal Reacted: 36.9 %

FRAGMENTED PLATE AFTER TRANSIENT

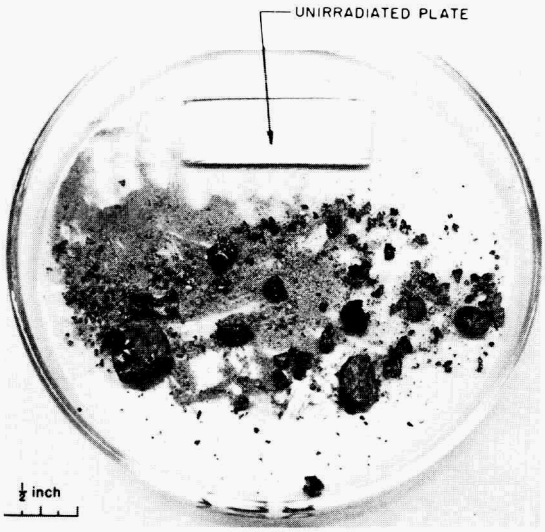

MACROGRAPH OF FRAGMENTS

5X

PARTICLE SIZE DISTRIBUTION
d_{sv} = 18.6 mils

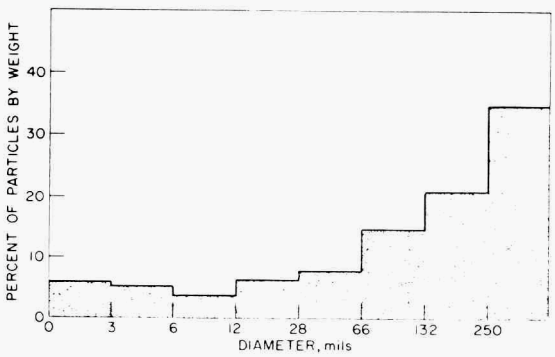

MICROGRAPH OF FRAGMENT

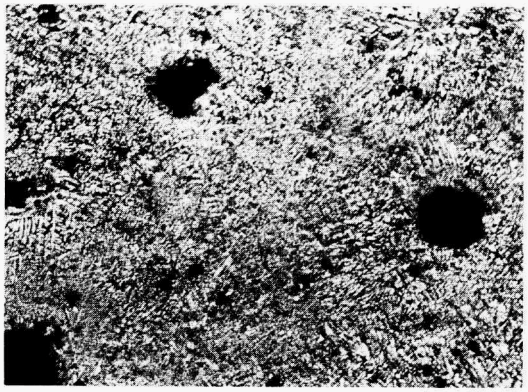

125X

Fig. 5.25. Results of Meltdown Experiments in TREAT on SPERT Fuel Samples Submerged in Water. Test CEN-120.

Fig. 5.26. Photomicrograph of Unirradiated SPERT 1-D Plate. Cross-sectional view showing both cladding and core. Etched with 0.5% HF.

entrapment of water by solidified metal is the initiating mechanism.[39] It appears, nevertheless, that water is momentarily trapped beneath a mound of metal at the bottom of the water tank. The rapid generation of steam then causes violent dispersal of the molten metal. The resulting rapid motion of hot particles greatly increases the heat transfer, forming steam very rapidly, and this process provides the bulk of the energy of the explosion.[34]

Aluminum is much less reactive than either zirconium or uranium at temperatures of the order of 1200°C. The vigorous burning of aluminum at 1750°C, however, makes aluminum more reactive than zirconium or uranium at higher temperatures. This is in accord with the explosion dynamometer tests, as indicated by the exceptional violence of the high-temperature aluminum-water reaction (see Fig. 5.4). The ignitions noted with aluminum probably occur when the vapor pressure of the aluminum (7 mm Hg at 1750°C) is sufficient to sustain vapor-phase combustion. The ultimate product of this kind of burning is α-alumina, which is partly in the form of a very porous mass and partly a finely divided powder. The delayed

ignitions occurring in the levitation studies between 1600 and 1750°C can also be explained in terms of a vaporization process. The following reaction occurs when aluminum vaporizes in the presence of aluminum oxide:[40]

$$4Al(g) + Al_2O_3(s) \rightarrow 3Al_2O(g) \ . \qquad (5.11)$$

Calculations based on thermodynamic data indicate that the vapor pressure of the suboxide Al_2O is 50 mm Hg at 1750°C, where immediate ignition occurs, and 7 mm Hg at 1600°C, where the delayed ignitions were first noted. The delay might be accounted for as the time required to build up sifficient solid oxide in order to generate suboxide vapor according to the above equation. The activation energy of the linear oxidation of aluminum (73.5 kcal/mole) is very similar to the heat of vaporization of aluminum (77 kcal/mole), and this provides further evidence that the reaction is controlled primarily by a varporization process. A similar coincidence between the activation energy for linear oxidation and the heat of sublimation for magnesium was taken as evidence for a vaporization-controlled reaction.[41]

The results obtained in the in-pile studies are not fully consistent with those obtained in laboratory studies. Considerably more reaction occurred with in-pile specimens in which the peak fuel temperature was believed to reach between 1200 and 1750°C than would be expected from the very low reaction rates indicated by the isothermal results. This may be due to the fact that the fuel specimens used in the TREAT studies and in many existing reactors is in the form of a dispersion of UAl_4 in an aluminum matrix. The UAl_4 clusters, visible in Fig. 5.26, are the sources of heat when nuclear heating is used. It seems likely that the resulting uneven heating vaporizes some of the aluminum, which can then react even though the average energy density generated within the fuel is equivalent to a temperature well below that which would produce metal vapor. This view is consistent with the results shown in Fig. 5.21, which indicate that dispersion fuels consisting of U_3O_8 in an aluminum matrix react to about the same extent as aluminum-uranium alloy fuels.

4. Stainless Steels

Isothermal Experiments. No systematic studies of the isothermal stainless steel-steam reaction at temperatures near melting have been reported. In a study of the reaction of metal wires with HCl and H_2O vapor, it was concluded that Inconel and stainless steel (18-8) did not react appreciably with water vapor at temperatures approaching their melting points.[42] Pure iron wires reacted with a 96% Ar–4% H_2O mixture and lost 0.002 to 0.05% in area per second over the temperature range 850 to 1120°C, with an apparent activation energy of 28 kcal/mole.

Nonisothermal Experiments. Dropping 10- to 15-g batches of molten type 304 stainless steel into water gave some metal-water reaction, although not as much as with zirconium.[20] No explosions were produced. Only a slight reaction was reported on pouring molten stainless steel into water.[21]

Experiments with Dispersed Metal. One test with molten stainless steel (type 303) at 2270°C in the explosion dynamometer indicated (see Fig. 5.4) that the explosion was nearly as vigorous as explosions obtained with molten zirconium.[7] Studies of the reaction by the electrical condenser discharge method[43] are summarized in Fig. 5.27. The most significant result of the study was the limited amount of reaction obtained with small particles (260 μ) at very high metal temperatures (3700°C) in heated water. The reactions of zirconium and uranium in heated water were more extensive under similar conditions. In addition, the stainless steel-water reaction was not much more extensive in heated water than it was in room-temperature water. These two results indicated that the reaction rate is controlled predominantly by a chemical rate law, even at very high temperatures. Gaseous diffusion of water vapor through the evolving hydrogen, shown to be of major importance in the zirconium-water reaction, appeared to be less important in the high-temperature stainless steel-water reaction.

In-Pile Meltdown Tests. Meltdown tests in TREAT were performed[25] with specimens of unclad stainless steel-UO_2 cermet fuel pins and plates and with stainless steel-clad mixed-oxide and pure-UO_2-core fuel pins. The results are summarized in Table 5.13. The extent of metal-water reaction as a function of fission energy input for the stainless steel-UO_2 cermets is plotted in Fig. 5.28. Included in the plot are the results for aluminum-U_3O_8 cermets. It is apparent from the figure that the cermets show nearly identical behavior over the limited energy range studied. At higher energies, it would be expected that the aluminum reaction would exceed the stainless steel reaction.

Results obtained with the oxide-core fuel pins, included in Fig. 5.9, indicate that the stainless steel-water reaction is less extensive than

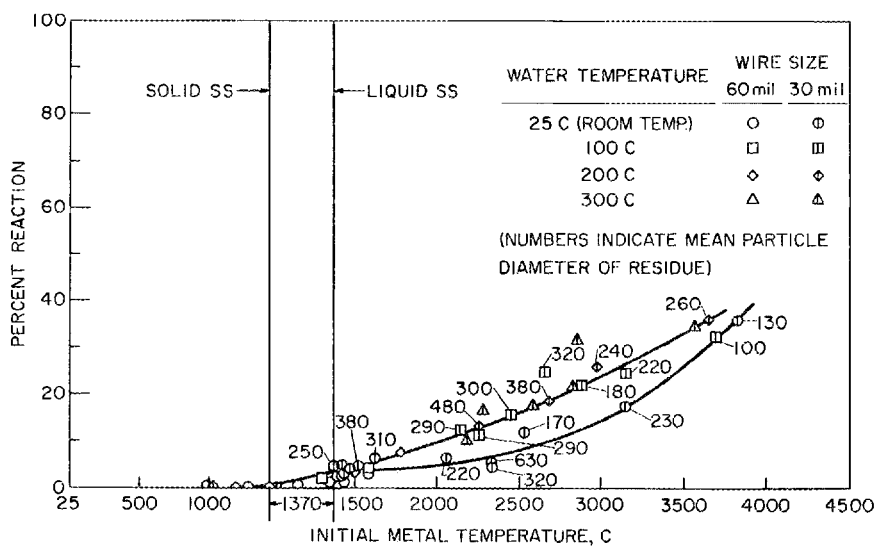

Fig. 5.27. Results of Studies of Type 316 Stainless Steel-Water Reaction by the Condenser Discharge Method. The particle diameters of the residue are given in microns.

Table 5.13. Results of Studies of Stainless Steel in Submerged Fuel Specimen Meltdown Tests in TREAT

Initial water temperature: 25°C
Initial helium overpressure: 20 psia

Fission Energy Input (cal/g)	Adiabatic Core Temperature (°C)	CEN Run Number	TREAT Characteristics		Appearance of Specimen After Transient	Mean Particle Diameter (mils)	Percent of Metal Reacted
			Period (msec)	Integrated Power (Mw-sec)			
Unclad Type 304 Stainless Steel and Uranium Oxide Cermet Fuel Pins[a,b]							
552		51	50	435	Fragmented	33	6.6
612		50	50	510	Fragmented	24	9.6
615		52	49	512	Fragmented	40	10.2
Unclad Type 304 Stainless Steel and Uranium Oxide Cermet Fuel Plates[a,c]							
550		54	51	368	Fragmented	10	5.2
725		53	52	490	Fragmented	11	9.1
732		55	51	495	Fragmented	17	11.0
Type 304 Stainless Steel-Clad Mixed-Oxide-Core Fuel Pins[a,d]							
296	1900	40	60	315	Cladding intact; core cracked	330[e]	0
395	2500	21	78	420	Cladding intact; core partly melted, cracked	330[e]	0
432	2600	48	72	460	Cladding partly fragmented; core fragmented	15	4.3
536	3200	24	65	560	Cladding partly fragmented; core fragmented		6.6
Type 304 Stainless Steel-Clad Urania-Core Fuel Pins[a,f]							
152	2000	63	121	120	Cladding intact; core cracked	330[e]	0.3
215	2700	67	290	185	Cladding intact; core cracked	330[e]	0.3
242	2700	65	50	190	Cladding fragmented; core fragmented	4	5.2
292	2900	66	97	230	Cladding fragmented; core fragmented	23	5.2
312	3100	69	64	245	Cladding fragmented; core fragmented	2	5.4
407	4200	61	116	320	Cladding fragmented; core fragmented	17	19.1
432	4500	62	49	340	Cladding fragmented; core fragmented	13	14.0
437	4600	60	47.5	344	Cladding fragmented; core fragmented	11	13.5
510	5400	71	42.5	400	Cladding fragmented; core fragmented	8	11.5
97	1300	72[g]	110	76	Cladding partly fragmented; core cracked	330[e]	0.7
178	2300	64[g]	115	140	Cladding partly fragmented; core cracked	330[e]	0.8

[a]From Liimatainen et al., ref. 25.

[b]Pin 90 wt % steel, 10 wt % UO_2 (93% enriched); dimensions were 0.34 in. in diameter and 0.50 in. long.

[c]Plate 90 wt % steel, 10 wt % UO_2 (93% enriched); dimensions were 0.5 × 1.0 × 0.1 in.

[d]Cladding 20 mils thick; ends capped; core 81.5 wt % ZrO_2, 9.1 wt % CaO, 8.7 wt % U_3O_8, 0.74 wt % Al_2O_3; dimensions were 0.33 in. in diameter and 0.50 in. long.

[e]Estimated values.

[f]Cladding 20 mils thick; core 20% enriched UO_2; dimensions were 0.33 in. in diameter and 0.50 in. long.

[g]Core saturated with water before test.

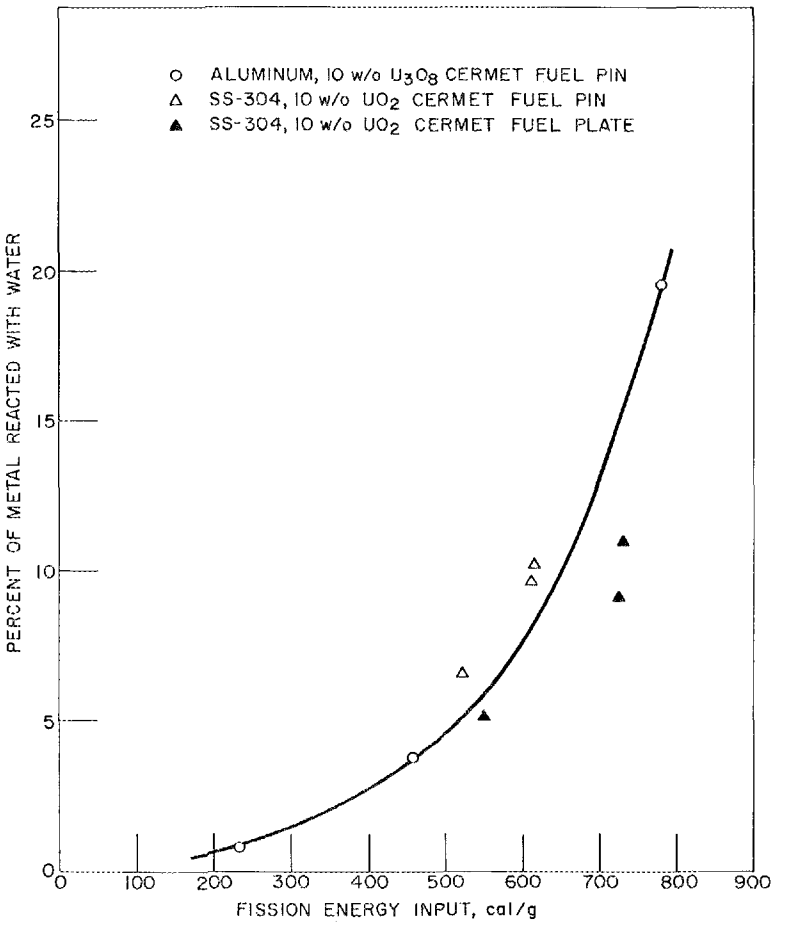

Fig. 5.28. Results of TREAT Meltdown Tests with Unclad Aluminum and Stainless Steel Cermet Fuel Specimens.

the zirconiun reaction but considerably more extensive than the aluminum reaction over the energy range studied. Comparison of the stainless steel-clad mixed-oxide-core fuel pins and the pure-urania-core fuel pins indicates that there were no significant differences in either the nature of the damage or the extent of the metal-water reaction. The threshold for fragmentation of the oxide-core specimens corresponded approximately with the melting points of the ceramic core material (2600 to 2700°C) for both the mixed oxide and the urania cores. A particularly striking example of this is shown by the macrograph of the cross section of a mixed-oxide-core fuel pin[25] (see Fig. 5.29). Energy calculations indicated that the core reached a temperature of 2500°C, while the macrograph indicated melting of the central region of the core. The stainless steel cladding remained intact during this transient. The nature of the damage produced in a very energetic transient with a urania-core specimen is indicated in Fig. 5.30 (ref. 25).

Two experiments were performed with urania-core specimens in which water was deliberately added to the core to simulate the case of defective

Energy:	395 cal/g
Period:	78 msec
Peak Adiabatic Core Temperature:	2500°C

10X Magnification

Fig. 5.29. Results of Meltdown Experiments in TREAT on Oxide-Core Stainless Steel-Clad Fuel Pins Submerged in Water. Test CEN-21, cross section.

Energy:	432 cal/g
Period:	49 msec
Peak Adiabatic Core Temperature:	4600°C
Amount of Metal Reacted:	13.5%

Fig. 5.30. Results of Meltdown Experiments in TREAT on Oxide-Core Stainless Steel-Clad Fuel Pins Submerged in Water. Test CEN-62.

cladding. In both cases, a hole developed in the cladding, even though the adiabatic core temperature was only 1300°C in one case.

The threshold for destruction of ceramic-core stainless steel-clad fuel pins (2600 to 2700°C adiabatic core temperature) was considerably higher than that obtained for aluminum and Zircaloy-2 clad specimens (1800°C adiabatic core temperature). This phenomenon may be related to

the greater high-temperature strength of stainless steel. It should be emphasized that the cladding did not reach the high core temperatures in these experiments.

5. Sodium (and NaK)

There are three products of the sodium-water reaction. In excess water, sodium hydroxide (NaOH) and hydrogen are formed, as indicated in Table 5.5. In excess sodium, sodium monoxide (Na_2O) and hydrogen are formed. The reaction of sodium with water can be considered irreversible. Figure 5.31 gives the results of calculations of equilibrium temperatures

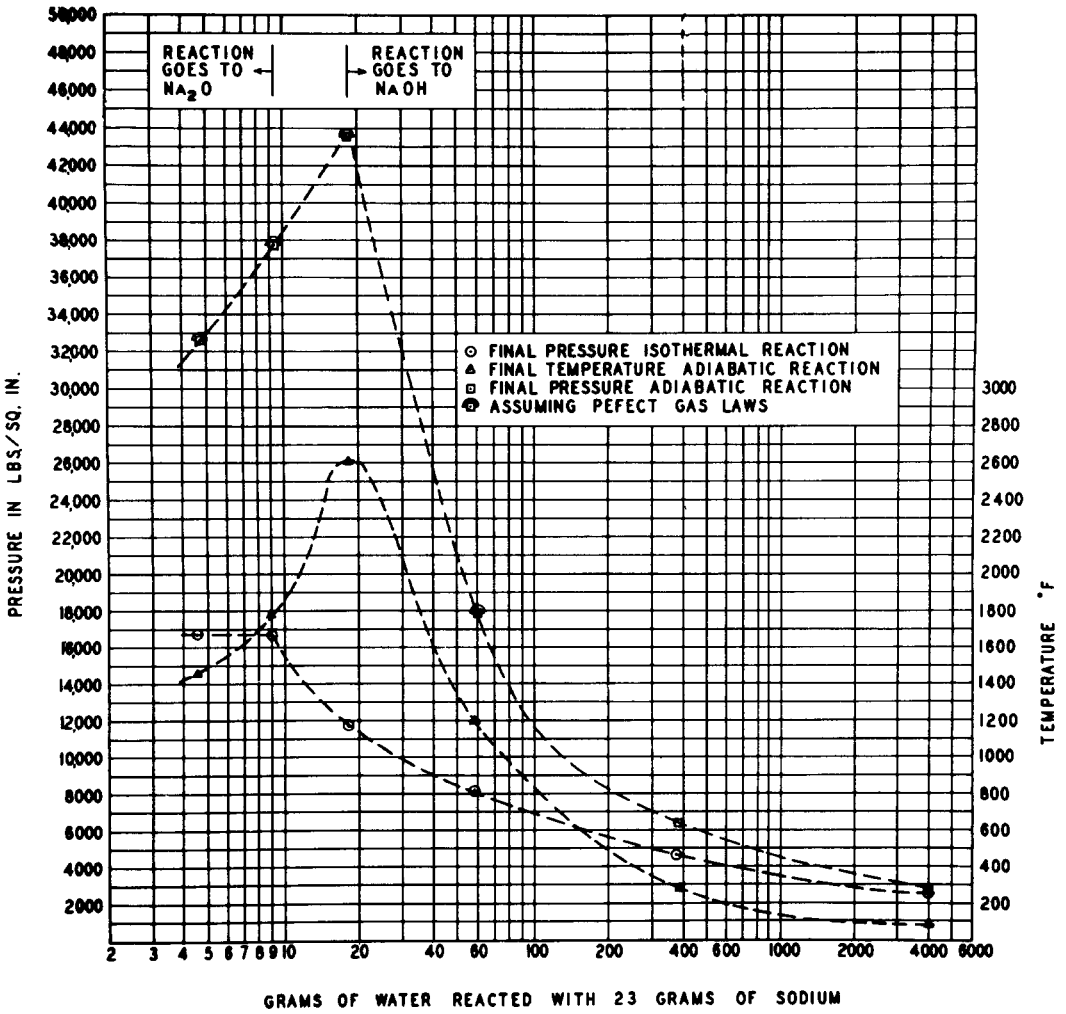

Fig. 5.31. Graph of Estimated Final Pressures and Temperatures Resulting from Reaction of One Mole of Sodium with Various Amounts of Water (From Liquid Metals Handbook, Sodium-NaK Supplement).

and pressures where complete reaction is assumed to occur in a rigid container with the hydrogen produced occupying the net volume between reactants and the oxide or hydroxide. It is apparent that the maximum pressure results from an adiabatic reaction of stoichiometric amounts of sodium and water.

The three reaction products can cause the following difficulties in reactor vessel and piping systems:[44]

Product	Difficulty
Na_2O	Plugging of sodium stream
NaOH	Corrosion of water or steam tubes if tube material is austenitic stainless steel or aluminum
H_2	Excessive pressure buildup or explosion if oxygen is also present

Isothermal Experiments. At low temperatures (<100°C) an initially rapid reaction between solid sodium and water vapor occurs, and then the rate decreases exponentially with time. At higher temperatures (100 to 300°C) the reaction rate of liquid sodium with water vapor conforms to the parabolic rate law, which is associated with protective films through which diffusional processes constitute the rate-determining step. At still higher temperatures (350 to 400°C), the film of NaOH is destroyed, with a resulting change in reaction rate.[45]

Nonisothermal Experiments and Experiments with Dispersed Metal. The reaction between molten sodium just above its melting point (~212°F) and water at 35 to 140°F is characterized by a rate[46] proportional to the surface area of contact. Data from tests with sodium droplets (30 to 300 mg of sodium) in water at room temperature and at 570°F are plotted in Figs. 5.32 and 5.33, respectively. If the sodium drops are assumed to be spherical, the rate constants (ref. 46, p. 18) can be calculated from Figs. 5.32 and 5.33 by the expression

$$V_e^{1/3} - (V_e - V)^{1/3} = \frac{akt}{3n^{1/3}} = 1.31kt \ , \qquad (5.12)$$

where

V_e = hydrogen that would be evolved if complete reaction of the sodium occurred, ml,
V = hydrogen evolved up to time t, ml,
a = a constant obtained by assuming that the surface area is proportional to the 2/3 power of the weight of sodium, thus, for a sphere, $a = (3/\rho_{Na})^{2/3} (4\pi)^{1/3} = 4.93 \ cm^2/g^{2/3}$,
k = reaction rate constant, $g/cm^2 \cdot sec$,
t = reaction time, sec,
n = stoichiometric equivalent, 1.94×10^{-3} g of sodium per cubic centimeter of H_2.

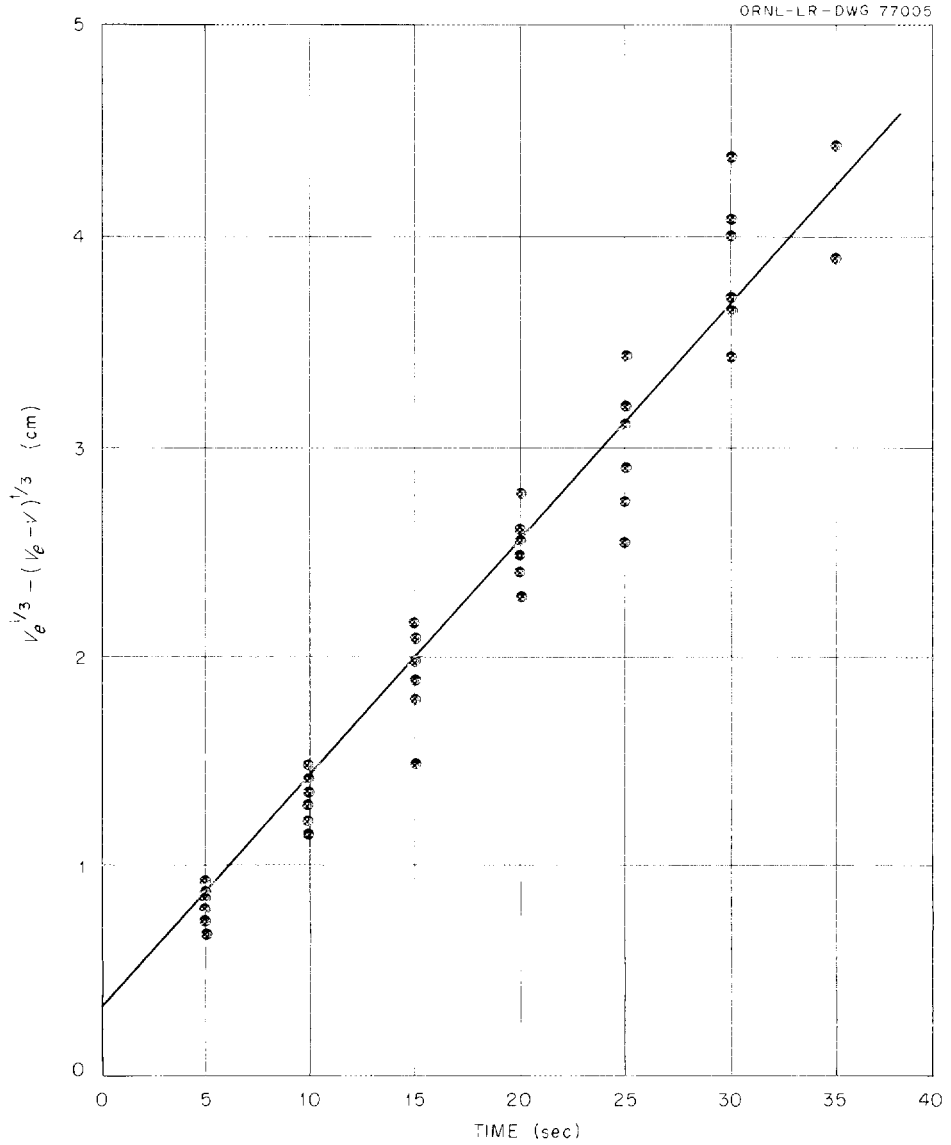

Fig. 5.32. Reaction of Sodium with Liquid Water. Composite of six runs at 5-sec intervals. Plot of $V_e^{1/3} - (V_e - V)^{1/3}$ versus time, where V_e = total volume of hydrogen evolved; V = instantaneous volume of hydrogen evolved. Sodium and H_2O initially at room temperature. (From Corrsin et al., ref. 46, p. 16.)

The reaction[46] of initially hot (~400 to 900°F) sodium with water is fast and unstable. Data from the reaction between sodium at 470°F and D_2O are included in Fig. 5.33. The rate of reaction of the type described above tends to increase with the rate of mixing of the reactants, which indicates that on a large scale, e.g., reactor accident conditons, the reaction would be dependent on hydrodynamic variables, in addition to chemical kinetics.

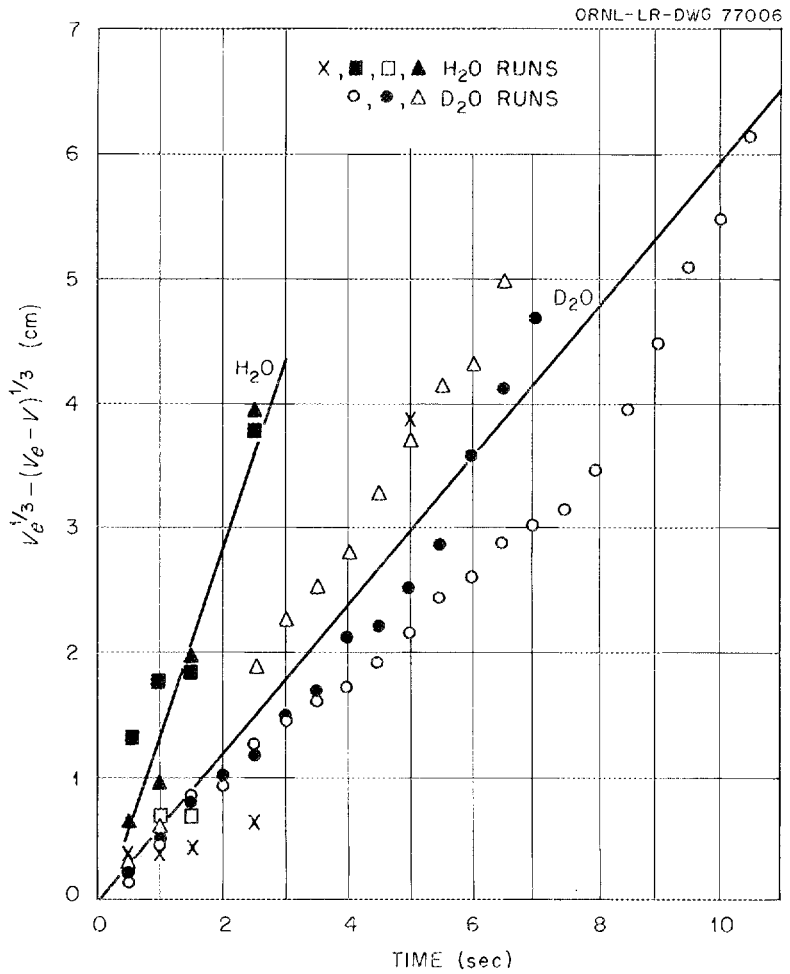

Fig. 5.33. Kinetics of the Reaction Between Molten Sodium at 570°F and Water at Room Temperature. (From Corrsin et al., ref. 46, p. 16.)

The reaction rate can be significantly slowed down by adding a film of oil or a foaming agent to the surface of the water on which the sodium droplets are floating.[46] The rate of reaction of sodium with water in isoamyl alcohol is a linear function of the water content over the range 0 to 10% water.[47]

The general conclusion of rapid kinetics was supported by experiments in which NaK and H_2O were mixed in 2 msec[48] and in another where NaK was contacted with a flowing stream of helium containing water vapor.[2] The reaction

$$NaK_2 + 3H_2O = 1.5H_2 + 2KOH + NaOH \qquad (5.13)$$

yielded the theoretical amount of hydrogen as fast as the reactants were mixed.[48] If oxygen is present, the record of pressure versus time shows

first a thermal maximum, followed by about a 40- to 80-msec induction period, at which time a hydrogen-oxygen explosion occurs. When helium containing from 100 to 400 ppm of water vapor (total pressure, 1 atm) was passed over molten sodium at 215 to 340°C, it was observed that the reaction rate approached the input rate of the water vapor and that the reaction rate also increased with the gas flow velocity. These observations suggested that the apparent reaction rates were limited by the mass transport of water vapor through the inert gas film.[2]

In another experiment, a thermal-convection NaK loop was connected to a similar water loop through a 0.5-in. triggering valve. With the NaK initially at 800°F and 30 psig and the water at 350°F and 400 psig a 4000-psi sharp-peak pressure was noted 20 sec after triggering.[44] However, the addition of a surge volume, equivalent to 8% of the NaK, eliminated the pulses and gave pressure fronts of from 400 to 600 psi. Motion pictures were made of sodium-water reactions both in water and in air. In the argon-blanketed case, there was no ignition or explosion, whereas with air there was both ignition of the metal and a violent hydrogen-oxygen explosion. From these empirical tests the following three safety recommendations were formulated for sodium or NaK systems:[49]

1. maintain oxygen content of blanket gas at less than 5%,
2. provide expansion volume on piping systems,
3. provide backup surge volumes with a venting device such as a rupture disk.

It is of interest that, in practice, leaks in sodium-water piping systems are usually so small (fine cracks or pinholes) that the leak is detected not by the direct evidence of the energy or pressure from the metal-water reaction but by subsequent plugging of a pump or valve.[50]

Other experiments have demonstrated that sodium-water reactions are not high-order explosions, since peak pressures are attained quite slowly, in milliseconds or seconds as contrasted to microseconds.[7] Results from dispersing 1 to 5 kg of NaK under 10 ft of water suggested that less than 0.3% of the exothermic reaction energy was evident in shock waves, while 16% went into formation of hydrogen gas bubbles; the remainder was dissipated into the water as heat.[51]

Discussion. In general, it is necessary to assume rapid and complete reaction when molten sodium and water are contacted. The thermodynamic heat of reaction will then be released; shock-wave energy can be considered negligible. Unlike the previous metal-water reactions discussed, no postaccident heatup period is required, since the metal reactant will be molten at reactor operating conditions.

5.2.1.7 Analysis of Cladding-Water Reaction During Reactor Accidents

The analysis of the rate and extent of metal-water reaction that would occur during a reactor accident is ultimately a synthesis of reactor kinetic calculations and chemical reaction calculations. While considerable knowledge exists in both areas, no rigorous means has been developed for analyzing an accident involving core meltdown. The principal stumbling block has been the uncertainty regarding the mechanism of fragmentation of the core and, in particular, the particle sizes produced. Other stumbling blocks include determinations of effective steam flow rate and heat

transfer coefficient. There appears to be no theoretical approach to the problem of predicting what particle sizes will be produced during a meltdown. Additional problems are presented by the lack of ability to determine steam flow rates and applicable heat transfer coefficients. Present knowledge in this area seems to be limited to the results obtained in small-scale meltdown experiments, particularly those conducted in TREAT. Two general classes of accidents, the loss-of-coolant and the nuclear excursion accidents, are discussed in the following paragraphs.

1. Loss-of-Coolant Accidents. An attempt has been made to combine reactor kinetic and chemical reaction rate calculations.[52,53] The calculations have indicated that the heat generated by the oxidation of zirconium cladding significantly increases the cladding temperature as soon as decay heat brings the temperature up to about 2000°F. Chemical rate equations for zirconium or Zircaloys, see Eq. (5.8), are available (while it can probably be assumed that aluminum and stainless steel do not react significantly at temperatures below their melting points). The resulting autocatalytic effect causes various amounts of cladding oxidation prior to melting and a large variation of temperature between the hottest and coolest areas in the core of the hypothetical reactor. The calculations indicated that 5 mils of a total of 30 mils of zirconium cladding would react in about 11 min before the cladding began to melt, a result similar to that obtained in analyzing a loss-of-coolant accident in the Shippingport reactor hazards evaluation.[19]

The analysis was carried a step further by attempting to evaluate the metal-water reaction occurring during and after the cladding melts.[19] The minimum particle size of droplets that would fall from the fuel plates into the pool of water below was estimated. The smallest thickness present in the PWR core was the 0.028-in. cladding on the blanket elements. It was then assumed that the molten droplet disengaged from the cylinder at a diameter at which the weight of the droplet equaled the surface tension holding the droplet. This gave a minimum droplet diameter of 2.38 mm, assuming a surface tension of 200 dynes/cm. A stepwise calculation of the curves of temperature vs time and extent of reaction vs time then yielded from 27 to 10.6% reaction on the basis of emissivities of 1.0 and 0.5, respectively. More recent calculations of the reaction of molten zirconium spheres with water would indicate about 9% reaction for a 2.38-mm droplet (see Fig. 5.12).

The approach involved the stepwise computation of terms, including decay heating and chemical reaction heating of the cladding. The more refined calculation[52] included terms to describe steam cooling as well. The procedures for estimating the curves for temperature vs time and extent of reaction vs time at temperatures below the melting point depend on a reliable chemical rate law and on estimating the heat transfer rates between the core and cladding and between the cladding and the steam atmosphere.

It is more difficult to predict the course of events when temperatures reach beyond the melting point of the cladding. It should be recognized that the metal oxides, which are continually forming, may act as effective containers and protective barriers for the molten metal. Simple melting and dripping of metal would not occur in this situation. It

would then be reasonable to assume that the chemical reaction continues to follow the same rate law without a significant increase in available surface area to temperatures considerably above the melting point of the cladding. If it is assumed that dripping occurs and a minimum droplet size is chosen, the maximum probable extent of reaction can be obtained from nuclear excursions simulated by the electrical condenser discharge method (see Figs. 5.5, 5.15, and 5.27) or by the TREAT method (see Tables 5.7, 5.11, 5.12, and 5.13).

2. Nuclear-Excursion Accidents. Experience gained from previous full-scale excursions, excluding the NRX incident, is limited to cores containing uranium-aluminum alloy and excursions having periods between 2.6 and 4.0 msec. The results of these excursions (Borax-1, SL-1, and SPERT-1) seem consistent with the conclusions reached during an evaluation of severe nuclear excursions in light water-cooled reactors.[54] It was concluded that for flat-plate metallic-aluminum fuel, melting would begin to occur only when the period of the excursion was 4.9 msec or less. It was also concluded that complete melting would occur for an excursion having a period of 3.3 msec or less, although this appears to ignore the wide flux variation from the edge of a reactor to the center. For a metallic zirconium core, the limiting periods were 12.2 and 8.6 msec, respectively. The narrow gap in excursion periods between no melting at all and complete melting implies that extensive melting and the possiblity of a massive metal-water reaction must be considered whenever the insertion of sufficient reactivity to achieve these short periods is credible. The differences in period between an aluminum core and a zirconium core resulted from the poorer thermal diffusivity of zirconium in comparison with aluminum. Steam void formation, the principal shutdown mechanism, was slower in the zirconium case.

A low-enrichment zirconium-clad UO_2-core fuel element was shown[54] to have a long thermal relaxation time so that Doppler broadening was the principal shutdown mechanism. Under these conditions it was concluded that the zirconium cladding would not reach the melting temperature, and consequently there was little likelihood of a massive metal-water reaction.

These calculations of nuclear excursions did not include terms to describe chemical heating or effects resulting from meltdown or fuel fragmentation.[54] At present, it appears that the nuclear characteristics of an excursion must be calculated separately from the chemical characteristics. Results of small-scale meltdown experiments can then be used to estimate fuel fragmentation patterns and the extent of metal-water reaction. TREAT meltdown studies with Zircaloy, aluminum, and stainless steel-clad oxide core fuel elements were correlated in terms of the adiabatic core temperature. The adiabatic core temperature (calculated from total fission energy input) would result from the nuclear analysis of the maximum credible excursion in a hazards analysis. The average particle sizes of residue and the extent of reaction can be estimated from Tables 5.7, 5.12, and 5.13 and from Fig. 5.9. The TREAT data apply strictly to excursions having periods between 40 and 100 msec. However, more rapid excursions would probably not differ greatly because of the lag in transferring heat from the oxide core to the cladding.

TREAT studies with cermet-core and metallic-core fuel elements were correlated in terms of the energy input to the entire specimen and can be

used directly only for excursions having periods in the region of 40 to 100 msec. More rapid excursions can be treated, approximately, on the assumption that the heating would be nearly adiabatic. In this case, it is necessary to estimate peak temperatures actually reached in TREAT experiments. This is done presently by noting indications of melting and changes in the character of reaction. Regions of solid and melted residue in the TREAT studies are indicated in Figs. 5.8, 5.16, and 5.21. The sharp jump in the zirconium reaction in Fig. 5.8 may be tentatively identified with the melting point of ZrO_2 (2600°C). The sharp jump has been shown in laboratory studies to result in greater subdivision of particles and more extensive reaction in room-temperature water (see Fig. 5.5). The threshold for extensive aluminum-water reaction at about 750 cal/g (see Fig. 5.21) may similarly be identified with the temperature (1750°C) at which aluminum ignites and burns in water, as determined in laboratory studies. It should be noted that the TREAT results are currently under study, and it is anticipated that a more rigorous estimate of the temperatures reached will be obtained from computer simulation of the experiments. It is also hoped that these studies will result in better methods for estimating the results of postulated reactor accidents.

An important consideration in applying TREAT results to nuclear excursion accidents is the wide variation of integrated flux across a reactor. The reactor must, therefore, be segmented in some way into regions of constant maximum temperature or fission energy input. The extent of metal-water reaction can then be estimated to a first approximation for each segment and the results summed to yield a total for the incident.

The rate of chemical reaction occurring during a nuclear excursion is more difficult to estimate than the total extent of reaction. The overall reaction rate depends primarily upon whether the reactive metal in the core is dispersed suddenly or over a period of time. Pressure transducers in the TREAT studies indicated that there were no violent pressure surges. Laboratory studies by the electrical condenser discharge method indicated that very rapid reactions occurred when very fine metal droplets were formed. Since fine particles were also formed in the TREAT studies, it appeared that the particles were formed over a period of time so that, while each fine particle reacted rapidly, the overall reaction was relatively slow. It has been suggested that the rate of reaction of the Zircaloy cladding on oxide core fuel elements could be estimated on the assumption that the particle formation rate is equal to the rate at which the cladding is melted.[3] Each particle would then react to the extent indicated in Fig. 5.12. Particles smaller than about 0.5 mm in room-temperature water and about 1.0 mm in heated water would react in a few milliseconds. Larger particles would react at rates indicated in Figs. 5.1 and 5.2.

A comparison between the extent of zirconium-water reaction indicated in Fig. 5.12 and results of TREAT runs with Zircaloy-2-clad mixed-oxide-core pins is given in Tables 5.9 and 5.10. It was assumed that the distribution of particle sizes of oxide and cladding metal together represented the distribution of metal particles alone. The anticipated reaction of each particle size group was then summed to give the total extent of reaction. The comparison of calculated reaction with experimental values (based on the measurement of evolved hydrogen) seems very reasonable in view of the many complicating factors.

There is a lack of experience regarding excursions initiated in a reactor operating at full power. Heat and mass transfer effects in saturated water differ markedly from those in subcooled water. Laboratory studies and preliminary studies in TREAT[24] have indicated that the zirconium-water reaction and the uranium-water reaction are more extensive in heated water, while the stainless steel-water reaction is nearly independent of water temperature. There is an indication that increasing the water temperature (steam pressure) causes a marked increase in the amount of aluminum-water reaction.

The following example is given to illustrate a method of estimating the extent of metal-water reaction which occurred during the SL-1 and SPERT-1 meltdowns. The calculation is based on TREAT meltdown studies summarized in Fig. 5.21. The following two assumptions were made:

1. The portion of core which became molten was assumed to be spherical with $x = 0$ at the center and $x = 1$ at the edge. Therefore, the volume was $4\pi/3$.

2. The energy density was assumed to vary linearly with the distance from the center of the sphere. This assumption is probably valid as a first approximation. This relationship was expressed as

$$E_x = E_{max} - Ax \ .$$

The maximum energy densities were taken from the literature[10,55] as

$$E_{max}(\text{SL-1}) = 500 \text{ cal/g}$$

and

$$E_{max}(\text{SPERT}) = 380 \text{ cal/g} \ .$$

The energy density at the edge of the sphere ($x = 1$) was taken as 220 cal/g, the energy required to heat aluminum to its melting point and completely melt it (energies based on $E = 0$ at 25°C). The equations for energy distribution were then determined to be

$$E_x = 500 - 280x \qquad \text{for SL-1}$$

$$E_x = 380 - 160x \qquad \text{for SPERT}$$

These equations were then used to calculate the energy distribution in the sphere by calculating the distance from the center of the sphere (x) that achieved energies corresponding to various temperatures. The fraction of sphere attaining the selected temperature or higher was then calculated as x^3. In this way the amount of metal that achieved various energy levels was calculated. This was done in steps of 100°C.

The extent of reaction was then determined from the TREAT data. This was done by assuming the following: (1) that the TREAT energy input of 220 cal/g corresponds to the complete melting of the material, (2) that the break point of 530 cal/g in the TREAT data corresponds to the temperature range of 1200 to 1400°C, and (3) that the marked increase in extent of reaction at 750 cal/g in the TREAT data corresponds to a temperature of 1750°C. The temperatures between these points were linearly interpolated. These assumptions were based on physical observations and metallographic examinations of the TREAT samples and on laboratory data. The graph in Fig. 5.21 has both TREAT energies and estimated temperatures on the abscissa. These calculations are summarized in Tables 5.14 and 5.15.

Table 5.14. Calculation of Aluminum Water Reaction in the SL-1 Excursion Based on 60 kg of Molten Core

E, Assumed Energy Density (cal/g)	Corresponding Temperature (°C)	X, Distance from Center of Sphere[a]	x^3, Volume Fraction	W, Mass of Sphere with Radius X (kg)	ΔW (kg)	Percent of Metal Reacted[b]	Weight of Metal Reacted (kg)
500	1700	0	0	0			
474	1600	0.093	0.0008	0.048	0.048	19.9	0.010
448	1500	0.186	0.0066	0.395	0.347	17.2	0.060
422	1400	0.279	0.023	1.39	0.99	11.0	0.109
396	1300	0.372	0.051	3.06	1.67	11.0	0.184
368	1200	0.472	0.105	6.29	3.23	11.0	0.355
342	1100	0.564	0.180	10.8	4.5	7.0	0.315
316	1000	0.658	0.284	17.0	6.2	3.4	0.211
290	900	0.750	0.422	25.3	8.3	1.2	0.100
264	800	0.843	0.600	35.9	10.6	0.6	0.064
238	700	0.9345	0.817	48.9	13.0	0.2	0.026
220	600	1.000	1.000	60.0	11.1	0.1	0.011
				Total metal consumed			1.445

Thus 1.445 kg × 18 Mw-sec/kg = 26.0 Mw-sec chemical energy

[a]Assumed molten mass.

[b]Based on information of the type shown in Fig. 5.21.

The estimates obtained in this manner are in excellent agreement with the values obtained by the postexcursion analyses of the SPERT and SL-1 debris. In both cases estimates of the extent of aluminum-water reaction were made from determinations of the amount of α-alumina. The analysis method yielded 3.5 Mw-sec of chemical energy release for SPERT[15] and 24 ± 10 Mw-sec for SL-1.[10] The calculation presented here yielded values of 2 Mw-sec for SPERT and 26 Mw-sec for SL-1.

Table 5.15. Nuclear Excursions of the SL-1 and SPERT Reactors

	SL-1	SPERT
Excursion parameters		
Reactor period, msec	4	3.2
Integrated power, Mw-sec	130	31
Peak energy density, cal/g	500	380
Core parameters		
Aluminum present in core, kg	185	51
Uranium present in core, kg	14	4
Peak core temperature, °C	>2060°C[a]	1200-1300°C
Percent of core melted	32	35
Chemical parameters		
Observed chemical energy release, Mw-sec	24 ± 10	3.5
Calculated chemical energy release, Mw-sec	26	2

[a]Vaporization temperature.

5.2.2 Oxidation Reactions

5.2.2.1 Graphite Oxidation

Oxidation could release a large amount of chemical energy if air contacted the moderator of a high-temperature gas-cooled graphite-moderated reactor. Although such reactors are normally cooled with a relatively inert gas, such as CO_2 below 600°C or helium, ingress of air following a coolant system rupture could result in uncontrolled oxidation heat release, commonly referred to as "runaway" oxidation, unless the containment building atmosphere was very depleted in oxygen or other preventive measures were taken. Low-temperature (~200°C max) air-cooled graphite-moderated reactors used for research and isotope production also have the possibility of runaway oxidation especially during "Wigner-energy" annealing operations. Since air-cooled graphite-moderated reactors are economically unattractive for power production and hence few, if any, such reactors will be constructed in the future, the graphite oxidation hazards of high-temperature reactors are emphasized in the following discussion.

Reference material pertaining to the general properties and performance of nuclear graphite and its use in nuclear reactors is available primarily from the USAEC, UKAEA, and French CEA reactor development programs. References 56, 57, and 58 are useful summaries of the work on gas-carbon reactions, nuclear graphite development and applications, and radiation effects on graphite. In addition, the Proceedings of the First through Fifth Conferences on Carbon and the new (1964) Carbon Journal

report information on all phases of graphite research conducted by educational institutions, the graphite industry, and the US, UK, and French governments.

1. Graphite-Air Oxidation Mechanisms. The oxidation mechanism* that controls the chemical reactivity of carbon and oxygen is generally agreed to be

$$2C_f + O_2(g) \rightarrow 2C(O) \rightarrow 2CO(g) \ , \qquad (5.14)$$

$$C_f + O_2(g) \rightarrow C(O_2) \rightarrow CO_2(g) \ , \qquad (5.15)$$

where C_f represents a carbon-free site capable of reaction, $C(O)$ and $C(O_2)$ represent a chemisorbed oxygen atom and molecule, and $CO(g)$ and $CO_2(g)$ represent the desorbed gaseous oxide. Both CO and CO_2 have been established as primary reaction products. In general the CO-to-CO_2 ratio increases rapidly with temperature, although other variables, such as the type of graphite, presumably have some effect.

The observed reaction rate – mass of carbon oxidized divided by the product of the unit external surface area and time – of a porous solid, like graphite, and a gas may be controlled by one or more of the following steps:

1. Mass transfer of the reactant and product gases across a stagnant gas film between the external graphite surface and the flowing gas stream,
2. Mass transfer of the reactant to an active site on the internal pore surface and of the products to the external surface,
3. Chemisorption of reactant at an active site, rearrangement of the chemisorbed species to a desorbable product, and desorption of the product from the surface.

Mass transfer to the external graphite surface, mass transfer within the internal pores, and the chemical reaction at the graphite surfaces occur simultaneously under all conditions. An ideal situation in which each of these rate-controlling mechanisms is limiting in different temperature regimes has been used[56] to illustrate the consequences of such rate-controlling conditions. In Fig. 5.34 the qualitative effect of temperature on the observed reaction rate is shown for this ideal situation, together with qualitative concentration profiles of the reactant gas. In zone I at the lowest temperature regime, the chemical reactivity is so low that the reactant concentration gradient in the gas stream and in the pore volume is essentially zero. The reaction rate in this zone increases with temperature as $\exp(-E_t/RT)$, where E_t is the true activation energy of the chemical reaction, R is the universal gas constant, and T is absolute temperature.

The zone II observed reaction rate is controlled by diffusion of the reactant gas to and the product gases from the active sites on the exposed

---

*Reference 56, from which this discussion is largely drawn, should be consulted for more detail.

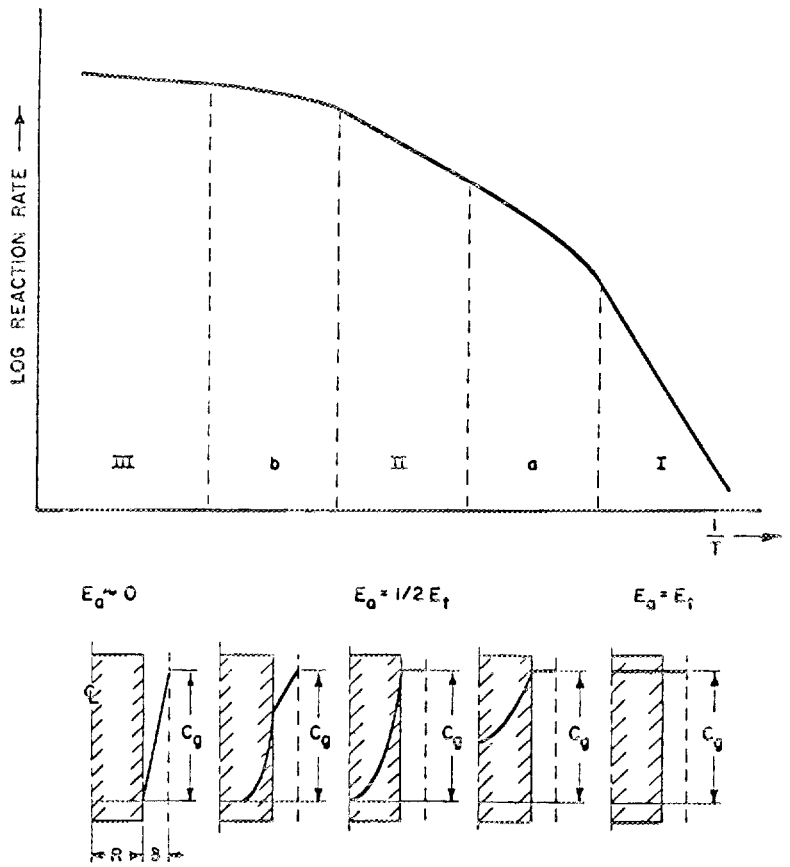

Fig. 5.34. Ideally, the Three Zones Representing the Change of Reaction Rate of a Porous Carbon with Temperature. (From ref. 56)

pore surface. The reactant gas concentration therefore decreases to essentially zero within the available depth of the exposed graphite. Assuming no change in the oxidation mechanism with temperature and uniform diffusion and chemical reactivity within the graphite, the apparent activation energy, E_a, in this zone should theoretically be one-half of true activation energy, E_t; that is, the slope of the log of the reaction rate versus 1/T in zone II should be one-half the slope in zone I.

The zone III reaction rate is controlled by mass transfer through the relatively stagnant surface film. Such a situation results because the chemical reactivity is so high at the highest temperatures that oxidation occurring only on the external graphite surface is sufficient to consume all the reactant gas that diffuses through the product gases in the film. The conditions that determine the establishment of a stagnant film depend on the transport properties of the gases and the flow velocity of the main gas stream. Since the transport properties vary only slightly with temperature, the reaction rate in zone III usually is controlled by the main stream flow conditions.

Graphite reaction research has verified the existence and importance of the three rate-controlling mechanisms described above. It should be

emphasized, however, that the behavior described above and illustrated in Fig. 5.34 is idealized from the standpoint that the three rate-controlling mechanisms do not overlap. Therefore the actual reaction rate dependence on temperature or inverse temperature may, in general, involve a more complicated overlapping of these steps and may even include the elimination of one reaction regime by combined or separate effects of the other two regimes.

2. Runaway Oxidation and Resulting Hazards. The runaway oxidation condition is the source of several potential hazards to a reactor containment system, regardless of the type of containment employed. ("Pressure" or "pressure-release," see Chapter 1, are the two basic types of containment system applicable for a gas-cooled power reactor.) A description of a runaway oxidation situation is presented below to illustrate the nature of the hazards that could result.

In the typical accident model a reactor coolant channel with one or more graphite surfaces is exposed to flowing gas containing air as a result of a coolant system rupture. A reactor scram is assumed to follow the coolant system depressurization. The flowing coolant is presumed to have a heat sink available to it so that the inlet coolant temperature is reduced to a value close to the normal inlet coolant temperature. In a typical graphite section taken perpendicular to the coolant channel, heat generation is by graphite oxidation, gamma radiation afterheat, and possibly stored Wigner-energy annealing. Radiative heat transfer from the fuel elements can add to the heat input of the adjacent graphite, which may be a supporting sleeve or moderator block. Heat is exchanged to or received from the graphite section by convection with the flowing gas and by radiation and conduction with surrounding materials. The rate of change of graphite temperature at any point is controlled by the unbalance in heat input and removal and is therefore a complicated function of time after scram, axial and radial core position, and the coolant-air mixture heat removal capability and oxygen partial pressure.

The time-temperature response at any position in the core graphite can follow any of the three basic response curves illustrated in Fig. 5.35. These curves are not intended to include all the possible temperature responses following a coolant system rupture. For example, the initial consequence of coolant depressurization may be a sharply increased heat load from the fuel element to the graphite surface of the coolant channel. The surface graphite temperature increase will, in most cases, be damped out by conduction across the graphite before the containment building air could displace the normal coolant gas and contact the core graphite. A short-term effect such as this is ignored in Fig. 5.35 to demonstrate the more important long-term effects that determine whether or not runaway oxidation could occur.

Curve A in Fig. 5.35 characterizes a graphite section that is cooled adequately to overcome all heat generation and heat input. Since the graphite oxidation rate decreases with decreasing temperature, the oxidation heat release for this situation decreases with time and runaway oxidation is positively prevented. The cooling characteristic of curve A is expected at the coolant inlet portion of the core where coolant and initial graphite temperatures are lower than in the remainder of the core.

The graphite temperature transient illustrated by curve B depicts a condition in which there is initially a period of insufficient cooling,

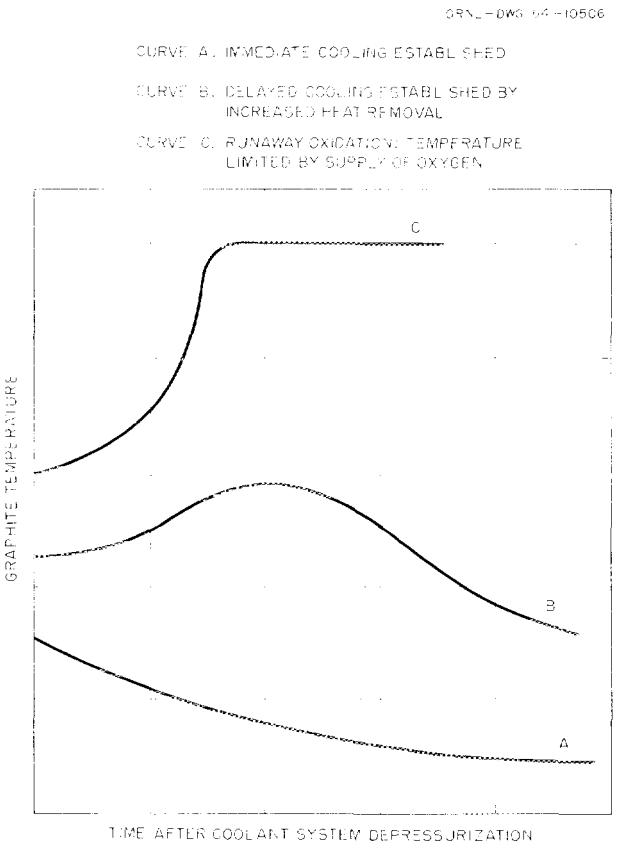

Fig. 5.35. Generalized Graphite Temperature-Time Responses Following Exposure to Air.

during which oxidation heat generation increases with the increasing temperature. The graphite heat balance gradually shifts so that cooling predominates from decreasing afterheat with time and also from increased heat transfer to the coolant channel. The coolant temperature at locations where continuous cooling occurs, as in curve A, decreases with time. As a result the coolant heat removal capability increases in the middle portion of the core. The main feature of the curve B temperature transient is its delayed cooldown result. Initially the graphite oxidation rate is not decreased by available heat removal mechanisms. The graphite heat capacity serves to absorb the excess heat input until changing conditions establish a net cooling situation.

The curve C temperature transient of Fig. 5.35 shows the runaway oxidation situation to be a rapidly increasing transient that results in uncontrollable oxidation at temperatures from 2200 to 3700°F. The relatively rapid temperature rise results from the high rate of oxidation heat release that is usually difficult to control by convection cooling above about 1300°F. The runaway oxidation temperature excursion is finally limited by the rate at which oxygen reaches the graphite surface through the stagnant gas film that forms because of the rapid evolution of hot reaction products, CO and CO_2. There are three characteristics of runaway oxidation that increase the hazards to a gas-cooled reactor containment system:

1. The high temperatures in the vicinity of runaway oxidation may cause metal-clad fuel elements to fail or even melt and thus increase the fission-product burden on the containment system.

2. Once runaway oxidation has started, it is difficult to "blow out" by increasing the mass flow rate of air. The oxidation heat release rate increases with increasing mass flow because the mass transfer of reactant and product gases increases; therefore the graphite temperature also increases with increasing mass flow rate of air. This result has been observed for nuclear grade and other types of graphite. The hazard of this aspect of runaway oxidation is the inability to cool the graphite, even with high air coolant flow rates.

3. The high graphite temperatures from runaway oxidation cause CO to be the predominant reaction product of the graphite surface reaction. The CO can subsequently be oxidized to CO_2 when contact with O_2 occurs in the gas stream. Thus the gas stream can be heated by the $CO \rightarrow CO_2$ heat of reaction in addition to the heat transferred to the gas by convection.

4. Depending on the coolant system rupture size and configuration, much of the graphite oxidation chemical energy could be transferred to the containment system and cause excessive pressure and temperature in the containment system.

3. Analysis of Air-Cooling Requirements to Prevent Runaway Oxidation. A gas-cooled graphite-moderated reactor must, in general, be designed to prevent runaway air oxidation following a primary coolant system rupture. This unique requirement must be satisfied simultaneously with the requirement for afterheat removal by forced or natural circulation of a gas coolant. There are three basic methods currently proposed or utilized to prevent runaway graphite oxidation, as listed in Table 5.16.

Table 5.16. Methods of Preventing Runaway Air-Graphite Oxidation in Gas-Cooled Power Reactors

Description of Method	Example
1. Provide sufficient air cooling from gas circulators in sound coolant loops	
2. Provide relatively inert gas (N_2) to purge out and prevent significant in-leakage of air during afterheat removal by forced circulation of purge gas by an "emergency cooling loop"	Experimental Gas Cooled Reactor (USAEC), Oak Ridge, Tennessee
3. Provide relatively inert atmosphere (N_2) in the containment vessel to reduce air in-leakage to a tolerable level	High Temperature Gas Reactor (General Atomic), Peach Bottom, Pennsylvania

The material in this section deals primarily with the first method of preventing runaway air-graphite oxidation. The conditions under which air cooling is desirable must usually be determined because air cooling may be (1) the most likely result of a depressurization accident and (2) the most attractive method for removing afterheat and cooling the core.

There are two basic approaches to the analysis of air-cooling requirements: the experimental and the computational. An exclusively experimental approach entails a full-scale experiment, such as an experiment in an in-pile loop in an operating graphite-moderated reactor in which air is passed through a coolant channel after a reactor scram. To be a valid experiment for a future reactor, the neutron exposure dose to the graphite would have to be accumulated to the level expected, axial temperature and neutron flux profiles would have to be very similar to the profiles expected, and provisions for maintaining adiabatic conditions should be included in the experiment design to minimize radial heat losses. The direct experimental approach has not been and probably will not be used because (1) it is virtually impossible to satisfy the above requirements in a test reactor environment, (2) in-pile testing is comparatively expensive, and (3) the large in-pile loop facilities required for full-scale graphite-channel experiments are not readily, if at all, available.

The computational method, based on a comprehensive experimental investigation, is recommended for determining the air-cooling requirements to prevent runaway air-graphite oxidation. This method consists of mathematically modeling the afterheat generation, heat transfer, and graphite-air oxidation mechanisms across a section of the air coolant flow and applying heat and oxygen mass balances along the path of the air coolant. The system heat balance may be based on the assumption of an adiabatic condition, in the case of a single fuel channel, or on a boundary heat loss condition, in the case of a pebble-bed reactor core configuration. The use of high-speed digital computers to calculate the temperature transients of a fuel-graphite system is an essential part of the computational method. Once a valid model is constructed and programmed, the effects of many variables on the oxidation characteristics during the calculated temperature transient can be determined more easily and quickly than with full-scale experiments. However, the computational method is no better than the model on which it is based. When simplifying assumptions are made either for lack of experimental information or to expedite the computational procedure, they must be made in a conservative manner. Therefore calculated results have the disadvantage of being somewhat nonrealistic, since they are dependent on the fidelity with which graphite-air oxidation under accident conditions can be simulated.

Heat and Oxygen Mass-Balance Equations. The basic equations in a graphite-air oxidation-transient calculation are the heat and oxygen mass-balance equations applied to the coolant, graphite, fuel element, and other components exchanging heat with the graphite or coolant. These equations are applied to an axial section of a fuel channel, that is, a section across which the coolant flow passes. The symbols used in the balance equations are defined below, and consistent units are given:

A = cross-sectional area, ft^2,
C_p = coolant heat capacity, $Btu/lb \cdot {}^\circ F$,
$\bar{G}$ = volumetric heat capacity, $Btu/ft^3 \cdot {}^\circ F$,

h = coolant heat transfer coefficient, Btu/hr·ft^2·°F,
ΔH = heat of oxidation, Btu per mole of graphite,
M = mole weight, lb/lb-mole,
P = perimeter, ft,
Q = heat input per unit distance along flow path, Btu/hr·ft,
T = temperature, °F,
t = time, hr,
W = coolant mass flow rate, lb/hr,
w = weight fraction of oxygen in coolant, lb of O_2 per lb of coolant,
X = distance along coolant flow path, ft,

and the subscripts are g for graphite, c for coolant, f for afterheat, ox for oxidation, rad for radiation, and cond for conduction.

A heat balance on an assumed isothermal graphite section in contact with air coolant gives the following equation:

$$A_g G_g \frac{dT_g}{dt} = Q_f + Q_{ox} + Q_{rad} + Q_{cond} - h_g P_g (T_g - T_c) \ . \qquad (5.16)$$

Heat inputs Q_{rad} and Q_{cond} could be positive or negative, depending on surrounding temperatures. Axial heat conduction between adjacent sections can often be ignored, since such heat exchange may be relatively insignificant. In such instances the Q_{cond} term in Eq. (5.16) may be dropped and the calculational procedure in digital calculation simplified considerably. Ignoring axial conduction is a conservative assumption, since it allows heat to "pile up" at the highest temperature locations where oxidation heat release is also highest.

Heat and oxygen mass balances for the coolant are given by

$$W_c C_p \frac{\partial T_c}{\partial X} = h_g P_g (T_g - T_c) = \sum_i h_i P_i (T_i - T_c) \qquad (5.17)$$

and

$$W_c \frac{\partial w}{\partial X} = - \frac{Q_{ox} M_{O_2}}{\Delta H} \ . \qquad (5.18)$$

The summation expression in Eq. (5.17) applies to all other surfaces with which the coolant has contact. Oxygen depletion in the coolant calculated by the use of Eq. (5.18) is based on the assumption of one mole of oxygen consumed per mole of carbon reacted, or complete oxidation of carbon to CO_2.

Oxidation Heat Release. The most distinctive characteristic of graphite-air oxidation calculations is the additional oxidation heat source, which varies with time and axial location as the graphite temperature and oxygen partial pressure in the coolant change. The local oxidation heat release rate, q_{ox} (Btu/hr·ft^3), is calculated by use of the expression

$$q_{ox} = \frac{\Delta H}{M_g} \rho_g K \left(\frac{wM_c}{0.21M_{O_2}}\right)^n , \tag{5.19}$$

where, in addition to terms defined above,

ρ_g = graphite density, lb/ft^3,
K = chemical reaction rate in 1 atm of air (ratio of mass of carbon reacting per hour to mass of carbon),
n = order of reaction, $0 \leq n \leq 1$, dimensionless.

The term $wM_c/0.21M_{O_2}$ is the mole fraction of air in any gas coolant containing air; the mole fraction of oxygen in air is 0.21. Oxidation heat input per unit of axial distance, Q_{ox}, is obtained simply from

$$Q_{ox} = q_{ox} P_g L = \frac{\Delta H}{M_g} \rho_g K \left(\frac{wM_c}{0.21M_{O_2}}\right)^n P_g L , \tag{5.20}$$

where L is the effective oxidation depth in feet. The most important variables of a particular type of graphite that influence the oxidation heat release are, from Eq. (5.20), K and L.

Heat of Reaction. The value of the heat of reaction, ΔH, used in Eq. (5.20) must be chosen to cover several exothermic reaction mechanisms. The possible exothermic reactions and heats of reaction (from ref. 59) in a graphite-air system are shown below:

Reaction	$\Delta H_{25°C}$ (kcal/g-mole)
$C + O_2 \rightarrow CO_2$	-94.052
$C + 1/2\ O_2 \rightarrow CO$	-26.416
$CO + 1/2\ O_2 \rightarrow CO_2$	-67.636

The primary reactions that yield CO_2 or CO release heat at the reaction site. Since oxidation of CO to CO_2 occurs in the gas phase, the corresponding heat of reaction could be released either in the graphite pores or in the flowing gas stream after CO mass transfer by diffusion. Investigations by Schweitzer and his co-workers[60] on the oxidation properties of air-cooled, graphite channels showed heat release in the air stream from CO-to-CO_2 oxidation to be significant at higher graphite temperatures. The several oxidation heat release mechanisms make an accurate oxidation heat release calculation impossible with the simple model proposed in Eqs. (5.16) through (5.20). A conservative value of ΔH = 94.052 kcal per mole of carbon reacted or 1.693×10^5 Btu/lb-mole is therefore used in Eq. (5.20). This value allows for the highest local heat release from the $C + O_2 \rightarrow CO_2$ reaction and makes runaway oxidation more likely than would actually be the case.

Graphite-Air Reaction Rate. The chemical reactivity of graphite depends on many variables, as discussed in a later section. The chemical reaction rate in air, K, for nuclear-grade graphite is controlled largely by its high purity (low ash content and low neutron cross section) and its

polycrystalline grain structure. In order to obtain a reasonable expression for the reaction rate, the results of Prados' investigation[61] are useful, since the reaction rate data cover a range of purity of several graphite specimens and a temperature range of 350 to 750°C. Observed reaction rates in air (fractional weight loss per hour) were corrected for diffusional control if necessary and converted to the reaction rate in one atmosphere of oxygen based on a first-order dependence on oxygen partial pressure. The results for the chemical reaction rate in oxygen, k, are shown in Fig. 5.36, with the sources of data indicated (refs. 62–67).

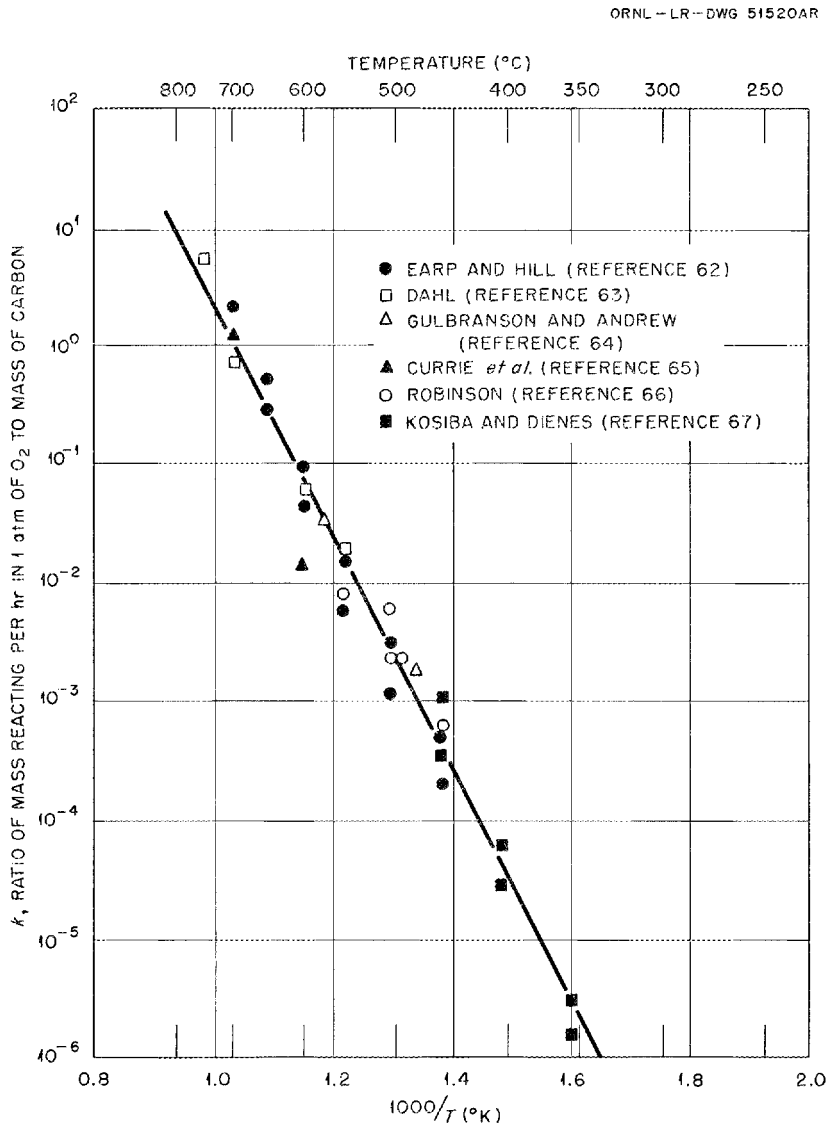

Fig. 5.36. Reaction Rate of Nuclear-Grade Graphite in 1 atm of Oxygen Versus 1/T. (From ref. 61)

Prados correlated these data with the expression $k = 7.24 \times 10^9 \exp(-22{,}100/T)$, for T in °K, which has a 44.0 kcal/g-mole activation energy. The corresponding reaction rate in 1 atm of air is

$$K\ (hr^{-1}) = 1.52 \times 10^9 \exp(-22{,}100/T)\ . \qquad (5.21)$$

The spread of the original data is within a factor of 6 of Eq. (5.21) and is mainly caused by differences in purity and structure within the nuclear-grade graphites. Equation (5.21) gives the general rate magnitude to be expected for nuclear-grade graphite in air; however, sufficient reaction rate measurements for a particular graphite are recommended, unless otherwise available, to confirm its reaction rate characteristics.

Variables Affecting the Reaction Rate. Certain conditions or environments are known to catalyze or inhibit the oxidation rate of graphite in air. The catalytic effects that could apply to reactor core graphite after a coolant system depressurization are neutron irradiation, gamma radiation, water vapor in the coolant, solid phase contaminants, and the size and orientation of the graphite crystals. Rate inhibition or reduction can result from exposure to halogen-containing gases or reduction in oxygen partial pressure from dilution or oxygen burnup. A brief description of these effects is included here with recommended methods of adjusting the reaction rate in air where possible. More detailed summaries of experimental investigations and theoretical implications of these effects are available from refs. 56, 57, and 68.

Neutron irradiation accelerates graphite oxidation rates by concentrating active sites for adsorption, according to Kosiba and Dienes.[69] This rate acceleration decreases as the temperature increases because of self-annealing of the carbon lattice. The effect of low-temperature (25 to 50°C) irradiation of AGOT graphite to an exposure of 4×10^{20} neutrons/cm^2 is shown in Fig. 5.37; the rate increases by a factor of 3 at 450°C (ref. 69). A linear increase in rate with neutron irradiation has been observed[70] to an exposure of 6×10^{20} neutrons/cm^2. The reaction rate after irradiation followed the expression

$$K = K_o(1 + 0.5n)\ ,$$

where K_o and K are rates before and after irradiation and n is neutron dose in units of 10^{20} neutrons/cm^2 (n = 1 for 10^{20} neutrons/cm^2). However, no significant data exist at temperatures above ~400°C and neutron doses of ~10^{22} neutrons/cm^2 that would apply to 20-year-life gas-cooled power reactors. Therefore in-pile graphite irradiations and monitoring of the reaction rate during reactor operation are necessary to provide pertinent reaction rate data.

The gamma-radiation catalytic effect is apparently caused by the gas-phase production of atomic oxygen and ozone (O_3), which is more reactive with graphite than molecular oxygen. This catalytic effect disappears at about 400°C, or at $K \cong 10^{-5}$ hr^{-1}, for gamma fluxes up to 10^6 r/hr, according to Nairn and Wilkinson.[70] The reaction rate increases in gamma fluxes of 2×10^5 and 6×10^5 r/hr are shown in Fig. 5.37; activation energies are reduced to 9.0 and 1.6 kcal/g-mole, respectively.[67] Gamma-radiation

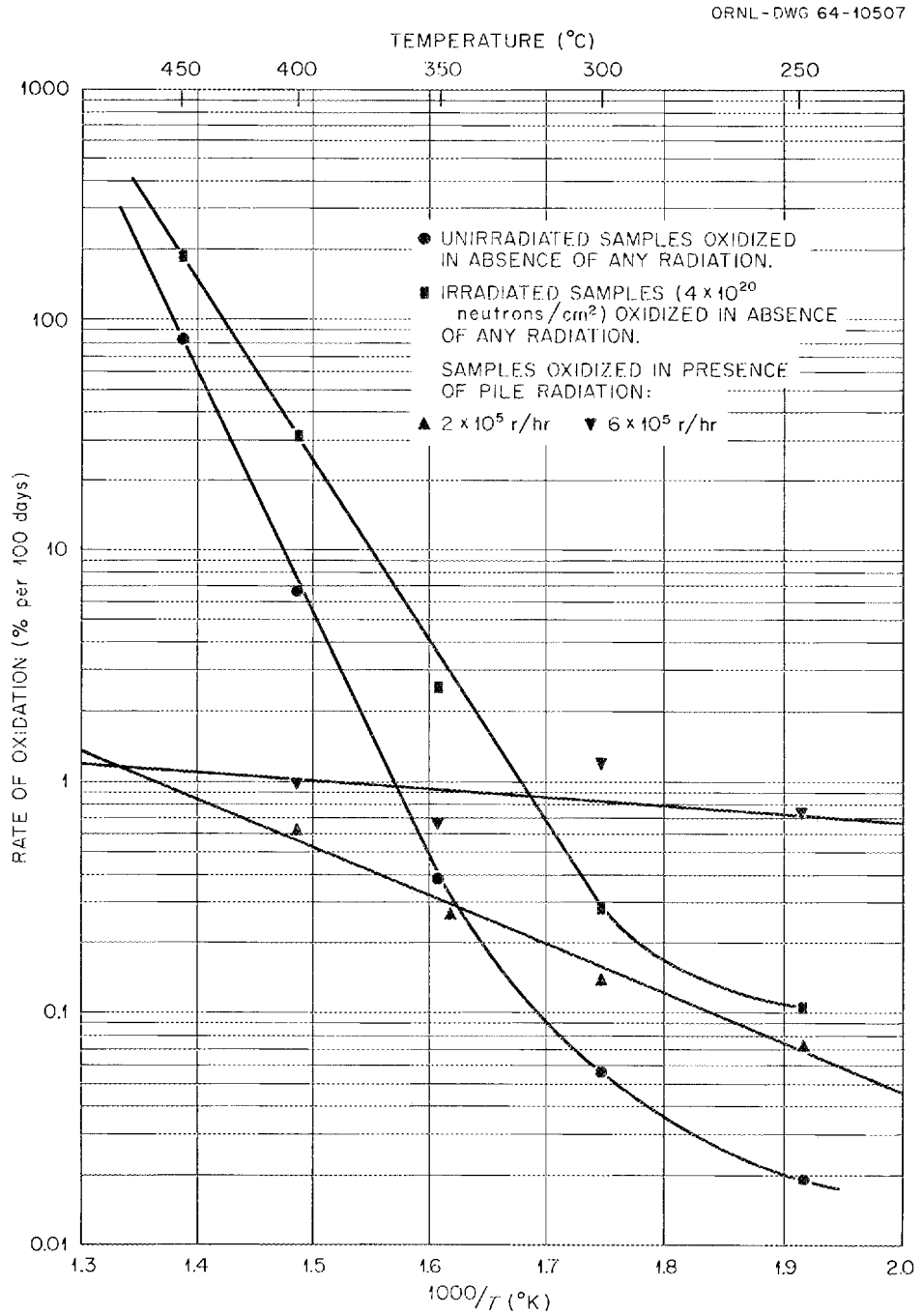

Fig. 5.37. Rate of Oxidation Versus 1/T for AGOT Graphite Oxidized Under Various Conditions. (From ref. 67)

catalysis may have little or no practical effect on graphite-air oxidation in high-temperature gas-cooled reactors because graphite temperatures may be above the threshold for gamma-radiation catalysis. Additional reaction rate data are required if gamma fluxes significantly exceed the 10^6 r/hr level to provide a firm basis for computational analysis. Two reaction rate expressions of the form,

$$K = a \exp(-E/RT) ,$$

can be used to represent the different activation energy reaction rates above and below the threshold temperature for describing this catalytic effect.

The presence of water vapor has been observed to catalyze graphite oxidation in air. However, this effect is significant at very low water vapor concentrations only and depends on the graphite purity. A very slight rate increase was observed by Dahl[71] at 600°C with 0.05 to 20 wt % water vapor; Lang and his co-workers[72] observed, at 620°C, a slight rate catalysis with unpurified graphite and rate inhibition with purified graphite in vapor with between 10.0 and 20,000 ppm (by volume) water. Water-vapor catalysis does not appear to be significant in the temperature range of an operating reactor.

The characteristics of a particular graphite that affect its reaction rate most strongly are its solid-phase contamination and its crystal size and orientation. Solid-phase contamination of graphite can either catalyze or retard the oxidation rate in air. Especially effective catalytic agents are (1) the oxides of iron, cobalt, nickel, copper, and manganese, (2) salts, except borates and phosphates, and (3) alkali metals. Heat treatment at 2500 to 3500°C volatilizes most of the impurities and leads to decreased oxidation rates, as Lang and his co-workers[72] and others have observed. Crystal size and orientation affect the air oxidation rate, since crystal edges are 10 to 200 times more reactive than the basal planes under many conditions. Heat treatment to above 2600°C orders the graphite crystals so that the relative exposure of crystal edges is reduced and leads to a reduction in oxidation rate. Data included in Fig. 5.36 show the scatter caused by these effects. Reaction rate measurements include, directly, the inherent effects of purity and crystal structure for a particular graphite.

Oxidation rate inhibition by halogen-containing gases is of interest in controlling potential runaway oxidation situations. Dahl[73] has investigated rate inhibition by chlorine; the rate reduction from chemisorption of chlorine to block active reaction sites was a factor of 1/5 in dry air. Phosphorus oxychloride ($POCl_3$) also shows promise for potential oxidation inhibition.[68] To date this approach has not been adopted as a practical measure for controlling graphite-air oxidation, although current research will probably result in a practical rate-inhibiting procedure.

The rate reduction with reduced oxygen partial pressure is described by the "order" of the reaction, as in Eq. (5.19). The order was concluded to be "first order, or close to first order" by Walker and his co-workers[56] over a wide range of graphites and temperatures. Data reported by Nairn and Wilkinson[70] show an order of 0.6 to 0.7 at 1 atm of air (21 vol % O_2) that increases toward an order of 1.0 with decreasing O_2. Therefore the

oxidation rate definitely decreases as the oxygen partial pressure decreases, and the order used to describe this effect is probably between 0.6 and 1.0 near 1 atm of air. The order has a significant effect on the oxidation heat release only when low flow of air allows significant oxygen burnup or when dilution of air occurs. Variation of the order, n, between 0.6 and 1.0 can be calculated from Eq. (5.20) to indicate the most serious situation.

In summary, the effects of the variables described above must be allowed for in the relationship used for determining the graphite-air oxidation rate, K. Some conditions, such as crystal size and orientation and solid-phase contamination, are fixed with the type of graphite chosen. Oxidation rate measurements in air therefore include such rate effects. The effects of water vapor in the air, neutron exposure, and gas-phase inhibitors may be included by adjusting the frequency factor, a, in the general oxidation rate expression,

$$K = a \exp(-E/RT) .$$

If necessary the gamma-radiation level effect is best described by a rate expression with a lower activation energy, E, that intersects the normal rate expression at about 400°C. Finally the possible catalytic effects of surface contamination by gas-borne impurities in the reactor coolant system are not usually allowed for before actual reactor operation because of a lack of applicable data. Therefore graphite sampling is used to monitor the oxidation rate of graphite exposed to reactor contamination and irradiation, and any observed catalytic effect is included in the analysis of air-cooling requirements.

Effective Oxidation Depth. The magnitude of the oxidation heat input per unit of axial distance, Q_{ox}, depends directly on the effective oxidation depth, L. When the oxidation rate is low, the oxidation profile is essentially uniform through the porous graphite, as shown in zone I of Fig. 5.34. The depth of graphite available for reaction is therefore the highest limiting value of L for a specific graphite geometry. As the oxidation rate increases in the absence of viscous flow across the graphite, the rate of diffusion of oxygen to the active carbon sites controls the rate of oxidation per unit of exposed surface area. The effective oxidation depth then becomes diffusion controlled, as shown in zone II of Fig. 5.34.

The physical interpretation of L with diffusion-controlled oxidation results from the solution of the steady-state diffusion equation in graphite for the oxygen concentration profile. The oxygen concentration decreases as exp (-X/L), with X being the distance from the graphite surface in contact with flowing gas. The total rate of oxidation within the graphite is therefore equivalent to that from a uniform oxygen concentration profile extending into the graphite a depth L. The theoretical calculation of L, in cm, is based on the following relations:

$$L = \left(\frac{D_p}{k_v}\right)^{1/2} , \qquad (5.22)$$

$$k_v = \frac{\rho_c RT}{M_c} k \ , \tag{5.23}$$

$$D_p = 0.178 \times 3600 \frac{\epsilon^2}{p_T} \left(\frac{T}{273}\right)^{1.75} \ , \tag{5.24}$$

where

D_p = effective in-pore diffusivity of O_2, cm^2/hr,
k_v = "volume" rate constant (ratio of moles of O_2 reacting per hr per volume of graphite to moles of O_2 per volume of gas),
k = chemical rate constant ratio of (mass of graphite reacting per hr per atm of O_2 to mass of graphite),
T = absolute temperature, °K,
ϵ = porosity of graphite (ratio of pore volume to total volume),
p_T = total pressure, atm.

The expression for L results from assuming a first-order reaction and uniform diffusion properties in the graphite. Equation (5.23) is based on the equivalence of 1 mole of carbon per mole of oxygen or complete oxidation to CO_2. The basis for Eq. (5.24) is

$$D_p = \epsilon^2 \times (\text{diffusivity of } O_2 \text{ in gas phase}) \ ,$$

from Walker et al.;[56] the temperature and pressure dependence are taken from gas-phase diffusion properties. Inserting Eqs. (5.23) and (5.24) into (5.22) gives a prediction of the general dependence of L, as follows:

$$L \propto \epsilon (p_T k)^{-0.5} \, T^{0.38} \ . \tag{5.25}$$

The effective depth of oxidation, as derived above, depends on several variables, some peculiar to the graphite and others to the oxidizing conditions. An additional complication is that oxidation within graphite increases the internal surface area available for reaction by increasing the pore size and unblocking originally closed pores.[56,72] These oxidation effects cause the reaction rate* and diffusivity to increase, possibly in a nonuniform fashion within the graphite. Experimental verification of an equation for the effective depth of oxidation is therefore important before this concept can be utilized in graphite-air oxidation analyses.

One such verification experiment was performed by Dahl[71] for National Carbon Co. nuclear grade-2 graphite for which the oxidation rate, K, had been determined. The following equation for L, proposed by Robinson[66] for PGA graphite with A = 0.033, was tested for its validity with sleeves and cylinders oxidized in 1 atm of air from 515 to 660°C:

---

*Increase of the reaction rate is observed directly by oxidizing thin samples in air; the rate increases to a steady value, which is used to determine the graphite-air oxidation rate, K.

$$L(\text{cm}) = A \left(\frac{T}{273}\right)^{0.38} K^{-0.5} \tag{5.26}$$

The results of this investigation were that

1. The dependence on T and K followed Eq. (5.26),
2. The depth constant, A, increased with oxidation as

$$A = 0.0023 + 0.014 \int_0^t K\, dt\ , \tag{5.27}$$

where A is in $(\text{cm/hr})^{1/2}$ and t is time in hours.

This relation held for oxidation at randomly varying temperatures and with oxidation burn-off increasing from zero to about 6%.

In summary, during diffusion-controlled air oxidation of graphite, the amount of graphite undergoing exothermic reaction can be reduced significantly from the entire mass of graphite present. However, sufficient experimental investigation must be performed to allow expressions for K and L to be formulated in terms of calculated variables such as T, K, and $\int_0^t K\, dt$. The experimentally confirmed expressions for K and L can then be used in computer calculation of graphite temperature transients along the length of a graphite-moderated reactor core.

5.2.2.2 Sodium Oxidation

In reactors that use sodium as a coolant, the possibility exists of accidentally exposing the sodium to air at a temperature sufficient to cause spontaneous ignition (exothermic oxidation reaction).[74] The ignition temperature could vary from 70 to 800°F, depending on conditions such as humidity, particle size, and oxide film thickness. Methods of exposure are categorized as follows: stagnant pool, pressurized spray, and explosive ejection. The method of explosive ejection, although the least likely, represents the greatest potential hazard for energy release to a system.

1. Thermodynamics of the Reaction. The reaction between sodium and oxygen (air) is dependent on the proportion of reactants.[75] For excess sodium,

$$2Na + \frac{1}{2} O_2 \rightarrow Na_2O$$

and

$$\Delta H_{25°C} = -4100 \text{ Btu/lb.}$$

For excess oxygen,

$$2Na + O_2 \rightarrow Na_2O_2$$

and

$$\Delta H_{25°C} = -4850 \text{ Btu/lb} .$$

Additional thermodynamic data needed for energy release calculations are listed below:

Heat of fusion, Btu/lb	49
Specific heat, Btu/lb·°F	0.3
Heat of combustion, Btu/lb	
Na_2O as product	4100
Na_2O_2 as product	4850
Melting point, °F	207
Boiling point, °F	1620

2. Rate of Reaction. Experimental studies[76] have indicated that the sodium-air reaction is primarily controlled by a diffusion process. Also, the activation energy in this case is zero. Since the reaction takes place on the surface of the sodium, it is independent of the number of sodium molecules. The combustion rate is therefore given by

$$B = kN_{O_2}T^{1/2} , \tag{5.28}$$

where k is the proportionality constant, N_{O_2} is the concentration of oxygen in the atmosphere, and T is the absolute temperature. The proportionality of the burning rate to the oxygen concentration has been indicated experimentally (ref. 76, p. 7; ref. 77), with a minimum of 4 to 5% oxygen required to support combustion. The water-vapor content of the air represents a complicating factor in that increased humidity decreases the required oxygen concentration for combustion (ref. 75, pp. 19-24). However, the effect is small in the normal humidity range for open air. In an atmosphere sufficiently free of water and hydrogen ($<\sim 10^{-4}$ mm of either), sodium will not burn.

Approximate combustion rates for pools of sodium burning in air were found to be 0.15 to 0.3 lb of sodium per minute per square foot of exposed surface (average rate based on total burning time) (ref. 75, p. 13). This rate increased with depth and decreased with surface area (Figs. 5.38 and 5.39). These data were obtained with air (21% oxygen), and the temperature of the burning sodium was approximately 1250 to 1350°F. It was estimated that nine-tenths of the sodium was burned during the first half of the time. Therefore, the combustion rate during the first half would be approximately 1.8 times the values plotted in Figs. 5.38 and 5.39.

The principal effect in explosive reactions is the rate of sodium surface exposure, which in turn is dependent on the particle size and the mass flow rate of the sodium into a reaction zone. Explosion-dispersion tests[78] using a hydrogen-oxygen explosion to drive and disperse molten sodium at 400°C into a steel vessel (72 ft^3) were conducted to simulate the most severe conditions for hazards evaluations. Peak pressures in these tests

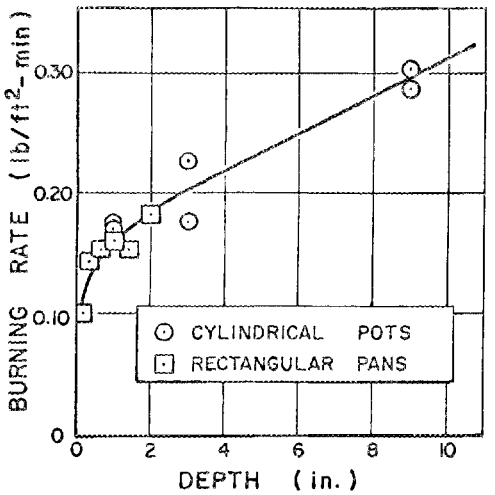

Fig. 5.38. Sodium Burning Rate Versus Depth of Pool. (From ref. 75)

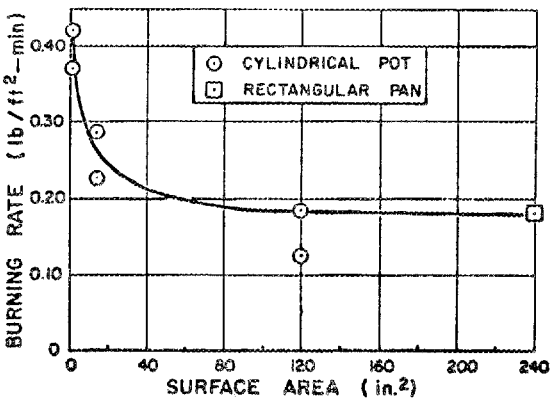

Fig. 5.39. Sodium Burning Rate Versus Pool Surface Area. (From ref. 75)

occurred within 30 to 200 msec from start of ejection and were immediately followed by a rapid pressure reduction (Fig. 5.40).

3. Extent of Reaction. A series of tests was conducted to determine the pressure rise resulting from a sodium-air reaction in a mockup of the gallery of the Sodium Reactor Experiment (ref. 75, p. 29). Molten sodium at 800 to 1000°F was forced through a spray (1/4-in. holes) by pressurized nitrogen into the mocked up gallery (48-ft^3 steel box). The tests indicated the effect on pressure rise of oxygen concentration, sodium temperature, drive pressure, and humidity, as shown in Fig. 5.41 and Tables 5.17 through 5.19.

Parameters studied in the explosion-dispersion tests[78] were (1) quantity of sodium, 200 to 1600 g, (2) distribution, 0.5 to 4 Na-to-O_2 molar ratio, (3) force of ejection, 8 to 22 cal per gram of sodium, and (4) humidity, 2 to 36 g of water vapor in the vessel atmosphere. Test results

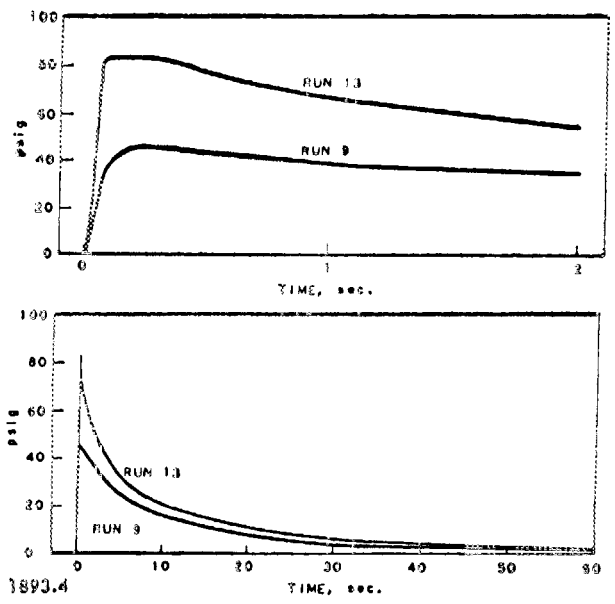

Fig. 5.40. Typical Experimental Pressure Profile for the Oxidation of Molten Sodium Sprayed Into Air. (From ref. 78)

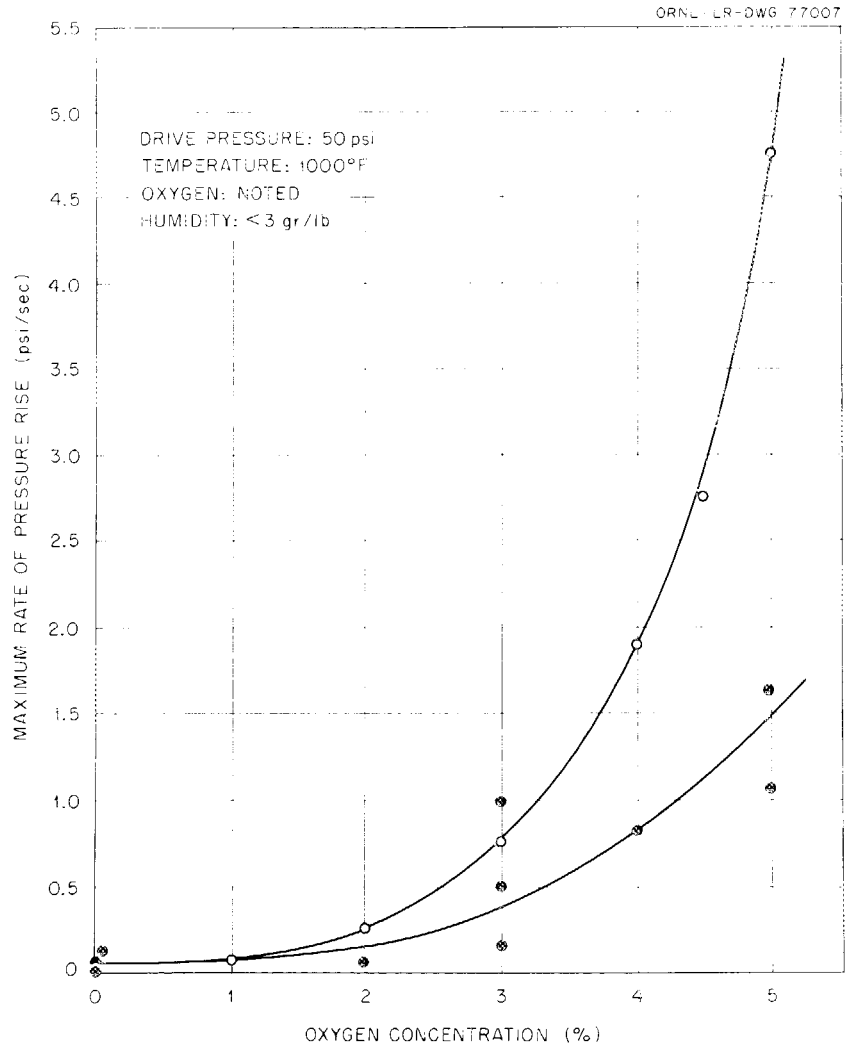

Fig. 5.41. Effect of Oxygen Concentration on Maximum Rate of Pressure Buildup in Gallery. (From ref. 75)

Table 5.17. Effect of Sodium Temperature on Pressure Increase in Gallery Mockup[a,b]

Sodium Temperature (°F)	Oxygen Concentration (vol %)		Maximum Temperature Observed in Gallery (°F)	Test Time (sec)	Maximum Pressure (psig)	Test Time (sec)	Maximum Rate of Pressure Increase (psi/sec)
	Initial	Final					
600	3.0	2.8	440	8	0.8	16.5	0.05
800	3.0	2.6	540	11	1.8	14.8	0.16
1000	3.1	2.5	950	17	3.0	33.0	0.17
1200	3.0	2.7	850	5.8	2.0	14.9	0.20

[a]From ref. 75, p. 34, Table VI.

[b]The following parameters were held constant: initial oxygen concentration, 3 vol %; driving pressure, 50 psi; and absolute humidity, <3 grains/lb.

Table 5.18. Effect of Drive Pressure on Pressure Increase in Gallery Mockup[a,b]

Drive Pressure (psi)	Oxygen Concentration (vol %)		Maximum Temperature Observed in Gallery (°F)	Test Time (sec)	Maximum Pressure (psig)	Test Time (sec)	Maximum Rate of Pressure Increase (psi/sec)
	Initial	Final					
30	3.0	2.6	850	6	2.5	21	0.26
50	3.1	2.4	850	5.8	2.0	15	0.20
60[c]	3.0		750	19.5	4.0	25	0.32

[a]From ref. 75, p. 34, Table VII.

[b]The following parameters were held constant: sodium temperature, 1000°F; initial oxygen concentration, ~3.0 vol %; and absolute humidity, <2 grains/lb.

[c]This run was made at a sodium temperature of 1200°F.

are compared with theoretical calculations of maximum pressure and temperature (based on instantaneous 100% reaction and no heat loss) in Fig. 5.42. In all cases the experimental values are only a fraction of the theoretical maximums because of heat loss to structural materials during mixing and reaction and incomplete reaction of the sodium. The unreacted sodium not only absorbs heat but transfers heat from the atmosphere by impingement on the vessel wall.

Table 5.19. Effect of Absolute Humidity on Pressure Increase in Gallery Mockup[a,b]

Initial Oxygen Concentration (vol %)	Absolute Humidity (grains/lb)	Maximum Temperature Observed in Gallery (°F)	Test Time (sec)	Maximum Pressure (psig)	Test Time (sec)	Maximum Rate of Pressure Increase (psi/sec)
3	<3	950	17	3	33	0.17
	80	1075	5	>3[c]	14.5	0.34
	300	1000	10.5	>4.8[c]	5.0	1.3
4	<3	1225	36	>4[c]	2.5	1.9
	210	1125	11.5	>3.5[c]	1.0	4.3

[a]From ref. 75, p. 35, Table VIII.

[b]The following parameters were held constant: sodium temperature, 1000°F; and driving pressure, 50 psi.

[c]Rupture disk burst.

4. Hazards Calculations. When explosion-dispersion experimental data, representing the most severe case for hazards evaluations, are extrapolated to an actual situation, an attempt is made to achieve optimum reaction conditions in the experimental system. This combination of conditions is extremely unlikely in a reactor accident. However, because of the greater mean diameter of a reactor vessel, the effective heat transfer rate to the wall during the pressure buildup period would be lower. Consequently, the peak pressure would be somewhat higher. Also, the rate of pressure falloff in a large vessel would be less because of the smaller ratio of the surface area available for cooling to total gas volume.

When the accident to be considered involves combustion of a pool of sodium, an appropriate burning rate at zero time can be assumed from the experimental data. If the oxygen supply is limited, combustion can be determined, as follows, until the oxygen concentration is depleted to approximately 4%. Thus

$$\frac{B(t)}{B(0)} = \frac{N_{O_2}(t)}{N_{O_2}(0)} \left[\frac{T(t)}{T(0)}\right]^{1/2} \tag{5.29}$$

and

$$N_{O_2}(t) = N_{O_2}(0) - b \int_0^t B(t')\, dt' , \tag{5.30}$$

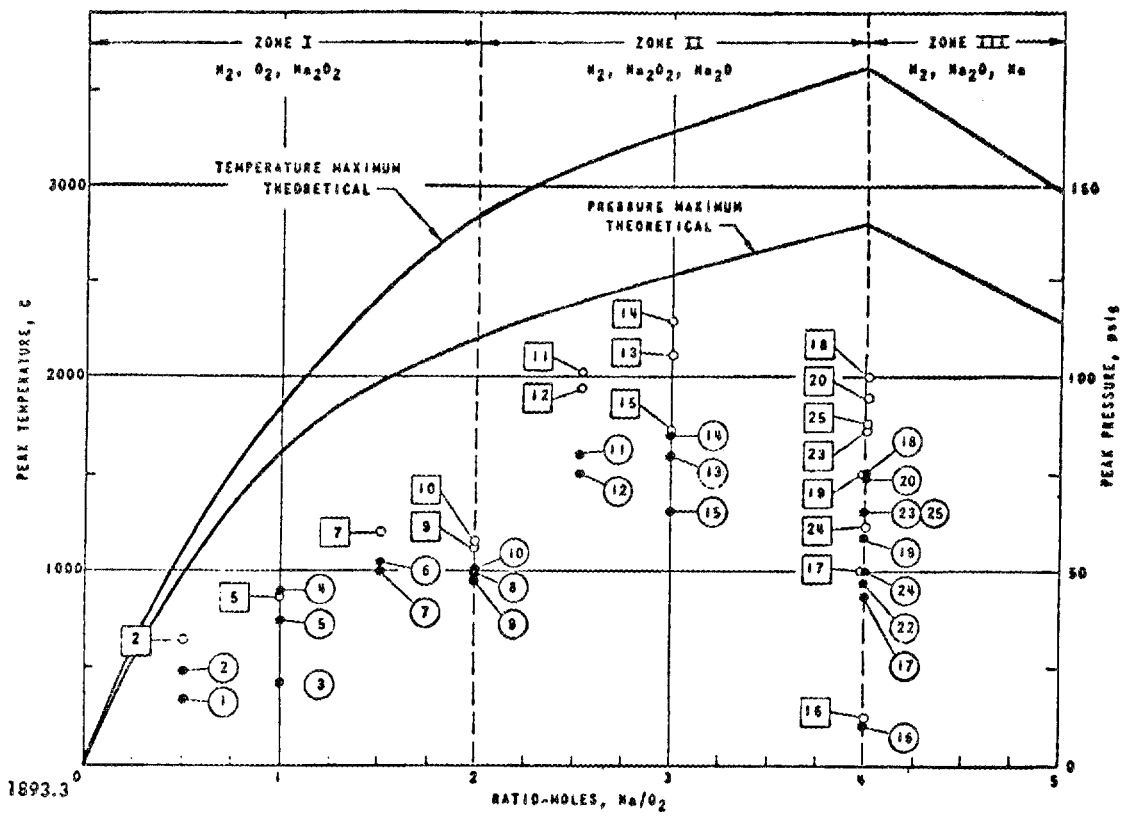

NOTES:

1. CURVES INDICATE MAXIMUM POSSIBLE PEAK PRESSURES AND TEMPERATURES BASED ON:
   (a) 100% REACTION OF SODIUM OR OXYGEN, WHICHEVER IS LIMITING.
   (b) INSTANTANEOUS REACTION (WHICH IMPLIES NO HEAT LOSS; OR, PERFECT DISTRIBUTION, INFINITE PARTICLE VELOCITY, AND INFINITESIMAL PARTICLE SIZE OF THE SODIUM).
   (c) THE FOLLOWING AVERAGE SPECIFIC HEATS ARE ASSUMED:
   $C_v(N_2) = 4.82 + 3.3 \times 10^{-4}t - 4.7 \times 10^{-8}t^2$ cal/mole°C
   $C_p(Na_2O_2) = 0.31$ cal/g °C
   $C_p(Na_2O) = 0.31$ cal/g °C
   $C_p(Na) = 0.31$ cal/g °C
   (d) INITIAL SYSTEM CONDITIONS
   P(ATMOSPHERIC) = 14.5 psi
   T(ATMOSPHERIC) = 20°C
   T(Na) = 600 C
   O_2(ATMOSPHERIC) = 20%

2. EXPERIMENTAL DATA ARE INDICATED AS FOLLOWS:
   (A) = EXPERIMENTAL PEAK PRESSURE (MEASURED), RUN A.
   [A] = EXPERIMENTAL PEAK TEMPERATURE (CALCULATED FROM MEASURED PEAK PRESSURE), RUN A.

Fig. 5.42. Peak Pressure and Temperature Versus Na-to-O_2 Molar Ratio. (From ref. 78)

where b is a conversion factor relating the total amount of sodium burned to the amount of oxygen consumed. Substitution and differentiation then give

$$\frac{dx}{dt} = \frac{x}{2T}\frac{dT}{dt} - \alpha x T^{1/2} , \qquad (5.31)$$

where $x = B(t)/B(0)$, and $\alpha = bB(0)/N_{O_2}(0)\ [T(0)]^{1/2}$.

5.2.2.3 Organic Coolants

Organic liquids used as coolants in reactors represent a possible combustion and/or explosion hazard, since their flash points are below the operating temperatures for most of these reactors. An additional hazard results from the radiation-induced degradation of the organic coolant to hydrogen, methane, ethane, propane, and similar gases, which have explosive properties.

1. Liquid Flammability. Materials that have been tested are (1) monoisopropylbiphenyl (MIPB), (2) Santowax-R, (3) biphenyl, (4) meta-terphenyl, (5) ortho-terphenyl, and (6) a eutectic mixture of (3), (4), and (5). Two types of exploratory tests were used to estimate combustion hazards: ignition of macroscopic quantities of a material in an open pan to simulate storage area problems and ignition of hot organic vapor escaping from a high-temperature system to simulate leaks in a reactor piping system. Results from exploratory experimental tests[79] are summarized in Table 5.20. The vapor tests were conducted at approximately 350°C and 350 psi and indicated that spontaneous self-ignition occurred. A more complete investigation[80,81] of Santowax-R produced the results given in Table 5.21. Thermodynamic and physical data for the various organic coolants are summarized in Table 5.22. Although heat of combustion data were not available for these compounds, data on similar compounds indicate a heat release of about 9.6 kcal/g.

In actual reactor installations, the combustion of organic coolants is extremely improbable.[82-84] Access of air to the coolant is difficult. Under accidental conditions that could lead to contact between air and coolant, the temperature would drop too low to sustain combustion of the coolant, a commercial mixture of terphenyls, such as Santowax-R.

2. Decomposition Gases. The principal gas produced by radiolytic decomposition of organic coolants is hydrogen. Results from a typical run in MORE,[85] along with flammability properties of the gases,[86] are included in Table 5.23.

The decomposition rate of the organic coolant is a function of the amount of energy absorbed by the coolant, which in turn is dependent on the geometry and materials of the core in question, the power level, and the high-boiler content of the coolant. Experimental data indicate that for the Piqua OMR, about 350 ft^3 of decomposition gases will be produced per hour.[85]

3. Hazards Calculations. Systems that operate with organic coolants are generally designed to preclude the occurrence of conditions favorable to explosion or combustion. The data presented here can be used to define such conditions.

Should combustion occur, a heat release of 9.6 kcal/g could be assumed as long as conditions conducive to combustion existed. Of major importance in this respect are temperature and oxygen supply. The burning rate should not exceed that of the more readily combustible hydrocarbon fuels, that is, several inches per hour.

5.2.2.4 Hydrogen-Oxygen Reaction

The reaction between gaseous hydrogen and oxygen in a reactor system presents potential explosion and combustion hazards. Either reaction would

Table 5.20. Organic Fire Characteristics[a]

Name of Organic Compound	Test Type	Response to							Comments
		Water	CO_2	Powder	Plate (red hot)	Torch	Electric Spark	Flash Back	
Santowax-R	Open pan	Good	Fair	Fair	No blaze	Ignited when hot	Ignited when boiling	No	Very hard to melt; black smoke with crystals; easy to ignite; water caused froth
meta-terphenyl	Open pan	Good	Fair	Fair	Not tried	Ignited when hot	Ignited when boiling	Yes	Melted slowly; hard to ignite; powder caused a froth
Biphenyl	Open pan	Good	Fair	Fair	No blaze	Ignited when boiling	Ignited when boiling	Yes	Hard to melt; hard to ignite; easiest to control; crystals in vapor
ortho-terphenyl	Open pan	Good	Poor	Fair	No blaze	Ignited when boiling	Ignited when boiling	Yes	Easy to melt; hard to ignite; lazy fire; burned with water in pan
Tertiary eutectic	Open pan	Good	Poor	Fair	No blaze	Ignited when hot	Ignited when boiling	Yes	Ignited before boiling; black, sooty smoke; easy to reignite
Monoisopropylbiphenyl	Open pan	Good	Poor	Poor	No blaze	Ignited when boiling	Ignited when boiling	No	Ignited only when boiling; hot fire; black, sooty smoke; only water would extinguish
Tertiary eutectic	Hot pressure	Good	Good	Good	No blaze	Ignited when sheltered	Ignited when sheltered	No	Vapor laden with liquid; incomplete combustion; easily extinguished
Monoisopropylbiphenyl	Hot pressure	Good	Good	Good	No blaze	Ignited every time	Ignited when deep in vapor	No	Very dense vapor; well vaporized; easily extinguished

[a]From ref. 79, p. 7, Table II.

Table 5.21. Combustion and Explosion Hazards of Santowax-R[a,b]

Property	Results	Comments
Dust explosion limits	0.035 oz/ft^3 of air, min	Similar to coal dust in this respect
Spontaneous ignition temperature for vapor	993°F at 0 psi delay time = 41 sec; 811°F at 100 psi delay time = 130 sec	Although these values were determined for para-terphenyl, they are considered applicable here
Vapor temperature limits of flammability	375–550°F at 0 psig	Derived from para-terphenyl data using vapor pressure ratio
Flammable concentration limits for vapor	0.48–3.7 vol %	These values are based on data for similar compounds, i.e., ratios of 0.53 ± 0.03 and 3.4 ± 0.5 times the stoichiometric concentration[c]

[a]From ref. 80, pp. 3–5; ref. 81.

[b]A commercially available mixture of terphenyls; about 30% para-terphenyl, 60% meta-terphenyl, 10% ortho-terphenyl, and <1% diphenyl.

[c]The stoichiometric concentration is that concentration at which, if an ideal combustion occurred, all the compound would be oxidized to CO_2 and H_2O and all the oxygen in the air would be reacted (0.96% for Santowax-R).

add heat to the system, whereas additional damage from shock waves and missiles could result from a detonation reaction.

1. Initiating Conditions. Hydrogen can be generated in a nuclear reactor by chemical reaction and by radiolytic decomposition of water. Possible chemical reactions involving reactor materials are

$$Zr + 2H_2O \rightarrow ZrO_2 + 2H_2 ,$$

$$2Al + 3H_2O \rightarrow Al_2O_3 + 3H_2 ,$$

$$U + 2H_2O \rightarrow UO_2 + 2H_2 ,$$

$$Fe + H_2O \rightarrow FeO + H_2 ,$$

$$C + 2H_2O \rightarrow CO_2 + 2H_2 .$$

These reactions are discussed in more detail in Section 5.2.1. Radiolytic decomposition occurs when water is exposed to ionizing radiation. A reasonable value appears to be that 1 molecule of hydrogen is produced per 100 ev of energy absorbed.[87] The overall reaction is represented by

$$H_2O + e^- + H_2 + \frac{1}{2} O_2 .$$

Table 5.22. Physical Properties of Organics[a]

	Monisopropyl-biphenyl[b]	Tertiary Eutectic[c]	meta-terphenyl[d]	ortho-terphenyl[d]	Biphenyl[e]	Santowax-R[d]	para-terphenyl[d]
Molecular weight	230.3	Mixture	230.3	230.3	154.2	230.2	230.3
Critical temperature, °F			1117	1039	924		1150
Melting point, °C	−70°F	10.5	87.45	56.25	69.5	145	212.7
Boiling point, °C	300	297.5	364	332	254.9	364	385
Flash point, °C	139	140	405	340	113	375°F	410
Fire point, °C	152	148	445	380	123	460°F	460
Heat of vaporization, Btu/lb			115	109	137		117
Specific gravity at 0°F or m.p.	0.9847	1.02	1.03	1.05	1.01	1.16	1.06
Heat capacity, Btu/lb·°F at 200°F	0.465	0.41	0.35	0.35	0.36	0.43 at 312°F 0.607 at 550°F 0.628 at 600°F	0.35
Viscosity, centipoises at 200°F	1.42	3.88	3.34	2.38	1.02	3.88	
Thermal conductivity, Btu/lb·ft·°F	~0.71	~0.65	0.062	0.063	0.070	0.074 at 312°F 0.067 at 550°F 0.066 at 600°F	0.076
Autoignition temperature, °F	845	~900	~900	~900	~900	~900	~900

[a]From ref. 79, p. 6-a, Table I.

[b]meta-terphenyl, 62%; para-terphenyl, 38%.

[c]Biphenyl, 30.9%; ortho-terphenyl, 47.5%; meta-terphenyl, 21.6%.

[d]$C_{18}H_{14}$.

[e]$C_{12}H_{10}$.

Table 5.23. Flammability Properties of Gases from the Radiolytic Decomposition of Organic Coolants

Gas	Self-Ignition Temperature (°F)	Flammable Range (vol %)	Flash Point (°F)	Relative Volume Produced in Decomposition (%)
Hydrogen	1085	4.1–74.2		65
Methane	1000	5.3–13.9		10
Ethane	950	3.3–10.6		10
Ethylene	1009	3.2–34		5
Propane	874	2.3–7.3		5
Propylene	927			2
Benzene	1000	1.4–8	12	
Toluene	1026	1.3–7	40	

2. Reaction. The reaction

$$2H_2(gas) + O_2(gas) \rightarrow 2H_2O(gas) ,$$

for which

$$\Delta H_{25°C} = -57.8 \text{ kcal/g-mole of } H_2O ,$$

proceeds as a deflagration or a detonation, depending on conditions. Deflagration (which encompasses the range from flammability to explosion) is characterized by subsonic flame propagation, the movement of which is governed by heat and mass transfer, whereas detonation is characterized by a highly stable shock wave propagated at a supersonic rate.

3. Unsaturated Gas Mixtures. A large quantity of published literature[88,89] may be summarized by the following statements:

1. The lower limit for flammability of hydrogen in air is 4.1% (at room temperature and 1 atm pressure for an upward propagation of the flame).
2. The lower limit for detonation of hydrogen in air at room temperature and 1 atm is 18.3%.
3. For downward propagation of the flame, the lower limit is increased by approximately a factor of 2 (to ~8%).
4. The lower limit for hydrogen-oxygen mixtures is essentially the same as that for hydrogen-air mixtures.
5. Increasing the pressure from 1 to 200 atm only slightly increases the lower limit of flammability.
6. Increasing the initial temperature of the gas mixture from room temperature to 500°C decreases the lower limit by one-third to one-half. The temperature effect is essentially linear.
7. Humidity has only a very small effect on flammability limits.

8. The addition of a diluent gas, for example, carbon dioxide, nitrogen, or helium, has little effect[90] on the lower flammability limit of hydrogen in the gas mixture (see Fig. 5.43a). The effect of steam is shown in Fig. 5.43b (ref. 91).

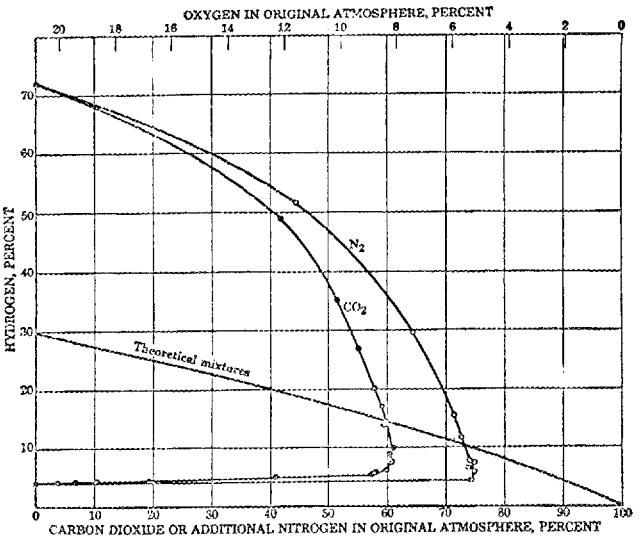

Fig. 5.43a. Limits of Flammability of Hydrogen in Air and Carbon Dioxide or Nitrogen. (From ref. 90)

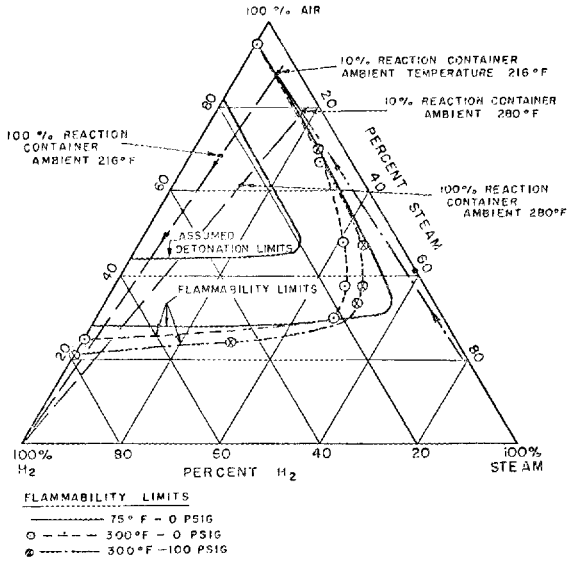

Fig. 5.43b. Flammability Limits of Hydrogen-Air Steam Mixtures. (From ref. 91)

4. Saturated $(2H_2 + O_2)$-Steam Mixtures. For some reactors, for example, the aqueous homogeneous, the environmental conditions are more closely simulated by a saturated mixture of steam with a gas having a stoichiometric ratio of hydrogen to oxygen. A comprehensive study[92] was performed to examine the reactions of knallgas*-steam mixtures for both light- and heavy-water systems. For experimental test conditions (reaction tubes ranging from 0.434 to 2.9 in. in diameter and from 7.5 to 14 ft in length; saturated water vapor at 100, 200, and 300°C; and spark, hot-wire, and shock ignition), the data indicated that (1) the lower limit for reaction of knallgas with saturated heavy steam mixtures was 19 ± 2.7 mole % for the conditions tested, (2) reflected detonation pressures during the unstable stages of detonation were approximately three times theoretical

*Stoichiometric mixture of hydrogen and oxygen $(2H_2 + O_2)$.

reflected pressures calculated from stable detonation equations, and (3) the lower limit for detonation of knallgas and saturated steam mixtures was estimated to be 30 mole %.

5. Hazards Calculations. Since the effect of heat release on containment is considered insignificant for most cases, the hazard results from shock-wave damage. Conservative concentration limits for a wide range of conditions are presented herein. Information on other conditions and more specific data are presented in refs. 90 and 92.

If situations involving explosive concentrations were unavoidable, the resulting pressures could be calculated either on the basis that the reaction heat release is the only effect or on the basis of shock-wave effects. Analytical techniques for these calculations are presented in Chapter 6. The heat release is obtained from heat-of-reaction data and total quantity of reactants, assuming that reactant concentrations remain within the flammability range.

5.2.3 Graphite-Steam Reactions

A reaction between graphite and steam would follow an internal rupture of a steam generator. Steam exposure could occur at either the system relief pressure or near the containment system pressure if the steam release was in connection with a coolant system depressurization. The potential hazard from the steam and graphite reaction arises from the generation of potentially explosive hydrogen and carbon monoxide (CO); the steam-graphite reaction is of itself endothermic.

5.2.3.1 Reactions in a Graphite-Steam Environment

The gasification reaction of the solid carbon is

$$C(\text{solid}) + H_2O(\text{gas}) \rightarrow CO(\text{gas}) + H_2(\text{gas}) \tag{5.32}$$

with

$$\Delta H_{25°C} = +31.4 \text{ kcal/g-mole of C.}$$

Thus CO has been identified as the primary reaction product. The "water-gas," or "shift," reaction

$$CO(\text{gas}) + H_2O(\text{gas}) \rightleftharpoons CO_2(\text{gas}) + H_2(\text{gas}) \tag{5.33}$$

can then proceed in the gas phase, with

$$\Delta H = -9.9 \text{ kcal/g-mole of CO .}$$

Secondary reactions that also occur in the presence of carbon, H_2, and CO are

$$C(\text{solid}) + 2H_2(\text{gas}) \rightleftharpoons CH_4(\text{gas}) \ , \tag{5.34}$$

with

$$\Delta H_{25°C} = -17.89 \text{ kcal/g-mole of C} \ ,$$

and

$$C(\text{solid}) + CO_2(\text{gas}) \rightleftharpoons 2CO(\text{gas}) \ , \tag{5.35}$$

with

$$\Delta H_{25°C} = +41.22 \text{ kcal/g-mole of C} \ .$$

Equilibrium conditions limit the generation of CO_2 and CH_4 as the temperature increases; hence H_2 and CO from Eq. (5.32) are predominant above about 770°C at 1 atm and above about 1000°C at 100 atm total pressure.[56]

5.2.3.2 Reaction Rate Kinetics

Dynamic rate data have been obtained by several investigators[93-96] in experiments using flow systems. The temperature range of interest was above 700°C because higher reaction rates for fuel gasification were the main objective of such studies. Hence little information is available in the operating temperature range of present gas-cooled reactors. The carbon structure used by these experimenters varied widely. For example, Pilcher and his co-workers[93] used electro-graphite of varying ash content (from 0.07 to 0.75%); Johnstone and his co-workers[94] and Blackwood and McGrary[96] used coconut charcoal (a porous industrial graphite).

Steam-graphite reaction rate investigations have yielded the following general observations of the effects of various reaction conditions at temperatures above 700°C:

1. Hydrogen pressure buildup retards the gasification reaction by chemisorption on the active carbon sites.[56]
2. The "shift" reaction, Eq. (5.33), reaches equilibrium rapidly.[94]
3. The reaction rate order, or dependence on H_2O pressure, varies from 0 to 1 depending on the type of graphite and reaction conditions.[56]
4. Reaction rates of graphite with H_2O, as with oxygen, increase with impurities and burn-off[94] and decrease with the degree of graphitization,[93] which controls the grain size and orientation.

The thermal reaction rate of graphite and steam is generally of the same order of magnitude as for graphite and CO_2. Graphite-steam and graphite-CO_2 reaction rates at total pressures below several atmospheres have the form

$$R = \frac{k_1 p_{H_2O}}{1 + k_2 p_{H_2} + k_3 p_{H_2O}} , \qquad (5.36)$$

where R is the ratio of the grams of carbon reacting per hour to the total grams of carbon and p_{H_2O} and p_{H_2} are the partial pressures in atmospheres of steam and hydrogen, respectively. The temperature dependent constants, k_1, k_2, and k_3, are interpreted as follows: k_1, reaction rate per atmospheres of H_2O, depends largely on the rate of adsorption of H_2O on the carbon surface; k_2, atmospheres of H_2^{-1}, is the adsorption-desorption equilibrium constant for H_2 on the carbon surface; k_3, atmospheres of H_2O^{-1}, depends primarily on the rate of reaction between adsorbed H_2O and carbon and the value of k_1. Rates for total pressures up to 50 atm were correlated by Blackwood and McGrary[96] by the expression

$$R = \frac{k_1 p_{H_2O} + k_4 p_{H_2} p_{H_2O} + k_5 p_{H_2O}^2}{1 + k_2 p_{H_2} + k_3 p_{H_2O}} . \qquad (5.37)$$

Available rate values for zero hydrogen pressure are shown in Fig. 5.44.

Reaction rates of graphite and steam in gamma radiation have not been obtained to any significant degree. Gamma radiation would be expected to form ionized and excited species of carbon, hydrogen, and oxygen. The gamma-radiation effect is not expected[57] to be significant above 500 to 600°C because of the much higher activation energy of the thermal reaction.

5.2.3.3 Hazards Calculations

Hydrogen generation rates from reactor core graphite in contact with steam could be calculated using a transient temperature calculation, such as discussed in Section 5.2.2.1 for graphite-air oxidation. The aim of such a calculation would be to determine the rate of hydrogen concentration increase within the primary coolant system, and subsequently to determine whether flammable hydrogen concentrations could exist in the primary coolant system before release or in the containment system after release. Hydrogen generation could be essentially limited by either (1) cooling the graphite to temperatures where the reaction rate is insignificant or (2) blanketing the graphite surfaces with an inert gas.

Conservative hydrogen generation calculations result from assuming 2 moles of H_2 per mole of carbon reacted and no reduction in the reaction rate from hydrogen pressure buildup as the reaction proceeds. However, lack of reaction rate and reaction depth data for nuclear graphite below 700°C makes calculations based on high-temperature data very conjectural and possibly unduly conservative. Therefore determinations of the surface reaction rates (weight of carbon gasified per unit surface area per unit of time) in an isothermal flow system are recommended for the type of graphite, geometry, and flow conditions of interest in a particular reactor system. Such an experimental approach should investigate the effects of temperature, pressure, and oxidation burn-off or exposure. If required, exposure of small graphite samples to steam in a gamma radiation field

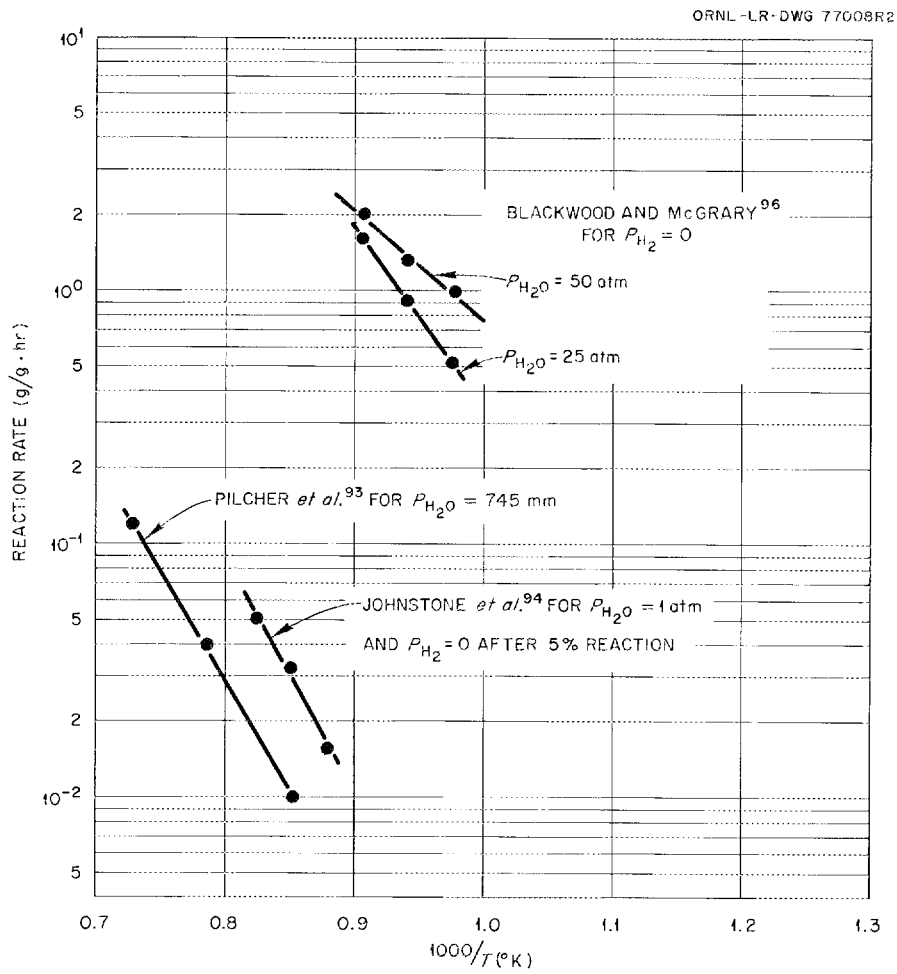

Fig. 5.44. Compilation of Rate Data on the Carbon-Steam Reaction.

could be used to determine the temperature or reaction rate at which the radiation effect becomes significant.

Surface reaction rate data were obtained for the graphite used in the EGCR in a superheated steam recirculating test loop.[97] The inner surface of a 1-in.-thick, 3-in.-ID, 29-in.-long graphite sleeve was exposed to flowing steam (Reynold's Nos. of ~2000 to 4000) at pressures from 50 to 300 psig. Reaction products were bled off and analyzed continuously for CO, CO_2, H_2, and CH_4. Test runs were made with the Speer 901-RYL sleeve graphite and the National Carbon Co. nuclear grade-2 moderator-block graphite; the stainless steel-clad fuel element bundle was also included with a Speer-type graphite sleeve. Surface reaction rates were calculated on the basis of the CO, CO_2, and CH_4 generation rates and the inner sleeve surface area exposed to steam. Figure 5.45 shows surface reaction rates for the Speer graphite sleeve with the fuel element present in the sleeve. Reaction rates for the moderator-block graphite fell within the 1 to 30% burn-off range shown on Fig. 5.45; steam flow rate and pressure were observed to have a small effect on the reaction rate compared with the burn-off effect.

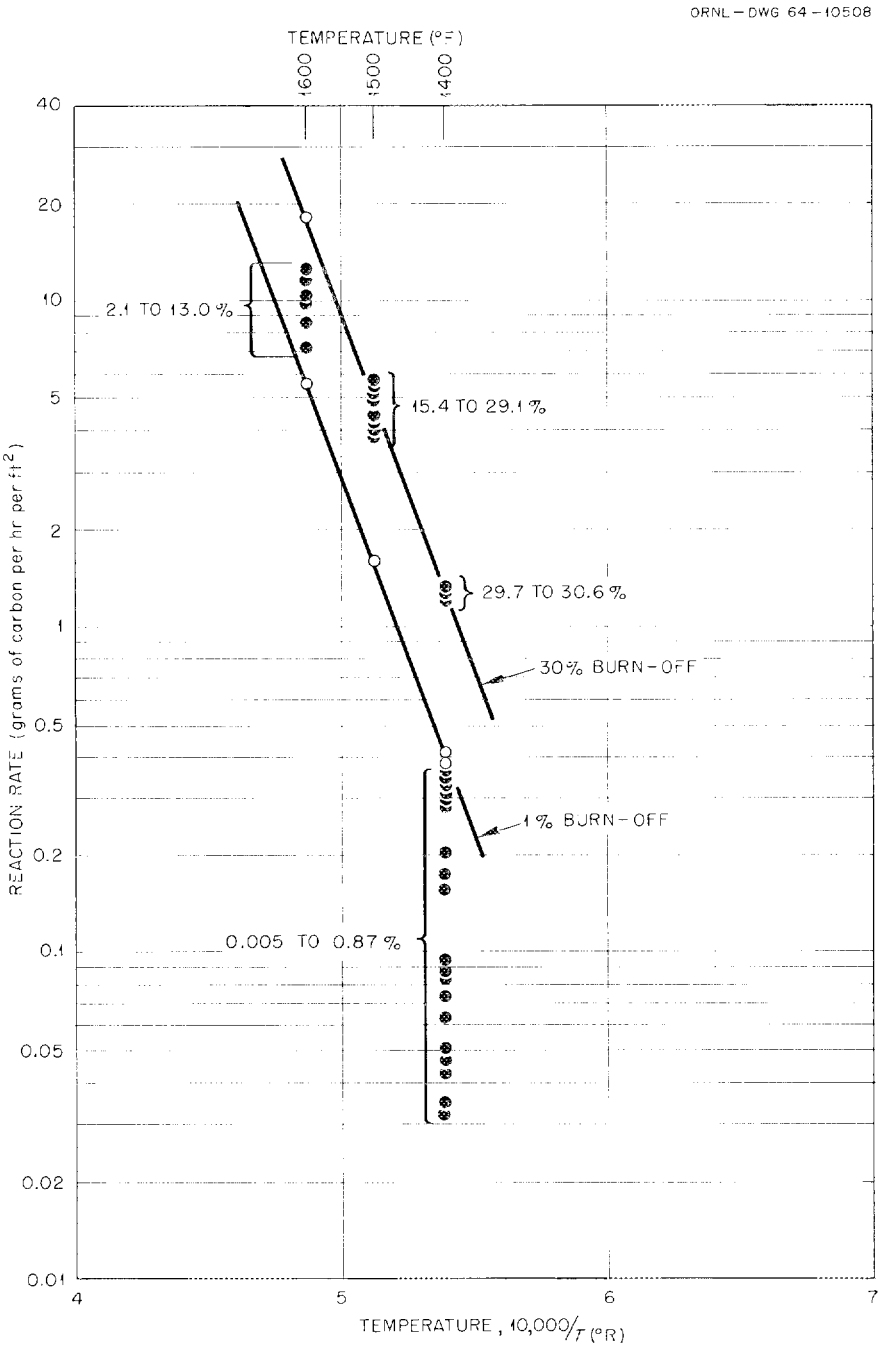

Fig. 5.45. Steam-Graphite Reaction Rate for EGCR Stainless Steel-Clad Fuel Element Graphite Sleeve VI; Speer 901 RYL Graphite.

5.3 NUCLEAR ENERGY

5.3.1 Fission Energy

Energy produced by nuclear fission appears as (1) kinetic energy of fission products, (2) kinetic energy of neutrons, (3) instantaneous gamma rays, (4) gamma rays from fission products, (5) beta particles from fission products, and (6) neutrinos. The heat generated by (1) and (5) is localized close to the place where the fission occurred; energy from (2), (3), and (4) is spread over a large region. Neutrinos do not generate measurable quantities of heat. Additional heat is generated by parasitic capture of fission neutrons, with resulting gamma-ray emission (capture gammas). For slow-neutron fission of U^{235}, the total heat[98] generated is about 200 Mev per fission (Table 5.24). For containment design it also appears adequate to assume an energy release of 200 Mev per fission[99] for U^{233} and Pu^{239}.

Table 5.24. Distribution of Fission Energy[a]

Source	Energy (Mev/fission)		
	Instantaneous	Delayed	Total
Localized release of heat			
Kinetic energy of fission fragments	165 ± 5		
Beta particles from fission products		7 ± 1	
Spread out in space			
Instantaneous gamma radiation	5 ± 1		
Gamma rays from fission products		6 ± 1	
Kinetic energy of neutrons	5 ± 0.5		
Total from fission (direct)			191 ± 6
Neutrinos (do not generate heat)	~10		
Capture gamma radiation (including decay of daughters)	5 ± 2	1 ± 1	
Total for heat generation			~200

[a]From ref. 98.

Data for design calculations are more useful in the better known engineering units (see Table 5.25). Thus

Table 5.25. Heat Generated by Fissionable Material

Conversion Factors	Heat Generated per Gram of Fissionable Material Consumed[a]
1.60×10^{-6} ergs/Mev	8.2×10^{17} ergs
3.83×10^{-14} cal/Mev	2.0×10^{10} cal
1.52×10^{-16} Btu/Mev	7.8×10^{7} Btu
4.45×10^{-20} kwhr/Mev	2.3×10^{4} kwhr

[a]Because of the small variation in molecular weights, this applies equally to U^{233}, U^{235}, and Pu^{239}.

$$\frac{A}{M} \times E_f \times C = \text{heat generated per gram of material} ,$$

where

A = Avogadro's number, 6.02×10^{23} molecules per gram-mole of material,
M = molecular weight of fissionable material, g/mole,
E_f = total energy released for heat generation, 200 Mev per fission,
C = conversion factor.

5.3.2 Power Excursions

5.3.2.1 Introduction

If sufficient excess reactivity were added to a reactor over a very short time, a rapid power rise could result that could destroy the reactor core with explosive violence. For such a catastrophic occurrence, reactor periods in the microseconds to milliseconds range are necessary, and the applicable kinetics equations are those that describe the superprompt critical condition.[100] In general, reactors have such extensive control systems and inherent shutdown mechanisms that catastrophic excursions are extremely remote and, therefore, do not represent a credible accident. Of particular note is the limitation on the size of possible accidents arising from natural constraints on achievable assembly rates of reactivity components. Although reactors have considerable excess reactivity, postulation of a credible means of inserting this reactivity simultaneously and instantaneously is quite difficult.

Reactor runaways are terminated either by buildup of sufficient negative reactivity in the core (self-shutdown mechanisms) or by disassembly (destruction) of the core. Self-shutdown mechanisms that exhibit significant negative reactivity effects in reactors are characterized by the following coefficients:

1. Temperature coefficient, which results from material expansion with increasing temperature and can refer to fuel, moderator, or other core materials.
2. Void coefficient, which results from formation of voids in the core as the result of liquid boiling or radiolytic gas formation.
3. Doppler coefficient, which results from an increased neutron absorption cross section in U^{238} (and others, such as Th^{232}) with increased temperature.

Of particular interest is the time behavior of these shutdown mechanisms; those in which the physical phenomena require relatively long times (greater than milliseconds) to become effective are of lesser importance. In the time period of microseconds to milliseconds, coolant flow, channel pressure drop, and thermal expansion of the coolant are of minor importance, whereas gamma and fast-neutron heating, thermal expansion of the fuel, microbubble formation, and Doppler broadening are the important physical mechanisms. Thus, those mechanisms that directly couple a specific neutronic effect with heating of the fuel by absorption of fission energy are truly prompt and may be more important than normally larger effects that have delays. In this manner the Doppler effect can be the most important shutdown mechanism in a reactor (one which contains relatively large amounts of U^{238}), even though the Doppler coefficient is generally an order of magnitude smaller than the overall steady-state temperature coefficient.

An ideal shutdown mechanism would be one that would be small for very long reactor periods and prompt and strongly negative for short reactor periods. The first requirement is that the reactivity addition necessary to bring the system to operating power be very low, and the second is protection against large excursions. In actual situations, however, many mechanisms normally of importance exhibit sizeable negative coefficients for long reactor periods but also have inherent delays that reduce their effectiveness for short periods.

Prediction of the excursions in existing reactors or those in the design stage generally consists of setting up the analytical equations applicable for specific accident conditions and solving them on a computer. This method, of course, defies generalization and must be evaluated for each individual situation. A description of an event of this type can be enormously complicated, involving intimate details of the design, construction, and operation of mechanical and instrumentation components of the system, as well as requiring information on the physical properties of the materials of the system and on the factors changing the neutronic properties of the system. The great variety of reacting systems adds to the complexity of the overall problem. Also, these calculations merely indicate the existence of dangerous conditions and do not predict energy releases. Thus the numerical analyses of catastrophic situations are reliable only to an order of magnitude because of the present crude understanding of the important physical mechanisms.

The transient calculations of thermal and fast reactors, while similar in many respects, differ sufficiently in the fast-burst range that they are discussed separately in the following sections, which were taken primarily from papers by Nyer and Okrent, respectively. The material presented here is not a complete discussion or review of the subject matter, inasmuch as the present state of knowledge is not adequate to avoid the

simplifying generalizations that so frequently characterize hazards calculations. However, an effort is made to include enough information to clarify the basic physical processes involved and to outline the analytical techniques that may someday be developed to the point where they alone may accurately characterize the nuclear energy in an incident. Until such time, however, the basis for making such analyses for hazards calculations must also be given.

5.3.2.2 Nuclear Excursion Models*

Despite the complexity and diversity of reactors, it has been observed that certain regularities are exhibited by the data obtained in reactor excursion experiments.[101] Furthermore, many similarities can be noted between the observed features of these excursions and the predictions of various simple mathematical models for reactor excursions.[101] The bases on which these models have been postulated vary from situation to situation. In some cases, it is possible to derive a model from a fundamental representation of a reactor system and thereby obtain a description of excursion behavior approaching the full detail outlined in the first paragraph. In other cases, the model serves as a convenient means of breaking the complete problem into parts that can be attacked individually. For example, a detailed calculation can be made in the part of the problem dealing with either the temperature coefficient or the Doppler coefficient; and this, if reducible to a convenient analytical form, may then be combined with a model. In many cases, the difficult task of computing excursion behavior directly from detailed considerations may be supplemented, or in some instances supplanted, by the use of an appropriate qualitative description. The models may range then from being pedagogical devices or handy means of correlating experimental data to theories of reactor excursion behavior.

The experimental situations to be described can, without any significant loss of generality, be limited to the two situations shown schematically in Fig. 5.46 for very fast bursts. In the first case (upper part of Fig. 5.46), it is assumed that the excursion is initiated by effectively adding reactivity to the reactor instantaneously, that is, as a reactivity "step." The initial reactor power is usually taken to be low and the initial reactivity state as delayed critical. In a short time the reactor power begins to rise exponentially with a constant period. Ultimately, the energy release produces effects that begin to cause a decrease in reactivity. As these reactivity losses continue, the power passes through a maximum and, on a typical fast transient, decreases to a low value. Although this idealized representation presents the essential character of a power excursion, an actual excursion may be rich in detail, with many other distinctive features being possible (see, for example, the features pointed out in a discussion by Horning and Corben[102]).

The lower part of the figure shows the behavior, on a linear plot, of the logarithmic derivative of the power (the reciprocal period), which is defined as the quantity α. It is only under special conditions that α, which is an observable feature of major importance, can be readily identified with the system reactivity. It will be assumed throughout this discussion that these conditions are satisfied so that either the computation of reactivity from α or the identification of α directly with the prompt reactivity[103] may be made.

---

*This section was condensed from a comprehensive summary by W. E. Nyer entitled Mathematical Models of Fast Transients; see Chap. 7, Vol, I, ref. 109.

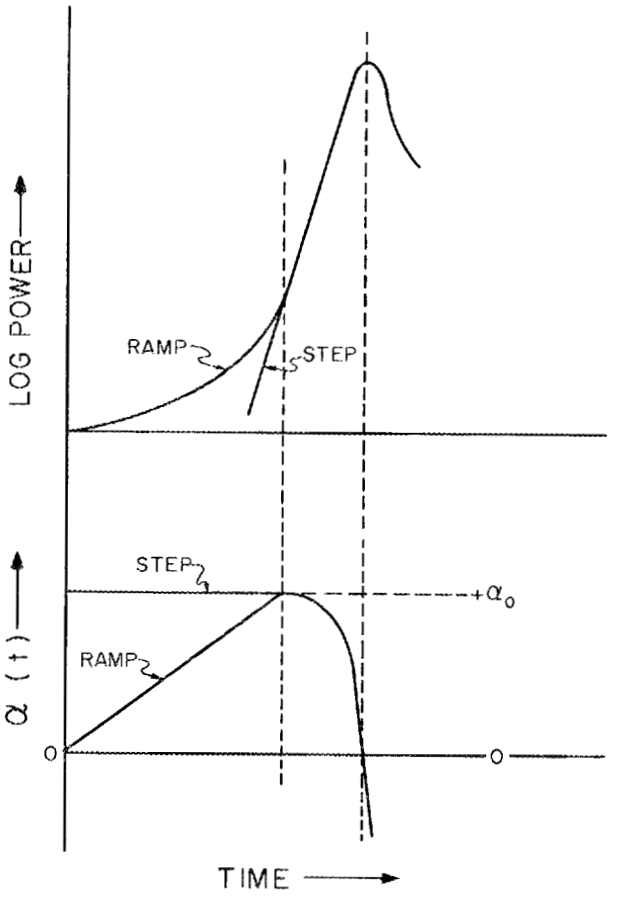

Fig. 5.46. Power and Reactivity Behavior During Reactor Excursions.

The second form of power burst, also shown in Fig. 5.46, is that in which the reactivity is introduced linearly with time under initial conditions assumed to be the same as for the step case. This linear or "ramp," addition of reactivity, shown as the curve labeled ramp on the lower part of the figure, corresponds to the gradually decreasing period for the power rise indicated on the ramp power curve (upper part of figure). In the next stage of the excursion, the energy release brings into effect, to a significant degree, the mechanisms that tend to decrease the reactivity. When the rate of reactivity loss rises to the point that it is equal to the rate of insertion, the reactor period has its minimum value, that is, α is maximum. From this point on, the development and final quenching of the burst is essentially the same as for a step transient in which the initial period is equal to the minimum period for the ramp test.

In both these cases the reactivity functions, α, are marked by two features. There is, initially, negligible departure of the reactivity from the input step or ramp. This is followed by a very rapid departure, which almost abruptly decreases the reactivity to zero. The difference between the step or ramp-inserted reactivity and the instantaneous reactivity at any time is called the compensated reactivity.

Although the physical factor of primary importance in such a burst is the time history of the energy release, from both the analytical and experimental points of view it is often more convenient to describe a burst in terms of its power history or other selected burst parameters. The latter can be simply the burst width taken at some fraction of the peak power, the energy release at some particular time, such as the power peak, the time in periods to the peak, or some combination thereof. These factors are not all of fundamental significance but are merely convenient ways of describing the shape of the burst. In any case, whichever factors are selected to characterize a burst, it then becomes important to describe the way in which they depend upon the reactivity insertion and upon the form of the relationship between the power history and the induced reactivity effects. The latter, of course, are determined by the intrinsic properties of the reactor.

One of the most useful models that permits such a description is also the simplest, and it was the first employed. This is the linear energy model, which has had various names associated with it (predominantly Fuchs,[104] Hansen,[105] and Nordheim[106]). This model may be regarded as a limiting form for many real situations, and because it is the starting point for other similar approaches, it will be described briefly. In this model,

$$\frac{\phi(t)}{\phi(t)} \equiv \alpha(t) \ , \tag{5.38}$$

where ϕ represents reactor power resource units.

The several nonlinear models that have been developed include (1) the zero delay model,[107] (2) the long delay model,[107,108] (3) the quadratic model[109] (zero delay with positive reactivity coefficients), and (4) several Doppler models[110,111] in which the Doppler coefficient of reactivity is a different function of the absolute temperature. None of these models will be described in detail here, since they are beyond the scope of this report. An excellent summary of this work is contained in the review by Nyer (Chap. 7 of ref. 112) from which the following discussions of burst shapes and comparison of models and data were taken.

5.3.2.3 Thermal Burst Shape Properties

It is often useful in the consideration of burst behavior to utilize the burst shape, particularly if it can be represented in a simple, closed form amenable to manipulations in hand calculations. In this section, two such simple approximate forms are described[108,113,114] to illustrate some of the systematics of bursts not previously discussed. A parameter to which particular attention is paid is the negative reactivity generated in the burst. This has frequently been called the "compensated reactivity," k_c.

Values of k_c (peak) calculated for a variety of postulated burst shapes have been compared with the values obtained by machine calculations using experimental power data and the neutron kinetics equations. From

these comparisons, several conclusions are evident. First, for approximate analyses the values obtained for k_c (peak) using approximations for the burst shape are often sufficiently accurate to justify the use of this more convenient means in preference to laborious machine calculations. Second, in some cases, analytical forms for the burst shape can be fit to the experimental burst shapes sufficiently well to be useful in calculations of other quantities of interest during a transient, such as temperature distributions, heat transfer, etc. (see, for example, the analysis of the SL-1 accident[114]). Thus, this approach may provide clues as to the nature of the feedback function. However, burst shape analysis alone does not provide the required information as to the form of the equation coupling power history with reactivity.

1. The Clipped Exponential Burst Shape Approximation. The clipped exponential burst shape approximation may be used to approximate a power burst up to the time of peak power. On the diagram shown in Fig. 5.47 the logarithm of the reactor power is plotted as a function of time, with the time of peak power taken as zero. An actual round-topped power burst is represented by the broken-line with peak power $\phi(0)$. The initial exponential rise of the actual burst is shown extended to the time of peak power, where it has the value $\phi_x(0)$. The solid curve made up of the extension of the initial exponential rise and the constant portion of magnitude $\phi(0)$ is the clipped exponential approximation. At the break in the curve, the first derivative of the power changes in a discontinuous fashion to zero.

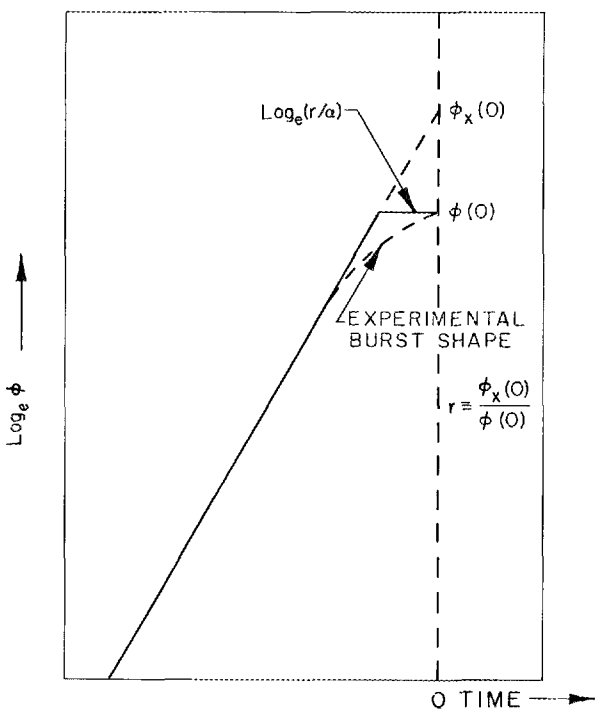

Fig. 5.47. Clipped Exponential Burst Shape Approximation.

The duration of the clipped portion is seen to be $\ln r/\alpha_0$, where r is defined as

$$r \equiv \frac{\phi_x(0)}{\phi(0)} . \tag{5.39}$$

Broad, flat-topped bursts will result in large r and long-duration clipped portions, whereas sharp bursts will have small r and short-duration clipped portions. Thus r can be used as a burst-shape parameter. The limiting form for very short bursts is simply an exponential with a vertical back side. This will be called an "exponential sawtooth."

The clipped exponential burst shape will, of course, never describe exactly an experimental burst shape. However, if it is matched to an experimental burst, as shown in Fig. 5.47, it will always be an overestimate of the energy to the time of peak power; and since the reactivity compensated at the time of peak power is dependent on burst shape, the clipped exponential will always provide an upper limit for the value of k_c (peak).

2. The Two-Term Burst Approximation. A better approximation that represents the entire burst can be made using a series of exponentials, as Corben and Forbes have done. The two-term model of Forbes[114] is described below. In this model it is assumed that the power burst can be represented by

$$\phi(T) = \phi(0) \left(a\ e^{\alpha_0 T} - b\ e^{c\alpha_0 T}\right) , \tag{5.40}$$

where a, b, and c are positive constants to be determined so that $\phi(T)$ satisfies three conditions: (1) $\phi(T)$ must coincide with the initial asymptotic power rise; (2) $\phi(T)$ must have the proper value at the peak ($T = 0$); and (3) $\phi(T)$ must have a zero time derivative at the power peak. As shown in Fig. 5.48, the two-term burst shape will be a round-topped burst and r can be defined as in Eq. (5.39).

Applying condition (1) to Eq. (5.40), it follows that for large negative values of T the second term in Eq. (5.40) may be assumed to be negligible, that is, for $T \ll 0$, the power is rising exponentially as $\phi(0)\ a\ e^{\alpha_0 T}$. Also

$$\phi(T) = \phi(0)\ r\ e^{\alpha_0 T} ,$$

from which it follows that $a = r$. From the second condition, at the time of peak power $T = 0$ and $\phi(T) = \phi(0)$, thus

$$\phi(0) = \phi(0)(r - b)$$

and $b = r - 1$. By applying the third condition to Eq. (5.40) and setting $d\phi/dt$ equal to zero,

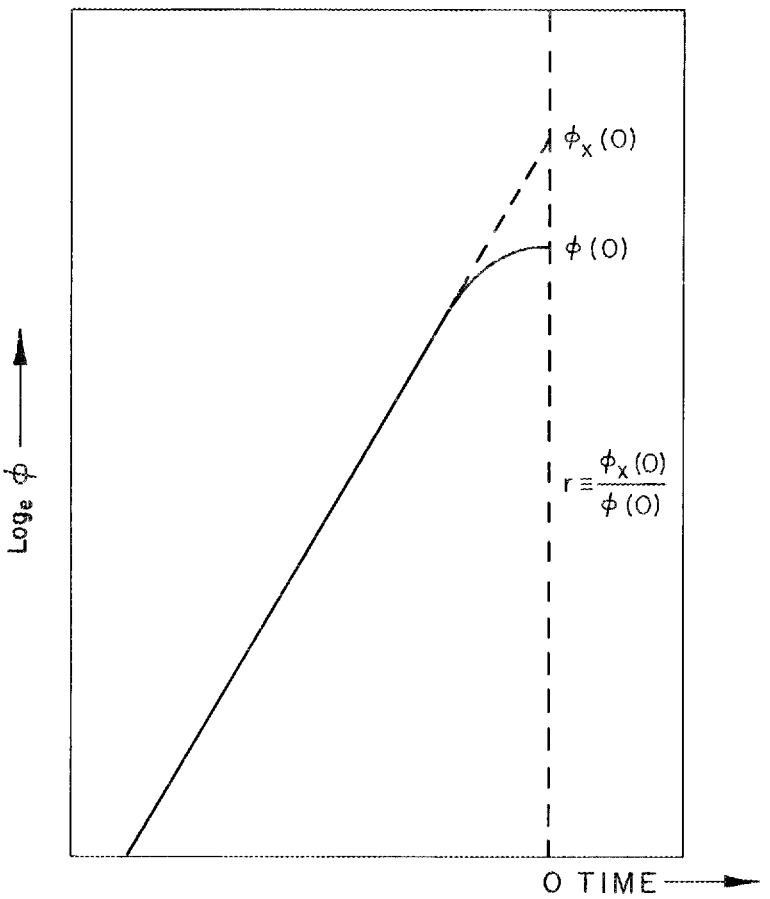

Fig. 5.48. Two-Term Burst-Shape Approximation.

$$\frac{d\phi}{dt} = 0 = \phi(0)\ \alpha_0 \left[r\ e^{\alpha_0 T} - (r - 1)\ c\ e^{c\alpha_0 T}\right],$$

from which

$$c = \frac{r}{r - 1}\ .$$

Substituting the above relations into Eq. (5.40) yields

$$\phi(T) = \phi(0) \left[r\ \exp(\alpha_0 T) - (r - 1)\ \exp\left(\frac{r}{r - 1}\ \alpha_0 T\right)\right]. \qquad (5.41)$$

The two-term burst shape is fairly restricted in its application for matching experimental burst shapes. As an illustration, the limiting burst shapes possible with the two-term model are (1) an exponential sawtooth for

$r = 1$ and (2) a somewhat broader burst shape for $r \rightarrow \infty$. These two limiting burst shapes are shown in Fig. 5.49, where they are compared with experimental burst shapes. The experimental bursts are from step-transient power excursions in the SPERT III reactor under the environmental conditions of atmospheric pressure, room temperature, and no forced coolant flow. It is evident from Fig. 5.49 that the shape of the power burst with $r \rightarrow \infty$ is still relatively sharp, as compared with the experimental bursts possible for subprompt critical bursts. As a result, integrating Eq. (5.41) and assuming the initial power to be arbitrarily small gives the result that the maximum energy to the time of peak power for the two-term model is $2\ \phi(0)/\alpha_0$ (for $r \rightarrow \infty$) and that the minimum energy is $\phi(0)/\alpha_0$ (for $r = 1$). Thus, the maximum energy is restricted to only a factor of 2 greater than the minimum energy, also implying a limit in the broadness of the burst shape.

3. Summary and Discussion. The two-term burst-shape description developed here approximates closely the SPERT experimental burst shapes only in the short-period (sharp-burst) region and thereby provides accurate estimates of the value of k_c (peak) for some cases. The range of α_0 for which this is true is small, and the use of the two-term burst shape is rather limited. On the other hand, although the clipped exponential burst shapes are never close approximations to experimental burst

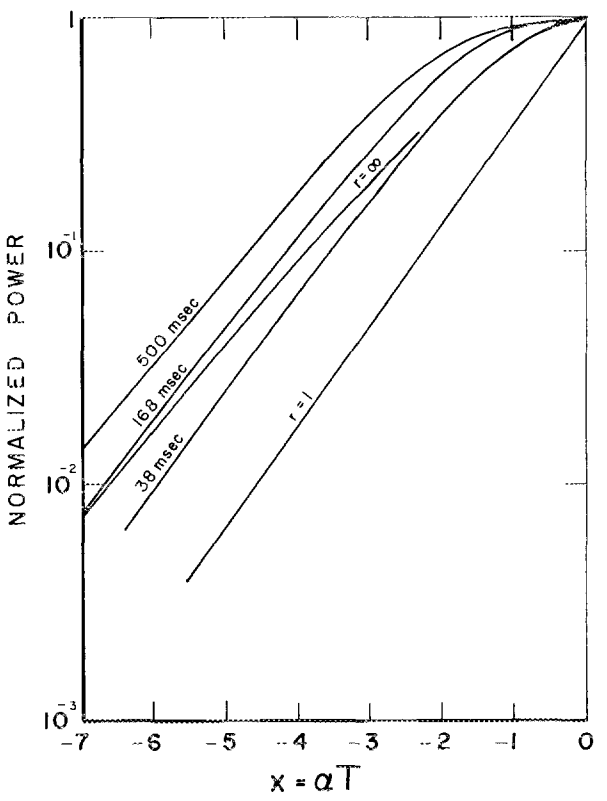

Fig. 5.49. Comparison of the Two-Term Approximation with Some Experimental Burst Shapes.

shapes, they always provide an upper limit for the value of k_c (peak) for any practical α_0, and from the viewpoint of attributing the self-shutdown to physical mechanisms, an upper limit for k_c (peak) is a useful quantity. The behavior of the compensated reactivity at peak power was examined using these burst-shape approximations, with the following results:

1. The shape of the k_c (peak) versus α_0 curve is dependent on the delayed-neutron parameters, the prompt-neutron lifetime, and the shape of the power burst.

2. The minimum in the k_c (peak) curve will appear for many reactor systems but will not be present in systems that have very long prompt-neutron lifetimes ($\simeq 7 \times 10^{-2}$ sec) or which exhibit extremely broad or extremely narrow power-burst shapes.

3. This type of reactivity compensation analysis provides little information as to the form of the coupling equation. Physical situations leading to sharp-topped bursts, predicted by r near unity, are those in which the reactivity compensation increases much more rapidly than the energy released by the reactor. Examples are threshold processes such as boiling, nonlinear expansion of moderator (such as water or steam), and systems whose reactivity changes are nonlinear functions of density or temperature. A linear energy shutdown model with a threshold leads to a sharp burst that approaches an exponential shape as the threshold is increased. Any reactor having nonlinear shutdown properties that can be represented by having $n \gg 1$ will also exhibit k_c (peak) versus α_0 behavior typical of small r results.

5.3.2.4 Some Comparisons of Thermal Models and Thermal Excursion Reactor Data

In the foregoing discussion the complexities of the reactor behavior were compressed into a single factor generically called the shutdown coefficient. This mathematical oversimplification is surprisingly successful in describing the behavior of actual systems. That is, the experimental reactors often behave as if they were governed by a single, or at most a few, quenching mechanisms obeying feedback laws of these simple forms. In this section a few of the main features of these models are compared with one another and with the excursion reactor data.

Table 5.26 summarizes the principal characteristics predicted by the various models. In addition, a burst-width parameter, W_B, is included. This is defined as the ratio of the product of the reciprocal period and the total energy of the burst to the power at the time of maximum. The symbols are those used above.

1. Energy Release Functions. A comparison of the energy-release functions with the reactivity for the shutdown models previously discussed is presented in Fig. 5.50. The abscissa is α_0, the initial step-inserted reactivity, and the ordinate is the energy release to time of peak power. The units are chosen for convenience in presentation. Under some conditions the values of the constants in the various expressions for $E(\alpha_0)$ may be such that the choice of form does not seriously alter the results. However, if the range in α_0 is sufficiently great, the differences become important.

Table 5.26. Comparison of Models

Parameter	Model					
	Linear	E^n, Zero Delay	Quadratic	$E^{1/2}$	ln E	$E^{-1/2}$
$\alpha(E)$	$\alpha_0 - CE$	$\alpha_0 - CE^n$	$\alpha_0 \pm b_1E - b_2E^2$	$\alpha_0 + B - B(1 + AE)^{1/2}$	$\alpha_0 - B \ln(1 + AE)$	$\alpha_0 - B + B(1 + AE)^{-1/2}$
$b(E)$	$-C$	$-nCE^{n-1}$	$\pm b_1 - 2b_2E$	$-\frac{1}{2} AB(1 + AE)^{-1/2}$	$\frac{-AB}{1 + AE}$	$-\frac{1}{2} AB(1 + AE)^{-3/2}$
$E(T_{max})$	$\frac{\alpha_0}{C}$	$\left(\frac{\alpha_0}{C}\right)^{1/n}$	$\frac{b_1}{2b_2}\left[\left(1 + \frac{4b_2\alpha_0}{b_1^2}\right)^{1/2} \pm 1\right]$	$\frac{\alpha_0(\alpha_0 + 2B)}{AB^2}$	$\frac{1}{A}\left(e^{\alpha_0/B} - 1\right)$	$\frac{\alpha_0(2B - \alpha_0)}{A(B - \alpha_0)^2}$
E_{final}	$\frac{2\alpha_0}{C}$	$\left[(n + 1)\frac{\alpha_0}{C}\right]^{1/n}$	$\frac{3b_1}{4b_2}\left[\left(1 + \frac{16b_2\alpha_0}{3b_1^2}\right)^{1/2} \pm 1\right]$ $\gtrsim \frac{3}{2} E(T_{max})$	$\frac{4}{A}\left[\left(\frac{9 + 3\alpha_0/B}{1 + 3\alpha_0/B}\right)^{1/2} - 1\right]^{-2} - \frac{1}{A}$	$\approx \frac{1}{A}\left(e^{\alpha_0/B+1}\right)$ for $AE_{final} \gg 1$	$\frac{4\alpha_0B}{A(B - \alpha_0)^2}$
$\phi(T_{max})$	$\frac{\alpha_0^2}{2C}$	$\frac{n}{n + 1}\left(\frac{\alpha_0^{n+1}}{C}\right)^{1/n}$	$\frac{b_1^3}{12b_2^2}(x^3 \pm 1) \pm \frac{b_1\alpha_0}{2b_2}$ $x = \left[1 + (4b_2\alpha_0/b_1^2)\right]^{1/2}$	$\frac{\alpha_0^2(\alpha_0 + 3B)}{3AB^2}$	$\frac{B}{A}\left(e^{\alpha_0/B} - 1 - \frac{\alpha_0}{B}\right)$	$\frac{\alpha_0^2}{A(B - \alpha_0)}$
$W_B = \frac{\alpha_0E_f}{\phi(T_m)}$	4	$\frac{n + 1}{n}(n + 1)^{1/n}$	$\approx \frac{9\alpha_0(x \pm 1)}{2(b_1^2/b_2)(x^3 \pm 1) \pm 18\alpha_0}$	≈ 4 for $\alpha_0 \lesssim B$	$\frac{\alpha_0}{B}\frac{e^{\alpha_0/B+1}}{e^{\alpha_0/B} - 1 - (\alpha_0/B)}$	$\frac{4B}{B - \alpha_0}$

Notes: ϕ = reactor power, $\alpha = \dot{\phi}/\phi$ = reciprocal period; E = energy release during excursion, $E(T_{max})$ = energy released in reaching maximum value of temperature, E_{final} = total energy released during excursion; $\phi(T_{max})$ = maximum power; W_B = burst width parameter; $b(e) = \partial\alpha/\partial E$ = "reactivity coefficient"; α_0 = initially injected value of α or the value of α at the start of the excursion.

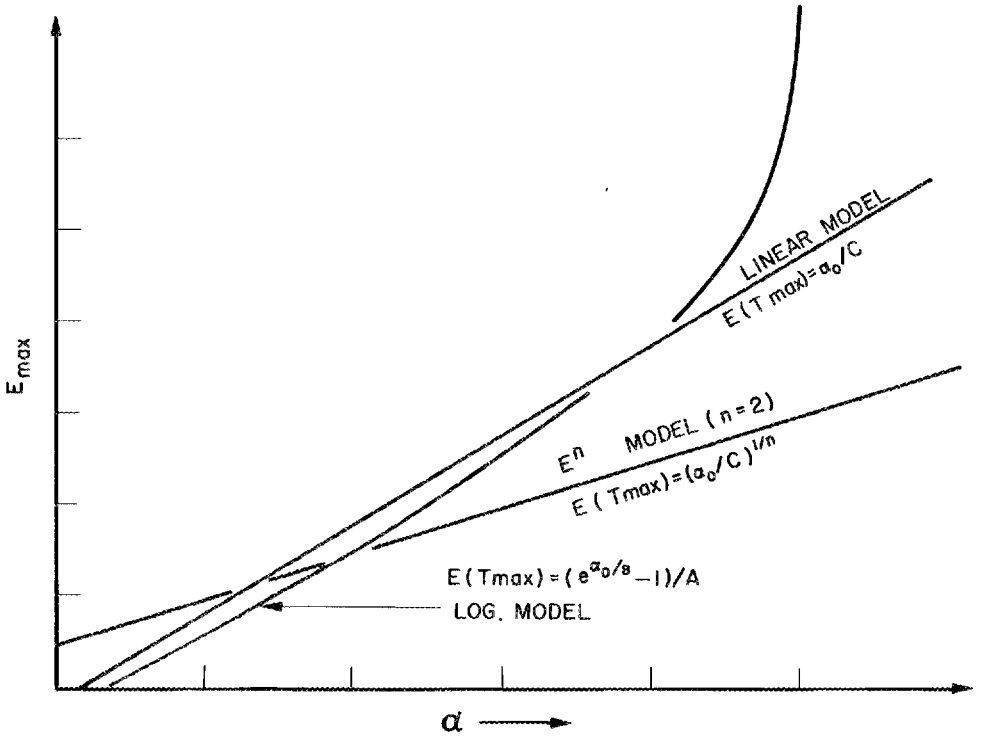

Fig. 5.50. E_{max} Versus α for Various Shutdown Models.

The curvature of these lines is determined by the type and complexities of the shutdown mechanism, whereas their displacement upward or downward is determined by the magnitude of the reactivity coefficient. One way of judging the relative importance of the two aspects, that is, curvature and displacement, is on the basis of how large α_0 can be made before the energy goes above some selected limit beyond which undesirable or even catastrophic effects occur. This limit could be represented by a horizontal line located approximately in the graph, say at the top of the figure, and could represent fuel plate melting or vaporization or some other effect. If this limit is taken to be the criterion, it is of lesser importance how the energy release function behaves below the limiting value provided it does not cross it or provided that the point of crossing is sufficiently far to the right that as a practical matter the step addition of the required α_0 is not realistic.

Figure 5.51 presents, for comparison, the energy-dependent behavior of the previously discussed forms of the shutdown coefficient. Here, also, the values of the constants in the various expressions for b may be such that the choice of form does not seriously alter the results. However, where the shutdown is due to a Doppler coefficient, the variation has been found to be significant[110] and may be sufficient to allow a clear choice between forms of the energy dependence.[115]

The excursion reactors exhibit or come rather close to exhibiting the behavior characteristics corresponding to the different feedback relations and energy versus α_0 functions represented in Figs. 5.50 and 5.51. Table 5.27 lists some important types of shutdown coefficients, along with the

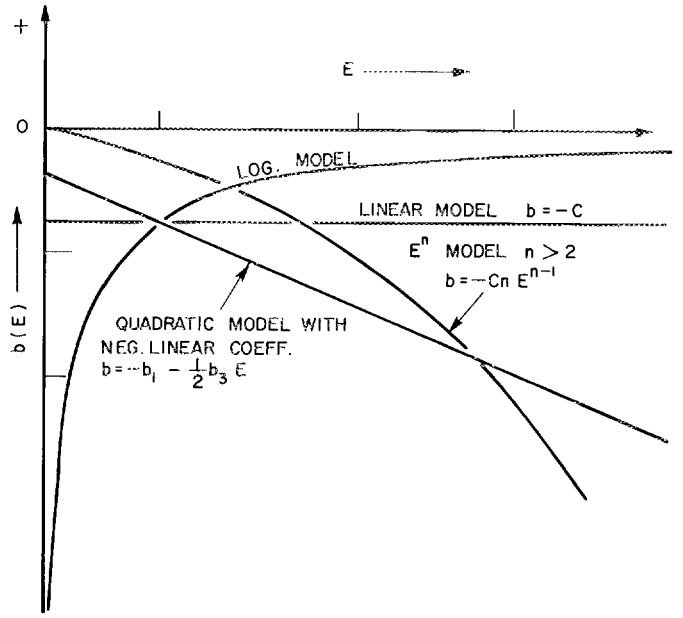

Fig. 5.51. Shutdown Coefficient b(E) Versus E for Various Models.

Table 5.27. Shutdown Coefficients with Various Excursion Reactor Examples

Shutdown Coefficient	Reactors
Prompt, negative, constant	Godiva, TRIGA, TREAT
Prompt and delayed, negative, increases with energy release	SPERT with metal plate cores, KEWB
Prompt, negative, decreases with energy release	SPERT with oxide core

reactors that most nearly display the related behavior. The first coefficient in the table is prompt and negative, and it remains constant during a burst independent of any temperature change, pressure change, or fuel expansion that might be caused by the energy release. To a degree, these characteristics are exhibited by the Godiva, TREAT, and TRIGA reactors; but the representation is far from perfect and could be expected to be worse in experiments with larger α_0 because of the increasing importance of time delays and because of possible threshold effects.

The second type of coefficient is prompt and negative, and it increases with energy release. There are no good examples, but there is one that at least has a similar component to an important degree. The SPERT metal-plate cores, which are highly enriched, have prompt and delayed components but nevertheless exhibit burst characteristics that can be associated with the type of coefficient that increases with energy release.

The last type of coefficient shown is prompt and negative, but it decreases with energy. The SPERT oxide core, which is a low-enrichment core, exhibits all these characteristics nicely.

The differences in type of shutdown coefficient manifest themselves as differences in the energy release function, such as shown in Fig. 5.50, and in other important ways, such as transient pressure pulses or temperature excursions. In each of these cases, reactor design changes that affect the shutdown mechanisms also affect the relative safety. However, the degree to which safety is affected depends on the form of the feedback relation and the exact nature of the particular shutdown mechanism, the accident under consideration, and the safety criterion. In some cases the net gain may be appreciable and, in others, relatively insignificant.

One interesting type of shutdown mechanism was left out of the table because no reactor exhibits it to a degree worthy of note. It is one that can be suggested as ideal: its reactivity effect is negative and small (effectively zero) for very long periods and the effect is prompt and strongly negative at short periods. The first requirement means that the reactivity investment needed to bring this fictitious system to power would be nil, and the second requirement is protection against the dangers of large excursions. This is in contrast with the behavior of many mechanisms normally of importance in existing reactors. These exhibit sizable negative coefficients for slow periods and also have important inherent delays that reduce their effectiveness when reactor periods become short.

As a consequence of both this normal behavior of reactivity coefficients and also for reasons of plant operating capability, the excess reactivity possessed by the plant at some time in its operating cycle may be many dollars. Since this investment in reactivity is a potential source for the initiation of a reactivity incident, it becomes important to consider the constraints that exist to limit the magnitude of such occurrences. One such constraint is that the reactivity addition must occur in a finite time rather than instantaneously. This has the important consequence already discussed that the reactivity that can be added is limited by the assembly rate, as well as by the total reactivity available. That is, to attain a given period, or what is the same thing, a given instantaneous level of reactivity, there is a minimum assembly rate that must be exceeded.

2. Reactivity Insertion Mechanisms. The importance of the reactivity insertion mechanism lies in the fact that for every mechanism there is a natural limitation on insertion rates; this applies equally to insertions by direct human actions, such as moving control rods by hand or dropping fuel assemblies into a core, and to insertions by more mechanical actions, such as the collapse of voids or accidental control rod withdrawal. In any event, for very large reactivity insertions, the assembly rate requirements, and concomitantly, acceleration requirements, become prohibitively high and establish an effective upper limit to the possible net reactivity additions and thus to the possible magnitudes of energy release. It is important to note that in actual cases the reactivity limit set by the attainable insertion rate is often substantially lower than the total available reactivity built into reactors.

These points are illustrated in qualitative fashion in Fig. 5.52 (ref. 116), which shows the reciprocal of the reduced prompt-neutron lifetime, α_R, on the abscissa. The assembly rate in dollars per second is on the

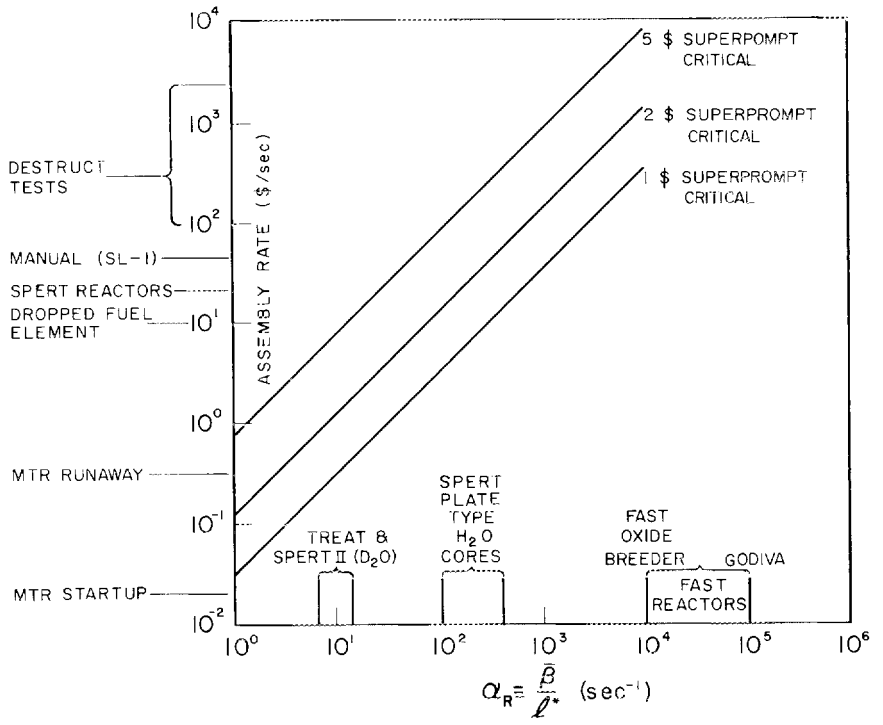

Fig. 5.52. The Degree of Superprompt Criticality Attainable as a Function of Assembly Rate and α_R.

ordinate. The lines show the assembly rates required to produce 1, 2, and 5 dollars superprompt criticality (reading from bottom to top) as a function of the characteristic reciprocal period. These lines were computed using the linear model but should apply qualitatively to many other, but perhaps not all, models, as well as any such consideration of assembly rates based on an extremely simplified picture of the reactivity feedback relationship. Many of the properties described may change markedly when time lags and nonlinearities are taken into account. The role of shutdown mechanisms in governing reactor safety is generally very complicated, but it is unlikely that there is a need to question the validity of certain features that emerge as general properties. First, in cases where stringent requirements are placed on the assembly rates that must be achieved in order to increase total reactivity insertion, even marginal gains in the reactivity coefficient may result in substantial increases in safety; thus, there is a strong motivation for improving the effectiveness of the coefficients by increasing their magnitude. Second, it is clear that the delays between the energy release and a reactivity loss may be more important than the magnitude of the coefficient; thus, there is also a strong motivation to understand the details of the mechanism and the feedback relationship determined thereby in order to make a realistic assessment of the effective coefficient under dynamic conditions and to point the way to shortening the delays.[117]

3. Results of Excursion Tests. A number of these characteristics are exhibited by the results obtained with excursion reactors and the

understanding of the physical mechanisms that operate during the bursts. The step-transient data from the excursion reactors can be compared in the following way. An experimentally determined quantity, ϵ, the effective dynamic energy coefficient of reactivity, is defined as the ratio of the reactivity compensated by the system to the nuclear energy release evaluated at the time of the power peak. Since a shutdown mechanism will usually have some characteristic time constant, it is to be expected that if ϵ is plotted as a function of reciprocal period that, for a system with a single self-shutdown mechanism, there would be a region of low α where ϵ would be relatively constant and could be determined by nontransient measurements. For a short enough period, the effective value would begin to decrease. If, however, another more effective mechanism began to act only at short periods, the value of the energy coefficient might level out or even rise; but ultimately, for short enough periods, the curve should drop again. A number of these features are exhibited in Fig. 5.53, which shows this coefficient as a function of reciprocal period for various systems.

The data for the various H_2O-moderated plate-type cores of SPERT and BORAX are contained within the cross-hatched area. In general, for these plate-type cores the effective energy coefficient decreases as the reciprocal period increases and then levels out or slightly rises as periods are reached where boiling is important; that is, as the time scale of the burst is shortened, the effectiveness of the thermal effects that depend on heat transfer rates decreases; but in the shorter period region, the threshold for the more effective mechanism of steam void formation is passed and the coefficient rises. The various SPERT cores are much alike, and there is really little variation in the coefficient. For this type of system over the range of period available, a coefficient of 6 ± 5¢/Mw-sec will describe all the cores for all practicable periods.

The effect on burst behavior of a threshold that brings a new, more powerful shutdown mechanism into operation is more dramatically exhibited by SPERT II data, which show a strong rise in the coefficient as the period decreases. These data lie in the range shown for SPERT H_2O-moderated plate-type cores and are shown by the heavy line running through the cross-hatched area. The increase in the coefficient is related to the fact that this system can shut down only by the generation of massive quantities of

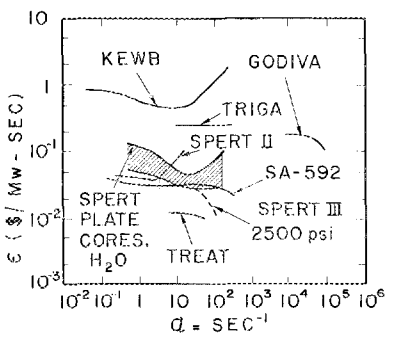

Fig. 5.53. Effective Dynamic Reactivity Coefficient for Excursion Reactors as a Function of α.

steam. However, at shorter periods than shown here, it would still be expected that the effective value of the steam coefficient would decrease. The SPERT III (plate-type cores) high-pressure runs, shown by the dashed line at the lower end of the SPERT band, show a marked decrease in ϵ. This is a result of the suppression of boiling as a shutdown mechanism by operating at a system pressure of 2500 psi. Actually, the SPERT III data show two things: (1) the effect of a threshold mechanism, such as boiling, in holding up the value of ϵ as it does in atmospheric pressure tests, and (2) when the threshold mechanism is absent, it illustrates the generally expected decrease in effectiveness of a shutdown mechanism as the period is shortened.

For this type of reactor, that is, the plate-type SPERT reactors, the principal mechanism for reactivity compensation is the decrease in effective moderator density arising, variously, from the thermal expansion of the water, thermal expansion of the fuel plates, and the formation of steam voids. Some of the shutdown mechanisms are prompt, but the primary ones involving heat transfer from the plate to the water are delayed.

For the aqueous homogeneous reactor KEWB, there are no delays due to energy transport as in the plate reactors, but there are delays inherent in void formation. The more prompt thermal effects present in the homogeneous reactor than those present in the plate reactor are partly responsible for the larger coefficient, which is about 50¢/Mw-sec in the prompt-critical range. The onset of the increasingly effective void formation at short periods causes an increase in the coefficient to the order of 2.5$/Mw-sec for 2-msec period tests. The existence of this threshold behavior in both KEWB and SPERT reactors tends to obscure the important fact that those mechanisms which involve a phase-change or the transport of energy by conduction or convection to produce a reactivity effect can have, even at relatively long periods, significant delays that are chiefly responsible for the difficulties in predicting reactivity effects. They produce a general tendency, already noted for the reactivity coefficient, to become less effective at very short reactor periods. This is, of course, opposite to one of the characteristics suggested as ideal for a shutdown mechanism.

In contrast, mechanisms that directly couple a specific neutronic effect with heating of fuel or moderator by absorption of fission fragments, neutron energy, beta rays, or gamma rays are truly prompt. The TREAT and TRIGA reactors are self-limiting by such a mechanism. In these systems the fuel-moderator mixture is essentially homogeneous. In TREAT, the time-lags in the transfer of heat from the uranium particle fuel to the graphite moderator can be expected to be significant at very short periods. The resultant delay in the quenching would be expected to lead to a decrease in the coefficient and higher energy yields. The experimental TREAT coefficient, as shown in Fig. 5.53 is nearly constant at ~1¢/Mw-sec. For TRIGA, the experimental value of the coefficient is about 25¢/Mw-sec over the entire range of tests shown here.

In many practical cases the changes in neutronic properties resulting from expansion, including that of the moderator, are also prompt. However, at short periods the kinetic effect may prevent the expansion from keeping pace with the temperature increases, and although the temperature rise is prompt, the reactivity effect may be delayed. This type of behavior is

exhibited in the well-known case of the Godiva reactor where delays in the expansion of the metal caused an observed decrease by a factor of 2 in the value of the coefficient. Since this occurs for periods shorter than about 20 μsec, it is not of practical importance to thermal reactors, but an analogous situation may exist in thermal systems where the shutdown mechanism requires the expulsion of a steam-water mixture. In fast reactors, expansion delays of this sort can also be expected when rod bowing or axial expansion of fuel rods contributes to reactivity effects. The dynamic coefficient for Godiva is several times larger than the coefficient for SPERT cores. However, this quantity is not in itself a reliable index for measuring reactor safety.

There is one more important mechanism on which there is excursion data. This is the Doppler effect, which is quite prompt, like the TRIGA and Godiva mechanisms, but which exhibits a saturation effect, that is, the coefficient decreases with energy release. Similar behavior was shown by other mechanisms because of delays, but in this case it is an inherent property. The light solid line at the bottom of Fig. 5.53, labeled SA-592, is for a low-enrichment oxide core in the SPERT I reactor. In this case the coefficient is approximately constant at about 3¢/Mw-sec for most of the tests. In this region, both the Doppler effect and conduction to the water moderator were operating. At higher α values, the loss of conduction heating effects and the decrease in effectiveness of the nuclear mechanism are evidenced by the decrease in the dynamic coefficient.

One important point should be noted here. Although Doppler coefficients are generally a factor of 10 smaller in magnitude than overall steady-state temperature coefficients, the dynamic value for this core is only slightly less than that for the other SPERT cores and, in fact, is larger at short periods than for the pressurized SPERT III case. This shows that the Doppler effect can be the most important shutdown mechanism, even in thermal reactors, because of its prompt nature.[115]

The reactors discussed represent a wide variety of types, but they are all relatively compact in size. It can be expected that larger systems will have characteristically different coefficients on this type of plot. A case in point is the reactor discussed by Greebler.[118] This reactor can be shown to have a dynamic coefficient of about 0.04¢/Mw-sec for an α of about 2000. This is about two decades below the value shown for the SPERT I oxide core. Actually, the coefficients for the two systems are comparable when stated in reactivity changes per degree rise, so the coefficient for the larger system should be smaller in proportion to its higher heat capacity. This emphasizes that broad conclusions about relative safety are difficult to make from this plot. There appears to be no way at present of putting relative safety into a single parameter and displaying it so conveniently.

4. Fast Control Systems. In the foregoing discussion, the quenching of bursts was treated as taking place solely by the action of inherent physical mechanisms, apart from any consideration of the possible contribution from mechanical control systems. Actually, the overall assessment of the performance and safety of a reactor requires consideration of both self-shutdown effects and control system action as modes of limiting excursions.

Some of the factors involved in evaluating safety when both modes of shutdown are considered may be illustrated by making use of the following

simple picture of the course of a fast excursion terminated solely by the action of the control system. Reactivity is considered to be inserted in a reactor at a very low initial power level. The power then rises exponentially on a constant period to a trip level where a demand for a scram is initiated by a sensor in the control system loop. The power continues to rise on the same exponential period until a later time when the power burst is terminated abruptly. This abrupt termination approximates the result of rapid movement of the control rods to a point of significant effectiveness. If the elapsed time, τ_d, between the call for scram and the actual power reduction is a constant, the maximum power level, ϕ_M, is given by

$$\phi_M = \phi_{trip}\, e^{\alpha_0 \tau_d} , \qquad (5.42)$$

where ϕ_{trip} is the power level at which the scram is demanded and α_0 is the reciprocal period.

Figure 5.54 shows schematically the calculated behavior of such a scram system with simple time delays of τ_d, $10\tau_d$, and $100\tau_d$ compared with self-shutdown characteristics representative of an enriched plate-type light-water-moderated and -reflected reactor in the superprompt-critical region. Generally, a downward displacement of the curves on the graph can be associated with an improvement in safety. For the case of self-shutdown, this is, in principle, accomplished by increasing the magnitude of the (negative) reactivity coefficient. For the case of control system shutdown, this is accomplished by lowering the trip level or decreasing the delay time. It can be seen that for certain combinations of these factors, self-shutdown can be more effective than the mechanical system in limiting the power burst. For other combinations the reverse is true.

The results obtained from experiments with ORNL Bulk Shielding Reactor II when assembled at NRTS are shown in Fig. 5.55. This was a

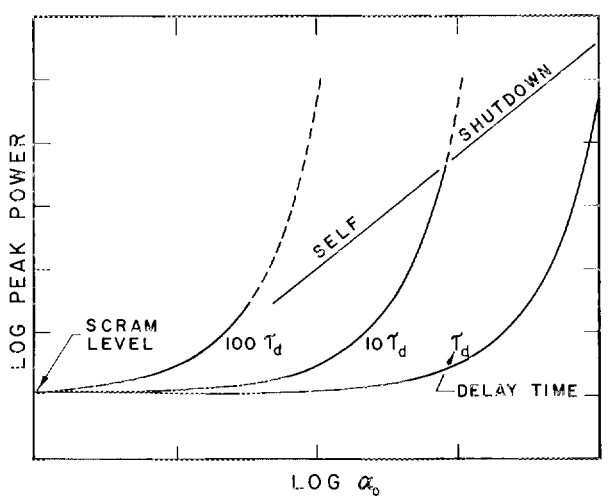

Fig. 5.54. Effect of Different Delay Times on Reactor Peak Power as a Function of the Reciprocal Period, α_0.

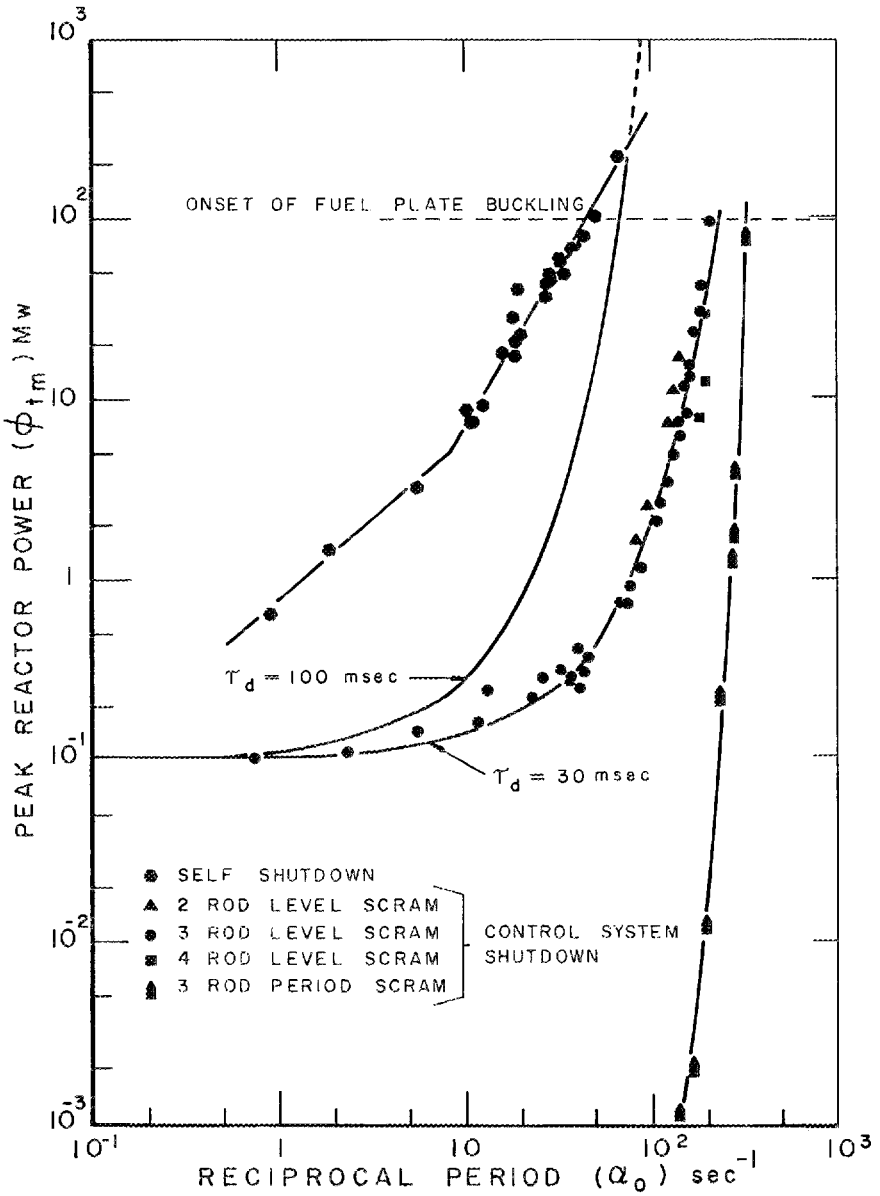

Fig. 5.55. Experimental and Calculated Values of Peak Power Versus Reciprocal Period for Various Shutdown Conditions.

plate-type reactor that also had a fast-acting safety system.[119,120] In these tests, the subcritical reactor at low initial power was subjected to step-by-step insertions of reactivity, and the resulting excursions were terminated either by the inherent quenching effects or by the control system. The results obtained with shutdown by the control system were well described by an expression of the form of Eq. (5.42) with τ_d = 30 msec. The considerable decrease in effectiveness that would have resulted from increasing the delay time to 100 msec was evident. The importance of the

delay was further indicated by the behavior of both types of control system scram, which exhibited an effective cutoff of their protective capability for reactivity insertions in which $\alpha_0 \tau_d \gg 1$. Clearly, the period scram provided valuable additional protection. Since the tests were conducted without a source in the system, the effectiveness of control system shutdown would have been improved under normal initial power conditions.

5.3.2.5 Energy in Fast Reactor Excursions

The term "severe accident" is used here to cover situations that would lead to an explosive release of nuclear energy in a fast reactor. Analysis of such accidents involves the calculation of those reactivity excursions that would not be terminated until some of the fuel had been vaporized and appreciable pressures had built up in the core. These pressures would cause the whole core or a portion thereof to expand, leading to a reduction of reactivity and a consequent termination of the excursion. A comprehensive review of fast reactor kinetics, including accident transients, was recently prepared by D. Okrent and W. McCarthy as part of the MIT study of "The Technology of Nuclear Reactor Safety."[112*] The material presented here is only a brief summary of some of the more salient conclusions of that review.

Assuming grossly pessimistic conditions, calculations made[121] for the EBR-II and Fermi reactors have led to the prediction of destructive effects equivalent to those that would be produced by an explosion of up to 400 and 500 lb of TNT, respectively. Containment structures provided for these two reactors have been designed to accommodate such an accident. Hence, both refinement of calculating methods and more careful analysis of the factors leading to a severe accident have been demanded.

Of course, the calculation of a severe accident in a real power reactor means dealing with complex geometry and irregularities in composition. The conditions and cause of the accident are generally not known precisely, and the course of the accident prior to the large nuclear burst is usually very complex. Nevertheless, idealized calculations provide some gage of the severity of the accident, and the evaluation and comparison of methods of calculation provide an estimate of the errors introduced by the mathematical techniques once an idealized form of the actual situation has been adopted.

Fast reactors gain reactivity if the fuel is rearranged in a denser configuration. About half the core of a typical fast power reactor is occupied by fuel alloy and solid structural material. The other half is the coolant. Hence very large amounts of reactivity are potentially available if the fuel alloy can be reassembled in a considerably denser configuration. The core is assumed to have lost its rigidity, and either the forces of gravity or those of a high velocity or high pressure fluid would cause much of the fuel to reassemble in a more reactive position.

---

*Chapter 10, Reactor Kinetics.

What turns out to be significant in estimating the explosive yield of a severe nuclear accident is not the total reactivity available but the rate at which it can be added to the assembly. It is assumed that a source of neutrons is always present and that the reactor is operating at low power at the beginning of the accident. (Otherwise, arbitrary amounts of reactivity could be introduced effectively as a step function.) The power rise is slight until prompt critical has been reached. Beyond this point the power rises as exp $[(\Delta k/l)t]$, where Δk is the reactivity above prompt critical and l is the prompt neutron lifetime. (Prompt neutron lifetime may range from several $\times 10^{-7}$ sec for large ceramic-fueled reactors to 10^{-8} sec for small highly enriched systems.) The time scale now becomes so short that heat conduction and delayed-neutron effects can be neglected. If the fuel is in a molten or pasty state, the usual reactivity loss mechanism associated with the fuel element expansion may be less significant; considerable energy may have to be added before the pressure buildup starts fuel movement and loss of reactivity at a rate sufficiently great to override the cause of the accident. (If the fuel element is initially intact, it is assumed that the initiating cause of the accident overrides any reactivity losses due to fuel expansion in the solid state; Doppler reactivity effects associated with fuel heating will be discussed later.) The maximum reactivity of the excursion (Δk_{max}) will be given very closely by the product of dk/dt, the rate at which reactivity is being added, and t_1, the time interval between prompt critical and the time when appreciable reactivity loss due to fuel motion begins. Once pressures are generated, the reactivity excursion is over in about 2 e-folding times, that is, in hundreds of microseconds, and very little additional reactivity can be added mechanically by the initiating cause. The pressures involved are so great that questions of mechanical strength are not important and can be ignored. Inertial effects are paramount in determining the acceleration of the fuel alloy.

The explosive energy yield depends strongly on Δk_{max} and therefore on the rate at which reactivity is being added, on the prompt-neutron lifetime, and on the ratio of the energy threshold for appreciable pressure generation to the initial power of the reactor. Other things being equal, the explosive energy increases with reactor size. Of course not all the energy generated is available for destructive work.

The temperature threshold for significant pressure generation is generally not the boiling point of the fuel at atmospheric pressure but that temperature where all the space freely available to the fuel is occupied by it as a single phase, usually as a liquid under pressure. As a consequence, the void present in the reassembled core becomes a crucial parameter. The fuel must expand until it occupies its original volume plus available void volume before appreciable motion in a macroscopic sense begins.

Most studies of hypothetical severe accidents in the past have dealt with reactivity addition rates in the range 0.05 to 7.5 $(\Delta k/k)$/sec. The corresponding maximum reactivities above prompt critical lie in the range 4×10^{-4} to 10^{-2} $\Delta k/k$.[121] However, any mechanism that can bring the reactor to superprompt critical may be of interest. For, should there be some autocatalytic effect, such as a positive Doppler coefficient of appreciable magnitude, the attainment of prompt criticality might automatically lead to explosive disassembly.

A partial list of initiating methods follows:

1. Loading or dropping a fuel element into a just-critical reactor.[122]
2. Scramming a control rod whose reactivity effect has been inadvertently reversed.
3. Rapid introduction of moderating material[123] or a loading error in some unusual experiment.
4. Large-scale inward bowing of fuel elements due to thermal stresses.[122,124]
5. Moving reflecting material toward the core of a bare or poorly reflected reactor.[125]
6. Removal of all neutron sources, in which case any slow reactivity insertion mechanism may simulate a step-function addition.[126]
7. Bunching of fuel, providing a self-multiplication effect.
8. Positive coolant void coefficient.[110,127–129]
9. Slumping of fuel material within its jacket.[110]
10. Inward net expansion of fuel upon heating. This might result from a central gap in a two-half critical assembly;[130] it might result from the net motion of a multipiece fuel element which had separated, possibly due to ratchet effects; it might result from the manner of support of a multipiece fuel element; or it could be the consequence of a void space at the core center, resulting from the previous transport of fuel material from hot to cool areas.
11. Positive Doppler coefficient.[110,131–134] As mentioned previously, a positive coefficient of this sort need not be large enough to initiate the accident and bring the reactor from delayed to superprompt critical. If it were the sole rapid-acting reactivity coefficient once the reactor attained prompt criticality, even a modest reactivity contribution could appreciably aggravate the accident.
12. Core meltdown and redistribution of fuel.

The energy yield in a fast reactor excursion may be calculated by the Bethe-Tait method[135] or by a direct numerical technique.[136] Since the Bethe-Tait method ignores the effect of expansion and wave motion on pressure, it can be expected to be most accurate for sharp explosions with small reactivity insertions. In Fig. 5.56 the total excess energy yield (defined in this case as the total energy generation less the energy generation up to the incidence of pressure generation at the core center) is plotted against $\Delta k_0^3/l^2$, with l as a parameter as calculated from the more accurate numerical technique.

5.3.2.6 Excursion Energy for Use in Accident Calculations

If sufficient excess reactivity is added to a reactor in a very short time, a rapid power rise could result that could destroy the reactor with explosive violence and could add to the energy content of the contained

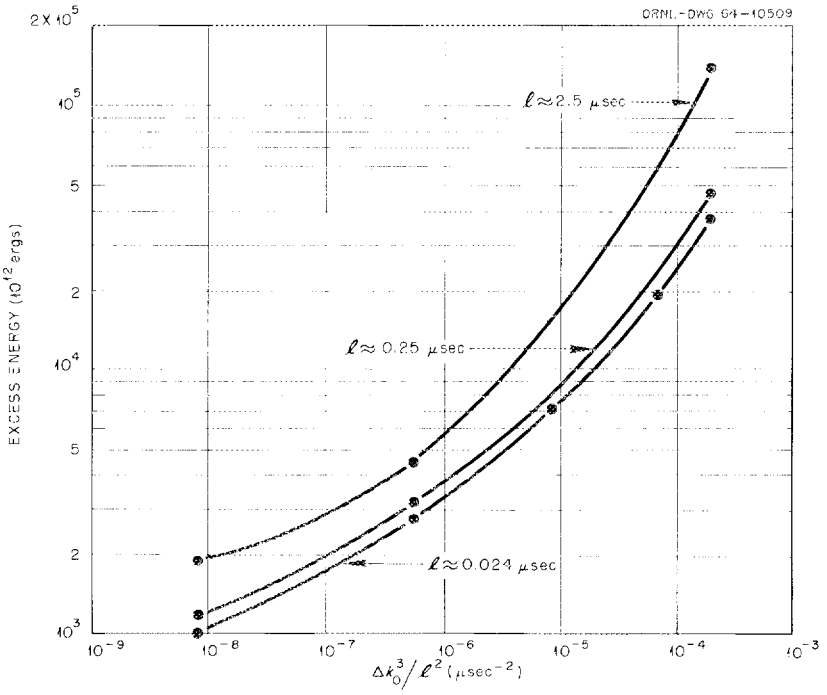

Fig. 5.56. Energy Yield in Excess of Threshold for Various Neutron Lifetimes; $E^* = 2100 \times 10^{12}$ ergs.

volume. For this to occur, the reactor would have to be in the superprompt critical condition. The preceding summary was taken from an excellent review of the large amount of experimental and theoretical work on the dynamics of superprompt critical reactors, which is contained in ref. 112, in particular, Chapter 7 on "Mathematical Models of Fast Transients" by Nyer. However, most of the work pertains to nondestructive excursions that are of no great interest in the present connection, since they do not necessitate the containment. There have been only a few explosive excursions of reactors, the BORAX I, the SL-1, and the SPERT I destructive tests on the enriched plate core and the low-enrichment oxide core.

Nyer concludes that "the experimental data on reactor excursions may be correlated, often very well, by simple models for shutdown by inherent processes or by control systems. However, the applicability of these models to different situations must rest on the degree to which they are understood in terms of the fundamental physical processes at work. Thus, detailed considerations are necessary, either to establish the need for detailed calculations, or to be assured that the simple models, may, instead, be applied and to what extent."

In lieu of experimental data on nuclear excursions, some of the early reactors were examined on the assumption that the contribution of the nuclear excursion to the energy content of the contained volume would be the energy content of the reactor at the time when 20% of the fuel reaches the vaporization point. For a thermal reactor, the destructive excursions seem to show that the nuclear excursion would be terminated rather rapidly

once the fuel vaporized, if not earlier, so this assumption is an upper bound. For a fast reactor, limits on the "credible" rates of reactivity insertions might substantiate this rough approximation.

1. Example of Excursion Calculation for a Thermal Reactor. To calculate the energy required to vaporize 20% of the core of the Yankee Reactor, the following information is necessary:*

Core weight, W_F	2.37×10^7 g of UO_2
Specific heat of solid UO_2, C_{p_S}	$18.45 + (2.431 \times 10^{-3}T) - (2.272 \times 10^5 T^2)$ in cal/mole·°C
Reactor operating temperature, T_0	268°C
Reactor operating pressure, P_0	2000 psig
UO_2 melting temperature, T_M	2760°C
UO_2 boiling temperature, T_B	3180°C at 1 atm, 4380°C at P_0
Heat of fusion, ΔH_F	16 kcal/g-mole
Heat of vaporization, ΔH_V	137 kcal/g-mole

From this information

$$Q_V = 0.2W_F \left[C_{p_S}(T_M - T_O) + \Delta H_F + C_{p_M}(T_B - T_M) + \Delta H_V\right]$$

$$= (0.2)(2.37 \times 10^7) \left[(0.081)(2760 - 268) + \frac{16,000}{270} + (0.100)(4380 - 2760) + \frac{137,000}{270}\right]$$

$$= 5.74 \times 10^6 \ (202 + 59.3 + 162 + 508)$$

$$= 5.3 \times 10^9 \text{ cal}$$

$$= 2.3 \times 10^4 \text{ Mw-sec} .$$

Obviously, this result is only approximate. A better calculational technique should evolve from the SPERT destructive test program.

---

*Although C_{p_S} is defined for $T < 2000°K$, average values from the formula are used over the entire temperature range owing to lack of any other data. The best estimate for T_M of many reported values is listed. No attempt was made to adjust to operating conditions. The value T_B (3180°C at 1 atm) was estimated from extrapolation of vapor-pressure data from J. Belle (Ed.), Uranium Dioxide: Properties and Nuclear Applications, pp. 197-98, U.S. Government Printing Office, Washington, 1961; T_B (4380°C at P_0) was estimated from the Clapeyron equation. The value of ΔH_F was obtained from H. H. Hausner and R. G. Mills, "Uranium Dioxide for Fuel Elements," Nucleonics, 15(7): 94-95 (July 1957). No attempt was made to adjust to operating conditions owing to lack of data. The value of ΔH_V was obtained from J. J. Katz and Eugene Rabinowitch, Chemistry of Uranium, USAEC Report TID-5292, 1958. No attempt was made to adjust to operating conditions owing to lack of data.

2. Calculation of Fast Excursion in EBR-II and Fermi. Using the Bethe-Tait approach, the maximum pressure and the ratio of maximum energy density (Q) to threshold energy density (Q^*) have been calculated for various reactivity insertion rates and three values of $(\gamma - 1)Q^*$, where γ is a parameter in the equation of state. The pressure in megabars and the term $[(Q/Q^*) - 1]$ are given for EBR-II in Table 5.28. The calculation for the Fermi reactor gives energy densities similar to those for EBR-II, since the increase in core radius is compensated in part by the increase of the prompt-neutron lifetime. However, the total energy produced in the Fermi reactor is larger, since the volume of the core is larger. To compare these two reactors, values of $(\gamma - 1) = 1$ and $Q^* = 10^{10}$ erg/g have been chosen, and the maximum reactivity, maximum pressure, and total energy developed have been calculated for widely varying reactivity insertion rates. The energy at the higher reactivity insertion rates is considerably in excess of that established for the respective maximum credible accidents. The results given in Table 5.29 were obtained by using the parameters as shown in Table 5.30.

Table 5.28. Maximum Pressure (p) Developed and Ratio of Excess Energy Density to Threshold Energy $(Q/Q^*) - 1$ in EBR-II for Various Reactivity Insertion Rates (in \$/sec = 0.0073/sec) Calculated Assuming Three Different Values for $(\gamma - 1)Q^*$ (in 10^{10} ergs/g)

dk/dt (\$/sec)	p (megabars)			$(Q/Q^*) - 1$		
10	0.036	0.064	0.109	0.95	0.84	0.72
20	0.048	0.079	0.137	1.27	1.04	0.90
50	0.074	0.119	0.21	1.96	1.56	1.37
100	0.103	0.167	0.27	2.7	2.2	1.76
200	0.163	0.27	0.38	4.3	3.6	2.5
500	0.32	0.45	0.67	8.3	5.9	4.4
1000	0.57	0.78	1.08	15.0	10.3	7.1
$(\gamma - 1)Q^*$, 10^{10} ergs/g	0.5	1	2	0.5	1	2

Table 5.29. Maximum Pressure (p) and Total Energy (E) Developed in EBR-II and the Fermi Reactor Assuming $(\gamma - 1) = 1, Q^* = 10^{10}$ ergs/g

dk/dt (\$/sec)	EBR-II			Fermi		
	$\Delta k_{max} \times 10^3$	p (megabars)	E (10^{16} ergs)	$\Delta k_{max} \times 10^3$	p (megabars)	E (10^{16} ergs)
10	0.55	0.064	0.65	0.82	0.073	3.4
20	0.79	0.079	0.72	1.18	0.099	4.0
50	1.26	0.119	0.91	1.89	0.157	5.3
100	1.81	0.167	1.13	2.70	0.22	6.7
200	2.60	0.27	1.63	3.86	0.31	8.9
500	4.16	0.45	2.4	6.22	0.58	15.1
1000	5.96	0.78	4.0	8.90	1.03	25.0

Table 5.30. Parameters for EBR-II and the Fermi Reactor

dk/dt ($/sec)	EBR-II	Fermi
$3\Sigma_{tr}\nu_0\Sigma_f$	1.43×10^{-2} cm^{-2}	0.80×10^{-2} cm^2
p_c	7.6 g·cm^{-3}	7.5 g·cm^{-3}
b	25.0 cm	44.3 cm
q	0.48	0.62
l	0.8×10^{-7} sec	2×10^{-7} sec

5.3.3 Delayed Neutrons

Delayed neutrons produce heat after a reactor has been shut down, although in most cases the amount is insignificant. The diffusion equation for the transient case may be solved to yield the following simplified equation:

$$\frac{\phi(t)}{\phi_0} \sim \frac{\rho}{\rho + \beta} \exp\left(-\frac{\rho + \beta}{l} t\right) + \sum_{i=1}^{m} \frac{\beta_i}{\rho + \beta} \exp\left(-\frac{\rho}{\rho + \beta} \lambda_i t\right) , \qquad (5.43)$$

where

$$\beta = \sum_{i=1}^{m} \beta_i ,$$

and

$\phi(t)$ = thermal-neutron flux as a function of time after shutdown,
ϕ_0 = constant flux up to start of shutdown,
λ_i = decay constant for ith group of delayed neutrons,
m = number of delayed-neutron groups,
ρ = reactivity.

Results calculated using Eq. (5.43) are presented in Fig. 5.57 (ref. 137).

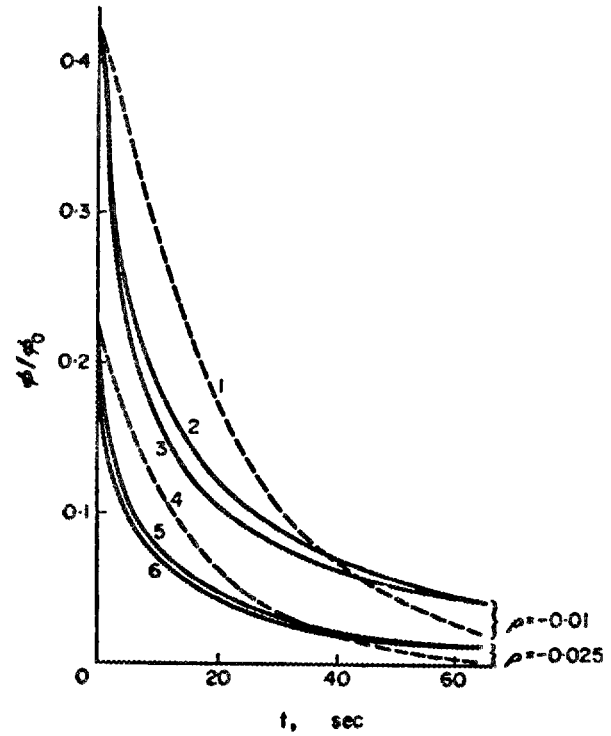

Fig. 5.57. Time Dependence of the Neutron Flux in the Shutdown Reactor. (From ref. 137)

5.3.4 Decay Heat Generation

Fission products in a nuclear reactor continue to release energy by radioactive decay after the chain reaction has subsided. The contribution of this heat source to the initial pressurization of the containment vessel is usually negligible; however, it may be significant to accident analysis through its contributions to core meltdown and to long-term containment pressure. If heat transfer mechanisms are sufficiently disrupted, decay heat could melt and even vaporize the fuel, thereby spreading fission products and possibly initiating chemical reactions that would release more heat.

Initially the decay heat represents 6 to 8% of the reactor's normal operating power level, with a subsequent decline determined by the average half-life of the mixture of fission products. In order to characterize the problem of heat generation from fission products, it is important to know, as a function of time, (1) the energy distribution of the fission-product gammas, (2) the energy release rate of the fission-product gammas, and (3) the energy release rate of the fission-product betas. Computation of these quantities requires that the time function of reactor fission rate, the total reactor operating time, and the time after shutdown be known and that the beta energy release rate and the energy and photon number release rates of a sufficient number of gamma energy groups be known as a function of time for an instantaneous fission event.

Simplified expressions, that is, those of Way-Wigner and Untermyer-Weills, exist but are not considered sufficiently accurate for less than a few hours after shutdown. To date, hazards evaluations of the existing power reactors have, in general, utilized the Way-Wigner expression for calculating decay heat generation. This was permissible because in most cases decay heat was relatively small compared with other heat sources.

A comprehensive survey of recent investigations of fission-product decay energy has been made[138] in which the most reliable information from the various sources[139–143] has been combined. Data on total energy release and gamma energy release after infinite reactor operation are presented in Figs. 5.58 through 5.61. Data from the total energy release curves can be converted to finite operating times by the relation

$$M(t_o,t_s) = M(\infty,t_s) - M(\infty,t_o + t_s),$$

where t_o is reactor operation time and t_s is time after shutdown. Gamma energy release can be obtained in a similar manner from the curves for $G(\infty,t_s)$. The rate of total heat release can then be obtained from

$$Q = \frac{P\ M(t_o,t_s)}{200} \text{ watts} = 49.8\ P\ M(t_o,t_s) \text{ cal/sec}\ , \qquad (5.44)$$

where P is the operating power (watts) of the reactor prior to shutdown, and $M(t_o,t_s)$ is the total energy release rate at t_s sec following constant reactor operation for t_o sec in Mev per fission.

Example. Calculate the total energy release rate at 10^4 sec after shutdown of a reactor that has operated for one month (2.6×10^6 sec) at 1 Mw:

$$t_s = 10^4 \text{ sec}\ ,$$

$$t_o = 2.6 \times 10^6 \text{ sec.}$$

From Fig. 5.58,

$$M(\infty,t_s) = M(\infty,10^4) = 1.9 \text{ Mev/fission},$$

and from Fig. 5.59,

$$M(\infty,t_o + t_s) = M(\infty,2.6 \times 10^6) = 0.4 \text{ Mev/fission}\ ,$$

$$M(t_o,t_s) = M(\infty,10^4) - M(\infty,2 \times 10^6) = 1.9 - 0.4 = 1.5 \text{ Mev/fission}\ ,$$

$$Q = \frac{P\ M(t_o,t_s)}{200} = \frac{10^6 \times 1.5}{200} = 7.5 \times 10^3 \text{ watts}\ .$$

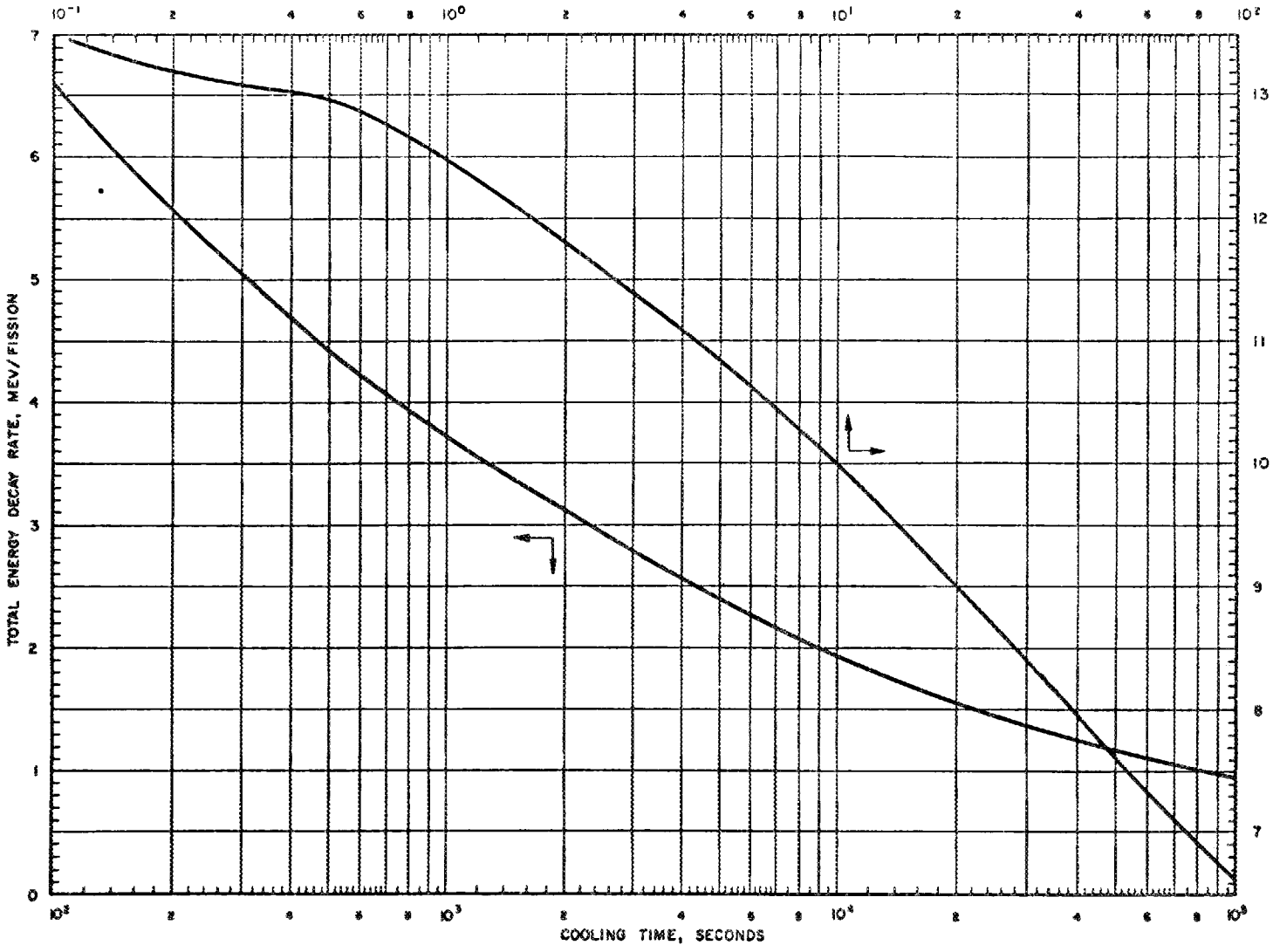

Fig. 5.58. Total Absorbable Energy Released by Fission Products Following Infinite Reactor Operation; Cooling Time, 10^2 to 10^5 sec. (From ref. 138)

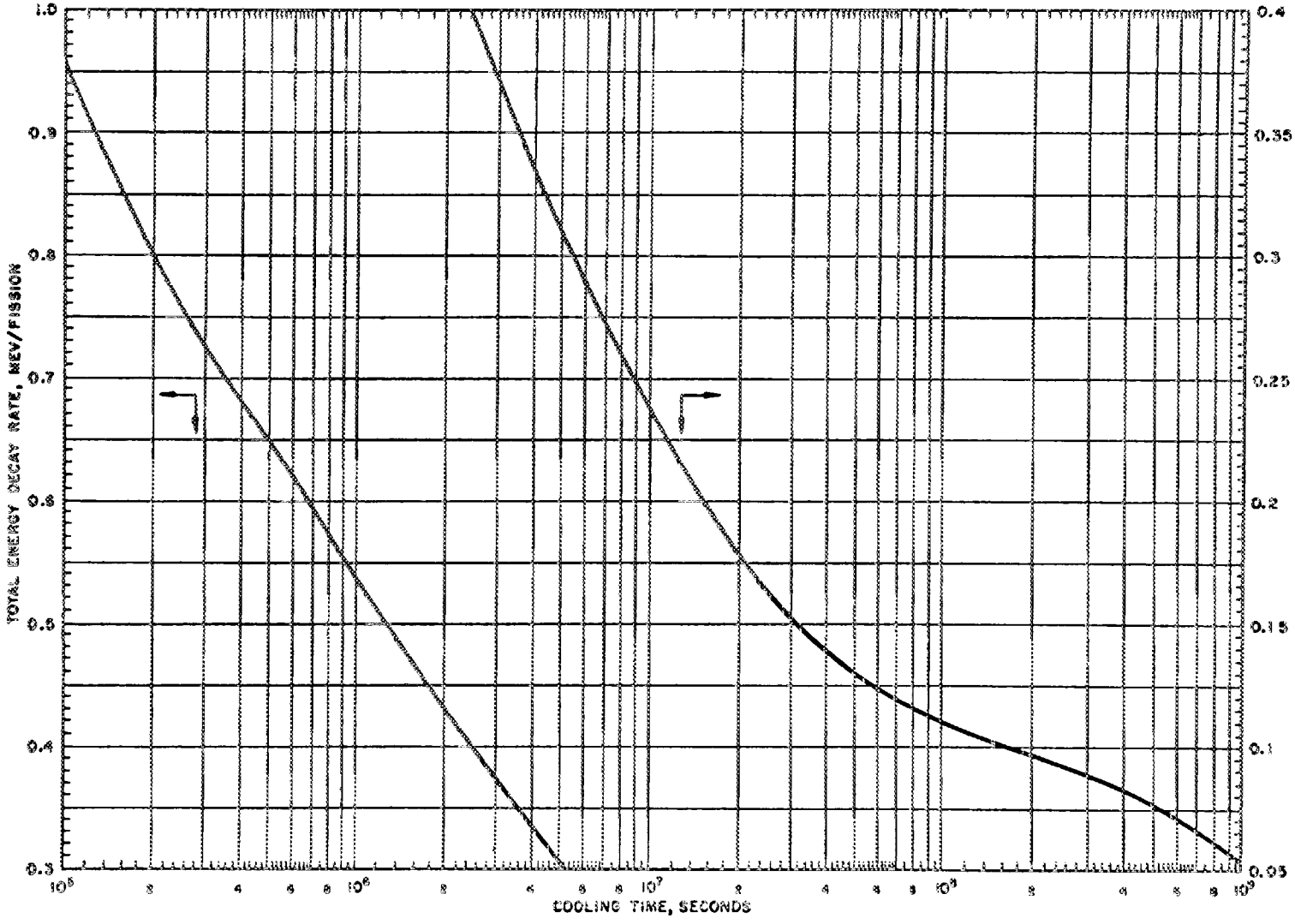

Fig. 5.59. Total Absorbable Energy Released by Fission Products Following Infinite Reactor Operation; Cooling Time, 10^5 to 10^9 sec. (From ref. 138)

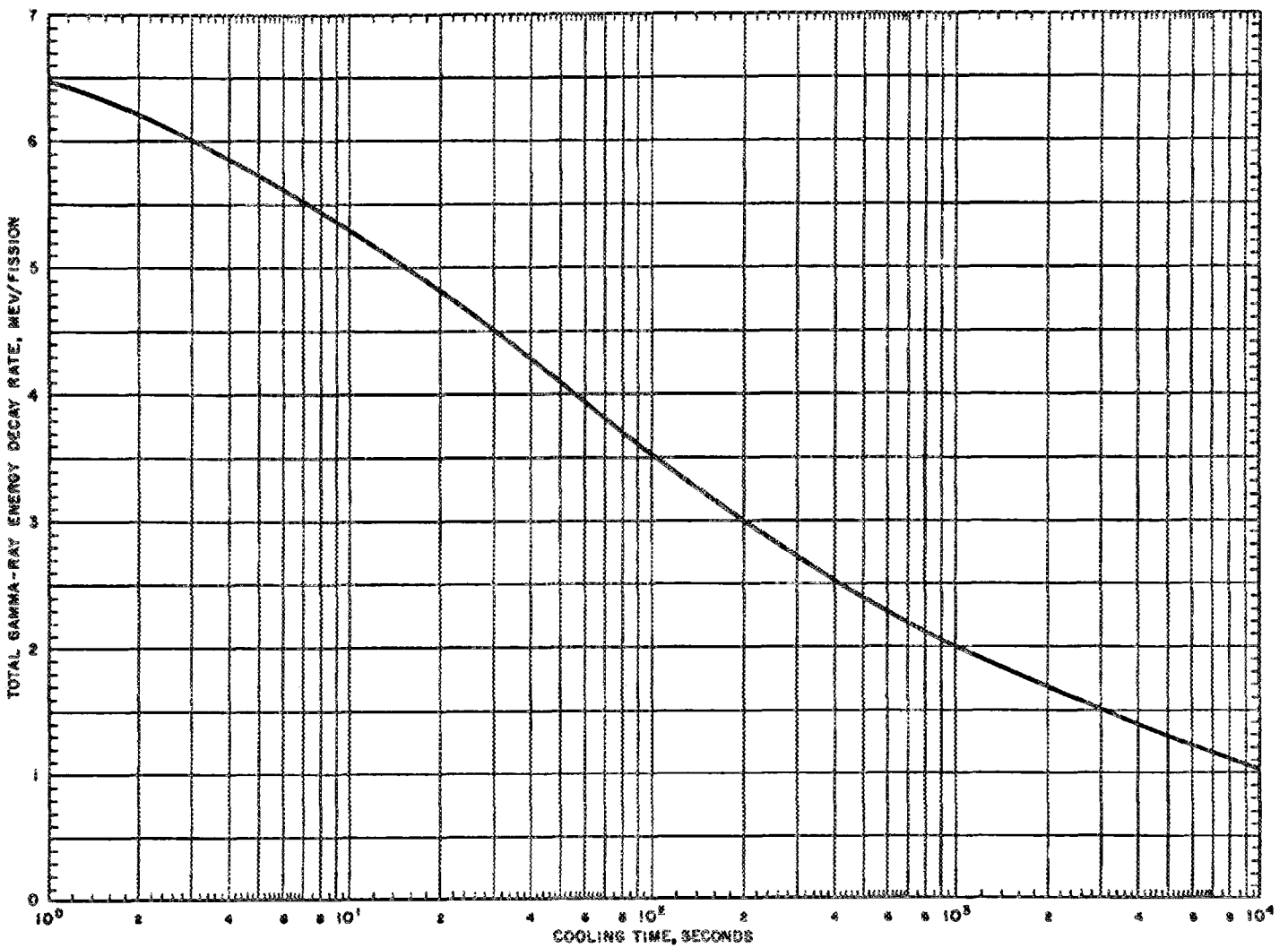

Fig. 5.60. Total Gamma-Ray Energy Released by Fission Products Following Infinite Reactor Operation; Cooling Time, 10^0 to 10^4 sec. (From ref. 138)

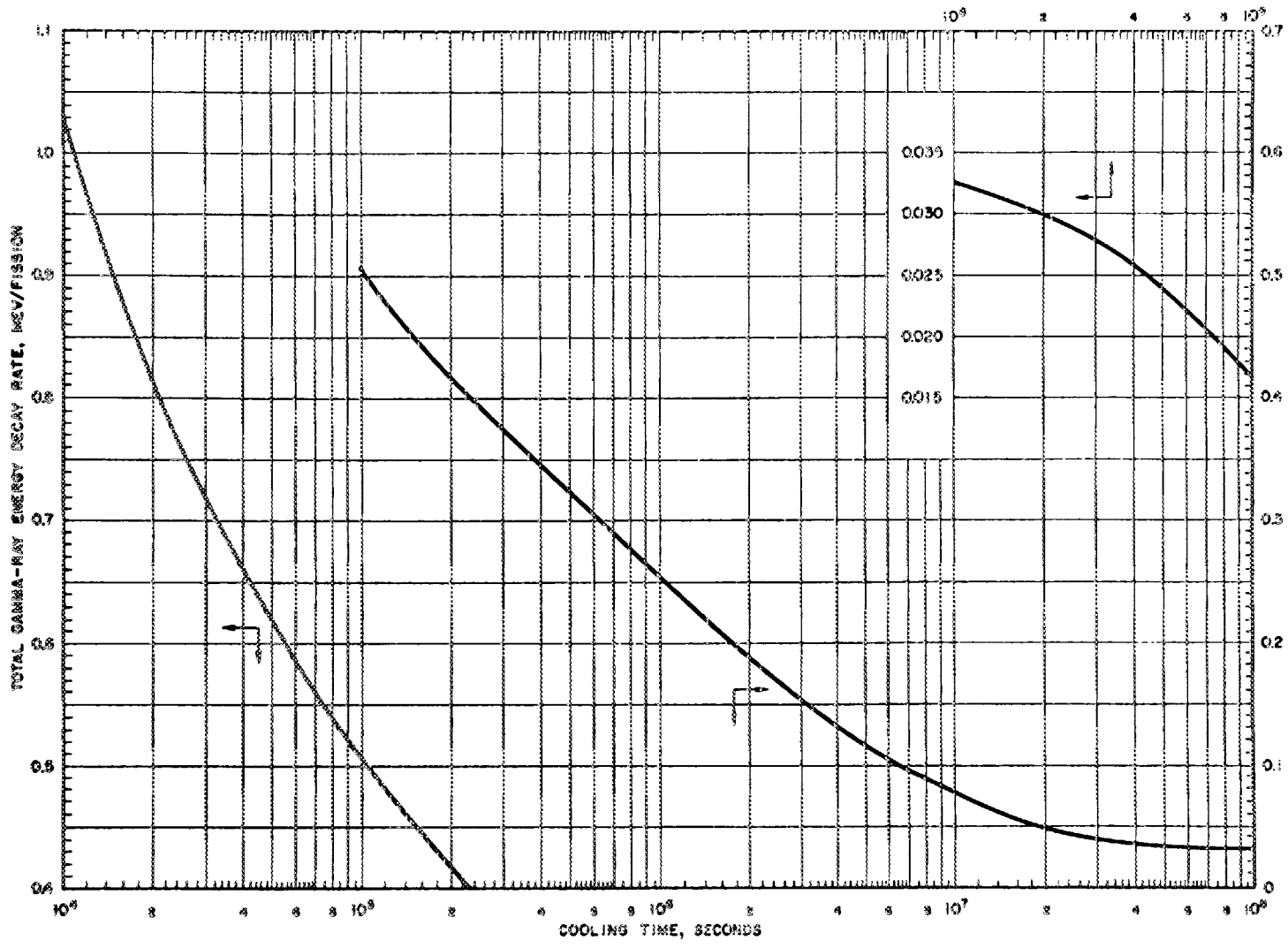

Fig. 5.61. Total Gamma-Ray Energy Released by Fission Products Following Infinite Reactor Operation; Cooling Time, 10^4 to 10^8 sec. (From ref. 138)

The gamma energy release rate $G(t_o,t_s)$ can be calculated similarly in the above example, and if the beta energy $B(t_o,t_s)$ is also desired it can be obtained by obtaining the difference:

$$M(t_o,t_s) = G(t_o,t_s) + B(t_o,t_s) \ .$$

The curves in Figs. 5.58 through 5.61 can be approximated by straight lines over various time intervals. These lines on a log-log plot can then be represented analytically by

$$M(\infty,t) = At^{-a} \ , \tag{5.45}$$

where A is the ordinate intercept and a is the slope. In Tables 5.31 and 5.32, the values for A and a and their deviations from the initial curves are listed for the total energy and gamma energy releases, respectively. Although the maximum deviations for energy release listed above are <10%, the deviation from the slope of the curve is often greater. For $t < 4 \times 10^6$ sec, the slope deviation is <20%, whereas for greater times this can range up to 40%. Such deviations cannot occur when $t_o > 4t_s$.

For hazards evaluations the total energy released from time of shutdown is also of interest:

$$M_{tot} = \int^{t_s} M(t_o,t_s)\ dt \ , \tag{5.46}$$

which represents the area under the curves in Figs. 5.58 through 5.61. Both rate and cumulative energy releases are presented in Table 5.33.

The effects of Bremsstrahlung, photoneutron production, flux magnitude, and neutron energy were investigated and considered within the accuracy of the experimental data and calculations.[144] Also, the fission-product spectrum and yield from U^{233} and Pu^{239} are sufficiently similar to those from U^{235} that no significant difference in decay heat generation should exist.[145,146]

For shutdown times greater than $\sim 10^4$ sec, the more simplified expressions developed by Way-Wigner[147] and Untermyer-Weills[148] are sufficiently accurate to be useful. The Way-Wigner formula,

$$Q_F(\tau,t) = 6.22\ [t^{-0.2} - (t + \tau)^{-0.2}] \ , \tag{5.47}$$

where $Q_F(\tau,t)$ is given in percent of operating power, is based on a statistical theory in which an average decay rate for the mass of fission products is assumed to be constant over the entire time interval.

An empirical formula developed by Untermyer and Weills was based on decay of fission products produced in natural uranium and, consequently, included contributions from U^{239} and Np^{239}:

Table 5.31. Constants for Total Power Emission Equation[a]

Applicable Time Interval (sec)	A	a	Maximum Positive Deviation	Maximum Negative Deviation
$10^{-1} \leq t < 10^{1}$	12.05	0.0639	4% at 10^{0} sec	3% at 10^{1} sec
$10^{1} \leq t \leq 1.5 \times 10^{2}$	15.31	0.1807	3% at 1.5×10^{2} sec	1% at 3×10^{1} sec
$1.5 \times 10^{2} < t < 4 \times 10^{6}$	26.02	0.2834	5% at 1.5×10^{2} sec	5% at 3×10^{3} sec
$4 \times 10^{6} \leq t \leq 2 \times 10^{8}$	53.18	0.3350	8% at 4×10^{7} sec	9% at 2×10^{8} sec

[a]From ref. 138, p. 10, Table II.

Table 5.32. Constants for Total Gamma Power Emission Equation[a]

Applicable Time Interval (sec)	A	a	Maximum Positive Deviation	Maximum Negative Deviation
$10^{0} \leq t < 1.5 \times 10^{2}$	6.710	0.1316	7% at 1.5×10^{2} sec	7% at 10^{1} sec
$1.5 \times 10^{2} \leq t \leq 10^{6}$	14.77	0.2919	7% at 1.5×10^{2} sec	6% at 4×10^{3} sec
$10^{6} < t < 3.5 \times 10^{7}$	536.4	0.5500	4% at 2×10^{7} sec	5% at 4×10^{6} sec
$3.5 \times 10^{7} \leq t \leq 4 \times 10^{8}$	0.4285	0.1405	2% at 4×10^{8} sec	1% at 3.5×10^{7} sec

[a]From ref. 138, p. 10, Table III.

Table 5.33. Energy Release Rate from Fission-Product Decay in a U^{235}-Fueled Reactor After Shutdown[a]

Operating Time, t_o (hr)	Shutdown Time, t_s (sec)	Q_γ (%)[b]	Q_β (%)[b]	Q_F (%)[b]	E_F (%-sec)[c]
10^0	10^0	2.53	2.35	4.88	6
	10^1	1.95	1.70	3.65	55
	10^2	1.06	0.93	1.99	250
	10^3	0.34	0.29	0.625	1,180
	10^4	0.01	0.005	0.015	3,150
	10^5				4,950
10^1	10^0	2.90	2.68	5.58	6
	10^1	2.32	2.03	4.35	55
	10^2	1.42	1.24	2.66	400
	10^3	0.66	0.55	1.21	1,880
	10^4	0.20	0.15	0.35	7,400
	10^5	0.023	0.007	0.030	16,200
	10^6	0.0025		0.0025	23,600
10^2	10^0	3.04	2.84	5.88	6
	10^1	2.46	2.19	4.65	55
	10^2	1.57	1.39	2.96	400
	10^3	0.81	0.71	1.52	2,480
	10^4	0.33	0.30	0.63	9,600
	10^5	0.088	0.060	0.148	33,500
	10^6	0.016	0.009	0.025	86,000
	10^7				200,000
	10^8				230,000
10^3	10^0	3.17	2.89	6.06	6
	10^1	2.59	2.24	4.83	55
	10^2	1.70	1.44	3.14	400
	10^3	0.93	0.76	1.69	2,480
	10^4	0.44	0.36	0.80	13,600
	10^5	0.185	0.123	0.308	51,500
	10^6	0.068	0.044	0.112	203,000
	10^7	0.007	0.005	0.012	481,000
	10^8				771,000

[a]Gamma energy release rate, Q_γ (τ,t) % of operating power; beta energy release rate, Q_β (τ,t) % of operating power; total energy release rate, Q_F (τ,t) % of operating power; cumulative energy release after shutdown, E_F (τ,t).

[b]Multiply by power/100 to obtain units of power.

[c]Multiply by power/100 to obtain units of energy, i.e., power-sec.

Table 5.33. (continued)

Operating Time, t_o (hr)	Shutdown Time, t_s (sec)	Q_γ (%)[b]	Q_β (%)[b]	Q_F (%)[b]	E_F (%-sec)[c]
10^4	10^0	3.22	2.94	6.16	6
	10^1	2.64	2.29	4.93	55
	10^2	1.75	1.49	3.24	400
	10^3	0.98	0.81	1.79	2,480
	10^4	0.492	0.412	0.904	13,600
	10^5	0.236	0.172	0.408	68,500
	10^6	0.110	0.088	0.198	260,000
	10^7	0.022	0.028	0.050	1,090,000
	10^8				2,270,000
10^5	10^0	3.22	2.97	6.19	6
	10^1	2.64	2.32	4.96	55
	10^2	1.75	1.52	3.27	400
	10^3	0.99	0.83	1.82	2,480
	10^4	0.497	0.436	0.933	13,600
	10^5	0.240	0.197	0.437	68,500
	10^6	0.113	0.113	0.226	370,000
	10^7	0.025	0.049	0.074	1,420,000
	10^8	0.003	0.012	0.015	4,150,000
∞	10^0	3.24	2.99	6.23	6
	10^1	2.66	2.34	5.00	55
	10^2	1.77	1.54	3.31	400
	10^3	1.00	0.87	1.87	2,480
	10^4	0.510	0.465	0.975	13,600
	10^5	0.254	0.225	0.479	68,500
	10^6	0.127	0.142	0.269	370,000
	10^7	0.038	0.079	0.117	1,822,500
	10^8	0.015	0.040	0.055	8,052,500

$$Q_F(\tau,t) = 10\{(t + 10)^{-0.2} - (t + \tau + 10)^{-0.2}$$

$$- 0.87[(t + 2 \times 10^7)^{-0.2} - (t + \tau + 2 \times 10^7)^{-0.2}]\} , \quad (5.48a)$$

where $Q_F(\tau,t)$ is given as percent of operating power. Estimated accuracy by Untermyer and Weills for their expression is listed below:

$1 \leq t \leq 10^2$ within ±50%
$10^2 \leq t \leq 10^4$ within ±30%
$10^4 \leq t \leq 10^6$ within ±10%
$10^6 \leq t \leq 10^8$ within ±50%

To obtain the heat generation from U^{235} fission products above, the heat from U^{239} and Np^{239} should be subtracted from the above expression:

$$Q_{U^{239}}(\tau,t) = 0.25\left[e^{-t/2040} - e^{-(t+\tau)/2040}\right] \tag{5.48b}$$

$$Q_{Np^{239}}(\tau,t) = 0.13\left[e^{-t/290,000} - e^{-(t+\tau)/290,000}\right], \tag{5.48c}$$

where both values are given as percent of operating power. A graphic comparison of the three methods presented here is shown in Fig. 5.62, which is based on an infinite reactor operating time.[147–149]

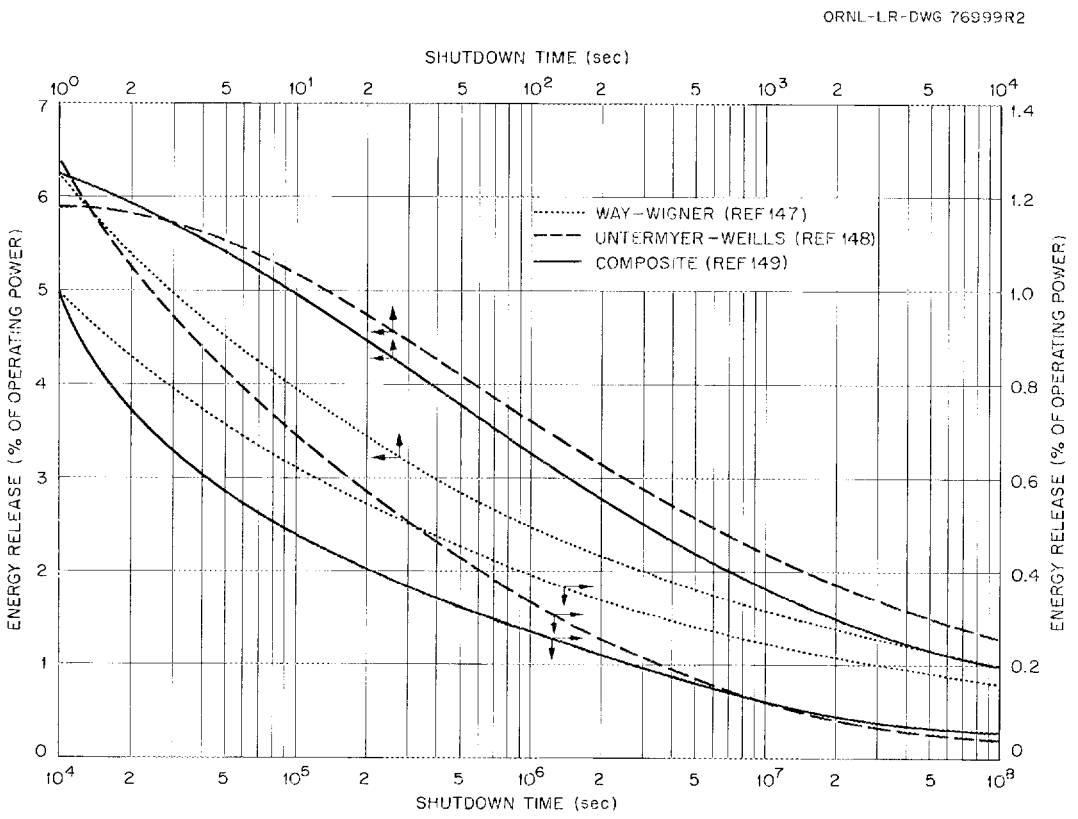

Fig. 5.62. Comparison of Methods for Obtaining Heat Generation Rate.

5.4 OTHER HEAT SOURCES

Additional sources of heat that exist in certain reactor systems and should be considered in containment design are described here, with references to specific data.

5.4.1 Heat Content of Materials

Large amounts of heat can accumulate in reactor materials as the result of operating conditions, and in some cases this may represent the major contribution to pressure buildup in the containment system in accident analysis; for example, flashing of coolant water in accidents involving primary coolant system ruptures in pressurized-water reactors. In other cases, significant contributions may be represented by heat transfer from high-temperature regions of core and structural materials as in Peach Bottom.

This energy is represented by both the sensible heat and the latent heat contained in the materials. Since the vast amount of data on this type of energy makes its inclusion here impractical, information concerning the source of the most accurate and usable figures presently available is summarized in the following section (see Table 5.34; refs. 150 to 168).

5.4.2 Stored Energy in Graphite (Wigner Energy)

Graphite, when exposed to a neutron flux, undergoes damage resulting from collisions between neutrons and carbon atoms. One of the effects of this damage (first theoretically predicted by Wigner) is the formation of excess energy in the crystalline structure of the graphite in the form of both simple and complex crystal lattice defects. Rearrangement of the atoms to eliminate these defects, for example, by heating, will release the energy as heat. Stored energy represents a hazard when its release (resulting from an abnormal temperature rise) would be sufficient to contribute to the course of an accident by causing the temperature to rise higher and more quickly than could be safely controlled.

Air-cooled low-temperature graphite-moderated research reactors require annealing operations during which the graphite temperature rise must be carefully controlled. The Windscale accident[169] illustrated the severe consequences of an uncontrolled release of Wigner energy in such a low-temperature reactor. Graphite employed in current and future high-temperature, gas-cooled power reactors will be subject to a much reduced degree of Wigner energy accumulation. However low-temperature locations, such as the reflector and coolant inlet section of the core, should be examined for the amount of stored Wigner energy.

The current status of experimental data and theoretical developments on Wigner energy problems has been presented by Nightingale and his coworkers.[57] The brief summary of the status of Wigner stored energy and release studies presented below is drawn from ref. 57, which should be consulted for a complete treatment of this subject.

Table 5.34. Heat Content of Reactor Materials

Material	Property	Parameter	Range	Principal Reference
Fluids				
Water (steam)	Enthalpy	Temperature Pressure	32-1600°F 0.2-5500 psia	J. H. Keenan and F. G. Keyes, Thermodynamic Properties of Steam, Wiley, New York, 1936
	Entropy	Temperature Pressure	32-1600°F 0.2-5500 psia	
	Specific heat, latent heats	Temperature Pressure	0-1600°F 0-5500 psia	
Heavy water[150,151]	Thermal conductivity	Temperature	10-60°C	H. Etherington (Ed.), Nuclear Engineering Handbook, 1st ed., Chap. 9, pp. 16-19, McGraw-Hill, New York, 1958
	Specific heat	Temperature	10-50°C	
	Latent heats	Temperature	3-220°C	
Air[152,153]	Heat capacity	Temperature Pressure	100-2400°F 1-100 atm	C. R. Tipton, Jr. (Ed.), Reactor Handbook, Vol. I, Materials, 2d ed., pp. 980-81, Interscience, New York, 1960
	Thermal conductivity	Temperature	100-1300°F	
Helium[153]	Heat capacity	Temperature Pressure	0-600°F 14.7-6000 psia	Ibid., Reactor Handbook, pp. 986-87
	Thermal conductivity	Temperature	0-1100°F	
Nitrogen[152]	Heat capacity	Temperature Pressure	60-5000°F 1-100 atm	Ibid., Reactor Handbook, pp. 989-90
	Thermal conductivity	Temperature	25-1800°F	
Carbon dioxide[152]	Heat capacity	Temperature Pressure	100-2000°F 1-100 atm	Ibid., Reactor Handbook, p. 985
	Thermal conductivity	Temperature	80-600°F	
Organics				
Polyphenyls	Heat capacity, thermal conductivity, latent heats	Temperature	200-800°F	Ibid., Reactor Handbook, pp. 946-48
Liquid metals				
Sodium (or NaK)	Enthalpy, entropy, specific heat	Temperature	0-900°C	C. B. Jackson (Ed.), Liquid Metals Handbook, Sodium-NaK Supplement, USAEC Report TID-5277, pp. 24-41, July 1, 1955
	Heat capacity	Temperature	0-1500°F	
	Thermal conductivity, latent heats	Temperature	200-1300°F	
Molten salts[154]	Heat capacity, enthalpy, latent heats	Temperature	Varies with composition	Op. cit., Reactor Handbook, pp. 446-47
Mercury[155]	Heat capacity	Temperature	0-450°C	Op. cit., Reactor Handbook, pp. 996-97
	Thermal conductivity, latent heats	Temperature	0-1200°C	
Bismuth[155]	Heat capacity	Temperature	271-1000°C	Op. cit., Reactor Handbook, pp. 996-97
	Thermal conductivity, latent heats	Temperature	300-700°C	
Potassium[155]	Heat capacity	Temperature	75-600°C	Op. cit., Reactor Handbook, pp. 996-97
	Thermal conductivity, latent heats	Temperature	200-600°C	

Table 5.34. (continued)

Material	Property	Parameter	Range	Principal Reference
Solids				
Stainless steel	Thermal conductivity, specific heat	Temperature	100–500°C	Op. cit., Reactor Handbook, pp. 567–85
Structural steel	Thermal conductivity, specific heat, latent heats	Temperature	Varies with composition	I. Lyman (Ed.), Properties and Selection of Metals, in Metals Handbook, Vol. I, 8th ed., pp. 422–23, American Society of Metals, Novelty, Ohio, 1961
Zirconium[156–159] (or Zircaloy)	Thermal conductivity	Temperature	25–400°C	Op. cit., Reactor Handbook, pp. 710–11
	Specific heat, latent heats	Temperature	200–1500°C	
Aluminum[155]	Thermal conductivity	Temperature	100–400°C	Op. cit., Reactor Handbook, pp. 484–85
	Specific heat	Temperature	150–600°C	
	Enthalpy, latent heats	Temperature	100–600°C	
Graphite	Thermal conductivity	Temperature	−100–2500°C	Op. cit., Reactor Handbook, p. 889
	Specific heat, enthalpy, entropy, latent heats	Temperature	25–1127°C	
Uranium[160–167]	Heat capacity, thermal conductivity, enthalpy, entropy	Temperature	10–1100°K	Op. cit., Reactor Handbook, pp. 112–13
Uranium dioxide[160,161,168]	Thermal conductivity	Temperature	0–850°C	Op. cit., Reactor Handbook, p. 293
	Specific heat	Temperature	100–1500°K	

5.4.2.1 Effect of Irradiation

The total stored energy increases with radiation dose and intensity and decreases with irradiation temperature. The neutron energy spectrum is also an important irradiation condition, since fast neutrons create more lattice defects than slow neutrons. The mechanisms of these effects are not completely understood.

The increase in stored energy with neutron exposure is shown in Fig. 5.63 (refs. 170 to 173) for temperatures from 30 to 450°C. The original data were taken from Hanford reactor irradiations of CSF graphite and British irradiations in Calder Hall, DIDO, and PLUTO reactors of PGA graphite. Stored energy, S, accumulates at a much lower rate at 300°C than at 30°C and also saturates at a much lower value. Although the higher temperature energy storage does not appear to reach a troublesome level, irradiations in the order of 50,000 Mwd/At are necessary to cover the expected life of central-station power reactors.

The neutron energy spectrum affects the stored energy and other radiation-damage properties. Equivalent dose, equivalent temperature, and damage flux concepts have been used to relate reactor design doses to existing stored energy versus neutron dose data from Calder and Hanford

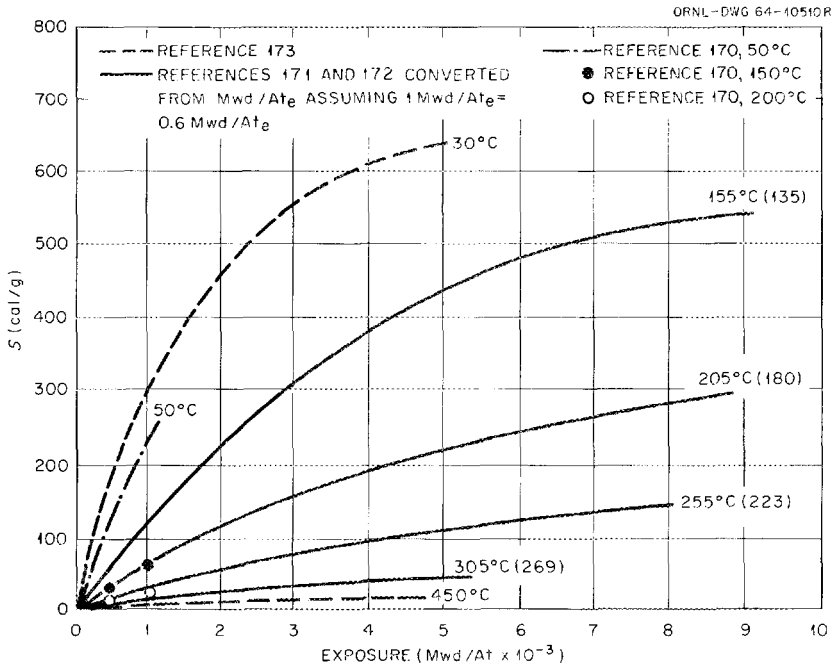

Fig. 5.63. The Accumulation of Total Stored Energy (S) at Several Irradiation Temperatures. Equivalent Calder irradiation temperatures are shown in parentheses for each curve. (From ref. 57)

reactors. For example, the equivalence of Calder Hall and Hanford irradiations has been determined[57] to be 1 Mwd/At (Hanford) = 0.6 Mwd/At$_e$ (Calder). Details of neutron energy spectrum effects on damage investigations are presented in ref. 57.

5.4.2.2 Energy Release

The release of stored energy has been investigated at low temperatures (~30°C) and high temperatures (>150°C) with neutron doses to approximately 5000 Mwd/At. The rate of release of energy stored during low-temperature irradiation as a function of annealing temperature exhibits a maximum near 200°C that broadens as the neutron dose increases,[174] as shown in Fig. 5.64. Hence the stored energy release rate (cal/g·°C) exceeds the specific heat of graphite from about 125°C to 300 to 400°C, depending on neutron dosage. Stored-energy release curves[171,172] for high-temperature irradiations exhibit a broad maximum, as shown in Fig. 5.65. The maximum release rate decreases with increasing irradiation temperature and occurs at higher annealing temperatures, as in Fig. 5.65. Thus higher annealing temperatures are required to release the stored energy from high-temperature irradiation.

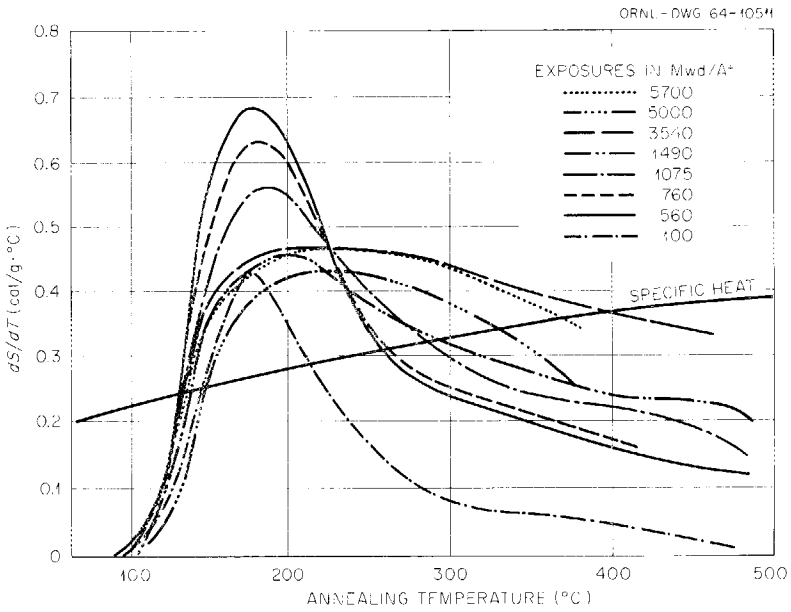

Fig. 5.64. Stored-Energy Release Curves[174] of CSF Graphite Irradiated Near 30°C. (From ref. 57)

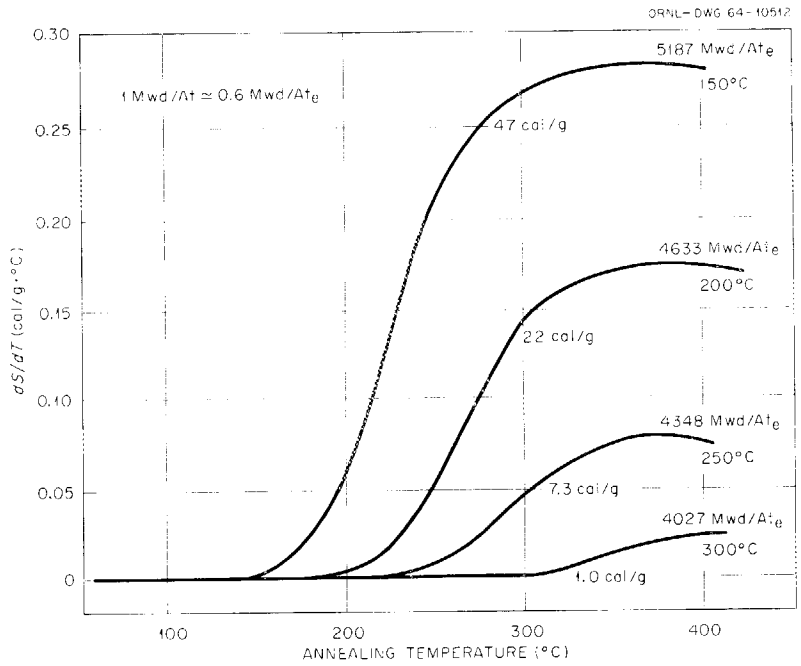

Fig. 5.65. The Effect of Irradiation Temperature on Stored-Energy Release Curves for High Exposures.[171,172] Numbers under the curves give the stored energy released to 400°C. (From ref. 57)

References

1. L. F. Epstein, Metal-Water Reactions: VII. Reactor Safety Aspects of Metal-Water Reactions, USAEC Report GEAP-3335, General Electric Co., Jan. 31, 1960.

2. S. C. Furman, Metal-Water Reactions: V. The Kinetics of Metal-Water Reactions - Low Pressure Studies, USAEC Report GEAP-3208, General Electric Co., 1959.

3. L. Baker, Jr., and L. C. Just, Studies of Metal-Water Reactions at High Temperatures: III. Experimental and Theoretical Studies of the Zirconium-Water Reaction, USAEC Report ANL-6548, Argonne National Laboratory, 1962.

4. L. F. Epstein, Correlation and Prediction of Explosive Metal-Water Reaction Temperatures, Nucl. Sci. Eng., 10(3): 247 (July 1961).

5. L. Baker, Jr., R. L. Warchal, R. C. Vogel, and M. Kilpatrick, Studies of Metal-Water Reactions at High Temperatures: I. The Condenser Discharge Experiment: Preliminary Results with Zirconium, USAEC Report ANL-6257, Argonne National Laboratory, 1961.

6. R. E. Wilson, L. Mishler, and C. Barnes, Metal-Water Reactions: Studies of the Aluminum-Water Reaction by the Levitation-Melting Method, Chemical Engineering Division Summary Report, Oct., Nov., Dec., 1962, p. 196, USAEC Report ANL-6648, Argonne National Laboratory, 1963.

7. H. M. Higgins and R. D. Schultz, The Reaction of Metals in Oxidizing Gases at High Temperatures, USAEC Report IDO-28000, Phillips Petroleum Co., 1957.

8. W. B. Lewis, The Accident to the NRX Reactor on December 12, 1952, Canadian Report DR-32, 1953.

9. D. G. Hurst, The Accident to the NRX Reactor: Part II, Canadian Report GPI-14, 1953.

10. General Electric Co., Final Report of SL-1 Recovery Operation, USAEC Report IDO-19311, 1962.

11. J. R. Buchanan, SL-1 Final Report, Nucl. Safety, 4(3): 83 (1963).

12. Phillips Petroleum Co., Report on the Nuclear Incident at the SL-1 Reactor, January 3, 1961, at the National Reactor Testing Station, USAEC Report IDO-19302.

13. J. R. Dietrich, Experimental Investigation of the Self-Limitation of Power During Reactivity Transients in a Subcooled Water-Moderated Reactor, BORAX-I Experiments, USAEC Report AECD-3668, 1954.

14. T. R. Wilson, An Engineering Description of the SPERT-1 Reactor Facility, USAEC Report IDO-16318, Phillips Petroleum Co., 1957.

15. Phillips Petroleum Co., Quarterly Technical Report, SPERT Project, Jan., Feb., March, 1963, USAEC Report IDO-16893, 1963.

16. Report on SPERT-1 Destructive Test Results, Trans. Am. Nucl. Soc., 6(1): 137-141 (June 1963).

17. W. A. Bostrom, The High Temperature Oxidation of Zircaloy in Water, USAEC Report WAPD-104, Bettis Atomic Power Laboratory, 1954.

18. A. W. Lemmon, Jr., Studies Relating to the Reaction Between Zirconium and Water at High Temperatures, USAEC Report BMI-1154, Battelle Memorial Institute, 1957.

19. B. Lustman, Zirconium-Water Reactions, USAEC Report WAPD-137, Bettis Atomic Power Laboratory, 1955.

20. M. Milich and E. C. King, Molten Metal-Water Reactions, USAEC Report NP-5813, Tech. Rpt. No. 44, DTI Extension, AEC, Oak Ridge, 1955.

21. H. M. Higgins, A Study of the Reaction of Metals and Water, USAEC Report AECD-3664, Hanford Atomic Products Operation, 1955.

22. W. C. Ruebsamen, F. J. Shon, and J. B. Chrisney, Chemical Reaction Between Water and Rapidly Heated Metals, USAEC Report NAA-SR-197, North American Aviation, Inc., 1952.

23. H. M. Higgins, The Reaction of Molten Uranium and Zirconium Alloys with Water, Report AGC-AE-17, Aerojet-General Corp., 1956.

24. R. O. Ivins, F. J. Testa, and P. Krause, Metal-Water Reaction Studies in TREAT, Chemical Engineering Division Summary Report, July, Aug., Sept., 1962, p. 191, USAEC Report ANL-6596, Argonne National Laboratory, 1962.

25. R. C. Liimatainen, R. O. Ivins, M. F. Deerwester, and F. J. Testa, Studies of Metal-Water Reactions at High Temperatures. II. TREAT Experiments: Status Report on Results with Aluminum, Stainless Steel-304, Uranium and Zircaloy-2, USAEC Report ANL-6250, Argonne National Laboratory, 1962.

26. W. M. Manning, J. J. Katz, and H. R. Hoekstra, Reactor Hazards, USAEC Report ANL-WMM-596, Argonne National Laboratory, 1950.

27. B. E. Hopkinson, Kinetics of the Uranium-Steam Reaction, J. Electrochem. Soc., 106: 102 (1959).

28. R. E. Wilson and P. Martin, Metal-Water Reactions: Isothermal Studies of the Uranium-Steam Reaction by the Volumetric Method, Chemical Engineering Division Summary Report, April, May, June 1962, p. 148, USAEC Report ANL-6569, Argonne National Laboratory, 1962.

29. W. F. Zelezny, Metal-Water Reactions: Rates of Reaction of Aluminum and Aluminum-Uranium Alloys with Water Vapor at Elevated Temperatures, USAEC Report IDO-16629, Phillips Petroleum Co., 1960.

30. D. Mason and P. Martin, Metal-Water Reactions: Pressure Pulse Method, Chemical Engineering Division Summary Report, July, Aug., Sept., 1961, p. 178, USAEC Report ANL-6413, Argonne National Laboratory, 1961.

31. R. E. Wilson and P. Martin, Metal-Water Reactions: Levitation Method, Chemical Engineering Division Summary Report, April, May, June, 1961, p. 208, USAEC Report ANL-6379, Argonne National Laboratory, 1961.

32. J. M. West and J. T. Weills, Reactor Engineering and Services Division Quarterly Report, Sept. 1-Nov. 30, 1950, p. 5, USAEC Report ANL-4549, Argonne National Laboratory, 1950.

33. R. B. Cox, H. M. Higgins, and E. G. Lucken, Research Development and Testing of Underwater Propulsion Devices, Report AGC-AE-464, Aerojet-General Corp., 1950.

34. G. Long, Explosions of Molten Aluminum in Water - Cause and Prevention, Metal Progr., 71: 107 (1957)

35. A. A. Shidlovskii, Explosive Methyl Alcohol-Water Mixtures with Magnesium and Aluminum, Zh. Prikl. Khim., 19: 371 (1946).

36. R. O. Ivins, F. J. Testa, and P. Krause, Studies of the Aluminum-Water Reaction in TREAT, Chemical Engineering Division Summary Report, Oct., Nov., Dec., 1962, p. 201, USAEC Report ANL-6648, Argonne National Laboratory, 1963.

37. R. O. Ivins, F. J. Testa, and P. Krause, Studies of the Aluminum Water Reaction in TREAT, Chemical Engineering Division Summary Report, Jan., Feb., March, 1963, p. 179, USAEC Report ANL-6687, Argonne National Laboratory, 1963.

38. R. C. Liimatainen, R. O. Ivins, and F. J. Testa, Metal-Water Reaction Studies in TREAT, Chemical Engineering Division Summary Report, Jan., Feb., March, 1962, p. 186, USAEC Report ANL-6543, Argonne National Laboratory, 1962.

39. L. F. Epstein, Recent Developments in the Study of Metal-Water Reactions, Progress in Nuclear Energy, Series IV, Vol. 4, p. 461, Pergamon Press, New York, 1961.

40. L. Brewer and A. W. Searcy, The Gaseous Species of the $Al-Al_2O_3$ System, J. Am. Chem. Soc., 73: 5308 (1951).

41. D. S. Gibbs and H. J. Svec, Kinetics of the Reaction Between Magnesium and Water Vapor, Report ISC-779, Iowa State College, 1956.

42. M. Farber, High-Temperature Reaction Rates of Several Metals with Hydrogen Chloride and Water Vapor, J. Electrochem. Soc., 106: 751 (1959).

43. L. Baker, Jr., R. Warchall, and R. Koonz, Metal-Water Reactions: Condenser-Discharge Method, Chemical Engineering Division Summary Report, July, Aug., Sept., 1962, p. 386, USAEC Report ANL-6596, Argonne National Laboratory, 1962.

44. Nuclear Development Corp. of America, Chemical Considerations in the Sodium Cooled D_2O Moderated Reactor (SDR), Report NDA-84-6, 1958.

45. P. B. Longton, Reactions of the Alkali Metals with Gases, British Report IGR-TN/C 418, pp. 10-13, December 1956.

46. L. Corrsin, H. Steinmentz, and B. Marano, Sodium-Water Reactor Rate Studies, Report NDA-84-19, Nuclear Development Corp. of America, 1959.

47. Knolls Atomic Power Laboratory Staff, Progress Report No. 45, USAEC Report KAPL-341, 1950.

48. M. Kilpatrick, L. Baker, and C. McKinney, Studies of Fast Reactions Which Evolve Gases. The Reaction of Sodium-Potassium Alloy with Water in the Presence and Absence of Oxygen, J. Phys. Chem., 57(4): 385 (1953).

49. N. R. Adolph, Recent Test Results of Sodium-Water Systems, Proceedings of Second United Nations International Conference on Peaceful Uses of Atomic Energy, Geneva, 1958, Vol. 7, p. 119, United Nations, New York, 1958.

50. J. R. Dietrich and W. H. Zinn, Solid Fuel Reactors, Addison-Wesley Publishing Co., Inc., Reading, Mass., 1958.

51. C. B. Jackson (Ed.), Liquid Metals Handbook, Sodium-NaK Supplement, USAEC Report TID-5277, 1955.

52. J. I. Owens, R. W. Lockhart, D. R. Iltis, and K. Hikido, Metal-Water Reactions: VIII. Preliminary Consideration of the Effects of a Zircaloy-Water Reaction During a Loss of Coolant Accident in a Nuclear Reactor, USAEC Report GEAP-3279, General Electric Co., 1959.

53. L. Baker, Jr., Metal-Water Reactions, Nucl. Safety, 7(1), Fall 1965.

54. J. I. Owens, Metal-Water Reactions: II. An Evaluation of Severe Nuclear Excursions in Light Water Reactors, USAEC Report GEAP-3178, General Electric Co., 1959.

55. R. O. Ivins, A Study of the Reaction of Aluminum Uranium Alloy Fuel Plates with Water Initiated by a Destructive Reactive Transient, Trans. Am. Nucl. Soc., 6(1): 101-102 (June 1963).

56. P. L. Walker, Jr., et al., Gas Reactions of Carbon, in Advances in Catalysis, Vol. XI, pp. 133-221, Academic Press, Inc., New York, 1959.

57. R. E. Nightingale et al., Nuclear Graphite, Academic Press, Inc., New York, 1962.

58. R. A. Wullaert et al., Effects of Radiation on Ceramic Materials — Carbon, in Effects of Radiation on Materials and Components, pp. 330-352, edited by John F. Kirchner and Richard E. Bowman, Reinhold Publishing Corporation, New York, 1964.

59. J. H. Perry et al., Chemical Engineer's Handbook, 3rd Ed., p. 237, McGraw-Hill, New York, 1950.

60. D. G. Schweitzer et al., Oxidation and Heat Transfer Studies in Graphite Channels, I. The Effect of Air Flow Rate on the $C-O_2$ and $CO-O_2$ Reactions, Nucl. Sci. Eng., 12: 39 (1962).

61. J. W. Prados, Graphite Oxidation, Nucl. Safety, 2(4): 8-13 (June 1961).

62. F. K. Earp and M. W. Hill, Oxidation of Carbon and Graphite, pp. 326-333 in Industrial Carbon and Graphite, Society of Chemical Industry, London, 1958.

63. R. E. Dahl, Preliminary Evaluation of Chlorine for Use as a Gas Cooled Reactor Safeguard, USAEC Report HW-63902 (Rev.), Hanford Atomic Products Operation, March 1960.

64. E. A. Gulbranson and K. F. Andrew, Reactions of Artificial Graphite, Ind. Eng. Chem., 44: 1034-1051 (1952).

65. L. M. Currie, V. C. Hamister, and H. G. MacPherson, The Production and Properties of Graphite for Reactors, Proceedings of the International Conference on the Peaceful Uses of Atomic Energy, Geneva, 1955, Vol. 8, pp. 451-473, United Nations, 1956.

66. P. J. Robinson, The Effects of Diffusional Control of Oxidation of Graphite on the Highest Safe Temperatures in Air, British Report IGR-143(RD/W), May 20, 1959.

67. W. L. Kosiba and G. J. Dienes, The Effect of Radiation on the Rate of Oxidation of Graphite, pp. 121-132 in US/UK Graphite Conference, London, USAEC Report TID-7565, 1957.

68. J. R. Beattie, J. B. Lewis, R. Lind, Graphite Oxidation and Reactor Safety, Third International Conference on the Peaceful Uses of Atomic Energy, Geneva, Switzerland, 1964, A/Conf.28/P/185, United Kingdom.

69. W. L. Kosiba and G. J. Dienes, The Effect of Displaced Atoms and Ionizing Radiation on the Oxidation of Graphite, Advances in Catalysis, 9: 398–405 (1957).

70. J. S. Nairn and V. J. Wilkinson, The Prediction of Conditions for Self-Sustaining Graphite Combustion in Air, pp. 229–247 in Proceedings of the US/UK Meeting on the Compatibility Problems of Gas-Cooled Reactors, February 24-26, 1960, USAEC Report TID-7597, March 3, 1961.

71. R. E. Dahl, Studies of the Combustion Characteristics of Large Graphite Blocks, USAEC Report HW-SA-2462, Hanford Atomic Products Operation, March 2, 1962.

72. F. M. Lang et al., Study of the Oxidation of Carbons by Air and Carbon Dioxide as a Function of their Structure and their State of Purity, Proceedings of the Fifth Conference on Carbon, Vol. I, pp. 171–193, Pergamon Press, Inc., New York, 1962.

73. R. E. Dahl, Evaluation of Chlorine Inhibition of Graphite Oxidation as a Gas-Cooled Reactor Safeguard, USAEC Report HW-67255, Hanford Atomic Products Operation, April 1961.

74. G. N. Lauben and R. L. Koontz, Sodium Fires and Release Characteristics of Particulates and Fission Products, Proceedings of the International Symposium on Fission Product Release and Transport Under Accident Conditions, USAEC Report Conf 650407 (to be issued).

75. J. D. Gracie and J. J. Droher, A Study of Sodium Fires, Report NAA-SR-4383, pp. 6–7, North American Aviation, Oct. 15, 1960.

76. E. Garelis, Sodium-Air Accident Study for a Sodium Cooled Reactor, USAEC Report AECU-4161, p. 5, Apr. 6, 1959.

77. C. O. Nelson and D. B. Nelson, Sodium-Air Reaction Experiments, Report KAPL-639, Knolls Atomic Power Laboratory, January 1952.

78. J. R. Humphrey, Jr., Sodium-Air Reactions as They Pertain to Reactor Safety and Containment, Proceedings of Second United Nations International Conference on the Peaceful Uses of Atomic Energy, Geneva, 1958, Vol. 11, pp. 177–185, United Nations, New York, 1958.

79. H. L. Floyd, Combustion Hazards of Organic Coolants, USAEC Report HW-58413, Hanford Operations Office, Dec. 19, 1958.

80. R. A. Sheldon, OMR Organic Fire and Explosion Hazard Study, 12eMW, Report NAA-SR-Memo-2917, North American Aviation, July 24, 1958.

81. G. W. Jones, Fire and Explosion Hazards of Contaminated Gases and Vapors, in Industrial Hygiene and Toxicology (Ed. by F. A. Patty), Chap. 13, Sec. 1, Interscience, New York, 1949.

82. J. Jacobson (Ed.), Preliminary Safeguards Report for the Piqua Organic Moderated Reactor, USAEC Report NAA-SR-3575 (Rev.), Atomics International, April 13, 1959.

83. Atomics International, Final Safeguards Summary Report for the Piqua Nuclear Power Facility, USAEC Report NAA-SR-5608, Aug. 1, 1961.

84. G. H. Hanson and F. K. Clements (Eds.), Experimental Organic Cooled Reactor Safety Analysis Report, Volumes I and II, USAEC Report IDO-16820, Phillips Petroleum Co., Nov. 30, 1963.

85. W. M. Hausser (Ed.), Preliminary Safeguards Report for the Piqua Organic Moderated Reactor, p. A-1, Report NAA-SR-3100, North American Aviation, Sept. 28, 1958.

86. N. I. Sax, Dangerous Properties of Industrial Materials, pp. 225–1281, Reinhold, New York, 1957.

87. T. H. Pigford, Explosion and Detonation Properties of Mixtures of Hydrogen, Oxygen, and Water Vapor, p. 15, USAEC Report ORNL-1322, Oak Ridge National Laboratory, Aug. 14, 1952.

88. A. F. Crawford and G. W. Jones, Limits of Inflammability of Gases and Vapors, U.S. Bureau of Mines Bulletin 279, Washington.

89. D. W. Kuhn et al., Explosion Limits in Mixtures of Hydrogen, Oxygen, Steam, and Helium, Report Y-731, Carbide and Carbon Chemicals Corp., Mar. 1, 1951.

90. H. F. Coward and G. W. Jones, Limits of Flammability of Gases and Vapors, U.S. Bureau of Mines Bulletin 503, pp. 15–24, Washington, 1952.

91. Z. M. Shapiro and T. R. Moffette, Hydrogen Flammability Data and Application to PWR Loss-of-Coolant Accident, USAEC Report WAPD-SC-545, Bettis Plant, September 1957.

92. J. A. Luker et al., The Formation of Detonation in Saturated Mixtures of Knallgas-Steam and in Stoichiometric Mixtures of Deuterium-Oxygen (Heavy Knallgas) Saturated with Deuterium Oxide (Heavy Water), Report CHE273-591F, Syracuse University Research Institute, January 1959.

93. J. M. Pilcher et al., Ind. Eng. Chem., 47: 1742 (1955).

94. H. F. Johnstone, C. Y. Chen, and D. S. Scott, Kinetics of the Steam-Carbon Reaction in Porous Graphite Tubes, Ind. Eng. Chem., 44(7): 1564–1569 (1952).

95. J. Gadsby, C. N. Hinskelwood, and K. N. Sykes, Proc. Roy. Soc., A 187: 129 (1946).

96. J. D. Blackwood and F. M. McGrary, The Carbon-Steam Reaction at High Pressure, Australian J. Chem., 11(1): 16-33 (1958).

97. R. E. Helms and R. E. MacPherson, Reaction of Steam with Large Specimens of Graphite for the Experimental Gas Cooled Reactor, USAEC Report ORNL-TM-984, Oak Ridge National Laboratory, November 1964.

98. S. Glasstone, Principles of Nuclear Reactor Engineering, p. 24, Van Nostrand, Princeton, N. J., 1955.

99. C. F. Bonilla, Nuclear Engineering, p. 361, McGraw-Hill, New York, 1957.

100. The Reactor Handbook, Vol. 1, Physics, p. 578, USAEC Report AECD-3645, March 1955.

101. J. C. Haire and G. O. Bright (Ed.), Proceedings of the 1960 Idaho Conference on Reactor Kinetics, USAEC Report IDO-16791, Phillips Petroleum Company, July 1962.

102. W. A. Horning and H. C. Corben, Theory of Power Transients in the Spert I Reactor (Final Report), USAEC Report IDO-16446, Phillips Petroleum Co., Aug. 20, 1957.

103. A. F. Henry, Application of Reactor Kinetics to the Analysis of Experiments, Nucl. Sci. Eng., 3: 52 (1958).

104. K. Fuchs, Efficiency for Very Slow Assembly, USAEC Report LA-596, Los Alamos Scientific Laboratory, Aug. 2, 1946.

105. G. E. Hansen, Burst Characteristics Associated with the Slow Assembly of Fissionable Materials, USAEC Report LA-1441, Los Alamos Scientific Laboratory, July 1952.

106. L. W. Nordheim, Physics Section II, pp. 32-36, Report CP-2589, Chicago University Metallurgical Laboratory, Feb. 28, 1945.

107. S. G. Forbes, Quarterly Progress Report, January, February, March, 1958, USAEC Report IDO-16452, Phillips Petroleum Co., Aug. 5, 1958.

108. R. W. Garner, Review of Several Models for Power Behavior and Reactivity Feedback in Reactor Excursion Studies, USAEC Report IDO-16636, Phillips Petroleum Co., Feb. 6, 1962.

109. W. E. Nyer, Quarterly Progress Report, January, February, March, 1959, USAEC Report IDO-16539, Phillips Petroleum Co., Nov. 20, 1959.

110. R. Greebler et al., Calculations of Doppler Coefficient and Other Safety Parameters for a Large Fast Oxide Reactor, USAEC Report GEAP-3646, General Electric Co., Mar. 23, 1961.

111. R. B. Nicholson, The Doppler Effect in Fast Neutron Reactors, USAEC Report APDA-139, Atomic Power Development Associates, June 1960.

112. J. G. Beckerley and T. J. Thompson (Eds.), The Technology of Nuclear Reactor Safety, Vol. 1, Reactor Physics and Control, MIT Press (to be published).

113. R. W. Miller, Quarterly Progress Report, April, May, June, 1958, USAEC Report IDO-16489, Phillips Petroleum Co., Jan. 19, 1959.

114. S. G. Forbes, Quarterly Progress Report, January, February, March, 1959, USAEC Report IDO-16539, Phillips Petroleum Co., Nov. 19, 1959.

115. A. H. Spano, Analysis of Doppler-Limited Power Excursions in a Water-Moderated Oxide Core, Nucl. Sci. Eng., 19(2): 172–186 (June 1964).

116. M. E. Thomas and W. E. Nyer, Some Special Features of Control Problems of Excursion Reactors, p. 434 in Symposium on Reactor Kinetics and Control Held at University of Arizona, (March 1963), USAEC Symposium Series, April 1964.

117. E. T. Clark, Initial Shut-Off in a Spert Type Transient, Trans. Am. Nucl. Soc., June 1957.

118. P. Greebler and D. B. Sherer, Excursion Shutdown Mechanism for Large Fast Oxide Reactors, Trans. Am. Nucl. Soc., 5(1): 158–159 (1962).

119. F. L. Bentzen, The Merits of Inherent Shutdown vs Mechanical Shutdown of a Plate-Type, Water-Moderated and Reflected Reactor in a Runaway Condition, USAEC Report IDO-16722, Phillips Petroleum Co., Nov. 3, 1961.

120. J. R. Tallackson, J. B. Ruble, R. T. Santoro, and R. E. Wintenberg, Performance Tests of the Oak Ridge National Laboratory Fast Safety System, USAEC Report ORNL-3393, Oak Ridge National Laboratory, Sept. 12, 1963.

121. W. J. McCarthy et al., Nuclear Accident Studies in Fast Reactors, Proceedings of Second United Nations International Conference on Peaceful Uses of Atomic Energy, Vienna, 1958, Vol. 12, p. 207, United Nations, New York, 1958.

122. L. J. Koch et al., Experimental Breeder Reactor II (EBR-II) Hazard Summary Report, USAEC Report ANL-5719, Argonne National Laboratory, 1957.

123. R. Daane, R. Mela, and J. DeFelice, Progress Report on the Study of Low Probability, High Hazard, Fast Reactor Accidents, Report NDA-14-107, Nuclear Development Corp., 1955.

124. F. W. Thalgott et al., Stability Studies on EBR-I, Proceedings of Second United Nations International Conference on the Peaceful Uses of Atomic Energy, Vienna, 1958, Vol. 12, p. 242, United Nations, New York, 1958.

125. W. R. Stratton, A Review of Criticality Accidents, in Progress in Nuclear Energy, Series IV, Vol. 3, p. 163, Pergamon Press, 1960.

126. T. F. Wimett and J. D. Orndoff, Applications of GODIVA II Neutron Pulses, Proceedings of Second United Nations International Conference on Peaceful Uses of Atomic Energy, Geneva, 1958, Vol. 10, p. 449, United Nations, New York, 1958.

127. S. Yiftah and D. Okrent, Some Physics Calculations on the Performance of Large Fast Breeder Power Reactors, USAEC Report ANL-6212, Argonne National Laboratory, 1960.

128. J. B. Nims and P. F. Zweifel, Sodium Temperature Coefficients in Fast Reactors, Trans. Am. Nucl. Soc., 2(2): 172 (1959). See also: Report APDA-135, Preliminary Report on Sodium Temperature Coefficient in Large Fast Reactors, Atomic Power Development Associates, 1959.

129. M. G. Bhide and H. H. Hummel, Reactivity Coefficients of Sodium in Some Large Fast Reactors, Proceedings of Symposium on Physics of Fast and Intermediate Reactors, Vol. II, p. 177, International Atomic Energy Agency, Vienna, 1961.

130. R. O. Brittan et al., Hazard Evaluation Report on ZPR-III, USAEC Report ANL-FWT-105, Argonne National Laboratory, 1955.

131. H. Feshbach et al., Estimation of Doppler Effect in Fast Reactors, Nucl. Sci. Eng., 1(1): 4-20 (March 1956).

132. H. A. Bethe, On the Doppler Effect in Fast Reactors, Report APDA-119, Atomic Power Development Associates, 1957.

133. R. B. Nicholson, The Doppler Effect in Fast Reactors, Report APDA-139, Atomic Power Development Associates, 1960.

134. D. Okrent, A Review of the Nuclear Aspects of Fast-Reactor Safety, Proceedings of Symposium on Physics of Fast and Intermediate Reactors, Vol. III, p. 155, International Atomic Energy Agency, Vienna, 1961.

135. H. A. Bethe and J. H. Tait, An Estimate of the Order of Magnitude of the Explosion when the Core of a Fast Reactor Collapses, British Report UKAEA-RHM (56)/113, April 1956. (Confidential)

136. D. Okrent et al., AX-1, A Computing Program for Coupled Neutronics — Hydrodynamics Calculations, USAEC Report ANL-5977, Argonne National Laboratory, 1959.

137. T. N. Zubarev and A. K. Sokolov, Calculation of the Heat Release in a Shut-down Reactor (Letter to the Editor), J. Nucl. Energy, Pt. A, 13: 72 (1960).

138. K. Shure, Fission Product Decay Energy, pp. 1–17 in Bettis Technical Review, Reactor Technology, Report WAPD-BT-24, Westinghouse Electric Corporation, December 1961.

139. J. R. Stehn and E. F. Clancy, Fission-product Radioactivity and Heat Generation, Proceedings of the Second United Nations International Conference on the Peaceful Uses of Atomic Energy, Geneva, 1958, Vol. 13, pp. 49–54, United Nations, New York, 1958.

140. I. J. MacBean, Energy Release from Fission Product Decay, British Report AERE-R-3033, September 1959.

141. J. F. Perkins and R. W. King, Energy Release from the Decay of Fission Products, Nucl. Sci. Eng., 3: 726–746 (1958).

142. F. C. Maienschein et al., Gamma Rays Associated with Fission, Proceedings of the Second United Nations International Conference on the Peaceful Uses of Atomic Energy, Geneva, 1958, Vol. 15, p. 366, United Nations, New York, 1958.

143. P. Spiegler, Energy Release from the Decay of Fission Products, Report NAA-SR-Memo-4126, North American Aviation, Inc., July 31, 1959.

144. W. E. Knabe and G. E. Putnam, The Activity of the Fission Products of U^{235}, Report APEX-448, General Electric Co., Oct. 31, 1958.

145. S. Katcoff, Fission Product Yields from U, Th, and Pu, Nucleonics, 16(4): 78–85 (1958).

146. Yu. I. Petrov, Gamma Radiation from U^{235} and Pu^{239} Fission Fragments, J. Nucl. Energy, Pt. A, 12: 129–132 (June 1960).

147. K. Way and E. P. Wigner, The Rate of Decay of Fission Products, Phys. Rev., 73: 1318 (1948).

148. S. Untermyer and J. T. Weills, Heat Generation in Irradiated Uranium, USAEC Report ANL-4790, Argonne National Laboratory, Feb. 26, 1962.

149. Final Report of SL-1 Recovery Operations, USAEC Report IDO-19311, Section IV, p. 19, Idaho Operations Office, July 27, 1962.

150. I. Kirshenbaum, Physical Properties and Analysis of Heavy Water, McGraw-Hill, New York, 1951.

151. J. R. Heiks et al., The Physical Properties of Heavy Water from Room Temperature to 250°C, Report MLM-934, Mound Laboratory, Jan. 12, 1954.

152. J. Hilsenrath et al., Tables of Thermal Properties of Gases, National Bureau of Standards Circular 564, Nov. 1, 1955.

153. C. F. Curtiss and J. O. Hirschfelder, Thermodynamic Properties of Air, Report CM-472, University of Wisconsin, June 1, 1948.

154. S. I. Cohen, W. D. Powers, and N. D. Greene, A Physical Property Summary for ANP Fluoride Mixtures, USAEC Report ORNL-2150, Oak Ridge National Laboratory, Aug. 23, 1956.

155. R. N. Lyon (Ed.), Liquid-metals Handbook, 2d ed., U.S. Government Printing Office, Washington, 1954.

156. J. P. Coughlin and E. G. King, High-temperature Heat Contents of Some Zirconium-containing Substances, J. Am. Chem. Soc., 72: 2262 (1950).

157. R. B. Holden and B. Kopelman, Heat Content and Specific Heat of Zirconium-Tin Alloy, Report SEP-128, Sylvania Electric Products, Inc., 1953.

158. G. Bing, F. W. Fink, and H. B. Thompson, The Thermal and Electric Conductivities of Zirconium and Its Alloys, Report BMI-65, Battelle Memorial Institute, Apr. 16, 1951.

159. H. W. Deem, Thermal Conductivity of Zirconium and Zirconium-Tin Alloys, Report BMI-849, Battelle Memorial Institute, July 10, 1953.

160. E. A. Long, W. W. Jones, and J. Gordon, The Heat Capacities of Uranium, UO_3, and UO_2 from 15°K to 300°K, J. Chem. Phys., 20: 695 (1952).

161. G. E. Moore and K. K. Kelley, High Temperature Heat Contents of Uranium, Uranium Dioxide, and Uranium Trioxide, J. Am. Chem. Soc., 69: 2105 (1947).

162. D. C. Ginnings and R. J. Corruccini, Heat Capacities at High Temperatures of Uranium, Uranium Trichloride, and Uranium Tetrachloride, J. Res. Natl. Bur. Standards, 39: 309 (1947).

163. J. M. North, A High-temperature Adiabatic Calorimeter — The Specific Heat of Uranium Between 100 and 800°C, British Report AERE-M/R-1016, 1952.

164. K. Mendelssohn and H. M. Rosenberg, Thermal Conductivity of Metals at Low Temperatures. II. The Transition Elements, Proc. Phys. Soc., 65(390A): 388 (1952).

165. W. W. Tyler, A. C. Wilson, and G. J. Wolga, Thermal Conductivity, Electrical Resistivity, and Thermoelectric Power of Uranium, Trans. Am. Inst. Mining Met. Engrs., 197: 1238 (1953).

166. H. W. Deem and R. A. Winn, Thermal Conductivity of Uranium-Zirconium Alloys, Report BMI-902, p. 22, Battelle Memorial Institute, February 1954. (Classified)

167. E. A. Long, W. M. Jones, and J. Gordon, The Heat Capacities of T Metal, TO_3, TO_2, from 15°K to 300°K. The Entropies at 298.1°K, USAEC Report A-329, Carbide and Carbon Chemicals Corp., Oct. 28, 1942.

168. W. D. Kingery et al., Thermal Conductivity. X. Data for Several Pure Oxide Materials Corrected to Zero Porosity, J. Am. Ceram. Soc., 37: 107 (1954).

169. Accident at Windscale No. 1 Pile on 10 October 1957, presented to Parliament by the Prime Minister, November 1957, British Report DFR/Inf/146.

170. J. M. Davidson, Stored Energy in Irradiated Graphite, pp. 11–20 in US/UK Graphite Conference, December 16–18, 1957, USAEC Report TID-7565, Pt. 1.

171. G. B. Greenough, Windscale Laboratories, unpublished data, April 1960.

172. J. C. Bell et al., Stored Energy in the Graphite of Power-Producing Reactors, Phil. Trans. Roy. Soc. London, Series A254, Vol. 1043, pp. 361–395, Feb. 8, 1962.

173. R. E. Nightingale et al., Damage to Graphite Irradiated up to 1000°C, Proceedings of the Second United Nations International Conference on the Peaceful Uses of Atomic Energy, Geneva, 1958, Vol. 7, pp. 295–300, United Nations, New York, 1959.

174. J. C. Bell and G. B. Greenough, Windscale Laboratories, unpublished data, April 1960.

6. ANALYTICAL TECHNIQUES AND PERTINENT EXPERIMENTAL DATA*

G. R. Fowles, Stanford Research Institute
B. L. Greenstreet, Oak Ridge National Laboratory
H. W. Hoffman, Oak Ridge National Laboratory
J. E. Mott, University of Tennessee
P. F. Pasqua, University of Tennessee
T. W. Pickel, Oak Ridge National Laboratory
M. A. Salmon, Armour Research Foundation
N. A. Weil, Armour Research Foundation

6.1 INTRODUCTION

Certain information necessary for the engineering design from a structural standpoint of reactor containment and engineered safeguards systems is compiled in this chapter. The available information on heat transfer thermodynamics, fluid dynamics, structural design, and missile protection that is unique to reactor containment is presented in a form that may be useful to the reactor containment design engineer. However, the engineering methods used to design reactor containment systems are for the most part conventional and need not be delineated. The problems peculiar to the design of containment systems are generally treated only in the journals and in technical reports. The purpose of this chapter is, then, to compile some of this information and to present it in a form that will be useful.

The removal of the heat generated in a power reactor is an acute problem under normal operating conditions. In the event of an accident it is even more important. The design of any containment system and its emergency heat-removal systems is dependent on the ability to predict, with a large degree of confidence, the various rates of heat transfer within the systems. Rates of heat transfer by conduction, convection, radiation, and boiling are discussed.

The pressure, volume, and temperature relations involved in calculations of the effects of release of the reactor contents into the containment vessel in the event of an accident are presented. The conditions or the properties of the fluids as they would exist in the containment vessel affect the ultimate design of this final barrier, which controls the release of radioactivity to the environment.

For the design of reactor containment systems, there are several hydraulic problems that must be considered. The linear momentum equation and Bernoulli's equation as used to determine jet impingement forces resulting from single-phase flow, working equations for two-phase flow, and shock transmission are discussed. A qualitative description of steam jet condensation is presented.

As a minimum requirement, containment vessels should be designed in accordance with Rules for Construction of Nuclear Vessels, Section III,

---

*The initial preparation of this chapter was done by J. E. Mott in late 1963. Since that time extensive revision has taken place, with the listed authors being major contributors.

ASME Boiler and Pressure Vessel Code, 1963 Edition (see Chap. 2 and App. C and D). A discussion of neutron embrittlement of steels may be found in Section 8.5. The code contains the most extensive and current material available on analytical techniques that are generally applicable. However, the calculation of stresses is, in general, based on an elastic analysis, even though the actual stresses may exceed the elastic limit of the material. Any attempt to incorporate elastic analysis techniques into this document would be needless repetition. On the other hand, much work is currently being done in the field of plasticity that will be directly applicable to ultimate strength analysis. This work is in the research and development stage and as such is not well enough developed to be incorporated into a code. This subject is therefore discussed here.

In order to evaluate the damage that may be done in the event of an accident to a nuclear power plant, it is necessary to predict the nature of the accident, the energy released, and the results of this release. Of particular interest in the design of containment systems is protection against missiles that may be generated either as the cause or the result of an accident. It is therefore necessary to determine which components may conceivably become missiles and to predict their maximum velocities. It is also necessary to design missile shields or other protective systems that will contain the missiles which may be generated. A second area of interest is the design of blast shields for dissipating much of the energy transmitted by a shock wave. These subjects are discussed in this chapter.

A compilation of computer codes designed to deal with the problems of reactor containment is included.

It should be noted that reactor containment problems have received attention only in the past few years, and therefore no strong body of reliable information has yet been developed. This is particularly true in the areas of two-phase critical flow, shock effects, dynamic loading, and missile protection. It is therefore imperative that conservative design procedures be employed and that extreme care be exercised in extrapolating existing information.

It was originally intended that a section on external loading be included in this chapter; however, it is felt that the recently released handbook Nuclear Reactors and Earthquakes[1] and conventional works on structural design cover this area satisfactorily.

6.2 HEAT TRANSFER PROBLEMS

T. W. Pickel

Removal of the heat generated in a power reactor is an important consideration under normal operating conditions, and in the event of an accident, it becomes an acute problem. The success of containment and other safeguards systems is dependent upon the designer's ability to predict, with a high degree of confidence, the various rates of heat transfer within the system. In general, the containment vessel is sized for the maximum credible accident. This usually involves dumping of the primary coolant, and frequently some secondary fluid at a rate determined by the assumed rupture, into the containment vessel. Heat transfer problems are involved in establishing the temperature of the fuel (from the standpoint

of over heating the fuel and the subsequent release and transport of fission products) and the temperature of the gas-vapor mixture in the containment shell (from the standpoint of pressure in the shell).

In the case of transfer of heat from the fuel elements to the coolant after an accident, the most common mechanism of heat transfer will be free convection or boiling of residual water. Heat transfer by radiation may be significant at high fuel cladding temperatures regardless of the type of convection. In most cases, emergency coolant loops will be used in which forced convection will be the controlling heat transfer mechanism.

After the contents of the primary system, and sometimes the secondary cooling system, flow into the containment vessel, heat is transferred to the containment shell and to structural members and equipment within the shell. Again natural convection is an important mechanism of heat transfer between the fluids and the surfaces of the shell and structural members. Condensation may occur on these surfaces and contribute to the transfer of heat. In some reactor systems, spray cooling and vapor suppression tanks are provided. Hence, simultaneous heat and mass transfer is important. Radiation may be important especially between the reactor vessel and structural or containment surfaces. Transfer of heat from the shell to the environment is accomplished primarily by natural convection and radiation, although in some cases this heat transfer is lessened by the presence of insulation.

6.2.1 Conduction

Fourier's Law gives the rate of heat conduction $dq/d\tau$ of $\dot{q}''A$ through a plane area A as

$$\frac{dq}{d\tau} = \dot{q}''A = -kA\,\frac{dT}{dx}\,, \tag{6.1}$$

where

q = quantity of heat transferred in heat units,
τ = time,
$\dot{q}''$ = heat flux in heat units per unit area per unit time,
A = area,
T = temperature,
x = distance measured normal to A and in the direction of the heat flow,
k = thermal conductivity of the material.

Thermal conductivities for most reactor materials may be found in refs. 2 and 3.

The general equation for unsteady-state conduction with internal heat generation, motion of the conduction field, and two- and three-dimensional shapes is

$$\frac{\partial T}{\partial \tau} = \alpha \nabla^2 T + \frac{\dot{q}'''}{\rho C} - \left(u_x \frac{\partial T}{\partial x} + u_y \frac{\partial T}{\partial y} + u_z \frac{\partial T}{\partial z}\right), \qquad (6.2)$$

where

$\dot{q}'''$ = internal heat generation in heat units per volume per unit time,
u = velocity,
ρ = density,
α = thermal diffusivity, $k/\rho C$,
C = specific heat,
∇^2 = Laplacian operator.

Steady-state conduction for several geometries is discussed by Bonilla.[4] Unsteady-state conduction is covered extensively by Carslaw and Jaeger,[5] whose text gives explicit solutions of many problems of practical interest, in addition to an excellent presentation of the theory and mathematics involved in these problems. Unsteady-state conduction is also covered by Hsu[6] and Jakob.[7]

Schneider[8] presents temperature response charts for several boundary conditions and body shapes and considers the relative magnitude of internal-to-surface conductance. The individual cases considered in each of these three categories are listed below:

A. BOUNDARY CONDITION

1. Constant surface temperature.
2. Variable surface temperature.
3. Constant ambient temperature.
4. Constant and variable heat input.
5. Radiation.

B. BODY SHAPE

1. Semi-infinite solid.
2. Single-layer plate.
3. Two-layer plate.
4. Cylinder.
5. Cylindrical cavity.
6. Cylindrical shell.
7. Sphere.
8. Spherical cavity.
9. Spherical shell.
10. Ellipse.
11. Ellipsoids.

C. INTERNAL AND SURFACE CONDUCTANCE

1. Finite internal conductance, infinite surface conductance.
2. Infinite internal conductance, finite surface conductance.
3. Finite internal and surface conductance.
4. Finite internal conductance.
5. Infinite internal conductance.

The charts represent analytical solutions for transient one-dimensional heat conduction. The density, specific heat, and thermal conductivity of the conducting material are assumed to be isotropic and constant.

6.2.2 Convection

Heat transfer by convection may occur as a result of fluid being forced past the heat transfer surface (forced convection) or the circulation of fluid caused by density gradients (free or natural convection). In transferring heat from fuel elements to coolant, forced convection is the normal heat transfer mechanism. However, free convection may be important during periods of pump failure or after partial loss of coolant. Where condensation is not occurring, free convection is the principle mechanism by which heat is transferred to the containment shell or structural members from the coolant and steam that are released by a system failure. Free-convection transfer may also occur in the transfer of heat from the containment shell to the surrounding atmosphere.

The transfer of heat by convection is characterized by the flow of heat through a film of the fluid. This is expressed by the following relation:

$$q = hA\,\Delta t\ , \tag{6.3}$$

where

q = heat transferred, Btu/hr,
h = heat transfer coefficient, Btu/hr·ft^2·°F,
A = area normal to the direction of heat flow, ft^2,
Δt = temperature drop across the film or difference in temperature of the bulk fluid and the surface, °F.

6.2.2.1 Forced Convection

The heat transfer relations for forced convection have been studied extensively, but because the mechanism is so complex, the best correlations have an accuracy of only ±20%. This uncertainty makes conservative design mandatory.

The data are normally correlated with various dimensionless numbers. A list of those used in the following tables is given below:

Nu = Nusselt number, hD/k,
Re = Reynolds number, DG/μ,
Pr = Prandtl number, $C\mu/k$,
Pe = Peclet number, DGC/k,
Gz = Graetz number, CGD^2/kL,

where

h = heat transfer coefficient, Btu/hr·ft^2·°F,
D = diameter, ft,
k = thermal conductivity, Btu/hr·ft^2 (°F/ft),
G = mass flow rate, lb/hr·ft^2 (in case g, Table 6.1, G is defined as lb/sec·ft^2),
μ = viscosity, lb/ft·hr,
C = specific heat at constant pressure, Btu/lb·°F,
L = length of flow channel, ft.

1. Turbulent Flow. Flow channels are usually long compared with the equivalent diameter, and the thermal entry length is short; therefore the heat-transfer coefficients for long tubes are usually desired. Heat-transfer correlations for the single-phase turbulent flow of nonmetallic fluids are given in Table 6.1. It should be noted that all fluid properties are evaluated at the film temperature:

$$t_f = \frac{1}{2}(t_b + t_w) ,$$

where t_b is the bulk fluid temperature and t_w is the wall temperature.

Table 6.2 shows the principal correlations for liquid metals in turbulent flow. The large discrepancies in these data are due to (1) differences in the wetting of the wall by liquid metals, (2) entrained gases, and (3) errors in temperature measurements.

2. Laminar Flow. In laminar flow the effect of the thermal entry length is greater than that for turbulent flow; therefore, the heat transfer coefficients for short channels are usually desired. The principal laminar-flow relations for short channels are listed in Table 6.3. The term Nu_{AM} (cases d and e) employs

$$h_{AM} = \frac{q}{A}\frac{1}{\Delta t_{AM}} ,$$

where Δt_{AM} is the arithmetic mean of the inlet and local Δt.

Tables 6.4 and 6.5 give long-channel values of h for the usual channel shapes. The flow mean Δt is the value defined by

$$\Delta t = \frac{q}{A}\frac{1}{h} .$$

The values of maximum Δt are useful in computing, from the flow mean Δt, the maximum temperature variation in the stream. The space mean Δt values give the volumetric average temperature of the fluid, which is useful in calculating the mass and buoyancy of the coolant in the tube. Because of

Table 6.1. Turbulent-Flow Heat Transfer for Nonmetallic Fluids[a]

Designation	Case	Limitations, etc.	Relation	Reference
a	Flow in long channels	$2{,}000 < Re < 300{,}000$	$Nu = 0.023\ Re^{0.8}\ Pr^{1/3} = Nu^0$	10
b	Local h in short channels; downstream distance L	$2{,}000 < Re < 60{,}000$	$Nu_L = \left[\frac{2.8}{Re^{0.06}}\left(\frac{L}{D}\right)^{-2.25/Re^{0.3}}\right] Nu^0$	11
c	Local h in short channels	$60{,}000 < Re$	$Nu_L = 1.5\ Nu^0$ at $L/D_e = 1$ $Nu_L = 1.1\ Nu^0$ at $L/D_e = 5$	
d	Flow in coils		$Nu = (1 + 3.5D/D_{coil})\ Nu^0$	10
e	Flow in wide concentric annuli	Heat transfer at outer surface	$Nu = Nu^0$ (using D_e)	12
f	Flow in wide concentric annuli	Heat transfer at inner surface	$Nu = 0.87\left(D_3/D_2\right)^{1/2} Nu^0$	13
g	Liquid in tubes with p′ % of gas by volume	Upflow with $25 < G < 100$ lb/ft^2·sec	$Nu = (1 + 6.1G^{-0.53} \log_{10} p')\ Nu^0$	14
h	Gases in long tubes at high Δt	$t_{0.4} = 0.4t_w + 0.6\bar{t}$	$Nu_{0.4} = 0.236[D\bar{u}(\rho/\mu)_{0.4}]^{0.78}$	15
i	Gases at high $\bar{u}$	Case a holds with $\Delta t = t_w - \bar{t} - \frac{\bar{u}^2}{2g_c JC_p} Pr^{1/2}$		10
j	Flow parallel to tube bundles	Ratio of axial spacing to diameter <1.3	$Nu = Nu^0$ (using D_e)	16
k	Flow parallel to tube bundles	Ratio of axial spacing to diameter = 1.46	$Nu = 1.4\ Nu^0$ (using D_e)	17

[a]From ref. 9.

Table 6.2. Turbulent-Flow Heat Transfer for Molten Metals[a]

Designation	Case	Limitations, etc.	Relation	Reference
a	Flow in a long tube	Constant q/A	$Nu = 7 + 0.025\ Pe^{0.8} = Nu^0$	18
a′	Flow in a long tube	Constant q/A	$Nu = 6.3 + 0.016\ Pe^{0.91}\ Pr^{0.3}$	19
b	Flow in a long tube	Constant t_w	$Nu = 4.8 + 0.025\ Pe^{0.8}$	18
b′	Flow in a long tube	Constant t_w	$Nu = 4.8 + 0.015\ Pe^{0.91}\ Pr^{0.3}$	19
c	Flow in a long tube	$50 < Pe < 20{,}000$	$Nu = 0.625\ Pe^{0.4}$	20
d	Local h in a short tube	Constant t_w	$Nu_L = 1.31(Pe\ D/L)^{0.455}$	21
e	Flow in a flat channel	One wall q/A = 0, other q/A constant	$Nu = 5.8 + 0.02\ Pe^{0.8}$ (using D_e)	18
f	Flow in a flat channel	Both walls with q/A constant	$Nu = 10.5 + 0.036\ Pe^{0.8}$ (using D_e)	18
g	Flow in a flat channel	Each wall with different constant q/A		18
h	Flow in a concentric annulus	$D_3/D_2 < 1.4$	Relation e, f, or g, as applicable	
i	Flow in a concentric annulus	$D_3/D_2 > 1.4$	$Nu_2 = 0.75(D_3/D_2)^{0.30}\ Nu^0$	
j	Flow in a concentric annulus	Constant q/A at D_2	$Nu_2 = (5.25 + 0.0175\ Pe)(D_3/D_2)^{0.53}$	22
k	Flow along an unbaffled bundle	D = tube or rod outer diameter	$Nu_D = 11.6(Pe_D)^{0.6}\ (D_e/L)^{1.2}$	22

[a]From ref. 9.

Table 6.3. Laminar-Flow Heat Transfer in "Short" Tubes[a]

Designation	Case	Limitations	Relations	Reference
a	Local h in a short tube, parabolic flow	Constant t_w; $Gz = CGD^2/kL > 12$	$Nu = 1.15\ Gz^{1/3}$	23
b	Local h in a short flat duct, parabolic flow	Constant t_w; $Gz' = CGD_e^2/kL > 70$	$Nu = 1.3\ Gz'^{1/3}$	23
c	Local h in a tube, plug flow	Constant t_w; $Gz = 1$, $Gz = 10$	$Nu = 1.3\pm$ $Nu = 3.7\pm$	24
d	Average h in a tube, actual flow	Constant t_w; $Re > 10$	$Nu_{AM} = 1.76\ Gz^{1/3} \left(\frac{\mu_b}{\mu_w}\right)^{0.14} \times \frac{2.25(1 + 0.01\ Gr^{1/3})}{\log Re}$	10
e	Average h in a flat duct, actual flow	Constant t_w; $Re > 10$; $D = D_e$	$\overline{Nu}_{AM}$ = 15% above relation d at same Gz	
f	Local h in a tube, parabolic flow	Constant q/A	Nu / Gz 4.36 / 0–10 5 / 34.4 6 / 73.7 8 / 191 10 / 378 14 / 632 19 / 2000	

[a]From ref. 9.

Table 6.4. Local Nusselt Number and Temperature Differentials in Streamlined Flow in Long Channels[a,b]

Channel Shape	Constant Heating Conditions	Velocity	Nu Based on Flow Mean Temperature[c]	Ratio of Δt_{max} to $\Delta t_{flow\ mean}$	Ratio of $\Delta t_{space\ mean}$ to $\Delta t_{flow\ mean}$
Round pipe	q/A	Parabolic	4.36[d]	1.636	0.727
	q/A	Uniform	8	2.013	1.000
	t_w	Parabolic	3.66		
	t_w	Uniform	5.80		1.000
Flat channel (infinite width)	q/A	Parabolic:			
		Heated one side	5.384	1.346	0.942
		Heated two sides	8.240	1.288	0.824
	q/A	Uniform:			
		Heated one side	6	1.500	1.000
		Heated two sides	12	1.500	1.000
	t_w	Parabolic:			
		Heated two sides	7.60		
	t_w	Uniform			
		Heated one side	4.94[e]	1.571	1.000[e]
		Heated two sides	9.88[e]	1.571	1.000[e]
Square	q/A	Uniform	6[f]	2.00[g]	
	q/A	Parabolic	3.68[f]		
Triangular[h]					
60° × 60° × 60°	q/A	Uniform	4[f]	3.00[g]	
45° × 45° × 90°	q/A	Uniform	2[f]	4.10[g]	
30° × 60° × 90°	q/A	Uniform	2[f]		
Rectangular					
a/b = 2	q/A	Parabolic	4.16[f]		
a/b = 3	q/A	Parabolic	4.78[f]		
a/b = 5	q/A	Parabolic	5.55[f]		
a/b = 10	q/A	Parabolic	6.77[f]		

[a] Length of Nu is D_e for all channels; axial conduction neglected.

[b] From ref. 9.

[c] From ref. 23.

[d] For gases with large Δt take k at $1.27\bar{t} - 0.27t_w$; similarly, for liquid metals, multiply 4.36 by $(\mu_b/\mu_w)^{0.14}$ (see ref. 25).

[e] To include axial conduction divide by $\{1 + [1 + (\pi\alpha/bu)^2]^{1/2}\}/2$.

[f] Based on mean wall temperature $\bar{t}_w$; conservative, since circulating currents are neglected.

[g] $[(t_w)_{max} - \bar{t}] / (\bar{t}_w - \bar{t})$.

[h] Liquid Metals Handbook (2d ed., R. N. Lyon, Ed.; 3d ed., C. B. Jackson, Ed.), Government Printing Office, Washington, D. C.

the viscosity change with temperature, the value of h for a liquid being heated or a gas being cooled will fall between the parabolic and uniform velocity cases.

6.2.2.2 Free Convection

1. Free-Convection Heat Transfer in Core Channels. In the event of a pump or blower failure or partial loss of coolant, free convection is the mechanism by which heat is removed from the fuel elements. The

Table 6.5. Local Nusselt Number for Streamlined Flow in Long, Concentric, Cylindrical Annuli Heated at Constant q/A on One Side[a]

Ratio of $D_{insulated}$ to D_{heated}	Uniform Velocity, Nu^b	"Parabolic" Velocity (μ Constant)	
		Nu^b	Ratio of Δt_{max} to $\Delta t_{flow\ mean}$
54.60	32.96	34.78	1.1
7.389	9.71	10.18	1.16
2.718	6.748	6.758	1.23
1.649	6.168	5.898	1.29
1.284	6.040	5.606	1.31
1	6	5.384	1.35
0.7788	6.036	5.222	1.37
0.6065	6.132	5.104	1.40
0.3679	6.442	4.962	1.46
0.1353	7.144	4.854	1.55
0	8	4.364	1.64

[a]From ref. 26.

[b]Nu based on D_e; $D_e = D_3 - D_2$.

characteristic parameters for free convection are the Nusselt number (Nu), Grashof number (Gr), and the Prandtl number (Pr).

The heat transfer by free convection at the inner surface of ducts having various cross-sectional geometries has been studied by Elenbaas.[25] His results are summarized by the various curves in Fig. 6.1, where

$$Nu = hr/k,$$
$$Gr = \rho^2 Bg(t_s - t_f)r^3/\mu^2,$$
$$Pr = C\mu/k,$$
$$r = \frac{2(\text{cross-sectional area})}{\text{wetted perimeter}}, \text{ ft},$$

B = coefficient of volumetric thermal expansion, 1/°F,
t_s = temperature of surface, °F,
t_f = temperature of the film, °F,
g = acceleration due to gravity, ft/hr^2.

The other physical properties are the same as previously defined. The ordinate in Fig. 6.1 is the Nusselt number, and the abscissa is $(r/h)GrPr$, where h is the height of the duct (the use of h for height applies only to this figure). The physical properties (with the exception of B) are to be taken at the surface temperature, t_s, and B is to be evaluated at the bulk fluid temperature, t_b.

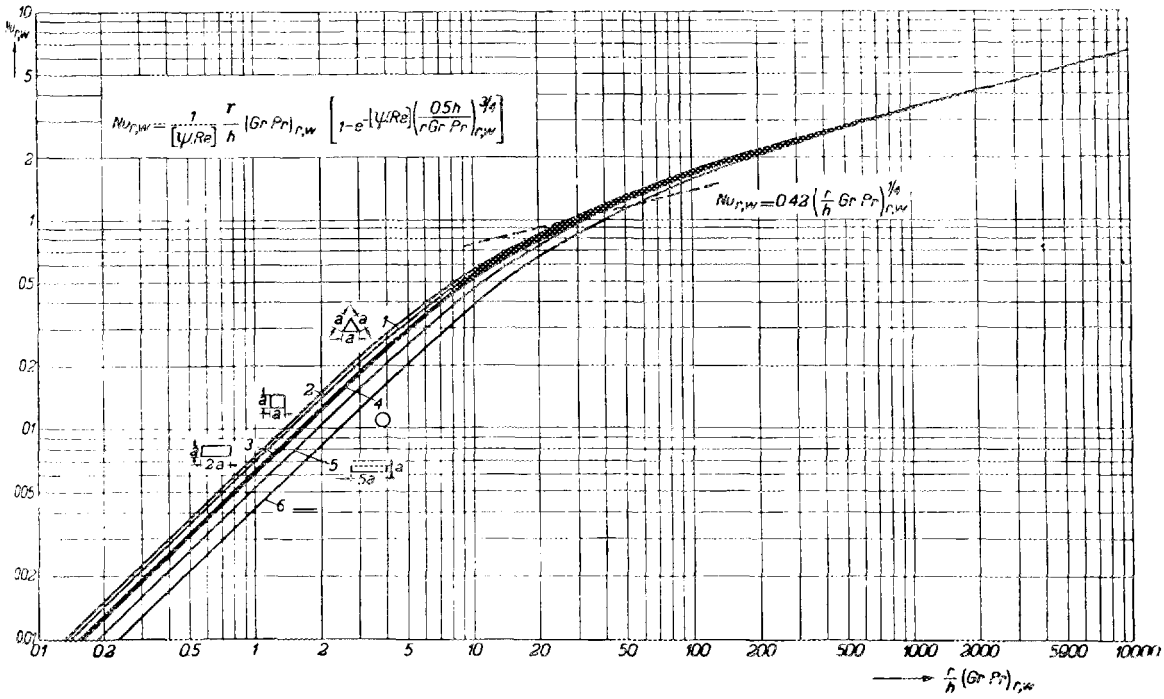

Fig. 6.1. Free-Convection Heat Transfer from the Interior Surfaces of Vertical Ducts Having Various Cross-Sectional Geometries. (From ref. 25)

In many reactors, thermal circulation may result when the pumping equipment fails. The flow rate and heat transfer rate in this type of system are directly related. This problem is covered by Bonilla.[27]

2. Free Convection Past External Surfaces. Free convection is an important mechanism in transferring heat from the released coolant to structural members and the containment shell and from the shell to the surrounding atmosphere. Table 6.6 gives empirical correlations for flow past horizontal and vertical surfaces with the physical properties evaluated at $t_f = (t_s + t_b)/2$. Here $Nu = hL/k$, $Gr = \rho^2 Bg(t_s - t_f)L^3/\mu^2$, and $Pr = C\mu/k$. Since the fluid involved is frequently air, simplified equations have been developed. The equations for air are listed in Table 6.7.

The type of flow is determined by the value of the Grashof number. The flow is laminar for values of Gr up to 10^8, passes through a transition region between 10^8 and 10^{10}, and becomes fully turbulent for values above 10^{10}.

6.2.3 Radiation

Radiation heat transfer may be important in transferring heat from fuel elements to coolant and from reactor vessel and other equipment to the containment shell and structural components. Radiation heat transfer

Table 6.6. Average Free-Convection Heat Transfer[a]

Case	Range	Relation
Vertical wall or large cylinder (L = height)	$10^4 < GrPr < 10^9$ $10^9 < GrPr < 10^{12}$	$Nu = 0.59(GrPr)^{1/4}$ $Nu = 0.13(GrPr)^{1/3}$
Horizontal cylinder ($L = D_o$) and sphere ($L = r$)	$10^3 < GrPr < 10^9$	$Nu = 0.53(GrPr)^{1/4}$
Horizontal square plates[b]		
1. Heated plate facing upward or cooled plate facing downward	$10^5 < GrPr < 10^{10}$ $10^7 < GrPr < 10^{10}$	$Nu = 0.54(GrPr)^{1/4}$ $Nu = 0.14(GrPr)^{1/3}$
2. Heated plate facing downward or cooled plate facing upward	$10^5 < GrPr < 10^{10}$	$Nu = 0.27(GrPr)^{1/4}$

[a]From ref. 28.

[b]For disks, replace L by 0.9 times diameter.

Table 6.7. Simplified Relations for Free Convection with Air as Fluid[a]

Case	Range	Relation
Vertical wall or large cylinder (L = height)	$10^4 < GrPr < 10^9$	$h_c = 0.29 \left[\frac{(t_s - t_b)}{L}\right]^{1/4}$
	$10^9 < GrPr < 10^{12}$	$h_c = 0.19\ (t_s - t_b)^{1/3}$
Horizontal cylinder ($L = D_o$) and sphere ($L = r$)	$10^3 < GrPr < 10^9$	$h_c = 0.27 \left[\frac{(t_s - t_b)}{L}\right]^{1/4}$
Horizontal square plates[b]		
1. Heated plate facing upward or cooled plate facing downward	$10^5 < GrPr < 10^7$	$h_c = 0.27 \left[\frac{(t_s - t_b)}{L}\right]^{1/4}$
	$10^7 < GrPr < 10^{10}$	$h_c = 0.22\ (t_s - t_b)^{1/3}$
2. Heated plate facing downward or cooled plate facing upward	$10^5 < GrPr < 10^{10}$	$h_c = 0.12 \left[\frac{(t_s - t_b)}{L}\right]^{1/4}$

[a]From ref. 28.

[b]For disks, replace L by 0.9 times diameter.

between two surfaces separated by a nonabsorbing medium may be expressed in the following form:

$$Q = AF_A F_\epsilon \sigma (T_1^4 - T_2^4) \ , \tag{6.4}$$

where

Q = rate of heat transmission, Btu/hr,
A = area of one of the two surfaces, ft^2,
F_A = shape or area factor,
F_ϵ = emissivity factor,
σ = Stefan-Boltzmann constant = 0.1714×10^{-8} Btu/ft^2·hr·°R^4,
T_1 = temperature of surface 1, °R.
T_2 = temperature of surface 2, °R.

Values for F_A and F_ϵ are given in Table 6.8 and Figs. 6.2, 6.3, and 6.4 for several arrangements of the two surfaces. In Table 6.8, ϵ_1 and ϵ_2 are the total emissivities of the two surfaces.

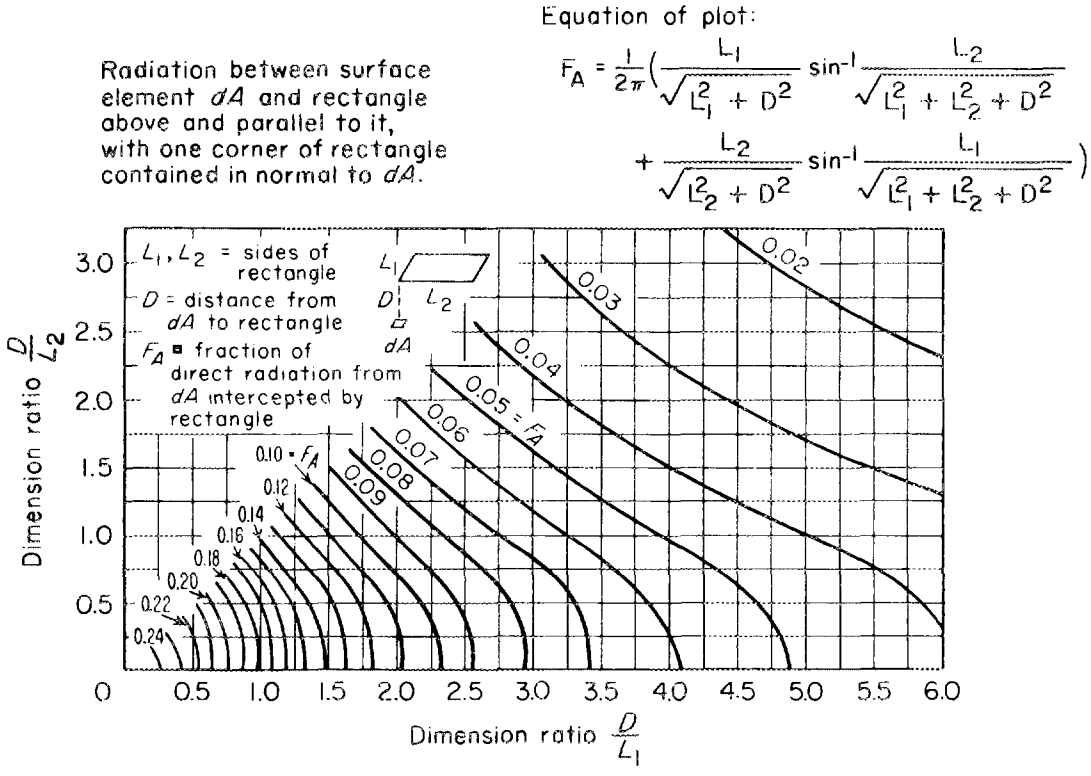

Fig. 6.2. Radiation Between Surface Element and Rectangle Above and Parallel to It. (From ref. 29)

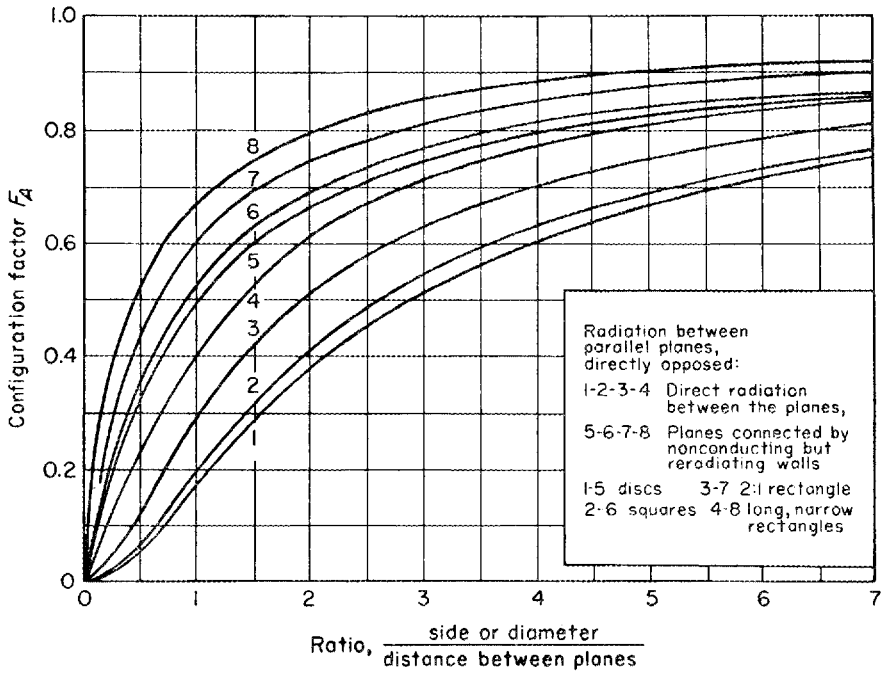

Fig. 6.3. Radiation Between Parallel Planes. (From ref. 29)

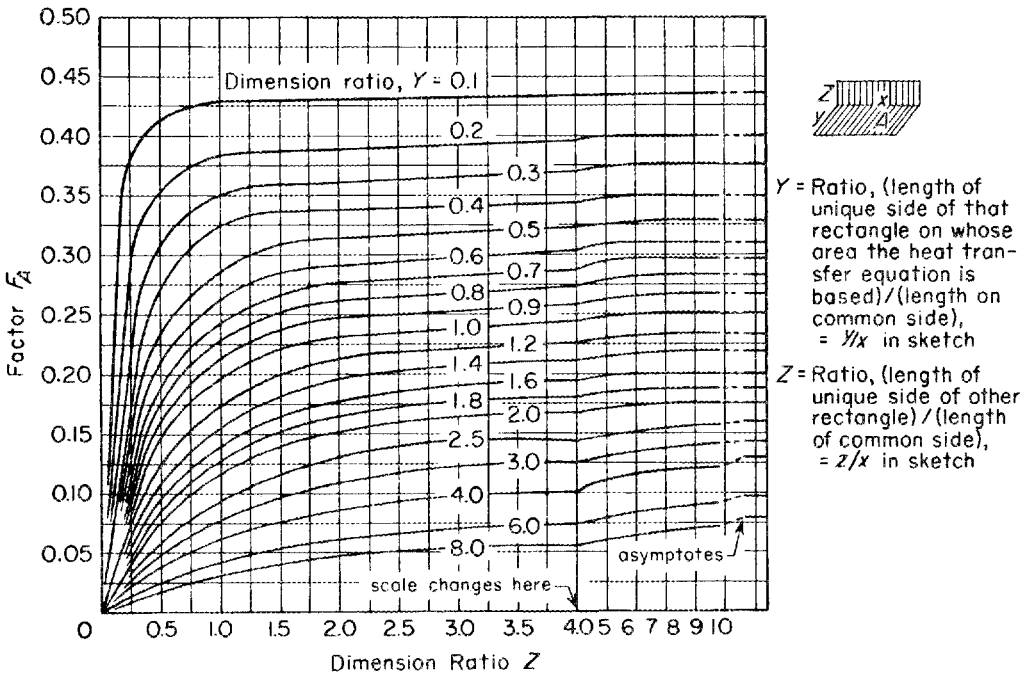

Fig. 6.4. Radiation Between Adjacent Rectangles in Perpendicular Planes. (From ref. 29)

Table 6.8. Radiation Between Solids[a]

Factors for use in equation

$$Q = AF_A F_\epsilon \sigma (T_1^4 - T_2^4) ,$$

where

Q = rate of heat transmission, Btu/hr,
A = area of one of the two surfaces, ft^2,
σ = the Stefan-Boltzmann constant, 0.1714×10^{-8} $Btu/ft^2 \cdot hr \cdot {}^\circ R^4$.

Serial No.	Surfaces Between Which Radiation Is Being Interchanged	Area, A	Area Factor, F_A	Emissivity Factor, F_ϵ
1	Infinite parallel planes	Either surface	1	$\frac{1}{\frac{1}{\epsilon_1} + \frac{1}{\epsilon_2} - 1}$
2	Completely enclosed body, small compared with enclosing body (subscript 1 refers to enclosed body)	A_1, see footnote (b)	1	ϵ_1
3	Completely enclosed body, large compared with enclosing body (subscript 1 refers to enclosed body)	A_1	1	$\frac{1}{\frac{1}{\epsilon_1} + \frac{1}{\epsilon_2} - 1}$
4	Intermediate case between cases 2 and 3 (incapable of exact treatment except for given shapes)	A_1	1	$\epsilon_1 > F_\epsilon > \frac{1}{\frac{1}{\epsilon_1} + \frac{1}{\epsilon_2} - 1}$
5	Concentric spheres or infinite cylinders, special case of 4	A_1	1	$\frac{1}{\frac{1}{\epsilon_1} + \frac{A_1}{A_2\left(\frac{1}{\epsilon_2} - 1\right)}}$ or $\frac{1}{\frac{1}{\epsilon_1} + \frac{1}{\epsilon_2} - 1}$, see footnote (c)
6	Surface element dA and area A_2; there are various special cases of case 6, with results presentable in graphical form; they follow as cases 7, 8, 9, etc.	dA	See below	$\epsilon_1\epsilon_2$
7	Element dA and rectangular surface above and parallel to it, with one corner of rectangle contained in normal to dA	dA	Given in Fig. 6.2	$\epsilon_1\epsilon_2$

[a]From ref. 29.

[b]Enclosed body must contain no negative curvature if A_1 is used; replace any "dimples" in surface by equivalent planes in evaluating A_1, and raise "effective" emissivity from ϵ_1 toward unity in proportion to depth of dimple.

[c]First form results if reflection is assumed to be completely diffuse; second, if reflection is completely specular; true value will be very much nearer first than second.

Table 6.8. (continued)

Serial No.	Surfaces Between Which Radiation Is Being Interchanged	Area, A	Area Factor, F_A	Emissivity Factor, F_ϵ
8	Element dA and any rectangular surface above and parallel to it; split rectangle into four parts having common corner above dA and treat as in case 7	dA	Sum of four F_A's determined as in case 7	$\epsilon_1\epsilon_2$
9	Element dA and circular disk in plane parallel to plane of dA	dA	Formula given in footnote (d)	$\epsilon_1\epsilon_2$
10	Element dA and semi-infinite surface, latter generated by line moving parallel to its original position and to plane of dA; pass plane through normal to dA, perpendicular to generating line of other surface; in this plane θ' and θ'' are angles made by lines connecting dA to edges of surface, with the normal to dA	dA	$\frac{\sin\theta' - \sin\theta''}{2}$, only plane angles are involved	$\epsilon_1\epsilon_2$
11	Two parallel circular disks with centers on same normal to their planes	A_b	Given in Fig. 6.3, line 1; formula given in footnote e	Exact treatment dependent on kind of reflection, unknown; F_ϵ lies between $\epsilon_1\epsilon_2$ and $\frac{1}{\frac{1}{\epsilon_1} + \frac{1}{\epsilon_2} - 1}$, for all cases, nearer the former when areas are close together; error is quite small, if ϵ_1 and ϵ_2 are not far from unity; applies to cases 11, 12, 13, and 14
12	Special case of case 11 with disks of same diameter	Either surface	Fig. 6.3, line 1	

[d]Case 9: R = (radius of disk)/(distance between planes); x = (distance from dA to normal through center of disk)/(distance between planes);

$$F_A = \frac{1}{2}\left\{1 - \frac{x^2 + 1 - R^2}{[x^4 + 2(1 - R^2)x^2 + (1 + R^2)^2]^{1/2}}\right\}.$$

[e]Case 11: radii of disks = a and b; distance between planes = K;

$$F_A = \frac{1}{2}\left\{1 + \frac{a^2}{b^2} + \frac{K^2}{b^2} - \left[\left(1 + \frac{a^2}{b^2} + K^2b^2\right)^2 - \frac{4a^2}{b^2}\right]^{1/2}\right\};$$

use area of disk with radius b.

Table 6.8. (continued)

Serial No.	Surfaces Between Which Radiation Is Being Interchanged	Area, A	Area Factor, F_A	Emissivity Factor, F_ϵ
13	Two equal rectangles in parallel planes and directly opposite each other	Either surface	Formula given in footnote (f); approximation: $F_A = (F_A' F_A'')^{1/2}$; see footnote (g); also Fig. 6.3, lines 3 and 4	
14	Two equal squares in parallel planes and directly opposite each other; special case of case 13	Either surface	Given in Fig. 6.3, line 2	(see previous cases)
15	Two rectangles with common side, in perpendicular planes	Either surface	Given in Fig. 6.4	Approximately $\epsilon_1\epsilon_2$
16	Parallel squares or disks connected by nonconducting but reradiating black walls	Either surface	Given in Fig. 6.3, lines 5 and 6	Approximately $\epsilon_1\epsilon_2$
17	Parallel rectangles connected by nonconducting but reradiating black walls	Either surface	Obtained from case 16 as case 14 from case 13; see footnote g and Fig. 6.3, lines 7 and 8	Approximately $\epsilon_1\epsilon_2$

[f] Case 13: ratios of sides to distance between planes = X and Y;

$$F_A = \frac{1}{\pi}\left[\frac{1}{XY}\log\frac{(X^2+1)(Y^2+1)}{(X^2+Y^2+1)} - \frac{2}{Y}\tan^{-1}X - \frac{2}{X}\tan^{-1}Y + 2\left(1+\frac{1}{Y^2}\right)^{1/2}\tan^{-1}\frac{X}{(Y^2+1)^{1/2}} + 2\left(1+\frac{1}{X^2}\right)^{1/2}\tan^{-1}\frac{Y}{(X^2+1)^{1/2}}\right].$$

[g] F_A' = factor obtained for case 14 for squares equivalent to smaller side of rectangle; F_A'' = factor obtained for case 14 for squares equivalent to larger side of rectangle; the approximation $F_A = (F_A' F_A'')^{1/2}$ introduces less than 1% error.

Several common gases and vapors (such as CO_2 and water vapor) exhibit emission and absorption effects of sufficient magnitude to be considered in heat transfer problems. For the net radiation heat transfer between a gas and a black surface, the following equation[29] may be used:

$$Q = \sigma A(\epsilon_g T_g^4 - \alpha_{g,b} T_s^4) \ , \tag{6.5}$$

where

Q = net heat transfer rate, Btu/hr,
σ = Stefan-Boltzmann constant = 0.1714×10^{-8} Btu/hr·ft^2·°R^4,
A = surface area, ft^2,
ϵ_g = emissivity of gas at temperature T_g,
$\alpha_{g,b}$ = absorptivity of gas at temperature T_g for radiation from a black body at temperature T_s.

The emissivity and absorptivity of the gas are functions of partial pressure, temperature, and mean beam length. Values of mean beam length for various geometrical shapes and graphs of emissivity for CO_2 and water vapor are given by Hsu,[29] Jakob,[30] and McAdams.[31]

The case of radiation heat transfer between two surfaces separated by an absorbing gas is discussed by Jakob[30] and McAdams.[31] The form of the equation is the same as the case where there is no absorbing medium present, with the quantity $F_A F_\epsilon$ changed to allow for the presence of the gas.

The relations presented are restricted to the net transfer between two surfaces. Many cases can be reduced to this situation without excessive loss in accuracy. However, some cases, where radiation effects are large and where there are more than two surfaces involved, will require a more precise analysis. A method of network analysis for radiation heat transfer has been presented by Oppenheim.[32]

6.2.4 Condensation

Condensation can be an extremely important factor in containment design if the maximum credible accident involves the release of steam or liquid coolant that may vaporize due to a reduction in pressure. In this case condensation may occur on the relatively cold containment shell wall and on cold structural members.

Condensation may be characterized by the formation of drops or by the formation of a continuous film. Dropwise condensation results in heat transfer coefficients four to eight times as high as film condensation.[26] Since it is difficult to maintain dropwise condensation on normal surfaces (surfaces that are not polished or coated), and since conservative heat transfer coefficients are desirable, only film-type condensation will be considered in this report.

6.2.4.1 Condensation Without Inert Gas Present

The theoretical equation of Nusselt for film-type condensation on vertical surfaces and laminar flow of condensate is[33]

$$h_m \left(\frac{\mu_f^2}{k_f^3 \rho_f^2 g}\right)^{1/3} = 1.47 \left(\frac{4\Gamma}{\mu_f}\right)^{-1/3}, \qquad (6.6)$$

where

h_m = mean value of the heat transfer coefficient with respect to the height of the condensing surface, Btu/hr·ft^2·°F,
μ_f = viscosity of condensate film evaluated at t_f, lb/ft·hr,
k_f = thermal conductivity of condensate evaluated at t_f, Btu·ft/°F·hr·ft^2,
ρ_f = density of condensate film evaluated at t_f, lb/ft^3,
g = acceleration due to gravity = 4.17×10^8 ft/hr^2,
Γ = mass rate of flow of condensate from lowest point on condensing surface divided by the breadth, lb/hr·ft; for a vertical tube the breadth is πD; for a horizontal tube the breadth is equal to the length of tube,
t_f = 1/4 saturation temperature + 3/4 surface temperature, °F.

Equation (6.6) applies to vertical surfaces where the value of $4\Gamma/\mu_f$ is below 1800. McAdams[33] recommends that the values of h_m obtained from this equation be multiplied by 1.28 for vertical tubes. For steam condensing at atmospheric pressure and with Δt ranging from 10 to 150°F, the preceding equation reduces to

$$h_m = \frac{4000}{L^{1/4}\ \Delta t^{1/3}}, \qquad (6.7)$$

where

L = length of vertical tube,
Δt = saturation temperature minus temperature of surface, °F.

With values of $4\Gamma/\mu_f$ exceeding 1800, McAdams[33] recommends the following relation for vertical surfaces:

$$h_m \left(\frac{\mu_f^2}{k_f^3 \rho_f^2 g}\right)^{1/3} = 0.0077 \left(\frac{4\Gamma}{\mu_f}\right)^{0.4}. \qquad (6.8)$$

For horizontal tubes the heat transfer coefficient is given by Nusselts equation[33]

$$h_m \left(\frac{\mu_f^2}{k_f^3 \rho_f^2 g}\right)^{1/3} = 1.51 \left(\frac{4\Gamma}{\mu_f}\right)^{-1/3} . \qquad (6.9)$$

Equation (6.9) applies for values of $4\Gamma/\mu_f$ below 4200.

6.2.4.2 Condensation with Inert Gas Present

When noncondensable gas is present, the heat transfer coefficients will be greatly reduced. In this case the temperature of the free surface film, t_f, will be equal to the saturation temperature of the vapor at a pressure equal to its partial pressure on that surface. The temperature t_f can be found from a heat balance, considering that the heat conducted through the liquid film must be equal to the sum of the heat transferred by convection from the bulk of the vapor-gas mixture to the free film surface and the heat liberated by condensation. To determine this, the amount of vapor that diffuses to the liquid surface must be known. The difference in partial pressure of the vapor in the bulk of the gas-vapor mixture and its partial pressure on the free liquid surface is the driving force for this diffusion. Using procedures presented by Jakob,[34] the temperature, t_f, may be found by trial and error. This value of t_f will vary along the height of the surface since the thickness of condensate film changes.

Figures 6.5 and 6.6 show the effect of air concentration on the condensing heat transfer coefficient for steam. The height of the vertical surface in this case is one meter.

6.2.4.3 Direct Contact of Liquid and Gas

In some containment systems water sprays are used to reduce the final pressure. In addition to cooling the gas, the spray may cause condensation. The effect of the spray is difficult to predict because the contact

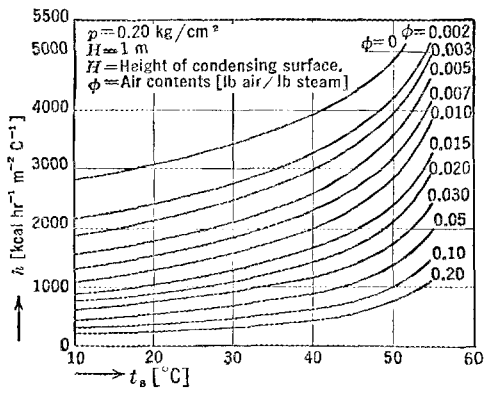

Fig. 6.5. Coefficient of Heat Transfer h in the Condensation of Steam Containing Air Versus Surface Temperature t_s. (From ref. 34)

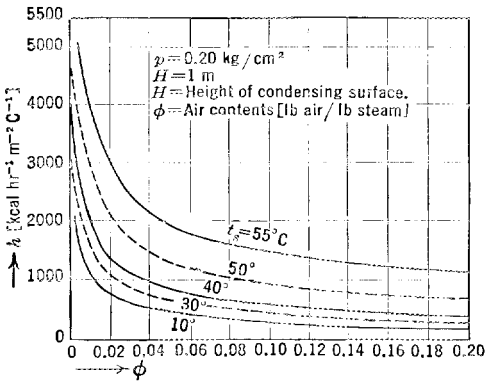

Fig. 6.6. Coefficient of Heat Transfer h in the Condensation of Steam Containing Air Versus Air Content ϕ. (From ref. 34)

surface between the two phases and the diffusion coefficients are uncertain. An estimate of the effect may be obtained by considering the data for vertical spray towers. The height of the spray tower is given by[33]

$$Z = Z_{oG} \int \frac{di_G}{i_L - i_G} , \qquad (6.10)$$

where

Z = height of vertical spray column, ft,
Z_{oG} = height of an overall mass-transfer unit, ft,
i_G = enthalpy for gas-vapor mixture, Btu/lb,
i_L = value of i_G based on temperature of bulk liquid, Btu/lb.

The height of an overall mass-transfer unit, Z_{oG}, depends on the gas and liquid mass flow rates. Values of Z_{oG} from 2.5 to 10 are given in refs. 33 and 35.

In addition to sprays, open water surfaces in the containment shell may be effective in condensing vapors. Kolflat[36] has presented experimental data showing the effect of liquid pools of cold water on the pressure in containment vessels after release of boiling water to the system. These data showed significant reductions in the final pressure when there were pools of cold water in the vessel.

6.2.5 Boiling

Boiling heat transfer may occur as liquid coolant is exposed to the fuel elements at a reduced pressure caused by a system failure, or it may occur in the containment shell when a superheated liquid is released to the containment system. Boiling heat transfer is characterized by several regimes. These are shown in Fig. 6.7 and discussed below.

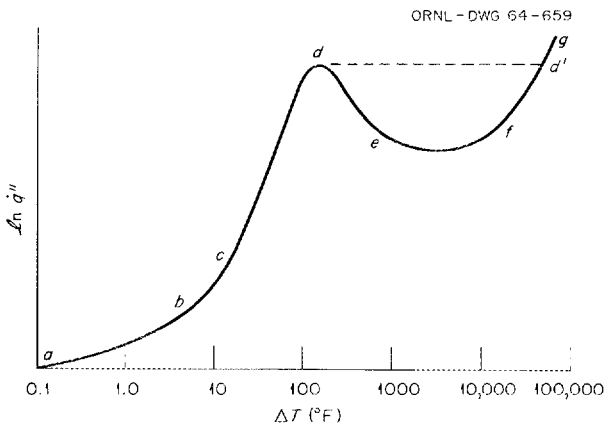

Fig. 6.7. Boiling Regimes.

In regime a-b, the heating-surface temperature is nearly equal to or only a few degrees greater than the liquid temperature. Thus there is little liquid superheat and no bubble formation, and heat transfer in regime a-b is by liquid convection only. The heat thus transferred is transported by the liquid rising to the surface, where some of it evaporates.

As the heating-surface temperature and thus Δt are increased, the heat flux increases and regime b-c is reached. In this regime the heat flux is still small, and only a small number of nucleation centers come into play; consequently, a small number of bubbles are formed. These bubbles rise quickly toward the surface and may collapse on the way. The slight agitation thus encountered causes $\dot{q}''$ (and h) to increase more rapidly with Δt. Again the effect of heat transfer is in the evaporation at the liquid top surface, as in regime a-b.

As Δt is further increased, regime c-d is reached. In this regime, the number of nucleation centers (and consequently the number of bubbles) increases rapidly with ΔT. The increasing number of bubbles causes considerable agitation and turbulence of the liquid in the boundary layer and, consequently, an increasing heat flux with ΔT. Regime c-d is called the nucleate-boiling regime and gives large rates of heat flux with moderate values of the temperature differences, ΔT, that is, moderate heating-surface temperature.

It should be noted here that, although this discussion pertains to nonflow saturated boiling, a similar mechanism occurs in flow systems if the bulk temperature is below saturation (for subcooled boiling), provided there is sufficient liquid superheat near the heating surface to initiate bubbles. These bubbles may collapse on or near the liquid top surface in the subcooled liquid, but they cause the same sort of liquid agitation and make large heat-transfer coefficients possible. The fact that bubble formation occurs in subcooled liquid means that local boiling at the heating surface can occur in pressurized-water reactors where the liquid bulk temperature is kept lower than saturation.

With reference to Fig. 6.7, the heat flux at point d is given various names; among them are maximum nucleate, critical, and peak heat flux. The temperature difference corresponding to point d is also called the maximum nucleate or the critical temperature difference.

As the temperature difference is increased beyond the critical value, regime d-e is reached. Here the bubbles become so numerous that they begin to coalesce and clump near the heating surface. In this case a portion of the heating surface gets blanketed with vapor, and the vapor blanket acts as a heat insulator (vapor is a poor heat-transfer agent). If ΔT is increased, the heat flux momentarily increases, causing more blanketing and a reduction in heat flux. The vapor blankets thus periodically collapse and reform. Operation in regime d-e is unstable. This regime is given various names, among which are the partial nucleate, unstable nucleate, partial film, mixed nucleate and film, and transition film boiling.

In regime e-f, a continuous blanket of vapor forms over the heating surface, and the heat transfer coefficient reaches a low value. Regime e-f is called the stable film or simply the film boiling regime.

In regime f-g the temperature of the heating surface is so high that thermal radiation from the surface comes into play. Thermal radiation is a strong function of temperature, and the heat flux rises rapidly with Δt. The exact location of point f depends, of course, on the thermal radiative emission and on the absorption characteristics of the surface and liquid. Regime f-g may be called the film and radiation regime.

If the heat flux is increased beyond that of point d in Fig. 6.7, the temperature difference changes abruptly from that at d to that at d′. The heating surface temperature at d′ is so high that it generally exceeds the melting point, and the surface is said to burn out. The heat flux corresponding to the temperature at burnout is called the burnout heat flux. This may be the heat flux corresponding to that at d or d′ but not necessarily so. Burnout may occur at any point on the curve, depending on the material of the heating surface and the operating conditions. In most cases, burnout occurs when the heat flux at point d is exceeded.

For nucleate pool boiling, Rohsenow and Choi[37] have developed the following equation from experimental data:

$$\frac{C_f \, \Delta t_x}{H_{fg} Pr^{1.7}} = K_{sf} \left[\frac{\dot{q}''}{\mu_f H_{fg}} \left(\frac{g_c \sigma}{g(\rho_f - \rho_g)} \right)^{1/2} \right]^{1/3} , \qquad (6.11)$$

where

C_f = specific heat of saturated liquid, Btu/lb·°F,
H_{fg} = latent heat of vaporization, Btu/lb,
Pr = Prandtl number of the saturated liquid,
g = acceleration of gravity, ft/hr^2,
g_c = conversion factor, numerically equal to g,
ρ_f = density of saturated liquid, lb/ft^3,
ρ_g = density of saturated vapor, lb/ft^3,
σ = surface tension of the liquid-to-vapor interface, lb/ft,
μ_f = viscosity of the liquid, lb/ft·hr,

Δt_x = temperature difference between the surface and the saturation temperature of the vapor, °F,
$\dot{q}''$ = heat flux, Btu/hr·ft^2,
K_{sf} = a constant that depends on the surface-fluid combination.

Values of K_{sf} are given in Table 6.9 for several surface-fluid combinations. Where the effect of convection heat transfer (either forced or

Table 6.9. Values[a] of K_{sf}

Surface-Fluid Combination	K_{sf}
Water-nickel	0.006
Water-platinum	0.013
Water-copper	0.013
Water-brass	0.006
CCl_4-copper	0.013
Benzene-chromium	0.010
n-Pentane-chromium	0.015
Ethyl alcohol-chromium	0.0027
Isopropyl alcohol-copper	0.0025
35% K_2CO_3-copper	0.0054
50% K_2CO_3-copper	0.0027
n-Butyl alcohol-copper	0.0030

[a]From ref. 37.

free) is superimposed on that caused by nucleate boiling, Rohsenow and Choi[37] suggest that the total heat flux be evaluated by

$$\dot{q}'' = (\dot{q}'')_c + (\dot{q}'')_b \ , \tag{6.12}$$

where

$(\dot{q}'')_c$ = heat flux due to convection in the absence of boiling, Btu/hr·ft^2,
$(\dot{q}'')_b$ = heat flux due to pool boiling, Btu/hr·ft^2.

The maximum heat flux for nucleate boiling, or peak heat flux, is given by[37]

$$\frac{(\dot{q}'')_{max}}{\rho_g H_{fg}} = 143 \left(\frac{\rho_f - \rho_g}{\rho_f}\right)^{0.6} \ . \tag{6.13}$$

Additional information on the effect of forced convection on peak heat flux, film boiling, effect of superheat, and effect of radiation is given in refs. 37, 38, and 39. The subject of burnout heat flux is covered by Gambill.[40]

6.3 PRESSURE, VOLUME, AND TEMPERATURE RELATIONS

P. F. Pasqua

Pressure, volume, and temperature relations are involved in the calculations leading to the design of the containment vessel. The conditions or the properties of the fluids as they would exist in the containment vessel in the event of an accidental release from the reactor affect the ultimate design of this final barrier that controls the release of radioactivity into the surroundings.

The problems associated with the determination of the final properties of the fluid in the containment vessel depend upon several factors, such as (1) the nature and mass of fluid and its state in the reactor before release into the containment vessel, (2) the rate of release of the fluid into the containment vessel and its interaction with the materials of the containment vessel, (3) the initial state and volume of the fluid in the containment vessel, (4) the likelihood and extent of any exothermic reactions, and (5) the expected load to be imposed by decay heat.

The pressure, volume, and temperature conditions of a system are determined through the use of equations of state, energy balances, and mass balances. These equations are interrelated and in many cases are very difficult to solve without making simplifying assumptions. As an example, assume that the reactor is of the boiling-water or pressurized-water type and that it is located within a containment vessel. The energy equation for the containment vessel as the <u>system</u> (the reactor is considered external to the system) is

$$\int_s \int_{\tau_1}^{\tau_2} \frac{\partial^2 Q}{\partial \tau \, \partial s} \, ds \, d\tau + \int_{\tau_1}^{\tau_2} e_f \, dm_f = U_{\tau_2} - U_{\tau_1} , \qquad (6.14)$$

where

$\int_s \int_{\tau_1}^{\tau_2} \frac{\partial^2 Q}{\partial \tau \, \partial s} \, ds \, d\tau$ = energy transferred as heat into and out of all surfaces of the system during the time $\tau_2 - \tau_1$,

$\int_{\tau_1}^{\tau_2} e_f \, dm_f$ = energy transferred into the system with the mass entering the system from the reactor,

U_{τ_2} = final internal energy of the fluid in the system (containment vessel),
U_{τ_1} = initial internal energy of the gas in the system.

The following assumptions are made for this problem:

1. The release of reactor fluid into the system is so rapid that heat transfer out of the system at the containment walls and heat transfer from the core into the vessel are not significant in calculating the maximum pressure rise.

2. With the above assumption, the system is changed to include the reactor; therefore, the second integral of Eq. (6.14) does not exist.

The energy equation is thus reduced to

$$U_{\tau_2} - U_{\tau_1} = 0 \ , \tag{6.15}$$

where the internal energies include reactor and containment vessel fluids.

In order to expand upon the problem, consider that the reactor, using water as the coolant or moderator or both, ruptures and releases its contents into the containment vessel, which contains a gas. The following additional assumptions are made:

1. The initial state of the water in the reactor is saturated liquid at a given pressure or temperature.
2. The mass or volume of water is known.
3. The initial state of the gas in the containment vessel is known.
4. The volume of the containment vessel is known.
5. The final mixture in the containment vessel is one of equilibrium between saturated water, saturated vapor, and gas.
6. There are no exothermic reactions within the system.

The problem is to determine the final state of the mixture in the containment vessel.

The total internal energy of the system is made up of the internal energy of the air in the containment vessel and the internal energy of the water in the reactor. Thus Eq. (6.14) becomes

$$M_a C_v (T_{a_1} - T_0) + M_w (u_1 - u_0) = M_a C_v (T_{a_2} - T_0) + M_w (u_2 - u_0) \ , \tag{6.16}$$

where

M_a = mass of air in containment vessel,
M_w = mass of water in reactor,
T_{a_1} = initial temperature of gas in containment vessel,
T_{a_2} = final temperature of gas in containment vessel,
T_0 = reference temperature,
C_v = specific heat of gas at constant volume,
u_1 = initial specific internal energy of water in reactor,
u_2 = final specific internal energy of water in containment vessel,
u_0 = reference internal energy.

Equation (6.16) reduces to

$$M_a C_v T_{a_1} + M_w u_1 = M_a C_v T_{a_2} + M_w u_2 \ . \tag{6.17}$$

The left-hand side of Eq. (6.17) is known if all the initial conditions are given; however, the final temperature of the gas (T_{a_2}) and the final internal energy of the water in the containment vessel are unknown. If it is assumed that the final condition in the containment vessel is one of equilibrium between gas, saturated vapor, and saturated liquid, Eq. (6.17) becomes

$$M_a C_v T_{a_1} + M_w u_1 = M_a C_v T_2 + M_w (u_{f_2} + x u_{fg_2}) \ , \tag{6.18}$$

where

T_2 = final equilibrium temperature,
u_{f_2} = specific internal energy of saturated liquid,
u_{fg_2} = specific internal energy change from saturated liquid to saturated vapor,
x = quality.

In Eq. (6.18) the properties of the water (u_{f_2}, u_{fg_2}) depend upon the final temperature (T_2), which in turn depends on the final pressure. An expression for the quality x is

$$x = \frac{\frac{V}{M_w} - v_{f_2}}{v_{fg_2}} \ , \tag{6.19}$$

where

V = volume of containment vessel,
v_{f_2} = specific volume of saturated liquid at T_2,
v_{fg_2} = specific volume change from saturated liquid to saturated vapor at T_2.

Thus it is seen that the final specific internal energies and the final quality depend upon the final temperature of the system.

There are several ways in which the final temperature and thus pressure can be determined. One method is a trial and error solution using the tables of Thermodynamic Properties of Steam.[41] The final temperature is assumed and, using the values of ref. 41, Eq. (6.19) is solved for the quality x. Using this quality and the assumed final temperature, Eq. (6.18) is checked for equality (or solved for T_2). If an inequality is found, then a different final temperature is assumed and the procedure is repeated.

Once the final equilibrium temperature has been determined, the final pressure in the containment vessel can be determined. The final pressure can be expressed as

$$P_2 = p_{s_2} + p_{a_2} ,$$

where

P_2 = final pressure in containment vessel,
p_{s_2} = partial pressure of the saturated vapor corresponding to T_2,
p_{a_2} = partial pressure of the gas corresponding to T_2.

Assuming the perfect gas equation of state for the gas,

$$p_{a_2} = p_{a_1} \frac{T_2}{T_{a_1}} ,$$

where p_{a_1} is the initial pressure of the gas in the containment vessel. Thus

$$P_2 = p_{s_2} + p_{a_1} \frac{T_2}{T_{a_1}} .$$

Equation (6.18) can be handled in a different manner through the use of nomographs. Dividing Eq. (6.18) by the mass of water gives

$$\frac{M_a}{M_w} C_v T_{a_1} + \frac{M_w}{M_w} u_1 = \frac{M_a}{M_w} C_v T_2 + \frac{M_w}{M_w} (u_{f_2} + x u_{fg_2}) = \frac{U}{M_w} \qquad (6.20)$$

or

$$u_{a_1} + u_{w_1} = u_{a_2} + u_{w_2} = \frac{U}{M_w} , \qquad (6.21)$$

where

$u_{a_1} = \frac{M_a}{M_w} C_v T_{a_1}$ (Btu/lb of H_2O),
$u_{w_1} = u_1$,

$$u_{a_2} = \frac{M_a}{M_w} C_v T_2,$$

$$u_{w_2} = u_{f_2} + x u_{fg_2} = u_{f_2} + u_{fg_2} \frac{V}{M_w} \frac{1}{v_{fg_2}} - \frac{v_{f_2}}{v_{fg_2}} .$$

In Figs. 6.8 through 6.11, u_{a_1} and u_{a_2} can be determined if the gas temperatures and mass ratio of gas to water are known. The initial pressure or temperature of the water in the reactor will fix u_{w_1}. By assuming the final temperature and knowing the ratio of the containment volume to the mass of water, the final u_{w_2} may be determined. The values determined must satisfy Eq. (6.20).

To illustrate the figures, assume the following:

T_{a_1} = 200°F (temperature of air),
M_w = 300 lb,
P_{w_1} = 1500 psia (saturation pressure),
V = 2000 ft^3,
P_{a_1} = 5 psia,
M_a = 41 lb.

The problem is to determine the final equilibrium pressure.

From Fig. 6.8, knowing that T_{a_1} = 200 and that

$$\frac{M_a}{M_w} = \frac{41}{300} = 0.137 ,$$

the initial internal energy of the air is

$$U_{a_1} = 16 \text{ Btu/lb of } H_2O .$$

From Fig. 6.9, at 1500 psia,

$$U_{w_1} = 611 \text{ Btu/lb of } H_2O .$$

Therefore, the total internal energy of the system per pound (mass) of water is

$$\frac{LI}{M_w} = 16 + 611 = 627 \text{ Btu/lb of } H_2O .$$

This total internal energy must be checked by the final conditions. Thus it is assumed that the final equilibrium temperature is

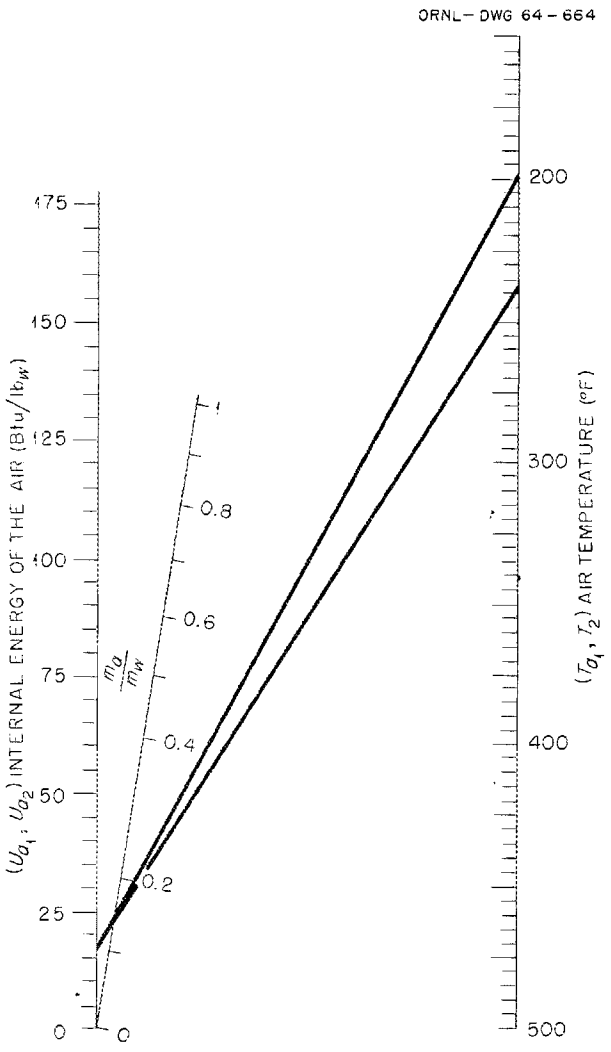

Fig. 6.8. Relation of Air Temperature, Mass Ratio, and Internal Energy of Air.

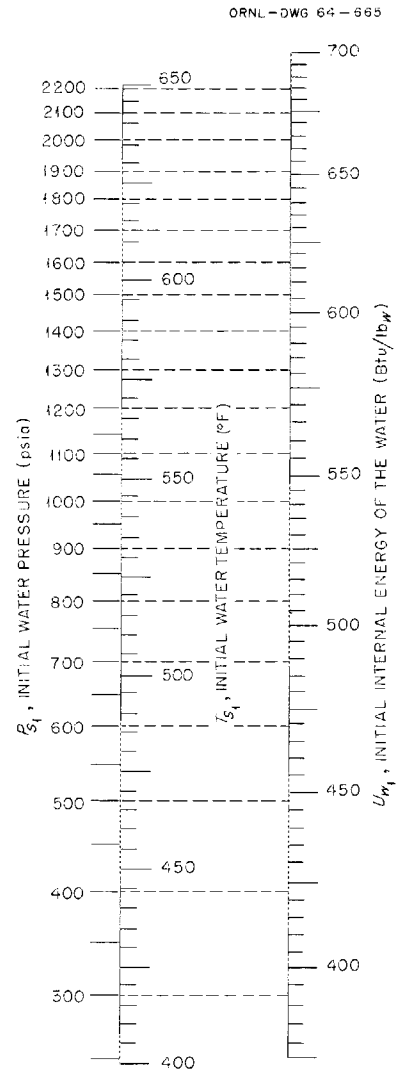

Fig. 6.9. Internal Energy of Saturated Water as a Function of Pressure or Temperature.

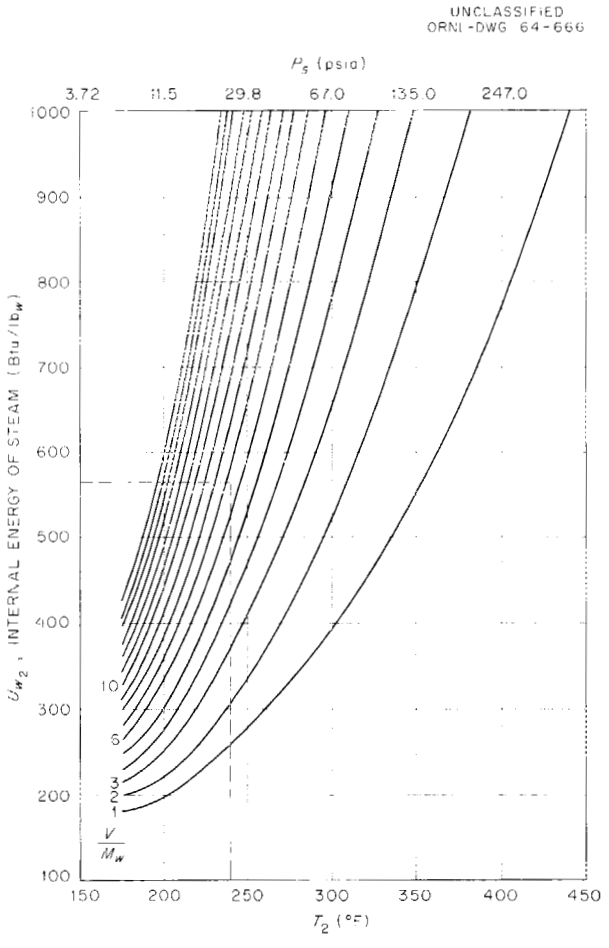

Fig. 6.10. Final Internal Energy of Water Mixture in Containment Vessel as a Function of Temperature and Ratio of Containment Volume to Mass of Water Mixture.

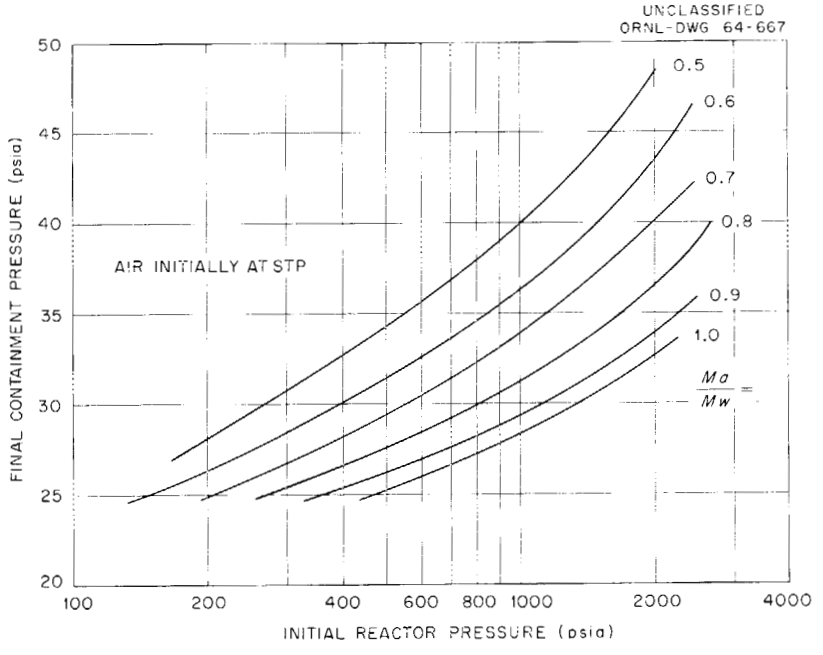

Fig. 6.11. Containment Vessel Conditions Following Reactor Accident.

$$T_2 = 240°F ,$$

and since

$$\frac{V}{M_w} = \frac{2000}{300} = 6.66 \text{ ft}^3/\text{lb of } H_2O ,$$

from Fig. 6.10,

$$U_{2_w} = 565 \text{ Btu/lb of } H_2O ,$$

and at 240°F, Fig. 6.8 gives

$$U_{2_a} = 18 \text{ Btu/lb of } H_2O .$$

Therefore

$$U_{2_w} + U_{2_a} = 565 + 18 = 583 \neq 627 .$$

Another trial at $T_2 = 245°F$ gives

$$U_{2_w} + U_{2_a} = 610 + 19 = 629 .$$

At $T_2 = 245°F$, the saturation pressure is approximately 27 psia. Therefore

$$P_2 = P_{s_2} + P_{a_1} \frac{T_2}{T_{a_1}} = 27 + 5 \left(\frac{705}{660}\right) \approx 33 \text{ psia} .$$

Equation (6.20) has been programmed in FORTRAN language and is presented in Table 6.10. Results from this program are shown in Fig. 6.11 for the initial conditions of saturated water in the reactor and air at standard temperature and pressure in the containment vessel. The program is written, however, so that any initial condition of water in the reactor and any initial condition of air in the containment vessel may be used. The other assumptions relating to Eq. (6.18) remain in this analysis.

It must be remembered that the analysis just made involving the final pressure in the containment vessel was for the condition of no transfer of energy as heat. Thus, the complexity of Eq. (6.14) could be reduced. The assumptions used in the analysis lead to a maximum pressure in the containment vessel.

If the assumption of no heat transfer is not appropriate, then an attempt should be made to solve Eq. (6.14). The first term in this

Table 6.10. FORTRAN Program for Eq. (6.20)

```
C     C CONTAINMENT VESSEL CONDITIONS FOLLOWING REACTOR ACCIDENT
C     C VARIABLES ARE DEFINED AS FOLLOWS...
C     C PRESS=SAT.PRESS.(PSIA)    TEMP=SAT.TEMP.(DEG.F.)
C     C VF=SP.VOL.OF SAT.FLUID(CU.FT./LBM)
C     C VG = SP. VOL. OE SAT. VAPOR (CU.FT./LBM )
C     C UF = SP. INTERNAL ENERGY OF THE VAPOR (BTU/LBM)
C     C UFG = SP. CHANGE IN INTERNAL ENERGY ON EVAP. (BTU/LBM)
C     C VFG = CHANGE IN SP. VOL. ON EVAP. (CU.FT./LBM)
C     C RAT = MASS RATIO (LBM AIR/LBM WATER)
C     C INITIAL REACTOR CONDITIONS...
C     C P1W=INITIAL PRESS OF SAT.FLUID IN REACTOR
C     C U1W =.CORRESPONDING SP. INTERNAL ENERGY
C     C INITIAL AIR CONDITIONS...
C     C TAIR = INITIAL AIR TEMP(DEG. F)
C     C PAIR= INITIAL AIR PRESS (PSIA)
C     C VAIR = INITIAL SP. VOL. OF AIR (CU. FT. / LBM)
C     C EN1 = TOTAL INITIAL INTERNAL ENERGY OF SYSTEM
C     C EN2 = TOTAL FINAL INTERNAL ENERGY OF SYSTEM
      DIMENSION PRESS(58),TEMP(58),VF(58),VG(58),UF(58),UFG(58),
     1P1W(30),U1W(30),RAT(20),VFG(58)
      READ 110,TAIR,PAIR,CV
      VAIR=53.35*(TAIR+460.)/(PAIR*144.)
      DO 5 K=1,58
    5 READ 10,PRESS(K),TEMP(K),VF(K),VG(K),UF(K),UFG(K)
      DO 6 I=1,20
    6 READ 20,RAT(I)
      DO23 J=1,30
   23 READ 50,P1W(J),U1W(J)
      PUNCH 90
      DO100 I=1,20
      PUNCH 30,RAT(I)
      PUNCH 40
      PUNCH 70
      DO 200 J=1,30
      EN1=RAT(I)*(TAIR+460.)*CV+U1W(J)
      K=1
   13 VFG(K)=VG(K)-VF(K)
      EN2=RAT(I)*CV*(TEMP(K)+460.)+UF(K)+(UFG(K)/VFG(K))*(RAT(I)*
     1VAIR-VF(K))
      IF(EN1-EN2) 9,9,14
   14 K=K+1
      IF(50-K)15,13,13
   15 PUNCH 80
      GO TO 100
    9 IF(K-1)84,84,85
   84 PUNCH 86,P1W(J)
      GO TO 200
   85 TA=TEMP(K)+TEMP(K-1)/2.
      UFA=UF(K)+UF(K-1)/2.
      UFGA=UFG(K)+UFG(K-1)/2.
      VFGA=VFG(K)+VFG(K-1)/2.
      VFA=VF(K)+VF(K-1)/2.
      ENA=RAT(I)*CV*(TA+460.)+UFA+((UFGA/VFGA)*(RAT(I)*VAIR))-VFA
      IF(EN1-ENA) 11,11,12
   11 K=K-1
      GO TO 17
```

Table 6.10 (continued)

```
 12   K=K
 17   P2=PRESS(K)+PAIR*((TEMP(K)+460.)/TAIR+460.)
      PUNCH 60, P1W(J), P2, TEMP(K)
200   CONTINUE
100   CONTINUE
110   FORMAT(F6.0,F7.1,F6.3)
 10   FORMAT(F5.1,F9.2,F7.3,F9.3,F10.2,F8.1)
 20   FORMAT(F6.3)
 50   FORMAT(F5.0,F8.1)
 90   FORMAT(51HCONTAINMENT PRESSURES VS.INITIAL REACTOR CONDITIONS)
 30   FORMAT(22HMASS(AIR)/MASS(WATER)=F6.3)
 40   FORMAT(40HINITIAL PRESS   FINAL PRESS   FINAL TEMP)
 70   FORMAT(38H (REACTOR)          (CONTAINMENT VESSEL))
 80   FORMAT(27HFINAL PRESS.EXCEEDS 100PSIA)
 86   FORMAT(F7.1,22H   FINAL PRESS.TOO LOW)
 60   FORMAT(F7.1,F17.1,F15.1)
      END

                    CARDS  0073
```

equation involves the heat transfer through all surfaces of the system during a specified time. One method of evaluating this integral is to treat the walls of the containment vessel as a semi-infinite slab that has been subjected to a sudden increase in temperature. A graphical technique known as the Schmidt plot is available for solving such problems. However, it should be recognized that the temperature at the surface of the slab is a variable that depends upon the amount of energy removed at the wall and the amount added to the system by the in-flow of reactor fluid.

The second integral of Eq. (6.14), the energy added to the system with the mass flowing into the system, depends upon many factors: the type and size of the break between the reactor and the containment vessel, the state of the material released, the pressure difference between the reactor and the containment vessel, and the type of flow assumed – equilibrium, two phase, critical, metastable, etc. As can be seen, the rate of mass release into the containment vessel, and its state, will affect the heat transfer and the final internal energy of the system.

No general solution to Eq. (6.14) is proposed because of the many different conditions that could prevail in a particular situation.

6.4 HYDRAULIC PROBLEMS

H. W. Hoffman

For the design of reactor containment systems, there are a variety of hydraulic problems that must be considered. The following sections include

(1) discussions of the linear momentum equation and Bernoulli's equation, both of which are used to determine jet impingement forces resulting from single-phase flow, (2) working equations for two-phase flow, and (3) shock transmission. A qualitative description of jet condensation is also presented.

6.4.1 Jet Impingement Forces

The linear momentum equation for steady flow through a control volume (Fig. 6.12) is derived for the x direction to begin the analysis. The resulting equation is in scalar form, but it is easily extended to vector form by considering the y and z directions.

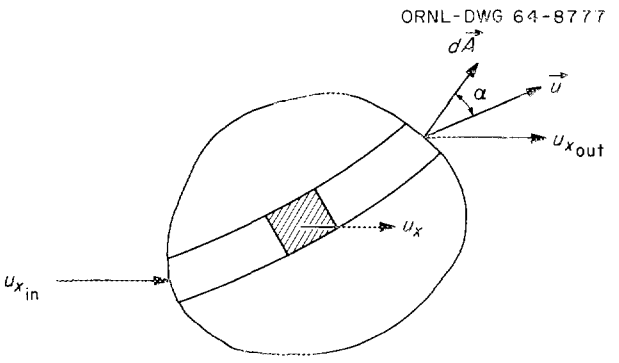

Fig. 6.12. Control Volume.

For the x direction, Newton's second law of motion for a particle is

$$\delta f_x = \frac{d}{dt}(u_x \delta_m) = \delta_m \frac{du_x}{dt} + u_x \frac{d\delta_m}{dt}, \tag{6.22}$$

where δf_x is the x component of force on the particle and u_x is the velocity in the +x direction. The last term drops out when the equation is applied to a given mass element as it flows through the control volume because δ_m is constant. The term on the right may be expanded as

$$\delta f_x = \delta_m \left(\frac{\partial u_x}{\partial s} \frac{ds}{dt} + \frac{\partial u_x}{\partial t} \right) . \tag{6.23}$$

For steady flow, $\partial u_x/\partial t = 0$. The mass element is written as $\rho\ \delta Q\ \delta t$, which represents the mass flowing through any section of the stream tube in steady flow. Thus

$$\delta f_x = \rho\ \delta Q \frac{\partial u_x}{\partial s}\, ds = \rho\ \delta Q\ \delta u_x\ . \tag{6.24}$$

Integration along the stream tube from entrance to exit gives

$$f_x = \rho\ \delta Q \int_{in}^{out} du_x = \rho\ \delta Q\ (u_{x_{out}} - u_{x_{in}})\ . \tag{6.25}$$

Summing for all stream tubes passing through the control volume gives the x component of force on the control volume:

$$F_x = \int \rho u_{x_{out}}\ dQ - \int \rho u_{x_{in}}\ dQ\ . \tag{6.26}$$

The above integrals are only carried out over those portions of the control volume where $u_x \neq 0$. By using the notation given in Fig. 6.12,

$$\delta Q = \vec{u} \cos \alpha\ dA\ ,$$

where α is the angle between the normal to the surface area element and the velocity vector at this point. Thus, Eq. (6.26) becomes

$$F_x = \int_A \rho u_x\ u \cos \alpha\ dA\ . \tag{6.27}$$

In vector notation, Eq. (6.27) becomes

$$F_x = \int_A \rho u_x\ \vec{u} \cdot d\vec{A}\ . \tag{6.28}$$

The y and z components, which may be obtained in a similar fashion, are

$$F_y = \int_A \rho u_y\ \vec{u} \cdot d\vec{A}\ , \qquad F_z = \int_A \rho u_z\ \vec{u} \cdot d\vec{A}\ . \tag{6.29}$$

The general, steady, linear momentum equation is obtained by adding the individual components vectorially:

$$\vec{F} = \int_A \rho\, \vec{u}(\vec{u}\cdot d\vec{A}) \ . \tag{6.30}$$

In many practical applications the coordinate system may be chosen so that only one or two of the scalar momentum equations need be considered. In addition, in some instances ρ and the velocity are constant over the inlet or outlet section. With V_x the average velocity over a section, and recalling that for steady flow $(\rho Q)_{in} = (\rho Q)_{out}$, the x-direction momentum equation becomes

$$F_x = \rho Q(V_{x_{out}} - V_{x_{in}}) \ . \tag{6.31}$$

When the velocity is not constant over the inlet or the outlet section, but the density is, the integrals in Eq. (6.26) may be written in the general form

$$\rho \int u_x \, dQ = \rho \beta_m V_x Q \ , \tag{6.32}$$

where β_m represents a momentum correction factor. If the velocity profile is known, either analytically or experimentally, β_m is found by solving

$$\beta_m = \frac{1}{A} \int_A \left(\frac{u}{V}\right)^2 dA \ . \tag{6.33}$$

Numerical values of β_m are readily obtainable in the literature. For example, for turbulent flow in pipes, β_m varies from 1.01 to 1.05, and for laminar flow in round tubes, $\beta_m = 4/3$.

Another equation that is useful in solving elementary flow problems is Bernoulli's equation. To derive Bernoulli's equation, it is first necessary to obtain a frictionless equation of motion, Euler's equation. The motion of a fluid particle along a streamline, as shown in Fig. 6.13, is considered.

Figure 6.13 shows the forces acting on a fluid particle of mass $\rho\, \delta s\, \delta A$ in the direction of its motion along a streamline. It is assumed that the viscosity is zero, which amounts to neglecting all frictional forces. From Newton's second law of motion, $\Sigma f_s = \delta_m a_s$, it is found that

$$\frac{1}{\rho}\frac{\partial p}{\partial s} + g \cos \alpha + a_s = 0 \ , \tag{6.34}$$

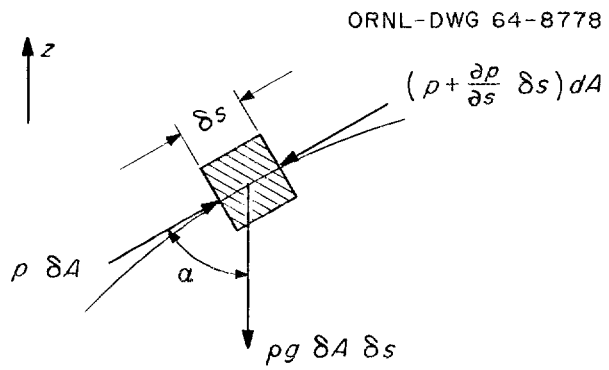

Fig. 6.13. Forces Acting on a Fluid Particle.

where a_s is the acceleration of the particle in the +s direction. As the particle moves a distance δs, it changes elevation by an amount δz, thus

$$\frac{\delta z}{\delta s} = \cos \alpha = \frac{\partial z}{\partial s} . \tag{6.35}$$

The acceleration $a_s = du/dt$, where $u = u(s,t)$. Consequently,

$$a_s = \frac{du}{dt} = \frac{\partial s}{\partial s}\frac{ds}{dt} + \frac{\partial u}{\partial t} . \tag{6.36}$$

To simplify, it is assumed that the motion is steady. Substituting Eq. (6.36), with $\partial u/\partial t = 0$, and Eq. (6.35) into Eq. (6.34), and noting that $ds/dt = u$, gives

$$\frac{dp}{\rho} + g\, dz + u\, du = 0 . \tag{6.37}$$

Equation (6.37) is Euler's equation of motion along a streamline for steady flow of a frictionless fluid.

Integration of Eq. (6.37) gives Bernoulli's equation:

$$gz + \frac{u^2}{2} + \int \frac{dp}{\rho} = \text{constant} . \tag{6.38}$$

Equation (6.38) is only valid if $\rho = \rho(p)$, and it only applies to motion along a given streamline, since the constant on the right generally varies from streamline to streamline.

If the fluid is incompressible, Eq. (6.38) becomes

$$gz + \frac{u^2}{2} + \frac{p}{\rho} = \text{constant} \ . \tag{6.39}$$

An expression similar to Eq. (6.39) is also obtainable by considering a nonrotational flow field and imposing all the other assumptions used in deriving Eq. (6.39), with the exception that the motion need not be limited to flow along a streamline. For this case, however, the constant on the right-hand side of Eq. (6.39) implies that the available energy is constant throughout the flow field.

To facilitate the use of Bernoulli's equation, it is often desired to use a one-dimensional analysis; that is, the flow is represented by a stream tube with average velocity, V. If the velocity is not uniform over the cross section of the stream tube, it is necessary to modify Eq. (6.39), since the kinetic energy per unit weight, $V^2/2g$, is not the average of $u^2/2g$ taken across the stream tube. To account for the difference, a kinetic-energy correction factor, β_k, is introduced so that $\beta_k(V^2/2g)$ is the average kinetic energy per unit weight passing through any cross section of the stream tube. The correction factor, β_k, is obtained by solving

$$\beta_k = \frac{1}{A} \int_A \left(\frac{u}{V}\right)^3 dA \ , \tag{6.40}$$

which is easily calculated if the velocity profile is known analytically or experimentally. For turbulent flow in a pipe, β_k ranges from 1.01 to 1.10 and is usually neglected; while for laminar flow in a pipe, $\beta_k = 2$.

Application of the above equations is demonstrated by the following examples:

Example 1. The mixing of two streams of fluid, as shown in Fig. 6.14, is considered to demonstrate an application of the linear momentum equation. For simplicity, it is assumed that both fluids are incompressible and have an identical density, ρ. To satisfy the steady-state continuity equation,

$$\rho_1 V_1 S_1 = \rho_2 V_2 S_2 \ .$$

But $\rho_1 = \rho_2$, and $A_1 = A_2$, therefore

$$V_1 = V_2 = \frac{1}{2} u_o + \frac{1}{2}\left(\frac{1}{2} u_o\right) = \frac{3}{4} u_o \ .$$

Since the velocity is not uniform across section 1, the momentum correction factor, β_m, must be calculated:

$$\beta_{m_1} = \frac{1}{A} \int_A \left(\frac{u}{V_1}\right)^2 dA \ .$$

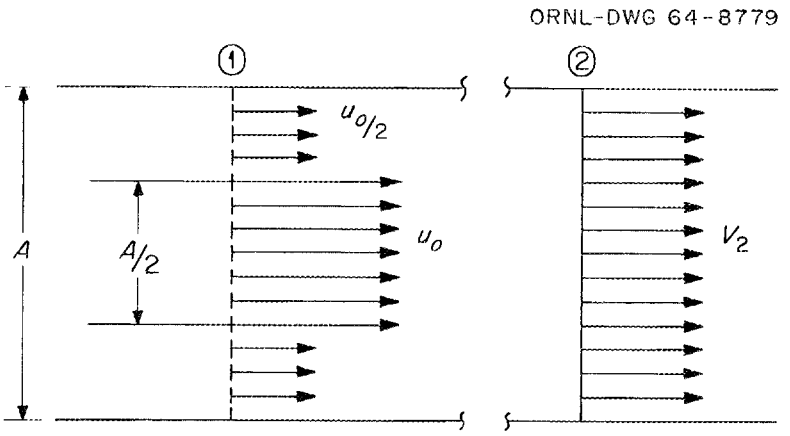

Fig. 6.14. Mixing of Two Streams of Fluid.

Since the flow is symmetrical, it is only necessary to integrate over one-half the channel width:

$$\beta_{m_1} = \frac{1}{A}\left[\int_0^{A/4}\left(\frac{u_o}{\frac{3}{4}u_o}\right)^2 dA + \int_{A/4}^{A/2}\left(\frac{\frac{u_o}{2}}{\frac{3}{4}u_o}\right)^2 dA\right] ,$$

or

$$\beta_{m_1} = \frac{10}{9} .$$

Since the velocity is uniform at section 2, $\beta_{m_1} = 1$.

A momentum balance between sections 1 and 2 is then, from Eq. (6.31),

$$(p_2 - p_1)A = \rho V_1 A(\beta_{m_1} V_1 - V_2) ,$$

but, $V_1 = V_2 = (3/4)u_o$, therefore

$$p_2 - p_1 = \rho V_1^2(\beta_{m_1} - 1) = \rho \frac{9}{16} u_o^2(\beta_{m_1} - 1) ,$$

$$= \rho \frac{9}{16} u_o^2 \left(\frac{10}{9} - 1\right) = \frac{1}{16} \rho u_o^2 .$$

The expression $p_2 - p_1$ represents the pressure increase resulting from the mixing of the two streams, neglecting all viscous forces.

Example 2. The problem is to find the tensile force exerted on the pipe shown in Fig. 6.15 by the converging section and to find the force exerted on wall section 3. The fluid has a specific gravity of 0.85. To determine the discharge, Bernoulli's equation is used:

$$z_1 + \frac{V_1^2}{2g} + \frac{p_1}{\gamma} = z_2 + \frac{V_2^2}{2g} + \frac{p_2}{\gamma} .$$

Since $z_1 = z_2$, $V_2 = (D_1/D_2)^2 V_1 = 9V_1$, and γ, the specific weight of the fluid, is 0.85×62.4, it is found that

$$\frac{V_1^2}{2g}(1 - 81) + \frac{100}{144 \times 0.85 \times 62.4} = 0 ,$$

or

$$V_1 = 14.78 \text{ ft/sec}, \qquad V_2 = 133 \text{ ft/sec}.$$

The flow rate, Q, is

$$Q = 14.78 \frac{\pi}{4}\left(\frac{1}{4}\right)^2 = 0.725 \text{ cfs} .$$

With the force exerted on the fluid by the converging section designated p_x, Eq. (6.31) gives

$$p_1A_1 - p_2A_2 - p_x = \rho Q(V_2 - V_1) ,$$

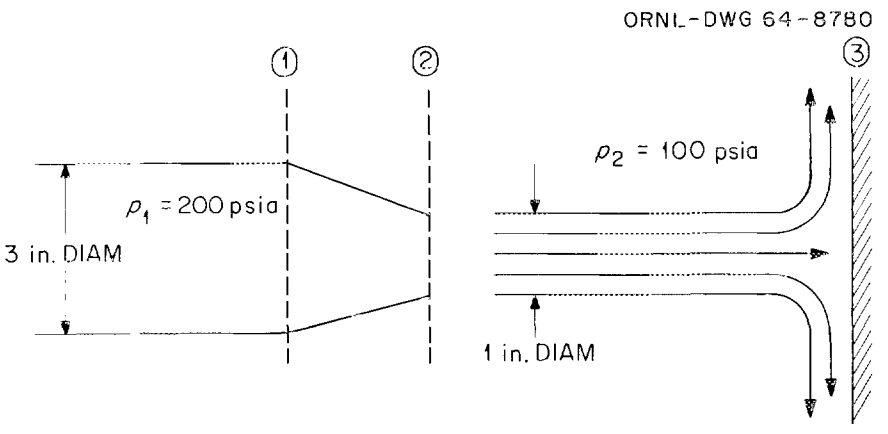

Fig. 6.15. Pipe Considered in Example 2.

$$200 \frac{\pi}{4} 9 - 100 \frac{\pi}{4} - p_x = 1.935 \times 0.85 \times 0.725 \ (133 - 14.78) \ ,$$

$$p_x = 1191.5 \text{ lb} \ .$$

Although p_x represents the force exerted by the converging section on the fluid, it does not represent the tensile force in the pipe, since the force on the exterior of the converging section due to p_2 has not been accounted for.

From Fig. 6.16, it can be seen that the net force in the x direction on the exterior of the converging section due to p_2 is

$$p_2 \frac{\pi}{4} (D_1^2 - D_2^2) = 626.25 \text{ lb} \ .$$

Thus, the tensile force in the pipe is

$$1191.5 - 626.5 = 565 \text{ lb.}$$

The difference between the force of the converging section on the fluid and the tensile force on the pipe is to be noted. The tensile force could have been readily obtained if it had been assumed that $p_2 = 0$ and $p_1 = 100$ (a pseudo gage pressure). Application of Eq. (6.31) directly yields

$$100 \frac{\pi}{4} 9 - p_x = 1.935 \times 0.85 \times 0.725 \ (133 - 14.78)$$

and

$$p_x = 565 \text{ lb.}$$

ORNL-DWG 64-8781

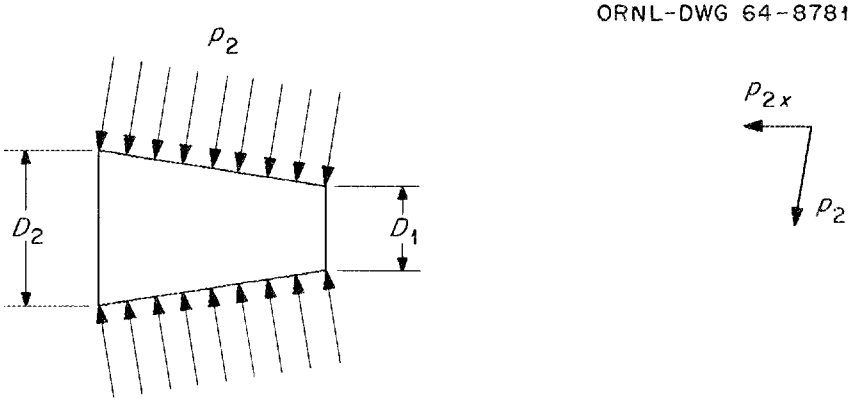

Fig. 6.16. Forces on Converging Section.

The jet impingement force action on surface 3 is calculated by using Eq. (6.31) between sections 2 and 3. Since $V_{x_3} = 0$ and $p_3 = p_2$, Eq. (6.31) gives

$$-F_x = \rho Q V_2$$

$$= 1.935 \times 0.85 \times 0.725 \times 133$$

$$= 158.5 \text{ lb.}$$

The force on section 3 is equal and opposite to F_x.

6.4.2 Two-Phase Flow

The simultaneous flow of a liquid and a gas or vapor is commonly defined in the literature as "two-phase flow," although this term can also apply to simultaneous flow of solids with gases or solids with liquids. In this section, the term "two-phase flow" will refer exclusively to the cocurrent steady-state gas-liquid flow. This type of flow is found in the coolant channels of boiling-water reactors and may be found in any pressurized-water circuit following a rupture in the system.

Because of the great difference in density and viscosity of the two fluids, the velocity of the gas phase is greater than the velocity of the liquid, giving rise to the so-called "slip," the difference of the average phase velocities. The ratio of the average velocities of the vapor and liquid is called the slip ratio. At the rupture of a line or a vessel, critical flow is likely to exist. The critical flow is obtained by dropping the downstream or back pressure until a maximum discharge is reached for a fixed upstream pressure and thermodynamic state of fluid. Further reduction of the back or receiver pressure will no longer affect the flow rate or the exit pressure.

The cocurrent flow of gas-liquid mixtures yields various flow patterns. The flow behavior and pressure drop of the system are dependent upon which of these flow patterns occurs. The gas-liquid flow may be divided into two general categories: (1) two-component flow in which the gas and liquid are different substances, or (2) one-component flow of a liquid and its vapor. One-component flow can be further divided into nonboiling and boiling categories. In nonboiling flow, the liquid and vapor in thermodynamic equilibrium are established upstream before entering a flow channel, with the flow thereafter being adiabatic. In boiling flow, the gas phase is generated by net boiling of the liquid phase due to heat addition in the channel.

The flow-pattern descriptions may be grouped into four categories: (1) vertical nonboiling flow, (2) horizontal nonboiling flow, (3) vertical boiling flow, and (4) horizontal boiling flow. The classification of flow patterns in gas-liquid flow is not standarized at present but depends largely upon individual interpretations of the visual appearance of particular flows.

In the case of vertical nonboiling flow, only symmetrical patterns are possible. The four patterns usually observed[42] are shown in Fig. 6.17. For horizontal nonboiling flow, there may be bubble, plug, stratified, wavy, slug, annular, and spray flow,[43] as shown in Fig. 6.18. Vertical boiling flow patterns have been classified by Wallis and Griffith[44] as bubbly, transitional, annular, dropwise, and streaky. There is little or no information on horizontal boiling flow patterns.

In the vertical channel, bubble flow consists in individual dispersed bubbles moving independently up the channel. Plug, or slug, flow occurs when patches of coalesced vapor fill most of the channel cross section as they move upward. Plug flow has been reported as being both a stable and an unstable transitional flow between bubble flow and the next type, annular flow. In annular flow the vapor forms a continuous phase that carries

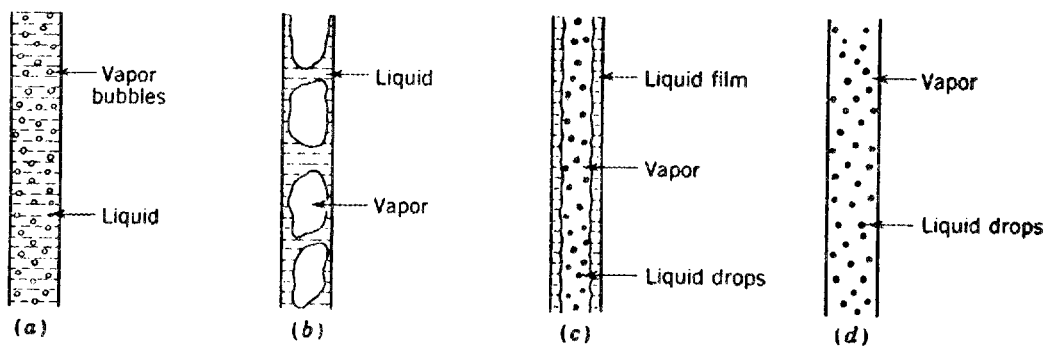

Fig. 6.17. Flow Patterns of Two-Phase Vertical Nonboiling Flow. (a) Bubble; (b) plug (slug); (c) annular (channelized); (d) fog. (From ref. 42)

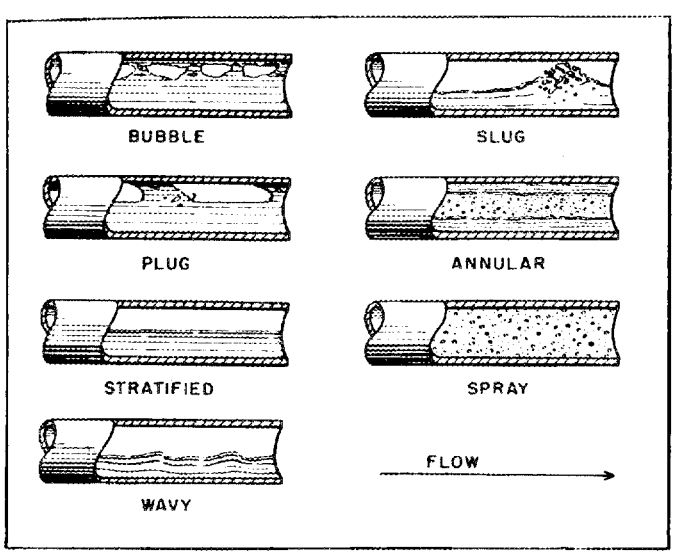

Fig. 6.18. Flow Patterns of Two-Phase Horizontal Nonboiling Flow. (From ref. 43)

only dispersed liquid droplets. The continuous phase travels up the channel core and leaves an annulus of superheated liquid adjacent to the walls. The fourth type shown in Fig. 6.17 is called fog, dispersed, or homogeneous flow. This is the opposite of the first type, bubble flow, in that in the latter case the vapor fills the entire channel and the liquid is dispersed throughout the vapor in the form of individual droplets.

In the horizontal channel, bubble flow consists in bubbles of gas moving along the upper part of the pipe at approximately the same velocity as the liquid. Plug flow occurs when alternate plugs of liquid and gas move along the upper part of the pipe. In stratified flow the liquid flows along the bottom of the pipe while the gas flows above over a smooth liquid-gas interface. Wavy flow is similar to stratified flow except that the gas moves at a higher velocity and the interface is disturbed by waves traveling in the direction of flow. In slug flow a wave is picked up periodically by the more rapidly moving gas to form a frothy slug that passes through the pipe at a much greater velocity than the average liquid velocity. In the annular flow, the liquid flows in a film around the inside wall of the pipe, and the gas flows at a high velocity as a central core. Most or nearly all the liquid is entrained as spray by the gas in the spray flow.

In the vertical boiling channel, air bubbles of all sizes exist in bubbly flow, with the interstices filled with water. The distribution of the two phases appears fairly uniform across the channel. The transitional flow is a mixture of bubbly and annular flow. Annular flow consists essentially of a core of air surrounded by bubbly layers on the walls. The bubbly layers form surface waves, some of which develop into crests and appear to be torn off to form droplets in the gas core. The dropwise flow in a vertical boiling channel is thought to be a flow pattern in which the water in the stream is in the form of drops swirling around at extreme turbulence. The streaky flow is similar to dropwise flow except that it is further obscured by shear stresses acting on the liquid layer.

Little is now known about the exact type of two-phase flow that takes place in high-pressure reactor systems. It is conceivable, however, that it is determined by the void fraction (volumetric ratio of vapor to vapor and liquid). It is also believed that the type of flow is a function of the Froude number (a measure of the ratio of inertia to gravity forces). Research on flow phenomena is being conducted at the University of Minnesota and at Hanford, as discussed in Chapter 12.

6.4.2.1 Quality and Void Fractions in a Nonslip Flow System

The quality x of a vapor-liquid mixture in a nonslip flow system, such as a homogeneous-model flow system, where no gross relative motion between the vapor and liquid phases exists, is defined as

$$x = \frac{\text{Mass of vapor in mixture}}{\text{Total mass of mixture}} . \qquad (6.41)$$

The void fraction α is defined as

$$\alpha = \frac{\text{Volume of vapor in mixture}}{\text{Total volume of vapor-liquid mixture}} . \qquad (6.42)$$

The relation between x and α in this system can be obtained by assuming a certain volume containing 1 lb of mixture in thermal equilibrium (Fig. 6.19). That volume will be equal to $(v_f + xv_{fg})$ ft^3, where v is the specific volume (lb/ft^3). In the notation used in this chapter, the subscripts f, g, and fg refer to saturated liquid, saturated vapor, and the difference between the two, respectively, which is the usual notation of steam practice.

In an equilibrium mixture the two phases are saturated liquid and saturated vapor, and the volume of vapor present is equal to its mass (lb) times its specific volume v_g. Thus α is given by

$$\alpha = \frac{xv_g}{v_f + xv_{fg}} . \tag{6.43}$$

This equation can also be written in the form

$$\alpha = \frac{1}{1 + \frac{1 - x}{x} \frac{v_f}{v_g}} , \tag{6.44}$$

where the specific volumes are all taken at the system pressure from appropriate tables of thermodynamic properties, such as the Keenan and Keyes steam tables.[41] Since the ratios of v_f/v_g are larger at low pressures, Eq. (6.44) serves to show the large values of α associated with low pressures for small values of x. Thus a small steam fraction by mass corresponds to a very large fraction by volume. The difference decreases at high pressure, however. Figure 6.20 shows calculated values for α versus x for light water at various pressures. Examination of the curves reveals the following:

1. For constant x, α decreases with pressure. As the pressure approaches the critical pressure (3206 psia for light water; 3212 psia for heavy water), α rapidly approaches x. At the critical pressure the two phases are indistinguishable and $\alpha = x$.
2. For any one pressure, $d\alpha/dx$ decreases with x.
3. At low values of x (such as those used in boiling-type reactors), $d\alpha/dx$ increases as the pressure decreases and becomes severely large at low pressure.

6.4.2.2 Slip Flow System

In the above calculations it was assumed that no relative motion existed between the two phases, that is, between vapor bubbles and the liquid. However, if a two-phase mixture is moving (e.g., in a vertical direction, as between fuel elements), the vapor, because of its buoyancy, has a tendency to slip past the liquid, that is, to move at a higher velocity than that of the liquid. A slip ratio S, usually greater than 1.0, is defined as the ratio of the velocity of the vapor V_g to that of the

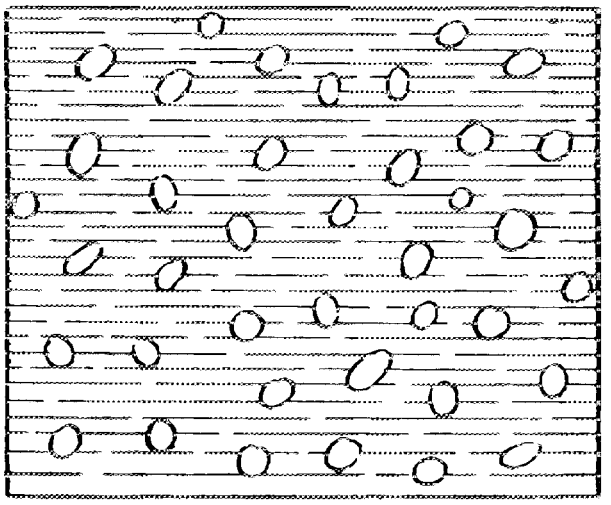

Fig. 6.19. Mixture of Liquid and Vapor in a Homogeneous Model Two-Phase Flow System. Mass mixture, 1 lb; composed of x lb of saturated vapor plus (1 − x) lb of saturated liquid; volume of mixture, $v_f + xv_{fg}$.

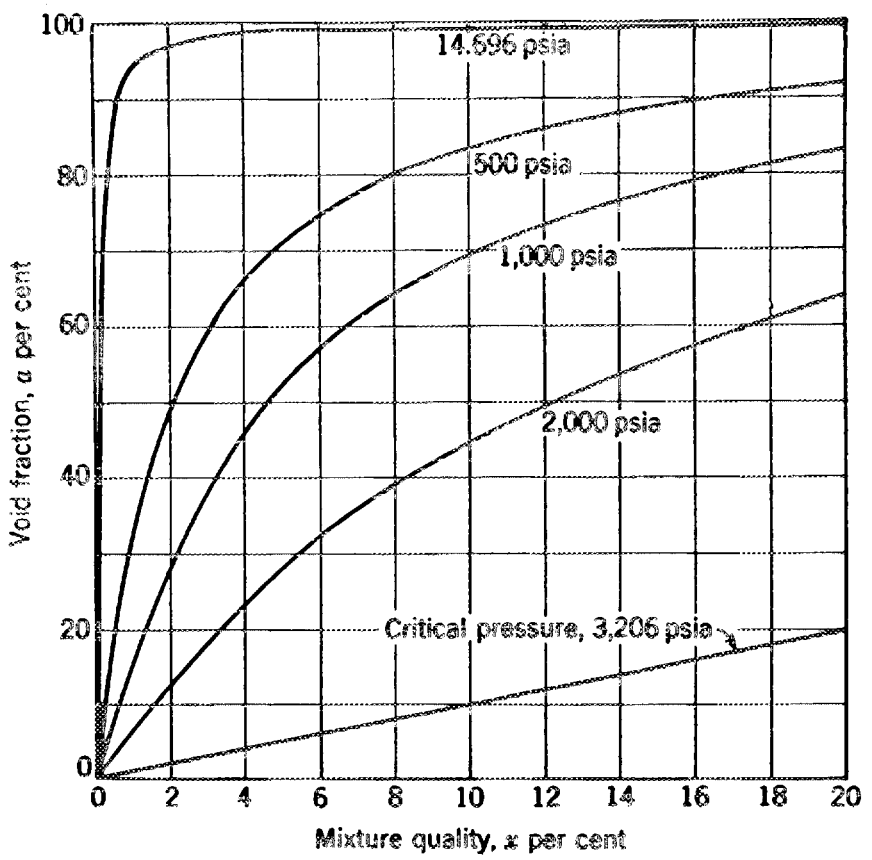

Fig. 6.20. α Versus x for a Nonflowing Water System. (From ref. 42) Used by permission of McGraw-Hill Book Company.

liquid V_f. Thus

$$S = \frac{V_g}{V_f} . \tag{6.45}$$

The ratio S modifies the relation between void fraction and quality developed in the previous section. This will now be shown with the help of Fig. 6.21, which illustrates, in (a), a two-phase mixture flowing upward in a channel. A certain section, between the dotted lines, small enough that x and α remain unchanged, is considered.

In this type of flow system the quality at any one cross section is defined by

$$x = \frac{\text{Mass flow rate of vapor}}{\text{Mass flow rate of mixture}} . \tag{6.46}$$

Thus, if the total mass flow of the mixture is $\dot{m}_{tot}$ (lb/hr), the vapor flow rate is $x\dot{m}_{tot}$ and the liquid flow rate is $(1 - x)\dot{m}_{tot}$, where x is the quality at the particular section in question. When the continuity equation is applied, the velocities of vapor and liquid are given by

$$V_g = \frac{v_g \dot{m}_{tot}}{A_g} x$$

and

$$V_f = \frac{v_f(1 - x)}{A_f} \dot{m}_{tot} ,$$

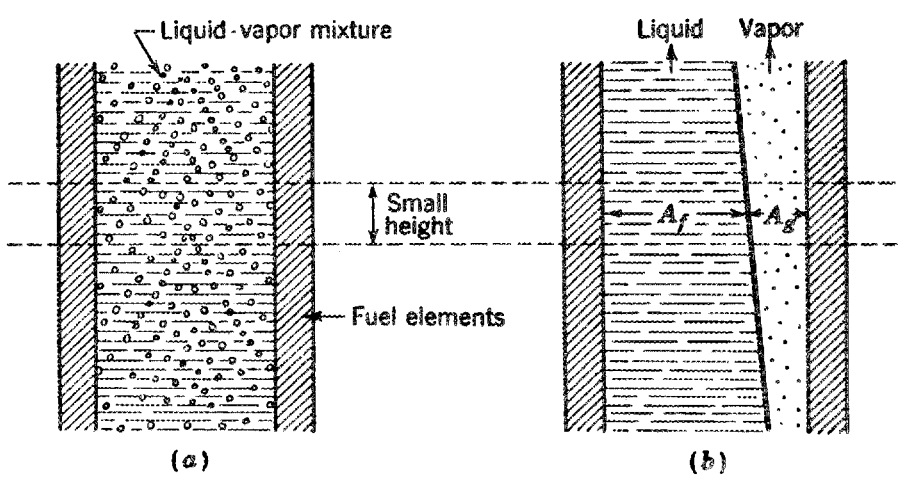

Fig. 6.21. Two-Phase Flow in a Heated Channel. (From ref. 42) Used by permission of McGraw-Hill Book Company.

where A_g and A_f are the cross-sectional areas of the two phases, perpendicular to flow direction, if the two phases are imagined to be completely separated from each other as in Fig. 6.21(a). Combining the above equations gives

$$S = \frac{V_g}{V_f} = \frac{x}{1 - x} \frac{A_f}{A_g} \frac{v_g}{v_f} . \tag{6.47}$$

The void fraction in the section considered is the ratio of the vapor-phase volume to the total volume within the section. In the small section of channel considered, this is the same as the ratio of cross-sectional area of vapor A_g to the total cross-sectional area of the channel. Thus

$$\alpha = \frac{A_g}{A_g + A_f}$$

or

$$\frac{A_f}{A_g} = \frac{1 - \alpha}{\alpha} .$$

Equation (6.47) then becomes

$$S = \frac{x}{1 - x} \frac{1 - \alpha}{\alpha} \frac{v_g}{v_f} . \tag{6.48}$$

This equation can be rearranged to give a relation between α and x, including the effect of slip, as

$$\alpha = \frac{1}{1 + \frac{1 - x}{x} \frac{v_f}{v_g} S} = \frac{1}{1 + \frac{1 - x}{x} \Psi} , \tag{6.49}$$

$$x = \frac{1}{1 + \frac{1 - \alpha}{\alpha} \frac{1}{\Psi}} , \tag{6.50}$$

where

$$\Psi = \frac{v_f}{v_g} S .$$

It is to be noted that the relation between α and x for no slip (S = 1) given by Eq. (6.43) is a special case of the general relation given by Eqs. (6.49) and (6.50).

The effect of slip is to decrease the value of α corresponding to a certain value of x below that which exists for no slip. This can be seen if Eqs. (6.49) and (6.50) are examined. At constant pressure and quality, the factor $(1 - \alpha)/\alpha$ is directly proportional to S. Thus, α decreases as S increases for a fixed x. A high S is thus an advantage from both the heat-transfer and moderation-effect standpoints. Figure 6.22 shows α versus x for light water at 1000 psia and several slip ratios.

The value of S has been experimentally found to decrease with both the system pressure and the volumetric flow rate and to increase with power density. It has also been found to increase with the quality at high pressures but to decrease with it at very low pressures.[45] Figures 6.23 to 6.25 show some of these effects. Figure 6.26 gives α versus $x\rho_f/\rho_g$ for various values of V_i^2/D, where V_i is the inlet velocity, at a pressure of 32 atm (ref. 46) from which S may be computed. As a function of the channel length, S has been found to increase rapidly at the beginning and then more slowly as the channel exit is approached. At the exit itself, turbulence seems to cause a sudden jump in the value of S.

Von Glahn[47] proposed the following empirical relation between x and α, which is based on much of the experimental data available at the time for water and which covers a wide range of operating conditions and channel geometries:

$$\frac{1}{x} = 1 - \left(\frac{v_g}{v_f}\right)^{0.67} \left[1 - \left(\frac{1}{\alpha}\right)^{(v_g/v_f)^{0.1}}\right] . \qquad (6.51)$$

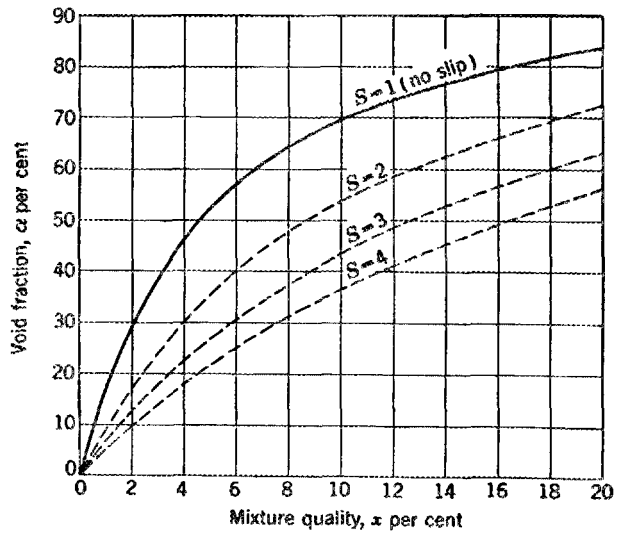

Fig. 6.22. α Versus x for Water at 1000 psia and Various Slip Ratios in a Flow System. (From ref. 42) Used by permission of McGraw-Hill Book Company.

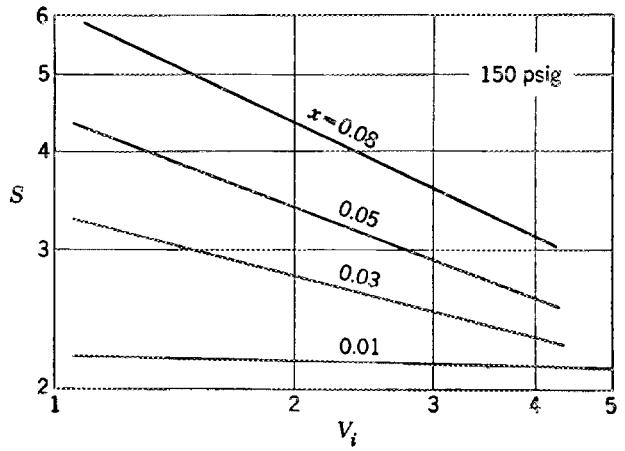

Fig. 6.23. Working Curves for Predicting Slip Ratios at 150 psig. (From ref. 42)

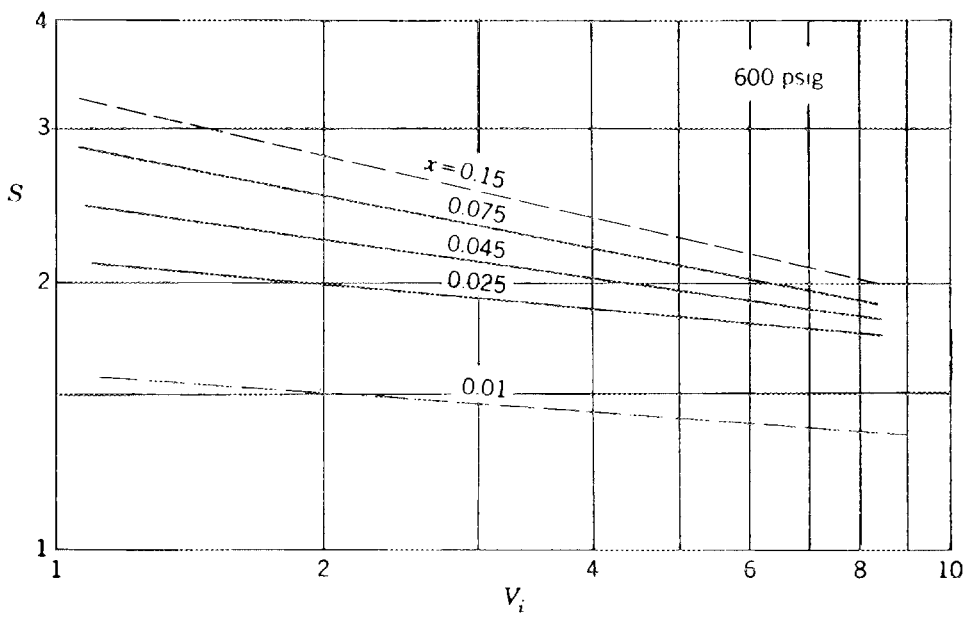

Fig. 6.24. Working Curves for Predicting Slip Ratios at 600 psig. (From ref. 42)

Experimental data or theoretical correlations for S covering all possible operating and design variables do not now exist. In containment studies, values for S may be estimated from data that closely approach those of interest. In this a certain amount of individual judgment is necessary. Otherwise, experimental values of S must be obtained under similar conditions. This procedure is usually expensive and time-consuming but may be necessary in some cases. In design work the usual procedure is to assume a constant value of S along the length of the channel.

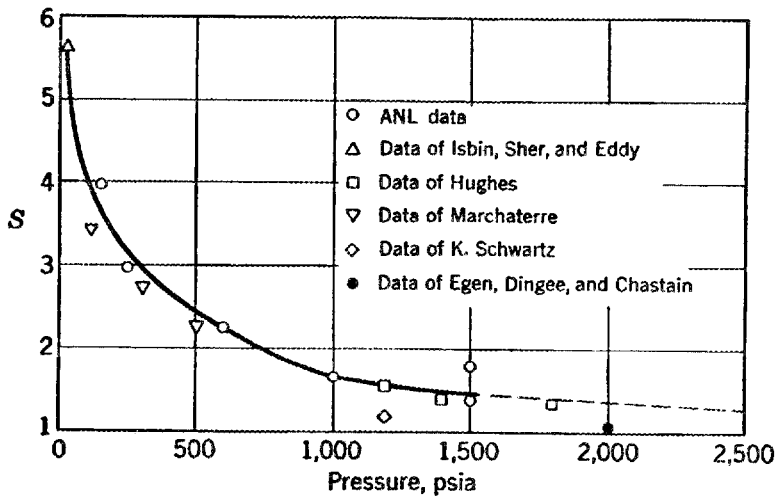

Fig. 6.25. Slip Ratio as a Function of Pressure for $V_i \approx 2$ ft/sec and $x \approx 0.05$. (From ref. 42)

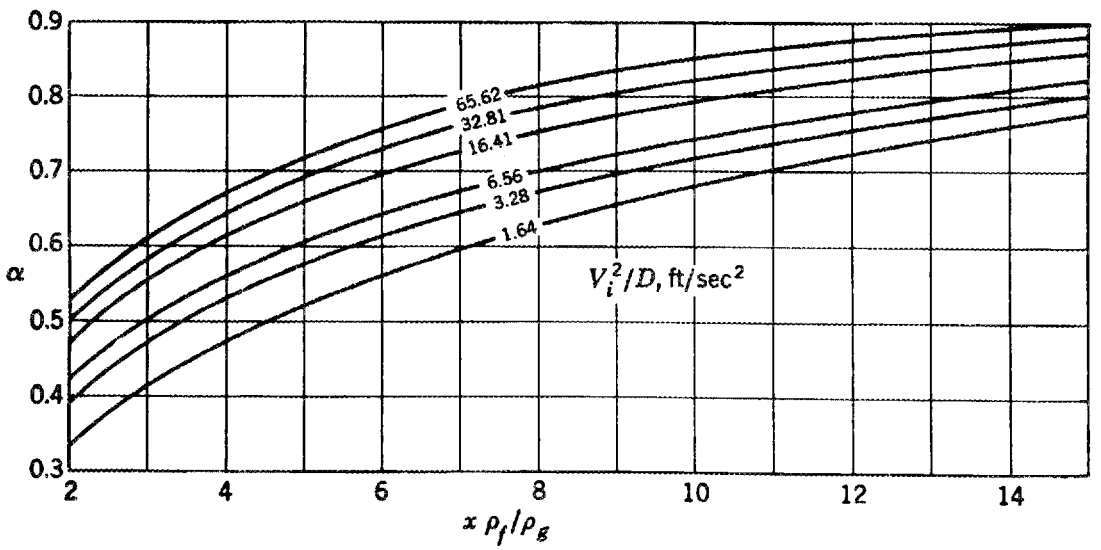

Fig. 6.26. Void Fraction as a Function of V_i^2/D and $x\rho_f/\rho_g$ for Vertical Tubes (p = 32 atm). (From ref. 42)

6.4.2.3 Friction Drop in a Boiling Channel

The pressure drop in a channel is the sum of the pressure drop in the nonboiling section Z_o and the pressure drop in the boiling section Z_b. In the nonboiling section, friction is due to single-phase flow and may be evaluated by standard methods used in such cases (e.g., the Darcy Formula). Thus the pressure drop due to friction in the nonboiling section may be given by

$$\Delta p_{sp} = f \frac{Z_o}{D_e} \frac{\rho V^2}{2g_c} , \qquad (6.52)$$

where

Δp_{sp} = single-phase pressure drop, lb/ft^2,
f = friction factor, dependent on Reynolds number and channel roughness, dimensionless,
D_e = equivalent diameter of channel, ft,
ρ = average density in nonboiling section, lb/ft^3,
V = average velocity in nonboiling section, ft/hr,
g_c = conversion factor, 32.174 lb_m-ft/lb_f-sec^2 or 4.17×10^8 lb_m-ft/lb_f-hr^2.

In the boiling height, however, the pressure drop due to friction is greater than that due to single-phase liquid flow of the same mass-flow rate. This higher pressure drop appears to be a function of the type of flow and results partly from the increased flow speeds. It can be experimentally determined by measuring the total pressure drops in two-phase flow and by subtracting the calculated pressure losses in the system, which include inlet, exit, contraction, acceleration, and friction losses due to the liquid phase only in the nonboiling section of the channel, if any.

Several attempts at finding a suitable correlation for two-phase friction pressure drop were made, with various degrees of success. Usually the two-phase friction drop was compared with a calculated friction drop, assuming that only saturated liquid existed in the channel. A friction multiplier, $\overline{R}$, greater than 1.0, was then used that was correlated with operating parameters. It is defined by

$$\overline{R} = \frac{\Delta p_{tp}}{\Delta p_{sp}} , \qquad (6.53)$$

where

$\overline{R}$ = two-phase friction multiplier,
Δp_{tp} = two-phase pressure drop in boiling height only.

The most widely accepted correlation for $\overline{R}$ is that of Martinelli and Nelson.[48] The correlation is based on previous correlations of two-phase turbulent flow by Martinelli and represents an extrapolation of pressure-drop data obtained for isothermal flow of air and various other liquids at low temperatures and pressures. The Martinelli-Nelson correlation is presented in the form of curves (Fig. 6.27) as a function of pressure and quality at the exit of the flow channel.

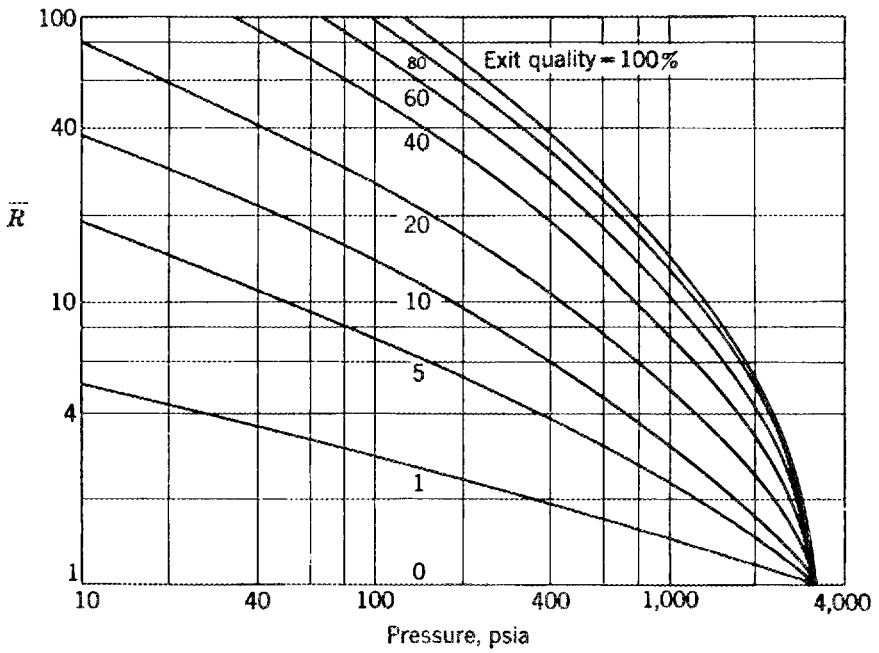

Fig. 6.27. Martinelli-Nelson Friction-Multiplier Correlation. (From ref. 42)

6.4.2.4 Acceleration Pressure Drop

Because the fluid undergoes an increase in volume as it vaporizes, it has to accelerate as it travels through the channel. If the pressure drop is small compared with the absolute pressure, the flow is effectively incompressible. In other words, although the specific volume of the mixture changes over wide limits, the specific volume of each phase is substantially constant along the tube.

Two extreme cases can exist. The actual conditions probably lie between these extremes: (1) liquid and vapor completely mixed (fog) and (2) liquid and vapor completely separated.

The acceleration pressure drop in the first case can be expressed as

$$\Delta p_a = \frac{G^2}{g_c}\left[(1 - x_c) + x_c\left(\frac{v_g}{v_f}\right) - 1\right] v_f = r_1 \frac{G^2}{g_c} . \qquad (6.54)$$

The second case, which is probably closer to actual conditions, may be evaluated by

$$\Delta p_a = \frac{G^2}{g_c}\left[\frac{(1 - x_c)^2}{1 - \alpha_c} + \frac{x_c^2}{\alpha}\left(\frac{v_g}{v_f}\right) - 1\right] v_f = r_2 \frac{G^2}{g_c} . \qquad (6.55)$$

The value of r_2 increases rapidly with x and only very slightly with the slip ratio S.

6.4.2.5 Expansion and Contraction Losses in Two-Phase Flow

Two-phase mixtures commonly encounter sudden area changes. As with friction, expansion and contraction pressure changes in two-phase flow are larger than those in single-phase flow because of the increased speed of the liquid caused by the presence of voids. It also follows that the higher the void fraction of a two-phase mixture, the higher the pressure change. Hanford analyses of the blowdown phenomenon are discussed in Chapter 12.

To aid in the analysis, the following relations are derived from the continuity equation and by reference to Fig. 6.21(b):

$$\dot{m}_g = x\dot{m}_{tot} = \rho_g A\alpha V_g$$

and

$$\dot{m}_f = (1 - x)\dot{m}_{tot} = \rho_f A(1 - \alpha)V_f ,$$

so

$$V_{f_1} = \frac{1 - x}{1 - \alpha_1}\frac{\dot{m}_{tot}}{\rho_f A_1} , \qquad V_{f_2} = \frac{1 - x}{1 - \alpha_2}\frac{\dot{m}_{tot}}{\rho_f A_2} , \tag{6.56}$$

$$V_{g_1} = \frac{x}{\alpha_1}\frac{\dot{m}_{tot}}{\rho_g A_1} , \qquad V_{g_2} = \frac{x}{\alpha_2}\frac{\dot{m}_{tot}}{\rho_g A_2} , \tag{6.57}$$

where the subscripts 1 and 2 refer to before and after the area changes, respectively, and the symbols have the same meaning as in the previous sections. The above relations assume that expansions or contractions are adiabatic so that $x_1 = x_2 = x$ and, since the pressure changes are small, the densities of the saturated liquid and vapor do not change.

1. Expansion. In the case of area expansion (Fig. 6.28), several methods have been suggested for calculation of the losses. Lottes[49] compared four of these and recommended one by Romie as the best available. This method is outlined below.

A force balance across the expansion region is written, as in single-phase flow, in which the upstream pressure p_1 is assumed to still act on the expanded area A_2 immediately after the expansion:

$$p_1A_2 + \frac{\dot{m}_{f_1}V_{f_1}}{g_c} + \frac{\dot{m}_{g_1}V_{g_1}}{g_c} = p_2A_2 + \frac{\dot{m}_{f_2}V_{f_2}}{g_c} + \frac{\dot{m}_{g_2}V_{g_2}}{g_c} . \tag{6.58}$$

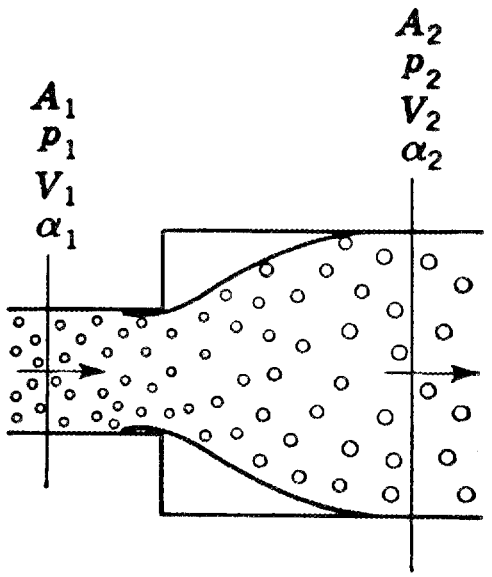

Fig. 6.28. Two-Phase Flow in Sudden Expansion. (From ref. 42) Used by permission of McGraw-Hill Book Company.

Using the relations of Eq. (6.56) and Eq. (6.57) and rearranging gives

$$p_2 - p_1 = \frac{\dot{m}_{tot}^2}{g_c}\left\{\frac{(1-x)^2}{\rho_f}\left[\frac{1}{(1-\alpha_1)A_1A_2} - \frac{1}{(1-\alpha_2)A_2^2}\right] + \frac{x^2}{\rho_g}\left(\frac{1}{\alpha_1A_1A_2} - \frac{1}{\alpha_2A_2^2}\right)\right\}. \qquad (6.59)$$

Based upon experiments by Petrick with air and water in vertical columns near atmospheric pressure, the following relation between α_1 and α_2 has been suggested:

$$\alpha_2 = \frac{1}{\frac{p_2}{p_1}\frac{1-\alpha}{\alpha_1}\left(\frac{A_2}{A_1}\right)^{0.2} + 1}. \qquad (6.60)$$

In reactor work the pressure changes are small compared with the operating pressures, so $p_2/p_1 \cong 1.0$. Equation (6.60) shows that at high pressures the void fraction decreases somewhat across an area expansion. Table 6.11 gives values of α_2 versus α_1 computed from Eq. (6.60) for two area ratios at high pressures. It can be seen that the decrease in void fraction is not large for area ratios of 0.5 or larger and is relatively greater the lower the initial void fraction. Where this change may be

Table 6.11. Effect of Area Expansion on Void Fraction in Vertical Air-Water Mixtures[a]

A_1/A_2	α_1 (%)	α_2 (%)	Change (%)
0.2	10	7.4	-26
	20	15.3	-23.5
	40	32.0	-20
	60	52.0	-13.3
0.5	10	9.0	-10
	20	18.0	-10
	40	36.6	-8.5
	60	57.0	-5

[a]From ref. 49.

ignored, that is, when $\alpha_1 = \alpha_2 = \alpha$, Eq. (6.59) reduces to

$$p_2 - p_1 = \frac{1}{g_c}\left(\frac{1}{A_1A_2} - \frac{1}{A_2^2}\right)\dot{m}_{tot}^2 \left[\frac{(1-x)^2}{\rho_f(1-\alpha)} + \frac{x^2}{\rho_g\alpha}\right] . \qquad (6.61)$$

The case of single-phase liquid flow may be obtained by putting $x = 0$ and $\alpha = 0$ in Eq. (6.61) and getting

$$p_2 - p_1 = \frac{1}{g_c}\left(\frac{1}{A_1A_2} - \frac{1}{A_2^2}\right)\frac{\dot{m}_{tot}^2}{\rho_f} . \qquad (6.62)$$

Since A_1 is less than A_2, the right-hand sides of Eqs. (6.61) and (6.62) are positive, indicating (in all cases) a pressure increase due to area expansions. It can also be seen that for the same total mass-flow rate and areas of flow, and since x is smaller than α, the pressure increases are larger in two-phase than in single-phase flow and are larger the larger the void fraction.

2. Contraction. As in single-phase flow, area contraction results in a vena contracta of area A_o following the contraction (Fig. 6.29). The fluid then expands to the reduced area A_2. As in single-phase flow the losses from the contraction to the vena contracta are negligibly small, and the contraction loss is assumed to be totally due to the expansion of the fluid from the vena contracta to the point where the fluid fills area A_2. In two-phase flow the vapor is able to accelerate more readily than the liquid, resulting in a considerable decrease in magnitude of the void fraction at the vena contracta. Beyond the vena contracta, however, shear

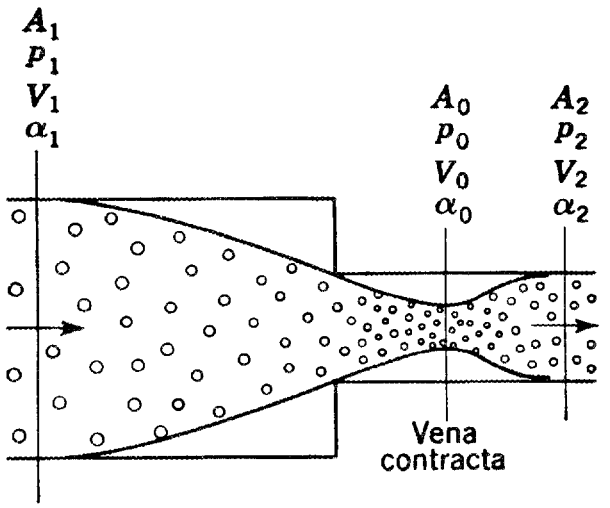

Fig. 6.29. Two-Phase Flow in Sudden Contraction. (From ref. 42) Used by permission of McGraw-Hill Book Company.

forces between liquid and wall and between liquid and vapor steady the flow and cause the void fraction at plane 2 to assume substantially the same value it had at plane 1.

If the pressure losses are attributed to the expansion length from plane 0 to plane 2, the contraction pressure change in single-phase flow can be shown[49] to be given by

$$p_2 - p_1 = \frac{\rho_f V_{f_1}^2}{2g_c} \left[1 - \left(\frac{A_1}{A_2}\right)^2 (k + 1)\right] , \tag{6.63}$$

where k is a dimensionless loss coefficient that is a function of A_2 and the area of the vena contracta A_o and is given by

$$k = \left(\frac{A_2}{A_o} - 1\right)^2 . \tag{6.64}$$

Since A_o is not known with certainty, k is usually given by

$$k = a \left[1 - \left(\frac{A_2}{A_1}\right)^2\right] , \tag{6.65}$$

where a is a dimensionless number less than unity. For single-phase flow, a has been reported to be between 0.4 to 0.5. Using the value 0.4 and combining Eqs. (6.63) and (6.65) gives, for single-phase flow,

$$p_2 - p_1 = 1.4 \frac{\rho_f V_{f_1}^2}{2g_c} \left[1 - \left(\frac{A_1}{A_2}\right)^2\right] . \tag{6.66}$$

Using $\dot{m}_{tot} = \rho_f A_1 V_{f_1}$, the above equation may be written in the form

$$p_2 - p_1 = \frac{1.4}{2g_c} \left(\frac{1}{A_1^2} - \frac{1}{A_2^2}\right) \frac{\dot{m}_{tot}}{\rho_f} . \tag{6.67}$$

In two-phase flow, it has been found[49] that the value of a is 0.2. If ρ_f is replaced by the density of the two-phase mixture, which is given by

$$\rho = (1 - \alpha)\rho_f + \alpha\rho_g , \tag{6.68}$$

and the product $\alpha\rho_g$ is ignored (being small at pressures far removed from critical), and if the pressure losses are attributed to the liquid alone, the pressure change in two-phase flow is given by

$$p_2 - p_1 = 1.2 \frac{\rho_f V_{f_1}^2}{2g_c} (1 - \alpha) \left[1 - \left(\frac{A_1}{A_2}\right)^2\right] , \tag{6.69}$$

where $\alpha = \alpha_1 = \alpha_2$, as indicated previously. The above equation may be modified, with the help of Eq. (6.57), to the form

$$p_2 - p_1 = \frac{1.2}{2g_c} \left(\frac{1}{A_1^2} - \frac{1}{A_2^2}\right) \dot{m}_{tot}^2 \frac{(1 - x)^2}{\rho_f(1 - \alpha)} . \tag{6.70}$$

Equations (6.68) and (6.69) show that since A_2 is less than A_1, contraction pressure changes in either single- or two-phase flow are negative, indicating a loss in pressure. A comparison of the two equations shows that, for the same total mass-flow rate and areas and for most values of α and x encountered in reactor work, the two-phase contraction pressure losses are larger than those in single phase and are larger the larger the void fraction.

6.4.2.6 Critical Flow

The design of efficient and economic reactor containment systems is in many instances dependent on predictions of critical-flow behavior for a reactor coolant. Typically, the primary coolant contains considerable energy and contamination in a water-cooled reactor. Upon a rupture of

some part of the primary coolant system, the escaping coolant must be contained in order to prevent the release of radioactive materials to the environs. Since the critical-flow phenomenon plays an important role in the rate of loss of the primary coolant, exact technical knowledge of its mechanism is needed for the design of efficient and economic containment and pressure-suppression systems. To date, however, no single design method has been proposed that will prove satisfactory over a wide range of two-phase flow conditions.

The available information on critical flow in tubes may be divided into three categories, classified according to a modified cavitation number, Ca′, as proposed by Fauske and Min.[50,51] This number is defined by

$$Ca' = \frac{2g_c \, \Delta p}{\rho_i V^2} \frac{L}{D}, \tag{6.71}$$

where

Δp = pressure difference between initial and exit pressure, lb/ft^2,
ρ_i = initial density of the saturated or subcooled fluid, lb/ft^3,
V = average velocity of the fluid, ft/sec,
L = length of tube, ft,
D = diameter or equivalent diameter, ft.

As indicated in Fig. 6.30, for a modified cavitation number less than 9,

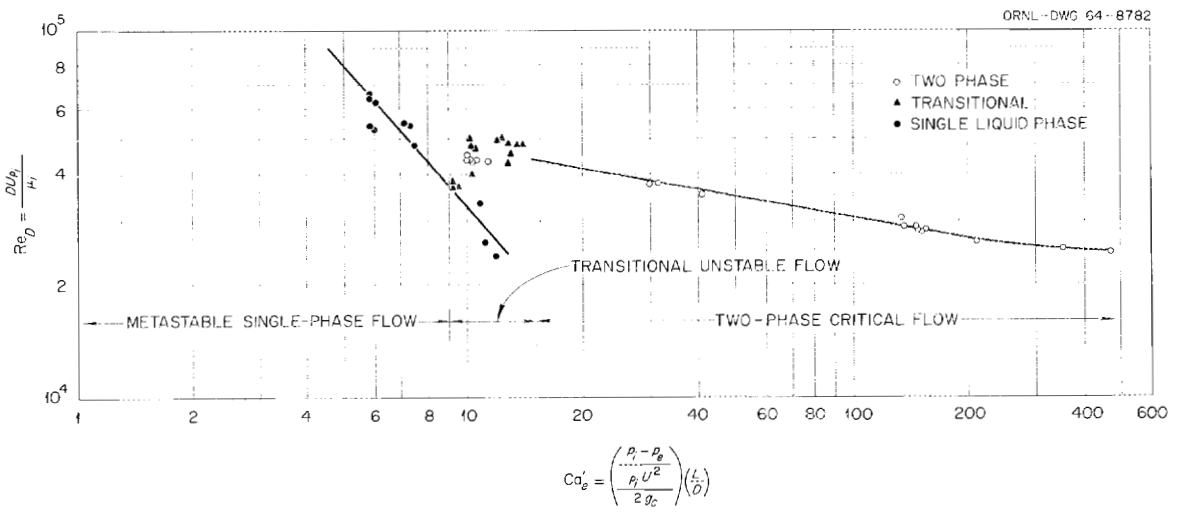

Fig. 6.30. Dimensionless Correlation Determining the Occurrence of Single-Phase and Two-Phase Flow Regimes and the Critical Discharge Flow Rates Through Short Tubes. (From ref. 51)

the fluid exhibits completely metastable single-phase flow.[51] When the modified cavitation number exceeds 15, two-phase flow exists. In the range of Ca′ between 9 and 15, unstable transitional flow occurs. There are, however, inconsistencies in these classifications. Isbin[52] recently performed tests on circular orifices (Ca′ = 0) in which a departure from metastable flow was found to exist. The mass-flow rate was less than that predicted for metastable flow. The assumption of metastable flow will yield high flow rates, giving conservative results for most cases of interest in containment studies.

6.4.2.7 Equilibrium Two-Phase Annular Critical Flow

Because of the recent work by Fauske,[53] critical-flow rates of the equilibrium critical flow in long tubes can be calculated with a large degree of confidence. Fauske developed a theoretical treatment based on the following assumptions: (1) annular flow (slip occurs), (2) thermodynamic equilibrium, and (3) isenthalpic expansion. He also postulated (1) that the specific volume v of the two-phase flow mixture was given by

$$v = \frac{x^2 v_g}{\alpha} + \frac{(1 - x)^2}{1 - \alpha} v_f , \tag{6.72}$$

(2) that the flow was critical when the flow rate no longer increased with increasing pressure differences, that is,

$$\frac{dG}{dp} = 0 , \tag{6.73}$$

and (3) that a condition of critical flow existed when the pressure gradient along the pipe proceeding to the exit had an absolute, finite maximum value for a given flow rate and quality. With these assumptions Fauske derived the following expressions for the slip ratio, S, void fraction, α, and mass velocity, G:

$$S_c = \left(\frac{v_g}{v_f}\right)^{1/2} , \tag{6.74}$$

$$\alpha_c = \frac{1 - x}{x} \left(\frac{v_f}{v_g}\right)^{1/2} + 1 , \tag{6.75}$$

$$G_c = \left(-g_c S \Big/ \left\{(1 - x + Sx)x \frac{dv_g}{dp} + \left[v_g(1 + 2Sx - 2x) + v_f(2xS - 2S - 2xS^2 + S^2)\right] \frac{dx}{dp} + S[1 + x(S - 2) - x^2(S - 1)] \frac{dv_f}{dp}\right\}\right)^{1/2} . \quad (6.76)$$

It is interesting to note that Eq. (6.74) sets an upper limit on the magnitude of the slip ratios, and the graph for the Eq. (6.74), as shown in Fig. 6.32, has the same shape as that in Fig. 6.25.

In Eq. (6.76), the derivatives, $dx/dp|_H$, $dv_g/dp|_H$, and $dv_f/dp|_H$ must be evaluated from a table of properties, such as that of Keenan and Keyes[41] for steam. The derivative dx/dp is approximated by $\Delta x/\Delta p$ determined at constant mixture enthalpy. For a given pressure p and quality x,

$$H = H_f + xH_{fg} , \quad (6.77)$$

$$\frac{dx}{dp} = -\frac{1}{H_{fg}}\left(\frac{dH_f}{dp} + x\frac{dH_{fg}}{dp}\right) , \quad (6.78)$$

and an approximate value for dx/dp is then

$$\frac{dx}{dp} \cong \frac{\Delta x}{\Delta p} = -\frac{1}{H_{fg}}\left(\frac{\Delta H_f}{\Delta p} + x\frac{\Delta H_{fg}}{\Delta p}\right) , \quad (6.79)$$

where H_{fg}, ΔH_f, and ΔH_{fg} can be found from a table of properties.[41]

The derivative dv_g/dp can be approximated by $\Delta v_g/\Delta p$ evaluated at constant mixture enthalpy. Actually, v_g is the specific volume of the saturated vapor and is a function of pressure; hence

$$\frac{dv_g}{dp} \cong \frac{\Delta v_g}{\Delta p} . \quad (6.80)$$

The value of dv_f/dp is approximated by $\Delta v_f/\Delta p$ determined at constant mixture enthalpy and is determined in the same fashion as dv_g/dp. Thus, with the aid of Eqs. (6.74) and (6.77) to (6.80), the critical mass velocity may be calculated from Eq. (6.76) and appropriate tables of properties. The results of Eqs. (6.74), (6.75), and (6.76) are plotted for water in Figs. 6.31, 6.32, and 6.33. Figure 6.34 shows a critical-flow envelope developed by means of the Fauske equations.

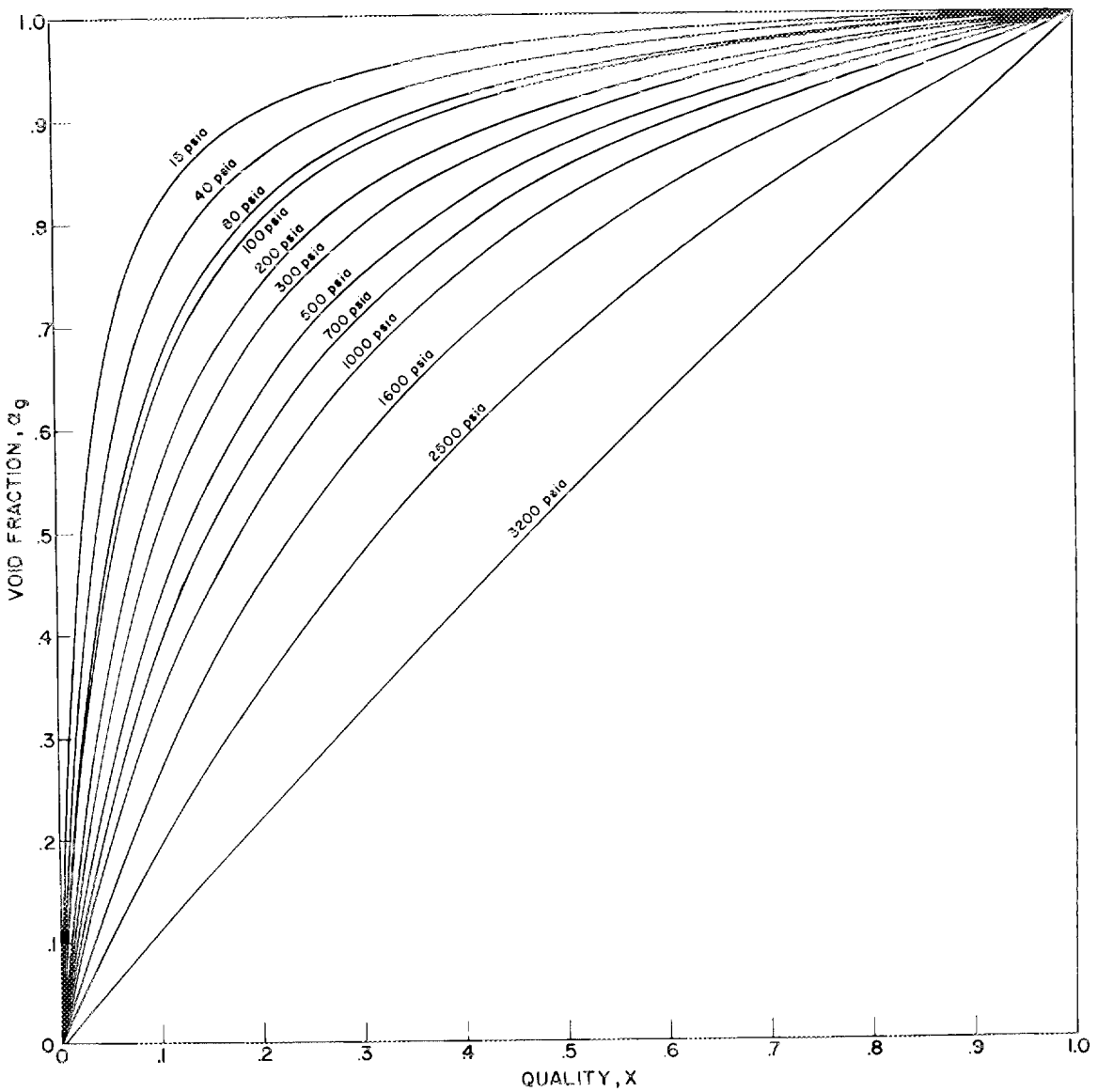

Fig. 6.31. Predictions of Void Fraction α_c at Critical Flow for Steam-Water Mixtures. (From ref. 53)

It should be noted that either Fig. 6.33 or 6.34 may be used to ascertain the critical mass velocity if the critical exit pressure P_e and the critical exit quality x are known. In most practical situations, neither P_e nor x is known; hence, a multiple trial and error procedure is necessary for estimating the critical exit pressure and quality before the critical discharge rate can be determined. The procedure is described in Section 6.4.2.11, Pressure-Flow-Time History.

The critical velocity is also of interest. For a single-phase system, it can be said that the maximum flow and critical pressure are reached when the velocity of the stream is equal to the velocity of sound in the

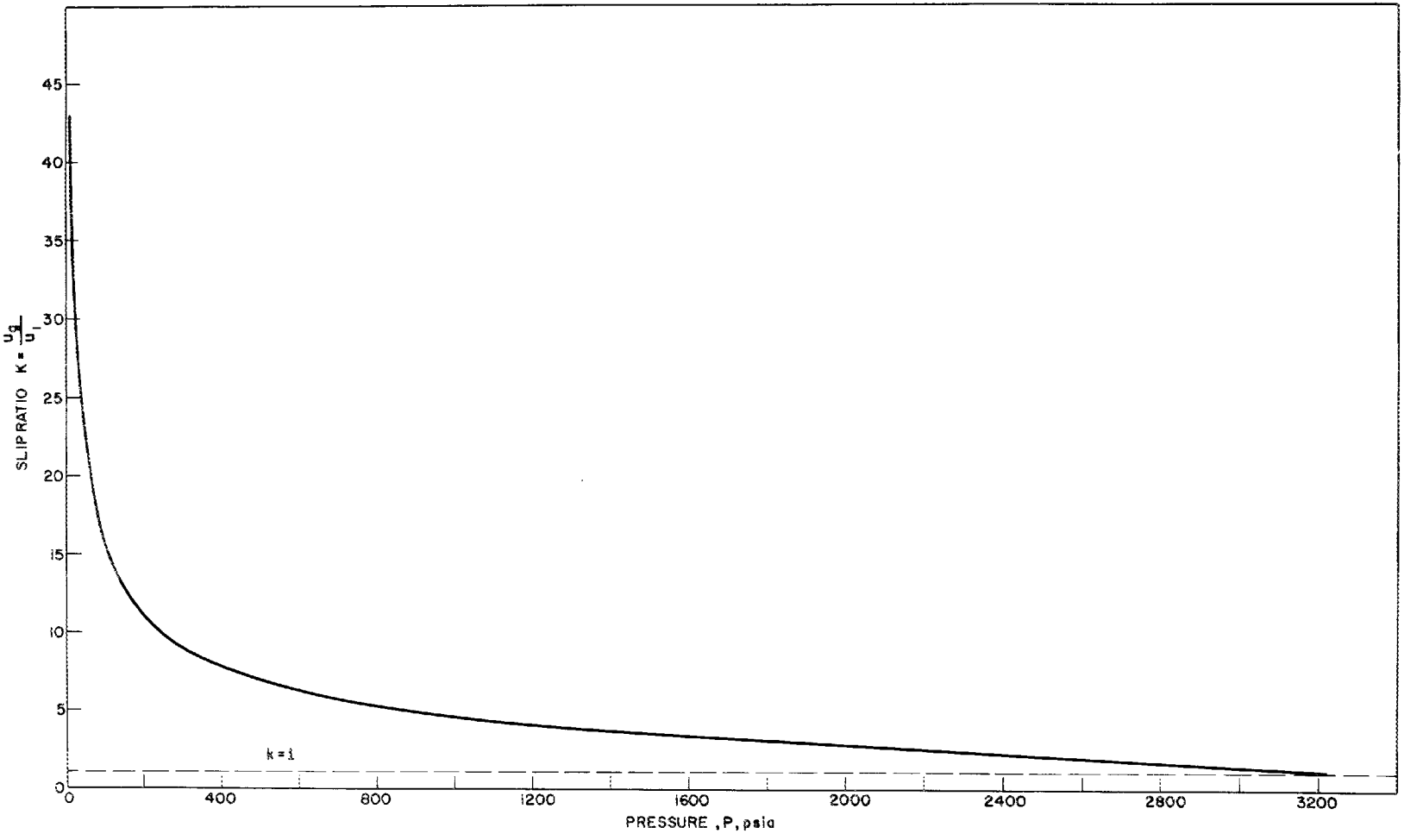

Fig. 6.32. Predictions of Slip Ratio S_c at Critical Flow for Steam-Water Mixtures. (From ref. 53.)

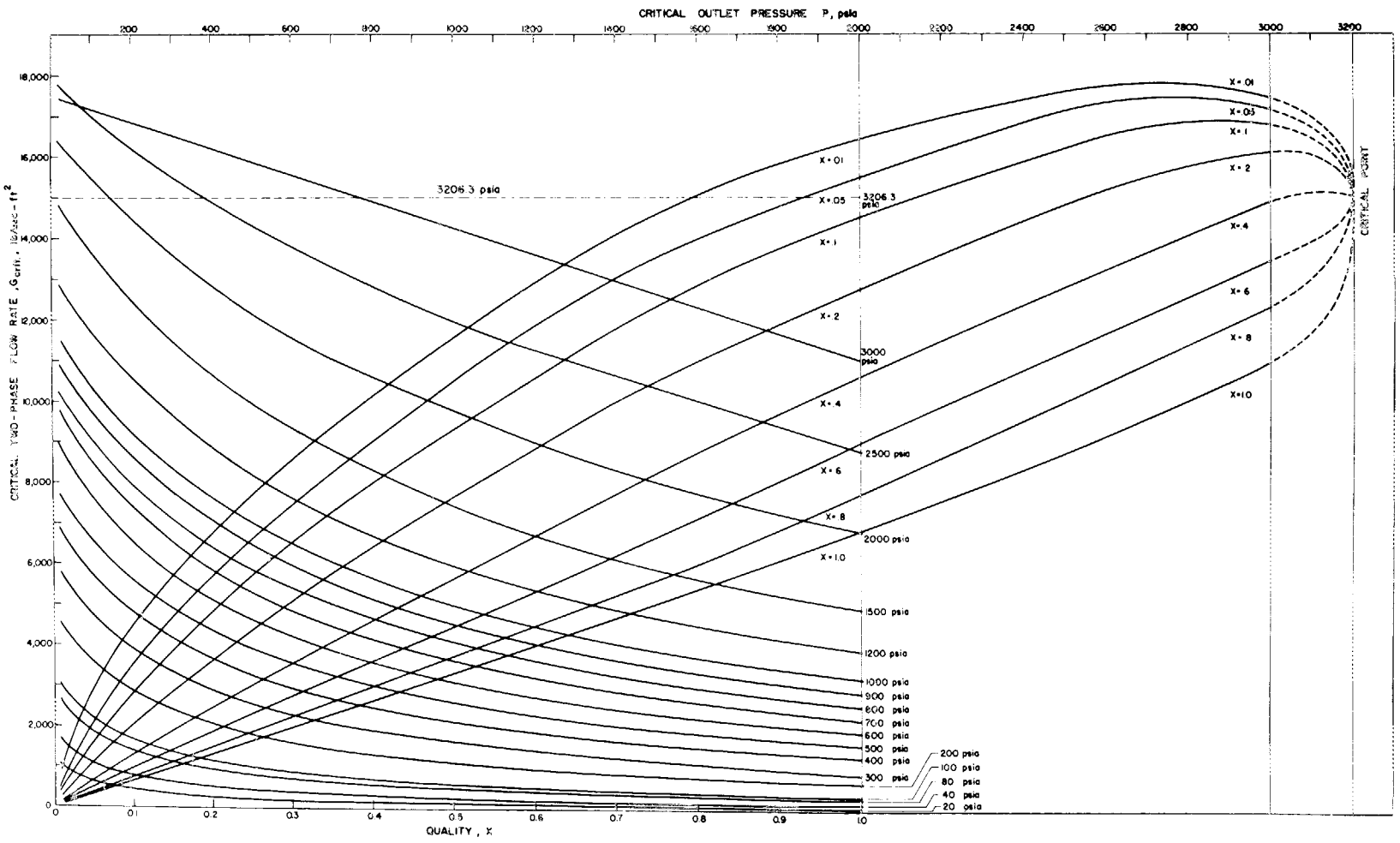

Fig. 6.33. Predictions of Critical Flow Conditions for Steam-Water Mixtures. (From ref. 53)

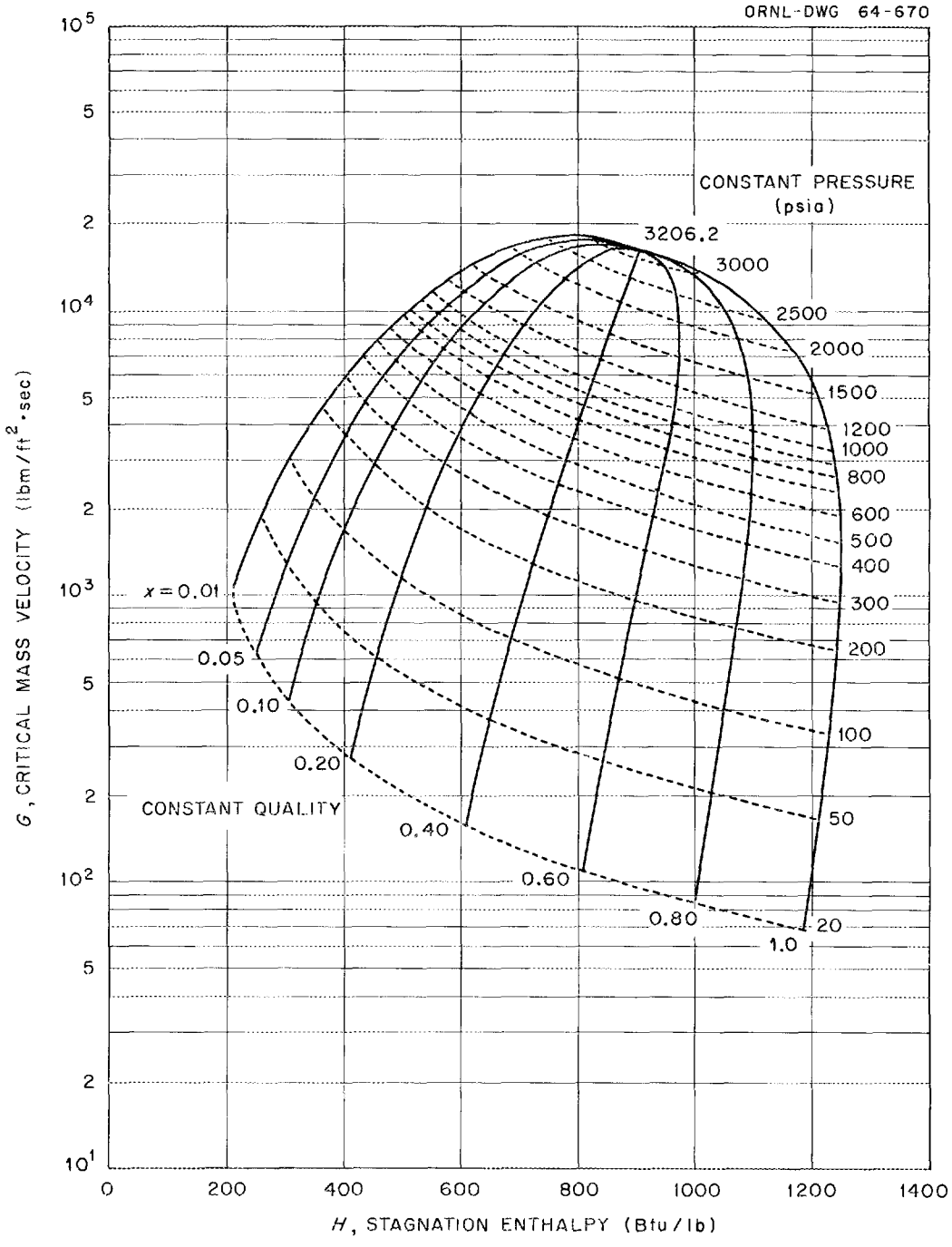

Fig. 6.34. Critical Flow Evelope for Light Water.

same medium. At this time, changes in the downstream pressure can no longer be transmitted up into the pipe. The absolute velocities calculated from the Fauske theory are below sonic velocities, except when the quality approaches 1.0. In Fig. 6.35, the linear vapor velocity is plotted versus quality, with pressure, p, as a parameter. Figure 6.35 shows that no sonic velocities occur for two-phase critical flow of steam-water mixtures. Therefore, the method of sonic velocities cannot be adopted to explain the maximum flows of two-phase mixtures.

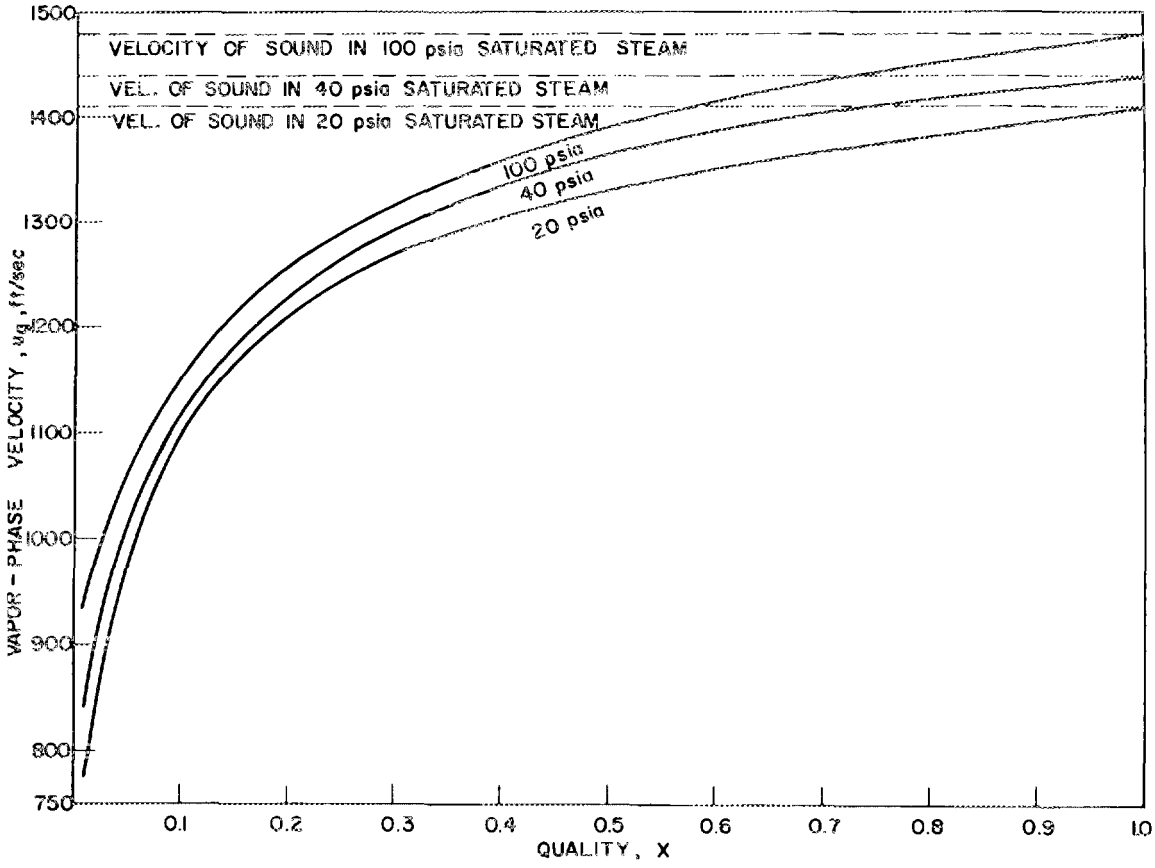

Fig. 6.35. Theoretical Prediction of the Vapor-Phase Velocity Compared with the Velocity of Sound. (From ref. 53)

6.4.2.8 Nonequilibrium or Metastable Two-Phase Critical Flow

The Fauske equilibrium annular model is believed to be achieved when the tube is sufficiently long to ensure that the flow will reach physical equilibrium. Fauske's experiments were run with L/D ratios of 400 or greater and a Ca′ of 3000, and the prediction by the method described in Section 6.4.2.7 checks with his experimental data quite well in that range. However, for short tubes with L/D in the neighborhood of 20 and a Ca′ of 300, the prediction based on Fauske's model is about 15% lower than the

measured rate.[50,51] The deviation between the predictions and the test data[50,51] becomes larger and larger as the L/D ratio decreases below 20 and Ca′ below 300. One contributing factor to this is that the actual quality of the metastable two-phase flow is much smaller than the quality calculated by assuming thermodynamic equilibrium. Since departure from thermodynamic equilibrium is very difficult to include in a mathematical model, Min et al.,[51] suggest the empirical correlations shown in Figs. 6.30 and 6.36. The modified cavitation number, Ca′, in Fig. 6.30 is based on the pressure difference between the initial pressure P_i and the critical exit pressure P_e. In most practical situations neither the critical exit pressure nor the critical velocity is known. For a given initial pressure P_i, back pressure P_b, and L/D ratio of the tube, it is necessary to ascertain the critical exit pressure from Figs. 6.30 and 6.36 by trial and error procedures before the critical discharge flow rate can be determined.

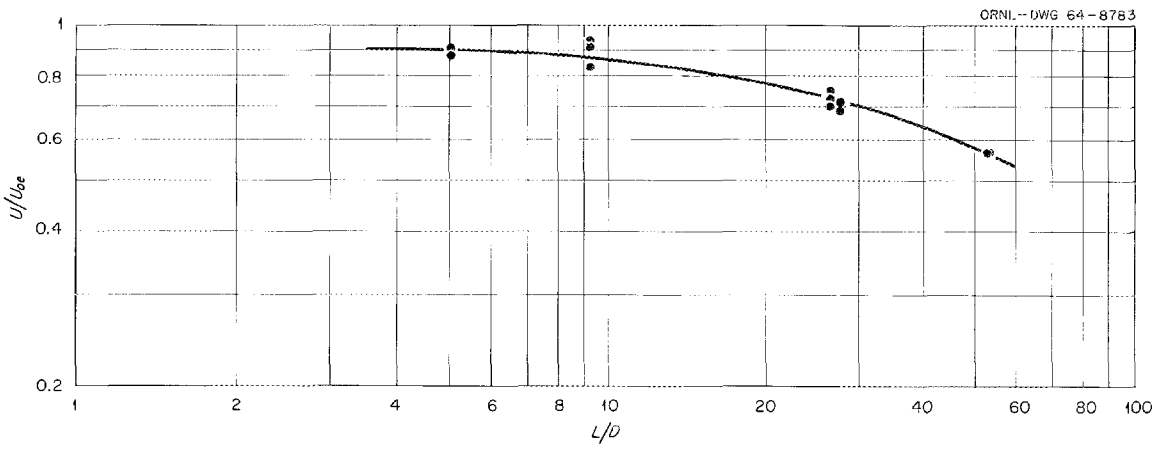

Fig. 6.36. Correlation of Dimensionless Velocity and Length-to-Diameter Ratio of Short Tubes. (From ref. 51)

For a given L/D ratio, Fig. 6.36 gives a value of u/u_o. Since u_o is the average velocity of the fluid flowing out from an orifice of the same size as that of the tube, it can be calculated from the following equation once a critical exit pressure is assumed:

$$u_o = c_d \left[\frac{2g_c}{\rho_i}(P_i - P_e)\right]^{1/2} , \qquad (6.81)$$

where

c_d = discharge coefficient or Euler Number, which can be estimated from ref. 54 or Fig. 6.37,

g_c = conversion factor, 32.2 lb_m-ft/lb_f-sec^2,

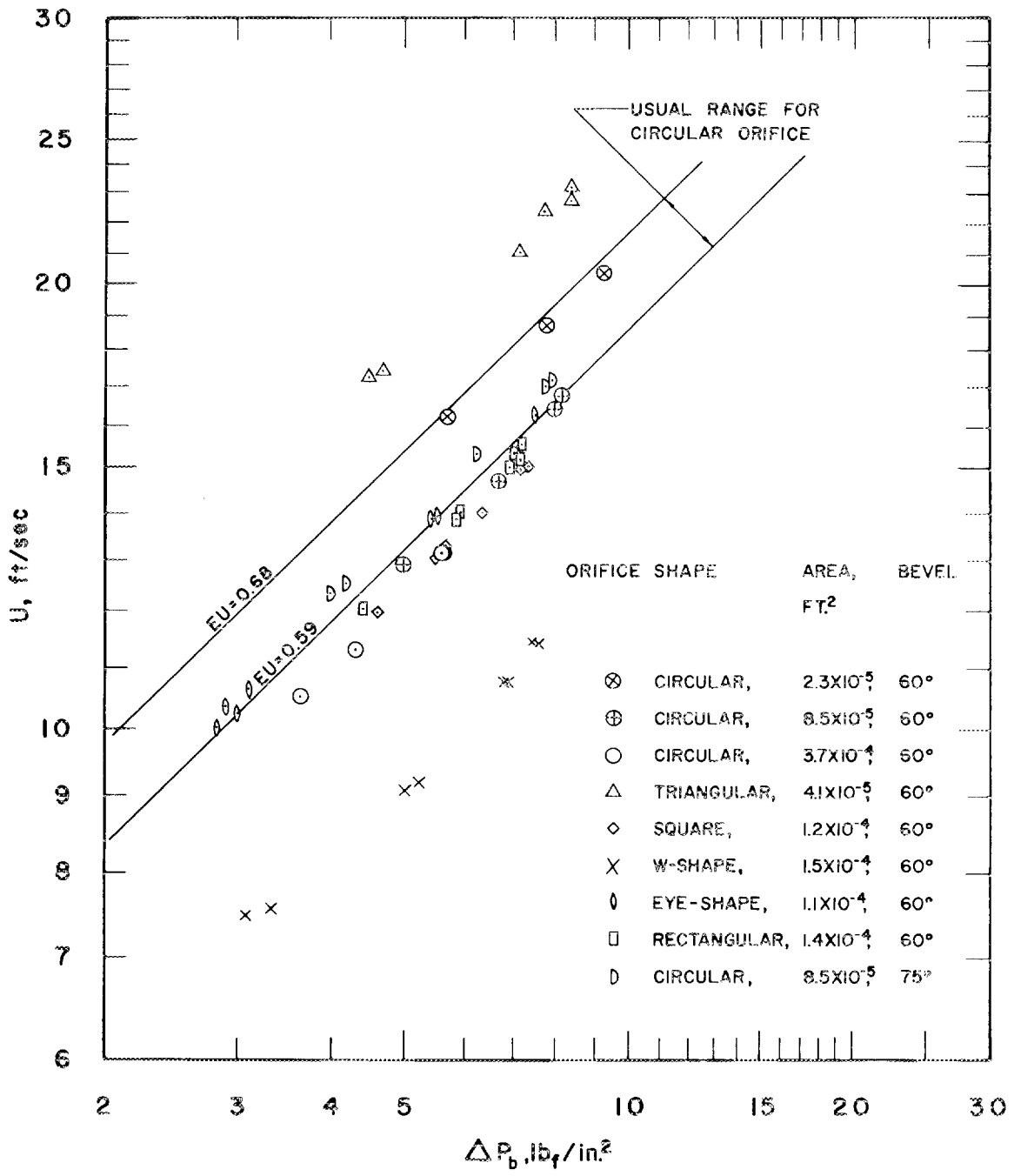

Fig. 6.37. Euler Number Variation for Various Apertures. (From ref. 51.)

ρ_i = initial density of the fluid in the vessel, lb/ft^3,
P_i = initial pressure of fluid in the vessel, lb/ft^2,
P_e = exit pressure, lb/ft^2.

Then u can be obtained from the value of U/U_{oe}. Once U is determined, a corresponding modified cavitation number, Ca', may be obtained from Fig. 6.30. This allows verification of the assumed critical exit pressure. If it is not correct, a new critical exit pressure is chosen, and the procedure is repeated. Once the correct value of critical exit pressure and velocity are found, the discharge rate can be evaluated.

6.4.2.9 Transitional Critical Flow

For a modified cavitation number between 9 and 14, from Eq. (6.72), unstable transitional flow also occurs, as shown in Fig. 6.30. In this range, single- and two-phase flows occur alternately. It has been postulated[50,51] that the contact time between wall and fluid may or may not be long enough to cause steady fluid flashing and hence produce a steady two-phase flow regime. Since the flow is unstable and oscillatory, the discharge rate is indefinite and hard to estimate. This can be seen in the region of transitional unstable flow in Fig. 6.30.

6.4.2.10 Metastable Flow

For a modified cavitation number smaller than 9, metastable flow may exist.[50,51] This is the situation when the saturated fluid discharges through a very short tube or an orifice. No critical phenomena are observed. The flow rate increases continuously as the back pressure is reduced.[50,51,55,56] The available evidence suggests that there is no time for heat transfer to take place between the phases, and the saturated fluid discharged from a very short tube or an aperture behaves as a single-phase incompressible fluid. The discharge flow rates become, therefore, much larger than could have been expected from equilibrium two-phase annular critical flow, nonequilibrium two-phase critical flow, or transitional flow.

Rates of discharge from very short tubes may be obtained from Fig. 6.36. The modified cavitation number in this case is based on the difference of initial and back pressure. Flow rates from various aperture configurations can be determined from Fig. 6.37. It is noted that for a fixed pressure, the Euler numbers or discharge coefficients for circular, triangular, rectangular, square eye-shaped, and W-shaped apertures depend on the configuration and cross-sectional area. For the same configuration, the larger the cross-sectional area, the smaller is the discharge or Euler number.[50,51]

Burnell[55] found that equilibrium conditions were never attained in nozzles and suggested empirical correlations, which depend on the value of the surface tension, to give the maximum flow rate for any given inlet

condition. The recommended relation for saturated liquids is

$$G_c = \left(\frac{2g_c p_i C}{v_i}\right)^{1/2} , \tag{6.82}$$

and for subcooled water,

$$G_c = \left\{\frac{2g_c[p_i - p_s(1 - C)]}{v_i}\right\}^{1/2} , \tag{6.83}$$

where

p_i = initial reservoir pressure, lb/ft^2,
p_s = saturation pressure for reservoir temperature, lb/ft^2,
v_i = specific volume for reservoir temperature, ft^3/lb,
C = coefficient (dependent on surface tension) = $0.264\sigma/49.2$,
σ = surface tension = $77.97 - 0.0778T$ for air-free water,
T = reservoir temperature, °F.

Mass velocities for water are shown in Fig. 6.38, with the values lying between the extremes of metastable and equilibrium flow. Figure 6.39 shows mass velocities for steam-water mixtures.

Where both steam and water exist in the reservoir, the steam behaves as a compressible fluid, and critical conditions can exist.[57] The theoretical treatment of such a flow has been extended by Edwards[58] to cover all wetness conditions. Figure 6.40 shows the results of this treatment for orifices. The flow rates plotted are based on effective flow area. Slight rounding of a sharp-edged orifice can affect the discharge considerably. The curve of saturated water flow in Fig. 6.40 is based on the assumption of $c_d = 1.0$.

6.4.2.11 Pressure-Flow-Time History

In computing the pressure-flow-time history after a rupture of a long tube in a high-pressure system, the following approximations appear to yield reasonable results. First, the fluid flowing through the piping follows an isenthalpic expansion. Second, the fluid in the pressurizer expands along a line of constant entropy. The flow is then assumed to follow a series of steady-state steps, each of which lasts for a small, finite time interval Δt. This technique requires multiple trial and error solutions composed of the following steps:

1. Determine the entropy and stagnation enthalpy.
2. Determine the saturation pressure corresponding to the stagnation enthalpy.
3. Assume a mass velocity G.
4. Calculate the length of pipe required for the pressure to reach the saturation pressure by a single-phase pressure drop, Eq. (6.52).

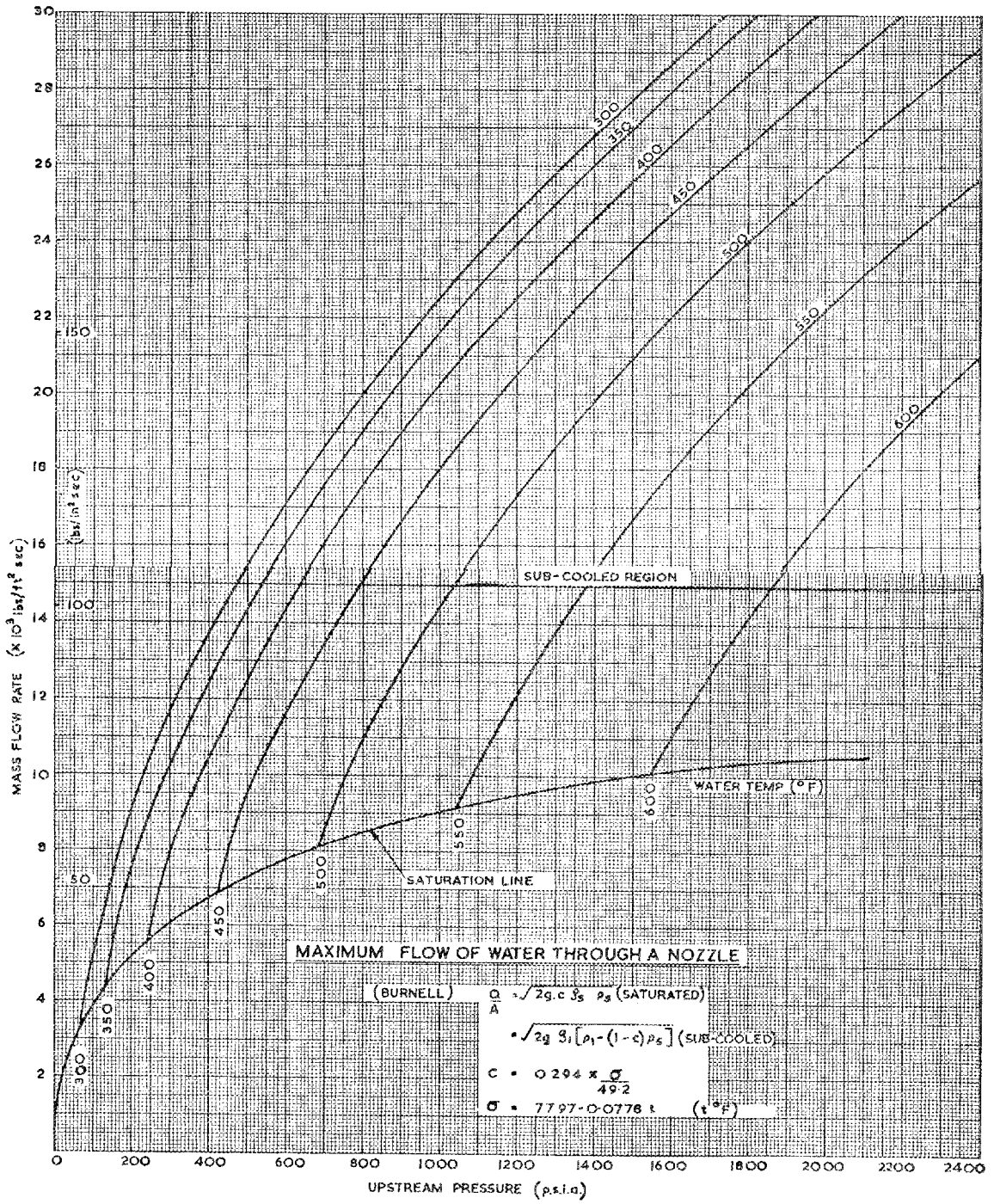

Fig. 6.38. Maximum Flow of Water Through a Nozzle. (From ref. 58.)

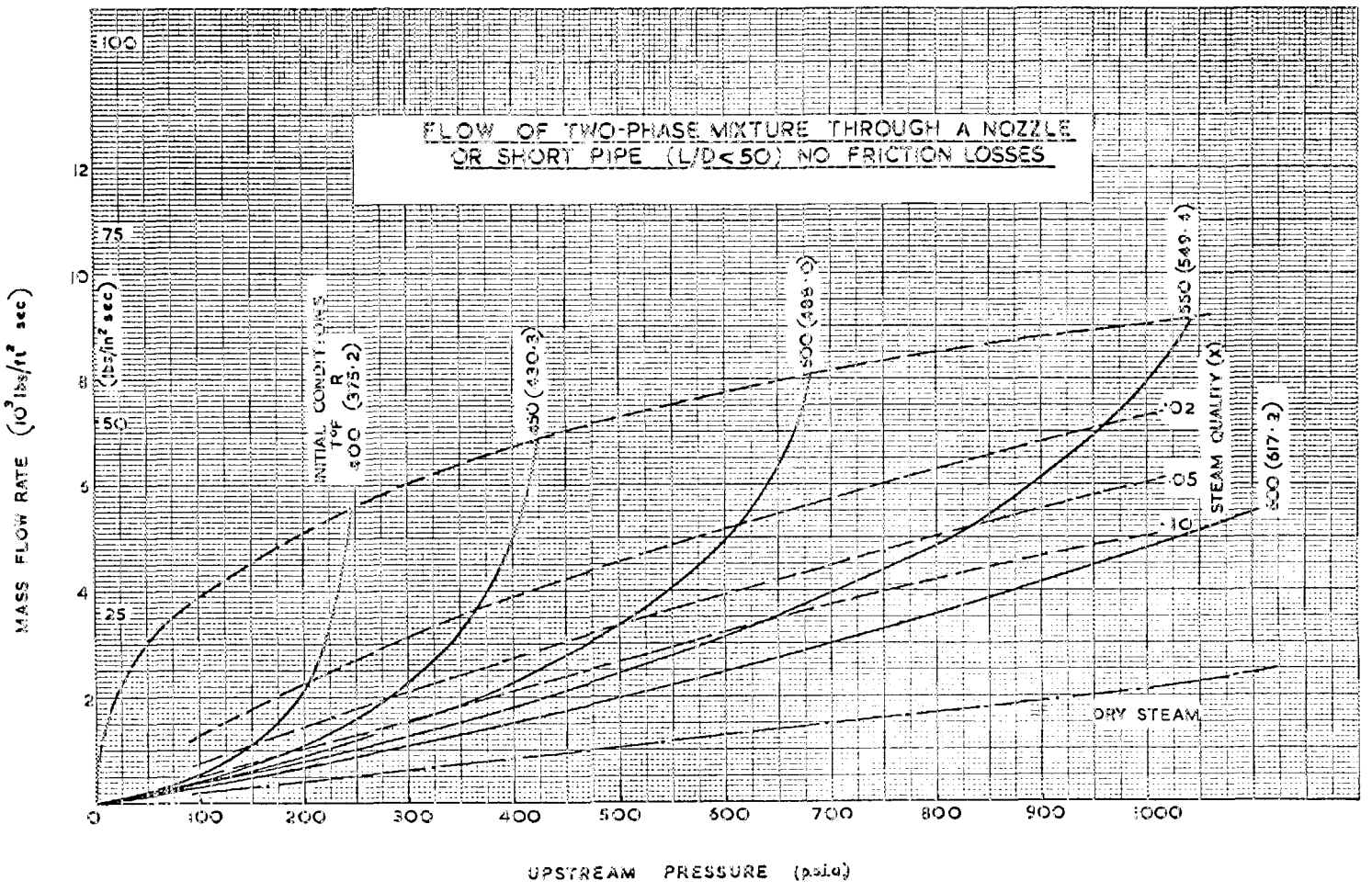

Fig. 6.39. Flow of Two-Phase Mixture Through a Nozzle or Short Pipe (L/D < 50), no Friction Losses. (From ref. 58.)

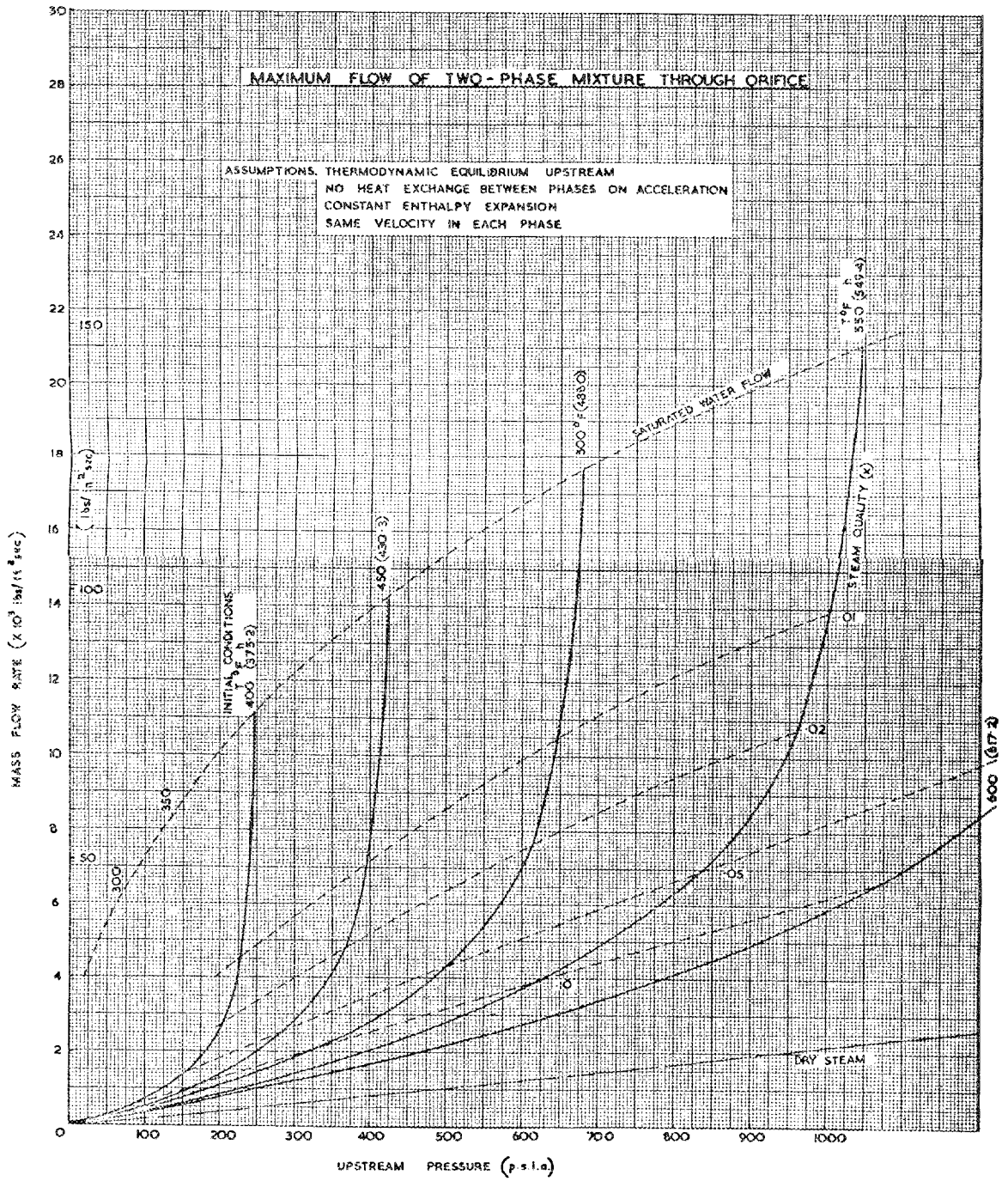

Fig. 6.40. Maximum Flow of Two-Phase Mixture Through Orifice. (From ref. 58.)

5. From the critical-flow envelope (Fig. 6.34), determine the critical pressure and quality.

6. Use the critical pressure and quality in Fig. 6.27 to obtain the Martinelli multiplier $\tilde{R}$.

7. Calculate the two-phase frictional pressure drop for the boiling section.

8. Determine the slip ratio S_c from Fig. 6.32 and void fraction α from Fig. 6.31.

9. Calculate the acceleration pressure drop by means of Eq. (6.55), using specific volumes v_f and v_g evaluated at the critical pressure.

10. Add the single-phase pressure drop, the two-phase frictional pressure drop, and the acceleration pressure drop to the critical pressure and compare this with the pressurizer pressure.

11. If the total pressure drop plus the critical pressure does not equal the pressurizer pressure, assume a new mass velocity and repeat steps 4 through 10.

12. Assuming steady flow, determine the mass that has left the pressurizer during time interval Δt.

13. Calculate the new pressurizer specific volume.

14. Determine the new pressurizer pressure corresponding to the initial entropy and the specific volume calculated in step 13.

15. Repeat steps 2 through 14 until the liquid level in the pressurizer falls below the exit pipe and the pressurizer has "blown down."

6.4.3 Shock Generation and Transmission

The theoretical treatment of the propagation of a shock wave in most materials must be grossly simplified, and an accurate treatment is probably beyond the present state of the art without substantially more theoretical and experimental work. The propagation of a shock wave in two media (air and water) has only recently been understood in something like adequate detail. The research in these two media was supported by an extensive body of thermodynamic properties. Comparable data do not exist for materials such as concrete and steel, which are commonly used in containment structures.

The problem at present is to seek out and simplify the principal features involved in a shock initiation. At present the best that can be expected is to establish the order of magnitude of the variables involved and to disclose proper lines for further research.

This section considers the basic laws of mechanics that govern shock and material velocities, describes shock transmission across an interface, gives semiempirical formulas that describe peak pressures, and cites pressure decay laws. In addition, the waste heat concept is used to describe the dissipation of energy behind a shock and to aid in understanding effective blast shields. The analysis is begun by considering the hydrodynamic variable at the shock front; namely, the Rankine-Hugoniot laws.

6.4.3.1 Rankine-Hugoniot Conservation Laws[59]

The Rankine-Hugoniot conditions across a shock front represent the conservation of mass, momentum, and energy. Although they are generally derived on the basis of a model of a sharp discontinuity in pressure and usually for a fluid like air, these restrictions by no means affect the general validity of the equations.

The concept of a sharp shock front is reasonable even when the initial energy release is not instantaneous. For example, consider the case shown in Fig. 6.41, where the initial release of energy is not instantaneous, and where it is propagated outward as a rising wave of pressure. Within a relatively short distance the pressure pulse will "shock up" and rapidly reach the configuration shown on the right. This steepening results from the fact that as the pressure increases the volume of the material decreases and the resistance to compression increases. These characteristics apply to almost all known materials.

In addition, the Rankine-Hugoniot conditions will be reasonable so long as the decay behind the shock front is slow enough that some meaning can be attached to the concept of "peak" variables and that there is no ambiguity in specifying the point behind the shock at which the peak density, pressure, and material velocity can be said to exist. The Rankine-Hugoniot conditions fail only if these variables are essentially "out of phase" with each other and their peaks occur at different locations in space.

Under these Rankine-Hugoniot conditions, conservation of mass gives

$$\rho_o U = \rho(U - u) \ , \tag{6.84}$$

where

U = shock velocity,
u = peak material velocity,
ρ = peak density behind the shock,
ρ_o = density in front of the shock.

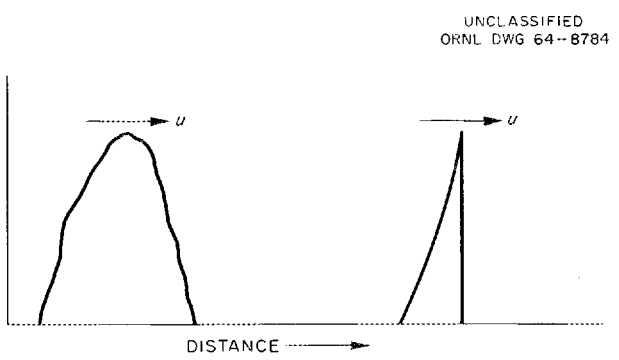

Fig. 6.41. Shocking Up of a Pressure Pulse.

This equation presupposes that the material in front of the shock is at rest.

Conservation of momentum across the shock requires that

$$p_o + \rho_o U^2 = p + \rho(U - u)^2 , \tag{6.85}$$

where p is peak absolute pressure behind the shock, and p_o is ambient pressure ahead of the shock. Like the law for conservation of mass, this equation does not depend on the equation of state of the material. If the shock "thickness" is not infinitesimal but has a finite width, both equations are still valid if all the variables are considered as average values for the time and space over which they are written.

With these two laws, the shock velocity is immediately deduced as

$$U^2 = \frac{p - p_o}{v_o - v} v_o^2 . \tag{6.86}$$

The material velocity is

$$u^2 = (p - p_o)(v_o - v) , \tag{6.87}$$

where v and v_o refer to the specific volume behind and ahead of the shock, respectively.

The total energy density behind the shock front is obtained by regarding the material behind the shock as a piston pushing with absolute pressure on 1 g of material of unit cross section and compressing it from an initial volume v_o to a final volume v. Here again there is no dependence on the equation of state nor the necessity for an absolutely sharp rise in the shock. Then

$$E_{tot} = p(v_o - v) . \tag{6.88}$$

The kinetic energy, E_k, for 1 g of material is, of course, $(1/2)u^2$. The internal energy is given by

$$\begin{aligned} E_i &= E_{tot} - E_k \\ &= p(v_o - v) - \frac{1}{2}(p - p_o)(v_o - v) , \end{aligned} \tag{6.89}$$

which becomes

$$E_i = \frac{1}{2}(p + p_o)(v_o - v) . \tag{6.90}$$

Equations (6.84) to (6.90) are often most useful in the general form, as stated. However, an equation of state is required in order to establish the relation between p and v behind the shock front.

An expression for the relation between pressure and volume across a shock front has been derived,[60] based on theoretical considerations, that is a good approximation for both solids and liquids. When applied to the specific case of water, this formula gave excellent results up to 250,000 bars, which is the highest known experimental value. This equation expresses the pressure as a function of the specific volume ratio, v_o/v, in the form

$$p - p_o = C \frac{\left(\frac{v_o}{v}\right)^b - 1}{\mu - \frac{v_o}{v}} . \tag{6.91}$$

Strictly speaking, μ is a variable; however, it approaches a value of 4 for almost any substance at high pressures. For any given material, C and b are constants. At low pressure, Eq. (6.91) reduces to

$$p - p_o = \rho_o c_o^2 \left(\frac{v_o}{v} - 1\right) , \tag{6.92}$$

where c_o is the sonic velocity evaluated at p_o. At high pressures, where μ approaches the numerical value of 4, Eq. (6.92) becomes

$$p - p_o = \frac{3}{b} \rho_o c_o^2 \frac{\left(\frac{v_o}{v}\right)^b - 1}{4 - \frac{v_o}{v}} . \tag{6.93}$$

For an ideal gas, the Rankine-Hugoniot equation is

$$\frac{v_o}{v} = \frac{\frac{\gamma + 1}{\gamma - 1} + \frac{p_o}{p}}{1 + \frac{\gamma + 1}{\gamma - 1} \frac{p_o}{p}} , \tag{6.94}$$

where γ is the ratio of the specific heats. The remaining hydrodynamic variables are readily deduced using the relation between pressure and density, as found in either Eq. (6.91) or Eq. (6.94), with the equations for material velocity, shock velocity, and energy density, Eqs. (6.86) to (6.90).

The general expression for material velocity in solids and liquids is

$$u^2 = C(v_o - v)\,\frac{\left(\frac{v_o}{v}\right)^b - 1}{\mu - \frac{v_o}{v}} \,. \tag{6.95}$$

In the elastic region, where Eq. (6.92) adequately expresses the relation between p and v, the material velocity becomes

$$u = \frac{p - p_o}{\rho_o c_o} \,. \tag{6.96}$$

Note the linearity of material velocity with pressure in this region. At high pressures, the material velocity is found to be proportional to the square root of the pressure. The material velocity in an ideal gas is

$$u^2 = \frac{c_o^2}{\gamma}\left(\frac{p}{p_o} - 1\right)\left(1 - \frac{v}{v_o}\right) , \tag{6.97}$$

where v/v_o may be found in Eq. (6.94).

The equation for the shock velocity for solids and liquids becomes, in general,

$$U^2 = Cv_o^2\,\frac{\left(\frac{v_o}{v}\right)^b - 1}{(v_o - v)\left(\mu - \frac{v_o}{v}\right)} , \tag{6.98}$$

which reduces, in the elastic approximation, to

$$U = C = c_o \,. \tag{6.99}$$

Even after the elastic approximation fails and as long as the shock equations are adiabatic, Eq. (6.99) is applicable. For an ideal gas, the shock velocity is given by

$$U^2 = \frac{\left(\frac{p}{p_o} - 1\right) c_o^2}{\gamma\left(1 - \frac{v}{v_o}\right)} \,. \tag{6.100}$$

The total energy behind the shock front is given closely by

$$E_{tot} = \frac{C\left[\left(\frac{v_o}{v}\right)^b - 1\right]\left(\frac{v_o}{v} - 1\right)}{\mu - \frac{v_o}{v}} \tag{6.101}$$

for solids and liquids and becomes

$$E_{tot} = \frac{p(p - p_o)}{\rho_o c_o^2} \tag{6.102}$$

in the elastic approximation. An important result here is that the pressure required for a given energy density at the shock front is given by

$$p = (\rho_o c_o^2 E_{tot})^{1/2} \quad . \tag{6.103}$$

Table 6.12 shows the variation of total energy with peak pressure for several different materials. The outstanding result shown in Table 6.12 is that a very small amount of energy is required in solid and liquid media to produce very strong pressure pulses.

Table 6.12. Total Energy of Shock Front at Various Peak Pressures for Several Materials[a]

Material	Energy per Unit Volume (cal/cm^3) at Indicated Peak Pressure			
	10 bars	100 bars	1000 bars	10,000 bars
Air	0.72	15.5	240	1910
Water	1.4×10^{-4}	1.4×10^{-2}	1.4	53
Concrete	5.5×10^{-6}	5.5×10^{-4}	5.5×10^{-2}	5.5
Steel	1.2×10^{-6}	1.2×10^{-4}	1.2×10^{-2}	1.2

[a]From ref. 61.

6.4.3.2 Wave Forms

In order to provide some insight into the duration of loading, expressions are needed to describe the decay of pressure behind the shock

front. Figure 6.42 illustrates two of the forms by which the pressure waves may be described.

The time of decay of pressure at the shock front has been derived[60] in the following form:

$$\frac{\partial p}{\partial \tau} = \frac{\left(\frac{u}{C} - \frac{U - u}{C} + 1\right)\frac{dp_s}{d\tau} + \rho U \frac{du_s}{d\tau} + \frac{\lambda \rho u U(U - u)}{r}}{1 - \frac{(U - u)^2}{C}} , \qquad (6.104)$$

ORNL-DWG 64-8785

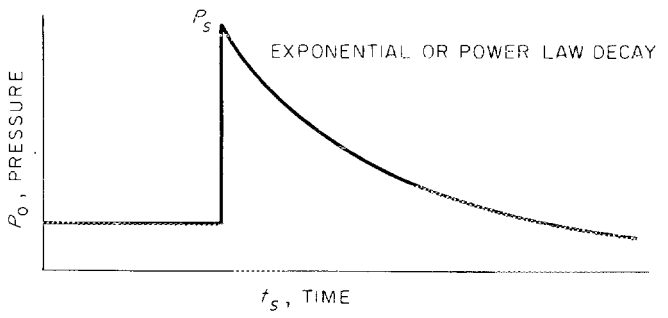

(*a*) EXPONENTIAL OR POWER LAW DECAY IS APPLICABLE AT HIGH PRESSURES; IT MAY DECAY BELOW AMBIENT OR LATER DEVELOP "NEGATIVE PRESSURES" IN A TENSION WAVE.

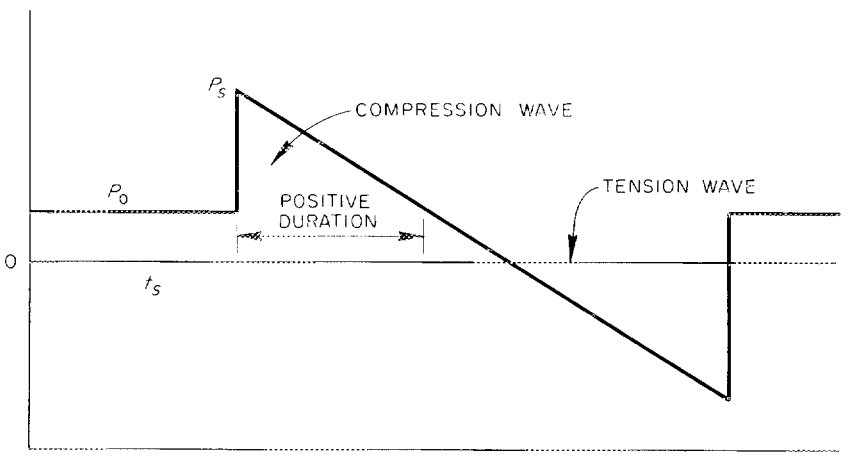

(*b*) THE N-WAVE IS APPLICABLE AT LOW PRESSURES; THE NEGATIVE PRESSURE IN THE TENSION WAVE CANNOT EXCEED THE TENSILE STRENGTH OF THE MATERIAL

Fig. 6.42. Pressure Wave Forms at Long Distances in Solid Media.

where

$dp_s/d\tau$ = time derivative of peak pressure across the shock front,
$du_s/d\tau$ = time derivative of peak material velocity across the shock front,
r = distance from the center of a spherical shock,
λ = divergence parameter, with the value of 2 for spherical shocks.

This equation may be simplified by use of the elastic approximation along with the two following assumptions: (1) over a wide range of pressures, the peak overpressure and time are related by

$$(p - p_o)\tau^n = \text{constant} , \tag{6.105}$$

where $n = 1 + \Delta > 1$; and (2) the shock has been running with sonic velocity for some time and has traveled a distance, r, from the center, given by

$$r = U\tau + C_1 , \tag{6.106}$$

where C_1 is a constant that represents the early radius-time history when the elastic approximation did not hold. With these approximations, Eq. (6.104) becomes

$$\frac{\partial p}{\partial \tau} = - \left[(n - 1) + \frac{nC_1}{r - C_1}\right] \frac{\rho_o c_o^3}{r} . \tag{6.107}$$

This equation is useful in making comparisons between shocks in different media at the same distance. Because of the term $\rho_o c_o^3$, the pressure decay behind the shocks is much more rapid for materials of high density and sonic velocity. The term in brackets is more or less insensitive to the type of medium in which the shock occurs, provided the material is isotropic.

Impulse Effects. The impulse of the pressure wave is as important as the peak pressure in damage criteria. The pressure impulse may be given by

$$\text{Pressure impulse} = \text{form factor} \cdot \frac{(p_s - p_o)^2}{\left(-\frac{\partial p}{\partial \tau}\right)_s} , \tag{6.108}$$

where the form factor is 1/2 for linear decay, $p = A - B\tau$; 1 for exponential decay, $p = A\, e^{-B}\, (\tau - \tau_s)$; and $B/(B - 1)$ for power-law decay, $p = A(\tau_s/\tau)^B$. The form factor that is applicable depends on the characteristics of the shock; that is, whether the peak pressure is much larger than or comparable to the ambient pressure. In any case, the form factors do not differ appreciably and may be regarded as essentially independent of

the medium. Combining Eq. (6.108) with Eq. (6.107) and assuming a form factor of 1, gives

$$\text{Pressure impulse} = \frac{(p_s - p_o)^2 \, r}{\left[(n - 1) + \dfrac{nC_1}{r - C_1}\right] \rho_o c_o^3} \quad . \tag{6.109}$$

In making comparisons among different media, it is noted that increases in sound velocity and density tend to decrease the impulse. However, Eq. (6.103) shows that the overpressure actually increases for the same total energy behind the shock when ρ_o and c_o increase. Applying this result and the observation that p is considerably larger than p_o, gives

$$\text{Pressure impulse} = \frac{E_{tot} r}{\left[(n - 1) + \dfrac{nC_1}{r - C_1}\right] c_o} \quad . \tag{6.110}$$

6.4.3.3 Shock Transfer Across an Interface

There are two types of interaction that are of interest in shock calculations. The first is the transfer relation across a liquid-gas interface. Upon arrival of the shock at the liquid-gas interface, reflection as a rarefaction wave throws a mass of liquid upward, mostly in the form of spray. The equations describing this type of transfer are given in Section 6.4.3.5.

The other interactions of interest here are transfers across fluid-solid or solid-solid interfaces. (For convenience, a liquid-solid interface is discussed.) With a perfectly rigid reflector, the material velocity behind the reflected wave in the liquid and behind the transmitted wave in the reflected medium are both zero. This yields the following relation:

$$\left(\frac{p_2}{p_1} - 1\right)\left(1 - \frac{v_2}{v_1}\right) = \left(1 - \frac{p_o}{p_1}\right)\left(\frac{v_o}{v_1} - 1\right) , \tag{6.111}$$

where the subscript o refers to ambient conditions; subscript 1 refers to conditions behind the incident shock, and subscript 2 refers to conditions behind the reflected shock. For an ideal gas, the pressure relation becomes

$$\frac{p_2 - p_o}{p_1 - p_o} = 1 + \frac{1 + \left(\dfrac{\gamma - 1}{\gamma + 1}\right)}{\dfrac{p_o}{p_1} + \left(\dfrac{\gamma - 1}{\gamma + 1}\right)} \quad . \tag{6.112}$$

Defining the pressure multiplication for a liquid as $\xi = p_2/p_1$ and with the assumption that $p \gg p_o$, the multiplication for a rigid surface is given by

$$\xi = \frac{\dfrac{v_o}{v_1} - \dfrac{v_2}{v_1}}{1 - \dfrac{v_2}{v_1}} \quad . \tag{6.113}$$

This equation is not explicitly a function of p_1, but it can be solved by an iterative process when used in conjunction with Eq. (6.93).

In the next higher approximation, it can be considered that the reflection processes are within elastic limits. This gives, for the pressure multiplication,

$$\xi = \frac{1 + \left(\dfrac{v_o}{v_1}\right)^{1/2}}{1 + \left(\dfrac{v_o'}{v_1}\,\dfrac{\rho_1 c_1^2}{\rho_2 c_2^2}\right)^{1/2}} \, , \tag{6.114}$$

where c_1 and c_2 are the sonic velocities in the media with the incident shock and the reflector media, respectively, and v_o' is the ambient specific volume in the reflecting medium.

The last approximation considers the reflector as an elastic medium, while the medium with the incident shock is above its elastic range. This approximation is closer to reality than the elastic-elastic approximation for a liquid-solid interface, since the elastic region for most liquids is an order of magnitude less than it is for solids. For example, the elastic region for water is valid up to 20,000 bars. The pressure multiplication for this case is

$$\xi = \frac{\dfrac{v_o - v_1}{v_1} + \xi^2 \dfrac{p_1}{a} \dfrac{v_o'}{v_o} \dfrac{v_o}{v_1}}{1 - \dfrac{v_2}{v_1} + 2\left[\dfrac{p_1}{a'}\left(\dfrac{v_o}{v_1} - 1\right) \dfrac{v_o'}{v_o} \dfrac{v_o}{v_1}\right]^{1/2}} \, , \tag{6.115}$$

where $a = \rho_o c_o^2$, and the prime denotes the reflector material ahead of the transmitted wave.

When a strong shock is transmitted from a liquid to a solid, it is necessary to compare the rate of work in the solid with the rate in the liquid during the same interval. The rate of work per unit area is given

by

$$\dot{W} = pu \ . \tag{6.116}$$

For an elastic medium, the material velocity behind the incident shock is related to its pressure, p_1, by

$$u_1 = p_1 \left(\frac{v_o}{a_1}\right)^{1/2} , \tag{6.117}$$

where $a_1 = \rho_o c_o^2$ (evaluated for properties of material having incident shock). Behind the transmitted shock in the reflecting medium, the material velocity is

$$u_2 = p_2 \left(\frac{v_o'}{a_2}\right)^{1/2} , \tag{6.118}$$

where p_2 is the pressure behind the transmitted shock in the reflecting medium, $a_2 = \rho_o' c_o'^2$ for the reflecting material evaluated at ambient conditions, and v_o' is the ambient specific volume for the reflecting medium.

Thus, using the elastic approximations for the material velocity, the rate of work becomes

$$\dot{W}_1 = p_1 u_1 = p_1^2 \left(\frac{v_o}{a_1}\right)^{1/2} \tag{6.119}$$

and

$$\dot{W}_2 = p_2 u_2 = p_2^2 \left(\frac{v_o'}{a_2}\right)^{1/2} , \tag{6.120}$$

and the ratio of work done is

$$\frac{\dot{W}_2}{\dot{W}_1} = \frac{p_2^2}{p_1^2} \left(\frac{v_o' a_1}{v_o a_2}\right)^{1/2} = \frac{p_2^2}{p_1^2} \frac{(\rho_o c_o) \text{ incident}}{(\rho_o' c_o') \text{ reflected}} \ . \tag{6.121}$$

6.4.3.4 Initial Pressure Generation

For an underwater explosion, Cole[62] gives the following empirical relation for peak pressure as a function of distance from the center of

the explosion:*

$$p_m = 1.47 \times 10^3 \left(\frac{W^{1/3}}{r}\right)^{1.13} , \qquad (6.122)$$

where

W = equivalent charge of TNT, lb,
r = radius from the center of the explosion, ft,
p_m = resulting peak pressure at distance r, bars.

The prompt energy release is assumed to be 1000 cal per gram of TNT, which is in accordance with customary usage with point-source explosions. The form of Eq. (6.122) makes it very useful for blast-shielding calculations. Experimental data on this phenomenon have been obtained by the Ballistics Research Laboratory, as noted in Chapter 12.

6.4.3.5 Spray Pressure

Upon the arrival of a shock wave at a liquid-gas interface, reflection as a rarefraction wave occurs. As a result of the reflection of the incident wave, a mass of liquid is thrown upward, mostly in the form of a spray. The particle velocity of the spray depends on the particle velocity behind the incident wave in the liquid. If it is assumed that the reflected wave is of strength about equal to the incident wave, superposition causes the particle velocity to double upon entry into the gas. Since the peak pressure within the liquid may be estimated from Eq. (6.122), and assuming the particle velocity in the liquid is given by Eq. (6.117), the particle velocity for the spray is

$$u = \frac{2p_m}{\rho_o c_o} . \qquad (6.123)$$

However, since the peak pressure does not occur at the same instant over the entire liquid-gas interface, the particle velocity will also vary. By referring to Fig. 6.43, the relation between the peak pressure at the interface on a vertical centerline through the explosion center and the

---

*It should be noted that in reality the TNT curve does not follow this simple power-law dependence on radius. It is known that the peak pressure versus distance curve for TNT has higher values and is steeper than the simple power-law curve at high pressures. At intermediate pressures, the slope gradually decreases until, at lower pressures, the power-law curve gives higher pressures and smaller slopes than are indicated by the curve for TNT. The TNT curve of constant exponent 1.13 is to be regarded as the average fit for the pressure-distance curve in the regions of practical interest.

ORNL DWG 64-8786

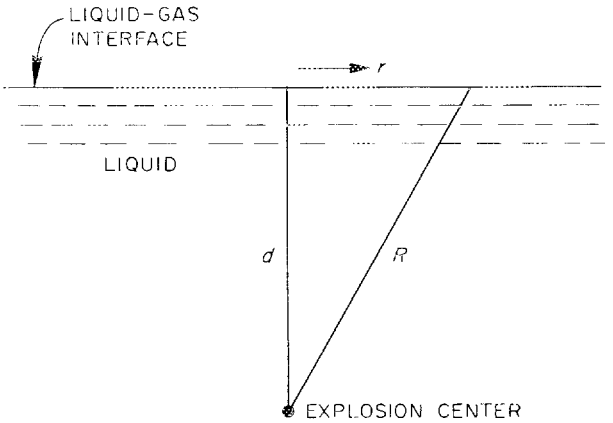

Fig. 6.43. Explosion Geometry.

peak pressure at any radial location r is

$$p_{m_r} = p_{m_o} \left[\frac{d}{(d^2 + r^2)^{1/2}} \right]^{1.13} . \tag{6.124}$$

The particle velocity of the spray is then found as a function of r by substituting Eq. (6.124) into Eq. (6.123). Thus,

$$u_r = \frac{2p_{m_o}}{\rho_o c_o} \left(1 + \frac{r^2}{d^2} \right)^{0.57} . \tag{6.125}$$

Figure 6.44 shows the variation of the particle velocity ratios (particle velocity at r = 0 divided by particle velocity at r) as a function of r/d. Because of the variation in the particle velocity over the free surface, it is easily seen that the subsequent impact of these particles against a solid surface will not yield a uniform pressure distribution on the impacted surface.

The dynamic pressure associated with the spray particles is

$$P_{d_r} = \frac{1}{2} \rho u_r^2 . \tag{6.126}$$

In Eq. (6.126), ρ is the spray density. Upon impact with a solid surface, and neglecting all frictional losses, the dynamic pressure given by Eq. (6.126) represents the loading on the impacted surface per unit area.

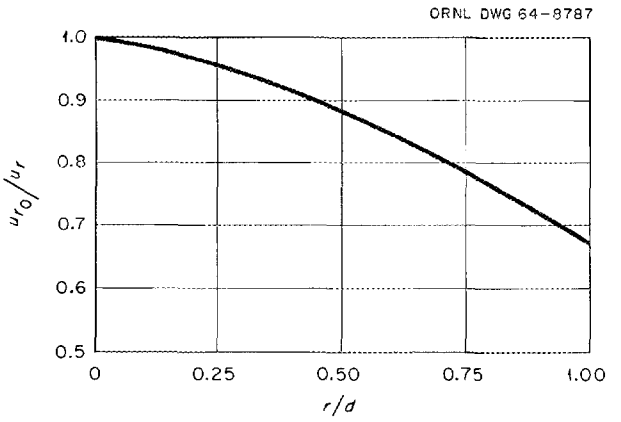

Fig. 6.44. Particle Velocity Ratio at the Liquid-Gas Interface as a Function of Radial Distance from Vertical Centerline of Explosion.

6.4.3.6 Energy Dissipation

Figure 6.45 illustrates the entropy, or waste heat, concept that is basic to the following discussion of energy dissipation. (This concept will also be used in Section 6.6.3 to describe effective blast shielding.) This figure is a conventional thermodynamic pressure-volume diagram for a unit mass of material. On this diagram, energies are portrayed as areas. The total energy is represented by the area of the rectangle below the pressure labeled p_s and between v_s and v_o:

$$E_{tot} = p_s(v_o - v_s) \ . \tag{6.127}$$

The kinetic energy is the triangle in the upper right of the total energy rectangle [see Eq. (6.87)]:

$$E_k = \frac{1}{2} u^2 = \frac{1}{2} (p_s - p_o)(v_o - v_s) \ . \tag{6.128}$$

The internal energy is the trapezoid occupying the rest of the rectangle:

$$E_i = \frac{1}{2} (p_s + p_o)(v_o - v_s) \ . \tag{6.129}$$

The curved line between p_o, v_o and p_s, v_s is the Rankine-Hugoniot curve that is the relation between pressure and specific volume [for example, Eq. (6.91)].

When a shock occurs, the material is irreversibly converted to the state p_s, v_s. From this point, the material will expand adiabatically to the original specific volume, v_o, essentially along the Rankine-Hugoniot wave. The area under the Rankine-Hugoniot curve represents the $\int p \, dv$

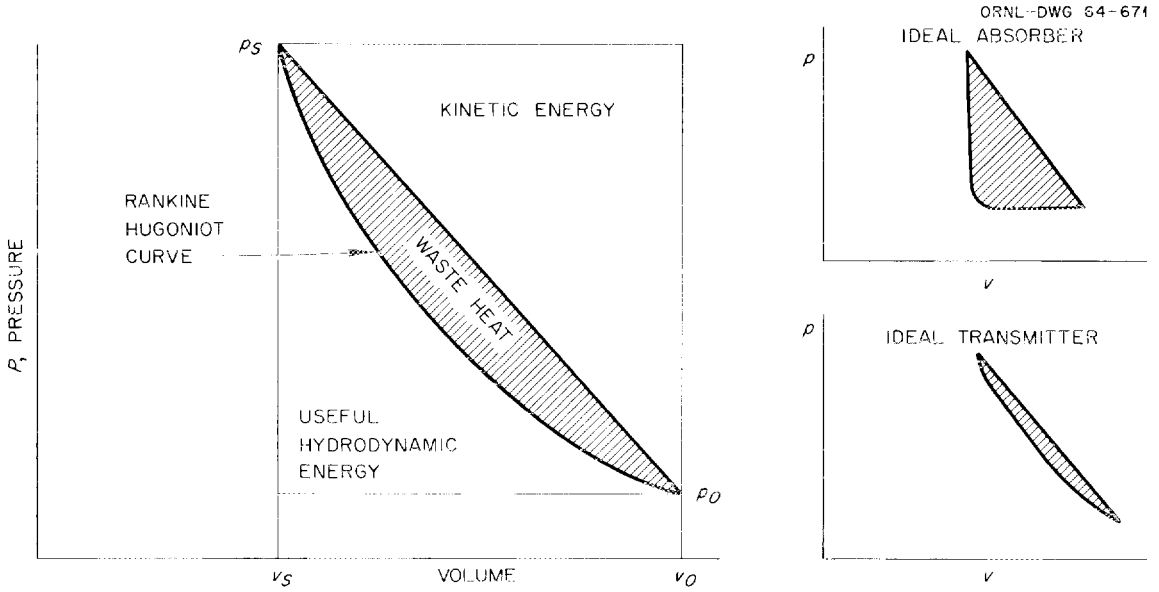

Fig. 6.45. The Waste Heat Concept. (From ref. 61)

energy given up through the expansion of the material and is shown as the "useful hydrodynamic energy" in Fig. 6.45. The shaded portion of this figure (labeled "waste heat") represents the energy dissipated by irreversible processes. It will be manifest as an increase in temperature of the material.

At high enough pressures, the Rankine-Hugoniot curve asymptotically approaches a limiting specific volume, and the waste heat area increases rapidly. As the pressure range is extended, the waste heat area approaches the area of the internal energy trapezoid, and the useful hydrodynamic energy fraction is correspondingly decreased. At some pressure, however, the irreversible heating will be so large that the material will be irreversibly converted to a gaseous state, in which case it will expand along an adiabatic line that lies above the Rankine-Hugoniot curve and will terminate in a final volume much larger than the initial volume. In such a case the waste heat is less severe than indicated by the corresponding waste heat area of Fig. 6.45. The maximum waste heat for a given material occurs near the point where the waste heat area is just sufficient to vaporize the material and decompose it to its elemental state. The waste heat concept is primarily a method of bookkeeping the energy and does not depend significantly on the details of the expansion process.

It is fairly easy to find or to fabricate materials that "crush down" to small volumes at relatively low pressures; these are the ideal absorbers. For such materials, the Rankine-Hugoniot curve is sharply bowed, as shown in Fig. 6.45 at the upper right. Nearly all the internal energy appears as waste heat, and little if any appears as useful hydrodynamic energy. The kinetic energy fraction is still transferred to the next particle through the conservation of momentum to sustain the shock. Finally, the subsequent expansion may be more complicated than shown here for a

variety of reasons: heat transfer between phases, slippage along crystal boundaries, phase changes, etc. The net result is to terminate the expansion curve closer to v_s than to v_o. These are equivalent to a hysteresis effect and lend further validity to the approximation that nearly all the internal energy is wasted behind the shock in an ideal absorber.

At low pressures, or in the elastic range, the Rankine-Hugoniot curve and waste heat approach the configuration shown as the "ideal transmitter." This is the domain of ordinary elastic or acoustic theory.

6.4.4 Jet Condensation

The venting of steam-air mixtures to a pool of water and the subsequent condensation of the steam have been considered in the design of pressure-suppression containment systems, and numerical evaluations have been made of the condensation of steam-air bubbles in a pool of water.[63] These evaluations have been made for the following initial conditions, which are applicable to current designs:

Initial temperature of bubble	280°F
Bulk water temperature	100°F
Initial bubble radius	0.25 in.
Pressure on bubble	18 psia

The effects of initial steam-mass fractions (0.2, 0.5, and 0.9) and heat-transfer coefficients have been included.

The results of the calculations have indicated that the presence of air in the steam-air bubble does not reduce the condensation rate sufficiently to increase the likelihood of appreciable steam carryover. For example, about 97% of the steam initially present in the steam-air bubble is condensed within 0.01 sec for an initial steam fraction of 0.9. Even with an initial steam-mass fraction of 0.2, about 80% of the steam condenses within 0.1 sec; beyond 0.5 sec, the excess steam carryover is not significant.

The values reported are for specific initial conditions; however, the numerical procedures outlined by Isbin, Nishiwaki, and Klein[63] may be used to investigate other conditions. It should be emphasized that the conclusions are based on an analytical evaluation of the problem and have not been verified experimentally. However, tests by Pacific Gas and Electric[64] have shown that, for the conditions of the Humboldt Bay Reactor, steam carryover is insignificant.

The equipment for these tests consisted of a 20-ft-diam tank containing water and means of discharging steady steam flows of up to 100,000 lb/hr at a supply line pressure of 100 psi. Injector pipes were from 4 to 14 in. in diameter. The tests demonstrated the extreme rapidity of steam-jet condensation. The jets stirred up the water vigorously, and complete condensation was obtained in all but a few tests where the injector pipe end was barely below the water surface. No large steam bubbles were observed. Jet condensation in these tests was found to be insensitive to the amount of air in the steam, to the temperature of the pool, and to the depth of the vent pipes as long as they were submerged.

6.5 STRUCTURAL PROBLEMS

B. L. Greenstreet
M. A. Salmon N. A. Weil

6.5.1 Introduction

Containment vessels should be designed in accordance with Rules for Construction of Nuclear Vessels, Section III, ASME Boiler and Pressure Vessel Code, 1963 Edition (see App. C and D). The code contains the most extensive and current material available on analytical techniques that are generally applicable. However, the calculation of stresses is, in general, based on an elastic analysis,[65] even though the actual stresses may exceed the elastic limit of the material. Any attempt to incorporate elastic analysis techniques into this report would be needless repetition and will therefore be omitted.

On the other hand, much work is currently being done in the field of plasticity that will be directly applicable to ultimate strength analysis. This work is in the research and development stage and is not well enough developed to be incorporated into a code. Therefore the current state of the art is discussed here. This section will be revised from time to time as new material is developed.

The basic assumptions made in the analyses are (1) that the shell is a membrane (its bending strength is neglected) and (2) that the shell material is rigid strain-hardening plastic (elastic displacements are neglected). The first assumption should lead to good results for unreinforced shells with large radius-to-thickness ratios under the distributed loadings that might result from a nuclear incident. Reinforcements, attachments, and openings present special problems outside the scope of these methods. Research on these problem areas is under way, and the results will be included in later editions. The assumption of rigid plastic material behavior is appropriate under the following conditions:

1. The specific problem being considered is that of a single application of an intense overload.
2. The structural material is a relatively ductile mild steel. (It has been shown experimentally that results of calculations based on the above conditions are within engineering accuracy.)
3. The elastic response to service loads has been determined and conforms to the applicable code requirements.

The following material, taken from a technical report[66] to be issued by IIT Research Institute (formerly Armour Research Foundation), gives the bases for plasticity analyses of various shell configurations and some theoretical and experimental results obtained to date.

6.5.1.1 Limitations of Analysis

Of all containment shell configurations, only the complete sphere and the infinite cylinder are readily amenable to exact analysis under both static and dynamic internal pressure loadings. This follows from the fact

that the deformed shape of these shells can be specified by a single coordinate (they are single-degree-of-freedom systems). However, other common containment shell configurations are, strictly speaking, infinite-degree-of-freedom systems. Since the equations are also nonlinear, the relatively simple methods of model analysis of dynamic response are inapplicable. The dynamic analysis must be made by step-by-step timewise integration of the equations of motion of a finite-degree-of-freedom model of the actual structure. The structure can be reduced to a system with a finite number of degrees of freedom either by the use of finite difference techniques or by the use of a lumped-parameter model arrived at from physical consideration. In either case the work involved in obtaining solutions for a range of types of containment shells with a range of material properties for a variety of dynamic loadings would be a task beyond the scope of this effort. Consequently, the major emphasis of the material in this section is on the development of approximate methods for the analysis of the response of containment shells as single-degree-of-freedom systems.

Before discussing the dynamic analysis, it is necessary to determine the static load response of shells of various types, since the method employed in the dynamic analysis is to assume that the static load resistance-displacement relationships also apply under dynamic loading. It turns out that the static load analyses are themselves quite involved, so it is necessary to develop simple approximate methods. A considerable effort is made, however, to check the accuracy of the approximate methods against both "exact" solutions and experimental results.

Since the material in this section is devoted to the problem of plastic deformation of shell structures, the appropriate materials properties are discussed first. The emphasis is on the plastic behavior in biaxial states of stress and the effects of strain rate on material properties. This is followed by presenting methods for the static analysis of various shell configurations. Both exact and approximate methods are given, and comparisons between the methods and experimental results are made. Extensive numerical results that cover the range of material properties of practical interest are given in graphical form. These results form the basis for the methods of analysis of dynamic response.

From results of work now in progress at IIT Research Institute (see Chap. 12), is planned, in future editions of this document, to expand the subsection on static methods of analysis and to include new sections on dynamic analysis, effect of openings, and the problem of shielding the shells against blast by use of crushable blast liners or shields.

An attempt is made throughout this section to eliminate as much of the mathematical development as possible and yet at the same time give the reader a full and, it is hoped, understandable account of the basis for the limitations of the methods presented. More detailed information than can be incorporated here will be found in refs. 66 through 132. An attempt has been made to conform to standard notations, as defined in refs. 68, 69, and 70. The most important definitions are included in the following list of nomenclature.

6.5.1.2 Nomenclature

H	Shell thickness
H_i	Original shell thickness
K	Strength coefficient in power law
L	Half-length of cylindrical portion of shell
l	L/R_i, length-to-diameter ratio
N_m	Meridional membrane stress resultant
n	Hardening exponent in power law
P	Internal pressure
p	Dimensionless pressure ratio, see Eq. (6.159) or Eq. (6.161)
R	Radial coordinate
R_1	Maximum radius of cylindrical portion of shell
r_1	R_1/R_i
R_i	Initial radius of cylindrical portion of shell
R_e	Radius of hemispherical cap
r_e	R_e/R_i
R_c	Circumferential radius of curvature
r_c	R_c/R_i
R_m	Meridional radius of curvature
r_m	R_m/R_i
β	σ_m/σ_c, biaxiality ratio
$\epsilon_c, \epsilon_m, \epsilon_n$	True strain in circumferential, meridional, and normal directions, respectively
σ_c, σ_m	Circumferential and meridional stresses
σ	Effective stress
σ_o	Initial yield stress in linear hardening law
λ	Hardening coefficient in linear hardening law

6.5.2 Mechanical Properties of Materials

This section is intended to provide the background in static and dynamic mechanical properties of materials sufficient for comprehension and optimum utilization of the containment vessel analyses presented in this section. Particular emphasis is given to the fundamentals of the plastic, static behavior of biaxially stressed metals and the effects of strain rate on material properties.

6.5.2.1 Fundamentals of the Plastic Behavior of Metals Under Biaxial States of Stress

A knowledge of material behavior under uniaxial stress is sufficient for the design of the simpler structural elements (beams and rods). For an understanding of the behavior of membrane shells in the plastic range, it is necessary to be able to predict material behavior in biaxial states of stress given the uniaxial stress-strain characteristics. Experimental and theoretical investigations have led to the generalization of the familiar concept of the yield point under uniaxial stress to the yield condition for biaxial states of stress. The tensile stress-strain curve gives

the relation between stress and strain during plastic flow under uniaxial stress. It turns out that during plastic flow under biaxial states of stress, the stresses are, in general, not uniquely determined by the strains. It is, however, possible to relate the strain increments to the stresses and the stress increments through the flow law and, in the special case where the biaxiality ratio remains constant, to obtain integrated stress-strain relations. Uniaxial stress-strain relations, the two commonly used yield conditions, and their associated flow laws are discussed in the following paragraphs.

6.5.2.2 Uniaxial Stress-Strain Relations

A typical, uniaxial, true stress-strain curve for mild steel is shown in Fig. 6.46. The stress-strain relation shows considerable curvature between the yield stress and the ultimate stress (maximum load) and then straightens out until the fracture load is reached.

Idealized uniaxial stress-strain curves are shown in Fig. 6.47. It is reasonable to neglect the elastic strains if they are small in comparison with the total strains; this neglect leads to the assumption of rigid plastic material behavior. A material is said to be perfectly plastic if flow occurs at a constant stress. If an increase in stress is required for continued plastic deformation, then the material is said to be strain hardening.

It is assumed that unloading in the plastic range immediately results in elastic strains and that the accompanying slope of the stress-strain curve will be the same as for the initial loading (Fig. 6.47). Since the same states of stress occur for unloading as for the original loading, it is clear that strain is not uniquely determined by stress.

Reloading of a specimen which was unloaded in the plastic range results in a yield stress equal in magnitude to the stress at which the unloading occurred. This means that the "current yield stress σ" for a strain-hardening material depends upon the plastic stress history.

Several empirical formulas (strain-hardening laws) have been proposed for fitting uniaxial true stress-strain curves. Because the curve usually becomes almost a straight line on a log-log plot, the power law

$$\sigma = K\epsilon^n \tag{6.130}$$

is often selected. Here, K and n are material constants called strength coefficient and strain-hardening exponent, respectively. This relation, due to Ludwik, usually differs significantly from the experimentally measured true stress-strain curve only for very small and very large strains. As is shown in Fig. 6.48, the tendency is to overestimate the actual stress for small strains and to underestimate it for large strains. This difference for small strains is essentially eliminated if elastic strains are neglected. Corrections for large strains are occasionally employed to make the empirical relation fit the data better.[71] Values of the constants K and n have been compiled for various steels (Table 6.13). Equation (6.130) is portrayed graphically in Fig. 6.49 for various values

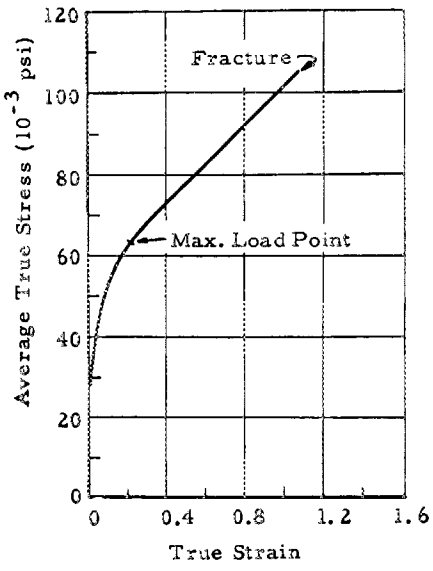

Fig. 6.46. True Stress-Strain Curve for 20°C Annealed Mild Steel.

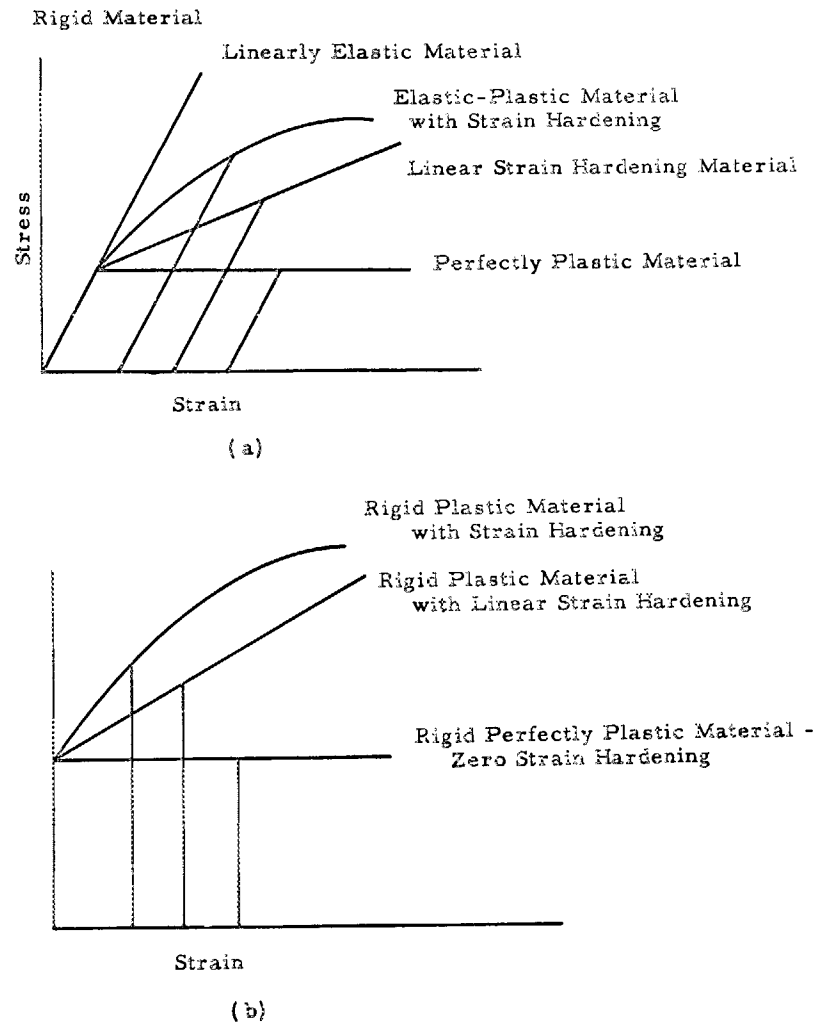

Fig. 6.47. Idealized Uniaxial True Stress-Strain Curves.

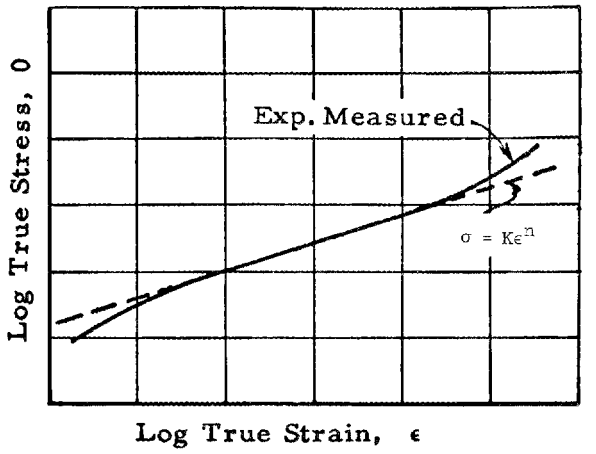

Fig. 6.48. True Tensile Stress-Strain Relation.

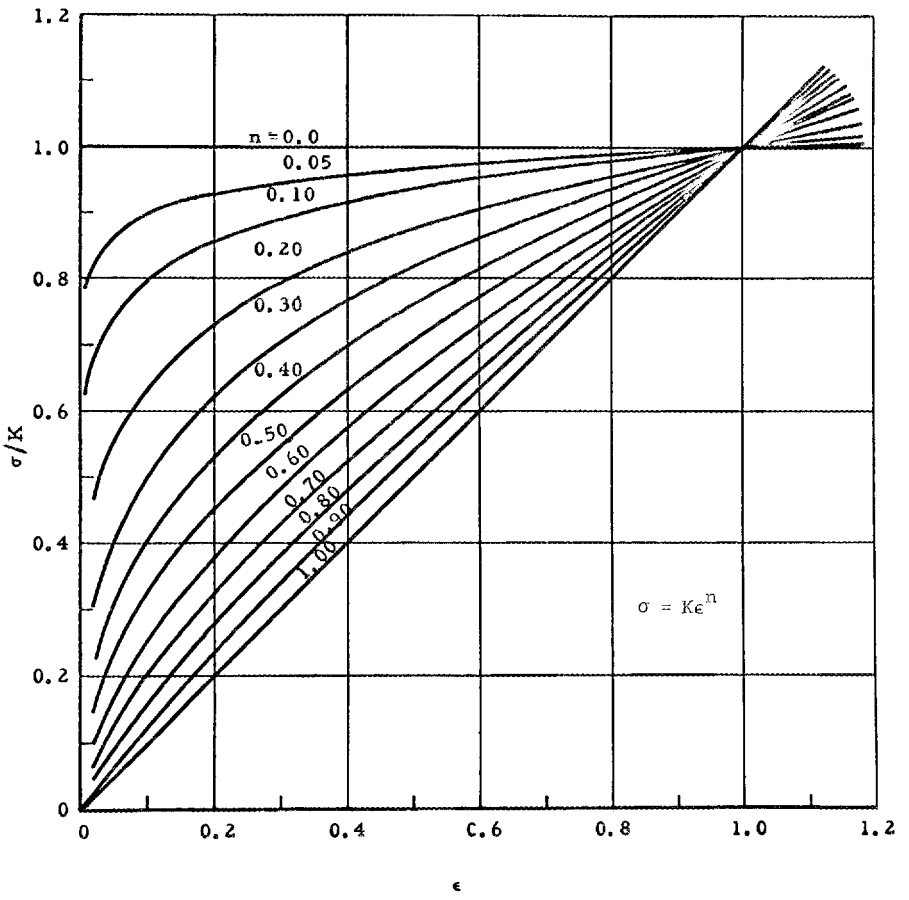

Fig. 6.49. Family of True Stress-Strain Curves for Power-Law Strain Hardening.

Table 6.13. Stress-Strain Properties in Simple Tension

Material	Ultimate True Stress (psi)	Ultimate True Strain	Constants of Power-Hardening Law, $\sigma = K\epsilon^n$		Linear-Hardening Law Values, $\sigma = \sigma_o (1 + \lambda\epsilon)$		Reference
			K	n	σ_o (psi)	λ	
A212, grade B, firebox steel	96,980	0.172	155,000	0.245	32,000	11.8	73
A295, grade C, firebox steel	76,550	0.215	117,000	0.278	27,500	8.3	73
Type 304 stainless steel	149,000	0.548	193,000	0.959	40,400	4.9	73
A302 steel	94,300	0.173	133,000	0.197	52,190	4.7	73
USS T-1 steel	141,500	0.123	178,700	0.087	119,800	1.5	73
0.15% carbon steel	74,000	0.250	108,000	0.285	32,700	5.1	73
SAE 4130 steel, annealed			169,400	0.118	106,700[a]	1.98	71
SAE 4130 steel, normalized, temper rolled			154,500	0.156	83,900[a]	2.41	71
Type 430 stainless steel, annealed			143,000	0.229	58,300[a]	3.27	71
0.05/0.07% phosphorus low-carbon steel			93,330	0.156	50,700[a]	2.44	71
Low-carbon rimmed steel, annealed			77,100	0.261	27,700[a]	4.08	71
Completely decarburized steel			75,500	0.284	24,800[a]	3.99	71

[a]Determined by 0.02 offset.

of the strain-hardening exponent. This relation is extremely versatile because the variation of n permits consideration of a wide range of stress-strain behaviors.

Stress-strain curves may also be fitted by a linear strain-hardening relation, which often leads to simplifications in analytical work. Such a relation can be written as

$$\sigma = \sigma_o(1 + \lambda\epsilon) \ , \tag{6.131}$$

where σ_o is the initial yield stress, and λ is a nondimensional hardening constant. Equation (6.131) can be adjusted to fit those portions of the actual stress-strain curve that are of interest in an analytical solution. Figure 6.50 shows the graphical representation of Eq. (6.131) for λ ranging from 0 to 12. In certain instances, for example, type 304 stainless steel (ref. 72), the linear relation provides a very close fit for all pertinent portions of the stress-strain curve (Fig. 6.51). The case $\lambda = 0$ in Eq. (6.131) corresponds to $n = 0$ in Eq. (6.130); the material behavior is then rigid plastic with yield stress $\sigma_o = K$.

The material constants σ_o and λ are given in Table 6.13. The values taken from ref. 73 were determined from the actual stress-strain curves,

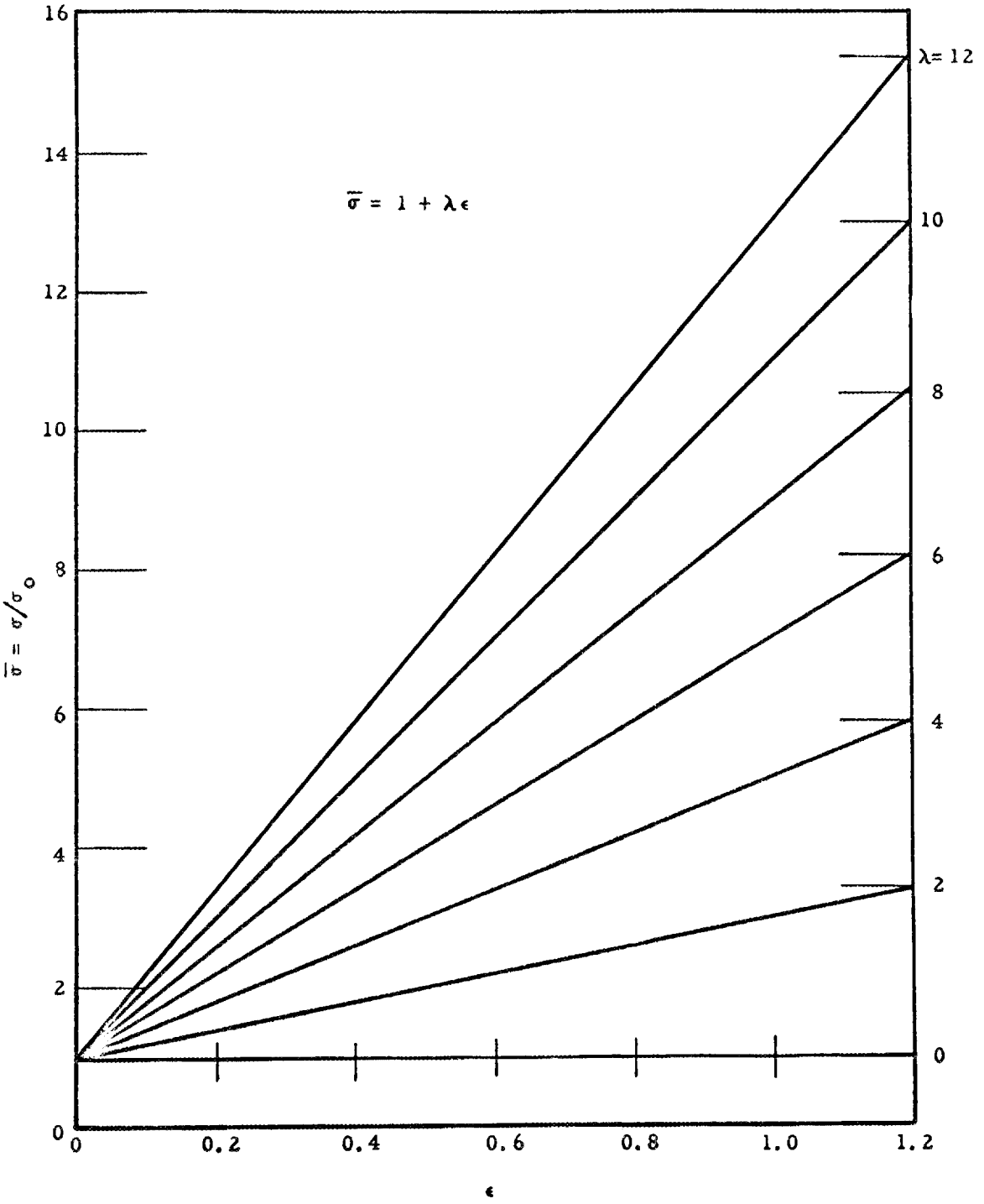

Fig. 6.50. Family of Nondimensionalized True Stress-Strain Curves for Linear Strain-Hardening Law for Various Values of λ.

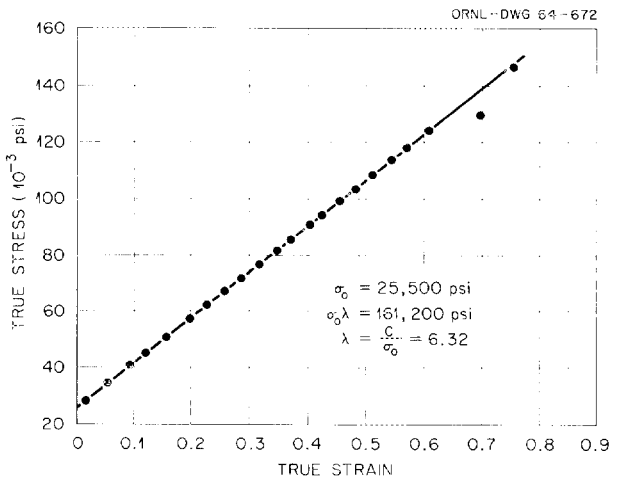

Fig. 6.51. True Stress-Strain Curve for Type 304 Stainless Steel Used in NOL Test.

whereas those from ref. 71 were found from the power-hardening law representation of the stress-strain curve. For the latter case, the initial yield stress was selected as the projection of the stress at 0.02 strain on the axis of zero strain (see Fig. 6.52).

6.5.2.3 Yield Criteria for Biaxial States of Stress

In uniaxial tension the yield stress is the limiting stress at which plastic flow occurs. For a work-hardening material the yield stress is affected by the loading that has been applied since the last annealing.

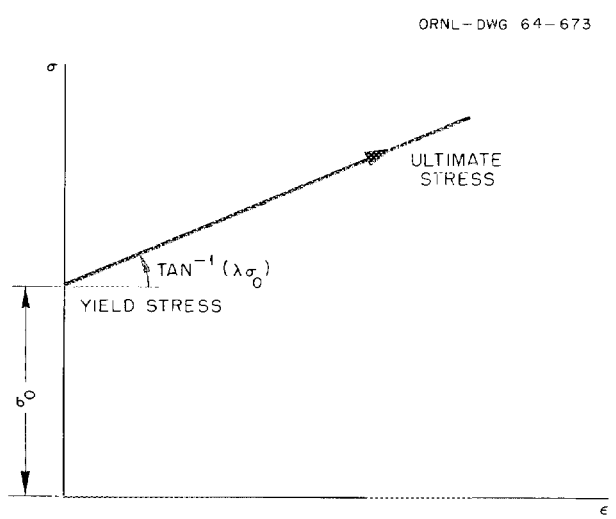

Fig. 6.52. Linear Strain-Hardening for Uniaxial Stress.

At stress levels below the yield stress, material behavior is elastic, but permanent plastic deformation is possible when the stress reaches the current yield stress.

It has been found experimentally that materials subjected to multiaxial states of stress behave elastically for certain values of the nonzero principal stresses, while at higher stress levels plastic flow occurs. If the principal stresses are denoted by σ_1, σ_2, and σ_3,* the condition that the material behave elastically can be expressed by the equation

$$f(\sigma_1, \sigma_2, \sigma_3) \leqq \sigma ,$$

where σ is the current tensile yield stress. The form of the yield function f must be based on experimental evidence. The two most commonly used theoretical yield criteria are the von Mises octahedral shear stress yield criterion

$$\tau_{oct} \leqq \sigma ,$$

and the Tresca or maximum shear stress criterion

$$(|\sigma_1 - \sigma_2|, |\sigma_2 - \sigma_3|, |\sigma_3 - \sigma_1|)_{max} \leqq \sigma .$$

For biaxial states of stress, σ_3 is always zero, and the yield criteria reduce to

$$(\sigma_1^2 - \sigma_1\sigma_2 + \sigma_2^2)^{1/2} \leqq \sigma \quad \text{(von Mises)} , \tag{6.132}$$

and

$$(|\sigma_1|, |\sigma_2|, |\sigma_1 - \sigma_2|)_{max} \leqq \sigma \quad \text{(Tresca)} . \tag{6.133}$$

For biaxial stresses, both criteria can be drawn as closed convex curves in the σ_1, σ_2 stress plane. Figures 6.53 and 6.54 (ref. 74) show a comparison between these two theoretical yield criteria and experimental data for two types of steel. Figure 6.53 shows data points at initial yielding, $\sigma = \sigma_y$, while data at ultimate load, $\sigma = \sigma_u$, are given in Fig. 6.54. Since the maximum difference between the Tresca and the von Mises yield criteria is about 15%, and since the experimental results generally fall somewhere between the two, the use of either criterion seems justified.

---

*Here the subscripts 1, 2, and 3 are used to denote direction only, and not relative magnitude.

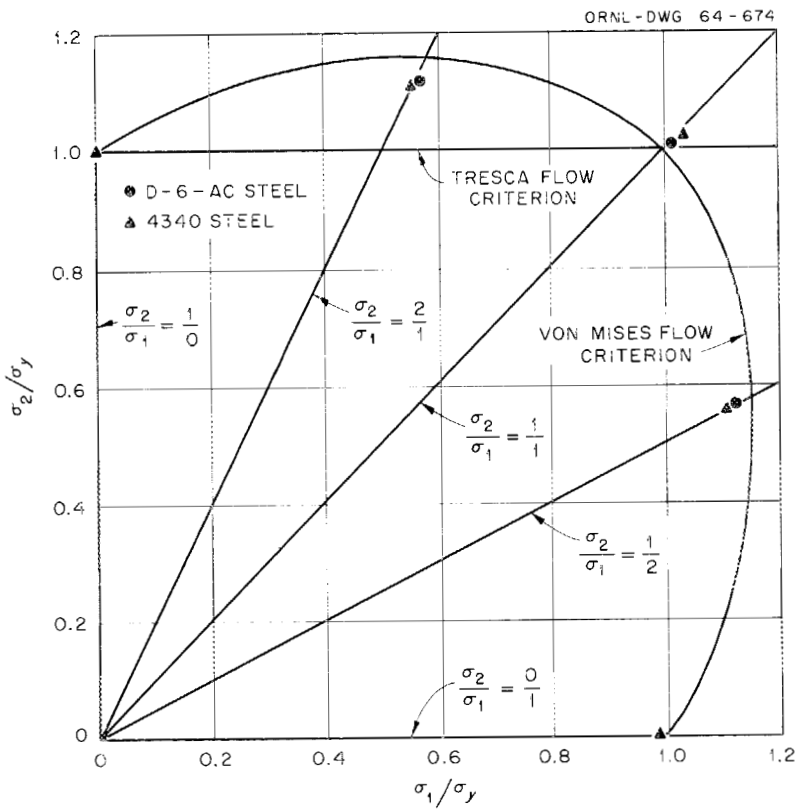

Fig. 6.53. Biaxial Yield Strength Data for Steel Cylinders.

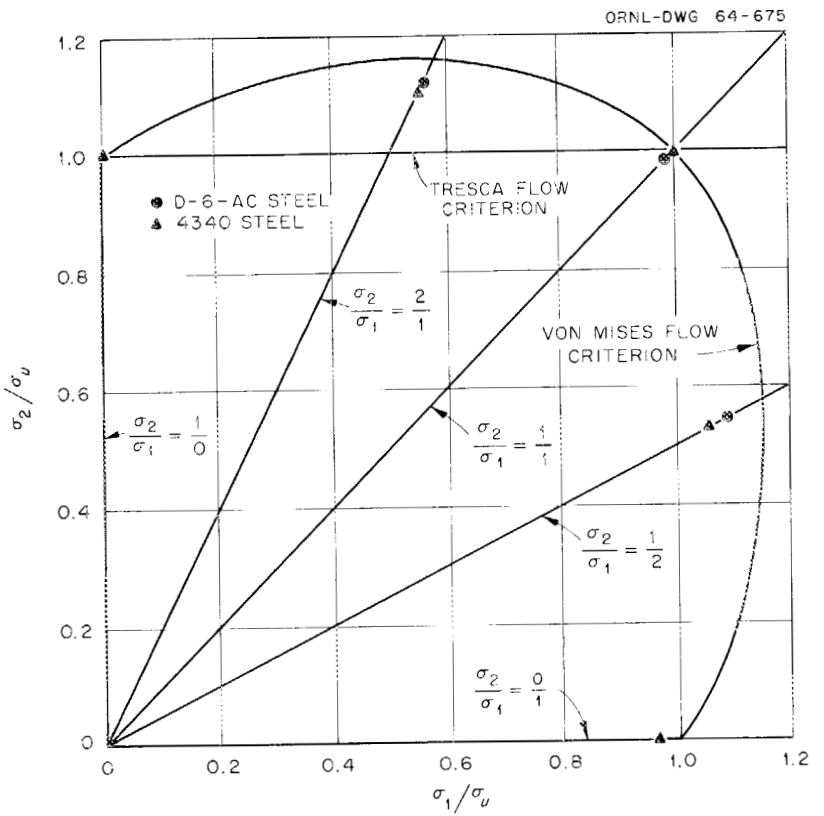

Fig. 6.54. Biaxial Ultimate Strength Data for Steel Cylinders.

6.5.2.4 Flow Rule

In plasticity, a relationship between strain rates and stresses is known as a flow rule. Flow rules are based upon the assumption of stable material, that is, the material cannot do work upon its existing loads or their increments. If a set of strain rate axes, $\dot{\epsilon}_1$, $\dot{\epsilon}_2$, $\dot{\epsilon}_3$, is superimposed on the stress axes, then the direction of the strain rate vector $\bar{\dot{\epsilon}}$, whose components are $\dot{\epsilon}_1\bar{i}$, $\dot{\epsilon}_2\bar{j}$, and $\dot{\epsilon}_3\bar{k}$, is determined by the condition of stability. The vector $\bar{\dot{\epsilon}}$ must always be directed along the outward normal to the yield surface at all points at which the slope of f is continuous and must be directed outward between adjacent normals at all points at which the slope of f is discontinuous.

It is known that the gradient vector

$$\bar{\nabla} f = \frac{\partial f}{\partial \sigma_1}\,\bar{i} + \frac{\partial f}{\partial \sigma_2}\,\bar{j} + \frac{\partial f}{\partial \sigma_3}\,\bar{k}$$

is normal to f. Therefore, the components of $\bar{\dot{\epsilon}}$ must be proportional to the components of $\bar{\nabla} f$. Thus, during plastic flow in the 1 and 2 directions, for the von Mises yield condition,

$$\frac{\dot{\epsilon}_1}{\dot{\epsilon}_2} = \frac{2\sigma_1 - \sigma_2}{2\sigma_2 - \sigma_1}\,, \tag{6.134}$$

while for the Tresca yield condition,

$$\begin{aligned} &\dot{\epsilon}_1 > 0, \quad \dot{\epsilon}_2 = 0 \quad \text{if} \quad \sigma_1 = \sigma > \sigma_2\,, \\ &\dot{\epsilon}_2 > 0, \quad \dot{\epsilon}_1 = 0 \quad \text{if} \quad \sigma_2 = \sigma > \sigma_1\,, \\ &\dot{\epsilon}_1 \geq 0, \quad \dot{\epsilon}_2 \geq 0 \quad \text{if} \quad \sigma_1 = \sigma_2 = 0\,. \end{aligned} \tag{6.135}$$

In either case the value of the third principal strain rate, $\dot{\epsilon}_3$, is determined from the condition that plastic deformation produces no volume change; that is,

$$\dot{\epsilon}_1 + \dot{\epsilon}_2 + \dot{\epsilon}_3 = 0\,. \tag{6.136}$$

This condition can be obtained directly from the general three-dimensional flow rule for any material whose yield criterion is independent of the hydrostatic component of stress by noting that $\bar{\nabla} f \cdot (\bar{i} + \bar{j} + \bar{k}) = 0$. Furthermore, Eq. (6.136) is in good agreement with experimental evidence.[75]

Only the relative magnitudes of the strain rates can be determined from Eqs. (6.134) and (6.135). In order to calculate actual strain rate magnitudes, another independent condition obtained from plastic work considerations must be used. The concept of effective strain is introduced by defining "ϵ" in terms of the current yield stress σ and the plastic

work W:

$$dW = \sigma \, d\epsilon \ . \tag{6.137}$$

Then, if the stress is some function of the effective strain (strain-hardening laws),

$$\sigma = F(\epsilon) \ , \tag{6.138}$$

and the rate at which plastic work is done can be written as

$$\dot{W} = \sigma \frac{\dot{\sigma}}{F'} \ , \tag{6.139}$$

where

$$F' = \frac{dF(\epsilon)}{d\epsilon} \ .$$

Plastic work can also be written in terms of the strain-rate components

$$\dot{W} = \sigma_1\dot{\epsilon}_1 + \sigma_2\dot{\epsilon}_2 + \sigma_3\dot{\epsilon}_3 \ . \tag{6.140}$$

Equations (6.139) and (6.140) can be equated to form the <u>condition of plastic flow</u>:

$$\sigma_1\dot{\epsilon}_1 + \sigma_2\dot{\epsilon}_2 + \sigma_3\dot{\epsilon}_3 = \sigma \frac{\dot{\sigma}}{F'} \ .$$

For biaxial states of stress ($\sigma_3 = 0$), this condition reduces to

$$\sigma_1\dot{\epsilon}_1 + \sigma_2\dot{\epsilon}_2 = \sigma \frac{\dot{\sigma}}{F'} \ . \tag{6.141}$$

The flow rule for the von Mises yield condition is obtained by substituting Eq. (6.134) into (6.141), thus

$$\begin{aligned} \dot{\epsilon}_1 &= \frac{2\sigma_1 - \sigma_2}{2\sigma} \frac{\dot{\sigma}}{F'} \ , \\ \dot{\epsilon}_2 &= \frac{2\sigma_2 - \sigma_1}{2\sigma} \frac{\dot{\sigma}}{F'} \ . \end{aligned} \tag{6.142}$$

The analogous relations for the Tresca yield are obtained using Eqs. (6.135) and (6.141); thus

$$\dot{\epsilon}_1 = \frac{\dot{\sigma}}{F'}, \quad \dot{\epsilon}_2 = 0 \quad \text{if} \quad \sigma_1 = \sigma > \sigma_2 ,$$

$$\dot{\epsilon}_2 = \frac{\dot{\sigma}}{F'}, \quad \dot{\epsilon}_1 = 0 \quad \text{if} \quad \sigma_2 = \sigma > \sigma_1 , \tag{6.143}$$

$$\dot{\epsilon}_1 + \dot{\epsilon}_2 = \frac{\dot{\sigma}}{F'} \qquad \text{if} \quad \sigma_1 = \sigma_2 = \sigma .$$

The flow laws, either Eq. (6.142) or Eq. (6.143), together with the incompressibility condition, Eq. (6.136), form the basis for incremental solutions to plasticity problems. By solving for σ_1 and σ_2 in Eq. (6.142) and substituting into Eq. (6.141), the following expression for $\dot{\sigma}$ is obtained in the case of a von Mises material

$$\dot{\sigma} = F' \frac{2}{(3)^{1/2}} (\dot{\epsilon}_1^2 + \dot{\epsilon}_1\dot{\epsilon}_2 + \dot{\epsilon}_2^2)^{1/2} . \tag{6.144}$$

Taking derivatives of both sides of Eq. (6.137) and combining the results with Eq. (6.144) gives the effective strain rate for a von Mises material

$$\dot{\epsilon} = \frac{2}{(3)^{1/2}} (\dot{\epsilon}_1^2 + \dot{\epsilon}_1\dot{\epsilon}_2 + \dot{\epsilon}_2^2)^{1/2} . \tag{6.145}$$

Then

$$\sigma = F \int \dot{\epsilon} \tag{6.146}$$

can be written as the expression relating the current yield stress to the strain history. An exact incremental solution entails the evaluation of the right-hand side of Eq. (6.146), above, at each material point throughout the deformation process. This usually requires the use of step-by-step methods of solution. In cases where the ratio of the principal stresses remains constant, Eqs. (6.134), (6.145), and (6.146) can be integrated directly to obtain the total stress-strain relations

$$\frac{\epsilon_1}{\epsilon_2} = \frac{2\sigma_1 - \sigma_2}{2\sigma_2 - \sigma_1} , \tag{6.147}$$

the original strain-hardening law

$$\sigma = F(\epsilon) \ ,$$

and the effective strain

$$\epsilon = \frac{2}{(3)^{1/2}} \left(\epsilon_1^2 + \epsilon_1\epsilon_2 + \epsilon_2^2\right)^{1/2} \ . \qquad (6.148)$$

Many solutions to plasticity problems have been obtained using these integrated stress-strain relations when, in fact, they were not applicable, that is, in cases where the ratios of the principal stresses changed during deformation. However, these so-called deformation theory solutions have often been in good agreement with experimental evidence. This combined with the fact that deformation theory solutions are almost always easier to obtain than exact incremental theory solutions has led to its wide use. Both methods are used in the analyses of the various types of shells considered in the following sections. Where possible, exact solutions are obtained, but even in these cases it is usually found necessary to employ deformation theory as well in order to obtain a sufficiently wide range of solutions.

More complete information on plasticity may be obtained from refs. 76 to 83.

6.5.2.5 Behavior of Materials Subjected to Dynamic Loading

The fact that the stress-strain behavior of most materials is affected by increased speed of deformation was recognized at an early date. Ludwik[84] included the influence of strain rate in his considerations of the resistance increases with both permanent strain and strain rate and concluded from his tests that the ultimate strength increases as the logarithm of the rate of strain.

Much of the experimental work in dynamic strength of materials is comparatively inexact and often provides only trends of the effect of strain rate on the uniaxial yield strength, uniaxial fracture strength, and final elongation of materials. Recently, experimental procedures have been devised to measure the actual uniaxial dynamic stress-strain curve. All the work indicates that the yield strength and flow stress are not independent of the rate of strain. In fact, although the plastic dynamic stress decreases with increasing temperature, the resultant of the simultaneously acting effects of strain rate and temperature experienced under the adiabatic conditions of high-speed plastic deformation of impact loads is generally an increase in plastic dynamic stress. This trend is indicated in the typical uniaxial stress-strain-strain rate graph in Fig. 6.55 (ref. 85). The plot shows compressive true stress against both true strain and true strain rate at room temperature for a 0.2% carbon steel that was cooled from 870°C.

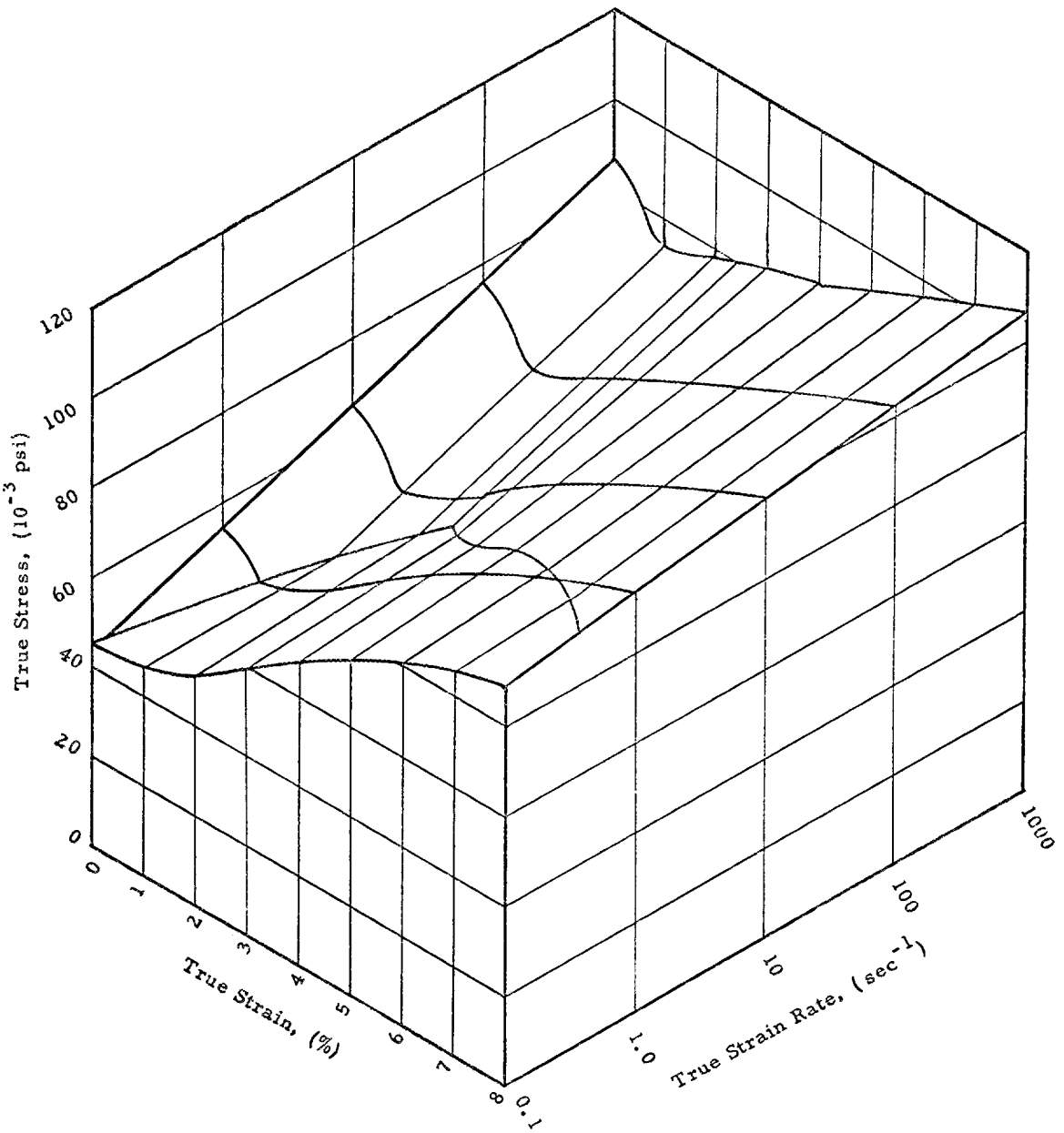

Fig. 6.55. Effect of Strain Rate on the Stress-Strain Curve for a 0.20% Carbon Steel Tested in Compression.

In the following paragraphs, the results of some experimental work on the material behavior effects of strain rates are discussed. It may be seen that these effects are dependent upon many factors, including rate of strain, material, temperature, and the type of test conducted. Also included in the following is a discussion of the correlation between effects of biaxial and uniaxial strain rates and a study of the magnitude of the strain rates that can be expected to occur in dynamically loaded spherical containment vessels.

1. Effects of Strain Rate on Material Properties

Low Rate of Strain. Conventional testing machines have been used to determine the effects of low rates of strain, for example, <1 in./in.·sec. Experiments by Puzicha and Krisch[86] show that the fracture strength and final elongation of austenitic steels decrease substantially with increasing strain rates, whereas they are known to increase or remain unaltered with increasing strain rates for carbon steels. These phenomena are illustrated in Fig. 6.56 for a typical carbon steel. In addition, very distinct increases in dynamic yield and ultimate strengths over the corresponding static strengths are shown in this figure.

Klinger[87] conducted low strain-rate tensile experiments on the high-strength steel SAE 4340 in the range from the annealed condition to a nominal ultimate strength of 220,000 psi. His results (Figs. 6.57 to 6.60)

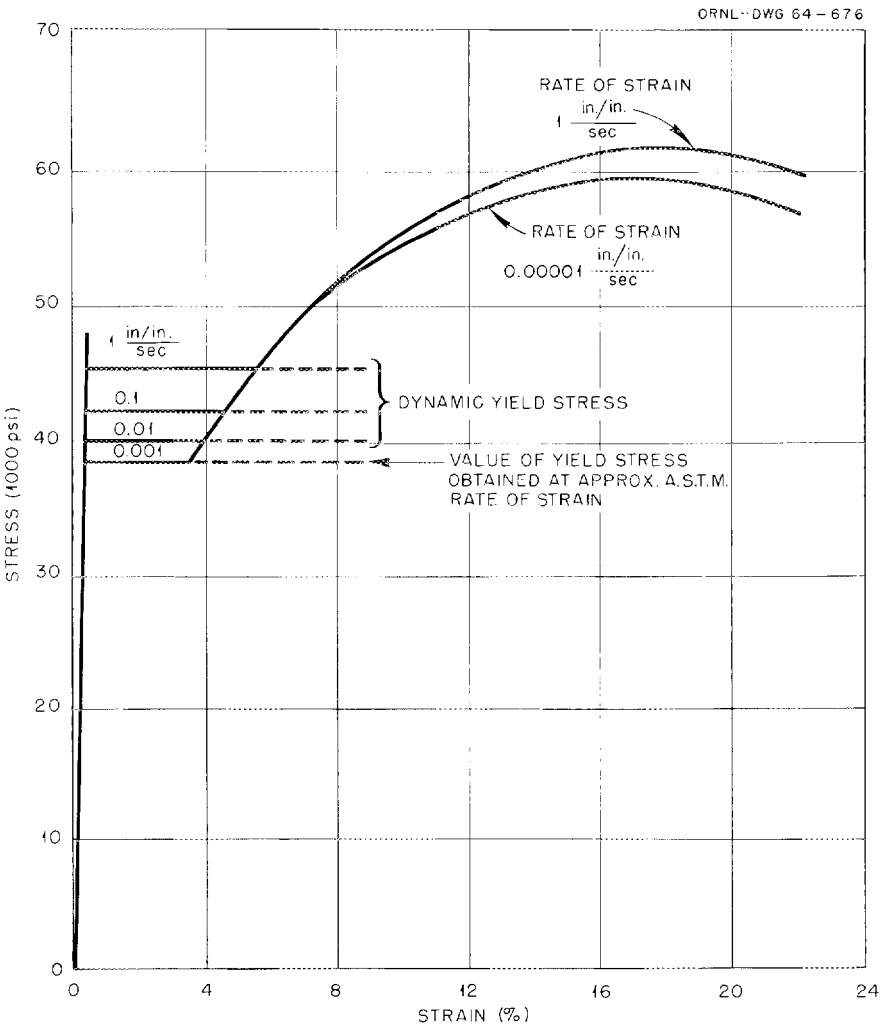

Fig. 6.56. Effect of Rate of Strain on Stress-Strain Curve for Carbon Steel.

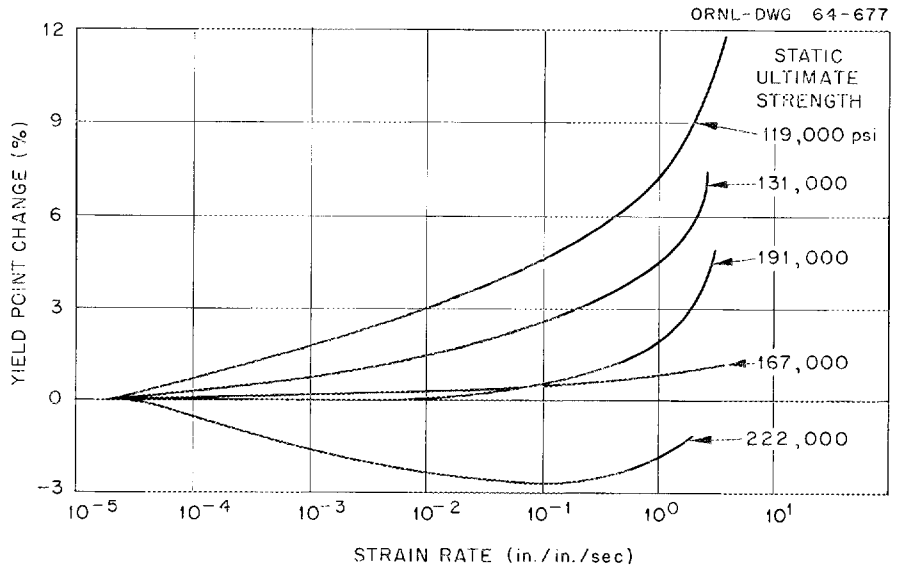

Fig. 6.57. Strain Rate Versus Change in Upper Yield Point for SAE 4340 Steel.

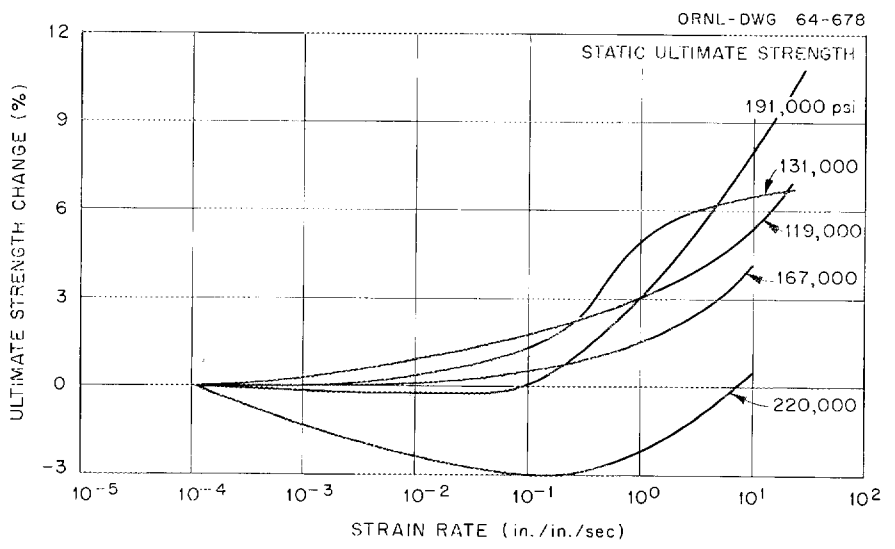

Fig. 6.58. Strain Versus Change in Ultimate Strength for SAE 4340 Steel.

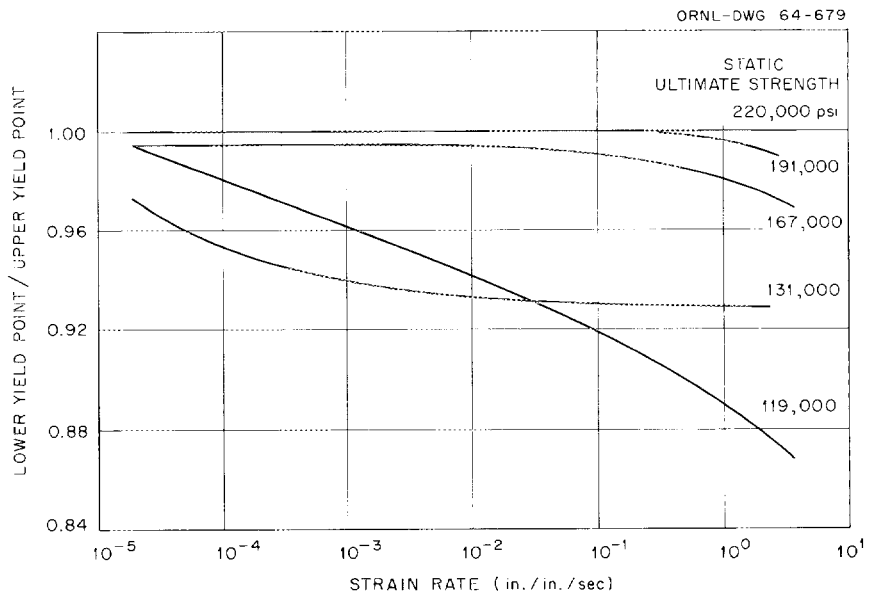

Fig. 6.59. Ratio of Lower Yield Point and Upper Yield Point Versus Strain Rate for SAE 4340 Steel.

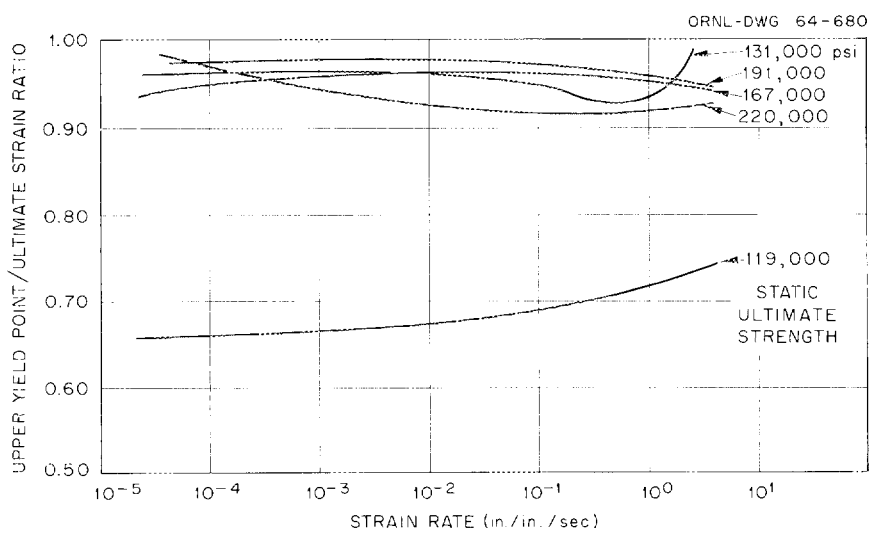

Fig. 6.60. Ratio of Upper Yield Point and Ultimate Strength Versus Strain Rate for SAE 4340 Steel.

indicate that, in general, the strength properties increase with increasing strain rate; moreover, this strain rate effect becomes markedly less as the strength level of the steel is increased. In fact, the 220,000-psi steels showed either no change or a loss in strength with increasing strain rate. No significant effect on the elongation at any strength level was noted.

Moderate Rates of Strain. For consideration of the effects of moderate strain rates, for example, up to 1000 in./in.·sec, modifications of standard testing machines must be made or different rapid-loading testing techniques developed. For example, dropping weights, Izod or Charpy pendulum machines, rotary impact machines, and explosive impact testers have all been used for this work. Since moderate "dynamic" conditions are usually associated with a wide spectrum of loading times and because there are limitations on individual testing methods, it is often necessary to apply several techniques to investigate completely the response of the loading-time range for a given specimen.

Stress-strain diagrams for moderate rates of strain were first determined by investigations of Manjoine and Nadai[88] and of Clark.[89] Both these works covered the range of strain rates from 100 to 1000 in./in.·sec. Manjoine and Nadai used a rotary impact machine and instrumentation yielding a force-elongation diagram on a cathode-ray oscillograph. The relative motion between the heads of the testing machine was used to indicate strain and strain rate. The stress on the specimen was indirectly determined by measuring the load on a load gage. Materials tested were copper, aluminum, and mild steel. Clark used the same instrumentation but did his work with an Izod pendulum.

Clark and Duwez[90] have pointed out that when the speed of deformation becomes too high, as may be the case for tension impact tests, the effect of wave propagation must be taken into account. Under these conditions an appreciable change of stress occurs during the time required for a small increment of strain to propagate throughout the specimen. This results in a strain rate that is not uniform along the specimen and makes it difficult to determine realistic strain rate effects. To eliminate the effect of wave propagation from their tests, Clark and Duwez used a hollow cylindrical specimen in which a circumferential strain was induced by internal fluid pressure. Their tests indicated the effect of strain rates as high as 200 in./in.·sec for specimens made of carbon steel, low-carbon manganese steel, and nickel-chromium steel. The ultimate strength for different rates of strain was determined from stress-time records. In the lower range of strain rates, it was possible to obtain an approximate evaluation of the proportional limit. The results shown in Figs. 6.61, 6.62, and 6.63 appear to indicate that the proportional limit increases with increasing nominal strain rate until it coincides with the nominal ultimate strength of the metal at rates in the neighborhood of 70 in./in.·sec. The ultimate strength increases until a strain rate of about 200 in./in.·sec is reached. This increase of ultimate strength is of the order of 45% for the carbon steel and about 30% each for the manganese and nickel-chromium steel.

Similar trends for the effect of moderate strain rates have been secured in tension impact tests. Baron[91] used such tests to obtain stress-strain curves for a number of steels at strain rates between 80 and 210 in./in.·sec. His results, presented for steels with the composition and

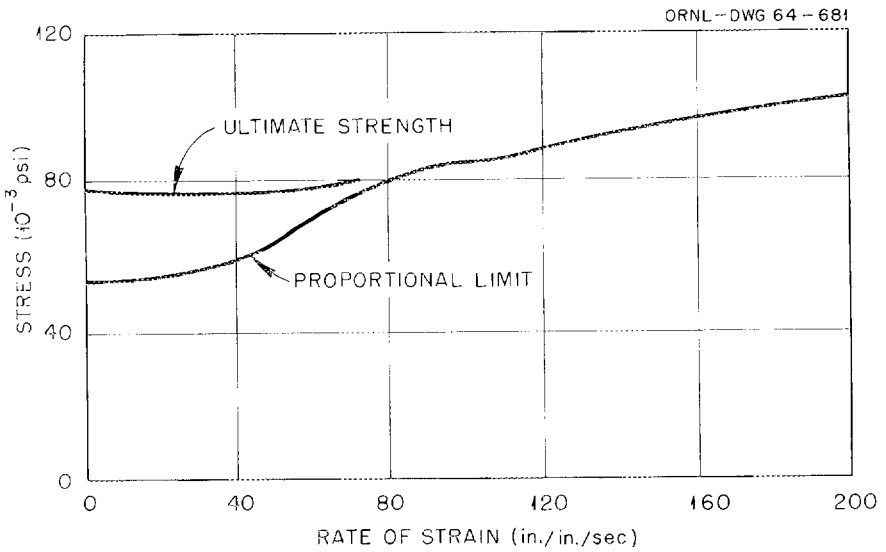

Fig. 6.61. Ultimate Strength and Proportional Limit Versus Rate of Strain for Low-Carbon Manganese Steel.

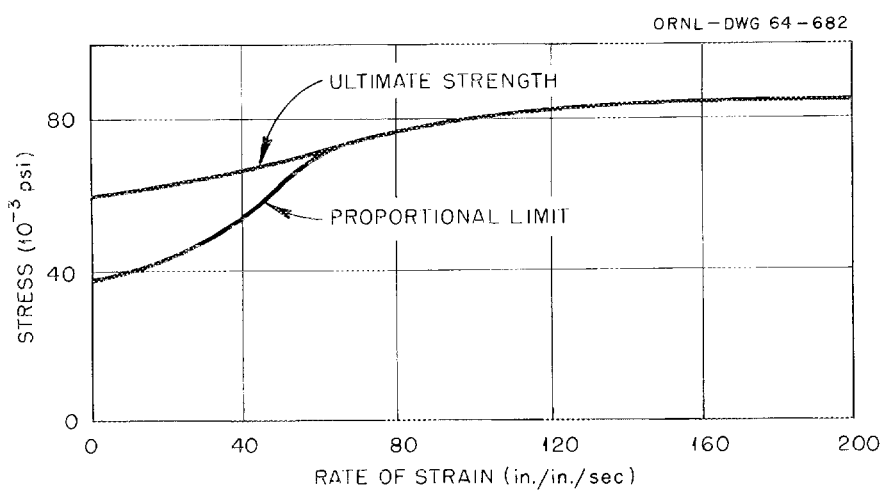

Fig. 6.62. Ultimate Strength and Proportional Limit Versus Rate of Strain for Carbon Steel.

heat-treatment details listed in Table 6.14, are shown in Fig 6.64. These graphs illustrate the contrasting dynamic responses of various steels. In particular, the curves indicate that the dynamic tensile fracture strengths of both carbon and austenitic stainless steels remain approximately the same as the static fracture strength. The elongation at fracture of a carbon steel appears to be independent of strain rate, whereas that for

Table 6.14. Composition and Heat-Treatment Details

Material	B.S. Specification	Analysis (%)									Condition
		C	Si	Mn	S	P	Ni	Cr	Mo	Nb	
Mild steel	En2A	0.20	0.01	0.52	0.031	0.041	0.03	0.06	0.01		Normalized at 900°C, annealed
0.34% carbon steel	En12	0.34	0.09	0.82	0.036	0.053	0.07	0.07	0.02		Hardened at 900°C, water quenched; tempered at 650°C; annealed
2.5% Ni-Cr-Mo steel A	En25	0.32	0.24	0.66	0.024	0.017	2.55	0.71	0.66		As received; hot rolled and tempered
2.5% Ni-Cr-Mo steel B	En25	0.30	0.24	0.62	0.014	0.024	2.53	0.65	0.62		Hardened at 830°C, oil quenched; tempered at 600°C; annealed
Stainless steel	En58	0.07	0.58	0.59	0.011	0.050	8.31	18.56	0.20	0.15	As received; softened and roller straightened

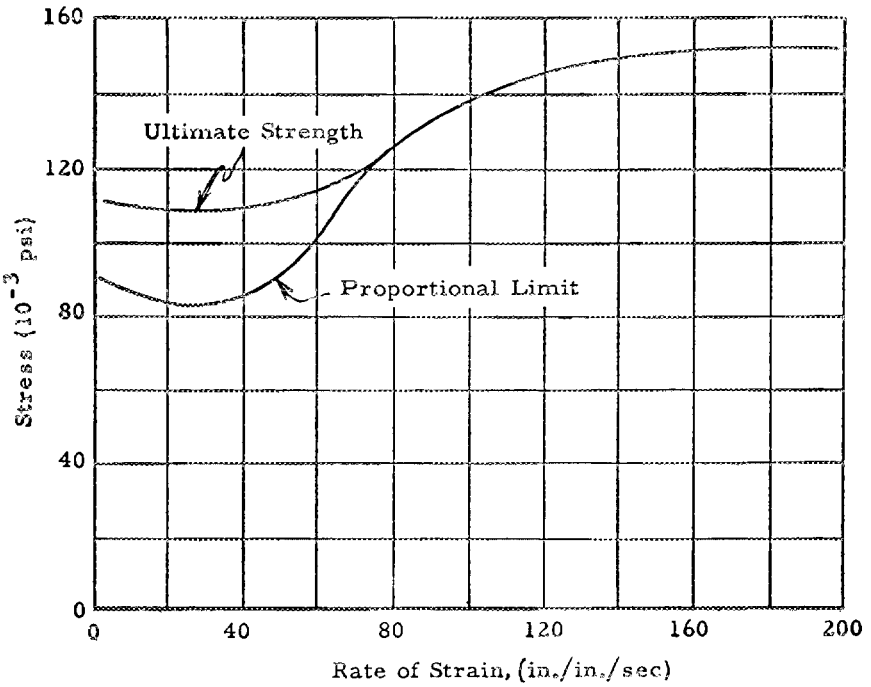

Fig. 6.63. Ultimate Strength and Proportional Limit Versus Rate of Strain for Nickel-Chromium Steel.

austenitic stainless steels decreases with an increase in strain rate. Both steels display a considerable increase in yield stress for increasing strain rate. Although the ultimate strength of the carbon steel shows a sizable increase as the strain rate is increased, the ultimate strength of the austenitic stainless steel remains unaffected.

As can be observed in Figs. 6.64(a,b), certain steels support extremely high dynamic loads elastically for a short time prior to yielding. This is the so-called "delay-time" effect for yield initiation. Campbell and Duby[92] found that mild steels subjected to impact loads yielded at a stress about 2 1/2 times the static upper yield stress. Medium carbon steels also display considerable delay-time effect.

High Rates of Strain. Austin and Steidel[93] developed a method for determining the dynamic tensile properties of materials at very high rates of strain (up to 22,000 in./in.·sec). They concluded, among other things, that the dynamic strength and ductility of SAE 1018 cold-rolled steel increase with increasing strain rate at room temperature. Their work was carried out on an explosive-impact tension tester which had provisions for direct measurement of load, impact velocity, and instantaneous changes of diameter as a function of time. A charge of gun powder was used to propel a projectile that was threaded to one end of a standard tension specimen; the other end was fixed. Their results (Fig. 6.65) indicate that the dynamic ultimate and fracture strengths of SAE 1018 cold-rolled steel increase continuously with increasing strain rates up to 22,000 in./in.·sec. Also, the percent reduction of area and percent elongation show that the

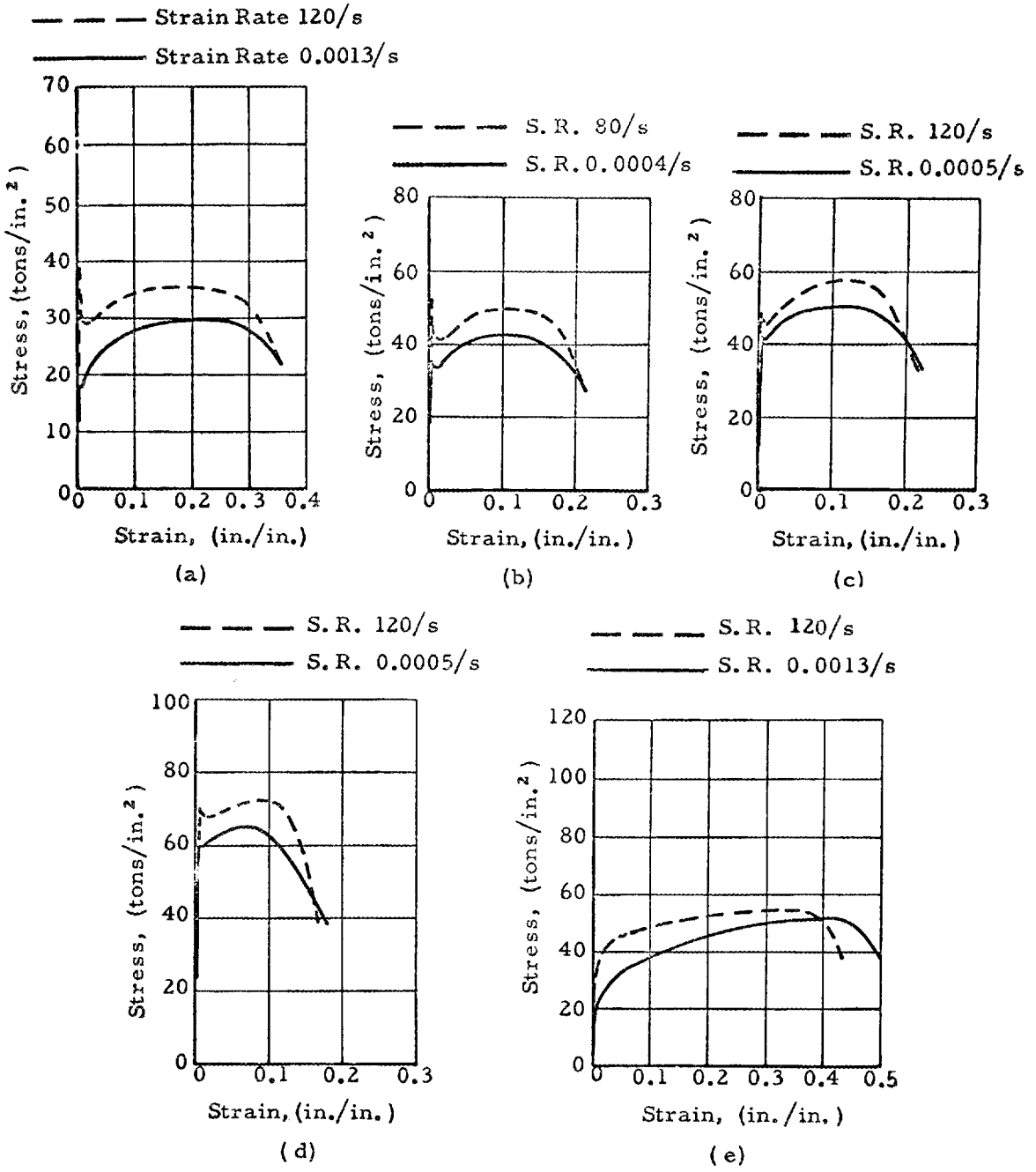

Fig. 6.64. Static and Dynamic Stress-Strain Curves at 20°C for (a) Normalized Mild Steel, (b) 0.34% Carbon Steel, (c) 2.5% Ni-Cr-Mo Steel A, (d) 2.5% Ni-Cr-Mo Steel B, and (e) Austenitic Stainless Steel.

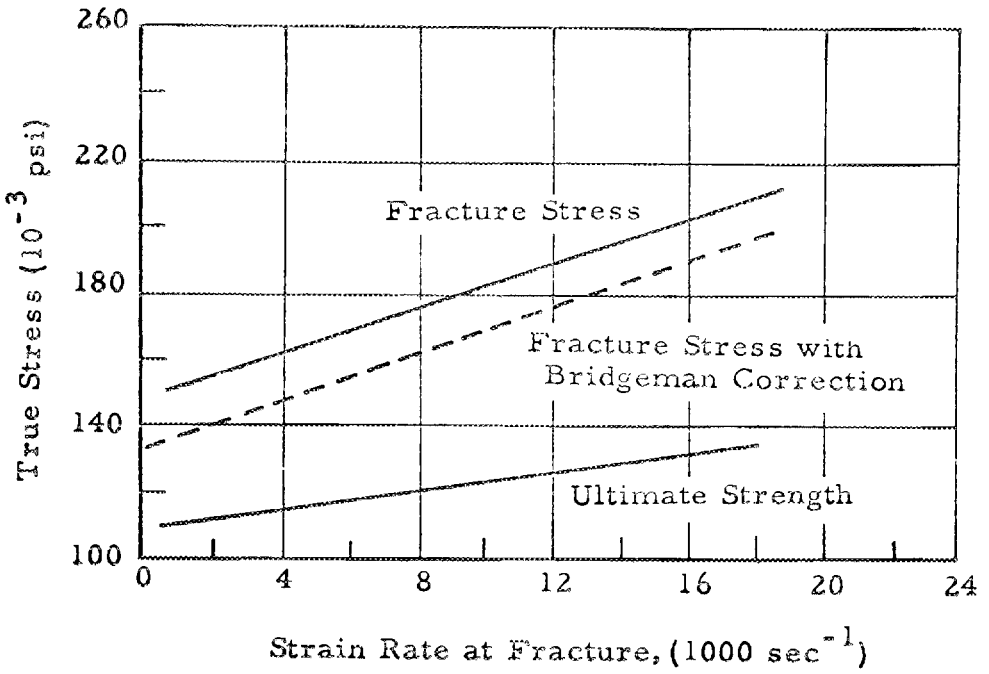

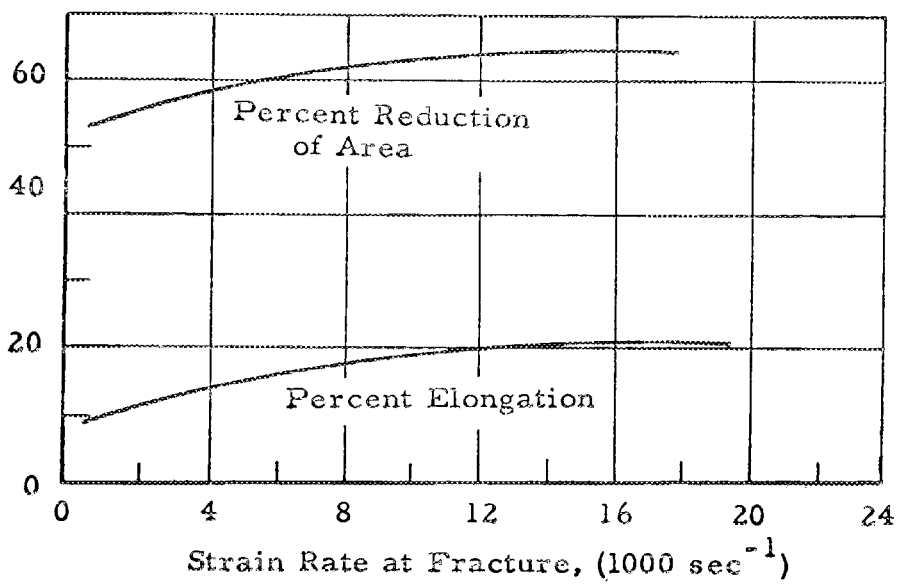

Fig. 6.65. Results of Explosive Impact Tests at Room Temperature on SAE 1018 Cold-Rolled Steel.

ductility increases with the strain rate but tends to approach a constant value at the higher rates.

Effects of Strain Rates in Biaxial States of Stress. The current state of knowledge of the effects of strain rates on the properties of steels under biaxial states of stress is rather limited. The correspondence between static uniaxial and static biaxial states of stress would seem to indicate that the trends shown in uniaxial dynamic tests are also applicable to biaxial states of stress.

Summary. As is shown in a following section, it is probable that low and moderate strain rates will be induced in the dynamically loaded containment vessels under consideration. It is evident from the investigations described in the previous sections that the stress-strain behavior of most steels is not independent of either low or medium strain rates. Hence, some allowance should be made for increases in both yield and ultimate stresses to account for the effects of strain rates.

In general, both the yield and ultimate stresses increase with increasing strain rate for steels; however, often the ultimate strength increases to a lesser extent than the yield stress until, at moderate rates of strain, the two are equal. In such a case the material behaves almost in a rigid plastic manner. These effects are particularly pronounced for mild, carbon, manganese, and nickel-chromium steels, where the ultimate strength and proportional limit coincide at strain rates of about 70 in./in.·sec. In the case of austenitic stainless steels, both the yield and ultimate strengths increase for low and moderate strain rates, whereas the fracture strength decreases. The strain rate effect on the stress-strain relation for heat-treated high-strength steels is relatively small, and the assumption of strain rate independence as a first approximation in analytical work appears to be sound.

2. Determination of Strain Rates for a Sphere

The magnitude of the strain rates involved in dynamically loaded containment vessels must be determined to ascertain the effects of strain rate on the stress-strain behavior of the vessel material. These effects, in turn, are used to alter parameters in the strength analysis of the vessel.

Strain rates for a sphere can be estimated with sufficient accuracy on the basis of a consideration of the response of a simple mass-spring system subjected to an initial peak triangular pulse loading. For a system with a constant restoring force, the equations of motion are

$$m\ddot{x} + R = F_o \left(1 - \frac{t}{t_o}\right) \text{ for } 0 \leq t \leq t_o \tag{6.149}$$

and

$$m\ddot{x} + R = 0 \text{ for } t_o < t \ , \tag{6.150}$$

where

x = displacement,
m = mass of the system,
R = constant restoring force,
F_o = peak force of the pulse,
t_o = pulse duration.

The maximum velocity occurs when the applied load has decreased to the value of the restoring force and is given by the formula

$$\frac{mv_m}{Rt_o} = \frac{1}{2}\,\frac{(q-1)^2}{q}\,, \tag{6.151}$$

where

v_m = maximum velocity,
$q = F_o/R$ = ratio of the peak applied force to the constant restoring force.

The maximum displacement x_m is related to the pulse duration t_o and the pressure ratio q by the formulas

$$\frac{2mx_m}{Rt_o^2} = \frac{4}{3}\,\frac{(q-1)^3}{q^2} \text{ if } q < 2 \tag{6.152}$$

and

$$\frac{2mx_m}{Rt_o^2} = \frac{1}{12}\,q(3\,q-4) \text{ if } q > 2\,. \tag{6.153}$$

For given values of maximum displacement and pulse duration, Eqs. (6.151), (6.152), and (6.153) determine the value of the maximum velocity and, hence, the maximum strain rate.

In the case of a rigid perfectly plastic sphere under internal pressure, the equations of motion corresponding to Eqs. (6.149) and (6.150) are

$$\gamma H_i\ddot{R} + \frac{2\sigma_o H_i}{R_i} = P_d\left(1 - \frac{t}{t_o}\right) \text{ for } 0 \leq t \leq t_o \tag{6.154}$$

and

$$\gamma H_i \ddot{R} + \frac{2\sigma_o H_i}{R_i} = 0 \quad \text{for } t_o < t \ , \tag{6.155}$$

where

P_d = peak pressure,
H_i = initial thickness of the sphere,
R = radius of the sphere,
R_i = initial radius of the sphere,
γ = mass density of the shell material,
σ_o = yield stress.

Equations (6.154) and (6.155), which are obtained by equilibrium of forces on the sphere, neglect the effects of shell thinning. The circumferential (and meridional) strain is expressed in terms of the displacement by the equation

$$e_c = \frac{R - R_i}{R_i} \ .$$

Equations (6.151), (6.152), and (6.153) now become, for the case of the sphere,

$$\begin{aligned} \frac{\gamma R_i^2 \, (e_c)_{max}}{\sigma_o t_o^2} &= \frac{4}{3} \frac{(\overline{P}_d - 1)^3}{\overline{P}_d^2} \quad \text{if} \quad \overline{P}_d < 2 \\ &= \frac{1}{12} \overline{P}_d \, (3 \, \overline{P}_d - 4) \quad \text{if} \quad \overline{P}_d > 2 \end{aligned} \tag{6.156}$$

and

$$\frac{\gamma R_i^2 \, (\dot{e}_c)_{max}}{\sigma_o t_o} = \frac{(\overline{P}_d - 1)^2}{P_d} \ , \tag{6.157}$$

where

$(e_c)_{max}$ = maximum circumferential strain,
$(\dot{e}_c)_{max}$ = maximum circumferential strain rate,
$\overline{P}_d = P_d R_i / 2\sigma_o H_i$ = ratio of the peak applied pressure to the static pressure required to cause failure.

For a given value of the maximum strain, Eqs. (6.156) and (6.157) can be used to determine the maximum strain rate. Graphs of these equations are given in Fig. 6.66. The dotted lines show the procedure for obtaining the value of $(\dot{\epsilon}_c)_{max}$ for specified values of the quantity

$$\frac{\gamma R_i^2 \, (e_c)_{max}}{\sigma_o t_o^2} .$$

To get some idea of the order of magnitude of the strain rates in spherical shells under transient loading, consider a steel sphere ($\gamma = 0.7323 \times 10^{-3}$ lb-sec/in.^{4}) with a diameter of 100 ft. For a maximum allowable strain of 0.05 and a yield stress of 50,000 psi the relations in Table 6.15 are obtained. In the right-hand column of the table, maximum thickness strain rates $(\dot{\epsilon}_t)_{max}$ are listed. For an incompressible material $(\dot{\epsilon}_t)_{max} = 2(\dot{\epsilon}_c)_{max}$.

Table 6.15. Strain Rates in Spherical Shells Under Transient Loading

Pulse Duration, t_o(sec)	Pressure Ratio, $\bar{P}_d$	Maximum Circumferential Strain Rate, $(\dot{\epsilon}_c)_{max}$ (in./in.·sec)	Maximum Thickness-Strain Rate, $(\dot{\epsilon}_t)_{max} = 2(\dot{\epsilon}_c)_{max}$
0.005	7.20	5.03	10.06
0.01	3.95	4.27	8.54
0.10	1.325	1.52	3.04
0.40	1.115	0.91	1.82

Clearly these strain rates can be classified as low or moderate, and hence the stress-strain behavior of the material will not differ significantly from that under static loading. For a particular material, Figs. 6.56 to 6.65 can be employed to estimate the increases, if any, in the yield and ultimate strengths.

Equations (6.156) and (6.157) show the effect of scale. That is, for fixed values of the pressure ratio and maximum strain, the strain rates, as well as the pulse duration, vary inversely with the radius. Thus, the strain rates would be twenty times as large for a sphere 5 ft in diameter, and the material properties might differ substantially from those under static load.

In summary, the results of the simplified analysis given above indicate that the effects of transient loading on material properties will be,

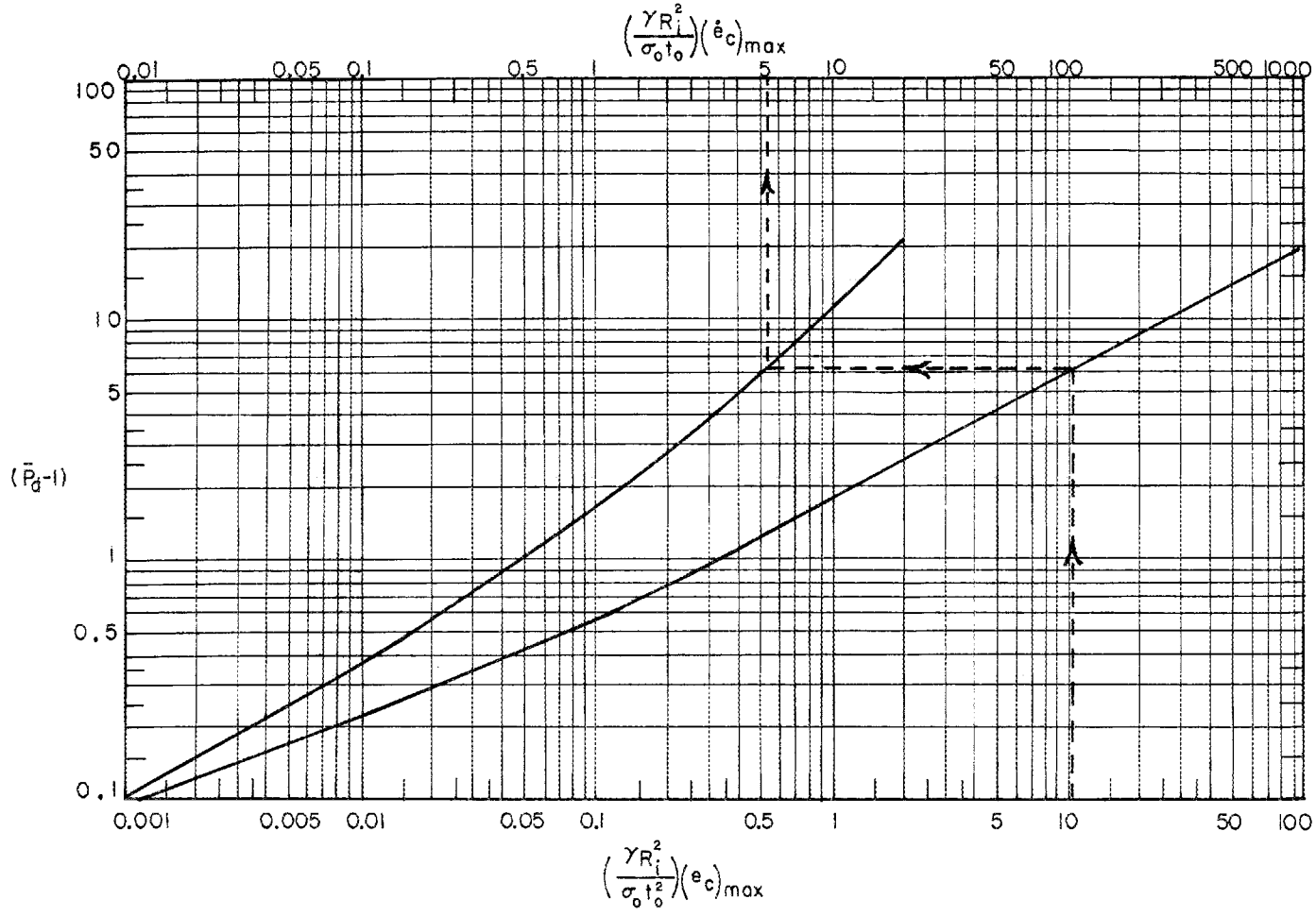

Fig. 6.66. Maximum Strain and Maximum Strain Rate Relation for a Sphere Under Internal Loading — Approximate Analysis.

in most instances, small for large spheres but may be quite important in small spheres or in small-scale test structures.

6.5.3 Static Plastic Strength of Thin Cylindrical Shells with Various End Closures Under Internal Pressures

The plastic strength of thin shells under internal pressure is of interest to the designer in those cases in which the structure is intended to withstand only a single application of the design load.

In the analysis of the deformation of thin shells under slowly applied internal pressure, the assumptions are made that the elastic strains and the bending strength of the shell can be neglected, since their effects are negligible at large strains. The shell is therefore assumed to act as an ideal membrane, and the shell material is assumed to be a rigid strain-hardening plastic solid. In the following, comparisons of exact theoretical solutions with test results are made for cylinders with rigid ends; approximate solutions for cylinders with rigid ends or hemispherical caps are developed and the results compared with available exact theoretical solutions and test results.

6.5.3.1 Comparison of Exact Solutions with Test Results

Exact solutions for the sphere and the infinite cylinder are available in the form of simple algebraic equations relating the pressure to radial displacement. Cylindrical shells of finite length are stronger than cylinders of infinite length but weaker than spherical shells. Exact solutions for cylindrical shells of finite length with rigid end closures, the geometry of which is shown in Fig. 6.67(a), have recently been obtained,[66,122] and much simpler approximate solutions to the same problem have been developed.[66] This approximate solution has also been extended[66] to apply to cylinders with two hemispherical heads, Fig. 6.68(a), and to cylinders with one rigid end cap and one hemispherical head, Fig. 6.69.

A series of tests[123] on small cylinders (8 in. diam, 0.100-in. wall) with these three types of end conditions has also been carried out to test the accuracy of the theories. The test specimens were of low-carbon steel (ASTM A 53-B) and were annealed dead soft after machining. The tensile test data for this material are shown in Fig. 6.70. The yield stress is 35,000 psi, and the ultimate strength is 56,000 psi. The power law of strain hardening

$$\sigma = K\epsilon^n \tag{6.158}$$

is seen to fit the data fairly well with the values $K = 108$ kips/in.^{2} and $n = 0.277$. Comparisons of the results of the tests of cylinders with rigid ends with the exact theories cited above are given in Figs. 6.71 through 6.75 for a range of values of the length-to-diameter ratio l. Values of the nominal circumferential stress, PR_i/H_i, are given for the range of dimensionless radial displacements, $r_1 - 1$, where P is the internal

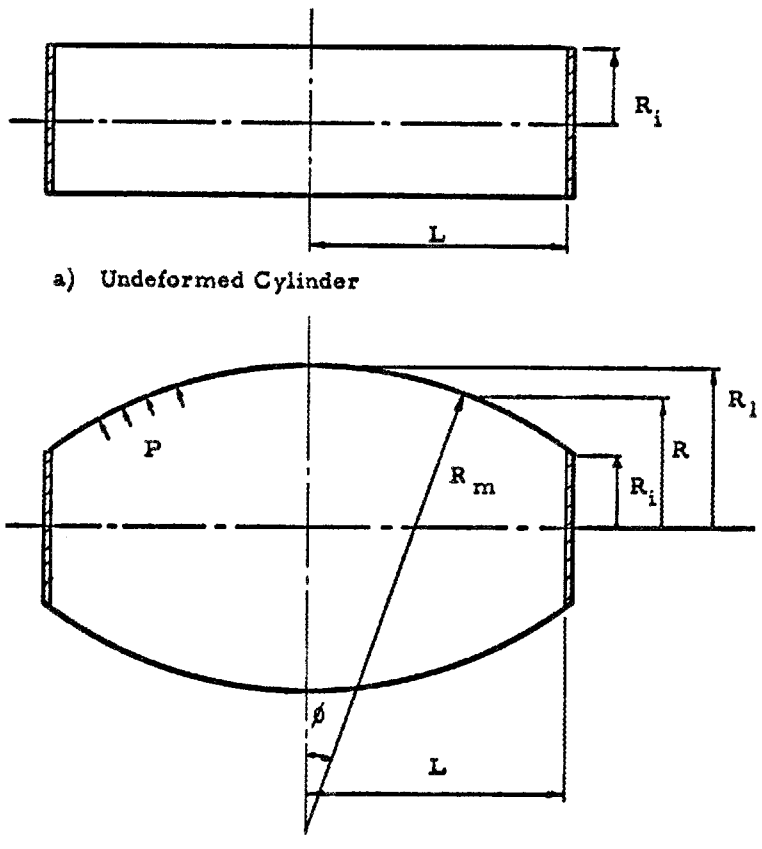

Fig. 6.67. Assumed Deformed Profile of Cylinder with Two Rigid Ends.

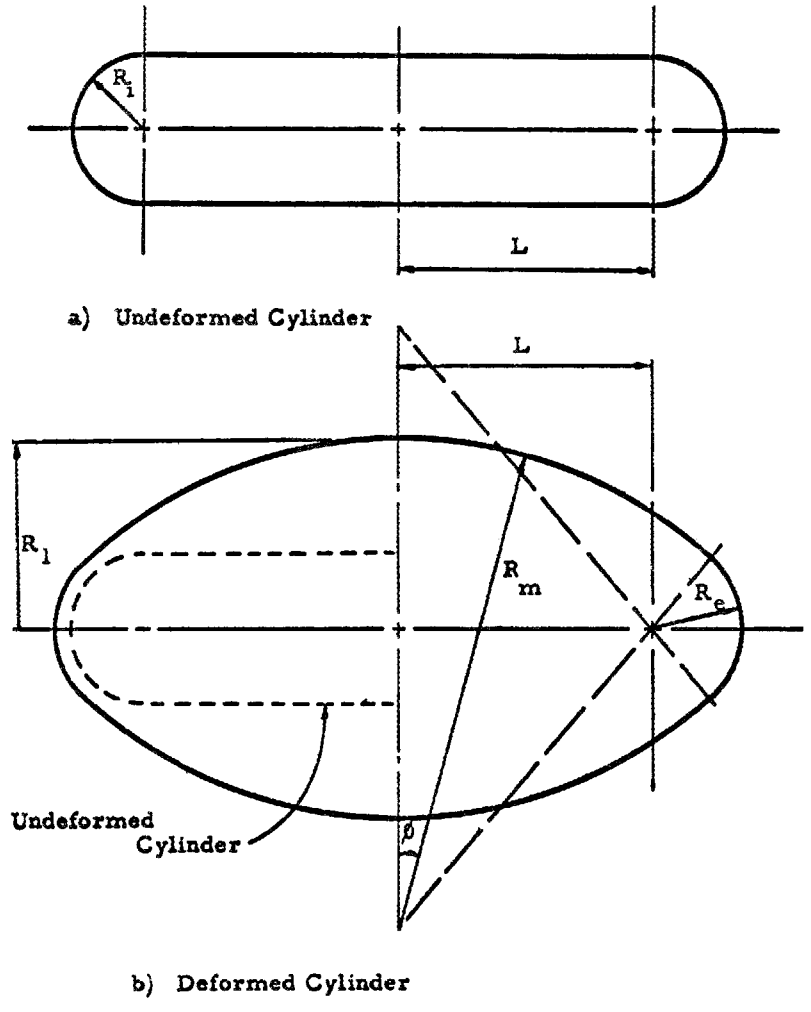

Fig. 6.68. Assumed Deformed Profile of Cylinder with Two Hemispherical Caps.

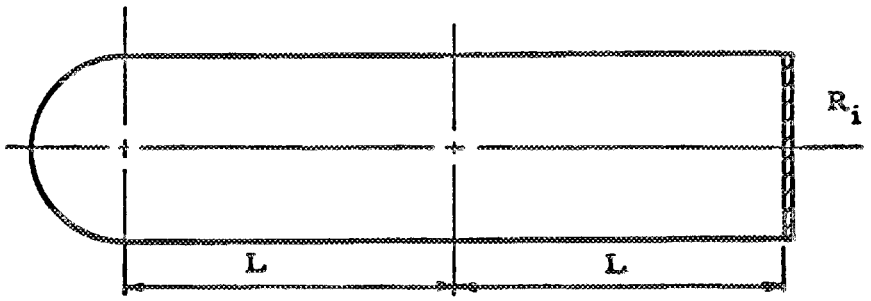

(a) Undeformed Cylinder

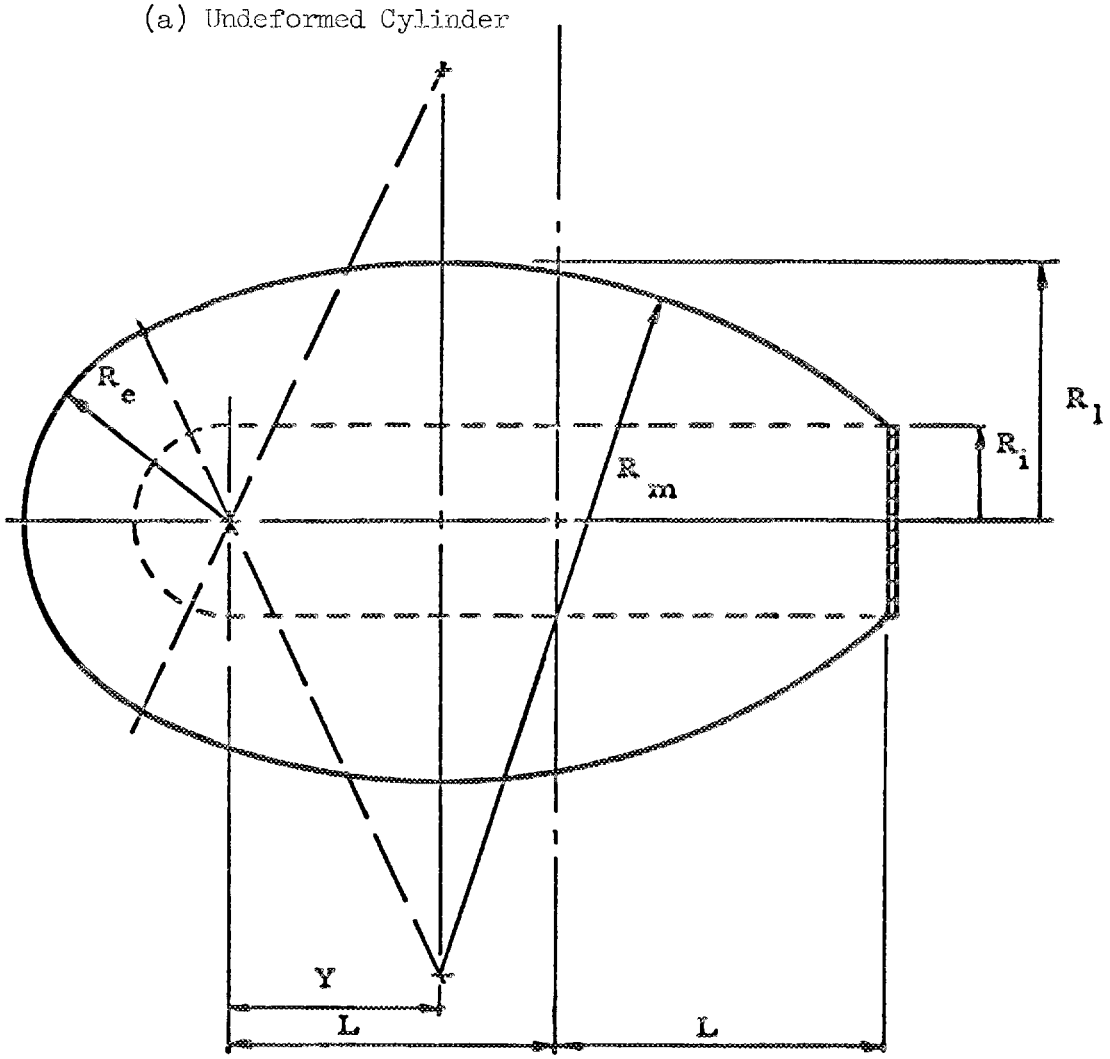

(b) Deformed Cylinder

Fig. 6.69. Assumed Deformed Profile of Cylinder with One End Rigid and One Hemispherical Cap.

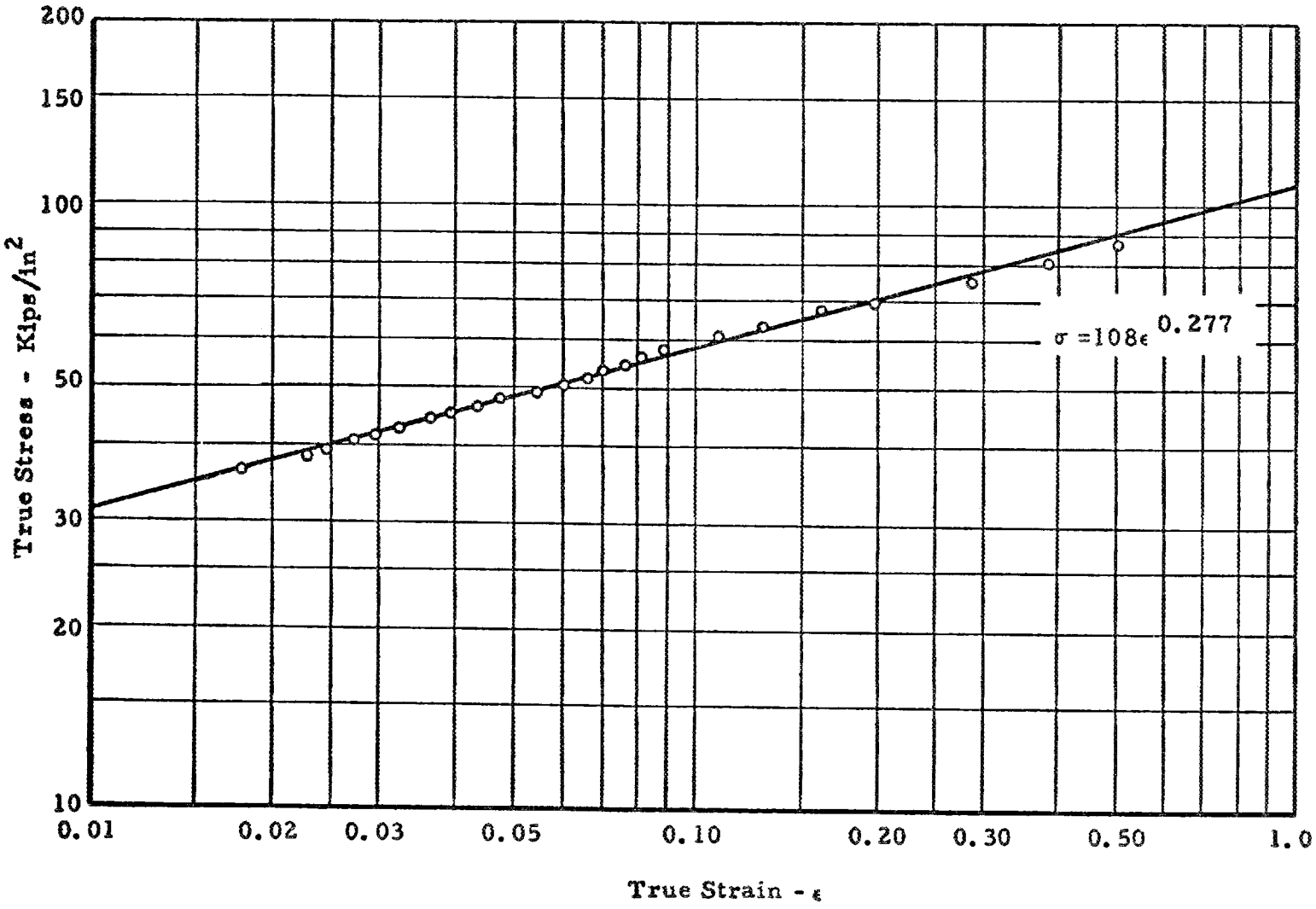

Fig. 6.70. Tensile Test Data for Mild Steel Circumferential Coupon.

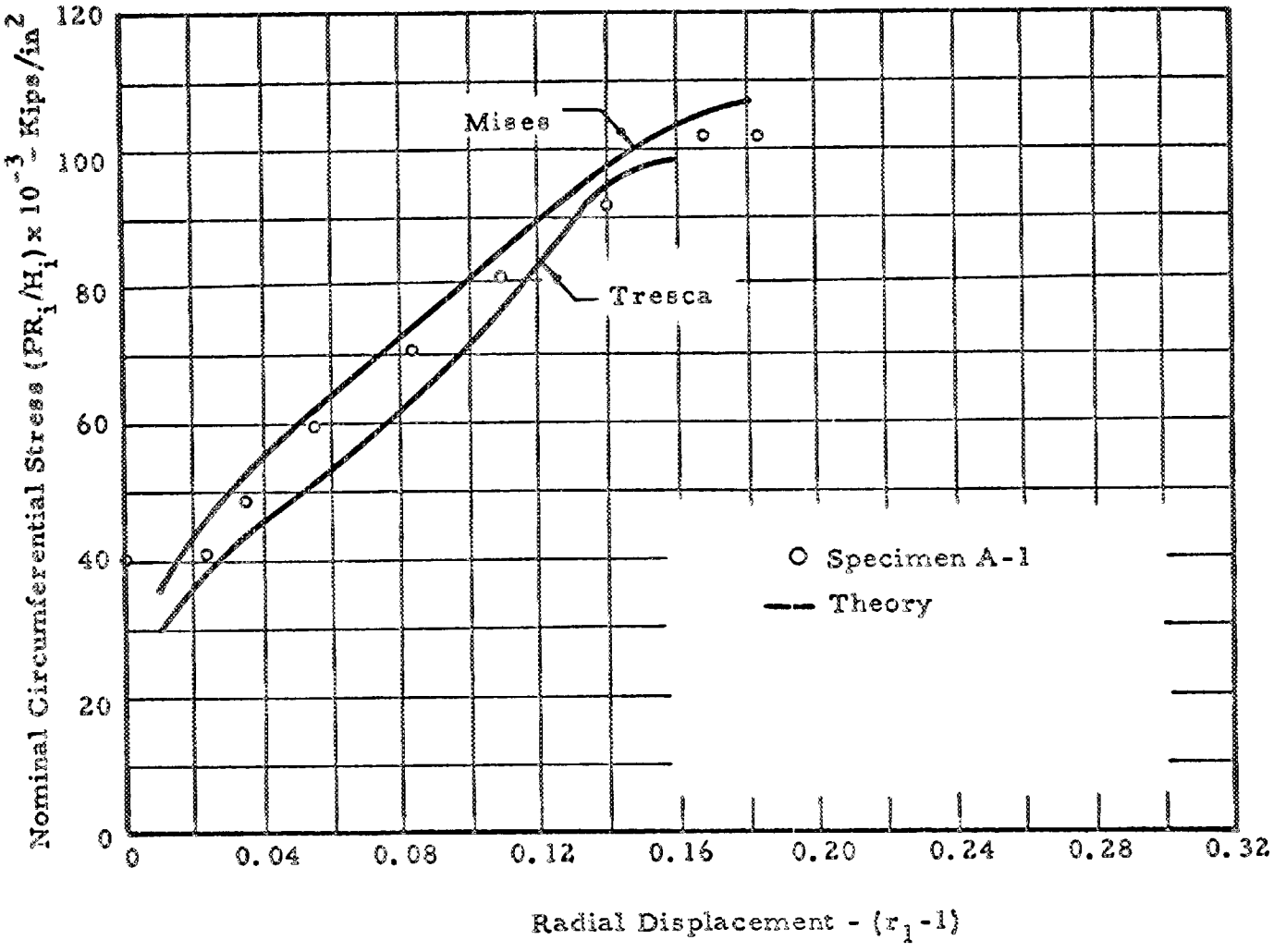

Fig. 6.71. Test Results for Mild Steel, l = 0.547.

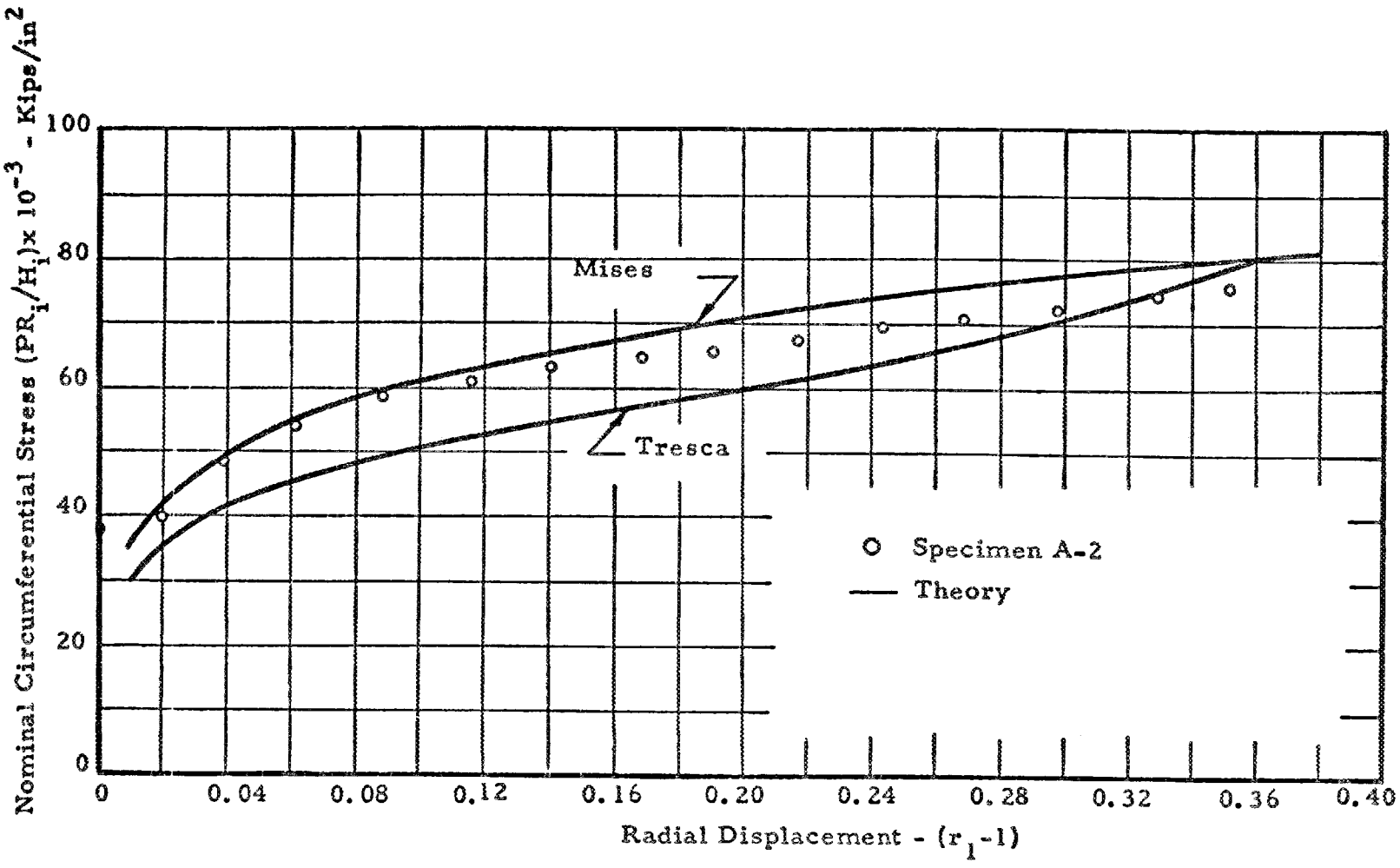

Fig. 6.72. Test Results for Mild Steel, l = 1.02.

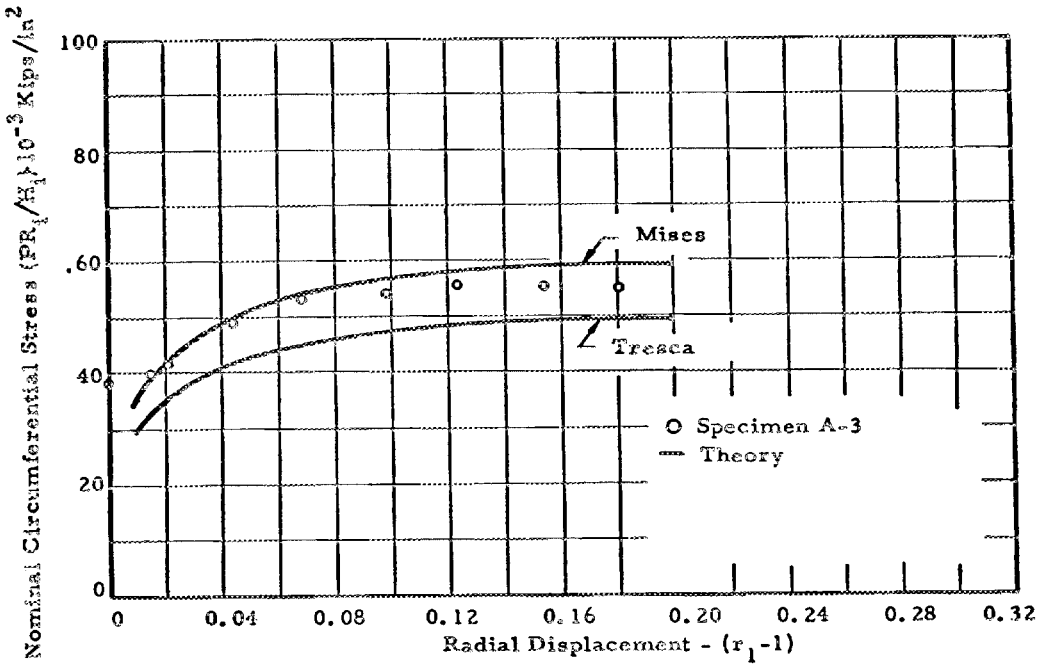

Fig. 6.73. Test Results for Mild Steel, l = 2.01.

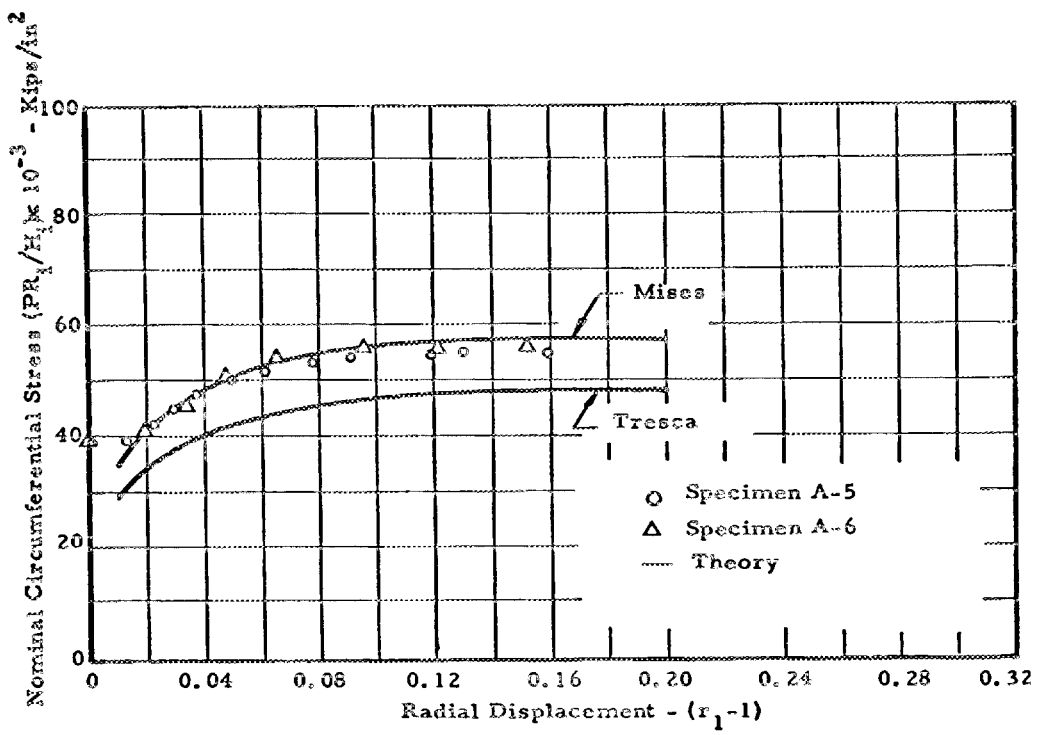

Fig. 6.74. Test Results for Mild Steel, l = 2.98.

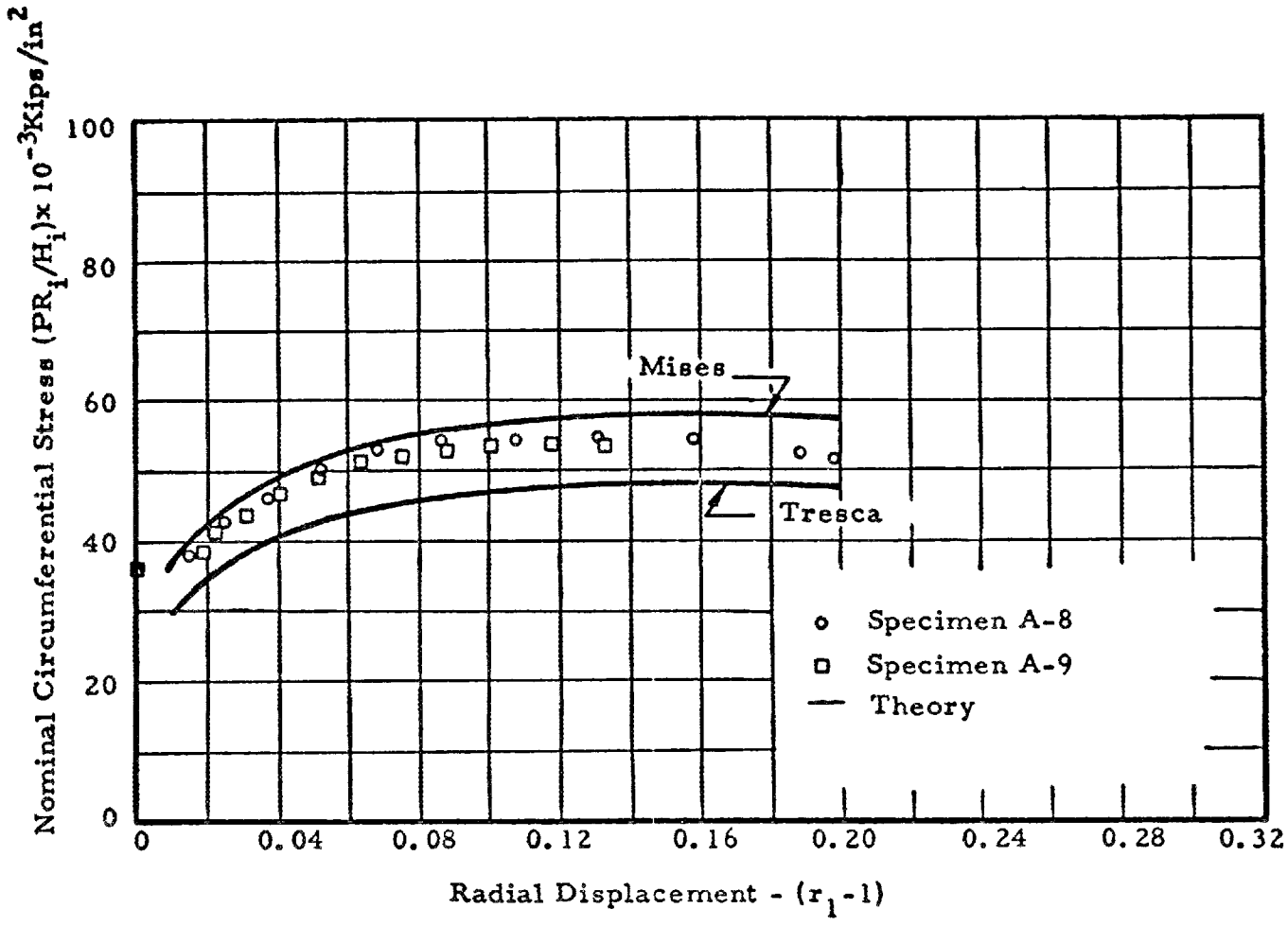

Fig. 6.75. Test Results for Mild Steel, l = 3.95.

pressure, R_i and H_i are the initial radius and thickness, and r_1 is the ratio of the maximum radius of the deformed cylinder to its initial radius. The quantity $r_1 - 1$ is equal to the engineering strain in the circumferential direction.

The theoretical curves labeled Mises were obtained by the method of ref. 122, a step-by-step incremental theory solution in which the material is assumed to obey the Mises yield criterion. The curves labeled Tresca were obtained by the exact method of ref. 66, which applies to materials that follow the Tresca yield criterion. The difference between the two solutions is greatest for the infinite cylinder, where they differ by the factor $[2/(3)^{1/2}]^{n+1}$, which for $n = 0.277$ amounts to about 20%. On the whole, the solutions based on the Mises yield criterion seem to agree more closely with the test results.

The test results show that the effect of rigid end restraint is negligible for values of $l \geqslant 2$ for the steel tested. End restraint does, however, greatly increase the strength of short cylinders ($l \leqslant 1$). The effects of variation in the value of the hardening exponent, n, are shown in Figs. 6.76, 6.77, and 6.78, where values of the pressure ratio

$$p = PR_i/KH_i \tag{6.159}$$

versus the center radius, r_1, are given for a range of values of l. These results were obtained using the method of ref. 122. The curves labeled $l = \infty$ are for infinite cylinders. Values of the strength coefficient K and the hardening exponent n for a number of steels are given in Table 6.13 above.

The true stress-strain curves for some steels (type 304 stainless steel, for example) can be best approximated by the linear law,

$$\sigma = \sigma_o\ (1 + \lambda\epsilon)\ , \tag{6.160}$$

in which σ_o is the initial yield stress in tension and the hardening coefficient λ is the slope of the dimensionless true stress-strain curve. Pressure ratio-center radius curves for values of $\lambda = 2$, 4, and 6 with a range of values of l are given in Fig. 6.79. In this case the pressure ratio is defined as

$$p = PR_i/\sigma_o H_i \tag{6.161}$$

and is simply the ratio of the applied pressure to the pressure required to cause initial yielding. The results shown in these figures were obtained using the incremental theory of ref. 122 for materials obeying the Mises yield condition.

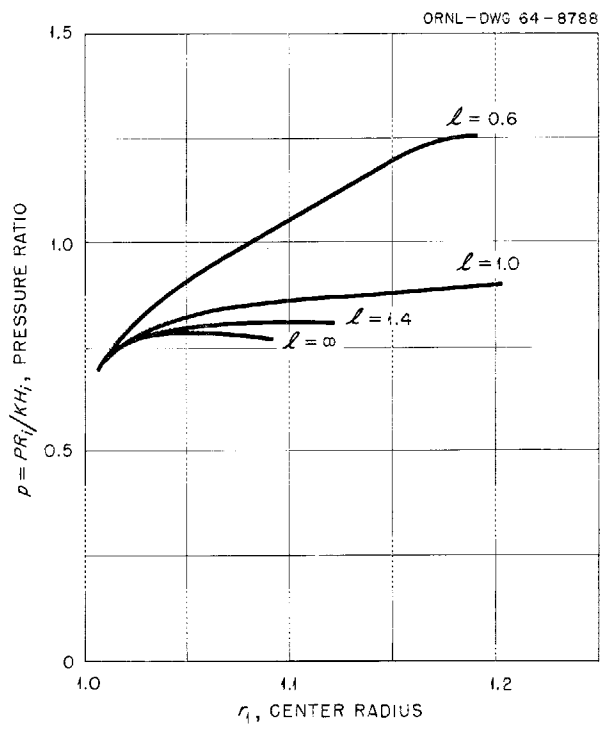

Fig. 6.76. Pressure Versus Center Radius for Cylinders with Rigid Ends; Exact Solution; Mises Yield Condition; Power-Law Strain Hardening, n = 0.1.

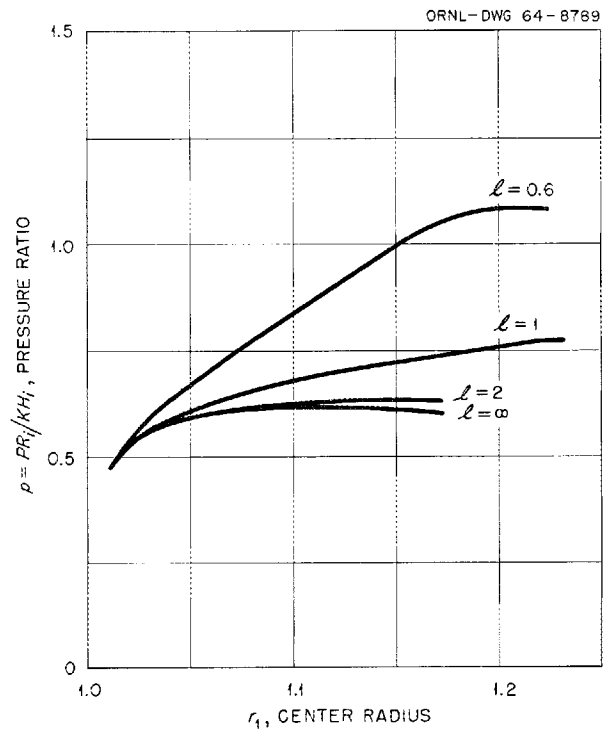

Fig. 6.77. Pressure Versus Center Radius for Cylinders with Rigid Ends; Exact Solution; Mises Yield Condition; Power-Law Strain Hardening, n = 0.2.

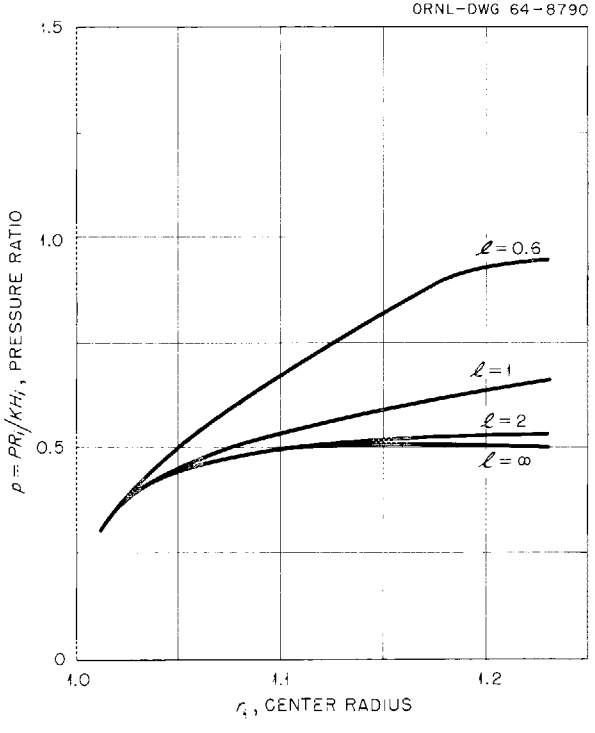

Fig. 6.78. Pressure Versus Center Radius for Cylinders with Rigid Ends; Exact Solution; Mises Yield Condition; Power-Law Strain Hardening, n = 0.3.

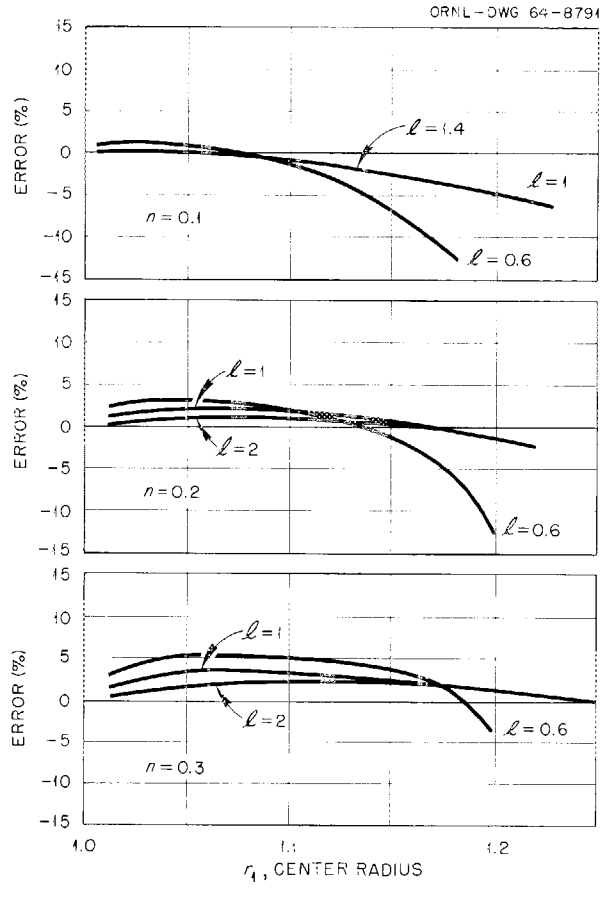

Fig. 6.79. Error in Approximate Solution for Cylinders with Rigid Ends; Mises Yield Condition; Power-Law Strain Hardening.

6.5.3.2 Approximate Theories

In order to reduce the computational effort required to obtain results by the exact incremental theories cited above, the following method for obtaining approximate solutions has been developed.[66,124,125] The method can also be applied to shells with one or two hemispherical heads, for which exact solutions are not available.

The basis of the analysis is the assumption that the profile of the deformed shell is a circular arc, as shown in Fig. 6.67(b), for shells with rigid ends. In the case of shells with either one or two spherical heads, the profile is assumed to be composed of two or three tangent circular arcs, as shown in Figs. 6.68(b) and 6.69(b). In all cases, the distance between the ends of the cylindrical portion of the shell is assumed to remain fixed. Test results[123] show this assumption to be very nearly true. The radii of these circular arcs are determined by the requirement that the equations of equilibrium be satisfied at the crown of the bulge of the cylindrical portion (at $R = R_1$ in the sketches) and at the pole of the end cap if the shell has a hemispherical head. The Mises yield condition and the stress-strain relations of deformation theory are assumed to apply.

Denoting the principal stresses, strains, and radii of curvature in the meridional and circumferential directions by $\sigma_m, \epsilon_m, R_m$ and $\sigma_c, \epsilon_c, R_c$, respectively, the Mises yield condition becomes

$$\sigma = (\sigma_c^2 - \sigma_c\sigma_m + \sigma_m^2)^{1/2} = F(\epsilon) \ , \tag{6.162}$$

where σ is the yield stress in tension and the function F is given by Eq. (6.158) for a material that hardens according to the power law, and by Eq. (6.159) for a material with linear hardening. The effective strain ϵ is, in the present case,

$$\epsilon = \frac{2}{(3)^{1/2}} (\epsilon_c^2 + \epsilon_c\epsilon_m + \epsilon_m^2)^{1/2} \ , \tag{6.163}$$

while the flow rule becomes

$$\frac{\epsilon_c}{\epsilon_m} = \frac{2\sigma_c - \sigma_m}{2\sigma_m - \sigma_c} \ . \tag{6.164}$$

If the stress biaxiality ratio β is defined as

$$\beta = \frac{\sigma_m}{\sigma_c} \ , \tag{6.165}$$

Eqs. (6.161) and (6.162) can be combined to give

$$\epsilon = \frac{2}{2-\beta}\,(1-\beta+\beta^2)^{1/2}\,\epsilon_c\ , \tag{6.166}$$

and Eq. (6.160) may be solved for the meridional stress

$$\sigma_m = \beta(1-\beta+\beta^2)^{-1/2}\,F(\epsilon)\ . \tag{6.167}$$

The incompressibility condition for this case is

$$\epsilon_c + \epsilon_m + \epsilon_n = 0\ , \tag{6.168}$$

where the thickness strain ϵ_n is

$$\epsilon_n = \log H/H_i\ , \tag{6.169}$$

where H/H_i is the ratio of the thickness of the deformed shell to its initial thickness. An expression for the current thickness in terms of β and ϵ_c is obtained by combining Eqs. (6.164), (6.165), (6.168), and (6.169), with the result

$$H = H_i\,e^{-\epsilon_c(1+\beta)/(2-\beta)}\ . \tag{6.170}$$

The meridional membrane stress resultant

$$N_m = \sigma_m H \tag{6.171}$$

is found, by combining Eqs. (6.167) and (6.170), to be

$$N_m = H_i\,e^{-\epsilon_c(1+\beta)/(2-\beta)}\,\beta(1-\beta+\beta^2)^{-1/2}\,F(\epsilon)\ . \tag{6.172}$$

The equation of equilibrium in the axial direction can be written in the form

$$N_m = \frac{PR_c}{2}\ . \tag{6.173}$$

Therefore, an expression for the pressure P is

$$P = \frac{2H_i}{R_c} e^{-\epsilon_c(1+\beta)/(2-\beta)} \beta(1 - \beta + \beta^2)^{-1/2} F(\epsilon) . \tag{6.174}$$

At the crown of the bulge of the cylindrical portion of the shell

$$R_c = R_1 \tag{6.175}$$

and

$$\epsilon_c = \log \frac{R_1}{R_i} = \log r_1 . \tag{6.176}$$

Substituting in Eq. (6.174) and rearranging terms gives

$$\frac{PR_i}{H_i} = 2 r_1^{3/(\beta-2)} \beta(1 - \beta + \beta^2)^{-1/2} F(\epsilon) \tag{6.177}$$

as the expression for the nominal circumferential stress in the cylinder, in which, by Eqs. (6.166) and (6.176), the effective strain is

$$\epsilon = \frac{2}{2 - \beta} (1 - \beta + \beta^2)^{1/2} \log r_1 . \tag{6.178}$$

A second independent equilibrium equation at the crown of the cylindrical portion of the shell is

$$\beta = \frac{\sigma_c}{\sigma_m} = \frac{r_m}{2r_m - r_1} , \tag{6.179}$$

where

$$r_m = \frac{R_m}{R_i} .$$

1. Cylinder with Two Rigid Ends. In the case shown in Fig. 6.67, r_m is found by geometry to be

$$r_m = \frac{l^2 + (r_1 - 1)^2}{2(r_1 - 1)} . \tag{6.180}$$

Equations (6.177) and (6.180) then give the pressure P directly as a function of the dimensionless radius r_1.

2. Cylinder with Two Hemispherical Heads. In the case illustrated in Fig. 6.68,

$$r_m = \frac{l^2 + r_1^2 - r_e^2}{2(r_1 - r_e)} , \tag{6.181}$$

where

$$r_e = \frac{R_e}{R_i} . \tag{6.182}$$

An additional equation is required to determine the unknown r_e, the dimensionless radius of the end caps.

In the spherical zone

$$\epsilon_c = \epsilon_m = \log r_e , \tag{6.183}$$

and the principal radii of curvature are each equal to R_e; thus, $\beta = 1$. The effective strain in the spherical zone is then found from Eq. (6.163) to be

$$\epsilon = 2 \log r_e . \tag{6.184}$$

Substitution of the appropriate values of β, R_c, ϵ_c, and ϵ into Eq. (6.174) gives

$$\frac{PR_i}{H_i} = \frac{2}{r_e^3} F (2 \log r_e) , \tag{6.185}$$

which is simply the formula for the stress in a spherical shell whose deformed radius is R_e and whose initial radius is R_i. The solution for a shell with two hemispherical caps is determined by Eqs. (6.177), (6.178), (6.179), (6.181), and (6.185). A trial and error procedure can be used to determine the pressure for a given value of r_1 for a particular shell of length l. A value of r_e is chosen and the two values of PR_i/H_i given by Eqs. (6.177) and (6.185) are computed. If the two values agree, the value of r_e is correct, if not, a new value of r_e is chosen.

3. Cylinder with One Rigid End and One Hemispherical Cap. In the case shown in Fig. 6.69, r_m is determined by geometry to be

$$r_m = \frac{y^2 + r_1^2 - r_e^2}{2(r_1 - r_e)} = \frac{(2l - y)^2 + (r_1 - 1)^2}{2(r_1 - 1)} , \tag{6.186}$$

where

$$y = \frac{Y}{R_i} .$$

The value of y for a given geometry can be found from Eq. (6.186) as

$$y = \left\{\xi \left[4l^2 (1 + \xi) - (r_1 - 1)(r_e + 1)\right]\right\}^{1/2} - 2l\xi \qquad \text{for } r_e > 1 \tag{6.187}$$

or

$$y = l - \frac{r_1 - 1}{2l} \quad \text{for} \quad r_e = 1 , \tag{6.188}$$

where

$$\xi = \frac{r_1 - r_e}{r_e - 1} . \tag{6.189}$$

Here, as in the case above, a trial and error method of solution is required.

4. Code. A computer code "ENDCON" was written to solve the above three problems. The results designated approximate solutions in the figures presented in Section 6.5.3.3 were obtained using this code. A Fortran listing of ENDCON is presented in Section 6.5.3.5.

6.5.3.3 Accuracy of the Approximate Theory

In the case of cylinders with rigid ends, comparisons of the results given by the approximate theory with the exact theoretical results of Figs. 6.76, 6.77, and 6.78 (power-law hardening) and of Figs. 6.80, 6.81, and 6.82 (linear hardening) are given in Figs. 6.79 and 6.83. Here the

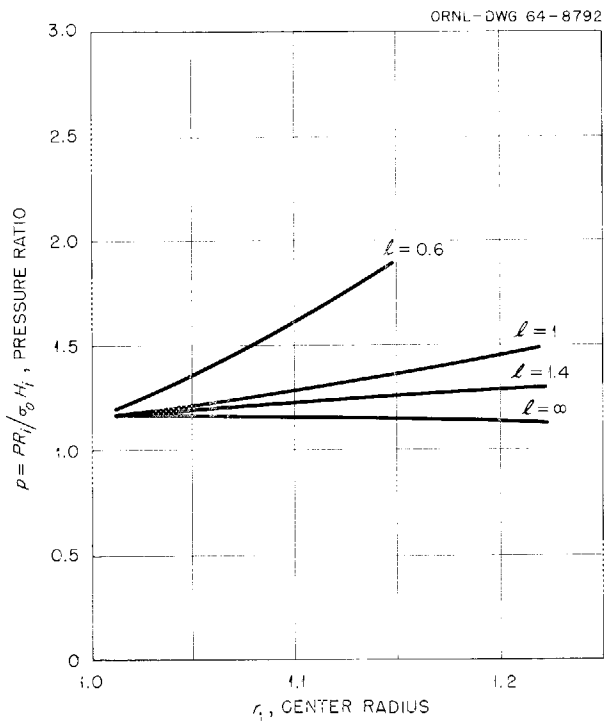

Fig. 6.80. Pressure Versus Center Radius for Cylinders with Rigid Ends; Exact Solution; Mises Yield Condition; Linear Strain Hardening $\lambda = 2$.

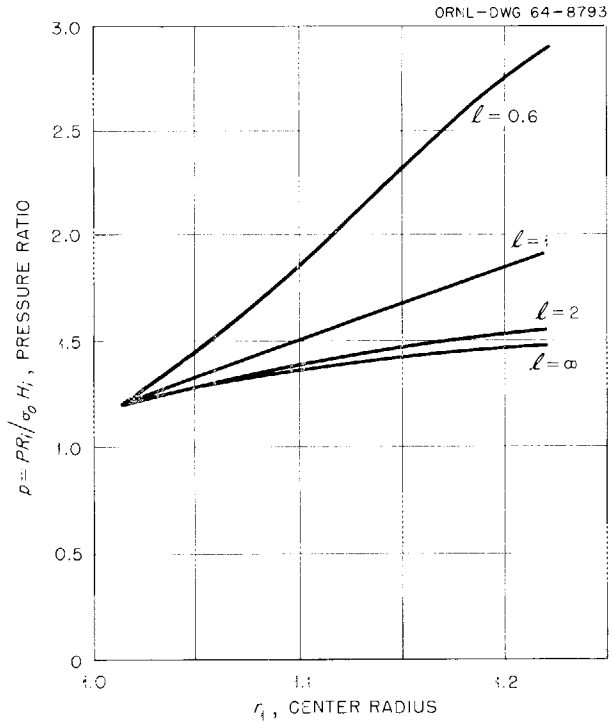

Fig. 6.81. Pressure Versus Center Radius for Cylinders with Rigid Ends; Exact Solution; Mises Yield Condition; Linear Strain Hardening $\lambda = 4$.

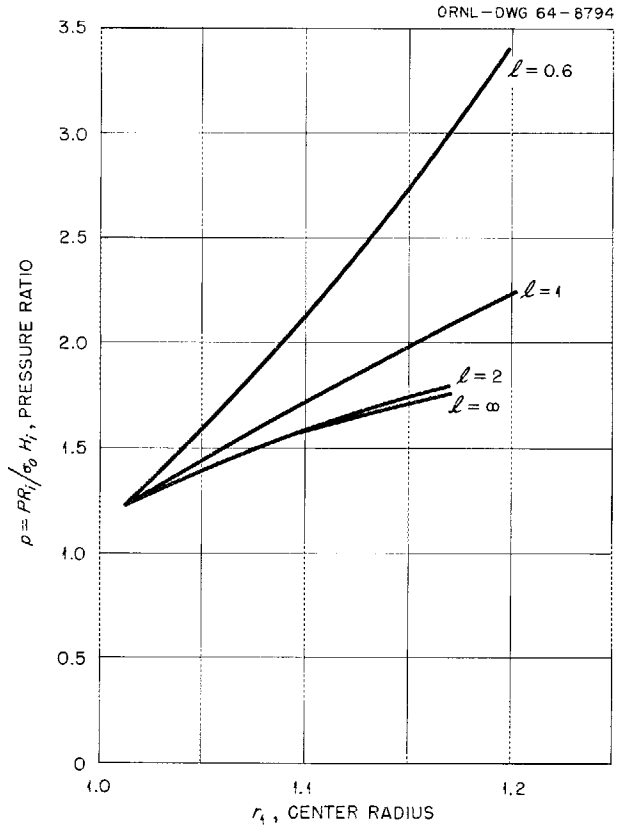

Fig. 6.82. Pressure Versus Center Radius for Cylinders with Rigid Ends; Exact Solution; Mises Yield Condition; Linear Strain Hardening, $\lambda = 6$.

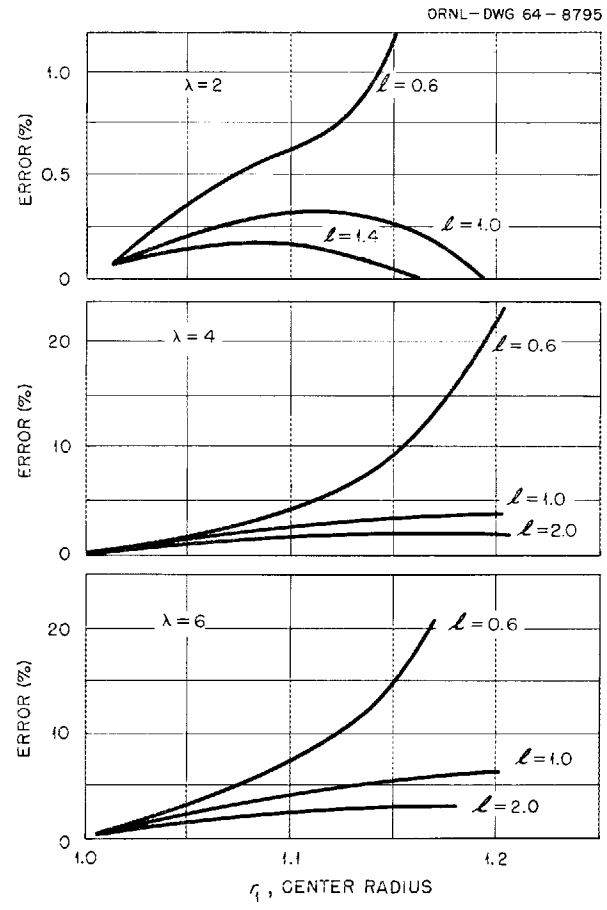

Fig. 6.83. Error in Approximate Solution for Cylinders with Rigid Ends; Mises Yield Condition; Linear Strain Hardening.

error (in percent) of the approximate theory is given as a function of r_1 for a range of values of n and λ with l as a parameter. The results show that the error in the approximate theory is less than 10% for values of the maximum circumferential strain ($r_1 - 1$) less than about 0.1.

A comparison of the approximate theory with some test results for cylinders with rigid ends is given in Fig. 6.84. The agreement is fairly good.

There are no exact theoretical results available at this time for cylinders with hemispherical end caps with which to compare the approximate theory; however, two tests in the series cited above were made on cylinders of this type. The test data, together with the approximate theoretical curves, are shown in Figs. 6.85 and 6.86. The results of a test on a cylinder with one end rigid and one hemispherical cap, and a length-to-diameter ratio of the cylindrical portion of $l = 2.31$, are shown in Fig. 6.85. In this case the effects of end restraint are negligible, as they are in cylinders with rigid end caps with $l > 2$ (see Figs. 6.73, 6.74, and 6.75). The results of a test of a cylinder with two hemispherical end caps and a length-to-diameter ratio of the cylindrical portion of $l = 1$ are shown in Fig. 6.86. The effects of end restraint are less than in the corresponding cylinder with rigid ends (Fig. 6.72), but there is an increase of about 10% over that of the infinite cylinder.

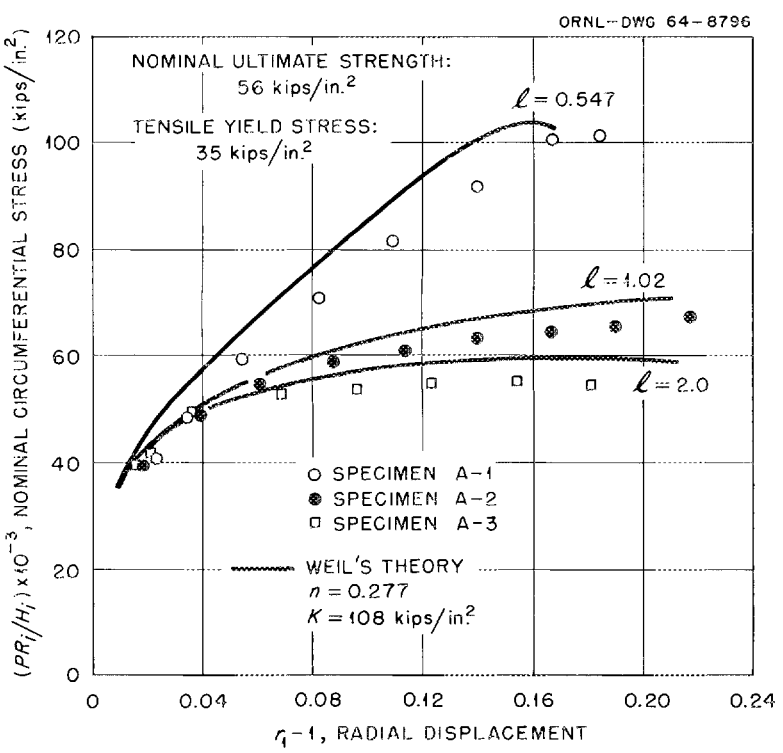

Fig. 6.84. Comparison of Results of Tests on Mild Steel Cylinders with the Approximate Theory.

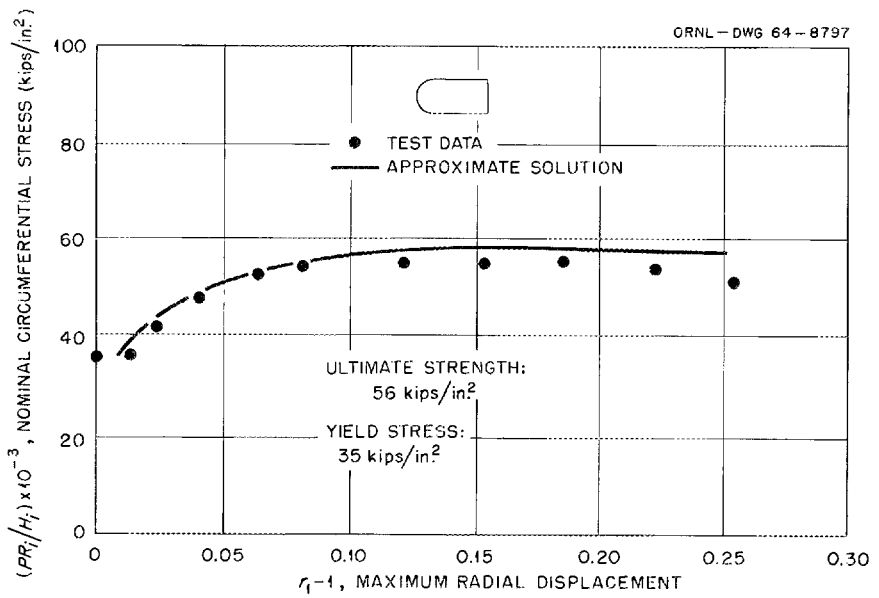

Fig. 6.85. Test Results for a Cylinder with One Hemispherical Cap; Mild Steel, l = 2.31.

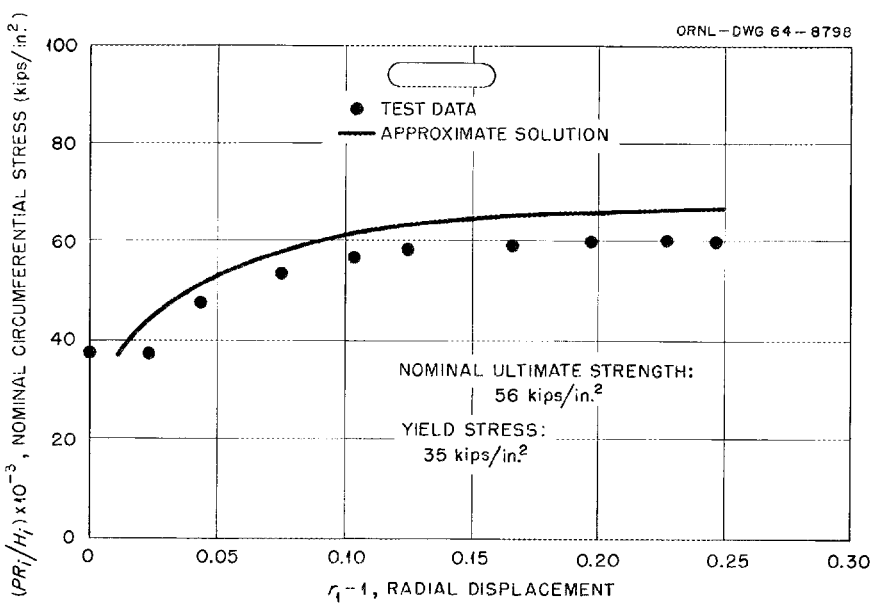

Fig. 6.86. Test Results for a Cylinder with Two Hemispherical Caps; Mild Steel, l = 1.0.

The effects of end restraint for the three types of end conditions are shown in Figs. 6.87, 6.88, and 6.89 for power-law hardening materials and in Figs. 6.90, 6.91, and 6.92 for materials with linear hardening. These curves were obtained by the approximate theory. The curves for the complete sphere designated $l = 0$ and for the infinite cylinder labeled $l = \infty$ are also shown. The formula for the latter case is obtained by substituting the values of R_c and ϵ_c from Eqs. (6.175) and (6.176), along with the value $\beta = 1/2$ into Eqs. (6.166) and (6.174) to obtain

$$\frac{PR_i}{H_i} = \frac{2}{(3)^{1/2}\, r_1^2}\, F\left[\frac{2}{(3)^{1/2}} \log r_1\right] . \tag{6.190}$$

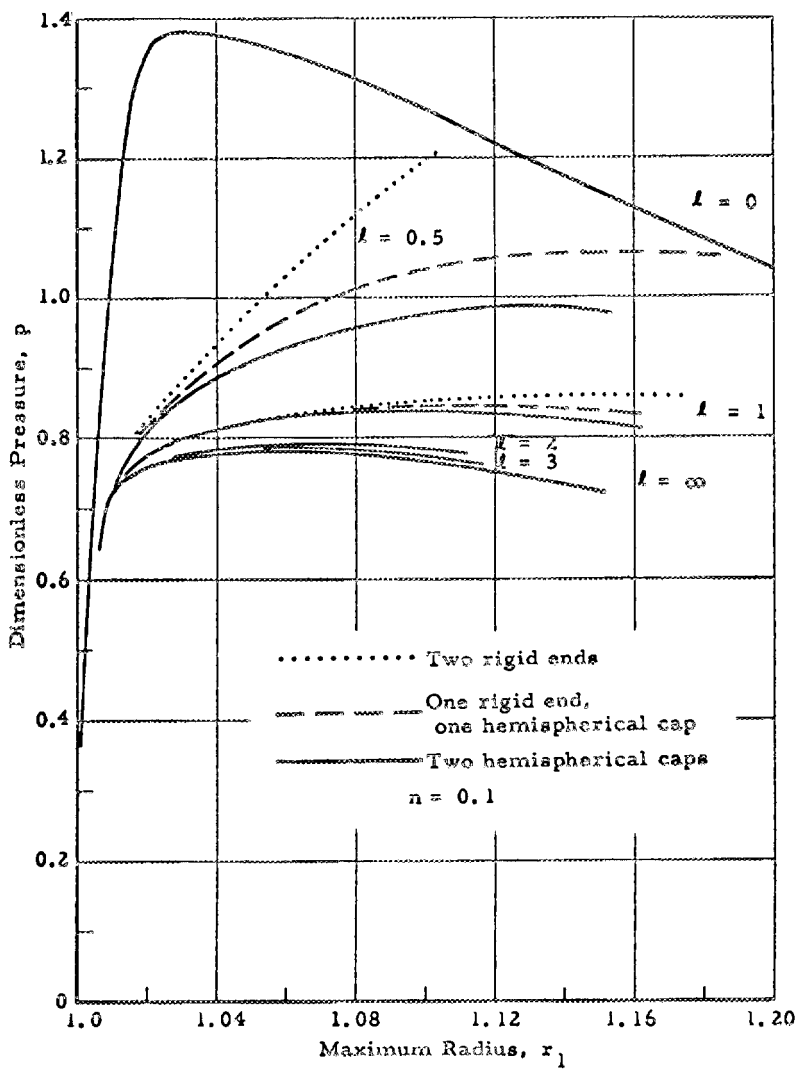

Fig. 6.87. Pressure–Maximum Radius Relation for Finite Cylinder; Power-Law Hardening Material; n = 0.1.

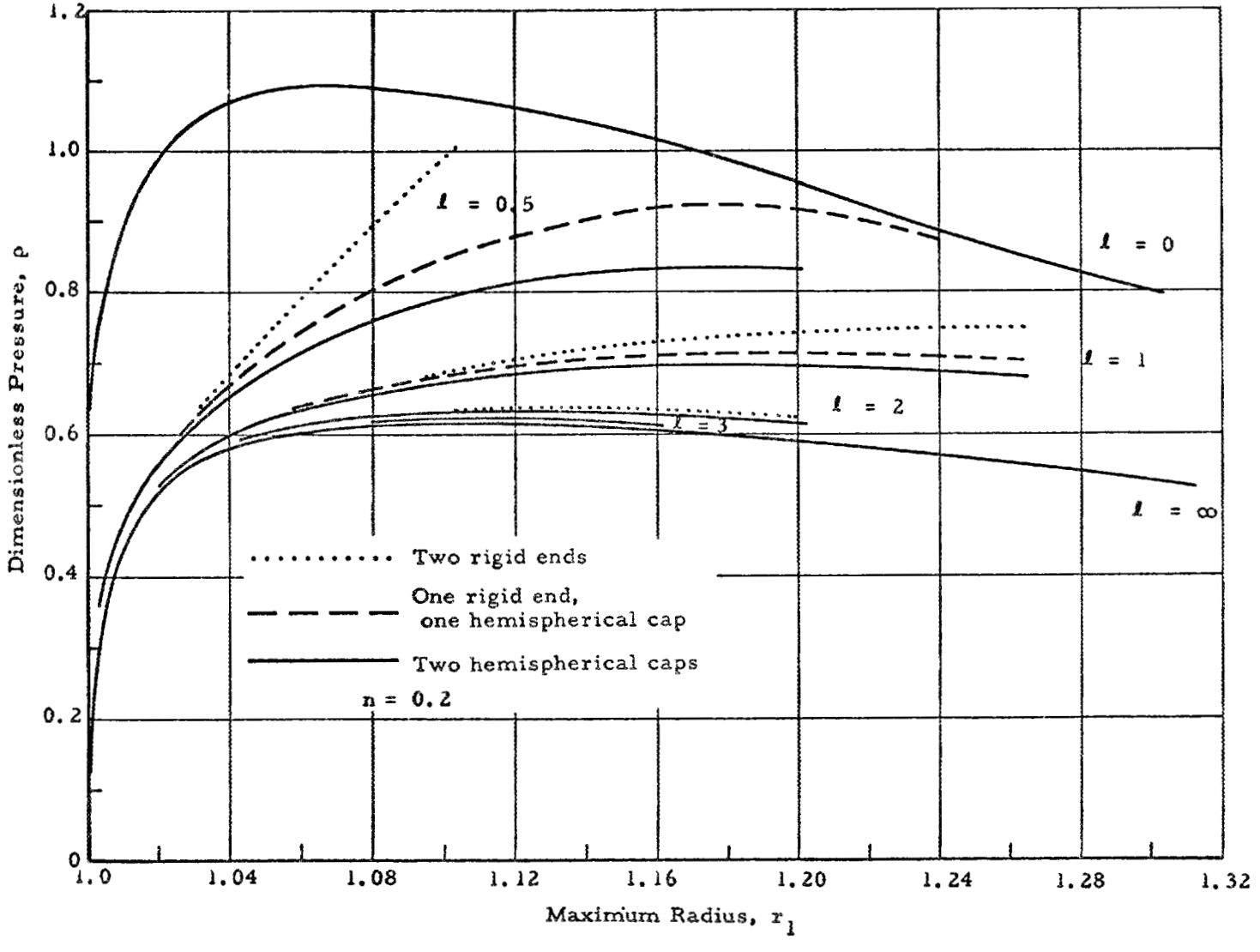

Fig. 6.88. Pressure–Maximum Radius Relation for Finite Cylinder; Power-Law Hardening Material; n = 0.2.

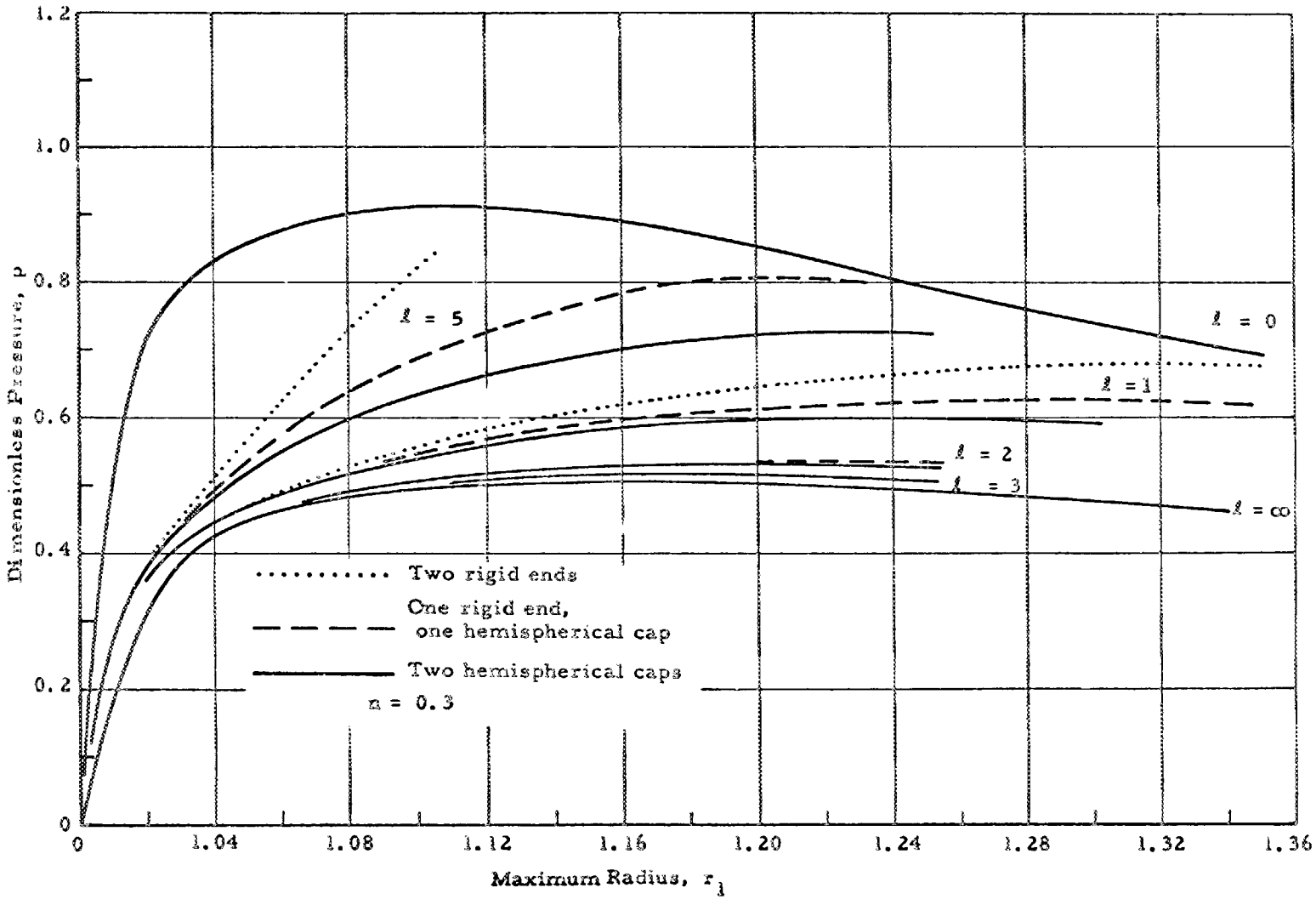

Fig. 6.89. Pressure—Maximum Radius Relation for Finite Cylinder; Power-Law Hardening Material; n = 0.3.

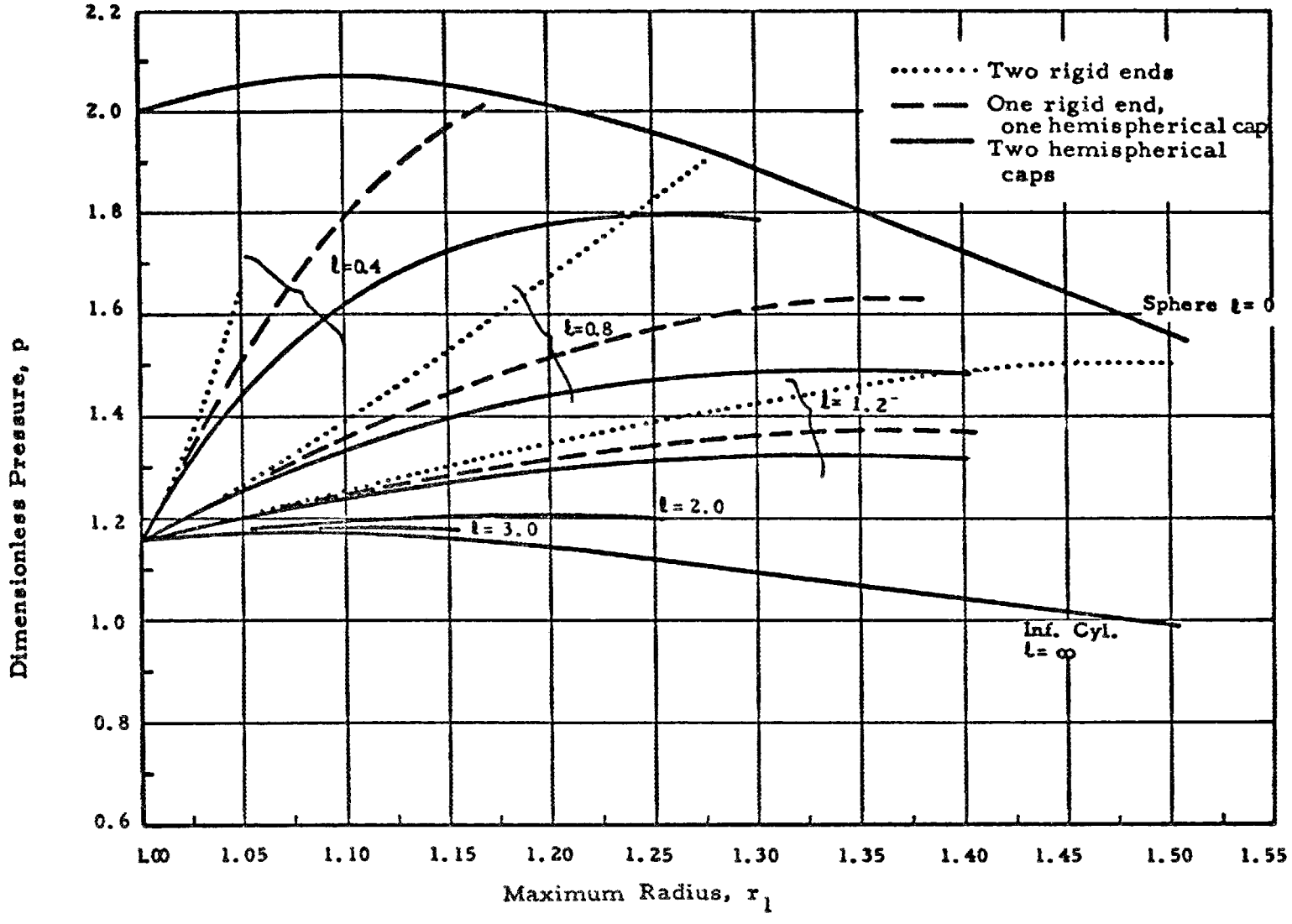

Fig. 6.90. Pressure-Maximum Radius Relation for Finte Cylinder; $\lambda = 2$.

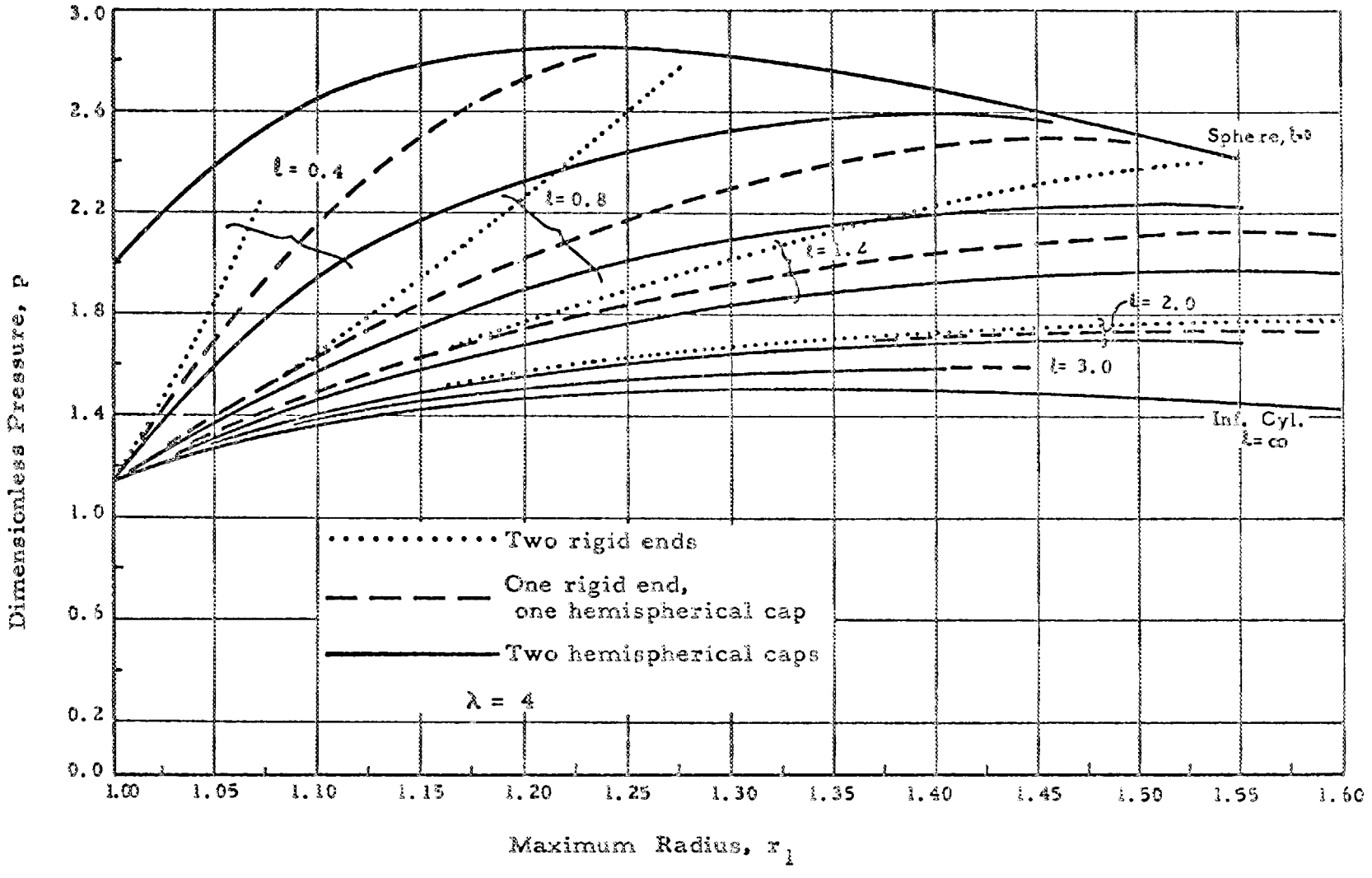

Fig. 6.91. Pressure–Maximum Radius Relation for Finite Cylinder; $\lambda = 4$.

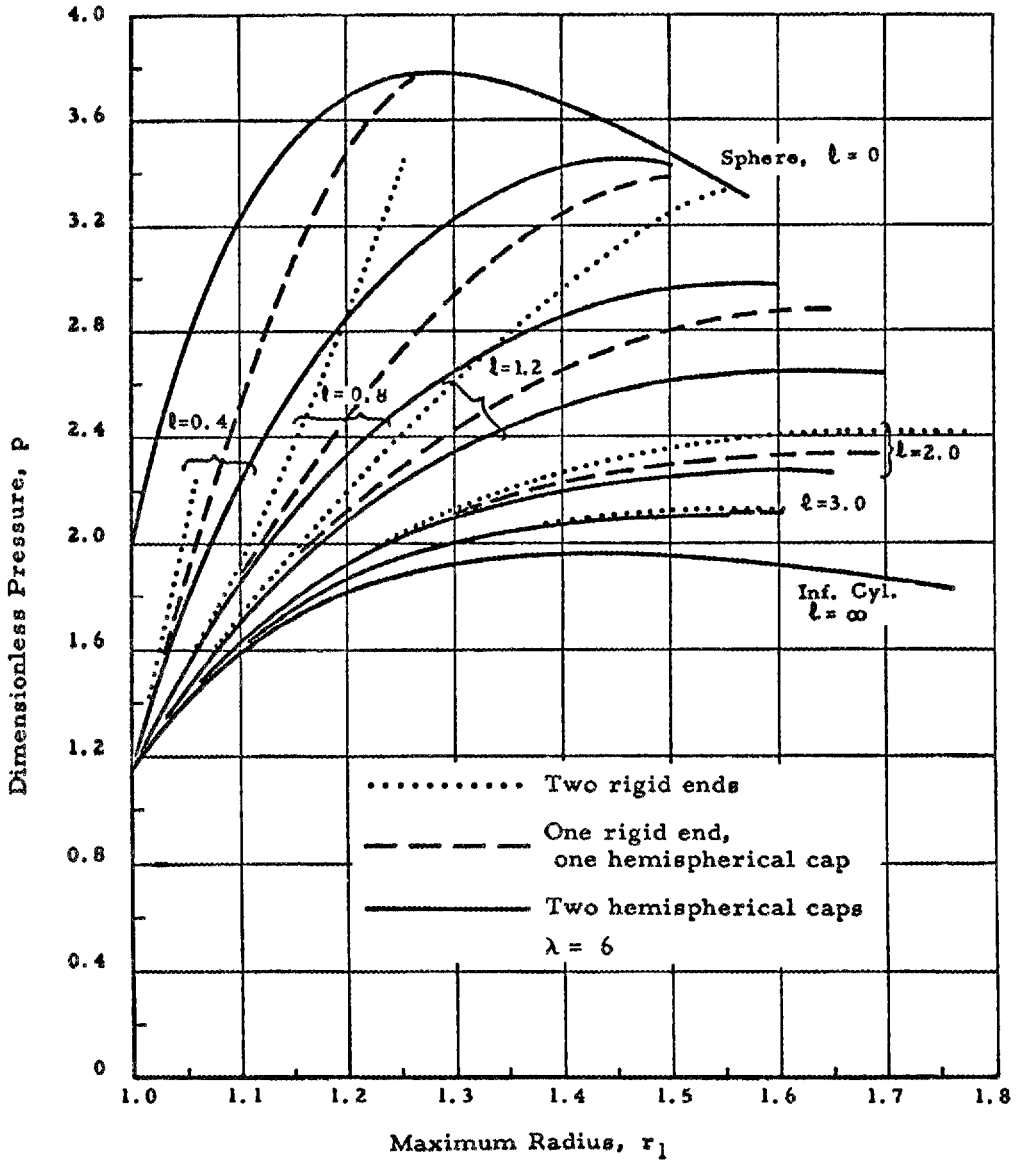

Fig. 6.92. Pressure–Maximum Radius Relation for Finite Cylinder; $\lambda = 6$.

6.5.3.4 Conclusions

Test results show that the strength under internal static pressure loadings of thin shells without openings is well in excess of that at initial yield. Fairly simple approximate analytical methods can predict this strength within about 10%. The degree to which this excess strength can be realized in actual practice, that is, in structures with openings, depends on the extent to which these openings reduce the ability of the structure to sustain large deformations without rupture.

6.5.3.5 ENDCON

The following is a Fortran listing and a sample set of data of the computer code used to calculate the approximate theory solutions referred to above.

```
*     LABEL
CENDCON                CYLINDER END CONDITIONS   APPROXIMATE SOLUTION
C     APPROX. ANALYSIS OF CYLINDERS WITH VARIOUS END CONDITIONS
C     REQUIRED INPUT
C     XLENT=LENGTH-DIAMETER RATIO OF CYLINDER
C     ROVRT=RADIUS-THICKNESS RATIO
C     STRESCO=STRENGTH COEF.(POWER LAW)=INITIAL YIELD STRS.(LINEAR LAW)
C     STRESCO KIPS PER SQ. INCH
C     XHRDCO=HARDENING EXP.(POWER LAW),HARDENING COEF.(LINEAR LAW)
C     RMAX=MAXIMUM  VALUE OF R1(MAX.RADIUS/INITIAL RADIUS)
C     DR=INCREMENT IN DIMENSIONLESS RADIUS
C     KECON=1(RIGID ENDS)=2(TWO HEMIS. CAPS)=3(ONE RIGID-ONE HEMIS.)
C     KHLAW=1 (POWER LAW) =2 (LINEAR LAW)
C     OUTPUT QUANTITIES
C     R1=DIMENSIONLESS RADIUS OF DEFORMED CYLINDER
C     RE= RADIUS OF END CAP
C     PRESS=INTERNAL PRESSURE PSI
C     EQ177=NOMINAL CIRCUMFERENTIAL STRESS GIVEN EQ.(6.177) KSI
C     Y=AXIAL COORDINATE OF CROWN OF BULGE
      COMMON STRSCO,XHRDCO,XLENT,KHLAW,R1,RE,Y,KECON
   30 READ INPUT TAPE 5,300,XLENT,STRSCO,XHRDCO,RMAX,DR,ROVRT,KECON,
     1KHLAW
  300 FORMAT(6F8.0,2I4)
      WRITE OUTPUT TAPE 6,301
  301 FORMAT(97H1          XLENT          STRSCO         XHRDCO         RMAX
     1      DR             ROVRT      KECON    KHLAW)
      WRITE OUTPUT TAPE 6,302,XLENT,STRSCO,XHRDCO,RMAX,DR,ROVRT,KECON,
     1KHLAW
  302 FORMAT(1H 6F13.3,2I8)
      WRITE OUTPUT TAPE 6,303
  303 FORMAT(62H0          R1             PRESS          EQ177          RE
     1      Y)
      Y=XLENT/2.
      R1=1.
      JMAX=(RMAX-1.)/DR
      DO 20 J=1,JMAX
      RE=1.
      KOUNT=1
      R1=R1+DR
      GO TO (1,9),KHLAW
C
C     POWER LAW
C
    1 GO TO(2,3,3),KECON
C
C     RIGID ENDS
C
    2 CALL CYLNDR(EQ177)
      RE=0.
      GO TO 19
    3 REUP=R1
      RELOW=1.
    4 RE=.5*(RELOW+REUP)
      CALL SPHERE(EQ185)
      CALL CYLNDR(EQ177)
      IF(EQ185-EQ177)5,6,5
    5 REUP=RE
      GO TO 7
    6 RELOW=RE
    7 DIFF=ABSF((REUP-RELOW)/REUP)
      IF(.00001 -DIFF)8,19,19
    8 KOUNT=KOUNT+1
      IF(200-KOUNT)100,100,4
C
C     LINEAR LAW
C
    9 RE=1.
      EQ185=2.
      CALL CYLNDR(EQ177)
      IF(EQ185-EQ177)3,19,19
```

```
   19 PRESS=EQ177/ROVRT*1000.
      WRITE OUTPUT TAPE 6,200,R1,PRESS,EQ177,RE,Y
  200 FORMAT(1H 5F13.3)
   20 CONTINUE
      GO TO 30
  100 WRITE OUTPUT TAPE 6,101
  101 FORMAT(18H FAILS TO CONVERGE)
      GO TO 30
      END
C
      SUBROUTINE CYLNDR(EQ177)
      COMMON STRSCO,XHRDCO,XLENT,KHLAW,R1,RE,Y,KECON
C
C     COMPUTE RM-RADIUS OF CYLINDER PROFILE
C
      GO TO (1,2,3 ),KECON
C
C     TWO RIGID ENDS EQ.(6.180)
C
    1 RM=(XLENT**2.+(R1-1.)**2.)/(2.*(R1-1.))
      GO TO 4
C
C     TWO HEMISPHERICAL CAPS EQ.(6.181)
C
    2 RM=(XLENT**2.+R1*R1-RE*RE)/(2.*(R1-RE))
      GO TO 4
C
C     ONE RIGID END -ONE HEMISPHERICAL CAP EQ.(6.186)
C
    3 IF(RE-1.)5,5,6
    5 Y=XLENT-(R1-1.)/(2.*XLENT)
      GO TO 7
    6 XSI=(R1-RE)/(RE-1.)
      Y=(XSI*(4.*XLENT**2.*(1.+XSI)-(R1-1.)*(RE+1.)))**.5-2.*XLENT*XSI
    7 RM=(Y*Y+R1*R1-RE*RE)/(2.*(R1-RE))
    4 BETA=RM/(2.*RM-R1)
C
C     COMPUTE EFFECTIVE STRAIN AT CROWN BY EQ.(6.178)
C
      EEF=2./(2.-BETA)*SQRTF(1.- BETA+BETA**2.)*LOGF(R1)
C
C     COMPUTE EFFECTIVE STRESS(FOFE) BY EQ.(6.158) OR EQ.(6.160)
C
      GO TO (8,9),KHLAW
C
C     POWER LAW EQ.(6.168)
C
    8 FOFE=STRSCO*EEF**XHRDCO
      GO TO 10
C
C     LINEAR LAW EQ.(6.160)
C
    9 FOFE=STRSCO*(1.+XHRDCO*EEF)
C
C     EVALUATE EQ.(6.177)
C
   10 EQ177=2.*R1**(3./(BETA-2.))*BETA/SQRTF(1.-BETA+BETA**2.)*FOFE
      RETURN
      END
C
      SUBROUTINE SPHERE(EQ185)
      COMMON STRSCO,XHRDCO,XLENT,KHLAW,R1,RE,Y,KECON
      GO TO (1,2),KHLAW
C
C     POWER LAW
C
    1 EQ185=2.*(2.*LOGF(RE))**XHRDCO/(RE**3.)*STRSCO
      RETURN
C
C     LINEAR LAW
C
    2 EQ185=2.*(1.+XHRDCO*2.*LOGF(RE))/(RE**3.)*STRSCO
      RETURN
      END
      DATA FOR SAMPLE PROBLEM
1.003   120.    .255    1.25    .01     41.11     2   1
2.31    120.    .255    1.25    .01     41.11     3   1
2.31     40.    4.66    1.25    .01     41.11     3   2
```

6.6 SHOCK AND MISSILE PROTECTION

B. L. Greenstreet
M. A. Salmon N. A. Weil

In order to evaluate the structural damage that would be done in the event of an accident in a nuclear power plant, it is necessary to predict the nature of the accident, the energy released, and the results of this release. Of particular interest in the design of containment systems is protection against missiles that might be generated. Such missiles could be either the cause or the result of an accident. It is therefore necessary to determine which components could conceivably become missiles and to predict their maximum velocities. It is also necessary to design missile shields or other protective systems that would contain all missiles that might be generated. A second area of interest is the design of blast shields to dissipate much of the energy contained in a shock wave.

6.6.1 Missile Generation

An object dislocated from a plant component and provided with potential energy originating from within the plant component or from a source at some distance (pressure waves) may develop into a missile through the conversion of this potential energy into kinetic energy. The missile may have enough energy when it contacts the vapor-containing shell to penetrate the vessel and thereby release fission products to the atmosphere.

The concentrated load caused by the missile may occur at the same time that the vapor containment shell receives the peak pressure load contemplated for the maximum credible accident. This combined load might cause excessive stresses in the vessel and result in rupture. Therefore protection of the vapor containment shell from the missile may be necessary.

Methods for preventing this additional load from occurring may be categorized as follows:

1. Eliminate the possibility of missile development by installing certain plant components that contain a considerable amount of stored energy, such as turbines, heat exchangers, etc., outside the vapor container (partial containment). Increase the material strength of plant components that are potential missile producers; this can be done by using larger safety factors in component design.

2. If a missile does develop, intercept or retard it before it contacts the vapor container wall.

Intercepting or retarding the missile in flight can be done in several ways. In the "static" approach, a hard wall, usually consisting of a steel plate or concrete slab, is placed in the potential path of the missile for converting part or all of the missile energy into harmless plastic deformation of the materials and heat on impact. In the "dynamic" approach, a flexible wall is used, for example, a steel mat, which absorbs part or all of the energy by wall motion.

A missile can also be retarded with liquid media. In all cases the objective is to slow the missile down to such an extent that upon arrival

at the vapor container shell its kinetic energy will be harmless. The following forms of missile interception have been applied in reactor plants:

1. Reinforced concrete lining of the vapor container shell.
2. Concrete walls between the potential missile and the vapor container wall.
3. Steel plates.
4. Removable steel mats.

If missile damage is anticipated, certain expenditures must be made to provide this missile protection for the containment shell. Since this may raise the total cost of containment a considerable amount, it is important to reduce this cost to a minimum by accurate determination of the minimum protection requirements.

A missile may have almost any shape and size (fragments with sharp edges, bolts, nuts, control rods, reactor vessel cover, complete pressurizer vessel, concrete spalls, etc.). The effects of missile impact on the shell are difficult to determine because of uncertain factors, such as shape, size, and weight of the missile, potential energy imparted to the missile at its origin and its resulting velocity and angle of impact, and irregularities in the shell material. Missiles can acquire velocity by the shock pressure from an explosion or by being struck by a jet of fluid issuing from a point of fracture and being propelled by that jet or, if the missile contains fluid at the time of rupture, it can be propelled by the expanding fluid.

6.6.1.1 Shock-Generated Missiles

The unbalanced pressure, P, acting on the missile is assumed to act for the length of time required for the shock wave to travel the length of the missile, that is,

$$\tau_o = \frac{L}{V} , \tag{6.191}$$

where L is the length of the missile normal to the shock wave, V is the shock velocity [see Eq. (6.86)], and τ_o is the time that the pressure acts.

It can be shown that the only significant force acting during the period of the shock force is the pressure force of the shock wave; and assuming that the pressure is constant over this time interval, the missile velocity can be obtained from the impulse-momentum relationship

$$V_o = \frac{PA\tau_o}{m} , \tag{6.192}$$

where

V_o = missile velocity at time τ_o,
P = unbalanced pressure exerted on missile,

A = area of missile on which P acts,
m = mass of missile.

The distance, x_o, that the missile travels during acceleration is

$$x_o = \frac{PA\tau_o^2}{2m} . \tag{6.193}$$

If, at the end of this period, the missile is still in a fluid, a period of negative acceleration follows for which

$$\frac{dV}{d\tau} = -\frac{C_d \rho A V^2}{2m} , \tag{6.194}$$

where C_d is the drag coefficient and ρ is the fluid density. The final velocity of the missile after traversing the remaining distance through the liquid is obtained by integrating Eq. (6.194) over the remaining distance, resulting in

$$V = \frac{V_o}{1 + \frac{C_d \rho A V_o (\tau - \tau_o)}{2m}} , \tag{6.195}$$

where

$$\tau - \tau_o = \frac{2m}{C_d \rho A V_o} \left\{ \exp \left[\frac{C_d \rho A}{2m} (x - x_o) \right] - 1 \right\} .$$

6.6.1.2 Self-Propelled Missiles

Pipes, pressurizers, or other hollow missiles that contain fluid at the time of rupture can be propelled by expansion of the fluid they contain. In order to calculate the final velocity the missile may attain, detailed knowledge of the expansion process and the critical discharge rates is required. A simple calculation will, however, yield conservative results. In this calculation it is assumed that the fluid in the missile expands isentropically to the ambient pressure and that the kinetic energy of the missile is equal to the change in internal energy of the fluid during this expansion. As an example, consider a section of 2-in. sched-160 pipe initially filled with saturated water at 500 psia. The initial internal energy is 447.6 Btu/lb. The final quality is 23.3%, and the final internal energy is 389 Btu/lb. There is therefore 58.6 Btu/lb or 45,600 ft-lb/lb of energy available to propel the missile. The weight of water per foot of pipe is 0.8 lb. Therefore the kinetic energy of the missile

is 36,500 ft-lb per foot of pipe. If it is assumed that the pipe, which weighs 7 1/2 lb/ft, and half the weight of the water are accelerated through the entire travel, the final velocity is 545 ft/sec. This is a conservative result since it has been assumed that all the energy of the fluid is transferred into kinetic energy of the missile at 100% efficiency.

6.6.1.3 Jet-Propelled Missiles

A credible missile upon being detached may be propelled by a jet of escaping fluid and continue in that jet of fluid until it strikes the wall of the vapor container. The jet, which has mass and velocity, imparts impulse to the missile.

The fluid expands into the vapor container and, when expanded to ambient pressure, reaches a peak velocity a few feet from the rupture. The missile is propelled by, and accelerated in, this jet of fluid. After the jet has reached vapor container pressure, the assumption is made that the jet continues to propel and accelerate the missile until the missile impinges on the vapor container wall at a distance of x feet.

A constant jet velocity, which is a conservative approximation, was assumed for the following analysis. The velocity of the jet may be calculated by the means described in Section 6.4.2.9.

The weight of fluid striking the missile decreases as the jet expands, starting with a maximum at the point of rupture and decreasing as the missile moves further and further from the rupture. Since the total mass flow rate in the jet remains constant, as the area of the jet increases, the weight of fluid actually striking the missile on its projected area continually decreases. Thus the final velocity of the missile depends on the angle of the jet.

Data obtained from the U.S. Department of Defense[133] indicate that the advancing front of a jet of air suddenly released from an orifice expands at an angle of 60 to 70° in going from the orifice pressure down to atmospheric pressure. On the other hand, in steam turbine practice, nozzles are designed with an angle of 10 to 15°, since with a greater angle the jet does not expand fast enough to maintain contact with the walls. With unconfined and uncontrolled expansion and with the jet issuing from a ragged opening, it is considered that the angle is more likely to approach the greater value.

With the assumption that the jet expands with angle 2β, the velocity equation becomes

$$\frac{dV}{d\tau} = \frac{d^2x}{d\tau^2} = \frac{\rho_f A_o V_f}{m} \frac{A_m}{A_j} (V_f - V) , \qquad (6.196)$$

where

ρ_f = density of jet fluid,
A_o = orifice area,
V_f = jet velocity at orifice,

A_m = cross-sectional area of missile,
m = mass of missile,
A_j = jet area at x
= $\pi\ (r_o + x \tan \beta)^2$ for circular jet,
r_o = radius of orifice,
V = missile velocity.

The solution of Eq. (6.196), which gives the velocity of the missile as a function of the distance traveled, is[134]

$$\left(1 - \frac{V}{V_f}\right) - \ln\left(1 - \frac{V}{V_f}\right) = K_1 - \frac{K_2}{r_o + x \tan \beta}\ , \qquad (6.197)$$

where

K_1 = constant depending on initial conditions
$= \left(1 - \frac{V_o}{V_f}\right) - \ln\left(1 - \frac{V_o}{V_f}\right) + \frac{K_2}{r_o}$ for initial velocity, V_o, at $x = 0$,

$$K_2 = \frac{\rho_f A_o A_m}{m\pi \tan \beta}\ .$$

Equation (6.197) may be solved either graphically or by numerical methods (trial and error or Newton's method) for the missile velocity after traveling a distance x in the jet.

The force on the missile is proportional to the weight of the fluid, and the acceleration is proportional to the weight of the fluid divided by the weight of the missile. Since the weight of the fluid striking the missile is proportional to the projected area, acceleration is, in turn, proportional to the area of the missile divided by the weight of the missile. The missile that has the greatest area-to-weight ratio will obtain the greatest acceleration and hence the greatest velocity. The area-to-weight ratios of some possible missiles are shown in the following tabulation:

Missile	Area-to-Weight Ratio
2-in. steel valve	0.60
Thermometer well	0.25
2-in. steel bar	0.14
2-in. steel pipe	0.15

6.6.1.4 Spalling

When a shock wave traverses a material, the shock front compresses and accelerates the matter through which it passes. If the pressure in the shock wave is large compared with the ambient pressure, the work done by the shock is partitioned approximately equally between kinetic and internal energy. The rate at which energy is delivered to the uncompressed material is

$$\dot{W} = pu = E_t \rho_o U \cong 2 \left(\frac{1}{2} u^2\right) \rho_o u \ . \tag{6.198}$$

When a shock such as this arrives at a free surface, the surface is rapidly accelerated, and, if two conditions are satisfied, a layer will be spalled from the material surface and projected outward. The two conditions are (1) that the pressure amplitude of the shock wave must be greater than the tensile strength of the material and (2) that the duration of the shock wave must be less than approximately twice the time required for the shock to traverse the body under consideration. If the duration of the shock wave is much greater than this, the body may be projected outward in one piece at a velocity determined by the total impulse delivered by the energy source. Suppose, however, that spalls do occur and that they are thin compared with body thickness; then one or more spalled layers will be projected from the surface at velocities depending on shock strength and material. Under these conditions the spalls would represent a threat to any surrounding container; and, according to previous work, the extent of threat depends on a damage parameter, L, equal to kinetic energy per unit diameter of projectile.[135] If all spalls have the same diameter (and this will depend on geometry), the extent of damage increases monotonically with

$$L = \frac{\frac{1}{2} \rho_o t d^2 W^2}{d} = \frac{1}{2} \rho_o t d W^2 \ , \tag{6.199}$$

where W, t, d, and ρ_o are spall velocity, thickness, width, and density, respectively. Since d was assumed to be constant,

$$L \propto \rho_o t W^2 \ . \tag{6.200}$$

Before comparing different materials, some criterion for equal shocks must be established, and it is perhaps most reasonable to suppose that the pressure-time history of the shock-generating mechanism is the same in each case. This implies that, except for attenuation, which may be controlling, the rate at which work is done is constant; that is, pu is constant. Then

$$W^2 = 4u^2 = \frac{4pu}{\rho_o u} = \frac{\text{constant}}{\rho_o u} , \qquad (6.201)$$

and

$$L \propto \rho_o t W^2 \propto \frac{t}{u} . \qquad (6.202)$$

Spall thickness depends in detail on shock wave structure and tensile strength. A fair approximation for the long wavelength shocks to be expected in reactor explosions is to regard the decay rate for pressure behind the shock front as linear over the distance of a spall thickness. Then spall thickness depends directly on dynamic tensile strength of the medium. It is interesting to compare concrete, the most common reactor shielding, with steel. Concrete has a static tensile strength of 100 to 400 psi compared with about 40,000 to 300,000 psi for steel. If both strengths rise by the same factor (about 3 for steel) for high rates of strain, spall thicknesses in concrete should be much less than those in steel for identical shocks. Since the shock velocity in steel is about twice that in concrete, it should be expected that $L_{steel} \approx 1000\ L_{concrete}$.

Shock waves in concrete will therefore not produce high energy spalls. The details of shock wave amplitude and shape are unimportant, except that the total impulse should not be enough to project the whole body out at high velocity. A high-amplitude shock will produce high-velocity spalls of powder size, while a low-amplitude shock will produce massive but low-velocity spalls.

The qualitative theoretical considerations above are backed up by the results of Stanford Research Institute studies of concrete breaching.[136] No fragments capable of breaching the usual reactor building were ever observed during extensive concrete demolition tests. Fragments of cubic-foot size were given velocities on the order of 50 ft/sec, and fist-size fragments were given velocities of less than 200 ft/sec.[137]

6.6.2 Penetrability of Shells*

A potentially serious hazard to the airtight integrity of the outermost containment shell is that posed by long, slender missiles generated during an excursion. Such missiles could conceivably be control rods or fuel rods channeled into the reactor core or lengths of pipe broken loose by the disruption of a pressure vessel. Fragments of the biological shielding, including reinforcing rod, might also constitute hazardous missiles.

---

*Work reported in this section was taken from a paper by G. R. Fowles, R. W. White, and N. B. Botsford, Poulter Laboratories, Stanford Research Institute, Menlo Park, Calif. Much of the work was performed by N. R. Zabel.

To assess the extent of the hazard from this source, knowledge is required of (1) the types of missiles likely to be generated and their velocities and (2) the criteria for penetration. Knowledge of the first depends strongly on the type of reactor and the magnitude of the excursion; at present the containment engineer must rely heavily for this information on theoretical estimates based on detailed study of the particular reactor under consideration. The second has been examined in a series of penetration experiments.

6.6.2.1 Penetration Experiments

1. Basic Tests. Most of the experiments were performed with flat-ended cylindrical rods fired end-on at thin mild steel plates supported in a heavy frame. The arrangement is shown in Fig. 6.93. A series of firings at slightly different velocities, with other parameters held constant,

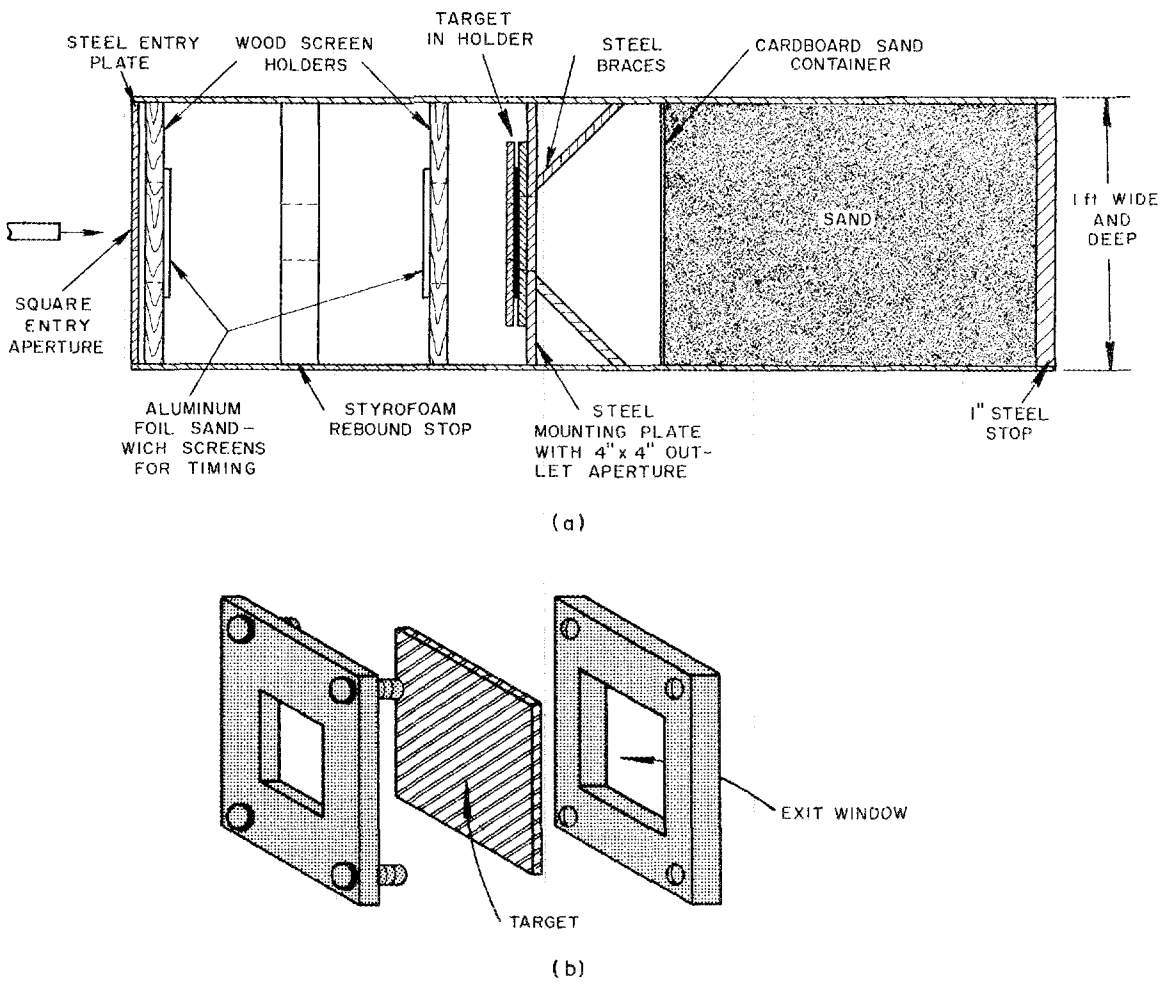

Fig. 6.93. Target Arrangement. (From ref. 135)

served to bracket the critical penetration velocity in each case. Figure 6.94 shows a case in which penetration was just achieved. For tool-steel projectiles, the following empirical relation was found:

$$\frac{E}{DF^2} = \frac{S}{46,500}\left(16,000\,\frac{T^2}{F^2} + 375\,\frac{WT}{F^2}\right), \qquad (6.203)$$

where

E = critical kinetic energy required for penetration, ft-lb,
D = rod diameter, in.,
S = ultimate tensile strength of target plate, psi,
T = target plate thickness, in.,
W = length of side of square window in the target frame, in.,
F = scale factor = W/W_s; W_s = 4 in.

A plot showing the agreement of the data with Eq. (6.203) is shown in Fig. 6.95. The data deviate from the formula somewhat, particularly at the higher (scaled) thickness values. Detailed examination of the

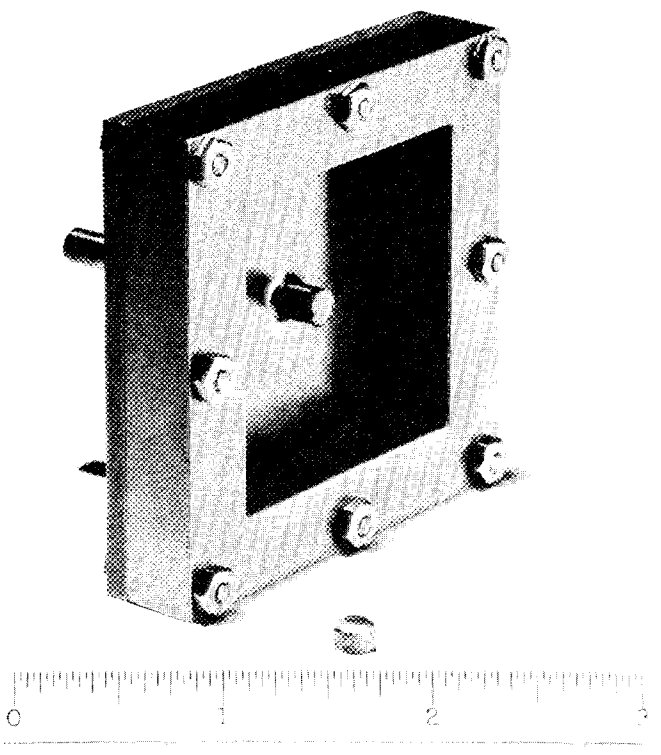

Fig. 6.94. Threshold Penetration. (From ref. 135)

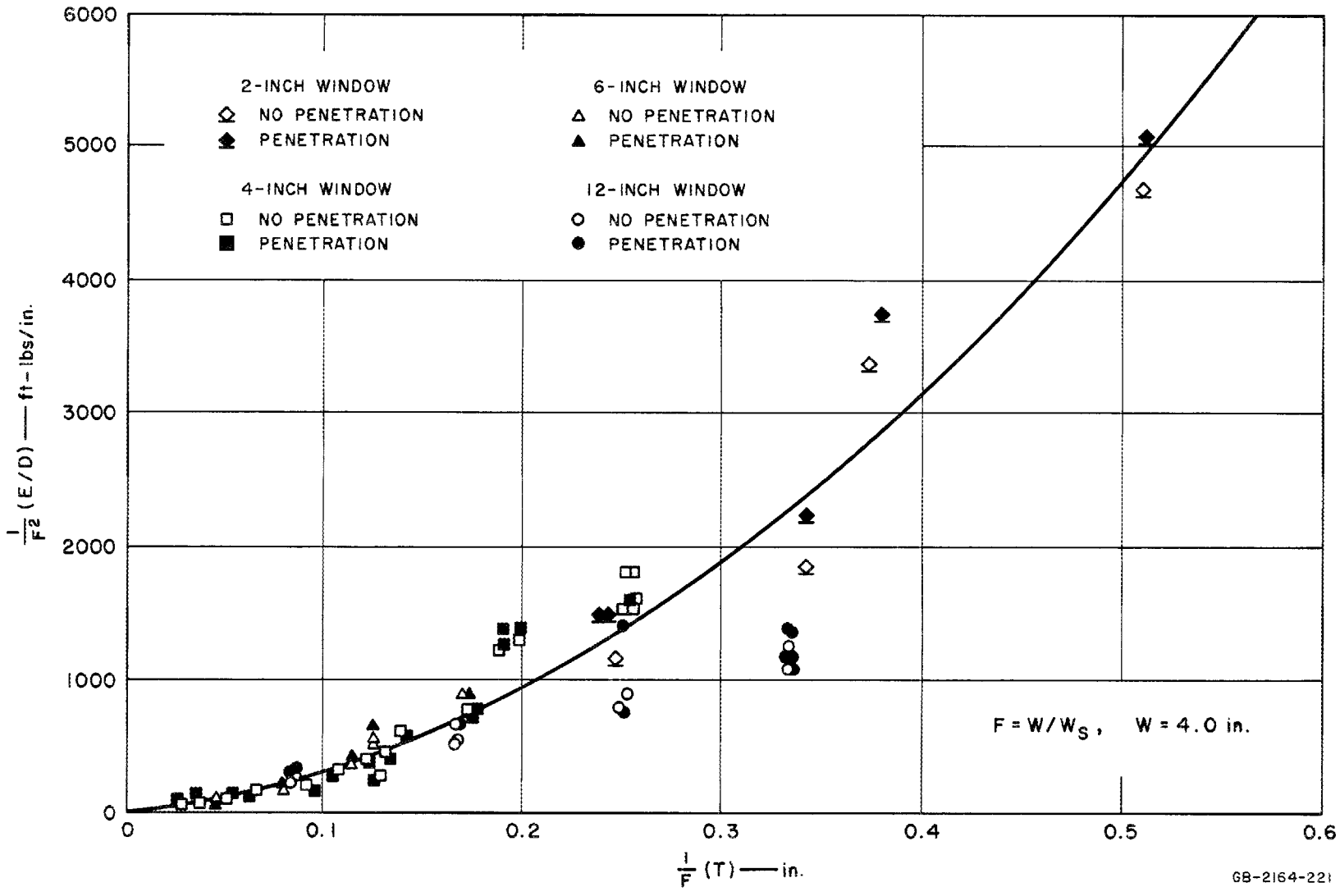

Fig. 6.95. Scaled Specific Energy for Penetration. (From ref. 135)

data indicates that some of this deviation is due to neglect of projectile length explicitly. [Projectile length enters Eq. (6.203) only in the calculation of kinetic energy.] However, the formula is simple to use; furthermore, it is probably adequate for most engineering purposes.

The formula can be used within the following ranges of variation of ratios of parameters:

$$0.1 < T/D < 0.8$$
$$0.002 < T/L < 0.05$$
$$10 < L/D < 50$$
$$5 < W/D < 8$$
$$8 < W/T < 100$$
$$0.2 < W/L < 1.0$$
$$70 < V_c < 400$$

where V_c is critical penetration velocity (ft/sec) and L is projectile length. These ratios are not all independent but must be satisfied simultaneously, since all combinations within the above limits were not tested. Some of these ranges are displayed graphically in Fig. 6.96. The points indicate the representative parameter ratios that were tested. Critical penetration velocities are indicated by the numbers shown next to the points.

2. Scaling. It may be noted that Eq. (6.203), as written, implies that the penetration phenomenon scales; that is, for a given target and projectile material the critical velocity for penetration is dependent only on ratios of geometrical parameters and not their absolute values. The validity of scaling was established in a series of experiments at the points labeled A, B, and C in Fig. 6.96. The scale factor was varied over a range of approximately 7 to 1, with all ratios of parameters held constant. The penetration velocity varied by less than 10% in each case. Because scaling holds, the range of validity of Eq. (6.203) is expressed in terms of ratios of geometrical parameters.

3. Projectile Materials. The effects of various projectile materials are compared in the graph shown in Fig. 6.97. The energy requirements for penetration clearly increases as the strength of the projectile decreases; this is believed to be due to plastic deformation of the end of the projectile on impact. Tool steel projectiles penetrated with the least energy of those investigated; and, since these suffered little deformation, they probably also represent the most hazardous case. Thus, hazard estimates based on the results for tool steel [Eq. (6.203)] should always be conservative. Concrete missiles are clearly much less hazardous than metal for T/D ratios greater than about 1:20.

4. Projectile Shape and Attitude. A limited number of tests to show the effect of a conical tip on the end of the rod showed that for cone angles greater than 90° the energy for penetration is equal to or slightly greater than that for a flat-ended projectile. For more sharply pointed rods, however, the energy for perforation (as distinct from complete penetration) is substantially less. For example, a rod with a 45° cone angle produced perforation with approximately half the energy required of a flat-ended rod of the same dimensions.

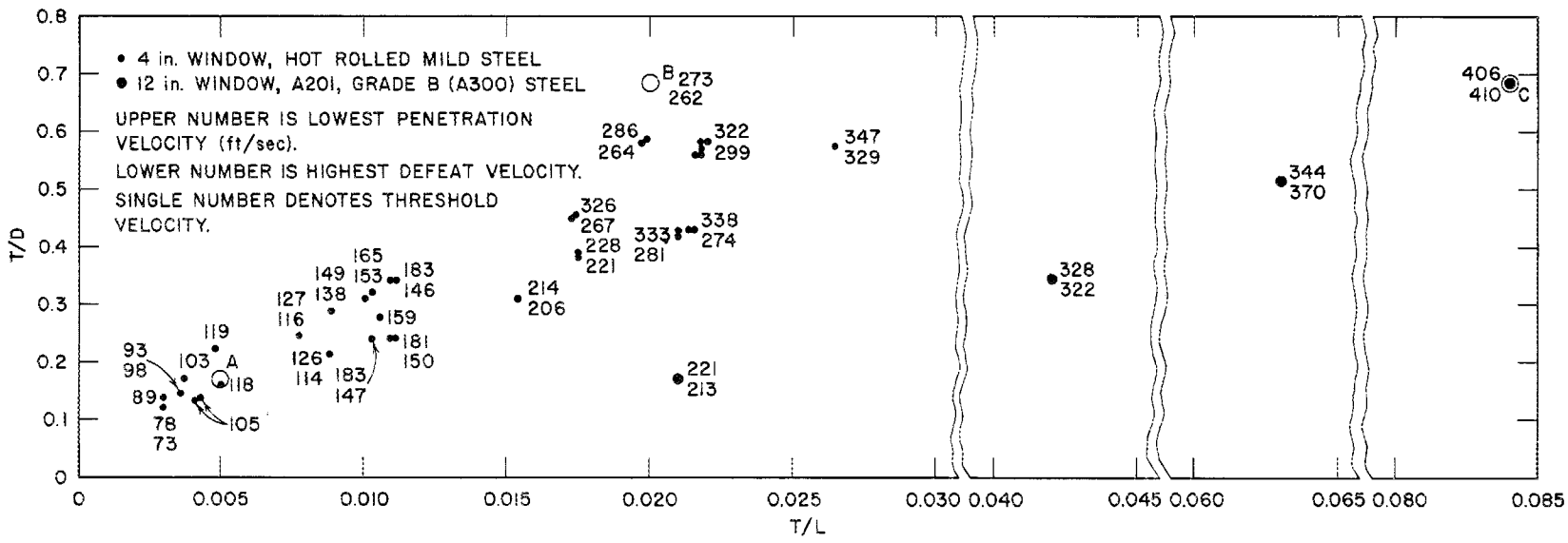

Fig. 6.96. Parameter Ratios Investigated. (From ref. 135)

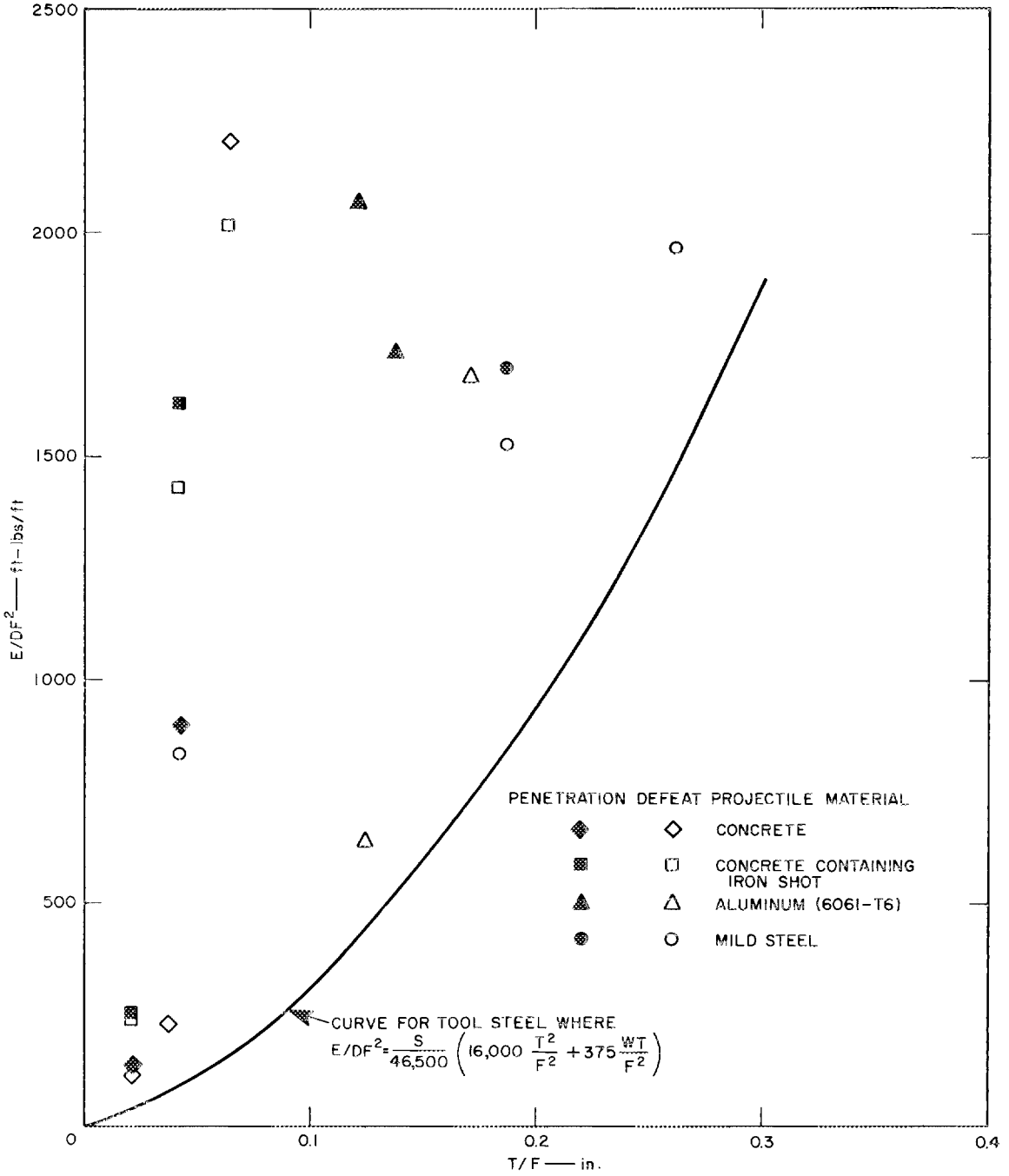

Fig. 6.97. Projectile Material Comparison. (From ref. 135)

Other tests in which the rod axis was inclined slightly (<15°) to the normal to the target showed no appreciable differences in penetration energy compared with tests at normal incidence.

5. Prestress of Target. In an excursion the containment shell might be prestressed by hydrostatic pressure before impact of a missile. Penetration tests with the target under tension, up to 6000 psi, showed that the effect of prestress is simply to reduce the effective ultimate tensile strength of the target. Thus, prestress can be accounted for in Eq. (6.203) by reducing S by the amount of prestress.

6. Window Size. The experiments were necessarily performed with the target mounted in a frame of finite size. Unfortunately, this size was not so large that variations in window size or, more accurately, variations in the ratio of window size to other geometrical parameters could be neglected. Consequently, window size must be considered in the application of Eq. (6.203) to real situations.

It should be noted that Eq. (6.203) does not extrapolate properly for values of W/L, W/D, and W/T substantially larger than those employed in the experiments; the formula predicts that the penetration energy increases indefinitely with W, with all other parameters held constant. A few tests, however, indicated deviations in penetration energy by no more than ±50% from predictions of Eq. (6.203) as the window size was made either very large or very small (larger windows required larger energy; smaller windows, less). Hence, a reasonable procedure for estimating the penetration hazard in cases where the ratio of window size to other parameters is greater than the range of validity of Eq. (6.203) would be to employ this equation with an assumed value of W such that $W/D \cong 8$. The value of critical penetration energy obtained by this procedure should always be conservative; that is, greater energy would be required to penetrate where the actual window size was larger than that assumed in the above ratio.

6.6.2.2 Conclusions

The experimental results lead to the following conclusions:

1. The most hazardous type of projectile is one of material that is hard when compared with mild steel, has either a sharply pointed end (cone angle less than 90°) or a flat end, and strikes the shell end-on.

2. Scaling is valid. Hence, results obtained in small-scale experiments can be applied on a larger scale, provided all ratios of geometrical parameters are held constant and provided the materials are the same.

3. The effect of an initial tensile stress in the shell is to reduce the effective ultimate tensile strength of the shell by the amount of the prestress.

4. Within the range of parameters listed, Eq. (6.203) provides a reasonably good prediction of the energy requirements for penetration of tool steel rods. This prediction is conservative for softer projectiles; it is generally overly conservative for concrete projectiles.

5. Where missiles with energies sufficiently large to penetrate the containment shell can be shown to exist, the containment shell should be protected as by interposing an adequate barrier between the shell and the potential missile. Shielding concrete frequently doubles for this purpose.

6.6.3 Blast Shielding[59]*

Figure 6.98 illustrates the generic idea in the use of blast shielding that was originally suggested by the waste heat concept (Section 6.4.3). The blast shield is designed to effect a bonafide conversion of hydrodynamic energy to thermal energy through the use of absorbing layers. The medium surrounding the core, the reactor shielding, and the reactor compartment may provide adequate absorber material. The thickness of the various layers is limited by considerations of the partition between internal and kinetic energy, the energy in the explosion, and the pressure level at which the absorber reaches its crushing strength and ceases to be efficient for absorption. Steel plates enclose the layers of the absorbing materials. Their function is to flatten out the shock front and to make the shock act more like a piston on the subsequent layers and to contain the absorbing materials.

---

*This Section is closely related to Section 6.4.3, Shock Generation and Transmission.

ORNL-DWG 64-8799R

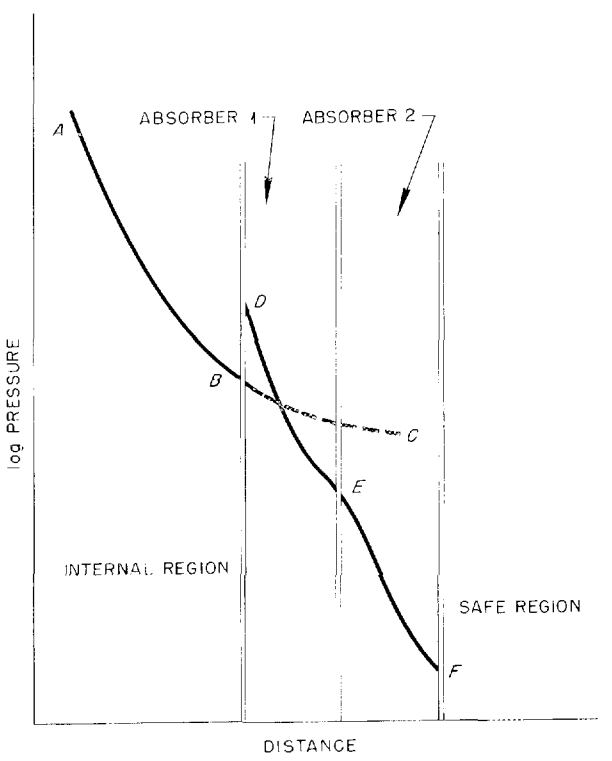

Fig. 6.98. The Waste Heat Concept.

A better insight into the mechanism of absorption may be obtained from Fig. 6.98 by following closely the sequence of events after an instantaneous energy release. As a result of the energy release, the internal region will be subjected to peak pressures, as shown by curve A-B. The decay of the peak pressure with distance may be predicted by Eq. (6.122). At point B, the internal region ceases to be an effective absorber (for example, for water this would be about 20,000 bars). As a result of pressure multiplication at the interface, the pressure in absorber 1 is boosted to point D. From this point, the pressure again decays to point E. As before, point E represents the lowest pressure at which material 1 is an effective absorber. At this point, a new absorbing material, 2, is used to reduce the pressure to point F, which is assumed to be a safe pressure. The dashed curves represent the decay of pressure with distance in the absence of the subsequent absorbing material layers. For example, curve B-C would represent the pressure decay if absorbers 1 and 2 were replaced with the internal region material.

Strictly speaking, an optimum shield can be tailor-made for any given pressure level and energy content, but, whatever shield is constructed, if the blast does not vaporize some of the absorber, it will be more efficient at higher energies and pressures than at low energies. Even though it will be less efficient for explosions below the design value, it will always reduce the pressure to some lower and safer level than for the larger explosion.

6.6.3.1 Blast Shield Theory

To effect a diminution in the energy of a shock, either a real absorptive mechanism must be provided or the energy must be distributed over a larger volume by some mechanism such as channeling. At a high enough pressure in any material, a shock becomes a highly irreversible process; the pressure level at which such irreversibility is important depends on the thermodynamic properties of the material through which the shock passes. Unfortunately, considering current reactor design, shock strengths in the range of a megabar in concrete or tens of kilobars in water are still elastic processes and, consequently, these materials act as transmitters. To capitalize on the irreversibility requires a suitable change of the materials through which the shock is passed.

Although the entropy change across shocks is well recognized, the difficulty is one of expressing or assessing this waste heat in a simple engineering fashion. This is especially true in the absence of a complete equation of state for the material up to the pressures in question. However, it appears that the Rankine-Hugoniot curve for the material may be valid to assess the magnitude of the waste heat at any reasonable pressure level below vaporization of the absorbing material.

The entire history of the thermodynamic behavior of the material in a blast wave and much of its dynamic behavior may be portrayed in a convenient form by use of the familiar pressure-volume plot shown in Fig. 6.99. It is similar to Fig. 6.45 but contains further details necessary for the exposition of the waste heat theory. The ambient conditions for the material before shock arrival are represented by the coordinate $p_o v_o$. The curved path along OAB is the Rankine-Hugoniot curve and represents, for various

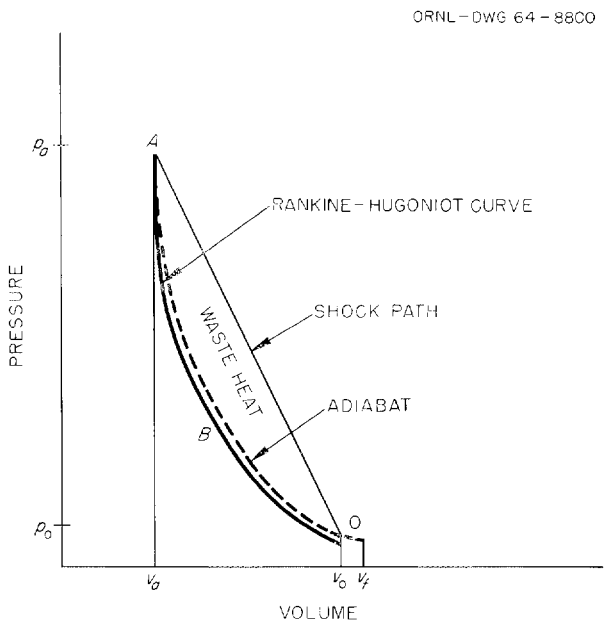

Fig. 6.99. The Waste Heat Concept.

shock strengths, the pv relations that must exist behind the shock front. For any given shock strength (point A), the material is effectively raised instantaneously to this state along the straight-line path, OA. The path OA does not mean that there is a constant rise across the shock front, but merely that the internal energy imparted by the shock to the material at pressure p_a may be conveniently represented by the area of the trapezoid, $v_0 O v_a A$.

After passage of the shock, the material expands, and the assumption is made, with considerable experimental justification, that the expansion is adiabatic. The p dv work done by the material in the expansion represents the energy given up by the particles. It is this energy that is transported forward and compresses more distant material at a later time.

The total work done during the adiabatic expansion is obviously the area under the curved adiabat from its initial shocked volume v_a to its final volume v_f when the material is returned to ambient pressure. The return to ambient pressure is not, of course, asymptotic; it is really a series of oscillations into negative-phase pressures beyond v_f until the final ambient pressures are reestablished. This happens essentially after the blast has decayed to insignificantly low overpressures. The difference between the area under the adiabat, which is the energy given up by the material, and the area under the internal energy trapezoid is the waste heat.

In general, the adiabat lies above the Rankine-Hugoniot curve, such as shown in an exaggerated way in Fig. 6.99. However, the difference is so small that the Rankine-Hugoniot wave may be used to depict the expansion process so long as the material is not raised to a sufficiently high pressure to result in subsequent vaporization upon expansion.

Another remarkable property of solid and liquid materials is that the temperature rise, even immediately behind the shock, is extremely small. In addition, their heat capacity is very large, and their coefficient of thermal expansion is small. Thus, even if substantial residual heat is left in these materials, their final specific volume, v_f, is nearly identical with their initial specific volume, v_o. Therefore, from a design standpoint, v_f may be assumed to be equal to v_o.

6.6.3.2 Absorption Mechanism

The mechanism for absorption of energy, with special regard for the process in an inhomogeneous medium, is considered briefly below. Air is a highly efficient transmitting medium for shocks at pressures in excess of 100 bars despite a high temperature. Solid and liquid media are efficient transmitters up to ranges near megabars. There is a question whether it is possible to construct a composite medium that has a waste heat fraction at pressure levels of interest (from 100 to 10,000 bars) that is larger than that of either material taken separately as a pure substance.

The absorption mechanism for a composite substance may be visualized by taking, for example, a composite material that contains equal volumes of air and some solid material. During the passage of the shock over the composite, the Rankine-Hugoniot equation would be written for each of the two phases. The solid or liquid phase would barely decrease in volume, and the temperature rise would be negligible. In the range of several hundred atmospheres, however, or even a few atmospheres for that matter, the temperature rise in the gas phase would be high. It may be estimated roughly from

$$\frac{T}{T_o} = \frac{\xi(\xi + \mu)}{(\mu\xi + 1)}, \tag{6.204}$$

where ξ is the pressure ratio, p/p_o, and μ is a constant for the gas. This equation implies the ideal gas law but, by virtue of the limiting density ratio in gaslike materials, this temperature ratio rapidly becomes ξ/μ. This means that for a pure substance, large p dv work is available by subsequent expansion. In the presence of the solid medium, however, the air may rapidly transfer its heat to the surrounding matrix of solid or fluid and lose this heat. Despite the fact that the mass of air is small, the very high temperatures, according to Eq. (6.204), represent substantial energy that may be transferred by conduction to the solid or liquid phase, where it then becomes unavailable for further p dv work. If the material is divided finely enough, thermodynamic equilibrium can be assumed, and the compression of the air may be considered as an isothermal process. The temperature rise in the mixture is relatively small, and the compression ratio across the shock is governed almost entirely by the initial air content.

Such a composite takes advantage of nearly all the high compressibility of air and yet is far less efficient than air for transmitting

shocks. The composite material would require an energy density in the order of a thousand times greater than that required for the solid to produce the same shock pressure. At a given pressure level, its material velocity would be higher and its shock velocities much lower than for the corresponding solid medium.

6.6.3.3 Criteria for Ideal Absorbers

Certain characteristics can be specified for an ideal absorber for the dissipation of energy. The ideal absorber should maximize the waste heat area or, more properly, the waste heat fraction. A composite material may be realized in a practical way by a suitable mixture of air and solids. This requirement is shown graphically in Fig. 6.100. The Rankine-Hugoniot curve would be initially flat, and at some compression ratio, shown as the value v_c, the material would become practically incompressible. From the standpoint of a waste heat fraction, it is not of prime importance what fraction of v_o is represented by v_c. In any case the waste heat area will be nearly identical with the internal energy trapezoid. From the standpoint of total absorption in calories per gram of material traversed, v_c would ideally be as close to zero as is possible. This would imply a large initial fraction of air present. There is a practical upper limit to the air fraction because, if the volume of air is too large, the final temperatures would be comparable with those of pure air. In that case the solid material would vaporize and the adiabat would no longer terminate at point v_o. The material would again become a very efficient transmitter of energy.

It may be noted in Fig. 6.100 that the lower branch of the Rankine-Hugoniot curve is concave downward over part of the region O YB. From previous considerations, it is clear that the slope of a line joining point O with any point on that segment of the Rankine-Hugoniot curve will be closely related to the shock velocity [see Eq. (6.86)]. From the shape of the curve shown in Fig. 6.100, it is clear that the shock velocity would actually decrease with increasing pressure in region YB. This, in turn, would imply that the shocking-up process could not be attained in this pressure region, and it would be expected that the pressure disturbance would show a slow rise instead of a sharp shock at these pressure levels.

To be effective for degradation of energy, the heat transfer in an inhomogeneous medium must be accomplished in a time considerably shorter than the shock duration. The time for thermal equilibrium is estimated by idealizing the mixture as composed of spheres of one material in a matrix of another.

A rough estimate for the temperature distribution gives the results that the interior of a wooden sphere 10^{-3} cm in diameter will be within 5% of the surface temperature in times of the order of 20 to 100 μsec. This means that the heat transfer from a material like air to a material like wood that has grain sizes on the order of 10^{-3} cm will be complete within 20 to 100 μsec.

These considerations of thermal conductivity suggest the following criteria for materials: (1) small grain size, particle size of 10^{-3} cm or

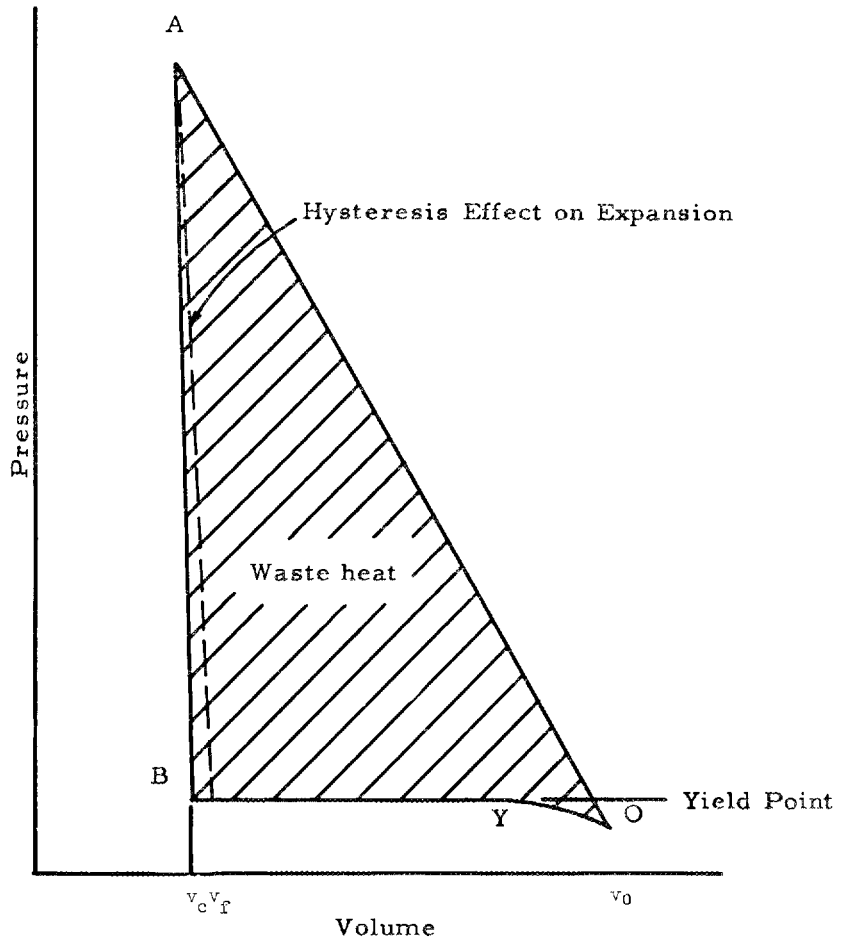

(1) Rankine-Hugoniot curve flat in Region YB (low yield point)
(2) AB nearly vertical (high final rigidity)
(3) High heat capacity and thermal conductivity
(4) Hysteresis (adiabatic expansion follows AB)

Fig. 6.100. Rankine-Hugoniot Curve for the Ideal Absorber. (From ref. 59)

less; (2) a high conductivity (like a metallic sponge); or (3) low densities and specific heat (like aluminum). It should be noted that the metals are, in general, more favorable than wood for these heat-transfer processes.

6.6.3.4 Reduction Factor Formula

Assuming an absorber with characteristics as portrayed in Fig. 6.100, the waste heat per gram of material is the internal energy of the shock

itself, as given by

$$\text{Waste heat} \cong E_i = \frac{1}{2}(p + p_o)(v_o - v) \ . \qquad (6.205)$$

If the material has been properly chosen so that the peak pressures involved fall on the vertical parts of the Rankine-Hugoniot curve, then the quantity $v_o - v$ is nearly independent of the peak pressure. This means, in turn, that the waste heat is directly proportional to the pressure of the incoming shock. As the wave is degraded in passing through the absorber, this pressure falls. Previous considerations have shown that there is no point in letting this pressure fall too low because of the corresponding decrease in its capacity to absorb energy. Moreover, an equal amount of energy is present as kinetic energy, and, even if all the internal energy is absorbed, one-half of the total energy will remain as kinetic energy of the absorbing material. There is no point in making the first absorbing layer much thicker than required to absorb the internal energy of the incoming shock.

At the end of this first absorbing layer, it seems advisable to insert a thin layer of a strong material, like steel, for several purposes. First of all, the possibility must be precluded of a break through the barrier channeling in the event of a weakness in the absorbing layer. In view of the enormous differential flow of energy to regions of light density or weakness, it can easily be visualized that such an absorber might readily "blow out" weak portions. The second purpose of the steel is to absorb the kinetic energy of the first layer. The steel then becomes the piston that transfers shock energy to the next succeeding layer.

In the second stage of the absorber, the behavior is still described by the critical portion of the Rankine-Hugoniot curve; hence, the $v_o - v$ volume change is independent of the pressure level. By this time the energy density should be one-half the energy density that entered the preceding layer; but, by the same token, the energy absorption ability of the second layer is also halved. Having calculated the thickness of material required for the first absorber, it will then be found that the thickness of the second absorber is identical with that of the first. After such a stage, a rigid barrier, like steel, is again placed for the same purposes as at the end of the first layer. Thus, successive stages of the blast shield count on a reduction in the peak pressure and the energy density by a factor of 2 until such time as the peak pressure falls below the yield point or flat portion of the Rankine-Hugoniot curve. At this time, the material in the absorber must be exchanged for one with a lower yield point.

It follows from these arguments that the number of stages, m, required in the blast shield will be given by the relation between the incident pressure at the face of the shield and the maximum tolerable pressure at the back of the shield, according to

$$\frac{\text{Incident pressure}}{\text{Maximum desired pressure}} = 2^n \ . \qquad (6.206)$$

6.6.3.5 Materials

Based on the criteria for ideal absorbers, given in Section 6.6.3.3, a number of materials may be considered. The criteria themselves immediately suggest wood as a likely material.

Metallic powders would have the advantage of high density and rapid heat transfer; but there is a danger that their thermal properties might be lost by oxidation, and there is considerable doubt that samples could be prepared in fine enough grain size in the bulk required for the blast shield. Fine sand would make an excellent material without the risk of decomposition on heating. In time, however, it would pack down and would probably not be fine enough for the purposes required. Plastic foams, such as those used for Christmas tree ornaments, are likely materials, but they might be too light and easily decomposed.

Wood offers considerable promise because its natural grain size and cell structure is probably fine enough to effect the heat transfer required. Wood shows a low yield point, especially if it is stressed across the grain. The density is high enough that a considerable amount of heat may be absorbed before decomposition occurs. In addition, crushed wood exhibits hysteresis which, as mentioned previously, is beneficial for blast shields. Of these materials, the hard woods would be expected to be the poorest from the standpoint of a yield point or overall compressibility. On the other end of the scale, balsa wood shows the lowest yield point and highest compressibility but is probably too expensive for use in the blast shield. Figures 6.101 to 6.104 (refs. 59 and 138) show compressibility curves for redwood, Celotex, vermiculite concrete, and aerated concrete.

The numerical results of tests on redwood conducted at the Armour Research Foundation[59] are given in Table 6.16, with the shock velocity as

Table 6.16. Compression Properties of Redwood[a]

Pressure (bars)	v/v_o, Volume Ratio (compression)	Volume Ratio (after pressure release)	Shock Velocity (cm/sec)
55	0.908	0.204	34,400
110	0.735	0.175	31,000
121	0.585		26,300
132	0.504		25,200
154	0.424		25,500
220	0.337	0.157	28,900
440	0.245	0.140	38,700
880	0.175	0.135	53,000
1320	0.15	0.126	64,100
1760	0.135		73,500
2200	0.13		82,000
2630	0.124	0.124	89,500

[a]From ref. 59.

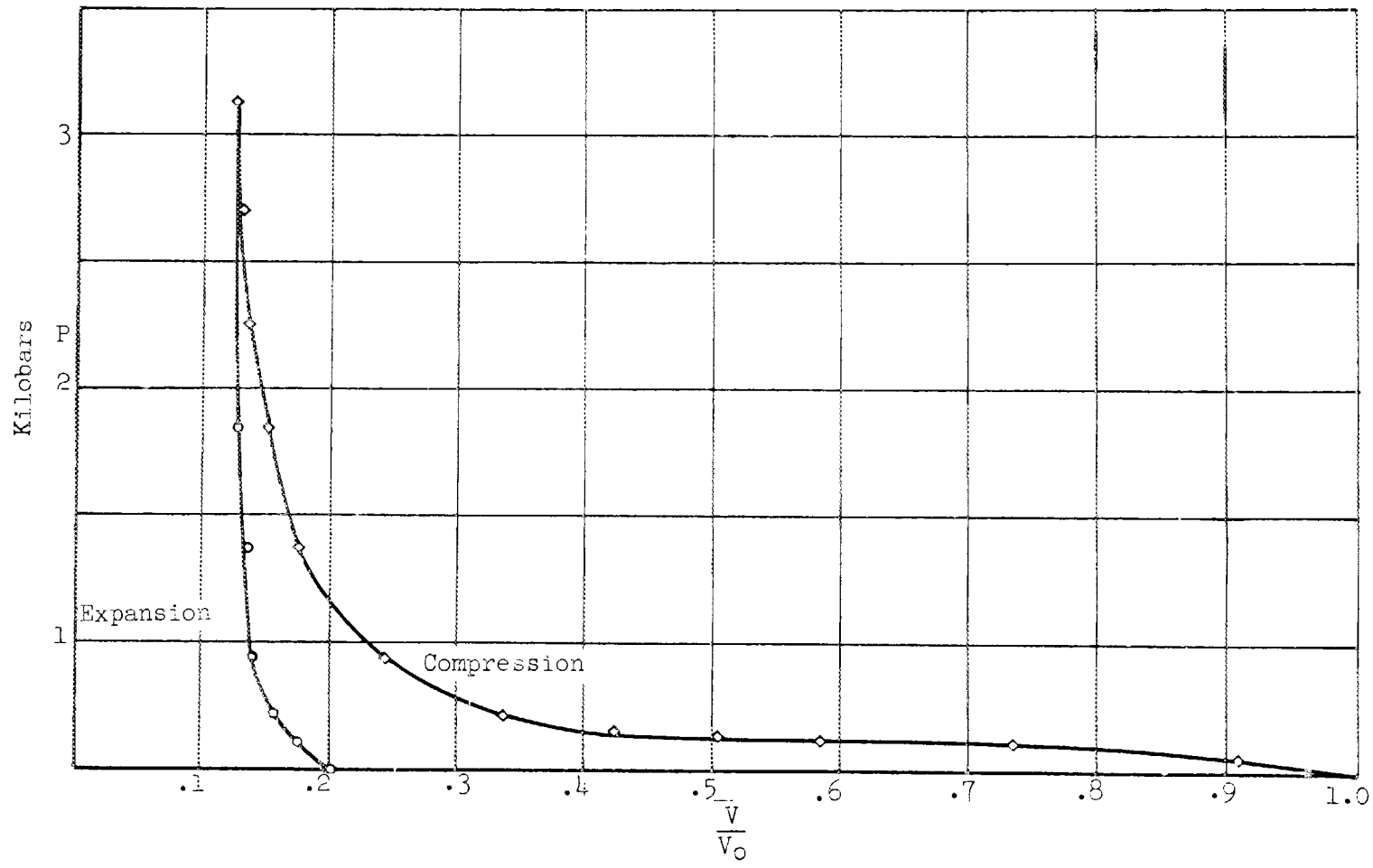

Fig. 6.101. Pressure-Volume Relations for Redwood. (From ref. 59.)

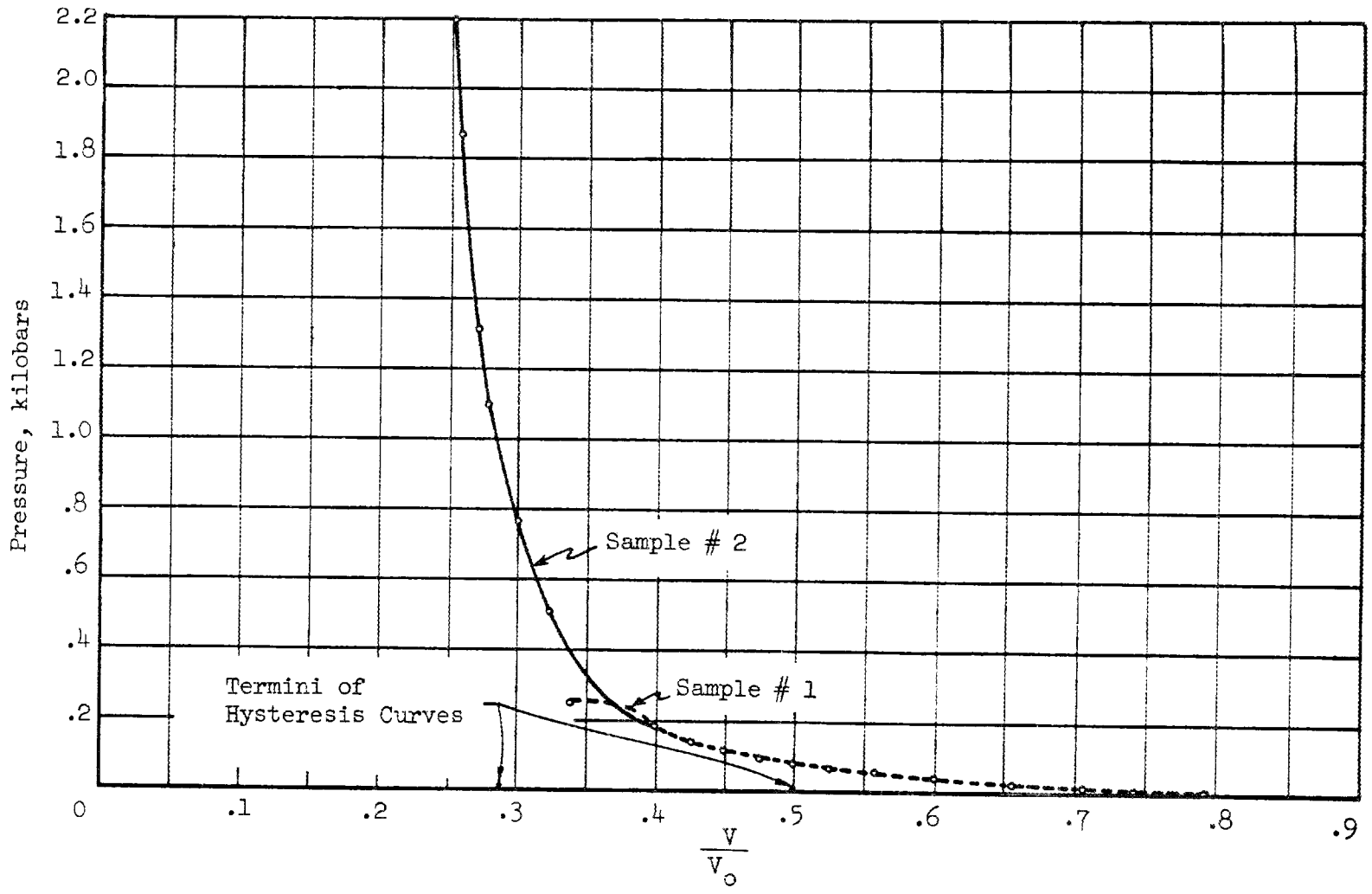

Fig. 6.102. Pressure-Volume Relations for Celotex. (From ref. 138)

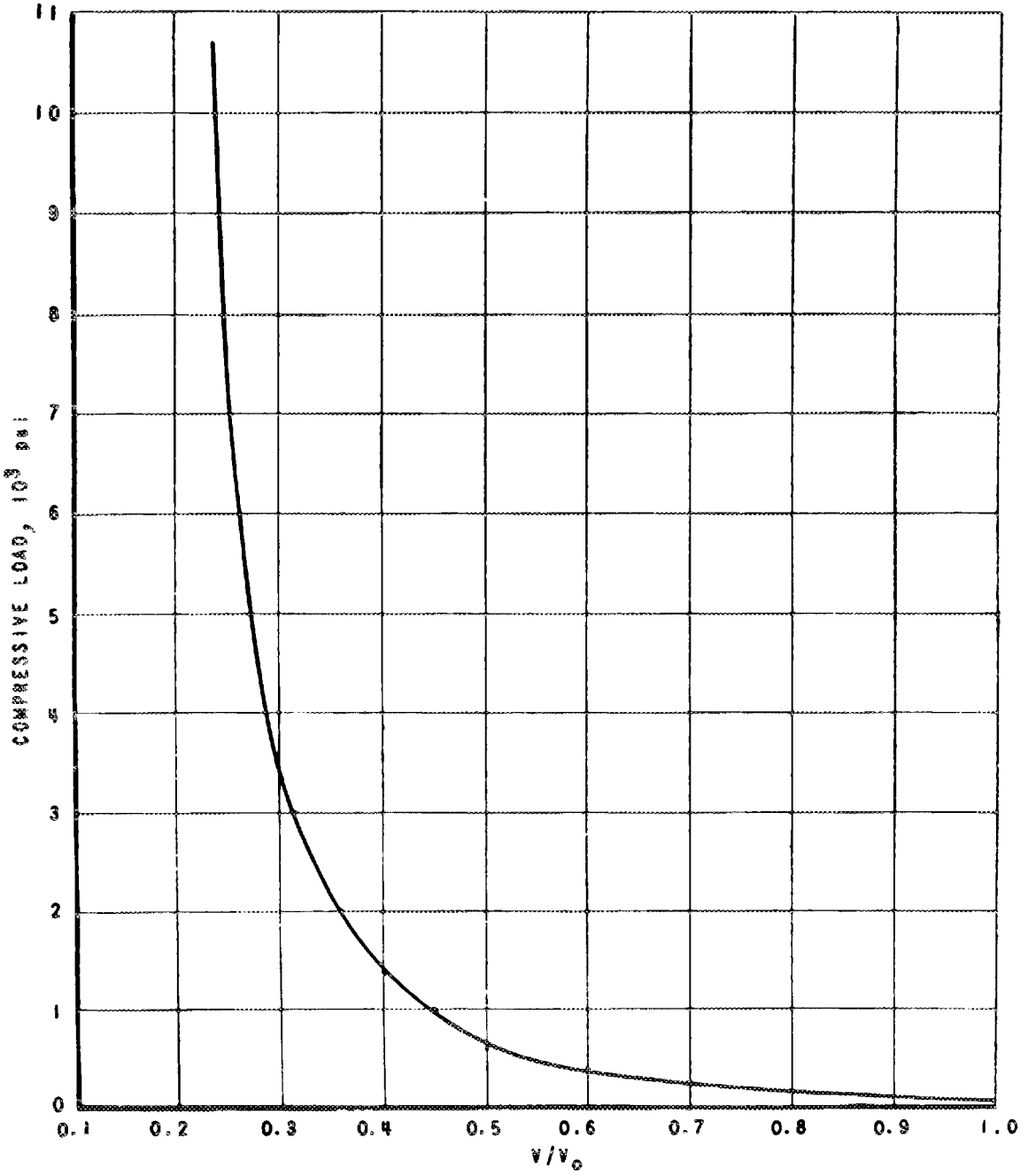

Fig. 6.103. Compressibility Curve for Vermiculite Concrete with a Density of 22 lb/ft^3. (From ref. 138)

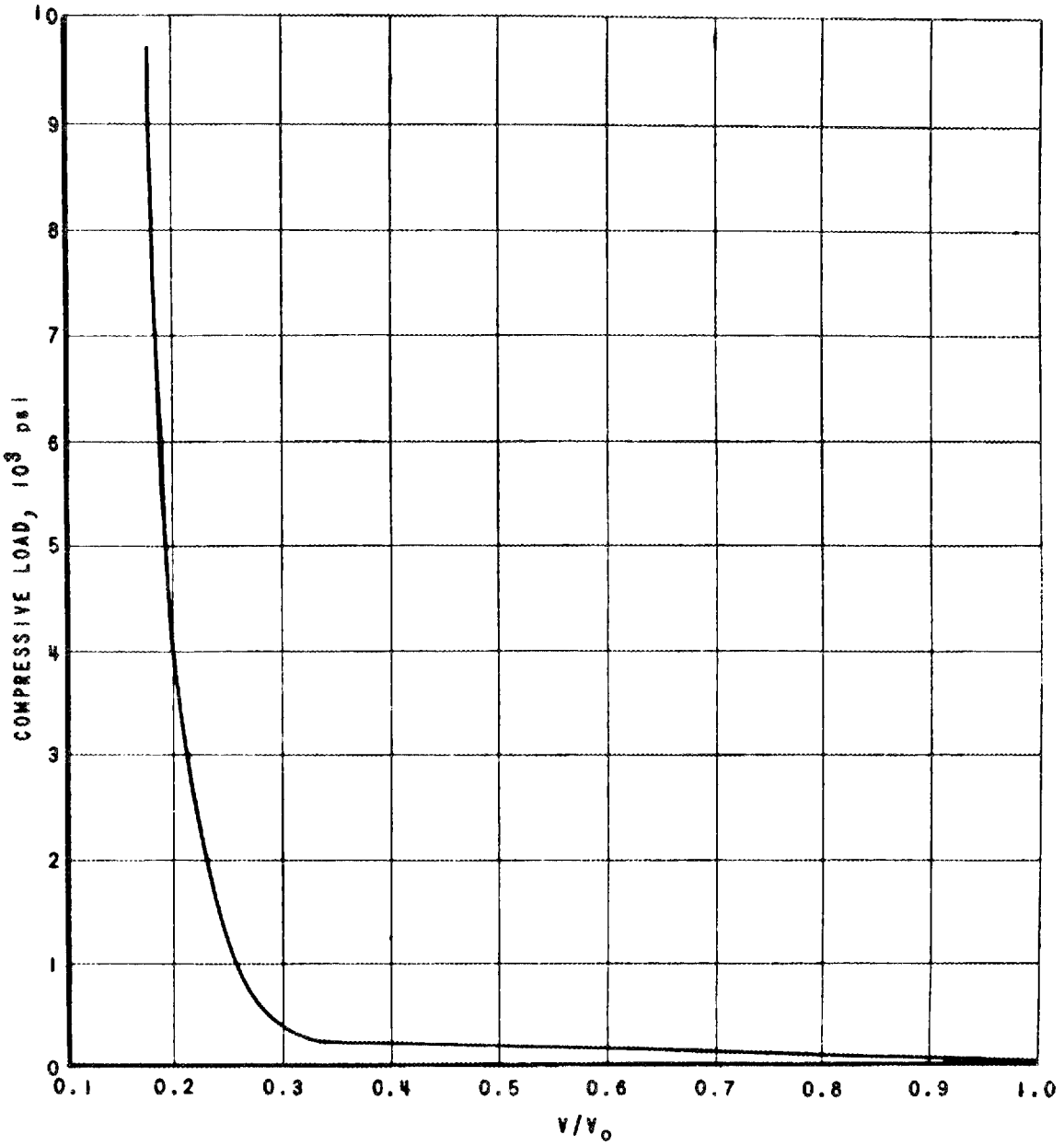

Fig. 6.104. Compressibility Curve for Aerated Concrete with a Density of 16.5 lb/ft^3. (From ref. 138)

a function of pressure. For all practical purposes, redwood has most of the properties of an ideal absorber. An important feature is the minimum in shock velocity for pressures on the order of 100 atm. This means that the shock-propagating characteristics are destroyed in redwood in this pressure range, and the pressure pulse that is transmitted can only be of a low-rise type; the shock discontinuity is absent.

An examination of Fig. 6.102 shows that although no true yield point is present for Celotex, the lower limit of pressure transmitted is likely to be considerably less than that for redwood. Considerable deflections occur for pressures as low as 60 psi, where the shock velocity is of the order of 6000 cm/sec. This is a remarkedly low value and is ideal from the standpoint of slowing down the shock in front of the shield and permitting back pressure to build up before the front is completely loaded. If a yield point exists in Celotex, it would seem to be at a pressure of 2 bars, or 30 psi. Since the Rankine-Hugoniot curve is concave upward in its entire history, a true shock would be transmitted in Celotex with no phenomena like the slow rise or acoustic wave (as in redwood).

Figure 6.103 indicates that vermiculite concrete has features similar to those of redwood, and, although it is not as close to an ideal absorber as redwood, it may have a sufficient fabrication advantage to make it preferable. Aerated concrete (Fig. 6.104) has features comparable with those of Celotex, and the choice of this material would be made on other considerations. A suitable design for a blast shield would use either redwood or vermiculite concrete in the earlier stages and one or two stages of either Celotex or aerated concrete at the end when the pressures are low.

6.6.3.6 Maximum Absorber Thickness

The determination of the maximum thickness of absorber required may be made on the basis of gross energy considerations. The assumption is made that all energy propagated from the explosions within a given solid angle remains within the solid angle. Any reduction in energy or pressure that occurs as a result of nonradial flow of energy is regarded as a safety factor in the shielding problem. The energy transmitted to the shield is calculated according to the methods in Section 6.4.3.

As an example, a shield composed of redwood in the earlier stages is considered. A shock is transmitted through concrete to the redwood. It is assumed that the shock has a pressure of 50,000 psi and an energy of 80 cal/cm^2. The least average pressure likely to be transmitted by redwood is the yield point of 100 bars. The p dv work done against such a pressure gives the maximum overall thickness. The amount the redwood would have to deflect to absorb this energy is

$$x_o - x = \frac{E}{p} = \frac{80 \text{ cal/cm}^2}{100 \text{ bars}} \times \frac{42 \text{ bars}}{\text{cal/cm}^3} \cong 33 \text{ cm} .$$

Since this calculation is on the basis of the unit cross section, a net deflection of 33 cm (~11 in.) would be sufficient to absorb the entire energy within the solid angle arriving at the shield. Since the actual pressures are likely to be considerably in excess of 100 bars and the final volume ratio for redwood is approximately 0.15, it appears a reasonable estimate that 1 ft of redwood could, in principle, absorb the entire energy from the explosion, or at least a major fraction of it. However, a blast shield based on this calculation would be overdesigned and would be

improper. The above design has not taken advantage of the ability of the wood to dissipate large quantities of energy as waste heat, and it does not recognize the equal partition of energy which requires that one-half the energy be transferred through the absorbing material as kinetic energy. The proper shield would consist of layers of the absorbing material. Each layer would dissipate energy and reduce the pressure until it reached a value where the compressibility curve (Rankine-Hugoniot curve) became horizontal. For redwood, this would be approximately 100 bars.

Before proceeding with the calculation of the individual layer thicknesses, it is useful to consider the sequence of events as the shock passes from concrete into the absorber redwood. Initially, a rarefaction occurs as the shock passes from concrete to wood. With a density of 2.7 g/cm^3 and the constant $a = 4.34 \times 10^5$ bars for concrete, the material velocity in concrete at this pressure level is calculated to be

$$u^2 = (p - p_o)(v_o - v) = \frac{v_o p^2}{a} = \frac{p^2}{\rho_o a}$$

$$= \frac{1}{2.7} \times \frac{(3.3 \times 10^3)^2}{4.34 \times 10^5} \times 10^6 \frac{\text{ergs}}{\text{bar}\cdot\text{cm}^3} = 9 \times 10^7 ,$$

or

$$u \cong 9000 \text{ cm/sec.}$$

According to the usual assumption, this material velocity is doubled by the rarefaction, and the pressure in redwood when the material velocity is 18,000 cm/sec is required. This may be obtained graphically from Fig. 6.101 with the final

$$u^2 = (1.8 \times 10^4)^2 = v_o p \left(1 - \frac{v}{v_o}\right) \times 10^6 .$$

For $v_o = 2.8$ cm^3/g,

$$115 = p \left(1 - \frac{v}{v_o}\right) .$$

This equation has a solution at $p = 185$ bars, where $v/v_o = 0.375$.

The initial shock of 185 bars is transmitted forward in the first stage of redwood. After traversing across the layer of redwood, this shock meets a steel-retainer piece (which is effectively a rigid material), and the reflection process is assumed to be acoustic (reflected = 2 × incident). A reflected shock of approximately 370 bars then moves backward through the

wood, and a transmitted shock of the same magnitude moves forward with the steel. Because this shock is well below the crushing strength for steel, the steel continues forward as a rigid body with negligible velocity. The reflected shock in the redwood meets the concrete, which is again a rigid body reflector. This pressure is insufficient to bring the concrete to rest. A twice-reflected shock moves forward from the concrete surface toward the steel at 740 bars, where it is again reflected, presumably to 1480 bars. By such a series of multiple reflections between concrete and steel surfaces, the pressure in the intervening layer of wood is eventually brought up to the pressures that existed in the concrete just prior to the entrance of the initial shock into the wood.

It is important to recognize that such a series of multiple reflections is intrinsic to reflections across a compressible medium. It is the means by which it is possible for a compressible medium to transmit shock pressures far in excess of its crushing strength.

If the thickness of wood absorber in the first layer were large enough, it might be supposed that entire absorption would occur. Nonetheless, by virtue of equal partition between kinetic and internal energy, it is clear that one-half the original total energy would remain as kinetic energy of the wood itself. For this reason, the maximum absorption reasonable to assume in any given layer is one-half the total energy transmitted to that layer. There is no point in making a layer of absorbing material that considerably exceeds this thickness. Therefore, for the example, there should be no attempt to absorb more than 40 cal/cm^2 in any of the first layer. The requirement for total absorber thickness, based on 80 cal/cm^2, was also based on the assumption that the least average pressure in the wood was 100 bars. The reflection process in the wood, by a series of multiple reflections, is accomplished by considerably less work than that under a single shock. It will be conservative to assume that the work done is the area under the Rankine-Hugoniot curve of Fig. 6.101, and it is readily verified that this area, up to 3300 bars, is approximately twice the area under the rectangle lying between $v/v_o = 0.15$ and 100 bars in height. Thus, the indicated thickness of the first layer is one-fourth the total previously calculated – approximately 8 cm or 3 in.

The thickness may also be justified in the following way. If the initial pressure through the wood is taken to be three times 3000 bars, corresponding to the pressure in concrete, the diminution in energy will be exceedingly rapid and pressures will be reduced to negligible values after the "optimum" thickness has been traversed. Hence, the average value of pressure is 1650 bars. Over this range, the final density ratio is $v/v_o \cong 0.15$, and by a single shock process the waste heat is calculated to be

$$\text{Waste heat} = E_1 = \frac{1}{2}\, p(v_o - v) = \frac{v_o}{2}\, p \left(1 - \frac{v}{v_o}\right)$$

$$= \frac{2.8}{2} \times 1650\ (0.85)$$

$$= 47 \text{ cal/g} .$$

To use up 80 cal would require 80/47 = 1.7 g of redwood, or a column, of unit cross section, 4.8 cm long. Under this exceedingly optimistic assumption, the thickness of the first layer would be approximately one-half the thickness of 3 in. determined on the basis of the more realistic assumption of nearly "adiabatic" compression for the wood.

6.6.3.7 Composite Design

The thickness of the steel plate separating the absorber layers is usually somewhat arbitrary, since the role of the steel plate is to effect the momentum transfer from layer to layer and to retain the layers. The optimum momentum transfer would occur at equal mass per unit area. This would indicate a steel thickness of 3/21 that of wood or approximately 1/8 in. But such a layer of steel is probably too thin to effect any smoothing in the blast wave through the wood, and 1 in. appears intuitively to be a reasonable thickness on the basis of this consideration.

Without considering the decay of the pressure wave in concrete and assuming it to be flat-topped, it is clear that the sequence of pressure multiplications across the first interface will eventually bring the pressure in the steel retainer plate to 3300 bars. In the same fashion as for the first layer, a greatly reduced pressure wave is transmitted to the second layer with multiple reflections across it. If the duration of the wave in concrete were long enough, eventually the second layer would be brought to 3300 bars, or a slightly lower value because of the greater distance from the explosion, through divergence. By the equipartition argument previously made, a reduction of more than two in the pressure transmitted across the layer could not be hoped for. Alternatively, it could be considered that the first layer was successful in reducing the pressure to one-half its original value. In that case, the calculations for the second layer would proceed with the same method as that used for the first layer, with half the energy densities and pressures. To the order of accuracy required, the thickness of the second layer will again be approximately 3 in. By a similar extension of this argument, the subsequent layers would also be of this thickness.

From the above calculations, it is clear that after traversing three layers it is entirely possible that the final pressures in wood might reasonably be reduced to the yield point of 100 bars or at least to the point where there would be no further advantage in curvature of the Rankine-Hugoniot curve. At this point, it appears reasonable to substitute a material such as Celotex, which has a much lower yield point. The sequence of calculations for Celotex would follow in much the same way as for wood with, of course, a much lower yield point involved.

6.7 COMPUTER PROGRAMS

Because of the complexity of most containment problems, digital computers have been used extensively in obtaining solutions to these problems. Tables 6.17 through 6.20 list a few computer codes that are applicable to reactor containment. All these codes, with the exception of "TOSS," may be

Table 6.17. Nuclear Codes

Name of Code	Machine	System	Description	Reference	Location
EQUIPOISE-1	IBM 704	FORTRAN II	Solves the two-group, two-dimensional, neutron diffusion equations in cylindrical geometry.	140	ANL
EQUIPOISE-2	IBM 7090	FORTRAN	Same as EQUIPOISE-1.	141	ANL
KARE	Philco 2000	TAC	Solves one- and two-dimensional diffusion equations in up to five energy groups in R-Z, X-Y with diagonal line, or uniform triangular mesh geometry. Complete life studies may be performed.	142	ANL or TUG
WHIRLAWAY	IBM 7090	FORTRAN	Solves the two-group, three-dimensional, neutron diffusion equation in X-Y-Z geometry.	143	ANL
RKC	Philco 2000	FORTRAN	Computes reactor startup transients in the range of reactor power levels where the temperature coefficient effect can be neglected. A constant shim rate or a time dependent table or both is used as a driving function.		TUG
DART	Philco 2000 with EAI 231R	FORTRAN-ALTAC	Provides a digital-analog system for computing reactor startup transients for use with the Philco 2000 in conjunction with an EAI 231R analog computer. The complete system provides an automatic solution for power-range startup transients on a reactor plant analog simulator.	144	TUG
KATE	Philco 2000	TAC	Determines the spectrum of thermal neutrons according to the Way-Wigner theory and averages various quantities important to reactor design over the spectrum. The blackness coefficients, mixed number density, diffusion constants, and macroscopic cross sections to be averaged are calculated directly.	144	ANL or TUG
MINK	Philco 2000		A service routine designed to automate the transcription of MUFT and KATE output data to KARE input cards.	144	TUG

obtained from either the Argonne Code Center, Argonne National Laboratory, or from TUG, the Philco 2000 Users Group, Computer Division, Philco Corporation, Willow Grove, Pennsylvania. "TOSS" may be obtained from Central Data Processing, Union Carbide Corporation, Nuclear Division, Oak Ridge, Tennessee.

Table 6.18. Gamma Heating Codes

Name of Code	Machine	System	Description	Reference	Location
NIGHTMARE	IBM 704	FORTRAN II	Calculation of gamma heating dose at any arbitrary target point within a cylindrical reactor using a source calculated by EQUIPOISE code.		ANL
GRACE-1	IBM 7090	FORTRAN	Calculation of gamma heating and gamma dose in multiregion finite or semi-infinite slab shields. A different buildup factor may be specified for each source region considered.	145	ANL
GRACE-2	IBM 7090	FORTRAN	Calculation of gamma heating and gamma dose in multiregion cylindrical and spherical shells. The source may be located in either the center region or in a concentric shell region surrounding it. It may be uniform, exponential, or have a polynomial variation.	146	ANL
2DGH	IBM 7090	FORTRAN	An extended version of NIGHTMARE with a larger number of mesh points and a two-dimensional material arrangement permitted.		ANL
SPAN-3	Philco 2000		Calculation of uncollided gamma flux, total gamma dose rate or total energy absorption in cylindrical shield region at points away from a source of gamma radiation. Fast neutron dose rate and thermal neutron flux may be calculated by use of an empirical point kernel.	147	TUG
CLOUD	IBM 7090	FORTRAN	Calculation of the external gamma-ray dose rate and total integrated dose resulting from the continuous release of radioactive materials to the atmosphere. Meteorological parameters, such as wind velocity, lateral and vertical diffusion parameters, stability parameters, and the presence of physical boundaries, such as ground surface and a temperature inversion layer, are considered.	148	ANL

One program that is not listed is "Hazard Calculation III," which is a runaway analysis for a gas-cooled reactor. It is used in the analysis of transients that occur rapidly and which cause fuel vaporization and explusion rather than meltdown. Information about this program may be obtained from ref. 139

Table 6.19. Stress Analysis Codes

Name of Code	Machine	System	Description	Reference	Location
BMS	Philco 2000	ALTAC	Stress analysis of cylindrical shells utilizing finite difference procedures to calculate deflections, slopes, and stresses along the length of a cylindrical shell, cone, or beam on an elastic foundation resulting from any type of axisymmetric loading. This also includes axial temperature distributions. It is possible to analyze a shell with variable thickness, radius, and modulus of elasticity whose end conditions are fixed, free, pinned, or attached to another elastic structure.	149	ANL or TUG
SEAL SHELL-1	Philco 2000	FORTRAN II	Determines stresses, deflections, and internal reactions in a thin shell of revolution loaded by pressure and axisymmetric forces or deflection at each end or both. The code has been successfully applied to such problems as (1) complete pressure vessel with hemispherical head, cylindrical sides, and a flat bottom, (2) an omega seal weld, (3) a bellows, and (4) a nozzle attached to a sphere.	150	ANL
SOR II	Philco 2000	ALTAC	Determines stresses, deflection, forces and strains in thin shells of revolution with arbitrary surface loadings.	151	ANL or TUG
TCUP	IBM 704 or Philco 2000	FORTRAN II	Determines the stresses, utilizing the linear theory of elasticity, in a long curved plate due to pressures on the curved surfaces and forces or deflections specified on the straight edges.	152	ANL or TUG

Table 6.20. Thermal Codes

Name of Code	Machine	System	Description	Reference	Location
TTD	Philco 2000	TAC	Solves the two-dimensional steady-state heat conduction equation with arbitrary heat generation rates in rectangular coordinates.	153	ANL or TUG
TIGER-2B	Philco 2000	ALTAC	Computes the transient as well as the steady-state temperature distributions in a three-dimensional field containing internal heat generation. Both the boundary temperatures and the internal heat generation can vary arbitrarily in both position and time. It can handle forced convection, free convection, and radiation boundary conditions.	154	TUG
FLOPSY-II	Philco 2000	FORTRAN	Computes the weight flow and pressure drop throughout a network of nodes and branches. It can handle both open and closed loop systems, and deals with resistances in series and in parallel.		TUG
HAFMAT	Philco 2000	ALTAC	Computes the distribution of flow to all paths of any flow system in which the flow geometry and heat addition must be specified for every flow path and the system boundary conditions must also be specified.		TUG
FUGUE	IBM 7090	FORTRAN	Computes steady-state wall and bulk fluid temperatures, void fractions, and local pressure in liquid-cooled closed channels in which the heating rate is specified.	155	ANL
TITE-1	IBM 704	FORTRAN	Computes the transient two-dimensional flow of water in a heated vertical rectangular channel having nonuniform axial and transverse heat flux distribution at the walls. The treatment includes the two-dimensional transfer of mass, momentum, and energy throughout the subcooled, nucleate, and bulk boiling regions of the coolant.	156	ANL
TITE-3	Philco 2000	ALTAC	Same as TITE-1.	157	TUG
STABLE-2	Philco 2000	ALTAC	Examines the hydraulic stability of a single boiling coolant channel in parallel with many other channels.	158	TUG
STABLE-3	Philco 2000	ALTAC	Extension of STABLE-2 to accommodate the simultaneous existence of both nonboiling and subcooled boiling regimes in the subcooled region of the coolant channel.	159	TUG
MOLE	Philco 2000	FORTRAN	Determines the temperature rise and surface temperature in a channel bounded by two heat-producing elements which in turn are bounded by two sinks of known temperature.		TUG

Table 6.20. (continued)

Name of Code	Machine	System	Description	Reference	Location
TARFSI	Philco 2000	FORTRAN	Performs the thermal analysis of the core during operation of the reactor fill system.		TUG
PRE	Philco 2000		Calculates the transient performance of pressurized-water nuclear power plant pressurizers, predicting the pressure, masses, volumes, and energies within the system.		TUG
ART-04	IBM 704	SAP	Predicts the behavior of a water-cooled and -moderated reactor with plate-type fuel elements during transients that are slower than a prompt excursion and during which reactor flow, inlet temperature, and control rod reactivity are specified as a function of time.	160	ANL
ART-05	Philco 2000	TAC	Same as ART-04.	160	ANL
STDY-3	IBM 704	FORTRAN	Performs the steady-state, parallel-channel thermal analysis of a rectangular water channel core with a plate-type fuel element in a pressurized-water reactor.	161	ANL
TANK	Philco 2000	FORTRAN	Computes the transient performance of a closed loop system consisting of two primary coolant loops, a single core channel with inlet and outlet plenums, pressurizer, and secondary steam system.	162	ANL or TUG
HILO	Philco 2000		Performs steady-state thermal analysis of one- and two-pass pressurized-water reactors.		TUG
PASS	Philco 2000		Evaluates the steady-state performance of pressurized-water reactor power plants under level attitude of ship and balanced-loop conditions.		TUG
TOSS	IBM 7090		Solves the heat transfer equations for the transient or steady-state temperature distribution or both of a three-dimensional irregular body with conductive or radiation boundary conditions.	163	UCNC
GHT	IBM 7090		Solves steady-state equations or transient equations or both for heat transfer and temperature distribution in three-dimensional irregular bodies with conductive or radiation boundary conditions.	164	UCNC

References

1. Nuclear Reactors and Earthquakes, USAEC Report TID-7024, August 1963.

2. H. Etherington (Ed.), Nuclear Engineering Handbook, pp. 9-2 to 9-22, McGraw-Hill, New York, 1958.

3. C. J. West, International Critical Tables of the Numerical Data of Physics, Chemistry, and Technology, McGraw-Hill, New York, 1933.

4. C. F. Bonilla (Ed.), Nuclear Engineering, pp. 370-383, McGraw-Hill, New York, 1957.

5. H. S. Carslaw and J. C. Jaeger, Conduction of Heat in Solids, Oxford University Press, London, 1950.

6. S. T. Hsu, Engineering Heat Transfer, pp. 54-107, Van Nostrand, Princeton, 1963.

7. M. Jakob, Heat Transfer, Vol. 1, pp. 251-321, Wiley, New York, 1949.

8. P. J. Schneider, Temperature Response Charts, Wiley, New York, 1963.

9. H. Etherington, op. cit., ref. 2, pp. 9-59 to 9-62.

10. J. H. Perry (Ed.), Chemical Engineers Handbook, 3d ed., McGraw-Hill, New York, 1950.

11. I. T. Aladev, Bull. Acad. Sci. USSR, Div. Chem. Sci. (English Transl.), 11: 1669 (1951).

12. C. C. Monrad and J. F. Pelton, Trans. Am. Inst. Chem. Engrs., 38: 593 (1942).

13. R. P. Stein and W. Begell, J. Am. Inst. Chem. Engrs., Vol. 4, March 1958.

14. H. Verschoor and S. Stemerding, General Discussion on Heat Transfer, pp. 201-203, Institute of Mechanical Engineers, London, 1951.

15. R. G. Deissler, ASME Paper 53-S-41, 1953.

16. D. A. Dingee et al., Report BMI-1026, Battelle Memorial Institute, 1955.

17. P. Miller et al., Nucl. Engr. Sci. Cong., Cleveland, 1955, Preprint 25.

18. C. B. Jackson, Liquid Metals Handbook, 3d ed., Government Printing Office, Washington, D.C., 1955.

19. C. A. Sleicher and M. Tribus, Proceedings of The Heat Transfer and Fluid Mechanics Institute, pp. 59–78, Stanford University Press, Stanford, Calif., 1956.

20. B. Lubarsky and S. J. Kaufman, Report NACA-TN-3336, National Advisory Committee for Aeronautics, Washington, D.C., 1955.

21. H. Poppendiek and W. B. Harrison, Chem. Engr. Prog. Symposium Series, 9: 23 (1954).

22. The Reactor Handbook, Vol. 2, Engineering, USAEC Report AECD-3645, pp. 277–286, March 1955.

23. R. H. Norris and D. D. Streid, Trans. Am. Soc. Mech. Engrs., 62: 525 (1940).

24. W. M. Kays, ASME Paper 54-A-151, 1954.

25. W. Elenbaas, Dissipation of Heat by Free Convection, Pts. I and II, Philips Res. Rept., Vol. 3, pp. 338–360 and 450–465, 1948.

26. L. M. Trefethen, Report NP-1788, Technical Information Service Extension, 1950.

27. C. F. Bonilla (Ed.), op. cit., ref. 4, pp. 448–454.

28. W. H. McAdams, Heat Transmission, 3d ed., pp. 167–182, McGraw-Hill, New York, 1954.

29. S. T. Hsu, op. cit., ref. 6, pp. 110–195.

30. M. Jakob, op. cit., ref. 7, Vol. II, pp. 120–135.

31. W. H. McAdams, op. cit., ref. 28, pp. 82–115.

32. A. K. Oppenheim, Radiation Analysis by the Network Method, ASME Paper 54-A-75; published in Trans. Am. Soc. Mech. Engrs., 78: 725–735 (May 1956); also published in Recent Advances in Heat and Mass Transfer, J. P. Hartnett (Ed.), McGraw-Hill, New York, 1961.

33. W. H. McAdams, op. cit., ref. 28, pp. 329–341 and 356–365.

34. M. Jakob, op. cit., ref. 7, pp. 588–613 and 689–692.

35. J. H. Perry (Ed.), Chemical Engineers Handbook, 4th ed., pp. 18–53 to 18–55, McGraw-Hill, New York, 1963.

36. A. Kolflat, Results of 1959 Nuclear Power Plant Containment Tests, Report SL-1800, Sargent & Lundy, March 1960.

37. W. M. Rohsenow and H. Y. Choi, Heat, Mass, and Momentum Transfer, pp. 223-232, Prentice-Hall, Englewood Cliffs, N. J., 1961.

38. C. F. Bonilla (Ed.), op. cit., ref. 4, pp. 402-431.

39. M. Jakob, op. cit., ref. 7, pp. 635-657.

40. W. R. Gambill, Generalized Prediction of Burnout Heat Flux for Flowing, Subcooled, Wetting Liquids, Chem. Engr. Prog. Symposium Series, 59(41): 71-87 (1963).

41. J. H. Keenan and F. G. Keyes, Thermodynamic Properties of Steam - Including Data for the Liquid and Solid Phases, 32d printing, Wiley, New York, 1959.

42. M. M. El-Wakil, Nuclear Power Engineering, McGraw-Hill, New York, 1962.

43. G. E. Alves, Co-Current Liquid-Gas Flow in a Pipeline Contactor, Chem. Eng. Progr., 50: 449-546 (1954).

44. G. B. Wallis and P. Griffith, Liquid and Gas Distributions in a Two-Phase Boiling Analogy, TR-13, Massachusetts Institute of Technology, Division of Industry Co-operation, 1958.

45. J. F. Marchaterre and M. Petrick, The Prediction of Steam Volume Fractions in Boiling Systems, Nucl. Sci. Eng., 7(6): 525 (June 1960).

46. S. S. Kutateladze, Heat Transfer in Condensation and Boiling (Translated from Russian publication of the State Scientific and Technical Publishers of Literature on Machinery, Moscow-Leningrad, 1952), USAEC Report AEC-tr-3770, Technical Information Service Extension, August 1959.

47. U. H. von Glahn, An Empirical Relation for Predicting Void Fraction with Two-phase Steam-Water Flow, Report NASA-TN-D1189, National Aeronautics and Space Administration, January 1962.

48. R. C. Martinelli and D. B. Nelson, Prediction of Pressure Drop During Forced-circulation Boiling of Water, Trans. ASME, 70: 695 (1948).

49. P. A. Lottes, Nuclear Reactor Heat Transfer, USAEC Report ANL-6469, Argonne National Laboratory, December 1961.

50. H. K. Fauske and T. C. Min, A Study of the Flow of Saturated Freon-11 Through Apertures and Short Tubes, USAEC Report ANL-6667, Argonne National Laboratory, January 1963.

51. T. C. Min, H. K. Fauske, and M. Petrick, Effect of Flow Passages on Two-Phase Critical Flow, paper prepared for Industrial and Engineering Chemistry Fundamentals, to be published.

52. H. S. Isbin, personal communication, June 1963.

53. H. K. Fauske, Contribution to the Theory of Two-phase, One-component Critical Flow, USAEC Report ANL-6633, Argonne National Laboratory, October 1962.

54. R. L. Daugherty and A. C. Ingersall, Fluid Mechanics, 5th ed., McGraw-Hill, New York, 1954.

55. J. G. Burnell, The Flow of Boiling Water Through Nozzles, Orifices, and Pipes, J. Inst. Engrs., Australia, 18: 41-48 (1946).

56. M. W. Benjamin and J. G. Miller, Flow of Saturated Water Through Throttling Orifices, Trans. ASME, 63: 657-669 (1942).

57. D. Anson, M. L. Horder, and A. J. Hugill, Flow Measurements in Geothermal Bores; a Preliminary Calibration of Critical Flow Nozzles and "Wet" Orifice Plates for Very Wet Steam, Report R.234, Dominion Physical Laboratory, D.S.I.R., New Zealand.

58. A. R. Edwards, The Discharge of Water-Steam Mixtures from Pipes and Orifices, paper prepared for the IAEA Symposium on Reactor Siting, Bombay, 1963, UKAEA, Risley, Warrington, Lancashire.

59. F. W. Porzel, Design Evaluation of BER (Boiling Experimental Reactor) in Regard to Internal Explosions, USAEC Report ANL-5651, Argonne National Laboratory, January 1957.

60. F. W. Porzel, Hydrodynamics of Strong Shocks, ARF Project Report No. M903, Armour Research Foundation.

61. F. W. Porzel, Hydrodynamic Problems of Reactor Containment, Proceedings of the Second International Conference on the Peaceful Uses of Atomic Energy, Geneva, 1958, Vol. 11, pp. 85-91, United Nations, New York, 1958.

62. H. Cole, Underwater Explosions, Princeton University Press, New Jersey, 1948.

63. H. S. Isbin, I. Nishiwaki, and L. A. Klein, Condensation of Steam in Steam-Air Bubbles Immersed in Water, University of Minnesota, Department of Chemical Engineering, Contract AT(11-1)-926, August 1960.

64. C. P. Ashworth, D. B. Barton, and C. H. Robbins, Pressure Suppression, Nucl. Eng., 7: 313 (August 1962).

65. W. E. Baker, "The Elastic-Plastic Response of Thin Spherical Shells to Internal Blast Loading," J. Appl. Mech., 27: 139 (1960).

66. N. A. Weil et al., Summary Report, Studies of Reactor Containment Structures, Report IITRI-578, pp. 22-29, Illinois Institute of Technology Research Institute, November 1964.

67. J. W. Melin and S. Sutcliffe, Development of Procedures for the Rapid Computation of Dynamic Structural Response, Civil Engineering Studies, Structural Research Series 171, University of Illinois, Urbana, Ill.

68. W. Flügge, Stresses in Shells, Springer, Berlin, 1960.

69. Subcommittee of Design Division, Pressure Vessel Research Committee, Uniform Notation System for Pressure Vessel Theory, Mech. Eng., 77: 505-507 (June 1955).

70. S. Timoshenko, Theory of Plates and Shells, McGraw-Hill, New York, 1940.

71. J. Marin, Mechanical Behavior of Engineering Materials, Prentice-Hall, New Jersey, 1962.

72. W. R. Wise, An Investigation of Strain Energy Absorption - Potential as the Criterion for Determining Optimum Reactor Vessel Containment Design, Report No. NOL-5748, U.S. Naval Ordnance Laboratory, 1958.

73. J. Marin and T. Weng, Strength of Thick-walled Cylindrical Pressure Vessels, Department of Engineering Mechanics, Pennsylvania State University, 1961.

74. G. Sachs, Material Problems in Solid Fuel Case Design and Manufacture, USAEC Report NP-11199, Technical Information Service Extension, 1960.

75. J. D. Lubahn and R. P. Felgar, Plasticity and Creep of Metals, Wiley, New York, 1961.

76. R. Hill, The Mathematical Theory of Plasticity, Clarendon Press, Oxford, 1950.

77. P. Hodge, Plastic Analysis of Structures, McGraw-Hill, New York, 1959.

78. J. N. Goodier and P. Hodge, Elasticity and Plasticity, Wiley, New York, 1958.

79. L. S. Marks, Mechanical Engineers Handbook, McGraw-Hill, New York, 1951.

80. W. Prager, On the Use of Singular Yield Conditions and Associated Flow Rules, J. Appl. Mech., 20: 183-188 (1953).

81. W. Prager and P. Hodge, Theory of Perfectly Plastic Solids, Wiley, New York, 1951.

82. E. W. Ross and W. Prager, On the Theory of the Bulge Test, Quart. Appl. Math., XII: 86-91 (1954).

83. H. Tresca, Memoire sur l'ecoulement des crops solides, Mem. pres. par. div. savants, 18: 733-799 (1868).

84. P. Ludwik, Elemente der Technologischer Mechanik, Springer, Berlin, 1909.

85. J. M. Krafft and A. M. Sullivan, Influence of Speed of Deformation on Strength Properties in the Post Lower Yield Stress-Strain Curve of Mild Steel, Ship Structure Committee Rept. 127 (Contract NObs-72046), 1960.

86. W. Puzicha and A. Krisch, "Der Einflu der Dehngeschwindigkeit auf die zugfestigkeit and Dehnung dustenitischer Stahle," Z. Metallk., 40: 93-98 (1949).

87. R. F. Klinger, Effect of Rate of Strain on the Tensile Properties of SAE 4340 Steel, Report WADC-TR-53-507, Wright Air Development Center, 1955.

88. M. J. Manjoine and A. Nadai, High-Speed Tension Tests at Elevated Temperatures, Proc. ASTM, 40: 822-839 (1940).

89. D. S. Clark, The Influence of Impact Velocity on the Tensile Characteristics of Some Aircraft Metals and Alloys, Report NACA-TN-868, National Advisory Committee for Aeronautics, 1942.

90. D. S. Clark and P. E. Duwez, Influence of Strain Rate on Some Tensile Properties of Steel, Proc. ASTM, 50: 560-575 (1950).

91. H. G. Baron, Stress-Strain Curves of Some Metals and Alloys at Low Temperature and High Rates of Strain, J. Iron Steel Inst. (London), 182: 354-365 (1956).

92. J. D. Campbell and J. Duby, Proc. Roy. Soc. (London) A, 236: 24 (1956).

93. A. L. Austin and R. F. Steidel, Jr., The Tensile Properties of Some Engineering Materials at High Rates of Strain, Proc. ASTM, 59: 1292-1308 (1959).

94. J. D. Campbell and J. Duby, Delayed Yield and Other Dynamic Loading Phenomena in a Medium-Carbon Steel, in Proceedings of the Conference on the Properties of Materials at High Rates of Strain, Institute of Mechanical Engineering, London, 1957.

95. D. S. Clark and G. Datnyler, Stress Relations Under Tension Impact Loading, Proc. ASTM, 38(II): 98-111 (1938).

96. D. S. Clark, The Behavior of Metals Under Dynamic Loading, Trans. Am. Soc. Metals, 46: 34 (1954).

97. A. H. Cottrell, Deformation of Solids at High Rates of Strain, in Proceedings of the Conference on the Properties of Materials at High Rates of Strain, London, 30th April-2nd May, 1957, pp. 1-12, Institute of Mechanical Engineers, London, 1957.

98. G. R. Cowper and P. S. Symonds, Strain-hardening and Strain-rate Effects in the Impact Loading of Cantilever Beams, ONR Contract Nonr-562 (10), NR-064-406, Grad. Div. of Appl. Math., Brown University Technical Report No. 28, September 1957.

99. T. E. Davidson and D. P. Kendall, A New Concept for Studying Pressure Vessel Configurations Under Very High Pressures and Loading Rates, Technical Report WVT-RI-6102-R, Watervliet Arsenal, Watervliet, N.Y., 1961.

100. A. G. H. Dietz and F. R. Eirich, High Speed Testing, Vol. 1, Interscience, New York, 1960.

101. R. W. Fenn, Jr., and J. A. Gusack, Effect of Strain Rate and Temperature on the Strength of Magnesium Alloys, Proc. ASTM, 58: 685-696 (1959).

102. D. H. Fisher, R. L. Carlson, and W. T. Lankford, The Effects of Strain Rate and Temper Rolling on the Strain-Aging Characteristics of Rimmed, Deep Drawing Steel, Proc. ASTM, 58: 932-942 (1958).

103. W. Goldsmith, Impact: The Theory and Physical Behaviour of Colliding Solids, E. Arnold, London, 1960.

104. D. B. Harris and M. P. White, Comparison of the Hardening Produced in a Yield-Point Steel by Uniaxial Loading Under Static and Under Dynamic Conditions, J. Appl. Mech., 21: 194 (1954).

105. J. A. Hendrickson, D. S. Wood, and D. S. Clark, The Effect of Rate of Stress Application and Temperature on the Upper Yield Stress of Annealed Mild Steel, California Institute of Technology, Dynamic Properties Laboratory, OOR Project No. 1235, Second Interim Technical Report, March 1957.

106. J. A. Hendrickson and D. S. Wood, The Effect of Rate of Stress Application and Temperature on the Upper Yield Stress of Annealed Mild Steel, Trans. Am. Soc. Metals, 50: 498-516 (1958).

107. J. E. Hockett, Compression Testing at Constant True Strain Rates, Proc. ASTM, 59: 1309-1319 (1959).

108. A. Kochendorfer, Calculation of Tensile Strength of Metals, and Its Dependence on the Strain Rate and Temperature, Z. Metallkunde, 38: 173-186 (1947).

109. S. L. Koh, Literature Summary: Behavior of Materials Under Impulsive Loading, Bibliography on Shock and Shock Excited Vibrations, Engineering Research Bull. No. 68, Pennsylvania State University, 1957.

110. F. P. Klier et al., The Properties of Constructional Metals as a Function of Temperature and Strain Rate in Torsion, Report WADC-TR-56-216 (PB 121912; ASTIA AD 110559), Wright Air Development Center, 1956.

111. R. F. Klinder, Tensile Properties of Some Aircraft Structural Materials at Various Rates of Loading, Proc. ASTM, 50: 1035-1050 (1950).

112. H. Kolsky, An Investigation of the Mechanical Properties of Materials at Very High Rates of Loading, Proc. Phys. Soc. London, 62: 676-700 (1949).

113. C. J. Maiden, Some Investigations of the Dynamic Strength of Low Carbon Steels, Proceedings of the Ordnance Corps Conference on High Loading Rate, 1959.

114. C. R. Manning, Jr., Application of Rate Temperature Parameters to Tensile Data for Magnesium Alloys and a Relation Between the Larson-Miller Constant and the Activation Energy, Report NASA-TN-D-172, National Aeronautics and Space Administration, 1960.

115. Y. Nakagawa, Yield Point Depends on the Rate of Strain: Its Theory, Bull. ASME, 2: 501-503 (1959).

116. N. H. Norris et al., Structural Design for Dynamic Loads, McGraw-Hill, New York, 1959.

117. H. J. Plass, Theory of Plastic Bending Waves in a Bar of Strain Rate Material, in Proceedings of the Second Midwestern Conference on Solid Mechanics, Purdue University Research Series, 129: 109 (1955).

118. J. S. Rinehart and J. Pearson, Behavior of Metals Under Impulsive Loads, The American Society of Metals, Cleveland, Ohio, 1954.

119. C. Riparbelli, On the Relation Among Stress, Strain, and Strain Rate in Copper Wires Submitted to Longitudinal Impact, Proc. Soc. Expl. Stress Anal., 14: 55-70 (1954).

120. F. B. Stulen, A Model for the Mechanical Properties of Metals, Mater. Res. Std., 2: 102-108 (1962).

121. J. A. Simmons, F. Hauser, and J. E. Dorn, Mathematical Theories of Plastic Deformation Under Impulsive Loading, University of California Publication in Engineering, Vol. 5, p. 7, University of California Press, Berkeley, 1962.

122. M. A. Salmon, Plastic Instability of Cylindrical Shells with Rigid End Closures, Report IITRI-528-19, Illinois Institute of Technology Research Institute, November 1964.

123. Studies of Reactor Containment, Report IITRI-528, p. 22-14, Illinois Institute of Technology Research Institute, November 1964.

124. N. A. Weil, M. A. Salmon, and C. J. Costantino, Approximate Burst Strength of Thin-Walled Cylinders with Hemispherical Caps, AIAA Journal, Vol. 1, No. 9, September 1963.

125. C. J. Costantino, M. A. Salmon, and N. A. Weil, Effect of End Conditions on the Burst Strength of Finite Cylinders, J. Appl. Mech., March 1964.

126. W. R. Wise and J. F. Proctor, Explosion Containment Laws for Nuclear Reactor Vessels, USAEC Report NOLTR-63-140, Naval Ordnance Laboratory (to be issued).

127. W. R. Wise, Jr., J. F. Proctor, and L. P. Walker, Response of Enrico Fermi Reactor to TNT Simulated Nuclear Accidents, USAEC Report NOLTR-62-209, Naval Ordnance Laboratory, Nov. 13, 1964.

128. R. J. Larson and W. Olson, Measurement of Air Blast Effects from Simulated Nuclear Reactor Core Excursions, USAEC Report WASH-747, September 1957.

129. E. R. Kilsby, Jr., A Survey of Water Reactor Primary System Conditions Pertinent to the Study of Pipe Rupture, USAEC Report GEAP-4445, General Electric Company, January 1964.

130. S. W. Tagart, Jr., Mechanical Design Considerations in Primary Nuclear Piping, USAEC Report GEAP-4578, General Electric Company, March 1964.

131. A. J. Brothers et al., A Review of Fracture Modes as Related to Primary Coolant System Rupture Study, USAEC Report GEAP-4446, General Electric Company, May 1964.

132. W. S. Gibbons and B. D. Hackney, Survey of Piping Failures for the Reactor Primary Coolant Pipe Rupture Study, USAEC Report GEAP-4574, General Electric Company, May 1964.

133. United States Department of Defense, Ballistic Research Laboratory, Paper No. 843, AFSQP No. 786.

134. T. S. Kress, Missile Analysis for GCR-ORR Loop 2, USAEC Report ORNL TM-854, Oak Ridge National Laboratory (to be published).

135. N. R. Zabel, Containment of Fragments from Runaway Reactor, Report SRIA-2, pp. 21-23, Stanford Research Institute, Oct. 1, 1958.

136. Fundamental Studies of Explosive Charges, Volume II: Concrete Breaching and Wood Cutting Charges, Engineer R. and D., SRI Project No. GU-1378, Contract DA-44-009-ENG-2512, June 12, 1957.

137. Progress Reports Nos. 2 and 3, SRI Project No. GU-2164, Contract No. AT(04-3)-115, Sept. 20 and Oct. 20, 1957.

138. H. O. Monson and M. M. Sluger, Containment of EBR-II, Proceedings of the Second United Nations International Conference on Peaceful Uses of Atomic Energy, Geneva, 1958, Vol. II, p. 137, United Nations, New York, 1958.

139. R. A. Becker, Runaway Analysis for a Gas-Cooled Reactor, Report APEX-585, General Electric Co., July 1960.

140. Melvin Tobias and T. B. Fowler, Equipoise – An IBM-704 Code for the Solution of Two-Group, Two-Dimensional, Neutron Diffusion Equations in Cylindrical Geometry, USAEC Report ORNL-2967, Oak Ridge National Laboratory, November 1960.

141. Melvin Tobias and T. B. Fowler, Equipoise – A Two-Dimensional, Two-Group, Neutron Diffusion Code for the IBM 7090 Computer, USAEC Report ORNL-CF-60-11-67, Oak Ridge National Laboratory, Nov. 21, 1960.

142. J. A. Archibald, Jr., KARE – A System of Diffusion Theory Programs for the Philco 2000, Vol. 1 (to be published).

143. T. B. Fowler and Melvin Tobias, Whirlaway – A Three-Dimensional Neutron Diffusion Code for the IBM-7090 Computer, USAEC Report ORNL-3150, Oak Ridge National Laboratory, August 1961.

144. H. J. Amster and J. B. Callaghan, Kate-1 – A Program for Calculating Wigner-Wilkins and Maxwellian Averaged Thermal Constants on the Philco-2000, Report WAPD-TM-232, Westinghouse Electric Corp., October 1960.

145. D. S. Duncan and A. B. Speir, Grace I, An IBM 704-709 Program Designed for Computing Gamma Ray Attenuation and Heating in Reactor Shields, Report NAA-SR-3719, North American Aviation, Inc., 1959.

146. D. S. Duncan and A. B. Speir, Grace II, An IBM-709 Program for Computing Gamma Ray Attenuation and Heating in Cylindrical and Spherical Geometries, Report NAA-SR-Memo-4649, North American Aviation, Inc., 1959.

147. W. H. Guilinger, N. D. Cook, and P. A. Gillis, Span-3 – A Shield Design Program for the Philco-2000 Computer, Report WAPD-TM-235, Westinghouse Electric Corp., February 1962.

148. D. S. Duncan, Cloud, An IBM-7090 Program for Computing Gamma-Ray Dose Rate from a Radioactive Cloud, Report NAA-SR-Memo-4822, North American Aviation, Inc., 1959.

149. D. C. Dight and R. F. Wojcieszak, BMS – Stress Analysis of Cylindrical Shells, Report KAPL-M-EC-10, Knolls Atomic Power Laboratory, Aug. 1, 1961.

150. C. M. Friedrich, Seal-Shell – A Digital Program to Determine Stresses and Deflections in Axisymmetric Shell of Revolution, Report WAPD-TM-277, Westinghouse Electric Corp., September 1961.

151. J. A. Mirabel and D. G. Dight, SOR II, A Program to Perform Stress Analysis of Shells of Revolution, Report KAPL-M-EC-19, Knolls Atomic Power Laboratory, June 1962.

152. D. S. Griffin and C. M. Friedrich, Stresses and Deflections in Thick, Curved Plates, Report WAPD-TM-258, Westinghouse Electric Corp., August 1961.

153. E. L. Wachspress, Cure, a Generalized Two-Space-Dimension Multigroup Coding for the IBM-704, Report KAPL-1724, Knolls Atomic Power Laboratory, April 1957.

154. A. T. Bray and S. J. MacCracken, Tiger 2: Digital Computer Program – Temperature from Internal Generation Rates, Report KAPL-M-DIG-TD-9, Knolls Atomic Power Laboratory, Feb. 28, 1959.

155. R. C. Noyes, F. Bergonzoli, and J. E. Gingrich, Fugue, a Non-Dimensional Method for Digital Computer Calculation of Steady State Temperature, Pressure, and Void Fraction in Pipe Flow with or Without Boiling, Report NAA-SR-5958, North American Aviation, Inc., 1961.

156. R. I. Miller and R. S. Pyle, Tite – A Digital Program for the Prediction of 2-Dimensional 2-Phase Hydrodynamics, Report WAPD-TM-240, Westinghouse Electric Corp., August 1960.

157. O. J. Marlowe, Nuclear Reaction Depletion Programs for the Philco-2000 Computer, Report WAPD-TM-221, Westinghouse Electric Corp., January 1961.

158. D. G. Dight, Stable-2 – Hydraulic Flow Stability Analysis, Report KAPL-M-EC-11, Knolls Atomic Power Laboratory, Oct. 15, 1961.

159. A. B. Jones and D. G. Dight, Hydrodynamic Stability of a Boiling Channel, Pt. 2, Report KAPL-2208, Knolls Atomic Power Laboratory, April 20, 1962.

160. J. E. Meyer, R. B. Smith, H. G. Gelbard, D. E. George, and W. D. Peterson, Art – A Program for the Treatment of Reactor Thermal Transients on the IBM-704, Report WAPD-TM-156, Westinghouse Electric Corp., November 1959.

161. R. S. Pyle, Stdy-3 – A Program for the Thermal Analysis of a Pressurized Water Nuclear Reactor during Steady-State Operation, Report WAPD-TM-213, Westinghouse Electric Corp., June 1960.

162. M. A. Ketcham, Tank – Transient Analysis of Plant Performance, Report KAPL-M-EC-9, Knolls Atomic Power Laboratory, July 1961.

163. David Bagwell, Toss – An IBM 7090 Code for Computing Transient or Steady State Temperature Distributions, USAEC Report K-1494, Union Carbide Nuclear Co., December 1961.

164. T. B. Fowler and E. R. Volk, Generalized Heat Conduction Code for the IBM 7090 Computer (GHT), USAEC Report ORNL-2734, Oak Ridge National Laboratory, October 1954; revised by ORNL CF-61-2-33, February 1961.